

Dynamics and
Control
of
Large
Electric
Power Systems



Marija Ilić - John Zaborszky

ISBN 0-471-29858-1

DYNAMICS AND CONTROL OF LARGE ELECTRIC POWER SYSTEMS

Marija Ilić & John Zaborszky



A Wiley-Interscience Publication
JOHN WILEY & SONS, INC.

New York • Chichester • Weinheim • Brisbane • Singapore • Toronto

This text is printed on acid-free paper. ☺

Copyright © 2000 by John Wiley & Sons, Inc. All rights reserved.

Published simultaneously in Canada.

No part of this publication may be reproduced, stored in a retrieval system or transmitted in any form or by any means, electronic, mechanical, photocopying, recording, scanning or otherwise, except as permitted under Section 107 or 108 of the 1976 United States Copyright Act, without either the prior written permission of the Publisher, or authorization through payment of the appropriate per-copy fee to the Copyright Clearance Center, 222 Rosewood Drive, Danvers, MA 01923, (978) 750-8400, fax (978) 750-4744. Requests to the Publisher for permission should be addressed to the Permissions Department, John Wiley & Sons, Inc., 605 Third Avenue, New York, NY 10158-0012, (212) 850-6011, fax (212) 850-6008, E-Mail: PERMREQ @ WILEY.COM.

For ordering and customer service, call 1-800-CALL-WILEY.

Library of Congress Cataloging in Publication Data:

Ilic, Marija D., 1951-

Dynamics and control of large electric power systems / Marija Ilić, John Zaborszky.

p. cm.

"A Wiley-Interscience publication."

Includes index.

ISBN 0-471-29858-1 (cloth : alk. paper)

1. Electric power systems—Control. 2. Systems analysis.

I. Zaborszky, John. II. Title.

TK1007.I45 2000

621.31—dc21

99-29004

CIP

Printed in the United States of America

10 9 8 7 6 5 4 3 2 1

PREFACE

Early in the twentieth century, electric power technology and theory represented the most difficult and advanced engineering areas. *Power systems* at that time were individual companies supplying some urban areas with a few generating stations. The rural inhabitants only heard of electric lights. Yet fast progress existed in equipment technology (e.g., the introduction of transformers) and theory (e.g., electromagnetic mathematical models developed for synchronous machines by Blondel, Park, and Concordia reduced to a simple form for short circuit and stability computations in the concept of transient and subtransient reactances; and the phasor transformation by Steinmetz).

Soon individual power companies were being interconnected by tie lines, creating systems based on networks of increasing size and complexity. This increased the computation burden and led to the early introduction of a hybrid lumped analog computer (network analyzer for networks with a maximum of approximately 25 generators). The *area control error* concept of Nathan Cohn in the late 1940's, followed by the seemingly first industrial use of digital computers in the late 1950's for generation dispatch, made possible a very fast growth of interconnections in the 1950's and early 1960's.

This latter development unfortunately overlooked proper design for emergency conditions. This led to the famous ten-state, one-week blackout of the Northeast U.S. in 1964. This in turn, however, led to a renewed interest in the theoretical base of the electric power system. Reinforced by the oil embargo of the 1970's, this interest generated ample research support in the 1970's and 1980's, resulting in the expansion of theory and technology in uncoordinated leaps and bounds.

One additional branch of major development since the 1970's has been power electronics use in high-voltage (HVDC) and the Flexible AC Transmission Systems (FACTS) and developments in many new and improved power system components.

Currently a deep reaching reorganization of the industry, from government "regulated" to a free-market style of "deregulated" electric power dispatch nationwide, creates some very difficult theoretical/political/economic problems, such as the price of free market trading of power across a very large, nonswitched network. All this still leaves the electric power system one of the most complex and challenging engineering systems, because of nonuniformity in size and character of its equipment (e.g., generators, transformers, transmission lines) and their nonlinearity. In contrast, the gigantic development during the second half of the twentieth century in complexity, size, and popular respect for electronics, computers, and communication systems is largely based on identical components repeated by the billions. Also, these components tend to be individually simple although they are based on highly sophisticated developments in mathematics,

physics, chemistry, etc. These fields also have great popular appeal through their multiple contact with ordinary people, whose only contact with power systems remains to be through the wall switch and wall plug.

It is the objective of this book to present an organized, comprehensive representation of the state-of-the-art electric power system dynamics, including the control concepts underlying the extremely complex power system field. It is our hope that the reader becomes excited about the challenges in modern power systems the way we have been over many years. The challenge to prove and advance the usefulness of near-real time computing, control, and communications for a system in which experimenting is virtually impossible remains enormous. So the area with its long but active history still remains one of the most exciting fields in engineering, both in theory and in technology. The authors hope that the book provides for the readers with proper background and foundation for understanding the dynamics of the system either as a student or in self study standing in his/her industrial or research activities.

Marija D. Ilić
Cambridge, MA

John Zaborszky
St. Louis, MO

CONTENTS

Preface	xvii
1 Introduction	1
1.1 Scope of the contents of the book	2
Acknowledgments	6
I Modeling the Structure and Components	7
2 Quasistationary Phasor Concepts	9
2.1 Time-domain representation for AC voltage, current, power, and energy	10
2.1.1 Basic power-flow concepts on single-phase transmission lines	13
2.1.2 Basic power-flow concepts on three-phase transmission lines	17
2.2 Definition of the phasor for AC quantities	19
2.2.1 Phasor interpretation of power	22
2.3 Classical stationary phasor calculus	23
2.4 The classical quasistationary phasor calculus	23
2.4.1 Some general comments	24
2.5 Summary of the characteristics of active- and reactive-power flow	24
2.5.1 Characteristics of active power $P(t)$ in the quasistationary region	24
2.5.2 Characteristics of the reactive power $Q(t)$ in the quasistationary region	25
2.5.3 Optimum performance of devices characterized by AC signals	26
2.6 Quasistationary phasor concepts for periodic signals	28
2.6.1 Time-domain representation for periodic voltage, current, power, and energy	28
2.6.2 Generalizing phasors to multiharmonic, that is, periodic, signals	33
2.6.3 Definition of vector phasors for periodic signals	35

2.6.4	Phasor interpretation of power	40
2.6.5	Conservation of reactive-power components	43
2.6.6	Circuit example	45
2.6.7	Reactive power in linear RLC circuits with power electronic switches	46
2.6.8	Optimum performance of devices characterized by periodic signals	47
2.6.9	Optimization example using vector-space algebra	49
2.6.10	Example of optimal performance for signals with harmonics	51
2.6.11	Summary of the characteristics of real- and reactive-power flow	53
2.6.12	Comparison with other reactive-power definitions	55
2.7	Vector representation for multiphase circuits	57
2.8	Chapter Summary	58
3	Analytical Dynamic Model of the Power System	61
3.1	Fundamental static and dynamic structures of the power-transmission system	65
3.1.1	Structure of the overall power-system model	65
3.1.2	Discussion of Figures 3.2 and 3.3	67
3.2	Particulars of the models of power-system components	68
3.2.1	Buses	69
3.2.2	HV-AC power-transmission lines	72
3.2.3	Bus-connected equipment with established models of uniform type	78
3.2.4	Bus-connected equipment with models consisting of many individual types, mostly primary controllers	135
Appendix 3.1	Conceptual derivation of algebraic coupling equations for generator and bus	162
Appendix 3.2	Model derivation (Eqs. 3.207) to (3.209)	162
4	Models for Computer-Aided Analysis and Control	169
4.1	Utilization of circuit theory methods	170
4.1.1	Classification of component types	170
4.1.2	Constituent relations for single-port components	171
4.1.3	Constituent relations for transmission lines	176
4.1.4	Computer formulation of the Kirchoff laws	179
4.1.5	Transmission network admittance matrix and its properties	183
4.1.6	Summary of a general DAE model	186

4.1.7	Models for horizontally structured large power systems	190
4.2	Non linear power system models in ordinary differential equation form	191
4.2.1	Coupled real-power–voltage dynamics for large-power systems (machine frame of reference)	192
4.2.2	Nonlinear power-system model in an ODE form (phasor frame of reference)	196
4.3	Elementary overview of stability problems in the power system	198
4.3.1	Static stability and static equilibria	201
4.3.2	Real-power static stability	201
4.3.3	Reactive-power static stability	202
4.3.4	Static stability limit	203
4.3.5	Small-signal-stability. Classification of equilibrium points	204
4.3.6	Transient stability	205
4.3.7	Transient stability in reactive power	206
4.3.8	Medium- and long-range or multiswing instability	208
4.3.9	Medium-range instability	208
4.3.10	Long-range instability in real power	208
4.3.11	Long-range instability in reactive power	209
II	Analysis of Stationary and Dynamic Processes	211
5	Stationary Analysis	213
5.1	Power-system equilibrium definition	213
5.2	Load-flow problem	215
5.2.1	Analytic properties of the load-flow equations	218
5.2.2	Real-power–reactive-power decoupling conditions	219
5.3	Decoupled real-power–angle load-flow problem	222
5.3.1	Linear resistive network interpretation of the DC load-flow problem	223
5.3.2	Nonlinear resistor network interpretation of the $P-\delta$ load-flow problem	225
5.3.3	Localized response property of the $P-\delta$ power network	235
5.3.4	$P-\delta$ load-flow problem in deregulated industry	245
5.4	Decoupled reactive-power–voltage $Q-V$ load-flow problem	258
5.4.1	Problem complexity as a function of load models used	259

5.4.2	Q–V problem with constant-power load models	261
5.4.3	Q–V load flow problem as a problem of a nonlinear resistive network with independent sources	261
5.4.4	<i>Q</i> –V load-flow problem as a problem of a linear resistive network with dependent sources	266
5.5	Low-voltage problems under heavy real-power transfers	274
5.5.1	Radial circuit fed by a constant-voltage source	276
5.6	Means of increasing real-power transfer	277
5.6.1	Load compensation and high-voltage problems	278
5.6.2	Line compensation as a means of increasing real-power transfer	283
5.7	Steady-state stability problem as a coupled <i>P</i> – <i>Q</i> problem	285
5.7.1	Two-bus system concepts	286
5.7.2	Methods for multibus systems	288
5.8	Numerical tools used in the solution of power-flow equations	290
5.9	Continuation methods	291
5.9.1	Introduction to the continuation paradigm	292
5.9.2	Problems with the embedding algorithm	296
5.9.3	Homotopy methods versus classical embedding algorithms	297
5.9.4	Tracking the paths	301
5.9.5	Choosing a homotopy method	303
5.9.6	Homotopy variations	303
5.9.7	Free-running versus forced homotopies	303
5.9.8	Globally convergent probability-1 homotopy algorithms	304
5.9.9	Applications of forced and free-running homotopy methods	305
5.9.10	Circuit applications	305
5.9.11	Applications of continuation methods to power systems	306
5.9.12	Homotopy software hompack	307
5.9.13	Power-flow problem and hompack	307
5.9.14	Simulation results	309
5.9.15	Homotopy applications to the <i>Q</i> –V problem	313
5.9.16	Coupled load-flow problem: bergen's example	316
5.9.17	Simulation conclusions	316
5.10	Chapter summary	320
Appendix 5.1	The Newton–Raphson method	321

6 Analysis of Linearized (Small-Signal) Dynamics	333
6.1 Objectives of small-signal analysis studies in power systems	335
6.1.1 Effect of models employed on stability analysis and its results	335
6.1.2 A multiparameter singularly perturbed model of an electric power system	337
6.2 Separation of fast angle and midrange voltage dynamics	340
6.2.1 Integral-manifold derivations	343
6.2.2 Relevant model for fast angle dynamics	347
6.2.3 Relevant model of midrange voltage dynamics	348
6.3 Slow voltage dynamics	349
6.3.1 Interactions of the OLTC control and midrange voltage dynamics	349
6.3.2 Approximate continuous model for midrange voltage dynamics	351
6.4 Slow frequency dynamics	352
6.4.1 Governor–turbine control of frequency dynamics	353
6.4.2 Real-power network constraints	355
6.4.3 Real-power–frequency dynamics of an interconnected system	358
6.5 Midrange voltage dynamics	359
6.5.1 Exciter control of reactive-power—voltage dynamics	359
6.5.2 Reactive-power network constraints	361
6.6 Interarea dynamics	363
6.6.1 Definition of the interarea variables	364
6.6.2 Fundamental relations relevant for analysis of the interarea dynamics	365
6.6.3 Computation of interarea variables	366
6.6.4 Modeling of the interarea dynamics	367
6.6.5 Dynamics of interarea variables on an interconnected power system	368
6.7 Model reduction at the interconnected system level	371
6.7.1 Time-scale separation in aggregate and coherent models	372
Appendix 6.1 Machine parameters and network data	374
Appendix 6.2 Singular perturbation method for model reduction	376

Appendix 6.3 Eigenmode-based model reduction: selective modal analysis	381
Appendix 6.4 Some relations between SP-and SMA-based model reduction techniques	384
7 Introduction to the Concepts and Structure of Comprehensive Power-System Dynamics	391
7.1 Nonlinear dynamic analysis of a minimal power system	393
7.1.1 A minimal power system model with (loss-less) generator and matched load	393
7.1.2 Parameter space	396
7.1.3 State space	396
7.1.4 Time histories of individual state variables	400
7.1.5 A guided tour through the parameter and state spaces and the time histories	401
7.1.6 Some observations	403
7.2 Voltage stability analysis of the rudimentary power system	405
7.2.1 Power-system model with generator, voltage control, transmission and matched load	406
7.2.2 Basic features of the structure of the state-space— parameter spaces	409
7.2.3 Exploration of changes caused by variations in the load model and the type of control used	427
7.2.4 Bifurcation analysis for the rudimentary power system	429
Appendix 7.1 Some aspects of the phase portrait (the flow of the vector field)	440
Appendix 7.2 Some aspects of bifurcations	442
8 Smooth Nonlinear Dynamics of the Large Power System	451
8.1 Historical sketch of the development of analytic tools for large comprehensive power-system dynamics	455
8.2 Dynamics of the DAE System	459
8.2.1 State-space structure of the DAE dynamics, Σ	462
8.2.2 Analysis of the stability regions	473
8.2.3 Structure of the parameter space	482
9 Dynamic Computation Analysis on Realistic Size (Thousands of Buses) Systems with Real-Life Examples	499
9.1 Computational aspects of the Hopf-bifurcation-related segment of the feasibility boundary	500
9.1.1 System description	500
9.1.2 Some aspects of the hopf bifurcation and its vicinity	501

9.1.3	Critical eigenvalue	502
9.1.4	Iterative technique for finding a Hopf-bifurcation point	504
9.1.5	Method for computing a hopf-bifurcation-related feasibility boundary	505
9.1.6	Computational analysis	507
9.1.7	Computation of the hopf-bifurcation-related segment	511
9.2	Use of large-scale computation results for studying the nature and interactions near the feasibility boundary	518
9.2.1	Effect of using lower-degree approximations	518
10	Large Smooth Systems with Embedded Discontinuous Nonlinear Constraints	523
10.1	Automatic-tap-changer-based control embedded in differential-algebraic equation systems	523
10.1.1	Physical features	524
10.1.2	Effect of the automatic tap changer on the feasibility boundary in parameter space	525
10.1.3	Transient phenomena connected with the tap changer in the state space	527
10.2	Dynamics of the large DAE power system with embedded hard limits	528
10.2.1	Modeling the large power system with hard limits	529
10.2.2	Conceptual introduction on small systems	531
10.2.3	Hard limits in the power-system model	540
10.2.4	State-space structure: region of attraction and stability boundary	541
10.2.5	Parameter-space structure: the boundary of small-signal stability	547
10.3	Summary	551
11	Beyond Quasistationarity and the Lumped-Parameter Model	555
11.1	Generalized time-varying phasor transformation	556
11.1.1	Low-pass phasor signals	559
11.1.2	Three-phase balanced phasor signals	560
11.2	Time-varying phasor and its properties	562
11.2.1	Parts of the power system for which phasors apply	568
11.2.2	Phasors in the G set the transmission system	570
11.3	Analysis of the transmission-line dynamics including distributed constants and line losses	571

11.4 Transmission-system equations (power balance)—models for the G set using time delays to represent partial differential equations	576
11.4.1 Transients in the G set	577
11.5 Power-system dynamic models	577
11.5.1 Some details and the precision of the model; available approximations	578
11.5.2 RLC-circuit approximation	579
11.5.3 Limitations imposed by the time-varying phasors	583
11.6 Chapter summary	586
III Control and Stabilization	589
12 Primary Control of Electric Power Systems	591
12.1 Available types of primary-control devices	592
12.1.1 Time-scale-separation-based classification	593
12.2 Generation-based primary control under normal operation	594
12.2.1 Fast continuous primary controllers	594
12.2.2 Generator-based control as a full-state optimal control-design problem	601
12.3 Generation control of power systems under stress	604
12.3.1 Remaining challenges in designing primary control of generators	605
12.3.2 Nonlinear control design for generators	610
12.4 Facts-based transmission system control	618
12.4.1 Static var compensator as a control means	619
12.5 Load-based control	631
12.6 Mechanically switched control	631
12.6.1 Modeling of switched-control-driven voltage changes	632
12.7 Chapter summary	634
13 Stationary Generation Control (Ignoring Congestion)	641
13.1 Principles of operation of the large interconnected system by decision and control	642
13.1.1 Some details of the decision and control phases	643
13.2 Basic structure of the generation-dispatch control	647
13.2.1 Basis for hierarchies in regulated generation control	655

13.2.2 Basis for hierarchies in deregulated generation control	657
13.3 Generation-dispatch economy	659
13.3.1 Generation dispatch in the regulated industry	661
13.3.2 Generation dispatch in the deregulated industry	668
13.4 Generation-based frequency control	676
13.4.1 Frequency control in the regulated industry	677
13.4.2 Frequency control in the deregulated industry	697
13.5 Reactive-power dispatch economy	715
13.5.1 Reactive-power dispatch in regulated industry	716
13.5.2 Reactive-power dispatch in the deregulated industry	720
13.6 Generation-based voltage control	727
13.6.1 Voltage control in the regulated industry	728
13.6.2 $P-\delta$ and $Q-V$ control: similarities and differences	742
13.7 Chapter summary	743
Appendix 13.1 Structure-based modeling for hierarchical control design	749
Appendix 13.2 Structure-based hierarchical control design	752
14 Stationary Generation Control (with Congestion)	757
14.1 Methods for transmission congestion flow control	759
14.1.1 Transmission line flow (congestion) control in regulated industry	760
14.1.2 Transmission line flow (congestion) management in deregulated industry	764
14.2 Re-examination of voltage control	778
14.3 Methods for efficient congestion control in very large power systems	778
14.3.1 Monitoring tests for determining the localized nature of voltage problems	779
14.3.2 \underline{D} Vector-based algorithm	784
14.3.3 Clusterwide approach with full information and flexible clustering	797
14.4 Efficient methods for controlling systemwide congestion	811
14.4.1 Textured-model algorithm	811
14.5 Chapter summary	819
Guide to using this book	824
Index	827

1 Introduction

This book offers an advanced presentation of modern electric power systems, starting from a brief review of their structure and their physical components, through modeling, analysis, computation, and control concepts. The authors strive to present a comprehensive account of power-system dynamics in a way that is accessible and useful to readers whose backgrounds range from moderate engineering and/or mathematical preparation to the highly advanced. This sounds like trying to be all things to all people, but it actually describes an organized and structured flow of the contents over the range of typical prospective users. All users should find an appropriate entry point from where they can proceed to strengthen the foundation of their knowledge, to find the guide for applying existing results toward various practical problems in planning and operating electric power systems, or to learn about a well-structured and precise theory as background in their research. The text will lead the readers from their entry point toward the highest level of understanding. It is hoped that they will keep the book at hand as a source, just as they have used a less advanced book written by one of the authors 40 years ago, which is still available in paperback.

Beyond comprehensiveness in this sense, the authors strive for strictly precise treatment of each subject both mathematically and in the physics–engineering sense. Great care is taken to avoid presenting “practical” techniques built on dubious theoretical foundations and also to avoid building elaborate mathematical structures on formulations with arbitrarily conjectured “mathematical” models of dubious physical and engineering validity and relevance. This is important because both of these traps often victimize the unwary. Approximations used in some cases are clearly defined and analyzed.

This book has two special features relative to other references in the area of advanced dynamics and control of the electric power systems. The first lies in a systematic treatment of large-power-system dynamics, with special emphasis on voltage–reactive-power dynamics and control. Since voltage changes cannot be studied independently of other phenomena, voltage dynamics is introduced as an integral part of the general system dynamics. Extensive results are provided for system conditions that can be directly interpreted in the voltage subspace. More generally, throughout the book foundations of operations and control of power systems are described by viewing these systems with a more general perspective as a class of large nonlinear dynamic systems and networks.

The second distinct feature of this book is that it is written keeping in mind that the operating rules of the electric power industry largely depend on the political structures in place. This is taken into consideration by introducing the

general structure of operation and control first and then describing particular subcases of regulated and competitive power industries. This approach is used to introduce foundations of the existing hierarchies in operating and controlling of a vertically integrated horizontally structured power industry of today, as well as to describe possible solutions for the competitive industry and to identify conceptual challenges in future operation and control of the latter.

1.1 SCOPE OF THE CONTENTS OF THE BOOK

The contents of the book and its organization will be outlined here briefly, chapter by chapter.

Part I Modeling the Structure and Components

Chapters 2 to 4 deal with modeling issues ranging from the issues and limitations of the commonly used quasistationary phasor calculus (Chapter 2) followed by a detailed study of the effect of harmonics present in the 60-Hz carrier, a detailed study of the structure of the power system for “regulated” and “deregulated” operation and the models of its components from transmission lines and generators to developments in flexible AC transmission systems (FACTS), and power electronic equipment both in forms needed for analysis (Chapter 3) and for use in computer-aided planning and operation (Chapter 4). Ties of the models with common circuit-theory concepts are also surveyed in Chapter 4.

Part II Analysis of Stationary and Dynamic Processes

The dynamics of the power system and the various tools and practices used for its analysis with increasing depth, scope, and sophistication is the subject of chapters 5 to 11 in this part. The stationary condition, as a special restricted case of dynamics, is the subject of Chapter 5. Next, dynamics of limited amplitude, that is, small signals — implying linearized mathematics — are analyzed by means of linear differential equations and matrix algebra in Chapter 6. This is a very rich field, which can be used within its limits of operating conditions for solving a large segment of practical problems, and it has a large literature base. However, the power system is inherently nonlinear. A large segment of problems, continually increasing in numbers with the steady increase of size and speed in today’s modern power systems, occur in conditions under which small-signal analysis becomes an inadequate approximation. This necessitates penetration into the much more complex and mathematically much more sophisticated world of the dynamics of very large systems. These systems are modeled by sets of nonlinear differential equations (some partial ones) constrained by sets of nondifferential (algebraic or instantaneous) equations such as load flow and also containing nonanalytic constraints such as hard limits and control action using tap changers, etc. The reader is guided through this more complex modeling in Chapters 7

to 10 in an organized, step-by-step fashion that is still constrained essentially to the use of quasistationary phasor calculus. After the dynamic analysis segment of the book, the world beyond quasistationarity and ordinary differential equations is explored in Chapter 11.

Some details follow:

In terms of stationary conditions in Chapter 5 beyond the conventionally studied numerical methods of the load-flow area, the emphasis here is on establishing conditions for real-power-transfer capability, including new methods for finding critical transmission lines for real-power transfer and the load-flow formulation and transmission-loss computation for the deregulated electric power systems. Power-transfer capability in terms of voltage collapse and existence of solutions for operationally acceptable voltage levels is also identified.

In Chapter 6, assuming that dynamics is restricted to small signals allows linearizing the differential and algebraic equations and, in some cases, the decoupling of angle (frequency)–power versus voltage–reactive-power dynamics. This leads to major model reduction and the use of frequency and real power as state variables instead of the more traditional frequency and phase angles. Assumptions are often used in the literature to separate these subprocesses which generate confusion, as pointed out in Chapter 6.

While the operation of the power system is in the stationary regime most of the time, sudden events such as the loss of generators, loads, transmission lines, or large-scale faults and the resulting relay operations result in major transient upheavals, which can lead to large-scale breakdowns or blackouts. Thus these phenomena are as vital for system security as is the stationary regime. Actually, ignoring this fact was the cause of the notorious northeastern United States blackout of 1964 and a more recent blackout in the western United States in 1996. A general theory of the large-size, nonlinear power system became available only recently (with major contribution of the teams of the authors), so until now the growth of the literature and software development was more vigorous for the stationary and small-signal regimes using largely nondynamic and linearized models. Developments on the general dynamic side will now become vigorous, and importance of dynamic models of loads, generators, and controls will intensify.

In Chapters 7 and 8 a comprehensive treatment of system dynamics is given that was developed only recently for the large-scale power system, incorporating both electromagnetic, or voltage, and electromechanical, or rotor-angle, dynamics. System dynamics beyond the small-signal region involves large changes in both state and parameter spaces in stationary and transient circumstances.

The treatment offered here, starting in Chapter 7, leads the reader to the full theory through first investigating a few small-scale stepping stones, that is, the study of minimal-size systems (i.e., generator and load), and “rudimentary” systems (consisting of generator, load, transmission, and control). Problems for these systems are solved directly and somewhat intuitively but without linearization or small-signal-type restrictions. A complete study of these minimal systems

in an intuitive but precise manner is used to make readers entering the field aware of the phenomena involved and help them to understand new or unfamiliar concepts such as feasibility and viability regions, and regions of attraction, which are major features in the dynamic behavior of today's heavily loaded systems.

Chapter 8 then offers to the reader who went through or bypassed the introduction a treatment of general power-system dynamics in the differential-algebraic equation (DAE) sense with mathematical depth, precision, and completeness combined with meaningful realistic physical and engineering usefulness. Numerous new concepts are introduced that will play a major role in the utilization of such studies as the field develops further. A study of bifurcation theory for large-power-system operations is included and developed with new concepts. This two-phase introduction through Chapters 7 and 8 was used in this book repeatedly, most notably in developing the models for synchronous machines in Chapter 3.

Chapter 9 then illustrates the usefulness of the theory of Chapters 7 and 8 by using it in a thorough analysis of a truly real and actual occurrence involving the Mid-America Interconnected Network (MAIN) region of the American interconnection that covers all of mid-America and by comparing the analytic results with existing extensive record from the event itself. Among other things, this study establishes the Hopf-bifurcation segment of the feasibility boundary, the proximity of which will establish the security of the operating conditions of the system in this vicinity. The size and complexity of this example illustrate the realism and application potential of the theory of Chapters 7 and 8 on a very-large-scale systems and open the door for developing technology for such applications.

Chapter 10 finally extends the theory beyond the DAE-type models to non-smooth constraints such as stepwise changing controls [e.g. on-load tap-changing (OLTC) transformers] and discontinuous, saturation-type limits. Thus Chapters 7 to 10 offer a deep, wide perspective; a precise and highly practical foundation; to concept tools and methods for analyzing problems of the modern heavily loaded power systems.

Chapter 11 offers a brief discussion on the limits of the conditions under which the quasistationarity holds when applied to typical transmission systems. Many phenomena of direct interest in this book cannot be studied by conventional phasor calculus without disregarding the quasistationarity assumption. As a result some conclusions in the literature based on the conventional models could be misleading. For accurate studies of such phenomena, time-varying phasors of two types are introduced in Chapter 11. In addition, a valid model would also need to accommodate the wave character of the long transmission line's response.

Part III Control and Stabilization

Part III is built on the foundations of the models and analysis introduced in the previous two parts, Chapters 3 to 11. Varied features of power-system control are discussed in Chapters 12 to 14. Solutions for many, very practical dynamic problems in this area are discussed. Chapters 12 to 14 deal with the problems of

power systems at two of the control levels and analyse many complex engineering problems created by the current deregulation process in the US.

Chapter 12 contains a detailed and precise introduction of the primary control of individual pieces of equipment in a geographically local sense such as generator governors and excitors. Chapter 12 is fully devoted to the design of primary-level controllers on power systems. Classification of these controllers into the generation-based controllers (such as governors, excitation systems, and power-system stabilizers) and the controllers switched mechanically or by power electronics present on a transmission network and the load side (such as switched capacitors and/or inductors, including FACTS) is introduced. At present, most primary controllers are entirely decentralized, that is, their control logic is based on strictly local measurements except for their setpoints which are assigned from the second level. They are typically designed to eliminate local deviations from the setpoints and are not based on any system control design. In closing, the chapter summarizes critical open questions necessary for ensuring small-signal stable operation of power systems.

In Chapter 13 we revisit fundamental principles of control-assisted operation of power systems. A conceptual setup for stationary generation control (such as the current automatic generation control (AGC)) as a hierarchical control problem is introduced, for both regulated and deregulated industries. First, the problem of economic dispatch and unit commitment to supply expected load demand is posed in the context of operating rules dictated by specific industry structures. This problem is formulated without explicit consideration for transmission-system-imposed constraints. The second part of the chapter introduces concepts for frequency and voltage regulation at systemwide and control-area levels. Concepts are introduced for both the regulated- and deregulated-industry structure. A possible market-based approach to the generation-based frequency and voltage regulation is described. This is a conceptually different paradigm from the vertically integrated industry; the desired technical performance is achieved by system users responding to the price of electricity instead of technical measurement.

In Chapter 14 the problem of stationary generation control is extended to account for transmission network constraints. This problem is again posed for an arbitrary industry structure, regulated and deregulated. The material concerns methods for scheduling generation to meet anticipated load in the most economic manner, consistent with the regulatory rules in place and within the acceptable operating constraints for maintaining system viability. The problem of observing transmission constraints when attempting to optimize use of generation becomes particularly intriguing in the deregulated industry in which generation, transmission, and distribution have often conflicting subobjectives. The role of on-line pricing for eliminating “congestion” on the transmission system as a means of ensuring that the system remains within the constraints is described as a novel concept likely to become essential for deregulated industry. Several examples are provided to illustrate how, for example, one could use the transmission price as a coordinating signal to effect decentralized decisions of individual system users

to approach the optimal power-flow solution. Much of the current restructuring debate concerns transmission-congestion pricing.

In the second part of this chapter effective computer methods for solving a security-constrained generation-control problem are described. The concepts are based on the idea that the effects of system input changes are typically within relatively small clusters. Methods for defining and computing these clusters are described first. Their use is illustrated for efficient reactive-power management in the regulated industry, as well as for creating the necessary database for managing transmission congestion in the deregulated industry. The chapter ends by introducing a textured model or algorithm for flexible parallel computing in the most severe cases when an event effects the entire system.

In summary, it is the authors' belief that the material in this book provides a strong scientific basis to power-system engineering. It is shown how the theory is translated into useful tools for power suppliers and consumers. It breaks with traditional structures that are largely based on what has been rather than what could be. The pursuit is devoted to the analysis and control of power systems that occur in the generation, transmission, and utilization of electrical energy. The material is organized in such a way that it could be understood by network and control theorists with little additional effort, and as such, it could be used as a starting reference for researchers with specialties in these areas who would like to challenge the state-of-the-art knowledge in their field by attempting to solve some of the open questions in operating electric power systems.

ACKNOWLEDGMENTS

This book covers a wide range of assorted aspects of power-system theory and practice. The material represented accordingly comes from many sources in the literature, including a substantial portion taken from contributions by the authors, their associates, and their students.

Accordingly due attributions are given chapter by chapter. No attempt will be made at this point to present a comprehensive list of this large heterogeneous set of acknowledgments. At the appropriate locations the sources of the material are identified through reference numbers under which publications and their authors are listed in comprehensive chapter bibliographies. In the case of material generated by the authors' teams the roles of the team members are discussed briefly as needed for clarification.

At this point the authors wish to express their deep appreciation for the extensive help received from their team members, their students, their institutions, their personnel, and last, but not least, their families.

PART I

Modeling the Structure and Components

2 Quasistationary Phasor Concepts

Phasors are the principal symbolic language of power-system studies, especially in the transmission-system area and also in some areas of general circuit theory. The validity of the commonly used form of phasor calculus is based on a “quasistationary” assumption to the effect that voltage, current, and power values are either constant in a steady-state condition of the system, or their variation is slow relative to 60 cycles in a quasistationary condition. This latter assumption is typically more than fulfilled in communications in which the frequency ranges of carrier and modulating frequencies are measured in multiple orders of magnitude. However, in power systems such automatic satisfaction is not to be taken for granted. Many decades of experience with simulating angle transients have shown that the quasistationary form of phasors gives a good approximation in that context. With the emergence of voltage stability as a major concern, connected with the increase of power transfer, complexity, and loading levels of the power system combined with the use of computers, the challenging power engineering problems are now moving outside the range of validity of the quasistationary assumption. This is shown in a recent analysis of the situation [1 to 3]. Unfortunately, the phasor as the symbolic language has become such an obvious and natural usage in the field that most engineers and researchers are unaware of its limitations. This has caused results of at least dubious validity in the literature.

It is implied that a book of this type should clarify the limitations of the validity of phasors as now used and extend the usage of phasors over the existing range of problems in the field. This is the motivation and objective of Chapters 2 and 11.

In the present chapter, first the physical time-domain relations of AC voltage, current, and power are reviewed in Section 2.2. This is followed by a very elementary graphical-physical illustration of the meaning of these basic concepts, which the reader may find useful in refreshing and in-depth understanding obscured by the routine use of phasors. Next, Section 2.3 gives a general definition of phasors and their classification into stationary, quasistationary, and time-varying categories. Use of the phasor definition for interpreting active (real) and reactive (imaginary) power is illustrated next.

The first ten chapters of this book treat cases that typically fall into the quasistationary class. In Section 2.3 a brief summary of classical stationary phasor calculus is provided. In Section 2.4 a brief summary of classical quasistationary phasor calculus is given. The later chapters in this book concerned with dynamics and control require awareness of the quasistationary assumption and the potential

need to use time-varying phasors. Accordingly this chapter is limited to discussing quasistationary phasors. Chapter 11 will analyze the more sophisticated time-varying phasors for systems. In Section 2.5 a summary of the characteristics of active- and reactive-power flows in the AC case is presented.

Included in Section 2.6 is the analysis of the important case of periodic i.e. non pure sinusoid carrier for voltage, current, and power signals. In Section 2.6.1 the basic time-domain representation for periodic signals is described. These are increasingly present in today's systems and are caused by power electronic (thyristor) equipment and certain nonlinearities. It is shown in Chapter 3 that typical constituent voltage–current characteristics of power-system components are nonlinear and therefore, a cause of harmonics even during normal system operation.

The presence of harmonics in modern electric power systems requires knowledge of generalized phasor concepts applicable to the periodic signals with higher-order harmonics. To meet this need, the material presented in Section 2.6 introduces concepts analogous to the phasor algebra described first for the single-frequency sinusoidal signals in Section 2.3. Basic notions of the root-mean-square (rms) value of a periodic signal with higher-order harmonics for currents and voltages are reviewed. It is revealed next in Section 2.6.4 that the average, or real-power, concept preserves a full physical meaning for these signals. Reactive power for periodic signals, on the other hand, has been a somewhat controversial topic in the past. In Section 2.6.4 rudiments of this controversy are described. A direct summary of the recent work [4,5] is given as a particularly attractive and elegant vector-space representation of all three power components (real, reactive and apparent). In Section 2.6.9 minimization of reactive power for periodic signals is described. It is explained in later parts of the book why understanding fundamentals is essential when designing control devices such as flexible AC transmission systems (FACTS). Finally, in Section 2.7, as a direct generalization of the vector phasor algebra for periodic signals, potential use of vector phasors for analyzing multiphase circuits is indicated.

2.1 TIME-DOMAIN REPRESENTATION FOR AC VOLTAGE, CURRENT, POWER, AND ENERGY

Consider the general time-varying AC voltage $e(t)$ and current $i(t)$ signals of the form

$$e(t) = \sqrt{2}E(t) \cos[\omega t + \delta(t)] \quad (2.1)$$

$$i(t) = \sqrt{2}I(t) \cos[\omega t + \delta(t) - \varphi(t)] \quad (2.2)$$

as illustrated in Figure 2.1, where E and I will be called the rms values and $\sqrt{2}E$ and $\sqrt{2}I$ peak values of voltage and current, respectively.

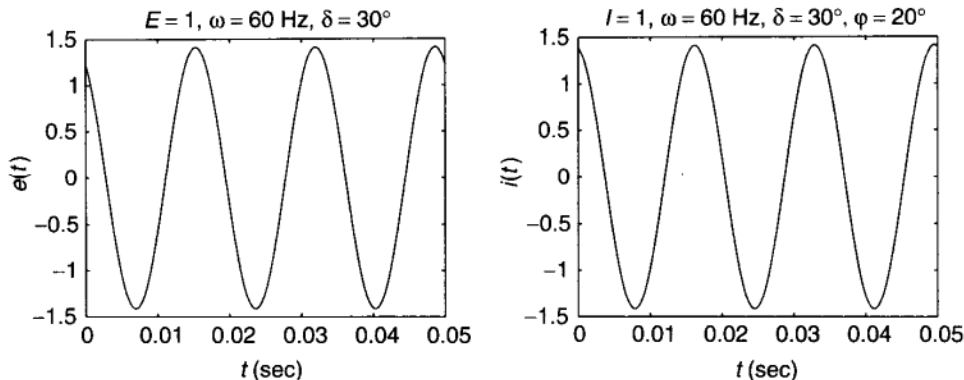


FIGURE 2.1 Typical voltage and current waveforms for an AC circuit.

These two equations are the actual and general time histories of, respectively, an AC voltage $e(t)$ and an AC current $i(t)$. Furthermore, in the stationary condition rms amplitudes $E(t) = E$ (in volts), $I(t) = I$ (in amperes), and the power factor angle $\varphi(t) = \varphi$ (in radians) are constant in time and the constant reference angle $\delta(t) = \delta$ is arbitrarily selected (between 0 and 2π rad). In the stationary case the only time variation enters through ωt , the sinusoidal variation of the 60-Hz (or 50 Hz in Europe and Japan) carrier. Then both voltage and current follow a pure sine wave of time history. This interpretation is still applicable as an approximation in a quasistationary region in which the time variation of the amplitude (E, I), phase (δ, φ), and frequency ($\omega, \dot{\varphi}$) are slow relative to 60 Hz. It is a coincidence of great practical significance that the quasistationary region of good approximation was found by wide ranging experience to cover the dynamic range of interest up to about 1970. Dynamic phenomena of interest in this period mainly concerned transient stability, generator and area swings etc., all involving mechanical (generator, load, etc.) inertias that are inherently relatively slow, below about (1/20) of the speed of the 60-cycle carrier.

Equations (2.1) and (2.2) in fact represent the original and classical definition of AC. In communication-type circuits in which modulated sinusoidal signals are also widely used, the ratio of the speed of signal to the speed of carrier typically spans many orders of magnitude. Hence in communications the quasistationary range as represented by Eqs. (2.1) and (2.2) precisely covers all problems that arise for all purposes.

On the AC power system, however, with the emerging importance of the voltage stability problem, the quasistationary approximation is not valid unconditionally any more (sine waves are too fast and distributed; there is a constant-time delay, etc.) and more refined techniques are required. Such techniques will be developed in Chapter 11 and used in portions of the remaining chapters.

Power being the commodity produced and distributed in power systems, power flow through line cross sections [Fig. 2.2(a)] or into equipment [Fig. 2.2(b)] is of primary interest. Let it now be assumed that the instantaneous voltage and current defined in Eqs. (2.1) and (2.2) are associated with each other in the fashion

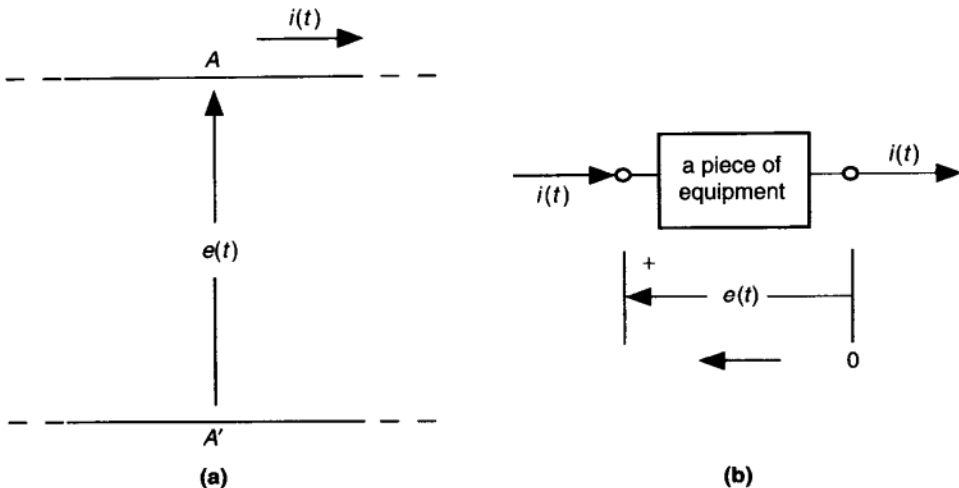


FIGURE 2.2 Cross section of (a) an AC line or (b) terminals of a piece of equipment.

of Figure 2.2(a) or 2.2(b). Then, from basic physics, the instantaneous power flow through a cross section ($A-A'$) [Fig. 2.2(a)] or into a piece of equipment [Fig. 2.2(b)] emerges after some trigonometric manipulations as

$$\begin{aligned}\mathcal{P}(t) = e(t)i(t) &= E(t)I(t) \cos \varphi(t)\{1 + \cos 2[\omega t + \delta(t)]\} \\ &+ E(t)I(t) \sin \varphi(t)\{\sin 2(\omega t + \delta(t))\}\end{aligned}\quad (2.3)$$

The energy transferred through $A-A'$ after $t = 0$ is then by basic physics:

$$w(t) = \int_0^t \mathcal{P}(t) dt \quad (2.4)$$

Furthermore, assuming smooth variations of E , I , φ , and δ and not showing their time dependence explicitly leads to the expressions for time derivatives of $i(t)$ and $e(t)$ as¹

$$\dot{e}(t) = \sqrt{2}\dot{E} \cos(\omega t + \delta) - \sqrt{2}E(\omega + \dot{\delta}) \sin(\omega t + \delta) \quad (2.5)$$

$$\dot{i}(t) = \sqrt{2}\dot{I} \cos(\omega t + \delta - \varphi) - \sqrt{2}I(\omega + \dot{\delta} - \dot{\varphi}) \sin(\omega t + \delta - \varphi) \quad (2.6)$$

Hence the instantaneous power flow [Fig. 2.2(b)] into a capacitor C is

$$\begin{aligned}\mathcal{P}_C(t) &= i_C(t)e_C(t) = C \dot{e}(t)e(t) \\ &= CE\dot{E}[1 + \cos 2(\omega t + \delta)] - CE^2(\omega + \dot{\delta})[\sin 2(\omega t + \delta)]\end{aligned}\quad (2.7)$$

¹ A single heavy dot \dot{i} will denote the time derivative of i .

and into the inductor is

$$\begin{aligned}\mathcal{R}_L(t) &= e_L(t)i_L(t) = L \dot{\mathbf{i}}(t)i(t) \\ &= LI\dot{i}[1 + \cos 2(\omega t + \delta - \varphi)] - LI^2(\omega + \dot{\delta} - \dot{\varphi})[\sin 2(\omega t + \delta - \varphi)] \quad (2.8)\end{aligned}$$

2.1.1 Basic Power-Flow Concepts on Single-Phase Transmission Lines

For a single-phase transmission line modeled as a π circuit,² as sketched in Figure 2.3, the following three equations will describe (and define the power flow)

$$\begin{aligned}\mathcal{P}_{ij}(t) &= e_{ij}(t)i_{ij}(t) \\ &= E_{ij}I_{ij}\cos\varphi_{ij}[1 + \cos 2(\omega t + \delta_{ij})] + E_{ij}I_{ij}\sin\varphi_{ij}[\sin 2(\omega t + \delta_{ij})] \quad (2.9)\end{aligned}$$

$$e_{ij}(t) = e_i(t) - e_j(t) = R_{ij}i_{ij}(t) + L_{ij}\dot{\mathbf{i}}_{ij}(t) = E_{ij}\cos(\omega t + \delta_{ij}) \quad (2.10)$$

$$\mathcal{P}_{Ci}(t) = e_i(t)i_{Ci}(t) \quad (2.11)$$

$$\mathcal{P}_{Cj}(t) = e_j(t)i_{Cj}(t) \quad (2.12)$$

where for the single-phase case in Figure 2.3 R_{ij} and L_{ij} represent the total resistance and inductance of the two lines of the single-phase transmission line, $\frac{1}{2}$ for each side. Conversely C_i and C_j are the line-to-ground capacitances of each one-half length of the single-phase transmission line. Let $w_C(t)$ and $w_L(t)$

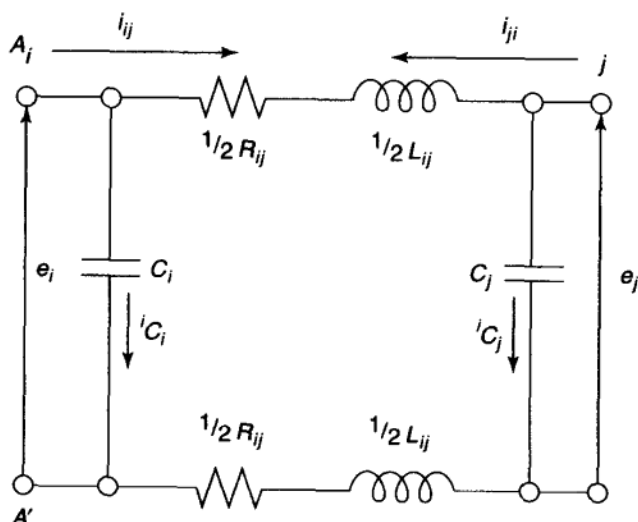


FIGURE 2.3 Nominal π -circuit model of a single-phase transmission line.

² Derivation of the π -circuit representation is given in Chapter 3 of this text.

represent the instantaneous energy contents of, respectively, the capacitor and inductor at t , then by basic physics and Eq. (2.4)

$$w_C(t) = \int_0^t \mathcal{P}_C(t) dt, \quad \mathcal{P}_C(t) = \frac{d w_C(t)}{dt} = \frac{1}{2} \frac{d}{dt} C e_C^2(t) \quad (2.13)$$

and

$$w_L(t) = \int_0^t \mathcal{P}_L(t) dt, \quad \mathcal{P}_L(t) = \frac{d w_L(t)}{dt} = \frac{1}{2} \frac{d}{dt} L i_L^2(t) \quad (2.14)$$

Caution is required when working with these energy terms because the integral form requires knowledge of the energy contents at $t = 0$. Without it the relations are undefined. The AC energy contents move in and out at a 120-Hz frequency by Eqs. (2.13) and (2.14); hence the often-used term of *stored* energy may be misleading.

Let us *discuss in more detail* the time variation of instantaneous power flow through a cross section $A-A'$ of a single-phase transmission line as indicated in Figures 2.2(a) and in 2.2(b) and the accumulating energy, say, to the right of the $A-A'$ cross section. The time variations of the instantaneous power flow $\mathcal{P}(t)$ is defined in Eq. (2.3) by two components

$$\mathcal{P}(t) = p(t) + q(t) \quad (2.15)$$

$$p(t) = EI \cos \varphi [1 + \cos 2(\omega t + \delta)] = \alpha(t) EI \cos \varphi \quad (2.16)$$

$$q(t) = EI \sin \varphi [\sin 2(\omega t + \delta)] = \beta(t) EI \sin \varphi \quad (2.17)$$

where both $\alpha(t)$ and $\beta(t)$ are double-frequency sinusoids. All $\mathcal{P}(t)$, $p(t)$, and $q(t)$ are instantaneous values of physical, that is, real-power (components) flows. Components $p(t)$ and $q(t)$, however, have rather different behavior over each 60-Hz cycle.

The energy transfers across $A-A'$ for each component $p(t)$ and $q(t)$ with reference to Eqs. (2.16), (2.17), and (2.4) are

$$w_p(t) = \int_0^t p(t) dt = EI \cos \varphi \left(t + \frac{1}{2\omega} \sin 2(\omega t + \delta) \right) - w_p(0) \quad (2.18)$$

$$w_q(t) = \int_0^t q(t) dt = -\frac{1}{2\omega} EI \sin \varphi \cos 2(\omega t + \delta) - w_q(0) \quad (2.19)$$

The two components $w_p(t)$ and $w_q(t)$ [just like $p(t)$ and $q(t)$] are very different in nature. Component $w_p(t)$ represents an energy flow to the right across cross section $A-A'$ in Figure 2.4(b) at the (power) rate $p(t)$. There it is converted into forms of energy (heat, light, mechanical energy output from motors, etc.) that which is not recoverable and is not recovered as electromagnetic energy on a 60-Hz basis, or else it is transferred into other parts of the network. As shown in Figure 2.4(a) for the case of a stationary single-phase line the value of $p(t)$ is

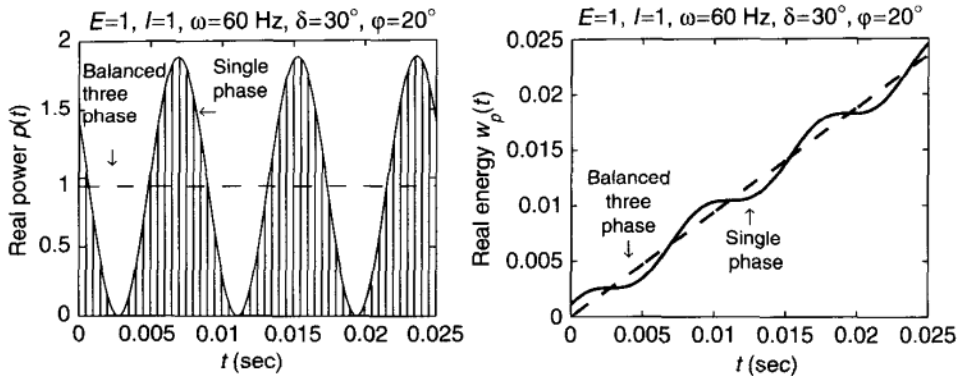


FIGURE 2.4 Real- or active-power component $p(t)$ and the resulting accumulated energy $w_p(t)$ as a function of time.

always positive, indicating unidirectional energy transfer to the right across $A-A'$ and a monotonically increasing accumulation $w_p(t)$ of the energy transferred to the right side of $A-A'$ [Fig. 2.4(b)].

On the other hand, $w_q(t)$ represents an amount of energy [the shaded area in Fig. 2.5(a) equaling the peak in Fig. 2.5(b)] with zero average flow and zero energy transfer at certain time instances that are an integer multiple of $(1/120)$ (i.e., half cycles of 60 Hz) seconds apart that is emerging between the two sides of $A-A'$. These energy forms are recoverable and are recovered within each cycle of the 60-Hz alternating current. Any amount of energy $w_q(t)$ that accumulates to the right of $A-A'$ during a half-cycle of 60 Hz (i.e., $(1/120)$ sec) as magnetic, that is, positive energy, is returned to the left of $A-A'$ as capacitive, that is, negative energy during the next half cycle.

The general character of the two types of power flow $p(t)$ and $q(t)$ will now be analyzed.

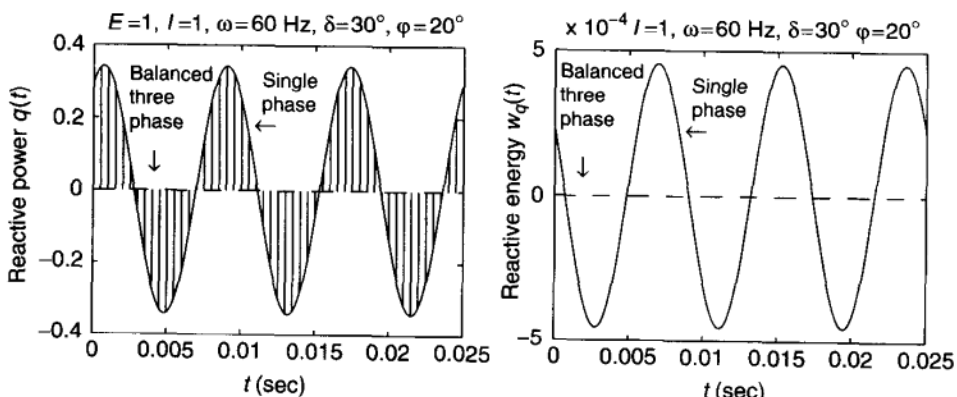


FIGURE 2.5 Instantaneous reactive power-flow component $q(t)$ and the resulting accumulating energy $w_q(t)$.

2.1.1.1 Real or Active Power P As may be observed in Figure 2.4(a) and Eq. (2.3) the value of $p(t)$ is always positive for $\varphi \leq \pi/2$ and so it is fluctuating at 120 Hz between zero and a peak value of $2EI \cos \varphi$ around a time average over each 60-Hz cycle of

$$P = EI \cos \varphi \quad (2.20)$$

with $\cos \varphi$ defined as a power factor term. The energy accumulation caused by $p(t)$ is accumulating monotonically and stepwise [the step size being $(1/120)P$ sec as shown in Fig. 2.4(b)]. We can then conclude that P represents a *real*, physical, constant average *power* flow that transfers real accumulating energy to the right of cross section $A-A'$. P then is correctly called the *real power*.

Note that most power equipment will not react noticeably at 60 Hz or 120 Hz. Thus in the steady state the only physical reality noted is the constant average power flow, the real power. The direction of the flow is defined by $\pm P$ for a specific but arbitrary reference direction assigned to $A-A'$.

2.1.1.2 Imaginary or Reactive Power Q The second term, $q(t)$, is a simple sine wave that swings at 120 cycles, but it has zero average and hence it transfers no net energy (over time periods measured in integer 60-Hz cycles) across $A-A'$. However, this component cannot be ignored (in fact, ignoring would make the problem undefined) since it describes instantly a physical nonzero power flow as shown in Figure 2.5(a) in a sine wave with a peak value of $EI \sin \varphi$.

So while $q(t)$ may seem to be a kind of phantom (for many engineers or else as a quantity that flows), as far as energy transfer is concerned its amplitude of

$$Q = EI \sin \varphi \quad (2.21)$$

called *reactive power* must be monitored.

From another viewpoint one can say that if $A-A'$ is embedded in a power system (large or small) to maintain a particular power flow P through it and to maintain a specific voltage E , it is necessary for a certain amount of power Q to oscillate across it. The amount of Q relative to P is related to power factor angle φ as per Eqs. (2.16) and (2.17). Its sign, set by the sign of $\sin \varphi$, implies which side of $A-A'$ is net inductive ($Q < 0$) and net capacitive ($Q > 0$) from the viewpoint of the reference direction assigned to $A-A'$. Note the inherent fact that the two sides across any cross section will always look, respectively, net inductive and net capacitive to an equal degree. So the energy connected with Q oscillates between capacitive and inductive stored energy.

Always remember that P flows but Q only oscillates. It may be correct to speak of a *reactive-power flow* as is often done in the literature as long as a convention is set for the meaning in terms of the power factor angle φ with respect to the reference direction across $A-A'$ and the fundamental oscillatory nature of Q is not forgotten. Thus P and Q are the two different phenomena that define the instantaneous flows $p(t)$ and $q(t)$, which in turn must add up to

the instantaneous values of $\mathcal{P}(t)$, or vice versa [see Eqs. (2.16) and (2.17)]. This condition determines instantaneous values of $e(t)$ and $\varphi(t)$.

2.1.2 Basic Power-Flow Concepts on Three-Phase Transmission Lines

Shown in Figure 2.3 is the nominal π -circuit representation of a single-phase transmission line. Three such circuits with a joint neutral line represent a *balanced three-phase circuit* (Fig. 2.6), if all three voltages and currents are equal in magnitude and E and I and displaced exactly 120° in phase. On such a circuit the current on the neutral line is identically zero; its resistance and reactance have no effect. In fact the same relations apply whether a neutral line is actually present or not as long as the balance exists:

$$e_a(t) = \sqrt{2}E \cos(\omega t + \delta), \quad i_a(t) = \sqrt{2}I \cos(\omega t + \delta - \varphi) \quad (2.22)$$

$$e_b(t) = \sqrt{2}E \cos(\omega t + \delta + 2\pi/3), \quad i_b(t) = \sqrt{2}I \cos(\omega t + \delta - \varphi + 2\pi/3) \quad (2.23)$$

$$e_c(t) = \sqrt{2}E \cos(\omega t + \delta + 4\pi/3), \quad i_c(t) = \sqrt{2}I \cos(\omega t + \delta - \varphi + 4\pi/3) \quad (2.24)$$

Then with reference to Eq. (2.3), the total, instantaneous three-phase power flowing through the cross section $A-A'$ at bus i of a balanced three-phase line is

$$\begin{aligned} \mathcal{P}_{ph}(t) &= \mathcal{P}_a(t) + \mathcal{P}_b(t) + \mathcal{P}_c(t) \\ &= EI \cos \varphi [3 + \cos 2(\omega t + \delta) + \cos 2(\omega t + \delta + 2\pi/3) \\ &\quad + \cos 2(\omega t + \delta + 4\pi/3) + EI \sin \varphi [\sin 2(\omega t + \delta) \\ &\quad + \sin 2(\omega t + \delta + 2\pi/3) + \sin 2(\omega t + \delta + 4\pi/3)] \\ &= \alpha 3EI \cos \varphi + \beta 3EI \sin \varphi \end{aligned} \quad (2.25)$$

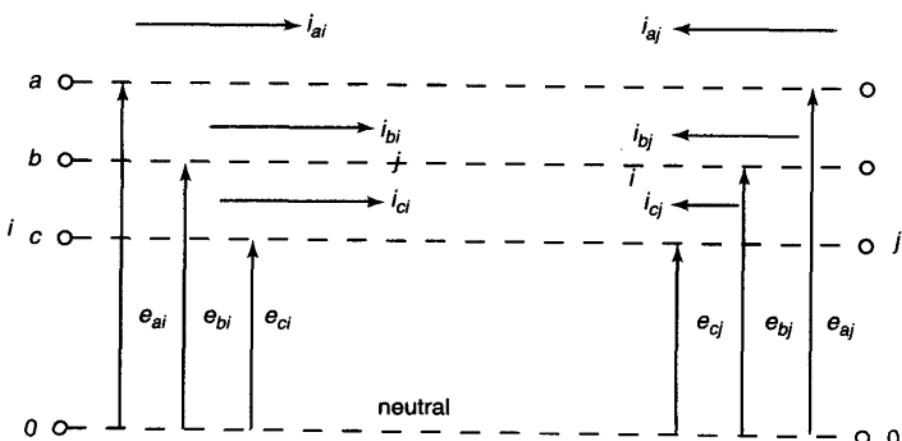


FIGURE 2.6 Sketch of voltages and currents on a three-phase transmission line.

Note the following:

- In a normalization (called per unit or p.u. [6,7]) commonly used in power system studies, the factor 3 drops out because the normalizing base power is also tripled. Hence, for a cross section $A-A'$ of a balanced three-phase line the instantaneous three-phase power flow is

$$\mathcal{P}_{\text{ph}}(t) = \alpha EI \cos \varphi + \beta EI \sin \varphi \text{ p.u. at all } t \quad (2.26)$$

- Since the sum of the three equal-amplitude, equally spaced sine waves is always equal to zero, in a balanced three-phase line in the steady state there will always be $\alpha = 1$ and $\beta = 0$. Thus for balanced three-phase line the power flow, as a physical quantity, Eq. (2.26), is a constant in time, that is, it has no modulated component in 60 Hz or 120 Hz [Fig. 2.4(a)]:

$$P = \mathcal{P}_{\text{ph}}(t) = EI \cos \varphi \text{ p.u.} \quad (2.27)$$

- Although oscillations of power and energy canceled out to zero for the balanced total three-phase power, Eq. (2.27), they are still present on the individual phases (Fig. 2.6) in the three-phase case. Thus, based on the same argument as in single phase, a reactive-power value arises for three-phase systems in the form

$$Q = EI \sin \varphi \text{ p.u.} \quad (2.28)$$

This total and constant three-phase quantity is then exchanged in 120-Hz oscillations between capacitive and inductive energy over the three phases, a situation explained most directly by the graphics of Figure 2.6.

- Corresponding results in Eqs. (2.20), (2.21) to (2.27), and (2.28) were obtained in Section 2.1.1.1 for stationary single-phase systems (E, I, δ, φ all constants). Quantities P and $w(t)$ are reinterpreted for three-phase systems as the actual physical power and energy values, respectively (they are time averages over integer numbers of cycles for single phase).

2.1.2.1 Summary The physical instantaneous power flow $\mathcal{P}(t)$ (the product of the instantaneous voltage and current), through a cross section of a single-phase AC line naturally divides into two instantaneous components: (1) Component $p(t)$, which is unidirectional, oscillates in any single phase at 120 Hz between zero and twice its average over one 120-Hz cycle, that is, P is known as the *real or active power*. In a balanced three-phase line the three-phase power, which is observable, is a constant, that is, P . So P is either an average or a constant physical flow for single- and three-phase systems. There is no practical difference since most power-system equipment does not respond noticeably at 120 Hz (except lights, but here human vision does the averaging). (2) The power component $q(t)$ by Eq. (2.15) simply is the difference between the actual total instantaneous flow $\mathcal{P}(t)$ and the oscillatory but unidirectional $p(t)$. So by definition $q(t)$ has

zero average and is simply an oscillation of power between the two sides of the cross section. The two sides automatically would appear, respectively, capacitive and inductive on the two sides of any cross section $A-A'$ with the amplitude of the oscillation in $q(t)$, Q being known as the reactive or imaginary power.

The $p(t)$ and $q(t)$ division of Eq. (2.3) as defined in Eqs. (2.16) and (2.17) has very useful practical features—separating the net power flow in $p(t)$ from accompanying zero mean oscillations. From another viewpoint, the power flow into any single-phase line (or in one phase of a three-phase line) is defined by four variables E , I , φ , and δ of which δ is referred to as constant but arbitrary reference. Expressions (2.20) and (2.21) convert these variables into E , P , Q , and δ , where δ is an arbitrary reference angle, which, however, must be the same within one problem solution.

2.2 DEFINITION OF THE PHASOR FOR AC QUANTITIES

Let $z(t)$ represent an AC signal such as $e(t)$ or $i(t)$ in Eqs. (2.1) and (2.2) and power in Eq. (2.3). The following then applies:

1. The time-domain representation is of the form

$$z(t) = z \cos(\omega t + \zeta) \quad (2.29)$$

where z and ζ may be time varying.

2. The definition of the phasor transformation \wp is

$$\wp z(t) = ze^{j\zeta} = \hat{z} \quad (2.30)$$

where \hat{z} is the phasor transform of $z(t)$

3. The inverse transformation of phasor \hat{z} is

$$\wp^{-1}\hat{z} = \text{Re}(\hat{z}e^{j\omega t}) = \text{Re}(ze^{j(\omega t+\zeta)}) = z(t) \quad (2.31)$$

Clearly this transformation and its inverse are unique except for the presence of an arbitrary number of $\pm 2\pi$ shifts in ζ which are typically inconsequential in practical problems. Note that \hat{z} is simply a fixed vector in the complex plane if z and ζ are constant in time and $\hat{z}e^{j\omega t}$ is a vector rotating at speed ω in the complex plane. The first is the transform of $z(t)$ and the second is a kind of semi-inverse transform (before taking the real part). Through extensive use in applying the phasor transforms as the mathematical description of AC quantities this static or rotating pair of vectors in the complex plane has become the basic meaning in the minds of most engineers of the concept of AC quantities, the more physical time domain form in Eq. (2.29) may be forgotten.

In some recent studies of periodic carriers it became convenient to use a three dimensional version of the diagram in Figure 2.7 with ω being the third axis

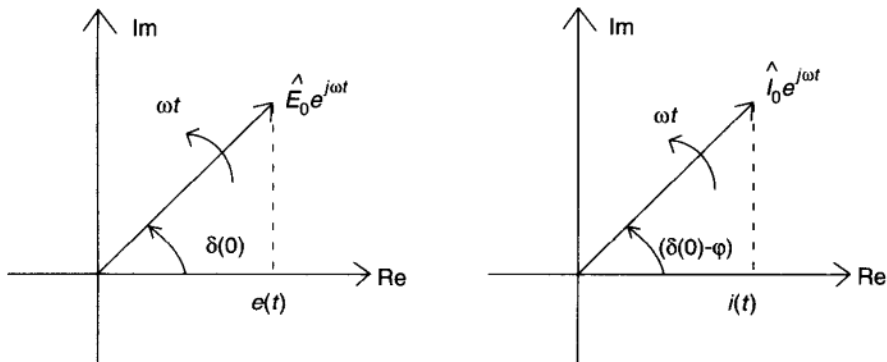


FIGURE 2.7 Sketch of the phasor relationship for cut set $A-A'$. \hat{E} and \hat{I} are the rms voltage and current phasors.

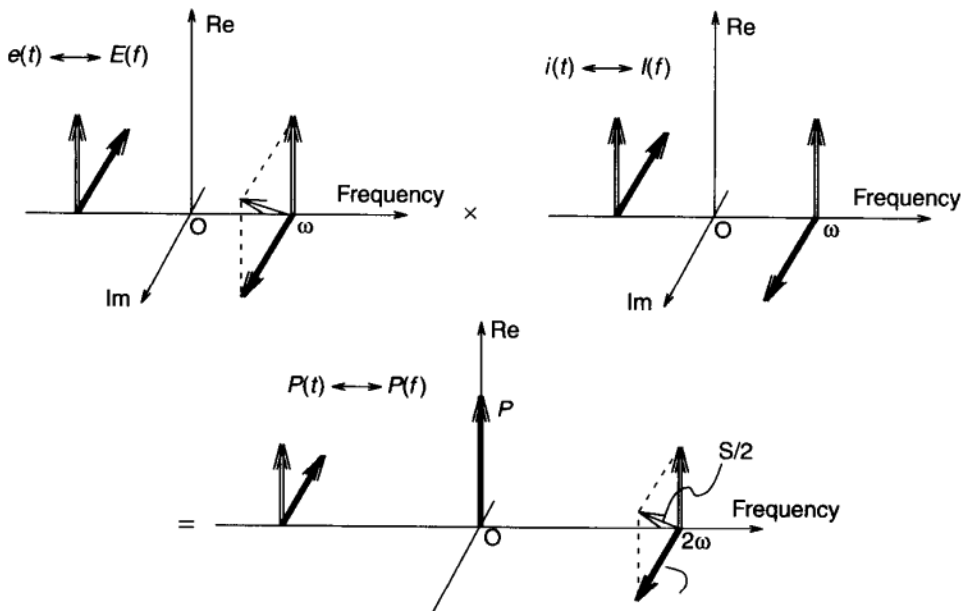


FIGURE 2.8 Frequency-domain view of power.

over the complex plane, as shown in Figure 2.8 [4,5]. Note that incorporating the $\omega < 0$ half plane makes Figure 2.8 symmetrical mathematically but one must not forget that the $\omega > 0$ half plane has physical meaning and the $\omega < 0$ half does not, it is purely mathematical.

Note that the physical, instantaneous voltage and current are then presented by the real parts of these rotating vectors, which is clear from Eqs. (2.1) and (2.2) as

$$\begin{aligned} e(t) &= \operatorname{Re}(\sqrt{2}\hat{E}e^{j\omega t}) = \operatorname{Re}(\sqrt{2}Ee^{j(\omega t+\delta)}) = \sqrt{2}E \cos(\omega t + \delta), \\ z &= \sqrt{2}E, \quad \zeta = \delta \end{aligned} \tag{2.32}$$

$$\begin{aligned} i(t) &= \operatorname{Re}(\sqrt{2}\hat{I}e^{j\omega t}) = \operatorname{Re}(\sqrt{2}Ie^{j(\omega t+\delta-\varphi)}) = \sqrt{2}I \cos(\omega t + \delta - \varphi), \\ z &= \sqrt{2}I, \quad \zeta = \delta - \varphi \end{aligned} \quad (2.33)$$

It is shown in Figure 2.7 that at the initial time ($t = 0$, i.e., $\omega t = 0$) $e(0) = E_0$ and $i(0) = I_0$. The entire \hat{E} and \hat{I} diagram rotates as a rigid unit as the projections of \hat{E} and \hat{I} onto the real axis each describe the sinusoidal time variation corresponding to the stationary version of Eqs. (2.1) and (2.2). This being the case, the $\hat{E}-\hat{I}$ diagram can be analyzed simply at $t = 0$ as in Figure 2.7. The time variation of 60-cycle sinusoids is uniquely implied by the complex-valued relationship at $t = 0$. In another form

$$\begin{aligned} \wp(e(t)) &= Ee^{j\delta} = \hat{E}_0 \\ \wp^{-1}\hat{E}_0 &= \wp^{-1}(Ee^{j\delta}) = \sqrt{2}E \cos(\omega t + \delta) \end{aligned} \quad (2.34)$$

$$\begin{aligned} \wp(i(t)) &= Ie^{j(\delta-\varphi)} = \hat{I}_0 \\ \wp^{-1}\hat{I}_0 &= \wp^{-1}(Ie^{j(\delta-\varphi)}) = \sqrt{2}I \cos(\omega t + \delta - \varphi) \end{aligned} \quad (2.35)$$

Note that E and I are the rms (or root mean square) voltage and current values and so $\sqrt{2}E$ or $\sqrt{2}I$ are the peaks or amplitudes of these AC instantaneous quantities.

Under the assumption that quantities E , I , δ , φ are smooth functions of time, it is easy to see how the admittance \hat{Y} , reactance \hat{X} , and impedance $\hat{Z} = R + \hat{X}$, concepts arise for time-varying phasors from Eqs. (2.32) and (2.33). For instance, for current flowing into capacitance C

$$\wp(i_C(t)) = \wp(C \dot{e}(t)) = \hat{I}_C = C \frac{d}{dt} E_C + \hat{Y}_C \hat{E}_C \quad (2.36)$$

where

$$\hat{Y}_C = j\omega C = \frac{1}{\hat{X}_C} \quad (2.37)$$

is the capacitive admittance and for voltage across inductance L

$$\wp(e_L(t)) = \wp(L \dot{i}_L(t)) = \hat{E}_L = L \frac{dI_L}{dt} + \hat{X}_L \hat{I}_L \quad (2.38)$$

where

$$\hat{X}_L = j\omega L = \frac{1}{\hat{Y}_L} \quad (2.39)$$

is the inductive reactance.

Note that the first term on the right-hand side in Eqs. (2.36) and (2.38) is missing from the conventional quasistationary phasor calculus in which differentiation simply involves multiplication by $j\omega$. In fact, the quasistationary assumption

in this example is simply neglecting or setting to zero the $dE(t)/dt$ and $dI(t)/dt$ terms. However, when such derivative terms are properly considered in the phasor equations for power it will be observed that *capacitors and inductors will have nonzero active power* (the change of the amount of swinging energy caused by the variation of voltage and current must come from real power) as follows:

$$\begin{aligned} P_C &= CE_C \dot{E}_C \\ Q_C &= CE_C^2(\omega + \dot{\delta}_C) \end{aligned} \quad (2.40)$$

and

$$\begin{aligned} P_L &= LI_L \dot{I}_L \\ Q_L &= LI_L^2(\omega + \dot{\delta} - \dot{\varphi}) \end{aligned} \quad (2.41)$$

Similar equations can be derived for the transmission-line power flows.

2.2.1 Phasor Interpretation of Power

The preceding shows that transformation to phasor analysis is really a major simplification that carries over to analysis involving power transfer and energy accumulation. So let us next define *complex power* based on Eqs. (2.34) and (2.35):

$$\hat{S}(t) = \hat{E}(t)\hat{I}(t)^* = P(t) + jQ(t) \quad (2.42)$$

$$P(t) = \text{Re}[\hat{E}(t)\hat{I}(t)^*], \quad Q(t) = \text{Im}[\hat{E}(t)\hat{I}(t)^*] \quad (2.43)$$

where symbol * stands for a conjugate of a complex valued variable.

Note that the concept of complex power has emerged as a lucky coincidence. P and Q have a physical meaning, respectively, as the actual physical power flow P through a cross section and the amplitude of a 120-Hz oscillation, Q , of energy between the two sides of the cut set. One side of a cut set $A-A'$ is inherently capacitive; the other is inductive. Coupling P and Q into an arbitrary complex power \hat{S} in a complex plane, is convenient computationally via Eq. (2.42). It is a mistake, however, as Figure 2.7 demonstrates, to try to associate it with some kind of physical entity. In mathematical transformations all terms will not automatically have physical identity.³ Equations (2.42) and (2.43) supply by accident through simple multiplication in the complex domain the physically meaningful but interdependent transforms $P(t)$ and $Q(t)$. Furthermore, the choice of \hat{E} and \hat{I}^* is entirely arbitrary, \hat{E}^* and \hat{I} are equally acceptable. This choice determines whether the inductive or capacitive reactive power will appear in Eq. (2.42) with positive or negative sign. Either choice is equally acceptable because there is no physical fact that would dictate this choice.

³ Think of the Laplace transform as an example.

Furthermore, the magnitude S of the complex-valued power \hat{S}

$$S = \sqrt{P^2 + Q^2} = EI \quad (2.44)$$

is sometimes referred to in the literature as the *apparent* power. It is easily shown that the apparent power is simply a product of the rms values of voltage and current, that is,

$$S^2 = E^2 I^2 \quad (2.45)$$

The units assigned to apparent power are MVA; given the fact that \hat{S} has no physical interpretation, the apparent power being the magnitude of \hat{S} lacks such interpretation, as well. It is often used in practice, however, as a meaningful measure of combined voltage and current rating for a particular device, given the nominal voltage level of the equipment.

2.3 CLASSICAL STATIONARY PHASOR CALCULUS

If all time derivatives \dot{E} , \dot{I} , $\dot{\delta}$, $\dot{\phi}$ are set to zero in Eqs. (2.5) and (2.6), then the defining equations of power flow in a strictly stationary system are directly obtained in both the time (Section 2.1) and phasor (Section 2.2) domains. These are the classical phasors as originally defined around the turn of the century for analyzing stationary conditions in power systems. These are used even today in computing stationary load flows in transmission networks—the most frequently used computation in power-system operation and planning. Here they appear as a special case of the newly defined time-varying phasor. So the equations defining a stationary phasor are Eqs. (2.29) to (2.45) with the derivatives \dot{E} , \dot{I} , $\dot{\phi}$ set to zero. Section 2.6 discusses an important extension of the stationary phasor case to signals composed of harmonics.

2.4 THE CLASSICAL QUASISTATIONARY PHASOR CALCULUS

It is pointed out here that either time-domain representation or stationary phasor calculus can be used as a quasistationary approximation and it is widely used so, including most of this book, applicable as an approximation for systems with sufficiently slow time variation of power flows. The order of the errors that define the limits of the validity of the quasistationary model were analyzed rigorously in Ref. [1 and 2]. It is shown later in the book that the quasistationary approximation is generally valid for electromechanical “transient stability” but not necessarily for voltage stability. In Chapter 11 the time-varying phasor is used beyond these limits. Stationary or quasistationary phasor calculus as defined here is an approximate tool used in most chapters of this book. Additional (introductory) discussion for more complex issues needed in some parts of later chapters is given later in Chapter 11.

2.4.1 Some General Comments

- When the basic definitions of phasor calculus are applied to linear electric circuits through the laws of Ohm and Kirchhoff, the conventional phasor calculus of reactances, inductances, susceptances, power-balance equations, etc., emerges. This is the universal language of AC power-system analysis today. This is common practice and will not be quoted here.
- Outside the quasistationary range where many voltage stability problems lie, more refined techniques are required for accurate analysis (discussed in Chapter 11).

2.5 SUMMARY OF THE CHARACTERISTICS OF ACTIVE- AND REACTIVE-POWER FLOW

Complex power as defined by phasors \hat{E} , and \hat{I}

$$\hat{S}(t) = EI \cos \varphi + jEI \sin \varphi = P(t) + jQ(t) \quad (2.46)$$

has no physical meaning as such, but Eq. (2.46) is a very useful mathematical concept. Its two components will now be discussed.

2.5.1 Characteristics of Active Power $P(t)$ in the Quasistationary Region

- $P(t)$ represents smooth unidirectional power flow through a cut set or into an equipment piece at all times (Fig. 2.2) for either single-phase or balanced polyphase circuits (the three-phase results shown here readily generalize to polyphase).
- For the voltage and current reference directions selected for Figures 2.2(a) and 2.2(b) and used in Eqs. (2.1) and (2.2) the reference direction of the power flow is positive from left to right in Figures 2.2, 2.4, and 2.6. The choice of the reference direction is, of course, completely arbitrary.
- For stationary single-phase cross sections or cut sets in Figures 2.2(a) and 2.2(b), this unidirectional power flow contains a time average (slowly drifting for a quasistationary case) over time intervals of integer multiples of $(1/120)$ sec with a 120-Hz sine wave of amplitude matching the average [Fig. 2.4(a)] superimposed. Thus the unidirectional flow $P(t)$ fluctuates between 0 and twice the average [Figure 2.4(a)].
- The averaging is automatically accomplished by equipment such as generators, motors, and loads with response that is slow compared to 60 cycles, that is, in the quasistationary range. For light the averaging is done by the human eye.
- For a balanced three-phase circuit (Fig. 2.6) the three-phase power flow is averaged instant by instant through the summation of three sine waves that are displaced 120° . So the total balanced three-phase power flow through a cross section or cut-set is physically constant in time.

- The unidirectional flow of $P(t)$ accumulates into a monotonically increasing (on a straight line for balanced three phase) physical quantity [Fig. 2.4(b)] of energy that subsequently may be distributed among pieces of equipment and/or converted into other types of energy such as heat, light, or mechanical power.
- Note that $P_{A-A'}(t)$ is unaffected by the circuit on the right of Figures 2.2(a) and 2.2(b) being inductive or capacitive as long as φ is the same size [$\cos(-\varphi) = \cos \varphi$].

2.5.2 Characteristics of the Reactive Power $Q(t)$ in the Quasistationary Region

- $Q(t)$ represents the amplitude of a smooth, sinusoidally varying power-flow component $q(t)$ through any cut set $A-A'$ or into an equipment piece.
- For the voltage and current reference directions selected for Figures 2.1 and 2.2 and used in Eqs. (2.1) and (2.2) the reference direction for positive power flow (whether instantaneous or average) will be from left to right.
- Since the instantaneous power flow in Q follows a sine wave the average power flow over an integer number of time intervals of $\frac{1}{120}$ sec duration (Fig. 2.5) is necessarily zero and the instantaneous total three-phase power flow is also zero [$Q(t) \equiv 0$ for balanced three-phase cut sets].
- This means that no net energy is transported across the cross section in balanced three-phase circuits or over $\frac{1}{120}$ sec intervals in single-phase circuits (including individual phases of balanced three-phase circuits); see Figure 2.6. Reactive power does not flow.
- Reactive power implies, however, a 120-Hz swinging of an amount of energy [see shaded areas in Fig. 2.5(a) in sine wave fashion] between the two sides of any single-phase circuit (or one phase of a three-phase circuit) across any cross section $A-A'$.
- Since there is a phase reversal for the current at the cut set (in for the left—out on the right in Fig. 2.6) the circuit has to be inductive on one side and capacitive on the other (equal reactance). So the reactive-power component $q(t)$ simply means a 120-Hz oscillation of energy between the capacitive circuit on one side (left side in Fig. 2.2) and the inductive circuit on the other. In alternate half-cycles the energy will accumulate in the net capacitive side or net inductive side, but there is no net energy flowing in reactive power over integer numbers of $\frac{1}{60}$ sec intervals.
- Remember then: Reactive power swings, but it does not flow, although *flow* is commonly used in a casual manner to identify which is the capacitive side or the inductive one. It will be used that way in some parts of this book.
- Q is *not* the imaginary power of the 2ω -frequency component.
- The most important thing to keep in mind is that active and reactive power are simply two different phenomena that sum into a single instantaneous power flow $\mathcal{P}(t)$ (or \hat{S} in phasors). P is a unidirectional (but fluctuating at

120 Hz from 0 to $2P$) power flow through a cross section or cut set $A-A'$ while Q is an oscillation without any net average flow across the same cross section. It is as simple as this. There is nothing mysterious about reactive power. The following section offers an illustrative example for the connection between reactive power and voltage.

- Looking at it from another angle, it takes two quantities [voltage $e(t)$ and current $i(t)$] to define the flow across the cross section $A-A'$. Here $e(t)$ and $i(t)$ are independently given. The combination P and Q is an alternative way, a transformation to define the instantaneous flow. Without Q the instantaneous power flow is not defined by P .

2.5.3 Optimum Performance of Devices Characterized by AC Signals

Recall from the preceding basic interpretation of real and reactive power through a cross section $A-A'$ that it is the real power that gets converted into real work. Because of this, given the design specifications of the device to the right of $A-A'$ in terms of its MVA rating (as a consequence of the specification of voltage and current rms values E and I), this device is most useful as measured in terms of the energy produced to perform real work when its real power P is maximized. It follows from Eq. (2.44) that, for given E real power P is maximized when the reactive power Q^2 is minimized. This is an important basic result to keep in mind when operating and planning electric power systems. It is easily proven that the optimum occurs when the power factor ($\cos \varphi$) of the device to the right of the cross section is 1, or, stated differently, when voltage and current waveforms $e(t)$ and $i(t)$ are in phase, or, furthermore, when the current phase angle φ in Eq. (2.2) is identically zero.

A classical illustration of this concept is the so-called maximum power-transfer theorem [8], whose simplest version is in the context of the following problem. Given an independent voltage source with a load connected through an internal impedance in series $\hat{Z}_s = R_s + jX_s$, it is required to find the load impedance that will take the maximum real power load P_{load} from the given source. The answer to this problem is that the optimum load impedance has the value $\hat{Z}_{\text{load}} = R_s - jX_s$. For this value of load impedance the reactive power into the cross section $A-A'$ seen by the source is zero. The typical compensation needed to change $i(t)$ to its optimal value $i^{\text{optimal}}(t)$ can be either shunt or series.

Variations of the same result can be used as a basis for several optimization problems of interest in power networks. Only some are given in this section. It is not hard to show that the following optimization problems are equivalent on the simplest, single generator single load, power system topology.

Problems

1. *Real-power transmission-loss minimization.* Find a reactive power compensation that will provide minimum real-power transmission losses for a given real-power input at the generator side P_g and its voltage rms value E . Its

mathematical formulation, with R_e resistance seen by the generator, is

$$\min_{i(t)} \frac{1}{T} \int_0^T R_e i^2(t) dt \quad (2.47)$$

subject to

$$\frac{1}{T} \int_0^T i(t) e(t) dt = P_g \quad (2.48)$$

and

$$E^2 = \frac{1}{T} \int_0^T e^2(t) dt \quad (2.49)$$

where T is an integer multiple of (1/120) sec. Here $e(t)$ stands for an independent voltage source whose rms value is E .

2. *Minimization of the reactive power out of a generator.* Find a reactive compensation that minimizes reactive-power input into the transmission grid, as seen at the source of energy (generator) terminals for specified P_g and E .
3. *Maximizing the real power delivered to a load.* Find a reactive compensation that maximizes P_{load} , for specified P_g and E .

All three problems are solvable as a simple calculus of variations problem [9], and have the identical solution

$$i^{\text{optimal}}(t) = \frac{P_g}{E^2} e(t) \quad (2.50)$$

*Proof:*⁴ The problem here is to minimize the expression (2.47) subject to the constraints (2.48) and (2.49). This is an isoperimetric variational problem. If the Euler–Lagrange equation is applied to the augmented functional

$$J = \frac{1}{T} \int_0^T [i_p^2(t) + \lambda i_p(t) e(t)] dt = \frac{1}{T} \int_0^T f(i_p(t)) dt \quad (2.51)$$

with λ being a Lagrange multiplier, the optimality condition is defined as

$$\frac{\partial f(i_p(t))}{\partial i_p(t) - (\partial f(i_p(t))/\partial i_p(t))} = 0 \quad (2.52)$$

Its solution is

$$-2i_p(t) + \lambda e(t) = 0 \quad (2.53)$$

⁴ Unpublished work with Prof. Branslava Peruničić, University of Sarajevo, 1986.

or

$$i^{\text{optimal}}(t) = Ke(t) \quad (2.54)$$

where

$$K = \lambda/2 \quad (2.55)$$

It is important to observe that the optimal compensation producing $i^{\text{optimal}}(t)$ cannot account for voltage operating constraints at the load port. This makes direct use of the maximum power-transfer theorem in electric power systems somewhat limited. Much is said in Chapter 14 on other methods that are used to solve voltage-constrained compensation problems in power networks.

2.6 QUASISTATIONARY PHASOR CONCEPTS FOR PERIODIC SIGNALS

In this section the basic time-domain and phasor representation of periodic signals with higher-order harmonics is introduced. These types of signals are increasingly present in today's electric power systems and are caused by various electronic power-switching equipment and certain inherent system nonlinearities, magnetic saturation, in particular. First, the time-domain representation of periodic voltage, current, and instantaneous power is defined in Section 2.6.1. This is followed by a notion of a generalized definition of *vector* phasors for periodic signals as possible symbolic language for efficient computations of quasistationary conditions. It is shown that a vector phasor is a direct generalization of the (scalar) phasors for AC signals. In Section 2.6.4 the use of this calculus for defining average (real), reactive, and complex-valued power entering an arbitrary cross section $A-A'$ or cut set characterized by the pair of voltage periodic signal $e(t)$ and current signal $i(t)$ as shown in Figure 2.2 is described.

Finally, minimization of reactive power into a cross section $A-A'$ with the objective of maximizing real power into it within the prespecified operating constraints on magnitudes of voltage $e(t)$ and current $i(t)$ is posed as a constrained optimization problem in Section 2.6.9. Within this section several illustrative examples are given to emphasize algebraic details when working with general periodic signals. These examples illustrate the potential use of the vector phasor calculus described here for optimal design of electronically controlled power components within an electric power system.

2.6.1 Time-Domain Representation for Periodic Voltage, Current, Power, and Energy

We begin by recalling that an arbitrary cross section shown in Figure 2.2(a) or a single port shown in Figure 2.2(b) are characterized by the pair of voltage $e(t)$ and current $i(t)$ signals at the cut set $A-A'$. The voltage and current are periodic with period T , such that $e(t+T) = e(t)$ and $i(t+T) = i(t)$. A Fourier series

expansion representation of a periodic voltage $e(t)$ containing n harmonics is

$$e(t) = \sum_{k=0}^{k=n} \sqrt{2}E_k \cos(k\omega t + \delta_k) = \sum_{k=0}^{k=n} e_k(t) \quad (2.56)$$

and, similarly, the representation of a periodic current is

$$i(t) = \sum_{k=0}^{k=n} \sqrt{2}I_k \cos(k\omega t + \delta_k - \varphi_k) \quad (2.57)$$

The representations (2.56) and (2.57) are a direct generalization of the AC voltage and current representation (2.1) and (2.2).

As always, the instantaneous power $\mathcal{P}(t)$ crossing cut set $A-A'$ is $\mathcal{P}(t) = e(t)i(t)$. With this in mind, if $e(t)$ and $i(t)$ signals consisting of a sum of sine waves at harmonic frequencies $k = 0, 1, \dots, n$ as given in Eqs. (2.56) and (2.57), respectively, are substituted into the general expression for instantaneous power (2.3), then it is easy to see following the reasoning leading to the Eqs. (2.15) to (2.21) that an equation of the form

$$\mathcal{P}(t) = \mathcal{P}_{kk}(t) + \mathcal{P}_{km}^+(t) + \mathcal{P}_{km}^-(t) = p(t) + q(t) \quad (2.58)$$

emerges for the instantaneous power flow, conveniently divided into three types of definitions:

$$\begin{aligned} \mathcal{P}_{kk}(t) &= \sum_k E_k I_k \cos \varphi_k [1 + \cos 2(k\omega t + \delta_k)] \\ &+ E_k I_k \sin \varphi_k \sin 2(k\omega t + \delta_k) = p_{kk}(t) + q_{kk}(t) \end{aligned} \quad (2.59)$$

$$\begin{aligned} \mathcal{P}_{km}^+(t) &= \sum_k \sum_{m, m \neq k} E_k I_m \cos \varphi_m \cos [(k\omega + m\omega)t + (\delta_k + \delta_m)] \\ &+ E_k I_m \sin \varphi_m \sin [(k\omega + m\omega)t + (\delta_k + \delta_m)] = p_{km}^+(t) + q_{km}^+(t) \end{aligned} \quad (2.60)$$

$$\begin{aligned} \mathcal{P}_{km}^-(t) &= \sum_k \sum_{m, m \neq k} E_k I_m \cos \varphi_m \cos [(k\omega - m\omega)t + (\delta_k - \delta_m)] \\ &+ E_k I_m \sin \varphi_m \sin [(k\omega - m\omega)t + (\delta_k - \delta_m)] = p_{km}^-(t) + q_{km}^-(t) \end{aligned} \quad (2.61)$$

Observe that despite the complexity of the above expressions, the average value P of instantaneous power $\mathcal{P}(t)$ is contributed to by only one term $\sum_k E_k I_k \cos \varphi_k$. All other terms average out to zero, and in this sense reflect components of instantaneous power that do not contribute to the average unidirectional power flow over time intervals that are integer multiples of $(1/60)$ sec.

These three equations can be interpreted in terms of interactions among specific harmonics. The terms $\mathcal{P}_{kk}(t)$ under the single summation are simply contributions of individual harmonics to the instantaneous power as though they were

acting independently from the other harmonics. The terms in \mathcal{P}_{km}^+ and \mathcal{P}_{km}^- under the double summation reflect oscillations of energy due to interactions among different harmonics. In other words, \mathcal{P}_{km}^+ and \mathcal{P}_{km}^- can be further differentiated into components that reflect interactions of individual harmonics $\mathcal{P}_{km}^+(t)$ at a frequency equal to the sum of the individual frequencies and into the components $\mathcal{P}_{km}^-(t)$, which reflect interactions at the frequencies that are differences of individual frequencies. Furthermore, within $\mathcal{P}_{km}^+(t)$ and $\mathcal{P}_{km}^-(t)$ themselves one could observe components $p_{km}^+(t)$ and $p_{km}^-(t)$ that are multiplied by $\cos \varphi_{km}$ and components $q_{km}^+(t)$ and $q_{km}^-(t)$ that are multiplied by $\sin \varphi_m$, respectively.

Notice that there is no average contribution of any of these components and as such none of them is directly useful in producing real work. An intriguing issue related to the reactive-power definition is to further extract from these subgroups of components of the instantaneous power the terms contributing to reactive power.

To establish this, observe that in Eq. (2.58) there are components whose individual terms contain $\cos \varphi_m$ and $\sin \varphi_m$, respectively. It is conjectured here that the reactive power can be interpreted directly in terms of the latter terms only.

Then the definition of active and reactive power for periodic functions can be stated as follows.

Definition 2.6.1.1 The active power P represents for the total periodic signal a unidirectional flow through a cross section $A-A'$ delivered

$$P = \sum_k E_k I_k \cos \varphi_k = \sum_k P_k \quad (2.62)$$

$$\begin{aligned} p(t) &= \sum_k E_k I_k \cos \varphi_k [1 + \cos 2(k\omega t + \delta_k)] \\ &\quad + \sum_k \sum_{m, m \neq k} E_k I_m \cos \varphi_{km} \cos [(k\omega + m\omega)t + (\delta_k + \delta_m)] \\ &\quad + \sum_k \sum_{m, m \neq k} E_k I_m \cos \varphi_{km} \cos [(k\omega - m\omega)t + (\delta_k - \delta_m)] \\ &= p_{kk}(t) + p_{km}^+(t) + p_{km}^-(t) \end{aligned} \quad (2.63)$$

Note that for $\varphi_k > \pi/2$ in some harmonics k , there would be $P_k < 0$, which then means that such harmonics deliver the energy against the mainstream.

Definition 2.6.1.2 The reactive power Q , which represents the amplitudes of sinusoidal energy oscillations with zero unidirectional flow of energy, can be defined as a matrix of the amplitudes of oscillation for individual contributions of pairs of harmonics $q_{km}^\pm(t)$ (including $q_{kk}(t)$)

$$[Q] = [Q_{kk}] + [Q_{km}^+] + [Q_{km}^-] \quad (2.64)$$

where $[Q_{kk}]$, $[Q_{km}^+]$, and $[Q_{km}^-]$ come from Eqs. (2.59), (2.60), and (2.61), respectively.

For sinusoidal (single harmonic) signals it was pointed out earlier in connection with Eqs. (2.16) and (2.17) that P and Q are two different phenomena which, as defined, always added up to the instantaneous power $\mathcal{P}(t)$, that is, $\mathcal{P}(t) = p(t) + q(t)$. $p(t)$ carries all the unidirectional power flow and in fact it is the largest monotonically varying function of the form $(1 + \cos(\omega t + \delta))$ that can be fitted into $\mathcal{P}(t)$. The rest of $\mathcal{P}(t)$, that is, $q(t)$, then represents a 120-Hz oscillation of power flow, which has zero average over any integer multiple of $(1/60)$ sec, and hence it carries no net energy flow. The point is that P and Q , although they are two components of a single function, are of different nature. P is the average power flow into cut set $A-A'$, and Q is the amplitude of a set of sinusoidal oscillations across this cut set. But together they define the instantaneous power flow. This is illustrated in Figure 2.9. This is the picture for signals consisting of one harmonic. Note that it is identical to Figures 2.4 and 2.5 plotted in a different format.

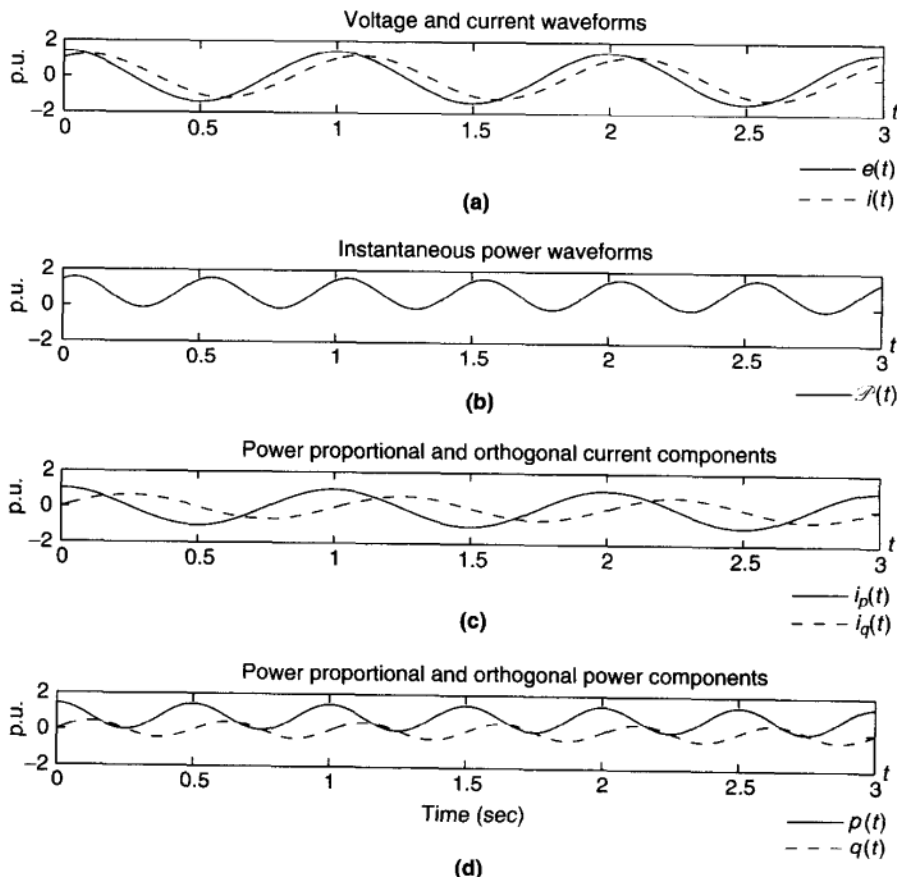


FIGURE 2.9 Single-frequency example waveforms.

Here, however, we face a signal containing a number of harmonics within a periodic function of basic period 60 Hz in a Fourier series. Components $p(t)$ and $q(t)$ for the case of a two-harmonic signal are shown in Figure 2.10. For multiharmonic signals, as just defined, the active power P is simply the sum of the active power flow of all nonempty harmonics. This fortuitous result follows from the linear, additive nature of $\mathcal{P}(t)$ according to Eq. (2.58), which justifies superposition of the integrals for individual harmonics. Not so advantageous is the situation with the amplitudes of the oscillations in $q_{kk}(t)$, $q_{km}^+(t)$ and $q_{km}^-(t)$ in Eqs. (2.60) and (2.61). The average flow of all such terms is zero, which gives no useful information. The amplitude of the oscillations are defined in Eqs. (2.59), (2.60) and (2.61), but only as entries in a matrix (2.64) with no apparent way to simplify them into a single meaningful Q reactive power for the entire signal.

This leaves us for the moment with a straightforward expression for the average real power flow, but only a large matrix of amplitudes for individual “reactive”-power oscillations for the harmonics and no obvious “reactive”-power value concept for the system. A solution may be the use of a norm for the matrix that would provide a measure of the size of the swinging energy but not its total

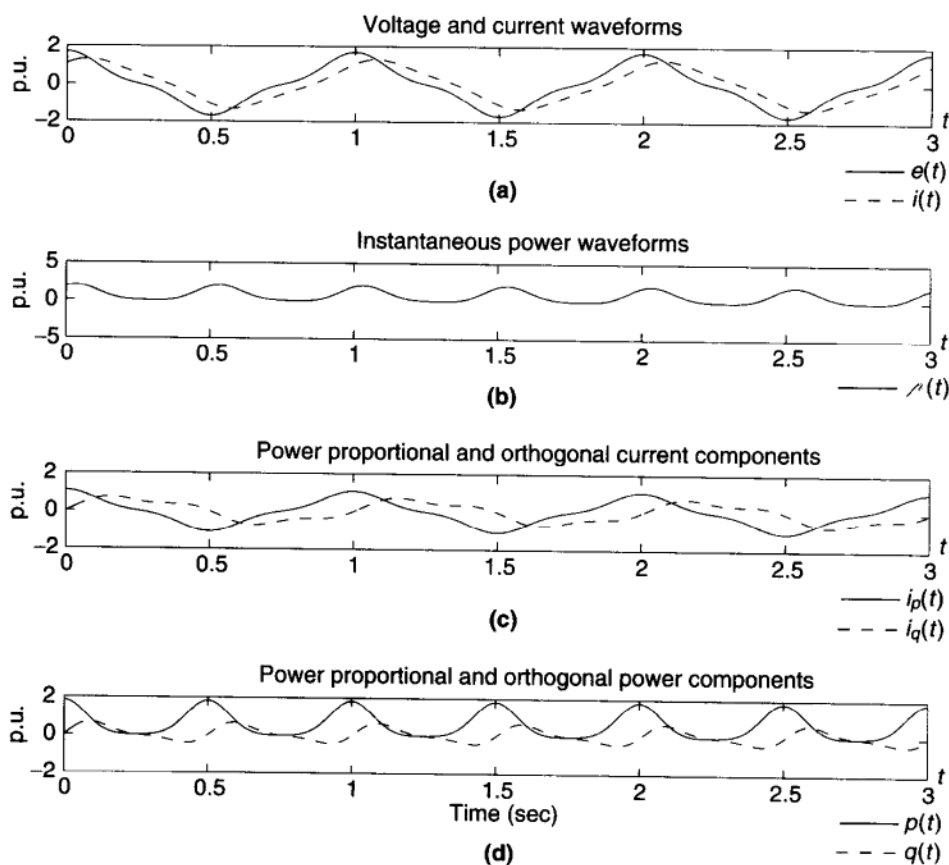


FIGURE 2.10 Two frequency example waveforms.

amount. These matters will be taken up again after extending the phasor concept to the multiharmonic signal.

2.6.2 Generalizing Phasors to Multiharmonic, that is, Periodic, Signals

Let us remember that the phasor transformation φ as defined in Section 2.3 Eqs. (2.33), (2.34), and (2.41) to (2.43), was arbitrarily selected for computational convenience by moving functions of time such as $e(t)$, $i(t)$, or $\mathcal{P}(t)$ into the complex plane. Such arbitrary transformations are always justified if, given mathematical precision, the results obtained in the transformed (here the complex) domain will transform back into the correct answers in the physical (here the time) domain. The transforms need not have a direct physical meaning in the transformed domain.

Faced with the situation that applies here, where functions $z_k(t)$ [such as $e_k(t)$, $i_k(t)$] are embedded in linear, summation-type relationships, a logical choice for a multiharmonic transformation is one with reference to the individual harmonic frequencies. The logical choice for a generalized transform is to apply Eqs. (2.33) and (2.34) directly and separately to individual harmonics of a function $z_k(t)$ as long as superposition applies to the individual harmonics of a function as it does on the power system (even to the power relations). This choice leads to a definition of a phasor transformation for a periodic system as follows.

Definition 2.6.2.1 Time-domain representation: Let the periodic function be defined by the Fourier series

$$z(t) = \sum_{k=1}^n z_k \cos(\omega_k t + \xi_k) \quad (2.65)$$

as exemplified by Eqs. (2.56), (2.57), and (2.58) for instantaneous voltage $e(t)$, current $i(t)$, and power $\mathcal{P}(t)$, respectively.

Definition 2.6.2.2 Phasor transformations from the time domain into the complex domain with the notation $\theta_k = \omega_k t$:

$$\varphi z(t) = \sum_{k=1}^{k=n} z_k e^{j\theta_k} = \hat{z} \quad (2.66)$$

where \hat{z} is the phasor transform of $z(t)$.

Definition 2.6.2.3 The inverse transform of \hat{z} into the time domain is

$$z(t) = \operatorname{Re} \left(\sum_{k=1}^n z_k e^{j\xi_k} e^{j\omega_k t} \right) \quad (2.67)$$

which can be carried out harmonic by harmonic.

It was pointed out in conjunction with Eqs. (2.56) to (2.58) that the phasor-domain representation (in the complex plane) for individual signals k simply consists of vectors of length z_k at an angle ζ_k . Clearly then for the periodic signal the phasor transform simply consists of the addition of the vectors of successive harmonics in the complex plane. So this is simply a static vector sum.

It also was explained with Eqs. (2.56) to (2.58) that in the engineering field it became customary to use a semi-inverse transform, which simply consists of the inverse transform before the "real part" Re is taken. That then leaves for a single harmonic a vector \hat{z} in the complex plane rotating at the speed of $\omega = 60$ cycles. For systems consisting of a number of components such as resistors, reactors, capacitors, and synchronous machines, an edifice of such complex vectors can be constructed.

The concept of the semi-inverse quite directly applies to the periodic function $z(t)$ as

$$z(t) = \sum_{k=1}^n z_k e^{j(\omega_k t + \zeta_k)} \quad (2.68)$$

This can be drawn for a given time such as $t = 0$ in a static vector diagram form. Of course if one wants to set it into rotation virtually every vector will move at its own speed, the further from the origin, the faster. This would be a rather complex vector diagram. But what is normally needed is a snapshot at some time t . Figure 2.11 displays the multiharmonic phasor form (compare to the one harmonic form in Figure 2.8) for voltage and current somewhat differently,

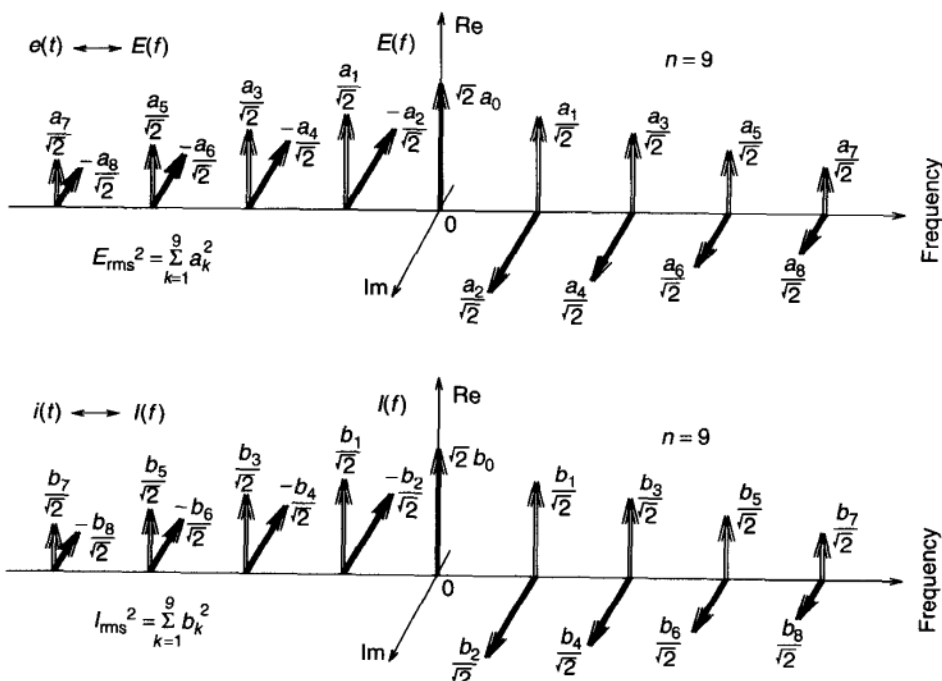


FIGURE 2.11 Vector-wise representation of reactive power in the single-frequency case.

emphasizing frequencies of the various harmonics rather than putting them on top of each other for a given instant of time. Coefficients a_i and b_i in this Figure represent the real and imaginary components of the vector representation for voltage and current, respectively.

Let us now define the Fourier sets of $e(t)$ and $i(t)$ in a vector from:

$$[\underline{e}(t)] = [e_1(t) \quad \cdots \quad e_n(t)]^T \quad (2.69)$$

and

$$[\underline{i}(t)] = [i_1(t) \cdots i_n(t)]^T \quad (2.70)$$

Also define the Fourier transformation vector as

$$\underline{\varphi} = [\varphi_1 \quad \cdots \quad \varphi_n]^T = [e^{j\omega t} \quad \cdots \quad e^{jn\omega t}]^T \quad (2.71)$$

Then the phasor transform of voltage and current can be written as

$$\hat{\underline{E}} = \underline{\varphi} \underline{e}(t) \quad (2.72)$$

and

$$\hat{\underline{I}} = \underline{\varphi} \underline{i}(t) \quad (2.73)$$

2.6.3 Definition of Vector Phasors for Periodic Signals

Thus vector phasors representing voltage $e(t)$ [Eq. (2.56)] and current $i(t)$ [Eq. (2.57)] of periodic signals are defined as

$$\begin{aligned} \hat{\underline{E}} &= [\hat{E}_1 \hat{E}_2 \quad \cdots \quad \hat{E}_n]^T \\ &= [E_1 e^{j\delta_1} E_2 e^{j\delta_2} \quad \cdots \quad E_n e^{j\delta_n}]^T \\ &= [(E_{c1} + jE_{s1}) \quad (E_{c2} + jE_{s2}) \quad \cdots \quad (E_{cn} + jE_{sn})]^T \end{aligned} \quad (2.74)$$

and

$$\begin{aligned} \hat{\underline{I}} &= [\hat{I}_1 \quad \hat{I}_2 \quad \cdots \quad \hat{I}_n]^T \\ &= [I_1 e^{j(\delta_1 - \varphi_1)} I_2 e^{j(\delta_2 - \varphi_2)} \quad \cdots \quad I_n e^{j(\delta_n - \varphi_n)}]^T \\ &= [(I_{c1} + jI_{s1}) \quad (I_{c2} + jI_{s2}) \quad \cdots \quad (I_{cn} + jI_{sn})]^T \end{aligned} \quad (2.75)$$

A direct relationship exists between this polar-coordinate-like representation of voltage and current signals and their rectangular-coordinate-like representation, as reviewed in Section 2.2.1 earlier for the pure sinusoidal case. In the periodic case *vector* rectangular representation of a complex-valued voltage phasor vector $\hat{\underline{E}}$ in *real-valued domain* is given as

$$\underline{E} \equiv [E_{c1} \quad E_{s1} \quad E_{c2} \quad E_{s2} \quad \cdots \quad E_{cn} \quad E_{sn}]^T \quad (2.76)$$

and the representation of a complex-valued current phasor vector $\hat{\underline{I}}$ is

$$\underline{I} \equiv [I_{c1} \quad I_{s1} \quad I_{c2} \quad I_{s2} \quad \cdots \quad I_{cn} \quad I_{sn}]^T \quad (2.77)$$

A periodic voltage represented in time domain as $e(t)$ is uniquely represented as a phasor vector $\underline{\hat{E}}$. The i th component of $\underline{\hat{E}}$ is an ordinary (AC) phasor rotating at the angular frequency $i\omega$, $i = 1, 2, \dots, n$. Note that, analogously to the AC phasor case, the physical interpretation of voltage $e(t)$ is

$$\begin{aligned} e(t) &= \operatorname{Re}[\sqrt{2}\underline{\hat{E}}^T \underline{\hat{\Phi}}^*(t)] \\ &= \operatorname{Re}[\sqrt{2}\underline{\hat{E}} * \underline{\hat{\Phi}}(t)] = \sqrt{2} \sum_{k=1}^{k=n} E_k \cos(k\omega t + \delta_k) \end{aligned} \quad (2.78)$$

where

$$\underline{\hat{\Phi}}(t) = [\hat{\Phi}_1(t) \quad \hat{\Phi}_2(t) \quad \dots \quad \hat{\Phi}_n(t)]^T = [e^{j\omega t} \quad e^{2j\omega t} \quad \dots \quad e^{nj\omega t}]^T \quad (2.79)$$

The corresponding real-valued representation of $\underline{\hat{\Phi}}$ is

$$\underline{\Phi}(t) = [\cos \omega t \quad \sin \omega t \quad \cos 2\omega t \quad \sin 2\omega t \quad \dots \quad \cos n\omega t \quad \sin n\omega t]^T \quad (2.80)$$

Similarly, a periodic current in time domain $i(t)$ can be represented as

$$\begin{aligned} i(t) &= \operatorname{Re}[\sqrt{2}\underline{\hat{I}}^T \underline{\hat{\Phi}}^*(t)] \\ &= \operatorname{Re}[\sqrt{2}\underline{\hat{I}} * \underline{\hat{\Phi}}(t)] = \sqrt{2} \sum_{k=1}^{k=n} I_k \cos(k\omega t + \delta_k - \varphi_k) \end{aligned} \quad (2.81)$$

This illustrates a generalized mapping from time domain into the complex-valued vector space, which is simply a mathematical transformation

$$\wp_H(e(t)) = \underline{\hat{E}} = [\hat{E}_1 \quad \hat{E}_2 \quad \dots \quad \hat{E}_n]^T \quad (2.82)$$

$$\wp_H(i(t)) = \underline{\hat{I}} = [\hat{I}_1 \quad \hat{I}_2 \quad \dots \quad \hat{I}_n]^T \quad (2.83)$$

and its inverse

$$\begin{aligned} \wp_H^{-1}(\underline{\hat{E}}) &= e(t) = \sqrt{2} \sum_{k=1}^{k=n} E_k \cos(k\omega t + \delta_k) \\ &= \sqrt{2}\underline{\hat{E}}^T \underline{\hat{\Phi}}(t) = \sqrt{2} \sum_{k=1}^{k=n} (E_{ck} \cos k\omega t + E_{sk} \sin k\omega t) \end{aligned} \quad (2.84)$$

$$\begin{aligned} \wp_H^{-1}(\underline{\hat{I}}) &= i(t) = \sqrt{2} \sum_{k=1}^{k=n} I_k \cos(k\omega t + \delta_k - \varphi_k) \\ &= \sqrt{2}\underline{\hat{I}}^T \underline{\hat{\Phi}}(t) = \sqrt{2} \sum_{k=1}^{k=n} (I_{ck} \cos k\omega t + I_{sk} \sin k\omega t) \end{aligned} \quad (2.85)$$

2.6.3.1 Concepts of rms Voltage and Current For the case of single frequency, transformation \wp_H and its inverse are identical to the ordinary mathematical transformation \wp [Eqs. (2.34) and (2.35)] of the AC case. Variables $\underline{\hat{E}}$ and $\underline{\hat{I}}$ are elements of the n -dimensional complex-valued space. In this space an inner (scalar) product of two variables $\underline{\hat{A}} = [\hat{A}_1 \quad \hat{A}_2 \quad \dots \quad \hat{A}_n]^T$ and $\underline{\hat{B}} = [\hat{B}_1 \quad \hat{B}_2 \quad \dots \quad \hat{B}_n]^T$ is defined as

$$\underline{\hat{A}} \cdot \underline{\hat{B}}^* \equiv [\hat{A}_1 \quad \hat{A}_2 \quad \dots \quad \hat{A}_n]^T [\hat{B}_1 \quad \hat{B}_2 \quad \dots \quad \hat{B}_n]^* = \sum_{k=1}^{k=n} \hat{A}_k \hat{B}_k^* \quad (2.86)$$

In this space the rms value of a periodic voltage $e(t)$, defined as the square root or the time average of the square of the voltage over integer cycles of the base harmonic,

$$E = \frac{1}{T} \int_0^T e^2(t) dt \quad (2.87)$$

can be directly shown to be

$$E = \sqrt{(\underline{\hat{E}} \cdot \underline{\hat{E}}^*)} = \sqrt{\left(\sum_k E_k^2 \right)} \quad (2.88)$$

Similarly, the rms value of a periodic current $i(t)$

$$I^2 \equiv \frac{1}{T} \int_0^T i^2(t) dt \quad (2.89)$$

is

$$I = \sqrt{(\underline{\hat{I}} \cdot \underline{\hat{I}}^*)} = \sqrt{\left(\sum_k I_k^2 \right)} \quad (2.90)$$

Note that the rms value of periodic signals such as $e(t)$ and $i(t)$ is contributed only by the individual harmonics and not by the mutual effects of components with different frequency carriers. This property is a direct corollary of the orthonormality property of $\underline{\hat{\Phi}}(t)$ defined in Eq. (2.79), that is

$$\frac{1}{T} \int_0^T \underline{\hat{\Phi}}_i(t) \underline{\hat{\Phi}}_j(t)^* dt = \begin{cases} 1, & i = j \\ 0, & i \neq j \end{cases} \quad (2.91)$$

or in complex-valued vector notation

$$\frac{1}{T} \int_0^T \underline{\hat{\Phi}}(t) \underline{\hat{\Phi}}^{*T}(t) dt = \underline{\mathbf{I}} \quad (2.92)$$

where $\underline{\mathbf{I}}$ is the identity matrix.

As in the case of AC signals, if a single port to the right of a cut set $A-A'$ consists of linear R,L,C elements, its constituent relation is of the form

$$\hat{\underline{E}} = \hat{\underline{Z}} \hat{\underline{I}} \quad (2.93)$$

where matrix $\hat{\underline{Z}}$ is an $n \times n$ complex-valued diagonal matrix whose diagonal terms are input impedances into the cross section computed for each single harmonic. This relation is a direct result of the superposition principle.

An analogous version of Eq. (2.93) can be stated in the $2n \times 2n$ dimensional space as

$$\underline{E} = Z \underline{I} \quad (2.94)$$

with \underline{E} and \underline{I} real-valued representations defined in Eqs. (2.76) and (2.77), and the Z matrix is a block-diagonal matrix with 2×2 nonzero blocks. The real-valued algebra of this type was introduced in Ref. [4]. Examples illustrating the use of this algebra are given throughout the rest of this chapter.

2.6.3.2 Examples of Linear RLC Circuits

Example 2.6.3.1 Single-phase example for a linear RLC circuit: This circuit consists of a series RL with $R = 1\Omega$ and $L = 0.1$ H connected to a single-frequency sinusoidal source. The voltage is 1 p.u. rms, with a frequency of 1 Hz, $e(t) = \sqrt{2} \cos(2\pi t)$. The complex-valued representation for this case is as in any standard AC case, and is directly based on using the phasors for AC signals. In particular, $\hat{\underline{E}} = 1e^{j0}$, $\hat{\Phi}(t) = e^{j\omega t}$. The complex-valued impedance is $\hat{\underline{Z}} = R + j\omega L$. The complex-valued current phasor is

$$\hat{\underline{I}} = \hat{\underline{Z}}^{-1} \hat{\underline{E}} \quad (2.95)$$

Similarly, in the real-valued two-dimensional vector space, voltage and current waveforms are represented as

$$\begin{aligned} e(t) &= \sqrt{2} \underline{E}^T \underline{\Phi}(t), & i(t) &= \sqrt{2} \underline{I}^T \underline{\Phi}(t) \\ \underline{\Phi}(t) &= [\cos(2\pi t) \quad \sin(2\pi t)]^T \end{aligned} \quad (2.96)$$

where

$$\begin{aligned} \underline{E} &= [1 \ 0]^T, & \underline{I} &= Z^{-1} \underline{E} \\ Z &= \begin{bmatrix} R & 2\pi L \\ -2\pi L & R \end{bmatrix} \end{aligned} \quad (2.97)$$

or

$$Z = \text{diag}(R) + LJ \quad (2.98)$$

with

$$J = \omega \begin{bmatrix} 0 & 1 \\ -1 & 0 \end{bmatrix} \quad (2.99)$$

Figure 2.9(a) shows the voltage and current waveforms, along with the instantaneous power waveform, $\mathcal{P}(t)$ in Figure 2.9(b). Figure 2.9(c) shows the two decomposed components of current, one component proportional to $e(t)$, thereby contributing to time average power, and the remaining component orthogonal to $e(t)$, contributing to Q . Figure 2.9(d) shows the two components of power, $P[1 + \cos(2\omega t)]$ and $Q \sin(2\omega t)$. Q , then, is the amplitude of the quadrature component of the power oscillation at twice the original frequency.

Note that the real-valued and complex-valued algebras are equivalent methods and could be used interchangeably.

Example 2.6.3.2 Example of a two-frequency waveform: Consider a simple voltage source whose time domain form is $e(t) = \sqrt{2} \cos(2\pi t) + 0.2\sqrt{2} \cos(6\pi t)$, connected to the same linear RL circuit used to illustrate basic relations in the AC case shown.

The complex-valued representation in this case amounts to defining a complex-valued vector phasor representing voltage source as $\underline{\underline{E}} = [1e^{j0} \ 0.2e^{j0}]$, and

$$\hat{Z} = \begin{bmatrix} R + j\omega L & 0 \\ 0 & R + 3j\omega L \end{bmatrix} \quad (2.100)$$

The complex-valued current phasor is simply computed using Eq. (2.93).

Analogously, in a four-dimensional real-valued vector space the same waveforms are represented as

$$\underline{\Phi}(t) = [\cos(2\pi t) \ \sin(2\pi t) \ \cos(6\pi t) \ \sin(6\pi t)]^T \quad (2.101)$$

where

$$\begin{aligned} \underline{\underline{E}} &= [1 \ 0 \ 0.2 \ 0]^T, & \underline{\underline{I}} &= Z^{-1}\underline{\underline{E}} \\ Z &= \begin{bmatrix} R & 2\pi L & 0 & 0 \\ -2\pi L & R & 0 & 0 \\ 0 & 0 & R & 6\pi L \\ 0 & 0 & -6\pi L & R \end{bmatrix} \end{aligned} \quad (2.102)$$

or

$$Z = \text{diag}(R) + LJ \quad (2.103)$$

with

$$J = \omega \begin{bmatrix} 0 & 1 & 0 & 0 \\ -1 & 0 & 0 & 0 \\ 0 & 0 & 0 & 3 \\ 0 & 0 & -3 & 0 \end{bmatrix} \quad (2.104)$$

Figures 2.10(a) and 2.10(b) show the resulting voltage, current, and power waveforms. The current is decomposed in Figure 2.10(c), and the resulting decomposition of power is shown in Figure 2.10(d).

2.6.4 Phasor Interpretation of Power

In Section 2.1 the concepts of real and reactive power (P and Q) were introduced as physical concepts in the time domain for single-harmonic AC signals. Then in Section 2.5 it was shown how the chance relationship $\hat{S} = \hat{E}\hat{I}^* = P + jQ$ produces their value when phasors are used. This form also gives some special emphasis to the fact that P and Q are describing different phenomena, P is an average flow, that is, power, and Q is a sustained oscillation of energy across a cross section (or cut set) in a network.

For the multiharmonic signals the concepts of real and reactive power were generalized by time-domain analysis in Section 2.6.1. As it developed, real power for such signals is still the average power flow across the cross section $A - A'$, which is a single number. Reactive power, however, is not a single number. It is shown in Eq. (2.64) to be a matrix of individual and not directly coupled oscillations of energy across the cross section $A - A'$ at a multitude of frequencies (sums and differences for all the pairs of harmonic frequencies). So reactive power does not automatically reduce to a single number.

After introducing multiharmonic phasors in Section 2.6.3 it can now be shown by direct, if tedious, algebraic maniulations that the $\hat{S} = P + jQ$ relationship generalizes to the periodic signal case where in the time domain or phasor definition

$$P = \frac{1}{T} \int_0^T e(t)i(t) dt = \operatorname{Re}(\underline{\hat{E}} \cdot \underline{\hat{I}}^*) = \operatorname{Re} \left(\sum_{k=1}^{k=n} \hat{E}_k \hat{I}_k^* \right) \quad (2.105)$$

becomes

$$\begin{aligned} P &= \operatorname{Re} \left(\frac{1}{T} \int_0^T (\underline{\hat{E}}^T \underline{\hat{\Phi}}^*) (\underline{\hat{I}}^T \underline{\hat{\Phi}}^*) dt \right) = \operatorname{Re} \left(\underline{\hat{E}}^T \frac{1}{T} \int_0^T \underline{\hat{\Phi}} \underline{\hat{\Phi}}^* dt \right) \underline{\hat{I}}^* \\ &= \operatorname{Re}(\underline{\hat{E}}^T \underline{\hat{I}}^*) = \operatorname{Re}[\hat{S}] \end{aligned} \quad (2.106)$$

It is concluded from Eq. (2.105) that the average (real) power of the instantaneous power associated with periodic signals equals the sum of average power associated with all individual harmonics.

Furthermore, by defining the phasor form of $[Q]$ as a cross (vector) product of \hat{E} and \hat{I}

$$[\hat{Q}] = [Q] = \operatorname{Im}[\hat{E} \times \hat{I}^*] \quad (2.107)$$

where the matrix $[Q]$ turns out to be equivalent to the reactive-power matrix in Eq. (2.64) derived from the time-domain definitions with physical interpretations as a matrix of energy oscillations across the cross section $A - A'$ at frequencies determined by the pairs of the harmonics present. Remember that S is an arbitrarily defined nonphysical quantity (sometimes called apparent power) and such manipulative proofs are all what is needed.

Thus for periodic functions the total real power P and the reactive power Q turn out to be, respectively, the real part of a scalar or dot product and a cross product of \hat{E} and \hat{I} , the latter being a matter of numerous energy oscillations determined by all pairs of harmonics and in phasor language it is the imaginary part of the vector product of \hat{E} and \hat{I} .

In order to obtain a single-number representation of the reactive power Q and avoid the complication of a matrix of oscillations at a multitude of frequencies, a single value for reactive power Q can be defined as a matrix norm of the reactive power matrix

$$Q = \sqrt{[\hat{Q}]^2} \quad (2.108)$$

For the preceding equations then it follows that

$$\hat{S} = P + jQ \quad (2.109)$$

including the formula

$$S^2 = P^2 + Q^2 \quad (2.110)$$

for their matrix norms, or

$$Q = \pm \sqrt{S^2 - P^2} \quad (2.111)$$

This definition was introduced by Fryze in Ref. [10]. Here it is introduced through the physical and mathematical connections of the time domain and the complex plane domain in phasor calculus as a physically meaningful quantity. The complex form of Eq. (2.109) recognizes the fact that using real-valued vector representations of voltage and current reactive power Q takes on the form

$$Q = [\underline{E}^T (\underline{E} \underline{I}^T - \underline{I} \underline{E}^T) \underline{I}]^{1/2} \quad (2.112)$$

The vector equation (2.112) can be written in terms of the elements of \underline{E} and \underline{I} ,

$$Q = \left(\sum_{j=1}^n \sum_{k=j+1}^n (E_j I_k - E_k I_j)^2 \right)^{1/2} \quad (2.113)$$

where E_i and I_i are the i th elements of the vectors \underline{E} and \underline{I} . In the Fourier basis, Eq. (2.113) expresses Q in terms of the rms values of the orthogonal cosine and sine frequency components of $e(t)$ and $i(t)$. Equations (2.112) and (2.113), however, are general and hold for any orthonormal decomposition. This is shown in Figures 2.12 and 2.13 respectively.

While it is not immediately obvious, Eq. (2.113) suggests that Q is the norm of a *vector product* of the real-valued voltage and current vectors \underline{E} and \underline{I} defined in Eqs. (2.76) and (2.77) [10,11]. This vector product, or cross product, of the two real-valued vectors is formed by cross-multiplying voltage components E_k

with current components I_j for each unique permutation of $j \neq k$. Each componentwise cross product is projected in an orthogonal direction \vec{l} according to an arbitrary rule, such as the right-hand rule commonly used for three dimensions:^{*}

$$\vec{l} = (\vec{j} \times \vec{k}) = -(\vec{k} \times \vec{j}) \quad (2.114)$$

A vector wise representation of the reactive power as a vector product is shown in Figure 2.12 for the single-frequency signals, and in Figure 2.13 for signals with harmonics.

The form of this cross product is called a two-form and is the exterior product of two one-forms, as discussed in detail in Ref. [13]. For our purposes, however, the cross product has m orthogonal elements given by $(E_j I_k - E_k I_j) \vec{l}$ equal to the projected area of the parallelogram (E, I) on coordinate axes \vec{j} and \vec{k} .

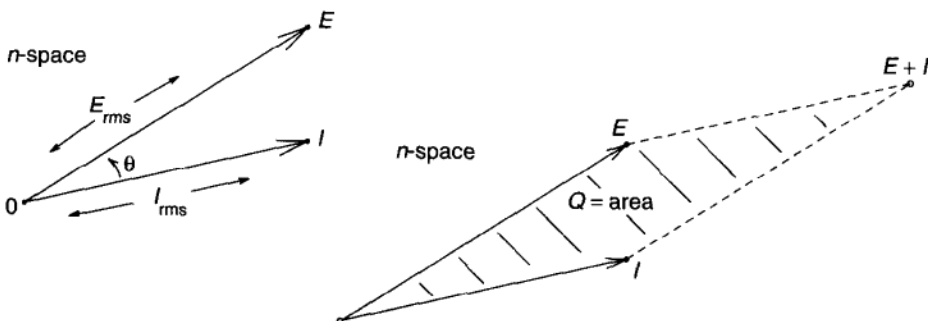


FIGURE 2.12 Vector-wise representation of reactive power in signals with harmonics.

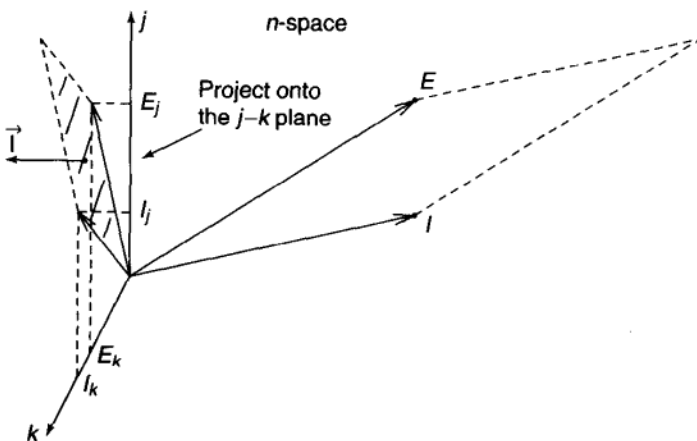


FIGURE 2.13 Frequency-domain interpretation of power components.

* The arrowed vector notation is to differentiate rectangular vector representation from the polar coordinate representation above.

$m = n(n - 1)/2$, corresponding to the unique permutations of $j \neq k$. These elements appear in the upper triangle of an antisymmetric matrix, \mathbf{R} , which will be referred to as the *reactive-power matrix*:

$$\mathbf{R} = (\underline{E}\underline{I}^T - \underline{I}\underline{E}^T) \quad (2.115)$$

As \mathbf{R} is antisymmetric, there are zeros on the main diagonal, and the negative of the upper triangle appears in the lower triangle.

Q in Eq. (2.113) is the root mean square of the m orthogonal elements of the cross product, and can be written as a norm. In matrix form, Q is the Frobenius norm of \mathbf{R} divided by $\sqrt{2}$. Alternately, for mathematical convenience, the m elements of cross product can be assembled into an m -vector, R , called the *reactive-power vector*, and Q is the two-norm of R .

Regardless of the notation, the cross product maps the n -vectors \underline{E} and \underline{I} to an m dimensional space, and Q is a norm of m orthogonal components in this space. Each component represents the interaction of two orthogonal frequency components of voltage and current. Each pair of orthogonal frequency components does not contribute to average power, but does contribute, orthogonally, to Q . While each component of Q is signed, according to the rule (2.114), Q cannot have a single-sign convention, because it is the norm of m orthogonal signed components.

For the special case of AC signals, voltage and current waveforms can be expressed as two-dimensional vectors or phasors. In this case, $n = 2$, so $m = 1$, and the cross product has a single component. This component is signed and corresponds to the classical definition of reactive power for sinusoidal signals. The single-sign convention is only possible when $m = 1$ and is not possible when harmonics are present.

It directly follows based on definition (2.112) that in the case of $n = 9$ the number of terms in Q equals 36. This can be seen from

$$E^2 = E_1^2 + E_2^2 + \dots \quad (2.116)$$

$$I^2 = I_1^2 + I_2^2 + \dots \quad (2.117)$$

$$S^2 = (E_1^2 + E_2^2 + \dots)(I_1^2 + I_2^2 + \dots) \quad (81 \text{ terms}) \quad (2.118)$$

$$P^2 = (E_1 I_1 + E_2 I_2 + \dots)^2 \quad (45 \text{ terms}) \quad (2.119)$$

$$Q^2 = S^2 - P^2 = (E_1 I_2 - E_2 I_1)^2 + \dots \quad (m = 36 \text{ terms}) \quad (2.120)$$

2.6.5 Conservation of Reactive-Power Components

For a generalized definition of power ρ , conservation implies that the sum of this power over all elements in a network is zero:

$$\sum_k \rho^k = 0 \quad (2.121)$$

where ρ^k is the power at element k .

Conservation of energy implies that instantaneous power is conserved at each instant of time. As the time-average operator is linear, it commutes with the summation in Eq. (2.121), so average power is also conserved:

$$\sum_k P^k = \sum_k \overline{p^k(t)} = \overline{\sum_k p^k(t)} = 0 \quad (2.122)$$

Other power definitions may not, however, obey conservation. S and Q , for example, are non-negative and cannot sum to zero unless all are zero. Tellegen's theorem can be used to prove conservation for a set of power definitions called generalized powers. As shown in Refs. [14–16], a particular power is a generalized power and will obey conservation if it can be expressed in the following form:

$$\rho^k = \Lambda_e(e^k) \Lambda_i(i^k) \quad (2.123)$$

where e^k and i^k are the voltage and current, respectively, at the k th circuit element, and Λ_e and Λ_i are linear operators, or more generally, Kirchhoff voltage and current operators. As in Eq. (2.122), applying a linear operator β to Eq. (2.123) preserves conservation and leads to a more general form for generalized powers:

$$\rho^k = \beta[\Lambda_e(e^k) \Lambda_i(i^k)] \quad (2.124)$$

The definition for Q in Eq. (2.121) cannot be written in the form of Eq. (2.124), and Fryze's definition for Q does not obey conservation. Each of the elements of the cross product, however, do take the required form, because the elements of the vectors \underline{E} and \underline{I} can be expressed as linear transforms of the voltage and current waveforms:

$$\underline{E} = \frac{1}{T} \int_0^T e(t) \Phi(t) dt \quad (2.125)$$

Each element in the reactive power vector R is a componentwise cross product, $E_j I_k - E_k I_j$, which is a linear combination of products of transformed voltage and current, as in Eq. (2.124). Therefore, the components of the cross product are generalized powers and obey conservation. Equation (2.122) can then be written in vector form

$$\sum_k R^k = \underline{0} \quad (2.126)$$

where $\underline{0}$ is the zero m -vector. This classification is independent of the specific decomposition of voltage and current, and will hold for any orthonormal basis $\Phi(t)$.

It is shown in Ref. [4] how to derive a simple coordinate rotation that provides an alternative vector decomposition of Q such that R of the port has only one nonzero element q , which is positive, by definition. As the other elements are zero,

$Q = \sqrt{q^2} = q$, but while Q does not obey conservation, q is an element of R and is a generalized power. Conservation, then, implies that $Q = q = \sum_k q^k$, where q^k is the same element of R^k , the reactive-power vector of the k th circuit element. As with the classical definition of reactive power in sinusoidal systems, this single-signed component of reactive power provides a measure that obeys conservation and can be used to indicate where the port reactive-power flows in the circuit.

2.6.6 Circuit Example

Figure 2.14 shows a one-port circuit example consisting of a linear RLC circuit in parallel with a switched resistive load. The triac switch is self-commutating with a 90° firing angle, so it is on for the latter half of each half-cycle. The circuit port is connected to a voltage source with a 1-Hz fundamental frequency and a small component of the third and fifth harmonics. The port current contains additional odd harmonics introduced by the switching discontinuity.

For the analysis, the voltage and current waveforms are decomposed with a Fourier basis consisting of normalized cosine and sine pairs of only the odd harmonics. For this example, the basis is truncated to length $n = 20$.

$$\underline{\Phi}(t) = \begin{bmatrix} \cos(\omega t) \\ \sin(\omega t) \\ \cos(3\omega t) \\ \sin(3\omega t) \\ \vdots \\ \cos(20\omega t) \\ \sin(20\omega t) \end{bmatrix} \quad (2.127)$$

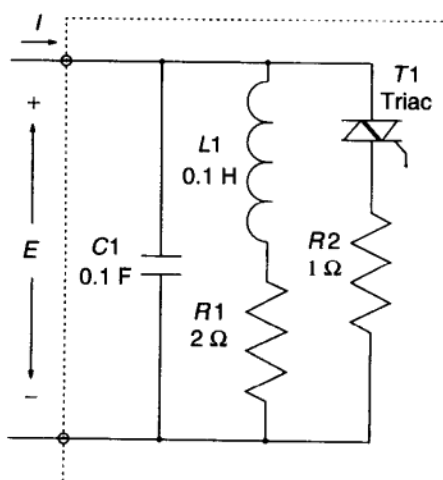


FIGURE 2.14 Example circuit.

For the linear circuit elements, the voltage and current relationships can be written as Ohm's law in vector form:

$$\underline{E} = Z \underline{I} \quad \text{or} \quad \underline{I} = Z^{-1} \underline{E} \quad (2.128)$$

where Z is an impedance matrix for the linear element. Z_R for resistive elements is the resistance R times the identity matrix. In the Fourier basis, Z_L and Z_C for inductive and capacitive elements are block-diagonal, antisymmetric matrices with zeros on the main diagonal, $Z_L = L J_\omega$ and $Z_C = (C J_\omega)^{-1}$, where L and C are the inductance and capacitance, and

$$J_\omega = \begin{bmatrix} 0 & \omega & 0 & 0 & 0 & 0 & \cdot \\ -\omega & 0 & 0 & 0 & 0 & 0 & \cdot \\ 0 & 0 & 0 & 3\omega & 0 & 0 & \cdot \\ 0 & 0 & -3\omega & 0 & 0 & 0 & \cdot \\ 0 & 0 & 0 & 0 & 0 & 5\omega & \cdot \\ 0 & 0 & 0 & 0 & -5\omega & 0 & \cdot \\ \cdot & \cdot & \cdot & \cdot & \cdot & \cdot & \cdot \end{bmatrix}$$

The impedance matrix for the linear RLC circuit is calculated as a parallel combination, $Z = [Z_{C1}^{-1} + (Z_{R1} + Z_{L1})^{-1}]^{-1}$, and the current vector is then calculated from Eq. (2.128).

To calculate the current in the switched resistive load, the vector for the $R2$ voltage is calculated using the Fourier transform, $E_{R2} = 1/T \int_0^T e_{R2}(t) \Phi(t) dt$. The current is then calculated from (2.128) using Z_{R2} .

Figure 2.15(a) shows the port voltage and current waveforms, while Figure 2.15(b) shows current waveforms of the RLC load and the switched resistive load. Table 2.1 shows the vectors representing the port voltage \underline{E} , the linear load current \underline{I}_{RLC} , the switched load current \underline{I}_{SW} , and the total current \underline{I} . The R vector is not shown, because it contains 190 elements. Table 2.2 lists P , S , Q , and q for each element in the circuit and for the port.

As shown in Table 2.2, the projection q is a signed measure of the contribution of each component to the total Q at the port.⁵ Whereas resistive elements do not contribute to reactive power, the triac does. Even though the switch is not an energy storage device, it generates reactive power, because the nonlinear switching characteristic generates current harmonics. For this example, the capacitor is contributing to the port reactive power, while the inductor is providing compensation.

2.6.7 Reactive Power in Linear RLC Circuits with Power Electronic Switches

Electric circuits consisting of linear R , L , and C devices and electronic switches represent an important first step towards analyzing circuits via vector algebra

⁵ For detailed treatment of q , see Ref. [4].

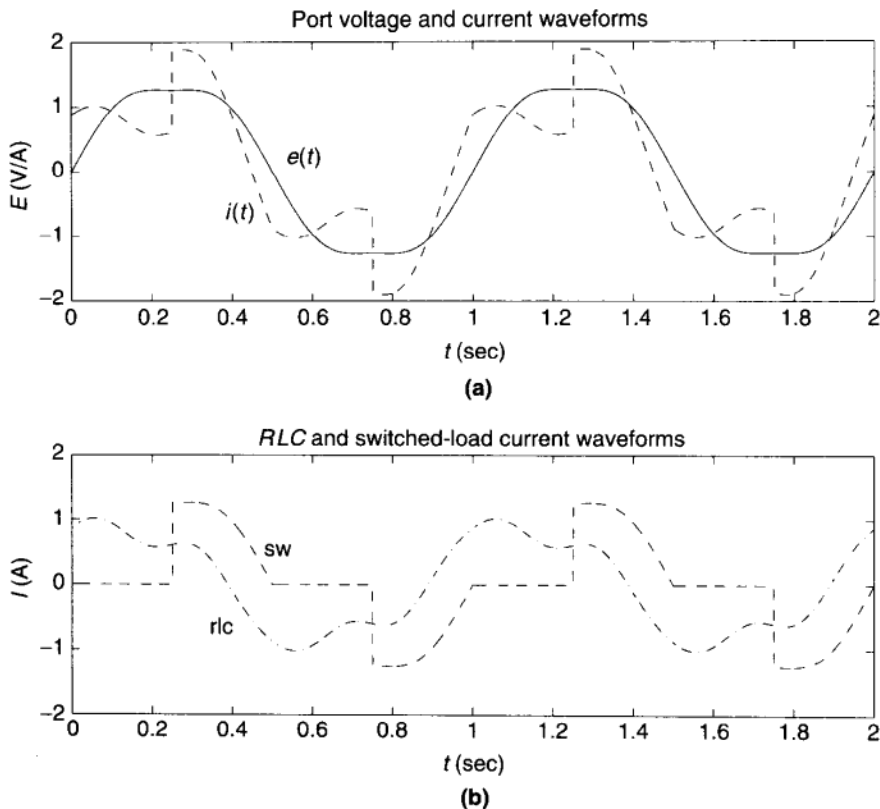


FIGURE 2.15 Example circuit waveforms.

introduced in Refs. [4,5]. Because of the linearity of their components they allow for introducing algebra fully defining the circuit behavior in steady state, which is analogous to the phasor algebra in the single-frequency case. One only needs to proceed with care when defining the equivalent of the circuit impedance when switches are present. A detailed approach of this type can be found in Ref. [5].

To illustrate this process, one should start with the possibly simplest relevant example of a linear *RLC* circuit with harmonics given in Figure 2.16. This is a circuit consisting of an independent AC voltage source, connected via a half-wave rectifier to a constant *RC* load. With current \underline{I} and voltage \underline{E}_L represented in vector space all power components are computed using vector-space-based algebra described before. For details of this computation the interested reader should see Ref. [5].

2.6.8 Optimum Performance of Devices Characterized by Periodic Signals

It follows in a straightforward way from the derivations in Section 2.5.3 that the optimality result holds true for any periodic signal, including signals with harmonics. If and only if voltage and current waveforms are mutually proportional with a real-valued constant of proportionality as stated in Eq. (2.54) will the

TABLE 2.1 Port Voltage, Current, and Rotation Vectors

<i>E</i>	<i>I_{RLC}</i>	<i>I_{SW}</i>	<i>I</i>
0.0000	0.4853	-0.3491	0.1363
1.0000	0.4551	0.4982	0.9533
0.0000	0.1635	0.3109	0.4744
0.1000	0.0265	0.0518	0.0783
0.0000	-0.0292	-0.0736	-0.1028
-0.0100	-0.0014	-0.0068	-0.0082
0.0000	0.0000	0.0965	0.0965
0.0000	0.0000	0.0018	0.0018
0.0000	0.0000	-0.0526	-0.0526
0.0000	0.0000	-0.0018	-0.0018
0.0000	0.0000	0.0580	0.0580
0.0000	0.0000	0.0018	0.0018
0.0000	0.0000	-0.0387	-0.0387
0.0000	0.0000	-0.0018	-0.0018
0.0000	0.0000	0.0413	0.0413
0.0000	0.0000	0.0018	0.0018
0.0000	0.0000	-0.0305	-0.0305
0.0000	0.0000	-0.0018	-0.0018
0.0000	0.0000	0.0320	0.0320
0.0000	0.0000	0.0018	0.0018

TABLE 2.2 Voltage and Current Projections and Reactive Power

	<i>P</i>	<i>S</i>	<i>Q</i>	<i>q</i>
<i>C1</i>	0.000	0.6600	0.6600	0.3416
<i>L1</i>	0.0000	0.1471	0.1471	-0.0598
<i>R1</i>	0.4577	0.4577	0.0000	0.0000
<i>T1</i>	0.0080	0.4971	0.4970	0.2454
<i>R2</i>	0.4955	0.4955	0.0000	0.0000
Total	0.9612	2.2575	1.3042	0.5272
Port	0.9612	1.0963	0.5272	0.5272

device whose current and voltage have harmonics operate optimally in the previously defined sense. This requires minimization of reactive power as defined in Ref. [10], instead of expressions like Budeanu's [17]. The use of this definition as a common measure of device performance as opposed to the measure presently used for single-frequency sinusoidal signals is justifiable, as shown in Section 2.6.4.

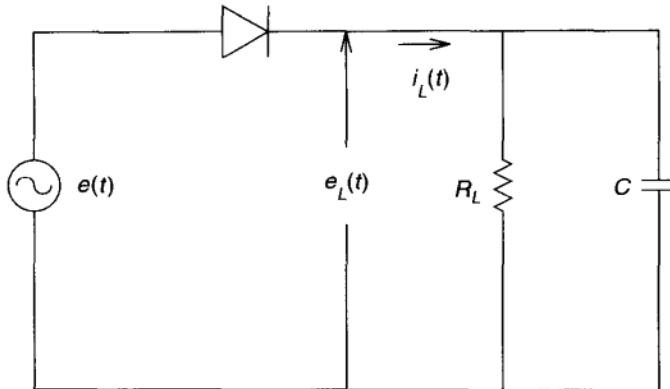


FIGURE 2.16 Half-wave rectifier.

2.6.9 Optimization Example Using Vector-Space Algebra

The next example shows how a projection of the reactive-power vector can be used to optimize a compensation circuit for the maximum power factor. Using the previous circuit example of Figure 2.14 as a load, the problem is to find the value of an inductor L_C , that when placed in parallel with the load, maximizes the power factor seen by the voltage source. This example is a constrained optimization in that compensation with a single inductor can improve the power factor but cannot achieve unity power factor.

The power factor is defined as the magnitude of average power divided by the apparent power:

$$\text{PF} = \frac{P}{S} = \frac{P}{\sqrt{P^2 + Q^2}} \quad (2.129)$$

Because the compensator is lossless and the voltage source is constant, P is not affected by compensation and remains constant. Maximizing the power factor, then, corresponds to minimizing Q at the port.

Q is not a generalized power and does not obey conservation, so the port Q is not simply the sum of load reactive power Q_L and compensator reactive power Q_C . The reactive-power vector, however, is a generalized power, so the port R vector is the sum of R_L and R_C , and the port Q is the norm of this vector sum:

$$Q = \|R_L + R_C\| \quad (2.130)$$

R_L and R_C are, in general, neither collinear nor orthogonal, but Eq. (2.130) can be simplified by decomposing the R vectors into collinear and orthogonal parts. For this example, R_C is decomposed into R_{C1} and R_{C2} , which are collinear with and orthogonal to R_L , respectively. This decomposition yields a quadrature decomposition of the compensator reactive power:

$$Q_C^2 = Q_{C1}^2 + Q_{C2}^2 = \|R_{C1}\|^2 + \|R_{C2}\|^2 \quad (2.131)$$

For the total Q seen by the source, Q_{C1} adds linearly with Q_L , and the sum adds in quadrature with Q_{C2} :

$$Q^2 = (Q_L + Q_{C1})^2 + Q_{C2}^2 \quad (2.132)$$

Equation (2.132) can be simplified by expanding the square and substituting from Eq. (2.131):

$$Q^2 = Q_L^2 + 2Q_L Q_{C1} + Q_{C1}^2 + Q_{C2}^2 = Q_L^2 + 2Q_L Q_{C1} + Q_C^2 \quad (2.133)$$

where Q_L is the constant-load reactive power, Q_{C1} is the projection of R_C in the direction of R_L , and Q_C is the total compensator reactive power. The projection, Q_{C1} , can be expressed in terms of the load reactive power matrix, \mathbf{R}_L as in Eq. (2.115).

$$Q_{C1} = E^T (\mathbf{R}_L / Q_L) I_C \quad (2.134)$$

As the compensator is lossless, $P_C = 0$, and $Q_C^2 = S_C^2$.

$$Q_C^2 = E^T E I_C^T I_C \quad (2.135)$$

Using Ohm's law, [Eq. (2.128)] I_C can be expressed in terms of the impedance matrix for the compensator inductance. This impedance matrix is proportional to L_C , the inductance:

$$I_C = Z_{LC}^{-1} E = \frac{1}{L_C} J_\omega^{-1} E \quad (2.136)$$

Now substituting Eqs. (2.134) to (2.136) into Eq. (2.133) yields a scalar quadratic equation in $1/L_C$:

$$Q^2 = Q_L^2 + 2E^T \mathbf{R}_L J_\omega^{-1} V \frac{1}{L_C} + E^T E E^T (J_\omega^{-1})^T J_\omega^{-1} V \frac{1}{L_C^2} \quad (2.137)$$

Inserting the values for the example circuit gives

$$Q^2 = 0.0256 \frac{1}{L_C^2} - 0.0490 \frac{1}{L_C} + 0.2779 \quad (2.138)$$

This equation has a single minimum, at $L_C = 1.05$ H, where $Q = 0.505$.

The compensated power factor is 0.885, improved from 0.877 by L_C . Due to the extreme harmonic content of the waveforms, the power factor cannot be improved beyond 0.885 without a more complicated compensator designed to better match harmonics in current to those of in voltage. The third and fifth harmonics, which exist in the voltage, could be adjusted by a linear network of tuned circuits, but nulling the higher harmonics in current would require a nonlinear or active compensator. In any case, Eqs. (2.133) to (2.135) would

still apply, but Z_{LC} in Eq. (2.136) would be a complicated function of control parameters. As Eq. (2.137) would no longer be quadratic, finding the global minima in closed form would be difficult. Still, for a small number of control parameters, the global minimum could be found numerically from Eqs. (2.133) to (2.135).

2.6.10 Example of Optimal Performance for Signals with Harmonics

This example⁶ can be viewed as very typical for developing high-voltage AC–DC conversion and FACTS technologies, since it illustrates creation of harmonic signals by switching, and possible compensation strategies for optimal performance in spite of presence of harmonics. The compensation described here is nonlinear in contrast to the commonly used linear compensation. As such, it is more powerful than a linear compensation. To show this, consider an independent, single-frequency sinusoidal source $e_s(t)$, with internal impedance $\hat{Z} = R + j\omega L$, connected via a balanced rectifier bridge to a DC load R . This configuration is given schematically in Figure 2.17.

The circuit dynamics are described by a differential equation of the form

$$|i(t)| = C \frac{de(t)}{dt} + \frac{e(t)}{R} \quad (2.139)$$

Let us assume that the current and voltage waveforms are represented as

$$i(t) = \sum_n \operatorname{Re}(\hat{I}_n e^{jn\omega t}) \quad (2.140)$$

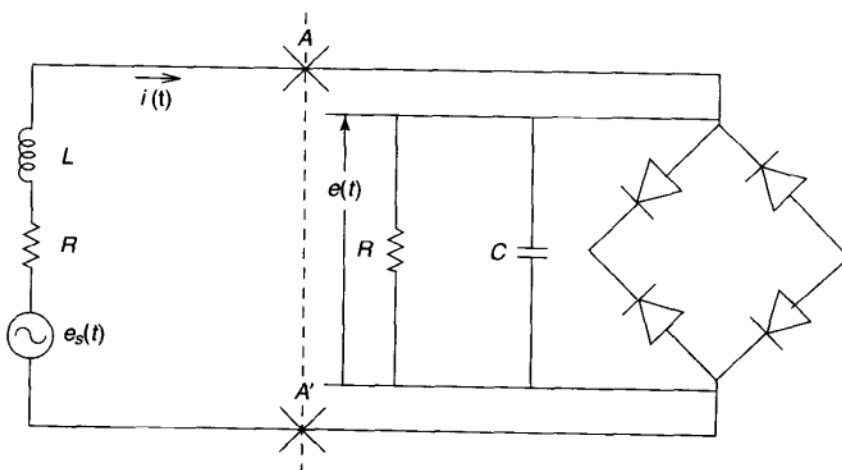


FIGURE 2.17 Rectifier-based AC-to-DC power converter.

⁶ Unpublished work with Prof. Branislava Perunicic, University of Sarajevo, 1987.

and

$$e(t) = \sum_m \operatorname{Re}(\hat{E}_m e^{j\omega t}) \quad (2.141)$$

where

$$\hat{E}_m = \frac{R\hat{I}_m}{1 + jRCm\omega} \quad (2.142)$$

The complex-valued power into the load is

$$\hat{S}^* = \sum_m \hat{I}_m \hat{E}_m^* = \sum_m \frac{RI_m^2}{1 + \omega^2 m^2 R^2 C^2} \quad (2.143)$$

with the rms values for voltage and current as

$$I^2 = \sum_m I_m^2 \quad (2.144)$$

and

$$E^2 = \sum_m \frac{R^2 I_m^2}{1 + \omega^2 m^2 R^2 C^2} \quad (2.145)$$

One possible compensation scheme that allows for most efficient real-power delivery to the load R is indicated in Figure 2.18. It is designed so that it provides for the voltage-current relationship $e^{\text{optimal}}(t) - i^{\text{optimal}}(t)$ of the compensated rectifier to meet the optimal operating condition defined above in Eq. (2.54), that is,

$$e^{\text{optimal}}(t) = \lambda i^{\text{optimal}}(t) \quad (2.146)$$

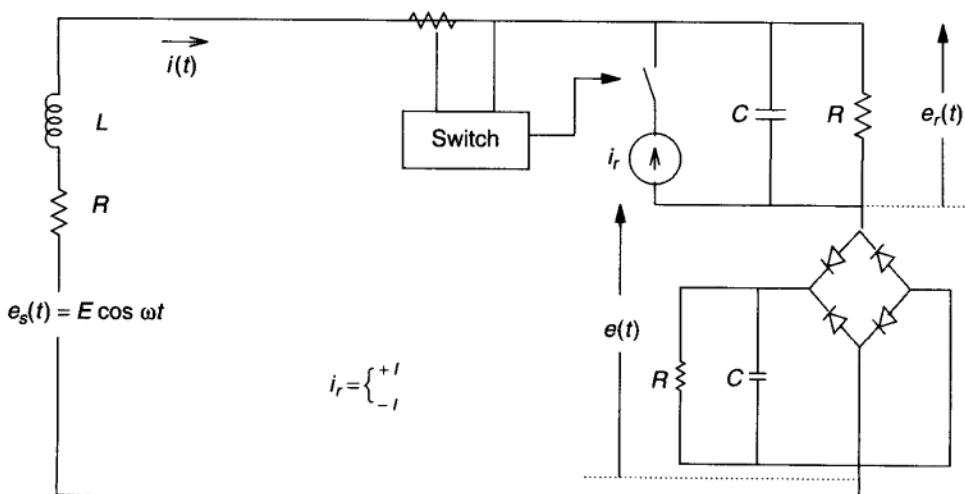


FIGURE 2.18 Compensation for optimal performance of an AC-DC converter.

The compensator given in Figure 2.18 operates according to the control law:
When

$$e_r(t) + e(t) - \lambda i(t) \geq 0 \quad (2.147)$$

then

$$i_r(t) = +I \quad (2.148)$$

and, similarly, when

$$e_r(t) + e(t) - \lambda i(t) \leq 0 \quad (2.149)$$

then

$$i_r(t) = -I \quad (2.150)$$

This control law falls under the general category of sliding mode controllers Ref. [18] with the sliding surface defined as

$$s(e(t), i(t)) = e_r(t) + e(t) - \lambda i(t) = 0 \quad (2.151)$$

It is interesting to note that, depending on switching frequency chosen to meet Eq. (2.151), only very-high-frequency content harmonics will be generated. The lower-frequency content from the compensated voltage and current waveforms will be eliminated automatically, as the compensation is done with the goal of optimizing real-power delivery to the load. In the limit of infinite switching frequency, harmonics will be eliminated in the same time as power delivery optimization is done.

2.6.11 Summary of the Characteristics of Real- and Reactive-Power Flow

When interpreting the real, reactive, and complex power of periodic signals some care must be taken in dealing with reactive power, in particular. Reactive power is *not* generalized as easily as the real power, since it is not simply sum of reactive power of individual harmonics. Moreover, Q is not a generalized power, and $Q \neq \sum_k Q_k$, where Q_k is the reactive power of the individual components k to the right of the cross section $A-A'$ of interest. It is not obvious how Q_k at each element contributes to the total Q into the crossection.

2.6.11.1 Real or Active Power P The average power into the port, P , and into the k th element P_k can be expressed using vector-space inner product

$$P = E^T I, \quad P^k = (E_k)^T I_k \quad (2.152)$$

Using vector-phasor algebra, the average power is the real part of the inner product of the vector-phasor voltage and current, that is, of the complex-valued power.

Time average power is a generalized power and obeys conservation, so $P = \sum_k P_k$. Thus there is an intuitive mechanism for showing where power flowing into the circuit is being dissipated. Now, as it may be observed in Figure 2.10, the value of the power component in phase with the voltage waveform $e(t)$ is always positive and is fluctuating around a time average over each cycle as defined in Eq. (2.152).

This average power is contributed to by individual harmonics themselves and not by the interactions among harmonics of different frequency. This result is obvious from the expression for the instantaneous power $\mathcal{P}(t)$ [Eq. (2.58)]. The same result is obtained using vector phasors for representing voltage, current, and power into an arbitrary cross section $A-A'$.

Real power for periodic signals basically shows the same inherent features as the average power of AC signals.

2.6.11.2 Imaginary or Reactive Power Q Reactive power into a cross section $A-A'$ characterized by the voltage and current vector phasors $\hat{\underline{E}}$ and $\hat{\underline{I}}$, respectively is *not* the imaginary part of the inner product of these two variables. It is, instead, the norm of a *vector (cross) product* of the corresponding real-valued voltage and current vectors \underline{E} and \underline{I} . Regardless of the notation used, the cross product maps the n -vectors to an m -dimensional [$m \equiv \frac{1}{2}n(n - 1)$] space. Each component represents the interaction of two orthogonal frequency components of voltage and current. Each pair of orthogonal frequency components does not contribute to average power but does contribute, orthogonally, to Q . While each component contributing to Q is signed, Q cannot have a single-sign convention, because it is the norm of m orthogonal signed components. It has been described based on the work in Ref. [4] that the $m = \frac{1}{2}n(n - 1)$ orthogonal components are conserved, where \underline{R} is an m -vector of these components and the magnitude of the reactive power is the norm of \underline{R} and does not obey conservation. Projections of \underline{R} , however, obey conservation and can provide useful measures when analyzing or compensating a circuit. One such measure is q , the projection of \underline{R} in the direction of \underline{R} , which is positive and equal to Q . While this definition seems trivial, the first example shows how such a projection can be used to analyze the flow of reactive power in a circuit. The second example shows how a similar projection is used to solve a constrained power-factor optimization problem.

The vector-space expressions for voltage and current provide a convenient notation for solving minimization problems, but the dimensionality does not arise purely from the notation. The underlying dimensionality arises from the terms in the expression $Q^2 = S^2 - P^2$. S^2 is the product of two n -term equations and has n^2 terms. P^2 is the square of one n -term equation and has $\frac{1}{2}n(n + 1)$ terms. The difference has $n^2 + \frac{1}{2}n(n + 1)$ terms, but $2n$ cancel, leaving $\frac{3}{2}n(n - 1)$ terms. These remaining terms are grouped in triples to form $m = \frac{1}{2}n(n - 1)$ perfect squares, corresponding to the m orthogonal components of Q .

The components of Q , then, do not correspond to the $2n$ orthogonal frequency components of instantaneous power, but instead arise from the definition of S . Q , then, is not a quantity bearing physical interpretation in terms of instantaneous

power, but is simply the m remaining orthogonal components of S not contained in P . Similarly, the usefulness of Q is not as a reflection of actual circulating powers, but as a measure of the overall useless component of S .

2.6.12 Comparison with Other Reactive-Power Definitions

The expression of Q as the norm of a cross product leads to a decomposition of Q into m orthogonal elements. As with the vector decomposition of the voltage and current, the reactive-power vector depends on the choice of basis functions, but the dimensionality m is fundamental to the cross product. Many other reactive power decompositions have been suggested, but the definitions suffer because they attempt to represent the m orthogonal conserved power components with fewer than m quantities.

Some definitions consist of linear combinations of the elements of R , which, like q , are projections of R and obey conservation. Each projection accounts for only one of the m dimensions in R ; the other $m - 1$ components must be accounted for if the total decomposition is to reflect the total inactive power. Other definitions combine orthogonal projections of R in quadrature, thus representing the magnitude contribution from several of the m components. The sign convention, however, is lost when components are combined in quadrature, and the resulting definition is not conserved.

The original Budeanu definition of reactive power is given in Ref. [17]

$$Q_B = \sum_i E_i I_i \sin(\theta_i) \quad (2.153)$$

where E_i , I_i , and θ_i are the rms voltage and current and the phase-angle difference of the i th harmonic. In the Fourier basis, each harmonic is represented with a cosine–sine pair, and each term in Eq. (2.153) represents the interaction of the cosine and sine components at a particular frequency. These terms appear as every other entry in the first upper diagonal in the reactive-power matrix \mathbf{R} . Equation (2.153) adds these terms linearly and ignores all other components, so Budeanu's definition is a projection of R in a fixed direction, and this projection has a sign and obeys conservation. The direction of the projection, however, is arbitrary and does not reflect any particular useful quantity, such as a power factor or $\sqrt{S^2 - P^2}$.

In order to account for the other components of R , Budeanu introduced distortion power,

$$D_B = \sqrt{S^2 - P^2 - Q_B^2} \quad (2.154)$$

D_B , then, is the norm of $m - 1$ orthogonal projections of R , which are also orthogonal to the Q_B projection. As D_B adds components in quadrature, the definition does not obey conservation. Because the direction of the Q_B projection is arbitrary, the D_B component has no generally useful interpretation.

Perhaps Budeanu intended that Q_B reflect the individual interactions of the $n/2$ frequencies and that D_B represent the cross terms between different frequencies. If so, Q_B should have been defined as the projection of R in the direction pointed by the $n/2$ components in the first upper diagonal of \mathbf{R} , and D_B should have been the projection of R in the direction pointed by the all the other elements in \mathbf{R} . The other $m - 2$ orthogonal projections would then have been zero, so the definition would have properly decomposed the total inactive power with two conserved quantities.

The Fryze reactive power, shown in Eq. (2.112), represents the total inactive power in a single signed-quantity. The magnitude is the norm of all the elements of R , which is useful because minimizing Q minimizes S , maximizing the power factor. The sign definition, however, is misleading in that the definition is a norm and is not conserved. Presumably, the sign was added to reflect the sign of the fundamental reactive-power component, which would be dominant in the nearly sinusoidal case. If the intention was to obtain a single conserved quantity to represent $\sqrt{S^2 - P^2}$, the definition should have been the projection of R in the direction of R , which is positive and equal to $\sqrt{S^2 - P^2}$. This is, in fact, the definition of q given in Ref. [4].

Page [19] defined capacitive reactive power and inductive reactive power, Q_C and Q_L , the two components of Q that could be compensated by a parallel capacitor and inductor. These powers are, in fact, projections of the R vector in the directions of R_C and R_L , the reactive-power vectors of a pure capacitance and pure inductance. Page correctly noted that these quantities can have a sign and are conserved, so a negative Q_C can be compensated by adding a capacitor in parallel. Page also noticed that the Q_C and Q_L are not generally orthogonal or parallel, and introduced a refinement to account for the cross terms.

Page's projections failed to account for the other $m - 2$ orthogonal components of R that must be considered if the compensation is to minimize the total Q . His projections help to solve for the best parallel L and C values, but do not adapt to other compensation topologies, such as series L and C values, or a linear network of L 's and C 's. A single-element parallel compensator does not necessarily provide substantial power factor improvement.

Wyatt [20] discusses the merits of an instantaneous expression of reactive power.

$$p_{\text{react},2}(t) = e(t) \frac{d}{dt} i(t) - i(t) \frac{d}{dt} e(t) \quad (2.155)$$

The time average of this quantity can also be interpreted as a measure of reactive power and can be expressed in vector notation. In the Fourier basis, $(d/dt)\Phi(t) = J_\omega^T \Phi(t)$, where J_ω is the block diagonal, antisymmetric matrix given in Section 2.6.6. As in Eq. (2.86), the time average of Eq. (2.155) simplifies by taking the constants outside the integral:

$$\frac{1}{T} \int_0^T p_{\text{react},2}(t) dt = E^T J_\omega I - E^T J_\omega^T I = 2E^T J_\omega I \quad (2.156)$$

Whereas Eq. (2.156) is not normalized, it is proportional to a projection of R . Like Budeanu's Q_B , the projection contains only interactions between the sine and cosine components of individual harmonics, but unlike Q_B , each component is scaled by its frequency.

In linear sinusoidal systems, reactive power can also be interpreted in terms of average electric and magnetic energy:

$$Q = 2\omega[\overline{w_m(t)} - \overline{w_e(t)}] \quad (2.157)$$

Because $w_m(t)$ and $w_e(t)$ both oscillate as $\cos(2\omega t)$ but are 180° out of phase, Eq. (2.157) can also be written in terms of the total reactive energy, $w(t) = w_m(t) + w_e(t)$ as

$$Q = \text{rms} \left(\frac{d}{dt}[w(t)] \right) \quad (2.158)$$

This expression has the advantageous interpretation that Q , in the sinusoidal case, is an rms measure of the oscillatory transfer of nonrecoverable energy. This fact, however, is a result of the 180° phase difference between $w_m(t)$ and $w_e(t)$, and no such relationship holds when harmonics are present or when nonlinear circuits are considered.

2.7 VECTOR REPRESENTATION FOR MULTIPHASE CIRCUITS

Multiphase periodic waveforms can also be represented as vectors given appropriate set of basis functions. By combining the vectors representing voltage and current in each phase into collective vectors, the entire set of waveforms can be represented as two constant vectors, \underline{E} and \underline{I} . While the results are general, this analysis will focus on the three-phase case.⁷

The set of phase voltage waveforms is assembled as a row vector, and expressed in terms of E and the basis functions

$$\begin{aligned} [e_1(t) & e_2(t) & e_3(t)] = \underline{E}^T \underline{\Phi}(t) \\ [i_1(t) & i_2(t) & i_3(t)] = \underline{I}^T \underline{\Phi}(t) \end{aligned} \quad (2.159)$$

Here E is length $3n$, and $\underline{\Phi}(t)$ is a $3n \times 3$ matrix of basis functions.

$$\underline{\Phi}(t) = \begin{bmatrix} \underline{\Phi}(t) & \underline{0} & \underline{0} \\ \underline{0} & \underline{\Phi}(t) & \underline{0} \\ \underline{0} & \underline{0} & \underline{\Phi}(t) \end{bmatrix} \quad (2.160)$$

⁷ Only real-valued vector representation of periodic signals is illustrated here; an equivalent complex-valued vector-phasor notation can be used, as described earlier in this chapter.

where $\underline{0}$ is an n -vector of zeros. Although $\underline{\Phi}$ is a rectangular matrix, the basis is still orthonormal:

$$\frac{1}{T} \int_0^T \underline{\Phi}(t) \underline{\Phi}^T(t) dt = \underline{I} \quad (2.161)$$

The total instantaneous power is the sum of instantaneous power in each phase:

$$\begin{aligned} p(t) &= [e_1(t) \quad e_2(t) \quad e_3(t)] \begin{bmatrix} i_1(t) \\ i_2(t) \\ i_3(t) \end{bmatrix}^T \\ &= \underline{E}^T \underline{\Phi}(t) \underline{\Phi}^T(t) \underline{I} \end{aligned} \quad (2.162)$$

Because $\underline{\Phi}$ is orthonormal, the time-average total power simplifies to a single scalar product, as in the single-phase case:

$$P = \frac{1}{T} \int_0^T \underline{E}^T \underline{\Phi}(t) \underline{\Phi}^T(t) \underline{I} dt = \underline{E}^T \underline{I} \quad (2.163)$$

Similarly, the multiphase rms value is again the two-norm, and the definition for total apparent power, $S = EI$, is the same as that in the single-phase case. $Q = \sqrt{S^2 - P^2}$ has the same form as Eq. (2.113) and can be interpreted as the norm of a cross-product vector R . Therefore, it is possible to construct a reactive-power measure q , that is a projection of R specific to the set of phase voltage and current waveforms at the port. This measure is signed, obeys conservation, and indicates how circuit elements contribute or compensate for the reactive power at the port. Extensive treatment of relations between the vector-space-based analysis described here and the traditional symmetrical components can be found in Ref. [5]. For the case of multiphase circuits with harmonics, see Refs. [4,21].

2.8 CHAPTER SUMMARY

In this chapter a brief reminder is given of the quasistationarity assumption under which most of the phenomena described in this book can be modeled and analyzed with near precision. Particularly, the fundamentals of real and reactive power under the quasistationarity assumption are reviewed. Reactive power is strongly coupled with voltage magnitude changes while real-power changes are strongly coupled to the voltage-angle changes. However, the cross-couplings are not automatically negligible. Generalization of phasors is presented next for periodic signals, which are represented as a series of basic frequency harmonics. This situation is important for representing reactive power changes when power electronic devices are present in the power system.

One encounters comments in the field to the effect that because three 120° displaced phases always add up to zero the three-phase reactive power is just

zero. If so, why are we putting reactive sources like capacitors, Static Var Compensators (SVCs), etc., on the system? The erroneous idea comes from not understanding that the active power and reactive power are entirely different in nature. Indeed, active power flows through cut sets or cross sections of lines. However, as explained before for single-phase circuits, reactive power contains no sustained flow; it represents a certain amount of energy swinging across the cut set at 120 Hz. The circuit on the two sides of any cut set is inherently capacitive on one side and inductive on the other. So reactive-power "flow" is no flow at all but a number identifying the amount of energy swinging across the cut set (expressed in peak MVA values at 120 Hz for convenience) with a + or - sign that tells one which side of the cut set has a capacitive circuit and conversely an inductive one.

How can two terms of \hat{S} be so different in nature? Remember that \hat{S} is an artificial concept, "complex power," without physical reality, created for convenience from a lucky coincidence ($\hat{S} = \hat{E}\hat{I}^*$). So there is no reason why its real and imaginary parts inherently cannot be of completely different nature as they indeed are. Note that again by lucky coincidence, both real and imaginary parts happen to have real physical meanings. Because it is a swing and not a flow, the amplitudes of the three-phase swings in reactive power simply add without any reference to the relation of the phase of the swings in time (each phase needs its own capacitor).

BIBLIOGRAPHY

1. Zaborszky, J. Some basic issues in voltage stability and viability, NSF Symposium on Bulk-Power Voltage Phenom. — Voltage stability and security, Potosi MO, 1988, pp. 1.17–1.60 (Editor Lester Fink).
2. Zaborszky, J., Schattler, H., and Venkatasubramanian, V., Limitations of the quasi-stationary dynamics and error due to phasor computations in network equations, Proc. Power Sys. Comput. Conf. (PSCC), France, August 1993 pp. 721–729.
3. DeMarco, C., and Verghese, G., Bringing phasor dynamics into the power system load flow, Proc. 1993 North American Power Symp., Howard University, Washington, D.C., October 1993, pp. 463–471.
4. LaWhite, N., and Ilić, M., Vector space decomposition of reactive power for periodic nonsinusoidal signals, IEEE Trans. on Circuits and Systems, Part I, vol. 44, April 1997 pp. 338–346.
5. LaWhite, N., Vector Algebra of periodic non-sinusoidal signals for decomposition of power components in single and multiphase circuits, masters degree thesis, Dept. of Electrical Engineering and Computer Science, MIT, 1995.
6. Concordia, C., *Synchronous Machines*, New York: Wiley, 1951.
7. Zaborszky, J., and Rittenhouse, J. W., *Electric Power Transmission*, Reynolds 1954. Available in paperback at Rensselaer University Bookstore, Troy, NY.
8. Desoer, C. A., and Kuh, E. S., *Basic Circuit Theory*, New York: McGraw-Hill, 1969.

9. Gelfand, I. M., and Fomin, S. V., *Calculus of Variations*, Englewood Cliffs, NJ: Prentice-Hall.
10. Fryze, S., Active, reactive and apparent powers in nonsinusoidal systems (in Polish), *Przeglad Elektrot.*, No. 7, pp. 193–203, 1931.
11. Zinovev, G. C., On reactive power in electric networks, *Sov. Acad. Sci. Rep. (Energy)*, No. 4: 80–86, 1987.
12. Mathis, W., and Marten, W., A unified concept of electrical power, *Proc. IEEE Int. Symp. Circuits Syst.*, 1989, pp. 499–502.
13. Arnold, V. I., *Mathematical Methods of Classical Mechanics*, 2nd ed. New York: Springer 1989, pp. 163–170.
14. Penfield, P. Jr., *Frequency-Power Formulas*, Cambridge, MA, and New York: MIT Press and Wiley, 1960.
15. Penfield, P. Jr., Spence, R. and Duinker, S. *Tellegen's Theorem and Electrical Networks*, Research Monograph No. 58, Cambridge, MA: MIT Press, 1970.
16. Milić, M., Integral representation of powers in periodic non-sinusoidal steady state and the concept of generalized powers, *IEEE Trans. Educ.*, August 1970: 107–109.
17. Budeanu, C. I., *Reactive and Fictitious Powers*, Roumanian National Institute of Energy, Publ. No. 2, 1927.
18. Utkin, V. I., *Sliding Modes and Their Application in Variable Structure Systems*, Moscow: MIR, 1978.
19. Page, C. H., Reactive power in nonsinusoidal situations, *IEEE Trans. Instrum. Meas.*, **IM-29**: 420–423, 1980.
20. Wyatt, J. L., Jr., and Ilić, M. D., Time-domain reactive power concepts for nonlinear, nonsinusoidal or nonperiodic networks, *IEEE Int. Symp Circuits Syst.*, **1**: 387–390, 1990.
21. Akagi, H., Kanazawa, Y., Fujita, K., and Nabae, A., Generalized theory of instantaneous reactive power and its application, *EE in Japan*, **103**: 483–490, 1983.
22. Wyatt, J., private communication.
23. Shepherd, W., and Zakikhani, P. Suggested definition of reactive power in nonsinusoidal systems, *Proc. IEE*, **119**: 1361–1362, 1972.
24. Kusters, N. L., and Moore, W. J. M., “On the Definition of Reactive Power under Nonsinusoidal Conditions,” *IEEE Trans. Power Appl. Syst.*, Vol. PAS-99, No. 5, Sept./Oct. 1980, pp. 1845–1854.
25. Filipski, P., A new approach to reactive current and reactive power measurement in nonsinusoidal systems, *IEEE Trans. Instrum. Meas.*, **IM-29**: 423–426, 1980.
26. Czarnecki, L. S., Considerations on the reactive power in nonsinusoidal situations, *IEEE Trans. Instrum. Meas.*, **IM-34**: 399–404, 1985.
27. Czarnecki, L. S., Minimization of reactive power under nonsinusoidal conditions, *IEEE Trans. Instrum. Meas.*, **IM-36**: 18–22, 1987.
28. Ofori-Tenkorang, J., Power components in non-sinusoidal systems: Definitions and implications on power factor correction, *LEES Technical Report No. TR94-001*, MIT, 1994.

3 Analytical Dynamic Model of the Power System

Viewed as a nationwide industry and business, the power system has a clear structure with definite engineering implications as sketched in Figure 3.1. The current organizational format is found in power companies that have their own generation, transmission and distribution facilities as shown in dashed line frame in Figure 3.1. They are individual business entities. They are connected by tie lines to their neighbors into a national system (with possible subdivision into power pools). Government regulated trading of power roughly on a days time scale is carried out under strict government supervision as in their dealings with their companies, large and small. To promote opportunities for competition, this organization is now in the process of changing into the pattern shown on the left of Figure 3.1. Three layers divide the industry vertically, rather than horizontally. At the generation level each company owns individually generating stations and sells its power to the widespread transmission company competitively. The distribution companies (these are local, like the current power companies) buy their power from the transmission companies and sell it to the individual loads, that is, customers, large and small. Alternatively, the generation companies sell directly to the distribution companies and deliver through the network of the transmission company.

This new reorganization subject to development and research is now in progress. Its effect is intended to be a more market-oriented competitive operation with commodities-exchange-type operation and less government regulation involved.

This means that the power field and particularly its dynamics are currently in a lively development stage. The technological and structural tools are the subject of this book. Today these developments have analytical and computational sides, both depending on precise modeling of the parts and the whole system. Analytical models are the subject of this chapter, while Chapter 4 deals with computational models. The analytical equivalent of the structure of Figure 3.1 is presented in Figures 3.2 and 3.3, followed by the analytical models of individual components.

It is common knowledge that the electric power-transmission system has a network structure of high-voltage transmission lines connecting nodes. The latter are known as buses. The equipment connected to each bus is complex in nature. Buses are the sole connection points to the transmission system of all equipment: (1) the sources, that is, generators; (2) the loads, either large and concentrated like an aluminum plant or distributed like the feeding point of subtransmission networks supplying a composition of smaller loads and eventually leading to distribution lines

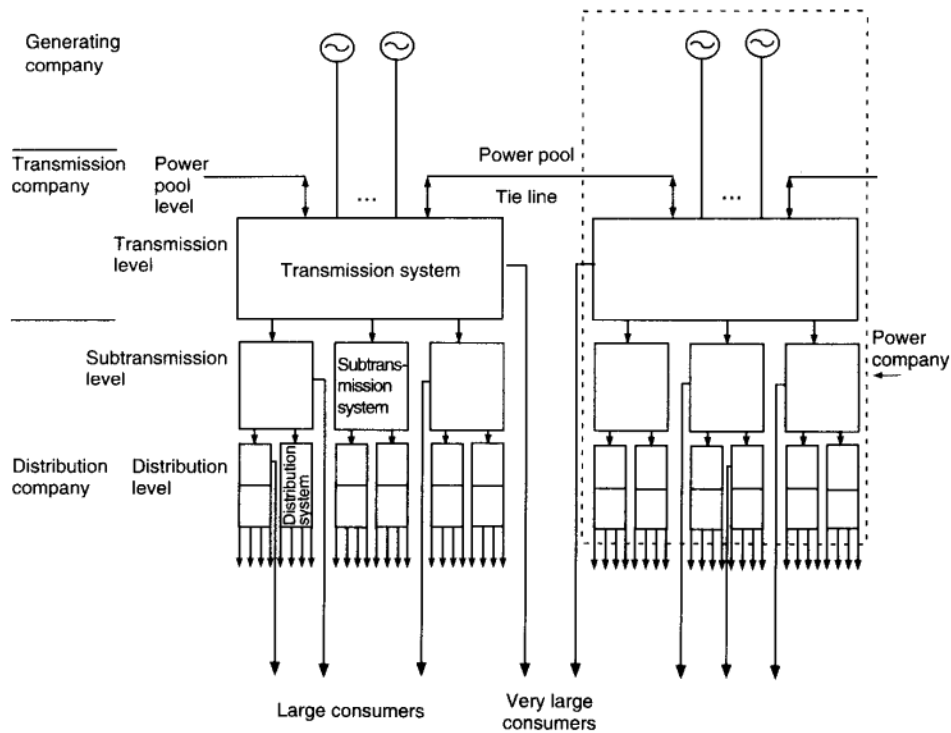


FIGURE 3.1 Basic traditional structure of a power system and the structural change now in progress.

on residential streets; (3) reactive-power storage devices like capacitor banks or reactors; (4) increasingly numerous power electronically switched devices (thyristors) such as static Var compensators (SVCs), the coupling equipment between the high-voltage AC (HV-AC) bus and the high-voltage DC (HV-DC) transmission lines, and currently developing flexible AC transmission systems (FACTS) devices; (5) series capacitor compensation; (6) lightning arrestors and other equipment connected to a bus by links other than transmission lines have no connection outside the transmission lines to any other bus; they form large islands of complex equipment connected to the outside world exclusively through the high-voltage lines (AC or DC) of the transmission network.

The network itself is sparse in the sense that its lines connect only at specific buses and for each bus there are typically not more than three or four transmission lines connected. Occasionally for heavily loaded areas this number of buses may rise to about a dozen. On the network side of the bus the only equipment is the lines themselves (HV-DC equipment such as rectifiers or inverters are considered here as part of the bus equipment) with power exchange at their terminal buses and a distributed discharge of resistive losses (typically small, less than 5%) along the lines.

All this presents a very rich but specially organized assortment of pieces of equipment involved in static or dynamic phenomena. In this book the first step

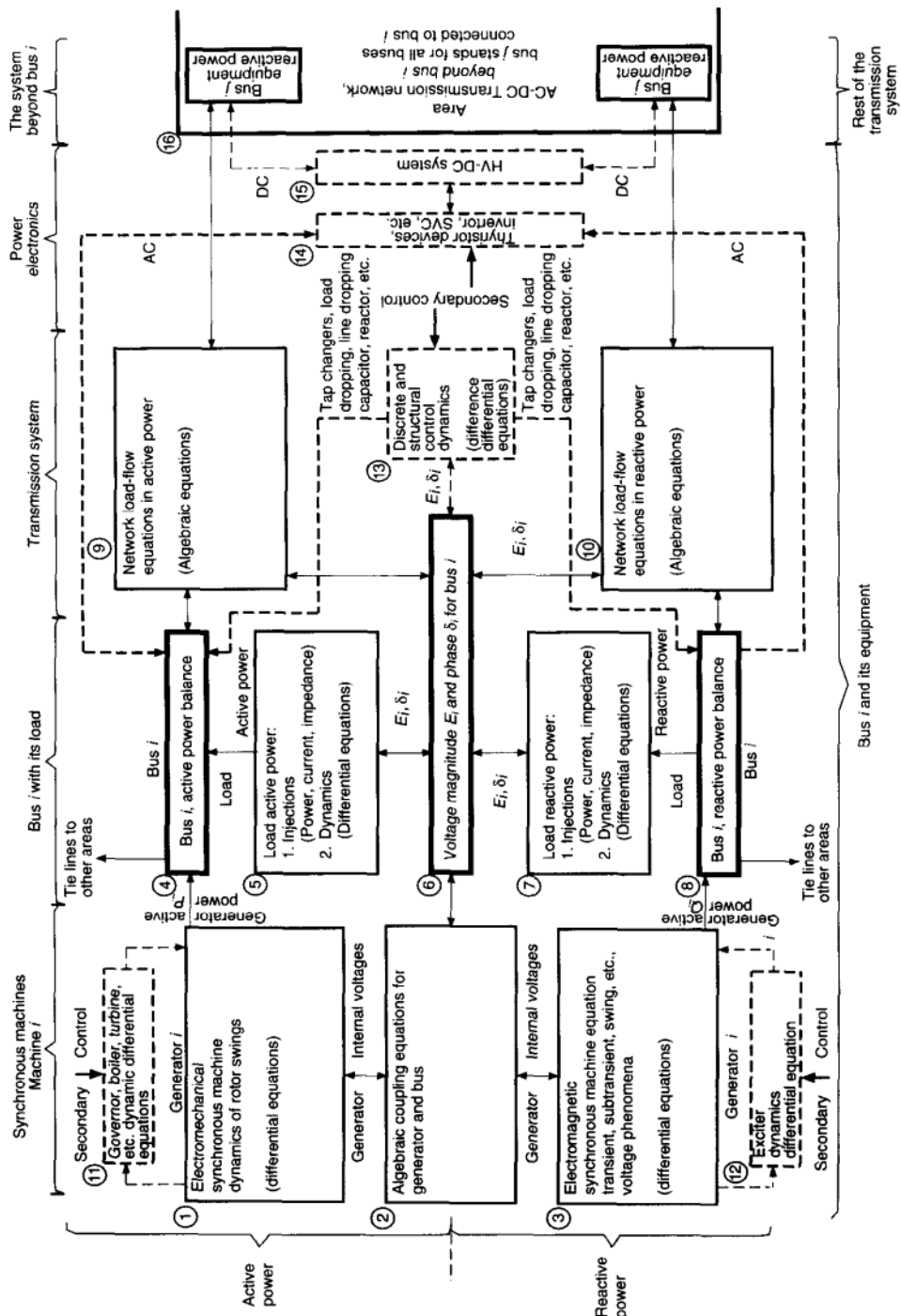


FIGURE 3.2 Structure of the overall power system model.

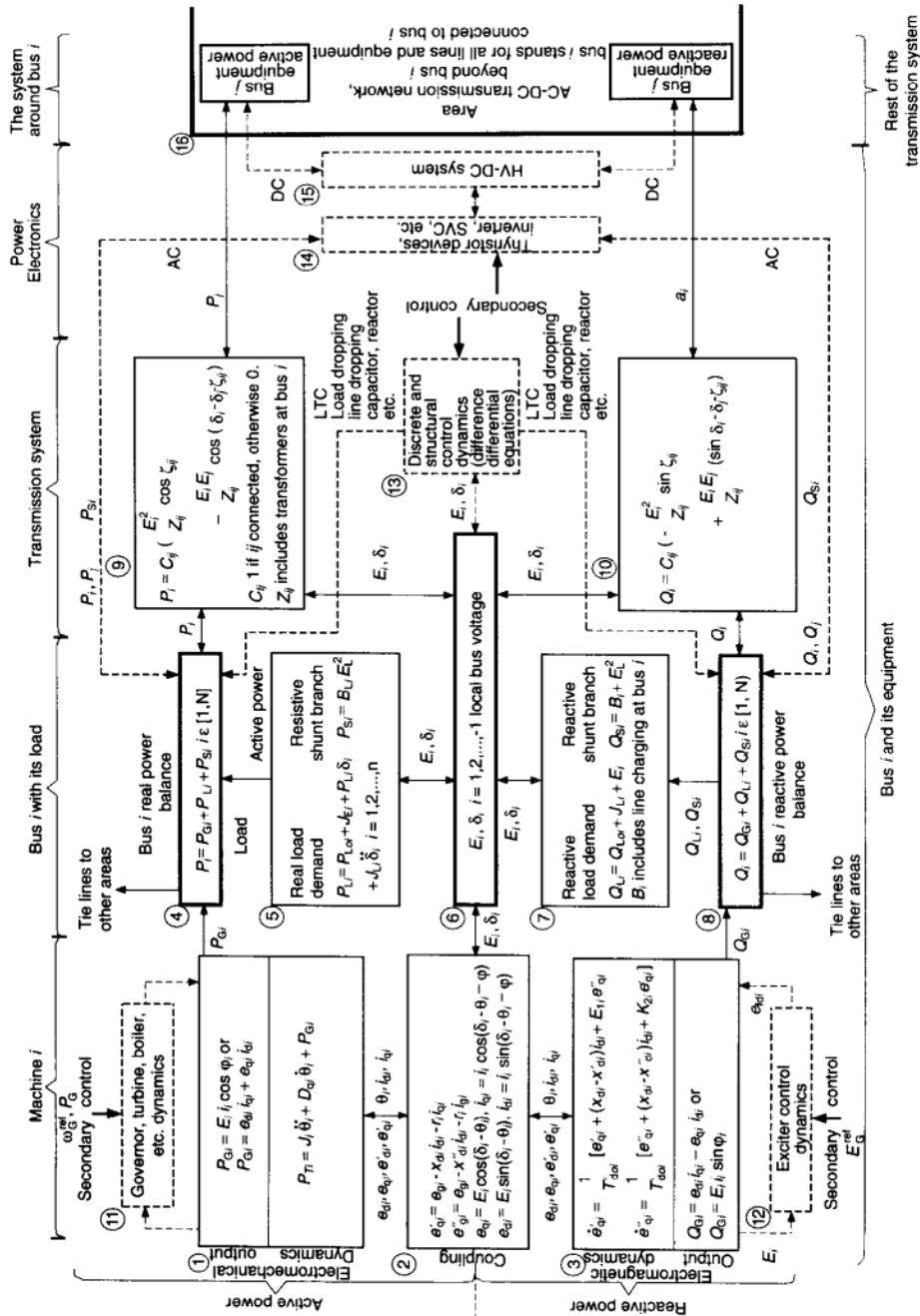


FIGURE 3.3 Overall model of the large power system (Model #1, Type 1).

will be to understand analytically modeling questions of the large variety of equipment. This is the subject of this chapter. The structure of the system is also treated in Chapter 4. To approach the equipment modeling issue properly it is necessary, however, to have a basic understanding of the system structure. Such a fundamental understanding is developed in the next section (Sec. 3.1).

3.1 FUNDAMENTAL STATIC AND DYNAMIC STRUCTURES OF THE POWER-TRANSMISSION SYSTEM

A variety of static and dynamic phenomena and problems connected with the interplay of reactive power and voltage with active power and rotor angle will be studied in this book. In these problems there is a great diversity of critical time periods, frequencies, and ranges of variation for both power and voltage. In many cases it is possible to decouple real and reactive power (i.e., phase angle and voltage) phenomena approximately. But making such approximations without thoroughly understanding the actual interactions will lead, and has lead, to results that are at least questionable. This situation is similar to ignoring the limitations of the quasistationary assumptions (see Chapter 2). Furthermore, almost every problem will critically engage a different set of static or instantaneous (algebraic equations) and dynamic (differential or difference equations) system components—hence a different mathematical model will emerge for almost every problem. This implies that, if models were developed individually for each problem a bewildering array of models would emerge. The reader would feel uncomfortable and insecure as to where they come from and how far their applicability extends.

In reality the entire system and its overall model are involved in all phenomena except that only some components participate importantly in each particular problem. Components too distant topographically or in frequency or in amplitude, etc., may affect a given problem only mildly, and so it may be possible to ignore them. To stay on firm ground, the best approach is to start with the overall system model and clearly understand its structure. Then it becomes relatively easy to select those aspects of the model that are needed for realism and accuracy in any problem. The reduced models resulting from this process are then well understood and easily placed into the context of the overall system.

3.1.1 Structure of the Overall Power-System Model

The structure of the overall power-system model is displayed in Figure 3.2 with the actual mathematical model presented in the same format in Figure 3.3. This structure can be best understood in terms of a set of ordering principles:

1. A vertical subdivision into, respectively, active- and reactive-power expressions (such a subdivision is dictated in the models by the use of *time-varying* phasor calculus that is the dominant language of power-system analysis).

2. Functional divisions are arranged in vertical bands:

- a. The bus active- (block 4), and reactive- (block 8) power balance, respectively, dominate the upper and lower subdivisions. The phasor bus voltage, (block 6), $\hat{E}_i(E_i/\delta_i)$ is a foundation for all bus-connected equipment; symbol E_i/δ_i is used interchangeably with $E_i e^{j\delta_i}$. The blocks for each bus i (4, 6, and 8) are highlighted to emphasize this fact.
- b. On the system side of the bus, the equipment consists of the AC (blocks 9 and 10) and DC (blocks 14 and 15) transmission lines of the network. Blocks 4, 6, 8, 9, and 10 bracket the left sides of Figures 3.2 and 3.3 and define the transmission-network model, typically used in load-flow or power-flow calculations.
- c. The well-understood but complex model of the generators, blocks 1 to 3, where box 2 in the middle represents the interconnection between real-power (and bus angle) and reactive-power (and bus voltage) dynamics. The interconnection, box 2, of the real- and reactive-power sides is strong and real and needs to be well understood before disjoint approximations are used properly.
- d. The static or dynamic models of the composite loads [active (block 5) and reactive power (block 7)] are not yet well understood, and theoretically conjectured models are very difficult to verify experimentally (you cannot subject a power system to a major fault just to experiment on a proposed model). The best that can be done currently is to use expressions derived from available disturbance records, and this is represented in blocks 5 and 7.
- e. An assortment of equipment connected to the bus, such as energy-storing components such as capacitors and reactors and a variety of power electronic devices such as SVCs (thyristor-controlled reactors), inverters, rectifiers, and discrete mechanically controlled devices such as tap changers are hinted at in blocks 13 to 15. This group of models is highly varied and much less standardized than those referred to earlier.

Proliferation of power-electronic- (thyristor) switched devices such as rectifiers, inverters, variable reactances (SVCs), and even more sophisticated technologies developing within the FACTS movement (block 14) is an important phenomenon in today's power systems. These devices are beginning to change the character of power-system operation. The same applies to the HV- DC network (block 15), which is on the verge of becoming a true network, rather than individual DC lines. The modeling structure offered in this chapter is ready to incorporate these developments without basic changes.

- f. Primary controls such as generator exciters and valve control actuators on the generators and discrete and structural control devices are included here as part of the piece of equipment that they control, in blocks 11 to 15. Most primary controls contain actuators and are feedback devices controlling to a piece of an equipment set point.

- g. The set points are generated in what is known as secondary control, for example, automatic generation control (AGC) [1], pilot point-based automatic voltage control (AVC) [2], or other corrective controls in stationary operation [3]. The latter are not shown, except for their entry points in Figure 3.2 or 3.3, but much of this text will be devoted to the theory and practice of secondary controls. Blocks 11, 12 and 13 are meant to contain only the primary controls themselves (exciter control and various discrete controls). Block 11 differs from 12 and 13 in that it contains, in addition to the direct primary control of the turbine torque (that is, the governor and governor mechanism), the mechanical dynamics of the equipment, such as the turbine or boiler, that tie to the system dynamically through the governor control valve.

First, the various components of the model in Figures 3.2 and 3.3 will be discussed in this section. Then the expressions for the applicable component models will be derived for incorporation into Figure 3.3. Typical primary-control models will also be introduced with references for the different types that may be encountered.

Space limitations dictate the use of relatively simple models in Figure 3.3 such as the balanced three-phase circuit. Realistic details in high precision are described in the next section. A set of replacement schemes for the generator model in Figure 3.3 for generator modeling of varied detail is given in Figure 3.27 in the section on generation modeling.

3.1.2 Discussion of Figures 3.2 and 3.3

Most of the structure shown in Figures 3.2 and 3.3 shows the primary details of equipment connected to one particular bus i and the connection of both high-voltage AC and DC lines (HV AC–DC) to bus i . From bus i both the AC and DC lines connect to a specific set of (typically less than 12) buses in the HV AC–DC power transmission network symbolized by blocks 9 to 16 in Figures 3.2 and 3.3. Thus the boxes denoted by “bus j ” within blocks 9 to 16 represent specific sets of pairwise interconnected structures identical in their character to the part of Figures 3.2 and 3.3 that is outside blocks 9 to 16. This, of course, represents a set of buses directly connected by AC and/or DC lines to bus i . This set is also known as the first tier of buses around bus i within the network. Thus all buses have the same basic structure of Figures 3.2 and 3.3 with some of the elements possibly empty (absent), for example, generator buses or load buses or even buses with no equipment except for line connections. The transmission network then in a circuit sense is a simple *sparse* network, where each node (i.e., bus) is connected to a limited number of other buses directly within a typically very-large-dimensional system of buses numbering in the tens of thousands. Note that Figures 3.2 and 3.3 represent the structure of the primary details of the analytic model of the large power system in stationary and dynamic conditions.

A horizontal symmetry axis bisects Figures 3.2 and 3.3; above it the real-power relations are represented, while reactive power resides below the axis. On

the axes are shown features that couple active- and reactive-power halves such as the bus i and the coupling equations within the active and reactive power sides of the generator model. The symmetry of the various functions is essentially complete in the structural sense as shown in Figure 3.2. There is also almost complete symmetry in mathematical detail shown in Figure 3.3, for, instance, in the transmission-system equations. The equations of real- and reactive-power dynamics in the generators are quite different, however, as shown in Figure 3.3. It should be emphasized that the display of, respectively, active and reactive power equations above and below the symmetry axes in Figures 3.2 and 3.3 should not be interpreted as two decoupled models. They are fully coupled through blocks 2, 6, 13, 14, and 15. In many instances it is possible to decouple active and reactive phenomena with good approximation since the interaction of the two is relatively weak. In other cases, however, reactive-power relations are vitally affected by active-power dynamics and vice versa. It is therefore vital to look at the full picture, the combined active- and reactive-power dynamics. In any case only a full understanding of the complete model will make feasible the confident and competent use of its parts. Accordingly, the full model is displayed in Figures 3.2 and 3.3 and studied in the associated sections. Theoretical conditions under which decoupling holds in stationary operation are introduced in Chapter 5. The concept of decoupling is more complex under dynamic conditions; various aspects of this notion are discussed in Chapters 6 to 10.

Accordingly, an overall model will first be developed here that can cover the entire range of static and dynamic phenomena for the range of problems considered in this text. The structural organization and mathematical specifics of such a model will now be introduced in connection to Figures 3.2 and 3.3.

3.2 PARTICULARS OF THE MODELS OF POWER-SYSTEM COMPONENTS

There are many components of the power system. The preceding discussion of Figures 3.2 and 3.3 suggests an organizational structure that will be followed in the next sections to give an organized set of descriptions of its various specific components:

1. Buses as the connection points of various equipment to the transmission network.
2. Components of the transmission system: specifically buses, AC lines, and DC lines.
3. Components connected to the buses such as generators, loads, transformers, and SVCs, which can be classified as:
 - a. Established components that have an established, basically uniform structure, such as generators, leading to a well-defined general model.

- b.** Established components that have a large variety of designs in the field such as excitation control, which cannot be readily reduced into a specific type of model.
- c.** Components that are still more or less in the developmental stage of modeling, like loads and many FACTS components and other devices, that involve power-electronic-based switching.

3.2.1 Buses

The buses (blocks 4 and 8 in Fig. 3.3) have no dynamics and no energy storage per se (energy storage devices, capacitor banks, or reactors are part of the equipment). Consequently, the only mathematical model required for bus i would be the two *power-flow balance equations* for active and reactive power

$$P_i = P_{Gi} + P_{Li} + P_{Si}, \quad i \in [1, n] \quad (3.1)$$

$$Q_i = Q_{Gi} + Q_{Li} + Q_{Si}, \quad i \in [1, n] \quad (3.2)$$

where n is the total number of buses. Here (with reference to Figs. 3.2 and 3.3) P_i and Q_i represent the combined power exchange over the transmission lines of the network terminating on bus i . P_{Gi} and Q_{Gi} are the combined power injection to bus i from directly connected generators (blocks 1 and 3), P_{Li} and Q_{Li} are load-power injections, and P_{Si} and Q_{Si} represent the total of any additional shunt branches at the bus such as capacitors, reactors, static Var compensators, or new types of FACTS devices.

It will be routinely assumed that all the rms voltages are normalized to a p.u. (per unit) form [4] and their phase angles are expressed on a common but arbitrary reference.

3.2.1.1 Selecting the Reference Angle for the Bus Voltages This seemingly simple task becomes rather complex for the power system. It depends on the method of system operation. The system considered in any problem can be isolated with no exchange of energy between the system and its environment. Such a system would exist, say, on New Zealand. At the other extreme the system studied may be firmly anchored to a very large system. A so-called "New England" study system would be an example with a single bus representing the connection to the entire U.S. interconnection. Intermediate cases with a variety of interconnections exist.

Much of the confusion results from the singularity of certain matrices (e.g., bus admittance matrix and the Jacobian or system sensitivity matrix, to be defined later in the text) that contain one row that is dependent on all the other rows. The most commonly used ways of selecting the voltage-phase-angle reference will be briefly stated here.

1. A *slack bus*, usually bus n , is assigned to serve as an anchor for the system with fixed references

$$\delta_n = 0, \quad E_n = \text{const, typically 1 p.u.} \quad (3.3)$$

Then the slack bus must have enough capacity to absorb without change in E_n and δ_n the balance of power

$$P_n = - \sum_{i=1}^{n-1} P_i - P_\ell, \quad Q_n = \sum_{j=1}^{n-1} Q_i \quad (3.4)$$

which, strictly speaking, implies an “infinite bus,” a connection to a source with infinite capacity. This condition, however is satisfied as long as the computed load for the slack bus is actually within its feasible and viable (to be defined later in the book) range. P_ℓ represents the system wide power losses on the transmission lines. These conditions along with the first $n - 1$ equations of Eqs. (3.1) and (3.2), that is,

$$P_i = P_{Gi} + P_{Li} + P_{Si}, \quad Q_i = Q_{Gi} + Q_{Li} + Q_{Si}, \quad i \in [1, n - 1] \quad (3.5)$$

where G stands for generator, L for load and S for assorted shunt equipment at the bus i , such as capacitor banks, inductors, SVC's etc. and knowledge of the time variations of P_{Gi} , P_{Li} , P_{Si} , Q_{Gi} , Q_{Li} , and Q_{Si} completely identify the power-flow relations on the system. Note that a slack bus is usually a dummy for computational convenience. The systems are operated traditionally by AGC in which no slack bus is used; the output of each generator is assigned by the controls. With use of slack bus, care must be taken that the resulting demand of power on it meets operating conditions. An infinite bus may be a good and desirable approximation for a small system (such as a single line feeding one bus, or the bus 10 “New England” system) that is dominated by one very large power source. Physically such a system is firmly anchored to the infinite bus, it is not autonomous.

2. An arbitrarily selected generator bus for reference δ_0 results in the equations being written in a coordinate system of *angle differences* $\delta_i - \delta_0$, rather than the δ_i actual values. This reduces the dimension of the system (eliminates the singularity of the original bus admittance matrix) and provides an isolated description of the relative behavior of the bus voltages and currents in the reduced space with no information of the *drifting* of the frequency in the full space. The latter is in the domain of AGC and its future replacements. So ignorance of the drift is of no consequence in many problems. For this reason this option is rather widely used.
3. An alternative representation uses the center-of-angle concept

$$\theta_c = \frac{\sum_{i=1}^N \theta_i J_i}{\sum_{i=1}^N J_i} \quad (3.6)$$

to represent an isolated system for angle reference on the system, where θ_i is the rotor angle of generator i and J_i is the machine-rotor inertia (if there is more than one generator per bus they need to be individually considered in the summations.) Then an additional dynamic equation arises:

$$\ddot{\theta}_c \sum_{i=1}^N J_i = \sum_{i=1}^N (P_{Gi} + P_{Li} + P_{Si}) - P_\ell = P \quad (3.7)$$

which along with Eq. (3.1) for $i \in [1, n - 1]$ and Eq. (3.2) for $i \in [1, n - 1]$ and the functions P_{Gi} , P_{Li} , P_{Si} , Q_{Gi} , Q_{Li} and Q_{Si} define the dynamics of an *isolated system*.

If $P \equiv 0$ for all t as may occur in a load-flow-type static condition, then items 1 and 2 give compatible results. But if $P \neq 0$, then the system Jacobian has a zero eigenvalue, which means that the center of angle is drifting because the entire isolated system is accelerating or decelerating. This latter phenomenon usually does not affect short-term stability results. Controlling the drift is in the realm of AGC for frequencies that act on a slow time scale, using P as control input. A detailed description of AGC is given in Chapter 13.

Using one of these three approaches properly as described usually leads safely to the right results. A detailed and thorough exposition of these matters is presented in Chapters 4 and 13. The latter portion of Chapter 13 also analyzes the ingenious AGC practice and its probable future developments resulting from the currently ongoing reorganization of the power industry.

When the system drift is of no interest, any arbitrary generator bus can be used as a reference angle, thus avoiding the computation of the center of angle. This is a common practice not always fully understood.

Thus the three fundamental operating modes,

1. Anchored system
2. Isolated system in the full space of δ_i with system frequency drift
3. Isolated system for the dynamics in the space of $\delta_i - \delta_0$.

are precisely defined and available for mathematical analysis. Practical systems may or may not approximate to a varying degree one or the other of these fundamentals. There are a few true isolated systems on large islands provided losses are considered as a load or as an approximation such as Australia, New Zealand, Ireland, Java, and Hawaii, but even some of the latter probably have some under-water cable connections to neighbors. Large continental systems will usually have some interconnections at the edges that may be sufficiently weak to allow the isolated model to be used as a good approximation. Even the U.S. system, for example, has strong ties to Canada and weaker ones to Mexico, but the latter would continue toward several countries to the south. Of course, there are no infinite buses either in the strict sense. The voltage and phase angle of a slack bus will also be slack in practice in the sense that they will respond to changes in the active

and reactive power drawn from them. Yet relative sizes may make the anchored model a good approximation. Matters of references, system drift, and related topics will be discussed in the following chapters, particularly in Chapter 13.

3.2.2 HV-AC Power-Transmission Lines

The principal elements of the power-transmission network are the transmission lines (blocks 9 and 10). On an AC system these can be viewed as waveguides, which leads to modeling in terms of Maxwell's equations [4, 5]. They also can be equivalently represented in terms of their R , L , and C values per unit length along the line. Physically the R , L , and C constants are distributed uniformly along the line. This approach leads to partial differential equations and boundary-value problems that can be equivalently reduced to ordinary differential equations with time delays. This approach is required for systems with long lines (Chapter 11).

For most power-system problems with lines of moderate length and within the quasistationary phasor range (see Chapter 2), a satisfactory approximation is possible by introducing R -, L -, and C -based parameters on approximate π or T circuits. The basic mathematical model of a transmission line will be introduced here in terms of the series and shunt resistances, inductances, and capacitance values per unit length of the line.

3.2.2.1 Basic Mathematical Model of a Transmission Line A basic transmission line consists of two parallel wires of arbitrary diameters, extending indefinitely in the $\pm y$ directions within a uniform medium (Figure 3.4). Cables are concentric cylinders, the space between being filled with uniform material. Thus, any cross section will appear identical to any other cross section. Internal magnetic fields will raise the current density inside a cylindrical solid conductor near its surface (known as the skin effect) and also in the area of conductors nearest to each other (this and the corona necessitate dividing the conductor into four parallel conductors on some high-voltage lines). These internal flux effects will increase with frequency. Yet for most practical circumstances on the power systems, all the line parameters (R , L , C , and G) can be viewed as constants.

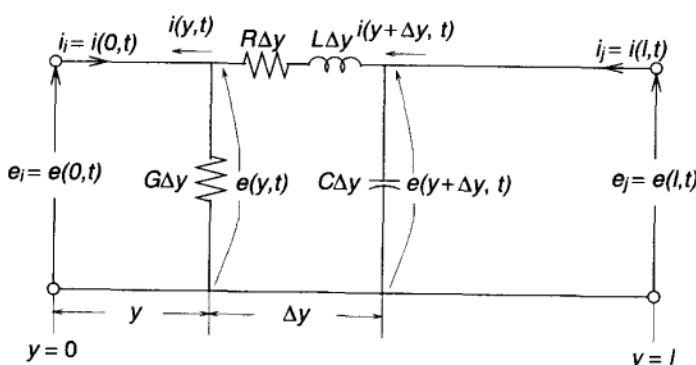


FIGURE 3.4 Transmission-line increment.

This assumption is made in this section. Refinements will be made in Chapter 11. Figure 3.4 represents a transmission line in which R , L , C , and G are constants along the line.

The voltage $e(y, t)$ decreases incrementally by $e(y + \Delta y, t) - e(y, t) = \Delta e(y, t)$ within an incremental length Δy , as there is a current $i(y, t)$ flowing through $R\Delta y$ and $L\Delta y$:

$$\Delta e(y, t) = R\Delta y i(y, t) + L\Delta y \frac{\partial i(y, t)}{\partial t} \quad (3.8)$$

The current increment over the Δy increment caused by G and C is

$$\Delta i(y, t) = G\Delta y e(y, t) + C\Delta y \frac{\partial e(y, t)}{\partial t} \quad (3.9)$$

which in the limit, as $\Delta y \rightarrow 0$, reduces to

$$\frac{\partial e(y, t)}{\partial y} = Ri(y, t) + L \frac{\partial i(y, t)}{\partial t} \quad (3.10)$$

and

$$\frac{\partial i(y, t)}{\partial y} = Ge(y, t) + C \frac{\partial e(y, t)}{\partial t} \quad (3.11)$$

Equations (3.10) and (3.11) are partial differential equations representing the distributed parameter nature of the line. Note that Figure 3.4 and Eqs. (3.10) and (3.11) are also applicable for a balanced three-phase line (or the upper half of the single-phase line) in which the neutral current is inherently zero, and hence there is no voltage drop in the neutral line even if there is a physical neutral conductor.

3.2.2.2 Lumped-Parameter Representation of Transmission Lines in the Quasistationary Range In this book transmission lines generally serve as the connections between buses, defining the relation between the bus voltages at the i and j ends of the line. Furthermore, in the quasistationary range these relationships depend only on constant parameters of the line such as the *characteristic impedance* and the *propagation constant* along with the line length. In some aspects these partial differential equations are needed for long transmission lines in dynamic conditions as will be presented in Chapter 11. For static and stationary conditions which cover most practical engineering problems lumped parameter model approximations apply.

These results, in fact, can be worked out by simple algebraic manipulations for both a π and a T circuit, as described next.

3.2.2.3 Transmission-Line Equations in Phasors for the Quasistationary Range The quasistationary phasor range covers most of the practical power engineering problems including those treated in this book. Accordingly it is desirable to look at the phasor form of the transmission-line equations. It will also be

observed that when the lines are of moderate length, lumped-parameter models described here give sufficiently accurate results.

In quasistationary phasors for connecting line i,j ,

$$e(y, t) = \operatorname{Re} \hat{E}(y) = \operatorname{Re} E(y) e^{j[\omega t + \delta(y) - \varphi(y)]} \quad (3.12)$$

$$i(y, t) = \operatorname{Re} \hat{I}(y) = \operatorname{Re} I(y) e^{j[\omega t + \delta(y) - \varphi(y)]} \quad (3.13)$$

Thus the stationary phasor form suppresses precisely the time dependence as discussed in Chapter 2 under the assumption of a steady-state condition in which the only time-dependent part of $e(y, t)$ and $i(y, t)$ is the 60-Hz carrier, whereas the amplitudes [$E(y)$ and $I(y)$] and phases [$\delta(y)$ and $\varphi(y)$] remain constant. These equations also give good approximation within the quasistationary range in which the magnitudes vary slowly enough. For the secure steady-state condition then with reference to Figure 3.4, in phasor notation Eqs. (3.8) and (3.9) become

$$\Delta \hat{E}(y) = [\hat{I}(y) + \Delta \hat{I}(y)] \hat{z} \Delta y \quad (3.14)$$

and

$$\Delta \hat{I}(y) = \frac{\hat{E}}{\hat{z}'} \Delta y \quad (3.15)$$

where, respectively, series and shunt impedances \hat{z} and \hat{z}' per mile are $\hat{z} = R + j\omega L$ and $\hat{z}' = G + j\omega C$. Clearly, when $\Delta y \rightarrow 0$ Eqs. (3.14) and (3.15) will precisely, for the actual steady-state system operation, converge to the following set of ordinary differential equations [omitting (y, t) and (y) dependences for notational simplicity]:

$$\frac{d\hat{E}}{dy} = \hat{z}\hat{I}, \quad \frac{d\hat{I}}{dy} = \frac{1}{\hat{z}'}\hat{E} \quad (3.16)$$

or

$$\frac{d^2\hat{E}}{dy^2} = \hat{z}\frac{d\hat{I}}{dy}, \quad \frac{d^2\hat{I}}{dy^2} = \frac{1}{\hat{z}'}\frac{d\hat{E}}{dy} \quad (3.17)$$

Combining Eqs. (3.16) and (3.17),

$$\frac{d^2\hat{E}}{dy^2} = p \frac{\hat{z}}{\hat{z}'} \hat{E}, \quad \frac{d^2\hat{I}}{dy^2} = \hat{p} \frac{\hat{z}}{\hat{z}'} \hat{I} \quad (3.18)$$

Define next

$$\hat{p} = l \sqrt{\frac{\hat{z}}{\hat{z}'}} \quad (3.19)$$

to be a so-called propagation constant. Note that for a lossless line ($R = G = 0$) $p = \sqrt{L/C}$ is real. For a line ij of length l connecting buses i and j boundary conditions become $\hat{E}_i = \hat{E}(y = 0)$, $\hat{I}_i = \hat{I}(l = 0)$, $\hat{E}_j = \hat{E}(y = l)$, and $\hat{I}_j = \hat{I}(y = l)$. With $\hat{Z} = l\hat{z}$ and $\hat{Z}' = (1/l)\hat{z}'$, let $\hat{Z}_0 = \sqrt{\hat{Z}\hat{Z}'}$ be called a line characteristic

impedance. The differential equations (3.18) are easily solved for the assumed solution form:

$$\hat{E}(y) = \hat{a}e^{\hat{p}y} + \hat{b}e^{-\hat{p}y} \quad (3.20)$$

$$\hat{I}(y) = \hat{c}e^{\hat{p}y} + \hat{d}e^{-\hat{p}y} \quad (3.21)$$

with \hat{a} , \hat{b} , \hat{c} , and \hat{d} dependent on the boundary conditions for voltage and current at a point y along the line as follows:

$$\hat{E}_i = \hat{E}_j \cosh \hat{p}\ell + \hat{I}_j \hat{Z}_0 \sinh \hat{p}\ell = \hat{A}\hat{E}_j + \hat{B}\hat{I}_j \quad (3.22)$$

$$\hat{I}_i = \frac{\hat{E}_j}{\hat{Z}_0} \sinh \hat{p}\ell + \hat{I}_j \cosh \hat{p}\ell = \hat{C}\hat{E}_j + \hat{D}\hat{I}_j \quad (3.23)$$

with the standard notations [4]

$$\hat{A} = \cosh \hat{p}\ell \quad (3.24)$$

$$\hat{B} = \hat{Z}_0 \sinh \hat{p}\ell \quad (3.25)$$

$$\hat{C} = \frac{1}{\hat{Z}_0} \sinh \hat{p}\ell \quad (3.26)$$

Equations (3.22) to (3.26) are convenient for analyzing single transmission lines [4]. In this book, however, the emphasis is on the system in which lumped-parameter models are more convenient. The latter will be summarized here.

Equivalent π -circuit Transmission-Line Model It is easy to show that for a lumped-parameter π circuit as in Figure 3.5 the relationships between the i -bus variables (\hat{E}_i, \hat{I}_i) and the j -bus variables (\hat{E}_j, \hat{I}_j) are

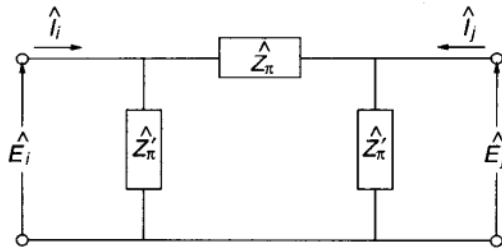
$$\hat{E}_i = \hat{E}_j \left(1 + \frac{\hat{Z}_\pi}{\hat{Z}'_\pi} \right) + \hat{I}_j \hat{Z}_\pi \quad (3.27)$$

$$\hat{I}_i = -\hat{E}_j \left(\frac{2}{\hat{Z}'_\pi} + \frac{\hat{Z}_\pi}{\hat{Z}'_\pi^2} \right) - \hat{I}_j \left(1 + \frac{\hat{Z}_\pi}{\hat{Z}'_\pi} \right) \quad (3.28)$$

Now postulating that Eqs. (3.27) and (3.28) are exactly equivalent to Eqs. (3.22) and (3.23), it is easy to show that the constants ($\hat{Z}_\pi, \hat{Z}'_\pi$) in the π circuit must be

$$\hat{Z}_\pi = \hat{Z} \left(1 + \frac{\hat{Z}}{6\hat{Z}'} + \frac{\hat{Z}^2}{120\hat{Z}'^2} + \frac{\hat{Z}^3}{5040\hat{Z}'^3} + \dots \right) \quad (3.29)$$

$$\hat{Z}'_\pi = 2\hat{Z}' \left(1 + \frac{\hat{Z}}{12\hat{Z}'} - \frac{\hat{Z}^2}{720\hat{Z}'^2} + \frac{\hat{Z}^3}{30240\hat{Z}'^3} + \dots \right) \quad (3.30)$$

FIGURE 3.5 π circuit.

where, of course, Taylor-series expansions of sinh and cosh were used. It then is precisely correct that for the quasistationary range, the equivalent π four-terminal network is indeed equivalent to the mathematical solution of Eqs. (3.22) and (3.23).

The series in Eqs. (3.29) and (3.30) converge rather rapidly, especially when the lines are relatively short, say under 300 miles. Hence in most power-system problems they can be approximated rather well by retaining only the first two terms in the series expansion and neglecting leakage reactance. Then also real and imaginary parts can be explicitly separated as follows:

$$\hat{Z}_\pi \cong rl \left(1 - \frac{x}{x'} \frac{l^2}{3} \right) + jxl \left[1 + \left(\frac{r^2}{xx'} - \frac{x}{x'} \right) \frac{l^2}{6} \right] + \dots \quad (3.31)$$

$$\hat{Z}'_\pi \cong -j \frac{2x'}{l} \left[\left(1 - \frac{x}{x'} \frac{l^2}{12} \right) + j \frac{r}{x'} \frac{l^2}{12} \right] + \dots \quad (3.32)$$

where x and r are in Ω per mile, x' is $\Omega \cdot$ miles, l is in miles, $\hat{z} = r + jx$, and $\hat{z}' = r' + jx'$.

As a guide, at a line length of 300 miles and a frequency of 60 cycles the error is only about 0.1% if all but the first three terms in the preceding series are neglected. Furthermore, very little error is incurred if it is assumed that

$$\hat{Z}' \cong -j \frac{1}{\omega C} \quad (3.33)$$

that is, the leakage impedance is assumed entirely reactive. Under this assumption, one can derive formulas for typical lines that are of the form

$$\hat{Z}_0 \cong k_0 \omega L \sqrt{1 - j \frac{R}{\omega L}} \quad (3.34)$$

and

$$\hat{p} \cong k_p \sqrt{-1 + j \frac{R}{\omega L}} \quad (3.35)$$

For open-air transmission lines $k_0 = k_p = 1$. For cables k_0 and k_p are constants dependent on the type of material used for making the cable. For ACSR cables, for example, at 60 Hz $k_0 = 485$ and $k_p = 2.66 \times 10^{-3}$ [4]. These relationships make it possible to compute close approximation values of \hat{Z}_T and \hat{Z}'_T without the need for determining the capacitive reactance C of the line. Derivation details for these formulas can be found in Ref. [4].

Equivalent T-Circuit Model For a lumped-constant T circuit like that shown in Figure 3.6, using the same process as for the π circuit, we obtain the following results:

$$\hat{I}_i = \hat{E}_j \frac{1}{\hat{Z}'_T} + \hat{I}_j \left(1 + \frac{\hat{Z}_T}{\hat{Z}'_T} \right) \quad (3.36)$$

$$\hat{E}_i = \hat{E}_j \left(1 + \frac{\hat{Z}_T}{\hat{Z}'_T} \right) + \hat{I}_j \left(2\hat{Z}_T + \frac{\hat{Z}_T^2}{\hat{Z}'_T} \right) \quad (3.37)$$

The \hat{Z}_T and \hat{Z}'_T constants are obtained using the Taylor-series expansion,

$$\hat{Z}_T = \frac{\hat{Z}}{2} \left(1 - \frac{\hat{Z}}{12\hat{Z}'} + \frac{\hat{Z}^2}{120\hat{Z}'^2} - \dots \right) \quad (3.38)$$

$$\hat{Z}'_T = \hat{Z}' \left(1 - \frac{\hat{Z}}{6\hat{Z}'} + \frac{7\hat{Z}^2}{360\hat{Z}'^3} - \dots \right) \quad (3.39)$$

If only two terms in the series expansion are retained, one obtains

$$\hat{Z}_T \approx \frac{1}{2}rl \left(1 - \frac{x}{x'} \frac{l^2}{12} \right) + j \frac{1}{2}xl \left[1 + \left(\frac{r^2}{x x'} - \frac{x}{x'} \right) \frac{l^2}{12} \right] \quad (3.40)$$

$$\hat{Z}'_T \approx -j \frac{x'}{l} \left[\left(1 + \frac{x}{x'} \frac{l^2}{6} \right) - j \frac{r}{x'} \frac{l^2}{6} \right] \quad (3.41)$$

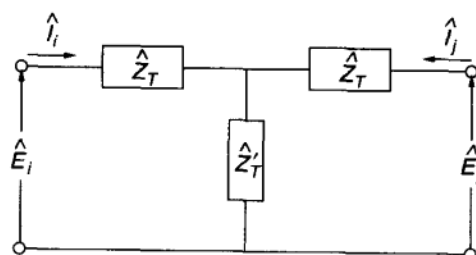


FIGURE 3.6 T circuit.

Nominal π - and T-Circuit Representations If lines are not longer than 100 miles

$$\hat{Z}_{\pi n} \cong \hat{Z} \quad (3.42)$$

$$\hat{Z}'_{\pi n} \cong 2\hat{Z}' \quad (3.43)$$

$$\hat{Z}_{Tn} \cong \frac{1}{2}\hat{Z} \quad (3.44)$$

$$\hat{Z}'_{Tn} \cong \hat{Z}' \quad (3.45)$$

Line representations with these parameters are frequently referred to as nominal π and T circuits for transmission lines. The circuits that have these coefficients are referred to as nominal π and T circuits of a transmission line to distinguish from the exact Taylor-series representation in Eqs. (3.29) and (3.30). For extremely short lines typical values of \hat{Z} and \hat{Z}' are very different ($\hat{Z} \cong 10 \Omega$, $\hat{Z}' \cong 50,000\Omega$), which allows one to neglect \hat{Z}' further. This results in the simplest model of transmission lines given in Figure 3.7.

3.2.3 Bus-Connected Equipment with Established Models of Uniform Type

The equipment discussed here is of well-established and quite uniform design, although the numerical values of the various parameters have no standardization. This feature makes power systems more challenging than telephone networks, for instance, in which standardized individual units number in the millions. Generators dominate in this class and will be discussed in the first subsection following.

3.2.3.1 Synchronous Machines The synchronous generators (blocks 1, 2, 3 in Figures 3.2 and 3.3) represent the most crucial and one of the most complex elements of the power system. Their overall dynamics involve the full scale of energy-storing elements from mechanical masses to electric and magnetic fields, all driven by a prime mover, normally a turbine and under direct primary control [6,7]. In this section the machine itself will be treated.

The dynamics separate to a certain extent into an electromechanical (block 1) and an electromagnetic (block 3) segment, which are, however, closely connected by a set of instantaneous relationships expressed as algebraic equations in block

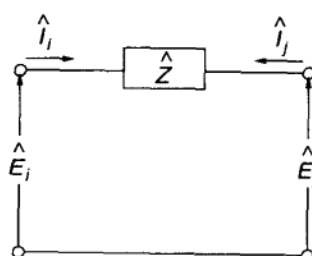


FIGURE 3.7 Nominal representation of a short line.

2. The turbine-governor (block 11) and exciter (block 12) provide direct primary controls, but they are of varying design and will be treated in Section 3.2.4.

3.2.3.2 Electromechanical Dynamics: The Shaft Power Balance Clearly the shaft power P_{Ti} coming in from the turbine (block 1, Figs. 3.2 and 3.3) must be divided among

1. The generator power injection, P_{Gi} , into bus i
2. The accumulating kinetic energy in the rotor inertia (turbine plus generator), J_i
3. The losses in the generator are represented as “viscous” damping D_i . For generator i

$$P_{Ti} = J_i \ddot{\theta}_i + D_i \dot{\theta}_i + P_{Gi} \quad (3.46)$$

Also, the following coupling equation connects the bus and generator side models (further discussed in Sec. 3.2.3.6):

$$P_{Gi} = E_i i_i \cos \varphi_i = e_{di} i_{di} + e_{qi} i_{qi} \quad (3.47)$$

assuming that $E_i \angle \delta_i$ is the terminal (bus) voltage, θ_i is the rotor phase angle (relative to synchronous reference), $i_i \angle (\delta_i - \varphi_i)$ is the generator current injection into the bus and e_{di} , i_{di} , and i_{qi} , e_{qi} are the Blondel components to be introduced next. These are the equations recorded in block 1 of Figure 3.3.

3.2.3.3 Electromagnetic Dynamics The electromagnetic dynamic model of the generator is a complex large-scale system that is very interesting and challenging (boxes 1 to 3, Fig. 3.3). It also is a classical model that was studied early in the century in classical developments by Blondel [8], Park [9], Concordia [10] and more recently by Woodson and White [6], Fitzgerald and coworkers [7], Willems [11] Verghese [12], and others.

Because of its complexity, importance, and interest, a two-stage approach (Parts A and B) is used in this text to introduce electromagnetic dynamics.

- A. An intuitive physical explanation introduces the basic concepts and basic mathematical formulations suitable for short-circuit computations.
- B. A precise mathematical treatment expands this into a general dynamic model formulation that is meant to be the foundation and starting point for solving nonlinear power-system problems.

This kind of a two-stage approach, which assures the reader of having the source material needed to make realistic and precise progress, is used also in other places of this text such as Chapters 7 and 8 for introducing large-system dynamics.

Before getting into Parts A and B, some general introductory material concerning principles of synchronous machine operation is presented. Since most electric power is generated, and in the case of large blocks consumed, as 3 phase

power, there are ordinarily three types of armature coils that are disposed and distributed around the stator to produce sinusoidally distributed magnetic excitation at 120° intervals.

A field structure rotates within a stator that supports and provides a magnetic flux path for armature windings. The exciting magnetic field is produced by a set of coils (the field winding) on the moving element or rotor.

A damper winding, amortisseur, usually consists of a set of copper or brass conductors placed in slots on the pole face and connected together at the ends of the machine. Its function is to permit the starting of a synchronous machine as an induction motor using the damper winding, which is equivalent to the squirrel cage of an induction motor rotor, and to assist in damping rotor oscillations.

The machine is ordinarily connected to a 3ϕ bus which is also being supplied by other synchronous machines, all running synchronously although with varying phase displacements. They are kept running in this condition by the electromagnetic forces in the machine under normal circumstances, as will be established in this chapter.

In the following Part A we describe the basics of physical processes in a synchronous machine. This is followed by a precise derivation of a synchronous machine model in Part B.

NOTATIONS

- \hat{i} Complex-valued current in p.u.
- \hat{E} Complex-valued phase voltage in p.u.
- \hat{Z} Complex-valued impedance in p.u.
- $\hat{S} = P + jQ$ Complex-valued 3ϕ power in p.u.
- $\hat{\psi}$ Complex-valued flux linkage in p.u.
- e_f Field excitation in p.u.
- i_f Field current in p.u.
- φ Flux in p.u.

The work in this book will typically be done in a normalized notation with per unit (p.u.) quantities expressed as ratios of the actual to base values, p.u. = (actual value)/(base value). The p.u. approach is commonly used in the literature and is discussed in ample detail in Ref. [4]. It depends on a well-reasoned set of references such that, for example, the base excitation current, its magnetomotive force and the magnetic field excited by the current, the magnetic flux linkage to armature coils, and the voltage induced by the current all have the same numerical values per unit in normal steady-state conditions. This is very useful because it eliminates messy coefficients from the equations. For the synchronous machines the following set of bases applies.

ORIGINAL BASE VALUES

- Base power kVA(3ϕ)
- Base voltage kV (line-neutral)

DERIVED BASE VALUES

$$\text{Base current } A = \frac{\text{Base power}}{3 \times (\text{Base voltage})}$$

$$\text{Base impedance } \Omega = \frac{\text{Base voltage}}{\text{Base current}}$$

GENERALIZATION

Base exciting current = Base magnetomotive force (mmf)

Base flux = The flux that induces the base voltage in the machine

Base damping current = k_T Base mmf

BASIC EQUATIONS IN P.U.

$$\hat{i} = \frac{\hat{E}}{\hat{Z}} \quad (3.48)$$

$$\hat{S} = P + jQ = \hat{E}\hat{i}^* \quad (3.49)$$

$$\psi = E, \quad \hat{\psi} = j\hat{E} \quad (3.50)$$

$$i_f = e_f \quad (3.51)$$

The values of the corresponding excitation (mmf), flux, and voltage are numerically equal in this p.u. system. Remember, however, that the same equations written in the proper physical units will also give the correct result if the appropriate proportionality constants are included [4].

Next, in Section 3.2.3.4 (Part A) a detailed intuitive physical analysis of a synchronous machine will be offered to help the reader to develop a clear conceptual picture of the numerous concepts and phenomena that play a role in the dynamics of the synchronous machine. Precise and straightforward mathematical modeling of relations for general synchronous machine dynamics will be offered in Section 3.2.3.5 (Part B).

3.2.3.4 Part A: Basics of Physical Processes in a Synchronous Machine

There are two alternative ways to describe a three-phase current or voltage:^{*}

1. Three rotating vectors 120° out of phase plus one stationary reference direction.
2. One rotating vector plus three stationary reference axes 120° out of phase.

A sketch of this is shown in Figure 3.8.

^{*} Note that in this section voltages and currents are represented by their amplitude and phase but *not* in the sense of phasors as defined in Chapter 2.

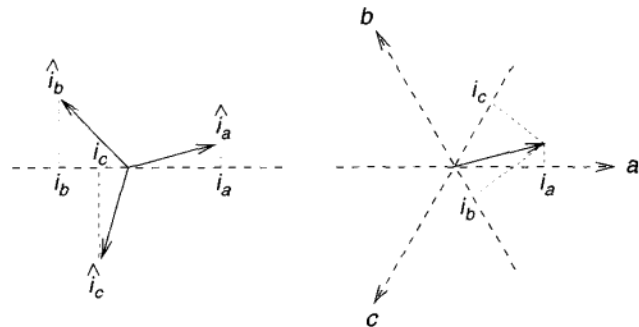


FIGURE 3.8 Two conceptually different ways of representing 3ϕ variables.

The second description has special significance in the case of synchronous machines in which there are actually three stationary phase coils sinusoidally distributed along the periphery on the armature, which represent three stationary reference directions. The three phase voltages are induced in three coils by one flux which is rotating at a synchronous speed with the rotor. Consequently, the three phase voltages can be interpreted as properties of one rotating flux¹ vector to the reference axes of the three phase coils. Similarly, the armature currents may be represented as the projections of a single current (or voltage) vector.

These considerations allow for representation of a three-phase machine with a single-vector diagram. Note that this is a different unified phase than arbitrarily picking one phase (usually phase a) to stand for the others.

This becomes further clarified if one ties these currents directly to the machine, rather than talking about the phasor diagram. More precisely, one may connect the phasor diagram to the machine, as shown in Figure 3.9. No saturation or

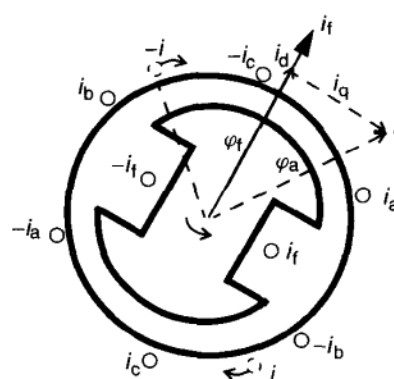


FIGURE 3.9 Single-vector-phasor diagram connected to the machine.

¹ Or voltage, since this is the same in the p.u. system introduced.

harmonics and a quasistationary operating regime are assumed, so the field-voltage relations are linear and superposition holds. The three armature coils are sinusoidally distributed along the periphery of the armature, displaced physically 120° . In Figure 3.9 the three phase coils i_a , i_b and i_c are replaced by a single virtual coil i (symbolized by the dashed circles in Fig. 3.9) which is stationary with respect to the vector, favoring a stationary representation of the generator in the $d - q$ coordinate system.

Note that the i vector rotates at velocity ω , and the rotor also rotates at the same velocity in electric degrees. Hence vector φ_f , representing the magnetic field excited by current i_f flowing in the de facto rotating field winding, and i , the equivalent rotating armature current vector, with its flux φ_a , will rotate synchronously. It is also known that the three-phase armature currents in the armature winding will create a sinusoidally distributed magnetomotive force (mmf) or magnetic field intensity (numerically equal in p.u.) that rotates at synchronous velocity and hence is stationary with respect to the rotor in Figure 3.9. It is then reasonable for analytical purposes to attribute the armature mmf to a single equivalent armature winding that carries current i and rotates synchronously with the rotor.²

In this view, the entire synchronous machine is reduced to equivalent coils and fields, all rotating synchronously. The entire machine in a sense is viewed from the rotor.

This $d - q$ system is static as long as the system is in a static condition. The static field current (represented by a vector i_f - not a phasor, in the sense of Chapters 2 and 11) identifies the size and the direction of the flux φ_f which it generates along the d axis. The equivalent, armature current i can also be decomposed into an i_d and i_q component respectively, which will produce their own field components φ_{ad} and φ_{aq} directed as shown by i_d and i_q .

Nothing is moving in this $d - q$ system during static system operation, so no induction is directly indicated in the $d - q$ space.

While we are talking about vectors here to identify direction and size of some quantities these are not, however, phasors in the $\hat{i} = ie^{j\omega t}$ sense as defined in Chapters 2 and 11. A transformation (the Blondel matrix) between these two will be established within the $d - q$ system, which is static, the stator is actually rotating backwards at a speed of $-\omega$. This rotation then causes any flux φ_{ad} and φ_{aq} components crossing the airgap to induce a voltage e_{ad} , e_{aq} etc in the actual coils a , b and c . These induced voltages are of the $e^{j\omega t}$ type and accordingly representable by conventional phasors are shown in this sense in Figure 3.10. The airgap then separates relations which fit well the circuit analysis on the network linking the buses, and the $d - q$ type of the static condition but also become dynamic in situations like short circuits on the bus side.

It is then further reasonable to decompose the armature current phasor i into its direct and quadrature components, one in phase with φ_f and the other 90° out of phase (see Figs 3.9 and 3.10). The equivalent armature coil then can also be

² Details on this simplification can be found in papers of Park and Concordia [9], [10].

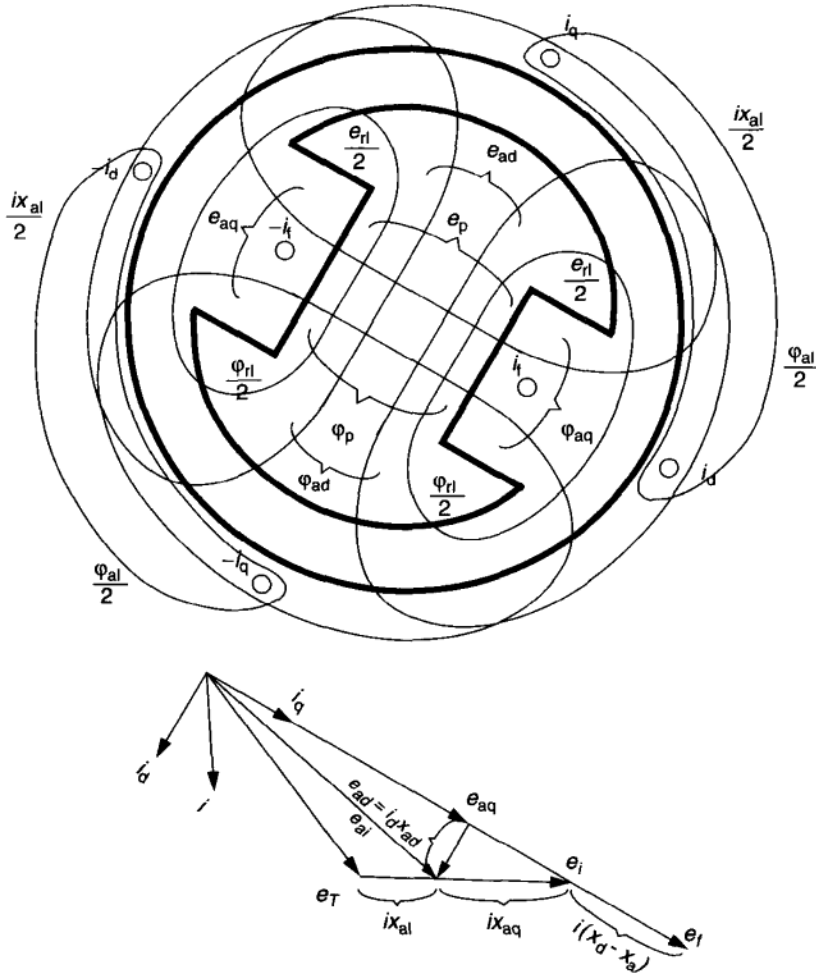


FIGURE 3.10 Components of the fluxes (or voltages in p.u.) in a machine without rotor damping.

decomposed into two such coils. Figure 3.10 displays in more detail the reference axes, currents, and voltages of a synchronous machine. Here subscript rl stands for rotor leakage, and subscript al for armature leakage.

Adding to the terminal (bus) voltage e_T the voltage drop $x_{ai}i$ corresponding to the armature leakage flux, the e_{ai} (so called air-gap voltage) may be determined. This is the voltage actually induced in the armature winding by the total flux φ_{ai} that penetrates the air gap. This flux may be decomposed (after neglecting saturation) into the direct-axis φ_d and quadrature-axis φ_q components. Since there is no excitation on the rotor in the quadrature axis, the quadrature-axis component of the air-gap flux will be determined entirely by the quadrature-axis component of the armature current, and consequently, it will be proportional to it, that is,

$$\varphi_q = x_{aq}i_q \quad (3.52)$$

The direct-axis component, on the other hand, is determined by the joint excitation of the field current and the direct-axis armature current

$$\varphi_d = i_f + x_{ad}i_d \quad (3.53)$$

Note that the proportionality factor between field current and flux is unity due to the way the p.u. system is selected. The same does *not* apply between armature current and flux since the base armature current was not defined with respect to the flux determined by it. Also, for salient pole machines

$$x_{aq} \leq x_{ad} \quad (3.54)$$

since the air gap is much larger in the quadrature axis. The excitation current i_f has the phase of the direct axis, of course. The field leakage flux φ_f is determined by the field excitation only; consequently

$$\varphi_f = k_i i_f \quad (3.55)$$

Adding the field leakage flux φ_{dl} to the direct-axis component of the air-gap flux, φ_d , the total pole flux in the direct axis φ_p may be determined:

$$\varphi_p = \varphi_d + k_i i_f \quad (3.56)$$

Owing to the way the p.u. system was related,

$$\varphi_{ai} = e_{ai} \quad (3.57)$$

that is, the air-gap flux is numerically equal to the voltage induced by it, at the bus and consequently, the flux and voltage are represented by vectors of equal lengths and 90° phase difference in Figure 3.10. The same applies to the components:

$$\varphi_d = e_q \quad (3.58)$$

$$\varphi_q = e_d \quad (3.59)$$

Similarly, one may attribute a voltage to the total pole flux:

$$\varphi_p = e_p \quad (3.60)$$

where e_p is the pole voltage due to the excitation i_f .³

Note: Remember that we are talking about the $d - q$ space here and not of complex-valued phasors. Furthermore the type of induction for e_q and e_d (second type, Part B) depends on the cutting of the flux lines rather than on the changing of

³ This is numerically the same with e_f in p.u. system.

the flux itself. In this type of induction the peaks of the exciting current, the flux and the induced voltage are all reached simultaneously (their vectors φ_d , φ_q and e_d , e_q are lined up in parallel-rather than with a 90° difference) as shown in Figures 3.9 and 3.10. Note that Eqn. (3.60) and others imply induction of the 1st kind with the customary 90° phase shift in the vector diagrams (no j in $d - q$ coordinates).

It must be observed, however, that neither e_p nor e_f are actual voltages. Both are fictitious. e_p represents the voltage that would be induced by the pole flux (which does not penetrate the armature winding actually) in the armature. e_f represents the voltage that would be induced in the armature by the excitation i_f with no current in the armature and without saturation. Since in this p.u. system the flux and (type 1 induced) voltage parts of the vector diagram are identical in dimensions and out of phase 90° , it is usually sufficient to indicate only the voltage part as is shown in Figure 3.11. Note also that in this figure yet another fictitious voltage is included, e_i . This is fictitious in an even larger sense than is e_p or e_f . Namely, e_p is the equivalent of an actually existing excitation. However, e_i is defined by an accidental point of intersection in the $d - q$ vector diagram of Figure 3.11, which has no physical voltage, flux, or excitation associated with it. Still, in the vector diagram e_i appears as some kind of electromotive force, and consequently it is sometimes convenient to use it as such. It should not be forgotten that it is only an ancillary calculated quantity without physical existence.

Balanced Short Circuit of an Alternator without a Damper Winding When a short circuit appears that is a dynamic change which will directly involve the changing of φ_p which was taken to be constant up to this point. The study of the transient short circuits of synchronous machines is based in many respects on the principle of constant-flux linkages [6]. This, as is well known, states that whatever

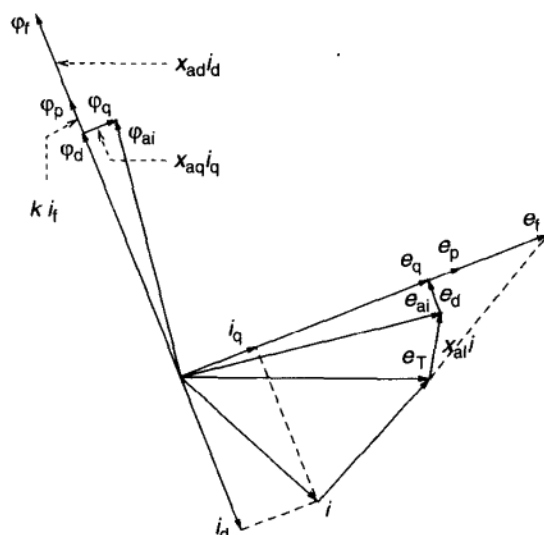


FIGURE 3.11 Relative position and sizes of flux and voltage diagrams.

change happens in an electromagnetic circuit the flux linkages immediately before and after change will be the same.

For example, consider a DC circuit shown in Figure 3.12 without leakage fields.⁴ In the steady state there will be a constant current in coil 1 and no current in coil 2 if both switches are closed. By opening S_1 current i_1 drops to 0, but then a current starts of equal flux linkage, that is, equal magnitude in coil 2 if coils 1 and 2 are equal so that the amount of flux linkages remains the same.

Current i_2 will flow with unchanged magnitude indefinitely if there is no resistance in the circuit of coil 2 (shown in Fig. 3.13). Actually, there will be resistance in the coil 2 circuit and consequently current i_2 will die down with the time constant of that circuit.

Now, applying the same principle to a sudden symmetrical short circuit at the terminals of a synchronous machine without a damper winding, an almost purely inductive current will start in the rotor excitation winding, which will have only a direct-axis component. This means that a new excitation suddenly appears in the direct axis to maintain the flux linkages at a constant value. This additional excitation in i_d has to be counterbalanced by a sudden increase in the excitation current, as may be observed in Figure 3.14.

This transient addition to the nominal excitation current i_{f0} dies down with time constant T'_d , the so-called transient time constant. Simultaneously, the armature

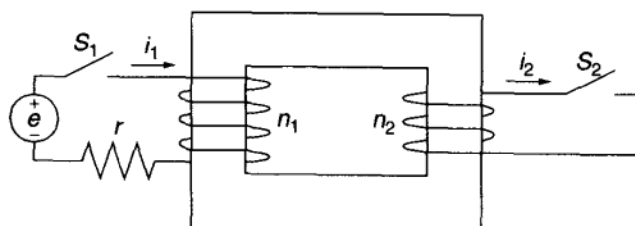


FIGURE 3.12 Principle of constant-flux linkages.

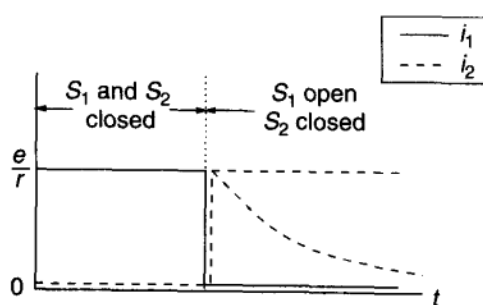


FIGURE 3.13 Current response to closing switch S_1 .

⁴ Leakage fields are fields that couple with only one or the other coil.

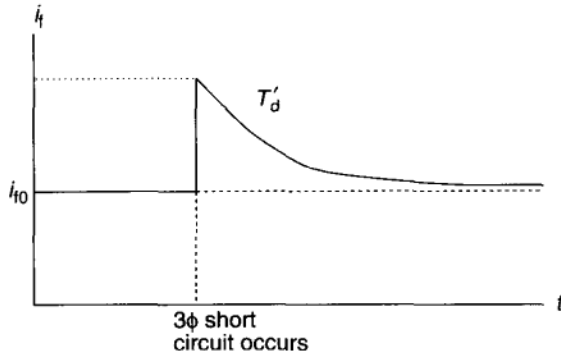


FIGURE 3.14 Field excitation under short-circuit conditions.

short circuit current will die down from its initial transient value i'_d to the steady-state short-circuit current i_d . Clearly, T'_d is determined by the resistance of the excitation circuit. When the machine is short-circuited at the terminals, all the voltage induced in the armature will be consumed as a voltage drop on the armature leakage reactance (neglecting the resistance of the armature). That is,

$$e_d = \varphi_d = i_d x_{al} \quad (3.61)$$

during the steady-state short circuit, and

$$e'_d = \varphi'_d = i'_d x_{al} \quad (3.62)$$

during the initial transient short circuit. Using Eq. (3.53)

$$\begin{aligned} i_d x_{al} &= i_{f0} - i_d x_{ad} \\ i'_d x_{al} &= i_f - i'_d x_{ad} \end{aligned} \quad (3.63)$$

Dividing the two equations by each other,

$$\frac{i_f}{i_{f0}} = \frac{i'_d}{i_d} \quad (3.64)$$

Consider next what happens to the different components of the flux in the case where a sudden short circuit is applied to the machine. Since each of the three flux components has linkages with some kind of closed circuit, each will be of the same magnitude immediately after the fault as immediately before.

Because the eddy-current paths in the laminated iron have practically zero time constant, the flux components that are only linked with such eddy-current paths, that is, the armature leakage flux φ_{al} and quadrature-axis flux φ_q , will die down or will follow the changes of the armature current instantaneously. On the other hand, the field winding has a large time constant (2 sec to 10 sec). Consequently,

the flux φ_p , which is linked with the field winding, will be unchanged after the short circuit and will change only relatively slowly.

Recall next that φ_p has two components,⁵ φ_d and φ_f . Of the two, φ_f is excited by i_f only [recall Eq. (3.55)], while φ_d is excited by the joint effect of i_f and i_d [Eq. (3.53)]. When a short circuit occurs both i_f and i_d are changed and consequently part of the flux φ_d will be shifted to the path of φ_f , which changes from ki_{f0} to ki_f .

Next these considerations will be applied to the case when a machine runs at no load and is suddenly short circuited at the terminals.

Short Circuit under No Load The vector diagram shown in Figure 3.15 is plotted for the voltages rather than the flux. As was shown in the p.u. system, $e_p = \varphi_p$, $e_d = \varphi_d$, and $e_f = \varphi_f$.

Immediately before the short circuit,

$$i_0 = 0 \quad (3.65)$$

$$e_{d0} = i_{f0} = e_T \quad (3.66)$$

$$e_p = e_{d0} + ki_{f0} \quad (3.67)$$

Immediately after the short circuit,

$$i = i'_d \quad (3.68)$$

$$i_f = e'_d + i'_d x_{ad} \quad (3.69)$$

$$e'_d = e_p - ki_f \quad (3.70)$$

$$e'_d = i'_d x_{al} \quad (3.71)$$

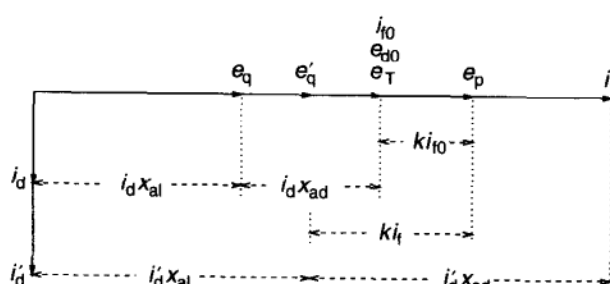


FIGURE 3.15 No-load conditions before short circuit.

⁵ Even though their sum must remain unchanged, initially the two components can undergo changes that compensate each other. This is because outside the field winding where the two components unite, neither has linkages with any closed coil (without a damper winding).

Finally, steady-state short-circuit conditions are defined:

$$i = i_d \quad (3.72)$$

$$i_{f0} = e_q + i_d x_{ad} \quad (3.73)$$

$$e_q = i_d x_{al} \quad (3.74)$$

From Eqs. (3.73) to (3.74) one obtains

$$i_{f0} = i_d(x_{ad} + x_{al}) \quad (3.75)$$

Define next a synchronous reactance

$$x_d = x_{al} + x_{ad} \quad (3.76)$$

then the steady-state short circuit current takes on the form

$$i_d = \frac{i_{f0}}{x_d} = \frac{e_T}{x_d} \quad (3.77)$$

From Eqs. (3.69) to (3.71) and (3.67) it follows that

$$i'_d x_{al} = e_{d0} + k i_{f0} - k e_d' + k i'_d x_{ad} \quad (3.78)$$

with Eqs. (3.66) and (3.71) gives

$$i'_d x_{al} = e_T + k e_T - k x_{al} i'_d - k i'_d x_{ad} \quad (3.79)$$

or

$$i'_d \left(x_{al} + \frac{k}{k+1} x_{ad} \right) = e_T \quad (3.80)$$

Defining next the transient reactance

$$x'_d = x_{al} + \frac{k}{k+1} x_{ad} \quad (3.81)$$

the transient short-circuit current is

$$i'_d = \frac{e_T}{x'_d} = \frac{e_0}{x'_d} \quad (3.82)$$

Pure Inductive Load before Short Circuit Derivations analogous to the no-load conditions lead to the following relations.

Immediately before the short circuit,

$$i = i_{d0} \quad (3.83)$$

$$i_{f0} = e_T + i_{d0}(x_{al} + x_{ad}) \quad (3.84)$$

$$e_{d0} = e_T + i_{d0}x_{al} \quad (3.85)$$

$$e_p = e_{d0} + k_i i_{f0} \quad (3.86)$$

Immediately after the short circuit,

$$i = i'_d \quad (3.87)$$

$$i_f = e'_d + i'_d x_{ad} \quad (3.88)$$

$$e'_d = e_p - k_i i_f \quad (3.89)$$

$$e'_d = i'_d x_{al} \quad (3.90)$$

Steady-state short-circuit conditions are defined:

$$i = i_d \quad (3.91)$$

$$i_{f0} = e_q + i_d x_{ad} \quad (3.92)$$

$$e_q = i_d x_{al} \quad (3.93)$$

A vector diagram representing these relations is shown in Figure 3.16. From Eqs. (3.92) and (3.93)

$$i_{f0} = i_d(x_{ad} + x_{al}) \quad (3.94)$$

and Eq. (3.84) one obtains

$$i_d = \frac{i_{f0}}{x_d} = \frac{e_T + x_d i_{d0}}{x_d} \quad (3.95)$$

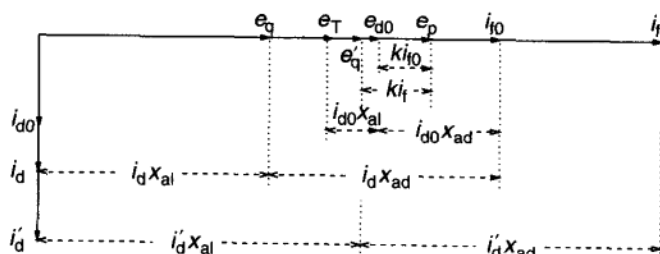


FIGURE 3.16 Short-circuit current vector diagram in the case of a purely inductive load.

From Eqs. (3.88) to (3.90) and (3.86)

$$i'_d x_{al} = e_T + i_{d0}x_{al} + k e_T + k i_{d0}x_{al} + k i_{d0}x_{ad} - k i'_d x_{al} - k i'_d x_{ad} \quad (3.96)$$

rearranging further into

$$i_d' \left(x_{al} + \frac{k}{1+k} x_{ad} \right) = e_T + i_{d0} \left(x_{al} + \frac{k}{1+k} x_{ad} \right) \quad (3.97)$$

and a familiar form

$$i'_d = \frac{e_T + i_{d0}x'_d}{x'_d} \quad (3.98)$$

General Load before Short Circuit The following relations are used for deriving short-circuit currents in a general case.

Immediately before the short circuit (see Fig. 3.17),

$$i = i_0 \quad (3.99)$$

$$i_{f0} = e_T + i_{q0}(x_{al} + x_{aq}) + i_{d0}(x_{al} + x_{ad}) \quad (3.100)$$

$$e_{d0} = e_T + i_{q0}(x_{al} + x_{aq}) + i_{d0}x_{al} \quad (3.101)$$

$$e_p = e_{d0} + k i_{f0} \quad (3.102)$$

Immediately after the short circuit,

$$i = i'_d \quad (3.103)$$

$$i_f = e'_d + i'_d x_{ad} \quad (3.104)$$

$$e'_d = e_d - k i_f \quad (3.105)$$

$$e'_d = i'_d x_a] \quad (3.106)$$

Steady-state short-circuit conditions are defined:

$$i = i_d \quad (3.107)$$

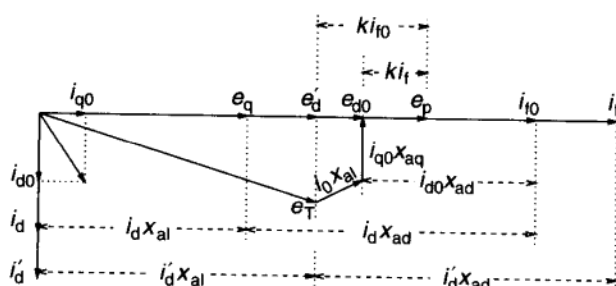


FIGURE 3.17 Short circuit during a general loading condition

$$i_{f0} = e_g + i_d x_{ad} \quad (3.108)$$

$$e_q = i_d x_{al} \quad (3.109)$$

Using these relations, and following similar algebraic steps as for a purely inductive load,

$$i_d = \frac{e_T + i_{q0}x_q + i_d x_d}{x_d} \quad (3.110)$$

and

$$i'_d = \frac{e_T + i_{q0}x_q + i_{d0}x'_d}{x'_d} \quad (3.111)$$

This means that the initial transient short-circuit current if the machine was loaded by current $i_0 = i_{d0} + j i_{q0}$ before the short circuit occurred is

$$i'_d = \frac{e_T + i_{q0}x_q + i_{d0}x'_d}{x'_d} \quad (3.112)$$

Similarly, the steady-state short-circuit current is

$$i_d = \frac{i_{f0}}{x_{al} + x_{ad}} = \frac{e_T + i_{q0}x_q + i_{d0}x_d}{x_d} \quad (3.113)$$

The following equations [Eqs. (3.114) to (3.116)] determine the initial value of the transient short-circuit current for synchronous machines without a damper winding. For the cases immediately before the fault the machine was unloaded [Eq. (3.114)], loaded by a pure inductor current [Eq. (3.115)] or loaded by an arbitrary current [Eq. (3.116)]:

$$i'_d = \frac{e_T}{x'_d} \quad (3.114)$$

$$i'_d = \frac{e_T + i_{d0}x'_d}{x'_d} = \frac{e'_d}{x'_d} \quad (3.115)$$

$$i''_d = \frac{e_T + i_{q0}x_q + i_{d0}x'_d}{x'_d} = \frac{e'_d}{x'_d} \quad (3.116)$$

These equations are represented by the vector diagrams shown in Figure 3.18. Common characteristics of Eqs. (3.114) to (3.116) are that all three determine the initial transient current as the ratio of a voltage and the transient reactance x'_d . The voltage values in these equations deserve more discussion.

The voltage in the numerator of Eq. (3.114) (short circuit, no load) is just the terminal voltage before the short circuit. The voltage in the denominator of Eq. (3.115) is a voltage

$$e'_d = e_T + i_{d0}x'_d \quad (3.117)$$

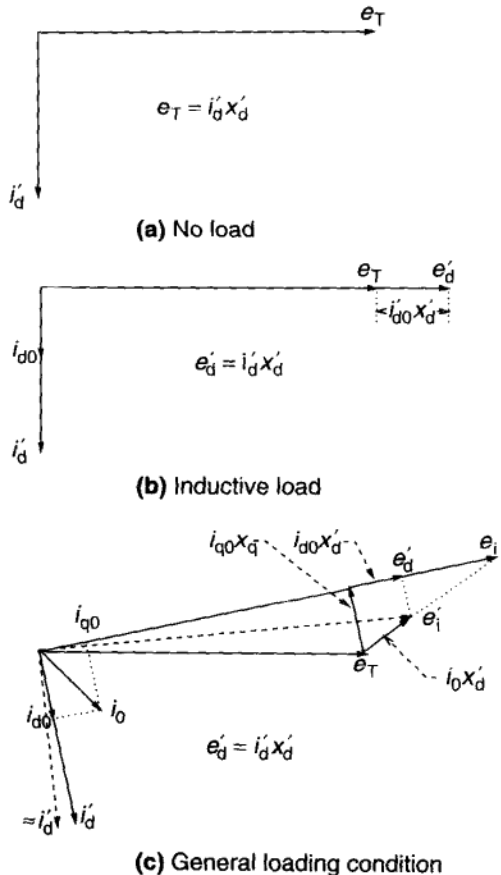


FIGURE 3.18 Initial transient short-circuit currents.

that is, a voltage composed of the terminal voltage previous to the fault and the voltage drop on the transient reactance due to the purely inductive current previous to the fault. This would be then a voltage behind the transient reactance previous to the fault (observe the same in Fig. 3.18).

Finally, the e_d' voltage defined by Eq. (3.116) and Figure 3.18 is the projection to the direct axis of voltage e_i' , that is the voltage behind the transient reactance previous to the fault. The magnitudes of e_i' and e_d' will not be significantly different. Consequently,

$$i_d' \approx \frac{e_i'}{x_d'} \quad (3.118)$$

is a fair approximation as far as the magnitude of the short-circuit current is concerned. As apparent from Figure 3.18, the *phases* of the currents i_d' and this approximation are considerably different. Since, however, in most short-circuit

calculations the phase angle is of secondary importance, it is customary to calculate the initial transient short-circuit current by the equation

$$i'_d = \frac{e'_i}{x'_d} \quad (3.119)$$

The voltage behind the transient reactance previous to the fault according to Figure 3.18 is

$$e'_i = e_T + i_0 x'_d \quad (3.120)$$

where i_0 is the load current before the short circuit. Equations (3.119) and (3.120) include both Eqs. (3.114) and (3.116) as special cases. This leads to the equivalent circuit for the synchronous machine with respect to the instantaneous transient short-circuit current shown in Figure 3.19. This equivalent circuit is often used, but it should not be forgotten that Eq. (3.119) just happens to be in the convenient form of Ohm's law. However, the "transient impedance", x'_d , is not actually a physical impedance but only an expression with the dimension of an impedance composed of the different machine constants. Consequently, the "voltage behind the transient reactance" e'_i is not a real physical voltage either, only a calculated quantity. Besides, e'_i is merely an approximation to replace the accurate, but also fictitious voltage e'_d . The switch transient current i_q in Eqn. (3.119) is a good approximation of the real physical initial short circuit current computed through a convenient line of artificial concepts.

The steady-state short-circuit current is given by Eqs. (3.77), (3.95), and (3.113) in the form

$$i_d = \frac{i_{f0}}{x_d} = \frac{e_T}{x_d} \quad (3.121)$$

that is, the ratio of the excitation voltage, or voltage behind the synchronous reactance e_T before the fault to the synchronous reactance x_d . Equations (3.119) to (3.121) determine the magnitude of the initial transient current and the final steady-state current. Naturally, the transition from the initial to the final state has to be determined also.

Consequently, the general layout of the electromagnetic circuits of the excitation and armature direct-axis coils of a machine when short circuited at the armature terminals is shown in Figure 3.20. As observed from this figure, the

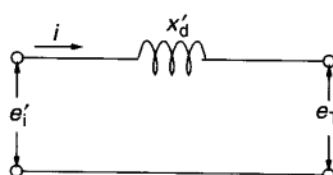


FIGURE 3.19 Simple equivalent circuit.

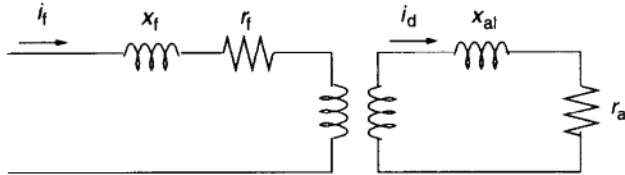


FIGURE 3.20 Conceptual layout under armature short-circuit conditions.

field-coil excitation e_f and the armature-coil current i_d are linked by the flux φ_d in much the same way as the primary and secondary windings of a transformer.

As anyone familiar with transients in electromagnetic circuits may see, this is an oscillatory circuit that has two time constants. However, if the resistance in the stator windings $r_a \ll r_f$ these two time constants will not be very different from each other and if $r_a = 0$ there will be only one time constant

$$T'_d = \frac{L_{f \text{ res}}}{r_f} \quad (3.122)$$

where $L_{f \text{ res}}$ is the resulting inductance of the whole field circuit as seen from the field winding. When the machine is short-circuited at the terminals, all magnetic fields within the machine derive entirely from the field current. Consequently, the resulting self-inductance $L_{f \text{ res}}$ as referred to previously can be calculated as the ratio of the total pole flux φ_p and the field current i_f , that is,

$$L_{f \text{ res}} = \frac{\varphi_p}{i_f} \quad (3.123)$$

This inductance can be expressed in the p.u. system adopted here by utilizing Eqs. (3.56), (3.53), and (3.55),

$$\varphi_p = i_f - x_{ad}i'_d + k_i f \quad (3.124)$$

and with Eq. (3.121)

$$i'_d = \frac{i_f}{x_d} = \frac{i_f}{x_{al} + x_{ad}} \quad (3.125)$$

or

$$\varphi_p = i_f \left(1 + k - \frac{x_{ad}}{x_{al} + x_{ad}} \right) \quad (3.126)$$

or with Eq. (3.85)

$$L_{f \text{ res}} = 1 + k - \frac{x_{ad}}{x_{al} + x_{ad}} \quad (3.127)$$

and with Eq. (3.121)

$$\begin{aligned} T'_d &= \frac{1+k}{r_f} \left(1 - \frac{x_{ad}}{(1+k)(x_{al} + x_{ad})} \right) \\ &= \frac{1+k}{r_f} \frac{x_{al} + kx_{ad}/(1+k)}{x_{al} + x_{ad}} = \frac{1+k}{r_f} \frac{x'_d}{x_d} \end{aligned} \quad (3.128)$$

If the armature is open-circuited

$$i_d = 0 \quad (3.129)$$

and using this instead of Eq. (3.125) becomes

$$T'_{d0} = \frac{1+k}{r_f} \quad (3.130)$$

with Eqs. (3.128) and (3.130), one obtains

$$T'_d = T'_{d0} \frac{x'_d}{x_d} \quad (3.131)$$

T'_{d0} is the time constant of the field winding with open-circuited armature winding. This can be measured, or calculated, from the design data easily. The time constant of the transient short-circuit current can be calculated from Eq. (3.131). Consequently, the three-phase short-circuit current of a synchronous alternator without damper winding may be expressed as

$$i_{sc} = (i'_d - i_d)e^{-t/T'_d} + i_d \quad (3.132)$$

where i_d , i'_d , and T'_d are determined by Eqs. (3.121), (3.119), and (3.131). It should be noted that Eq. (3.132) applies only to the base-frequency AC short-circuit current of round-rotor machines.

Subtransient Reactance: Effects of a Damper Winding Consider one additional circuit on the rotor, a damper circuit as shown in Fig. 3.21 represented by a simple circuit. No direct source of current is included in this closed circuit. It is however inductively tied to the excitation coil. This tie may result in a current i_r (for rotor damper winding) in a dynamic situation, like a short circuit. In static situation when $i_f = \text{const}$ there will be $i_r = 0$. An appropriate base for i_r to be measured in p.u. will be established later. This simple representation will be used

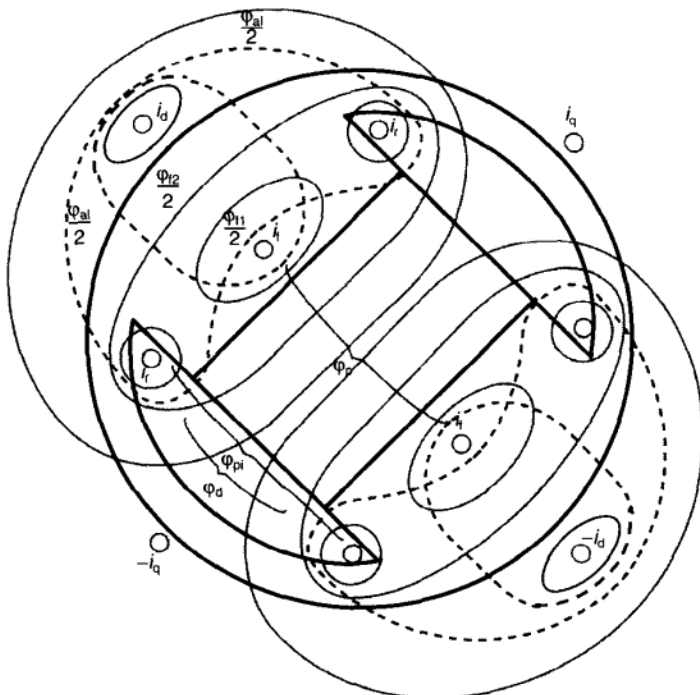


FIGURE 3.21 Conceptual sketch of relative positions of fluxes of various coils, indicated as single loops.

here to introduce the concepts of subtransient short circuit current component and of subtransient reactance.⁶

Under this model the pole flux is jointly determined by currents in the main excitation winding, i_f , the damper winding i_r and the direct axis armature winding i_{ad} like

$$\varphi_d = i_f + i_r - i_{ad}x_{ad} \quad (3.133)$$

and

$$\varphi_{f1} = k_1(i_f + i_r) \quad (3.134)$$

$$\varphi_{f2} = k_2 i_f$$

$$\varphi_I = k_r i_r$$

$$k_1 + k_2 = k \quad (3.135)$$

⁶ The actual damper winding is either a squirrel-cage type embedded in the laminated steel rotor surface in salient pole machines, or simply the eddy currents in solid steel bodies of round-rotor machines. In either case, a multiplicity of frequencies is present dynamically, but these always fall in a narrow band so that a single average circuit approximation is justified. This was recognized in the early literature [10, 12].

The fluxes $\varphi_{al} = k_{al}(i_r - i_d)$ and $\varphi_{af} = k_{af}(i_f - i_d)$ will be relatively small and could be neglected in order to simplify the calculation. Immediately before the short circuit $i_r = 0$, assume a purely inductive load i_{d0} . Then

$$\begin{aligned}\varphi_{p0} &= \varphi_{d0} + \varphi_{f10} + \varphi_{f20} + \varphi_{af0} \\ &= i_{f0} - i_{d0}x_{ad} + i_{f0}(k_1 + k_2) + (i_{f0} - i_{d0})k_{af}\end{aligned}\quad (3.136)$$

and

$$\begin{aligned}\varphi_{pl0} &= \varphi_{d0} + \varphi_{f10} + \varphi_{f10} + \varphi_{al0} \\ &= i_{f0} - i_{d0}x_{ad} + i_{f0}k_1 - i_{d0}k_{af}\end{aligned}\quad (3.137)$$

Immediately after the short circuit

$$\begin{aligned}\varphi_p &= \varphi_d + \varphi_{f1} + \varphi_{f2} + \varphi_{af} \\ &= i_f + i_r - i_d''x_{ad} + (i_f + i_r)k_1 + i_fk_2 + (i_f - i_d'')k_{af}\end{aligned}\quad (3.138)$$

and

$$\begin{aligned}\varphi_{pl} &= \varphi_d + \varphi_{f1} + \varphi_I + \varphi_{al} \\ &= i_f + i_r - i_d''x_{ad} + k_1(i_f + i_r) + k_r i_r + k_{al}(i_r - i_d'')\end{aligned}\quad (3.139)$$

Consequently, using the principle of constant-flux linkages,

$$\begin{aligned}\varphi_{p0} &= \varphi_p \\ \varphi_{pl0} &= \varphi_{pl}\end{aligned}\quad (3.140)$$

implying further

$$\begin{aligned}i_{f0}(1 + k) - i_{d0}(x_{ad} + k_{af}) &= (i_f + i_r)(1 + k_1) \\ &\quad + i_f(k_2 + k_{af}) - i_d''(x_{ad} + k_{af})\end{aligned}\quad (3.141)$$

$$\begin{aligned}i_{f0}(1 + k_1) - i_{d0}(x_{ad} + k_{af}) &= (i_f + i_r)(1 + k_1) \\ &\quad + i_r(k_r + k_{af}) - i_d''(x_{ad} + k_{af})\end{aligned}\quad (3.142)$$

and since the machine is short-circuited at the terminals with short-circuit current i_d'' flowing,

$$e_d = \varphi_d = i_f + i_r - i_d''x_{ad} - i_d''x_{al}\quad (3.143)$$

From Eqs. (3.141) and (3.142) with $k'_2 = k_2 + k_{af}$ and $k'_r = k_r + k_{If}$

$$i_{f0} \frac{1+k}{k'_2} - i_{d0} \frac{x_{ad} + k_{af}}{k'_2} = (i_f + i_r) \frac{1+k_1}{k'_2} + i_f - i_d'' \frac{x_{ad} + k_{af}}{k'_2} \quad (3.144)$$

and

$$i_{f0} \frac{1+k_1}{k'_r} - i_{d0} \frac{x_{ad} + k_{al}}{k'_r} = (i_f + i_r) \frac{1+k_1}{k'_r} + i_r - i_d'' \frac{x_{ad} + k_{al}}{k'_r} \quad (3.145)$$

Adding the last two equations obtains

$$\begin{aligned} & i_{f0} \left(\frac{1+k}{k'_2} + \frac{1+k_1}{k'_r} \right) - i_{d0} \left(\frac{x_{ad} + k_{af}}{k'_2} + \frac{x_{ad} + k_{al}}{k'_r} \right) \\ &= (i_f + i_r) \left(\frac{1+k_1}{k'_2} + \frac{1+k_1}{k'_r} \right) + i_f + i_r \\ & \quad - i_d'' \left(\frac{x_{ad} + k_{af}}{k'_2} + \frac{x_{ad} + k_{al}}{k'_r} \right) \end{aligned} \quad (3.146)$$

or

$$\begin{aligned} & i_{f0} \frac{k'_r + k_1 k'_r + k_1 k'_2 + k'_2}{k'_2 k'_r} - i_{d0} \frac{x_{ad} k'_r + x_{ad} k'_2 + k_{al} k'_2 + k'_r k_{af}}{k'_2 k'_r} \\ &= (i_f + i_r) \left(\frac{k'_r + k'_r k_1 + k'_2 + k_1 k'_2}{k'_2 k'_r} + 1 - i_d' \frac{k'_r x_{ad} + k'_2 x_{ad} + k_2 k'_{al}}{k'_r k_{af} k_2 k_1} \right) \end{aligned} \quad (3.147)$$

or

$$\begin{aligned} & i_{f0} (k'_r + k_1 k'_r + k_1 k'_2 + k'_2) - i_{d0} [x_{ad} (k'_r + k'_2) + k_{al} k'_2 + k_{af} k'_r] \\ &= (i_f + i_r) (k'_r + k'_r k_1 + k_1 k'_2 + k'_2 + k_2 k'_r) - i_d'' (x_{ad} (k'_r + k'_2) + k_{al} k_2 + k_{af} k'_r) \end{aligned} \quad (3.148)$$

Next, with the notation

$$K_1 = k'_r + k_1 k'_r + k_1 k'_2 + k'_2 = k_r (1+k) + k_2 (1+k_1) \quad (3.149)$$

and

$$K_2 = x_{ad} (k'_r + k'_2) + k_{al} k'_2 + k_{af} k'_r \quad (3.150)$$

one obtains

$$i_{f0} K_1 - i_{d0} K_2 = (i_f + i_r) K_1 - i_d'' K_2 \quad (3.151)$$

or

$$i_f + i_r = i_{f0} - i_{d0} \frac{K_2}{K_1} + i_d'' \frac{K_2}{K_1} \quad (3.152)$$

which substituted into Eq. (3.143) gives

$$i_d'' \left(x_{al} + x_{ad} - \frac{K_2}{K_1} \right) = \left(i_{f0} - i_{d0} \frac{K_2}{K_1} \right) + i_d'' \frac{K_2}{K_1} \quad (3.153)$$

or

$$i_d'' = \frac{e_T + i_{d0}x_d''}{x_d''} \quad (3.154)$$

where

$$x_d'' = x_d - \frac{K_2}{K_1} \quad (3.155)$$

is a subtransient reactance and $(e_T + i_{d0}x_d'')$ is the voltage behind the subtransient reactance. i_d'' is the subtransient short-circuit current, and x_d'' is a subtransient reactance.

Subtransient reactance is further expressed in terms of physical machine constants

$$\begin{aligned} x_d'' &= x_d - \frac{K_2}{K_1} = x_{al} + x_{ad} - \frac{x_{ad}(k'_r + k'_2) + k_{al}k'_2 + k_{af}k'_2}{k'_r(1+k) + k'_2(1+k_1)} \\ &= x_{al} + x_{ad} \left(1 - \frac{k'_r + k'_2}{k'_r(1+k) + k'_2(1+k_1)} - \frac{k_{al}k_2 + k_{af}k'_2}{k_r(1+k) + k_2(1+k_1)} \right) \\ &\quad + x_{al} + x_{ad} \frac{kk'_r - k_1k'_2}{k'_r(1+k) + k'_2(1+k_1)} - \frac{k_{al}k'_2 + k_{af}k'_2}{k'_r(1+k) + k'_2(1+k_1)} \end{aligned} \quad (3.156)$$

Observe next that

$$\frac{kk'_r - k_1k'_2}{k'_r(1+k) + k'_2(1+k_1)} = \frac{k + k_1k_2/k_r}{1 + k + k_1k'_2/k_1 + k'_2/k'_r} \leq \frac{k}{1+k} \quad (3.157)$$

Since the order of magnitudes

$$\frac{k}{2} \approx k_1 \approx k_2 \approx k_r \approx 0.1 - 0.001 \quad (3.158)$$

this implies

$$x_d'' \leq x_d' \quad (3.159)$$

resulting in a larger subtransient short-circuit current than the transient short-circuit current.

A vector diagram representing prefault, transient, and subtransient currents is shown in Figure 3.22. The time responses of the components are shown in

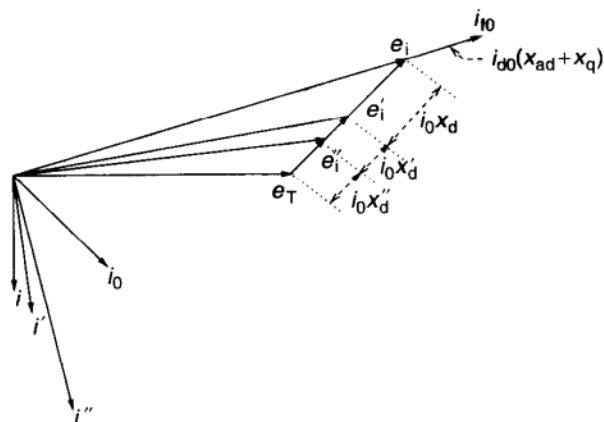


FIGURE 3.22 Relations among subtransient, transient, and steady-state short-circuit currents.

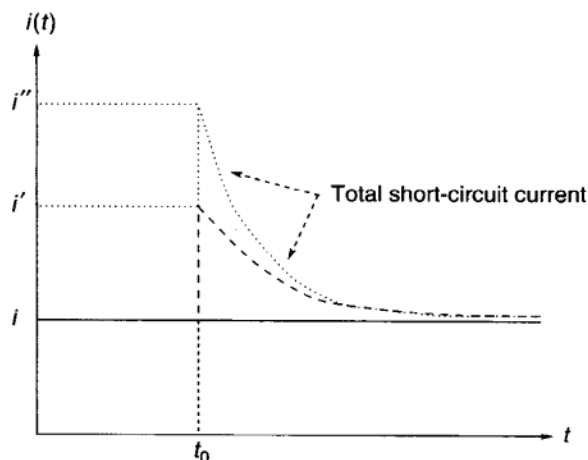


FIGURE 3.23 Relations among time histories of the sizes of subtransient, transient, and steady-state currents and their sum, the total short-circuit current.

Figure 3.23. The initial values are next summarized:

$$i = \frac{i_{f0}}{x_d} \quad (3.160)$$

$$i' = \frac{e'_i}{x'_d} = \frac{e_T + i_0 x'_d}{x'_d} \quad (3.161)$$

$$i'' = \frac{e''_i}{x''_d} = \frac{e_T + i_0 x''_d}{x''_d} \quad (3.162)$$

The current i'' in the damper winding will have a relatively very short time constant $T_d'' \approx 0.05$ sec whereas $T_d' \approx 5$ sec. Consequently, the current i'' will adjust itself at a time when there is still no appreciable change in i_f . After i'' dies down the situation is the same as if there were no damper winding. This situation is described by the transient short-circuit current. The time history of the short circuit current is

$$i(t) = (i'' - i')e^{-t/T_d''} + (i' - i)e^{-t/T_d'} + i \quad (3.163)$$

and the time constants are

$$T_d' = T_{d0}' \frac{x_d'}{x_d} \quad (3.164)$$

$$T_d'' = T_{d0}'' \frac{x_d''}{x_d} \quad (3.165)$$

Actual machines will have a damper winding that does not consist of merely one turn but rather a partial or full squirrel cage, or wound-rotor machines with eddy current paths in the rotor. Such dampers represent a multiplicity of circuits that are linked to each other and to the excitation and armature circuits and that also have their own leakage fluxes and impedances. A single winding approximation as used in the preceding sketches and in the single impedance values like x_{al} was introduced early by Concordia as an approximation justified by the fact that the impedances of individual conductors in a squirrel cage or of eddy current circuits are close to each other in magnitude.

DC Component of the Balanced Short-Circuit Current With a balanced short circuit applied to the machine suddenly, the total flux in the direct axis will remain constant as discussed in connection with Figure 3.12 according to the principle of constant-flux linkages. A magnetic flux may link with two or three coils, one of which is instantly closed at a time ($t = 0$), say by a short circuit. A sudden shift of current magnitude may then occur in all coupled circuits while the magnetic flux will remain momentarily constant and later gradually change to a transient in a lossy circuit or remain constant in a lossless circuit such as in Figure 3.12.

When this principle is applied to a synchronous machine that is suddenly short-circuited in all three of its phases the total main flux through the rotor will remain momentarily constant but its components

1. Excitation current i_f
2. Three-phase armature currents i_a, i_b, i_c

will jump in opposite directions as in Figure 3.12. The rotation of the machine introduces a new complication by dividing the flux into a stationary and a rotating component. Specifically, the field current will jump up, and since machine is rotating, this increased excitation will continue inducing increased 60-cycle

transient (and subtransient) AC currents until they die down with their respective time constants as discussed before. The sudden compensating excitation current in the armature circuit will leave behind a magnetic field at a fixed position in the armature maintained by the compensating instantaneous current jump of the short-circuited armature coils (as in the simpler circuit in Fig. 3.12). This magnetic field component will remain fixed in the armature in its position at the instant of the short circuit and it will be maintained at its fixed value as i_2 in Figure 3.12 in a lossless situation, thus forming a DC component in the AC armature currents. The distribution of the currents between the phases will of course depend on the instantaneous position of the armature at the instant of the short circuit. In the actual lossy system this constant current will of course decay and disappear, but while there it will maintain its "DC", that is, unidirectional nature. It is known as the DC component of the synchronous machine short circuit. It can be readily analyzed along the lines of this thinking, but this will be left to the reader to save space here.

3.2.3.5 Part B: Precise Analysis and Modeling of Electromagnetic Processes in Synchronous Machines Section 3.2.3.4 developed, through a purely intuitive reasoning using the most basic tools of algebra and physics, a dynamic model of a synchronous machine useful in dynamic analysis of short circuits. The most useful product of this reasoning is a set of concepts such as synchronous, transient, and subtransient reactances and associated time constants for computing the synchronous, transient and subtransient components of short-circuit currents. These special concepts are based on the structure of the circuits on synchronous machines established a long time ago. These concepts also fit the short-circuit computation well for synchronous generators, which represent the bulk of computations connected with power-system operations and design. Thus this approach is quite effective on the power system in developing well-understood ad hoc concepts.

Of course, the needs of the power-system dynamic studies are broadly general and are of a scale far beyond the needs of computing short-circuit currents. The dynamic analysis of stability of the large nonlinear power system both in small-signal and large-signal conditions, sustained oscillations connected with voltage collapse, slow oscillations of large areas across the system, and system security in stationary and dynamic conditions are only a few of the problems in this currently very active area of power-system studies and development. These studies will be discussed throughout the text.

This wide area of power-system analysis has to be built and must depend on a precise and well-defined generator model of full scope. Such a model is developed in this section, which also gives a systematic study of various levels of simplification of the model by approximation.

While the short-circuit-based model (which is precise and is proven even through its intuitive algebraic approach) can and has been "generalized" to other types of events, these extensions lead to various degrees of model precision.

The most desirable approach is then through a direct and precise development based on a precise formulation of the problem. This will now be offered in

Part B. For definitions and conceptual understanding references will be made to the intuitive work in Part A.

3.2.3.6 Electromagnetic Generator Dynamics Electromagnetic generator dynamics (blocks 2 and 3 in Figs. 3.2 and 3.3) has been a topic of much classic work Refs. [6–10] on synchronous machines to only mention a few. Commonly used state variables are almost exclusively expressed with respect to the rotating reference frame described at the beginning of Part A (Sec. 3.2.3.4.) Only very recently have attempts been made to rewrite synchronous machine dynamics with respect to the stationary network reference frame. In this chapter we use the most common electromagnetic dynamics with respect to the rotating reference frame. Reference to the second option is made later in this text, in Chapter 6. The mathematical transformation used to represent instantaneous state variables in the rotating reference frame known as the Blondel or Park transformation is described next.

The Blondel transformation is a linear transformation that converts the instantaneous AC quantities e_a, e_b, e_c of the three stator phases into DC quantities e_d, e_q, e_0 , which are stationary with respect to the rotor; in other words, they rotate at synchronous speed along with the rotor [9] (see also the intuitive concept building in Part A):

$$e_d = \frac{2}{3}[e_a \cos \theta + e_b \cos(\theta - 120^\circ) + e_c \cos(\theta + 120^\circ)] \quad (3.166)$$

$$e_q = -\frac{2}{3}[e_a \sin \theta + e_b \sin(\theta - 120^\circ) + e_c \sin(\theta + 120^\circ)] \quad (3.167)$$

$$e_0 = \frac{1}{3}(e_a + e_b + e_c) \quad (3.168)$$

Note that $e_0 = 0$ for symmetrically balanced three-phase systems, the only case considered in this text, unless stated otherwise.

The inverse transformation

$$e_a = e_d \cos \theta - e_q \sin \theta + e_0 \quad (3.169)$$

$$e_b = e_d \cos(\theta - 120^\circ) - e_q \sin(\theta - 120^\circ) + e_0 \quad (3.170)$$

$$e_c = e_d \cos(\theta + 120^\circ) - e_q \sin(\theta + 120^\circ) + e_0 \quad (3.171)$$

The same transformation applies to the currents.

Clearly the transformation is invertible (orthonormal) everywhere with a non-singular determinant invertible everywhere, which is $2\sqrt{3}$ and $1/2\sqrt{3}$ for all t . All components e and i are considered quasistationary. That is, if they vary with time, the variation is very slow with respect to the 60-Hz frequency. This is typically true for problems discussed in this text. See Chapters 2 and 11 for detailed analysis of quasistationarity.

The transformed system, stationary as viewed from the rotor, is shown in Fig. 3.24. This is a conceptual rendering in which all coils are represented by single turn coils. There are three layers of coils on two axes identified

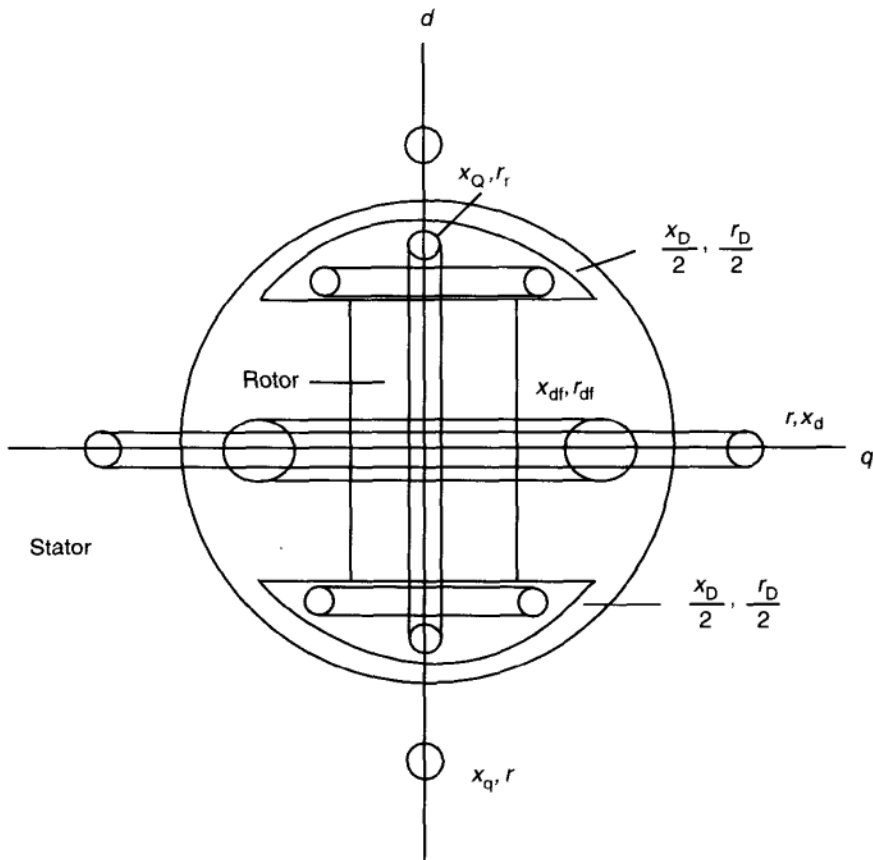


FIGURE 3.24 Sketch of circuits of a linear synchronous generator as viewed from the rotor.

TABLE 3.1 Stator and Rotor Coils on a Round-Rotor Machine Typical for Steam-Turbine Generators

	Direct axis	Quadrature axis
Field excitation winding (transient time range)	f	none
Rotor damper winding (subtransient time range)	D	Q
Armature coil winding	d	q

by subscripts as denoted in Table 3.1. Definitions and verbal explanations of concepts were offered in Part A.

Because the magnetic fields are symmetrical around the d or q axes, there is no shared flux linkage between the coils of these two axes; that is coils d and q are not coupled inductively in a direct way. Remember that strictly speaking

there is no damper winding as such. Damping is provided either by the eddy currents in wound-rotor (steam-turbine) generators and a squirrel-cage structure in salient pole machines. Each corresponds to a multiplicity of higher frequencies but as their frequency distribution peak is narrow, the customary approximation (going back to Park and Concordia) with a single winding as used here is well justified.⁷ Also note that multipole machines as used in water turbines can be built with more than one damper winding [7]. This case is not specified here, to save space and complexity, but it can be readily added if applicable within the structure offered here. Armature coils likewise are distributed in slots around the perimeter of the stator to ensure a sinusoidal variation of flux linkage around the rotor surface 120° displaced for the three phases. These matters are discussed in introductory texts on synchronous machines [10, 7].

When the rotation of the rotor is considered, however, two kinds of inductive effects emerge.

Induction of the first kind results from changes (very slow in the transient and subtransient range compared to 60 cycles) of the fluxes of the *d* and *q* axes. *Induction of the second kind* results from the movement of the *d*-axis coils relative to the *q*-axis field and vice versa.

These inductions will now be studied separately and then superimposed on the basis of the assumed linearity of the circuits and fields (this ignores saturation).

Induction of the First Kind This induction follows the basic pattern of induction between two coils coupled by a magnetic link (without leakage fluxes) as shown in Figure 3.25. Flux linkages in Figure 3.25 are

$$\psi_i = I_i x_i + I_j x_{ij} = \psi_{ii} + \psi_{ij} \quad (3.172)$$

$$\psi_j = I_i x_{ij} + I_j x_j = \psi_{ij} + \psi_{jj} \quad (3.173)$$

where x_i , x_{ij} , and x_j are magnetic permeances in p.u.

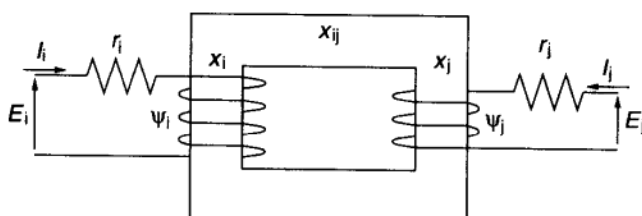


FIGURE 3.25 Basic coupled circuit.

⁷ When choosing two instead of one damper winding coil on the *q* axis, a different model evolves [13, 14].

Note: The two versions on the right-hand side of Eqs. (3.172) and (3.173) do not imply termwise equality; or inverted and decomposed,

$$I_i = y_i \psi_{ii} + y_{ij} \psi_{ij}, \quad \psi_{ij} = A(x_{ij} + x_i) \psi_i = A(x_{ij} + x_j) \psi_j \quad (3.174)$$

$$I_j = y_{ij} \psi_{ij} + y_j \psi_{jj}, \quad A = \frac{1}{x_i x_j - x_{ij}^2} \quad (3.175)$$

Note that (without saturation) in properly selected p.u. normalization magnetic permeances, electric reactances and inductances are numerically the same and will be identified by the letter x . Magnetic reluctances and electric admittances will be similarly identified by y . $\dot{\psi}_i$ and $\dot{\psi}_j$ are the induced (first kind) voltages in coils i and j , respectively. Induced voltages e_i and e_j can then be expressed as

$$E_i = \dot{\psi}_i + I_i r_i = \dot{\psi}_i + r_i y_i \psi_{ii} + r_i y_{ij} \psi_{ij} \quad (3.176)$$

$$E_j = \dot{\psi}_j + I_j r_j = \dot{\psi}_j + r_j y_{ij} \psi_{ij} + r_j y_j \psi_{jj} \quad (3.177)$$

Signs on the right-hand side depend on the selection of reference directions for voltage current and mutual reactance, as shown in Figure 3.25 (so current flowing is i).

Applying these relations to the multiple circuits of Figure 3.24 in superposition one obtains

$$y_d \psi_{dd} + y_{df} \psi_{df} + y_{dD} \psi_{dD} = i_d, \quad \psi_d = \psi_{dd} + \psi_{df} + \psi_{dD} \quad (3.178)$$

$$y_q \psi_{qq} + y_{qQ} \psi_{qQ} = i_q, \quad \psi_q = \psi_{qq} + \psi_{qQ} \quad (3.179)$$

$$y_D \psi_{DD} + \psi_{Df} \psi_{Df} + y_{dD} \psi_{dD} = i_D, \quad \psi_D = \psi_{DD} + \psi_{Df} + \psi_{dD} \quad (3.180)$$

$$y_{qQ} \psi_{qq} + y_Q \psi_{QQ} = i_Q, \quad \psi_Q = \psi_{QQ} + \psi_{qQ} \quad (3.181)$$

$$y_f \psi_{ff} + y_{df} \psi_{df} + y_{Df} \psi_{Df} = i_f, \quad \psi_f = \psi_{ff} + \psi_{df} + \psi_{Df} \quad (3.182)$$

Induction of the Second Kind It can be observed in Figure 3.24 that the flux ψ_d , which is lined up with the d axis is not linking with the armature coil x_q around the q axis. That is, flux linkage between the two is zero. However since the armature coils are moving with a velocity of $\dot{\theta}$ relative to the flux ψ_d , the flux linkage will actually increase at a rate of $\dot{\theta}$. Rate of increase of flux linkage is proportional to voltage (equal in p.u.) so a voltage

$$e_d = -\psi_q \dot{\theta} \quad (3.183)$$

will be induced in the q -axis coil and conversely a voltage

$$e_q = \psi_d \dot{\theta} \quad (3.184)$$

will be induced in the d -axis coil. Remember that θ is the rotor angle. These inductions take the role of the imposed voltages in Figure 3.25.

Combination of Inductions of the First and Second Kinds The combination of Eqs. (3.176) to (3.182) and (3.183) to (3.184) produces the following basic set of differential equations assuming that $r_D = r_Q = r_r$ and $r_d = r_q = r$.

$$\dot{\psi}_f = -r_f y_f \psi_{ff} - r_f y_{df} \psi_{df} - r_f y_{Df} \psi_{Df} + e_f, \quad \text{slow} \quad (3.185)$$

$$\dot{\psi}_D = -r_r y_{dD} \psi_{dD} - r_r y_{Df} \psi_{Df} - r_r y_D \psi_{DD}, \quad \text{fast} \quad (3.186)$$

$$\dot{\psi}_Q = -r_r y_{qQ} \psi_{qQ} - r_r y_Q \psi_{QQ}, \quad \text{fast} \quad (3.187)$$

$$\dot{\psi}_d = -r y_d \psi_{dd} - r y_{dD} \psi_{dD} - r y_{df} \psi_{df} + e_d - \psi_q \dot{\theta}, \quad \text{ultrafast} \quad (3.188)$$

$$\dot{\psi}_q = -r y_q \psi_{qq} - r y_{qQ} \psi_{qQ} + e_q - \psi_d \dot{\theta}, \quad \text{ultrafast} \quad (3.189)$$

where the concepts slow, fast, and ultrafast identify the typical speed class of the reaction of the various flux linkages on the synchronous machine. These differential equations suggest the presence of three layers of basic, typical time constants (momentarily neglecting the coupling) with the associated time scales in the singular perturbation sense [15]:

$$\begin{array}{ccc} \frac{1}{r_f y_f} \gg \frac{1}{r_r y_D} \approx \frac{1}{r_r y_Q} \gg \frac{1}{r y_d} \approx \frac{1}{r y_q} & & \\ \text{transient} & \text{subtransient} & \text{subsubtransient} \\ \text{slow} & \text{fast} & \text{ultrafast} \end{array} \quad (3.190)$$

Thus the following assumption suggests itself⁸:

$$\frac{\dot{\psi}_d}{r y_d} \cong \frac{\dot{\psi}_q}{r y_q} = 0$$

Then combining Eqs. (3.176) to (3.182) with Eqs. (3.185) to (3.187), one obtains

$$e_d = -\psi_q \dot{\theta} - r i_d \quad (3.191)$$

$$e_q = +\psi_d \dot{\theta} - r i_q \quad (3.192)$$

$$e_D = \dot{\psi}_D + r_r i_D = 0 \quad (3.193)$$

$$e_Q = \dot{\psi}_Q + r_r i_Q = 0 \quad (3.194)$$

$$e_f = \dot{\psi}_f + r_f i_f \quad (3.195)$$

⁸This approximation is not critical for the model derivation presented here; for phenomena of interest in which this may be important, the stator dynamics $\dot{\psi}_d$ and $\dot{\psi}_q$ in Eqs. (3.188) and (3.189), respectively, could also be preserved.

where e_d and e_q are the d and q components of the bus voltage; e_D and e_Q are the components of the voltages in the damper winding that are short-circuited on themselves, and e_f is the excitation voltage. And by eliminating the components of the flux linkages by use of Eqs. (3.178) to (3.182), the following is obtained for the total flux linkages:

$$\begin{bmatrix} \psi_d \\ \psi_D \\ \psi_f \\ \psi_q \\ \psi_Q \end{bmatrix} = \begin{bmatrix} x_d & x_{dD} & x_{df} & 0 & 0 \\ x_{dD} & x_D & x_{Df} & 0 & 0 \\ x_{df} & x_{Df} & x_f & 0 & 0 \\ 0 & 0 & 0 & x_q & x_{Qq} \\ 0 & 0 & 0 & x_{Qq} & x_Q \end{bmatrix} \begin{bmatrix} i_d \\ i_D \\ i_f \\ i_q \\ i_Q \end{bmatrix} \quad (3.196)$$

As long as saturation is neglected, the magnetic field and current relations are linear; thus superposition applies. This is the basis of the development leading to Eqs. (3.191) to (3.196).

It is important to understand, however, the composition of the flux linkages ψ and the relative magnitudes of their various components.

Based on physical orthogonality of the d , D and q , Q axes, respectively, there is no coupling between the direct-and quadrature-axis fields, as is stated in Eq. (3.196). The direct-axis flux linkages ψ_d , ψ_D , and ψ_f (or fluxes, the same numerically in p.u.) are jointly excited by the three currents i_d , i_D and i_f . However the coupling between the coils carrying currents i_d , i_D , and i_f is not leakproof. Accordingly each of ψ_d , ψ_D , and ψ_f divides into two types of components.

One is ψ_{dm} , the linkage with the main field, which is linking with all three direct-axis coils. It is jointly excited by all three currents i_d , i_D , and i_f , that is, $\psi_{dm} = (i_d + i_D + i_f)x_{dm}$, where x_{dm} is the total permeance of the magnetic path of the main flux. Similar relations apply to ψ_q and ψ_Q , of course. In addition to the main flux, each coil and its current, i_d , i_D , and i_f , link individually or in pairs with flux lines that do not link with one or two of the other coils. Such flux components linking with only one or two coils are called leakage fluxes (implying the fact that they are parasitic on the main flux, which is the one that does the work). This decomposition would modify the matrix in Eq. (3.196) into

$$\begin{bmatrix} x_{dm} + x_{al} & x_{dm} + x_{dD\ell} & x_{dm} + x_{df\ell} & 0 & 0 \\ x_{dm} + x_{dD\ell} & x_{dm} + x_{D\ell} & x_{dm} + x_{Df\ell} & 0 & 0 \\ x_{dm} + x_{df\ell} & x_{dm} + x_{Df\ell} & x_{dm} + x_{f\ell} & 0 & 0 \\ 0 & 0 & 0 & x_{qm} + x_{q\ell} & x_{qm} + x_{qQ\ell} \\ & & & x_{qm} + x_{qQ\ell} & x_{qm} + x_{q\ell} \end{bmatrix} \quad (3.197)$$

There is a hierarchy of magnitudes of these reactances (permeances) in Eq. (3.197). The main field reactances x_{dm} and x_{qm} are by far the largest (usually $x_{dm} > x_{qm}$, known as saliency). The self-leakage reactances x_{al} , $x_{D\ell}$, $x_{f\ell}$, $x_{Q\ell}$, and $x_{q\ell}$ are much smaller. The leakage coupling or mutual terms $x_{dD\ell}$, $x_{df\ell}$, $x_{Df\ell}$ and $x_{qQ\ell}$ are much smaller yet.

The reason for this separation in size is that most of the magnetic reluctance comes from those parts of the flux lines that cross air gaps; because iron has very

high permeability, iron cores contribute little reluctance. Even the crude sketch of Figure 3.24 would reveal that the main flux needs to cross only the short air gap between the rotor and stator while leakage fluxes must pass largely through air, and coupling leakage fluxes are located almost entirely in air. (Precise values for actual machines are readily obtained by a computer flux plotting of which there is a substantial literature and a large library of programs.) This means low permeances, or reactances for $x_{(\cdot)\ell}$ and even lower ones for $x_{(\cdot)(\cdot)\ell}$. This situation gives an opportunity for judicious approximations, which will be presented later. The complete model that follows contains all the details of Eqs. (3.185) to (3.189) as well as the traditionally defined or state variables:

$$e'_q = \frac{x_{df}x_D - x_{dD}x_{Df}}{x_fx_D - x_{Df}^2} \Psi_f \quad (3.198)$$

$$e''_q = e'_q + \frac{x_fx_{dD} - x_{df}x_D}{x_fx_D - x_{Df}^2} \Psi_D \quad (3.199)$$

$$e''_q = -\frac{x_{Qq}}{x_Q} \Psi_Q \quad (3.200)$$

$$e_{fd} = \frac{x_{df}}{r_f} e_f \quad (3.201)$$

e'_q , e''_q , e_{fd} , and e_{fd} are the classical notations for these classically defined quantities. They correspond to current IEEE notational guides [16] and are the result of the normalization procedure intended to result in 1-p.u. values of the base mmf, base voltage, and base flux (the flux that induces the base voltage in the machine). This normalization is carried out in a similar fashion as the p.u. normalization for voltages and currents in power networks [4, 13]. In the steady state e'_q becomes the voltage behind the transient reactance (slow variable ~ 5 sec) while e''_q and e_d become the voltage behind the subtransient reactances (fast variable ~ 0.1 sec) and e_{fd} represents the excitation voltage. e_d , e_q , and i_d , i_q denote the d and q components of, respectively, the bus voltage and current. All these variables are expressed in per-unit values (assuming no saturation).

At this point it is possible to distill Eqs. (3.185) to (3.201), after considerable algebraic manipulation into the complete model of electromagnetic dynamics of the generator described in the following sections. (Appendix 3.2 summarizes some details of this algebra for those who are interested. Tedious manipulations are simple and straightforward.)

3.2.3.7 Complete Model of the Electromechanical and Electromagnetic Dynamics of a Synchronous Generator: Type I

1. Electromechanical dynamic equations (block 1 in Fig. 3.3):

$$P_T = J\ddot{\theta} + D\dot{\theta} + P_G \quad (3.202)$$

2. Coupling equations between the generator and bus (block 2, Fig. 3.3):

a. For the generator side:

$$e_q = e_q'' + x_d'' i_d - r_i_q \quad (3.203)$$

$$e_d = e_d'' - x_q'' i_q - r_i_d \quad (3.204)$$

For the conceptual derivation of these two equations, see Appendix 3.1.

b. For the bus side:

$$e_q = E \cos(\delta - \theta), \quad i_q = i \cos(\delta - \theta - \varphi) \quad (3.205)$$

$$e_d = E \sin(\delta - \theta), \quad i_d = i \sin(\delta - \theta - \varphi) \quad (3.206)$$

where E is the magnitude of the terminal (bus) voltage, δ is its phase angle (a phase), and θ is the phase angle of the direct axis (i.e., the rotor), while φ is the power factor angle of the terminal current i .

Note that the use of $e_q'' - e_q'$ as effectively a state variable (it could be given as a separate symbol, but it would be unconventional) substantially simplifies the equations. It also makes physical sense since this difference is connected to the damper winding flux [Eq. (3.199)].

3. Electromagnetic dynamic equations. (block 3 in Fig. 3.3):

$$\begin{aligned} T'_{d0} \dot{e}'_q &= - \left(1 + \frac{x_d - x'_d}{(x'_d - k_6 x_{al})^2} (x'_d - x''_d) \right) k_1 e'_q \\ &\quad + \frac{x_d'' - k_6 x_{al}}{(x'_d - k_6 x_{al})^2} (x_d - x'_d) k_2 (e''_q - e'_q) \\ &\quad + \frac{x_d'' - k_6 x_{al}}{x'_d - k_6 x_{al}} k_4 e_{fd} \\ &\quad + \left(\frac{x_d'' - k_6 x_{al}}{x'_d - k_6 x_{al}} \right)^2 (x_d - x'_d) k_3 i_d \end{aligned} \quad (3.207)$$

$$\begin{aligned} T''_{d0} (\dot{e}''_q - \dot{e}'_q) &= \frac{x'_d - x''_d}{(x''_d - k_6 x_{al})} k_5 e'_q - (e''_q - e'_q) \\ &\quad + (x_d - x''_d) i_d \end{aligned} \quad (3.208)$$

$$T''_{q0} \dot{e}''_d = -e''_d - (x_q - x''_q) i_q \quad (3.209)$$

There are two classes of constants present in these equations.

1. *Primary or Standard Constants.* These are defined in the traditional and standard means established by IEEE [16], as follows:⁹

⁹ For interpretation of these constants in the context of short-circuit dynamics, see Sec. 3.2.3.4.

$T'_{d0} = \frac{x_f}{r_f}$	Transient time constant
$T''_{d0} = \frac{x_D}{r_D} \left(1 - \frac{x_{Df}^2}{x_f x_D} \right)$	Subtransient time constant in the d axis
$T''_{q0} = \frac{x_Q}{r_Q}$	Subtransient time constant in the q axis
x_d	Synchronous reactance
x_{ae}	Armature leakage reactance (3.210)
$x'_d = x_d - \frac{x_{df}^2}{x_f}$	Transient reactance
$x''_d = x_d - \frac{x_D x_{df}^2 - 2x_{df} x_D x_{dD} + x_f x_{dD}^2}{x_f x_D - x_{Df}^2}$	Subtransient reactance in the d axis
$x''_q = x_q - \frac{x_{Qq}^2}{x_Q}$	Subtransient reactance in the q axis

These constants can be obtained in the design phase by finding the initial set of constants (x_D , x_{df} , x_{dD} , etc.) using flux-plotting programs or by measurements on the actual machines for which standard practices are prescribed [3].

Note: It should be pointed out that this set of constants is a derived set which emerged in mostly intuitive development during short circuit studies during the first half of this century such as outlined in Section 3.2.3.4 (part A). Using this particular set is therefore arbitrary. This is convenient since concepts such as transient and subtransient reactances and voltages are firmly embedded in common usage, although they are derived rather than physical concepts. Other choices could be used; for instance, for a mathematical model to be used in mathematical dynamic analysis, direct use of physical quantities e_d , e_q , e_D , e_Q , x_d , x_q etc. in Eqs. (3.186) through (3.189) may be preferable. So it is not a necessity to transform these tediously into Eqs. (3.207) and (3.209). But the latter form uses concepts e'_q , x'_d , x'_q etc. which, while not physical, are firmly embedded in common thinking and so the results in terms of these have much more intuitive impact.

2. *Secondary or Corrective Constants k_1 through k_6 .* These constants ensure precise dynamic relations (3.192 to 3.206), which include the main (x_{dm} , x_{qm}), leakage (x_{ae} , x_{de} , x_{Qe} , x_{qe} , $x_{d\ell}$, $x_{q\ell}$, $x_{d\ell e}$), and mutual leakage (x_{dDe} , x_{qQe} , x_{dfe}) reactances as defined in Eq. (3.197).* All these reactances can also be determined directly by flux-plotting techniques, although no standard measurements have been established for them:

$$k_1 = \frac{(x'_d - k_6 x_{ae})^2 + (x_d - x'_d)(x'_d - x''_d)k_2 k_5}{(x'_d - k_6 x_{ae})^2 + (x_d - x'_d)(x'_d - x''_d)} \quad (3.211)$$

*The authors wish to give special thanks to Professor V. Venkatasubramanian, for his help in his student days in working out the details of this section.

$$k_2 = \frac{(x'_d - k_6 x_{a\ell}) k_4 - (x''_d - k_6 x_{a\ell}) k_3}{(x'_d - x''_d)} \quad (3.212)$$

$$k_3 = \frac{z_1^2 z_2^2}{x_{df}^2 z_4^2}, \quad k_4 = \frac{z_1 z_2}{x_{df} z_4} \quad (3.213)$$

$$k_5 = \frac{x_{Df} z_4}{z_2 z_3}, \quad k_6 = 1 - \frac{x_{dD\ell}}{x_{a\ell}} \quad (3.214)$$

where,

$$z_1 = x_{dD} x_f - x_{df}^2, \quad z_2 = x_{df} x_D - x_{dD} x_{Df} \quad (3.215)$$

$$z_3 = x_{dD} x_f - x_{df} x_{Df}, \quad (3.216)$$

$$z_4 = x_{dD} x_f x_D - x_{dD} x_{Df}^2 - x_D x_{df}^2 + 2x_{Df} x_{df} x_{dD} - x_f x_{dD}^2 \quad (3.217)$$

There will be instances when the use of the complete set of dynamic equations (3.207) to (3.209) will be needed, for example, when analysis of the effects of certain approximations are sought. However it was pointed out in conjunction to Eq. (3.197) that $x_{(\cdot)m} \gg x_{(\cdot)\ell} \gg x_{(\cdot)(\cdot)\ell}$; that is, the mutual leakage reactances are much smaller than the leakage or especially the main field reactances. In most practical situations the assumption that

$$x_{(\cdot)(\cdot)\ell} = x_{fd\ell} = x_{dD\ell} = x_{qQ\ell} = 0 \quad (3.218)$$

will be well justified. Importantly, when this assumption is made then all the constants k_i in Eqs. (3.211) to (3.214) become unity:

$$k_i = 1, \quad i \in \{1, 6\} \quad (3.219)$$

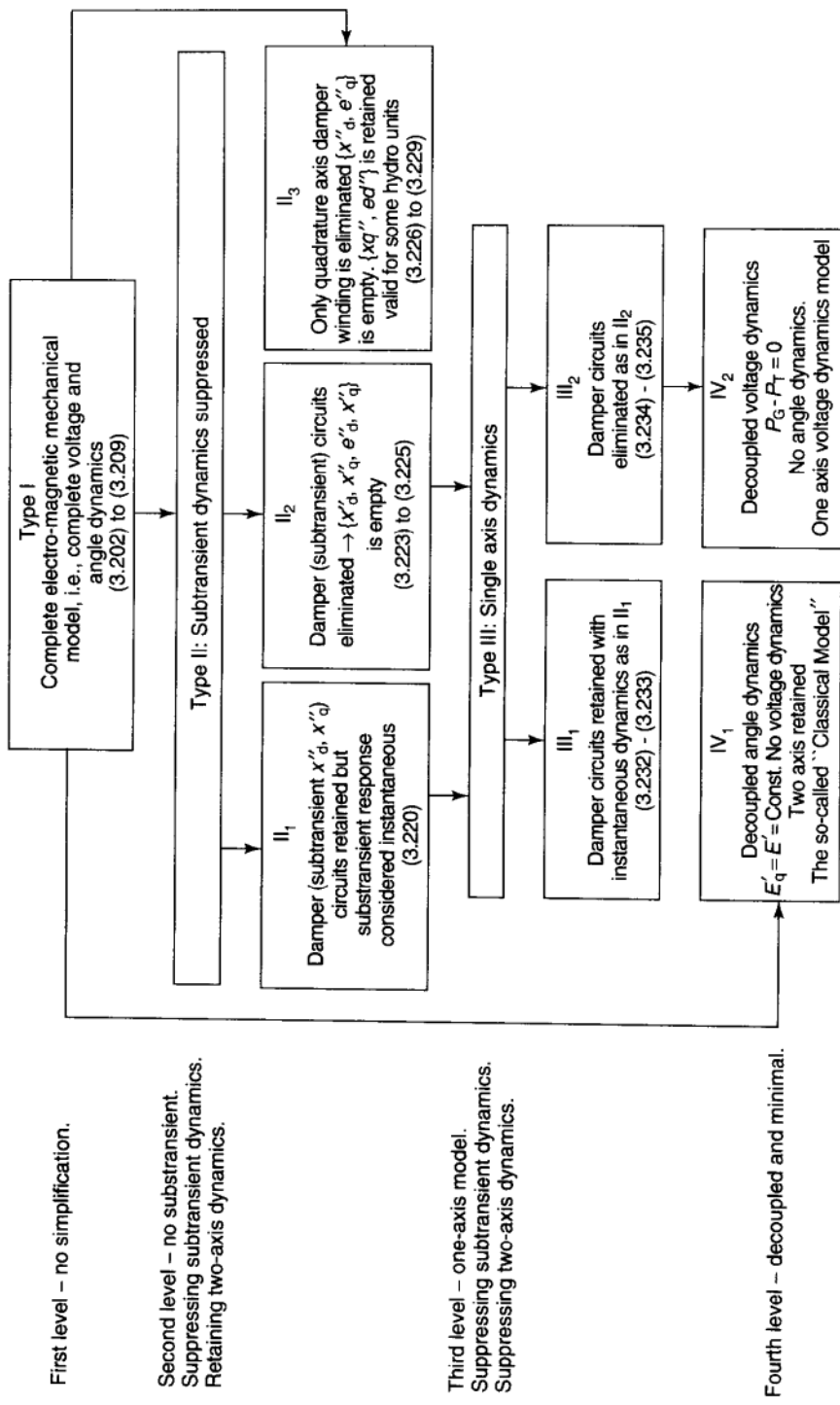
Therefore, the type I, or complete electromagnetic-mechanical model of the synchronous machine is for most practical problems the complete electromagnetic dynamic equations of the synchronous machine as given by the set of equations (3.202) and (3.207) to (3.209) with $k_i = 1, i \in \{1, 6\}$. In conjunction with the electromechanical dynamic model, these equations thus will be referred to as the type I dynamic model (blocks 1, 2, 3 in Figs. 3.2 and 3.3) of the synchronous machine (Table 3.2).

A vector-diagram representation of the complete electromagnetic model for steady-state 60-cycle conditions $\dot{e}'_q = \dot{e}''_q = \dot{e}''_d = 0$ is shown in Figure. 3.26. This special case matches the classical form of this complete diagram given by Concordia [10] for steady-state 60-cycle conditions.

3.2.3.8 Simplifying the Electromagnetic Model of the Synchronous Machine

The type I model of the synchronous machine as defined in Eqs. (3.207) to (3.219) is a set of nonlinear differential equations. Although it may not be

TABLE 3.2 Four levels of Simplification of Generator Electromagnetic Dynamics



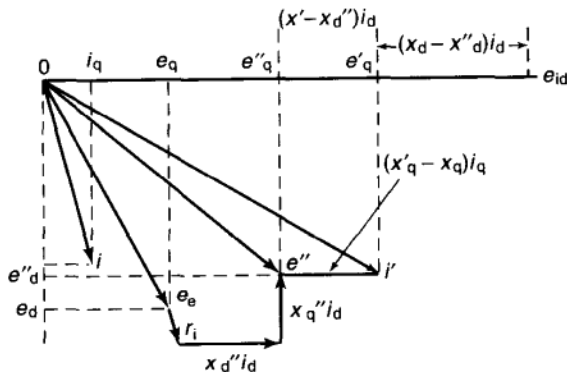


FIGURE 3.26 Steady-state ($\dot{e}_d'' = \dot{e}'_q = \dot{e}''_q = 0$) vector diagram of the complete model (type I) with damper windings.

excessively complex, it has three features that are analytically and computationally inconvenient especially because of their very large number in the systems,¹⁰ described as follows.

1. Two time scales are present, a transient one with a typical time constant of 5 sec and a subtransient one with a typical time constant of 0.05 sec. While both of these must be considered in some problems, it is often justified to suppress the fast, subtransient, component. The three models of this nature will be labeled as type II (Table 3.2).
2. Two separate coordinate systems are used on the generators (e_d , e_q , d and q axes) and the system side (phasor $E\angle\delta$, magnitude, E , and angle δ) Fig. 3.31. Each of these offer major advantages on their respective subsystems. This injects into the problem formulation a rather inconvenient transformation that complicates both analysis and computation. A direct connection between the e_d , e_q and $E\angle\delta$ forms, which obviates the presence of two different coordinate systems within one problem, will be presented in Section 3.2.3.9. Furthermore, in many problems, where it is justifiable, there is good reason to approximate the generator with a single-axis model. Models of this nature will be labeled as type III in Table 3.2.
3. Electromagnetic dynamics is coupled with electromechanical dynamics (block 2 in Figs. 3.2 and 3.3). This severely raises the number of coupled variables and ties a somewhat heterogeneous portion of a problem together. However, the coupling between phase angle and real power, on the one hand, and voltage magnitude and reactive power, on the other hand, is strong but it is weak between the two pairs. This suggests a decoupling of the two models. The two minimal models for electromechanical dynamics (sometimes called the

¹⁰ In drawing such a diagram or doing other applications, one must remember that the specific reference directions in Eqs. (3.202)–(3.269) are selected, as implied by Fig. 3.25 with reference current entering the armature. References with reverse direction are also used in the literature. Properly and consistently used leads a vector diagram as in Fig. 3.26.

“classical” model) and a corresponding model for electromagnetic dynamics are labeled as type IV in Table 3.2.

It should be mentioned that in the literature it is not uncommon to use the electromagnetic parts of type II or type III models and simply ignore the electromechanical dynamics or vice versa. This approach seems rather questionable.

Dynamic equations (mostly electromagnetic since the electromechanical variables do not change) will now be listed in the format of Table 3.2. These various types affect the equations in the first column of Figure 3.3. Popularly used approximations are shown in Figure 3.27 in a tabular form. All are described in the following text.

Type II: Suppressing the Subtransient Dynamics As indicated in Table 3.2 for type II, subtransient is being suppressed in the literature in at least three ways.

TYPE II₁: ASSUMING THAT SUBTRANSIENT IS INSTANTANEOUS This approach (block 2, Fig. 3.3) assumes that the damper windings are present on the machine but their dynamics is very fast, introducing $T''_{d0} = T''_{q0} = 0$ into the dynamics of the coupled model of Eqs. (3.207) to (3.209). Equations (3.208) and (3.209) become algebraic equations. These then can be used to eliminate e_d'' and e_q'' in Eq. (3.206). This results in the following approximation:

1. The electromagnetic dynamic equation (block 3 in Fig. 3.3) becomes

$$T'_{dq}\dot{e}'_q = -e'_q + \frac{x_d'' - x_{a\ell}}{x_d' - x_{a\ell}}(x_d - x_d')i_d + \frac{x_d'' - x_{a\ell}}{x_d' - x_{a\ell}}e_{fd} \quad (3.220)$$

2. The coupling equations between generator and bus (Block 2, Fig. 3.3) become the following.

- a. For the generator side,

$$e_q = \frac{(x_d' - x_{a\ell})}{(x_d'' - x_{a\ell})}e'_q + x_d'i_d - ri_q \quad (3.221)$$

$$e_d = -x_qi_q - ri_d \quad (3.222)$$

- b. For the bus side, see Eqs. (3.205) and (3.206).

Note that e_d'' and e_q'' are now instantaneous (algebraic) internal variables. If for some reason they are needed, they can be computed from Eqs. (3.203) and (3.204), which are still valid.

Clearly, suppressing the fast time or subtransient component results in major simplification, Eqs. (3.220) to (3.222), as compared to Eqs. (3.207) to (3.209). Note further that the model, Eqs. (3.220) to (3.222), is the transient or slow component of the dynamics separated from the subtransient or fast component by way of considering the latter instantaneous as an approximation. This type

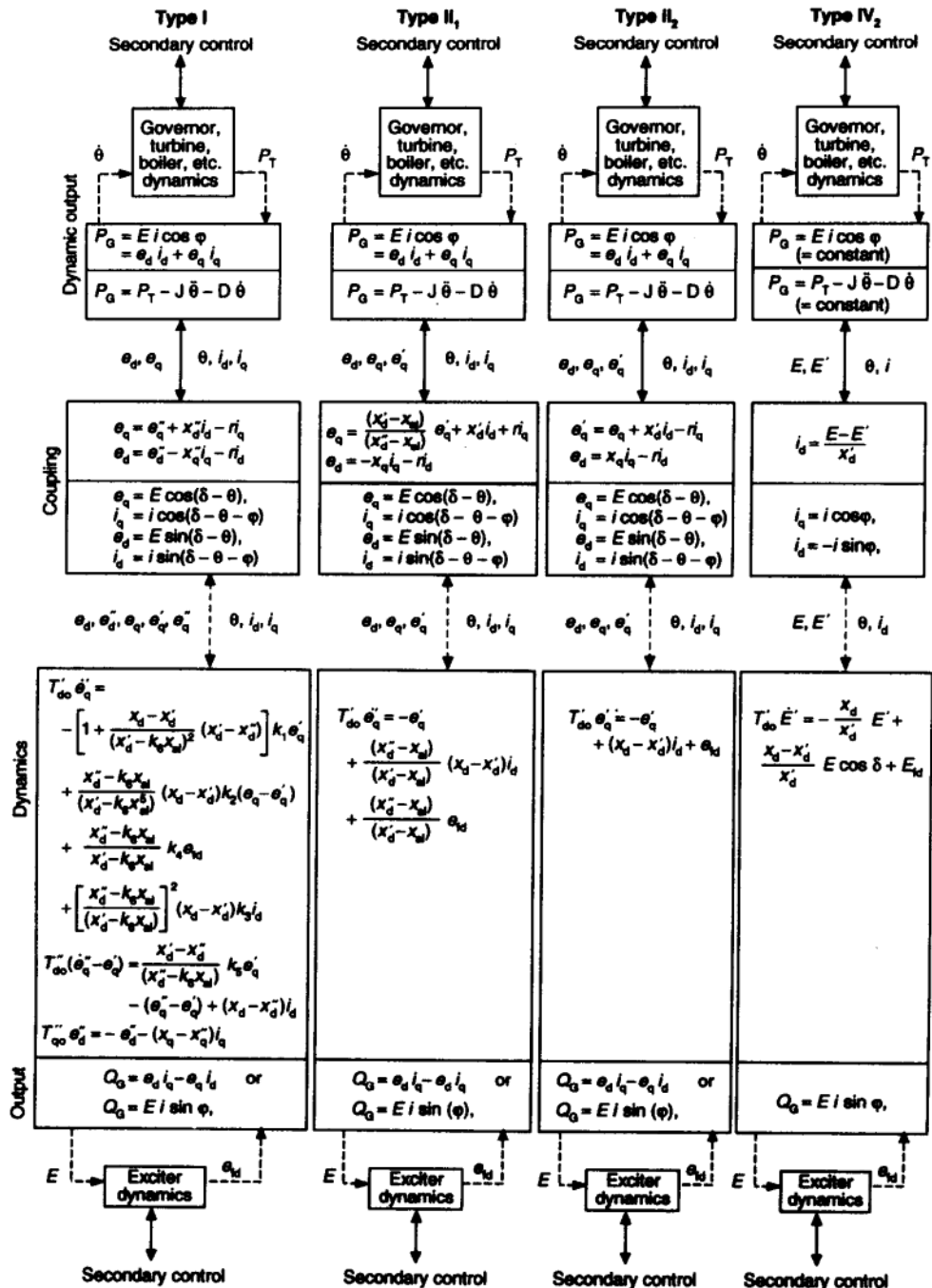


FIGURE 3.27 Replacement of first columns in Figure. 3.3 for four popular approximations listed in Table 3.2.

of dynamic separation is the subject of singular perturbation methods. In the language of singular perturbation, Eqs. (3.220) to (3.222) represent the zero-order integral manifold approximation of the exact model. This is the most that can be done without specifying the system connected to the generator terminals. When this system is specified it is sometimes possible to use a first-degree approximation that incorporates a first-degree correction term to improve the approximation inherent in neglecting the fast or subtransient dynamics [14].

TYPE II₂: ASSUMING THE ABSENCE OF DAMPING CIRCUITS An alternative way to suppress the subtransient component is to claim that there are no damper windings. Consider that e_d'' , e_q'' , x_d'' , and x_q'' are simply nonexistent. Going back to Eqs. (3.207) to (3.209) with this modification, Eqs. (3.208) to (3.209) simply disappear along with certain terms in Eq. (3.207). These result in the following approximation:

1. The electromagnetic dynamic equation (blocks 3, in Fig. 3.3) becomes

$$T'_{d0}\dot{e}'_q = -e'_q + (x_d - x'_d)i_d + e_{fd} \quad (3.223)$$

2. The coupling equations between generator and bus (block 2, Fig. 3.3) become as follows.

- a. For the generator side,

$$e'_q = e_q + x'_d i_d + r i_q \quad (3.224)$$

- b. For the bus side (see Eqs. (3.205) and (3.206)).

Note that the definitions for e'_q and e_{fd} also simplify to

$$e'_q = \frac{x_{df}}{x_f} \psi_f, \quad e_{fd} = \frac{x_{df}}{r_f} e_f \quad (3.225)$$

The vector diagram applicable to the type II₂ model is shown in Figure. 3.28.

Note that type II₂ model is less precise generally than the type II₁ model since it eliminates the damper circuits rather than just treating them like they were even faster than they actually are.

TYPE II₃: AN ARBITRARY SIMPLIFICATION OF ELECTROMAGNETIC DYNAMICS BY OMITTING ONLY THE QUADRATURE-AXIS DAMPER CIRCUIT Type II dynamics retains only the slow or transient component of electromagnetic machine dynamics, which is a reasonable approximation in terms of actual orders of magnitude as was explained in the preceding section. In type II₁ dynamics the subtransient time constant T''_{d0} is replaced by an instantaneous response $T''_{d0} = 0$. In type II₂ dynamics the damper windings (subtransient) are effectively removed from the machine. In recent years extensive use has also been made in the literature of a model that

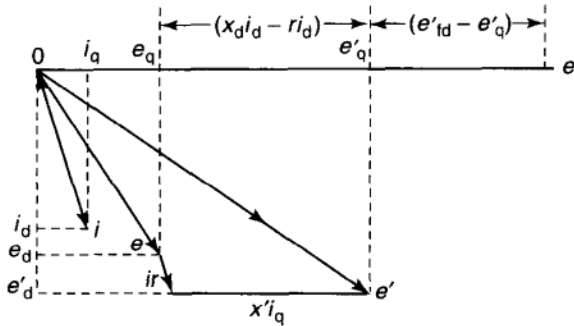


FIGURE 3.28 Steady-state ($\dot{e}'_q = 0$) vector diagram of the electromagnetic dynamic model (type II₂) without the damper winding. See Footnote 10 on page 116.

omits only the direct-axis subtransient component but retains the quadrature-axis subtransient. This corresponds to removing the quadrature-axis damper winding. (This is physically true or possible only on some hydrodynamic units).

This halfway measure seems very arbitrary. The assumptions that x''_q , and e''_q are absent and Eqs. (3.207) to (3.209) modify into the following.

1. Electromagnetic dynamic equations (block 3, Fig. 3.3):

$$T'_{d0}\dot{e}'_q = -e'_q - (x_d - x'_d)i_d + e_{fd} \quad (3.226)$$

$$T''_{q0}\dot{e}''_d = -e''_d + (x_q - x''_q)i_q \quad (3.227)$$

See also Figure. 3.29.

2. Coupling equations between generator and bus Block 2, Figs. 3.3 and 3.28:

a. For the generator side,

$$e'_q = e_q + x'_d i_d + r i_q \quad (3.228)$$

$$e''_d = e_d + x''_q i_q + r i_d \quad (3.229)$$

b. For the bus side see Eqs. (3.205) and (3.206).

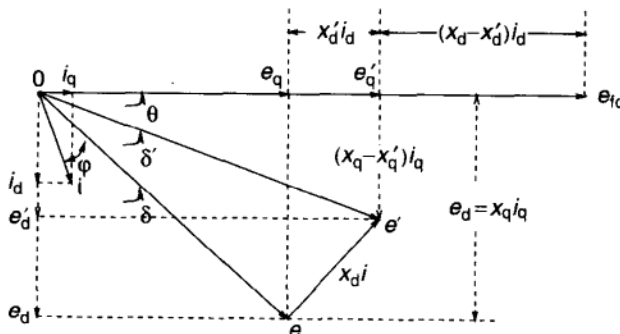


FIGURE 3.29 Stationary vector diagram for type II₃ dynamics.

Also note that the definitions for e'_q and e_{fd} are modified as shown in Eq. (3.225). The vector diagram applicable to the type II₃ model is shown in Figure 3.29.

When this type II₃ model is used in the literature (often referred to as a two-axis flux decay model), another notational simplification is commonly made, that is, e''_d and x''_q are replaced, respectively, by e'_d and x'_q . This is possible because there is no main rotor circuit on the quadrature axis so the symbols e'_d and x'_q are vacant. However, basically, the single prime is used for quantities connected with the main rotor concepts and, the double prime stands for the damping circuit. This latter simplification will not be used in this section but in Chapters 6 and 12 it is used to make comparisons with other work in this part of the literature easier for the reader.

Type III One-Axis Models To eliminate the quadrature-axis components in the model the argument can be made reasonably well that the phase angle $\theta - \delta'$ between the machine axis θ and the phase of the voltage behind the transient reactance is both small and does not change very much. This leads to the assumptions

$$e'_q = e' \cos(\theta - \delta') \cong e' \quad (3.230)$$

$$e'_d = e' \sin(\theta - \delta') \cong 0 \quad (3.231)$$

It is also assumed as in type II₁ dynamics that $T''_{do} = T''_{qo} = 0$ and in type II₂ dynamics that

$$e''_q = e''_d = x''_q = x''_d \equiv 0$$

Again the two types III₁ and III₂ are analogous to the II₁ and II₂ results.

TYPE III₁: ONE-AXIS MODEL ASSUMING THAT SUBTRANSIENT IS INSTANTANEOUS

1. The electromagnetic dynamic equations (block 3, Fig. 3.3) are

$$T'_{do} \dot{e}'_q = -e'_q + \frac{x''_d - x_{a\ell}}{x'_d - x_{a\ell}} (x_d - x'_d) i_d + \left(\frac{x''_d - x_{a\ell}}{x'_d - x_{a\ell}} \right) e_{fd} \quad (3.232)$$

2. The coupling equations between generator and bus (block 2, Fig. 3.3) are as follows.

a. For the generator side,

$$e_q = \frac{x'_d - x_{a\ell}}{x''_d - x_{a\ell}} e'_q - x'_d i_d - r_{i_q} \quad (3.233)$$

b. For the bus side see Eqs. (3.205) and (3.206).

TYPE III₂ ONE-AXIS MODEL ASSUMING THAT SUBTRANSIENT CIRCUITS ARE ABSENT

1. Electromagnetic dynamic equations (block 3, Fig. 3.2):

$$T'_{do} \dot{e}'_q = -e'_q - (x_d - x'_d) i_d + e_{fd} \quad (3.234)$$

2. Coupling equations between generator and bus (block 2, Fig. 3.3):

- a. For the generator side:

$$e'_q = e_q + x'_d i_d + r i_q \quad (3.235)$$

- b. For the bus side see Eqs. (3.205) and (3.206).

Type IV: Minimal, Decoupled Voltage, and Angle Dynamics The final step of simplification inherently decouples the electromagnetic dynamics from the electromechanical ones. It is then the coupling equations between the electrical and mechanical side (blocks 1 and 3, Fig. 3.3):

$$P_G = E i \cos \varphi = e_d i_d + e_q i_q \quad (3.236)$$

$$Q_G = E i \sin \varphi = e_d i_q - e_q i_d \quad (3.237)$$

which disappear. This of course is a major simplification, but the price is a model that may not be precise enough under some circumstances. Good judgment needs to be used.

Actually two models result: one for the angle dynamics and one for the voltage dynamics. Both the electromechanical dynamics and the electromagnetic dynamics are included here for completeness as type IV₁ and type IV₂, respectively in Table 3.3.

TYPE IV₁: SIMPLIFIED DECOUPLED ANGLE DYNAMICS (SOMETIMES CALLED “CLASSICAL MODEL”) The basic assumption here (see block 2, Fig. 3.3) is that the voltage behind the transient reactance is constant, $e'_q = E' = \text{const}$, which along with the assumption of no damper winding made for the type III₂ model means that there are no voltage dynamics. Thus the simple circuit and vector diagram in Figure 3.30 describe the entire model. The “dynamic equation” is incorporated in Table 3.3, which also compares complementary types IV₁ and IV₂.

TYPE IV₂: SIMPLIFIED DECOUPLED VOLTAGE DYNAMICS The basic assumption here is complimentary to the assumption on which the type IV₁ model is based. It is assumed that the bus power P_G is constant and that the turbine power P_T is matching it exactly. If so, because there is only one section, then $\theta = \text{const}$, and there are no angle dynamics. The dynamic state equation given in Table 3.3 is derived by starting with the voltage dynamics given in Eq. (3.223), using

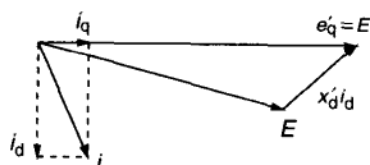
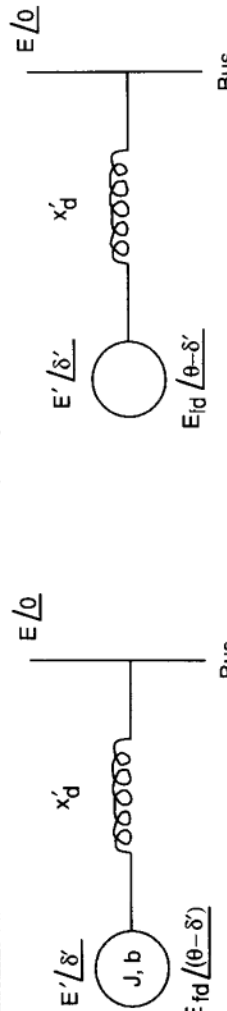


FIGURE 3.30 Vector diagram of a constant voltage behind transient reactance (type IV₁) model.

TABLE 3.3 Two Complementary Simplified Models for Stability Studies (Types IV₁ and IV₂)

SIMPLIFIED ("CLASSICAL") MODEL FOR ROTOR ANGLE STABILITY (IV ₁)	SIMPLIFIED MODEL FOR VOLTAGE STABILITY (IV ₂)
<u>Assumptions:</u>	<u>Assumptions:</u>
1) Generator and infinite bus with constant voltage. 2) Voltage behind transient reactance, E' , fixed. 3) $\dot{\theta} = \dot{\delta}'$ and $\dot{\theta} = \dot{\delta}'$ so $\theta - \delta'$ is const, where θ is rotor phase, δ' is phase of E' . Then one axis rotor angle dynamics results $\ddot{\delta}' + D\dot{\delta}' = P_T - \frac{1}{x'_d} E' E \sin \delta'$	1) Generator and load without rotating machine. 2) Turbine shaft power, P_T exactly matches load power injection $P_L = P_T$. 3) $\cos(\theta - \delta') = \text{const} = 1$ that is $\theta - \delta'$ is small and constant. Then one axis voltage dynamics results $T_d \dot{E} = - \frac{x_d}{x'_d} E' + \frac{x_d - x'_d}{x'_d} E \cos \delta + E_{fd}$
	<p>This assumption means that the phase of the voltage behind the transient reactance is rigidly tied to rotor angle or, equivalently, lined up with it at $\theta = \delta'$.</p>
4) Equivalent Circuit	4) Equivalent Circuit 

relationship (3.224) as

$$e'_q = E_q + x'_d i_d = E \cos \delta + x'_d i_d$$

which when further combined with the internal voltage relations $e'_q = E'$, $i_d =$

$$\frac{e'_q - E_q}{x'_d} = \frac{E' - E \cos \delta}{x'_d}$$

leads to type IV₂ model in Table 3.3.

This table juxtaposes type IV₁ and IV₂ models and shows them to be counterparts. These highly simplified final models can be very useful for initial exploration. In fact, most of the angle stability studies through the 1960s were based on this “classical model”, type IV. Now that interest has developed in voltage stability, corresponding a fundamental inquiry can be carried out in voltage, leading to the type IV₂ simplification.

The final arbitrary thought models Type IV₁ and IV₂ are derived by eliminating the direct coupling between the electromagnetic and electromechanical subprocesses. However, by making both δ and E' states and considering models IV₁ and IV₂ together as a model IV coupling could be restored approximately in a single model.

3.2.3.9 Unifying the d- and q-axis Representation of the Generators with the Phasors of the Transmission System via the Blondel Transformation The basic structure of the power system is displayed in Figures 3.2 and 3.3, and some of the details were discussed earlier in this chapter. It will be useful, however, to look at this chapter from a different viewpoint in an even more concise sketch as shown in Figure 3.31. Three components arise.

1. *Transmission*, that is, a network of high-voltage transmission lines connecting buses (nodes), is at the core of the system (see the sketch in Fig. 3.31). All states or signals within are modulated AC (or appear to be such at the end points for high-voltage DC lines, SVC) and also at the terminals of the generator. It has a sparse connection matrix (from 2 to 10 lines per bus), even for large systems. This part is represented by a set G of equations (blocks 9 and 10 in Figs. 3.2 and 3.3).
2. *Equipment* such as generators, loads, and various mechanically switched and power electronically switched devices are connected to individual buses (blocks 1 to 3 in Fig. 3.2). Each item has its own dynamics in various forms, usually the differential equations throughout this chapter. None of the equipment is physically in a modulated AC form, and there is no direct coupling between individual items outside their connection to the buses. The equipment dynamics are symbolically represented in Figure 3.31 as set F .
3. Since the mathematical form of describing the dynamics is thus quite different for transmission and the attached equipment, conversion equations (e.g., Blondel transformation) are typically needed for the interaction between the G and F sets (Fig. 3.31). As seen from the preceding discussion and reinforced later, the mathematical representation, or language, used in the G and F sets are quite different.

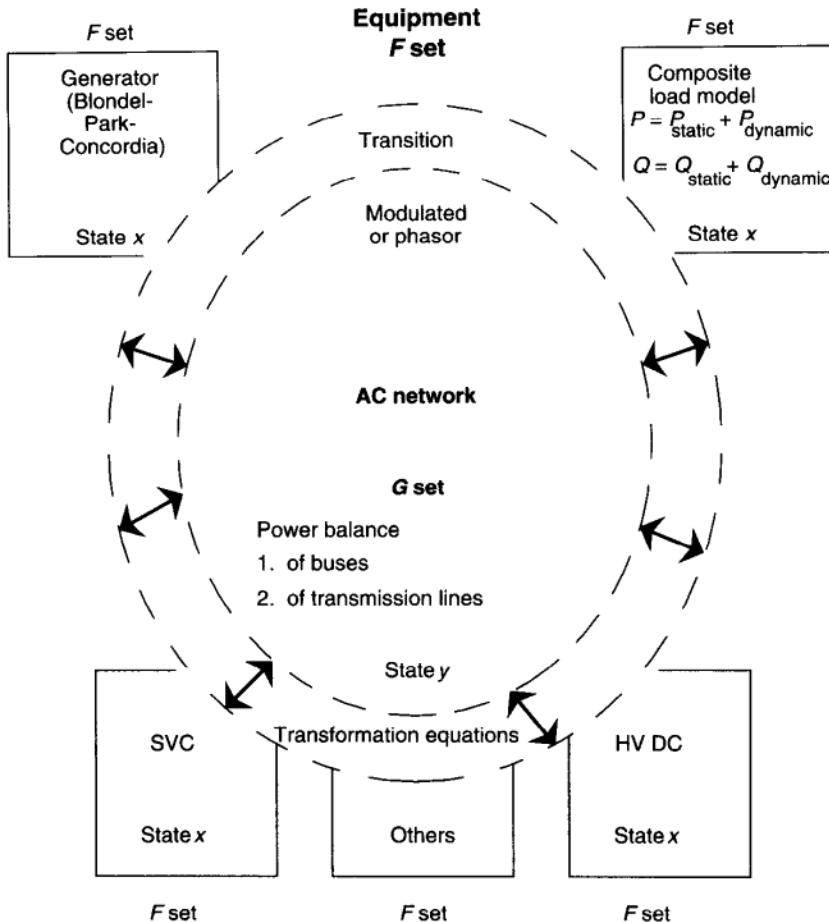


FIGURE 3.31 Sketch of the overall power-system structure.

4. The G set uses phasors $E\angle\delta$, $I\angle\delta + \varphi$, etc. to describe the electrical state variables (Chapter 2). For instance, consider a balanced three-phase signal $e(t)$ of the form

$$\underline{e}(t) = \begin{pmatrix} e_a(t) \\ e_b(t) \\ e_c(t) \end{pmatrix} = \begin{pmatrix} \sqrt{2}e_a(t) \cos[\omega t + \delta_a(t)] \\ \sqrt{2}e_b(t) \cos[\omega t + \delta_b(t)] \\ \sqrt{2}e_c(t) \cos[\omega t + \delta_c(t)] \end{pmatrix} \quad (3.238)$$

Among these three phase signals, the set of all balanced three-phase signals can be distinguished. Precisely we say that $e(t)$ is balanced if there exist smooth scalar functions $E : \mathbb{R} \rightarrow \mathbb{R}$ and $\theta : \mathbb{R} \rightarrow \mathbb{R}$ such that

$$\begin{aligned} \underline{e}(t) &= \begin{pmatrix} e_a(t) \\ e_b(t) \\ e_c(t) \end{pmatrix} = \begin{pmatrix} \sqrt{2}E(t) \cos[\omega t + \delta(t)] \\ \sqrt{2}E(t) \cos[\omega t + \delta(t) - (2\pi/3)] \\ \sqrt{2}E(t) \cos[\omega t + \delta(t) + (2\pi/3)] \end{pmatrix} \\ &= \sqrt{3}B(t) \begin{pmatrix} E(t) \cos \delta(t) \\ E(t) \sin \delta(t) \\ 0 \end{pmatrix} \end{aligned} \quad (3.239)$$

where $B(t)$ is the orthonormal matrix,

$$B(t) := \sqrt{2/3} \begin{pmatrix} \cos(\omega t) & -\sin(\omega t) & 1/\sqrt{2} \\ \cos(\omega t - 2\pi/3) & -\sin(\omega t - 2\pi/3) & 1/\sqrt{2} \\ \cos(\omega t + 2\pi/3) & -\sin(\omega t + 2\pi/3) & 1/\sqrt{2} \end{pmatrix} \quad (3.240)$$

Observe that, as is commonly known, a balanced three-phase signal has two independent state variables $E(t)$ and $\delta(t)$.

Note that the $d - q$ representation is valid originally for the region in the interior of one synchronous machine which is in its complete model.

Now for the balanced signals, we can define the associated time-varying phasor $E(\cdot)$ by inverting the linear transformation $B(t)$ in Eq. (3.239). For the balanced three-phase signals we represent the phasor operator by the symbol \mathcal{P} . The phasor representation $\mathcal{P}(e(t)) := E(t)$ of a balanced sinusoidal three-phase signal $e(t)$ is

$$\begin{aligned} \mathcal{P}(e(t)) = E(t) &=: e_d(t) + j e_q(t) \\ &=: E(t) \cos \delta(t) + j E(t) \sin \delta(t) \\ &=: E(t) e^{j\delta(t)} = E(t) \angle \delta(t) \end{aligned} \quad (3.241)$$

This relation applies strictly to the bus voltage where the generator terminals are physically connected. Mathematically, the transformation and Eq. (3.241) can be applied to internal voltages of either G or F to eliminate the transformation belt in Figure 3.31. One must remember, however, that G and F have different type of dynamics (RLC network model and respectively generator models of type I through IV) even if displayed in the same type of coordinates. Accordingly

1. Converting the F region coordinates into phasor form will not make them actually phasors since their dynamics is still that of F , that is the internal dynamics of the generator. This fact would make the manipulation of the system in the phasor form even more complicated than handling the transformation belt of Figure 3.31. An exception is the use of the brutally simplified approximation model Type IV₁ (the classical model) which is already reduced to a RLC format.
2. More promising is to go in the opposite direction and convert the interior dynamics of the G set (the transmission system) to the $d - q$ format. In fact, the dynamics of the generator already has some (RLC) components (armature leakage reactance and the transformer between the bus and the generator) incorporated and handled in the $d - q$ fashion. Then if the G set is converted into the $d - q$ coordinates this established practice could simply be expanded into the G set. This model is used in Chapter 4, Section 4.2.1.

Certain facts should be kept in mind. The B transformation is a mathematical transformation. When it is applied to a physical quantity such as e it should not be expected that the transformed quantity will have direct physical meaning. Yet if a mathematical analysis is carried out in the transformed domain correctly, then the inverse transform of the result back into the original coordinates will

present the correct physical solution. Think of the use of Laplace transforms. The Laplace transform as such has no direct physical meaning (although after using it a long time, one may get the feeling that it does), yet results obtained in the s domain give the right physical meaning after inverse-transforming them into the physical, time domain.

Similarly here the phasor quantities have physical meaning in the G but not in the F domain, and in fact their use in the F domain in a physical sense is undesirable, as it causes complexity (in fact the Blondel–Park effort tries to get away from this). The converse, the use in the G domain of the Blondel coefficients, which are physical in the F domain, but not in the G domain, may lead to simplifications through unifying the representation across the entire system. However, if shunt capacitances are present, then the coefficients in the transformed system do not have “physical” meaning. As with the Laplace transform, this should not prevent doing mathematical manipulations. The inverse transform then gives the answer in “physical” terms.

3.2.3.10 Load Dynamics Realistic dynamic modeling of composite loads is one of the great unsolved (possibly unsolvable) problems of the electric power field. No model so far can give good results, although substantial effort was expended throughout the years, both by using synthetic analysis of composite loads and by overall statistical descriptions and estimations. The intensity of these efforts has escalated strongly in recent years, but the practical validity of the proposed models remains dubious and unproven. Simple conjectured models, such as constant load injection or constant impedance, were used extensively in simulation studies. These crude approximations of the load model often make contributions in the literature of questionable validity.

Load modeling is not a subject of this book but it is necessary to state some appropriate models and try to make it as realistic as possible. There is a fundamental difference between modeling the composite load and modeling power equipment such as generators, transformers, capacitors, reactors, SVC, HV DC, converters, and inverters. Some of this equipment is quite complex (such as generators and power electronics or thyristor devices like the thyristor-controlled reactances known as SVC). Their structure, however, is well known and their dynamics and static behavior are well understood. Also these are large pieces of equipment connected to the buses in very limited numbers. So precise models are readily written and if necessary simplified with good approximations at varying levels.

The load, that is, the composite load connected to a bus, however, consists of millions of individual components of many different types and sizes, for example, incandescent and fluorescent lights, induction motors, thyristor controlled motors, heaters, many types of electrical and electronic control devices (e.g., control of central heating), synchronous motors, fans, and other air moving equipment, to mention just a very few types. This complex melange is connected to the transmission-system bus through a very large (county size or larger) network of several levels, that is, subtransmission, high- and low-voltage distribution all the way down to a bedside lamp. Traditionally there is no interconnection of

generators through the sub-transmission network (and if there is, then it becomes transmission) but in the age of cogeneration small generators would also feed into this “composite load.” Furthermore, the subtransmission distribution network is far from being passive. It has its own automatic voltage control devices as well as protection, such as overcurrent relays and fuses. Motors in industrial plants are often subject to undervoltage dropping. Emergency load dropping commands from the transmission side may result in deenergization of substantial sections of the load on subtransmission and distribution.

There would be a few well-identified and very large loads such as an aluminum or steel plant and a hydraulic pumped storage station. Such loads are connected either directly to the transmission bus or to a high level of subtransmission. These can be treated as individual entities for which precise individual models can be worked out.

3.2.3.11 Modeling of a Composite Load through its Components In principle, more or less precise models for the individual items of the composite load can be produced. Also in principle, a detailed model for the entire composite-load system with its internal controls, etc. (as outlined), can be written, although such a program would be of gargantuan proportion and of little practical use since the detailed data are simply not available.

Next, one could postulate the percentage share of each type of load (e.g., fluorescent lights and induction motors) and try to derive a “composite” model, but again the percentage data information is not available, and to analyze the interaction of the various types (concentrated in artificial groups) through the subtransmission distribution network would be a virtually unsolvable task. Nevertheless, considerable effort along these lines has been reported in the literature. Of special interest is a recent 1993 IEEE Task Force Report [17] that gives a detailed but still qualitative description of the variety of components as described before. It gives some typical ranges for quantities such as the dropout voltage of various motor loads but prudently avoids presenting mathematical models for the various load components. It does, however, offer a sampling of reputable papers from the recent literature in its list of references.

3.2.3.12 Overall Fitted Modeling of Composite Load An approach more realistic than the mathematical modeling of components would be to record the voltage and frequency dependence of the composite load on line and then fit a model of an appropriate nature to it. This still is easier said than done. First, such a model would strictly speaking be applicable only for the location where the measurements are taken. Second, it may be possible to perform such measurements on actual composite loads and typify them only over a limited band of voltage or frequency (tolerable to the customer while data are collected) by organized experiment (e.g., [18]). Such a band may cover conditions that arise in studies of viability as in Chapters 5 and 14. Third, however, no organized experiments on the live system are feasible for large transient conditions such as those studied in parts of Chapters 6 through 12. In this latter situation voltage

and frequency models could be retrofitted from oscillograms taken during actual large disturbances.

With all these difficulties this latter approach—fitting overall or blanket composite-load models from actual measurements on the composite load itself—seems most promising, both from the viewpoint of feasibility and accuracy. This approach will be discussed here briefly.

What we have then is the load as an empirical function of voltages and/or frequency that needs to be fitted with a mathematical expression “optimally” in some sense. The result must also be general in the sense that case-by-case fitting is not required. In fact, the form of possible models will be discussed here. Two assumptions will be made.

Assumption 1 The composite load as a function of the bus voltage and frequency is smooth (continuous and differentiable) and hence it can be approximated effectively by smooth or analytic functions. This is a physical reality. (Loss of extra large units is an isolated disturbance that locates dynamic response, treated separately.)

Assumption 2 It is assumed (as an approximation) that a superposition principle applies to the composite bus load that is active and reactive, static and dynamic components are not coupled, and furthermore the dependency of these components on the bus voltage and the frequency are not coupled.

$$P_L = P_D + P_S \quad (3.242)$$

$$Q_L = Q_D + Q_S \quad (3.243)$$

where P_S and Q_S are the static power demands, while P_D and Q_D are the dynamic power demands and

$$P_S(E, \omega) = P_S(E_0, \omega_0) + \Theta P_E(E - E_0) + \Theta P_\omega(\omega - \omega_0) \quad (3.244)$$

$$Q_S(E, \omega) = Q_S(E_0, \omega_0) + \Theta Q_E(E - E_0) + \Theta Q_\omega(\omega - \omega_0) \quad (3.245)$$

In an alternative formulation,

$$P_S(E, \omega) = P_{S\omega}(E_0, \omega - \omega_0)P_{SE}(E - E_0, \omega_0) \quad (3.246)$$

$$Q_S(E, \omega) = Q_{S\omega}(E_0, \omega - \omega_0)Q_{SE}(E - E'_0, \omega_0) \quad (3.247)$$

where E_0 and ω_0 are the nominal variables at the operating point.

While these components are not strictly independent, this division seems inevitable at the present state of knowledge. Fortunately it also is a good approximation since on the power system the couplings neglected are also inherently quite weak. Since this section is dealing with one bus at a time the bus indexing i (Fig. 3.3) will be omitted as in other sections of this chapter.

3.2.3.13 Static Load Components: Options on Fitted Models Since the composite load varies in a smooth manner with voltage and frequency it can be fitted with appropriate smooth functions. There could be two principal options.

Option 1 Fitting with a noninteger exponential using notations from Ref. [17] and Eqs. (3.246) and (3.247),

$$P_{SE} = P_{SE0} \left(\frac{E}{E_0} \right)^{kpe} \quad (3.248)$$

$$Q_{SE} = Q_{SE0} \left(\frac{E}{E_0} \right)^{kqe} \quad (3.249)$$

and similarly for the frequency terms,

$$P_{S\omega} = P_{S\omega0} \left(\frac{\omega}{\omega_0} \right)^{kp\omega} \quad (3.250)$$

$$Q_{S\omega} = Q_{S\omega0} \left(\frac{\omega}{\omega_0} \right)^{kq\omega} \quad (3.251)$$

This form is fairly convenient for computation but less so for analysis in which E and ω themselves are functions. Large software packages like EPRI-ETMSP [19] offer it in their menus. Some typical experiments are listed in Ref [18] for a blend of option 1 for E and option 2 for f , that is, ω . Historically this option seems to be more popular in mechanical than in electrical engineering.

Option 2 Fitting with a Taylor-series expansion around the nominal operating point (E_0, ω_0)

$$\begin{aligned} P_S(E, \omega) &= P_S(E_0, \omega_0) + \sum_{k=1}^{\infty} \frac{1}{k} \left. \frac{dP_s}{dE} \right|_{E_0} (E - E_0)^k \\ &\quad + \sum_{k=1}^{\infty} \frac{1}{k} \left. \frac{\partial P}{\partial \omega} \right|_{\omega_0 E_0} (\omega - \omega_0)^k \end{aligned} \quad (3.252)$$

$$\begin{aligned} Q_S(E, \omega) &= Q_S(E_0, \omega_0) + \sum_{k=1}^{\infty} \frac{1}{k} \left. \frac{dQ_s}{d\omega} \right|_{E_0 \omega_0} (E - E_0)^k \\ &\quad + \sum_{k=1}^{\infty} \frac{1}{k} \left. \frac{dQ}{d\omega} \right|_{\omega_0 E_0} (\omega - \omega_0)^k \end{aligned} \quad (3.253)$$

With the available best level of information it would be unjustified in most cases to continue the series beyond $k = 2$, which leaves

$$\begin{aligned} P_S(E, \omega) &= P_S(E_0, \omega_0) + \left. \frac{dP_s}{dE} \right|_{\omega_0 E_0} (E - E_0) + \frac{1}{2} \left. \frac{d^2 P_S}{dE^2} \right|_{\omega_0 E_0} (E - E_0)^2 \\ &\quad + \left. \frac{dP_S}{d\omega} \right|_{\omega_0 E_0} (\omega - \omega_0) + \frac{1}{2} \left. \frac{d^2 P_S}{d\omega^2} \right|_{\omega_0 E_0} (\omega - \omega_0)^2 \end{aligned} \quad (3.254)$$

and a similar representation for $Q(E, \omega)$

$$\begin{aligned} Q_S(E, \omega) &= Q_S(E_0, \omega_0) + \frac{dQ_S}{dE} \Big|_{\omega_0 E_0} (E - E_0) + \frac{1}{2} \frac{dQ_S^2}{dE^2} \Big|_{\omega_0 E_0} (E - E_0)^2 \\ &\quad + \frac{dQ_S}{d\omega} \Big|_{\omega_0 E_0} (\omega - \omega_0) + \frac{1}{2} \frac{d^2 Q_S}{d\omega^2} \Big|_{\omega_0 E_0} (\omega - \omega_0)^2 \end{aligned} \quad (3.255)$$

Note that the cross terms are omitted in agreement with Assumption 2. For a given operating point (E_0, ω_0) Eqs. (3.254) and (3.255) can be rewritten under the decoupling assumption as

$$P_S(E) = P_{L0} + ME + GE^2 \quad (3.256)$$

$$Q_S(E) = Q_{L0} + KE + BE^2 \quad (3.257)$$

These terms have physical meanings beyond being coefficients of a Taylor series. Specifically, the terms P_{L0} and Q_{L0} represent, respectively, active- and reactive-power load injections. Terms ME and KE may be interpreted as active and reactive current injection components, which at fixed voltage generate the respective power components in proportion to the bus voltage. Finally GE^2 and BE^2 are the active- and reactive-power components of a shunt admittance, $G + jB$. The latter then represents an *impedance load*, which is frequently used as the sole load model.

Of course these injections and impedances are physical only in principle. The true meaning of the three terms is a truncated Taylor approximation of a formation known only by measurement and experiment. So one should not go looking for the current injection into the system or system impedance in a physical sense as is customary in some of the literature.

For the frequency, similar second-degree representations can be used. They follow directly from Eqs. (3.254) and (3.255), again under the real-power–voltage decoupling assumption. However the active and reactive powers are less sensitive to frequency variations than to voltage variations so a first-degree expansion may be adequate:

$$P_S(\omega) = P_0 + N(\omega - \omega_0) + H(\omega - \omega_0)^2 \cong P_0 + P_0 K_{pf}(f - fs) \quad (3.258)$$

$$Q_S(\omega) = Q_0 + L(\omega - \omega_0) + C(\omega - \omega_0)^2 \cong Q_0 + Q_0 K_{qf}(f - fs) \quad (3.259)$$

where the second form is written in the notation of Ref. [17]. The typical parameters for the model of the form

$$P = P_0 \left(\frac{E}{E_0} \right)^{K_{pv}} [1 + K_{pf}(f - f_0)] \quad (3.260)$$

and

$$Q = Q_0 \left(\frac{E}{E_0} \right)^{K_{qv}} [1 + K_{qf}(f - f_0)] \quad (3.261)$$

are given as Table 3.4 [18]. This model represents a reasonable static load model for computations and some of the static analysis of the type of Chapters 5 and 14. Note that the model used in Table 3.4 is a blend of expansion for f and noninteger exponent for E . For most analytical work the noninteger exponent creates difficulties and an expansion-type model may be more convenient.

It appears futile at this time to try to identify P_{L0} , M , G , Q_{L0} , K , and B in Eqs. (3.256) and (3.257) from direct modeling of the component of the bus load. The best route is to conduct measurements on the system itself by varying the voltage and measuring active and reactive power at various static voltage levels. The resulting curves are then easily fitted with coefficients as in Eqs. (3.256) and (3.257). Various terms, potentially power injection P_{L0} and/or Q_{L0} and constant impedance G and/or B , are quite commonly used individually, mostly motivated by their convenience for analysis but without any factual or physical justification.

The representation in Eqs. (3.256) and (3.257) was suggested in 1981 by Kalinowsky and Forte [18] on the basis of extensive experimental studies performed on the live Consolidated Edison system (New York City) at three substations. These studies gave credence to the proposed representation although the voltage range that can be used on a live system (0.95 p.u. to 1.02 p.u. in this case) did not allow any numerical identification of the quadratic coefficients.

The experiments covered three substations. Among them the composition of loads varied widely: 10% to 60% residential, 30% to 40% small commercial, and 60% to 100% large commercial and industrial. The locations of the substations were in Manhattan (two networks), Brooklyn, and Queens.

Thus these results seem to give a representative basis for the model in Eqs. (3.256) and (3.257). According to Kalinowsky and Forte the value of the higher-order terms is higher for megavolt-ampere than for megawatt consumption because fluorescent lights have this characteristic. A special study of fluorescent characteristics is included in the paper. The presence and realism of a quadratic term is quite visible (at least in reactive power) in these laboratory tests since the voltage was varied over a much wider range than was possible on the live system. Conceivably the share of fluorescent light load could be lower at locations other than New York City.

The model of Ref. [18] is shown on Figure 3.3. Note that the two injection terms (P_i , Q_i) and the constant admittance terms (P_z , Q_z) are separated in Figure 3.3 as follows:

$$P_S = P_i + P_z, \quad P_i = P_{L0} + ME, \quad P_z = GE^2 \quad (3.262)$$

$$Q_S = Q_i + Q_z, \quad Q_i = Q_{L0} + HE, \quad Q_z = BE^2 \quad (3.263)$$

This is convenient because, as was explained above, the constant admittance shunt branches at bus i include line charging and capacitors or reactors along with the load in the general system model shown in Figure 3.3.

Currently several major companies such as the New York Power Pool and Ontario Hydro are conducting major studies on their systems, so gradually refined results will be presented in the future (and probably summarized in future IEEE

TABLE 3.4 Typical Load Voltage and Frequency Parameters [18]

	<i>p.f.</i>	<i>Kpv</i>	<i>Kqv</i>	<i>Kpf</i>	<i>Kqf</i>
Residential					
Elec. heating					
Northeast					
Summer	0.90	1.2	2.7	0.7	-2.3
Winter	0.99	1.7	2.6	1.0	-1.7
North-Central					
Summer	0.90	1.1	2.6	0.8	-2.3
Winter	0.99	1.7	2.6	1.0	-1.7
South					
Summer	0.87	0.9	2.4	0.9	-2.1
Winter	0.97	1.5	2.5	0.9	-1.8
West					
Summer	0.92	1.3	2.7	0.8	-2.2
Winter	0.99	1.7	2.5	1.0	-1.5
Nonelec. heating					
Northeast					
Summer	0.91	1.2	2.8	0.7	-2.3
Winter	0.93	1.6	3.1	0.7	-1.9
North-Central					
Summer	0.91	1.3	2.8	0.7	-2.3
Winter	0.96	1.5	3.0	0.8	-1.7
South					
Summer	0.89	1.1	2.5	0.9	-2.0
Winter	0.97	1.6	2.9	0.8	-1.6
West					
Summer	0.94	1.4	2.9	0.7	-2.1
Winter	0.97	1.5	2.8	0.9	-1.3
Commercial					
Elec. heating					
Summer	0.85	0.5	2.5	1.2	-1.6
Winter	0.90	0.6	2.5	1.5	-1.1
Nonelec. heating					
Summer	0.87	0.7	2.5	1.3	-1.9
Winter	0.90	0.8	2.4	1.7	-0.9
Industrial					
Primary aluminum	0.85	0.1	0.6	2.6	1.6
Steel mill	0.90	1.8	2.2	-0.3	0.6
Power plan aux.	0.83	0.6	2.0	1.5	0.6
Agricultural pumps	0.80	0.1	1.6	2.9	0.6
	0.85	1.4	1.4	5.6	4.2

Task Force reports) resulting in gradually more refined data. Many researchers are also pursuing work in this direction [20], [21]. It is doubtful, however, that comprehensive load models will ever go beyond classification of the type for middle-income residential in the northeast, for example. It is most unlikely that utilities will ever be able to justify the cost and effort to obtain refined quantitative data by type (e.g., residential activity) of load composition on the specific areas of the data type "middle income residential," so researching the type of specific detailed models on such components may be futile.

3.2.3.14 Dynamic Load Components The genesis of dynamic load components is even less understood than that of the static ones. Also, the effect here is more divergent for active power and reactive power. Accordingly, these will be separately discussed.

3.2.3.14.1 Load Dynamics in Active Power It was recognized since the mid-1960s that energy accumulating in the system inertia plays an important role in the performance of load frequency control here [22 to 25]. This would imply a dynamic model of bus load power

$$P_D = D_L \dot{\theta} + J_L \ddot{\theta} \quad (3.264)$$

Remember that torque and power are the same numerically in per unit at rated frequency. The variations of frequency are small compared to the rate $\dot{\theta} = \omega_s$. Thus in Eq. (3.264) $D_L \dot{\theta}$ represents the deviation of the kinetic energy [neglecting the $\dot{\theta}^2$ term in $(\omega_s + \dot{\theta})^2$]. The term $J_L \ddot{\theta}$ represents the rate of change of the kinetic energy stored in the load inertias.

Note that Eq. (3.264) represents a dynamic equation much in the nature of Eq. (3.46) and can be incorporated in system stability studies in a similar role [22].

Data for D_L and J_L are not easily obtained, however. The best route seems to be the use of automatic fault oscillograph records after sudden changes such as losses of major generators or lines. At the slower levels statistical analysis of the random part of load frequency control records can be applied [23 to 25].

It should be noted that Eq. (3.264) only displays the dynamic dependence on the angular velocity deviation $\dot{\theta}$ from the synchronous speed ω_s . Certainly the composite load on the bus will also depend on the bus voltage E in some dynamic ways beside the static found in Eq. (3.256). In the absence of a detailed understanding of the dynamics of the load model, a refined picture is far in the future. About the best one could do is to consider the angle and voltage dynamics decoupled (there is a well-known tendency of such a decoupling of the steady-state load-flow equations). Accordingly Eq. (3.264) is proposed in this text as the electromechanical dynamic model. In fact in certain problems D_L and/or J_L may be considered small based on the numerical values and the time scale of the phenomenon studied. Then, this component of the load dynamics can be neglected.

3.2.3.14.2 Electromagnetic Load Dynamics First, one should realize that the dynamics of the bus load P_L in E that result from the line inductances and capacitances on the bus side should be expected to be instantaneous in the same sense

and for the same reason that the electromagnetic dynamics of the transmission system is taken as instantaneous. In both cases the energy-storage elements are electric and magnetic fields around, respectively, the transmission and distribution lines, all of which have very short time constants and small resistive components and hence fast dynamics. Accordingly and as an approximation, the assumption is made that this component of the load dynamics (sometimes called parasitic) is instantaneous. There are problems, however, where this dynamics plays a vital role such as in switching- and lightning-caused overvoltages and in behavior around singularities (Chapter 11). Furthermore, the lumped-constant representation of the transmission lines is not valid except in the 60-cycle steady state, a fact easily forgotten.

There are dynamic components in voltage that fall more in the framework of problems considered here. Active and reactive power of induction machines certainly have strongly coupled dynamic responses in frequency $\dot{\theta}$ and voltage \dot{E} . The well-known induction motor dynamics has been transcribed into an equivalent-system-size machine [26], but the usefulness of this is questionable because the induction-machine component of the load is hard to determine and it would not act as a single machine. Other dynamic components abound; fluorescent lights certainly supply a dynamic voltage component. The dynamics of thyristor-controlled motors are becoming important as well as the dynamics produced by automatic devices such as low-voltage protection of motors. In the face of this variety, the best policy again appears to be a generalized representation, trying to cover the overall dynamics with a low-degree (first or at most second) representation. Some recent realistic and competent studies [27] done in different countries strongly support this approach. They display, for example P and Q step responses in a form analogous to a well-damped linear second-degree response.

Based on this observation electromagnetic load dynamics models of the following general form will be used:

$$\ddot{P}_D + \alpha \dot{P}_D = \beta P_D + kE \quad (3.265)$$

$$\ddot{Q}_D + C \dot{Q}_D = d Q_D + h E \quad (3.266)$$

Coefficients again may be found from studies of fault oscillograms. Note that for many situations first-degree dynamics (with the second derivative omitted) will be quite satisfactory. Note also that most load dynamics proposed in the literature are formulated as $\dot{E} = f(P, E)$ rather than the form $\dot{P} = f(P, E)$ proposed here. This alternative formulation is questionable since physically the voltage is the input to which the power responds dynamically.

3.2.4 Bus-Connected Equipment with Models Consisting of Many Individual Types, Mostly Primary Controllers

The components of the power system discussed in Section 3.2 so far (boxes 1 through 15 in Figs. 3.2 and 3.3) have dynamics which have basically a physical

and mathematical structure that is consistent with specifications of all manufacturers and all interconnected areas. Even within these models, however, the coefficients of the components are variable without any standardization or quantization. This latter fact differentiates the power system from such systems as the telephone system in which components would tend to be identical, numbering in the millions. With respect to the dynamics of primary-control devices such as governors and excitors (blocks 11 to 13 in Figs. 3.2 and 3.3), which are directly associated with individual component manufacturers' practices, not only the coefficients but also the basic structure and nature of the model will be variable. Some primary-control devices such as capacitors, reactors, automatic tap changers, load dropping, and line switching (block in Figs. 3.2 and 3.3) will also act in discrete steps rather than continuously as do all components mentioned in blocks 1 to 10 in Figures 3.2 and 3.3.

It has been customary to refer to primary devices that respond to deviation in real power or voltage phase angle from the desired set point as the *real-power controllers*. Similarly, devices that respond to the error in voltage magnitude or reactive power are referred to as *voltage controllers*. This is potentially misleading since any change in system input generally affects the entire coupled system dynamics. Further analytic work is needed to justify the claim that a particular device in a particular application primarily affects real power or voltage only. To start with, this customary terminology should be understood as described here without drawing immediate conclusions regarding the major impact of these devices on the interconnected system dynamics.

A close look into a variety of primary controllers reveals the fact that most of the primary controllers available for system stabilization are voltage controllers. The devices that are capable of controlling real-power dynamics directly in the fastest time framework following major system changes have been sparse until very recently. Most representative devices of this sort have been fast-valving, generation-dropping, and/or load-shedding devices. This situation is being drastically changed with the influx of HV-DC technologies, which are ideal for the purpose of direct control of real power and by the development of electronic devices, which result in tap changing of transformers, including phase shifters, at a high speed. This is replacing the present practice of OLTCs moving as slowly as 1 tap per 100 seconds. In this process additional opportunities to improve performance emerge. This device is referred to as a controllable phase shifter. Versions of this technology are emerging, called a unified power controller (UPC) adopted by industry [28, 29]. One should keep in mind, however, that the HV-DC and FACTS-type devices can only change the distribution of network flow rather than the actual injection or withdrawal of real power.

More traditional primary controllers (the majority of these now in operation) available for fast control are voltage controllers. Controlling voltage depends largely on the control of reactive power sources. Some of these are specifically installed for the purpose. Historically the first such devices were synchronous condensers joined around 1950 by static shunt capacitor banks and later by reactors for transmission lines. Thyristor-controlled reactances (TCRs), advanced

versions of SVCs, are the latest and most flexible entries still in the process of coming into their own. Transformers with taps that can be changed (to control voltage or phase) have been available a long time out. Their reliability is still improving, particularly with the inclusion in the 1960s of vacuum switches to interrupt the differential current. Capacitor banks, reactors, and automatic tap changers are by nature structural control devices, since they affect the structure and parameters of the admittance matrix representing the transmission grid.

To conclude, the primary-controller components are installed on the system with the prime purpose of facilitating the operation of the standard components, such as synchronous machines and the transmission system. As such, they are primarily devices used for responding to local deviations in voltage and frequency at the locations of standard components from their values set at the system level. Because their main function is to respond to the error in voltage and/or frequency relative to the setpoint they can be generally categorized as control devices. This is true although not all of these devices respond in an automatic way. Some are preprogrammed according to the off-line studies or anticipated load changes on the system. A majority of these devices respond in an automated way to a signal deviation.

Because of a wide variety of these components and their nonuniform design, it is hard to classify them further into subgroups. Here one possible classification is used according to the frequency of use and the underlying control technology:

1. Semistandardized Continuous Controls of Synchronous Machines. These devices are governors the main purpose of which is to regulate frequency of each generator locally and exciter systems that control the terminal voltage of each generator locally. These devices are routinely used on each synchronous machine. They are briefly described later in subsections on

- Governor and turbine dynamics
- Exciter dynamics
- Synchronous condensers

2. Semistandardized Structural Control Devices. These devices consist of a wide group of reactances of different types connected to the system as either shunts or devices in series with the transmission lines. They are switched in and out of the system in response to voltage or frequency deviations. The switching technology is primarily mechanical, and furthermore it is not always automated. The representative subgroups of these devices are as follows:

- Capacitors and reactors
- Series capacitors
- On-load tap-changing transformers
- Phase-shifting transformers
- Load dropping
- Line dropping
- Generator dropping and fast valving

All devices in this group share a common property that they change in a discrete manner, both in amount and time. They share this property with the newest technologies of electronically switched devices.

3. Electronically Switched Devices—Flexible AC Transmission Systems. This last large group of controls on the system is based on fast electronically based switching. The term used at present in referring to these devices is flexible AC transmission systems (FACTS). Power electronics technology provides a means for rapid control of power-transmission systems. Modern implementation of traditional, semistandardized control devices using thyristor switches and fast electronic controls has led to devices such as static Var compensators (SVCs) for transmission voltage control, controllable series capacitors (CSCs) for transmission-line impedance control, and phase shifters (PSHs) for transmission-angle adjustment [29]. The use of recently developed gate-turn-off (GTO) thyristors allows for advanced, all solid-state, and uniform implementation of SVCs, CSCs, and PSHs. This technology is very varied, and only equipment representative of the functional concepts is described in this section under the following subgroups:

- Static var compensator (SVC)
- Controllable series capacitor (CSC)
- Phase shifter (PSH)
- HV-AC or HV-DC control technology

These components are described next according to the classification just described.

3.2.4.1 Semistandardized Continuous Controls of Generators This section is devoted to components that have nonstandardized models but describe continuously acting dynamics, most importantly governors and the associated mechanical dynamics of turbines and boilers (block 11) and exciters (block 12). Because of the large variety of the devices and their models IEEE committees periodically issue surveys of the types in use and record their appropriate models. The latest of these surveys is given in Ref. [30] for governors and Ref. [31] for exciters. Synchronous condensers can be viewed as a specific design of fast generator controls. It will only be appropriate to summarize in the next sections the models for the simplest types described in these references. The reader is referred for more detail to the references cited or their updated versions, which are certain to follow in the future.

3.2.4.1.1 Governor and Turbine Dynamics The types of turbines and governors used vary greatly among manufacturers and also with a single manufacturer. Turbines may have two or three pressure stages. The lower-pressure stage is sometimes split into two parallel turbines, and there may or may not be a reheater between stages [30]. Usually all stages are on the same shaft driving a single generator. This complex is controlled by the governor, which in turn controls a valve usually through a hydraulic servomotor driven by a (usually two-stage) hydraulic amplifier. The governor itself is controlling the actual turbine speed

(frequency) to a set point or reference input that is provided through the governor speed changer by a secondary control such as automatic generation control (AGC) [4] or an emergency stabilizing control. The governor-controlled valve is the steam inlet into the high-pressure end of the turbine. It usually consists of a bank of valves (four to six) that are operated in sequence. The total steam flow into the turbine represents of course the turbine input power; the shaft power will be "proportional" to it in the steady state. Whatever the proportionality factor, the turbine efficiency is a nonlinear function of the steam temperature and pressure as well as the power level. One typical design is shown in Figure 3.32.

All this adds up to a complex dynamic system. It would be impractical to try to incorporate all these complexities in system dynamic studies, and in fact their effect on the overall system performance would not justify a full-scale analysis of these details especially where reactive power is the primary concern, as it is in this text. Nevertheless, the effects cannot always be neglected either.

Four basic models are presented in Ref. [30]. These are

1. Speed-governing systems for steam turbines
2. Steam turbine systems
3. Speed-governing systems for hydroturbines
4. Hydroturbine systems

Using this information a simple model and a description of a model for the governor mechanism for a steam turbine follows. It should be mentioned that there are two basic types of governor mechanisms.

1. A typical mechanical-hydraulic speed-governing system consists of a speed governor, a hydraulic amplifier, a hydraulic servomotor, and governor-controlled valves.
2. An electrohydraulic speed-control mechanism provides flexibility through the use of electronic circuits in place of mechanical components in the low-power portions.

The general speed-governing model of Figure 3.33 may be used to represent either a mechanical-hydraulic system or an electrohydraulic system by means of an appropriate selection of parameters. Table 3.5 contains a listing of typical parameters for this block diagram for the speed-governing system previously discussed. This model shows the load reference that is the input from the secondary control. This reference value is combined with the increments due to speed deviation to obtain the total power at the governor-controlled valve P_{GV} , subject to the time constant T_3 , introduced by the servometer mechanism.

Universal models are convenient for computer program development and as a basis for data files. All of the commonly encountered steam-turbine configurations may be represented by the block diagram of Figure 3.34. Table 3.6 shows relationships between the parameters of Figure 3.35.

Six common steam-system configurations are listed and the coefficients of the corresponding mathematical models are shown in Figure 3.35. The time

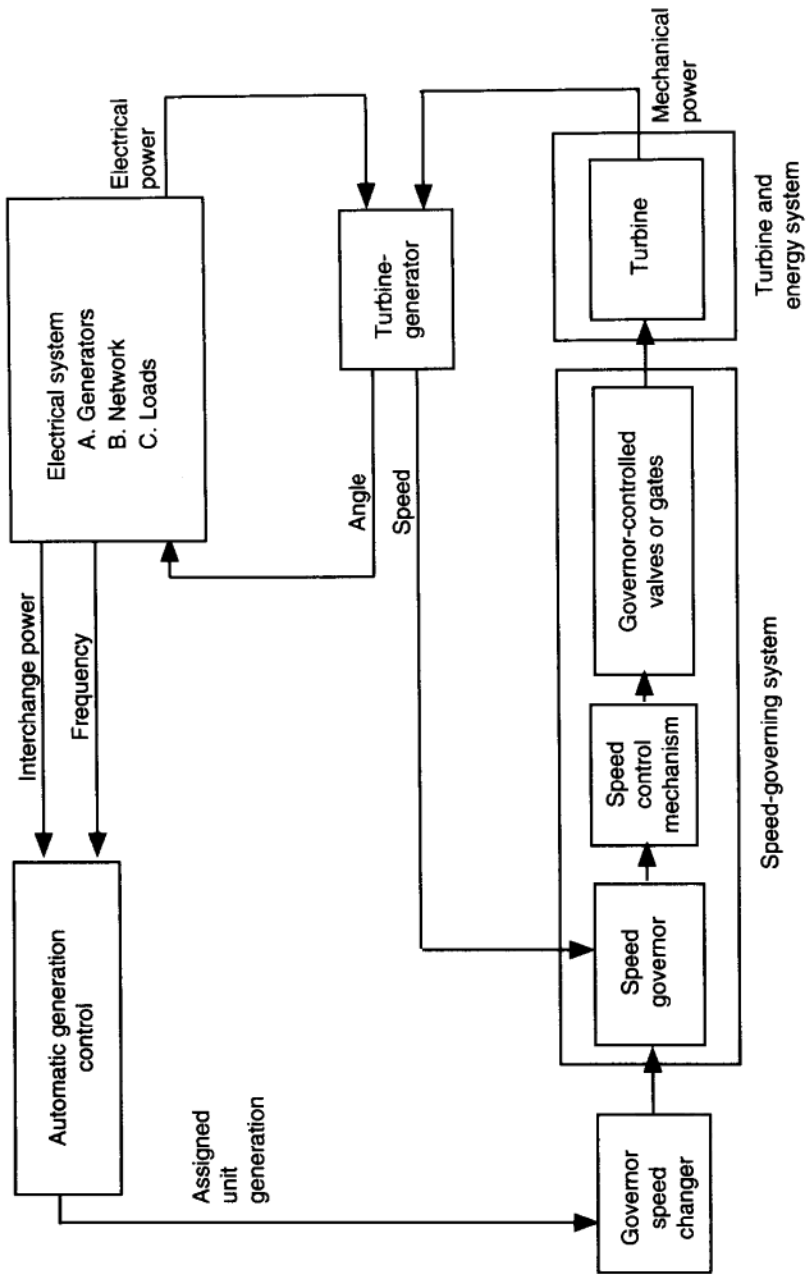


FIGURE 3.32 Functional block diagram showing the location of the speed-governing system and turbine relative to the complete system.

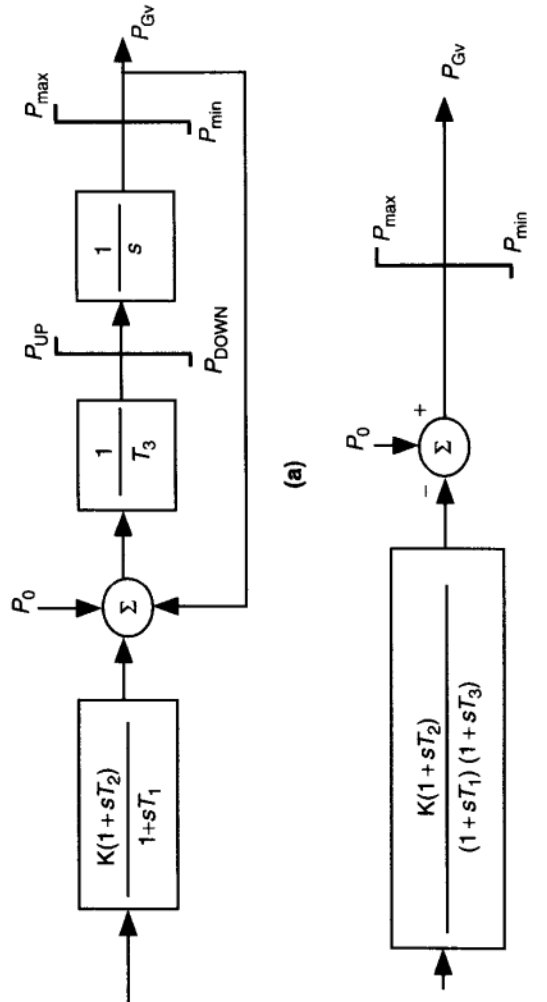


FIGURE 3.33 General model for the speed-governing system.

TABLE 3.5

System	Time Constants (sec)		
	T_1	T_2	T_3
Mechanical-hydraulic	0.2–0.3	0	0.1
General Electric electrohydraulic with steam feedback	0	0	0.025
General Electric electrohydraulic without steam feedback	0	0	0.1
Westinghouse electrohydraulic with steam feedback	2.8**	1.0**	0.15
Westinghouse electrohydraulic without steam feedback	0	0	0.1

^aRate inputs are normally 0.1 p.u. per second except for the mechanical hydraulic system

constants T_{CH} , T_{RH} , and T_{CO} represent delays due to the steam chest and inlet piping, reheaters, and crossover piping, respectively. The fractions F_{VHP} , F_{HP} , F_{IP} , and F_{LP} represent portions of the total turbine power developed in the various cylinders that are turbine units at various pressure levels. P_{T1} and P_{T2} are the turbine shaft powers on one and two shafts, respectively. Typical values for time delays and cylinder fractions are presented in Table 3.7. Extraction steam taken at various turbine stages to heat feedwater usually does not have significance for stability studies and is not shown in these models, although it is represented in some stability programs. This table contains quantities that apply to steam systems. Models and typical values are based on a per-unit system in which power, speed, valve or gate position, pressures, and flows are in per unit of rated values. Time constants are in seconds. Models for hydraulic turbines are also included in Ref. [11].

3.2.4.1.2 Exciter Dynamics The exciter generates the field current i_{fd} of a generator or the voltage e_{fd} applied to the field coil (see block 12, Fig. 3.34). These two are proportional in the steady state (the resistance of the field coil being the proportionality factor) and numerically equal in p.u. but not necessarily dynamically. In the early years of electric power industry, the field voltage e_{fd} was left constant with occasional manual adjustments. Currently, however, the field voltage is typically adjusted by a feedback control to regulate the terminal voltage E of the machine. Types of excitation dynamics are then determined by

1. The nature of the source of DC voltage e_{fd}
2. The nature of the feedback control arrangement

Three distinctive types of excitation systems are identified by the IEEE [31] on the basis of excitation power source:

- *Type DC excitation systems*, which utilize a direct current generator with a commutator typically at the end of the generator shaft as the source of excitation system power.
- *Type AC excitation systems* which use an alternator and either stationary or rotating rectifiers to produce the direct current needed for the generator field.

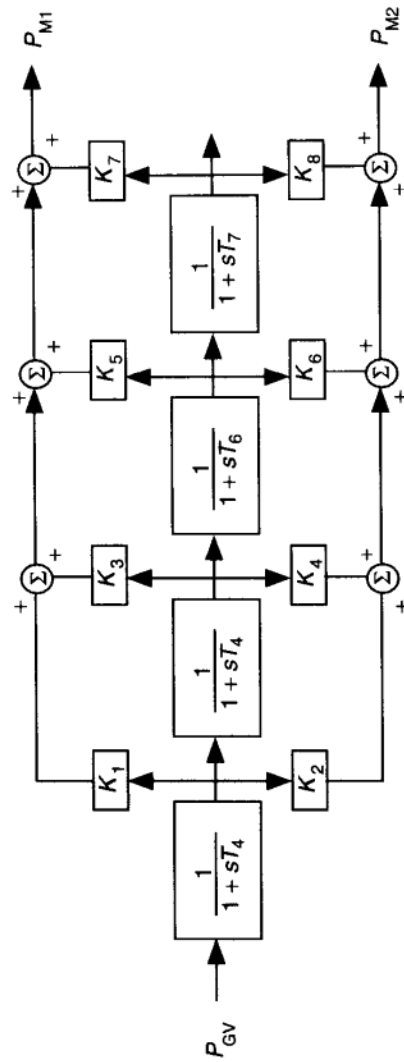


FIGURE 3.34 General model for turbine systems.

TABLE 3.6 Interpretation of Parameters Used in General Model for Turbines in Figure 3.25 [30]

System Description	Time Constants				Fractions							
	T_4	T_5	T_6	T_7	K_1	K_2	K_3	K_4	K_5	K_6	K_7	K_8
Nonreheat	T_{CH}				1	0	0	0	0	0	0	0
Tandem-compound, single-reheat	T_{CH}	T_{RH}	T_{CO}		F_{HP}	0	F_{IP}	0	F_{LP}	0	0	0
Tandem-compound, double-reheat	T_{CH}	T_{RH1}	T_{RH2}	T_{CO}	F_{VHP}	0	F_{HP}	0	F_{IP}	0	F_{LP}	0
Cross-compound, single-reheat	T_{CH}	T_{RH}	T_{CO}		F_{HP}	0	0	F_{IP}	$F_{LP/2}$	$F_{LP/2}$	0	0
Cross-compound, Single-reheat	T_{CH}	T_{RH}	T_{CO}		F_{HP}	0	F_{IP}	0	0	F_{LP}	0	0
Cross-compound, double-reheat	T_{CH}	T_{RH1}	T_{RH2}	T_{CO}	F_{VHP}	0	0	F_{HP}	F_{IP2}	F_{IP2}	F_{LP2}	F_{LP2}
Hydro	0	$T_{W/2}$			-2	0	3	0	0	0	0	0

- *Type ST excitation systems* in which excitation power is supplied through transformers and grid controllers (thyristor rectifiers).

A general functional block diagram for a generator excitation control system is given in Figure 3.36.

Clearly, there will be a wide variety of dynamic models for both the DC sources and the feedback control devices. Only the type DC1 exciter will be presented here in Figure 3.37, taken from Ref. [31]. This represents the traditional generator DC exciter at the end of the shaft under traditional linear feedback control supplemented by a rate limiter for the type of Figure 3.38. The lead-lag network $(1 + sT_C)/(1 + sT_B)$ provides for damping and stabilization.

All this is well within the tradition of 1950s control technology. In some analytical work in recent years it became customary to eliminate the leadlag network ($T_C = T_B = 0$) and represent the remaining part of Figure 3.37 by a three-state variable model as follows:

$$T_E \frac{de_{fd}}{dt} = -(S_E(e_{fd}) + K_E)e_{fd} + V_R \quad (3.267)$$

$$T_F \frac{dV_F}{dt} = -V_F + \frac{K_F}{T_E}[V_R - (S_E + K_E)e_{fd}] \quad (3.268)$$

$$T_A \frac{dV_R}{dt} = -V_R + K_A(V_S + V_{err} - V_F) \quad (3.269)$$

where $V_{err} = E - E_r$ the difference of the bus voltage E and the set point voltage E_r . Equations (3.267) to (3.269) represent dynamics of the main exciter, stabilizing transformer and amplifier, respectively. T_E , T_F and T_A are time constants of

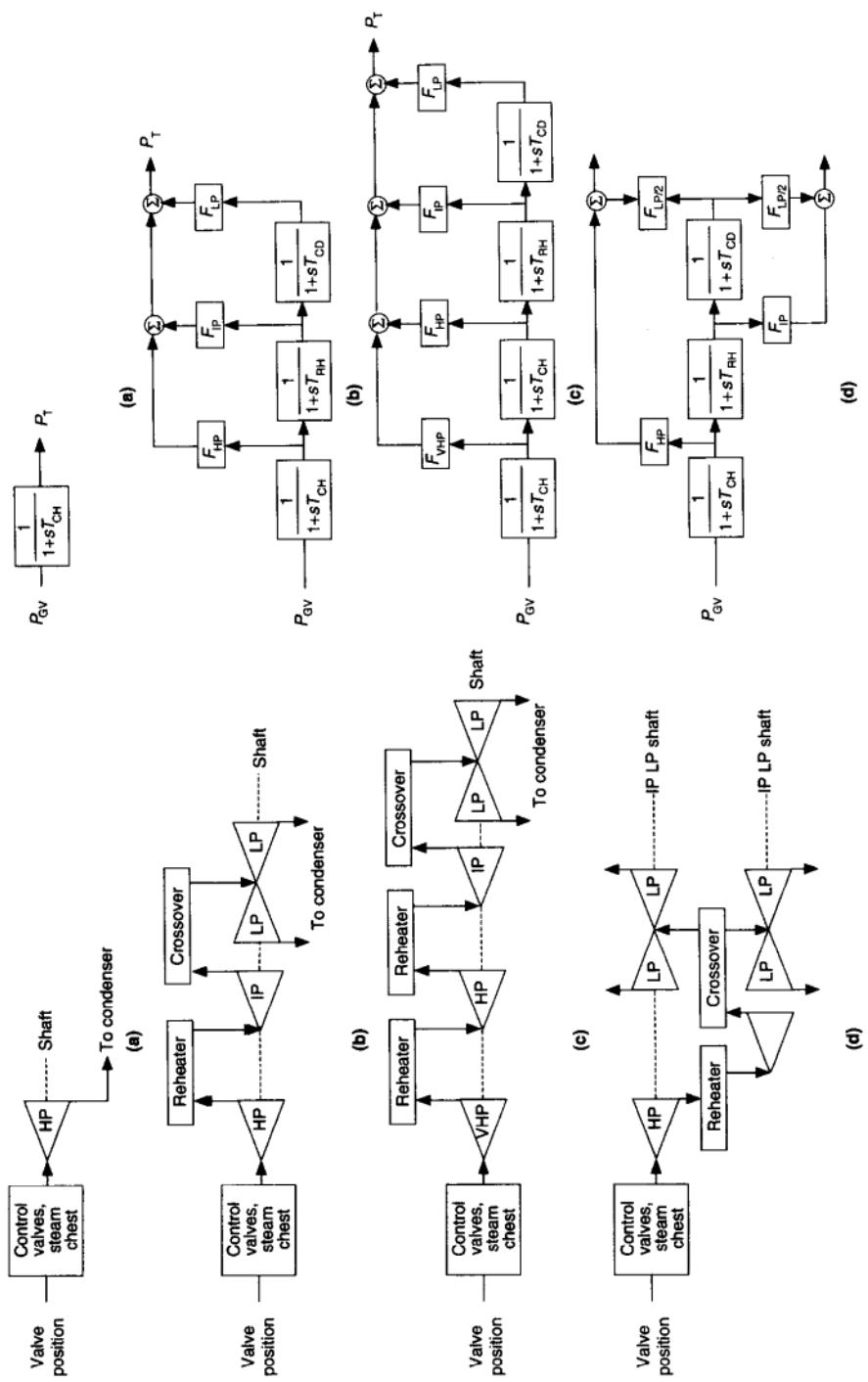


FIGURE 3.35 Common steam-system configurations and their approximate linear models.

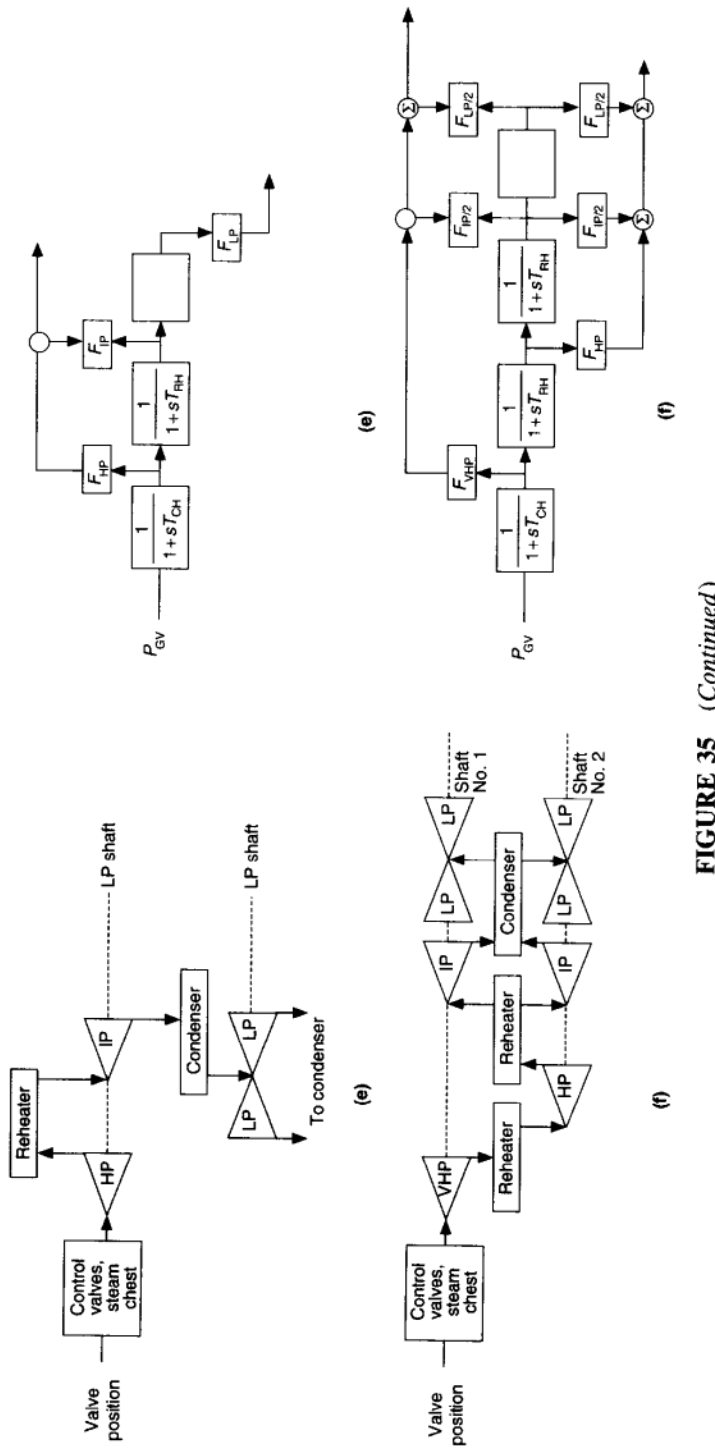
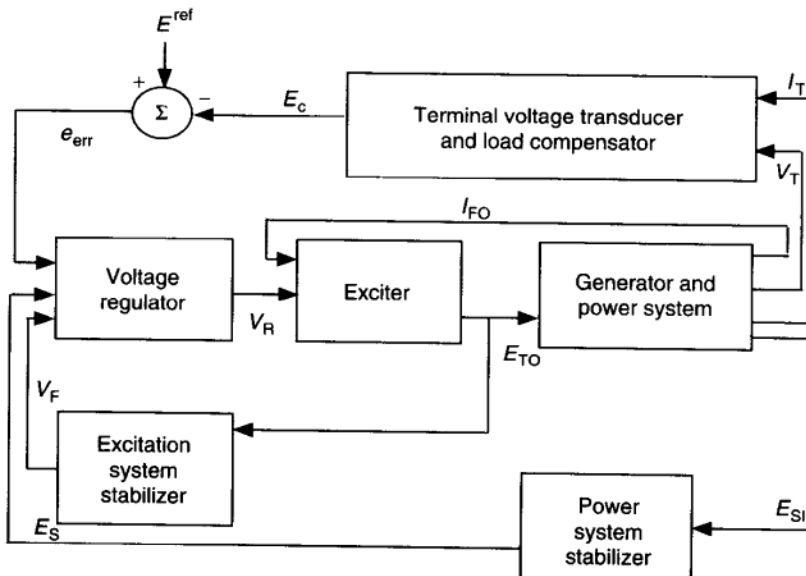


FIGURE 35 (Continued)

TABLE 3.7 Typical Parameters for Steam-Turbine Models in Figure 3.25 [30]

Steam-System Configuration	Typical Cylinder Fractions				Typical Time Constants					
	F_{VHP}	F_{HP}	F_{IP}	F_{LP}	T_{CH}	T_{RH1}	T_{RH2}	T_{CO}		
Nonreheat					0.2–0.5					
Tandem-compound single-reheat		0.3	0.4	0.3	0.1–0.4	4–11		0.3–0.5		
Tandem-compound double-reheat	0.22	0.22	0.30	0.26	0.1–0.4	4–11	4–11	0.3–0.5		
Cross-compound single-reheat		0.3	0.3	0.4	0.1–0.4	4–11		0.3–0.5		
Cross-compound single-reheat		0.25	0.25	0.5	0.1–0.4	4–11		0.3–0.5		
Cross-compound double-reheat	0.22	0.22	0.28	0.28	0.1–0.4	4–11	4–11	0.3–0.5		

**FIGURE 3.36** General functional block diagram for the generator excitation control system.

the excitation system dynamics associated with its internal variables e_{fd} , V_F and V_R respectively. $S_E(e_{fd})$ represents saturation of the exciter $S_{E\max}$ and $S_{E\min}$ are limits within which the exciter dynamics are linear. The corresponding internal variable is within $V_{R\max}$ and $V_{R\min}$ shown in Table 3.8. K_E is its linear path. K_A is the path of the voltage regulator.

Typical model parameters for excitation systems are given in Table 3.8. A second stage of approximation is reached by setting $T_F = T_A = 0$. This leaves a

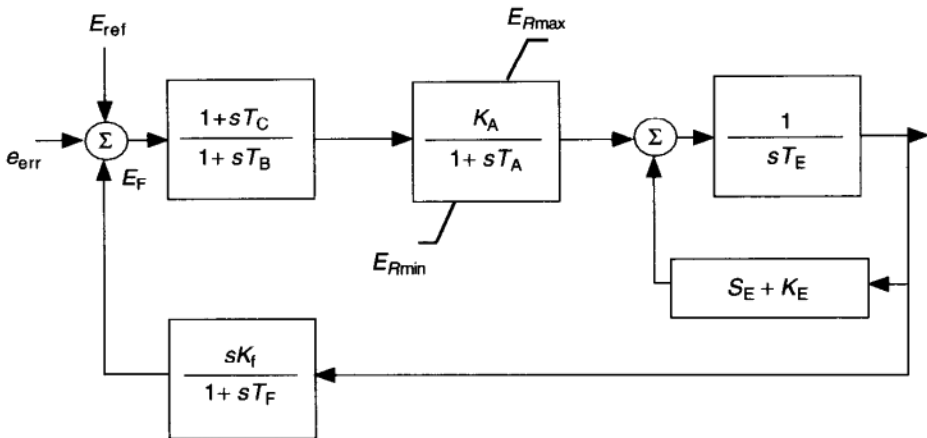


FIGURE 3.37 DC1 type exciter.

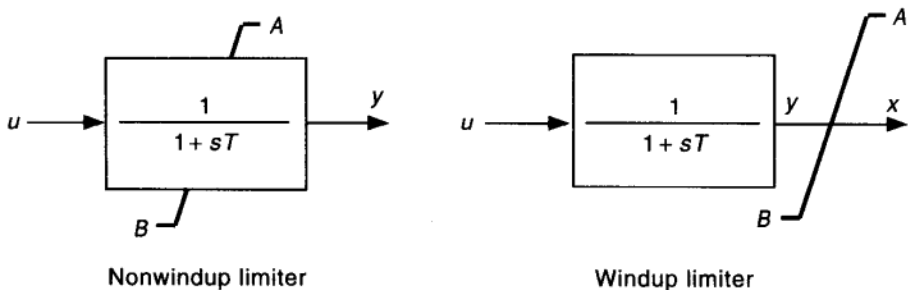


FIGURE 3.38 Limiter.

simple direct feedback through an amplifier, K_A , with a single state variable e_{fd} resulting in the first-order dynamical model of the form

$$\frac{T_E - K_A K_F \frac{de_{fd}}{dt}}{S_E + K_E} = -e_{fd} + \frac{K_A}{S_E + K_E} (V_S + V_{err}) \quad (3.270)$$

Note that while such simplifications make the analysis simpler, they also may limit the validity of the results. Direct feedback control is certainly feasible but stability considerations will severely limit the control gain and hence the speed of control response to unrealistically low values. The same is true in a milder form for the three-state model, which is lacking the stabilizing effect of the lead-lag network.

Furthermore, note that hard limits that occur in many parts of the power system are frequent in various controls and in excitation controls in particular. Two basic types exist: a nonwindup type that puts a limit on one particular state in the system (Fig. 3.38), and a windup limit in which an actuation output that is a function of several states is limited. The effect of such hard limits is studied in Chapter 10. It should not be forgotten that while many generators still have the old-fashioned exciters described here, the use of the newer, much more flexible

TABLE 3.8 Typical Parameters for the Westinghouse Brushless Excitation Systems

IEEE Type 1			IEEE Type AC1		
$T_R = 0$ sec			$R_R = 0$ sec		
$K_A = 400$			$K_A = 400$		
$T_A = 0.02$ sec			$T_A = 0.02$		
$e_{fd\max} = 3.9$ p.u.			$K_E = 1.0$		
$e_{fd\min} = 0.0$ p.u.			$K_F = 0.03$		
$K_E = 1.0$			$T_F = 1.0$ sec		
$K_F = 0.03$			$T_B = T_C = 0.0$ sec		
$T_F = 1.0$ sec			$K_C = 0.2$		
			$K_D = 0.38$		
	3600 rpm	1800 rpm		3600 rpm	1800 rpm
$V_{R\max}^a$	7.3	8.2	$V_{R\max}^a$	7.3	8.2
$V_{R\min}^a$	−6.6	−7.4	$V_{R\max}^a$	−6.6	−7.4
$S_E\max$	0.86	1.1	$S_E\max$	0.1	0.12
$S_E\min$	0.5	0.5	$S_E\min$	0.03	0.03
T_E	0.8	1.3	T_E	0.8	1.3

^aValues given assume E_{FD} (full load) = 3.0 p.u. If not, multiply the value by E_{FD} (full load)/3.0.

and much faster thyristor types is spreading. Theoretical work should account for their presence in order to be realistic.

3.2.4.1.3 Synchronous Condensers Not much needs to be said in supplement of the earlier section on synchronous machines. Synchronous condensers are fairly normal synchronous machines except that they are not used to generate or absorb (as synchronous motors would) real power. They are not connected to turbine shafts or drive shafts, and $P_G = 0$ except possibly for some power taken for the excitors and losses. They are used as reactive sources, only mostly as capacitative sources. For this purpose they are run in an underexcited condition, that is, with low e_{fd} values. Since they have no attached turbines or other inertias, their total inertia is that of the generator, which is relatively small. Consequently in stability swings they move at a high frequency with low energy compared to the generators.

3.2.4.2 Semistandardized Switching Structural Controls Using Mechanical Switching These devices are reactive elements such as capacitors and/or reactors, connected either in series with the transmission lines, or as shunts between a given power system bus and the ground. They typically have a localized function of maintaining a particular bus voltage within the prespecified threshold. Depending on the type of device, this is achieved by adjusting the number of shunt capacitor

or reactor banks in response to voltage deviation at the bus of interest. As such they change in discrete steps and at a discrete random times only when voltage deviations exceed acceptable threshold. Also, the tap-changing transformers perform the same task by adjusting mechanically the number of active taps on the secondary side of a transformer in response to the secondary bus voltage.

A typical schematic of a controlled shunt capacitor is shown in Figure 3.39, series capacitor is shown in Figure 3.40, and an on-line tap changer (OLTC) transformer in Figure 3.41. The common feature of these devices is that they lead to change in transmission network parameters as they respond to voltage changes on the system. Typically these changes are carried in discrete steps and at discrete times.

One possible mathematical description of a voltage-controlled capacitor at bus i is given as

$$C_i(k+1) = C_i(k) - e_i r_i (E_i(k) - E_i^{\text{ref}}), \quad i = 1, 2, \dots, n_c \quad (3.271)$$

where n_c is the number of capacitor banks on the system, e_i is the per-cycle change in tap positions of capacitor banks,¹¹ and r_i is a relay-type function with

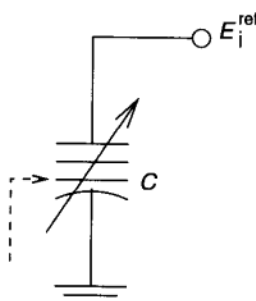


FIGURE 3.39 Mechanically switched shunt capacitor for controlling voltage at bus i .

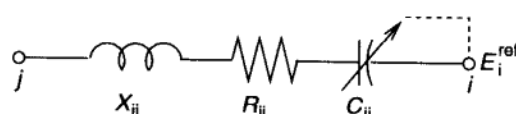


FIGURE 3.40 Mechanically switched series capacitor for controlling voltage at bus i .

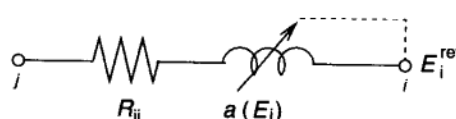


FIGURE 3.41 Mechanically switched OLTC for controlling voltage at bus i .

¹¹ Capacitor banks typically have significantly fewer number of tap positions than OLTCs.

a dead zone defined as

$$r_i(E_i - E_i^{\text{ref}}) = \begin{cases} +1 & \text{if } (E_i - E_i^{\text{ref}}) \geq \Delta E \\ -1 & \text{if } (E_i - E_i^{\text{ref}}) \leq -\Delta E \\ 0, & \text{if } |E_i - E_i^{\text{ref}}| \leq \Delta E \end{cases} \quad (3.272)$$

A mathematical model for representing an OLTC is of a similar form; a tap position $a_i(k+1)$ at the $(k+1)$ st discrete step is related to the tap position at the previous step as

$$a_i(k+1) = a_i(k) - d_i r_i(E_i(k) - E_i^{\text{ref}}), \quad i = 1, 2, \dots, n_T \quad (3.273)$$

where n_T is the number of OLTC transformers and d_i is the per-cycle change in tap positions of the transformers.

It is straightforward to see the effect of the tap ratio $a = E_1/E_2$ on the admittances of the π model of the line connecting buses 1 and 2 in which an OLTC is present. As a changes, both series \hat{Y}_{12} and shunt \hat{Y}_{10} and \hat{Y}_{20} admittances change according to

$$\hat{Y}_{12} = \frac{1}{a} \hat{Y}_{\text{nom}} \quad (3.274)$$

$$\hat{Y}_{10} = \frac{1-a}{a^2} \hat{Y}_{\text{shunt}}^{\text{nom}} \quad (3.275)$$

$$\hat{Y}_{20} = \frac{a-1}{a} \hat{Y}_{\text{shunt}}^{\text{nom}} = -a \hat{Y}_{10} \quad (3.276)$$

This admittance structure is sketched in Figure 3.42. It follows from these formulas that as a tap position changes, the relative amount of shunt reactances and capacitances at the ends of the line vary in such a manner that they are always opposite in sign. This further explains the fundamental function of a transformer as a control device; this device does not inject any power, it only redistributes power. A similar mathematical description of a mechanically controlled series capacitor holds true.

A phase-shifting transformer, on the other hand, is a different device than a basic OLTC transformer. This device effectively changes a complex-valued tap position, since both the voltage magnitude and angle change as the phase-shifting transformer switches. This device provides a quadrature voltage injection, which varies typically to regulate a phase angle across the line in which the transformer is located. Depending on the actual design, a phase-shifting transformer can regulate both voltage phase angle and magnitude, or only the voltage angle.

While this model is not frequently used, it can be shown that dependence of the admittance model of a phase-shifting transformer is identical to the model used in Figure 3.42 with the only difference of using a complex-valued (instead of real-valued) transformer ratio $\hat{a} = \hat{E}_1/\hat{E}_2$. It is curious to recognize that this structural change of admittance parameters results in a nonsymmetric matrix of

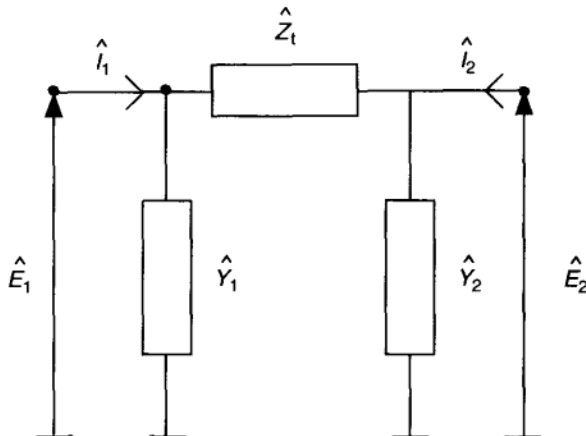


FIGURE 3.42 Equivalent of an OLTC.

the interconnected grid. This is important to recognize, since the majority of up-to-date analytic work assumes a symmetric admittance matrix. Because of this, the presence of phase-shifting transformers requires significant new analytic developments.

It is important to notice that these models of mechanically switched reactances are written by neglecting the transient response of the device itself. While this is justified for many operating regions, it is important to keep in mind that the model described by Eq. (3.272) itself may become questionable for extremely fast processes on the system related to voltage-collapse phenomena.

3.2.4.3 Disconnecting Components from the System: Load, Line, and/or Generator Dropping A slightly different subgroup of semistandardized switching on the system for controlling systemwide dynamics is based on disconnecting standard system components when the system cannot operate satisfactorily with them present on the system. These control actions are practiced when the controls such as standardized switching of capacitors and reactors are not sufficient to maintain voltage and frequency within the prespecified operating limits.

Load dropping (load shedding) is usually done when there is a severe generation deficiency on the system, and it is practiced both in response to locally observed frequency deviation and in response to voltage deviation.

Generation dropping is practiced in a rare event of generation excess on the system.

Line dropping is practiced for dealing with both generation excess and deficiency; in contrast to load and generator dropping, which change the net power injection into the system, this action only reroutes the existing power throughout the system, it does not contribute to the total generation–load mismatch elimination.

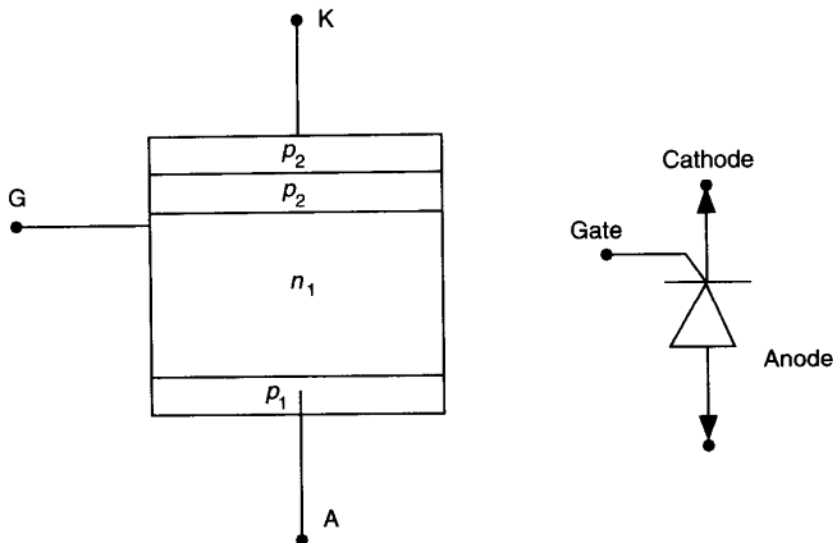


FIGURE 3.43 Symbol and structure of a thyristor.

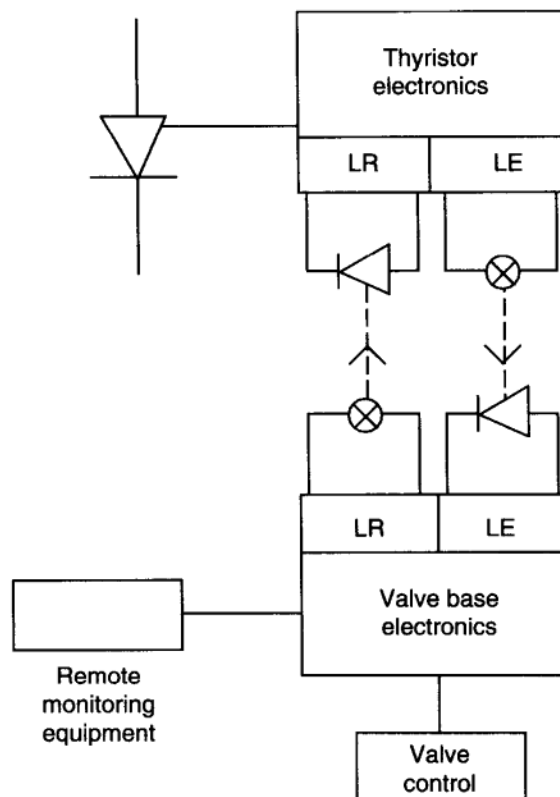


FIGURE 3.44 Valve-firing scheme. LR denotes the light receiver, LE the light emitter.

Load dropping and generation dropping are often intended for balancing systemwide mismatch on the system and are not always intended to have a localized effect.¹² At least one method will also be described that is capable of line switching for systemwide voltage control. With this in mind, we do not describe the mathematics of these actions here. They are listed in this chapter primarily for completeness. The control logic for these actions is not standardized.

3.2.4.4 Electronic (Thyristor) Devices Most of the devices in this group are based on the same principles as those implemented in mechanically switched devices, described before. The main difference is the replacement of mechanical switching by faster, electronic switching.

In order to provide at least a minimum background in this area, we briefly summarize the role of a thyristor in these technologies. Once this is provided, it becomes straightforward to model electronically controlled devices such as capacitors and reactors.

3.2.4.5 Thyristor as the Basic Power Electronic Switch Thyristor is now a generic term applicable to the whole range of four-layer (*P-n-P-n*) semiconductor switches [12]. It is also known commercially as a silicon-controlled rectifier (SCR). The structure of a thyristor with the three terminals and its electronic symbol are shown in Figure 3.45.

The voltage rating of a thyristor is now in the range of 5 kV, while the current rating has gone up to 3000 A. While the current ratings are adequate (no need for parallel connections), the voltage rating is insufficient to make up the high-voltage valve. Thus a series connection of thyristors is necessary. This, unfortunately, introduces design and protection problems.

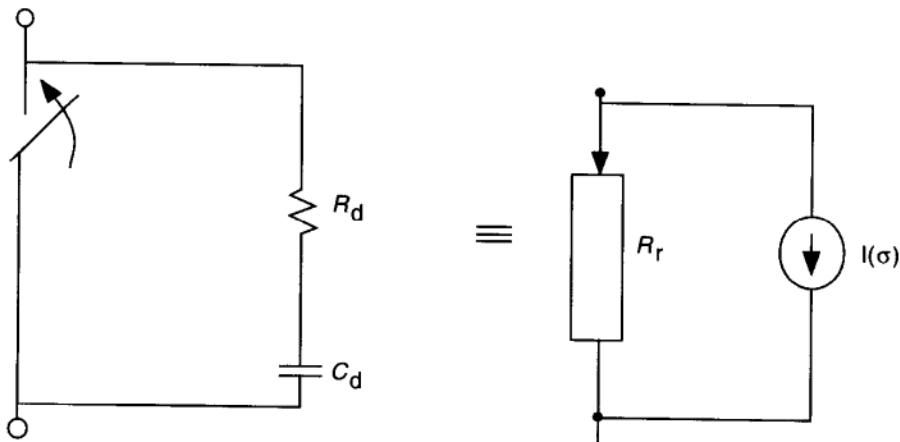


FIGURE 3.45 Thyristor valve model.

¹²This is in contrast to all other primary devices, whose role at least at present is highly localized.

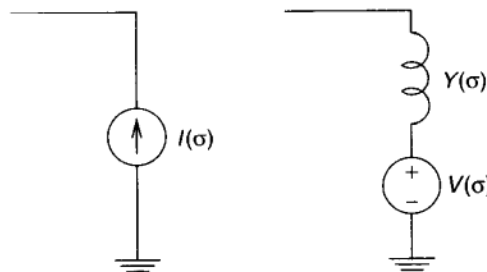


FIGURE 3.46 Equivalent network models of a thyristor switch.

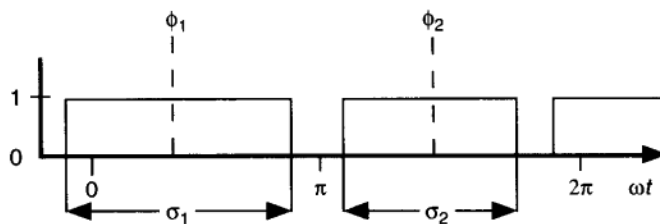


FIGURE 3.47 The switching function.

A thyristor valve consists of a number of thyristors in series to provide a required voltage. The basic valve-firing scheme is given in Figure 3.46. The valve control generates firing signals. Each thyristor level receives the signal directly from a separate fiber-optic cable. It has been generally agreed that a valve can be represented by a controllable switch in parallel with the snubber circuit as shown in Figure 3.47. The switch is closed when the valve turns on and is open when the valve turns off. The dynamics of the turn-on and turn-off processes can be usually neglected. The snubber dynamics are not significant under most operating conditions.

A simple method of modeling a switch is to replace it by a variable resistance or impedance. This model is used in the electromagnetic transient program (EMTP). An advantage of this modeling is that circuit topology remains invariant, while the parameters are time dependent. In steady state the firing signals are generated at a time interval T/p , where T is the period of the AC voltage and p is the pulse number.

Another possible model for the thyristor valve is based on models for switching in low-power electronics [32], [33]. The state of the valve is represented by the currents through the inductor and voltage across the capacitor of the snubber circuit, and the switch is represented by a time-varying switching function $H(t)$. For example, a model of a thyristor-controlled reactor is

$$\begin{bmatrix} \dot{I}_R \\ \dot{V}_C \end{bmatrix} = \begin{bmatrix} -\frac{R_R}{L_R} & \frac{H(t)}{L_R} \\ -\frac{1}{C} & 0 \end{bmatrix} \times \begin{bmatrix} I_R \\ V_C \end{bmatrix} \quad (3.277)$$

It has been shown in Ref. [34] that the equivalent-network model for the thyristor-controlled switch takes on the form of a time-on σ -dependent current injection model or voltage model as shown in Figure 3.48. The switching function $H(t)$ is given in Figure 3.49.

A standard averaging method in low-power electronic circuits for a state-space model of the form in Eq. (3.277) can also be applied in electric power systems. This allows for capturing relevant average effects of switching on the electronically switched devices on the dynamics of the interconnected power system. This is

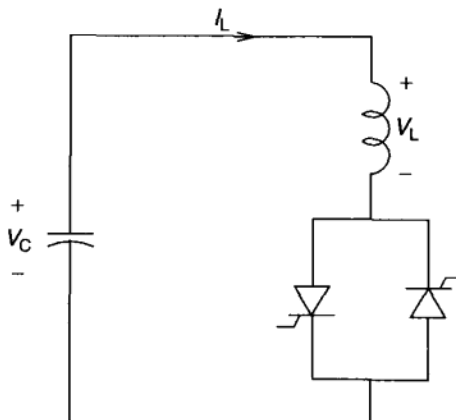


FIGURE 3.48 Thyristor-controlled reactor (SVC).

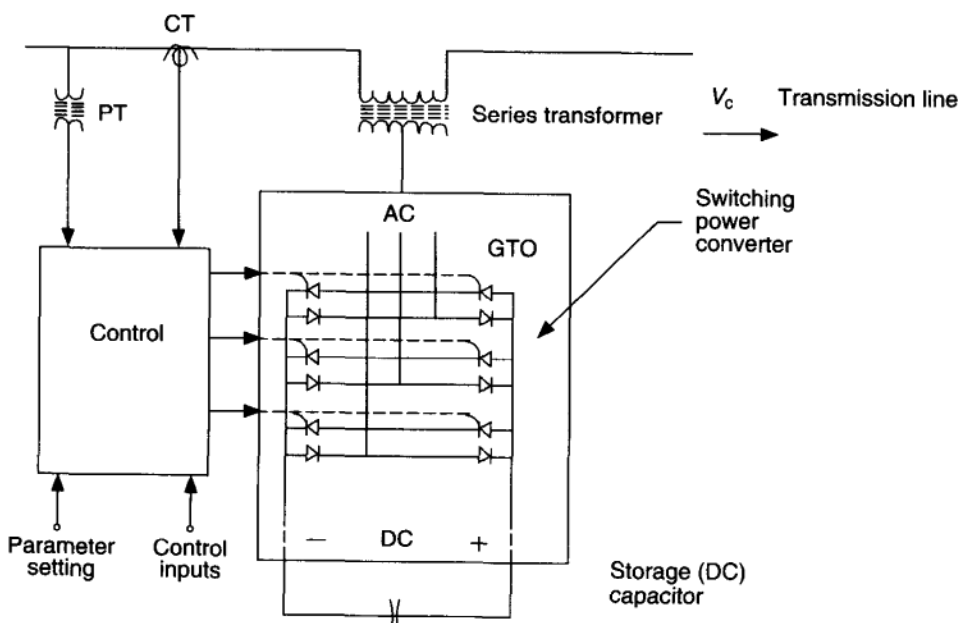


FIGURE 3.49 Schematics of a controllable series capacitor.

most often justifiable because of the significant difference in time constants associated with the switching circuits, on one side, and time constants of synchronous machines, on the other side.

A state-space averaged model of the model in Eq. (3.277) is of the general form

$$\dot{x} = [\sigma A_1 + (1 - \sigma)A_2]x + [\sigma B_1 + (1 - \sigma)B_2]u \quad (3.278)$$

where σ is the on-time of the switching function $H(t)$, A_1 and A_2 are the time-invariant system matrices of the two systems evolving over each period of time, and B_1 and B_2 are the corresponding control matrices, respectively. A good treatment of state-space averaging method applications to low-power electronic circuitry can be found in Refs. [32,35]. Unfortunately, no reference of a tutorial nature for a similar modeling of electronically switched circuitry implemented on large-scale power systems is available.

Partial modeling of this type in context of FACTS technologies can be found in Refs [32,36]. The same author provides an initial setup for stability studies of dynamics resulting from interactions of power electronic circuits and variable voltage sources in Ref.[37]. We return to this work when modeling and analyzing dynamics of the interconnected system in Chapter 6 and control design in Chapter 12.

With this basic notion of a thyristor-based switch it is straightforward to represent simplest versions of a static var compensator (SVC), controllable series capacitor (CSC), and a phase shifter (PSH). The actual technological developments in the area of electronic switching are into the direction of replacing standard thyristors by the gate-turn-off (GTO) thyristors, which are capable of regulating the turn-off time, in addition to the turn-on time [31, 38 to 40]. The following description of these devices is done without describing the details of technological advances associated with the GTO thyristors and implications of this on the design of these devices. The interested reader can find systematic reports in this area in Refs. [29, 41].

3.2.4.6 Thyristor-Controlled Reactor (SVC) The shunt-connected SVC, using conventional thyristor switches, is already firmly established equipment for transmission-line compensation [42]. As shown in Figure 3.49, the SVC is usually composed of thyristor-switched capacitors and thyristor-controlled reactors. With proper coordination of the capacitor switching and reactor control, the Var output can be varied continuously and rapidly between the capacitive and inductive rating of the equipment. More advanced designs of SVCs can be found in Ref. [42].

The simplest version of an SVC can be thought of as being a TCR connected in parallel to a load \hat{Z}_L of a power system [36]. This is normally called a phase-controlled or a thyristor-controlled reactor. The phase-controlled current through the reactor is controlled by delaying the firing angle α of the thyristors [36, 42].

Controllable series capacitor In principle, thyristor-switched capacitors in series connection, shown in Figure 3.50, could provide fast control of the effective

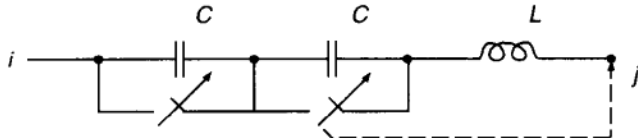


FIGURE 3.50 Possible model for a thyristor-controlled series capacitor.

impedance of a transmission line to which it is connected for direct control of power transmitted on this line. The first successful significant implementation of this technology was in the north west United States. One of the most recent implementations of this type can be found on the American Electric Power (AEP) system.

A possible mathematical model of this device is in terms of an electronically controlled switch connected in series with the transmission line, as sketched in Figure 3.50. The firing angle of the thyristor switch is determined, based on the voltage at bus E_i^{ref} controlled by a capacitor.

This potentially very powerful device has not been implemented widely in practice because of several hidden problems. These problems are seen through interactions of the series capacitor switching and the generator dynamics [43]. Moreover, protection of series capacitors is more complex.

Controllable phase shifter Although there is no high-power solid-state phase shifter in service, the principles for using a phase-shifting transformer with a thyristor tap changer are the same as for the mechanically switched phase-shifting transformer.

A thyristor-controlled phase-shifting transformer is shown in Figure 3.51.

HV-AC and HV-DC control components One of the main advantages of an HV-DC link is fast controllability of transmitted power through the control of firing angles of the converters. A schematic of a DC link is given in Figure 3.52.

The conversion from AC to DC and vice versa is done in HV-DC converter stations by using three-phase bridge converters. The configuration of the bridge is as shown in Figure 3.53. This is a six-pulse converter. The 12-pulse converter is composed of two bridges in series supplied from two different transformers with voltages differing in phase by 30° . The pulse number of a converter is defined as the number of pulsations of direct voltage per cycle of alternating voltage. The opening of the switch occurs at the zero-current value. (This is the simplest version of a firing angle control, referred to as constant α control. It is shown in Figure 3.58. More advanced versions of firing-angle control will be studied in context of system wide control in Chapter 12.)

The output voltage of the converter consists of a DC component and a ripple, the contents of which are determined by the pulse number. At any instant two valves are conducting in the six-pulse bridge, one from the upper, the other from the lower commutation group. The firing of the next valve results in the turning off of the valve that is already conducting. Each valve conducts 120° , and the

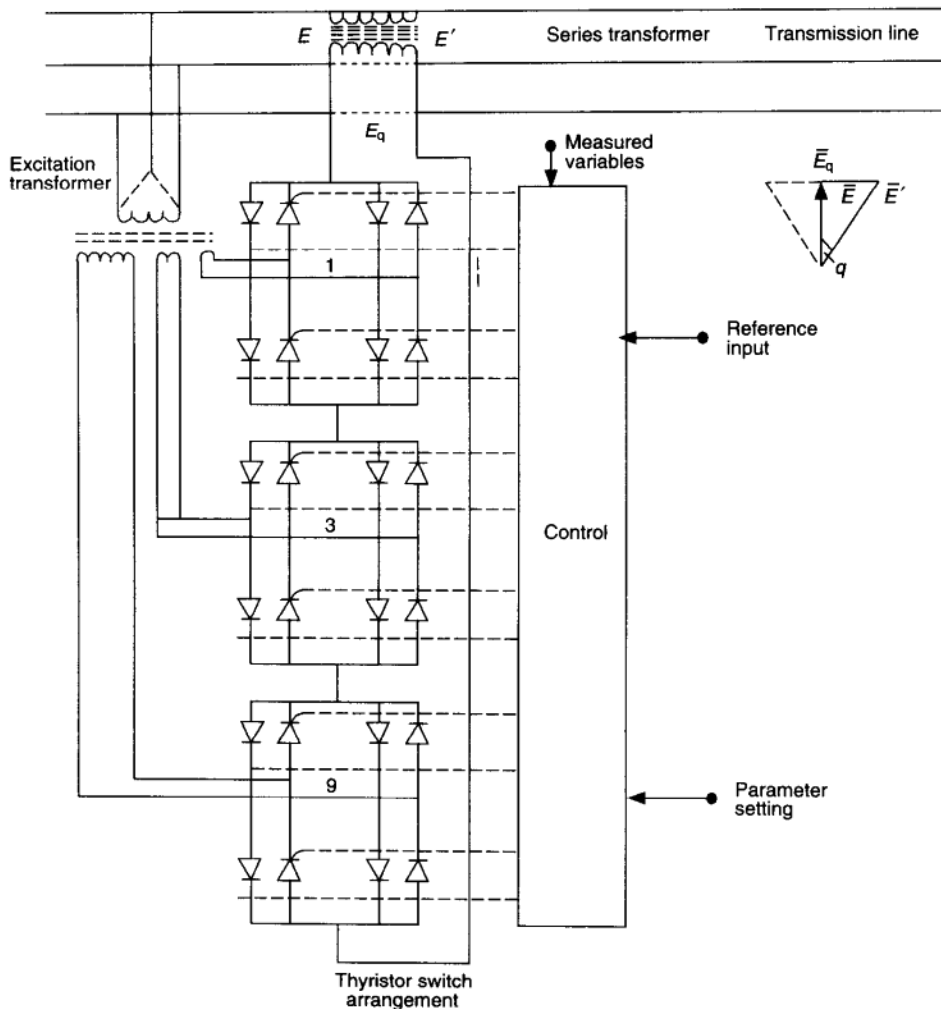


FIGURE 3.51 Thyristor-controlled phase-shifting transformer scheme for transmission-angle control.

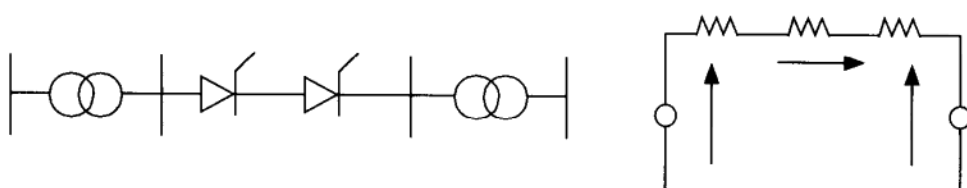


FIGURE 3.52 Schematic of a DC link.

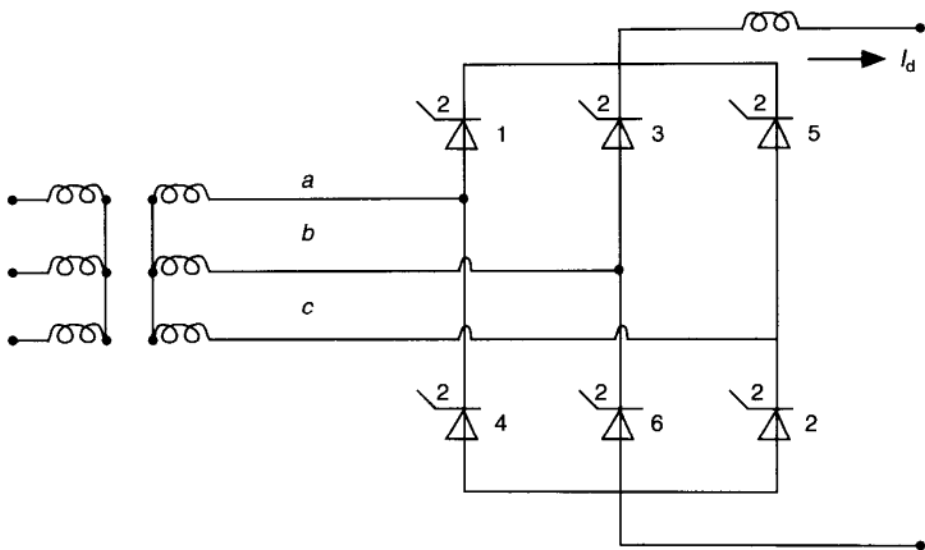


FIGURE 3.53 Graetz-circuit – three-phase bridge converter.

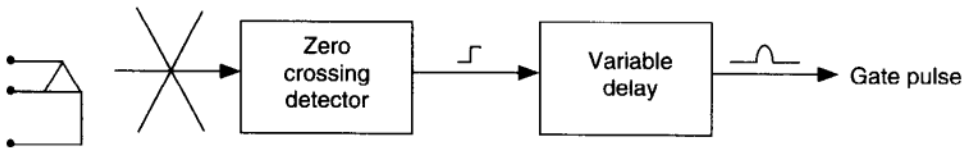


FIGURE 3.54 Constant- α control.

interval between consecutive firing pulses is 60° in steady state. Assuming the firing of a valve is delayed by an angle α (that is, α after the zero crossing of the commutation voltage) it is easily shown that the DC (average) voltage is

$$E_d = \frac{3\sqrt{2}}{\pi} E_{LL} \cos \alpha \quad (3.280)$$

where E_{LL} is the peak line-to-line AC voltage. By controlling the firing angle α of thyristors in the valve, one directly controls the DC voltage and therefore the DC (average, real) power through the link.

The control functions required for the HV-DC link are typically performed using a hierarchical control structure shown in Figure 3.55. The master controller for a bipole is located at one of the terminals and is provided with a power order (P^{ref}) from the system controller at the energy control center level. The master controller transmits the current order (I^{ref}) to the pole control units, which in turn provide a firing-angle order to the individual valve groups (converters).

Similar to the mathematical modeling of one thyristor valve, the pair of valves used on a DC link can be modeled with various degree of accuracy. The simplest model is to assume no dynamics associated with the valves, and an a priori given

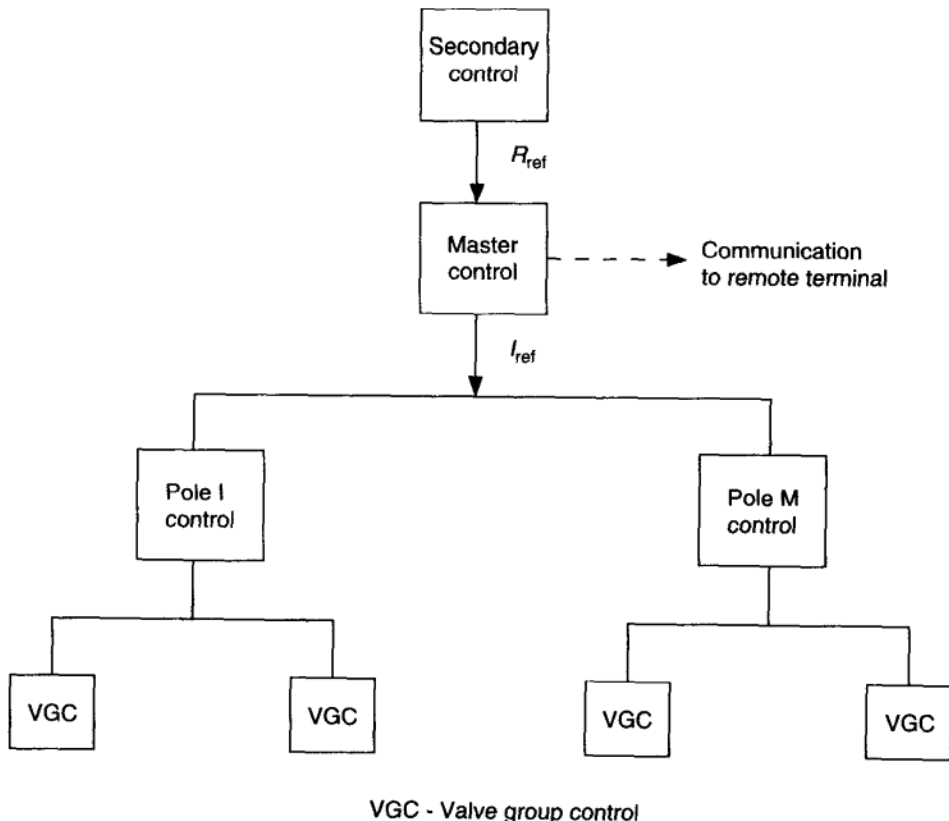


FIGURE 3.55 Hierarchical control structure for a DC link.

firing angle α . More accurate models would lend themselves to dynamical models suggested in Ref. [36].

Protection devices: relays This group of devices is essential in every large power system [43, 44]. They are often referred to as silent sentinels, without which the system components would become prone to a variety of destruction. Almost every major component has individual protection, which basically allows the device to be connected as long as operating conditions are such that they are not detrimental to its hardware.

Most relays are based on steady-state concepts in that they react to the variable characterizable in 60-Hz terms only, that is, by means of time-invariant phasors. Only recently has there been significant technological development towards microprocessor-based relaying that uses time-varying phasors [45].

Whereas it is beyond the scope of this text to describe basic principles of relaying, it is important to recognize that they are indirectly modeled on the interconnected system by introducing inequality constraints on a variety of system variables. Only mathematical solutions within the constraints admissible by the relays present on the system are directly useful.

In this sense, relays are modeled indirectly by stating operating inequality constraints on system variables. Unfortunately, much analysis is done without taking into consideration the constraints imposed by protection. One should be very aware of this generic deficiency of much work on power system analysis and control [46].

APPENDIX 3.1 CONCEPTUAL DERIVATION OF ALGEBRAIC COUPLING EQUATIONS FOR GENERATOR AND BUS

After neglecting the ultrafast dynamics in Eqs. (3.188) and (3.189) one obtains a reference system based on Figure 3.25, which makes the current flowing out of the armature a negative number.

$$ri_d + e_d - \psi_q = 0 \quad (3.1.1)$$

$$-ri_q - e_q - \psi_d = 0 \quad (3.1.2)$$

Also, in the steady state, Eq. (3.209) takes on the form

$$-e_d'' - x_q i_q + x_q'' i_q = -e_d'' + ri_d - e_d + x_q'' i_q = 0 \quad (3.1.3)$$

leading to the Eq. (3.204)

$$e_d = e_d'' - ri_d - x_q'' i_q \quad (3.1.4)$$

It directly follows from the state equation (3.208) that under steady-state conditions

$$0 = -e_q'' + (x_d' - x_d'') i_d = -e_q'' + x_d' i_d - x_d'' i_d \quad (3.1.5)$$

Using the expression for e_q from Eq. (3.1.2) above, one obtains the second coupling variable of interest Eq. (3.203), that is,

$$e_q = e_q'' + x_d'' i_d - ri_q \quad (3.1.6)$$

APPENDIX 3.2 MODEL DERIVATION (Eqs. 3.207) TO (3.209)

To derive state equation (3.209), start with Eqs. (3.191) to (3.194) and assume $\dot{\theta} \equiv 1$, that is the rotating speed ω is close to the nominal, whose normalized value is 1. Define next a state variable as in Eq. (3.199),

$$e_d'' = -\frac{x_{Qq}}{x_Q} \psi_Q \quad (3.2.1)$$

This state variable is a quadrature-axis component of the normalized flux linkage of the damper winding. The normalizing procedure for synchronous machines

is quite involved, and consequently, it is not straight-forward to understand the reasoning related to the introduction of the normalized state variables for synchronous machines. The main objective of the normalization is, similar to the normalization for power and voltage on the transmission side, to obtain standardized values for base voltage, base flux, and base mmf close to 1 p.u. For more details, see Refs. [10, 28]. Differentiation of Eq. (3.2.1) with respect to time and combined with Eq. (3.194) leads to

$$\frac{x_Q}{x_{Qq}} \dot{e}_d'' = -\dot{\psi}_Q = r_Q i_Q \quad (3.2.2)$$

From Eq. (3.196) one obtains

$$i_Q = \frac{1}{x_Q} \psi_Q - \frac{x_{Qq}}{x_Q} i_q \quad (3.2.3)$$

which, in turn, when combined with equation (3.2.2), results in

$$\frac{x_Q}{r_Q} \dot{e}_d'' = -e_d'' d - (x_q - (x_q - \frac{x_{Qq}}{x_Q})) i_q \quad (3.2.4)$$

Define next a subtransient reactance in the q axis

$$x_q'' = x_q - \frac{x_{Qq}^2}{x_Q} \quad (3.2.5)$$

and a subtransient time constant in the q axis

$$T_{q0}'' = \frac{x_Q}{r_Q} \quad (3.2.6)$$

leading to

$$T_{q0}'' \dot{e}_q'' = -e_d'' - (x_q - x_q'') i_q \quad (3.2.7)$$

which is indeed the state equation (3.209) which we intended to derive.

Similarly, but a bit more algebraically involved, we derive next equation (3.223). To do this, let us define next a state variable representing normalized field flux linkage

$$e'_q = \frac{(x_{df}x_D - x_{dD}x_{Df})}{(x_f x_D - x_{Df}^2)} \psi_f \quad (3.2.8)$$

and a state variable which is a linear combination of e'_q and the normalized flux linkage in the D axis of the damper winding

$$e_q'' = e'_q + \frac{(x_f x_{dD} - x_{df} x_{Df})}{(x_f x_D - x_{Df}^2)} \psi_D \quad (3.2.9)$$

From Eq. after differentiating with respect to time and combining with Eq. (3.193) one obtains

$$\frac{x_f x_D - x_{Df}^2}{x_f x_{dD} - x_{df} x_{Df}} (\dot{e}_q'' - \dot{e}_q') = -r_D i_D \quad (3.2.10)$$

Also, from Eq. (3.196)

$$\begin{aligned} \psi_D &= x_{dD} i_d + x_D i_D + x_{Df} i_f \\ \psi_f &= x_{df} i_d + x_{Df} i_D + x_f i_f \end{aligned} \quad (3.2.11)$$

which, after eliminating i_f gives

$$i_D = \frac{x_f}{x_D x_f - x_{Df}^2} \psi_D - \frac{x_{Df}}{x_D x_f - x_{Df}^2} \psi_f - \frac{x_f x_{dD} - x_{Df} x_{df}}{x_D x_f - x_{Df}^2} i_d \quad (3.2.12)$$

Insert Eq. (3.298) into (3.296) to obtain

$$\begin{aligned} \frac{x_D x_f - x_{Df}^2}{r_D x_f x_{dD} - x_{Df} x_{df}} (\dot{e}_q'' - \dot{e}_q') &= \frac{x_{Df}}{x_D x_f - x_{Df}^2} \psi_f \frac{x_f}{x_f x_D - x_{Df}^2} \psi_D \\ &\quad + \frac{x_f x_{dD} - x_{Df} x_{df}}{x_D x_f - x_{Df}^2} i_d \end{aligned} \quad (3.2.13)$$

or

$$\begin{aligned} \frac{x_D - x_{Df}^2}{r_D} (\dot{e}_q'' - \dot{e}_q') &= \frac{x_f x_{dD} - x_{df} x_{Df}}{x_D x_f - x_{Df}^2} \frac{x_{Df}}{x_f} \psi_f - \frac{x_f x_{dD} - x_{df} x_{Df}}{x_D x_f - x_{Df}^2} \psi_D \\ &\quad + \frac{x_f x_{dD} - x_{Df} x_{df}}{x_D x_f - x_{Df}^2 x_f} i_f \end{aligned} \quad (3.2.14)$$

Define next a damper winding subtransient time constant in the d axis:

$$T_{d0}'' = \frac{x_D}{r_D} \left(1 - \frac{x_{Df}^2}{x_f} \right) \quad (3.2.15)$$

which, together with Eq. (3.2.14) leads to

$$T_{d0}'' (\dot{e}_q'' - \dot{e}_q') = \frac{x_f x_{dD} - x_{df} x_{Df}}{x_D x_f - x_{Df}^2} \frac{x_{Df}}{x_f} \psi_f - (e_q'' - e_q') + \frac{x_f x_{dD} - x_{Df} x_{df}}{(x_D x_f - x_{Df}^2) x_f} i_d \quad (3.2.16)$$

Next, we claim that the coefficient $B = (x_f x_{dD} - x_{df} x_{Df})^2 / (x_D x_f - x_{Df}^2) x_f$ multiplying i_d equals $x_d' - x_d''$ where the constant

$$x_d' = x_d - \frac{x_{df}^2}{x_f} \quad (3.2.17)$$

is known as a transient reactance, and the constant

$$x_d'' = x_d - \frac{x_D x_{df}^2 - 2x_{df}x_{Df}x_{dD} + x_f x_{dD}^2}{x_f x_D - x_{Df}^2} \quad (3.2.18)$$

is a subtransient reactance in the d axis. It is fairly straightforward to show the claim that $B = x_d' - x_d''$. Equation (3.2.16) is of the form in Eq. (3.223) provided

$$\frac{x_f x_{dD} - x_{df} x_{Df}}{x_{df} x_D - x_{dD} x_{Df}} \frac{x_{Df}}{x_f} = \frac{x_d' - x_d''}{x_d'' - k_6 x_{al}} k_5 \quad (3.2.19)$$

To show this, start by using relation between B and $x_d' - x_d''$, which leads to

$$\begin{aligned} \frac{x_f x_{dD} - x_{df} x_{Df}}{x_{df} x_D - x_{dD} x_{Df}} \frac{x_{Df}}{x_f} &= \frac{x_d' - x_d''}{x_f x_{dD} - x_{Df} x_{df}} \frac{x_D x_f - x_{Df}^2}{x_{df} x_D - x_{dD} x_{Df}} x_{Df} \\ &= \frac{x_d' - x_d''}{z_2 z_3} x_{Df} (x_D x_f - x_{Df}^2) \end{aligned} \quad (3.2.20)$$

Note that by definition

$$k_5 = \frac{x_{Df} z_4}{z_2 z_3} \quad (3.2.21)$$

which further implies

$$\frac{x_f x_{dD} - x_{df} x_{Df}}{x_{df} x_D - x_{dD} x_{Df}} \frac{x_{Df}}{x_f} = (x_d' - x_d'') k_5 \frac{x_D x_f - x_{Df}^2}{x_{dD} x_f x_D - x_{dD} x_{Df}^2 + 2x_{Df} x_{df} x_{dD} - x_f x_{dD}^2 - x_D x_{df}^2} \quad (3.2.22)$$

Also,

$$x_d'' = \frac{x_d x_f x_D - x_{Df}^2 x_d - x_D x_{df}^2 + 2x_{df} x_{Df} x_{dD} - x_f x_{dD}^2}{x_f x_D - x_{Df}^2} \quad (3.2.23)$$

leading to

$$\frac{x_f x_{dD} - x_{df} x_{Df}}{x_{df} x_D - x_{dD} x_{Df}} \frac{x_{Df}}{x_f} = \frac{x_d' - x_d''}{x_d'' - (x_d - x_{dD})} k_5 \quad (3.2.24)$$

The relation $x_{dD} x_d - x_{dD} = x_{al} - x_{dDI}$ follows directly by definition from the current-flux relations (3.196) and (3.197) [$x_d - x_{dD} = (x_{dm} + x_{al}) - (x_{dm} + x_{dDI})$]. Now, using the definition for $k_6 = 1 - \frac{x_{dDI}}{x_{al}}$, the desired relation (3.2.19) follows, which, in turn, reads to the dynamic equation (3.223).

Finally, to derive the state equation (3.207), start with the definition of the state variable in Eq. (3.198), differentiate both sides of this relation with respect to time, and use the state equation (3.195) to obtain

$$\frac{x_f x_D - x_{Df}^2}{x_{df}} x_D - x_{dD} x_{Df} \dot{\bar{e}}_q' = \frac{r_f}{x_{df}} e_{fd} - r_f i_f \quad (3.2.25)$$

Now, define the transient time constant

$$T'_{d0} = \frac{x_f}{r_f} \quad (3.2.26)$$

and perform the following algebraic manipulation:

$$\begin{aligned} -\frac{x_D x_f}{x_f x_D - x_{Df}^2} &= -\left(1 + \frac{x_{Df}^2}{x_f x_D - x_{Df}^2}\right) \\ &= -\left(1 + \frac{x_{Df}^2 x_f (x_d - x'_d)}{(x_f x_D - x_{Df}^2) x_{Df}^2}\right) \\ &= -\left(1 + (x_d - x'_d) \frac{x_{Df}^2 x_f^2}{x_{df}^2} (x_f x_{dD} - x_{Df} x_{df})^2\right) \frac{x_f x_{dD} - x_{Df} x_{df}^2}{x'_d - x''_d} \\ &= -\left(1 + \frac{x_d - x'_d}{c_1^2} (x'_d - x''_d)\right) \end{aligned} \quad (3.2.27)$$

where

$$c_1 = \frac{x_{df} (x_f x_{dD} - x_{Df} x_{df})}{x_{Df} x_f} \quad (3.2.28)$$

Also, from Eqs. (3.296) and (3.297)

$$i_f = -\frac{x_{Df}}{x_D x_f - x_{Df}^2} \psi_f + \frac{x_D}{x_D x_f - x_{Df}^2} \psi_f + \frac{x_{dD} x_{Df} - x_{df} x_D}{x_f x_D - x_{Df}^2} i_d \quad (3.2.29)$$

which when combined with (3.2.25) obtains

$$\begin{aligned} T'_{d0} \dot{e}'_q &= -\frac{x_D x_f}{x_f x_D - x_{Df}^2} e'_q + \frac{(x_{df} x_D - x_{dD} x_{Df}) x_f x_{Df}}{x_f x_{dD} - x_{df} x_{Df}} (x_f x_D - x_{Df}^2) (e''_q - e'_q) \\ &\quad + \frac{x_{df} x_D - x_{dD} x_{Df}}{x_f x_D - x_{Df}^2} \frac{x_f}{x_{df}} e_{fd} + \frac{x_{df} x_D - x_{dD} x_{Df}^2}{(x_f x_D - x_{Df}^2)} x_f i_d \end{aligned} \quad (3.2.30)$$

After tedious algebraic manipulations, similar to the steps taken in performing intermediate steps when deriving the previous state equation, one obtains the state equation (3.207).

BIBLIOGRAPHY

1. Cohn, N., *Control of Generation and Power Flow on Interconnected Systems*, New York: Wiley, 1966.
2. Paul, J.P., et al., Improvements of the secondary voltage control in France, Proc. IFAC Symp. on Power Syst. Power Plant Control, Beijing, 1986.
3. Zaborszky, J., Prasad, K., Whang, K.W., Operation of the large interconnected power system by decision and control, *IEEE Trans. Power Apparatus Syst.*, PAS-99: 37–45, 1980.

4. Zaborszky, J., and Rittenhouse, J., *Electric Power Transmission*. Reynolds 1954. Available in paperback at Rensselaer University Bookstore, Troy, NY.
5. Woodson, H., and Melcher, J.R., *Electromechanical Dynamics*, New York Wiley, 1968.
6. White, D., and Woodson, H., *Electromechanical Energy Conversion*, New York: Wiley, 1959.
7. Fitzgerald, A., Kingsley, C., and Umans, S., *Electric Machinery*, New York: McGraw-Hill, 1983.
8. Blondel, A., *Synchronous Motors and Converters*, New York: McGraw-Hill, 1913.
9. Park, R.H., Two-reaction theory of synchronous machines—Generalized method of analysis: Part I, *AIEE Trans.* 48, 912–926, 1929.
10. Concordia, C., *Synchronous Machines: Theory and Performance*, New York: Wiley, 1951.
11. Willems, J.L., A system theory approach to unified electrical machine analysis, *Int. J. Control.*, **15**: 401–418, 1972.
12. Liu, X., Vergheze, G., Lang, J., and Onder, M., Extending the Blondel–Park transformation to generalized electrical machines, Proc. 12th IMACS World Congress, Paris, July 1988.
13. Padiyar, K.R., *Power System Dynamics*, London: Wiley, 1996.
14. Sauer, P.W., and Pai, M.A., Modeling and simulation of multimachine power system dynamics, in Leondes, C.T.(Ed) *Adv. Control Dynamic Syst.* **43**: Academic Press, 1991.
15. Kokotović, P., Khalil, H., and O'Reilly, J., *Singular Perturbation Methods in Control: Analysis and Design*, New York: Academic Press, 1986.
16. IEEE Guide for Synchronous Generator Modeling Practices in Stability Analyses, IEEE Standard 1110–1991, November 1991.
17. IEEE Task Force on Load Representation for Dynamic Performance Analysis, *IEEE Trans. Power Syst.*, **8**: 472–482, 1993.
18. Kalinowsky, S. A., and Forte, M. N., Steady state load voltage characteristic field tests at the area substations and fluorescent lighting component characteristics, *IEEE Trans. Power Apparatus Syst.*, **PAS-100**: 3087–3094, 1981.
19. Electromagnetic Transients Program, User's Guide, EPRI EL-6421- 1989.
20. Hill, D.J., Load recovery in voltage stability analysis and control, Proc. Workshop Bulk Power Syst. Voltage Phenom. III, Davos, Switzerland, August 1994.
21. Begovic, M., Load structure: Identification and impact on voltage stability, Proc. Workshop Bulk Power Syst. Voltage Phenom. III, Davos, Switzerland, August, 1994.
22. Zaborszky, J., Huang, G., Zheng, B., and Leung, T. C., On the phase portrait of a class of large nonlinear systems such as the power system, *IEEE Trans. Automatic Control*, **33**: 4–15, 1988.
23. Zaborszky, J., and Singh, J., A re-evaluation of the normal operating state control of the power system using computer control and system theory. Part I: Estimation, Proc. IEEE Power Indust. Comput. Appl. (PICA) Conf., Cleveland, OH, May, 1979.
24. Mukai, H., Singh, J., Spare, J.H., and Zaborszky, J., A re-evaluation of the normal operating state control of the power system using computer control and system theory. Part II: Dispatch targeting, *IEEE Trans. Power Apparatus Syst.*, 309–317, 1981.

25. Kambale, P., Mukai, H., Spare, J., and Zaborszky, J., A re-evaluation of the normal operating state control of the power system using computer control and system theory. Part III: Tracking and dispatch targets with unit control, *IEEE Trans. Power Apparatus Syst.*, 1903–1912, 1983.
26. Thomas, R.J., and Tiranuchit, A., Dynamic Voltage Instability, Proc. 26th IEEE Conf. Decision Control, December 1987. pp. 53–58.
27. Concordia, C., and Ihara, S., Load representation in power system stability studies, *IEEE Trans. Power Apparatus and Syst. PAS-101*, pp. 969–977, 1982.
28. Kappenman, J., and Norr, S., Static phase-shifter application and concepts for the Minnesota-Ontario interconnection, Proc. Third EPRI Workshop on FACTS, 1994.
29. Proc. FACTS Conference I—The Future in High-Voltage Transmission, EPRI Report TR-100504, 1992, Palo Alto, CA, 1992.
30. IEEE Committee Report, Dynamic models for steam and hydro turbines in power system studies, *IEEE Trans. Power Apparatus Syst., PAS-92*: 1904–1915, 1973.
31. Excitation system models for power system stability studies, IEEE Committee Report, *IEEE Trans. Power Apparatus Syst., PAS-100*: 494–509, 1981.
32. Kassakian, J., Schlecht, M., and Verghese, G., *Power Electronics*, Addison-Wesley, 1990.
33. Lasseter, R., Interaction of power systems with thyristor controlled reactors and other FACTS devices, EPRI Report TR-100504, Section 2.7.
34. Bohmann, L.J., and Lasseter, R., Equivalent circuits for frequency response of a static Var compensator, *IEEE Trans. Power Syst., PWRS-1*: 68–74, 1986.
35. Perreault, D., and Verghese, G., Time varying effects and averaging issues in models for current-mode control, *IEEE Trans. Power Electron.*, 12: 453–461, 1997.
36. Lasseter, R.H., and Lee, S.Y., Digital simulation of static Var transients, *IEEE Trans. Power Apparatus Syst., PAS-101*: 1982.
37. Yacamini, R., and de Oliveira, J.C., Comprehensive calculation of convertor harmonics with system impedances and control representation, *IEE Proc.*, 133: 95–102, 1986.
38. Bose, B.K., Evaluation of modern power semiconductor devices and future trends of converters, *IEEE Trans. Indus. Appl.*, 28: 403–412, 1992.
39. Hingorani, N., and Stahlkopf, K., High-power electronics, *Sci. Am.*, Nov., 78–85, 1993.
40. Chen, D., Power semiconductors: Fast, tough, and compact, *IEEE Spectrum*, Sept., 30–35, 1987.
41. *FACTS3—The Future of High-Voltage Transmission*, EPRI Proc., October 1994.
42. Gyugyi, L., Solid state control of AC power transmission, in EPRI Report TR-100504, Section 1.7.
43. Anderson, P., Agrawal, B., and Van Nes, J., *Subsynchronous Resonance in Power Systems*, New York: IEEE Press, 1990.
44. Applied Protective Relaying, Westinghouse Electric Co., Coral Springs, FL 33065, 1982.
45. Phadke, A., Thorp, J., and Horowitz, S., Impact of adaptive protection on power system control, Proc. Power Syst. Control Conf., Lisbon, Portugal, 1987.
46. Dobraca, F., Pai, M.A., and Sauer, P.W., Relay margins as a tool for dynamical security analysis, *J. Electric. Power Energy Syst.* 12: 226–234, 1990.

4 Models for Computer-Aided Analysis and Control

Having introduced in Chapter 3 physically based analytic models of individual components and the basic structure of an electric power system, it is necessary to provide models for its systematic computer-aided analysis and control. Conceptually, modeling of a power network for computer-aided studies is based on the same principles as of any other electric circuit [1–3]. In the first part of this chapter a computer-aided circuit model of an interconnected electric power network is developed by using general concepts from modeling electric circuits.

As it is well known, to establish a computer-aided circuit model, one needs constituent relations in terms of computer-aided characterization at each component level. It is recognized in this chapter, based on physical modeling in Chapter 3, that general computer-aided models at each component level can be expressed in terms of dynamics of the local states and local input and output variables only. These input and output variables are subject to algebraic constraints defined by Kirchhoff's laws. Combination of dynamic models of individual components and these algebraic constraints leads to a computer-aided model of an interconnected electric power system. The most general computer-aided model takes on the form of coupled, nonlinear differential-algebraic equations (DAEs) [4,5].

Because of the intended use of these models for system analysis and control design in later chapters, the constituent relations are expressed using a state-space-based modeling approach, typical in modeling general dynamic systems and given in Chapter 3. Moreover, instead of just declaring *system* state, input and output vectors, further subgrouping of these variables into *component*, or *local* state, input and output subvectors is done. This is helpful for systematic introduction of the power system control principles. In particular, decentralized control design at the lowest level of hierarchy is quite straightforward as long as the structure of the system model is retained [6]. It is with this in mind that notation for these subvectors at each component level is preserved.

In the second part of this chapter we introduce an elementary and intuitive overview of types of stability problems of direct interest in electric power systems as a basic motivation for the analysis and control design material in the remainder of this text.

4.1 UTILIZATION OF CIRCUIT THEORY METHODS

The power system consists of an entirely electrical power transmission network that connects nodes, that is, buses. Equipment components such as generators, loads, capacitors, reactors, and electronically switched devices are not strictly electrical and are connected directly to a bus and so they interact with equipment at other buses only through a power transmission network. No direct connection or interaction exists between pieces of equipment located at different buses.

The power transmission network is an electric circuit with nodes and branches typical of any other electric circuit. One unusual feature is its three-phase nature, three conductors and a neutral. The signals are modulated 60-cycle sine waves. The neutral carries the sum of the three phase current signals in reverse direction across any cut set over the four lines. If these add up to zero identically as it would in normal system conditions for three equal sine waves spaced at 120° in phase, the 3 phase current is known as balanced.

The equipment connected to the buses is widely varied in character, for example, rotor shaft position and power for generators. These can be represented, however, in electrical terms (power, voltage, current) at the interface with a bus as it is shown in Figures 3.2 and 3.3. Consequently, Kirchoff's constraints and methods apply, although they are commonly expressed in the form of power balance at buses since power is the input and output common in the electric power systems, as explained in Chapter 3. Of course, a system state $x(t)$ (a vector) is any set of variables which in their entirety at any time t_0 uniquely determine the entire system condition at all times $t > t_0$ given the system inputs for $t > t_0$. This leaves a choice of selecting the actual state variables depending on the type of the problem. So for instance in stationary conditions such as load flow on the transmission network, $e(t)$ and $i(t)$ are often chosen to exploit the advantages of linearity of the transmission network itself. For dynamic problems which involve the equipment at the buses power and voltage in phasor form are preferred (Chapter 2).

Note: For readers familiar with classical computer-aided packages for simulating electronic circuits, such as SPICE [7], it is important to recognize that certain major single port components in power systems do not lend themselves in a straightforward way to circuit representations.

4.1.1 Classification of Component Types

To introduce a model for computer-aided analysis recall from Chapter 3 that each electric power system consists of two types of fundamental components.

1. Single-port equipment (such as synchronous machines and loads, incorporated with their less standardized primary controllers, such as governors, excitors, switched shunt capacitors and reactors)

2. Two-port transmission components [high-voltage transmission lines connecting buses (nodes) and their primary controllers such as series capacitors, phase-shifting transformers, and on-line tap changers (OLTCs)].

The equipment components from the first category and their controllers are single ports and are connected by the transmission lines, which are two-port devices. The network topology in which these one- and two-port devices are interconnected is planar, meaning that all equipment is connected between specific buses and the neutral, with the transmission lines in a plane defined by the network buses. An analytical description of devices in categories 1 and 2 is introduced next.

4.1.2 Constituent Relations for Single-Port Components

As established in Chapter 3, the dynamics of any single-port component connected to bus i can be written as

$$\dot{x}_i = \tilde{f}_i(x_i, u_i, y_i, p_i) \quad (4.1)$$

where x_i is a local dynamic state vector, u_i is a local control input vector into the component if there is a local controller present, and y_i is a vector of local coupling variables through which local dynamics of individual components directly interact. Vector p_i stands for parameters of a component i . Dynamics of the various components, in particular synchronous generators and loads, are introduced in Chapter 3.¹

Strictly speaking, this form applies only to system components with continuous and smooth dynamics. All realistic components have some dynamics, that is, they do not respond instantaneously to changes. However, models of loads often neglect their dynamic response, that is, it is assumed that $\dot{x}_i \equiv 0$. Here, we take a more general approach to load modeling based on the physically based load behavior described in Chapter 3. This flexibility is particularly important in light of the fact that voltage-related instabilities are known to be strongly dependent on the actual load model used.

As shown in Figure 3.2, system components, such as primary controllers connected in parallel to synchronous generators and loads, enter the model in Eq. (4.1) by affecting dynamics of a local control vector u_i . The primary task of local controllers is to stabilize the local output variables y_i to their desired set point values y_i^{ref} that are typically set by a higher level stationary generator control introduced in Chapter 13.

¹ The general notation in this chapter is based on representing variables associated with individual components by using subscripts; variables representing all system devices do not have any superscripts.

A local continuous control u_i is typically designed in response to a local error signal²

$$e_i = y_i - y_i^{\text{ref}} \quad (4.2)$$

With a local controller of this form, the closed-loop local dynamics of a common component connected to bus i takes on a general form

$$\dot{x}_i = f_i(x_i, y_i, y_i^{\text{ref}}, p_i) \quad (4.3)$$

If a local controller is of the switching type, one obtains instead of the continuous differential equation form (4.3), a slightly more complicated form for the closed-loop dynamics

$$\dot{x}_i = \tilde{f}_i(x_i, y_i, u_i, p_i) \quad (4.4)$$

with control

$$u_i[(k+1)T] = u_i(kT) - d_i r_i[e_i(kT)] \quad (4.5)$$

acting only at discrete times kT , $k = 1, 2, \dots$

The local controller is typically governed by a relay-type switching function. Closed-loop local dynamic models of equipment controlled continuously and by switching are represented by general models of the form in Eqs. (4.3) to (4.5). Examples of the equipment characterized in this general manner are

- A synchronous machine equipped with a governor and exciter
- A load controlled by a switched-type controller connected in parallel with it (shunt capacitor and/or reactor)
- Tap changers

Consider such a power system consisting of n components characterized individually by Eq. (4.3). Define the *system* states and input and output variables of the corresponding variables defined for individual components³:

$$x_{\text{EQ}} \triangleq \begin{bmatrix} x_1 \\ \vdots \\ x_n \end{bmatrix}, \quad u_{\text{EQ}} \triangleq \begin{bmatrix} u_1 \\ \vdots \\ u_n \end{bmatrix}, \quad y_{\text{EQ}} \triangleq \begin{bmatrix} y_1 \\ \vdots \\ y_n \end{bmatrix} \quad (4.6)$$

² As described in Chapter 3, present state of the art of primary controllers relies entirely on local output error measurements e_i . In Chapter 12 we depart from this assumption fundamental to the present hierarchical control of power systems; several recent design concepts described are based on coordinated measurements.

³ Modern power systems contain both types of primary devices described by Eqs. (4.3) and (4.5), resulting in system state variables being a mix of continuous and discrete variables. Chapter 10 is analyzing the response to the nonsmooth (discrete) events.

Subscript EQ in Eqn. (4.6) stands for (single port) equipment. Since Eq. (4.3) describes each component, a dynamical model for the entire system takes on the form

$$\dot{x}_{\text{EQ}} = \tilde{f}(x_{\text{EQ}}, y_{\text{EQ}}, u_{\text{EQ}}, p_{\text{EQ}}) \quad (4.7)$$

where the nonlinear function defined as

$$\tilde{f}(x_{\text{EQ}}, y_{\text{EQ}}, u_{\text{EQ}}, p_{\text{EQ}}) \triangleq \begin{bmatrix} \tilde{f}_1(x_1, u_1, y_1, p_1) \\ \vdots \\ \tilde{f}_n(x_n, u_n, y_n, p_n) \end{bmatrix} \quad (4.8)$$

Equation (4.8) defines a set of coupled nonlinear differential equations of easily recognizable structure; each function \tilde{f}_i depends explicitly on variables associated with component i only. This model also provides a basis to view the interconnected system as consisting of individual components whose input–output characteristics are given in terms of u_i and y_i relations defined at each component level.

The output variables are generally port voltages \hat{E}_i defined at each port i , and input variables are currents into the single ports \hat{I}_i as indicated in Figure 4.1.⁴ Or, using vector notation for the entire system, it follows that

$$u_{\text{EQ}} \equiv [\hat{I}_1 \quad \dots \quad \hat{I}_n]^T \quad (4.9)$$

and

$$y_{\text{EQ}} \equiv [\hat{E}_1 \quad \dots \quad \hat{E}_n]^T \quad (4.10)$$

Example 4.1.1: Constituent relations of a synchronous machine Obtaining the actual model of the form in Eq. (4.3) for synchronous machines is a particularly laborious process. As shown in Chapter 3, a model of each synchronous

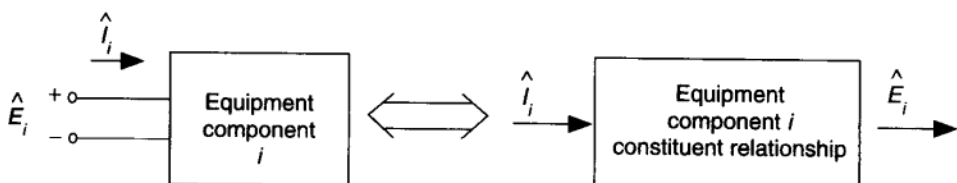


FIGURE 4.1 Equipment component as a single-port circuit element.

⁴ Both \hat{E}_i and \hat{I}_i are in fact state dependent variables (i.e., none of the two are independent inputs); because of this, the choice of input and output variables for system equipment and transmission lines is nonunique.

machine connected to bus i is of the form

$$\frac{dx_i^{dq}}{dt} = f_i(x_i^{dq}, y_i^{dq}, y_i^{\text{ref}}, p_i) \quad (4.11)$$

where x_i^{dq} , y_i^{dq} , y_i^{ref} , and p_i are vectors representing local dynamic state variables expressed in the dq reference frame, local output variables expressed in the dq reference frame, set point values for the output variables, and parameters of the specific equipment, respectively.⁵ This formula covers all types of synchronous machine models, independent from their complexity, ranging from type I through type IV shown in Table 3.2.

For creating a mathematical model of the interconnected system it is important to realize that the local state x_i^{dq} , input u_i^{dq} , and the output y_i^{dq} variables are routinely expressed in the dq reference frame,

$$u_i^{dq} = [i_i^d \quad i_i^q]^T \quad (4.12)$$

and

$$y_i^{dq} = [e_i^d \quad e_i^q]^T \quad (4.13)$$

Also, typically⁶

$$y_i^{\text{ref}} = [E_i^{\text{ref}} \quad P_{Ti}] \quad (4.14)$$

The local output variables are related to the local state variables by the coupling equations at the equipment side. In the case of synchronous machines, these are the two algebraic equations that result from assuming the dynamics of the flux linkages in the stator winding to be instantaneous.⁷ An example of coupling equations is given in Chapter 3 [Eqs. (3.203) to (3.204)]. These coupling equations are of a general form

$$0 = g_i(x_i^{dq}, y_i^{dq}, p_i) \quad (4.15)$$

In order to relate equipment variables to the variables on a transmission system, these need to be expressed with respect to the same reference frame. This issue is discussed in Section 3.2.3.5. Transformation from a dq into phasor reference frame is based on relations (3.205) and (3.206), which are restated here for completeness. Complex-valued phasor voltage (output variables) $\hat{E}_i = E_i e^{j\delta_i} =$

⁵ See Figure 3.3.

⁶ When dynamics of a turbine or governor is included P_{Ti} becomes a state variable in a closed-loop primary dynamics; see Chapter 13.

⁷ This assumption is not critical for the modeling approach adopted here; see Ref. [8].

$[E_i \cos \delta_i \quad E_i \sin \delta_i] = [E_{ci} \quad E_{si}]^8$ is related to the same voltage expressed in machine reference frame, $\hat{E}_i = [e_{di} \quad e_{qi}]$, as

$$\begin{aligned} e_{di} &= -E_{ci} \sin \theta_i + E_{si} \cos \theta_i \\ e_{qi} &= E_{ci} \cos \theta_i + E_{si} \sin \theta_i \end{aligned} \quad (4.16)$$

This relation can be thought of as transforming local output variables y_i in the network (phasor) coordinates to the same output variables y_i^{dq} in the dq coordinates via the rotation matrix $T(\theta_i)$, that is, an alternative form follows directly,

$$y_i^{dq} = T(x_i^{dq})y_i = T(\theta_i)y_i \quad (4.17)$$

where the transformation matrix⁹ $T(\theta_i)$ stands for

$$T(\theta_i) = \begin{bmatrix} -\sin \theta_i & \cos \theta_i \\ \cos \theta_i & \sin \theta_i \end{bmatrix} \quad (4.18)$$

This matrix is essential for mapping variables from a dq reference frame into the network reference frame and vice versa. It can be shown that the inverse of this matrix is the same matrix transposed, that is, this matrix is unitary.

Based on the preceding, one identifies x_i^{dq} and y_i as local state and output variables of a synchronous machine. As derived in Chapter 3, similar relations hold for mapping the equipment input variables (currents) from the dq to the network reference frame.

Note: In electronic circuits it would suffice to have currents and voltages only as input and output variables, and not power. However, since an electric power system network is primarily concerned with power delivery, both real and reactive power into a port could be made part of the input (independent parameter) variables. They are functions of current and voltage at a port and are not designated explicitly as input variables in Eq. (4.12). For purposes of stating power relations explicitly, this could be replaced by another vector of input variables

$$u_i = [P_i \quad Q_i]^T \quad (4.19)$$

Yet another important distinction of the “dynamic” power system models relative to the circuit theory models comes from representing dynamics of time-varying phasors rather than dynamics of the instantaneous variables. Derivatives of certain variables with respect to time represent dynamics of phasor magnitude and angle, and not of the instantaneous variables.

⁸ The same notation used as in Chapter 2.

⁹ This is the Blondel transformation introduced in Chapter 3 for the case of balanced three-phase systems.

Example 4.1.2: Constituent relations of a load Equipment components, such as loads, whose dynamics may be assumed to be negligible for many of the phenomena studied in this text can be simply characterized by a vector of output variables analogous to the output variables used for synchronous machines. Their constituent relation of an algebraic form¹⁰ as introduced in Section 3.2.3.10, Eq. (3.244) is

$$0 = f_{Li}(u_{Li}, y_{Li}, y_{Li}^{\text{ref}}, p_{Li}) \quad (4.20)$$

with

$$u_{Li} = [P_{Li} \quad Q_{Li}]^T \quad (4.21)$$

$$y_{Li} = [E_{ci} \quad E_{si}]^T \quad (4.22)$$

and

$$y_{Li}^{\text{ref}} = [E_i^{\text{ref}}] \quad (4.23)$$

While most of the small loads do not have primary-control equipment to maintain y_{Li}^{ref} , many larger industrial loads are amenable to controlling their own output variable. (It is discussed later in Chapter 14 that this may become an important function for maintaining operating conditions within the prespecified operating limits. Qualitative difference exists between the effect of regulating E_{Li}^{ref} and regulating the load power factor. The reasons for this are discussed in Chapter 14.)

Equations (4.20) to (4.23) represent the most often used load model. However, depending on the type of phenomenon analyzed, this model may not be adequate. At least in concept, given local state, input and output variables of a load connected to a bus, the load model lends itself to the form characteristic of an electric machine [Eq. (4.1)]. For example, to analyze the impact of an induction-machine type load model on voltage dynamics, a model of this type is commonly used.¹¹

4.1.3 Constituent Relations for Transmission Lines

As established in Chapter 2, physical single-phase or physically balanced three-phase two-port devices (transmission lines) can each be fully modeled by single-phase circuits with the ground or neutral side connection having zero impedance. For the physically single-phase case the impedance on the phase side is then doubled. For the physically balanced three-phase case the zero-impedance neutral line (or an absent neutral line which is equivalent provided the system is balanced) is equivalent to the physical cancellation of equal vectors displaced by 120°.

¹⁰ Notice no explicit role of x_i in static devices since the device dynamics are neglected.

¹¹ In addition, for analyzing fast phenomena it has been shown that using a constant-power model could result in dynamic instabilities [8]. For such studies it becomes necessary to model fast dynamics of the load using time-varying phasors, much in the same sense as when modeling dynamics of a generator or dynamics of a lumped-parameter transmission line.

So for balanced three-phase case the actual impedance is used on the phase side of the single-phase model. In most of this text the single-phase models with a zero-impedance neutral line will stand for balanced three-phase circuits, but with the above convention most of the results will also stand for the physical single-phase circuit. Unless otherwise stated, the so called one-line diagrams will represent such single-phase models with zero impedance on the neutral side and double impedance on the other of an actual single phase circuit. It has been shown in Chapter 3 that transmission lines are basically four-terminal (two-port) devices. A schematic view of a transmission line as a four-terminal, two-port device connecting any two nodes i and j is shown in Figure 4.2.

Most often transmission lines are modeled in this text as devices that respond instantaneously to changes in operating conditions at their terminals. In this case, a constituent relation of a two-port device is static as described in Chapter 3.

However, transmission lines actually have dynamics governed by the time constants of their RLC lumped-parameter representation, which under certain operating conditions lead to dynamic interactions between the transmission lines and synchronous generators; an example of this kind is the problem of subsynchronous resonance. For analyzing this phenomenon a more adequate representation of transmission lines is obtained by incorporating dynamics of the series inductor current and shunt-capacitor voltages of the π -circuit model of a transmission line. It turns out that use of time-varying phasors introduced in Chapters 2 and 11 is particularly handy for this, resulting in a dynamic transmission-line model with the state variables being time-varying phasors of the inductor current and capacitor voltages. This model is used in Ref. [13] for designing advanced generator and/or transmission-line control to suppress subsynchronous resonance problem. It is for applications of this sort that two different models of transmission lines are given, a static model and a lumped-parameter model with the line dynamics included. These models are described next.

4.1.3.1 Static Model (Lumped Parameter) The constituent relations of a transmission line are described in Chapter 3 and are summarized here for completeness. Constituent relations of each transmission line connecting buses i and j are of the form

$$\begin{aligned}\hat{I}_i &= \hat{Y}_{ii}\hat{E}_i + \hat{Y}_{ij}\hat{E}_j \\ \hat{I}_j &= \hat{Y}_{ji}\hat{E}_i + \hat{Y}_{jj}\hat{E}_j\end{aligned}\quad (4.24)$$

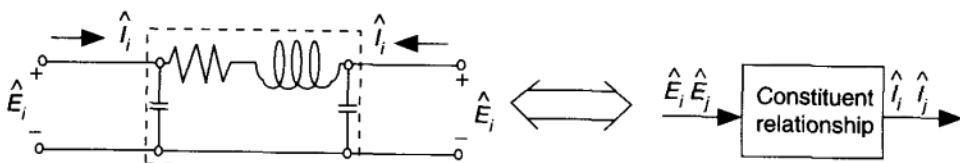


FIGURE 4.2 A transmission line as a two-port device.

The complex-valued power into a transmission line ij at bus i and, similarly, complex-valued power into the same transmission line ij at bus j are

$$\begin{aligned}\hat{S}_{ij} &= \hat{E}_i \hat{I}_i^* \\ \hat{S}_{ji} &= \hat{E}_j \hat{I}_j^*\end{aligned}\quad (4.25)$$

The general form of Eq. (4.25) is

$$\hat{S}_{ij} = f_{ij}(\hat{E}_i, \hat{E}_j, p_{ij}) \quad (4.26)$$

where \hat{E}_i and \hat{E}_j are voltages at buses i and j in their phasor form, and p_{ij} denotes the transmission-line parameters in the π -circuit model of a line shown in Chapter 3, Figure 3.5. The output variables y_{ij} at ports i and j of the transmission line connecting equipment components between buses i and j are defined to be complex-valued currents¹² \hat{I}_i and \hat{I}_j and bus voltages are inputs \hat{E}_i and \hat{E}_j , or vice versa, respectively,

$$y_{ij} = [\hat{I}_i] \quad (4.27)$$

and

$$u_{ij} = [\hat{E}_i \quad \hat{E}_j]^T \quad (4.28)$$

The notation \hat{I}_i stands for the total current into port i of a transmission line ij ; when shunt capacitances are neglected in the π line model $\hat{I}_i = \hat{I}_{ij}$; otherwise, $\hat{I}_i \equiv \hat{I}_{ij} + \hat{I}_{i0}$, where \hat{I}_{i0} stands for the line current through a shunt capacitor at bus i .

4.1.3.2 Dynamic Model (Lumped Parameter) A systematic dynamic model can be obtained by viewing a lumped-parameter π circuit shown in Figure 3.5 as any other RLC two-port circuit characterized by the time-varying phasor dynamics of inductor current [Eq. (2.36)] and capacitor voltages [Eq. (2.37)] derived in Chapter 2. Local state variables of a transmission line are chosen much in the same way as the state variables in two-port electric circuits. In the case of a π -circuit model of a transmission line the local state vector is

$$x_{ij} = [\hat{I}_{ij} \quad \hat{E}_i \quad \hat{E}_j]^T \quad (4.29)$$

Using the formulas in Chapter 3 for a transmission line one obtains

$$L \frac{d\hat{I}_{ij}}{dt} = -\hat{Z}_{ij} \hat{I}_{ij} + \hat{E}_i - \hat{E}_j$$

¹² When necessary, currents \hat{I}_i and \hat{I}_j are referred to as \hat{I}_{ij} and \hat{I}_{ji} , respectively.

$$\begin{aligned} C \frac{d\hat{E}_i}{dt} &= -\hat{Y}_C \hat{E}_i + \hat{I}_{i0} \\ C \frac{d\hat{E}_j}{dt} &= -\hat{Y}_C \hat{E}_j + \hat{I}_{j0} \end{aligned} \quad (4.30)$$

where \hat{I}_{i0} and \hat{I}_{j0} are currents through the corresponding shunt capacitances in the J_i -circuit of a transmission line. The same as in the static model (4.24), currents \hat{I}_i and \hat{I}_j into the sending end of a transmission line i and receiving end j , respectively, are output variables between the two-port devices of the line and the devices directly connected to buses i and j . The model given by Eq. (4.30) is of the same general form as the dynamic model of a single-port dynamic model, when one keeps in mind that $\hat{I}_i = -\hat{I}_j$, i.e.,

$$\dot{x}_{ij} = f_{ij}(x_{ij}, y_{ij}, p_{ij}) \quad (4.31)$$

It is a simple matter to see that when shunt capacitors are neglected in the lumped-parameter π -circuit model of a line, voltages \hat{E}_i and \hat{E}_j take on the role of port inputs instead of states.

Time responses of states x_{ij} in transmission lines are short relative to the natural response of synchronous machines and are often neglected. If they are assumed instantaneous, the model in Eq. (4.30) degenerates into the static model in Eq. (4.24). The model in Eq. (4.24) is routinely used in this book, except when explicitly said otherwise. The vector notation for the output variables of all transmission lines present on the system is simply

$$\begin{aligned} y_{TL} &= [y_{12} \quad y_{13} \quad \cdots \quad y_{(n-1)n}]^T \\ &= [\hat{I}_{12} \quad \hat{I}_{13} \quad \cdots \quad \hat{I}_{(n-1)n}]^T \end{aligned} \quad (4.32)$$

and for the input variables

$$\begin{aligned} u_{TL} &= [u_{12} \quad u_{13} \quad \cdots \quad u_{n(n-1)}]^T \\ &= [\hat{E}_1 \quad \hat{E}_2 \quad \hat{E}_3 \quad \cdots \quad \hat{E}_{(n-1)} \quad \hat{E}_n]^T \end{aligned} \quad (4.33)$$

4.1.4 Computer Formulation of the Kirchoff Laws

Any lumped-parameter network obeys three basic laws: the Kirchoff voltage law (KVL), the Kirchoff current law (KCL), and the constituent characteristics of individual components and devices. So far we have established in this chapter constituent relations of individual components and devices. The Kirchoff laws are linear algebraic constraints on branch voltages and currents arising from the interconnection of components and are independent of the constituent relations of the components.

A complete description of the network model contains information about devices connections, the reference directions for device currents and voltages (network topology), and device characterization. A well-established approach to providing information about the network topology of an arbitrary electric network

is by drawing a *directed graph* associated with a given network according to the following: replace each two-terminal device by a line segment, called a branch, with an arrow in the same direction as the assumed positive current through that branch. This arrow also serves as the branch voltage reference: The positive voltage terminal is assumed to be at the tail of the arrow. By adopting such an associated reference, there is no need to carry two sets of references, one for the currents and the other for the voltages [1,3].

While a directed graph completely describes a lumped-parameter network, it is not in a form suitable for storing in a computer. It is known that the information contained in a directed graph can be completely stored in a matrix called an *incidence matrix* [1,3]. For a directed graph with n nodes and b branches, the incidence matrix is an $n \times b$ matrix $A_a = [a_{ij}]$, where

$$a_{ij} = \begin{cases} 1 & \text{if } j \text{ incident at } i, \text{ and the arrow is away from } i \\ -1 & \text{if } j \text{ is incident at } i, \text{ and the arrow is toward node } i \\ 0 & \text{if branch } j \text{ is not incident at node } i. \end{cases} \quad (4.34)$$

Observe further that since every branch is connected to two distinct nodes, it follows that every column of an incidence matrix A_a has exactly two nonzero elements, a 1 and a -1 , with the rest being zeros. Therefore, one could delete one row of this matrix without losing nonrecoverable information. A matrix obtained from A_a (complete incidence matrix) is called a *reduced incidence matrix* and is denoted by A . The reduced incidence matrix is an important concept since both KCL and KVL are easily written using this matrix.

In particular, the maximum set of independent KCL equations can be expressed as [2]

$$Ai = 0 \quad (4.35)$$

where i is the vector of all branch currents. This equation simply says that the sum of all currents into any given bus equals zero, that is, a network node does not store energy.

Furthermore, the $n - 1$ columns of A are linearly independent if and only if the branches corresponding to these columns form a tree in the directed graph of a network. Topology of *any size* electric power network is relatively simple, in the sense that a very simple (normal) tree can be constructed which consists of branches connecting individual buses to the neutral line. This tree is symbolically represented in Figure 4.3, corresponding to a three-bus power system in Figure 4.4. Currents in this normal tree correspond to the currents in single-port devices connected to the buses. Currents in the rest of the branches are linearly dependent and constrained according to the KCL given in Eq. (4.35). For example, for the three-bus power network shown in Figure 4.4, its directed graph is shown in Figure 4.5 and its reduced incidence matrix is

$$A = 2 \begin{bmatrix} 1 & 1 & 0 & 1 & 1 & 0 & 0 & 0 & 0 & 1 & 0 & 0 \\ -1 & 0 & 1 & 0 & 0 & 0 & 1 & 1 & 0 & 0 & 1 & 0 \\ 0 & 0 & 0 & -1 & 0 & 1 & -1 & 0 & 1 & 0 & 0 & 1 \end{bmatrix} \quad (4.36)$$

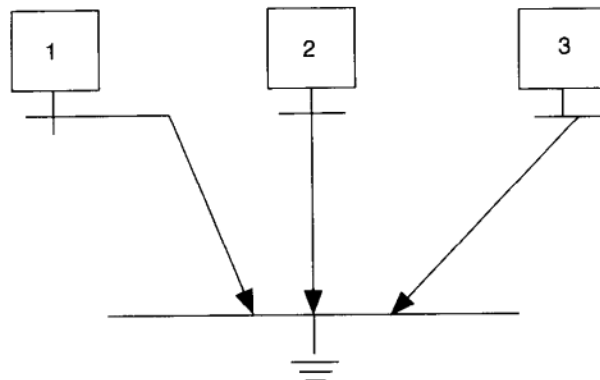


FIGURE 4.3 Normal tree in the graph of a three-bus system.

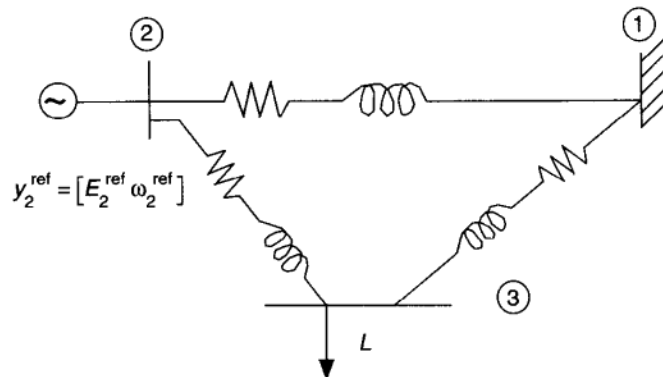


FIGURE 4.4 A three bus example.

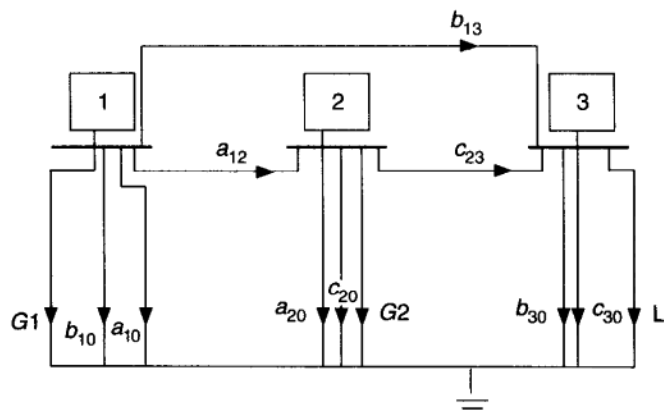


FIGURE 4.5 Directed graph associated with the three-bus system.

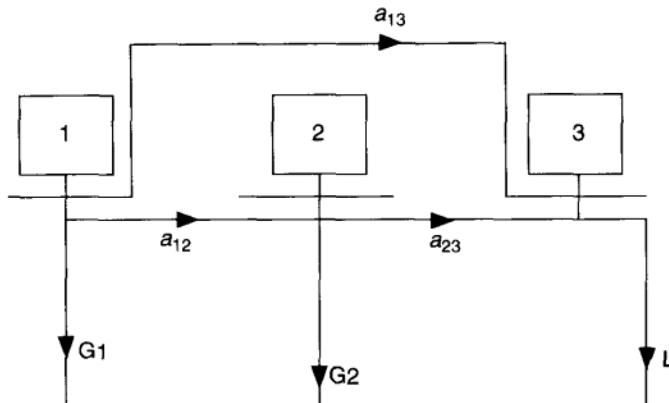


FIGURE 4.6 Directed graph associated with the three-bus system—no shunt capacitances.

A directed graph and the corresponding reduced incidence matrix when shunt capacitances in π -circuit lumped-parameter models of the transmission lines are neglected are shown in Figure 4.6, and the reduced incidence matrix is

$$A = \begin{matrix} 1 \\ 2 \\ 3 \end{matrix} \left[\begin{array}{cccccc} 1 & 1 & 0 & 1 & 0 & 0 \\ -1 & 0 & 1 & 0 & 1 & 0 \\ 0 & -1 & -1 & 0 & 0 & 1 \end{array} \right] \quad (4.37)$$

Similarly, the KVL in the case of the simple topology with a normal tree shown in Figure 4.3 states that the branch voltage vector e is a linear combination of the nodal voltage vector e_n , the elements of which are nodal voltages measured between individual nodes and the neutral line (ground). Mathematically,

$$e = A^T e_n \quad (4.38)$$

The KCL and KVL stated formally for an electric power network, as for any other electric network, imply constraints on the variables used in defining constituent relations of system components and devices. In particular, the transmission network imposes algebraic constraints on the coupling variables y_{EQ} and y_{TL} given in Eqs. (4.10) and (4.32) and the input variables u_{EQ} and u_{TL} defined in Eqs. (4.9) and (4.33). If the graph branches are ordered to include equipment components first, and line components next (as in the three-bus network example), then the KCL equation (4.35) applied to the power network states becomes

$$A[u_{EQ} \quad y_{TL}]^T = 0 \quad (4.39)$$

Equation (4.38) applied to a directed graph of an arbitrary power network is used implicitly by writing simple fundamental loops associated with the normal tree. The KVL for such simple network topology basically states that the voltage difference \hat{E}_{ij} across a transmission line connected to buses i and j equals the

difference of nodal voltages \hat{E}_i and \hat{E}_j . Defining voltage differences across all transmission lines,

$$\hat{E}_{\mathcal{L}} \equiv [\hat{E}_{12} \quad \hat{E}_{13} \quad \dots \quad \hat{E}_{(n-1)n}]^T \quad (4.40)$$

the KVL equation (4.38) takes on the form

$$\hat{E}_{\mathcal{L}} = A^T y_{EQ} \quad (4.41)$$

All network constraints here are written in terms of currents and voltages. However, since the purpose of a power system is to move power around, the power balance equations are often preferable. They directly follow from the KCL equation after taking the complex conjugate of this relation and multiplying it by the complex-valued diagonal matrix, the elements of which are elements of y_{EQ} , that is,

$$\text{diag } (y_{EQ}) A ([u_{EQ} \quad y_{TL}]^T)^* = 0 \quad (4.42)$$

Equation (4.42) simply states that at each bus of a transmission network the algebraic sum of power flowing into a bus from all locally connected equipment and all transmission lines is zero. Equation (4.42) states in computer-aided form the power-balance equations at all buses in a power network, and written explicitly in terms of phasors, that is as complex-valued currents and voltages, takes the form

$$\text{diag } (\hat{E}) A [\hat{I}_1 \quad \hat{I}_2 \quad \dots \quad \hat{I}_n \quad \hat{I}_{12} \quad \hat{I}_{13} \quad \dots \quad \hat{I}_{(n-1)n}]^T = 0 \quad (4.43)$$

Equation (4.43) effectively represents load flow equations under the assumption that certain variables are specified and others need to be computed. The simplest case of specifying the power-flow vector out of individual equipment components leads to a load-flow formulation

$$\text{diag } (\hat{E}) [\hat{I}_{12} \quad \hat{I}_{13} \quad \dots \quad \hat{I}_{(n-1)n}]^{*T} = [\hat{S}_1 \quad \hat{S}_2 \quad \dots \quad \hat{S}_n]^T \quad (4.44)$$

which further, after using the static characterization of transmission lines in Eq. (4.24) becomes

$$\text{diag } (\hat{E}) \hat{Y}_{bus}^* [\hat{E}_1 \quad \hat{E}_2 \quad \dots \quad \hat{E}_n]^{*T} = [\hat{S}_1 \quad \hat{S}_2 \quad \dots \quad \hat{S}_n]^T \quad (4.45)$$

where \hat{Y}_{bus} is known as the power system bus admittance matrix and its terms are easily built by inspection.

4.1.5 Transmission Network Admittance Matrix and its Properties

The system admittance matrix is of the form

$$\hat{Y}_{bus} = A \hat{Y} A^T \quad (4.46)$$

where \hat{Y} is a $b \times b$ diagonal matrix, the elements of which represent branch admittance in a power system ordered according to the branch graph enumeration of a power system. For further understanding of the material in later chapters, Chapter 13 in particular, it is important to observe an essential fact related to the structure of the bus admittance matrix of any power system: the matrix \hat{Y}_{bus} has an inherent modeling (not numerical) singularity, that is, it is always rank-1 deficient. This claim can be simply shown by recalling how one builds matrix \hat{Y}_{bus} by inspection [3]. This rank deficiency occurs when the power flows $[\hat{S}_1 \hat{S}_2 \dots \hat{S}_n]$ into all individual equipment components are modeled as independent from the actual local states of the equipment. In this setup the transmission portion of the system appears completely separated from the ground, since all inputs into it are treated as independent (flow) sources from the actual equipment states. In reality this is not the case (see the constituent relations of equipment and transmission lines), but when modeling equipment components as independent flow sources, this potentially misleading interpretation evolves.

Note: It is important to recognize that this singularity is not analogous to the singularity of any electric circuit prior to defining ground. The analogy is more appropriate with transistor circuits that are represented by the incremental models with independent current sources. When the parasitic parallel elements are neglected a transistor circuit could require an additional reference [1].

Equation (4.45) is valid for computing all power flows into the transmission system $[\hat{S}_1 \hat{S}_2 \dots \hat{S}_n]$ for a power system with n buses given all bus voltages $[\hat{E}_1 \hat{E}_2 \dots \hat{E}_n]$. The inverse problem, however, cannot be solved uniquely. Given a full set of n bus power injections $[\hat{S}_1 \hat{S}_2 \dots \hat{S}_n]$, there is no way to compute $[\hat{E}_1 \hat{E}_2 \dots \hat{E}_n]$ because the inverse problem is not well posed mathematically, that is, the matrix \hat{Y}_{bus} is singular. Note, however, that physically on a live system all these quantities can be readily measured. So there is no mystical “structural singularity”, only an improperly formulated mathematical problem.

Think of a bus to bus transmission line. Given the voltages ($E_i e^{j\delta_i}$ and $E_j e^{j\delta_j}$), the current and the power at the line ends can be directly and unequivocally computed. Furthermore, changing the reference angle or the voltage reference will not be a problem as long as the *differences* between line ends are the same, because

$$\hat{I}_{ij} = \frac{\hat{E}_i - \hat{E}_j}{\hat{Z}_{ij}} \quad (4.47)$$

where \hat{Z}_{ij} is a transmission-line impedance. In a set of n buses or nodes of a network there are only $n - 1$ independent differences since with $n - 1$ phasor differences the n th difference can be computed. Thus from $n - 1$ phasor differences of bus voltages all line currents can be computed uniquely. Furthermore

$$\Delta\hat{E}_i = \hat{E}_i - \hat{E}_k, \quad i = 1, 2, \dots, n - 1 \quad (4.48)$$

are equivalent and convertible information, where $k = n$ is any of the system buses chosen as a reference. Thus writing Eq. (4.47) in matrix form

$$\hat{I} = \hat{\mathcal{Y}}\Delta\hat{E} \quad (4.49)$$

where $\hat{\mathcal{Y}}$ is an $(n - 1) \times (n - 1)$ nonsingular matrix, we would have a formulation that is invertible.

We now have a mathematically well-posed problem for the same physical situation without singularities. The price to pay, however, is a transformation (noninvertible) from the easily known phasor voltages \hat{E}_i to the phasor voltage differences $\Delta\hat{E}_i$ and to $\hat{\mathcal{Y}}$. A full analysis of this is given in Section 3.2.1.

It should be observed further that the transmission network, defined in Eq. (4.48) and (4.49) is an *isolated system* of order n with no interaction with the outside world beyond its own $(n - 1) \times (n - 1)$ phasor "home". Even the reference \hat{E}_k at bus k is internal because it is tied to one of the system buses. Introducing an arbitrary external (i.e., not in the system) reference, say for δ_k , would bring in outside information and disrupt the isolation of the system.

Accordingly, care must be taken in selecting the references E_k and δ_k to preserve the isolated nature of the system. This means that an *internal* reference (one connected to the system itself) must be used. One would first think of the internal system neutral bus as such a reference. As explained in Chapter 2 on a balanced three-phase quasistationary system the phasor voltage on the neutral line is identically zero with not even the 60-Hz carrier visible. This implies two facts:

1. $E = 0$ is an *internal* state for the n -bus system connected with the neutral bus as a node and hence assigning it as a reference is legitimate and it will preserve both the isolation of the system and the number of independent \hat{E}_i states for the voltage.
2. Because the neutral voltage for balanced three phase systems including the carrier is identically zero, its phase is undefined. So for the angle the neutral bus cannot serve as a reference. Several ways of resolving this problem are described in Chapter 3, Section 3.2.1.1.

The moral is that the system will behave as an independent system which will react to any internal changes (in voltage, current, power etc.) in a manner uniquely and inevitably, responding to such changes and keeping a constant frequency assuming that the net total power input-output balance is zero. If the net power is non zero the entire system, its center of angle (Section 3.2.1.1), will be drifting and thus the system frequency will be changing. This frequency change however is typically very slow and small but important when controlling the system frequency is the issue such as it is in automatic generation control (AGC in its classical or present approaches, see Chapter 13). This means that except for system frequency control isolated system models are quite precise

for internal dynamic events within the system. See Section 3.2.1.1 for detailed analysis and a choice of models.

4.1.6 Summary of a General DAE Model

In summary, a computer-aided model of any electric power system in the quasi-stationary operation consists of sets of differential equations for the equipment connected to the buses and algebraic or load-flow equations for transmission network.

While none of this appears to be any different from modeling electronic circuits, some caution is required in deciding how detailed models for each component should be used for the problem of interest. A particular example of this problem is deciding which components are dynamic and which are static for the problem of interest.

As shown in Chapter 3, models of synchronous machines range over a wide variety depending on the purpose of the model (i.e., the degree of desired approximation). Load models are subject to the same considerations. Similarly, as pointed out in this chapter, transmission lines are most often modeled as static devices for the purposes of this text, without any dynamics. However, when necessary the dynamics of lumped-parameter transmission lines lend itself to the same general computer formulation in terms of state equations as the dynamics of synchronous machines. Very long transmission lines require a treatment as boundary value problems with partial differential equations or by time delay equations as presented in Chapter 11.

When one attempts to study an unusual phenomenon it is generally safe to start with dynamics as detailed as possible and apply systematic ways for simplifications. In Chapter 6 systematic approaches to model simplification often used in the small signal analysis of dynamic systems are described in detail.

Some caution is required in converting input and output variables of synchronous machines from a dq into a phasor reference frame (coordinate system). As shown in Chapter 3, Section 3.2.3.5 it is common practice to write the dynamics of synchronous machines in a dq (machine) reference frame, convert their input and output variables from the dq reference frame into a network reference frame, and write network constraints using a phasor network reference frame. In some very recent literature machine dynamics are formulated using a network (rather than machine) reference frame; more work is needed to understand potential benefits of using this modeling approach.

Finally, one should understand the implications of writing power-balance equations (4.42) instead of current-balance equations (4.35). This difference is more fundamental than it seems at first sight, since power relations are *quadratic functions of nodal voltages*. A typical stationary analysis of a power network requires computation of nodal voltages $[\hat{E}_1 \hat{E}_2 \dots \hat{E}_n]$ for specified power injection into the nodes $[\hat{S}_1 \hat{S}_2 \dots \hat{S}_n]$, as defined in Eq. (4.45). This analysis is known as the load-flow analysis problem, which is studied in detail in Chapter 5. This analysis is much more complex than the nodal analysis for linear *RLC* circuits,

such as the transmission-line models, when sources are specified as independent current sources. The complication is a direct consequence of writing power-balance equations as quadratic functions of nodal voltages [Eq. (4.45)], instead of linear KCL equations relating independent current sources to nodal voltages. This choice however is dictated by the practical fact that the commodity one deals with on the system is power and choosing a simple linear network model would introduce a need to convert the results into a *power flow*. So practice has opted for the bus power balance-line power balance. This is all observed in Chapter 3.

Because of a large number of components of the same type, the tendency is to use simple models, resulting in a fewer number of dynamic equations. This generally results in models consisting of constituent relations of all individual equipment components with dynamics of the general form [Eq. (4.7)], all components with dynamics that are negligible for the phenomena studied [Eq. (4.20)], all transmission lines [Eqs. (4.24)], the coupling equations at the equipment and bus sides [Eqs. (4.15) and (4.17)], and the power-balance equations at all buses [Eq. (4.42)], that is,

$$\dot{x} = \tilde{f}(x, u, y, p), \quad x(t_0) = x_0 \quad (4.50)$$

$$0 = g(x, u, y, p) \quad (4.51)$$

where

$$x = [x_1 \ x_2 \ \dots \ x_n]^T \quad (4.52)$$

and

$$u = [u_{EQ} \ \dots \ u_{TL}]^T \quad (4.53)$$

and

$$y = [y_{EQ} \ \dots \ y_{TL}]^T \quad (4.54)$$

This model [Eqs. (4.50) to (4.54)] is referred to as a differential-algebraic equations (DAE) model or a descriptor form model of an interconnected power system [4, 5, 9].

Example 4.1.3: Model of a small power system This system consists of two generators and a single load as shown in Figure 4.4. One of the generators, bus 1, is assumed to have unlimited real power and is therefore modeled as an ideal voltage source of magnitude E_1 and phase angle 0° (system slack bus), whose frequency is maintained at its value independent of system changes. Generator 2 which has a limited amount of real-power reserves, is connected to the bus 1. Its dynamical model is characterized by the type II₂ synchronous machine model described in Chapter 3 as follows:

$$\frac{d\theta_2}{dt} = \omega_2 - \omega_0 \quad (4.55)$$

$$\frac{d\omega_2}{dt} = P_{T2} - P_{G2} \quad (4.56)$$

$$\frac{de'_{q2}}{dt} = -e'_{q2} + (x_{d2} - x'_{d2})i_{d2} + e_{fd2} \quad (4.57)$$

Similarly, dynamics of the exciter of generator 2 are defined by Eqs. (3.267) to (3.269) as

$$\frac{dV_{F2}}{dt} = \frac{1}{T_F} \left(-V_{F2} + \frac{K_F}{T_E} (V_R - (S_E + K_E)e_{fd2}) \right) \quad (4.58)$$

$$\frac{de_{fd2}}{dt} = \frac{1}{T_E} [-(K_E + S_E(e_{fd2}))e_{fd2} + V_{R2}] \quad (4.59)$$

$$\frac{dV_{R2}}{dt} = \frac{1}{T_A} \left[K_A \left(V_{F2} - \frac{K_F}{T_F} e_{fd2} - E_2 + E_{ref2} \right) - V_{R2} \right] \quad (4.60)$$

Coupling equations between the generator and bus 1 on the generator side are an example of the general equations (3.205) to (3.206) and restated here for the generator connected to bus 2 are

$$e_{q2} = e'_{q2} + x'_{d2}i_{d2} - ri_{q2} \quad (4.61)$$

$$e_{d2} \approx 0 \quad (4.62)$$

On the bus side, the general coupling equations (3.203) to (3.204) [illustrated in Eq. (4.15)] effectively convert terminal bus voltage represented in the *dq* (synchronously rotating) reference frame into the voltage and current phasors needed for the one-line diagram system representation in the network frame of reference. They are restated here for completeness as

$$e_{q2} = E_2 \cos(\delta_2 - \theta_2), \quad i_{q2} = I_2 \cos(\delta_2 - \theta_2 - \varphi_2) \quad (4.63)$$

$$e_{d2} = E_2 \sin(\delta_2 - \theta_2), \quad i_{d2} = I_2 \sin(\delta_2 - \theta_2 - \varphi_2) \quad (4.64)$$

The real power out of generator 2 is

$$P_{G2} \approx e_{q2}i_{q2} = E_2I_2 \cos \varphi_2 \quad (4.65)$$

$$Q_{G2} \approx -e_{q2}i_{d2} = E_2I_2 \sin \varphi_2 \quad (4.66)$$

Recall that E_2 is the magnitude of the terminal bus voltage, δ_2 is its phase angle, and θ_2 is the phase angle of the direct axis, while φ_2 is the power factor angle of the terminal current I_2 . The load model connected to bus 3 is most often represented as a constant real-reactive power device. Characteristics of steady-state system operation could under certain conditions become strongly dependent

on the load model chosen. Here a real-reactive-power load model representation is assumed. Notationally this is simply expressed by stating that

$$P_{L3} = P_3 \quad (4.67)$$

$$Q_{L3} = Q_3 \quad (4.68)$$

where P_3 and Q_3 are given values. Constituent relations (4.55) to (4.68) together with the network constraints form a sufficient number of relations to define everything else on the system, given its input variables and all transmission system parameters. Depending on the type of specific device models chosen, input specifications could be different. Specific bus constraints (4.42) for the power system given in Figure 4.4 are

$$P_{L3} + jQ_{L3} = P_{31} + jQ_{31} + P_{32} + jQ_{32} \quad (4.69)$$

and

$$P_{G2} = P_{21} + P_{23} \quad (4.70)$$

Equations (4.69) and (4.70) represent power balance equations at buses 3 and 2, respectively¹³.

In this example, for generator model type II₂, the output variables needed to be specified for generator 2 are P_{T_2} and E_2^{ref} . If loads are defined as truly static devices via Eqs. (4.67) to (4.68), their characterization can be viewed as parametric; as the loading changes, load inputs P_{L3} and Q_{L3} change. Similarly, the transmission network is characterized by specifying its static relation only, since its dynamics are assumed instantaneous.

A particular choice of state x_2 , output y_2 , and input u_2 variables depends on the level of complexity of the constituent relations employed for representing generators and other system components. For example, the type II₂ model of a generator requires more state variables than type III. For type II₂ the state vector of each generator i is

$$x_2^{dq} = [\theta_2 \quad \omega_2 \quad e'_{q_2} \quad V_{F_2} \quad e_{fd_2} \quad V_{R_2}]^T \quad (4.71)$$

the secondary control vector (see Fig. 3.2) in Chapter 3 is

$$y_2^{\text{ref}} = [E_2^{\text{ref}} \quad P_{T_2}]^T \quad (4.72)$$

¹³ Notice that only the real part of the power balance equation at a generator 2 is used. This is because the reactive-power generation (Q_{G2}) is not specified a priori. This is in contrast to the power balance equation at a load bus 3 for which both real and reactive demand are specified.

and the generator output variables are

$$y_2^{dq} = [e_2^d \quad e_2^q]^T \quad (4.73)$$

Input variables at generator 2 port are

$$u_2^{dq} = [i_2^d \quad i_2^q]^T \quad (4.74)$$

The output variable of the load bus is

$$y_{L3} = [\hat{E}_3] \quad (4.75)$$

and the input variable is

$$u_{L3} = [\hat{I}_3] \quad (4.76)$$

or, more frequently,

$$u_{L3} = [P_3 \quad Q_3]^T \quad (4.77)$$

Output variables associated with the individual transmission lines in this example are

$$y_{TL} = [\hat{I}_{12} \quad \hat{I}_{13} \quad \hat{I}_{23}]^T \quad (4.78)$$

or

$$y_{TL} = [\hat{S}_{12} \quad \hat{S}_{13} \quad \hat{S}_{23}]^T \quad (4.79)$$

Similarly, the input variables associated with transmission lines are

$$u_{TL} = [(\hat{E}_1 - \hat{E}_2) \quad (\hat{E}_1 - \hat{E}_3) \quad (\hat{E}_2 - \hat{E}_3)]^T \quad (4.80)$$

System input and output variables are defined as containing all input and output variables of the generators, loads and transmission lines, as described earlier.

4.1.7 Models for Horizontally Structured Large Power Systems

For understanding principles of hierarchical power-system operation and control in normal operation, it is convenient to introduce at this point an extension of the model in Eqs. (4.50) to (4.51). This model is derived under the assumption that the system is operated as one. However, as electric power systems have expanded, they have evolved into an interconnected grid whose subsystems are often owned and managed by different entities. Examples of such subsystems are utilities within an electric power pool and pools within a large geographic region. The existence of these administrative divisions has implications on the type of real-time operations and control principles of the interconnected system as the operating conditions vary. As described later in Chapter 13, these principles are hierarchical with a division of functions according to administrative separation.

To pose the problems of operation and control for such systems, one needs to partition system variables accordingly. Most individual components, both single-port and two-port devices, are owned by administratively structured subsystems. It is relatively rare that a particular synchronous machine is jointly owned by more than one subsystem. Under certain circumstances very long transmission lines interconnecting particular subsystems are also jointly owned. This joint ownership may sometimes interfere with the operating strategies made by subsystems themselves.

At least for analysis and control design purposes in this text an assumption is made that the individual equipment physically located within a given subsystem is identifiable as a component belonging to the same subsystem.¹⁴ For purposes of analyzing and controlling a particular area, it becomes necessary to model each subsystem of interest as a dynamic model driven by the input and output variables from the neighboring, directly connected subsystems and subsystem variables themselves. Subsystems are typically interconnected by tie lines (large transmission lines). The variables into the subsystem (region, area) I , F^I are tie-line currents, or power flows, on lines directly connected to the buses within the subsystem.¹⁵

If system coupling and input variables u are partitioned into output variables within the region and inter-regional coupling variables denoted here as F^I these equations take on a generic form¹⁶

$$\dot{x}^I = \tilde{f}^I(x^I, y^I, F^I, p^I) \quad (4.81)$$

$$0 = g^I(x^I, y^I, F^I, p^I) \quad (4.82)$$

This partitioning is illustrated in detail in Chapter 13. A particular case of the model in Eqs. (4.81) to (4.82) is Eqs. (4.50) to (4.51) when $F^I \equiv 0$.

4.2 NON LINEAR POWER SYSTEM MODELS IN ORDINARY DIFFERENTIAL EQUATION FORM

The most general model of an interconnected power system is shown to consist of a set of coupled ordinary differential equations (ODEs) subject to various algebraic constraints. These models are very difficult to use for simulations, analysis, and control. It is, therefore, important to understand assumptions under which it is justifiable to simplify this model into a better understood dynamic models of so-called (standard) state space form comprising only ODEs. Lack of systematic models of this type has been a serious obstacle to introducing systematic control

¹⁴ This assumption is not so easily justifiable in a competitive power industry, see Chapter 13.

¹⁵ All variables with superscript I represent corresponding vectors in area I . Note that in the case of tie-line flow, this is *not* the net tie-line flow but the vector of flows on individual tie lines.

¹⁶ The F^I can represent power flow or current.

design at the primary level for electric power systems. Basic questions regarding controllability and observability of models based on the design of the control have not been given necessary attention in the area of the power systems. Consequently, as shown in Chapter 12, the overall situation concerning applications of modern control theory to the electric power systems is usually restricted to very small examples. To bridge this serious gap partially we describe a recently introduced state-space form of a non linear model that lends itself to systematic analysis and control.

4.2.1 Coupled Real-Power–Voltage Dynamics for Large-Power Systems (Machine Frame of Reference)

In the general case of simultaneous occurrence of large swings in both the magnitude and phase angle of voltages on the transmission network that is typically seen during an interarea oscillation, transmission lines may operate with large phase-angle differences. Under these conditions, the magnitude of the bus voltages can be quite significant in determining the level of power transfer during an oscillation. Thus the assumption that the swing dynamics are insignificant when modeling the voltage dynamics of a system (and *vice versa*) may not be justified in this case. Here we provide a summary of a recently developed model by Jeffrey Chapman in his doctoral work Refs. [11, 12], which provides modeling of the interconnected power system for the purpose of evaluating stability and control design, specifically when the decoupling does not hold.

4.2.1.1 Assumptions Made It is shown in this section that it is possible to establish a general state-space form model of a large power system under the following two assumptions:

1. The loads are assumed to have constant impedance.
2. Saliency in synchronous machines is negligible.

The first assumption allows the admittance matrix that represents the transmission network to be reduced via Kron's reduction, so that a system with m generators utilizes an $m \times m$ reduced bus admittance matrix. As described in Chapter 3, neither the constant-impedance nor the constant-power load model accurately reflects the actual behavior of system loads, however, in transient stability work, constant-admittance loads are often used, and we will follow that convention here.

The implications of the second assumption are less transparent and are described as part of model derivation. In the following development, a type II₃ (two-axis flux-decay) model is used for the generators. Each of the $m = k + 1$ generators is modeled by a fourth-order set of coupled nonlinear differential equations. All variables are expressed in the synchronously rotating frame that underlies Blondel transformed coordinates. Generators are coupled via the machine currents i_d and i_q , which depend on the machine voltages e'_d and e'_q .

and the rotor angle θ (where underlines denote vector quantities). The machine equations of type II₃ are repeated here for completeness:

$$\dot{e}'_d = \frac{1}{T'_{q0}} [-e'_d + (x_q - x'_q)i_q] \quad (4.83)$$

$$\dot{e}'_q = \frac{1}{T'_{d0}} [-e'_q - (x_d - x'_d)i_d + e_{fd}] \quad (4.84)$$

$$\dot{\theta} = \omega - \omega_0 \quad (4.85)$$

$$\dot{\omega} = \frac{1}{J} \left[P_T - P_G - \frac{D}{\omega_0} (\omega - \omega_0) \right] \quad (4.86)$$

$$= \frac{\omega_0}{2J} \left(P_T - e'_q i_q - e'_d i_d - (x'_q - x'_d)i_d i_q - \frac{D}{\omega_0} (\omega - \omega_0) \right) \quad (4.87)$$

The solution for the Blondel transformed machine currents i_d and i_q may be expressed most simply using a block-matrix form. Initially, the state variables are grouped into block form, so that for a system with m machines, we have

$$\begin{bmatrix} e'_d \\ e'_q \end{bmatrix} = [e'_{d_1} \quad \dots \quad e'_{d_m} \quad e'_{q_1} \quad \dots \quad e'_{q_m}]^T \quad (4.88)$$

We now define the well-known transformation from the phasor network frame of reference (uppercase subscripts) to the machine frame of reference (lowercase subscripts) in block form as

$$\begin{bmatrix} E_D \\ E_Q \end{bmatrix} = T(\theta) \begin{bmatrix} E_d \\ E_q \end{bmatrix} \quad (4.89)$$

where

$$T(\theta) = \begin{bmatrix} S(\theta) & C(\theta) \\ -C(\theta) & S(\theta) \end{bmatrix} \quad (4.90)$$

$$T^{-1}(\theta) = \begin{bmatrix} S(\theta) & -C(\theta) \\ C(\theta) & S(\theta) \end{bmatrix} \quad (4.91)$$

$$S(\delta) = \text{diag } (\sin(\theta_1) \dots \sin(\theta_m))$$

$$C(\theta) = \text{diag } (\cos(\theta_1) \dots \cos(\theta_m))$$

Here θ_i is the rotor angle of the i^{th} generator in the Blondel transformed coordinates, measured relative to an arbitrary systemwide reference. Since this is just a coordinate rotation, $T^T T = I$. Now, assuming that loads may be represented as a constant admittance, the complex-valued bus admittance matrix \hat{Y}_{bus} can be ordered such that all nonmachine buses occupy the bottom of the full admittance matrix, followed by Kron's reduction to eliminate load buses, yielding

the complex reduced matrix \hat{Y}_r . The real-valued block-form reduced admittance matrix Y_r is then formed:

$$\begin{aligned} Y_r &= \begin{bmatrix} \operatorname{Re}\{\hat{Y}_r\} & -\operatorname{Im}\{\hat{Y}_r\} \\ \operatorname{Im}\{\hat{Y}_r\} & \operatorname{Re}\{\hat{Y}_r\} \end{bmatrix} \\ &= \begin{bmatrix} G_r & -B_r \\ B_r & G_r \end{bmatrix} \end{aligned} \quad (4.92)$$

Note that G_r and B_r are symmetric.

The currents i_d and i_q are now expressed in terms of the generator terminal voltages E_D and E_Q and matrix Y_r as follows:

$$\begin{bmatrix} i_d \\ i_q \end{bmatrix} = T(\underline{\theta})^{-1} Y_r T(\underline{\theta}) \begin{bmatrix} E_D \\ E_Q \end{bmatrix} \quad (4.93)$$

The following scalar equations relate the terminal voltage to the machine states (the so-called “internal” voltages) (Eqns. (3.228) and (3.229) with r neglected):

$$E_d = e'_d + x'_q i_q \quad (4.94)$$

$$E_q = e'_q - x'_d i_d \quad (4.95)$$

These can be written for an m -machine system as the vector equation

$$\begin{bmatrix} E_d \\ E_q \end{bmatrix} = \begin{bmatrix} e'_d \\ e'_q \end{bmatrix} + X \begin{bmatrix} i_d \\ i_q \end{bmatrix} \quad (4.96)$$

where

$$\begin{aligned} X &= \begin{bmatrix} \mathbf{0} & \mathcal{X}q' \\ -\mathcal{X}d' & \mathbf{0} \end{bmatrix} \\ \mathcal{X}d' &= \operatorname{diag}(x'_d) \\ \mathcal{X}q' &= \operatorname{diag}(x'_q) \end{aligned} \quad (4.97)$$

Note that here and in all that follows, capital script letters are used exclusively to denote diagonal matrices [e.g., in Eq. (4.97), \mathcal{X}_q is diagonal, but X is not]. Substituting Eq. (4.96) into Eq. (4.93):

$$\begin{bmatrix} i_d \\ i_q \end{bmatrix} = T^{-1} Y_r T \left(\begin{bmatrix} e'_d \\ e'_q \end{bmatrix} + X \begin{bmatrix} i_d \\ i_q \end{bmatrix} \right) \quad (4.98)$$

or

$$[I - T^{-1} Y_r T X] \begin{bmatrix} i_d \\ i_q \end{bmatrix} = T^{-1} Y_r T [T^{-1} Y_r^{-1} T - X] \begin{bmatrix} i_d \\ i_q \end{bmatrix} = T^{-1} Y_r T \begin{bmatrix} e'_d \\ e'_q \end{bmatrix} \quad (4.99)$$

where the dependence of the transform upon θ has been suppressed for notational convenience. Finally, premultiplying by $[T^{-1}Y_r^{-1}T - X]^{-1}T^{-1}Y_r^{-1}T$ and factoring, we have

$$\begin{bmatrix} \dot{i}_d \\ \dot{i}_q \end{bmatrix} = T^{-1}[Y_r^{-1} - TXT^{-1}]^{-1}T \begin{bmatrix} \dot{e}'_d \\ \dot{e}'_q \end{bmatrix} \quad (4.100)$$

This expression may be simplified if $\dot{\mathcal{E}}_q' = \dot{\mathcal{E}}_d'$, that is, when saliency is ignored. Specifically, when $\dot{\mathcal{E}}_q' = \dot{\mathcal{E}}_d'$, the matrices T and X commute, so that $XTT^{-1} = XTT^{-1} = X$, and

$$\begin{bmatrix} \dot{i}_d \\ \dot{i}_q \end{bmatrix} = T^{-1}(Y_r^{-1} - X)^{-1}T \begin{bmatrix} \dot{e}'_d \\ \dot{e}'_q \end{bmatrix} \quad (4.101)$$

Denoting this matrix by \bar{Y}_r , we have

$$\begin{bmatrix} \dot{i}_d \\ \dot{i}_q \end{bmatrix} = T^{-1}\bar{Y}_rT \begin{bmatrix} \dot{e}'_d \\ \dot{e}'_q \end{bmatrix} \quad (4.102)$$

This can be expressed in a more general form, where the context will determine whether saliency has been ignored.

$$\begin{bmatrix} \dot{i}_d \\ \dot{i}_q \end{bmatrix} = Y_m(\underline{\delta}) \begin{bmatrix} \dot{e}'_d \\ \dot{e}'_q \end{bmatrix} = \begin{bmatrix} Y_{m11} & Y_{m12} \\ Y_{m21} & Y_{m22} \end{bmatrix} \begin{bmatrix} \dot{e}'_d \\ \dot{e}'_q \end{bmatrix} \quad (4.103)$$

It can be shown via simple algebraic manipulations that $(Y_r^{-1} - X)^{-1}$ from Eq. (4.101) is precisely the reduced admittance matrix that is calculated when the machine transient reactance is included as part of the network and the generator terminal bus is eliminated by matrix reduction. The (standard) state-space form of the model now directly follows by:

- Combining eqs. (4.83) to (4.85) and (4.103) to describe dynamics of voltage variables e'_d and e'_q in the general form
- Writing dynamics of each generator ω and θ as defined in Eqs. (4.85) and (4.86) with Eq. (4.103) in which the currents i_d and i_q are defined in a matrix form to obtain the dynamics of electromechanical variables

$$\dot{\underline{\theta}} = \underline{\omega} - \underline{\omega}_0 \quad (4.104)$$

$$J[\dot{\underline{\omega}}] = [P_T] - EY_m(\underline{\delta}) \begin{bmatrix} \dot{e}'_d \\ \dot{e}'_q \end{bmatrix} - \frac{D}{\omega_0}[(\underline{\omega} - \underline{\omega}_0)] \quad (4.105)$$

In eq. (4.105) matrices J , D and E denote for diagonal matrices the terms of which are machine inertia constants, machine damping coefficients, and voltages e'_d and e'_q , respectively.

It is interesting to conclude that a nonlinear model of coupled power system dynamics is obtainable in a state-space form (consisting of only ODEs, with the algebraic constraints fully eliminated) under some fairly mild assumptions such as neglected saliency of the machines. The critical step in the preceding derivation is the nonsaliency assumption in synchronous machine models. The load-modeling assumption made could be eliminated through structure-preserving approaches in which some form of load-model dynamics is considered. On the other hand, when general nonlinear static load models are used, only a linearized model can be represented in its state-space form as described in Chapter 6.

4.2.1.2 State-Space Model with Constant-Flux Linkage behind the Transient Reactance It is straightforward to realize that the commonly used model for stability studies of electromechanical transients directly follows from Eq. (4.105) when $e'_d = 0$ and $e'_q = \text{const}$, where const stands for the prespecified voltage behind the transient reactance.

4.2.2 Nonlinear Power-System Model in an ODE Form (Phasor Frame of Reference)

The model of Section 4.2.1 is quite simple and effective in representing the dynamics of a single machine. However, if quantities such as the total system power or reactive power are to be considered, it may be more attractive to consider modeling the dynamics in the phasor frame of reference. For example, suppose that the generator transient voltages are expressed in block form in the phasor frame of reference:

$$\begin{bmatrix} \underline{E}_D \\ \underline{E}_Q \end{bmatrix} = [E_{D_1} \quad \dots \quad E_{D_m} \quad E_{Q_1} \quad \dots \quad E_{Q_m}]^T \quad (4.106)$$

Then, expressing the machine currents in the same frame of reference, we have

$$\begin{bmatrix} i_D \\ i_Q \end{bmatrix} = \bar{Y}_r \begin{bmatrix} \underline{E}_D \\ \underline{E}_Q \end{bmatrix} = \begin{bmatrix} \bar{G}_r & -\bar{B}_r \\ \bar{B}_r & \bar{G}_r \end{bmatrix} \begin{bmatrix} \underline{E}_D \\ \underline{E}_Q \end{bmatrix} \quad (4.107)$$

Because the change of coordinates preserves power relationships, we have these scalar relationships for real and reactive power (with transient saliency ignored) leaving a given internal generator bus:

$$P_G = E_D i_D + E_Q i_Q \quad (4.108)$$

and

$$Q_G = -E_D i_Q + E_Q i_D \quad (4.109)$$

From this it is easy to see that the sum of the power of all generator buses is given by

$$P_{\text{tot}} = [\underline{E}'_D \quad \underline{E}'_Q] \begin{bmatrix} \bar{G}_r & -\bar{B}_r \\ \bar{B}_r & \bar{G}_r \end{bmatrix} \begin{bmatrix} \underline{E}'_D \\ \underline{E}'_Q \end{bmatrix} \quad (4.110)$$

Since this is a quadratic form, the antisymmetric part is eliminated, which leaves the total real power in the network

$$P_{\text{tot}} = [\underline{E}'_D \quad \underline{E}'_Q] \begin{bmatrix} \bar{G}_r & 0 \\ 0 & \bar{G}_r \end{bmatrix} \begin{bmatrix} \underline{E}'_D \\ \underline{E}'_Q \end{bmatrix} \quad (4.111)$$

Similarly, the total reactive power Q_{tot} (taken at the “terminals” of the transient machine voltage) may be written as

$$\begin{aligned} Q_{\text{tot}} &= [\underline{E}_D^T \quad \underline{E}_Q^T] \begin{bmatrix} 0 & -I \\ I & 0 \end{bmatrix} \begin{bmatrix} \bar{G}_r & -\bar{B}_r \\ \bar{B}_r & \bar{G}_r \end{bmatrix} \begin{bmatrix} \underline{E}_D \\ \underline{E}_Q \end{bmatrix} \\ &= [\underline{E}'_D \quad \underline{E}'_Q] \begin{bmatrix} -\bar{B}_r & -\bar{G}_r \\ \bar{G}_r & -\bar{B}_r \end{bmatrix} \begin{bmatrix} \underline{E}'_D \\ \underline{E}'_Q \end{bmatrix} \\ &= [\underline{E}'_D \quad \underline{E}'_Q] \begin{bmatrix} -\bar{B}_r & 0 \\ 0 & -\bar{B}_r \end{bmatrix} \begin{bmatrix} \underline{E}'_D \\ \underline{E}'_Q \end{bmatrix} \end{aligned} \quad (4.112)$$

While it is intuitively satisfying that the total power transmitted must be determined only by the resistive component of the network, it is perhaps more interesting and not immediately obvious that the total reactive power transmitted from the machine voltage “terminals” is determined only by the reactive part of the network. Note that as long as the transmission network does not contain too much shunt capacitance, the matrix $-\bar{B}_r$ is positive definite, that is, Q_{tot} is a positive-definite quadratic function.

The simple form of Eqs. (4.111) and (4.112) suggests that it may be advantageous to investigate the behavior of energy-type functions in the network frame of reference. For this reason it is of interest to formulate the dynamics of the generators in terms of the state variables E_D and E_Q :

$$\begin{aligned} \begin{bmatrix} \dot{\underline{E}}_D \\ \dot{\underline{E}}_Q \end{bmatrix} &= - \left(\begin{bmatrix} T_1 & 0 \\ 0 & T_1 \end{bmatrix} + \begin{bmatrix} \mathcal{X}_1 & 0 \\ 0 & \mathcal{X}_1 \end{bmatrix} \begin{bmatrix} -\bar{B}_r & -\bar{G}_r \\ \bar{G}_r & -\bar{B}_r \end{bmatrix} \right) \begin{bmatrix} \underline{E}_D \\ \underline{E}_Q \end{bmatrix} \\ &\quad - \begin{bmatrix} \mathcal{C}(2\underline{\delta}) & \mathcal{S}(2\underline{\delta}) \\ \mathcal{S}(2\underline{\delta}) & \mathcal{C}(2\underline{\delta}) \end{bmatrix} \left(\begin{bmatrix} T_2 & 0 \\ 0 & T_2 \end{bmatrix} \right. \\ &\quad \left. + \begin{bmatrix} \mathcal{X}_2 & 0 \\ 0 & \mathcal{X}_2 \end{bmatrix} \begin{bmatrix} -\bar{B}_r & -\bar{G}_r \\ \bar{G}_r & -\bar{B}_r \end{bmatrix} \right) \begin{bmatrix} \underline{E}_D \\ \underline{E}_Q \end{bmatrix} \\ &\quad - \begin{bmatrix} 0 & -\Omega \\ \Omega & 0 \end{bmatrix} \begin{bmatrix} \underline{E}_D \\ \underline{E}_Q \end{bmatrix} + \begin{bmatrix} \mathcal{C}(\underline{\delta}) \\ \mathcal{S}(\underline{\delta}) \end{bmatrix} T_{d0}^{-1} \underline{E}_{fd} \end{aligned} \quad (4.113)$$

This may be done by applying the transform (4.89) to the dynamic equations (4.83) and (4.85). We make the following definitions:

$$\begin{aligned} T_1 &= \frac{1}{2} \left(\frac{1}{T'_{d0}} + \frac{1}{T'_{q0}} \right) \\ T_2 &= \frac{1}{2} \left(\frac{1}{T'_{d0}} - \frac{1}{T'_{q0}} \right) \\ \bar{x}_d &= \frac{x_d - x'_d}{T'_{d0}} \\ \bar{x}_q &= \frac{x_q - x'_q}{T'_{q0}} \\ x_1 &= \frac{\bar{x}_d + \bar{x}_q}{2} \\ x_2 &= \frac{\bar{x}_d - \bar{x}_q}{2} \\ \tilde{\omega} &= \omega - \omega_0 \\ \Omega &= \text{diag } (\tilde{\omega}_1 \dots \tilde{\omega}_m) \end{aligned}$$

Now, with the obvious definitions for the block-diagonal matrices represented by capital script letters and with considerable algebraic manipulation, one arrives at the matrix equation (4.113). The model in Eq. (4.113) is in a state-space form potentially very convenient for robust control design [10]. Quantities P_{tot} and Q_{tot} may serve as natural measures of control performance.

4.3 ELEMENTARY OVERVIEW OF STABILITY PROBLEMS IN THE POWER SYSTEM

The main use of models introduced in this chapter is for analysis and control of different dynamical phenomena taking place over a variety of time horizons. This text is devoted to both detailed analysis and control design. However, prior to engaging in very rigorous studies, we offer in this section a purely intuitive conceptual development to establish the whole perspective of phenomena involved and to introduce the concepts that are needed. Because of the highly simplified, even oversimplified, nature of the examples offered in this section it is emphasized that they should not be used beyond conceptual development.

Keeping in mind the fact that much analytic work was developed in the past only for electromechanical phenomena, it is important to put in perspective the parallelism of the phenomena related to the electromagnetic voltage changes. Voltage instability, although recently emphasized, is not a single phenomenon.

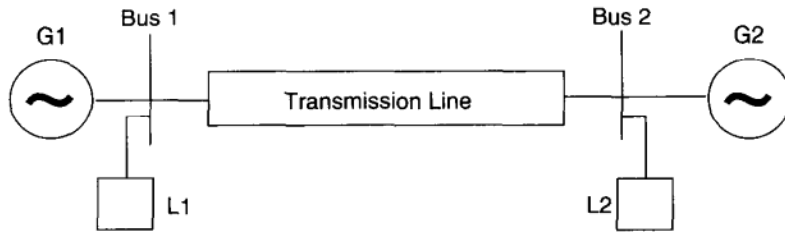


FIGURE 4.7 One-line diagram of a two-bus power system.

To make understanding of the concepts easier, a brief and purely intuitive presentation is given in this section using only two machines with no shunt branches. General mathematical relations are presented in later chapters. Real- and reactive-power cases are presented in parallel in this introductory section, using the better-known real-power relations for illustrating the corresponding ones for reactive power.

Let us consider the system of Figure 4.7 for which the following relations apply in real and reactive power,

$$\hat{E}_1 = E_1 \angle \delta_1 = 1 \angle 0^\circ, \quad \hat{E}_2 = E_2 \angle \delta_2, \quad \hat{Z}_{12} = Z_{12} \angle \zeta_{12} \quad (4.114)$$

given the following:

1. Power-flow equations and electromechanical dynamics of machines at buses 1 and 2 are, respectively (the type IV₁ generator model in Chapter 3, Table 3.3),¹⁷

$$\begin{aligned} P_1 &= \frac{1}{Z_{12}} [E_1^2 \cos \zeta_{12} - E_1 E_2 \cos(\delta_1 - \delta_2 - \zeta_{12})] \\ &\quad + J_1 \frac{d^2 \delta_1}{dt^2} + D_1 \frac{d\delta_1}{dt} \end{aligned} \quad (4.115)$$

$$\begin{aligned} P_2 &= \frac{1}{Z_{12}} [E_2^2 \cos \zeta_{12} - E_1 E_2 \cos(\delta_1 - \delta_2 - \zeta_{12})] \\ &\quad + J_2 \frac{d^2 \delta_2}{dt^2} + D_2 \frac{d\delta_2}{dt} \end{aligned} \quad (4.116)$$

$$Q_1 = \frac{1}{Z_{12}} [E_1^2 \sin \zeta_{12} - E_1 E_2 \sin(\delta_1 - \delta_2 + \zeta_{12})] \quad (4.117)$$

$$Q_2 = \frac{1}{Z_{12}} [E_2^2 \sin \zeta_{12} - E_1 E_2 \sin(\delta_1 - \delta_2 - \zeta_{12})] \quad (4.118)$$

¹⁷ The machine model here is of type IV, described in Chapter 3. More complex models are not typically used for introducing the basic concepts of system stability.

2. Electromagnetic dynamics of equipment at bus 1 and 2 are, respectively [the type (IV₂) generator model in Chapter 3, Table 3.3],

$$F_1 \left(E_1, E_2, \frac{dE_1}{dt}, p \right) = 0, \quad F_2 \left(E_2, E_1, \frac{dE_2}{dt}, p \right) = 0 \quad (4.119)$$

where the derivative terms represent, respectively, the rotor dynamics and machine damping and the dynamics of magnetic fields and exciter. The symbol p stands for assorted parameters.

The dynamic equations (4.115) to (4.119) can be either

- In a stationary, steady state or equilibrium state defined by all time derivatives being equal to zero
- In a dynamic state as defined by Eqs. (4.115) to (4.119).

Note that in either condition the system is assumed to be defined by these equations, including the deviations even when some or all derivatives are zero. In the power field the term *static* describes a problem formulation in which it is assumed implicitly that no dynamics exist (or that changes are at an infinitesimally slow pace), that is, all time derivatives are identically zero. This reduces Eqs. (4.115) to (4.119) to a set of algebraic equations also known as the load-(or power-) flow equations. In the absence of dynamics, the question is whether these equations have solutions and how many. In fact, the load-flow computation is the most used commercial program in the power industry.

The term *stationary* is used for a condition in which all derivatives are zero in the sense that the dynamics are not excited but are still present and could become active. The term *static*, on the other hand, relates to conditions in which no dynamics are present.

Note that typically the power system operates in a stationary condition with slowly varying loads on the scale of minutes and a minimal (about 1%) random load fluctuation. So, most of the time, dynamics play no role, and hence it is logical to disregard them in static and stationary studies as is done in Chapter 5. Dynamic conditions can then be separately investigated as is done in Chapters 6 through 12. For purposes of fostering intuition, it should be observed that in the absence of the derivative terms (i.e., in static conditions) eqs. (4.115) to (4.119), the general character of the equations is applicable to a network of nonlinear springs. The operator would consider such a system to behave normally or stably if it acts with a positive spring constant. In this text we refer to this behavior as the stable behavior of the system, stretched by increasing force. Negative spring constant behavior would represent unstable behavior.

Note that there exists another, more recent traditional designation in power systems. It is customary in at least part of the literature to call the behavior locally stable around equilibrium the *dynamic* stability. This practice is somewhat confusing because it conflicts with usage in mathematics, where all behavior

defined by the dynamic equations is called dynamic. So *dynamic* will not be used in this text in a sense restricted to local dynamics around equilibrium. The phrase *small signal stability* has also been used recently for this type of stability analysis; we adopt this term, for example, in Chapter 6 in the sense of local stability as used for mathematical analysis. The latter could be confusing because of the presence of local stability in the geographic location sense.

4.3.1 Static Stability and Static Equilibria

When all derivatives are set to zero identically (this is equivalent to eliminating all system dynamics, resulting in a static system) in eqs. (4.115) to (4.119), a set of nonlinear algebraic equations results. These are known as the load-flow equations; a solution of these equations is known as a load-flow solution or an equilibrium point (potential operating point when stable). For a given system (a given line in this case) the equilibrium point (that is, values of $\delta_1 - \delta_2$ and $E_1 - E_2$) will depend on a given set of parameters (that is, loads P_1, P_2, Q_1, Q_2). Of course, typically there are more parameters than free state variables. In this case there are four parameters and two free variables $E_1 - E_2$ and $\delta_1 - \delta_2$; thus these solutions will not exist for every arbitrary parameter set. In fact, one could specify two parameters arbitrarily, for instance, the real- and reactive-power flows P_2, Q_2 to find $E_1 - E_2$ and $\delta_1 - \delta_2$. This is well known in setting up data for load-flow calculations. It is also common, but not always justifiable, to use the so-called decoupled load flow, that is constant $E_1 - E_2$ for finding $\delta_1 - \delta_2$ from P_2 , Eq. (4.116); fix $\delta_1 - \delta_2$ for finding $E_1 - E_2$ from Q_2 , Eq. (4.118). This is based on the relative independence of the P_1, δ_1 pair from the Q_1, E_1 pair. Decoupled load flow is useful and helpful provided it is used with care and where it is applicable. This decoupling assumption is useful here for reviewing concepts of steady-state (static) real- and reactive-power stability as they have evolved historically. The following highly simplified discussion will be used for developing conceptual insight into various aspects of stability and particularly parallels between real- and reactive-power phenomena.

4.3.2 Real-Power Static Stability

Assume bus voltages E_1 and E_2 such that $E_1 - E_2 = \text{const}$; then by Eqs. (4.115) and (4.116) the angles δ_1 and δ_2 vary with the power P_2 drawn from bus 2 as

$$\delta_1 - \delta_2 - \zeta_{12} = \cos^{-1} \left(\frac{-P_2 Z_{12} + E_2^2 \cos \zeta_{12}}{E_1 E_2} \right) \quad (4.120)$$

in a manner shown in Figure 4.8.

This is a well-known transmission law, a sinusoidal dependence of real power delivered on the phase-angle difference. There is no load-flow solution, that is, no equilibrium beyond the value $P_2 = P_2^{\max}$. Below P_2^{\max} there are two load-flow solutions, that is, two equilibria. At the equilibrium at δ_e^s the line behaves like

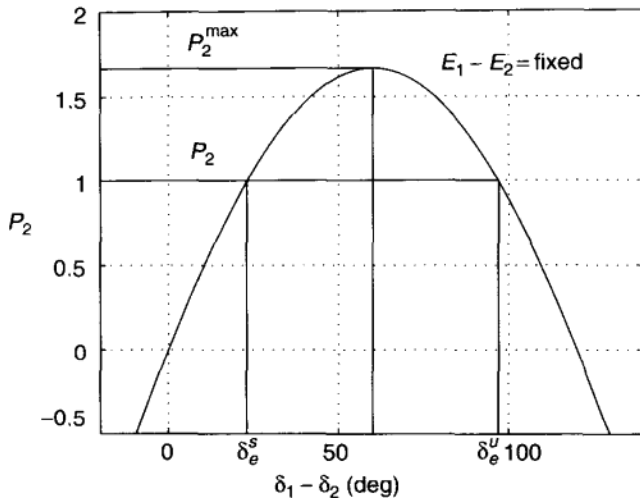


FIGURE 4.8 Real-power–phase-angle dependence.

a normal (nonlinear) spring. Increased P_2 power is needed to increase or stretch $\delta_1 - \delta_2$ and at reduced P_2 a decrease of $\delta_1 - \delta_2$ takes place. In each case the force counteracts the change. Such a situation is considered statically stable. At the other, statically unstable, load-flow value δ_e^u the line behaves opposite of the normal spring. Anomalous behavior occurs at $P_2 = P_2^{\max}$, which is known as the static stability limit characterized by a single equilibrium point.

4.3.3 Reactive-Power Static Stability

Assume that the difference of angles δ_1 and δ_2 is fixed; then by eqs. (4.117) and (4.118) the voltage difference $E_1 - E_2$ varies with reactive power Q_2 drawn from bus 2 as

$$\begin{aligned} a &= \sin \zeta_{12} & b &= E_1 \sin(\delta_1 - \delta_2 - \zeta_{12}), & c &= Q_2 Z_{12} \\ \Rightarrow E_2 &= -\frac{-b \pm \sqrt{b^2 - 4ac}}{2a} \end{aligned} \quad (4.121)$$

in the manner of Figure 4.9.

It should be observed that the basic character of the reactive power versus $E_1 - E_2$ curve for positive $E_1 - E_2$ is exactly the same as the character of Figure 4.8 for the real-power and positive-angle differences. All the observations made in Figure 4.8 can be repeated in Figure 4.9. Trying to draw too much reactive power (larger than Q_2^{\max}) from the line would result in nonexistence of a load-flow solution just as in case of real power. Here E_e^s is a practical operating point as is δ_e^s for real power. Q_2^{\max} is the static stability limit for reactive power just as in the case of real power. Here E_e^s and E_e^u are, respectively, statically stable and unstable operating points just as in the case of real power. One difference is that

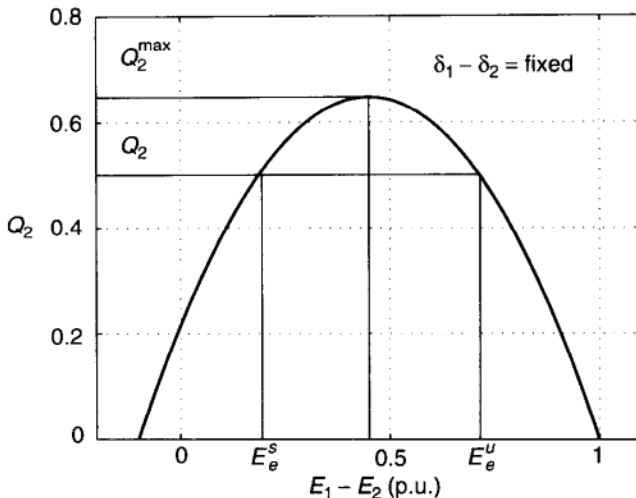


FIGURE 4.9 Reactive-power–voltage dependence.

the curve is a quadratic function for voltages, while it is a sinusoidal curve for phase angles.

4.3.4 Static Stability Limit

The engineering meaning of the static stability limit for the small system of Figure 4.7 is pretty clear from Figures 4.8 and 4.9 for either real or reactive power. However, in preparation for criteria applicable to a large system with many machines, it is important to observe some features that can serve as a foundation for setting up criteria that are applicable to the general large system. Two such observations are particularly important.

1. If one defines an arbitrarily small neighborhood in the parameter space (P or Q) of the unique static stability limit for either real or reactive power, that is,

$$|\Delta P| = |P^{\max} - P| < \varepsilon \quad \text{or} \quad |\Delta Q| = |Q^{\max} - Q| < \varepsilon \quad (4.122)$$

where $\varepsilon > 0$, there always will be either two equilibria or none, regardless how small $\varepsilon > 0$ is. Such an equilibrium is called a static bifurcation point. (Note that the results around a bifurcation point critically depend on certain knowledge of parameters and inputs, that is, a small deviation from the given parameters implies qualitatively different results. Detailed discussion of this is given in Chapters 6 to 11.)

2. The derivatives $\partial P / \partial \delta$ and $\partial Q / \partial E$ are zero at the static stability limit (the Jacobian matrices are singular in higher-dimension, multibus systems) and thus are small in the neighborhood. So smallness of such derivatives would also indicate the nearness of the bifurcation point.

To summarize, in the absence of dynamic effects with equations that are all algebraic, the question of stability or instability in the dynamic sense does not arise. However, as stated above, traditional power-system terminology would consider the static equilibrium stable if the system behaves like a normal spring, that is, it reacts to an increased load demand P_2 by increasing torque angle $\delta = \delta_1 - \delta_2$. In this case the sensitivity or spring constant $\partial\delta/\partial P_2 \geq 0$. An unstable static equilibrium in the traditional sense is connected with a negative spring constant or negative definite sensitivity matrix. A similar parallel described previously holds for static voltage stability.

4.3.5 Small-Signal-Stability. Classification of Equilibrium Points

Let us now assume that the dynamics of both active and reactive power are present in Eqs. (4.115) to (4.119), that is, the derivatives $d^2\delta_2/dt^2$, $d\delta_2/dt$, and dE_2/dt are no longer identically zero while E_1 and δ_1 remain fixed. But let us also assume that dynamic phenomena will only be studied in a small neighborhood of each equilibrium point where the system is approaching a linear behavior, that is,

$$|\delta_2 - \delta_{e2}^s| < \varepsilon \quad (4.123)$$

or

$$|\delta_2 - \delta_{e2}^u| < \varepsilon \quad (4.124)$$

and

$$|E_2 - E_{e2}^s| < \varepsilon \quad (4.125)$$

or

$$|E_2 - E_{e2}^u| < \varepsilon \quad (4.126)$$

where $\varepsilon > 0$ is arbitrarily small and the superscript s denotes stable and u denotes unstable equilibria. Let us further assume that the initial state, δ_{20} or E_{20} , is perturbed from the respective equilibria, δ_{e2}^s , δ_{e2}^u , E_{e2}^s , and E_{e2}^u by a small distance Δ , that is, respectively,

$$|\delta_{20} - \delta_{e2}^s| < \Delta \quad (4.127)$$

or

$$|\delta_{20} - \delta_{e2}^u| < \Delta \quad (4.128)$$

and

$$|E_{20} - E_{e2}^s| < \Delta \quad (4.129)$$

or

$$|E_{20} - E_{e2}^u| < \Delta \quad (4.130)$$

where $\Delta > 0$ and $\Delta \leq \varepsilon$. Then the equilibrium point δ_{e2}^s or E_{e2}^s is locally stable if for an arbitrarily small ε there exists a Δ such that a trajectory starting at δ_{20} or

E_{20} never goes further away than ε and it converges to δ_{e2}^s or E_{e2}^s . Otherwise, point δ_{e2} or E_{e2} is dynamically locally unstable. The linearized form of the dynamic model will be applicable to the analysis. Observe that the derivatives $\partial P_2 / \partial \delta_2 < 0$ and $\partial Q_2 / \partial E_2 < 0$ at, respectively, δ_e^s and E_e^s . This indicates an asymptotic return to the equilibrium at least from a small distance. Observe the opposite situation at the unstable equilibrium. Clearly, for the simple example in Figure 4.7 there is one locally stable equilibrium for either active (δ_{e2}^s) or reactive (E_{e2}^s) power below, respectively, P_2^{\max} or Q_2^{\max} that behaves exactly like the other. Each also possesses a (dynamically) unstable equilibrium. So again, in small-signal stability there is an exact parallel between active- and reactive-power behavior. However, when details are examined in most cases, the coupling between the two needs to be considered. In mathematical terms, the preceding definition is that of local stability. (In recent power systems literature the term *local* is reserved for geographic locality, hence the mathematically local counterpart is replaced by the term *small signal*).

4.3.6 Transient Stability

Transient stability is a concept unique to power system theory. It is tied to specific disturbances and it may include specific countermeasures in the way of selective protection and other emergency control or security measures. More specifically,

1. Disturbance a happens (e.g., a short circuit in a specific place or a loss of a specific line).
2. Countermeasure b follows (e.g., clearing of a fault within a critical time t_{cr} by dropping a specific line).
3. The system has transient stability for this occurrence or contingency if following events a and b , it will settle down to a stable and viable equilibrium point (may be different from the original) without losing synchronism or voltage collapse.

This can be described in general mathematical terms to the effect that the system has transient stability for events a and b if the state reached at the conclusion of events a and b is within the region of attraction of the stable equilibrium point applicable for the system condition as it exists at t_{cr} after events a and b . (The system may have lost components compared to the condition prior to a .) So transient stability is a global dynamic concept that will involve large changes (not local neighborhoods of equilibria) and potential topological changes of the system. Two simple examples based on Figure 4.7 will illustrate this concept for active and reactive power. The well-known active-power example will help to explain the practically unknown reactive-power counterpart.

4.3.6.1 Transient Stability in Active Power

Let it be assumed that the simple system of Figure 4.7 is operating with E_1 and δ_1 constant at a specific load level of P'_2 as shown in Figure 4.10 when generation $\Delta P''_2$ is lost at bus 2 so that the

load at bus 2 increases to P_2'' and the system moves from its stable equilibrium point p_1 to point p_2 , which is not an equilibrium since the transmission line keeps transferring P_2' MW as δ_2 is initially unchanged because of the inertia of the machinery at bus 2. Since there is more load now at bus 2 than is delivered by the transmission line, the machine at bus 2 starts slowing down, thus δ_{12} is increasing. So does the transmission-line power output at bus 2 along the sine curve in Figure 4.10. The power balance is restored at point p_3 but now machines at bus 2 are running slower than at bus 1 and hence δ_{12} keeps increasing. Beyond point p_2 , however, there is more transmitted power than load so machines at bus 2 start speeding up again and will catch up with the machine 1 speed at point p_4 . [The reader could check that p_4 is determined by the areas of triangles ($p_1-p_2-p_3$) and ($p_3-p_4-p_5$) being equal, which means that equal energy was spent on acceleration and deceleration.] Since there is still more transmission output power p_5 than load p_4 , the speeding continues, so δ_{12} is now decreasing. The lossless system (as assumed here) will keep oscillating between points p_1 and p_5 at a frequency of up to 3 Hz. The actual lossy system settles down eventually to the stable equilibrium point p_3 from where it may eventually be returned to p_1 by readjusting real generation at bus 2. So the system has transient stability for this disturbance. If the values of P_2' and P_2'' are changed, transient stability is preserved until point p_4 moves beyond the position of p_6 , before the speed of machine 2 catches up with the speed of machine 1. Past point p_6 , the machine at bus 2 is again decelerating so $\delta_1 - \delta_2$ keeps increasing and synchronizing is lost. Then the system does not have transient stability for the assumed disturbance.

4.3.7 Transient Stability in Reactive Power

Now let us see how the familiar preceding scenario evolves for reactive power as shown in Figure 4.11. Again power generation, this time the reactive power

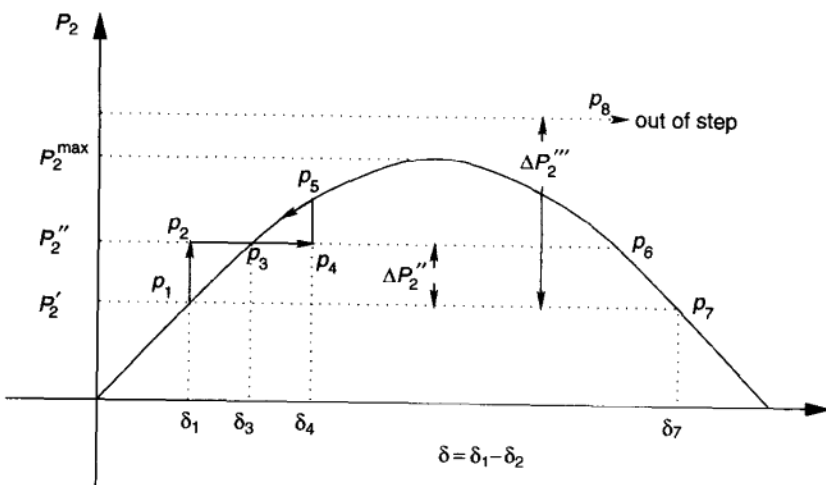


FIGURE 4.10 Transient stability in real power

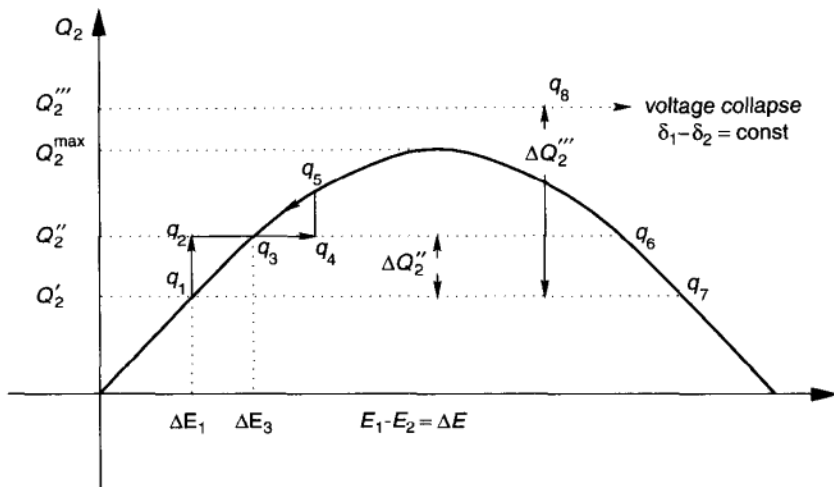


FIGURE 4.11 Transient stability in reactive power

($\Delta Q_2''$), say, the power supplied by the generator, is reduced at bus 2. In Figure 4.11, this means moving from point q_1 to q_2 . Then there is more (inductive) reactive power taken at bus 2 than is supplied by the transmission line at the existing voltage $E_1 - E_2$. This will result in a reduction of voltage E_2 at bus 2 until $E_1 - E_2$ increases to point q_3 , where the reactive power supplied by the line matches the demand Q_2'' . There will still be energy in the dynamics, electromagnetic energy in the case of Figure 4.11. Just as in the real-power case this may drive the voltage $E_1 - E_2$ to an overshoot position q_4 . Point q_4 is analogous to p_4 on the real-power side. $E_1 - E_2$ eventually settles to q_3 , if q_4 is to the left of q_6 , in which case the system has transient stability for a change of injection from Q_2' to Q_2'' . If, however, q_4 is to the right of q_6 , then E_2 keeps decreasing and a voltage collapse occurs. All this follows the pattern of real power shown in Figure 4.10 quite closely. For a more detailed representation of the reactive-power dynamics, the response will become distorted but it retains its basic character. Furthermore, if the reactive-power injection is increased to Q_2''' up to point q_8 , which is above the static-dynamic stability limit at Q_2^{\max} , then the system is transiently unstable and E_2 collapses directly just as in the equivalent situation in real power.

These two cases also provide a simple example of a dynamic stability oscillation in a nonlinear system.

It is interesting to point out that the Belgian blackout of 1982 mirrors the pattern of Figure 4.11. In a somewhat simplified account, the Belgian system at the time (as a result of a tie line to France being open) was effectively a single, long, crescent-shaped, radial transmission path from south to north with some large nuclear plants at the north end and a concentration of other generation plants in the south. In an operation aimed at disconnecting these nuclear plants, the operators, following common practice, reduced the real power to zero

and then opened the circuit breakers. Reactive power was not reduced to zero since historically this was not necessary. Thus when the plants were dropped a substantial amount of reactive-power support was lost and the system condition moved to an equivalent of point q_8 in Figure 4.11. Voltage collapse followed.

It is hoped that these simple examples will help the reader to acquire an intuitive concept of transient stability for reactive-power in a framework similar to active power transient stability but with important differences. Again one should emphasize that these two phenomena are not merely similar, they are closely coupled and need to be studied jointly in most situations.

Note: In this intuitive sketch the reactive power is treated and referred to as something that flows and integrates with time in energy. This is not true, as no net flow is produced, but energy is bouncing back and forth, that is, it oscillates between capacitive and inductive forms on the respective sides of any cut set. This was explained in Chapter 2. It was also shown that a fictitious "flow" language can be used by identifying the position of the energy as a "flow direction," positive if the circuit is inductive in the reference direction chosen for the flow and vice versa for capacitive circuit. The quantity of the oscillating energy proportional to the peak flow of the reactive-power component of the flow is simply taken as the *rate of the flow*, that is, *reactive-power flow*.

For an exercise the reader should prove that the physical oscillation phenomenon will produce the same results as shown in Figure 4.11.

4.3.8 Medium- and Long-Range or Multiswing Instability

If the system survives the danger of the critical first swing or immediate voltage breakdown as described in the preceding discussion of the transient stability, then the nature of the phenomenon is changed as slower-moving processes begin to define the events. This phase of the occurrence or contingency may be more severe and critical than the first fast swing or immediate voltage-collapse condition. Again active- and reactive-power aspects will be juxtaposed.

4.3.9 Medium-Range Instability

A typical case of voltage stability is connected with automatic tap changers and will be discussed later in Chapters 6 and 12. Automatic tap changers control reactive power, and they are discrete control elements, which implies a rather complex situation. A somewhat more detailed discussion of long-term instability is given next.

4.3.10 Long-Range Instability in Real Power

It is important to recognize that in long-range stability, voltage, current, and power values are defined simply in terms of their magnitude and frequency (in many cases frequency will also remain constant). Invariably, phase angle plays no role at these time scales, frequency takes over its role. This occurs randomly, which creates a random deviation of negligible magnitude.

The phenomena that play a role fall mostly in three categories.

1. The slower-responding components of the turbine generator itself: Governors will open and close valves in response to variations in frequency. This in turn produces a fairly fast response of increasing (decreasing) steam flow at decreasing (increasing) pressure using the energy stored in the drums of one type of boiler. Other (types of) boilers lack this dynamic component but eventually all will respond by changing feedwater and fuel intake. This latter response is quite slow, however.
2. Coupled to such activities in the turbine generator, particularly governor action, the fast swings of individual machines will be superceded by coherent swings of more or less large clusters of machines against each other (including interarea oscillations) at a much slower pace of several seconds per cycle.
3. The swings described in phenomenon 2 can also be excited by dynamically uncoordinated control activities, potentially with sufficient violence to cause system instability and breakup. The principal causes are the dispersed underfrequency load-shedding relays, which are capable of producing destructive frequency and voltage swings. Even with rate measurements, these independently controlled devices act without real consideration of the existing system dynamics. Coordinated load shedding would be the answer here. Systematic modeling for capturing potential instabilities of this type is introduced in Chapter 6.

After the few examples of problems with active power, one should now discuss the corresponding phenomena for reactive power.

4.3.11 Long-Range Instability in Reactive Power

The sources of longer-range stability problems in voltage and reactive power may again develop as a longer-range manifestation of the initial response to a disturbance.

1. It may be observed in connection with the voltage reduction at bus 2 in the transient case (Figure 4.11) that decreasing voltage will result in increasing the excitation of the generator at bus 2. In fact, it is customary to force the excitation to levels that can only be permitted for a short time because of the thermal limitations of the generator. This means that such emergency excitations will soon need to be reduced, which reverts to the original problem of insufficient reactive-power balance point q_8 in Fig. 4.11 over wide system areas, unless other sources of reactive power are available and activated on time.
2. The load reactive power initially decreases in response to voltage reduction, thus giving initial help to the system. This effect is often offset by the voltage increase produced by the emergency excitation control of phenomenon 1. It is further aggravated by automatic tap changing transformers between transmission and subtransmission, which will try to raise subtransmission and distribution voltage levels and to move the accompanying load reactive-power demand back to normal in the face of the shaky reactive-power balance on

the transmission level. This adds up to a long-range voltage stability problem that develops following the initial transient stability period.

3. As was described in the preceding section, the dynamic limitations of underfrequency decentralized load shedding could result not only in frequency swings but also in severe subsequent voltage problems. Similar localized load shedding for low voltage is now being contemplated by several utilities. While load shedding for reactive-power problems can be a valuable remedy when properly applied, inadequate dynamic coordination can result in even more severe long-range or trailing problems in voltage and reactive power.

In summary, models for analysis of various types of instabilities classified here are not well established yet. Much of the analysis in Chapter 6 was written keeping in mind the need for developing models that are relevant for analyzing various instabilities, assuming that linearized models are valid. In Chapters 7 to 9 more general modeling and analysis are introduced for system studies under large disturbances.

BIBLIOGRAPHY

1. Chua, L. O., Lin, P-M., *Computer-Aided Analysis of Electronic Circuits: Algorithms and Computational Techniques*, Englewood Cliffs, NJ: Prentice-Hall, 1975.
2. Desoer, C. A., Kuh, E. S., *Basic Circuit Theory*, New York: McGraw-Hill, 1969.
3. Bergen, A. R., *Power System Analysis*, Englewood Cliffs, NJ: Prentice-Hall, 1986.
4. Sincovec, R. F., Erisman, A. M., Yip, E. L., Epton, M. A., "Analysis of descriptor systems using numerical algorithms," *IEEE Trans. Automatic Control*, **AC-26**: 139–147, 1981.
5. Crow, M. L., Waveform relaxation methods for the simulation of systems of differential/algebraic equations with applications to electric power systems," Ph.D. thesis, University of Illinois at Urbana-Champaign, 1990.
6. Saeks, R., DeCarlo, R., *Interconnected Dynamical Systems*, New York: Marcel Dekker, 1981.
7. Vladimirescu, A. *The Spice Book*, John Wiley & Sons, 1993.
8. Allen, E., Ilić, M., "Interaction of transmission network and load phasor dynamics," *IEEE Trans. Circuits Systems*, 1999 (to appear).
9. Venkatasubramanian, V., Schattler, H., Zaborszky, J., "A stability theory of large differential algebraic systems—A taxonomy," Report SSM 9201—Part I, 1992. Washington University, St. Louis, MO.
10. *Simulink User's Manual*, Natick, The Mathworks Inc., MA 1994.
11. Chapman, J.W., "Feedback linearizing generator excitation control for enhanced power system stability," Master thesis, MIT, 1993.
12. Chapman, J., "Power system control for large-signal stability: Security, robustness, and transient energy," Ph.D. thesis, MIT, 1996.
13. Allen, E., Chapman, J., Ilić, M., "Effects of torsional dynamics on nonlinear generator control," *IEEE Trans. on Control Systems Technology*, Vol. 2, March 1996.

PART II

Analysis of Stationary and Dynamic Processes

5 Stationary Analysis

One of the basic questions in operating and planning electric power systems concerns conditions under which a stationary solution exists. In Section 4.3 of Chapter 4 an elementary notion of this problem was introduced for a two-bus power system. In this simplest case it is straightforward to derive solutions in their closed form and to state explicit bounds on variations in load demand within which solutions are guaranteed to exist.

Answering the same question for a power system of general topology, on the other hand, is a major theoretical challenge. No closed-form equilibria solutions are known. Moreover, only operationally meaningful solutions are acceptable. This limits use of general theoretical tools as one attempts to develop nonconservative bounds on system inputs within which solutions of interest exist. As a consequence of this, most studies are numerical.

In this chapter we first review theoretical results that are useful for defining conditions under which a solution of interest is guaranteed to exist. While this problem has a long history, it has recently gained major new importance as the electric power industry undergoes restructuring. The transmission-system providers are required to post so-called *available power transfer* capability (ATC) publicly. In Section 5.3.4 we pose industry restructuring-related stationary analysis problems. In the second part of this chapter nonstandard numerical methods are described for computing system equilibria when the system is close to its steady-state stability boundaries.

5.1 POWER-SYSTEM EQUILIBRIUM DEFINITION

As system inputs (demand and generation) vary or unexpected equipment contingencies occur, the basic question of whether the system could sustain its operation under the new conditions arises. This is basically the question of the existence of a new equilibrium and its properties. In electric-power-system studies this problem is also known as a steady-state stability problem. Recalling from Chapter 2 that all variables are represented in their phasor form relative to the synchronously rotating reference frame, it is straightforward to understand that a new equilibrium is reached when no further changes in voltage magnitudes and angles occur (although the actual instantaneous voltages vary sinusoidally at the nominal frequency). Consequently, any stationary model of an interconnected power system, thought of in terms of state, input, and output variables, takes on

the form

$$0 = f(x, y, y^{\text{ref}}, p) \quad (5.1)$$

and

$$0 = g(x, y, y^{\text{ref}}, p) \quad (5.2)$$

This model is the result of combining the dynamic model in Eqs. (4.50) to (4.51) with the defining equation for stationary operation

$$\frac{dx}{dt} = 0 \quad (5.3)$$

A stationary-analysis problem viewed in this framework becomes the problem of studying equilibria of the dynamical model given in Eqs. (4.50) and (4.51). The model in Eqs. (5.1) to (5.2) serves as the starting model for analysis of system state, input, and output variables at equilibrium. An unconstrained equilibrium can be found by solving Eqs. (5.1) and (5.2) for x in terms of given y^{ref} and p . In practice, only an operationally acceptable equilibrium is of interest [1].

Example 5.1.1 To illustrate defining equations for stationary operation, consider the same three-bus example given in Chapter 4 as Example 4.1.1, Figure 4.4. By setting all derivatives on the left-hand side of Eqs. (4.55) to (4.60), we obtain specific form of Eq. (5.3) for this system:

$$0 = \omega_2 - \omega_0 \quad (5.4)$$

$$0 = P_{T2} - P_{G2} \quad (5.5)$$

$$0 = -e'_{q_2} + (x_{d_2} - x'_{d_2})i_{d_2} + e_{fd_2} \quad (5.6)$$

and, similarly, from Eqs. (3.267) to (3.269),

$$0 = \frac{1}{T_F} \left(-V_{F_2} + \frac{k_F}{T_F} e_{fd_2} \right) \quad (5.7)$$

$$0 = \frac{1}{T_E} \{ [-K_E + S_E(e_{fd_2})]e_{fd_2} + V_{R_2} \} \quad (5.8)$$

$$0 = \frac{1}{T_A} \left[K_A \left(V_{F_2} - \frac{K_F}{T_F} e_{fd_2} - E_2 + E^{\text{ref}_2} \right) - V_{R_2} \right] \quad (5.9)$$

All other equations describing coupling between the generator variables and the corresponding variables at the bus side and the constituent relations for the transmission line as well as the topological constraints are identical to their algebraic characterization stated in Example 4.1.1 in Chapter 4.

5.2 LOAD-FLOW PROBLEM

Generally, a slight difference exists between this general formulation of the power-system stationary operation and the most frequently used characterization of the stationary power-system operation via the load-flow equations [2]. The simplest interpretation of the load- (power-) flow equations directly follows from Eq. (4.45) in Chapter 4: given power injections into all buses $[\hat{S}_1 \dots \hat{S}_n \hat{S}_{n+1} \hat{S}_{n+k}]$, compute bus voltages $[\hat{E}_1 \dots \hat{E}_n \hat{E}_{n+1} \hat{E}_{n+k}]$. Recall that these equations are basically (power-) flow balance equations resulting from the familiar nodal equations in electric circuits [3].

However, it does not generally follow from the constituent relations that for $dx/dt = 0$ a device would inject constant (complex-valued) power. As a matter of fact, this is largely not the case. When loads are modeled as devices whose complex-valued power $[\hat{S}_1 (= P_1 + jQ_1) \dots \hat{S}_n (= P_n + jQ_n)]$ is specified, major differences between the load-flow formulation and Eqs. (5.1) and (5.2) come from modeling assumptions made in characterizing the stationary operation of generators. The load-flow formulation assumes that both exciter and governor have unlimited control, so that they maintain voltages at the generator buses $[E_{n+1} \dots E_{n+k}]$ at any value set by the secondary-level voltage regulation and their electrical power output $[P_{n+1} \dots P_{n+k}]$ at the set-point value specified by a higher level control. For this reason generators are often referred to in load-flow computations as *PV* buses, since their steady-state specifications are parametric in terms of real power and voltage. These specifications are used instead of a more general stationary characterization of generators illustrated in Eqs. (5.4) to (5.9).

To differentiate among stationary specifications of loads, generators, and the slack bus for load-flow calculations, three types of bus characterizations used for the load-flow formulation are listed in Table 5.1. With the bus enumeration $1, \dots, n$ for loads, $n+1, \dots, n+k$ for generators, and 0 for the slack generator and their parametric characterization as in Table 5.1, a sufficient number of equations for defining a load-flow problem of an interconnected system is given by equations stating $2n$ real- and reactive-power balances at all load buses and k real-power balances at generator buses. They are of a general form

$$P_i = \sum_{j \in K_i} \left(\frac{E_i^2}{Z_{ij}} \cos \zeta_{ij} - \frac{E_i E_j}{Z_{ij}} \cos(\delta_{ij} - \zeta_{ij}) \right), \quad i = 1, \dots, n \quad (5.10)$$

$$Q_i = \sum_{j \in K_i} \left(\frac{E_i^2}{Z_{ij}} \sin \zeta_{ij} - \frac{E_i E_j}{Z_{ij}} \sin(\delta_{ij} - \zeta_{ij}) \right), \quad i = 1, \dots, n \quad (5.11)$$

$$P_i = \sum_{j \in K_i} \left(\frac{E_i^2}{Z_{ij}} \cos \zeta_{ij} - \frac{E_i E_j}{Z_{ij}} \cos(\delta_{ij} - \zeta_{ij}) \right), \quad i = n+1, \dots, n+k \quad (5.12)$$

where K_i is the set of all nodes directly connected to node i . The load-flow problem formulation (5.10) to (5.12) provides a sufficient number of equations

TABLE 5.1 Bus Characterization Typical in Load Flow

Bus Type	Slack Bus	<i>PQ</i> Bus	<i>PV</i> Bus
Known variables	E, δ	P, Q	P, E
Explicitly unknown variables		E, δ	δ
By-products	P, Q		Q

implicitly expressed in terms of unknown load voltages and phase angles, and angles of generator terminal voltages, given all generator voltages, generator real power, and load real and reactive power.

This basic load-flow problem formulation assumes sufficient generation control (primary control) to maintain the specified voltages and real power. In actuality, each generating unit only provides real power within the limits

$$\underline{P}_{Gi}^{\min} < P_{Gi} < \underline{P}_{Gi}^{\max}, \quad i = n + 1, \dots, n + k \quad (5.13)$$

These limits are result of limited mechanical power of generator–turbine–governor units.

Limits that directly affect the ability of generators to maintain their terminal voltages at the set-point values defined by a higher-level control are the result of the physical limits on field voltage sources:

$$e_{fdi}^{\min} < e_{fdi} < e_{fdi}^{\max}, \quad i = 0, n + 1, \dots, n + k \quad (5.14)$$

This limit cannot be directly expressed in the load-flow formulation. Instead, limits on the reactive-power output of generating units are typically specified as

$$Q_{Gi}^{\min} < Q_{Gi} < Q_{Gi}^{\max}, \quad i = 0, n + 1, \dots, n + k \quad (5.15)$$

to reflect the limitations in maintaining the specified terminal voltage. It is impossible to convert limits of type (5.14) into limits of type (5.15) prior to knowing the system voltages; therefore these two specifications are not equivalent. It is mainly because of discrepancies of this type that potentially different stationary solutions are obtained when solving Eqs. (5.1) and (5.2) subject to explicit input inequality constraints (5.13) and (5.14) and when solving Eqs. (5.10) to (5.12) subject to inequality constraints (5.13) and (5.15).

In addition to accounting for the available control limits, a practically acceptable load-flow solution must lie within the prespecified bus voltage

$$E_{Li}^{\min} \leq E_{Li} \leq E_{Li}^{\max}, \quad i = 1, \dots, n \quad (5.16)$$

$$E_{Gi}^{\min} \leq E_{Gi} \leq E_{Gi}^{\max}, \quad i = 0, n + 1, \dots, n + k \quad (5.17)$$

and line-flow limits

$$P_{kl} \leq P_{kl}^{\max} \quad k, l = 1, \dots, n+k \quad (5.18)$$

The limit specifications are result of the requirements for individual equipment protection (generator, customer, transmission lines) as well as for the stable system operation. These specifications are known as the system security constraints. Typical bus voltage limits for the extra high voltage (EHV) transmission network in normal operation are $\pm 2\%$ and are often system specific.

In summary, the load-flow problem formulation (5.10) to (5.12) subject to constraints (5.13) and (5.15) could be viewed as a particular case of the more general equations (5.1) and (5.2) subject to constraints (5.13) and (5.14) [4,5]. The conventional characterization of generators as constant PV buses implies that constraints (5.13) and (5.14) on the governors and excitors are not violated. When this is not the case, considerable differences could result between the load-flow solution and the stationary solutions computed using Eqs. (5.1) and (5.2).

Note: The load-flow equations should be understood simply as nodal equations defining stationary sinusoidal operation, expressed in terms of (complex-valued) power instead of in terms of (complex-valued) currents. This is because current injections into buses of a power network are not explicitly characterized. Instead, power injections are often specified. As it was discussed in Chapter 4, this difference creates a qualitatively new algebraic problem and requires different techniques, more specialized than the techniques commonly used for solving nodal equations in electric circuits [6]. An interesting analogy of these two problems can be found in Ref. [7]. Analytical properties and possible network interpretation of the load flow equations are studied later in this chapter.

Example 5.2.1 The conventional load-flow equations (5.10) to (5.12) take on the following form for a small power system shown in Figure 4.4:

$$\begin{aligned} P_{D3} &= \frac{E_3^2}{Z_{31}} \cos \zeta_{31} - \frac{E_3 E_1}{Z_{31}} \cos(\delta_{31} - \zeta_{31}) \\ &\quad + \frac{E_3^2}{Z_{32}} \cos \zeta_{32} - \frac{E_3 E_2}{Z_{32}} \cos(\delta_{32} - \zeta_{32}) \end{aligned} \quad (5.19)$$

$$\begin{aligned} Q_{D3} &= \frac{E_3^2}{Z_{31}} \sin \zeta_{31} - \frac{E_3 E_1}{Z_{31}} \sin(\delta_{31} - \zeta_{31}) \\ &\quad + \frac{E_3^2}{Z_{32}} \sin \zeta_{32} - \frac{E_3 E_2}{Z_{32}} \sin(\delta_{32} - \zeta_{32}) \end{aligned} \quad (5.20)$$

$$\begin{aligned} P_{G2} &= \frac{E_2^2}{Z_{21}} \cos \zeta_{21} - \frac{E_2 E_1}{Z_{21}} \cos(\delta_{21} - \zeta_{21}) \\ &\quad + \frac{E_2^2}{Z_{23}} \cos \zeta_{23} - \frac{E_2 E_3}{Z_{23}} \cos(\delta_{23} - \zeta_{23}) \end{aligned} \quad (5.21)$$

The control-limit-imposed constraints in this example take on the form

$$P_{G2}^{\min} < P_{G2} < P_{G2}^{\max} \quad (5.22)$$

$$Q_{G2}^{\min} < Q_{G2} < Q_{G2}^{\max} \quad (5.23)$$

In the case of a three-bus system the operating constraints (5.16) to (5.18) take on the form:

$$E_{D3}^{\min} < E_{L3} < E_{D3}^{\max} \quad (5.24)$$

$$E_{G2}^{\min} < E_{G2} < E_{G2}^{\max} \quad (5.25)$$

and

$$P_{kl} < P_{kl}^{\max} \quad (5.26)$$

for $k, l \in 1, 2, 3; k \neq l$.

5.2.1 Analytic Properties of the Load-Flow Equations

The general structure of the load-flow equations (5.10) to (5.12) was studied by Galiana and coworkers [8,9]. In this work also the analytic concept of a stationary stability margin as a measure of system's proximity to the limits outside which a solution to the load flow does not exist for systems other than the simplest two-bus systems was defined for the first time. Here we briefly summarize this load-flow formulation.

The quadratic nature of the load-flow equations when complex-valued voltages are represented in rectangular coordinates is formalized. To present this, denote the complex-valued bus voltage \hat{E}_i at bus i by

$$\hat{E}_i = E_{ci} + jE_{si} \quad (5.27)$$

and let

$$e = [E_{c1} \quad E_{c2} \quad \cdots \quad E_{c,n+k+1}]^T \quad (5.28)$$

$$f = [E_{s1} \quad E_{s2} \quad \cdots \quad E_{s,n+k+1}]^T \quad (5.29)$$

A typical complex-valued power balance equation (5.10) to (5.12) at bus k can be expressed as a quadratic function

$$z_k = x^T J_k x \quad (5.30)$$

with the vector x defined by

$$x = [e \quad f]^T \quad (5.31)$$

and the symmetric matrix J_k given by

$$J_k = \frac{1}{2} \begin{bmatrix} GH_k + H_k G & BH_k - H_k B \\ -BH_k + H_k B & GH_k + H_k G \end{bmatrix} \quad (5.32)$$

if $z_k = P_{Tk}$. For the case $z_k = Q_{Lk}$

$$J_k = \frac{1}{2} \begin{bmatrix} BH_k - H_k B & GH_k - H_k G \\ -GH_k + H_k G & BH_k - H_k B \end{bmatrix} \quad (5.33)$$

where matrices G and B are real and imaginary parts, respectively, of the bus admittance matrix $\hat{Y}_{\text{bus}} = G + jB$ [Eq. (4.46)], while the matrix H_k has 0s everywhere except in the kk location where it takes value 1. Finally, if the injection is $z_k = E_k^2 = E_{ck}^2 + E_{sk}^2$, then J_k will have 0's everywhere except for the kk and $(n+k)(n+k)$ elements, which are equal to 1.

For a general network it is difficult to characterize bounds on system inputs z within which a solution x to the load-flow problem

$$z = F(x), \quad x \in \mathbb{R}^{2n+k} \quad (5.34)$$

would be guaranteed to exist. In Refs. [8,9] and in Chapters 8 to 10 the region of all inputs for which the solution to Eq. (5.34) exists is referred to as a stationary or feasibility region $R_z = \{z : F(x) = z\}$. The distance between the chosen operating point and the boundaries of R_z (measured in terms of some norm measure) is referred to as a steady-state stability margin. An illustration of this in context of a two-bus system is the distance $|P^{\max} - P|$ and/or $|Q^{\max} - Q|$ in Figures 4.8 and 4.9. As pointed out earlier, a more practical modified definition would require inclusion of limits on both z and x , that is,

$$z^{\min} < z < z^{\max} \quad (5.35)$$

and

$$x^{\min} < x < x^{\max} \quad (5.36)$$

component-wise, so that Eq. (5.34) holds.

This general formulation of the load-flow problem as given in Eq. (5.34) is quite elegant and has provided a basis for further development in characterizing qualitative properties of state variables x for given ranges on z without actually solving numerically for x [10].

Another possible approach to deal with the overall complexity of the load-flow computations for very-large-power systems is to view the problem as a problem of solution existence and uniqueness in nonlinear DC electric networks. This is described next, following the introduction of the real-power–reactive-power decoupling assumption, typically made when posing the steady-state stability problem as two separate (decoupled) network problems.

5.2.2 Real-Power–Reactive-Power Decoupling Conditions

The foundation for the real-power–reactive-power decoupling assumption can be illustrated from the simplest case of a two-bus example introduced in Chapter 4,

Figure 4.7. The sensitivity of the real power P_2 delivered to the load with respect to change in phase-angle difference δ_{12} from Eq. (4.116) is

$$\frac{\partial P_2}{\partial \delta_{12}} = \frac{1}{Z_{12}} E_1 E_2 \sin(\delta_{12} - \zeta_{12}) \quad (5.37)$$

Similarly, the sensitivity of the real power P_2 with respect to the change in voltage magnitude E_2 follows from the same equation (4.116):

$$\frac{\partial P_2}{\partial E_2} = \frac{E_1}{Z_{12}} \cos(\delta_{12} - \zeta_{12}) \quad (5.38)$$

Highly inductive lines have $\zeta_{12} \simeq 90^\circ$, therefore typically for voltages close to 1 p.u. it follows from Eqs. (5.37) to (5.38) that

$$\left| \frac{\partial P_2}{\partial (\delta_1 - \delta_2)} \right| \gg \left| \frac{\partial P_2}{\partial E_2} \right| \quad (5.39)$$

This relationship forms the basis for analyzing changes in phase-angle differences as related to real-power injections, while assuming that voltages do not change significantly.

Similarly, the sensitivity of the reactive power Q_2 with respect to the change in the voltage magnitude E_2 follows from Eq. (4.118):

$$\frac{\partial Q_2}{\partial E_2} = \frac{1}{Z_{12}} [2E_2 \sin \zeta_{12} - E_1 \sin(\delta_{12} - \zeta_{12})] \quad (5.40)$$

and the sensitivity of the reactive power Q_2 with respect to the change in phase angle difference δ_{12} as

$$\frac{\partial Q_2}{\partial \delta_{12}} = \frac{1}{Z_{12}} [-E_2 E_2 \cos(\delta_{12} - \zeta_{12})] \quad (5.41)$$

Again, keeping in mind that $\zeta_{12} \simeq 90^\circ$, it follows from Eqs. (5.40) and (5.41) that

$$\left| \frac{\partial Q_2}{\partial E_2} \right| \gg \left| \frac{\partial Q_2}{\partial \delta_{12}} \right| \quad (5.42)$$

for voltages close to 1 p.u. This relationship forms the mathematical basis for analyzing the dependence of the reactive power on voltage changes, assuming that changes in angle differences have insignificant effects.

Note that as the phase-angle difference δ_{12} increases, or as voltages E_1 and E_2 deviate significantly away from 1 p.u., the decoupling assumption becomes less accurate. In addition, for lines with a non-negligible resistance to inductance ratio (i.e., $\zeta_{12} > 90^\circ$), the decoupling assumption is not as reliable as for the lossless lines [2].

A systematic generalization of decoupling conditions (5.39) to (5.42) for a multibus system is described next. Consider the relationship between changes in voltage and angles due to changes in real and reactive power defined by linearizing the load-flow equations (5.10) to (5.12) around a given operating point:

$$\begin{bmatrix} \Delta P \\ \Delta Q \end{bmatrix} = \begin{bmatrix} \frac{\partial P}{\partial \delta} & \frac{\partial P}{\partial E} \\ \frac{\partial Q}{\partial \delta} & \frac{\partial Q}{\partial E} \end{bmatrix} \begin{bmatrix} \Delta \delta \\ \Delta E \end{bmatrix} = J(\delta, E) \begin{bmatrix} \Delta \delta \\ \Delta E \end{bmatrix} \quad (5.43)$$

It follows directly from this relationship that exact changes in voltages and angles can be computed as

$$\begin{bmatrix} \Delta \delta \\ \Delta E \end{bmatrix} = J(\delta, E)^{-1} \begin{bmatrix} \Delta \delta \\ \Delta E \end{bmatrix} \quad (5.44)$$

Notice that the difference between the exact Jacobian inverse and its decoupled version

$$J(E, \delta)^{-1} - \hat{J}(E, \delta)^{-1} = J(E, \delta)^{-1} - \begin{bmatrix} \frac{\partial P}{\partial \delta} & 0 \\ 0 & \frac{\partial Q}{\partial E} \end{bmatrix}^{-1} \quad (5.45)$$

can be computed directly by employing the formula for block matrix inversion [11]:

$$J(\delta, E)^{-1} = \begin{bmatrix} E \Delta^{-1} F & -E \Delta^{-1} \\ -\Delta^{-1} F & Q_E^{-1} C T^{-1} D Q_E^{-1} \end{bmatrix} \quad (5.46)$$

where

$$\begin{aligned} P_\delta &= \frac{\partial P}{\partial \delta}, & P_E &= \frac{\partial P}{\partial E}, & Q_\delta &= \frac{\partial Q}{\partial \delta}, & Q_E &= \frac{\partial Q}{\partial E} \\ \Delta &= Q_E - Q_\delta P_\delta^{-1} P_E, & \Gamma &= P_\delta - P_E Q_E^{-1} Q_\delta \\ E &= P_\delta^{-1} P_E, & F &= Q_\delta P_\delta^{-1} \end{aligned}$$

With a typical p.u. normalization employed in computing load-flow solutions it can be shown that the order of magnitude¹ $O(P_\delta) = O(Q_E) = O(1)$ and $O(Q_\delta) = O(P_E) = O(\varepsilon)$, where $\varepsilon \ll 1$. Depending on specific operating conditions this order of magnitude estimate could lead to different levels of inaccuracies when relying on decoupled real-power reactive-power computations, which directly assume $\varepsilon \equiv 0$. It can be shown that typically

$$J(\delta, E)^{-1} - \hat{J}(\delta, E)^{-1} = O(\varepsilon^2) \quad (5.47)$$

¹ The order of magnitude of a matrix is typically measured in terms of a matrix norm [11].

Note: The basic question underlying this commonly made real-power–reactive-power decoupling assumption can be related to the conditions under which changes in real power do not affect voltage dynamics significantly, and similarly, changes in reactive power do not greatly affect angle dynamics. One possible mathematical formulation of this statement could be derived by establishing conditions under which eigenmodes associated with the angle dynamics can be decoupled from the eigenmodes associated with the voltage dynamics. This concept is analyzed in detail in Chapter 6.

The simplest connection between the decoupling conditions derived using the eigenmode analysis of system dynamics and the condition (5.47) can be made by recalling that under certain modeling assumptions given in Refs. [4,5] the system matrix defining linearized system dynamics is identical to the load-flow Jacobian $J(\delta, E)$. In this case, the eigenmodes of the load-flow Jacobian can be used to characterize small changes in system dynamics. It is shown in Chapter 6 that for this case a direct application of the general Gershgorin circle theorem [11] to the load-flow Jacobian leads to conditions similar to Eq. (5.57) under which voltage dynamics can be decoupled from angle dynamics.

However, both condition (5.47) and the Gershgorin theorem-based approach used in Chapter 6 are, strictly speaking, only valid for small changes. A particularly important restriction is that all variables remain within the prespecified limits. In other words, these techniques do not allow for change of bus type from PV to PQ when limits on the reactive-power output of a PV bus are exceeded, for example. This is critical to incorporate when any physical limitations on primary controllers are exceeded. In applying the results discussed here it is important to observe this fact, since once the bus type is changed, the number of equations describing PV and PQ buses changes and the derived condition must be re-tested for a different set of equations. This is sometimes overlooked.

The use of a decoupled load flow generally results in some loss of accuracy in analytical or numerical conclusions of interest. This is particularly the case if the system is subject to significant changes. For some theoretical estimates of decoupling error, see Refs. [12] and [13].

In what follows we establish conditions under which solutions to the decoupled load-flow problems ($P-\delta$ and $Q-V$) are guaranteed to exist. This problem is also known as the problem of steady-state stability limits in a large electric power system. It is of great practical importance to understand the theoretical limits on real- and reactive-power inputs for which phase-angle differences across all transmission lines and bus voltages remain within the prespecified operating limits.

5.3 DECOUPLED REAL-POWER–ANGLE LOAD-FLOW PROBLEM

Recall from Chapter 4 that in a simple two-bus power system the largest power delivered to a load is

$$P_2^{\max} = E_1 E_2 B_{12} \quad (5.48)$$

If the power demand P_2 at receiving end 2 of the line is larger than this, then power transfer is not feasible. The limit P_2^{\max} is known as the power associated with the steady-state stability limit. For $P_2 < P_2^{\max}$ there exist two solutions to the voltage-phase-angle difference $\delta_{12} = \delta_1 - \delta_2$ across the transmission line:

$$\delta_{12} = \sin^{-1} \left(\frac{P_2}{E_1 E_2 B_{12}} \right) \quad (5.49)$$

At least one solution exists only as long as $P_2/E_1 E_2 B_{12} \leq 1$. The decoupled $P-\delta$ problem in the case of a two-bus system is fully understood.

In this section the same problem is studied for the case of general power networks. While an explicit solution cannot be found, it is of great practical importance to understand theoretical limits on real-power inputs for which a solution exists for phase-angle differences across all transmission lines, and it is furthermore within the prespecified operating limits.

Here we first review a resistive network interpretation of the linearized $P-\delta$ load-flow equations (DC load-flow problem) developed in Refs. [14–18].

Next, the linearizing assumption is relaxed and the problem of finding a solution to the AC decoupled $P-\delta$ load flow is interpreted as a nonlinear circuit problem [19–21]. Emphasis is placed on nonconservative measures of feasible real-power transfers. As we proceed, notice that answers to the questions regarding bounds on system input and topology changes for which the unique solution exists cannot be provided by simply employing numerical packages for solving load flow. A typical load-flow program cannot detect the cause of divergence, it only detects that a solution is not computable by means of a specific numerical algorithm. We seek here, instead, to establish bounds on power inputs within which a solution is guaranteed to exist. Moreover, when it does not exist, the critical transmission-line bottleneck is identified.

5.3.1 Linear Resistive Network Interpretation of the DC Load-Flow Problem

Separating the real- and reactive-power components of the load-flow equations (5.10) to (5.12) and assuming all voltages E_i specified, one obtains (decoupled) AC real-power-flow equations

$$P_i = \sum_{j \in K_i} \left(\frac{E_i^2}{Z_{ij}} \cos \zeta_{ij} - \frac{E_i E_j}{Z_{ij}} \cos(\delta_{ij} - \zeta_{ij}) \right), \quad i = 1, \dots, n \quad (5.50)$$

$$P_i = \sum_{j \in K_i} \left(\frac{E_i^2}{Z_{ij}} \cos \zeta_{ij} - \frac{E_i E_j}{Z_{ij}} \cos(\delta_{ij} - \zeta_{ij}) \right), \quad i = n+1, \dots, n+k \quad (5.51)$$

The decoupled real-power-phase-angle problem is defined as the problem of finding phase-angle differences (δ_{ij}) for specified real-power demand $[P_1 \dots$

$P_n]$ at loads $i = 1, \dots, n$ and real-power generation $[P_{n+1} \dots P_{n+k}]$ at generator buses $i = n + 1, \dots, n + k$, and the specified angle at the slack bus δ_0 . This is a nonlinear problem, and it generally has multiple solutions [22–24]. The practical problem of direct interest to secure power-system operation is concerned with the bounds on real-power input changes ΔP_i , $i = 1, \dots, n + k$ around a nominal steady state for which an operationally acceptable solution exists and is characterized by

$$\delta_{ij}^{\min} < \delta_{ij} < \delta_{ij}^{\max} \quad (5.52)$$

for all i, j . Since the general answer to this question is difficult, we first present the state of the art for a linearized version of this problem. This formulation summarizes results from Refs. [14–19].

Suppose that the resistive part of transmission lines is negligible relative to its inductive part. Let $A \in \mathbb{R}^{N \times l}$ ($N = n + k$) be the reduced incidence matrix of the system obtained by deleting all shunts and the ground node. The slack bus is taken as the reference. Let $[b]$ be the diagonal matrix with elements $\{B_{ki}|k \neq i, k, i = 0, \dots, N\}$ and define $B \in \mathbb{R}^{N \times N}$ which is the imaginary part of the bus admittance matrix \hat{Y}_{bus} [Eq. (4.46)] as

$$B = A[b]A^T \quad (5.53)$$

The DC (linearized) load-flow equations (5.50) and (5.51) when neglecting resistive losses take on the form

$$\Delta P_k = \sum_{i=0}^N E_i E_k B_{ki} \Delta \delta_{ki}, \quad k = 1, \dots, N \quad (5.54)$$

or, written in a matrix form

$$\Delta P = C_p \Delta \delta \quad (5.55)$$

with $\Delta P = [\Delta P_1 \dots \Delta P_n \Delta P_{n+1} \dots \Delta P_{n+k}]$ and $\Delta \delta = [\Delta \delta_1 \dots \Delta \delta_n \Delta \delta_{n+1} \dots \Delta \delta_{n+k}]$, and $C_p = A[b][E]A^T$, where $[E]$ is an $l \times l$ diagonal matrix with elements $E_i E_k$. Typically $[E]$ is approximated by an identity matrix for voltages assumed to be close to 1 p.u. This is also done in what follows (although this is not essential for the derivations presented.) Under this assumption Eq. (5.55) becomes

$$\Delta P = B \Delta \delta \quad (5.56)$$

Observe that the same linearized real-power–phase-angle load-flow equations (5.54) can be derived by simply combining (1) Kirchhoff's flow equations

$$P = Ap \quad (5.57)$$

(2) Kirchhoff's voltage equations

$$\theta = A^T \delta \quad (5.58)$$

and (3) the constituent relations for transmission-line flows p

$$p_{ij} = E_i E_j B_{ij} \sin \theta \simeq E_i E_j B_{ij} \theta \quad (5.59)$$

which collectively results in Eq. (5.54). This formulation is analogous to the nodal equations representing a linear resistive network whose branch parameters are $C_{ik} = E_i E_k B_{ik}$, and in which currents and voltages are replaced by real-power flows and phase angles, respectively. This analogy is summarized in Table 5.2.

Recognizing this interpretation and recalling that resistive networks with positive resistors and independent voltage and current sources *always have a unique solution* [3, 25] guarantees existence of the solution for phase angles under small changes of input power [18].

Given the change in real-power inputs ΔP , approximate changes in phase angles $\Delta\delta$ are easily computed using the DC load-flow equation (5.56) as

$$\Delta\delta = B^{-1} \Delta P = X \Delta P \quad (5.60)$$

Recall again that this formulation assumes linearization of nonlinear constituent relations (5.59), which is only meaningful for small phase-angle differences. For large changes in phase angles, problems may arise in certain ranges of operating conditions. This is discussed next.

5.3.2 Nonlinear Resistor Network Interpretation of the $P-\delta$ Load-Flow Problem

The nonlinear formulation is obtained by recalling the constituent relation for a transmission line $i-j$

$$p_{ij} = E_i E_j B_{ij} \sin \delta_{ij} \quad (5.61)$$

Combining network constraints (5.57) and (5.58) with the nonlinear constituent relations (5.52) of the transmission lines, one obtains

$$\Delta P_i = E_i \sum_{j \in K_i} E_j B_{ij} (\sin(\delta_{ij} + \Delta\delta_{ij}) - \sin \delta_{ij}), \quad i = 1, \dots, n+k \quad (5.62)$$

TABLE 5.2 Analogy between the Decoupled Real-Power-Angle Problem and an Electric Resistive Network

	Electric network	Lossless decoupled real-power network
Independent sources	Ideal voltage sources; ideal current sources	Slack bus; real-power sources
Constituent relations	Conductors $i_{kj} = G_{kj} E_{kj}$	Lossless transmission lines $p_{kj} = B_{kj} E_k E_j \sin \delta_{kj} \simeq B_{kj} \delta_{kj}$
Kirchhoff's flow law	$I = A_i$	$P = A p$
Kirchhoff's voltage law	$V = A^T E$	$\theta = A^T \delta$

or

$$\Delta P_i = \sum_{j \in K_i} c_{ij} v_{ij} (\Delta \delta_{ij}) \quad (5.63)$$

where

$$v_{ij} (\Delta \delta_{ij}) = \sin(\delta_{ij} + \Delta \delta_{ij}) - \sin \delta_{ij} \quad (5.64)$$

$$c_{ij} = E_i E_j B_{ij} \quad (5.65)$$

Next, create a linear system of equations of the form

$$\Delta P_i = \sum_{j \in K_i} \Delta \delta_{ij} g_{ij} c_{ij} \quad (5.66)$$

where

$$g_{ij} = \frac{\sin(\delta_{ij} + \Delta \delta_{ij}) - \sin \delta_{ij}}{\Delta \delta_{ij}} \quad (5.67)$$

If we examine solutions of Eq. (5.62) for which Eq. (5.52) holds, then it is only necessary to consider g_{ij} in Eq. (5.66) which are bounded by

$$g_{ij}^{\min} \leq g_{ij} \leq g_{ij}^{\max} \quad (5.68)$$

where

$$g_{ij}^{\min} = \min \left(\frac{\sin \delta_{ij}^{\min} - \sin \delta_{ij}}{\delta_{ij}^{\min} - \delta_{ij}}, \frac{\sin \delta_{ij}^{\max} - \sin \delta_{ij}}{\delta_{ij}^{\max} - \delta_{ij}} \right) \quad (5.69)$$

$$g_{ij}^{\max} = \max \left(\frac{\sin \delta_{ij}^{\min} - \sin \delta_{ij}}{\delta_{ij}^{\min} - \delta_{ij}}, \frac{\sin \delta_{ij}^{\max} - \sin \delta_{ij}}{\delta_{ij}^{\max} - \delta_{ij}}, \cos \delta_{ij} \right) \quad (5.70)$$

Every solution to Eq. (5.62) with the voltage-phase-angle constraint of Eq. (5.52) then corresponds to a solution of Eq. (5.66) with some set of coefficients bounded by (5.68).² Therefore the system of nonlinear equations (5.62) has a linear resistor network analogy of the form

$$\underline{\Delta P} = H_P \underline{\Delta \delta} \quad (5.71)$$

The off-diagonal elements of H_P are

$$h_{ij} = c_{ij} g_{ij} \leq 0 \quad (5.72)$$

² This solution is unknown, though.

and the diagonal elements are

$$h_{ii} = - \sum_{j \in K_i, i \neq j} c_{ij} g_{ij} \geq 0 \quad (5.73)$$

The matrix H_P can be thought of as a conductance matrix of a resistive network with the same topology as the underlying power network.

5.3.2.1 Conditions for the Existence of a Solution The problem of real-power static stability at bus α on an arbitrary size power network can be regarded as the question of bounds on the generator or load real-power change at node α , ΔP_α , such that a unique solution exists that does not violate constraints given in Eq. (5.52) [21]. The results presented in this section are obtained in close collaboration with Professor Martin Hasler ETH, Zürich, Switzerland.

In order to be able to answer this question, consider a solution δ_{ij} of Eq. (5.62) with a new generator or load power increment at bus α , ΔP_α , but with all other power inputs unchanged. Then the increments $\Delta\delta_{ij}$, interpreted as branch voltages of a nonlinear resistor network, constitute a solution of a linear resistor network. This solution is obtained from the nonlinear resistive circuit by replacing the nonlinear resistor connecting nodes i and j with a linear resistor whose conductance g_{ij} is given as

$$g_{ij} = \frac{\sin(\delta_{ij} + \Delta\delta_{ij}) - \sin \delta_{ij}}{\Delta\delta_{ij}} \quad (5.74)$$

and by short-circuiting the voltage source corresponding to the slack bus and by removing all current sources except the source at bus α whose current becomes ΔP_α .

Suppose that for a power deviation ΔP_α all linear resistive circuits whose conductances satisfy Eq. (5.68) have solutions that obey the branch voltage-phase-angle constraint (5.52). Then there exists exactly one solution of the nonlinear resistor circuit with power ΔP_α injected into node α and nominal inputs into the other nodes that also satisfies the branch voltage constraint.

This can be explained as follows. Modify the nonlinear resistor characteristics v_{ij} in Eq. (5.64) to \hat{v}_{ij} where

$$\hat{v}_{ij}(\Delta\delta_{ij}) = \begin{cases} \sin \delta_{ij} + \Delta\delta_{ij} \frac{\sin \delta_{ij}^{\min} - \sin \delta_{ij}}{\delta_{ij}^{\min} - \delta_{ij}} & \text{for } \delta_{ij} + \Delta\delta_{ij} < \delta_{ij}^{\min} \\ \sin(\delta_{ij} + \Delta\delta_{ij}) - \sin \delta_{ij} & \text{for } \delta_{ij}^{\min} \leq \delta_{ij} + \Delta\delta_{ij} \leq \delta_{ij}^{\max} \\ \sin \delta_{ij} + \Delta\delta_{ij} \frac{\sin \delta_{ij}^{\max} - \sin \delta_{ij}}{\delta_{ij}^{\max} - \delta_{ij}} & \text{for } \delta_{ij} + \Delta\delta_{ij} > \delta_{ij}^{\max} \end{cases} \quad (5.75)$$

The modified resistor characteristics are then strictly monotonic. Therefore the modified nonlinear resistive circuit has exactly one solution [21]. This solution is again a solution of a linear resistive circuit [Eq. (5.66)], the conductances of

which satisfy Eq. (5.68). Now, if all linear resistive circuits with conductances satisfy the voltage-phase-angle constraint (5.52), then the unique solution of the linear circuit corresponding to the solution of the modified nonlinear circuit also exists. Given that the nonlinear v_{ij} in Eq. (5.63) is equal to \hat{v}_{ij} for $\delta_{ij}^{\min} \leq \delta_{ij}$ such that $\Delta\delta_{ij} \leq \delta_{ij}^{\max}$, this proves the existence and the uniqueness of the solution of Eq. (5.66), satisfying Eq. (5.52).

For fixed conductances, \underline{g} , we can easily determine $\Delta P_{\alpha}^{\max}(\underline{g})$ and $\Delta P_{\alpha}^{\min}(\underline{g})$. Suppose we compute the solution $\Delta \bar{\delta}_{ij}(\underline{g})$ of the circuit with conductances \underline{g} and the source value $\Delta \bar{q} \bar{P}_{\alpha} = 1$. The solution for arbitrary ΔP_{α} is then $\Delta \delta_{ij}(\underline{g}) = \Delta P_{\alpha} \Delta \bar{\delta}_{ij}(\underline{g})$. This allows us to determine the bounds for ΔP_{α} . Accordingly, we define

$$\Delta P_{\alpha}^{\max}(\underline{g}) = \begin{cases} \frac{\delta_{ij}^{\max} - \delta_{ij}}{\Delta \bar{\delta}_{ij}(\underline{g})} & \text{if } \Delta \bar{\delta}_{ij}(\underline{g}) > 0 \\ +\infty & \text{if } \Delta \bar{\delta}_{ij}(\underline{g}) = 0 \\ \frac{\delta_{ij}^{\min} - \delta_{ij}}{\Delta \bar{\delta}_{ij}(\underline{g})} & \text{if } \Delta \bar{\delta}_{ij}(\underline{g}) < 0 \end{cases} \quad (5.76)$$

$$\Delta P_{\alpha}^{\min}(\underline{g}) = \begin{cases} \frac{\delta_{ij}^{\min} - \delta_{ij}}{\Delta \bar{\delta}_{ij}(\underline{g})} & \text{if } \Delta \bar{\delta}_{ij}(\underline{g}) > 0 \\ -\infty & \text{if } \Delta \bar{\delta}_{ij}(\underline{g}) = 0 \\ \frac{\delta_{ij}^{\max} - \delta_{ij}}{\Delta \bar{\delta}_{ij}(\underline{g})} & \text{if } \Delta \bar{\delta}_{ij}(\underline{g}) < 0 \end{cases} \quad (5.77)$$

Hence, for $\Delta P_{\alpha} \in [\Delta P_{\alpha,ij}^{\min}(\underline{g}), \Delta P_{\alpha,ij}^{\max}(\underline{g})]$, the solution of the circuit satisfies $\delta_{ij}^{\min} \leq \delta_{ij}(\underline{g}) \leq \delta_{ij}^{\max}$. Since the bound must be satisfied on each branch, we can write

$$\Delta P_{\alpha}^{\max}(\underline{g}) = \min_{ij} \Delta P_{\alpha,ij}^{\max}(\underline{g}) \quad (5.78)$$

$$\Delta P_{\alpha}^{\min}(\underline{g}) = \max_{ij} \Delta P_{\alpha,ij}^{\min}(\underline{g}) \quad (5.79)$$

Now for any \underline{g}_{ij} satisfying Eq. (5.68)

$$\Delta P_{\alpha}^{\max} = \min_{\underline{g}_{ij}} \Delta P_{\alpha}^{\max}(\underline{g}_{ij}) \quad (5.80)$$

$$\Delta P_{\alpha}^{\min} = \max_{\underline{g}_{ij}} \Delta P_{\alpha}^{\min}(\underline{g}_{ij}) \quad (5.81)$$

Thus we have converted a problem involving a single nonlinear resistive circuit into a problem involving an infinite number of linear resistive circuits.

Fortunately, certain general circuit theoretic properties allow us to limit the number of circuit analyses to a finite number. First, consider $\Delta P_{\alpha,ij}^{\max}(\underline{g})$ and $\Delta P_{\alpha,ij}^{\min}(\underline{g})$ as functions of $\Delta \bar{\delta}_{ij}(\underline{g})$ as shown in Figure 5.1. As \underline{g} varies within

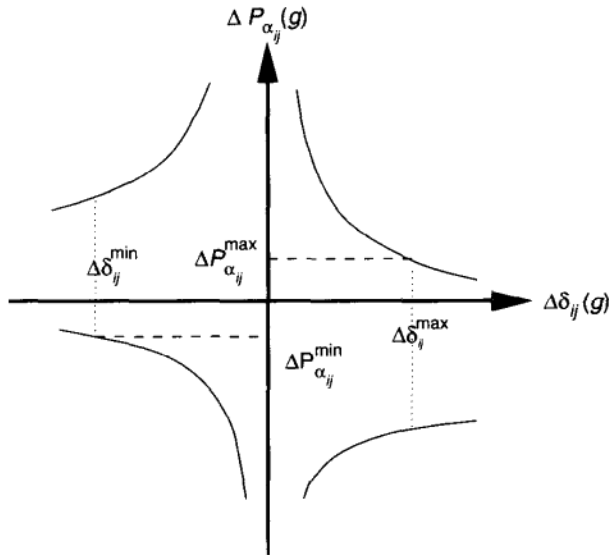


FIGURE 5.1 $\Delta P_{\alpha,ij}^{\max}(g)$ as the function of $\Delta \delta_{ij}(g)$.

$[g_{kl}^{\min}, g_{kl}^{\max}]$ the values $\Delta \bar{\delta}_{ij}(g)$ fill out the interval $[\Delta \bar{\delta}_{ij}^{\min}, \Delta \bar{\delta}_{ij}^{\max}]$. Clearly, the bounds $\Delta P_{\alpha,ij}^{\min}$ and $\Delta P_{\alpha,ij}^{\max}$ are reached at $\Delta \bar{\delta}_{ij}^{\min}$ and/or $\Delta \bar{\delta}_{ij}^{\max}$. Hence, we have to determine $\Delta \bar{\delta}_{ij}^{\min}$ and $\Delta \bar{\delta}_{ij}^{\max}$.

The change of voltage phase angle $\Delta \delta_{ij}$ of line $i-j$ with respect to the change in input ΔP_α in an arbitrary resistive circuit, with a given ΔP_α , is a function of g_{kl} . This function has the form [25,26]

$$\Delta \delta_{ij}(g) = \frac{Ag_{kl} + B}{Cg_{kl} + D} \Delta P_\alpha \quad (5.82)$$

where A, B, C , and D depend on all conductances, except g_{kl} . Hence, for $\Delta P_\alpha = 1$

$$\frac{\partial \Delta \bar{\delta}_{ij}(g)}{\partial g_{kl}} = \frac{AD - BC}{(Cg_{kl} + D)^2} \Delta P_\alpha \quad (5.83)$$

As long as $Cg_{kl} + D \neq 0$, $\Delta \bar{\delta}_{ij}(g)$ is increasing, decreasing, or constant in g_{kl} . Thus, when only g_{kl} is varied, $\Delta \bar{\delta}_{ij}(g)$ takes its extreme values at the end points of the interval $[g_{kl}^{\min}, g_{kl}^{\max}]$.

Repeating this procedure for all conductances g_{ij} , we conclude that $\Delta \bar{\delta}_{ij}^{\max}$ and $\Delta \bar{\delta}_{ij}^{\min}$ are reached at a vertex of the hypercube defined by

$$g_{ij}^{\min} \leq g_{ij} \leq g_{ij}^{\max} \quad (5.84)$$

Therefore, in order to determine the margin for ΔP_α , only 2^l analyses of linear circuits instead of infinitely many need be carried out, with l being the number of branches in the entire network.

In Ref. [21] a criterion is given for a nonlinear resistive circuit that allows us to decide whether a branch voltage or current is (as a function of a source voltage or current elsewhere in the circuit)

- Always strictly increasing
- Always strictly decreasing
- Always constant
- Nonmonotonic — increasing, decreasing or constant depending on circuit parameters

Here, *always* means *independently of the parameters of the circuit elements*, as long as the circuit elements belong to the same class (e.g., strictly increasing resistors). For a precise formulation, see Ref. [25]. We do not review this criterion here, but only illustrate its meaning in the context of steady-state stability limits.

Example 5.3.1 In the power-system example shown in Figure 5.2 one could show using the monotonicity test of Ref. [25] that all dependences on g_{ij} are strictly monotonic.

Given the monotonic dependence, if we fix our attention on a particular branch kl , we can determine which linear circuit among the infinitely many satisfying Eq. (5.68) will give the highest δ_{ij} for fixed ΔP_α , and which one has the lowest. These two linear circuits are the bounds on ΔP_α within which branch kl satisfies the constraints (5.52). This analysis must be carried out for each branch. The tightest bounds will give the overall safety margin on P_α .

Note that this procedure allows us to identify the critical transmission line. The nominal load-flow solution and line flows for the system given in Figure 5.2

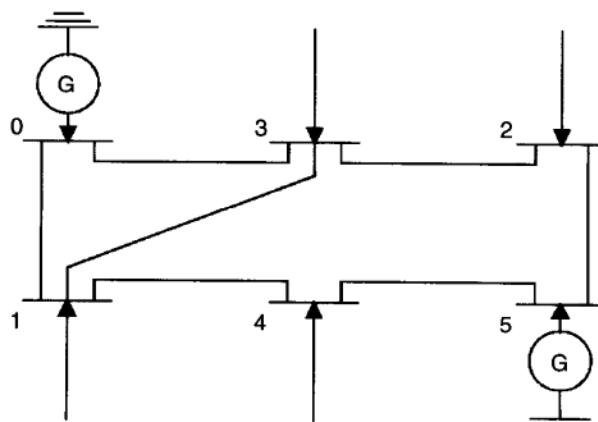


FIGURE 5.2 Six-bus example that exhibits monotonic response.

are shown in Tables 5.3 and 5.4. The line parameters $c_{ij} = (E_i E_j)/(X_{ij})$ for this circuit are $c_{01} = 2.0165$, $c_{03} = 2.8469$, $c_{13} = 2.4520$, $c_{14} = 3.2673$, $c_{23} = 7.5087$, $c_{25} = 1.0429$, and $c_{45} = 1.6935$. The voltage-phase-angle differences at the nominal load-flow solution are $\delta_{01} = 0.2063$, $\delta_{03} = 0.1630$, $\delta_{13} = -0.0433$, $\delta_{14} = -0.0018$, $\delta_{23} = -0.0474$, $\delta_{25} = -0.1874$, and $\delta_{45} = -0.1815$.

Steady-state stability limit at bus 2 We are interested in the steady-state real-power stability limit ΔP to load 2, given ± 0.3491 radians constraints on the phase angles. Using the monotonicity-based combinatorial search for the worst vertex on the hypercube determined by Eq. (5.68), one finds out that the critical line is 03 for the load increase at bus 2. The number of linear analyses required in estimating ΔP_2 is reduced to 16 from 128 ($= 2^7$) when taking into account the monotonicities. The estimated ΔP_2 is obtained to be

$$-0.7480 \leq \Delta P_2 \leq 2.0582 \quad (5.85)$$

An extensive load-flow calculation yields

$$-0.7495 \leq \Delta P_2 \leq 2.1017 \quad (5.86)$$

TABLE 5.3 Nominal Load-Flow Solution for the Monotonic System

Bus type	E_i	$\angle E_i$ (rad)	P_i (p.u.)	Q_i (p.u.)
0. Slack bus	1.0500	0.0000	0.8750	0.3252
1. PQ load	0.9948	-0.2063	-0.5250	-0.0499
2. PQ load	0.9955	-0.2104	-0.5500	-0.1299
3. PQ load	1.0032	-0.1630	0.0000	0.0001
4. PQ load	0.9853	-0.2046	-0.3000	-0.1799
5. PV generator	1.1000	-0.0230	0.5000	0.3527

TABLE 5.4 Line Flow Data for the Monotonic Circuit

From ^a <i>i</i>	To ^a <i>j</i>	Resistance R_{ij} (p.u.)	Reactance X_{ij} (p.u.)	Real power P_{ij} (p.u.)	Reactive Power Q_{ij} (p.u.)
0	1	0.000	0.518	0.4131	0.1546
0	3	0.000	0.370	0.4619	0.1706
1	3	0.000	0.407	-0.1062	-0.0182
1	4	0.000	0.300	-0.0057	0.0315
2	3	0.000	0.133	-0.3558	-0.0491
2	5	0.000	1.050	-0.1943	-0.0808
4	5	0.000	0.640	-0.3057	-0.1487

^aNumbers in this column refer to the first column in Table 5.3.

5.3.2.2 Algorithms for Computing $P-\delta$ Steady-State Stability Limits in Monotonic Nonlinear Power Networks Based on the preceding analysis, one could arrive at several important features of monotonic networks for reducing complexity of finding the steady-state stability limit. Initially, the necessary step is for a given power network to perform a combinatorial test [25] that determines if the network has a monotonic response. This test may be time consuming for large networks. However, it is strictly topological and needs to be only done once.

Next, provided that the power network has a monotonic response one could proceed as follows:

- One could use small-signal sensitivity-based approaches, such as distribution factors to estimate the steady-state stability limit. The most important factor here is that in circuits with monotonic response the *sign* of large sensitivity is determined by the *sign* of the small-signal sensitivity and is independent of operating conditions.
- One could use a method described in Refs. [21,25] for reducing the number of linear circuits needed to find the corner on the hypercube defined in Eq. (5.68) such that constraints (5.68) are met.

All of these possibilities would contribute significantly to the computational efficiency in determining steady-state stability problems. Here only the results of using distribution factors are shown for the same circuit given in Figure 5.2.

A distribution-factor-based method routinely used by power utilities shows the effect on line kl , which we describe by $\delta_{kl} = \delta_k - \delta_l$, of a change in real power, ΔP_i , on the generator or load at i :

$$\frac{D_{kl,i}}{B_{kl}} = \frac{\Delta\delta_{kl}}{\Delta P_i} \quad (5.87)$$

where $\Delta\delta_{kl}$ is the change in the angle difference on line kl and ΔP_i is the change in real power at bus i . In order to apply the distribution factors we first linearize the system around a nominal operating point. We start with the matrix equation that is obtained by solving Eq. (5.56) for δ in terms of P :

$$[\Delta\delta] = [c][\Delta P] \quad (5.88)$$

where $\Delta P_k = 0$ for $k \neq i$, and the distribution factors are given by

$$D_{kl,i} = c_{ki} - c_{li} \quad (5.89)$$

if $k, l \neq 0$, or

$$D_{0l,i} = -c_{li} \quad (5.90)$$

Example 5.3.2 For the six-bus example analyzed here, $D_{01,2} = -0.1564$, $D_{03,2} = -0.2405$, $D_{13,2} = -0.0841$, $D_{14,2} = -0.0334$, $D_{23,2} = 0.1186$, $D_{25,2} =$

0.1048, and $D_{45,2} = -0.0645$. Suppose $\Delta P_2 = 0.005$ (about 9% deviation from its nominal value). Then the expected angle differences δ_{ij} are given by

$$\delta_{ij} = \bar{\delta}_{ij} + D_{ij,2}\Delta P_2 \quad (5.91)$$

Hence, we obtain $\delta_{01} = 0.2055$, $\delta_{03} = 0.1618$, $\delta_{13} = -0.0437$, $\delta_{14} = -0.0019$, $\delta_{23} = -0.0468$, $\delta_{25} = -0.1868$, and $\delta_{45} = -0.1819$. Compared to the values obtained from the load-flow program $\delta_{01} = 0.2055$, $\delta_{03} = 0.1618$, $\delta_{13} = -0.0437$, $\delta_{14} = -0.0019$, $\delta_{23} = -0.0468$, $\delta_{25} = -0.1868$, and $\delta_{45} = -0.1819$, the result is very good.

However, suppose that we employ this method to obtain the power deviation at node 2, ΔP_2 . In order not to violate the line constraint, ΔP_2 must vary within an interval

$$\frac{\delta_{ij}^{\min} - \bar{\delta}_{ij}}{D_{ij,2}} \leq \Delta P_2 \leq \frac{\delta_{ij}^{\max} - \bar{\delta}_{ij}}{D_{ij,2}} \quad (5.92)$$

Given that $-\delta_{ij}^{\min} = \delta_{ij}^{\max} = 0.3491$ using the distribution factor method, we get the safety margin for load 2,

$$-0.7739 \leq \Delta P_2 \leq 2.1294 \quad (5.93)$$

which is not so accurate compared to Eq. (5.86) or (5.85). In many cases the linearization overestimates the safety margin, which can lead to serious consequences.

5.3.2.3 Nonmonotonic Response of a Nonlinear Power Network Now consider a simple power system shown in Figure 5.3, the system data and the solution of which is given in Tables 5.5 and 5.6. Based on the results in Ref. [25], $\delta_{13}(P_2)$, $\delta_{14}(P_2)$, $\delta_{15}(P_2)$, and $\delta_{34}(P_2)$ are expected to be either monotonic or nonmonotonic functions depending on parameter values.

Indeed, as we vary the real-power generation at bus 2, P_2 , from -3.6 p.u. to 3.6 p.u. the angle difference, δ_{14} is modified in an unpredictable manner. Shown in Figure 5.4, δ_{14} initially increases from 0.0222 to 0.0287, then stays constant at 0.0287 for a while and eventually decreases to -0.0026 [26]. It is critical

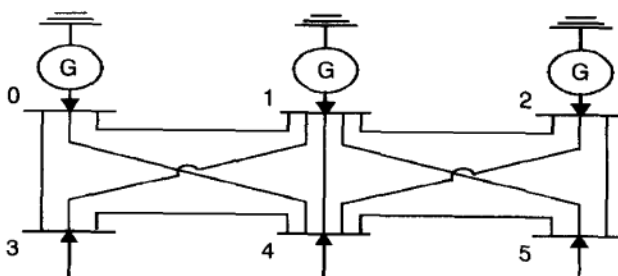


FIGURE 5.3 Six-bus network, whose response is nonmonotonic.

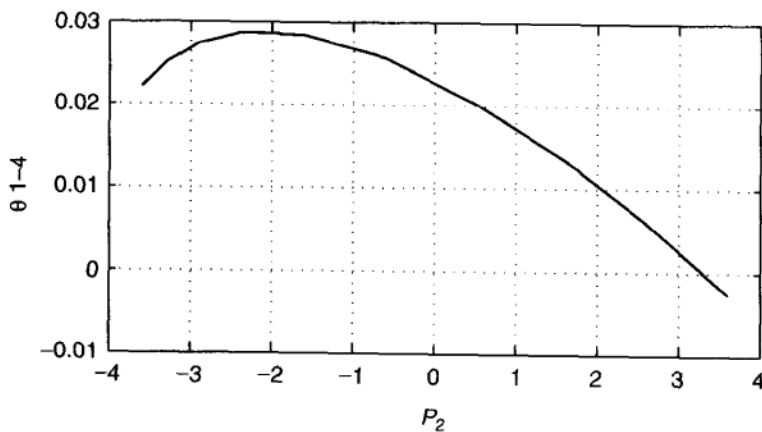
TABLE 5.5 Load-Flow Solution in a Nonmonotonic Circuit

Bus type	$ E_i $	$\angle E_i$ (rad)	P_i (p.u.)	Q_i (p.u.)
0. Slack bus	1.05000	0.0000	1.09272	0.16873
1. PV generator	1.05000	-0.0689	0.50259	1.34391
2. PV generator	1.07000	-0.0671	0.60028	0.58755
3. PQ load	0.98849	-0.0747	-0.70000	-0.70000
4. PQ load	0.99311	-0.0886	-0.70000	-0.70000
5. PV load	1.03383	-0.0961	-0.70000	-0.70000

TABLE 5.6 Line Flows in the Nonmonotonic Circuit

From ^a <i>i</i>	To ^a <i>j</i>	Resistance	Reactance	P_{ij}	Q_{ij}
0	1	0.100	0.200	0.30870	-0.17987
0	3	0.050	0.200	0.44394	0.18782
0	4	0.080	0.300	0.34008	0.08347
1	2	0.050	0.250	-0.02365	-0.13714
1	3	0.050	0.100	0.30687	0.43469
1	4	0.100	0.300	0.15374	0.25031
1	5	0.070	0.200	0.36389	0.57537
2	4	0.120	0.260	0.19304	0.19106
2	5	0.020	0.100	0.38327	0.27785
3	4	0.200	0.400	0.02279	-0.05677
4	5	0.100	0.300	-0.01731	-0.20042

^aNumbers in this column refer to the first column in Table 5.5.

**FIGURE 5.4** Nonmonotonic dependence of the line flow on power input changes.

to observe that in a circuit with nonmonotonic behavior the steady-state stability limit that is demanded at a particular system input cannot be computed only once. Also it is assumed that lower power injections would necessarily cause line flows within the transmission constraints independent of the operating conditions, that is, other power injections into the system. This finding leads one to a conclusion that in this case it is not very meaningful to compute the steady-state stability limit independent of the other power injections into the system.

5.3.3 Localized Response Property of the $P-\delta$ Power Network

As the real power inputs to the $P-\delta$ network change either intentionally (for purposes of maintaining state and output variables within the operating constraints) or unintentionally (a consequence of generator outages, an increase or decrease in load demand at a specific bus, or transmission-line outage seen as a simultaneous change of two inputs), a system operator needs to compute the effect of these changes on system-wide conditions quickly.

Generally, two types of effects of these power input changes are of interest: (1) the effect on the individual bus voltage state, such as phase angle δ_i (state variables), and (2) the effect on the line flows, that is phase-angle differences δ_{kl} (output variables). Here we analyze both types of sensitivities. The main intent is to show that when posed correctly these effects are localized as long as the $P-\delta$ power network behaves as a nonlinear positive resistive network.

We show first how changes in bus voltage phase angles δ_i are effected in a tier-wise manner around the location α at which a power input change ΔP_α occurs. Next the effect of power input changes on the line flows is analyzed. To do this, first a so-called distribution factors matrix is defined; this is basically an input-output sensitivity matrix. More caution is needed here as a localized response property of the phase-angle difference δ_{kl} with respect to the power input change at a bus is studied. To start with, when a power change takes place at a single bus, a localized response is not obvious since the entire imbalance created by this change is compensated by the slack bus. Depending on where this bus is located, the effects may be system-wide. This slack-bus-related asymmetry was recognized some time ago in Ref. [27]. The localized response is much easier to detect when the system is subject to a transmission line outage or to a balanced power injection at two different buses. Potential applications of this property for effective stationary generation control are shown later in Chapter 14.

5.3.3.1 Localized Changes in Phase Angles (States) Many algorithms for fast evaluation of real-power change propagation throughout a large system are based on the property that the effects of change seen through changes in voltage phase angles decrease monotonically as the electrical distance from a triggering event increases [18, 19, 28, 29]. This property is also often used by system operators in their decision making for corrective actions as described later in Chapter 14.

It is fairly straightforward to formalize this so-called localized response of a transmission network to real-power input changes, keeping in mind the resistive network interpretation of the $P-\delta$ power network. In order to state this

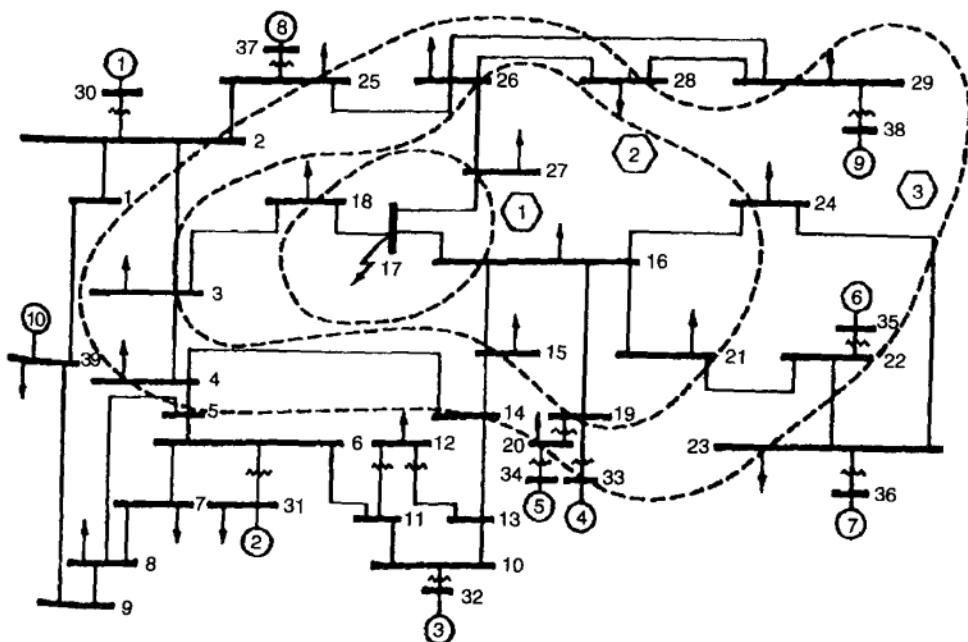


FIGURE 5.5 Tier-based bus enumeration.

property rigorously, it is convenient to introduce change-dependent (triggering-event-dependent) bus enumeration. We assume that buses are partitioned into tiers [29,30]. A bus for which the real-power injection changes constitutes tier 1; the buses directly connected to tier 1 constitute tier 2; and so on. This concept is illustrated for a simple power system in Figure 5.5.

The vectors P and δ (respectively, ΔP and $\Delta \delta$) are partitioned accordingly with P_k and δ_k (respectively, ΔP_k and $\Delta \delta_k$) representing the subvectors corresponding to the buses in each tier k . Let the outermost be tier N . We then state this localized response formally as follows [18,19,21].

Theorem 5.3.1 Let a $P-\delta$ network be partitioned into tiers around a given set of buses [18]. Suppose the changes ΔP_1 are such that $\Delta \delta$ lies in the regions defined by Eq. (5.68). Then we have

$$\|\Delta \delta_1\|_\infty \geq \|\Delta \delta_2\|_\infty \cdots \geq \|\Delta \delta_N\|_\infty \quad (5.94)$$

where $\|\cdot\|_\infty$ denotes the superior norm and $\Delta \delta_k$ is the vector of changes in phase angles in tier k . This theorem says that the maximum change in phase angle in tier 1 is not less than the maximum change in phase angle in tier 2, etc.

Proof: First of all, note that it is enough to show that

$$\|\Delta \delta_{k-1}\|_\infty \geq \|\Delta \delta_k\|_\infty \quad (5.95)$$

Note also that by the fact that each nonlinear $P-\delta$ network has an equivalent linear resistive network interpretation, it is sufficient to show the result for the linear circuit defined by its conductance matrix B .

Lemma 5.3.1 In the case of the linear problem it is enough to show Eq. (5.95) for $k = N$, where N is the number of tiers.

Proof: For $k < N$, one can by star-mesh transformation eliminate the nodes in tier $k + 1$ through tier N without affecting the solutions in tiers 1 through k . Also the reduction will only introduce new lines between buses in tier k and thus not affect the tier structure of the network.

Proof of theorem (for the linear case): Because we have ordered the network tier-wise, we have the following block tridiagonal system of equations directly resulting from Eq. (5.54) after the tier-based bus reenumeration

$$\begin{bmatrix} B_{11} & B_{12} & 0 & 0 & \cdots & 0 \\ B_{21} & B_{22} & B_{23} & 0 & \cdots & 0 \\ 0 & B_{32} & B_{33} & B_{34} & \cdots & 0 \\ \vdots & \vdots & \vdots & \vdots & \vdots & \vdots \\ \vdots & \vdots & \vdots & \vdots & \vdots & \vdots \\ 0 & 0 & 0 & \cdots & B_{N(N-1)} & (B_{NN}) \end{bmatrix} \begin{bmatrix} \Delta\delta_1 \\ \Delta\delta_2 \\ \Delta\delta_3 \\ \vdots \\ \Delta\delta_{N-1} \\ \Delta\delta_N \end{bmatrix} = \begin{bmatrix} \Delta P_1 \\ 0 \\ 0 \\ \vdots \\ 0 \\ 0 \end{bmatrix} \quad (5.96)$$

whence

$$B_{N(N-1)}\Delta\delta_{N-1} + B_{NN}\Delta\delta_N = 0 \quad (5.97)$$

$$\Delta\delta_N = (-B_{NN}^{-1}B_{N(N-1)})\Delta\delta_{N-1} \quad (5.98)$$

Hence

$$\|\Delta\delta_N\|_\infty \leq \| -B_{NN}^{-1}B_{N(N-1)} \|_\infty \|\Delta\delta_{N-1}\|_\infty \quad (5.99)$$

where

$$\| -B_{NN}^{-1}B_{N(N-1)} \|_\infty = \max_i \sum_j \|(-B_{NN}^{-1}B_{N(N-1)}_{ij})\| := v \quad (5.100)$$

Denote by $\underline{1}$ the vector all of whose components are 1. From elementary properties of the admittance matrix it follows that every element of B_{NN} is non-negative and every element of $B_{N(N-1)}$ is nonpositive. Hence

$$v = \max_i \sum_j \|(-B_{NN}^{-1}B_{N(N-1)}_{ij})\| = \max_i \|(-B_{NN}^{-1}B_{N(N-1)}\underline{1})_i\| \quad (5.101)$$

Since the sum of entries in each row is greater than or equal to zero,

$$B_{NN}\underline{1} + B_{N(N-1)}\underline{1} \geq 0 \quad (5.102)$$

where \geq denotes a component-wise inequality. Multiplying Eq. (5.102) on both sides by B_{NN}^{-1} , every entry of which is non-negative,

$$\underline{1} + B_{NN}^{-1}B_{N(N-1)}\underline{1} \geq 0 \quad (5.103)$$

or

$$-B_{NN}^{-1}B_{N(N-1)}\underline{1} \geq \underline{1} \quad v \leq 1 \quad (5.104)$$

which proves the theorem.

Although this result appears to hold unconditionally for the linearized real-power change propagation, under the assumption of negligible real-power losses, its generalization to lossy transmission systems indicates additional restrictions on operating regions in which a similar property holds. These results can be found in Ref. [19].

5.3.3.2 Localized Changes in Phase-Angle Differences (Outputs) One of the frequently used approximate methods for assessing the effect of changes in real-power injections ΔP_i on changes in real-power line flows ΔP_{kl} is known as a distribution factor method. This method is typically used to avoid violation of the line-flow limits defined in Eq. (5.18). A distribution factor $D_{kl,i}$ is defined as the sensitivity of the power flow in line kl of interest with respect to the power injection at bus i , that is,³

$$D_{kl,i} = \frac{P_{kl}}{P_i} \quad (5.105)$$

These sensitivities are computed by using the line constituent relation (5.59):

$$P_{kl} = M_{kl}^T \delta \quad (5.106)$$

where M_{kl} is the sensitivity vector of the line power with respect to bus voltage-phase-angle changes, the elements of which are zero except the i th and j th are B_{ij} and $-B_{ij}$, respectively; δ is a vector of the voltage phase angles of all buses including generators, loads, and the slack buses. If the DC load-flow equations (5.56) are written assuming bus n as a slack bus, then the phase angles relative to this bus can be solved according to Eq. (5.60) as

$$\delta_{-n}^{\text{rel}} = B_{-n}^{-1} P_{-n} \quad (5.107)$$

³ The Δ symbol is omitted for notational simplicity.

where the subscript $-n$ denotes a vector without its n th element or in a matrix form with, correspondingly, its n th row and column eliminated. The actual phase angles can be rewritten by simply adding the relative angles and the phase angle of the reference bus:

$$\begin{aligned}\delta &= \left[\frac{\delta_{-n}^{\text{rel}}}{0} + \delta_n \underline{1} \right] \\ &= \left[\begin{array}{c|c} B_{-n}^{-1} & 0 \\ \hline 0 & 0 \end{array} \right] P + \delta_n \underline{1}\end{aligned}\quad (5.108)$$

where δ_n is the phase angle of bus n . Then, combining Eqs. (5.108) and (5.56), the power flow on line k to l can be expressed in terms of real-power injections:

$$\begin{aligned}P_{kl} &= M_{kl}^T \left[\begin{array}{c|c} B_{-n}^{-1} & 0 \\ \hline 0 & 0 \end{array} \right] P + \delta_n M_{kl}^T \underline{1} \\ &= D_{kl}^{n,T} P\end{aligned}\quad (5.109)$$

The second term is identical to zero because of the fact that $M_{kl}^T \underline{1} = 0$. Thus the distribution factor D_{kl}^n with bus n as the reference bus is obtained as

$$D_{kl}^n = \left[\begin{array}{c|c} B_{-n}^{-1} & 0 \\ \hline 0 & 0 \end{array} \right]^T M_{kl}\quad (5.110)$$

Observe that the n th element in this relation corresponding to the prespecified reference bus is always zero. Namely, the distribution factors computed with respect to the reference bus n , D_{kl}^n will be different from those computed with respect to the bus m , D_{kl}^m , if $n \neq m$. However, they are always related as follows [31]:

Lemma 5.3.2 The distribution factors calculated with respect to different reference buses differ from each other by a shift factor which equals to the m th element of D_{kl}^n or the n th element of D_{kl}^m with negative sign, that is,

$$D_{kl}^n - D_{kl}^m = \beta_{kl}^{m,n} \underline{1}\quad (5.111)$$

and

$$\beta_{kl}^{m,n} = D_{kl}^n(m) = -D_{kl}^m(n)\quad (5.112)$$

where $D_{kl}^n(m)$ denotes the m th element of the vector D_{kl}^n .

Proof: By the fact that the matrix B is rank-one deficient, only differences between elements $D_{kl}^n(m)$, of the distribution factors D_{kl}^n have unique solutions,

that is,

$$D_{kl}^n(m) - D_{kl}^n(n) = D_{kl}^m(m) - D_{kl}^m(n) \quad (5.113)$$

Also based on these derivations, $D_{kl}^n(n) = D_{kl}^m(m) = 0$; therefore, $D_{kl}^n(m) = -D_{kl}^m(n)$. As $D_{kl}^n(m)$ and $D_{kl}^m(n)$ are determined, the relation of vectors D_{kl}^n and D_{kl}^m follows Eq. (5.111).

5.3.3.3 Distribution Factors and Localized Response While it is intuitively appealing that a change in power injection at bus i would cause larger (in magnitude) real-power-flow changes in lines electrically closer to the location of the change than in lines further away, this property is not obvious when computing the distribution factors defined in Eq. (5.107) for an arbitrary choice of a slack bus. To the contrary, all imbalances are compensated at the location of the slack bus. It is for this reason that a transformation of inputs into balanced input pairs was proposed some time ago in Ref. [27].

Recently a novel type of distribution factor was introduced in Ref. [31] for computing the sensitivity of a line flow in kl with respect to the balanced pairs of power injections. These newly defined distribution factors capture a localized property of the transmission network response to a change in bus power injections [18,19,28]. This property refers to the fact that sensitivities of line flows with respect to the power injections at the electrically closer buses are higher than those with respect to the injections at the electrically distant buses.

Here we briefly summarize these distribution factors. Even though different $\beta_{kl}^{m,n}$'s do not result in different impacts of individual transactions on the line flow P_{kl} , $\beta_{kl}^{m,n}$ does affect the actual numerical values of the line-flow sensitivities to the power injections at individual buses. For line distribution factors to represent relative contributions of the injections at individual buses to the line flow in a line of interest accurately, the magnitudes of sensitivity of P_{kl} with respect to injection at buses i and j should satisfy

$$\begin{aligned} \left| \frac{\partial P_{kl}}{\partial P_k} \right| &> \left| \frac{\partial P_{kl}}{\partial P_i} \right| \\ \left| \frac{\partial P_{kl}}{\partial P_l} \right| &> \left| \frac{\partial P_{kl}}{\partial P_i} \right| \quad \text{if } i \neq k, l \end{aligned} \quad (5.114)$$

These inequalities effectively define the physical property of the localized response of a line flow in transmission line $k-l$ with respect to power injections at different buses. To show this, consider $(\partial P_{kl})/(\partial P_k) = a$, $(\partial P_{kl})/(\partial P_l) = b$, and $(\partial P_{kl})/(\partial P_i) = c$. $|a|$, $|b|$, and $|c|$ represent the magnitudes of the contribution of power injected into buses k , l , and i with respect to the line flow P_{kl} ; the signs determine the flow direction. A meaningful magnitude of a line-flow distribution factor is one that satisfies Eq. (5.114), which is effectively a localized response property of a transmission line flow with respect to injection at various buses; buses further away, k , should have smaller (in magnitude) impact on line flow

than k and l .⁴ This usually does not show if one chooses an arbitrary reference bus to calculate distribution factors. To ensure that Eq. (5.114) holds, it has been proposed in Ref. [31] to choose a very specific shift factor β_{kl} so that values of distribution factors at bus k and bus l have the same magnitudes but opposite signs, that is

$$\beta_{kl} = -\frac{D_{kl}^n(i) + D_{kl}^n(j)}{2} \quad (5.115)$$

This β_{kl} makes $|a| = |b| > |c|$, so Eq. (5.114) is always satisfied. Consequently, the choice of β_{kl} results in a transparent localized response property of a power network with respect to balanced pairs of power injections. With this result in mind, the new distribution factors for transmission line from i to j are defined in Ref. [31] as follows:

$$D_{kl} = D_{kl}^n + \beta_{kl} \mathbf{1} \quad (5.116)$$

5.3.3.4 Distribution-Factor-Based Clustering Given the values of distribution factors at all buses of the network, one could separate these buses into two groups: one group with positive distribution factors and the other with negative distribution factors. Recall that the sign of distribution factors only determines if injection increases or decreases the flow in the line of interest.

Next, it follows from Eq. (5.105) that if all buses associated with a particular bilateral transaction⁵ have similar distribution-factor values, the net impact of that transaction on the congested line is very small. In order to reduce complexity, the transactions that have an impact less than a certain percentage, for example, 5%, could be neglected. Based on this, one can then define clusters of buses that affect the power flow in a line of interest in a similar way. These were introduced in Ref. [31] to compute so-called congestion clusters of buses contributing the most to a specific line-flow limit violation (“congestion”).

DEFINITION 5.3.1 The congestion cluster 1 for line $k-l$ consists of a set of buses i the distribution factors of which are very large and are electrically closest to the line of interest.

DEFINITION 5.3.2 The congestion clusters number 2, 3, and higher for line $k-l$ consist of sets of buses i whose differences of distribution-factor values with respect to line $k-l$ are smaller than 5%.

⁴ This follows from the inequality $a > c > b$, which always holds if the power flows from bus k to l because only the portion of P_i that reaches bus k or l enters line $k-l$; therefore, $|a - c|$ or $|b - c|$ cannot be larger than $|a - b|$. In other words, the power transaction between buses k and l should have a larger portion contributing to the line flow connecting these two buses than any other transactions; if the flow direction changes, the relation is the opposite, that is, $a < c < b$.

⁵ The term bilateral *transaction* is used here to represent a pair of balanced power injections.

It follows from these two definitions that buses in the first congestion cluster generally have distribution factors much larger (in magnitude) than the buses in the higher enumerated clusters. Ultimately, buses that are electrically very far away from the line $i-j$ will have relatively small distribution factors, and their impact on the congested line may be negligible. This localized effect cannot be seen without introducing an appropriate shift factor defined in Eq. (5.115).

As a result of the creation of these congestion clusters on a very large power-system network that contains thousands of buses, one only has to look at the clusters instead of the individual buses. These simplifications are important for effective on-line congestion management by both system users and system providers. Methods for managing system inputs to ensure line flows within the operating constraints based on this concept are described in Chapter 14.

Example 5.3.3 Here we illustrate the newly introduced line distribution factors and their use for clustering on the IEEE 39-bus system [31]. For this system only two lines are analyzed.

In the case 1, the line of interest is the line connecting buses 16 and 19 as shown in Figure 5.6. Since this line is the only connection to the rest of the network for the subset of buses 19, 20, 33, and 32, these buses form a separate cluster, cluster 2, if the line 16–19 is congested. The distribution factors are

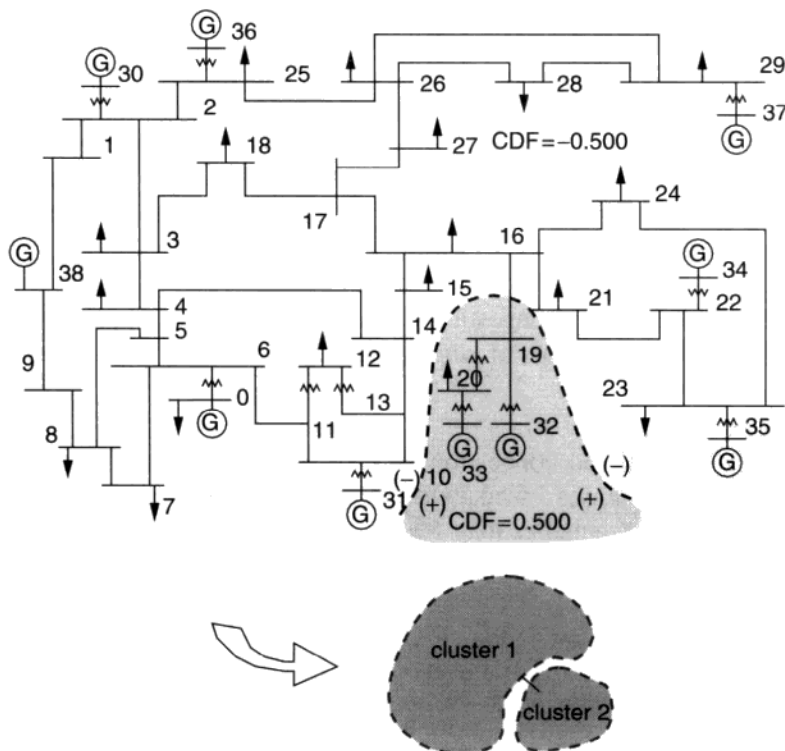


FIGURE 5.6 Congestion case 1: Line 16–19.

0.500 for buses in this cluster and -0.500 for the other buses. In other words, if a bilateral transaction occurs between buses only within cluster 1 or cluster 2, there will be no power flow through the congested line; if a bilateral transaction is made across clusters, 100% of the transaction will flow through the congested line. In this case, there are only two clusters and the boundary is the congestion interface line 16–19.

The second case of congestion clusters is more generalized. Consider the line 4–14 as shown in Figure 5.7. Unlike case 1, buses on both sides of the congestion interface are still connected to each other via other uncongested lines. The distribution-factor values for each bus and cluster are listed in Table 5.7. In this case, cluster 1 is the congestion-sensitive cluster and the other three clusters are less sensitive congestion clusters. All buses in cluster 4 are connected to the rest of the system via bus 16; therefore they all have the same distribution-factor values as bus 16.

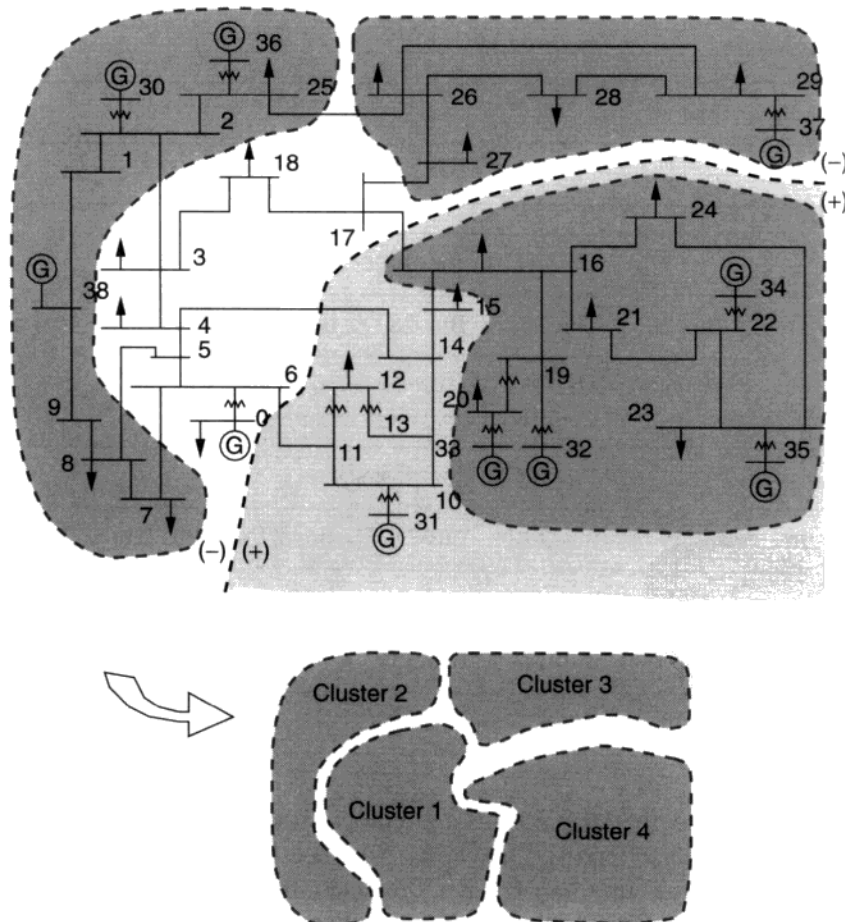


FIGURE 5.7 Congestion case 2: Line 4–14.

TABLE 5.7 Congestion Distribution Factors (CDFs) and Clusters for the IEEE 39-Bus System (Case 2: Line 4–14)

CDF for congestion-sensitive cluster (cluster 1)						
Bus 3	Bus 4	Bus 5	Bus 6	Bus 10	Bus 11	Bus 12
-0.1512	-0.3372	-0.1280	-0.0894	0.1087	0.0449	0.1087
CDF for cluster 2						
Bus 1	Bus 2	Bus 7	Bus 8	Bus 9	Bus 25	Bus 30
0.1210	-0.1254	-0.1041	-0.1115	-0.1157	-0.1120	-0.1254
Bus 36	Bus 38					
-0.1120	-0.1184					
CDF for cluster 3						
Bus 26	Bus 27	Bus 28	Bus 29	Bus 37		
-0.0606	-0.0364	-0.0606	-0.0606	-0.0606		
CDF for cluster 4						
Bus 16	Bus 19	Bus 20	Bus 21	Bus 22	Bus 23	Bus 24
0.0668	0.0668	0.0668	0.0668	0.0668	0.0668	0.0668
Bus 32	Bus 33	Bus 34	Bus 35			
0.0668	0.0668	0.0668	0.0668			

We remark here that the 39-bus system is still a relatively small system compared to a realistic power network. All buses in this system are tightly connected. Therefore, in some congestion cases, the entire system is a single congestion cluster 1. This indicates that significant simplifications can only be seen on very large networks; for examples of this, see Ref. 31.

5.3.4 $P-\delta$ Load-Flow Problem in Deregulated Industry

The problem of establishing bounds on system inputs so that an operationally acceptable (secure) solution to the $P-\delta$ problem exists is important independent of the specific industry structure in place. Nevertheless, a stationary analysis problem formulation varies, depending on the specific industry structure-dependent operating rules.

Here we give a brief summary of the load-flow-analysis-related problems of direct interest for operating a transmission system in which system inputs are defined in the electricity market. Only balanced transactions (power sales and purchases) between parties are handled by a transmission system provider. The balancing process generally takes place through separate trades in the electricity markets.

A system operator must establish measures of how much a transmission system can accommodate and the order in which the requests for using the system are served. One way in which the required stationary analysis in the regulated industry differs from the analysis necessary to answer these questions in the deregulated industry is that a so-called available transfer capability (ATC) is a nonunique, operating-rule-dependent notion. Depending on the rules under which requests for transmission are served, the bounds on secure power injections at specific bus locations will vary.

In what follows we first recall a definition of a transmission-system capacity⁶ related to the basic notion of secure operating regions. Next, we briefly summarize several possible notions of transmission capability recently introduced in Refs. [32,33] and Chapter 3 of Ref. [34]. The concepts reviewed in this section were published in direct collaboration with Professor Francisco Galiana during his sabbatical visit at MIT.

5.3.4.1 Security Regions and Available Transfer Capability The concept of security regions is very useful in conceptualizing and, under certain conditions, in explicitly characterizing the multidimensional security margins of power networks in terms of controllable parameters. The security margins are crucial in defining any type of power interchange and its corresponding capability. One can conceptualize security regions under steady-state or transient-state conditions or both transient and steady-state conditions [32].

In its most general form, a security region S is a set of vector quantities, $\theta(t) = (x(t), y(t), d(t))$, for which the power network satisfies all steady-state and transient operational requirements under both the existing network topology and a set of contingency-degraded network topologies. In order to understand the most general concept of a security region consider that a power system can be characterized by a set of differential-algebraic equations of the form given earlier

⁶ Apparently replaced by the term available transfer capability (ATC) in the present industry restructuring debate.

in Eqns. (4.50) and (4.51)

$$\frac{dx(t)}{dt} = f(x(t), y(t), d(t), t) \quad (5.117)$$

and

$$g(x(t), y(t), d(t), t) = 0 \quad (5.118)$$

with

$$f(x(0), y(0), d(0), 0) = 0 \quad (5.119)$$

that is, where everything is in stable equilibrium at $t = 0$. The quantity x is the dynamic equation state vector (machine and load dynamics) while y is the load-flow state vector (P and Q injections, voltage magnitudes and phase angles, power flows, phase-shifters, tap-changers). The vector d is a disturbance and parameter vector, which in its most general form can be assumed to represent all bus-load model parameters as well as all fault and contingency data, machine parameters, and any other system parameter.

Equations (5.117) to (5.119) model the load flow and the system dynamics for the existing as well as for all possible contingency network topologies and system dynamics. The disturbance vector $d(t)$ describes all disturbances including faults, load changes, and outages with respect to which the system must remain stable. In addition to the stability requirements, the system variables must satisfy a number of steady-state operational inequalities for line flows and voltage and frequency limits. Both the steady-state stability and the stability requirements can be expressed in the form⁷

$$h(x(t), y(t), d(t), t) \leq 0 \quad (5.120)$$

Then the security region S can be defined as the set of initial states $\theta(0) = (x(0), y(0), d(0))$ that satisfy Eqs. (5.117) to (5.120) for the set of disturbances defined by $d(t)$, $t \geq 0$, namely,

$$S = \left\{ \theta(0) \left| \begin{array}{l} \frac{dx(t)}{dt} = f(\theta(t), t), \\ h(\theta(t), t) \leq 0 \end{array} \right. \right\} \quad (5.121)$$

To find such a limit, even for a simple system, normally requires a sequence of simulations that repeatedly vary the generation level (control) until it becomes impossible to meet all security constraints. A general tool to mechanize the recursive simulation process and find arbitrary boundaries of the security region for arbitrary power systems is reported in Ref. [10].

An extensive analytic solution for the security boundary problem in the state and parameter space is presented in Chapters 7 and 8 for the differential-algebraic

⁷ The inequalities are time-varying since the system variables have different limits during the transient and steady-state conditions.

equation problem on very large systems with constraints i.e. hard limits introduced in Chapter 10 and use on a very large (8000 bus) system for computational but non simulation type, solution of the security boundary problem is demonstrated in Chapter 9. Security boundary is defined as the boundary of a intersection of the viability (the region where operating constraints, or hard limits like (5.120) are satisfied) and the feasibility (the region where the operating point can move within the parameter-state space without losing stability during contingencies or just regular operation) boundaries. An alternate definition for the security boundary moves it back from the surface just described by a fixed margin as is done in Chapters 7–10.

One should remember in planning operating practices that it is impractical to compute and store very large dimensional surfaces for security for a realistically large number of contingencies like the 8000 bus system in Chapter 10.

5.3.4.2 Alternative Definitions of Available Transfer Capability More precise definitions of transmission capability are clearly needed, one which can accommodate the existing regulated power exchanges as well as multilateral interchanges in potential future open networks. Four definitions are discussed, each of which provides a different perspective of the kind of exchanges that the network can provide.

DEFINITION 5.3.3 The system transmission capability (STC) is the maximum total generation, incremental above a normal point of operation that can be securely⁸ transmitted to the set of loads. The STC is essentially the conventional definition of the transmission capability.

DEFINITION 5.3.4 The bus transmission capability (BTC) is the maximum amount of power at a given network bus, incremental above a given operating point, that can be securely injected into or extracted from the network regardless of its destination or origin. The BTC can be calculated for each bus.

The BTC is the maximum possible generation (or load) at each bus, incremental from a given operating point, regardless of the bus or buses to which (from which) this power is delivered (received). The BTC defines an upper bound on the capability to send to or receive power from any other buses in the network regardless of the consequences that operation at this bus maximum may have on the capability to send to or receive power from other network buses. Normally, it will not be possible to operate at this maximum since it may sharply reduce the transmission capability of other buses. Nevertheless, the BTC does provide a measure of transmission capability unique to each bus, which could be useful

⁸ Securely implies that all steady-state and transient operational and contingency conditions are met. In this chapter only steady-state security conditions are studied. Chapters 7 and 8 offer the most general treatment of system security.

to assess the degree to which a bus can participate in power interchanges. For example, the BTC can serve as an upper bound on any potential interchange transaction to or from this bus.

DEFINITION 5.3.5 The bilateral transmission capability (BITC) is the maximum amount of power at a given network bus, incremental above a given operating point, that can be securely injected into (extracted from) the network and transmitted to (from) another specific bus. The BITC can be calculated for each pair of generation and load buses.

The BITC is a special case of the BTC assuming a purely bilateral exchange of power between two specified buses. Once again, the BITC establishes an upper bound on the possible power exchanges through the network between two buses regardless of the possible impact that operation at this maximum would have on other potential interchanges. In solving for the BITC, the load flow permits real-power changes from the given operating point in only the sending (ΔP_i) and receiving buses (ΔP_j) so that

$$\Delta P_i + \Delta P_j = \Delta P_{i,j}^{\text{loss}} \quad (5.122)$$

where $\Delta P_{i,j}^{\text{loss}}$ is the incremental transmission loss due to the transaction between buses i and j . Again, one important application of the BITC is a bound on any potential bilateral power exchanges between two buses. The BITC also can be generalized to multilateral exchanges involving sets of sending and receiving buses.

DEFINITION 5.3.6 The uniform bus transmission capability (UBTC) is the maximum amount of power at a network bus, incremental above a given operating point, that can be securely injected into or extracted from the network assuming a uniform allocation of transmission resources to each generation bus. The UBTC can be calculated for each bus or for pairs of generator and load buses.

In a single regulated utility, the uniform allocation of resources to the generators is normally done through economic dispatch. In an open system, the motivation for the UBTC is to prevent any single generator from hoarding the available transmission capability at the expense of other possible transactions. Under this approach, each generating bus would be assigned a “fair” percentage of the available transmission capability that would be used up to its maximum possible absolute power level dependent on the capability of the network and consistent with all other generation buses also trying to maximize their output. Variations of this definition include (1) leaving the loads free to find the best possible UBTC; (2) requiring specific multilateral exchanges between specified groups of generators and loads.

The function to be optimized in order to find the system transmission capability, STC, is,

$$\text{TC}(\theta) = \sum_{j=1}^{k+1} \Delta P_{G,j} \quad (5.123)$$

where $k + 1$ is the number of generators (including slack) and $\Delta P_{G,j}$ is the incremental output of generator j from its existing operating point. In this case, the loads may be assumed to be free to vary with respect to the present operating point perhaps within some prespecified limits, or they may be required to vary uniformly. The value of the STC will be higher for loads allowed to be free than for that for loads that are forced to vary uniformly. For an elaborate illustration of the relations between transmission capability and security regions, see Ref. [10].

5.3.4.3 Available Transfer Capability and Security Constraints All four definitions of transmission capability can be systematically expressed in terms of the security region S defined in Eq. (5.121) as follows. Let TC be a generic term for any of the transmission capability definitions. Thus, as defined earlier, TC is some type of incremental power injection and therefore a function of θ , $\text{TC}(\theta)$.

DEFINITION 5.3.7 The ATC is a maximum power transfer within the requirements of the security region, and it can be computed as

$$\text{ATC} = \max_{\theta \in S} \text{TC}(\theta) \quad (5.124)$$

Methods introduced earlier are directly applicable to estimating ATC in various industry setups.

5.3.4.4 Possible Mathematical Framework for Stationary Analysis in Deregulated Industry

Next, we summarize a mathematical framework and a set of methods for the analysis of the various types of existing and potential future transactions recently given in Refs. [32,33] and Chapter 3 of Ref. [34]. The framework is consistent with existing models and tools of power-network analysis, namely, load flow. The framework makes it possible to analyze systematically all aspects of power-system operation and planning in the world of transactions, including loss allocation, transmission network usage, congestion management, and the calculation of available transfer capability or ATC.

We begin by proposing a general method for characterizing bilateral transactions between any type of trading entity, be it generator, load, pool, or marketer. Similarly, the notion of a transactions network is presented as a means of ensuring that all possible transactions are consistent with the physical bus loads and generators and that, at each node, the power balance is satisfied.

It will be generally assumed throughout this section that bilateral transactions are independently determined by market forces and that they therefore represent the system inputs. It is shown in Ref. [34], Chapter 3, that all transactions,

regardless of how they are obtained, including the optimal pool transactions, have bilateral generator-to-load (or bus-to-bus) equivalents. The calculation of these equivalent bus-to-bus transactions is necessary to be able to allocate a component of the transmission network usage and losses to individual contracts.

5.3.4.5 Framework for the Analysis of Power Transactions In contrast with the physical network that is composed of lines, transformers, and other real devices conducting real power flows from generators to loads, the virtual transaction network models power transactions among financial entities. Through the virtual network, the transactions define the real power generations and loads. These then fix the real power flows within the physical network, which ultimately define the security of the network. Note, however, that a set of generation levels and loads do not uniquely define a set of transactions.

The general transaction network consists of three types of *financial entities*: (1) the *individual generator-serving entities* represent the selling interests of individual physical generators; (2) the *individual load-serving entities* represent the buying interests of retail loads; and (3) the *trading entities*, which are of three types: (a) *group generator-serving entities* serve the selling interests of groups of individual generators, (b) *group load-serving entities* serve the buying interests of groups of individual loads, and (c) *pure trading entities* trade for their own profit with individual or group entities of any kind. An example of a virtual network of transactions is shown in Figure 5.8. The individual generator-serving entities are G1 through G4, the individual load-serving entities are D1 through D4, while E1 is a group generator-serving entity, E4 is a group load-serving entity, and E2 and E3 are pure trading entities. Generator G1 represents an independent power producer trading directly with D1, E1, and E4. Generators G2 and G3 are

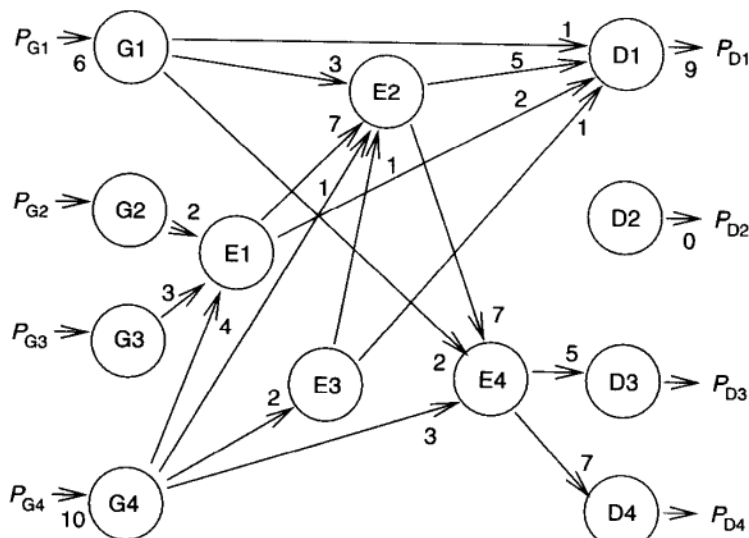


FIGURE 5.8 Example of a virtual network of transactions.

uniquely represented by trading entity E1, which sells to E2 and D1. Finally, the load-serving entity E4 is supplied by G1 and G4 and by the pure trading entity E2. Note that load D2 does not trade with anyone as it has zero consumption.

5.3.4.6 Transaction matrices The market defines the transaction network according to the type of bilateral trades that take place. The values of these trades can be represented by the following variables and relations:

1. GD_{ik} is the contract for power sold by generator i to load k . DG_{ik} is the contract for power bought by load k from generator i . If transmission losses are a separate ancillary service, then

$$GD_{ik} = DG_{ik} \quad (5.125)$$

or, in matrix form, defining the matrices of contracts, GD and DG ,

$$GD = DG \quad (5.126)$$

Generally, $GD_{ik} \geq 0$, that is, generators usually sell to loads and not vice versa, however, if the interests of loads and generators are handled by serving entities, then these could also trade with each other and the above inequality need not necessarily apply.

2. GE_{ik} is the contract for power sold by generator i to trading entity k . With no losses, $GE_{ik} = EG_{ik}$ which is the contract for power bought by trading entity k from generator i . In matrix form, without losses, then

$$GE = EG \quad (5.127)$$

3. ED_{ik} is the contract for power sold by trading entity i to load k , which must be equal to DE_{ik} which is the contract for power received by load k from trading entity i . In matrix form,

$$ED = DE \quad (5.128)$$

4. EE_{ik} is the contract for power sold by trading entity i to trading entity k . Since there are no losses in such transactions, it follows that this contract must be equal to the negative of the contract for power sold by entity k to entity i ,

$$EE_{ik} = -EE_{ki} \quad (5.129)$$

or, in matrix form,

$$EE = -EE^T \quad (5.130)$$

Because a trading entity will not trade with itself, it is assumed that $EE_{ii} = 0$. The reciprocal nature of the EE -type transactions does not apply to GD

or GE transactions; that is, the power sold by generator i to load k , GD_{ik} , has no relation whatsoever to the power sold by generator k to load i , GD_{ki} .

5. It is also possible for generator-serving entities to trade with other generator-trading entities and likewise for load-serving entities. In this case, one can define the quantities GG_{ik} and DD_{ik} to characterize such trades. It is, however, possible to declare that the matrices GG and DD are zero without loss of generality if one considers the generator and load-serving entities as just another set of trading entities. In this case, the GG and DD matrices would be part of the EE matrix of trading entity contracts.

From the definitions of bilateral matrices among generators, loads, and trading entities, it is possible to express the physical generators and loads in terms of the contracts. We assume that the network has N_b buses and that at each bus there can exist both a generator and a load. Similarly, the number of trading entities is taken to be N_e . Then, assuming $GG = 0$ as just argued, the power generated at bus i , P_{gi} , can be expressed as

$$P_{gi} = \sum_{k=1}^{N_b} GD_{ik} + \sum_{j=1}^{N_e} GE_{ij} \quad (5.131)$$

or, in matrix form,

$$P_g = GDu_b + GEu_e \quad (5.132)$$

where u_b is a vector of 1's of dimension N_b while u_e is a vector of 1's of dimension N_e . Next, the power balance for an arbitrary load at bus i , P_{di} , yields

$$P_{di} = \sum_{k=1}^{N_b} DG_{ki} + \sum_{j=1}^{N_e} DE_{ji} \quad (5.133)$$

which in equation form becomes

$$P_d = DG^T u_b + DE^T u_e \quad (5.134)$$

Finally, pure trading entities do not directly generate or consume power, so that any trading entity i must sell all of its purchases to either other trading entities or to loads,

$$\sum_{j=1}^{N_b} EG_{ij} = \sum_{k=1}^{N_e} EE_{ik} + \sum_{j=1}^{N_b} ED_{ij} \quad (5.135)$$

This can be put in matrix form as

$$-EG^T u_b + EEu_e + EDu_b = 0 \quad (5.136)$$

All of these bilateral matrices and relations can be systematically represented by the transaction matrix T ,

$$T = \begin{bmatrix} 0 & GD & GE \\ DG^T & 0 & DE^T \\ -EG^T & ED & EE \end{bmatrix} \quad (5.137)$$

such that

$$\begin{bmatrix} P_g \\ P_d \\ 0 \end{bmatrix} = \begin{bmatrix} 0 & GD & GE \\ DG^T & 0 & DE^T \\ -EG^T & ED & EE \end{bmatrix} \begin{bmatrix} u_b \\ u_b \\ u_e \end{bmatrix} \quad (5.138)$$

Note that the diagonal blocks GG and DD have been assumed to be zero without loss of generality according to the arguments previously offered. Under lossless assumptions, Eq. (5.138) can be expressed in terms of the purchased quantities only, that is, DG , DE , and EG by using Eqs. (5.126) to (5.128). Then

$$T = \begin{bmatrix} 0 & DG & EG \\ DG^T & 0 & DE^T \\ -EG^T & DE & EE \end{bmatrix} \quad (5.139)$$

and

$$\begin{bmatrix} P_g \\ P_d \\ 0 \end{bmatrix} = \begin{bmatrix} 0 & DG & EG \\ DG^T & 0 & DE^T \\ -EG^T & DE & EE \end{bmatrix} \begin{bmatrix} u_b \\ u_b \\ u_e \end{bmatrix} \quad (5.140)$$

As an example, for the transaction network of Figure 5.8 the transaction matrix takes the form

$$T = \begin{bmatrix} 0 & 0 & 0 & 0 & 1 & 0 & 0 & 0 & 0 & 3 & 0 & 2 \\ 0 & 0 & 0 & 0 & 0 & 0 & 0 & 0 & 2 & 0 & 0 & 0 \\ 0 & 0 & 0 & 0 & 0 & 0 & 0 & 0 & 0 & 3 & 0 & 0 \\ 0 & 0 & 0 & 0 & 0 & 0 & 0 & 0 & 0 & 4 & 1 & 2 \\ 1 & 0 & 0 & 0 & 0 & 0 & 0 & 0 & 0 & 2 & 5 & 1 \\ 0 & 0 & 0 & 0 & 0 & 0 & 0 & 0 & 0 & 0 & 0 & 0 \\ 0 & 0 & 0 & 0 & 0 & 0 & 0 & 0 & 0 & 0 & 0 & 0 \\ 0 & 0 & 0 & 0 & 0 & 0 & 0 & 0 & 0 & 0 & 0 & 5 \\ 0 & 0 & 0 & 0 & 0 & 0 & 0 & 0 & 0 & 0 & 0 & 0 \\ 0 & -2 & -3 & -4 & 2 & 0 & 0 & 0 & 0 & 7 & 0 & 0 \\ -3 & 0 & 0 & -1 & 5 & 0 & 0 & 0 & -7 & 0 & -1 & 7 \\ 0 & 0 & 0 & -2 & 1 & 0 & 0 & 0 & 0 & 1 & 0 & 0 \\ -2 & 0 & 0 & -3 & 0 & 0 & 5 & 7 & 0 & -7 & 0 & 0 \end{bmatrix} \quad (5.141)$$

5.3.4.7 Load-Flow Equations in Terms of Transaction Matrices For simplicity, we assume that the load-flow equations are governed by a relation between the net power injections, denoted by the N_b -dimensional vector⁹ P , and

⁹ $N_b = n + k + 1$, including the slack bus.

the voltage phase angles δ of the same dimension,¹⁰ that is

$$P = P_g - P_d = P(\delta) \quad (5.142)$$

where $P(\cdot)$ is a function of the angles δ representing the load-flow equations. Using Eq. (5.140), one can express the load-flow equations in terms of the specified bilateral contracts. For the lossless case, this becomes

$$P = (DG - DG^T)u_b + (EG - DE^T)u_e = P(\delta) \quad (5.143)$$

while the lossy case is discussed in a subsequent section.

The importance of Eq. (5.143) lies in its ability to express network quantities such as transmission flows in terms of the market-specified bilateral contracts. From such a relation, as is shown next, one can derive how each individual contract affects the flows in the network and hence how usage-based tariffs can be systematically set up. In more elaborate variations of this load-flow model, it is also possible to establish a relationship between the bilateral contracts and reactive power injections and voltage magnitudes.

5.3.4.8 Power-Flow Distribution Factors in Terms of Transaction Matrices

One way to model the impact of a bilateral transaction on the network is to examine the power-flow distribution factors in terms of the transaction matrices. Because of the special nature of the problem, it is useful first to go through the derivation of the flow distribution factors.

Under DC-load-flow assumptions, the term $P(\delta)$ reduces to $B\delta$ (recall Eg. (5.56) earlier), where B is the symmetric load-flow Jacobian matrix. From Eq. (5.143),

$$\delta = B^{-1}[(DG - DG^T)u_b + (EG - DE^T)u_e] \quad (5.144)$$

If we denote the vector of network line power flows as P_f and its relation to the angles through (recall Eg. (5.106))

$$P_f = M\delta \quad (5.145)$$

where M is a matrix dependent on the network topology and the line susceptances, then

$$P_f = MB^{-1}[(DG - DG^T)u_b + (EG - DE^T)u_e] \quad (5.146)$$

The transaction participation factors are found by solving Eq. (5.146) as a linear combination of each individual contract. This can be readily done for the generator to load contracts DG_{ik} since the term $(DG - DG^T)u_b$ can be split into the sum of N_b^2 terms,

$$(DG - DG^T)u_b = \sum_{i=1}^{N_b} \sum_{k=1}^{N_b} u_{ik} DG_{ik} \quad (5.147)$$

¹⁰ That is, no specific angle is arbitrarily selected as the reference.

where u_{ik} is a vector of dimension N_b with all entries equal to zero with the exception of entry i , which is equal to 1, and entry k , which equals -1 . Since the term $B^{-1}u_{ik}$ exists,¹¹ the vector of flow participation factors corresponding to contract DG_{ik} is then given by

$$PP_{ik} = MB^{-1}u_{ik} \quad (5.148)$$

so that component of the vector of line flows, P_f , due to the generation-to-load contracts becomes

$$P_f = \sum_{i=1}^{N_b} \sum_{k=1}^{N_b} PP_{ik} DG_{ik} \quad (5.149)$$

An illustrative example of the generation-to-load transaction participation factors is that of a three-bus system with identical line susceptances and with a generator and load at each bus. The vector of line flows then becomes

$$P_f = \begin{bmatrix} \frac{2}{3} \\ -\frac{1}{3} \\ \frac{1}{3} \end{bmatrix} (DG_{12} - DG_{21}) + \begin{bmatrix} -\frac{1}{3} \\ \frac{2}{3} \\ \frac{1}{3} \end{bmatrix} (DG_{23} - DG_{32}) + \begin{bmatrix} \frac{1}{3} \\ \frac{1}{3} \\ \frac{2}{3} \end{bmatrix} (DG_{13} - DG_{31}) \quad (5.150)$$

The flow participation factors corresponding to the contracts EG_{ik} and DE_{ik} are not as evident, however. Whereas it can be shown that the term $(EG - DE^T)u_e$ is in the range space¹² of B , Eq. (5.146) cannot be solved for the effect on the flows of each individual EG_{ik} and DE_{ik} contract, given that the corresponding vector is not in the range space of B . Intuitively, this is correct, since a contract between a generator and a trading entity only specifies where the power is injected into the network but not the bus or buses where this power is consumed. Thus unless one knows to what other entity the power bought by an entity is sold, one cannot calculate its impact on the power flows. The difficulty is that the power bought by a trading entity may be sold in part to some loads and in part to numerous other trading entities, which, in turn, may also trade this power in many ways. Eventually the power sold by a generator to a trading entity finds its way to the loads. However, the original power is split into fractions that depend on the number and type of entity-to-entity and entity-to-load contracts.

Although the individual impact of generator-to-entity or entity-to-load transactions on the power flows cannot be evaluated, their combined impact can. This is done by showing that all transactions involving trading entities can be reduced to an equivalent parallel set of generation-to-load transactions, the impact of

¹¹ This is true since u_b belongs to the null space of B as well as being orthogonal to u_{ik} , thus implying that u_{ik} belongs to the range space of B .

¹² This is true since it can be shown that u_b is orthogonal to $(EG - DE^T)u_e$ by the fact that the combined power bought from all generators by all the trading entities, $u_b^T [EG] u_b$, must equal the combined power sold by all trading entities to the loads, $u_b^T [DE^T] u_e$.

which can be analyzed through the generator-to-load transaction participation factors computed earlier. This approach essentially says that each generator-to-load transaction gets assigned a correction, the total of which accounts for the effect of all transactions with and among trading entities. Any charges for network usage due to transactions involving trading entities thus get passed on to the equivalent generator-to-load transactions, which, it can be argued, are the ultimate payers for all transmission costs incurred. For details of this, including examples, see [34].

5.3.4.9 Incremental Power-Balance Equation The key relation in the subsequent loss allocation analysis is the incremental power-balance equation, which takes the form

$$\sum_{i=1}^{N_b} \alpha_i dP_i = 0 \quad (5.151)$$

where dP_i is the net power injection at bus i given by

$$dP_i = dP_{Gi} - dP_{Di} \quad (5.152)$$

The parameters α_i can be found in two ways: one is from the load-flow equations and the other from the sensitivity coefficients of the loss with respect to the injections. These two equivalent methods are presented here.

From the power-flow equations of Eq. (5.142), it follows that under incremental changes,

$$dP = dP_G - dP_D = \left[\frac{\partial P(\delta)}{\partial \delta} \right] d\delta \quad (5.153)$$

Since the load-flow Jacobian matrix ($\partial P / \partial \delta$) is singular (normally of full rank -1), there exists a nonzero vector α such that

$$\left[\frac{\partial P(\delta)}{\partial \delta} \right]^T \alpha = 0 \quad (5.154)$$

Thus, from Eqs. (5.153) and (5.154) this value of α , corresponding to a vector spanning the null space of the transpose Jacobian, satisfies the incremental power-balance equation.

An alternative way of deriving the parameter vector α is to start with the standard power-balance relation,

$$\sum_{i=1}^{N_b} dP_i = dP_L \quad (5.155)$$

where P_L stands for the system transmission losses. If we let bus k be the slack bus, from standard load-flow sensitivity analysis, it is well known that dP_L can

be expressed in terms of $N_b - 1$ of the incremental injections with the exclusion of the slack-bus incremental injection dP_k . Then

$$dP_L = \sum_{i=1}^{N_b} \left[\frac{\partial P_L}{\partial P_i} \right]_k dP_i \quad (5.156)$$

where $[\partial P_L / \partial P_i]_k$ is the sensitivity of the losses P_L with respect to P_i with bus k as the slack. Note that the k th sensitivity coefficient is 0. Thus from Eqs. (5.155) and (5.156),

$$\sum_{i=1}^{N_b} \left(1 - \left[\frac{\partial P_L}{\partial P_i} \right]_k \right) dP_i = 0 \quad (5.157)$$

from which it follows that, within an arbitrary nonzero constant, a possible set of values for α_i is

$$\alpha_i = 1 - \left[\frac{\partial P_L}{\partial P_i} \right]_k \quad (5.158)$$

We note in passing that since the choice of the slack bus is always arbitrary, from Eq. (5.157), the following useful identity can be easily proven:

$$\frac{1 - \left[\frac{\partial P_L}{\partial P_i} \right]_k}{1 - \left[\frac{\partial P_L}{\partial P_j} \right]_k} = 1 - \left[\frac{\partial P_L}{\partial P_i} \right]_j \quad (5.159)$$

5.3.4.10 Distribution-Factor-Based Congestion Clustering The sensitivity of system constraints with respect to the power quantities injected into different buses as the transactions are implemented generally depends on both the power quantity injected and on the electrical distance of the power injection to the system constraint of interest. Because of this, it is necessary to develop sensitivity indicators that are easy to understand and to use by both transmission providers and by the system users. We next summarize the notion of congestion clusters recently introduced in Ref. [31] for this purpose.

The simplest specification necessary is the power quantity $P_{Gi} = P_{Lj}$ of the bilateral transaction requiring the use of the transmission system between a seller at bus i and the user at bus j .

DEFINITION 5.3.8 Mathematically, each bilateral transaction between a power seller at bus i and power purchaser at bus j is of the following form:

$$C_k = (0 \quad 0 \quad P_{Gi} \quad 0 \quad \dots \quad 0 \quad -P_{Lj} \quad 0 \quad 0 \quad \dots)^T \quad (5.160)$$

where

$$P_{Gi} - P_{Lj} = 0 \quad (5.161)$$

P_{Gi} and P_{Lj} stand for injections into bus i and taken out at bus j respectively.

DEFINITION 5.3.9 Similarly, a multilateral contract involving more than one supplier and/or one consumer can be expressed as:

$$\underline{C}_k = (0 \quad 0 \quad P_{G_i} \quad P_{G_{i+1}} \quad \dots \quad 0 \quad -P_{L_j} \quad -P_{L_{j+1}} \quad \dots)^T \quad (5.162)$$

where

$$\sum_i P_{G_i} - \sum_j P_{L_j} = 0 \quad (5.163)$$

Because each (multi) pair of candidate transmission users has to be balanced, it must satisfy the equality

$$\underline{1}^T \underline{C}_k = 0 \quad (5.164)$$

where $\underline{1}$ is a vector with all elements equal to 1. Then the distribution factors for the transmission line from k to l proposed in Ref. [31] can be obtained as

$$D_{k,l} = D_{k,l}^n + \beta_{k,l} \underline{1} \quad (5.165)$$

where

$$\beta_{k,l} = -\frac{D_{k,l}^n(k) + D_{k,l}^n(l)}{2}, \quad (5.166)$$

Then, for transaction k specified by \underline{C}_k [Eq. (5.160)], the portion of the line flow $P_{i,j}$ on the transmission connecting buses i and j contributed by this transaction, $P_{k,l}^i$, can be calculated as

$$P_{k,l}^i = D_{k,l}^T \underline{C}_k \quad (5.167)$$

Based on these derivations it follows that the magnitude of a CDF at each bus computed for a transmission line indicates the sensitivities of the line flow with respect to the power injection of a bilateral transaction; the sign of the CDFs at each bus indicates if the power injection at that bus will increase or relieve the congestion of the line of interest.¹³

5.4 DECOUPLED REACTIVE-POWER-VOLTAGE $Q-V$ LOAD-FLOW PROBLEM

Under the real-reactive-power decoupling assumption, the reactive-power–voltage problem is defined as the problem of determining load voltages $E_1 \dots E_n$ for specified reactive power load demand $Q_1 \dots Q_n$; generator voltages $E_0 \dots E_{n+1} \dots E_{n+k}$ are assumed known, as long as sufficient reactive power

¹³ Of course, the actual impact of a transaction is determined by both power sending and receiving buses and follows the formula (5.167).

reserves at generators are available.¹⁴ Under the decoupling assumption all phase angles are assumed to be specified parameters in the problem of interest. A mathematical formulation of the reactive-power–voltage problem follows directly from the load-flow equations (5.11) defining the reactive-power balance at all loads which are restated here as

$$E_i^2 \left[\left(\sum_{k \neq i} B_{ik} \right) - b_i \right] - E_i \sum_{k \neq i} E_k B_{ik} \sin(\delta_{ik} - \zeta_{ik}) - Q_i = 0, \quad i = 1, \dots, n \quad (5.168)$$

where b_i is the shunt capacitance at bus i , and $B_{ik} = Z_{ik}$. Typical inequality constraints directly relevant for reactive-power–voltage support are

$$Q_{G^i}^{\min} < Q_{G^i} < Q_{G^i}^{\max}, \quad i = 0, n + 1, \dots, n + k \quad (5.169)$$

$$E_i^{\min} < E_i < E_i^{\max}, \quad i = 0, 1, \dots, n + k \quad (5.170)$$

As it was introduced in Section 4.3 of Chapter 4 for a two-bus system, reactive-power steady-state stability problems are directly related to the operating conditions under which a voltage solution may not exist within the given operating limits. Similarly to the P – δ problem discussed earlier, in this section the prime concern is with solution existence.

5.4.1 Problem Complexity as a Function of Load Models Used

The main theoretical challenge arises here because loads are modeled as nonlinear constant-power models. It is a simple exercise to show that in the case when loads are modeled as either constant-impedance or constant-current devices, the reactive-power–voltage problem defined in Eq. (5.168) degenerates into a linear problem of the form

$$Ax = c \quad (5.171)$$

where matrix A and input vector c are defined in the following way [30]:

1. In the case of assumed constant-impedance load models and a lossless transmission system ($\zeta_{ij} \simeq \pi/2$)

$$Q_i = B_{Di} E_i^2, \quad B_{Di} = \text{const}, \quad i = 1, \dots, n \quad (5.172)$$

¹⁴ When the limits on reactive-power generation are reached, a generator bus becomes effectively a load bus, implying change in the number of equations and unknowns.

Eq. (5.168) degenerates into

$$\left(\sum_{j=1}^{j=n} B_{ik} - b_i + B_{Di} \right) E_i - \sum_{j=1}^n B_{ij} E_j \cos \delta_{ij} = \sum_{j=0, n+1}^{n+k} B_{ij} E_j \cos \delta_{ij} \quad (5.173 \& 5.174)$$

The matrix representation of these equations is of the form (5.171), where

$$A = B + \text{diag}(B_{Di}) \quad (5.175)$$

and

$$B = \begin{bmatrix} B_{11} - b_1 & -B_{12} \dots & B_n \\ -B_{21} & (B_{22} - b_2) \dots & -B_{2n} \\ -B_{n1} \dots & & B_{nn} - b_n \end{bmatrix} \quad (5.176)$$

and

$$c^T = [c_1 \dots c_n] \quad (5.177)$$

with

$$c_i = \sum_{j=0, n+1}^{n+k} B_{ij} E_j \cos \delta_{ij} \quad (5.178)$$

and the unknown vector x being a vector of load bus voltages

$$x^T = [E_1 \dots E_n] \quad (5.179)$$

Clearly, as long as network and load parameters are such that matrix A remains nonsingular, the problem of voltage solution nonexistence is avoided. The only remaining question is if the voltage solution to equation of the form (5.171) is within prespecified operating limits, Eq. (5.170), and if it is achievable within the reactive power generation limits, Eq. (5.169).

2. Similarly, in the case of constant-current load models of the form

$$Q_{Di} = \text{Im } \hat{S}_{Di} = E_i I_i \sin \varphi_i \quad (5.180)$$

with φ_i being the load-power factor angle, current I_i is a const (under the constant-current load model assumption), and the power factor $\varphi_i = \text{const}$ (under the real-power-reactive-power decoupling assumption). The reactive-power load-flow equations take on the form of linear equations (5.171) in unknown voltages

$$E = [E_1 \dots E_n]^T \quad (5.181)$$

with the system matrix equal B as defined in Eq. (5.176), and the known vector c

$$c^T = [I_i \sin \varphi_1 \dots I_n \sin \varphi_n]^T \quad (5.182)$$

These particular cases of the reactive-power–voltage problem formulation under simplifying load modeling assumptions show an obvious dependence of any theoretical results concerning the reactive-power–voltage problem on the load models assumed. Any deviation from the assumed load model, all three of which are primitive and arbitrary approximations of an actual load, Chapter 3, could lead to quite different solutions. The hope is that the system would operate in regions with low sensitivity of voltage solution to the choice of load model. Otherwise, there would be too much risk involved in employing theoretical results for estimating regions within which a robust, technically acceptable voltage solution exists. More studies are needed to establish robustness conditions with respect to the load models. The most frequent modeling assumption of constant reactive-power loads leads to a genuine nonlinear problem, the solution of which may not exist, or it may be nonunique. This problem is studied next.

5.4.2 Q–V Problem with Constant-Power Load Models

The reactive-power–voltage (Q – V) problem can be formulated as a nonlinear network problem in two slightly different ways:

- As a nonlinear resistive network with independent sources;
- As a linear resistive network with dependent sources.¹⁵

Both formulations can be found in the recent literature. For completeness we review both in this section. As in the P – δ problem, these formulations are relevant for determining nonconservative bounds on changes in reactive power inputs for which a feasible voltage solution exists. Developments similar to the real-power–phase-angle formulation as a nonlinear resistive network have been reported in Ref. [35]. We first present these results, and indicate their potential use for establishing bounds on reactive-power input changes for which a voltage solution within the prespecified bounds is guaranteed to exist. Next, we review the Q – V problem formulation as a linear resistive network with dependent sources first introduced in Ref. [36].

5.4.3 Q–V Load Flow Problem as a Problem of a Nonlinear Resistive Network with Independent Sources

It is generally less obvious how the reactive-power–voltage problem could be thought of as a resistive network problem than it was in the case with the

¹⁵ Recall that the real-power–phase-angle problem is inherently a problem of nonlinear resistive networks with independent sources.

$P-\delta$ problem formulation [35]. To show this, start with the decoupled reactive-power–voltage load-flow equations (5.168), the form of which under the assumption of negligible transmission line resistances becomes

$$Q_i = -E_i \sum_{k \in K_i} E_k c_{ik} \quad (5.183)$$

where

$$c_{ik} = c_{ki} = B_{ik} \cos \delta_{ik} \quad (5.184)$$

and

$$c_{ii} = B_{ii} - b_i = \sum_{k \in K_i} B_{ik} \quad (5.185)$$

To clarify the sign convention¹⁶ in Eq. (5.183) notice that for inductive transmission lines $B_{ik} < 0$ and capacitive shunts $b_i > 0$, where b_i is a shunt connection at bus i . Because the E_i 's are voltage magnitudes and as such are always positive, write

$$E_i = e^{x_i} \quad (5.186)$$

to form

$$Q_i = - \sum_{k \in K_i} e^{x_i + x_k} c_{ik} \quad (5.187)$$

or

$$Q_i = - \sum_{k \in K_i} f(x_i + x_k) c_{ik} \quad (5.188)$$

Similarly as in the real-power–phase-angle studies, we are concerned with perturbations around the nominal steady state, and therefore we write Eq. (5.188) in a (finite) incremental form as

$$\Delta Q_i = - \sum_{k \in K_i} [f(x_i + x_k + \Delta x_i + \Delta x_k) - f(x_i + x_k)] c_{ik} \quad (5.189)$$

or

$$\Delta Q_i = - \sum_{k \in K_i} h_{ik} (\Delta x_i + \Delta x_k) c_{ik} \quad (5.190)$$

where the function h_{ik} is defined as

$$h_{ik} = e^{x_i + x_k} (e^{\Delta x_i + \Delta x_k} - 1) \quad (5.191)$$

¹⁶ Conventions for reference direction are not consistent throughout the existing literature.

It can be seen that $h_{ik}(\Delta x_i + \Delta x_k)$ is monotonously increasing and restricted to the first and third quadrants in $\Delta x_i + \Delta x_k$. We create a linear system of equations of the form

$$\Delta Q_i = - \sum_{k \in K_i} (\Delta x_i + \Delta x_k) c_{ik} g_{ik} \quad (5.192)$$

where $g_{ik} = g_{ki}$. If we examine solutions of Eq. (5.190) for which $|\Delta x_j| < r$, $j = 1, \dots, n$, then it is only necessary to consider g_{ik} in Eq. (5.192), which are bounded by

$$E_i E_k \frac{e^{-2r} - 1}{-2r} \leq g_{ik} \leq E_i E_k \frac{e^{2r} - 1}{2r} \quad (5.193)$$

Every solution to Eq. (5.190) with bounded Δx_i then corresponds to a solution of Eq. (5.192) with some set of coefficients bounded by inequalities (5.193). We show next that the set of equations (5.190) has a resistive-network interpretation. To put the linear system (5.192) in more recognizable form, rewrite it as

$$-\Delta Q = H_Q \Delta x \quad (5.194)$$

where

$$h_{ik} = c_{ik} g_{ik} = g_{ik} B_{ik} \cos \delta_{ik} \quad (5.195)$$

and

$$h_{ik} = - \sum_{k \in K_i, k \neq i} c_{ik} g_{ik} + 2c_{ii} g_{ii} \quad (5.196)$$

The conventions involved in Eq. (5.183) produce nonpositive off-diagonal entries in the admittance matrix for the power system. If we associate $-\underline{\Delta Q}$ with a set of currents and $\underline{\Delta x}$ with the set of node voltages, then the matrix can be thought of as a conductance matrix of a resistive network with the same topology as the power system. Nodes i and k in the resistive network are connected with positive conductance $-g_{ik} B_{ik} \cos \delta_{ik}$. The conductance to ground at node i is given by

$$h_{ii} = 2g_{ii}c_{ii} + 2 \sum_{k \in K_i} c_{ik} g_{ik} \quad (5.197)$$

$$h_{is} = 2g_{ii} \left(-b_i - \sum_{k \in K_i} B_{ik} \right) + 2 \sum_{k \in K_i} g_{ik} B_{ik} \cos \delta_{ik} \quad (5.198)$$

To verify that the conductances h_{ii} are typically negative, consider perturbations small enough so that

$$g_{ik} \cong E_i E_k \quad (5.199)$$

In this case

$$h_{ii} \cong -2Q_i \quad (5.200)$$

The typical load bus (PQ bus) in the power system has $Q_i > 0$ so that for small disturbances the equivalent resistive network is composed of positive resistors to ground at the nodes corresponding to load buses. The DC-load-flow assumptions of small angles δ_{ik} and voltage magnitudes near unity give for small perturbations

$$h_{ii} \cong -2B_i \quad (5.201)$$

Estimates of the size of perturbations r , for which the shunt connections remain negative, can also be obtained. If we assume

$$-b_i - \sum_{k \in K_i, k \neq i} B_{ik} > 0 \quad (5.202)$$

which is typical at PQ buses, the h_{ii} is maximized if g_{ii} takes on the maximum value possible while each g_{ik} is the minimum. For example, for the voltage-reduction case

$$h_{ii} \leq Q_{is} + \frac{1 - e^{2r}}{2r} Q_{i2} \quad (5.203)$$

where

$$Q_{is} = 2E_i^2 \left(b_i - \sum_{k \in K_i} B_{ik} \right) \quad (5.204)$$

and

$$Q_{i2} = 2 \sum_{k \in K_i, k \neq i} E_i E_k B_{ik} \cos \delta_{ik} \quad (5.205)$$

Since Q_{is} is available from the diagonal entry of the Jacobian of the load-flow solution and

$$Q_i = -\frac{Q_{is} + Q_{i2}}{2} \quad (5.206)$$

the range of r for which Eq. (5.203) is negative can be computed directly. For the American Electric Power Co. AEP 14-bus system given in Ref. [37] the bounds on r at the load buses were computed. The corresponding voltage bounds ranged from 22% to 65%.

Due to presence of shunt capacitances a resistive-network interpretation of the reactive-power–voltage problem is more involved than in the $P-\delta$ problem. To see this, recall the first formulation of an equivalent linear problem (5.194).

For a solution to this resistive network to exist it is necessary for its equivalent conductance matrix H_Q in Eq. (5.194) to preserve a positive-definiteness property. This matrix can be analyzed by rewriting it as

$$H_Q = \bar{B} - \bar{C} \quad (5.207)$$

where \bar{B} is an admittance-like matrix corresponding to the positive resistors only and \bar{C} is a diagonal matrix representing negative conductances to ground. From Eq. (5.192) $\bar{B}_{ik} = g_{ik} \cos \delta_{ik}$, where the g_{ik} satisfy Eq. (5.193).

Instead of requiring diagonal dominance conditions for this, otherwise admittance-like matrix, it is sufficient to guarantee for H_Q to be an M matrix [38,39]. Such an H_Q matrix is called an M matrix if it can be written as

$$H_Q = sI - A, \quad \rho(A) \leq s, \quad A \leq 0 \quad (5.208)$$

where $\rho(A)$ is the spectral radius of A and $A \leq 0$ means that every element of A is non-negative. If $\rho(A) \leq s$, then H_Q is a nonsingular M matrix. There exists a large number of equivalent conditions to the statement “ H_Q is a nonsingular M matrix”. For example, the following are equivalent:

1. H_Q is a nonsingular M matrix
2. $H_Q^{-1} > 0$
3. All the principle minors of H_Q are positive
4. There exists a positive diagonal matrix D such that $H_Q D$ is strictly diagonally dominant

It has been shown in Ref. [35] that one could establish an upper bound on the largest shunt capacitor, which could be added to a primarily inductive transmission network in order to improve voltages without reversing the M -matrix properties of matrix H_Q in Eq. (5.207). This bound is defined as

$$b_i \leq \frac{1}{\frac{x_{ii} + x_{ij}}{(x_{mi} - x_{ji})}} \quad (5.209)$$

for all j and m , where x_{ij} are components of the impedance matrix $X = B^{-1}$ of the inductive part of the network.

This bound is very important since it provides an estimate of the largest effective capacitive support, without reversing qualitatively the response of a primarily inductive network. For example, one can find throughout the literature references to capacitive support that did not improve voltage support as expected [40–45]. Based on this analysis one may conclude that one possible cause for this situation in practice is when matrix H_Q loses its positive definiteness if some capacitances are larger than defined in Eq. (5.209).

Under the condition of H_Q preserving the positive-definiteness property for operating regions within r the Q – V dependence is similar to the P – δ dependence within monotonic operating regions as defined earlier. One could develop an algorithm similar to the algorithm introduced in Ref. [46] for determining bounds on ΔQ_α at any bus α within which voltage solution is guaranteed to exist.

An alternative, less combinatorial approach to finding these bounds is presented next. The approach is based on formulating the Q - V problem as a linear resistive-network problem with dependent sources.¹⁷

5.4.4 Q - V Load-Flow Problem as a Problem of a Linear Resistive Network with Dependent Sources

In order to clarify differences between the problem formulation of the Q - V nonlinear problem as a nonlinear resistive network problem with independent sources [35] summarized earlier, on one side, and the formulation given in [36,37], which is presented in this section, on the other side, the following should be recognized. A general nonlinear resistive-network problem can be thought of as an algebraic problem of n coupled equations in n unknowns of the form

$$g_1(x_1, \dots, x_n) = c_1 \quad (5.210)$$

$$g_2(x_1, \dots, x_n) = c_2 \quad (5.211)$$

$$g_n(x_1, \dots, x_n) = c_n \quad (5.212)$$

where each function g_i depends on *all* unknown variables. Whereas conditions under which a solution to this general problem exists are not known, by recognizing a linear resistive-network structure of the problem class of interest here, it becomes possible to solve this problem in terms of bounds on changes within which a unique solution is guaranteed to exist.

It has been shown in Ref. [37] that the Q - V problem can be formulated based on a particular subclass of the general algebraic problem, Eqs. (5.210) to (5.212), of the form

$$Ax + f(x) = c \quad (5.213)$$

Here each nonlinear function f_i is a function of one variable x_i only. This problem and conditions for its solution existence have been studied extensively in the area of nonlinear monotone networks [47]. In [36,37] the nonlinear reactive-power–voltage problem was formulated as a problem of type (5.213). Here we briefly review this formulation.

Starting with Eq. (5.168), add and subtract $\lambda_i E_i^2$, divide by E_i , and put all terms involving generator voltages on the right-hand side to obtain

$$[(B_{ii} - b_i) - \lambda_i]E_i \sum_{j=1}^n B_{ij}E_j \cos \delta_{ij} + \lambda_i E_i - \frac{Q_i}{E_i} = \sum_{j=0, j=n+1}^{n+k} B_{ij}E_j \cos \delta_{ij} \quad (5.214)$$

¹⁷ This alternative is not possible for the P - δ problem formulation, since the real-power line flows are function of voltage-phase-angle differences, and as such they vary as the operating conditions vary.

or put in a matrix form

$$(\hat{B} - \Lambda)\underline{x} + \underline{f}(\underline{x}) = \underline{c} \quad (5.215)$$

where Λ is a diagonal matrix with the i th diagonal entry equal to λ_i . We note that because $B_{ij} \geq 0$, $E_i > 0$, $-90^\circ < \delta_{ij} < 90^\circ$, we have $c \geq 0$. The function $f(x)$ has the form

$$[f_1(x_1) : \cdots : f_n(x_n)]^T \quad (5.216)$$

where $f_i(x_i) = \lambda_i x_i - Q_i/x_i$. Hence if the load at node i is capacitive, Q_i will be positive and $f_i(x_i)$ will be monotonically increasing for all $x_i \geq 0$ and have a zero at $(Q_i/\lambda_i)^{1/2}$. If the load at node i is inductive, Q_i will be negative and from

$$\frac{df_i(x_i)}{dx_i} = \lambda_i + \frac{Q_i}{x_i^2} \quad (5.217)$$

we see that $f_i(x_i)$ has a minimum at $x_i = (-Q_i/\lambda_i)^{1/2}$ and is monotonically increasing for $x_i > (-Q_i/\lambda_i)^{1/2}$. We also observe that

$$f_i\left(\left(\frac{-Q_i}{\lambda_i}\right)^{1/2}\right) = \lambda_i \left(-\frac{Q_i}{\lambda_i}\right)^{1/2} - \frac{Q_i}{(-Q_i/\lambda_i)^{1/2}} = 2\lambda_i \left(\frac{-Q_i}{\lambda_i}\right)^{1/2} > 0 \quad (5.218)$$

for $\lambda_i > 0$. So $f_i(x_i) > 0$ and monotonically increasing for $x_i > (|Q_i|\lambda_i)^{1/2}$ for all i . The functions f_i for Q_i positive and negative are shown in Figure 5.9.

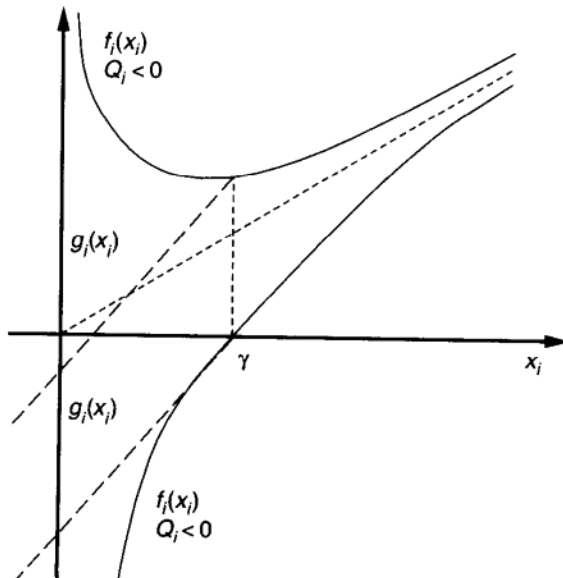


FIGURE 5.9 Nonlinearities in the Q – V decoupled load flow.

Now let $\hat{\lambda} = \max_i \lambda_i$ and $\tilde{\lambda}_i = \hat{\lambda} - \lambda_i$ and let $\tilde{\Lambda}$ be the diagonal matrix with the i th diagonal entry given by $\tilde{\lambda}_i$.¹⁸ Then we can write $[\tilde{B} - \Lambda] = [\tilde{B} + \tilde{\Lambda} - \hat{\lambda}I]$. It is assumed that $\tilde{B} + \tilde{\Lambda}$ has a positive inverse. To see that this is reasonable, consider \tilde{B}_1 which results from neglecting all b_i in \tilde{B} . This corresponds to the conductance matrix of a network of positive resistors, which is known to have positive inverse. Hence $\tilde{B}_1 + \tilde{\Lambda}$ will have a positive inverse if $\tilde{B}_1 - sI + \tilde{\Lambda}$ does, where s is the largest capacitive susceptance in the system. But it is proved in Ref. [38] that $(\tilde{B}_1 - sI + \tilde{\Lambda})^{-1} > 0$ if $s < \lambda_{\min}[B_1]$. Then we see that $(\tilde{B}_1 - sI + \tilde{\Lambda})^{-1} > 0$ since $\tilde{\Lambda}$ is non-negative diagonal. Letting $B = \tilde{B} + \tilde{\Lambda}$ we can write

$$[\tilde{B} - \Lambda] = [\tilde{B} + \tilde{\Lambda} + \hat{\lambda}I] = [B - \hat{\lambda}I] \quad (5.219)$$

Then Eq. (5.219) can be written as

$$[B - \hat{\lambda}I]\underline{x} + \underline{f}(\underline{x}) = \underline{c} \quad (5.220)$$

Now let $\lambda_i = |Q_i|/\gamma^2$ and define

$$g_i(x_i) = \begin{cases} f_i(x_i), & x_i \geq \gamma \\ x_i - \gamma + \frac{|Q_i| - Q_i}{\gamma}, & x_i < \gamma \end{cases} \quad (5.221)$$

Then we see that $\underline{g}(\underline{x})$ maps \mathbb{R}^n onto \mathbb{R}^n , is monotonically increasing for all \underline{x} , coincides with $\underline{f}(\underline{x})$ for $\underline{x} \geq \gamma$, and $\underline{g}(\underline{x}) > 0$ for $\underline{x} \geq \gamma$. The functions $g_i(x_i)$ are shown in Figure 5.9 for Q_i positive and negative. From this point on, $\gamma = 0.8$ is used, as 0.8 is a reasonable lower limit on the voltage magnitudes of interest. This formulation is used as a starting point for establishing sufficient conditions under which the unique voltage solution exists.

5.4.4.1 Conditions Under Which the Unique Solution Exists The investigation of existence and uniqueness of the voltage solution starting with formulation (5.220) must proceed in two stages. First we note that the system

$$(B - \hat{\lambda}I)\underline{x} + \underline{f}(\underline{x}) = \underline{c} \quad (5.222)$$

can be studied directly using the following result of Willson [47]: Consider the equation

$$A\underline{x} + \underline{f}(\underline{x}) = \underline{c} \quad (5.223)$$

where $\underline{f}(\underline{x})$ is of the form

$$[f_1(x_1) : f_2(x_2) : \cdots : f_n(x_n)] \quad (5.224)$$

¹⁸To start with, λ_i has no specific interpretation.

and its maps \mathbb{R}^n onto \mathbb{R}^n , and each f_i is monotonically increasing. Then it is necessary and sufficient that $A \in P_0$ for Eq. (5.223) to have a unique solution for all $\underline{c} \in \mathbb{R}^n$. In the case of symmetric matrices, as is our concern here, the class of P_0 matrices coincides with positive-semidefinite matrices. A more complete discussion of P_0 matrices is given in Refs. [38,39].

Given our construction of $\underline{g}(\underline{x})$ it is necessary and sufficient that $(B - \hat{\lambda}I) \in P_0$ in order to ensure a unique solution to Eq. (5.223), for all \underline{c} . Since B is symmetric, $B - \hat{\lambda}I$ is equivalent to $B - \lambda I$ positive semidefinite or $\hat{\lambda} \leq \lambda_{\min}[B]$. Note that if we set $\hat{\lambda} < \lambda_{\min}[B]$ then $(B - \hat{\lambda}I)^{-1} > 0$. We can then conclude the following.

Theorem 5.4.1 If

$$\max_i |Q_i| \leq \gamma^2 \lambda_{\min}[B] \quad (5.225)$$

then the decoupled reactive-power flow problem [Eq. (5.168)] has at most one solution with load bus voltage magnitudes greater than γ .

Proof: The inequality (5.225) guarantees a unique solution to Eq. (5.223). If this solution has every voltage magnitude greater than γ , then it corresponds to a solution to Eq. (5.168). Since Eq. (5.223) has a unique solution, there can be at most one such solution to Eq. (5.168).

The test is reasonable in the physical sense for the inductive loads. Large inductive loads depress the voltage at the load bus and Eq. (5.225) gives a measure of the size of the load versus the desired minimum voltage level γ . Since the capacitive loads ($Q_i > 0$) were already represented via monotonically increasing nonlinearities, it is possible to give a stricter version of Theorem 5.4.1 where $\max_i |Q_i|$ is replaced by $\min_i |Q_i|$. We have chosen $\max_i |Q_i|$ in order to ensure $g_i(x_i) > 0$; $x_i > \gamma$, which is needed to obtain the bounding results that follow.

The existence and uniqueness of the reactive-power-flow problem for $x_i > \gamma$ could be obtained if we determine conditions so that Eq. (5.223) has a solution with $\underline{x} > \gamma$. Bounds on solutions obtained by Willson are either computationally burdensome or amount to the condition that matrix $(B - \hat{\lambda}I)$ satisfies weak row sum dominance conditions. Unfortunately, even B may not satisfy the dominance conditions in the Q – V power system problem, so bounds must be obtained that use the structure of the power system problem if we are to be successful. To obtain appropriate bounds, multiply Eq. (5.223) by $B - \hat{\lambda}I$ to form

$$\underline{x} + \underline{h}(\underline{x}) = \underline{e} \quad (5.226)$$

where $\underline{h}(\underline{x}) = (B - \hat{\lambda}I)^{-1} \underline{g}(\underline{x})$ is strictly monotonically increasing and positive for $x_i > \gamma$ and $\underline{x} \in (\underline{e} - \underline{h}(\underline{e}), \underline{e})$.

Lemma 5.4.1 If $\underline{e} > \gamma$ and $\underline{e} - \underline{h}(\underline{e}) > \gamma$ then the solution of Eq. (5.223) lies in $(\underline{e} - \underline{h}(\underline{e}), \underline{e})$, that is, $x_i > \gamma$.

Proof: Let x^* be the solution of Eq. (5.223) and write

$$(B - \hat{\lambda}I)\underline{x}^* + \underline{g}(\underline{x}^*) = \underline{c} \quad (5.227)$$

or

$$(B - \hat{\lambda}I)[\underline{e} - \underline{x}^* + \underline{g}(\underline{e}) - \underline{g}(\underline{x}^*)] = \underline{g}(\underline{e}) \quad (5.228)$$

but since \underline{g} is strictly monotonically increasing there exists a positive diagonal matrix D such that

$$\underline{g}(\underline{e}) - \underline{g}(\underline{x}^*) = D(\underline{e} - \underline{x}^*) \quad (5.229)$$

so

$$(B - \hat{\lambda}I + D)(\underline{e} - \underline{x}^*) = \underline{g}(\underline{e}) \quad (5.230)$$

or, since $\underline{e} > \gamma$, $\underline{g}(\underline{e}) > 0$ and $\underline{e} > \underline{x}^*$. [If $(B - \hat{\lambda}I)^{-1} > 0$, then $B - \lambda I + D > 0$ since the terms in D represent positive conductances to ground.] If $\underline{x}^* < \underline{e}$ then $\underline{h}(\underline{x}^*) < \underline{h}(\underline{e})$ so

$$\underline{x}^* - [\underline{e} - \underline{h}(\underline{e})] = \underline{h}(\underline{e}) - \underline{h}(\underline{x}^*) > 0 \quad (5.231)$$

implies

$$\underline{x}^* > \underline{e} - \underline{h}(\underline{e}) \quad (5.232)$$

This lemma represents a test to determine whether Eq. (5.223) has a solution with $x_i > \gamma$. It remains to establish the conditions under which we can guarantee that $\underline{e} - \underline{h}(\underline{e}) > \gamma$. It can be seen that \underline{c} is linear in the source voltage magnitudes and also that Eq. (5.228) is a strictly monotonically increasing function of \underline{c} . Let

$$(B - \lambda I)\underline{x} + \underline{g}(\underline{x}) = \underline{c} \quad (5.233)$$

$$(B - \lambda I)\underline{y} + \underline{g}(\underline{y}) = \underline{d} \quad (5.234)$$

with $\underline{d} > \underline{c}$ then as in Lemma 5.4.1

$$(B - \lambda I + D)(\underline{y} - \underline{x}) = \underline{d} - \underline{c} \quad (5.235)$$

and $\underline{y} > \underline{x}$. The next step is to adjust the source voltage magnitudes until

$$\underline{e} - \underline{h}(\underline{e}) > \gamma.$$

It is sufficient to establish a minimum level for all the sources. Let

$$\underline{c} = \alpha \underline{c}_1 \quad (5.236)$$

where \underline{c}_1 is the value of c when all sources are set equal to one. If \underline{e}_1 is the corresponding value of \underline{e} , then α must satisfy

$$\alpha \underline{e}_1 - \underline{h}(\alpha \underline{e}_1) > \gamma \quad (5.237)$$

For $\alpha e_1 > \gamma$ we can write

$$h(\alpha e_1) = \alpha \lambda (B - \lambda I) \underline{e} - \frac{1}{\alpha} (B - \lambda I)^{-1} q \quad (5.238)$$

where q is a vector with i th entry $q_i = Q_i/e_i$. The inequality (5.237) is then

$$\alpha[\underline{e}_1 - \lambda(B - \lambda I)^{-1} \underline{e}_1] + \frac{1}{\alpha} (B - \lambda I)^{-1} Q > \gamma \quad (5.239)$$

There will always be an α satisfying Eq. (5.239) if

$$\underline{e}_1 > \lambda(B - \lambda I)^{-1} \underline{e} \quad (5.240)$$

Lemma 5.4.2 Given any c_1 there is some α^* such that

$$\alpha \underline{e}_1 - h(\alpha e_1) > \gamma \quad (5.241)$$

for $\alpha > \alpha^*$ if $\gamma < \lambda_{\min}[B]$.

Proof. For arbitrary $c_1 \geq 0$, \underline{e}_1 is arbitrary non-negative vector. From the subinvariance theorem [39], if e_1 satisfies $T e_1 \geq s e_1$ for a non-negative irreducible matrix, then s is greater than the Perron–Frobenius eigenvalue of T . Since $(B - \lambda I)^{-1}$ has the largest eigenvalue

$$\lambda_{\max}[(B - \lambda I)^{-1}] = \frac{1}{\lambda_{\min}[B] - \lambda} \quad (5.242)$$

we have $\lambda_{\min}[B] > 2\lambda$. The conclusion of this lemma is that although $\lambda < \lambda_{\min}[B]$ is sufficient to guarantee the solution of Eq. (5.168) with $x_i > \gamma$ for some α we need the additional requirement $\lambda < \lambda_{\min}[B]/2$ in order to get $\underline{e} - h(\underline{e})$ to be greater than α . We now state the main result.

Theorem 5.4.2 If

$$\max |Q_i| < \frac{\gamma^2}{2} \lambda_{\min}[B] \quad (5.243)$$

there exists an α^* such that the decoupled reactive-power flow problem has a unique solution with load-bus voltage magnitudes greater than γ if the source voltages are all greater than α^* . Furthermore, given a set of source voltage satisfying $E_i > \alpha^*$ the unique solution to Eq. (5.168) satisfies

$$\underline{e} - h(\underline{e}) < \underline{e} \quad (5.244)$$

The value of α^* is obtained from Eq. (5.241). The theorem gives conditions on the loads and source-voltage magnitudes to guarantee a physically reasonable

solution. In addition, it gives an upper bound \underline{e} for the solution. A further exploration of the reactive-power–voltage formulation discussed here can be found in Ref. [46]. This work has led to a less conservative vector criteria for the voltage solution to be above prespecified voltages $[E_1, E_2, \dots, E_n]$. This is stated as the following.

Theorem 5.4.3 [46] For load voltages $[E_1, E_2, \dots, E_n]$ to be above the prespecified lower bound \underline{E}^{\min} it is sufficient that, as the operating conditions on the system change

1. Matrix $(H - \hat{\lambda}I)$ remains positive definite and
2. The vector $\underline{D} < \underline{0}$, component-wise, or

$$\underline{D} = (H - \hat{\lambda}I)\underline{E}^{\min} - \underline{c} + \underline{g}(\underline{e}) < 0 \quad (5.245)$$

where

$$H_{i,i} = B_{ii} - b_i \quad (5.246)$$

$$H_{ij} = -B_{ij} \cos \delta_{ij} \text{ for } i \neq j \quad (5.247)$$

$$\lambda_i = \frac{|Q_i|}{(E_i^{\min})^2} \quad \hat{\lambda} = \max_i \lambda_i \quad (5.248)$$

$$\hat{\lambda}_i = \hat{\lambda} - \lambda_i \quad (5.249)$$

Proof. A direct consequence of the conditions for Eq. (5.215) to have the unique solution and condition (5.232) in Lemma 5.4.1. Vector \underline{D} has some characteristics that obviously make it an excellent candidate to indicate deviations from the desired solution. They are

1. When $\underline{E}^{\min} = \underline{E}^{\text{load flow}} \rightarrow \underline{D} = 0$.
2. For any load i , $D_i > 0$ is an indicator of a trouble location, with regard to voltage.
3. Having $D_i \ll 0$ is an indication that node i has more than enough reactive-power support to maintain the prespecified load voltage.

In order to appreciate the full potential of these results for effective voltage monitoring and control, it is important to recognize that the condition (5.245) can be met without performing matrix inversion. Namely, as the loading conditions and network parameters change, the matrix H and the parameter \underline{c} also change. However, computing their impact on the value of vector \underline{D} is simple, because it involves relatively few multiplications and additions. As the voltage generator settings change the vector changes, and computing this effect is also simple.

In principle, the only significant computational effort involved is recomputing the impact on the component $\underline{g}(\underline{e})$. However, this is not essential, since the following approximation holds:

Lemma 5.4.3

$$\underline{g}(\underline{e}) \cong g(1) \quad (5.250)$$

The justification for this approximation is that the vector \underline{e} is always close to the vector 1, since it corresponds to the upper voltage limit. To make this result better justified, $\underline{g}(\underline{e})$ is expanded into a Taylor series. Combining Eqs. (5.245) and (5.250),

$$g_i(e_i) = \frac{|Q_i|}{(E_i^{\min})^2} - \frac{Q_i}{e_i} \quad (5.251)$$

Taking the partial derivative with respect to e_i ,

$$\frac{\partial g_i(e_i)}{\partial e_i} = \begin{cases} \frac{Q_i}{(E_i^{\min})^2} + \frac{Q_i}{(e_i)^2} & \text{for } Q_i > 0 \\ \frac{Q_i}{(E_i^{\min})^2} + \frac{Q_i}{(e_i)^2} & \text{for } Q_i < 0 \end{cases} \quad (5.252)$$

Furthermore, the second derivative is

$$\frac{\partial^2 g_i(e_i)}{\partial^2 e_i} = \frac{2Q_i}{e_i^3} \quad (5.253)$$

Hence, a Taylor-series expansion of $g_i(e_i)$ in powers of $e_i - 1$ follows,

$$g_i(e_i) - g_i(1) = \left(-\frac{Q_i}{(E_i^{\min})^2} + \frac{Q_i}{1^2} \right) (e_i - 1) \quad (5.254)$$

assuming all reactive loads at load busses are negative, that is inductive. From this Taylor series, it can be concluded that the error in the proposed approximation is of the order of the square of voltage changes, which is negligible, relative to the order of D, for all practical purposes. The vector $g(1)$ is defined by

$$g_i(1) = \frac{|Q_i|}{E_i^{\min,2}} - Q_i \quad (5.255)$$

Hence, although the dependency of $\underline{g}(\underline{e})$ on the actual voltages has been avoided, $g(1)$ is still dependent on the voltage bound defined by E_i^{\min} . However, $g(1)$ is nevertheless simple to calculate, using Eq. (5.255). In light of our earlier discussion regarding the dependence reactive-power–voltage problem formulation on the load model chosen, it is important to recognize that a similar approximation to Eq. (5.250) is applicable to load models other than the constant-power model.

It is a simple exercise to recognize that no approximations are involved in computing Eq. (5.255) for constant-impedance and constant-current load models.

Therefore, the problem formulation given here is sufficiently general for developing algorithms with nonuniform load models. An actual development of Theorem 5.4.3 into a very practical algorithm for voltage monitoring and control the usefulness of which was demonstrated on very large power systems, is discussed in the next chapter of this book.

We close this section by emphasizing the importance of developing the least conservative possible vector-type criteria for solution to the steady-state problems in general and here in particular to the reactive-power–voltage problem. For example, it is a simple exercise to show the conservativeness of the scalar criterion like that defined in Eq. (5.243) relative to the vector criterion like that defined in Eq. (5.245). Estimates on reactive-power bounds obtained using the vector criterion are very close to the limits obtained by the load-flow simulations. As the reactive-power inputs approach limits defined in Eq. (5.245), the load-flow simulations are likely to experience convergence problems. Note that none of the results presented up to this point are subject to any optimality criterion. Only feasibility of the voltage solution has been studied.

5.5 LOW-VOLTAGE PROBLEMS UNDER HEAVY REAL-POWER TRANSFERS

As the real-power transfer increases, voltage at the receiving end decreases. In Ref. [45] the question of the critical voltage while attempting to increase power transfer is computed in terms of short-circuit currents at terminals of the load.

It is important to have an understanding of the voltage reduction problem in terms of an engineering quantity such as a short-circuit load current. This is particularly important for understanding the motivation for choosing critical load voltages to monitor (on the French system “pilot points” [47] are loads with the largest short-circuit currents). In Chapter 13 the pilot-point-based monitoring and steady-state control concept are reviewed as one of the very few automated voltage-regulation methods successfully implemented in practice, which are based on the reduced set of data measurements rather than a full set of measurements. Typically, pilot-point loads are chosen as loads whose short-circuit current is largest. To understand a rationale for this choice one needs to analyze relationships between the critical voltage and the short-circuit currents.

Consider a load fed through a two-terminal system given in Figure 5.10. With the notation of line and load impedances adopted directly from Ref. [45] the line current can be expressed in terms of the short-circuit current at load terminals

$$\hat{I}_{ee} = \frac{\hat{E}_1}{\hat{Z}_L}. \quad (5.256)$$

as

$$I_{ee} = \frac{E_1}{\sqrt{(Z_L \cos \beta + Z \cos \varphi)^2 + (Z_L \sin \beta + Z \sin \varphi)^2}} \quad (5.257)$$

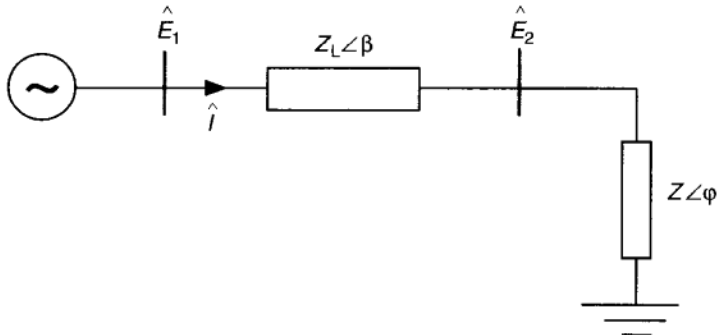


FIGURE 5.10 Load fed through a two-terminal system from a constant-voltage source.

$$I = \frac{I_{ee}}{\sqrt{1 + (Z/Z_L)^2 + 2(Z/Z_L) \cos(\beta - \varphi)}} \quad (5.258)$$

The three-phase average (real) power supplied to the load is then

$$P_2 = 3E_2 I \cos \varphi = \frac{3ZI_{ee}^2 \cos \varphi}{1 + (Z/Z_L)^2 + 2Z/Z_L \cos(\beta - \varphi)} \quad (5.259)$$

Variations of current, voltage, and real power at the load terminals as a function of load admittance for voltage E_1 and constant phase φ reach a maximum relative to increasing Z_L , and afterwards they decrease. The maximum power corresponds to the value of load impedance of

$$\frac{Z}{Z_L} = 1 \quad (5.260)$$

resulting in the maximum possible power delivered

$$P_2^{\max} = \frac{E_1^2}{Z_L} \frac{\cos \varphi}{4 \cos^2[(\beta - \varphi)/2]} \quad (5.261)$$

and the corresponding current and load voltages

$$I_{\text{crit}} = \frac{I_{ee}}{2 \cos[(\beta - \varphi)/2]} \quad (5.262)$$

and

$$E_{2\text{crit}} = \frac{E_1}{2 \cos[(\beta - \varphi)/2]} \quad (5.263)$$

The index “crit” represents the largest current I and the smallest load voltage E_2 , whereas the maximum real power is satisfactorily delivered to the load.

When $P_2 < P_2^{\max}$, two operating points may be found. The operating point corresponding to the higher current and the same power flow is at the smaller load impedance. This is because the transmission losses are higher for the same power delivered. Note that condition (5.260) is identical to the condition of the local maximum power transfer.

5.5.1 Radial Circuit Fed by a Constant-Voltage Source

An approximate computation of the critical voltage at the receiving end of a radial circuit fed by one constant voltage source is proposed in Ref. [45]. To state this result, let us consider such a radial circuit shown in Figure 5.11.

Using these results for the two-terminal system, it follows that

$$\hat{E}_1 - \hat{E}_2 = \hat{Z}_{ee} \hat{I}_{eq} \sqrt{3} \quad (5.264)$$

where \hat{Z}_{ee} is the short-circuit impedance of the system at point B and \hat{I}_{eq} is the equivalent current flowing from A to B . For critical cases, in the same sense as for the two-terminal bus system,

$$|\hat{E}_1 - \hat{E}_2| = E_2$$

resulting in the case of a radial circuit

$$|(\hat{E}_1 - \hat{E}_3) + (\hat{E}_3 - \hat{E}_4) + (\hat{E}_4 - \hat{E}_5) + (\hat{E}_5 - \hat{E}_2)| \sum_j \hat{Z}_{kj} \hat{I}_{kj} \sqrt{3} \quad (5.265)$$

thus obtaining

$$|\hat{E}_1 - \hat{E}_2| \cong \sum X_{kj} P_{kj} E_j \quad (5.266)$$

or

$$E_{2\text{crit}} \cong \sum \frac{XP}{E}$$

The summation in this equation can be made over any path that connects the point at which voltage is constant to the end of the radial line, and P and E are the active power and voltage measured at the same end of the line.

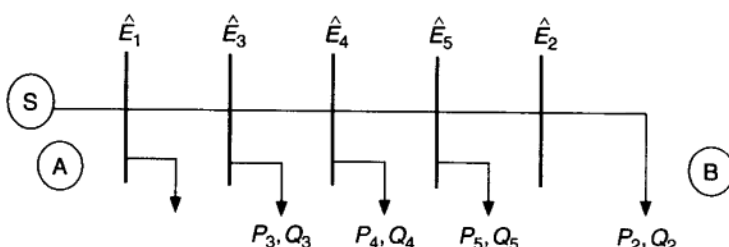


FIGURE 5.11 Radial circuit fed by one constant voltage source only.

A further generalization of computing the critical voltage at any bus A of the radial circuit fed by more than one constant voltage source is introduced in Ref. [45]:

$$E_{A\text{crit}} = \frac{P_{ee1}}{P_{ee}} \sum_{\text{path trajectory } S_1A} \frac{XP}{E} + \frac{P_{ee2}}{P_{ee}} \sum_{\text{path trajectory } S_2A} \frac{XP}{E} + \dots \quad (5.267)$$

The sum of XP/E over each of any paths that connect a source K_iB to point A is weighted by the short-circuit contribution of each source P_{eei}/P_{ee} . The reasoning that leads to this equation can be found in Appendix A of Ref. [45].¹⁹

When the source substation can no longer hold its voltage constant, because it has reached its limit two possibilities for computing the new critical voltage $E_{A\text{crit}}$ at any point A of a radial circuit are proposed:

1. If there exist other substation sources that are capable of maintaining their voltages constant, formula (5.267) for the critical voltage of a two-terminal bus circuit is applied, resulting in the new critical voltage at the same point A . This is most likely going to be a lower voltage than that before the limit was reached because the path over which the other source is connected to it is often electrically further in the sense of having higher $\sum(XP/E)$.
2. A much worse scenario than 1 is when there are no other source substations left that could maintain their voltage constant. This inevitably leads to the voltage collapse. If voltage E_1 in Figure 5.11 is not directly controlled, an increased load demand corresponds to reduction of impedance Z and therefore to an increase of current for a constant E_1 and a drop of voltage E_2 . In order to bring current I back to its initial value, voltage E_1 must be reduced, leading to another drop of E_2 . If the transformer on-load tap-changers try to increase the voltage E_2 , their action leads to a reduction of impedance of the load “seen from the substation,” leading to another drop of voltage E_2 and of real power delivered, etc. This is one of the familiar scenarios related to “malfunctioning” of OLTC’s during voltage collapses reported in the past [48, 50]. One corrective strategy in this case suggested in Ref. [45] is to maintain constant current of the generating units that are not capable of maintaining constant voltage.

5.6 MEANS OF INCREASING REAL-POWER TRANSFER

There are at least two ways to increase real-power transfer. They are based on load compensation or transmission-line compensation. The well-known maximum-power-transfer theorem is often used in electric circuits for estimating the maximum possible real power that could be delivered to a compensated load.

¹⁹ This quantity can be thought of as one possible measure of electrical “distance” between points on a general radial circuit.

The question of using the maximum-power-transfer theorem for determining the “best” compensation in power networks has also been studied in the past, notably by Belgian researchers [49,50].²⁰ It is typically posed as the question of matching a given sinusoidal source \hat{E} whose internal impedance is \hat{Z}_0 by the “best” load \hat{Z}_L [3]. The concept of “best” is identified with delivering maximum (real) average power P_L to a load for given \hat{E} and \hat{Z}_0 . The answer to this question is well known, and it can be summarized by stating that the “best” load is that which satisfies

$$\hat{Z}_L = \hat{Z}_0^* \quad (5.268)$$

where the asterisk denotes a complex conjugate. A concise generalization of this theorem and the conditions under which the result holds when applied to multiport networks can be found in Ref. [51].

This theorem is particularly relevant for understanding stationary operation of power systems as affected by the voltage–reactive-power compensation. At the operating conditions defined by Eq. (5.268) under which the maximum power transfer occurs, the source does not deliver any net reactive power to the combined internal source impedance \hat{Z}_0 and the load impedance \hat{Z}_L . It follows that a source is capable of delivering maximum real power from its terminals into the network when its reactive-power output is zero. Loosely speaking, in operating power systems the “better” reactive-power compensation, the more real-power transfer from the source into the network is possible.

However, a direct application of this theorem to the design and operation of an electric power network is not possible for two reasons: The first reason comes from the fact that only under extremely simplifying modeling assumptions given in Chapter 3 (type IV model) can a generator be thought of as a single-port device with voltage source behind the transient reactance X as posed in Ref. [49]. The second reason comes from the fact that for typical parameters of transmission lines the bus load voltages at the maximum-power-transfer level are unacceptably high. The follow-up analysis of the maximum-power-transfer theorem as related to the efficient power system operation is given using the type IV generator model. This allows for representing each generator as a voltage source behind a reactance. Complications related to high voltages are elaborated in more detail. We briefly review the results from Refs. [51, 52] as related to the topic of this chapter.

5.6.1 Load Compensation and High-Voltage Problems

For simplicity we only describe maximum-power-transfer problem in context of the simplest power network topology. Consider an electric power system

²⁰To start with, a direct application of the maximum-power-transfer theorem to multiport power systems cannot be pursued, since the \hat{Z}_0 matrix is not positive definite (in the complex-valued domain) if the internal resistance of the generator is neglected as is most often the case. To circumvent this problem Calvaer proposed in Ref. [49] a version of the maximum-power-transfer theorem as applied to power networks that does not require nonsingular \hat{Z}_0 .

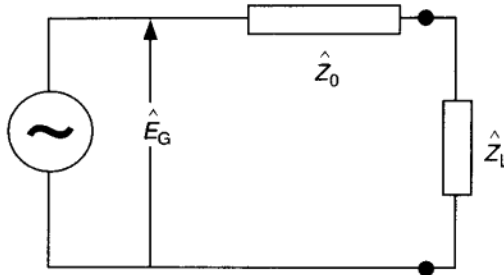


FIGURE 5.12 Small power system.

represented in Figure 5.12. The generator model is thought of as a constant-voltage source behind a synchronous reactance [49]. The ultimate goal of an efficient power network is to enable as much average (real) power delivery to loads from generators as possible.

The answer to this question is that the best load is when

$$X = R \quad (5.269)$$

Again this result does not follow directly from Ref. [51]; it is derived, instead, based on generalizations developed in Ref. [49]. Note, however, that the maximum power occurs when the load-voltage magnitude takes on the value

$$E_L = E_G \frac{\sqrt{R^2 + X^2}}{2R} \quad (5.270)$$

It follows from Eqs. (5.269) and (5.270) that operating the simplest power network at its maximum power transfer would lead to severe overvoltages typically higher than 2 p.u. This is the main reason for not operating electric power systems close to its theoretical feasibility limits. A new, interesting interpretation [53] of the condition discussed in Ref. [49] is as follows.

Consider a single transmission line the parameters of which are R and X , connecting a directly controlled terminal voltage of the generator E_G , which is required to deliver specified real and reactive power P_L and Q_L , respectively, to the load. The load-flow equations for (both real and reactive) power are given as

$$P_L = G(E_L E_G \cos \delta - E_L^2) + B E_L E_G \sin \delta \quad (5.271)$$

$$Q_L = B(E_L E_G \cos \delta - E_L^2) + G E_L E_G \sin \delta \quad (5.272)$$

Using the notation

$$a = RP_L + XQ_L \quad (5.273)$$

and

$$b = XP_L - RQ_L \quad (5.274)$$

for parameters reflecting the effects of the given line and load, a solution to the coupled equations (5.271) to (5.272) can be expressed as

$$2E_L^2 = E_G^2 - 2a \pm \sqrt{E_G^4 - 4(aE_G^2 + b^2)} \quad (5.275)$$

By further normalizing power and voltage as

$$p = \frac{XP_L}{E_G^2} \quad (5.276)$$

$$e = \frac{E_L}{E_G} \quad (5.277)$$

$$q = \frac{Q_L}{P_L} \quad (5.278)$$

$$r = R/X \quad (5.279)$$

Eq. (5.275) takes on the form

$$2e^2 = 1 - 2p(r + q) \pm \sqrt{1 - 4(r + q)p + (1 - rq)^2 p^2} \quad (5.280)$$

For real-valued solutions of Eq. (5.280) to exist, it is necessary that

$$1 - 4[(r + q)p + (1 - rq)^2 p^2] \geq 0 \quad (5.281)$$

which leads to the constraints on delivered real power to the load as

$$p_{\min} \leq p \leq p_{\max} \quad (5.282)$$

where

$$p_{\max} = \frac{-(r + q) + \sqrt{(1 + r^2)(1 + q^2)}}{2(1 - rq)^2} > 0 \quad (5.283)$$

$$p_{\min} = \frac{-(r + q) - \sqrt{(1 + r^2)(1 + q^2)}}{(1 - rq)^2} \quad (5.284)$$

Value p_{\max} represents the maximum power the load can receive for a given q , while p_{\min} is the maximum power the load can send. Voltages corresponding to these two values, respectively, are

$$e_{\max} = \sqrt{\frac{1}{2} - (r + q)p_{\max}} \quad (5.285)$$

$$e_{\min} = \sqrt{\frac{1}{2} - (r + q)p_{\min}} \quad (5.286)$$

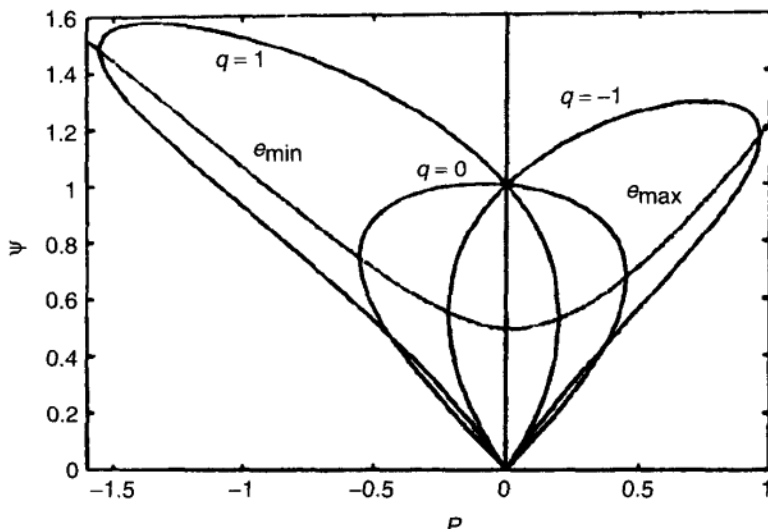


FIGURE 5.13 Parametric dependence of a load-flow solution on r and q .

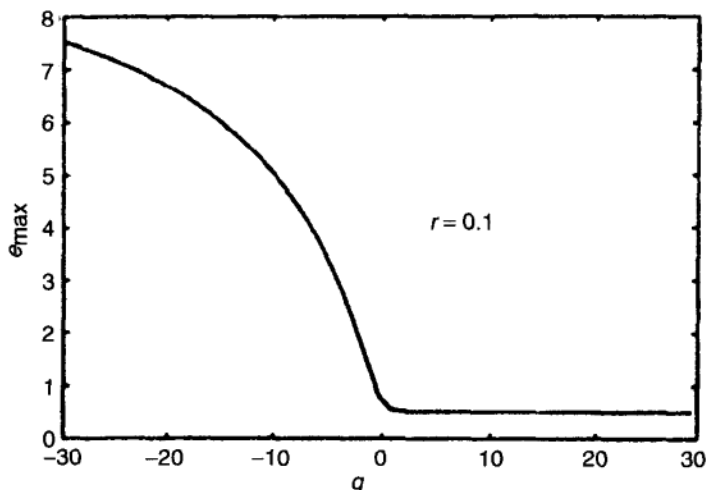


FIGURE 5.14 Extreme feasible power and voltage as a function of q .

Next a parametric dependence of the solution on r and q is shown in Figure 5.13. Since the curves on this figure are drawn for a fixed r and q , the importance of reactive power in maximum power transfer can be understood by asking for what q and/or r values p_{\max} reaches its maximum. To analyze this question, let us first plot p_{\max} , P_{\min} , and θ_{\max} as a function of q , keeping r fixed (Fig. 5.14). It can be seen from these figures that the p_{\max} maximum occurs somewhere for

$q < 0$ at

$$p_{\max} = \frac{-(r+q) + \sqrt{(1+r^2)(1+q^2)}}{2(1-rq)^2} > 0 \quad (5.287)$$

Let us fix r first. Then the p_{\max} maximum occurs when

$$\frac{dp_{\max}}{dq} = 0 \quad (5.288)$$

which is at

$$rq = -1 \quad (5.289)$$

A symmetric result for fixed q and varying r leads to the identical condition (5.288). We refer to p_{\max} for an arbitrary q as a local maximum: the p_{\max} that corresponds to the choice of parameters $q = -1/r$ we refer to as the global maximum. Now, let us define p_{\max} for any (fixed) q to be the local maximum power delivered to the given load: also let us define the p_{\max} for $q = -1/r$ to be the global maximum, as shown in Figure 5.15. At the global maximum

$$q = -\frac{1}{r}, p_{\max} = \frac{1}{4r}, e_{\max} = \frac{\sqrt{1+r^2}}{2r} \quad (5.290)$$

and $\tan \delta = 1/r$. At the global maximum

$$P_{\text{loss}} = G(E_G^2 + E_L^2 - 2E_G E_L \cos \delta) \quad (5.291)$$

$$Q_{\text{loss}} = B(E_G^2 + E_L^2 - 2E_G E_L \cos \delta) \quad (5.292)$$

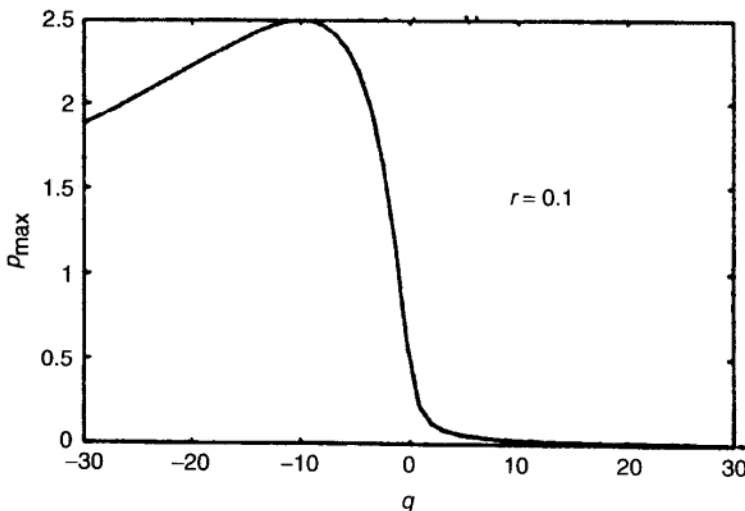


FIGURE 5.15 Global maximum.

from which it follows that

$$P_{\text{loss}} = P_{\text{max}} = P_L \quad (5.293)$$

and

$$Q_{\text{loss}} = -Q_{\text{max}} = Q_L \quad (5.294)$$

Conditions for the maximum power transfer using the constant-impedance load model directly follow from these derivations. Next, by viewing the load model as an impedance load, that is, $\hat{Z}_L = R_L + jX_L$, at the maximum $R_L = R$, $X_L = -X$, that is, the maximum power transfer occurs when the load impedance is $\hat{Z}_L = \hat{Z}^*$, the impedance of the transmission line.

Next, let us investigate fundamental load characteristics at a local maximum. Define the complex-valued line impedance (generator reactance included) as

$$\hat{Z} = R + jX = Ze^{j\zeta} \quad (5.295)$$

and the load impedance $\hat{Z}_L = R_L + jX_L = Z_L e^{j\zeta_L}$. It can be shown that when $Z_L/Z = 1$, a local maximum occurs. In conclusion, since $R \ll X$ for actual transmission lines, the global maximum voltage will be $e_{\text{max}} \gg 1$, which is unacceptable. Only the local maximum (for a given $q \neq -1/r$) is operationally acceptable. Calvaer's result [49] is a particular case of this more general result. Furthermore, it can be seen that at the global maximum the load power factor becomes unacceptably low for typical transmission-line parameters ($X \gg R$), that is,

$$\alpha = \frac{P_L}{\sqrt{P_L^2 + Q_L^2}} = \frac{R}{\sqrt{R^2 + X^2}}$$

5.6.2 Line Compensation as a Means of Increasing Real-Power Transfer

It can be seen from the derivations just presented that the efficiency of the given source in delivering real power to a load depends on both transmission-line and load characteristics. Usually the system is designed to accommodate wide ranges of load changes, which are often outside the direct control of power-system operators.

This situation raises the question of maximum efficiency of transmission lines themselves in accommodating a load connected to its terminals. This question is addressed next. To begin with, it is shown in Ref. [54] that if a line is terminated at its characteristic impedance \hat{Z}_0 [Chapter 3, Eq. (3.23)], its internal reactive-power requirements are completely balanced; consequently, no reactive power from external sources is required. The line current in this condition is the minimum possible for any given load; consequently, the line loss is minimum. The voltage drop along the line is relatively small in this operating condition, consisting simply of a purely ohmic, exponential attenuation. The power transmitted in this

condition is

$$P^n = \frac{E_R^2}{Z_0} \quad (5.296)$$

and is called the natural power. Here E_R is the voltage magnitude at the receiving end of the line.

It is an important fact that the characteristic impedance of all single, high-voltage lines differs not more than about $\pm 10\%$ from 400Ω ; consequently the approximate value of the three-phase natural power is

$$P^n = 2.5E^2 \text{ kW} \quad (5.297)$$

if E is the line-to-line voltage in kilovolts. For this equation values of P^n for various voltages are shown in Table 5.8.

These values are rather small. The transmission of 25,000 kW over a distance of more than 200 miles would hardly be economical. Since, on the other hand, according to Table 5.8, only power values close to the natural power can be transmitted over large distances, a limit is soon reached in which either the natural power has to be raised or the load has to be distributed on parallel lines. The most obvious way of increasing the natural power is by increasing the voltage, since the natural power increases with its square (voltage upgrade). The increase of transmission voltages, however, is accompanied by considerable difficulties, and it becomes cumulatively more expensive as the voltage increases; consequently there is a need for investigating the possibilities of reducing the characteristic impedance of the lines. As defined in Chapter 3, the characteristic impedance of a line given as

$$\hat{Z}_0 = \sqrt{\hat{Z}\hat{Z}'} = Z_0 \angle \eta \quad (5.298)$$

derives from the line constants \hat{Z} and \hat{Z}' and ultimately from the line dimensions. But the line dimensions cannot be changed widely since conductor distances are limited by consideration of insulation levels and corona. Furthermore, the line constants are proportional to the logarithm of the line dimensions; consequently, any change in the line dimensions is reflected only in a much smaller proportion in

TABLE 5.8 Load-Carrying Capability of Transmission Lines in Multiples of the Natural Load

Line-to-line voltage (kV)	Approximate natural power (kW)
100	25,000
200	100,000
300	225,000

the line constants. This then leaves the actual addition of capacitors or induction coils as the only possible way of changing the characteristic impedance of a line.

Such additional reactances can be practically applied only in a lumped form, and there are four possibilities for such an application [54]. It can be shown that adding shunt capacitors or series capacitors would have desirable effects on characteristic impedance. Although the method of adding shunt capacitances is very popular, it could have detrimental effects on steady-state stability of the system with very long transmission lines. Earlier in this chapter bounds on the amount of shunt compensation were derived (Eq. (5.209)) to avoid steady-state reactive power instability.

The application of series capacitors seems most promising. This results in a reduction of line inductance and consequently in a reduction of both the magnitude of the characteristic impedance Z_0 and its propagation factor η . Serious practical difficulties in implementing this solution have been associated with the protection against overvoltages. Since the capacitors are in series with the line, the full line current must pass through them. This results in large overvoltages on the capacitors during short circuits. No entirely satisfactory protection against these overvoltages has been developed yet. The other problem with adding series capacitance comes from the danger of subsynchronous resonance [55].

It has been shown recently in Refs. [56, 57] that a transmission line is most efficient when it has an impedance whose magnitude remains unchanged as one interchanges the sending-end variables with the receiving-end variables, and, furthermore, a phase angle that remains unchanged in absolute value (but not in sign) as one interchanges the load side with the feed side. This implies that the transmission-line impedance should, when transferred from end to end, become the complex conjugate. Under these conditions the magnitude of line impedance can be expressed as a function of general line parameters (Eqs. (3.22) to (3.23), Chapter 3) as

$$Z = \sqrt{\frac{AB^* + BA^*}{CA^* + AC^*}} \quad (5.299)$$

Some of these possibly well-known facts have to be kept in mind as the existing transmission system is being enhanced by various FACTS technologies.

5.7 STEADY-STATE STABILITY PROBLEM AS A COUPLED $P-Q$ PROBLEM

A conventional generation scheduling for supplying specified load has primarily been in terms of real power only, motivated by a direct relationship between the real-power output and the energy cost at which customers are charged. In recent times the trend to transfer large amounts of energy over far electrical distances for economic reasons has been particularly emphasized within a single utility and more so in the interutility tradings [58]. The effect of these transfers on

system steady-state operation is not pronounced when relatively small amounts of energy are transferred. However, it is possible to find more and more frequent instances of energy transfers that result in a steady-state operation considerably different from the operation from which the system was rated at its original design stage. A direct consequence of this is a shift of a steady-state operating point closer to the system's steady-state transfer limits. Employing analysis tools described earlier in this chapter shows that the system is then closer to its steady-state real-power transfer limits (assuming voltages do not change significantly). A similar analysis of proximity measures to the limits of the reactive-power–voltage solution existence shows significant deviations in these measures as well (not including the real-power effects on voltage).

Moreover, the operating scenarios associated with large energy transfers are emerging as examples in which it is not sufficient to analyze real-power transfer separately from voltage changes and, similarly, voltage changes independently from the effect of real-power changes. Otherwise, unrealistic analyses are performed, indicating larger transfer limits than would be the case when the coupling is accounted for. Cases have been documented in the literature [59] indicating voltage problems caused by increased real-power transfers. If commonly employed remedies for low voltages, such as capacitor banks, are used, voltage at the receiving end will be maintained close to nominal values as the energy transfer increases. At a certain level of energy transfer a small increment leads to a sudden voltage drop.

Theory supporting the derivation of steady-state limits within which solutions to the coupled P – Q steady-state problem exist is not well understood. For example, a nonlinear network interpretation of the coupled P – Q problem, similar to the nonlinear network interpretation of the decoupled P – δ and Q – V subproblems, has not been introduced yet. It remains an important open problem.

We briefly review here the often-used P – V -curve-based conditions and their relation with the network-based conditions for ensuring steady-state stability developed in Sections 5.3 and 5.4. Many recent references concerning reactive power steady state instabilities are in the literature concerning the topic of voltage collapse.

Research approaches in this area could be grouped into two different categories: (1) a two-bus theory of voltage collapse and (2) its generalization to multibus systems. An elementary overview of the two-bus theory was provided in Section 4.3 together with other notions of system instabilities. Here several other relations are discussed.

5.7.1 Two-bus System Concepts

Although the concepts of steady-state real- and reactive-power stability limits have historically evolved under the decoupling assumption, this assumption is not essential for a small two-bus system since a closed-form solution to the coupled load-flow equations is easily found as shown in Section 5.6.1. Most of the classical references concerning Q – V steady-state instabilities and voltage

collapse are presented under the assumption of a constant-load power factor, instead of the decoupling assumption.

This distinction between the P - Q decoupling and constant-load power-factor assumptions is relevant for understanding the implications of various types of reactive-power-voltage compensation devices on possible power transfer. It is described in detail in Chapter 12 that one could use two qualitatively different types of controllers for regulating reactive-power consumption:

1. Various system components are equipped with direct voltage control (these could range from various designs for voltage regulators on generators, through shunt capacitor control of load and series capacitors on transmission lines).
2. The same components could be compensated so that their power factors remain constant.

Typical P - V curves assume a second scenario of a fixed-load power factor instead of direct voltage control at the load.

5.7.1.1 Constant-load-voltage Control It is useful to observe that in the case when the load has direct voltage control, the P - Q decoupling assumption is automatically met when analyzing real-power steady-state stability problem. This further implies that under constant-voltage control at the load bus, only real-power steady-state stability problems may occur. In this case, as described in Section 4.3, a desired network response would be seen in the increase of the phase-angle difference as P_2 increases (recall Fig. 4.36), whereas the voltage remains unchanged. If the required real power at the load is larger than P_2^{\max} , an undesired real-power steady-state stability problem occurs. Strictly speaking, with this type of load control no Q - V power steady-state stability problem will occur as long as the voltage-control limits are met and as long as the logic of the load-control device is designed to ensure constant load voltage as the system operating conditions vary. For operating regions in which the Q - V power network behaves as a positive resistive network the control logic is not critical. More advanced control is described in Chapter 12 for other regions.

5.7.1.2 Constant-power-factor Control As described in Section 5.5 in the summary of Barbier's work, in the case of a load power-factor control, various Q - V -related steady-state stability problems may take place, in addition to the P - δ steady-state stability problems. Moreover, the actual ranges within which the network responds in a qualitatively unchanged way (say, as a positive resistive network) will depend on how the load is actually controlled.

When the operating conditions are outside those within which the Q - V power network is equivalent to a positive resistive network, caution must be taken in designing load power-factor control. The same issues arise when partial load shedding is done for ensuring that the voltages remain within the acceptable operating limits. Under some unusually demanding conditions it may happen

that a reduction in reactive-power load may not lead to the expected voltage increase. It is for such reasons that understanding the basic nature of power-network response to changes in system inputs is critical.

Understanding the difference between direct voltage control and power-factor control from the point of view of the transmission network's response to input changes is generally very important when the system experiences unusual stress. It can be shown that having load-voltage control rather than constant-power-factor control virtually eliminates the Q - V steady-state instability problems. Again, this is the case as long as the load-voltage-control logic is sufficiently adaptive to maintain load voltage as desired, even for operating regimes when the network responds differently than expected. In Chapters 14 and 12 stationary and dynamic voltage-control algorithms are described, respectively. It is shown how simple decision algorithms can be developed for deciding if the system is in the operating regions in which the transmission responds as a positive resistive network or if it has a more complicated response. This knowledge is then used for developing a control logic that is sufficiently effective to maintain voltages within their operating limits.

5.7.2 Methods for Multibus Systems

As it is well known, typical voltage-related problems of multiload-multigenerator systems are associated with large electrical distances between generators and loads, relatively large energy transfers, and limited reactive-power support close to loads. To predict these problems, many generalizations of analytical conditions that are well understood for two-bus systems have been attempted in the past. These are based primarily on analyzing load-flow equations of multibus power systems. Issues are more complex than with the two-bus systems because, instead of being able to express load voltages explicitly in terms of power demand and network parameters, it is impossible to find a closed-form solution for such relations.

In this chapter sufficient conditions for load-flow voltages to remain within the acceptable limits are reviewed under the decoupling assumption. Notice that in discussing load-flow-related analytical results only sufficient instead of necessary conditions are available because of the nonlinear nature of the load-flow problem. A direct consequence of relying on sufficient conditions is the danger of developing many extremely conservative measures, potentially useless in practice. This basically means that many analytical tools will lead to conditions that are hard to satisfy; moreover, if the same conditions are used for corrective strategies, the results will indicate need for excessive control. It is with this in mind that conservativeness issue is addressed here.

5.7.2.1 Graphical Methods It is established in Chapters 7 and 8 that the point, at the tip of the nose curve, i.e. the P - V curve is a saddle mode bifurcation point. This bifurcation point is also present in multibus systems and is studied throughout theoretically and in its practical manifestations in Chapters 7 and 8,

for respectively two bus and multibus systems. However for readers who seek an intuitive link to the multibus systems such an approach is used in this section.

Issues concerned with generalizing the concept of P - V curves to multibus systems are very complex. The main complication comes from the interconnected character of the network, since any single change affects everything else on the system. It is hard to give a good interpretation of mutual effects taking place on the system by drawing a family of curves resulting from a single change at a time. To be more specific, while considering a contingency of a single line outage on an already heavily loaded system, it becomes apparent that in response to this change, voltage set-point values of various voltage controllers, as well as real-power schedules, may change as a result of corrective actions that a system operator may take to remedy voltage problems. It is practically impossible to draw families of curves that would be ready for any combination of these actions occurring in this situation. (Recall that every single P - V curve is currently generated for a single-generator, single-load case, given all other parameters constant, such as the position of an on-load tap-changing transformer and set point of the terminal voltage on the generating unit.)

Often-made claims that only particular buses and lines are of interest are not sufficient for justifying the direct application of two-bus system techniques to only a particularly chosen generator-load pair of the interconnected system while ignoring the effects of changes on the rest of the system. As a matter of fact, if an approach of this type is taken, it becomes very important to identify the most critical buses. Unfortunately, it is plausible that the choice of critical buses changes with operating conditions.

More justifiable may be approaches of creating P - V curves for interconnections of interest by performing extensive load-flow calculations that take into consideration the effect of the rest of the network, for a given scenario, that is, with everything else fixed [60,61]. These curves are then used for monitoring the closeness to voltage-related problems when the operating conditions, for example, power flow in a particular line of interest, change.

5.7.2.2 Methods Based on the Load-Flow Sensitivity Matrix (Jacobian) The main idea of studying properties of the load-flow Jacobian (Eq. (5.43)) for the interconnected system in order to anticipate voltage changes can be understood by recalling the basic theory for two-bus systems. A positive-resistive-network property of a power network will produce a voltage reduction with increased reactive power demand and vice versa. A mathematical formulation of this property for a two-bus system, assuming real-reactive-power decoupling has been generalized to multibus systems by exploiting the notion of M matrices [47].

First, several results are known under the decoupling assumption. It follows directly from Eq. (5.208) that for the Q - V network to behave similar to a positive resistive network, it is sufficient that matrix H_Q be an M matrix. At any given operating point this matrix is numerically identical to the Jacobian of the decoupled Q - V equations. At any other operating point, limits on maximum value of shunt capacitances are defined via the inequality (5.209) so that the

$Q-V$ network behaves like a positive resistive network. As the operating conditions and network topology change significantly, the eigenstructure of the matrix H_Q could qualitatively change.

The analysis of the $Q-V$ problem as the nonlinear network problem of the form (5.213) offers similar conditions under which the network behaves “as expected.” In contrast to the analysis of the decoupled $P-\delta$ network problem in which it is sufficient to meet diagonal dominance property of the corresponding Jacobian, the decoupled $Q-V$ network problem does require computation of the minimum eigenvalue for monitoring positive definiteness of the matrix relevant for the desired network response.²¹

A virtually identical condition is required in the network-based conditions because at the nominal operating point this condition amounts to the condition that the Jacobian of the $Q-V$ equations remains positive definite.

5.8 NUMERICAL TOOLS USED IN THE SOLUTION OF POWER-FLOW EQUATIONS

Solving the power-flow equations (5.10) to (5.12) numerically is viewed as the problem of solving a set of $2n + k$ nonlinear equations with $2n + k$ unknowns:

$$F(x) = 0 \quad (5.300)$$

Finding the zeros of a general nonlinear function $F : \mathbb{R}^N \rightarrow \mathbb{R}^N$, that is finding an $x^* \in \mathbb{R}^N$ such that $F(x^*) = 0$, is a classical problem, difficult to solve explicitly. One has to resort to iterative methods, starting from an initial guess, x^0 , and proceeding with the calculation of successive approximations to the solution by applying an appropriate iteration function. Iterative methods may converge more slowly than analytical techniques and more importantly suffer from ill-conditioned situations such as numerical instabilities and bifurcations. However, for large problems with inherent nonlinearities such as those encountered in power system analysis, iterative techniques are the only applicable methods. This section is based entirely on the M.Sc. thesis work of Mary Tolikas, MIT [62].

The issues associated with applying a numerical technique to a particular problem are as follows.

1. *Choice of a method appropriate to the problem under consideration.* The type of equations to be solved, the amount of nonlinearity inherent, and the number and type of solutions required should influence the choice of a numerical method.
2. *Conditions under which the method will converge to the required solution(s).* These conditions are dependent on an initial guess. A starting point too “far

²¹ Recall that the presence of shunt capacitances b_i is the reason for the Jacobian associated with the decoupled $Q-V$ problem not having the diagonal dominance property.

away" from the actual solution may result in no convergence. Moreover, the choice of appropriate measures and tolerances that provide the criteria on whether or not convergence has been achieved should be carefully made.

3. *The rate of convergence, that is how fast the iterative scheme will converge to the final solution x^* .* This also depends on the proximity of the initial guess to the actual solution.
4. *Computational speed.* This becomes an important issue for on-line applications, where results are required quickly so that corrective measures may be taken.
5. *Computer storage.* This depends on available resources and problem size.

These issues are well understood for the Newton–Raphson and Gauss–Seidel methods, as applied in the solution of power–flow equations. A brief summary is given in the Appendix 5.1 of this chapter.

A numerical alternative that has recently drawn the attention of the engineering world in order to alleviate the problems plaguing conventional numerical techniques is that of continuation algorithms. These algorithms are particularly attractive for computing steady-state solutions in the operating regions close to stability margins because convergence to multiple solutions and global convergence are their strengths. Given the novelty of this approach to the power engineering community, the general continuation paradigm is presented here next in considerable detail. Following this general introduction to the continuation methods, its applications to solving load flow equations are formulated.

In the next section a sufficient criterion for a solution to exist to the given non linear problem is presented. This is the condition of the positive-definite inner product, which, furthermore, has a passivity interpretation for non linear resistive networks. This result forms the basis for developing similar conditions under which the numerical solution can be found, when it exists, given the earlier interpretation of decoupled load-flow problems as non linear resistive networks in operating regions of interest.

Simulation results using HOMPACK, a software package implementing continuation methods, are shown. The performance of different homotopies is evaluated and compared for simple academic examples of power systems. The choice of a starting point and a homotopy function is shown to affect convergence to certain types of solutions.

5.9 CONTINUATION METHODS

Most of the traditional methods used in the solution of a system of nonlinear equations do not converge for starting points that are too far away from the solution. In this section, a set of methods is presented as a better alternative to conventional techniques. Continuation methods may increase the domain of convergence of a solution. They may also be used to bring the initial guess closer to the solution and within the region of convergence of conventional iterative

schemes, such as the Newton–Raphson scheme, so that these may be further employed.

5.9.1 Introduction to the Continuation Paradigm

Consider the simple diode example, shown in Figure 5.16 for ease of reference. The KCL equation at node 1 may be solved for the diode voltage v_d using the Newton–Raphson method, but, as demonstrated in the appendix of this chapter, overflow problems may occur for inappropriate initial guesses.

Consider solving this problem in a different manner. Assume that the voltage source is initially zero (i.e., a short circuit). Gradually step up the voltage to its final value of 10 V. At each step calculate the voltage at node 1 by using the previous solution as an initial guess. This approach, known as the *source stepping algorithm*, is illustrated in Figure 5.17. Starting off with $\alpha = 0$ (and no source), the diode voltage is found by inspection to be zero. Changing α by a small, positive amount results in a new, nonlinear problem, which may be solved by the Newton–Raphson method with an initial guess equal to the solution of the previous step (zero in this case). The process is repeated until αV_s reaches 10 V (with $\alpha = 1$).

Figure 5.17, a plot of the solutions to the intermediate problems versus α , illustrates these ideas. Each point in the α - x plane represents the solution to a different circuit topology and hence a different nonlinear problem to be solved. Via this transformation, $\alpha = 0$ maps to a circuit topology with a trivially found operating point X_{initial} . A slightly increased α corresponds to a slightly different topology with solution x_1 . The solution x_1 may be obtained by a Newton–Raphson step using x_{initial} as the initial guess and so on.

A similar approach to the same problem is that of G_{\min} stepping. A resistor $G(1 - \alpha)$ is connected across the diode as shown in Figure 5.18. α is initially set

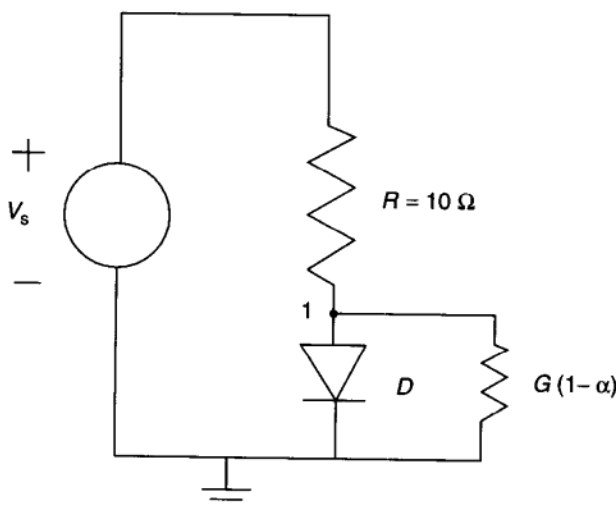


FIGURE 5.16 Source-stepping for the diode circuit.

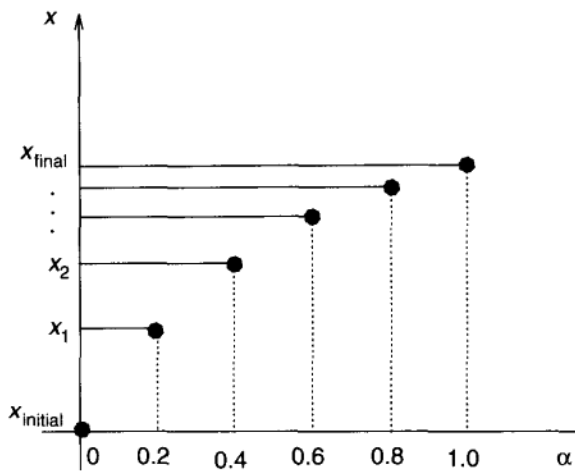


FIGURE 5.17 Plot of the diode voltage for various voltage excitations.

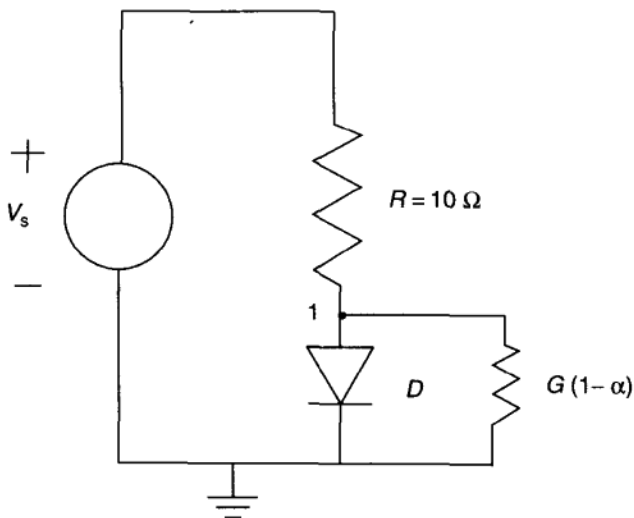


FIGURE 5.18 G_{\min} stepping for the diode problem.

to 1 so that a short circuit is effectively placed across the diode. This gives rise to an easily solved topology, where the voltage at node 1 is zero. By gradually decreasing α to 0 and solving the intermediate problems, the resistance across the diode gradually becomes an open circuit (assuming G has a high enough value). The system topology is deformed to that of the original problem. Figure 5.19 illustrates the effect of G_{\min} stepping on the circuit's operating point. At each step, the solution is the intersection of the diode characteristic (fixed in the i_d-v_d plane) and the load line of the remaining circuit (with varying slope in the i_d-v_d plane).

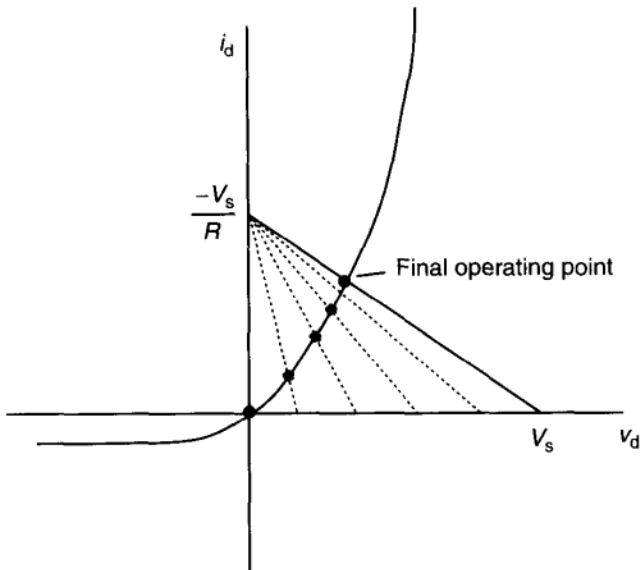


FIGURE 5.19 Effect of G_{\min} stepping on the circuit's operating point.

Gradually deforming a simple (usually linear) problem to a nonlinear one forms the basis of the continuation method. The earliest application of the continuation technique for the numerical solution of equations appears to have been made by Lahaye (1934) for a single equation, using Newton's method to move along the solution curve. Since then the method has found wide application in engineering and applied mathematics for solving fixed-point problems, systems of nonlinear equations, integral equations, etc.

In strict mathematical terms the continuation or embedding methods may be formulated as follows. Suppose the zeroes of the nonlinear equation

$$F(x) = 0 \quad (5.301)$$

are required. A parameter $\lambda \in [0, 1]$ is introduced, which is usually referred to as the *continuation parameter*. This results in increasing the initial problem dimension by 1 and gives rise to a new mapping, for example,

$$H(x, \lambda) = (1 - \lambda)G(x) + \lambda F(x) \quad (5.302)$$

where $H : \mathbb{R}^N \times [0, 1] \rightarrow \mathbb{R}^N$, $G : \mathbb{R}^N \rightarrow \mathbb{R}^N$ is a trivial map with known solution x^0 , and $F : \mathbb{R}^N \rightarrow \mathbb{R}^N$ is the nonlinear problem to be solved.

The continuation idea involves deforming the simple problem (trivial mapping) $G(x)$ with a known solution x^0 to the given problem $F(x)$ [whose solution(s) x^* are required], by gradually varying λ from 0 to 1. In other words, starting from

$$H(x^0, 0) = G(x^0) = 0 \quad (5.303)$$

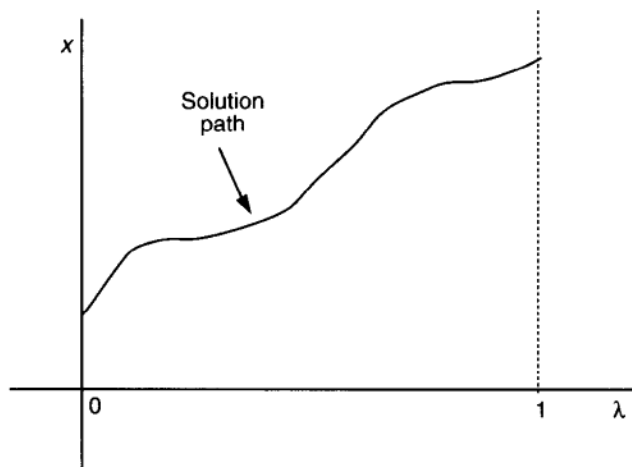


FIGURE 5.20 Typical solution path generated using continuation.

one gradually results in

$$H(x^*, 1) = F(x^*) = 0 \quad (5.304)$$

through increasing λ by fixed, positive steps $\Delta\lambda$. In general, the series of deformed problems $H(x, \lambda) = 0$ yield a solution $x = x(\lambda)$, which depends continuously on λ . x describes a space curve in \mathbb{R}^N , linking the initial point $(x^0, 0)$ to the final required solution $(x^*, 1)$. This is illustrated in Figure 5.20 for a function $F : \mathbb{R} \rightarrow \mathbb{R}$.

These steps form the simplest continuation algorithm, known as the embedding algorithm. The interval $[0,1]$ is partitioned into k equal subintervals $\Delta\lambda$ such that $\Delta\lambda = 1/k$. Starting at a known solution point, the homotopy path is traced by incrementing the continuation parameter and solving the problems

$$H(x, \lambda_i + \Delta\lambda) = 0, \quad i = 1, \dots, k \quad (5.305)$$

for x , by some iterative method that uses the solution x^{i-1} of the $(i-1)$ th problem as a starting approximation to solve the i th problem. If $\lambda_{i+1} - \lambda_i$ is sufficiently small, then, hopefully, x^{i-1} will be a sufficiently good approximation to x^i so that convergence will occur. The general algorithm is the following.

EMBEDDING ALGORITHM

```

start
initialize constants
Set λ = 0;
Set starting point (x0, 0);
Set Δλ;
while λ ≤ 1

```

```
Solve  $H(x, \lambda) = 0$  iteratively;
Set  $\lambda = \lambda + \Delta\lambda$ ;
end
```

A Newton–Raphson method could be employed in the inner loop to solve

$$H(x, \lambda) = 0 \quad (5.306)$$

iteratively, resulting in the step

$$x^{i,k+1} = x^{i,k} - \left(\frac{\partial H(x^{i,k}, \lambda_i)}{\partial x} \right)^{-1} H(x^{i,k}, \lambda_i) \quad (5.307)$$

Other iterative methods may be adopted in the solution of that loop.

The simple embedding algorithm does not work well in general, for reasons given next. Experiments have shown, however, that the method never works. This could be due to a number of ill-conditioned cases that may arise, which are outlined in the next section.

5.9.2 Problems with the Embedding Algorithm

The questions and problems arising in employing the classical continuation algorithm are the following.

- How is it assured that a solution path connecting the trivial solution to the final solution exists? In other words, once a starting point has been established, how is it ascertained that a solution to the next problem exists in that neighborhood? There may be no solution of $H(x, \lambda_i + \Delta\lambda) = 0$ near (x, λ_i) for a small enough $\Delta\lambda$.
- The path may diverge to infinity as $\lambda \rightarrow 1$. As shown in Figure 5.21, the path may never reach the $\lambda = 1$ level; it may become unbounded. Hence the method may never yield a solution to the required problem. Another ill-conditioned case that may arise is also that of returning back to the $\lambda = 0$ level before a final solution has been obtained.
- The method will fail when turning points of the curve with respect to λ are encountered, as illustrated in Figure 5.22, that is, the problem $H(x, \lambda_i + \Delta\lambda) = 0$ is still prone to bifurcations, becoming numerically unstable at local turning points of H .
- The Newton step might fail if $\Delta\lambda$'s are not sufficiently small. The number of subintervals k should be small to guarantee that the solution to the previous problem is a good enough guess for the next problem. If that is not the case, the Newton–Raphson step used in the inner loop of the embedding algorithm will never converge.

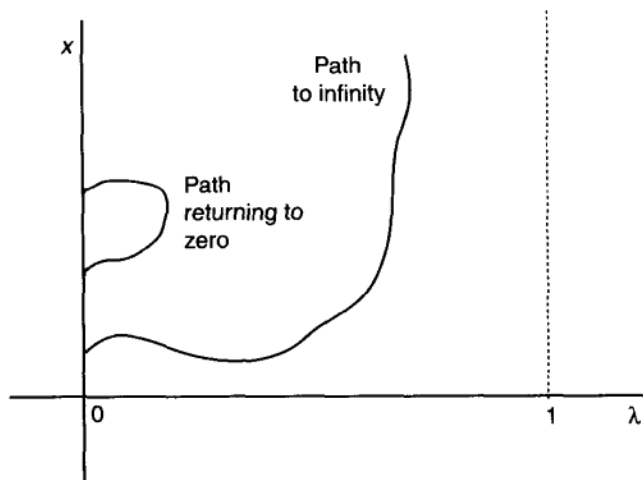


FIGURE 5.21 Solution path diverges to infinity.

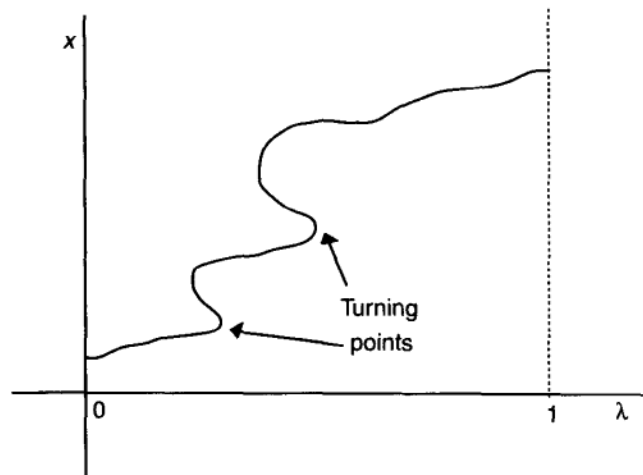


FIGURE 5.22 Turning points in the solution path.

It may therefore be concluded that the classical continuation methods may exhibit the same problems as conventional techniques. Homotopy methods, presented next, offer more sophisticated forms of continuation and exhibit more robust and numerically stable characteristics.

5.9.3 Homotopy Methods Versus Classical Embedding Algorithms

Homotopy methods overcome most of the problems associated with the classical embedding algorithms. The distinction lies in the fact that the homotopy zero

curves are always smooth, well-behaved paths. Moreover, bifurcation points and other ill-conditioned cases may be avoided. This section takes a closer look at the problems associated with classical continuation, and theoretical results from nonlinear analysis are given to prove that such problems may never occur for appropriately defined homotopy methods. The following nomenclature is adopted.

Define $H^{-1} = \{(x, \lambda) | H(x, \lambda) = 0\}$ as the set of all solutions $(x, \lambda) \in \mathbb{R}^{N+1}$ to the system of equations $H(x, \lambda) = 0$. The solutions for fixed λ are further denoted as $H^{-1}(\lambda) = \{x | H(x, \lambda) = 0\}$ so that $H^{-1}(0)$ consists of all the starting points and $H^{-1}(1)$ consists of the required solutions to $F(x)$. In general, H^{-1} is arbitrary, consisting of all possible solution points that lie over the region where H is defined. This does not necessarily imply that they are ordered according to a particular configuration, that is they may not be connected by a path.

The first issue addressed is that of ensuring that at least one path will exist connecting the trivial solution to the final solution. This encompasses the task of determining whether H^{-1} consists of well-behaved paths that do not intersect themselves. The key to ensuring this is found in the implicit function theorem, as follows.

Theorem 5.9.1 Suppose $H : \mathbb{R}^{N+1} \rightarrow \mathbb{R}^N$ is continuous on an open neighborhood $D \subset \mathbb{R}^{N+1}$ of a point (x^0, λ^0) for which $H(x^0, \lambda^0) = 0$. Assume that $(\partial H)/(\partial x)$ exists in a neighborhood of (x^0, λ^0) , and is continuous and nonsingular at (x^0, λ^0) . Then there exist open neighborhoods $S_1 \subset \mathbb{R}^N$ and $S_2 \subset \mathbb{R}^N$ of x^0 and λ^0 , respectively, such that for any $\lambda^0 \in S_2$, the equation $H(x, \lambda) = 0$ has a unique solution $x^* = H^{-1}(\lambda) \in S_1$ and H^{-1} is continuous.

The proof of this theorem may be found in Ref. [63]. Its importance is that it ensures that all points $(x, \lambda) \in H^{-1}$ near (x^0, λ^0) are on a continuous differentiable path. A path therefore exists connecting the initial point $(x^0, 0)$ to a neighboring point $(x^1, \Delta\lambda)$. Using the same argument, one can show that a continuous differentiable path exists, connecting $(x^1, \Delta\lambda)$ to a neighboring point $(x^2, 2\Delta\lambda)$. This argument may be repeated until the neighborhood of the final point $(x^*, 1)$ has been reached. This, however, holds as long as $(x^0, 0)$ is a regular zero point of H , that is, as long as the Jacobian $(\partial H/\partial x)(x^0, 0)$ has full rank N .

The next issue is that of ensuring that the path will always reach a solution, assuming of course that such a solution exists, and will never tend to infinity. Given a homotopy H defined over a region $D \subset \mathbb{R}^N$ we have to prove that the path defined by $H(x, \lambda) = 0$ goes to $x^* \in D$. The theorems presented next are related to existence theorems in nonlinear analysis. They are applied to ensure that the solution path c generated by H and linking the starting point to the required solution cannot go beyond the boundary of the region over which H is defined. If c is already inside that region, it cannot escape from it and cannot tend to infinity. One then is able to force it to go to the required solution, which is assumed to exist within the region D under consideration. The start of all theoretic arguments lies with the following theorem.

Theorem 5.9.2 (Brouwer's fixed point theorem) [63] Let $S_N = x \in \mathbb{R}^N : \|x\| < 1$ and $\bar{S}_N = x \in \mathbb{R}^N : \|x\| \leq 1$, where $\|\cdot\|$ is the Euclidean norm. Any continuous mapping $f : \bar{S}_N \rightarrow \bar{S}_N$ has a fixed point in $x_0 \in \bar{S}_N$.

In other words, considering a closed unit sphere \bar{S}_N and a continuous mapping f defined within that sphere, there exists $x^0 \in \bar{S}_N$ such that $f(x^0) = x^0$. By further defining a homotopy mapping $H : \bar{S}_N \times [0, 1] \rightarrow \bar{S}_N$ such that

$$H(x, \lambda) = (1 - \lambda)x + \lambda F(x) \quad (5.308)$$

it may be shown that there exists a path along which the Jacobian $(\partial H)/(\partial x)$ has rank N , emanating from $(0, 0)$ and reaching $(\bar{x}, 1)$, where \bar{x} is a fixed point of f . This results established for a unit sphere S_N (and \bar{S}_N) may be generalized to a region of radius r .

Various proofs and versions of the above theorem may be found in Ref. [64]. One of its versions is applied to the zero-finding problem

$$F(x) = 0 \quad (5.309)$$

that is addressed here.

Theorem 5.9.3 Let $F : \mathbb{R}^N \rightarrow \mathbb{R}^N$ be smooth. Suppose $F(x)^T \cdot x \geq 0$ when $|x| = 1$. Moreover, suppose that $H : \mathbb{R}^N \times [0, 1] \rightarrow \mathbb{R}^N$, where

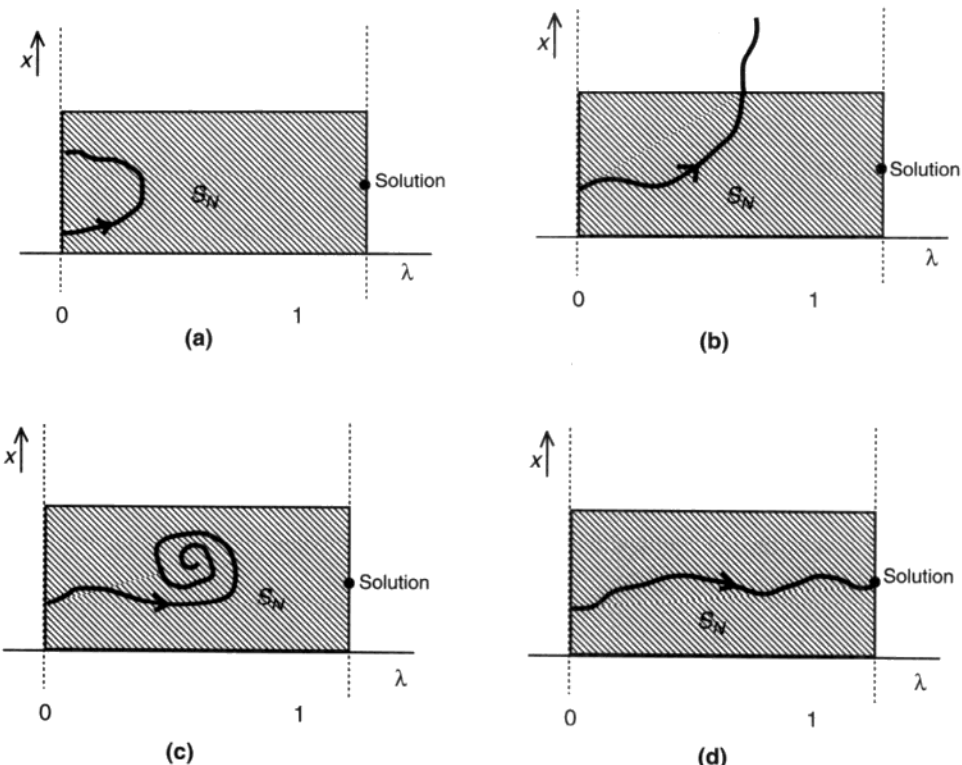
$$H(x, \lambda) = (1 - \lambda)x + \lambda F(x) \quad (5.310)$$

is regular. Then there exists $|x| \leq 1$ such that $F(x) = 0$.

The condition $F(x)^T \cdot x \geq 0$ is known as the inner-product condition. Here the significance of this theorem and the implications of the inner-product condition to homotopy convergence is stressed by presenting its proof.

Proof: The fact that H is regular at $\bar{\lambda}$ means that at all $(x, \bar{\lambda}) \in H^{-1}$, the Jacobian $(\partial H/\partial x)(x, \bar{\lambda}) \neq 0$, which further implies that all possible paths are well behaved. No spirals and no bifurcation points are present. How is it ascertained that the path will reach a solution within the region under consideration, S_N ? Consider all possible cases that may arise, as illustrated in Figure 5.23.

- The path may return and ‘hit’ the $\lambda = 0$ level as illustrated in Figure 5.23(a). But this can never happen since, at $\lambda = 0$, H has a unique starting point, defining a unique solution at that λ level.
- The path could tend to infinity before it reaches a solution, as shown in Figure 5.23(b). Contradiction may be used to prove that this ill-conditioned case may never occur: Suppose an \bar{x} may be found on the path such that

FIGURE 5.23 Different path behaviors within S_N .

$\bar{x} \in \partial S_N$, that is, \bar{x} is on the boundary of the unit ball S_N and the path is just about to exit this region and diverge to infinity. Then

$$H(\bar{x}, \lambda) = 0 \quad (5.311)$$

Consider now

$$H(\bar{x}, \lambda)^T \bar{x} = (1 - \lambda)\bar{x} + \lambda F(\bar{x})^T \bar{x} \quad (5.312)$$

which can be written as

$$H(\bar{x}, \lambda)^T \bar{x} = (1 - \lambda)\bar{x}^2 + \lambda F(\bar{x})^T \bar{x} = 0 \quad (5.313)$$

Since $F(\bar{x})^T \cdot \bar{x} \geq 0$ by assumption, $H(\bar{x}, \lambda)^T \bar{x}$ is positive and not zero. This leads to contradiction, because by Eq. (5.311), this should be 0, for every x . Hence H^{-1} cannot have a point on ∂S_N and the path will never cross the boundary towards infinity.

- The path might spiral, as shown in Figure 5.23(c). Regularity of H however, ascertains that this may never happen.

Hence the path is forced to reach the required solution at $\lambda = 1$, and the zero of $F(x)$ may be found, as illustrated in Figure 5.23(d).

5.9.4 Tracking the Paths

In the embedding algorithm, the path is followed by increasing the continuation parameter λ monotonically from 0 to 1, by fixed positive steps $\Delta\lambda$. It is necessary to choose an extremely small $\Delta\lambda$ in order for the algorithm to succeed. This may be attributed to the fact that λ may not be suited as a parameter for the curve. For typical homotopy methods, however, λ can both increase and decrease along the path with no adverse effect. In other words, the continuation parameter does not vary monotonically as the path length is increased. This is accomplished by parametrizing with respect to the path length s , so that $\lambda = \lambda(s)$ and $x = x(s)$. The problem of solving $H(x(s), \lambda(s)) = 0$ may then be changed to an initial-value problem, an idea first introduced by Davidenko in 1953 for the solution of a wide variety of problems including integral equations, systems of equations, and eigenvalue problems. This is derived by differentiating the homotopy equation $H(x, \lambda) = 0$ with respect to arc length s , as shown next.

The algorithm based on the ordinary differential equation (ODE) for tracking homotopy paths is presented here [65]. It has been adopted for all simulations here since it offers robustness and reliability, with the tradeoff of cost.

Assume the zero-finding problem

$$F(x) = 0 \quad (5.314)$$

is to be solved, with $F(x)$ in C^2 [i.e., $F(x)$ is twice continuously differentiable]. We may define a homotopy map $H(x, \lambda)$ such that the Jacobian matrix of H has full rank along the path. Assume H is given by Eq. (5.308). The zero curve can then be parametrized with respect to arc length s . One may then write

$$\lambda = \lambda(s), \quad x = x(s) \quad (5.315)$$

along the path so that

$$H(\lambda(s), x(s)) = 0 \quad (5.316)$$

Differentiating Eq. (5.316) with respect to s ,

$$\frac{d}{ds} H(\lambda(s), x(s)) = \frac{dH}{ds} \begin{pmatrix} \frac{d\lambda}{ds} \\ \frac{dx}{ds} \end{pmatrix} = 0 \quad (5.317)$$

with

$$\left\| \begin{pmatrix} \frac{d\lambda}{ds} \\ \frac{dx}{ds} \end{pmatrix} \right\|_2 = 1 \quad (5.318)$$

and initial conditions

$$\lambda(0) = 0, \quad x(0) = 0 \quad (5.319)$$

Then, the path is the trajectory of the initial value problem, given by Eqs. (5.317) to (5.319). $(d\lambda/ds, dx/ds)$ is a unit tangent vector on the path. From Eq. (5.317), the tangent spans the one-dimensional kernel of the $N \times (N + 1)$ Jacobian matrix of H . In other words, $(d\lambda/ds, dx/ds)$ is orthogonal to all rows of (dH/ds) and can be calculated by applying the fact that the $\ker(dH/ds)$ has exactly two vectors of unit norm ($\pm z$). These two vectors correspond to the two possible directions of traversing the path so that

$$\left(\frac{d\lambda}{ds}, \frac{dx}{ds} \right) = \pm \frac{z}{\|z\|_2} \quad (5.320)$$

The sign defines the orientation of the path and is chosen to maintain an acute angle with the previous tangent vector on the path. z is further computed by using Householder transformations [66] to QR factorize the Jacobian dH/ds in Eq. (5.317), so that

$$Q \frac{dH}{ds} P^T P z = 0 \quad (5.321)$$

where Q is a product of Householder reflections and P is a permutation matrix. This is of the form

$$\begin{pmatrix} x & \dots & x & x \\ 0 & \ddots & \vdots & \vdots \\ & & x & x \end{pmatrix} P z = 0 \quad (5.322)$$

By setting $Pz = 1$ and using back substitution, z [and hence $(d\lambda/ds, dx/ds)$] can be calculated. A predictor–corrector method [67,68] is then employed for the solution of the problem. More specifically, assuming a point on the path p_i , a new point p_{i+1} may be computed by using a predictor step such as

$$p_{i+1} = p_i + h \begin{pmatrix} \frac{d\lambda}{ds} \\ \frac{dx}{ds} \end{pmatrix} \quad (5.323)$$

where $h > 0$ is an appropriately chosen step size. Corrective action is then taken by solving the following optimization problem for w_{i+1} :

$$\|w_{i+1} - u_{i+1}\| = \min_{H(w)=0} \|w - u_{i+1}\| \quad (5.324)$$

Hence, consecutive points closest to the actual path are obtained until the final solution is reached.

5.9.5 Choosing a Homotopy Method

The choice of a homotopy method depends on the type of problem to be solved. The next sections present different homotopy variations that directly affect the exact path generated. Moreover, two distinct ways of embedding the continuation parameter in the initial problem are outlined.

5.9.6 Homotopy Variations

The convex or fixed point homotopy

$$H(x, \lambda) = (1 - \lambda)G(x) + \lambda F(x) \quad (5.325)$$

is only one of a series that may be used to implement the continuation paradigm. Other homotopy varieties include

$$H(x, \lambda) = F(x) - (1 - \lambda)F(x^0) \quad (5.326)$$

where at $\lambda = 0$, any initial point x^0 may be adopted. At $\lambda = 1$, the required solution is obtained.

The modified stimulus homotopy

$$H(x, \lambda) = (1 - \lambda)G(x) + F(\lambda x) \quad (5.327)$$

requires that at $\lambda = 0$

$$G(x) + F(0) = 0 \quad (5.328)$$

has a trivially found solution. This does not present a problem for the lossless $P-\theta$ or $Q-V$ decoupled load-flow problems, since in the first case

$$F(0) \propto \sin(0 \times \theta) = 0 \quad (5.329)$$

and in the latter case

$$F(0)\alpha(0 \times |V|^2) = 0 \quad (5.330)$$

and hence the solution of Eq. (5.328) becomes that of

$$G(x) = 0 \quad (5.331)$$

Each homotopy mapping defines a different path connecting the starting point to the desired solution. Adopting a homotopy function H is not a trivial task, since it is equation- (problem-) dependent. In the follow-up simulations all three homotopies are considered, resulting in different behavior and paths for the solution of the same examples.

5.9.7 Free-running versus forced homotopies

Embedding a homotopy parameter into a nonlinear equation is a crucial step in constructing various homotopies. In addition to the mapping $F(x)$ satisfying the

inner-product condition, the Jacobian matrix of the newly formed set of equations should not vanish anywhere along the homotopy path.

Two general ways to embed a homotopy parameter are as follows:

- Free-running case (artificial parameter homotopy): λ has no relation to system parameters.
- Forced case (natural parameter homotopy): λ has a physical meaning (often it is a system parameter).

In the free-running case, the continuation parameter λ has no physical meaning. It is just a real-valued variable (varying from 0 to 1 in the embedding algorithm) with no connection to the physical system under consideration. Free-running homotopy methods use the implicit function theorem [68] to ensure smooth paths. They may not be based on physical intuition but provide well-behaved paths to the solution(s) that normally do not require any sophisticated tracking algorithms. In the forced case, the continuation parameter is chosen to be a physical parameter varying in the system. The system equations in this case are of the form

$$F(x, p) = 0 \quad (5.332)$$

where p is the physical parameter varying in the system. Employing a forced continuation algorithm would mean setting the homotopy mapping to be

$$H(x, \lambda) = F(x, p) = 0 \quad (5.333)$$

with $\lambda = p$ and tracing this path for a prespecified change in the parameter λ . The solution path is then the trajectory of the system for the particular variation in the parameter p . It is interesting to note that defining a physical parameter as the continuation parameter in the homotopy problem may involve a careful normalization, usually based on physical intuition rather than preset rules. The forced case also has the disadvantage that it may give rise to ill-conditioned paths suffering from bifurcations, which may be difficult to trace numerically.

5.9.8 Globally Convergent Probability-1 Homotopy Algorithms

Recent mathematical developments have led to a new class of homotopy methods, known as globally convergent probability-1 homotopy methods. These methods ensure bifurcation-free paths provided the inner-product condition introduced in Theorem 5.9.3 is satisfied. They introduced a real vector $a \in \mathbb{R}^N$ in the trivial map $G(x)$ of Eq. (5.302), so that

$$H(x, \lambda) = (1 - \lambda)(x - a) + \lambda F(x) \quad (5.334)$$

Hence, at $\lambda = 0$, the initial solution is $x^0 = a$. The introduction of a ensures that the method will almost always converge to a solution of $F(x) = 0$ for an

arbitrary choice of starting point a . That is where the term “globally convergent probability-1” method comes from.

To summarize these theoretical results, the following criteria should be satisfied by the homotopy mapping and the problem to be solved, for a successful homotopy algorithm:

- The Jacobian $\partial H / \partial x$ is nonsingular at $H^{-1}(0)$.
- The initial problem is trivial to solve and has a unique solution.
- The final problem is the problem to be solved.
- The inner product $F(x)^T \cdot x \geq 0$ should hold for all x 's on the boundary of the region considered.
- $H_a^{-1}(0)$ is bounded.

5.9.9 Applications of Forced and Free-Running Homotopy Methods

Homotopy methods are in general robust, accurate, numerically stable, and almost universally applicable. They are suitable for nonlinear problems for which initial solution estimates are difficult to obtain, such as those encountered in the electric power-system analysis. Moreover, homotopy methods can find all solutions to a given problem, but in general all supporting theory establishes conditions for obtaining only one solution (the first one encountered by the path). They may be made globally convergent, that is, they may be made to converge to a solution from an arbitrary starting point. They are expensive on serial computers but their implementation on parallel computers results in improved efficiency because of a large amount of inherent parallelism [65]. Various applications of homotopy methods are presented next in the context of circuits and power systems.

5.9.10 Circuit Applications

In the area of electric circuits, homotopy methods have been applied in finding the DC operating points of transistor circuits. These circuits are described by a set of nonlinear algebraic equations, and the application of Newton's method for their solution exhibits the same convergence problems as those ones described in the appendix of this chapter. The equations solved in this case are the KCL equations at each node of the circuit and the unknowns solved for are the node voltages. Different homotopy methods have successfully been applied in generating the solutions required [69,70]. Yamamura and Horiuchi in Ref. [71] present another version of a homotopy algorithm that employs rectangular subdivisions for the solution of nonlinear resistive networks. This algorithm has its roots in the simplicial-type homotopy algorithms in Ref. [67]. These methods are not considered here because they have been reported [71] to be computationally inefficient for large-scale systems and therefore inappropriate for conventional power systems. An extensive treatment may be found in Ref. [67].

5.9.11 Applications of Continuation Methods to Power Systems

Continuation methods have successfully been employed in the solution of the load-flow equations describing power systems at steady state. Among the first applications of continuation in power systems problems was that of Thomas, Barnard, and Meisel [72], which addressed the problem of solving the load-flow equations by both forced and free-running algorithms. The continuation parameter, α in this case, is allowed to vary arbitrarily or has some physical meaning attached to it. Parametrization of the variables x and α is, however, done with respect to time, assuming continuity of all variables involved. Both methods are used in Ref. [72] to generate load-flow trajectories under prespecified load changes and multiple singular points.

A continuum of power-flow solutions for a load-change scenario has been generated by Ajjarapu and Christy [73]. A continuation power flow has been applied for steady-state stability analysis of power systems, starting at some base load and resulting at the critical point of the P - V curve. This is another demonstration of the forced continuation case, which requires the user to define where to go and how things are changing in the system. Adopting such an approach requires sophisticated tracking algorithms since such scenarios (driving the system to a bifurcation point) are prone to numerical instabilities.

In Ref. [74], a Newton homotopy is employed to prove that no solution exists to an ill-conditioned load-flow problem of an 11-bus system. The simulation results presented in this case may demonstrate this observation, but no theoretical results are presented linking nonconvergence and nonexistence of a solution to the homotopy method employed. Moreover, the homotopy mapping adopted in Ref. [74], may give rise to ill-conditioned cases and is inappropriate for power-system applications.

Last but not least, Guo and Salam [75] compute the zeros of power-flow equations by an embedding-based method. The work presented aims at eliminating traceable homotopy curves that do not converge to a solution. A unique feature is that the continuation parameter is allowed to vary in the complex plane between $0 + j0$ and $1 + j0$, increasing monotonically with the path length.

The application of the continuation method in electric-power-system analysis, although successful, requires further exploration. No conclusions have yet been drawn on the convergence properties of the method for the particular nonlinearities present in the power-flow problem. The effectiveness of different homotopy algorithms needs to be further examined. As a result, this section takes a step back and questions the application of globally convergent probability-1 homotopy methods in the decoupled power-flow problem. It explores how the choice of a homotopy mapping affects the number, as well as the nature of the solutions obtained. The specific type of nonlinearities inherent in the load-flow equations, namely trigonometric and quadratic, should influence this choice accordingly. Convergence and existence issues are directly studied.

5.9.12 Homotopy Software HOMPACK

Before proceeding with the choice of a homotopy software package to be used in the solution of electric-power-flow equations, one has to identify the aims of the simulation and the specifics of the analysis to be performed. Those aims could include

- Obtaining one specific solution to a particular system of power-flow equations
- Obtaining multiple solutions to such a system by tracking a single path
- Determining points where the dynamic and/or the numerical stability properties of the solutions change, that is, obtaining critical points such as bifurcation points or limit points
- Obtaining solutions for a specified sequence of values of a particular physical parameter varying in the system
- Using branch switching at a bifurcation point

Depending on the aims, an appropriate software code has to be adopted or developed. For example, the task of obtaining solutions for a specified sequence of values of a parameter defines the need for a program implementing forced homotopy techniques, as opposed to the free-running case. Ajjarapu and Christy [73] has presented such an algorithm by using the load as the continuation parameter.

Here attention is placed on the first three of the previously mentioned aims. This requires consideration and application of free-running homotopy methods. Such methods are applied here for the load-flow analysis of small, power-system examples. The objective is to examine the convergence properties of different homotopy mappings for the type of nonlinearities present in the power-flow equations so that the “best” homotopy mapping can be chosen and conclusions can be drawn on the application of the method to larger, more realistic power systems. Speed is not an issue; it is the basic convergence behavior of different paths that is addressed and examined.

5.9.13 Power-Flow Problem and HOMPACK

5.9.13.1 Introduction to HOMPACK HOMPACK [65], a software package implementing autonomous homotopies, has been used here for all simulations. The package has already been applied successfully in the solution of the nonlinear equations describing nonlinear resistive and transistor circuits [76,70]. It consists of a library of subroutines for solving sets of nonlinear equations and is specifically designed for probability-1 globally convergent homotopies. For the zero-finding problem

$$F(x) = 0 \quad (5.335)$$

HOMPACK assumes that $F(x)$ is a C^2 map (twice continuously differentiable) such that for some $r > 0$, $F(x)^T \cdot x \geq 0$ whenever $|x| = r$. The equation is then

solved by following the zero curve of a user-defined homotopy map, such as

$$H(x, \lambda) = (1 - \lambda)(x - a) + \lambda F(x) = 0 \quad (5.336)$$

emanating from $\lambda = 0, x = a$.

There are many algorithms within HOMPACK for tracking the homotopy path. The algorithm employed in all simulations is the ODE-based algorithm, where the zero curve H is parametrized by arc length s . The details of this algorithm are given in Ref. [65] and have been outlined previously. It was shown that the problem of tracing the path translates to that of solving an initial-value problem. This tracking algorithm may have the disadvantage of being expensive since it involves a large number of Jacobian evaluations, but it has generally proven to be one of the most reliable and robust [65], an observation which justifies its choice.

5.9.13.2 Definition of a Continuation Run Within HOMPACK HOMPACK provides the option of formulating a user-customized homotopy. In order to be able to run a specific homotopy equation $H(x, \lambda)$ for a particular set of equations, a subroutine has to be written and adjusted accordingly. Each subroutine is written in C and compiled with the rest of the code. For the solution of a homotopy equation of the form

$$H(x, \lambda) = (1 - \lambda)(x - a) + \lambda F(x) \quad (5.337)$$

the functions performed by the subroutine are as follows.

- Definition of the homotopy mapping H at point (x, λ) . The homotopy function considered is defined explicitly, together with its Jacobian entries, $\partial H / \partial x$ and $\partial H / \partial \lambda$, which in the case of Eq. (5.337) are given by

$$\frac{\partial H}{\partial x} = (1 - \lambda) + \lambda \frac{\partial F}{\partial x} \quad (5.338)$$

$$\frac{\partial H}{\partial \lambda} = (x - a) + F(x) \quad (5.339)$$

respectively. Every time the routine is called at each step, values for these components are calculated.

- The starting solution is provided explicitly. Considering again the homotopy of Eq. (5.337), the starting solution would be

$$x^0 = a \quad (5.340)$$

Note that x^0 has to be unique for $\lambda = 0$.

- Specific error measures and appropriate tolerances are provided that correspond to how closely the user requires the path to be followed and may be critical for the convergence of the method.

Furthermore, HOMPACK allows for a respectable amount of user intervention to control the process. This may be done by changing all or some of the following parameters:

- The initial point on the path via changing a
- The step length, which is defined as the “distance” between two points or the difference between two consecutively calculated solution points on the path
- The number of steps (HOMPACK stops after this preset number of continuation steps has been exceeded)
- Tolerance criteria, which provide the criteria for convergence

Bifurcations and turning points of the path defined by $H(x, \lambda) = 0$ should not occur; otherwise HOMPACK will fail. That is why the choice of a becomes critical. The randomness with which the starting point is chosen should yield a smooth path. If a is such that H is not regular, ill-conditioned cases may arise.

5.9.13.3 Output and Result Postprocessing HOMPACK generates two output data files. The first data file includes the solution path points; the second file encompasses error tolerances used at each step, the total number of iterations at each run (that may be further used for efficiency comparisons between different methods), and convergence flags.

5.9.14 Simulation Results

In order to assess the performance of different homotopy methods, two test examples of power systems form the basis of all simulations presented here. HOMPACK, briefly described earlier, has been compiled and run for all simulations on a VAXstation 3100 work station. The following two homotopy mappings have been considered for the decoupled, as well as coupled, load-flow equations of two examples:

$$H_1(x, \lambda) = (1 - \lambda)(x - a) + \lambda F(x) \quad (5.341)$$

$$H_2(x, \lambda) = (1 - \lambda)(x - a) + F(\lambda x) \quad (5.342)$$

5.9.14.1 Power-System Examples Considered

1. Single-machine-infinite-bus case. The simple case of a synchronous generator connected to an infinite bus via a transmission line is considered in this example. The load-flow equation describing the system is given by the following equations, assuming a lossless inductive transmission line:

$$P_2 = \frac{E_1 E_2}{X} \sin \delta \quad (5.343)$$

where P_2 is the mechanical power input to the generator, E_1 is the voltage magnitude at the generator bus, E_2 is the voltage magnitude at the infinite bus, δ is the angle by which E_1 leads E_2 , and X is the transfer reactance between the buses, that is, the reactance to which the machine reactance, together with the network reactance, is reduced.

2. *Two-machine-one-load case.* The example presented here is found in Ref. [77]. It consists of two generators connected to a load. Figure 5.24 illustrates the system topology and particular parameters used in all simulations. The equations describing the system under different assumptions follow.

- For the $P-\delta$ problem:

$$P_2 = E_2 E_1 B_{21} \sin(\delta_2 - \delta_1) + E_2 E_3 B_{23} \sin(\delta_2 - \delta_3) \quad (5.344)$$

$$P_3 = E_3 E_1 B_{31} \sin(\delta_3 - \delta_1) + E_3 E_2 B_{32} \sin(\delta_3 - \delta_2) \quad (5.345)$$

The numerical values of the line parameters and all other variables, assumed known, are given in Figure 5.24. The unknowns in this case are the angles δ_2 and δ_3 , that is, the angle difference $\delta_2 - \delta_3$.

- For the $Q-V$ problem:

$$Q_3 = -[E_3 E_1 B_{31} \cos(\delta_3 - \delta_1) + E_3 E_2 B_{32} \cos(\delta_3 - \delta_2) + E_3^2 B_{33}] \quad (5.346)$$

In this case, the unknown variable is the voltage magnitude E_3 , with all other parameters known.

- For the coupled problem:

$$P_2 = E_2 E_1 B_{21} \sin(\delta_2 - \delta_1) + E_2 E_3 B_{23} \sin(\delta_2 - \delta_3) \quad (5.347)$$

$$P_3 = E_3 E_1 B_{31} \sin(\delta_3 - \delta_1) + E_3 E_2 B_{32} \sin(\delta_3 - \delta_2) \quad (5.348)$$

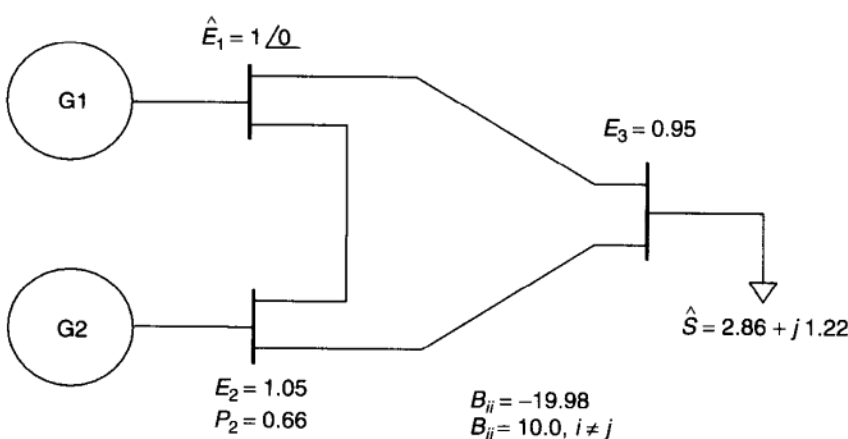


FIGURE 5.24 Two-machine-constant-power-load example.

$$Q_3 = -[E_3 E_1 B_{31} \cos(\delta_3 - \delta_1) + E_3 E_2 B_{32} \cos(\delta_3 - \delta_2) + E_3^2 B_{33}] \quad (5.349)$$

This is the combination of the two previous cases, with unknowns δ_2 , δ_3 , and E_3 .

5.9.14.2 Homotopy Applications to the $P-\delta$ Problem The decoupled $P-\delta$ problem exploits trigonometric nonlinearities. In this section results for the two example systems are presented.

5.9.14.2.1 Single-Machine-Infinite-Bus (SMIB) Case: Results and Observations Fixing X , the electrical power out of the machine and the voltage at the machine bus, yields an equation for δ . This equation can be more generally written as

$$\sin \delta = k \quad (5.350)$$

where

$$k = \frac{P^{\max}}{E_1 E_2} \quad (5.351)$$

This equation exhibits the trigonometric nonlinearity characteristic of the $P-\delta$ problem. Although simple, it provides a good starting point for the analysis, since it features three important characteristics, depending on the value of the constant k :

- Multiplicity of solutions for $-1 < k < 1$. An infinite number of solutions exist for this range of k . Although power-system analysis is usually restricted in the range $-\pi \leq \delta \leq \pi$, the possibility of generating multiple solutions should be investigated.
- No solution for $|k| > 1$.
- Bifurcation point for $k = 1$. This is an operating point where the Newton-Raphson step would fail, since the Jacobian at this point is zero.

CASE OF $-1 < k < 1$ (MULTIPLICITY OF SOLUTIONS) All simulations have been performed for $k = 0.5$. Although in this case one is generally interested in solutions between 0 and π , multiple solutions may be generated in one run (Fig. 5.25). The solutions to the problem are the points of intersection of the plotted path with the $\lambda = 1$ level. Both homotopies converge for arbitrary values of the trivial solution a producing smooth paths leading to multiple solutions. The first solution obtained in all runs is always a stable one.

Case of $k = 1.0$ (bifurcation point) Both homotopy methods H_1 and H_2 calculate the bifurcation points without resulting in numeric instabilities. Figure 5.26 illustrates the effectiveness of the method at points where the application of the

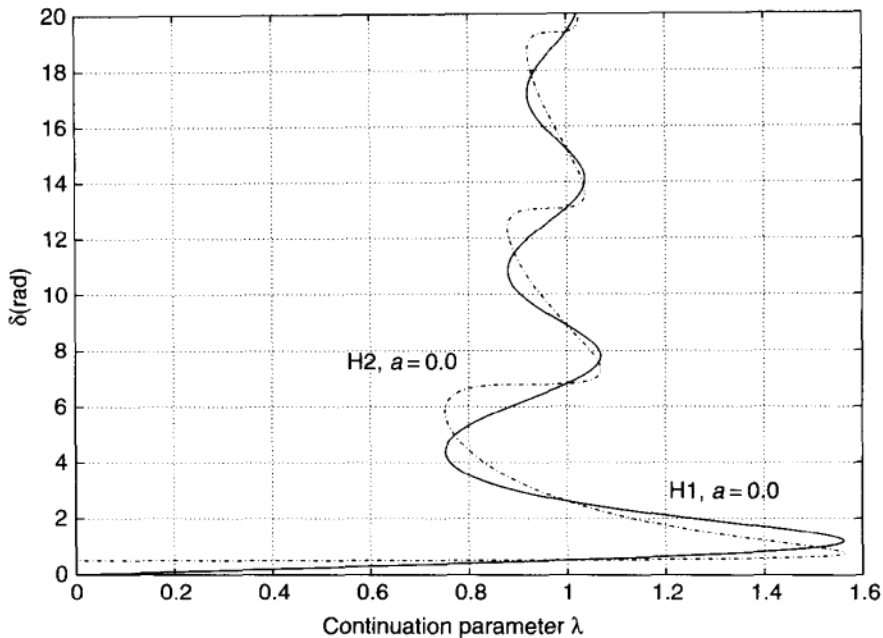


FIGURE 5.25 SMIB case: Finding multiple solutions using different homotopies.

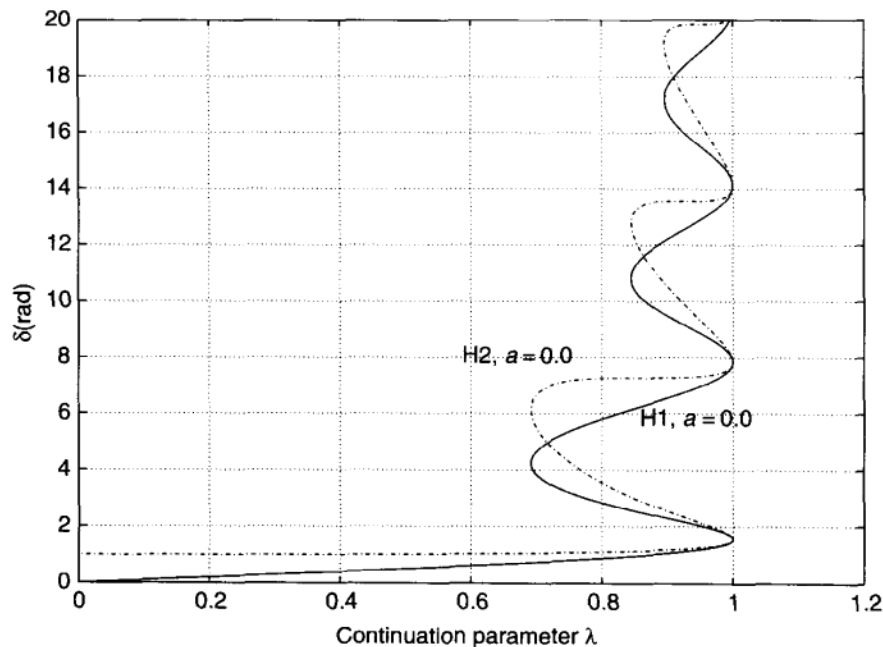


FIGURE 5.26 SMIB case: Calculation of the bifurcation point using different homotopies.

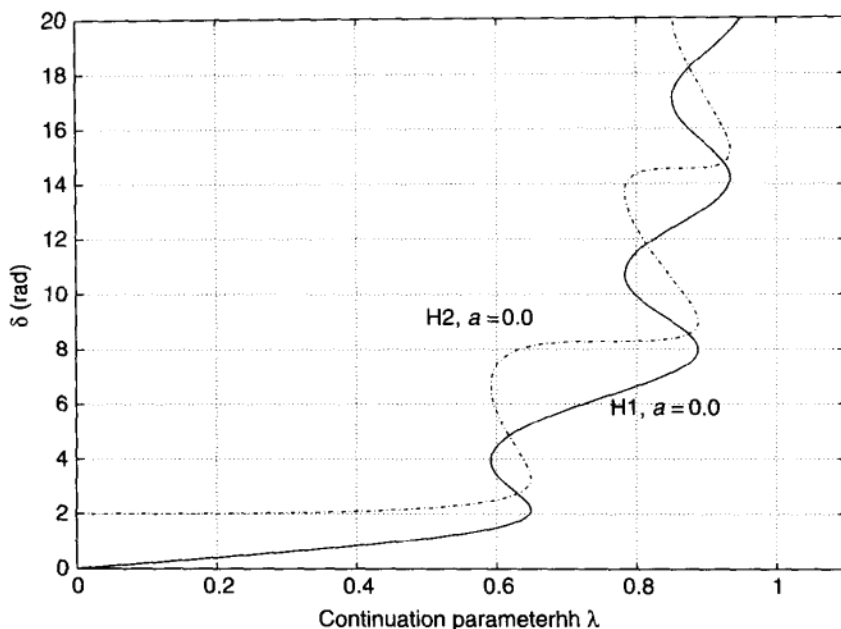


FIGURE 5.27 SMIB case: Both homotopy paths for no solution.

Newton–Raphson step would fail. Note again that multiple solutions may be generated, and one is not restricted to modulo 2π .

Case of $k = 2.0$ (no solution) Figure 5.27 gives homotopy paths for the case in which the system has no solution. The paths never reach the $\lambda = 1$ level, but instead keep increasing in length towards infinity.

TWO-MACHINE–CONSTANT-POWER-LOAD EXAMPLE The second example consists of two machines connected to a constant power load already introduced in Figure 5.24. This problem is one dimension higher in complexity than the SMIB case. The two real-power-flow equations are solved for the angles δ_2 and δ_3 . Results from homotopies 1 and 2 lead to some interesting observations as shown in Figures 5.28 to 5.31. The number of solutions generated, as well as the actual solution itself, depend on the choice a . For example, in Figure 5.28 the choice $a = 0.0$ yields only one solution, whereas in Figure 5.29 choice $a = -3.0$ yields multiple solutions. The second homotopy shows better convergence properties. Although it generates a more entangled and longer path, it provides a bigger range of distinct solutions for a larger range of a 's, as illustrated in Figures 5.30 and 5.31.

5.9.15 Homotopy Applications to the Q – V Problem

The equations describing the Q – V problem exploit quadratic nonlinearities. Such a problem may be generated using Bergen's example system of Figure 5.24. The

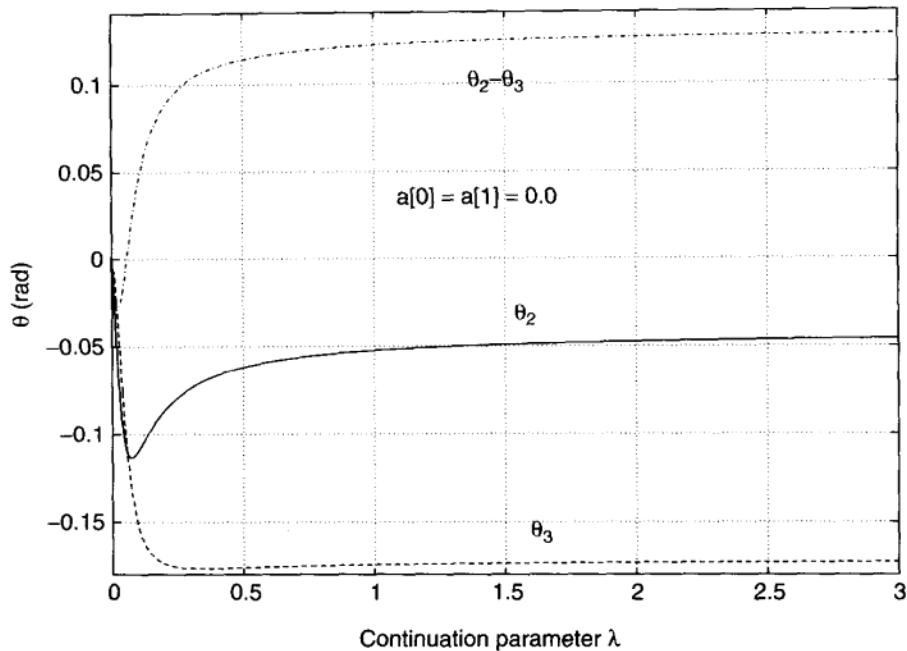


FIGURE 5.28 Two-machine–constant-power-load example: Obtaining one solution with H_1 .

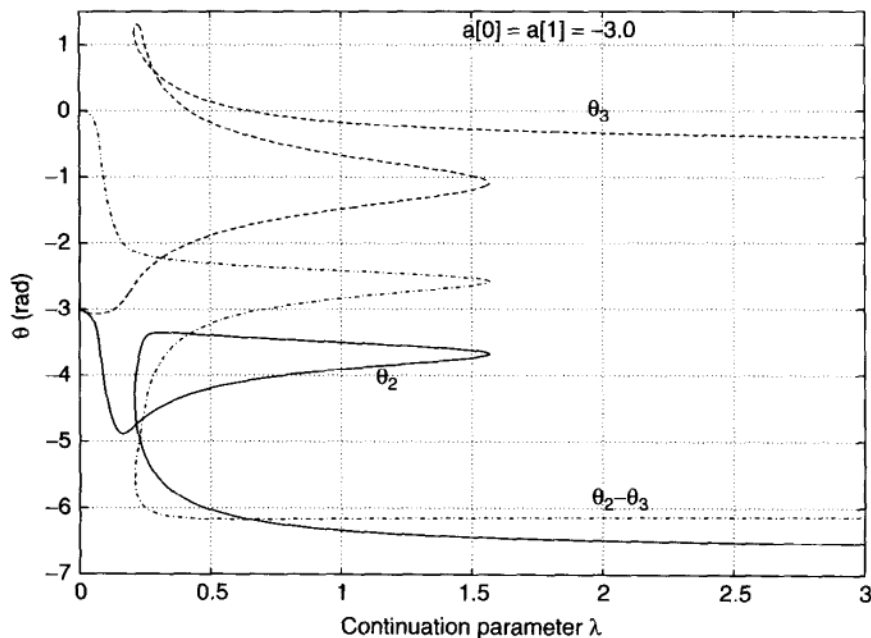


FIGURE 5.29 Two-machine–constant-power-load example: Obtaining multiple solutions with H_1 .

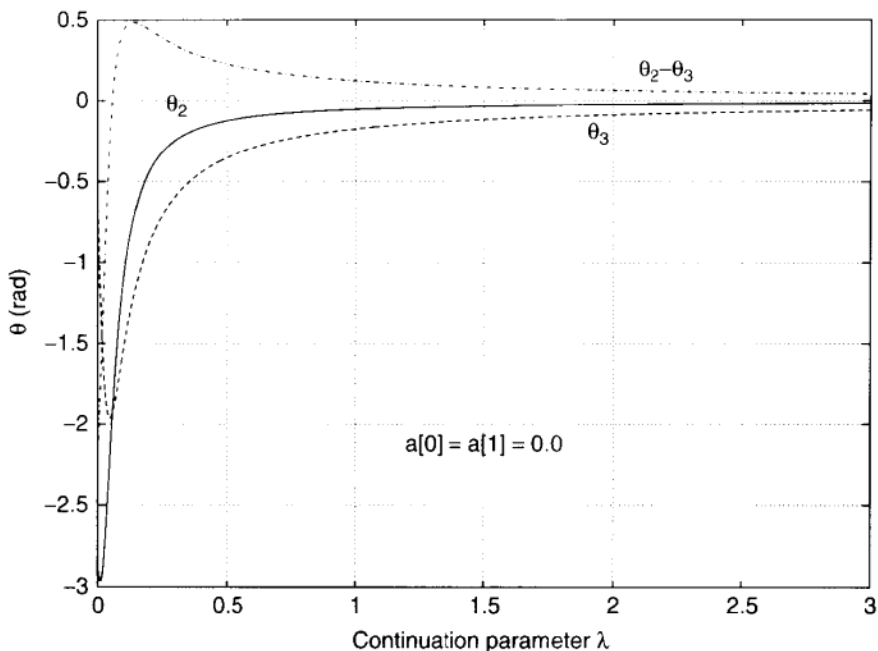


FIGURE 5.30 Two-machine–constant-power-load example: Obtaining one solution with H_2 .

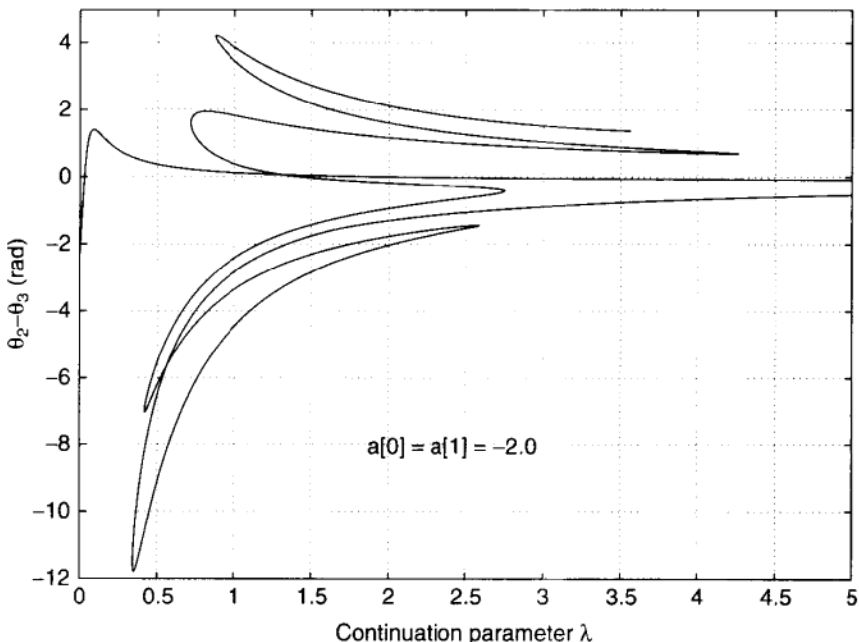


FIGURE 5.31 Two-machine–constant-power-load example: Obtaining multiple solutions with H_2 .

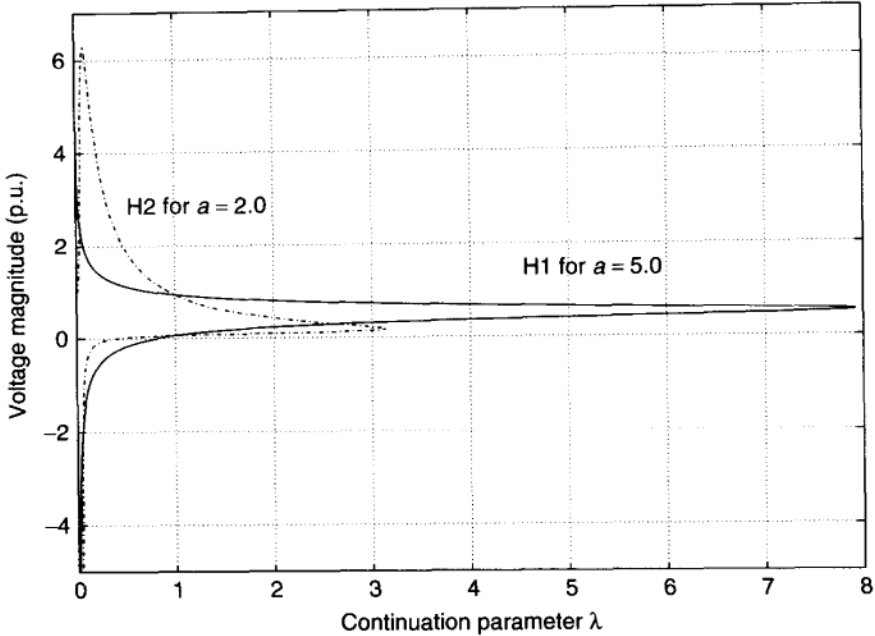


FIGURE 5.32 Two-machine—constant-power-load Q — V example: Generation of both solutions applying both homotopies.

equation described is quadratic in E_3 . The phase-angle differences are assumed known, $\delta_{31} = -0.174$ rad and $\delta_{32} = -0.122$ rad.

Homotopies 1 and 2 have been applied for its solution. Figure 5.32 illustrates the effectiveness of both homotopies for this type of nonlinearity. Generation of both solutions has been achieved for different starting points. The latter homotopy converges to both solutions for a considerably larger range of starting points than the former, an observation that was also made in the P — δ case too. Hence it would be expected that the second homotopy would be more effective in the coupled case presented next.

5.9.16 Coupled Load-Flow Problem: Bergen's Example

Results for the coupled load-flow problem of Bergen's example are included here for completeness and for the purpose of illustrating that the coupling of trigonometric and quadratic nonlinearities may not have as good convergence properties as the decoupled case. Figures 5.33 to 5.36 illustrate representative paths leading to solutions. The second homotopy equation is found to converge for more initial points a , as in the decoupled case.

5.9.17 Simulation Conclusions

This section summarizes results and observations made for all simulations. The first important point is that bifurcation points do not give rise to numerical

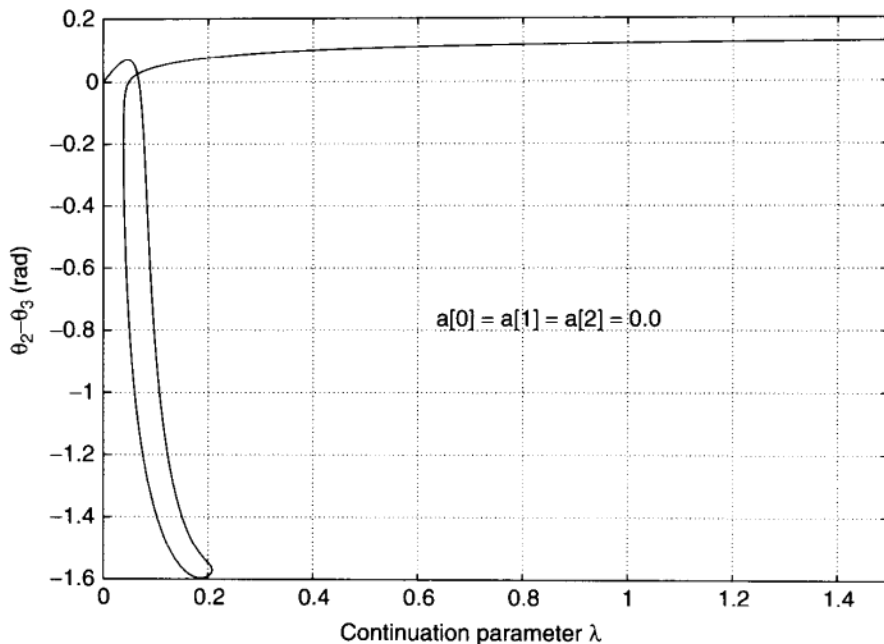


FIGURE 5.33 Coupled Bergen's example using H_1 : Obtaining the phase-angle difference.

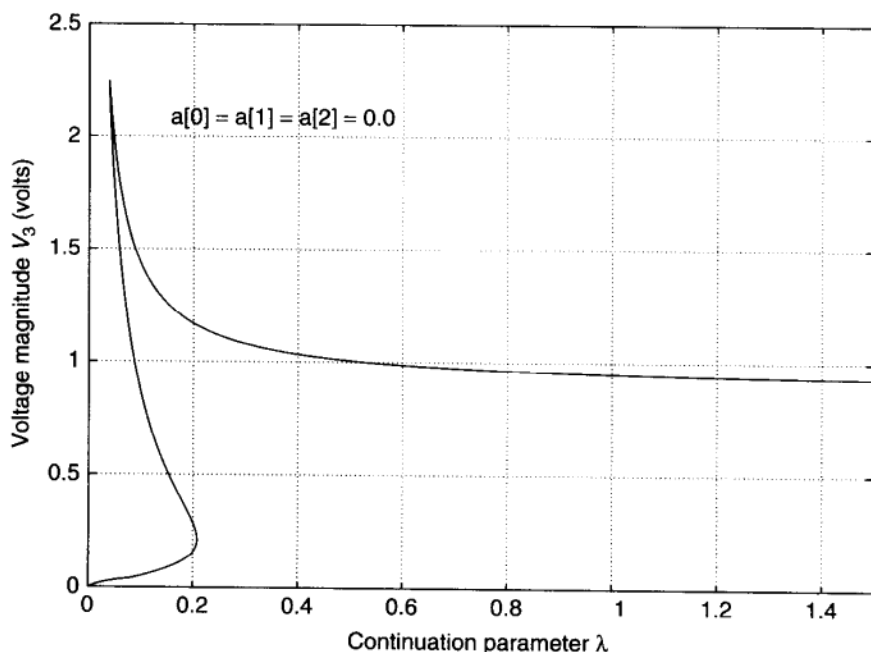


FIGURE 5.34 Coupled Bergen's example using H_1 : Obtaining the voltage magnitude.

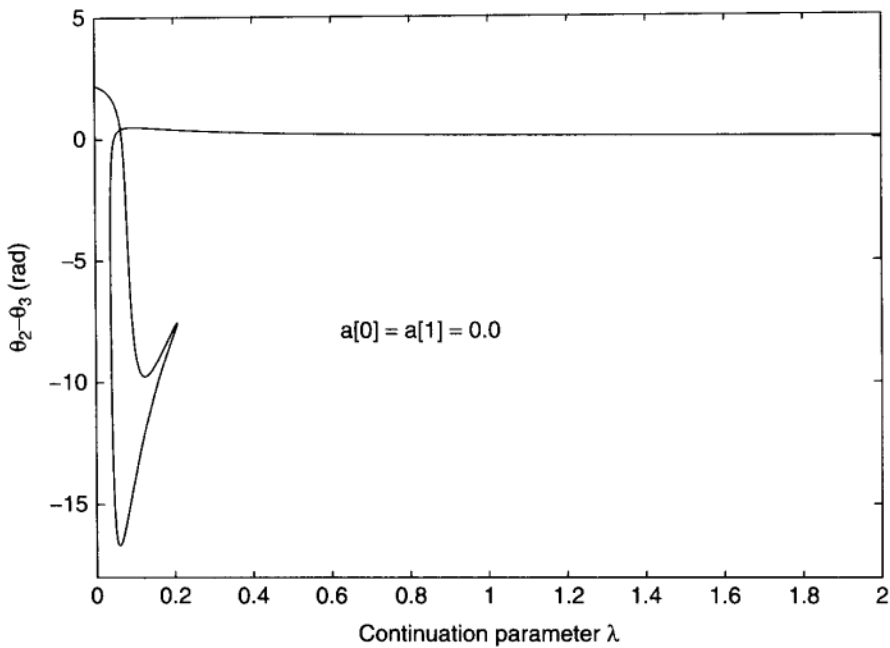


FIGURE 5.35 Coupled Bergen's example using H_2 : Obtaining the angle difference.

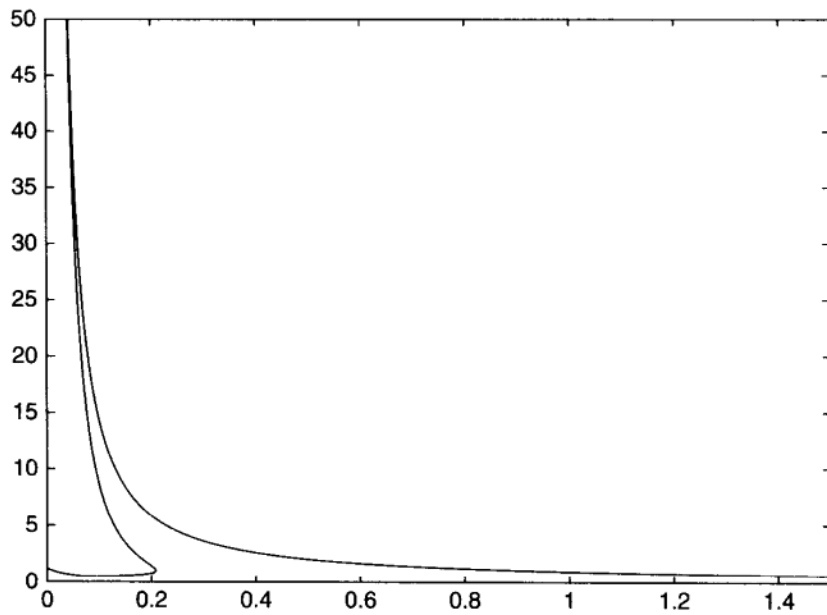


FIGURE 5.36 Coupled Bergen's example using H_2 : Obtaining the voltage magnitude.

instabilities, as would be the case with the Newton–Raphson method. Moreover, generation of multiple solutions with a single path is possible but, for the set of examples considered, this is dependent on the following features.

- *Type of homotopy mapping.* The second nonlinear homotopy

$$H_2(x, \lambda) = (1 - \lambda)(x - a) + F(\lambda x) \quad (5.352)$$

generates multiple solutions for a wider range of starting points than

$$H_1(x, \lambda) = (1 - \lambda)(x - a) + \lambda F(x) \quad (5.353)$$

for all decoupled problems. Notice, however, that the supporting theory (implicit function theorem, versions of Brouwer's fixed-point theorem) can be conclusive for only one of the solutions and more specifically for the one that the path encounters first. This is because the inner-product condition and the regions it defines guarantee only the existence of one solution.

- *Starting point on the path.* This plays a significant role on whether a single solution or multiple solutions will be generated. For the single-machine–infinite-bus case, both homotopies will generate multiple solutions for almost all a so that the following, more general statement can be made: Both homotopy mappings generate multiple solutions for both ill-conditioned and well-behaved single-machine–infinite-bus systems, irrespective of the initial guess. In other words, both homotopy methods are globally convergent, with a probability of 1 for the trigonometric nonlinearity presented by the simplest power system example. For a multidimensional P – δ problem, homotopy H_2 generates multiple solutions for a wider range of starting points. This is also true in the case of the Q – V problem.

More generally, both mappings are successful in generating at least one solution to the trigonometric nonlinearities presented in the P – δ problem. The convergence characteristics of both methods, however, are significantly different in the case of the Q – V problem, where the difference between the two homotopies is even more striking. H_1 converges to at least one solution for almost all a (except from a very small radius around zero). H_2 is globally convergent for starting points greater than zero, yielding both solutions with a single path. The fact that one of the solutions (the one in the lower part of the P – V curve) is unstable, renders the generation of both solutions with a single path and for almost all a an attractive characteristic.

From an efficiency point of view, the choice of a starting point for the path influences the path length and the number of iterations needed to reach the destination. This material focuses on small academic examples. Drawing any conclusions on the speed of the algorithm based on these examples would be inconclusive, since much larger electric power systems would have to be tested

out for a fair comparison of speed between homotopy methods and other conventional numerical techniques.

Finally, the most salient observation is that the methods converge only to stable operating points. Unstable points may be generated only after a stable point has been found.

5.10 CHAPTER SUMMARY

The general analysis for stationary operation of any dynamical process is concerned with properties of system equilibria. In the power-system literature a system equilibrium is most often identified with a solution to the power-flow equations.

In this chapter a conventional load-flow problem formulation is reviewed as a particular case of the equations defining system equilibrium under certain modeling assumptions. Once the basic definition of steady-state system operation is clarified, theoretical conditions are reviewed that allow for the steady-state voltage problem to be studied separately from the steady-state real-power problem.

Under the decoupling assumption made we proceed by reviewing first the decoupled real-power-angle $P-\delta$ problem as a nonlinear network problem. Conditions for existence of the unique solution to this problem are introduced. This is an important practical problem for determining the bounds on power that can be transferred on a given system.

Other general properties of real-power-change propagation are defined together with the supporting theoretical conditions for them to hold. In particular, a localized response property of real-power-change propagation is defined and proven, because it is commonly used in simplifying system analyses. It is important to be aware of the conditions under which this assumption does not hold, and, when violated, could lead to inaccurate conclusions.

Moreover, so-called distribution factors are reviewed as a means of computing sensitivities of real power line flows on changes in system inputs (generation and/or load). These are further used to set the basis for determining clusters of nodes (system inputs) which contribute in a similar way to a line flow of interest. These formulae are essential for information structures needed in transmission congestion management (Chapter 14). The problem of real power load flow is posed for both coordinated and competitive electric power industry.

Next, the decoupled reactive-power-voltage $Q-V$ problem is formulated as a nonlinear network problem. Conditions on network topology and its parameters and on system generation and demand are stated under which an operationally acceptable voltage solution exists. Conditions under which reactive-power-change propagation is similar to the real-power propagation are formulated and proven. Several relevant qualitative differences between the decoupled real-power and decoupled reactive-power problem are described.

The last section of this chapter is devoted to the numerical techniques for computing steady-state solutions. An extensive treatment is provided on the continuation methods and their application to simulations of scenarios for which conventionally used numerical methods do not converge.

APPENDIX 5.1 THE NEWTON–RAPHSON METHOD

The Newton–Raphson step, obtained by the Taylor-series expansion of F about an operating point, is given by

$$x^{k+1} = x^k - J(x^k)^{-1}F(x^k) \quad (5.354)$$

where x^{k+1} and x^k are the values of x at the $(k + 1)$ th and k th steps, respectively, and $J(x^k)^{-1}$ is the inverse of the Jacobian, $\partial F/\partial x$, at x^k .

This step is more easily understood in the one-dimensional case, where F becomes a function F in one variable x . Assuming that F is differentiable, that is, that F has a definite slope at each point in \mathbb{R} , a Taylor-series expansion yields an exact expression for F , by making use of the mean value theorem [78]. Hence, for $\tilde{x} \in [x^0, x]$

$$F(x) = F(x^0) + \frac{\partial F(x^0)}{\partial x}(x - x^0) + \frac{1}{2} \frac{\partial^2 F(\tilde{x})}{\partial x^2}(x - x^0)^2 \quad (5.355)$$

Ignoring the second-order term and setting $F(x) = 0$ yield the Newton step given in Eq. (5.354). Note that in the multidimensional case, the derivation is more involved since no vector mean value theorem may be defined and employed in this case. As a result, an exact Taylor-series expansion like that in Eq. (5.355) may not be written. The Taylor-series expansion is only approximate for multidimensional problems; second- and higher-order terms are commonly ignored.

The Newton–Raphson method converges quadratically, a characteristic that when combined with special programming techniques and matrix manipulations results in a fast and attractive solver. Quadratic convergence implies that errors in successive steps obey an inequality of the form

$$\|x^{k+1} - x^*\| \leq c \|x^k - x^*\|^2 \quad (5.356)$$

where $c < 1$ and $\|\cdot\|$ is the Euclidean norm.

However, the success of the method is guaranteed under certain assumptions and restrictions. Following are simple examples of functions in which the Newton–Raphson method fails to converge.

Singular Jacobian Case

Consider the steady-state power curve. At the point of maximum power transfer ($\delta = \pi/2$), the derivative is equal to zero and the tangent to the curve at that point has zero slope. At that point, the Newton–Raphson step (5.354) fails.

In the multidimensional case such a problem occurs when the Jacobian $J(x^k)$ is singular. The point x^k is called a bifurcation point. The Jacobian singularity present at such a point leads to numerical instabilities, which yield erroneous results. It is in general impossible to predict when the Jacobian will become singular, especially for multivariable systems that are both large in size and

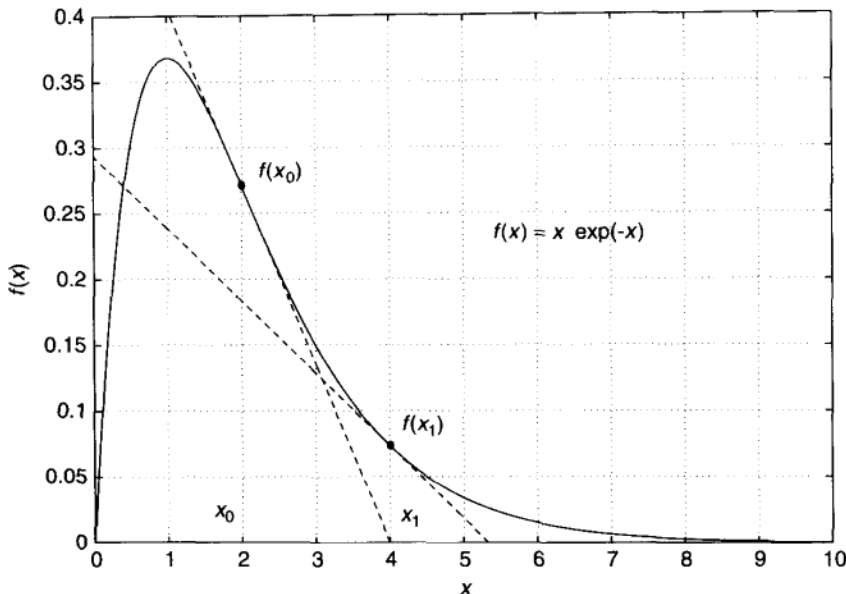


FIGURE 5.37 Convergence problem with an initial guess away from the solution.

highly nonlinear. Hence, one is forced to use the Newton–Raphson method, although the method might never converge in the end.

Initial Guess Outside the Region of Attraction of the Solution

The Newton–Raphson method fails to converge if the initial guess, x^0 , is too “far away” from the solution. The region of attraction of a solution is often hard to determine, especially for systems where no information about the solution is given *a priori*.

To illustrate how the choice of an initial guess affects convergence, consider the case of Figure 5.37, a plot of $F(x) = xe^{-x}$. The value of x^{i+1} in the method is the intersection of the x axis with the tangent to the curve at $F(x^i)$. The tangent at $x^0 = 2.0$ intersects the x axis at a point x^1 far away from the root, $x^* = 0$. Successive iterations yield guesses that recede from the solution, instead of converging to it. Hence $(0, 1)$ defines a region of attraction for the solution, $x^* = 0$ in this example. In other words, the Newton–Raphson method will only converge for $0 < x^0 < 1$. An initial guess outside this region results in no convergence.

Expanding this in multidimensional space is not a trivial task. Distances and regions of attraction are hard to visualize and even harder to estimate. A lot of consideration has to be given to the proper choice of a starting point.

Limit Cycle Problem

Another ill-conditioned case, although not very frequent in the power-system framework, is that of oscillating about the solution. Consider the case of $F(x) = \tan^{-1}(x)$ of Figure 5.38. There will be a limit value of the initial guess x^0 for

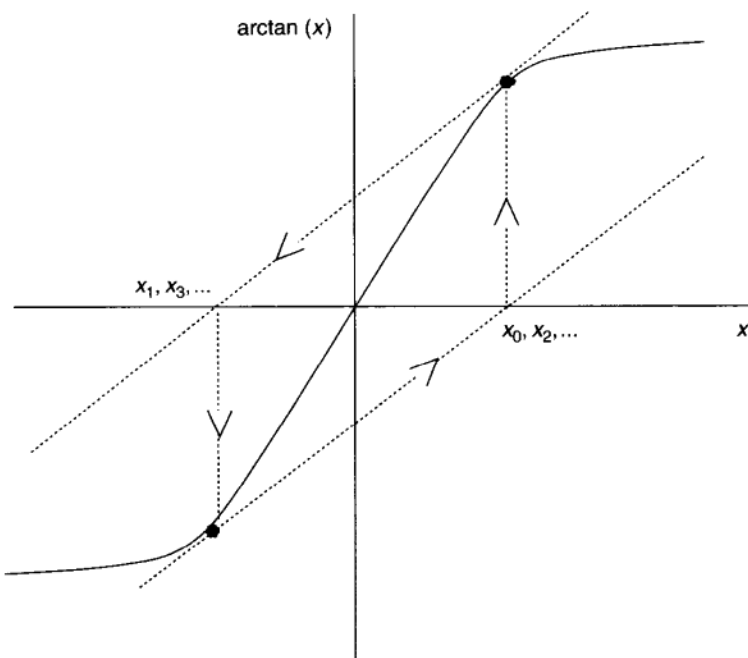


FIGURE 5.38 Limit cycle problem.

which the subsequent guesses will oscillate about the final solution, as illustrated. This problem occurs for all initial guesses on the boundary of the region of attraction of the solution, defined by the dashed-line parallelogram. If the initial guess were to fall inside that region, convergence would be guaranteed. Then comes the question of what “inside” really means in the multidimensional case. This question is difficult to answer because, in this case, regions and boundaries are hard to visualize and interpret.

Overflow Problem

This ill-conditioned case is better illustrated through an example of a constant-voltage source connected to a diode via a resistor, as shown in Figure 5.39. Kirchoff's current law at node 1 yields

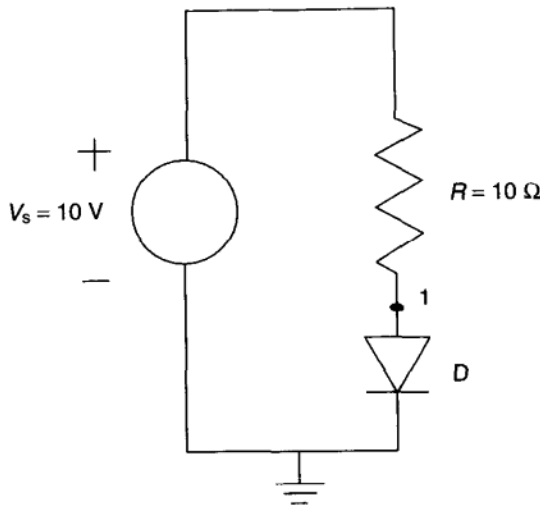
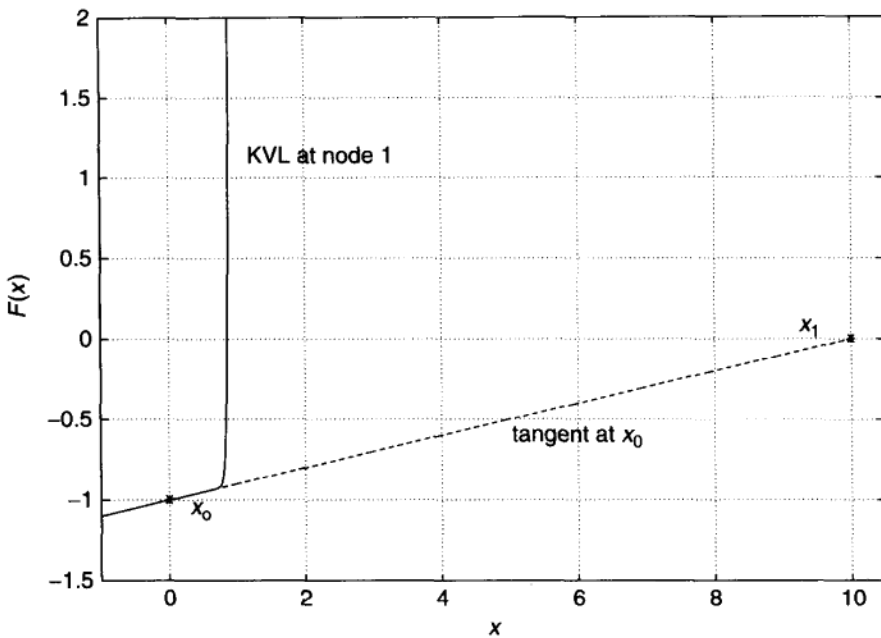
$$F(x) = I_s(e^{x/V_t} - 1) + 0.1(x - 10) = 0 \quad (5.357)$$

where x is the unknown voltage at node 1, I_s is the diode saturation current, and V_t is the diode voltage, $= 0.025$ V.

$F(x)$ is plotted in Figure 5.40. Choosing $x^0 = 0$ yields a voltage $x^1 = 10$. A numerical overflow occurs, as illustrated in the figure because

$$I_d = I_s(e^{10.0/0.025} - 1) \quad (5.358)$$

is a very large number. The diode example is also considered in Chapter 2 to present another methodology for solving the equations describing a physical system and to illustrate the basics of the continuation method.

**FIGURE 5.39** Diode circuit.**FIGURE 5.40** Numerical overflow.

Application of the Newton–Raphson Method in the Solution of the Load-Flow Problem

An interesting aspect of the Newton–Raphson method is that, under certain modeling assumptions, the Jacobian matrix at a given operating point provides a linearized mathematical model of the power system at that operating point [5].

This becomes an advantage when combined with small-signal stability analysis, where the stability of the system is assessed in the neighborhood of an equilibrium point. The position of the Jacobian eigenvalues in the s plane determines the stability of the nonlinear model in that neighborhood.

The computation time (αn^3) and storage requirements (αn^2) of the Newton-Raphson method would be prohibitive for very large systems, such as commercial power systems, if conventional matrix techniques were to be employed. In load-flow analysis, however, use is made of the sparsity of the system Jacobian matrix. This sparsity is preserved by ordered triangular factorization, and sparse matrix techniques are further applied resulting in very efficient solutions. An efficiency-related drawback of the method is that the coefficients of the Jacobian matrix are functions of the unknowns E and δ and hence not constant. As a result, the matrix has to be recalculated at each iteration, unless special techniques evaluating the rate of change of these variables have been incorporated. If E and δ are not changing rapidly over a certain region, the Jacobian need only be recalculated after an appropriate number of iterations.

In Ref. [79] an extensive survey on the application of the Newton-Raphson to large power-system problems is given. The issues of speed, accuracy, and convergence are directly addressed. The number of iterations required for solution is not dependent on the type or the size of the problem for problems with a flat voltage start, that is, for problems in which the initial guess for voltage magnitude and phase angles is 1 and 0, respectively. Round-off errors that arise in the direct solution of the system of simultaneous equations is the only limiting factor in the accuracy of the power-flow solution.

It has already been stressed that the initial guess should not be far away from the solution required. This condition may not be restrictive for conventional power systems, where a flat voltage start is usually sufficient; voltage magnitudes are usually set equal to their scheduled values or to the magnitude of the slack-bus voltage. Voltage-phase angles are often set to the slack-bus reference angle. In some situations, however, such guesses may not be a good idea. Such cases are likely to arise in the competitive electric power systems, as well as under large system contingencies. The operating point of the system, following such severe contingencies, may be too "far away" from the flat voltage start and thus too difficult to predict. The Newton-Raphson method may never converge.

Nonlinear Relaxation Methods

The most commonly used relaxation techniques are the Gauss-Seidel and the Gauss-Jacobi methods, which may be used in the solution of both linear and nonlinear sets of algebraic equations. They differ only in the information they use at each iteration. The algorithms for these methods are briefly outlined below.

In the Gauss-Jacobi method each x_i^k is calculated using values for all other unknowns from the previous iteration. In the Gauss-Seidel method, however, the new information is used as soon as this is made available, that is, the latest iteration values are adopted as soon as they have been calculated. The algorithms

listed will only work if the equations $F(x)$ in the inner loops have unique solutions in the specific domain under consideration. If the problem to be solved is nonlinear, the Newton–Raphson method may be used in the inner loops to solve for the individual nonlinear equations, resulting in the following inner loops: Gauss–Jacobi–Newton method:

$$x_i^{k+1} = x_i^k - \left(\frac{\partial F_i(x^k)}{\partial x_i} \right)^{-1} F_i(x^k) \quad (5.359)$$

Gauss–Seidel–Newton method:

$$x_i^{k+1} = x_i^k - \left(\frac{\partial F_i(x^{k,i})}{\partial x_i} \right)^{-1} F_i(x_i^{k+1}) \quad (5.360)$$

where

$$x^{k,i} = (x_1^{k+1}, x_2^{k+1}, \dots, x_{i-1}^{k+1}, x_i^k, x_{i+1}^k, \dots, x_N^k)^T$$

Relaxation methods present linear convergence, that is,

$$\|x^{k+1} - x^*\| \leq \gamma \|x^k - x^*\| \quad (5.361)$$

where $\gamma < 1$, as opposed to the quadratic convergence of the Newton–Raphson step.

The system Jacobian may be decomposed into its diagonal, strictly lower-triangular and strictly upper-triangular matrices, so that

$$J(x) = D(x) + L(x) + U(x) \quad (5.362)$$

This may be written as

$$J(x) = B(x) - C(x) \quad (5.363)$$

In the Gauss–Seidel method $B = L + D$ and $C = -U$, whereas in the Gauss–Jacobi method $B = D$ and $C = -(L + U)$. Convergence for nonlinear relaxation methods is governed by the following theorem [80].

Theorem 5.11.1 Given $F: \mathbb{R}^n \rightarrow \mathbb{R}^n$, assume that F is continuously differentiable in an open neighborhood S of x^* , such that $F(x^*) = 0$. If $B(x^*)$ is nonsingular and $\rho(B(x^*)^{-1}C(x^*)) < 1$, then there exists an open ball $S^* \subset S$ such that the nonlinear relaxation methods converge to x^* for any initial guess $x^0 \in S^*$.

$\rho(B(x^*)^{-1}C(x^*)) \leq 1$ is the spectral radius of $B(x^*)^{-1}C(x^*)$. It is important to note that this result is only valid for initial guesses close enough to the solution. The spectral radius condition of the above theorem holds if the matrix $B-C$ is strictly diagonally dominant, that is, if the sum of the off-diagonal elements

of each row is less than the diagonal element of the same row. The speed of convergence depends on the spectral radius of each iteration. The smaller the radius, the more dominant the diagonal, the more rapid the convergence. Diagonal dominance is further related to the coupling between the system variables. Consider, for example, the simple case of a system of two linear equations in two unknowns:

$$a_{11}x_1 + a_{12}x_2 = b_1 \quad (5.364)$$

$$a_{21}x_1 + a_{22}x_2 = b_2 \quad (5.365)$$

The spectral radius for the Gauss–Seidel method is given by $|a_{12}a_{21}/a_{11}a_{22}|$, which should be less than 1 for convergence. If both $a_{12} \neq 0$ and $a_{21} \neq 0$, x_1 and x_2 are coupled. If, on one hand, the product $a_{12}a_{21}$ is large compared to $a_{11}a_{22}$, the variables are tightly coupled. On the other hand, if the product $a_{12}a_{21}$ is small compared to $a_{11}a_{22}$, the variables are loosely coupled. Such conditions may be used to partition the system into groups of equations of tightly coupled variables, which may be solved independently of other blocks.

Relaxation Newton methods are good for solving nonlinear systems whose Jacobian matrix is diagonally dominant and the initial guess for each inner loop is close enough to the solution. Their advantage is that the largest residual is known at each step and readjustment of the corresponding x is performed to reduce this residual to zero. This, however, requires more computing time and hardware [81]. The application of such methods in the load-flow problem is plagued by the fact that they converge more slowly than the Newton–Raphson method, especially as one gets closer to the solution. Moreover, the number of iterations increases with problem size, an attribute that renders these methods inappropriate for conventional power systems. However, less storage space is required than with the Newton–Raphson method.

In Ref. [82] another formulation of the load-flow problem is presented. The definition of blockwise strictly diagonally dominant nonlinear mappings is presented, and sufficient conditions are established for convergence of block Jacobi and block Gauss–Seidel iterations. This method converges for initial guesses that are considerably farther from the flat start than the Newton–Raphson method.

REFERENCES

1. IEEE Guide for Synchronous Generator Modeling Practices in Stability Analysis, IEEE Standard 1110–1991.
2. Stott, B., Review of load-flow calculation methods, *Proc. IEEE*, **62**: 916–929, 1974.
3. Desoer, C. A., and Kuh, E. S., *Basic Circuit Theory*, New York: Mc Graw-Hill, 1969.
4. Venikov, V. A., Stroev, V. A., Idelchik, V. I., and Tarasov, V. I., Estimation of electric power system steady-state stability in load flow calculations, *IEEE Trans. Power Apparatus Syst.* **PAS-94**: 1034–1041, 1975.

5. Sauer, P. W., and Pai, M. A., Power system steady-state stability and the load-flow Jacobian, *IEEE Trans. Power Apparatus Syst.*, **5**,: 1374–1381, 1990.
6. Chua, L. O., and Lin, P. M., *Computer-Aided Analysis of Electronic Circuits: Algorithms and Computational Techniques*, Englewood Cliffs, NJ, Prentice-Hall, 1975.
7. Sauer, P. W., Hajj, I. N., Pai, M. A., and Trick, T. N., Computer methods in electric network analysis, IEEE Paper No. 83 WM 023–9, 1983.
8. Galiana, F. D., and Lee, K., On the steady-state stability of power systems, Proc. Power Industry Computer Applications (PICA) Conf., 1977, pp. 201–210.
9. Jarjis, J., and Galiana, F. D., Quantitative analysis of steady-state stability in power networks, IEEE Paper No. F 79 753–5, 1979.
10. Marceau, R., Malihot, R., and Galiana, F., A generalized shell for dynamic security analysis in operations planning, *IEEE Trans. Power Syst.*, **8**,: 1099–1106, 1993.
11. Varga, R. S., *Matrix Iterative Analysis*, Englewood Cliffs, NJ, Prentice-Hall, 1962.
12. Kaye, R. J., and Wu, F., Analysis of linearized decoupled Flow Approximations for steady-state security assessment, *IEEE Trans. circuits and syst.*, vol. **CAS-31**: 623–636, 1984.
13. Schultz, D. K., Error on the Q-V decoupled load flow, M.Sci. thesis, Cornell University, 1984.
14. Fischl, R., and Puntel, W. R., Computer aided design of electric power transmission networks, Paper C 72 168–8, presented at the 1972 PES Winter Meeting, New York, NY, 1972.
15. Wu, F. F., and Sullivan, R. L., Nonlinear resistive circuit models for power system steady-state analysis, Proc. 14th Allerton Conf., Univ. of Illinois, Urbana, IL, 1976, pp. 261–268.
16. Sauer, P. W., and Christensen, J. P., Power system network analysis using an electronic circuit modeling approach, Proc. 1983 IEEE Intl. Symp. Circuits Syst., Newport Beach, CA, 1983, pp. 1176–1179.
17. Sauer, P. W., and Christensen, J. P., Active linear RC circuit models for power system analysis, *Electric Machines Power Syst.*, **9**: 103–112, 1984.
18. Narasimhamurthi, N., and Ilić, M. D., A proof of localized response of large interconnected power systems in steady state, Proc. Allerton Conf., 1980, pp. 997–1002.
19. Ilić, M. D., Spong, M. W., Fischl, R., “The No-gain Theorem and Localized Response for the Decoupled $P - \theta$ Power Network with Active Power Losses Included”, *IEEE Trans. on Circuits and Systems*, vol. **CAS-32**, no. 2, pp. 170–177, February 1985.
20. Ilić, M., Network-theoretic conditions for existence and uniqueness of steady state solutions to electric power circuits”, Proc. *ISCAS'92*, San Diego, pp. 2821–2828, 1992.
21. Hasler, M., Wang, C., Ilić, M., and Zobian, A., Computation of static stability margins in power systems using monotonicity, Proc. *ISCAS'93*, Chicago, pp. 2196–2199, 1993.
22. Tavora, C., Smith, O., “Equilibrium Analysis of Power Systems”, *IEEE Trans. on PAS*, vol. **PAS-91**, pp. 1131–1137, 1972.
23. Sekine, Y., Yokoyama, A., “Multisolusions for Load-Flow Problem of Power System and Their Physical Stability”, Proc. of the 7th PSCC, pp. 819–826, 1981.

24. Klos, A., Krener, A., "The Non-uniqueness of Load-Flow Solutions", Proc. of the PSCC, vol. 5, no. 2, pp. 3–1/8, 1975.
25. Hasler, M., and Wang, C., Monotonic dependence on sources in nonlinear resistive circuits, AEU, *Intel. Jo. Electron. Commun.* vol. **46**: 242–249, 1992.
26. Ilić, M. D., Yoon, Y. T., and Zobian, A., Available transmission capability and its value under open access, *IEEE Trans. Power Syst.* **12**: 636–645, 1997.
27. Zaborszky, J., Huang, G., and Lin, S. Y., Control of reactive power and voltage in emergencies, *IFAC Automatica*, **21**: 237–246, 1985.
28. Winokour, M., and Cory, B. J., Identification of strong and weak areas for emergency state control, presented at the IEEE/PES Winter Mtg., Dallas, TX, 1984, Paper No. 84WM 022–0.
29. Zaborszky, J., Whang, K. W., and Prasad, K. V., Fast contingency evaluation using concentric relaxation, *IEEE Trans. Power Apparatus Syst.*, **PAS-99**: 28–36, 1980.
30. *Reactive Power: Basics, Problems and Solutions*, IEEE Tutorial Course, 87 EH 0262-6-PWR, 1987.
31. Yu, C-N., and Ilic, M., Congestion clusters-based markets for transmission management, Proceedings of the IEEE PES Winter Meeting, New York, NY, 1999.
32. Ilić, M. Galiana, F. D., Fink, L. H., Bose, A., Mallet P. Othman, H. Transmission Capacity in Power Networks, Electrical Power and Energy Systems, vol. 20, pp. 99–110, 1998.
33. Galiana, F. D. and M. D. Ilić, "A Mathematical Framework for the Analysis and Management of Power Transactions Under Open Access," *IEEE Transactions on Power Systems*, PWRS-13, 681–687, May 1998.
34. Ilić, M., F. D. Galiana and L. Fink (eds.) *Electric Power Systems Restructuring: Engineering and Economics*, Kluwer Academic Publishers, 1998.
35. Ilić, M. D., Thorp, J. S., and Spong, M. W., Localized response performance of the decoupled Q-V network, *IEEE Trans. Circuits Syst.* **CAS-33**: March 316–322, 1986.
36. Thorp, J. S., Ilić, M. D., and Schultz, D. K., Existence and uniqueness of a solution to the reactive power problem for an electric power network, Proc. IEEE Int'l. Sympo. Circuits Syst. (ISCAS), pp. 372–376, 1984.
37. Thorp, J. S., Ilić, M., and Schulz, D., Reactive power-voltage problem: Conditions for the existence of solution and localized disturbance, *Intl. J. Electrical Power Energy Syst.* **8**: 66–74, 1986.
38. Seneta, E., *Non-Negative Matrices*, New York: Wiley, 1973.
39. Berman, A., and Plemmons, R. J., *Non-negative Matrices in the Mathematical Sciences*, New York: Academic Press, 1979.
40. Reppen, D. N., "Incipient System Voltage Collapse Analysis", Power Technologies, Inc., Schenectady, N. Y., Final Report no. R60-91, June 1991.
41. Dessel, P., Glavitch, H., "Estimating the Voltage Stability of a Power System", Proc. of the 1985 PICA Conf., pp. 424–430.
42. Nagao, T., et al, "Analytical Method and Operation Index for Voltage Stability of Bulk Power Systems", *Trans. on IEE of Japan*, vol. 116-B, no. 11, November 1990.
43. Lachs, W. R., "Voltage Collapse in EHV Power Systems", IEEE paper no. A 78 057–2, January 1978.

44. Medanić, J., Ilić, M. D., Christensen, J., "Discrete Models of Slow Voltage Dynamics for Under Load Tap-Changing Transformer Coordination", IEEE Trans. on Power Systems, vol. PWRs-2, no. 4, 1987, pp. 873–882.
45. Barbier, C., and Barret, J. P., An analysis of phenomena of voltage collapse on a transmission system, RGE-Special Issue, July 1980, pp. 3–21.
46. Ilić, M. I., and Stobart, W., Development of a smart algorithm for voltage monitoring and control, IEEE Trans. on Power Systems PWRS-5, 1183–1193, 1990.
47. Willson, A. N., *Nonlinear Networks: Theory and Analysis*, City: IEEE Press, 1974.
48. Yorino, N., Sasaki, H., Masuda, Y., Tamura, Y., et al, "An Investigation of Voltage Instability Problems", IEEE Trans. on Power Systems, vol. 7, no. 2, 1992, pp. 600–611.
49. Borremans, P., Calvaer, A., deReuck, J. P., Goosen, J., VanGeert, Van Hecke, J., and Van Ranst, A., Voltage stability—Fundamental concepts and comparison of practical criteria, CIGRE Paper No. 38–11,?
50. Van Cutsum, T. Lecture notes on Reactive power, DSI Inc. Course, Monaco, 1990 (private exchange).
51. Desoer, C. A., The Maximum Power Transfer for n-ports, *IEEE Trans. Circuit Theory*, **CT-20**: 328–330, 1973.
52. Calvaer, A. J., On the maximum loading of active linear electric multiports, *Proc. IEEE*, **71**: 282–283, 1983.
53. Ilić, M. D., and Liu, X., Some optimality notions of voltage profile for the steady-state operation of the electric power systems, Proc. of the Workshop on Bulk Power System Voltage Phenomena III, Davos, Switzerland, 1994.
54. Zaborszky, J., and Rittenhouse, J. W., *Electric Power Transmission*, Reynolds, 1954. Available in paperback at Renssaelear University Bookstore, Troy, N.Y.
55. Anderson, P., Agrawal, B., and Van Ness, J., *Subsynchronous Resonance in Power Systems*, New York: IEEE, 1990.
56. Papazoglou, T. M., On the maximum efficiency of a long transmission line, *Intel. Jo. Electrical Power Energy Syst.*, **12–1**: J 69–70, 1990,
57. Papazoglou, T. M., On the maximum efficiency of transmission lines: Part II, *Intel. Jo. Electrical Power Energy Syst.* **16–5**: 349–351, 1994.
58. Gutman, R., Application of line loadability concepts to operating studies, *IEEE Trans. Power Syst.*, 1426–1433, 1988.
59. Donohue, T. J., and Rana, R. D., Analytical study of the loadability of AEP's AMOS-MATT Funk 345 kV circuit, *Proc. Am. Power Confe.* 1988.
60. Yan, H. H., Willson, J. D., "The PJM Approach to Detect, Analyze and Operate the System Considering Reactive Problems", 87 EG0262-6-PWR, Tutorial Course.
61. *Voltage Stability of Power Systems; Concepts, Analytical Tools, and Industry Experience*, IEEE Tutorial Course, 90 HO 358-2-PWR, 1990.
62. Tolikas, M., The application of homotopy methods in the analysis of electric power systems, M.Sci. thesis MIT, 1992.
63. Ortega, J. M., and Rheinboldt, W. C., *Iterative Solutions of Nonlinear Equations in Several Variables*, New York: Academic, 1969.
64. Istrătescu, V. I., *Fixed Point Theory, An Introduction*, Dordrecht: Reidel, 1981.

65. Watson, L. T., Billups, S. C., and Morgan, A. P., HOMPACK: a suite of codes for globally convergent homotopy algorithms, *ACM Trans. Mathe. Software*, **13**: 281–310, 1987.
66. Golub, G. H., and Van Loan, C. F., *Matrix Computations*, 2nd ed. Baltimore, MO: Johns Hopkins University Press, 1991, pp. 211–213.
67. Allgower E. L., and Georg, K., *Numerical Continuation Methods, An Introduction*, Springer-Verlag Series in Computational Mathematics, New York: Springer, 1990, pp. 1–15, and 346–382.
68. Garcia, C. B., and Zangwill, W. I., *Pathways to Solutions, Fixed Points and Equilibria*, Englewood Cliffs, NJ: Prentice-Hall, 1981, pp. 1–23.
69. Trajković, Lj., Melville, R. C., and Fang, S. C., Passivity and nogain properties establish global convergence of a homotopy method for DC operating points, *Proc. IEEE Int. Symp. Circuits and Systems*, New Orleans, LA, 1990, pp. 914–917.
70. Trajković, Lj., Melville, R. C., and Fang, S. C., Finding DC operating points of transistor circuits using homotopy methods, *IEEE Int. Symp. Circuits Systems*, Singapore, 1991, pp. 758–761.
71. Yamamura, K., and Horiuchi, K., A globally and quadratically convergent algorithm for solving nonlinear resistive networks, *IEEE Trans. Comput.-Aided Design*, Vol. **9**: 487–499, 1990.
72. Thomas, R. J., Barnard, R. D., and Meisel, J., The generation of quasi steady-state load flow trajectories and multiple singular point solutions, presented at the *IEEE Winter Power Meeting*, New York, 1971.
73. Ajjarapu, V., and Christy, C., The continuation power flow: A tool for steady state voltage stability analysis, presented at the *2nd Intl. Workshop Bulk Power Syste. Voltage Phenom. Voltage and Security*, Maryland, 1991.
74. Okumura, K., Terai, K., and Kishima, A., Solution of ill-conditioned load flow equation by homotopy continuation method, *Proc. IEEE Int. Symp. Circuits Systems*, Singapore, 1991, pp. 2897–2899.
75. Guo, S. X., and Salam, F. M. A., The imbedding-based method: computing the zeroes of models of power systems, *Proc. IEEE Int. Symp. Circuits Systems*, Singapore, 1991, pp. 868–871.
76. Trajković, Lj., Melville, R. C., and Fang, S. C., Improving DC convergence in a circuit simulator using a homotopy method, presented at *Custom Integra. Circuits Confe.*, San Diego, CA, 1991.
77. A. R. Bergen, *Power Systems Analysis*. Englewood Cliffs, NJ: Prentice-Hall, Inc., 1986, pp. 150–179.
78. Bers, L., and Karal, F., *Calculus*. Holt, Rinehart and Winston, 1976, pp. 352–355.
79. Tinney, W. F., and Hart, C. E., Power flow solution by Newton's method, *IEEE Trans. Power Apparatus Syste.* **PAS-86**: 1447–1460, 1967.
80. Saleh, R. A., and Newton, A. R., *Mixed Mode Simulation*. Kluwer Academic, 1990, pp. 52–64.
81. Stagg, G. W., and El-Abiad, A. H., *Computer Methods in Power Systems Analysis*., New York: McGraw-Hill, 1968.
82. Ilić-Spong, M., Katz, I. N., Dai, H., and Zaborszky, J., Block diagonal dominance for system of nonlinear equations with application to load flow calculations in power systems, *Mathematical Modeling*, **5**: 275–297, 1984.

6 Analysis of Linearized (Small-Signal) Dynamics

This chapter concerns modeling and analysis of power-system dynamics assuming validity of model linearization. The term *small-signal stability analysis* or *dynamic stability* is then used in electric power systems to refer to the analysis of a linearized dynamic model around an equilibrium point [1]. Such an analysis is usually carried out to determine the system sensitivity with respect to small deviations in initial conditions of the state and its inputs and/or parameter perturbations. Of particular interest is the system response to persistent random fluctuations in load demand.

The starting model is derived by linearizing a general nonlinear dynamic model [Eqs. (4.50) to (4.54)]

$$\begin{aligned}\dot{\tilde{x}} &= f(\tilde{x}, \tilde{y}, \tilde{u}, \tilde{p}) \\ 0 &= g(\tilde{x}, \tilde{y}, \tilde{u}, \tilde{p})\end{aligned}\tag{6.1}$$

around an equilibrium (x_0, y_0, u_0, p_0) . Here the tilde stands for the actual values of states \tilde{x} , outputs \tilde{y} , inputs \tilde{u} , and parameters \tilde{p} . The general form of the linearized dynamics is

$$\dot{x} = Ax + B_1u + B_2p\tag{6.2}$$

where $x = \tilde{x} - x_0$, $u = \tilde{u} - u_0$, and $p = \tilde{p} - p_0$. Also,

$$\begin{aligned}A &= \left[\frac{\partial f}{\partial x} - \frac{\partial g}{\partial y}^{-1} \frac{\partial g}{\partial x} \right] \\ B_1 &= \left[\frac{\partial f}{\partial u} - \frac{\partial g}{\partial y}^{-1} \frac{\partial g}{\partial u} \right]\end{aligned}$$

and

$$B_2 = \left[\frac{\partial f}{\partial p} - \frac{\partial g}{\partial y}^{-1} \frac{\partial g}{\partial p} \right]$$

are evaluated at the operating point (x_0, u_0, y_0, p_0) .

Note that the small signal stability concerns situation in power systems where local has geographical meaning (like the Lake of the Ozark power plant) and a mathematical meaning for the small (infinitesimal) neighborhood of equilibrium

points. Dynamic however has a very wide use and it should not be, tied to a limited problem ideas in power engineering.

Depending on how detailed model in Eqs.(4.50) to (4.54) is used, the resulting linearized model (6.2) may or may not be applicable to studies of particular physical phenomena. Care must be taken when simplifying these models. To start with, any disturbance affects all system states, and their exact changes can be analyzed using only a full-order model. Despite this fact, much effort has been devoted to model the reduction of power system dynamics. As in modeling any other dynamic system, this is typically done to avoid unnecessary complexity whenever possible.

The model-reduction techniques in power systems have yet another, implied, purpose. A typical question concerns conditions under which angle dynamics may become separable from voltage dynamics [2], and, moreover, conditions under which angle instability occurs independently of voltage instability and vice versa [3]–[7]. This question has been the focus of research as some real-life power systems have experienced voltage-related operating problems.

Model-reduction techniques have yet another conceptual importance in power systems. In a horizontally structured power system consisting of often weakly connected subsystems, it is possible to derive a relatively low-order model relevant for understanding interactions among the subsystems (interarea dynamics), as well as detailed models relevant for understanding dynamics inside each subsystem (intraarea dynamics.)

In this chapter we first study conditions under which linearized system dynamics can be decoupled into subprocesses of direct interest. We show how under these conditions the elementary classification of a two-bus power-system dynamics into fast (angle), midrange (voltage), and long-range (frequency and/or voltage) subprocesses described in Chapter 4, Section 4.3 can be generalized to larger power systems. Relevant models for subprocesses are introduced.

Next, the problem of model reduction in a very large power system is studied using the same model-reduction techniques. We stress the important distinction between the notion and physical importance of an interarea variable defined for a given horizontal structure of a large system into subsystems, on one hand, and the slow model resulting from similar dynamic motions of groups of machines, independent of administrative borders within an interconnection, on the other.

The model reduction of power-system dynamics is based on two commonly used techniques for model simplification of many other dynamic systems, namely, the singular perturbation (SP) and selective modal analysis (SMA) techniques. These are briefly summarized in Appendixes 6.2 and 6.3, respectively. Some relations between the two are given in Appendix 6.4.

Once the models are introduced, the small-signal stability analysis of these models is straightforward. Basic analysis uses the elementary result that, given $u = 0$ and $p = 0$, the system of time-invariant linear differential equations (6.2) will have a stable response to initial conditions $x(0) \neq 0$ when all eigenvalues of system matrix A are in the left-half plane. More involved sensitivity techniques are needed to analyze the robustness of system dynamics with respect to parameter uncertainties [8].

6.1 OBJECTIVES OF SMALL-SIGNAL ANALYSIS STUDIES IN POWER SYSTEMS

Recall that a system response to an arbitrary small disturbance in state x , input u , and/or parameter p is determined by the dynamic model given in Eq. (6.2). Depending on the relative sensitivities of particular modes to a specific disturbance, the system response could range from exhibiting fast frequency instabilities before any significant voltage changes are seen, through a stable frequency response followed by the slower oscillations in voltage dynamics, etc. The small-signal response to disturbances is determined by both the natural (open-loop) system response and by the various controllers. Different components respond at the rates determined by their own time constants, much in the same way as in any other dynamic system.

One of the main objectives of systematic small-signal power-system analysis is to establish sufficiently complete models for capturing phenomena of interest in real-life power systems. However, basic concern that instability may occur at an unexpected rate of response requires a systematic approach to model reduction and establishment of conditions under which different subprocesses can be studied independently. When in doubt, one should always start with as complete model of a power system as possible and check if the conditions under which a given reduced-order model is used are applicable to the problem of interest. The starting model is usually of a very high order. Various model-reduction techniques are typically used to create a lower-order model capable of reproducing a phenomenon of direct interest.

This thinking leads to the development of reduced-order models relevant for analyzing conditions under which a power system could have unstable frequency in response to a small disturbance, even before voltages begin to vary and before controllers react; models relevant for analyzing voltage oscillations that may occur after real power is fully matched; models relevant for designing controllers capable of stabilizing open-loop response of the system, etc. These reduced-order models are only valid under certain assumptions about the subprocesses that are neglected. For example, one could use type IV₁ models to represent the dynamics of the generators to study conditions under which a fast frequency instability may take place. Hidden in choosing this model is a strong assumption that loads and transmission lines (and all other equipment, including transformers) respond instantaneously and in a stable fashion to the class of disturbances under a particular study. This model is then not capable, by definition, of capturing the problem of so-called subsynchronous resonance reflected in instabilities of the state variables defining transmission line dynamics, such as the time-varying phasors $\hat{I}_L(t)$ and $\hat{E}_C(t)$ in the equivalent π -circuit model of a line (Chapter 3).

6.1.1 Effect of Models Employed on Stability Analysis and its Results

As one would expect, stability-analysis results depend on modeling assumptions made when defining the starting dynamic model (6.1). We recall from Chapter 3

that the only components typically modeled as truly dynamic are synchronous machines, turbines, and their local controllers, such as governors and excitors. Loads are typically modeled as static devices. It is because of this that the level of model complexity at the interconnected system level is generally determined by the level of complexity of models used for representing dynamics of the generator–turbine–governor (G-T-G) units and voltage controllers.¹

Recall from Chapter 3 that the closed-loop dynamics of any electric power system can be thought of as consisting of generators locally controlled and interconnected to the loads through a transmission network, as shown in Figure 6.1. This is a simplified version of the general power-system structure shown in Figure 3.3, in which components relevant for modeling closed-loop system dynamics with primary generation-based controllers are kept.

Local generator controllers are governors controlling their mechanical power output deviations P_T in response to the frequency deviations ω_G around the set-point values ω_G^{ref} and excitation systems controlling field voltage deviations e_{fd} in response to the terminal voltage deviations E_G (also denoted E_t) from the set values E_G^{ref} . The relevant output variables on the generator side affecting the transmission network and the loads are real power P_G , reactive power Q_G , frequency ω_G , and terminal voltage E_G . The quantities P_L , Q_L , ω_L , and E_L are corresponding variables at the load side. During normal operating conditions, governors and excitation systems respond automatically to the random load fluctuations. The turbine–generator sets have their own dynamics of producing P_G and Q_G , which combined with the governor and excitation systems dynamics forms what is referred to in this text as the (local) primary dynamics of the governor–turbine–generator (G-T-G) sets. For frequency ranges of interest in normal operating conditions, the network is modeled as an algebraic constraint imposed on generator and load outputs. Most uncertainty is seen in load models. They are typically modeled as sinks of constant real power P_L and reactive power Q_L . The main purpose of the primary frequency and voltage controllers is to cancel out the effects of fast load fluctuations in P_L and Q_L .

The dynamics of generation-based controllers, on the other hand, interact in various ways with the switched-type network and load controllers, all evolving at

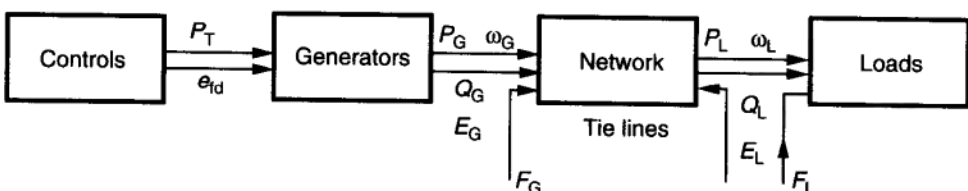


FIGURE 6.1 Structure of an electric power system.

¹ None of the analysis in this book is critically dependent on modeling other components as static devices. Any other devices when modeled as dynamic components can be incorporated into the model of the interconnected system by following the general modeling described in Chapter 4.

different rates. In this chapter we study this complex closed-loop system dynamics in response to small perturbations under which linearization holds.

In the past, most analyses have been concerned with frequency dynamics over very short time intervals following a perturbation. With the increase of voltage-related instabilities it has become important to establish rigorous theoretical conditions under which these subprocesses within the power-system dynamics are separable.

Techniques based on singular perturbation (Appendix 6.2) and selective modal analysis (Appendices 6.3 and 6.4) have been used for systematic model reduction of general power-system dynamics by many researchers. As a first step, a general problem of model reduction in power systems over a variety of time horizons starting from the transient time through midterm and long-term dynamics can be thought of as a multiparameter singular perturbation problem [9,10].

6.1.2 A Multiparameter Singularly Perturbed Model of an Electric Power System

A multiparameter singularly perturbed model of a dynamic system is typically represented as [9,10]

$$\begin{aligned}\dot{y} &= A_y y + A_{yz_1} z_1 + A_{yz_2} z_2 + \cdots + A_{yz_m} z_m \\ \varepsilon_1 \dot{z}_1 &= A_{z_1 y} y + A_{z_1 z_2} z_2 + \cdots + A_{z_1 z_m} z_m \\ &\vdots \\ \varepsilon_m \dot{z}_m &= A_{z_m y} y + A_{z_m z_1} z_1 + \cdots + A_{z_m z_m} z_m\end{aligned}$$

In this model full state vector $x(t)$ is partitioned into a slow substate $y(t)$ and faster substates $z_1(t), z_2(t), \dots, z_m(t)$, and $\varepsilon_m < \varepsilon_{m-1} < \dots < \varepsilon_1 \ll 1$.

For purposes of modeling the linearized dynamics of electric power system in this form we start by recognizing the inherent temporal separation of various phenomena in response to deviations of $x(t), u(t), p(t)$ from the assumed equilibrium and/or in response to exogenous disturbances $d(t)$. This inherent time scale separation of relevant subprocesses is summarized in Table 6.1.

Depending on the load model used, the effect of load deviations can be studied as a change in parameter, or the load could have its own dynamics, or it could be represented as an exogenous system disturbance.

A typical engineering approach to the small signal stability analysis of power systems has been to assume when studying $z_i(t)$ ($i = 1, 2, 3$) that all other $z_j(t)$, $j > i$ are stabilizable and that $z_i(t)$, for $j < i$ together with $y(t)$ remain constant. For example, when analyzing possible angle instability in response to parametric changes or perturbation in initial frequency around an equilibrium of interest ($z_3(t)$, in Table 6.1), it is generally assumed that the transmission network instantaneously (without any dynamics in $z_4(t)$) reacts to changes in system conditions, which, in turn, implies no SSR problems present. At the same time, all other

TABLE 6.1 Typical Phenomena of Interest

Subprocess of interest	Typical rate of response	Variable of interest	Typical cause	Control means
Subynchronous resonance (SSR)	Very fast (m sec to sec)	$z_4(t) = [\hat{I}_L(t) \hat{E}_C(t)]$	Interplay between rotor shafts and transmission	Excitation systems, power system stabilizers, FACTS
Angle instability	Fast (10^{-2} sec to sec)	$z_3(t) = [\omega_G(t) \delta_G(t)]$	Deviations in p and $x(0)$	Excitations systems, power system stabilizers, FACTS, fast valving
Voltage instability	Midrange (1–10 sec)	$z_2(t) = [e'_q(t)]$	Inadequate network design and/or excitation control	Excitation systems
Frequency deviations	Slow (>10 sec)	$\omega_L(t)$	Persistent deviations in real power load	Governor control
Voltage deviations	Slow (>10 sec)	$z_1(t) = e'_q(t)$	Persistent deviations in reactive power load	On-load tap changing transformers, capacitor banks
Frequency drift	Very slow ($10^{-1} - 10^4$ sec)*	$y(t) = \omega_L(t)$ $y(t) = \omega_L(t)$	Slow persistent real power load deviations	Secondary level frequency regulation, AGC
Load voltage drift	Very slow ($10^{-1} - 10^4$ sec)*	$y(t) = E_L(t)$ $y(t) = E_L(t)$	Slow persistent reactive power load deviations	Secondary level voltage regulation, AVC

*System-dependent designs.

slower phenomena ($z_2(t)$, $z_1(t)$ and $y(t)$) are assumed unchanged for the time horizon of interest.

To justify this approach one must, however, check if the conditions for decoupling the two (or more) subprocesses closest in their rates of response are met. Moreover, even when these conditions are met, one should recognize that the subprocesses are always corrected up to a certain degree and that it is therefore, desired to develop lower (reduced)-order models in terms of the variable of direct interest while accounting for the effect of the suppressed subprocesses in the higher order model approximations. Over the past 10–20 years much analytic effort has been devoted to developing such systematic model reduction procedures for simplifying complex dynamics of the electric power systems.

In this chapter we illustrate these model reduction techniques to reflect the temporal separation indicated in Table 6.1.

In what follows we first illustrate in Section 6.2 the process of separating closed-loop dynamics in a small three-bus example driven by its generator-excitator dynamics to analyze if the system will remain stable before the governor-turbine control activates. A detailed integral-manifold derivation is illustrated to define conditions under which fast frequency dynamics are separable from the electromagnetic (voltage) dynamics and to show the process of incorporating effects of other variables on the variables of direct interest. The problem of small-signal instabilities in the decoupled real-power–frequency dynamics model is characterized as the fast frequency instability problem. Similarly, unstable reactive-power–voltage model derived is characterized as the (midrange) voltage instability.

Next, in Section 6.3 a linearized model for studying slow closed-loop generator-excitator reactive power dynamics controlled by the OLTCs responding to load voltage deviations caused by slow reactive power load changes is described assuming that real power is balanced. It is illustrated that even when midrange voltage dynamics can be stabilized one could have long-range voltage instability caused by inadequate network voltage control devices such as on-line tap changers (OLTCs) as the reactive power demand varies. A reduced-order model relevant for capturing the OLTC-created (midterm) voltage instability is described using the same general model-reduction concepts. Understanding this systematic model reduction for studies of voltage–reactive power dynamics is particularly important since this is a newer, less-studied phenomenon.

This is followed by deriving in Section 6.4, a reduced-order model for studying slow linearized closed-loop real power dynamics of a governor-turbine-generator set responding to frequency deviations caused by real power load changes assuming that voltages do not affect the outcome significantly.

In Section 6.5 slow voltage-reactive power model driven by the reactive power load variations is introduced.

We emphasize that the proposed classification of various types of small-signal instabilities is dependent on the system. It indicates, for instance, that in typical power systems one could separate a subprocess driven by slower governor-turbine control from the subprocess driven by generally fast excitation

systems. However, it is important to keep in mind that the classification is not general. It is based on typical features of vertically integrated and horizontally structured interconnected grids. As the small-scale distributed generation penetrates lower-voltage-level portions of the grid, the relative dynamics of subprocesses may be significantly different. This is the subject of future research.

6.2 SEPARATION OF FAST ANGLE AND MIDRANGE VOLTAGE DYNAMICS

This section presents an illustration of the typical use of the singular perturbation method (Appendix 6.2) for separating two subprocesses evolving at different rates. Conditions under which a separation is meaningful are established for the simple three-bus system shown in Figure 4.4. This example is used throughout this chapter to illustrate various aspects of small-signal analysis in power systems, and it originates from the Ph.D. thesis of Fong Mak [3,5].

The illustration is carried out starting from a full-order model of system dynamics resulting from the interactions of the synchronous-machine dynamics and the primary voltage control, that is, the voltage regulator dynamics. This model is reduced to two lower-order models: first, the model for fast frequency or real-power dynamics (fast, boundary-layer model), and second, the model of midrange closed-loop voltage dynamics (slow subsystem).

The basic components of the system are two generators, a load, and a network switching device such as an OLTC transformer. As pointed out by Concordia [11], the small-signal instability problems have been studied by different people using extreme scenarios, some of which introduce primarily electromechanical instability [12], and others in which voltage problems dominate [13]. The simplest example of the angle (electromechanical) instability problem caused by high demand in real power can be illustrated on a power system consisting of a single synchronous generator connected to an infinite bus [12]. Similarly, a problem dealing with only voltage (electromagnetics) can be illustrated on a simple power system consisting of one synchronous generator connected to a static load [13]. In order to study time evolution and mutual effects between these electromechanical and electromagnetic subprocesses without loss of generality, it is necessary to study a system consisting of at least two generators and one load.

Recall from Chapters 3 and 4 that one could represent dynamics of a power system in two qualitatively different ways. The first approach is to include dynamics of each generator. The second approach is to introduce a reference bus and express system dynamics relative to this bus [14]. This reference bus may be a slack bus which results in an anchored system. Analysis results should be interpreted accordingly. The role of a reference bus in context of model reduction becomes particularly confusing when analyzing long-term interarea oscillations. An elaborate treatment of this modeling issue is given in Section 6.4. To avoid confusion in this example the second generator is modeled as the reference bus, that is, as an ideal voltage source for which both voltage phase angle

and magnitude are given. Furthermore, to deemphasize at this stage issues related to the reference bus, parameters of the transmission system given in Figure 4.4 are chosen in such a way that the load bus is much closer electrically to the generator bus than to the infinite bus. In this way any disturbance at the load bus will have a greater impact on the generator bus. An OLTC is also included as part of the system under study to illustrate its role in the long-range closed-loop voltage dynamics later in this chapter.

First, we illustrate a typical application of a SP-based model reduction starting from the fourth-order lossless model of synchronous machine (type II₃), combined with the dynamics of an IEEE type 1 excitation system, both described in Chapter 3. We restate this model here with notation identical to that in Chapter 3, including replacement of e_d'' with e_d' as explained in Chapter 3 for type II₃ model.

Closed-loop dynamics of a generator with its IEEE type 1 excitation system are given by combining models of type II₃ electromagnetic dynamics [Eqs. (3.226) and (3.227)], electromechanical dynamics [Eq. (3.202)], and the excitation system dynamics [Eqs. (3.268) to (3.270)], respectively,

$$\dot{e}'_d = \frac{1}{T'_{q0}}[-e'_d + (x_q - x'_q)i_q] \quad (6.3)$$

$$\dot{e}'_q = \frac{1}{T'_{do}}[-e'_q - (x_d - x'_d)i_d + e_{fd}] \quad (6.4)$$

$$\dot{\theta} = \omega_o(\omega - 1) \quad (6.5)$$

$$\dot{\omega} = \frac{1}{2J}[-(e'_d i_d + e'_q i_q) - D(\omega - 1) + P_T] \quad (6.6)$$

$$\dot{V}_R = \frac{1}{T_A} \left(K_A V_F - \frac{K_A K_F}{T_F} e_{fd} - V_R - K_A E_t + K_A E^{\text{ref}} \right) \quad (6.7)$$

$$\dot{e}_{fd} = \frac{1}{T_E}[-(K_e + S_E)e_{fd} + V_R] \quad (6.8)$$

$$\dot{V}_F = \frac{1}{T_F} \left(-V_F + \frac{K_F}{T_F} e_{fd} \right) \quad (6.9)$$

where $S_E = A_{\text{sat}} e^{(B_{\text{sat}} e_{fd})}$ and the stator algebraic equations (3.228) to (3.229) are

$$E_d = e'_d + i_q x'_q \quad (6.10)$$

$$E_q = e'_q - i_d x'_d \quad (6.11)$$

These equations are fully equivalent to equations in Chapter 3, including an arbitrary notation change from e_d'' , x_q'' , and T_{q0}'' to e'_d , x'_q , and T'_{q0} , which is commonly used to match this literature.

In the model of Eqs. (6.3) to (6.9), interactions of the generator with the rest of the system are only through the variables i_d , i_q , and E_t , which are functions

of states, network parameters, and the operating conditions. Since two types of load models, constant impedance and constant power, are considered, they are discussed separately.

Constant-power load In general, variables i_d and i_q are computed using the network relation

$$[\hat{I}] = [\hat{Y}]_{\text{bus}}[\hat{E}] \quad (6.12)$$

where \hat{Y}_{bus} is the bus admittance matrix, which includes the internal nodes of the machine. For the three-bus example with $T'_{qo} = \infty$ and $x_q = x'_d$, the network constraints are given as

$$\begin{bmatrix} \hat{I}_G \\ I \\ 0 \\ 0 \\ -\hat{I}_L \end{bmatrix} = \left[\begin{array}{cc|cc} \frac{1}{jx'_d} & 0 & -\frac{1}{jx'_d} & 0 & 0 \\ 0 & \frac{1}{jx_1} + \frac{1}{jx_2} & -\frac{1}{jx_1} & 0 & -\frac{1}{jx_2} \\ \hline -\frac{1}{jx'_d} & -\frac{1}{jx_1} & \frac{1}{jx'_d} + \frac{1}{jx_1} + \frac{1}{jx_{12}} & -\frac{1}{jx_{12}} & 0 \\ 0 & 0 & -\frac{1}{jx_{12}} & \frac{1}{jx_{12}} - y_T t^2 & -\frac{t}{jx_T} \\ 0 & -\frac{1}{jx_2} & 0 & -\frac{t}{jx_T} & y_T + \frac{1}{jx_2} \end{array} \right] \times \begin{bmatrix} \hat{E}_1 \\ \hat{E}_2 \\ \hat{E}_3 \\ \hat{E}_4 \\ \hat{E}_5 \end{bmatrix} \quad (6.13)$$

where

$$\hat{E}_1 = e'_q \angle \delta, \quad \hat{E}_2 = 1 \angle 0,$$

$$\hat{E}_L = (P_L + jQ_L)/\hat{I}_L^*, \quad \hat{I}_G = (i_d + ji_q)e^{j(\delta - (\pi/2))}$$

As pointed out earlier in Chapter 3, i_d and i_q can be computed explicitly when the transient reactance is neglected. There exist two solutions for \hat{I}_L in Eq. (6.13) for any given P, Q load, implying two solutions for both i_d and i_q . But only one of the solutions is operationally acceptable.

Constant-impedance load For the constant-impedance-load model, i_d and i_q are also computed using Eq. (6.13). A simpler approach is adopted, however, where the Thevenin equivalent circuit is introduced as seen from a generator's side and characterized by the equivalent impedance $R_e + jX_e$ and voltage $E'_\infty, \delta'_\infty$, to compute i_d and i_q . The detailed expressions for $R_e, X_e, E'_\infty, \delta'_\infty$ in terms of the network parameters are given in Appendix 6.1 and their derivations can be

found in Refs. [3,5]. Variables i_d , i_q , and E_t are then obtained in the closed form as functions of the state variables, tap changer position $t(k)$ and load parameters R_L and X_L . They obey the following expression:

$$i_d = \frac{R_e e'_d + (X_e + x'_d) e'_q - [R_e \sin(\delta - \delta'_{\infty}) + (X_e + x'_d) \cos(\delta - \delta'_{\infty})] E'_{\infty}}{R_e^2 + (X_e + x'_d)^2} \quad (6.14)$$

$$i_q = \frac{-(X_e + x'_d) e'_d + R_e e'_q + [-R_e \cos(\delta - \delta'_{\infty}) + (X_e + x'_d) \sin(\delta - \delta'_{\infty})] E'_{\infty}}{R_e^2 + (X_e + x'_d)^2} \quad (6.15)$$

The terminal voltage of the generator E_t , which plays a critical role in voltage studies with respect to the rest of the system, is

$$E_t = \sqrt{E_d^2 + E_q^2} \quad (6.16)$$

It should be noted that i_d and i_q admit only one solution for each operating condition for loads modeled as a constant impedance. Moreover, any changes in load, that is, changes in R_L and X_L , or changes in tap position $t(k)$ will be reflected through R_e , X_e , E'_{∞} , and δ'_{∞} . Hence, the system can be thought of as one machine connected to a pseudoinfinite-bus network.

6.2.1 Integral-Manifold Derivations

The time-scale separation between state electromechanical and electromagnetic variables was first recognized and examined in Ref. [2]. In [3,5] the integral-manifold technique described earlier is used to derive this reduced-order model. This derivation is summarized next.

One way to recognize the time-scale separation formally is based on introducing a new “transient speed” [15] defined as

$$\omega_t = \sqrt{2J\omega_0}(\omega - 1) \quad (6.17)$$

The small parameter ε is defined as

$$\varepsilon \stackrel{\Delta}{=} \sqrt{\frac{2J}{\omega_0}} \quad (6.18)$$

and the parameters α_a , α_e , and α_q as

$$\alpha_a \stackrel{\Delta}{=} \frac{T_A}{\varepsilon}, \quad \alpha_e \stackrel{\Delta}{=} \frac{T_E}{\varepsilon}, \quad \alpha_q \stackrel{\Delta}{=} \frac{T'_{q0}}{\varepsilon} \quad (6.19)$$

Thus the parameters T_A , T_E , and T'_{q0} are assumed to be very small. The regulator gain K_F is assumed to be $O(\varepsilon)$ of T'_{d0} , T_F . With these definitions, the model of

Eqs. (6.3) to (6.11) is

$$\varepsilon \alpha_q \frac{de'_d}{dt} = -e'_d + (x_q - x'_q)i_q \quad (6.20)$$

$$\varepsilon \frac{d\delta}{dt} = \omega_t \quad (6.21)$$

$$\varepsilon \frac{d\omega_t}{dt} = -e'_d i_d - e'_q i_q - \frac{D\omega_t}{\sqrt{2J\omega_0}} + P_T \quad (6.22)$$

$$\varepsilon \alpha_e \frac{de_{fd}}{dt} = -(K_E + S_E)e_{fd} + V_R \quad (6.23)$$

$$\varepsilon \alpha_a \frac{dV_R}{dt} = K_A V_F - \frac{K_A K_F}{T_F} e_{fd} - V_R - K_A E_t + K_A E_{ref} \quad (6.24)$$

$$T'_{d0} \frac{de'_q}{dt} = -e'_q - (x_d - x'_d)i_d + e_{fd} \quad (6.25)$$

$$T_F \frac{dV_F}{dt} = -V_F + \frac{K_F}{T_F} e_{fd} \quad (6.26)$$

$$E_d = e'_d + i_q x'_q \quad (6.27)$$

$$E_q = e'_q - i_d x'_d \quad (6.28)$$

$$E_t = \sqrt{E_d^2 + E_q^2} \quad (6.29)$$

$$i_d = \frac{R_e e'_d + (X_e + x'_d)e'_q - [R_e \sin(\delta - \delta'_{\infty}) + (X_e + x'_d) \cos(\delta - \delta'_{\infty})]E'_{\infty}}{R_e^2 + (X_e + x'_d)^2} \quad (6.30)$$

$$i_q = \frac{-(X_e + x'_d)e'_d + R_e e'_q + [-R_e \cos(\delta - \delta'_{\infty}) + (X_e + x'_d) \sin(\delta - \delta'_{\infty})]E'_{\infty}}{R_e^2 + (X_e + x'_d)^2} \quad (6.31)$$

In view of Eqs. (6.20) to (6.26), it is clear that the predominantly fast variables (z in 6.2.2), (Appendix 6.2) are e'_d , δ , ω_t , e_{fd} , and V_R , and the predominantly slow variables (y in 6.2.1), (Appendix 6.2) are e'_q and V_F . To express the predominantly fast variables $z = (e'_d \ \delta \ \omega_t \ e_{fd} \ V_R)^T$ in terms of the slow variables $y = (e'_q \ V_F)^T$, one looks for the series expansion

$$e'_d(y) = E'_{d0}(y) + \varepsilon E'_{d1}(y) + \varepsilon^2 E'_{d2}(y) + \dots \quad (6.32)$$

$$\delta(y) = \delta_0(y) + \varepsilon \delta_1(y) + \varepsilon^2 \delta_2(y) + \dots$$

$$\omega_t(y) = \omega_{t0}(y) + \varepsilon \omega_{t1}(y) + \varepsilon^2 \omega_{t2}(y) + \dots$$

$$e_{fd}(y) = E_{fd0}(y) + \varepsilon E_{fd1}(y) + \varepsilon^2 E_{fd2}(y) + \dots$$

$$V_R(y) = E_{R0}(y) + \varepsilon E_{R1}(y) + \varepsilon^2 E_{R2}(y) + \dots$$

that is, the manifold M_ε (Eq. (6.2.3), Appendix 6.2) is defined as

$$M_\varepsilon : \quad z = \phi(y, \varepsilon) \quad (6.33)$$

The manifold condition (Eq. (6.2.5), Appendix 6.2) repeated here as

$$\varepsilon \frac{\partial \phi}{\partial y} \dot{y} = g(y, \phi(y, \varepsilon)) \quad (6.34)$$

and applied to Eqs. (6.20) to (6.26) gives

$$\varepsilon \begin{bmatrix} \frac{\partial e'_d}{\partial e'_q} & \frac{\partial e'_d}{\partial V_F} \\ \frac{\partial e'_q}{\partial \delta} & \frac{\partial V_F}{\partial \delta} \\ \frac{\partial e'_q}{\partial \omega_t} & \frac{\partial \omega_t}{\partial \delta} \\ \frac{\partial e'_q}{\partial V_F} & \frac{\partial V_F}{\partial \delta} \\ \frac{\partial e'_{fd}}{\partial e'_{fd}} & \frac{\partial e'_{fd}}{\partial V_F} \\ \frac{\partial e'_q}{\partial V_R} & \frac{\partial V_R}{\partial V_F} \\ \frac{\partial e'_q}{\partial e'_q} & \frac{\partial V_F}{\partial e'_q} \end{bmatrix} \begin{bmatrix} \frac{de'_q}{dt} \\ \frac{dV_F}{dt} \end{bmatrix} = \begin{bmatrix} \frac{1}{\alpha_q} [-e'_d + (x_q - x'_q)i_q(\delta, e'_q)] \\ \omega_t \\ -e'_d i_d(\delta, e'_q) - e'_q i_q(\delta, e'_q) - \frac{D\omega_t}{\sqrt{2J\omega_0}} + P_T \\ \frac{1}{\alpha_e} [-(K_E + S_E)e_{fd} + V_R] \\ \frac{1}{\alpha_a} \left(K_A V_F - \frac{K_A K_F}{T_F} e_{fd} - V_R - K_A \right. \\ \left. E_t(\delta, e'_q) + K_A E_{ref} \right) \end{bmatrix} \quad (6.35)$$

Expanding Eq. (6.35) in the powers of ε and equating terms associated with the $\varepsilon = 0$ term, ε term, ε^2 term, etc., defines terms in the series expansion (6.32). Hence, the reduced-order model suitable for representing the full-order system dynamics for sufficiently small ε is

$$\ddot{\bar{e}}'_q = \frac{1}{T'_{d0}} [-\bar{e}'_q - (x_d - x'_d)i_d(\bar{e}'_q, \bar{\delta}(\bar{e}'_q)) + \bar{e}_{fd}(\bar{e}'_q, \bar{V}_F)] \quad (6.36)$$

$$\dot{\bar{V}}_F = \frac{1}{T_F} \left(-\bar{V}_F + \frac{K_F}{T_F} \bar{e}_{fd}(\bar{e}'_q, \bar{V}_F) \right) \quad (6.37)$$

where $\bar{\delta}(\bar{e}'_q)$ and $\bar{e}_{fd}(\bar{e}'_q, \bar{V}_F)$ are the series expansions taking into account the order of complexity and accuracy in the reduced model derivation.

When the predominantly fast variables, in particular, the electromechanical variables, are asymptotically stable, the general required assumptions sufficient for manifold existence are met. Furthermore, if the zeroth-order approximation is all that is required, then a type II₃ machine model with IEEE type 1 exciter can be reduced to the following second-order model

$$\frac{d\bar{e}'_q}{dt} = \frac{1}{T'_{d0}} [-\bar{e}'_q - (x_d - x'_d)i_d(\bar{e}'_q, \bar{\delta}_0(\bar{e}'_q)) + \bar{e}_{fd0}(\bar{e}'_q, \bar{V}_F)] \quad (6.38)$$

$$\frac{d\bar{V}_F}{dt} = \frac{1}{T_F} \left(-\bar{V}_F + \frac{K_F}{T_F} \bar{e}_{fd0}(\bar{e}'_q, \bar{V}_F) \right) \quad (6.39)$$

with the zeroth-order approximation for the fast variables taken to be

$$\bar{\omega}_{t0} = \sqrt{2J\omega_0}(\omega - 1) = 0 \quad (6.40)$$

$$\bar{e}'_{d0} = (x_q - x'_q)i_q(\bar{e}'_q, \bar{\delta}_0(\bar{e}'_q)) \quad (6.41)$$

where the saturation function is $S_E \cong A_{\text{sat}}(1 + B_{\text{sat}}e_{\text{fd}})$. Then \bar{V}_{R0} and $\bar{e}_{\text{fd}0}$ are given by

$$\bar{V}_{R0} = (K_E + A_{\text{sat}})\bar{e}_{\text{fd}0}A_{\text{sat}}B_{\text{sat}}\bar{e}_{\text{fd}0}^2 \quad (6.42)$$

$$\bar{e}_{\text{fd}0} = \frac{-\hat{b} \pm \sqrt{\hat{b}^2 - 4\hat{a}\hat{c}}}{2\hat{a}} \quad (6.43)$$

with

$$\hat{a} = \frac{T_F A_{\text{sat}} B_{\text{sat}}}{K_A K_F}$$

$$\hat{b} = \frac{T_F (K_E + A_{\text{sat}})}{K_A K_F} + 1$$

$$\hat{c} = \frac{T_F}{K_F} [-\bar{V}_F + E_t(\bar{e}'_q, \bar{\delta}_0(\bar{e}'_q)) - E_{\text{ref}}]$$

and $\bar{\delta}_0$ needs to be computed iteratively from

$$\bar{e}'_d(\bar{e}'_q, \bar{\delta}_0(\bar{e}'_q))i_d(\bar{e}'_q, \bar{\delta}_0(\bar{e}'_q)) + \bar{e}'_q i_q(\bar{e}'_q, \bar{\delta}_0(\bar{e}'_q)) = P_T \quad (6.44)$$

This zeroth-order model is valid for both the constant-impedance and constant-power loads. The difference is in the way of computing $\bar{\delta}_0$ iteratively. Moreover, in the case of the constant-impedance load model with e'_d dynamics neglected totally, that is, with the assumption that $x_q = x'_d$, $\bar{\delta}_0$ can be explicitly computed as follows:

$$\bar{\delta}_0 = \delta'_\infty + \cos^{-1} \left(\frac{ac \pm \sqrt{(ac)^2 + (b^2 + c^2)(b^2 - a^2)}}{b^2 + c^2} \right) \quad (6.45)$$

with

$$a = \frac{T_m}{E'_\infty e'_q} [R_e^2 + (X_e + x'_d)^2] - \frac{R_e e'_q}{E'_\infty}$$

$$b = X_e + x'_d$$

$$c = -R_e$$

Notice from Eqs. (6.43) and (6.45) that there are two solutions for $\bar{e}_{\text{fd}0}$ and $\bar{\delta}_0$, respectively; therefore, there will be four sets of possible solutions even with the

TABLE 6.2 Four Sets of Possible Equilibria

Solution	$\bar{\delta}_0$	$\bar{\omega}_0$	\bar{E}_{fd0}	\bar{V}_{R0}	$\lambda \left(\frac{\partial g}{\partial y} \right)$
1	0.07	0	1.88	0.08	$-0.01 \pm j 1.24$ $-1.05 \pm j 1.02$
2	0.07	0	-0.11×10^5	0.0433×10^5	$-0.01 \pm j 1.243$ $-1.05 \pm j 1.02$
3	2.94	0	4.84	0.23	1.23 -1.25 $-1.06 \pm j 1.02$
4	2.94	0	-0.11×10^5	0.43×10^5	1.23 -1.25 $-1.06 \pm j 1.02$

constant-impedance load model and with e'_d dynamics neglected. However, in general, only one of the four possible solutions results in a physically acceptable solution. For illustrative purposes, the four sets of zeroth-order equilibrium points for a particular initial loading condition of the full-order model with $R_L = 1.0$, $X_L = 1.0$, $\delta^0 = 0.0742$, $\omega^0 = 1.0$, $e_{fd}^0 = 1.8793$, $V_R^0 = 0.0877$, $e_q^0 = 1.1634$, and $V_F^0 = 0.3$ are examined. The four sets of zeroth-order approximated initial equilibrium points are shown in Table 6.2.

From Table 6.2 it appears that only the first two sets of equilibrium points could be candidates for the stable manifold M_0 . This is because the values of the angle δ^0 of 2.936 rad of equilibrium sets 3 and 4 clearly show the unstable solutions and also because their $\lambda(\partial g/\partial z)$ have unstable eigenvalues. Furthermore, only the first equilibrium point is acceptable because it is reasonably close to the equilibrium point of the full-order system. Besides, the discrepancy between the equilibrium points (e_{fd}^0 and V_R^0 in particular) of the full-order system and the zeroth order manifold (\bar{e}_{fd0} and \bar{V}_{R0}) is small compared to the second set of equilibrium points.

In view of the general Assumptions 6.2.1 and 6.2.2 in Appendix 6.2, it follows that the $\text{Re}\lambda(\partial g/\partial z)$ evaluated for $\varepsilon = 0$ along M_0 has to be strictly negative for the period of interest. Since the cases studied are transiently stable, this assumption is satisfied. Now, one is in a position to propose the following two reduced-order models.

6.2.2 Relevant Model for Fast Angle Dynamics

The most widely used model for studying fast angle responses is the so-called "classical" model which in the case of the three-bus system is directly derived by assuming $e'_q = \text{const}$ and $e'_d = 0$. A more accurate transient response of the fast variables is obtained by defining the boundary-layer dynamics for zeroth-order

approximation. This model is derived by using Eq. (6.35) and is given in slow time $\tau = \frac{t}{\varepsilon}$ as

$$\frac{d\hat{e}'_d}{d\tau} = \frac{1}{\alpha_q} [-\hat{e}'_d + \bar{e}'_d(0) + (x_q - x'_q)i_q(\bar{e}'_q(0), \hat{\delta} + \bar{\delta}(0))] \quad (6.46)$$

$$\frac{d\hat{\delta}}{d\tau} = \hat{\omega}_t + \bar{\omega}_t(0) \quad (6.47)$$

$$\begin{aligned} \frac{d\hat{\omega}_t}{d\tau} &= -[\hat{e}'_d + \bar{e}'_d(0)]i_d(\bar{e}'_q(0), \hat{\delta} + \bar{\delta}(0)) \\ &\quad - \bar{e}'_q(0)i_q(\bar{e}'_q(0), \hat{\delta} + \bar{\delta}(0)) - \frac{D(\hat{\omega}_t + \bar{\omega}_t(0))}{\sqrt{2J\omega_0}} + P_T \end{aligned} \quad (6.48)$$

$$\frac{d\hat{e}_{fd}}{d\tau} = \frac{1}{\alpha_e} \{ -(K_E + S_E)[\hat{e}_{fd} + \bar{e}_{fd}(0)] + \hat{V}_R + \bar{V}_R(0) \} \quad (6.49)$$

$$\begin{aligned} \frac{d\hat{V}_R}{d\tau} &= \frac{1}{\alpha_a} \left(K_A \bar{V}_F(0) - \frac{K_A K_F}{T_F} [\hat{e}_{fd} + \bar{e}_{fd}(0)] - [\hat{V}_R + \bar{V}_R(0)] \right. \\ &\quad \left. - K_A E_t(\bar{e}'_q(0), \hat{\delta} + \bar{\delta}(0)) + K_A E_{ref} \right) \end{aligned} \quad (6.50)$$

6.2.3 Relevant Model of Slow Voltage Dynamics

The reduced-order model relevant for reactive-power–voltage dynamics studies is defined using \bar{e}'_q and \bar{V}_F as the state variables as

$$\frac{d\bar{e}'_q}{dt} = \frac{1}{T'_{d0}} [-\bar{e}'_q - (x_d - x'_d)i_d(\bar{e}'_q, \bar{\delta}_0(\bar{e}'_q)) + \bar{e}_{fd0}(\bar{e}'_q, \bar{V}_F)] \quad (6.51)$$

$$\frac{d\bar{V}_F}{dt} = \frac{1}{T_F} \left(-\bar{V}_F + \frac{K_F}{T_F} \bar{e}_{fd0}(\bar{e}'_q, \bar{V}_F) \right) \quad (6.52)$$

where $\bar{\delta}_0$ and \bar{e}_{fd0} are the zeroth-order manifold reflecting the effect of changes of variables on the e'_q and V_F dynamics.

Sufficient conditions for stability of this midrange voltage dynamics are derived in Ref. [5] using basic eigenvalue conditions for stability of the second-order linear time-invariant system represented in Eqs. (6.51) and (6.52). For the case of the simple three-bus example studied, these conditions are:

- (i) $(\partial E_t / \partial e'_q) > 0$,
- (ii) $0 < (\partial e_{fd} / \partial V_R) < (T_F / K_F)$ and
- (iii) $(\partial i_d / \partial x'_d) > -c(x_d - \partial e'_q)$.

Conditions (i) to (iii) have a physical interpretation in the sense that (i) and (ii) define sufficient conditions for adequate voltage regulator and excitation system desire, and condition (iii) reflects the requirement that the Thevenin

impedance of the transmission system as seen from the generator terminals remains inductive. Condition (ii) could be violated in practice if very high gain controller is designed, while condition (iii) could be violated if the capacitive load power factor compensation is too large. Condition (i) reflects the basic requirement implied in the PID control design that the output variable (E_t) increases as the controlled state (e'_q) increases.

It is known that under very high power transfer conditions, for example, condition (i) could become violated if a constant gain controller is not tuned for such conditions.

Therefore, the violation of conditions (i) to (iii) could create a scenario for voltage-related instability even though angle response per se is stabilizable.

6.3 SLOW VOLTAGE DYNAMICS

Next, a mathematical model relevant for capturing the interactions of midrange voltage dynamics with the control actions of an OLTC transformer is derived. The OLTCs and other types of load and network controllers, which are typically of slow switched character, interact in an interesting way with the voltage dynamics of generators controlled by the fast and continuous excitation systems. Combining the effect of these controllers with the relevant voltage dynamics is of importance for understanding potential voltage instabilities that have been reported as the main causes of several voltage-related blackouts.

In the past, dynamics of switching devices (load control) have been much slower than the voltage dynamics of generators. Under such pronounced time-scale separation and assuming that midrange generator voltage dynamics are asymptotically stable, the long-range voltage dynamics are primarily result of inadequate switching logic of OLTCs [16]. For purposes of posing this problem, a slow closed-loop dynamic model comprising midrange closed-loop continuous dynamics and the discrete dynamics governed by the OLTC is derived next. The model is *hybrid* (i.e., discrete–continuous) due to the discrete nature of the controller acting on a continuous system model.

A variety of open questions concerning the effect of feedback on stabilizing otherwise unstable dynamics with present controllers calls for at least posing a model that allows for raising questions about the dynamic interactions of generators and switching devices. Specific control design questions of this type are studied in Chapter 12 in this text. Here only the process of extracting the model relevant for posing the question of OLTC control logic is described.

6.3.1 Interactions of the OLTC Control and Midrange Voltage Dynamics

A steady-state equivalent π -circuit of an OLTC introduced in Chapter 3 is used by assuming its dynamics to be instantaneous and stable relative to the studied dynamics. Its operation and detailed modeling are described in Ref. [17]. Note that since the natural dynamics of the generator are much faster than the tap

actions of the transformer, which have a typical operating cycle of 10 sec to 100 sec, the steady-state model represents a reasonable model for the time range of interest. However, with this steady-state model, there is no mechanism to predict interactions of the midrange voltage dynamics and the OLTC actions.

As described in Chapter 3, the tap positions of the transformer change according to the following discrete logic [16]

$$\mathbf{t}(k+1) = \mathbf{t}(k) - d(k)f(E_L(k) - E_L^{\text{ref}}), \quad k = 1, 2, \dots \quad (6.53)$$

where $\mathbf{t}(k)$ is the tap position in the k th operating cycle, and $d(k)$ denotes the step size in the change of the tap position during one operating cycle. The relay type function $f(E_L(k) - E_L^{\text{ref}})$ is the control function governing the actions of the transformer and is given by

$$f(E_L(k) - E_L^{\text{ref}}) = \begin{cases} 1, & E_L(k) - E_L^{\text{ref}} > \Delta E \\ 0, & |E_L(k) - E_L^{\text{ref}}| \leq \Delta E \\ -1, & E_L(k) - E_L^{\text{ref}} < -\Delta E \end{cases} \quad (6.54)$$

where ΔE is a prespecified threshold of allowable load voltage deviation prior to tap-changer actions. Thus if $|E(k) - E^{\text{ref}}| < \Delta E$, no action results, and the tap position is unchanged.

It follows from studying the reduced order model for midrange voltage dynamics prior to the OLTC actions that this model is not very sensitive to changes in mechanical variables (angle) under the assumption of their asymptotic stability. This means that in incorporating the effect of discrete load control actions of the OLTC, the zeroth-order model for the generator's voltage dynamics would be sufficiently accurate. If such model (Eqs. (6.51) and (6.52)) is used for representing the generator's midrange voltage dynamics, the closed-loop dynamic model with the load controls included becomes

$$\begin{aligned} \frac{d\bar{e}'_q}{dt} = & \frac{1}{T_{d0}} [-\bar{e}'_q - (x_d - x'_d)i_d(\bar{e}'_q, \bar{\delta}_0(\bar{e}'_q)) \\ & + \bar{e}_{fd0}(\bar{e}'_q, \bar{V}_F)] \end{aligned} \quad (6.55)$$

$$\frac{d\bar{V}_F}{dt} = \frac{1}{T_F} \left(-\bar{V}_F + \frac{K_F}{T_F} \bar{e}_{fd0}(\bar{e}'_q, \bar{V}_F) \right) \quad (6.56)$$

$$\mathbf{t}[(k+1)\Delta] = \mathbf{t}(k\Delta) - d(k\Delta)f(E(k\Delta) - E^{\text{ref}}) \quad (6.57)$$

$$f(E_L(k\Delta) - E_L^{\text{ref}}) = \begin{cases} 1, & E_L(k\Delta) - E_L^{\text{ref}} > \Delta E \\ 0, & |E_L(k\Delta) - E_L^{\text{ref}}| \leq \Delta E \\ -1, & E_L(k\Delta) - E_L^{\text{ref}} < -\Delta E \end{cases} \quad (6.58)$$

The dynamics of \bar{e}'_q are coupled with the changes in tap position through the variables i_d and e_{fd0} . The basic property of this closed-loop dynamic model

is that it is a hybrid model (continuous-discrete) with a much slower discrete control acting on the continuous dynamics of the system.

Since the OLTC actions are treated as a sequence of changing parameters, there is no mechanism in this hybrid model to predict the slow voltage instability associated with the OLTC dynamics. The dynamic stability of model, Eqs. (6.55) to (6.58), associated with OLTC actions is regarded as the parametric stability as suggested in Ref. [16].

6.3.2 Approximate Continuous Model for Slow Voltage Dynamics

Virtually no techniques exist for studying hybrid models in a direct way. Two possible indirect ways to study these dynamics are as follows:

1. Discretize the model of the continuous system dynamics at the same sampling rate as that at which a tap changer acts,
2. Approximate a discrete model by its continuous counterpart in slow time τ and study the closed-loop model as a continuous nonlinear model.

As noted earlier, a variety of open questions with respect to the effect of feedback on stabilizing otherwise unstable dynamics with present controllers calls for at least posing a model that considers the dynamic interactions of generators and switching devices. In this section, a singular perturbation method is used to derive such a reduced-order model.

It can be shown on the same small three-bus power system studied that, following the method suggested in Ref. [16], the load-voltage dynamics due to changes in tap position governed by Eq. (6.57) take on the form

$$E_L[(k+1)\Delta] = E_L(k\Delta) + B_{LL}^{-1}E_t(k\Delta)B_T \cos \delta_{21} f(E_L(k\Delta) - E^{\text{ref}}) \quad (6.59)$$

where $E_L(k\Delta)$ is the load voltage at step k of the OLTC and $E_t(k\Delta)$ is the terminal voltage of the generator sampled at the same instant. The network parameters $B_T = 1/x_T$ and $B_{LL} = (1/X_L) + (1/x_T) + (1/x_2)$. Here x_{12} is small and is neglected in the derivation. Equation (6.59) should be understood in the following way: Voltage E_L may change each cycle if the load-voltage violation larger in magnitude than ΔE exists. If not, the voltage will maintain the same value. In this sense, the count k can be equated with the sampling time. A continuous approximation of Eq. (6.59) is obtained by writing

$$\frac{E_L((k+1)\Delta) - E_L(k\Delta)}{\Delta} = \frac{B_{LL}^{-1}E_t(k\Delta)}{\Delta} B_T \cos \delta_{21} f(E_L(k\Delta) - E^{\text{ref}}) \quad (6.60)$$

When the finite difference on the left-hand side is replaced by the derivative with basic time unit Δ , Eq. (6.60) becomes

$$\left. \frac{dE_L}{dt} \right|_{t=k\Delta} = \mu B_{LL}^{-1} E_t B_T \cos \delta_{21} f(E_L - E^{\text{ref}}) \quad (6.61)$$

where $\mu = (1/\Delta)$. As it can be seen from Eq. (6.61), the load-voltage dynamics are coupled with the generator dynamics through the terminal voltage E_t . The term $\cos \delta_{21}$ in Eqn. (6.61) is assumed to be known under the real/reactive power decomppling approximation.

For the mid- and long-range voltage stability studies, the slower voltage dynamics governed primarily by the load control actions will be relevant. However, the effects of the (faster) system dynamics through E_t need to be taken into account rigorously. The standard form for deriving conditions under which the dynamics given in Eq. (6.61) will determine the mid- and/or long-range voltage stability of the system is obtained by re-writing the coupled model in Eqs. (6.55), (6.56), and (6.61) in the slow time t_s . The time scale of dynamic t in Eqs. (6.55) and (6.56) is related to the slow time t_s as

$$t_s = \frac{t}{\mu} \quad (6.62)$$

Then, Eqs. (6.55), (6.56), and (6.61) become

$$\mu \frac{d\bar{e}'_q}{dt_s} = \frac{1}{T'_{d0}} [-\bar{e}'_q - (x_d - x'_d)i_d(\bar{e}'_q, \bar{\delta}_0(\bar{e}'_q)) + \bar{e}_{fd0}(\bar{e}'_q, \bar{V}_F)] \quad (6.63)$$

$$\mu \frac{d\bar{V}_F}{dt_s} = \frac{1}{T_F} \left(-\bar{V}_F + \frac{K_F}{T_F} \bar{e}_{fd0}(\bar{e}'_q, \bar{V}_F) \right) \quad (6.64)$$

$$\frac{dE_L}{dt_s} = B_{LL}^{-1} E_t B_T \cos \delta_{21} f(E_L - E^{\text{ref}}) \quad (6.65)$$

Introducing the slow variable to be E_L and the fast variable \bar{e}'_q leads to studies that allow for further model reduction. The reduced model is then suited for studying the coordination issues among OLTC dynamics by taking the dynamics of a machine into account. Detailed conditions under which a stable integral manifold $\bar{e}'_q(E_L)$ exists and under which it can be approximated by its zeroth-order manifold are subject for future work. For detailed simulations using this model, see [3, 5].

6.4 SLOW FREQUENCY DYNAMICS

Another important class of reduced-order models is needed for studying the long-range slow frequency dynamics resulting from interactions of generator dynamics and its local turbine-governor control. Under the assumptions made while deriving the integral manifold for separating fast angle dynamics from the midrange voltage dynamics one can model e'_q as a constant. This forms a starting model for analyzing long-range frequency changes as affected by the governor-turbine control. The modeling approach in this section is based on Refs. [18] and [19].

6.4.1 Governor-turbine Control of Frequency Dynamics

Let us assume first that voltage regulators maintain terminal voltages of all machines almost constant. The main question of interest concerns a model derivation for analyzing the effects of governor-turbine control on generators' dynamics in response to load perturbations. The design objective is to regulate frequency oscillations over the 1 to 2 minute range following a change in real-power demand according to a prespecified performance criterion. Various control methods for meeting this objective are studied later in Chapter 12.

A block diagram representing a single governor-turbine-generator (G-T-G) unit is shown in Figure 6.2.

In this subsection closed-loop primary dynamics of each individual G-T-G unit are considered [18] to [23]. In general, the complexity of the equations may vary, depending on the complexity of the actual type of a G-T-G unit and modeling assumptions. Only its structure is important for the concepts in this work, which is common to all designs and is illustrated here using simple G-T-G models.

Recall from Chapter 3, type IV₁ classical model of generator dynamics given via

$$J\dot{\omega}_G + D\omega_G = P_T - P_G \quad (6.66)$$

the turbine dynamics

$$T_u \dot{P}_T = n(P_T, a) \quad (6.67)$$

and the dynamics of the governor as

$$T_g \dot{a} = m(a, \omega_G^{\text{ref}}, \omega_G) \quad (6.68)$$

where J , D , T_u , T_g are moment of inertia of the combined G-T-G unit, its damping coefficient, and time constants of the turbine and governor, respectively. P_T and P_G are the mechanical and electric power of the turbine and generator, respectively. The generator state variable is its frequency ω_G ; the state variable of the turbine is P_T which corresponds to the part of the mechanical power directly regulated by the valve opening a , which is a state variable of the governor in its closed-loop operation. ω_G^{ref} is the set point value for the governor.

Viewing each generator as a separate block of the system, its linearized local dynamics is described in a state-space form by defining its state variables as

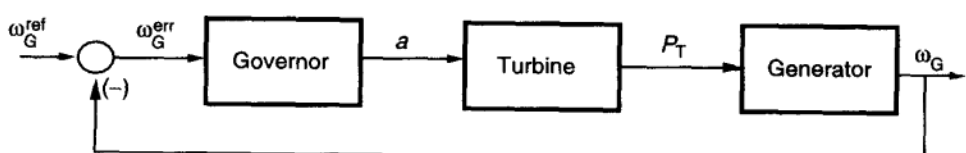


FIGURE 6.2 Primary frequency control loop of a G-T-G unit.

deviations in frequency, mechanical power, and valve position, respectively, that is,

$$x_G = [\omega_G \quad P_T \quad a]^T \quad (6.69)$$

A detailed derivation in this section is done first using the linearized model of each G-T-G unit²:

$$J\dot{\omega}_G + D\omega_G = P_T + e_T a - P_G \quad (6.70)$$

$$T_u \dot{P}_T = -P_T + K_t a \quad (6.71)$$

$$T_g \dot{a} = -ra - \omega_G + \omega_G^{\text{ref}} \quad (6.72)$$

ω_G^{ref} is a fixed constant within each primary response time interval (secondary control is activated only at some discrete times kT_s), and therefore $\omega_G^{\text{ref}} = 0$ for the time domain of interest in this section. With this and the definition for local states (6.69), one can rewrite the local primary dynamics, Eqs. (6.70) to (6.72), for each G-T-G unit as

$$\begin{aligned} \dot{x}_G &= \begin{bmatrix} -D/M & 1/M & e_T/M \\ 0 & -1/T_u & K_t/T_u \\ -1/T_g & 0 & -r/T_g \end{bmatrix} x_G \\ &+ \begin{bmatrix} -1/M \\ 0 \\ 0 \end{bmatrix} P_G \equiv A_G x_G + c_M P_G \end{aligned} \quad (6.73)$$

A_G is the system matrix of each generator. Properties of the system matrix A_G determine the response of each generator to its real-power demand while maintaining its frequency within the steady-state error determined by its droop characteristic [23]. It is important to notice that the dynamics of a stand-alone G-T-G unit defined via Eqs. (6.66) to (6.68) does not depend explicitly on the generator angle δ_G . However, the real-power generation P_G is not an independent variable of the interconnected system. It can be seen from Figure 6.1, with the flow F_G from the neighboring areas being zero, that this power has to be instantaneously matched with the power flows into the transmission network P_G^N . In an interconnected system, P_G is matched with the line flows into the transmission lines within the area P_G^N and the tie-line flows F_G from the neighboring areas. Because the area line flows are explicit functions $P_G^N(\delta_G, \delta_L)$ of generator δ_G and load δ_L phase angles in the same area, it is necessary to augment the local state-space x_G , which characterizes the dynamics of a single generator when introducing a multimachine power system model.

Common practice has been to use δ_G as an additional state variable for this purpose. It was proposed in Refs. [19] to [22] to use the real power out of a generator P_G instead. The process of defining the model of a multimachine

² All symbols corresponding to state variables represent *deviations* from an operating point around which a linearized model is derived rather than actual values.

system using $(x_G$ and P_G) as state variables is described next. It is suggested that these variables are more convenient for modeling, analyzing, and designing the control of interarea dynamics. It will be shown that the interarea variables are simple linear combinations of P_G in each area. Understanding the interarea dynamics is essential for establishing conditions under which hierarchical control of large power systems introduced in Chapter 13 works well.

6.4.2 Real-Power Network Constraints

Without loss of generality we illustrate our derivations on an interconnected power system partitioned only into two areas, as shown in Figure 6.3. A model of the interconnected system is obtained by subjecting the individual machine models Eqs. (6.70) to (6.72), of all machines to the transmission network constraints that relate real-power generation P_G to the real-power flows in the transmission lines of each area P_G^N and the real-power flows from the neighboring area F_G . The only direct coupling of each machine to the rest of the system is through this real-power output P_G .

Recall from Chapters 3 and 4 [Eq. (4.45)] that the network constraints are typically expressed in terms of nodal-type equations that require complex-valued power into the network \hat{S}^N to be equal to the complex-valued power $\hat{S} = P + jQ$ injected into each node,

$$\hat{S}^N = \text{diag}(\hat{E})\hat{Y}_{\text{bus}}^*\hat{E}^* = \hat{S} \quad (6.74)$$

where $\hat{S}^N = P^N + jQ^N$ is the vector of transmission network line flows into all nodes and \hat{Y}_{bus} is the admittance matrix of the network. $\hat{E} = Ee^{j\delta}$ is the vector of all nodal voltage phasors with magnitude E and phase δ . The real part of this equation has the structure

$$P^N = P^N(\delta, E) = P \quad (6.75)$$

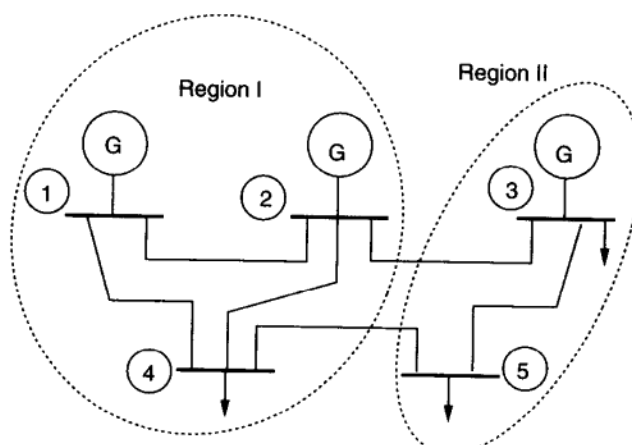


FIGURE 6.3 An interconnected five-bus power system.

Furthermore, the real power injected into each generator terminal on the interconnected system generally is the sum of the generator power output P_G and the real-power flow from the neighboring areas F_G , that is, $P = F_G + P_G$. With this, Eq. (6.75) takes on the structural form of interest as

$$P_G^N(\delta, E) = F_G + P_G \quad (6.76)$$

Similarly, since the real power from the load into the network can be written as the difference of real-power flow injected into the network at the load bus F_L and the real power absorbed by the load P_L , the network constraints (6.75) at the load nodes are expressed as

$$P_L^N(\delta, E) = F_L - P_L \quad (6.77)$$

According to the schematic representation of Figure 6.3, tie-line flows into the network are assumed to have a positive direction. The separation of the power injection P into the part of the intra-area injections by various components inside the area P_G and the part from the interconnecting tie lines with the neighboring subsystems F_G is essential for establishing structure-based models of the interconnected systems introduced here.

Note: The term *structure-based* is often used in this text to emphasize that variables directly relevant for various hierarchical levels can be expressed explicitly in terms of variables at each specific level, for example, variables relevant for the primary level are only local (equipment) level variables (x_G and P_G), while variables relevant for secondary-level regulation will be the interarea variables, which are determined at each area level.

Linearizing these equations under the decoupling assumption ($\partial P^N / \partial E = 0$), one obtains

$$F_G + P_G = J_{GG}\delta_G + J_{GL}\delta_L \quad (6.78)$$

$$F_L - P_L = J_{LG}\delta_G + J_{LL}\delta_L \quad (6.79)$$

where $J_{ij} = \partial P_i^N / \partial \delta_j$, $i, j \in \{G, L\}$, where $\{G, L\}$ represents a set of all generators and loads in the area, respectively. All variables denote deviations from their nominal values around which the linearization is done. Assuming J_{LL} to be invertible under the normal operating conditions,³ we define

$$C_\omega = -J_{LL}^{-1}J_{LG} \quad (6.80)$$

to express frequency deviations at loads ω_L in terms of frequency deviations at generators ω_G and fluctuations in load power. It follows from Eq. (6.79) that

$$\delta_L = C_\omega \delta_G + J_{LL}^{-1}(F_L - P_L) \quad (6.81)$$

³ This assumption is relaxed in later chapters of the text concerned with various degrees of abnormal system operation.

or by differentiating it with respect to time

$$\omega_L = C_\omega \omega_G + J_{LL}^{-1}(\dot{F}_L - \dot{P}_L) \quad (6.82)$$

Relationship (6.82) defines the explicit dependence of load frequencies on generator frequencies and system disturbances ($\dot{F}_L - \dot{P}_L$) determined by the network constraints. Combining Eqs. (6.81) and (6.78) and defining

$$K_P = J_{GG} + J_{GL}C_\omega \quad (6.83)$$

and

$$D_P = J_{GL}J_{LL}^{-1} \quad (6.84)$$

result in

$$P_G = K_P \delta_G + D_P F_L + F_e \quad (6.85)$$

Here F_e represents the effective tie-line flow as seen by each generator and is given as

$$F_e = D_P F_L - F_G \quad (6.86)$$

Similarly, Eq. (6.82) becomes

$$\omega_L = C_\omega \omega_G + J_{LL}^{-1}(\dot{F}_L - \dot{P}_L) \quad (6.87)$$

Keeping in mind that the main objective of the model derivation in this section is to pose the robustness (small-signal stability) problem of closed-loop real-power dynamics with respect to changes in initial conditions and in response to fast fluctuations in load demand \dot{P}_L (and \dot{F}_L in systems consisting of more than one area), we proceed by developing a state-space formulation of the real-power dynamics, in which the state variables representing dynamics of G-T-G units are augmented by adding the real-power P_G as a system-state variable for each G-T-G unit. This is done by differentiating Eq. (6.85) with respect to time⁴ and combining it further with Eq. (6.87). This results in

$$\dot{P}_G = K_P \omega_G + \dot{F}_e - D_P \dot{P}_L \quad (6.88)$$

which is of the form typically used when analyzing linear dynamic systems; with P_G as a state variable, Eq. (6.88) states that the rate of state-variable change (\dot{P}_G) with respect to time is proportional to (another state variable) ω_G and to a disturbance $d(t)$ (rate of change of load demand \dot{P}_L and or rate of change of effective tie-line flows \dot{F}_e into an area in a multiarea system). It is shown in the remainder of this section that this equation, combined with the dynamics

⁴ For rigorous interpretation of differentiation of algebraic constraints with respect to time, see Ref. [24].

of G-T-G units, obtains formulation of real power dynamics in its closed-loop state-space form. A closed-loop state-space form referred to here is

$$\dot{x}(t) = Ax(t) + Cd(t) \quad (6.89)$$

where $x(t)$ is system state and $d(t)$ is system disturbance. The primary control $u(t)$ is already included, because A represents closed-loop system matrix.

6.4.3 Slow Real-Power-Frequency Dynamics of an Interconnected System

Consider a single region with m generators within an interconnected system. The state-space formulation of the linearized dynamics of all G-T-G units on the system Eq. (6.73), together with the network constraint Eq. (6.88), forms the closed-loop dynamic model of the interconnected system. Local dynamics of generators are related through variations in P_G only. This is seen by defining

$$x_G = \begin{bmatrix} x_G^1 \\ \vdots \\ x_G^m \end{bmatrix}, \quad P_G = \begin{bmatrix} P_G^1 \\ \vdots \\ P_G^m \end{bmatrix}, \quad \omega_G = \begin{bmatrix} \omega_G^1 \\ \vdots \\ \omega_G^m \end{bmatrix} \quad (6.90)$$

and

$$A_G = \begin{bmatrix} A_G^1 & & \\ & \ddots & \\ & & A_G^m \end{bmatrix}, \quad C_M = \begin{bmatrix} c_M^1 & & \\ & \ddots & \\ & & c_M^m \end{bmatrix} \quad (6.91)$$

The generator frequencies are part of the local generator states, given by

$$\omega_G = Ex_G \quad (6.92)$$

with the matrix $E = \text{block diag}(e, e, \dots, e)$ and $e = [1 \ 0 \ 0]$.

The standard state-space model of the single region within the interconnected system in terms of the tie-line flows explicitly takes on the form

$$\dot{x} = \begin{bmatrix} \dot{x}_G \\ \dot{P}_G \end{bmatrix} = \begin{bmatrix} A_G & C_M \\ K_P E & 0 \end{bmatrix} \begin{bmatrix} x_G \\ P_G \end{bmatrix} + \begin{bmatrix} 0 \\ \dot{F}_e \end{bmatrix} + \begin{bmatrix} 0 \\ -D_P \end{bmatrix} \dot{P}_L \quad (6.93)$$

This model is of the general form (6.89) and as such lends itself to well-established analysis and control methods for linear time-invariant dynamic systems.

The system matrix for the region is

$$A = \begin{bmatrix} A_G & C_M \\ K_P E & 0 \end{bmatrix} \quad (6.94)$$

The system-state variables within each area (intra-area variables) are

$$x_{\text{new}} = \begin{bmatrix} x_G \\ P_G \end{bmatrix} \quad (6.95)$$

instead of more commonly used state-space variables

$$x_{\text{old}} = \begin{bmatrix} x_G \\ \delta_G \end{bmatrix} \quad (6.96)$$

With these new state variables the general structure of an interconnected power system is given in Eq. (6.93). The model in Eq. (6.93) is equivalent to the more frequently used model in terms of x_{old} . One of the reasons for using this model is to stress that the general structure of the system matrix A does not depend on the level of complexity of the G-T-G unit. Only the order of A changes as A_G changes.

6.5 MIDRANGE VOLTAGE DYNAMICS

As in the real-power–frequency dynamics case, a structure-based decomposition approach is taken here to derive a model representing voltage dynamics at each area level. A remarkable feature is that although the reactive-power–voltage model has a seemingly parallel structure to the long-range real-power–frequency model, these two models represent fundamentally different systems. While the real-power–frequency dynamics are structurally singular, this is *not* the case for reactive-power–voltage dynamics, unless a specific numerical singularity occurs.

The modeling singularity of real-power–frequency dynamics is due to the fact that the real power across a transmission line depends on the phase-angle *difference* across the line. A constant offset on both angles makes no difference for real-power transfer. However, the reactive power across a transmission line is not a function of the voltage difference only, so that a constant offset on both voltages does change the reactive-power flow. Due to the nonexistence of zero modes in the decoupled voltage dynamics, there is no need for a direct interarea flow control except for unusual operating conditions in which voltage dynamics become numerically singular.⁵

6.5.1 Exciter Control of Reactive-Power–Voltage Dynamics

The general structure of the reactive-power–voltage control of power systems can be represented by Figure 6.4. The excitation system controls the field-voltage input to the generator using the error signal between the measured generator terminal voltage and a given set-point value. The goal is to maintain the generator terminal voltage at the prespecified setting.

As in the real-power–frequency control case, the dynamics of all generators are coupled together through the transmission network via the reactive-power outputs of all generators. The transmission network imposes an algebraic

⁵ The occurrence of a numerical singularity is very relevant for understanding various aspects of voltage-collapse phenomena; this is studied in great detail in Chapters 7 to 11.

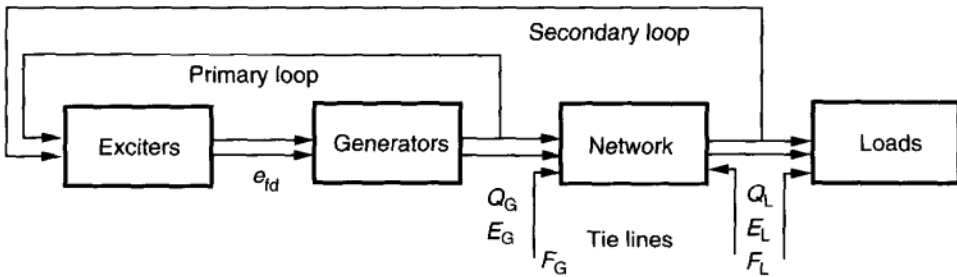


FIGURE 6.4 Typical structure of reactive-power–voltage control.

constraint on the total reactive-power injections into the network and couples all the generator power outputs together. It also couples generators to the loads.

Let us first consider the local dynamics of an individual excitation system and a generator set. A schematic block diagram for the excitation control system is shown in Figure 6.5.

As described in Chapter 3, a typical excitation system consists of the regulator, exciter, and the excitation feedback compensator. The regulator is described by

$$T_A \dot{V}_R = K_A V_F - \frac{K_A K_F}{T_F} e_{fd} - V_R - K_A (E_G - E_G^{\text{ref}}) \quad (6.97)$$

where e_{fd} is the field voltage of the exciter, E_G the generator terminal voltage, and E_G^{ref} the set-point value for the generator terminal voltage. The exciter dynamics can be modeled in the following form:

$$T_e \dot{e}_{fd} = -(K_e + S_e) e_{fd} + V_R \quad (6.98)$$

Generator dynamics are typically given by (type IV₂ model in Chapter 3)

$$T'_{d0} \dot{e}'_q = -e'_q - (x_d - x'_d) i_d + e_{fd} \quad (6.99)$$

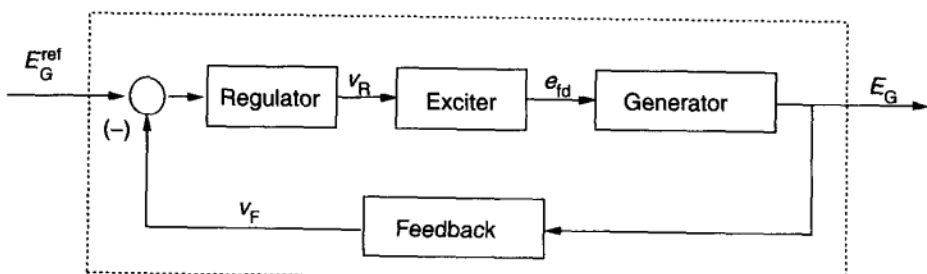


FIGURE 6.5 Typical excitation system

After neglecting the effects of damper winding, that is, $e'_d = 0$, where i_d is the reactive current out of a generator, this current is obtained as

$$i_d \simeq \frac{Q_G}{e'_q} \quad (6.100)$$

because $Q_G = e'_q i_d - e'_d i_q$

Finally the compensator is of the form

$$T_F \dot{V}_F = -V_F + \frac{K_F}{T_F} e_{fd} \quad (6.101)$$

Define the local states of each generator as

$$x_G = [V_R \quad e_{fd} \quad e'_q \quad V_F]^T \quad (6.102)$$

One can write Eqs. (6.97) to (6.101) together in a nonlinear state-space form as

$$\dot{x}_G = f(x_G, Q_G, E_G^{\text{ref}}) \quad (6.103)$$

recognizing that $E_G = e'_q$ because $E_G = \sqrt{e'^2_q + e'^2_d}$ if $e'_d = 0$. This model of local dynamics is of the general form Eq. (4.7). In this model, the generator reactive-power output Q_G is the power flow in the general local dynamics model Eq. (4.7). This variable couples dynamics of all generators connected through the network. This coupling, known as the network constraints, is discussed next.

6.5.2 Reactive-Power Network Constraints

As in the real-power-frequency case, the generator reactive power outputs Q_G are determined by the interactions with other generators and loads via the transmission network. Derivations here are very similar to those for the real-power-frequency dynamics. Consider an administrative region with m generators and n loads within an interconnected system. Similar to Eq. (6.75), the reactive-power-voltage constraints are the imaginary part of Eq. (5.118) and are of the form

$$Q^N = Q^N(\delta, E) \quad (6.104)$$

where

$$\delta \stackrel{\Delta}{=} \begin{bmatrix} \delta_G \\ \delta_L \end{bmatrix}, \quad E \stackrel{\Delta}{=} \begin{bmatrix} E_G \\ E_L \end{bmatrix} \quad (6.105)$$

are the nodal voltage angles and magnitudes. Define the reactive-power tie-line flows from the neighboring areas into all generator nodes and all load nodes as

$$F_G \stackrel{\Delta}{=} \begin{bmatrix} F_G^1 \\ \vdots \\ F_G^m \end{bmatrix}, \quad F_L \stackrel{\Delta}{=} \begin{bmatrix} F_L^1 \\ \vdots \\ F_L^n \end{bmatrix} \quad (6.106)$$

Then it is obvious that $Q_G^N = F_G + Q_G$. The network constraints for the reactive-power-balance Eq. (6.104) can be further written as

$$Q_G^N(\delta, E) = F_G + Q_G \quad (6.107)$$

The same relationship is true for the load buses, that is,

$$Q_L^N = F_L - Q_L \quad (6.108)$$

the network constraint (6.104) at the load nodes are expressed as

$$Q_L^N(\delta, E) = F_L - Q_L \quad (6.109)$$

assuming again that the positive direction for tie-line flows is injection into the network and the positive direction for loads is leaving the network. Similar to the real-power-frequency case, we separate reactive-power injections into the part of the injection from the generators or loads and the part from the interconnecting tie lines with the neighboring regions. These represent algebraic constraints to the network variables such as the bus voltage vector E .

Next, under the real-reactive power decoupling assumption, differentiating the above constraints yields

$$\dot{F}_G + \dot{Q}_G = J_{GG}\dot{E}_G + J_{GL}\dot{E}_L \quad (6.110)$$

$$\dot{F}_L - \dot{Q}_L = J_{LG}\dot{E}_G + J_{LL}\dot{E}_L \quad (6.111)$$

where

$$J_{ij} = \frac{\partial Q_i^N}{\partial E_j}, \quad i, j = G, L \quad (6.112)$$

are the Jacobian matrices evaluated at the given equilibrium operating point. Assuming J_{LL} to be invertible under the normal operating conditions, we define

$$C_E = -J_{LL}^{-1}J_{LG} \quad (6.113)$$

to express voltage deviations at loads E_L in terms of voltage deviations at generators E_G and fluctuations in load power. It then follows from Eq. (6.111) that

$$\dot{E}_L = C_E \dot{E}_G + J_{LL}^{-1}(\dot{F}_L - \dot{Q}_L) \quad (6.114)$$

where

$$E_G \stackrel{\Delta}{=} \begin{bmatrix} E_G^1 \\ \vdots \\ E_G^m \end{bmatrix} \quad (6.115)$$

Relationship (6.114) defines the explicit dependence of load voltages on generator voltages and system disturbances ($\dot{F}_L - \dot{Q}_L$) determined by the network constraints. Combining Eqs. (6.114) and (6.110) and defining

$$K_Q \stackrel{\Delta}{=} J_{GG} + J_{GL}C_E \quad (6.116)$$

and

$$D_Q \stackrel{\Delta}{=} -J_{GL} J_{LL}^{-1} \quad (6.117)$$

result in

$$\dot{Q}_G = K_Q \dot{E}_G - \dot{F}_e + D_Q \dot{Q}_L \quad (6.118)$$

Here F_e represents the effective reactive tie-line flow as seen by each generator and is defined as

$$F_e \stackrel{\Delta}{=} F_G + D_Q F_L \quad (6.119)$$

Equation (6.118) defines the relationship among the generator reactive-power outputs Q_G , generator voltages E_G , the tie-line flows into the subsystem \dot{F}_e , and the reactive-power load variations \dot{Q}_L through the network characteristics specified by the two important matrices K_Q and D_Q .

It should be noted that any (portion of) network is fully characterized by the three matrices K_Q , C_E , and D_Q , with K_Q reflecting the effect of the generator voltages on the generator reactive-power outputs, C_E relating the generator voltages to the load voltages, and D_Q representing different electrical distances of loads at different locations seen by the generators. It can be shown that the matrix K_Q does not have a modeling singularity associated with matrix K_P for the real-power–frequency dynamics, although under extreme operating conditions numerical singularities are possible.⁶

6.6 INTERAREA DYNAMICS

The interconnected power systems are often horizontally structured in the sense that their analysis and design are accomplished by observing administrative borders between the subsystems (regions). An unexpected dynamic problem can occur under certain conditions through increased efforts to transfer electric power across vast geographical and electrical distances. There have been documented instances of low-frequency oscillations between two specific power plants located in two administratively different subsystems. These are known as the interarea oscillations.

We stress that it is conceptually meaningful to define a particular linear combination of states in each subsystem that has only dynamics when the subsystems are physically interconnected. In this section we formalize the notion of these variables.

Keeping in mind that Eq. (6.93) is true for any single area within an interconnected system, we obtain a dynamic model for each area explicitly in terms of

⁶ These are the subject of studies in Chapters 7 to 11.

the tie-line flows among the areas as

$$\dot{x}^i = A^i x^i + \begin{bmatrix} 0 \\ \dot{F}_e^i \end{bmatrix} + \begin{bmatrix} 0 \\ -D_p^i \end{bmatrix} \dot{P}_L^i \quad (6.120)$$

for $i \in I, II, \dots, R$. This form implies that the dynamics of state variables in each area i are directly dependent of state variables in the same area, the dynamics of loads (disturbance) in the same area, and the dynamics of tie-line flows into the area \dot{F}_e^i . As shown before, this formulation is a direct consequence of the basic power-balance equations once the dynamics at the component level are expressed in terms of the new state variables. Notice, however, that this formulation accounts for the electrical distances of load and tie lines from the machines according to values of K_p^i and D_p^i . It *cannot* be written by inspection.

6.6.1 Definition of the Interarea Variables

To extract the interarea dynamics, we introduce the generalized interarea variables in the following.

DEFINITION The interarea variables $z(t)$ are variables that satisfy

$$z(t) = \text{const} \quad (6.121)$$

when all interconnections among the subsystems S^i , $i = I, \dots, R$ are removed, and the system is free of disturbances.

It has been shown in Refs. [19]–[22] that in the case of weakly connected power systems the interarea variables as defined here are directly related to the slow variables of the aggregate model in Ref. [25]. However, it is suggested here that by starting with a structure-based general definition (6.121) one could introduce an aggregate model that does not necessarily assume weak interconnections, and it is also easier to compute or interpret when one is interested in mid- to long-range interarea dynamics only.

Note from this definition that the interarea variables $z(t)$ are local variables associated with each region. The interarea variables for area i are a function of the state variables of area i only. Note also that for a linear system, it is expected that the interarea variables $z(t)$ can be expressed as a linear combination of state variables $x(t)$. This linear dependence is expressed as

$$z^i(t) = P^i x^i(t), \quad i = I, II, \dots \quad (6.122)$$

with the “participation factor” P^i satisfying

$$P^i A^i = 0 \quad (6.123)$$

(Notice that symbol z used here to represent the inter-area variables is *not* related to the variable $z(t)$ in Appendix 6.2 nor to the variables $z_i(t)$ used in Table 6.1.)

6.6.2 Fundamental Relations Relevant for Analysis of the Interarea Dynamics

Possibly the strongest reason for using the new state-space variables x_{new} [Eq. (6.95)] comes from the fact that the interarea dynamics within an interconnected system have a rather straightforward interpretation in terms of power generated within the individual areas.⁷ This is shown in the following.

A closer look at the model in Eq. (6.93) expressed in terms of the new state variables reveals that the properties of the long-range real-power–frequency dynamics are directly determined by the properties of the network matrix K_P under certain weak assumptions regarding states x_G at each component level. Furthermore, under the same assumptions the basic properties of the interarea dynamics are directly determined by examining the structure of the network matrix K_P . To show this, we first review several basic properties of the system Jacobian J in Eqs. (6.78) to (6.79) and the matrix K_P .⁸ These properties are used to propose a general definition and interpretation of the interarea dynamics and are given in the following propositions.

Proposition 6.6.1 For any isolated power system (lossy or lossless),

1. $J\mathbf{1} = 0$, that is, the row sum of J is 0, where matrix J is the Jacobian $\partial P^N(\delta, E)/\partial \delta$.
2. $C_\omega \mathbf{1} = \mathbf{1}$, that is, the row sum of C_ω in Eq. (6.80) is 1.
3. $K_P \mathbf{1} = 0$, that is, the row sum of K_P is 0. This is equivalent to K_P being singular with $\mathbf{1}$ as the right eigenvector corresponding to its 0 eigenvalue.
4. $\mathbf{1}^T J^b = 0$ and $\mathbf{1}^T J = \mathbf{1}^T J^g$, that is, the column sum of J is equal to the column sum of J^g , where J^g is part of the Jacobian contributed by losses, and J^b is its main part representing the loss-less transmission network, $J = J^b + J^g$.
5. $\mathbf{1}^T J = 0$ and $\mathbf{1}^T K_P = 0$, for a lossless network, that is, $\mathbf{1}^T$ is also the left eigenvector corresponding to the 0 eigenvalue.

Here $\mathbf{1} = [1 \cdots 1]^T$.

Proposition 6.6.1 is a direct consequence of the fact that the row sum of the incidence matrix is 0 (see Chapter 4).

⁷ On the other hand, the interarea dynamics appear to be very difficult to model, analyze, and stabilize when using x_{old} [Eq. (6.96)]. The interarea dynamics are expressed as a linear combination of voltage phase angles, with the computation of coefficients defining what amounts to an aggregate variable that is extremely computationally involved [25].

⁸ In the case of a lossless power system, and with voltage magnitudes 1 p.u. and voltage-phase-angle differences 0, J is identical to the imaginary part of the bus admittance matrix \hat{Y}_{bus} . Properties stated here are easily understood in relation to the general properties of the bus admittance matrix discussed in Chapter 4, Section 4.1.5.

6.6.3 Computation of Interarea Variables

Next, using the preceding definition of interarea variables, the basic structure of the model in Eq. (6.120) and properties of matrix K_p listed in these propositions, we study the existence and uniqueness of transformation P^i , $i = I, \dots, R$ as well as the computational complexity involved in deriving P^i .

Proposition 6.6.2 There exists a unique P^i (up to a scalar) whose dimension is $1 \times (n_G^i + n^i)$, where n_G^i is the number of generators in the area i , and n^i is the number of local state variables of all generators in the area i .

Proof: Consider area i , which is connected to the others. Matrix A^i is structurally rank-deficient since K_p^i is rank-deficient as shown in Proposition 6.6.1. It is also known that matrix K_p^i is generally of rank $n_G^i - 1$ if there are n_G^i generators in the area, that is, K_p^i is structurally rank-deficient only by 1. Since we are only interested in the interarea dynamics (and not in the local dynamics of each generator), take the form for P^i as

$$P^i = [0 \quad p^i] \quad (6.124)$$

where p^i is a matrix to be determined from the condition (6.123). With this form, Eq. (6.123) becomes

$$p^i K_p^i = 0 \quad (6.125)$$

Clearly p^i is the *left eigenvector of matrix K_p^i* corresponding to its 0 eigenvalue. This also proves the uniqueness of p^i up to a scalar.

In general, it is desired to have stable local dynamics, that is, the governor control design is such that each matrix A_G^i is of full rank. This assumption is normally met since local controls are typically designed such that local dynamics are stable for the expected range of real-power outputs P_G .

Under this condition local dynamics do not contribute to the interarea variables defined in Eq. (6.121). This is reflected in Eq. (6.124) by the component 0, which corresponds to the local states. If this is not the case, then local dynamics do contribute to the interarea dynamics. The question of governor control design (and, more generally, generation-based primary controls) so that x_G 's can be stabilized for the range of anticipated variations in P_G is studied in Chapter 12.

Next, we discuss the calculation of p^i . It is emphasized that eigenanalysis is not necessary, since Eq. (6.125) can be easily solved by a simple Gauss elimination-like method. For a lossless network, computation of p^i is trivial. Recall from Propositions 6.6.1 and 6.6.2 that $p^i = p^{bi} = \mathbf{1}^T$. For a lossy network, we discuss an approximate formula for p^i as an alternative to the numerical Gauss method. Let us write p^i as

$$p^i = p^{bi} + p^{gi} = \mathbf{1}^T + p^{gi} \quad (6.126)$$

where $p_b^i = \mathbf{1}$ corresponds to the eigenvector of the lossless K_P matrix, and p_g^i is added to account for losses. Condition (6.125) becomes

$$p^i K_P^i = (p^{bi} + p^{gi})(K_P^{bi} + K_P^{gi}) = 0 \quad (6.127)$$

Recognizing that $p^{bi} K_P^{bi} = 0$, and neglecting second-order terms due to losses, one obtains

$$p^{gi} K_P^{bi} = -p^{bi} K_P^{gi} \quad (6.128)$$

Furthermore, without loss of generality, one could assume the form for p^{gi} to be

$$p^{gi} = [0 \quad p_2^g \quad \cdots \quad p_{n_G}^g]^i \quad (6.129)$$

because the transformation p^i is unique only up to a constant scalar, and one can always choose the first element of p^i to be the first element of p^{bi} ; therefore first element of p^{gi} is always 0.

It can be shown that for the choice of p^{gi} as in Eq. (6.129), the solution to Eq. (6.128) becomes

$$p^{gi} = -p^b K_P^g E_1 E_2 [(E_1 E_2)^T K_P^b (E_1 E_2)]^{-1}|^i \quad (6.130)$$

where $E_1 = I_{n_G^i \times n_G^i}$ without the first column and $E_2 = I_{(n_G^i - 1 \times n_G^i - 1)}$ without the first column.

It is interesting to note that when matrix K_P^i has rank lower than $n_G^i - 1$, there exists the possibility of having more than one interarea variable per area. These additional interarea variables are simply caused by the nonexistence of a solution to the static network constraints (5.118) and are independent of the relative inertia and damping coefficient values of generators as well as of the type of governor controls. Although an open question remains about the feasibility of such operating points, a near loss of rank would be of definite practical interest. For example, one scenario of additional loss of rank in the matrix K_P^i would be when the system operates at unusually high real-power transfers. The interarea oscillations have been recognized in context of this operating mode [27, 28].

6.6.4 Modeling of the Interarea Dynamics

It is clear that to define the interarea dynamics one needs only to compute p^i — a participation factor at the level of subsystem i using formula (6.130). This algorithm leads to introducing only one interarea variable $z^i(t)$ associated with each area i . Its form is obtained by combining relations (6.124) and (6.122) as

$$z^i(t) = p^i P_G^i \quad (6.131)$$

that is, the interarea variable $z^i(t)$ is simply a combination of the generator power outputs of each area i . This particular combination will remain constant if interactions are removed. This is actually another form of expressing the regional power-balance condition. As tie-line flows vary, the combination will also vary. We refer to the model defining changes in the interarea variable $z^i(t)$ as the *interarea dynamics* model.

By introducing definition (6.121) it directly follows from Eq. (6.120) that the interarea dynamics model takes on the form

$$\dot{z}^i(t) = P^i \begin{bmatrix} 0 \\ \dot{F}_e^i(t) \end{bmatrix} + P^i \begin{bmatrix} 0 \\ -D_P^i \end{bmatrix} \dot{P}_L^i(t) = p^i (\dot{F}_e^i(t) - D_P^i \dot{P}_L^i(t)) \quad (6.132)$$

We see that the interarea variables $z^i(t)$ vary due to the tie-line power flow injections, for a constant power load.⁹ Equation (6.132) defines exactly the relationship between these two. From here we also see that the fundamental cause of the interarea dynamics lies in the interarea power exchanges. All this can only be seen through the model using power as part of system state variables, as introduced in x_{new} . This kind of interaction among the regions is referred to as the *interarea power interactions*.

It follows from formula (6.131) that the interarea variable $z^i(t)$ is defined as a linear combination of generator power output deviations P_G^i in area i only. In the case of a lossless power network $p^i = \mathbf{1}^\top$, leading to

$$z^i(t) = p^i P_G^i(t) = \sum_{j=1}^{n_G^i} P_{Gj}^i(t) = \text{total generation of area } i \quad (6.133)$$

for $i = I, II, \dots, R$. This implies that $z^i(t)$ is constant, assuming a constant real-power load model and no losses in an isolated power network.

6.6.5 Dynamics of Interarea Variables on an Interconnected Power System

Writing the model given in Eq. (6.132) for each area leads to an aggregate model of the interconnected system

$$\dot{z}(t) = p(\dot{F}_e(t) - D_P \dot{P}_L(t)) \quad (6.134)$$

with $p = \text{diag}(p^1, \dots, p^R)$ and

$$z(t) = \begin{bmatrix} z^1(t) \\ \vdots \\ z^R(t) \end{bmatrix}, \quad F_e(t) = \begin{bmatrix} F_e^1(t) \\ \vdots \\ F_e^R(t) \end{bmatrix}, \quad P_L(t) = \begin{bmatrix} P_L^1(t) \\ \vdots \\ P_L^R(t) \end{bmatrix} \quad (6.135)$$

⁹ The reader should keep in mind that this claim is made under the assumption that x_G can be stabilized to within a threshold of x_G^{ref} assigned by a secondary level control as P_G varies. Ensuring that this assumption is met is a question of primary governor control design at the generator level.

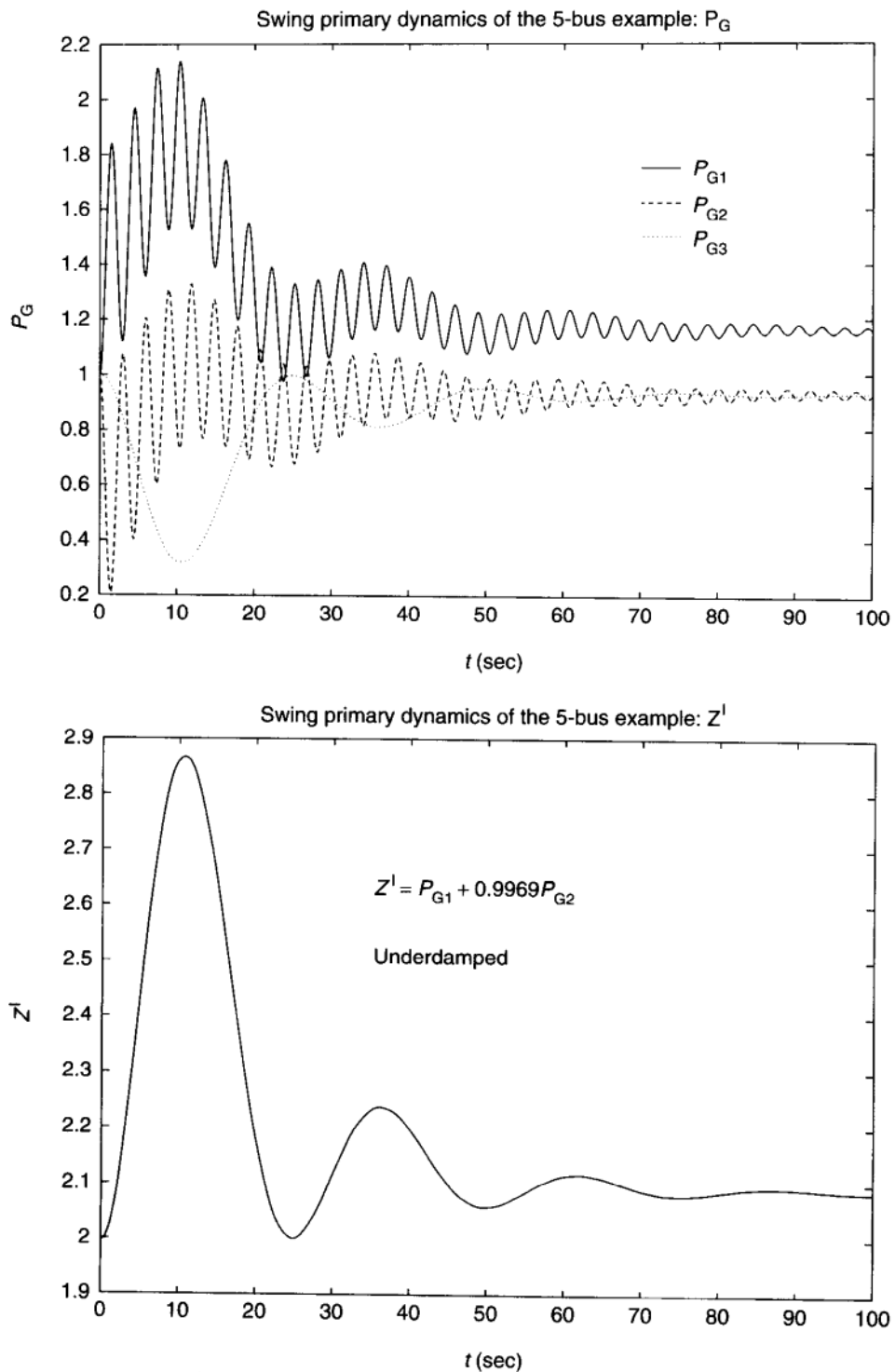
Obviously, $\dim z = R$, corresponding to the number of subsystems of the interconnected system. This results in relatively low order and a simple model that is relevant for stabilizing interarea dynamics, assuming that local control stabilizes fast dynamics.

It is seen from the model in Eq. (6.134) that the dynamics of interarea variables are the result of changes in tie-line flows and changes in loads. The aggregate model (6.134) of the interconnected system offers an exact quantification of the participation of tie-line flow changes and/or load changes in the dynamics of interarea variables $z(t)$. On the other hand, the variables $z(t)$ themselves reflect participation of generation changes in each area i directly in variable $z^i(t)$. As shown in the preceding section, the participation factors are extremely easy to compute in the case of lossless networks and can be built by inspection. The approximate formulas (the only approximation involves neglecting second-order effects of losses) for computing participation factors on the lossy system do not require left-eigenmode computations. They only involve computing load-flow sensitivity matrices such as K_p^i for each area and a matrix inversion according to formula (6.130) for each area separately. This provides for qualitative computational savings relative to many other methods concerned with the interarea dynamics. A unique property of the aggregate model (6.134) is that it is defined in terms of physically measurable variables such as the tie-line flows. An interpretation of the dynamics of interaction variables in terms of eigenmode-based analysis and comparison with other methods can be found in Ref. [21].

It can be seen from model in Eq. (6.132) that the interarea dynamics are strictly disturbance-driven. Consequently, the only swings in $z^i(t)$ occur as a result of cumulative effect of load disturbances and disturbances outside an area. No interarea instability takes place as long as governors stabilize their own local states for prespecified ranges of changes in P_G .

6.6.5.1 Numerical Example A small five-bus electric power system divided into two subsystems as shown in Figure 6.3 is used to illustrate the interarea dynamics studied. Parameters of the system are as follows: generator masses $J_1 = 10$, $J_2 = 5$, $J_3 = 3$; $D = 10$, and $B_{ij} = 1$ for all lines. The state variables P_{Gj} , $j = 1, 2, 3$, and $z^i(t)$ for the undamped case are given in Figure 6.6. It can be seen that the generator power outputs have fast components (corresponding to the intra-area dynamics) and a slow component (corresponding to the interarea dynamics). The frequency of the slow interarea dynamics is captured by the interarea variables $z^I(t)$ and $z^{II}(t)$ as shown in the same Figure 6.6 [note that $z^{II}(t) = P_{G3}$, since region II has only one generator]. The interarea variables $z^I(t)$ and $z^{II}(t)$ of the interconnected system change at a rate corresponding to the mode that is a result of interconnecting the two subsystems.

It is interesting to note that although P_{G1} and P_{G2} have a higher oscillatory frequency, their weighted sum according to formula (6.131) does not change at the isolated system level. The weighting coefficients are $p^I = [1 \ 0.9969]$ and $p^{II} = 1$ (since area II has only one generator).

**FIGURE 6.6** State variables.

6.7 MODEL REDUCTION AT THE INTERCONNECTED SYSTEM LEVEL

There exists yet another basis for the separation of subprocesses and model reduction that is essential only for very large interconnected power systems. This is in addition to the separation of subprocesses described earlier in this chapter that are governed by considerably different time constants at a component level.

Model reduction is done for very large electric power systems with different objectives. They are primarily intended to provide:

- Modeling one's own system in sufficient detail, while "equivalencing" the rest of the power system by a very-low-order model [28] to [30] and [31] to [32].
- Developing low-order "aggregate" models for very large systems, essential for dynamic interactions among different utilities [25].

In this section only the basic principles underlying these techniques are described. No attempt is made to summarize various research results in detail.

Two qualitatively different approaches are known for obtaining such models. The first approach uses singular perturbation-based thinking that there exist subprocesses that evolve at a fast time scale within each area, and that other, interarea, subprocesses are slower [33]. This premise suggests the possibility of modeling a very-high-order model to recognize such a time-scale separation. A close look into the problem suggests further that this separation is caused by either nonuniform relative inertia of synchronous generators or nonuniform electrical connections. In the first case, it is fairly straightforward to understand why different groups of machines act in concert that is, in coherency; all machines with similar inertia constants will respond at a similar rate to a system perturbation. This leads to a formation of coherent groups of machines that are geographically and electrically distant from each other.

The second case is much more intriguing: Imagine an electric power system with machines that have almost identical constants of inertia but fairly nonuniform interconnections. It is not obvious a priori at all if such a system could exhibit processes that are separable in time. Nor is it obvious how these may be separated. The networks are highly meshed, and it is not intuitively clear how this separation takes place. It can be shown basically that any system can be brought into a nonexplicit singular perturbation-form in Eq. (6.2.25), Appendix 6.2. This form does not provide a guarantee that the substates will be separated in time. However, it is necessary for the rank of the system matrix $A(0)$ to be rank-deficient for transforming the nonexplicit form (6.2.25) into the explicit forms (6.2.1) and (6.2.2). All electric-power-system models exhibit a fascinating property that the system matrix has at least one structural zero. The cause of this was explained earlier in Chapter 4. This is in the very roots of time-scale-separated processes associated with any electric power system. The procedure outlined in Section 6.7.1 clearly implies that the states that contribute the most to this rank

deficiency caused by a structural zero eigenvalue are candidates for “slow” variables in each group. As a matter of fact, the number of groups is indicated by the number of states that participate the most in this mode. In this sense it is numeric and depends strongly on the actual strength of interconnections, which determines the smallest singular values of the matrix $A(\varepsilon)$ (Appendix 6.2). This fundamental aspect of separating processes into intra- and interarea processes, for any given system partitioning, was recognized only recently.

6.7.1 Time-Scale Separation in Aggregate and Coherent Models

To introduce the basic framework, consider a simple power system given in Figure 6.7. Assume that $J_2/J_1 \ll 1$ and $J_3/J_1 \ll 1$. The linearized model of this interconnected system is of the form¹⁰

$$J_1 \frac{d^2\delta_1}{dt^2} = B_{11}\delta_1 + B_{12}\delta_2 + B_{13}\delta_3 \quad (6.136)$$

$$J_2 \frac{d^2\delta_2}{dt^2} = B_{12}\delta_1 + B_{22}\delta_2 + B_{23}\delta_3 \quad (6.137)$$

$$J_3 \frac{d^2\delta_3}{dt^2} = B_{13}\delta_1 + B_{23}\delta_2 + B_{33}\delta_3 \quad (6.138)$$

Here J_i stands for inertia of the i th generator and B_{ij} represents the susceptance of a transmission line connecting nodes i and j . Two cases are of direct interest:

- Uniform B_{ij} , nonuniform J_i
- Nonuniform B_{ij} , uniform J_i

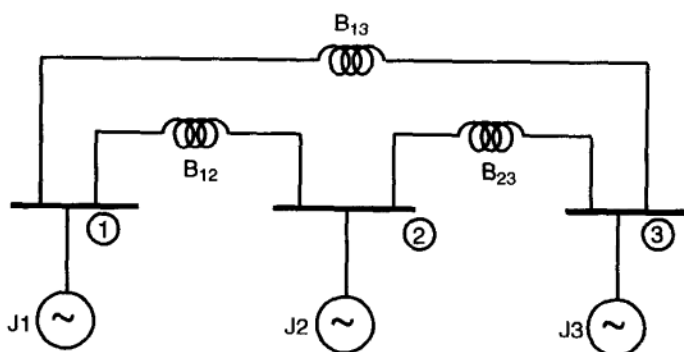


FIGURE 6.7 Power-system model.

¹⁰ This model directly follows from the general model in Eqs. (4.105) and (4.104) when e'_q is assumed constant and damping coefficients of the machines D_i and line conductances G_{ij} are neglected.

Case 1: Uniform B_{ij} , $J_2 = J_3$. Define

$$t_d = \sqrt{\frac{J_1}{B_{12}}} t \quad (6.139)$$

and

$$\varepsilon = \beta \frac{J_2}{J_1} \quad (6.140)$$

Equations (6.136) to (6.138) take on an explicit singularly perturbed form

$$\frac{d^2y}{dt^2} = Ay + Bz \quad (6.141)$$

$$\varepsilon \frac{d^2z}{dt^2} = Cy + Dz \quad (6.142)$$

Here z consists of δ_2 and δ_3 , and y is δ_1 . The slow motion of this system is represented sufficiently accurately by the dynamics of the first machine. This result is intuitively clear, since it implies that the machine with the largest inertia moves in the slowest manner. One can proceed with general SP-based model reduction described earlier for retaining the “slow” variable y .

Case 2: Nonuniform B_{ij} , uniform J_i . Assume $B_{12} = B_{23} = p$ and $B_{13} = \varepsilon$. In this case the resulting model is in a nonexplicit SP form:

$$\frac{d^2x}{dt^2} = \left(\begin{bmatrix} -p & p & 0 \\ p & -2p & p \\ 0 & p & -p \end{bmatrix} + \varepsilon \begin{bmatrix} -1 & 0 & 1 \\ 0 & 0 & 0 \\ 1 & 0 & -1 \end{bmatrix} \right) x \quad (6.143)$$

Presence of the zero eigenvalue determines the existence of subprocesses that are separated in time, independently from the actual strength of system interconnections. This means that there exists at least one state that responds more slowly than the others. Typically it is a linear combination of states determined by the similarity transformation defined in Eq. (6.2.26).

It is essential to observe that the coherency-based model reduction described here is based on a full model that has all generators present. The process becomes ill-posed once the equations are rewritten relative to a prespecified reference machine. This is because the structural singularity is the foundation of time-scale-separated processes in interconnected power systems.

We find the analogy with basic RC circuits particularly helpful for understanding fundamentals of process separation caused by nonuniform interconnections. It suffices to compare the two RC circuits in Figures 6.8 and 6.9 [25]. Following the same modeling procedures described here, one can easily find that the first circuit is the only one that exhibits time-scale-based separation of

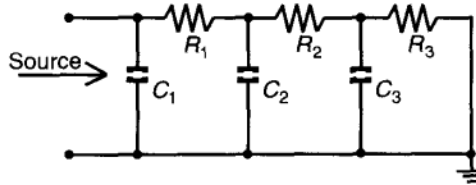


FIGURE 6.8 *RC* circuit that exhibits time-scale separation.

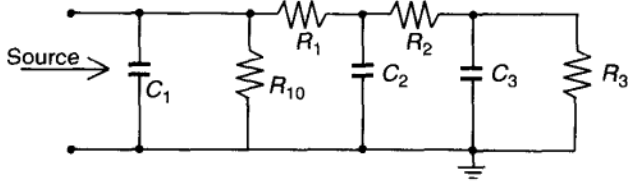


FIGURE 6.9 *RC* circuit that does not exhibit time-scale separation.

processes due to its inherent zero eigenvalue; the second circuit does not have this property.

For specific algorithms for model reduction in large power systems using selective modal analysis (SMA) methods see Refs. [34–36]. Also, for a specific singular perturbation–(SP) based algorithm for computing a model relevant for coherency studies see Refs. [14, 25, 37].

APPENDIX 6.1 MACHINE PARAMETERS AND NETWORK DATA

Another way of interpreting the three-bus system as a Thevenin equivalent of the three-bus system is shown in Figure 6.1.1. Note that E'_∞/δ'_∞ are network-parameter-dependent variables and are given by

$$E'_\infty = \sqrt{(E_\infty + I_{1y}x_1)^2 + (-I_{1x}x_1)^2} \quad (6.1.1)$$

$$\delta'_\infty = \tan^{-1} \left(\frac{-I_{1x}x_1}{E_\infty + I_{1y}x_1} \right) \quad (6.1.2)$$

where

$$I_{1x} = \frac{E_\infty(a_4 + a_5a_7 - b_5b_7)}{(a_4 + a_5a_7 - b_5b_7)^2 + (b_4 + b_5a_7 + a_5b_7)^2}$$

$$I_{1y} = \frac{-E_\infty(b_4 + b_5a_7 + a_5b_7)}{(a_4 + a_5a_7 - b_5b_7)^2 + (b_4 + b_5a_7 + a_5b_7)^2}$$

$$a_7 = \frac{-a_4a_5(t-1)^2 - a_6b_6(t-1)}{[a_5(t-1)]^2 + b_6^2}$$

$$\begin{aligned}
b_7 &= \frac{a_5 a_6 (\mathbf{t} - 1)^2 - b_6 a_4 (\mathbf{t} - 1)}{[a_5 (\mathbf{t} - 1)]^2 + b_6^2} \\
a_6 &= -\frac{x_T}{\mathbf{t}} - a_3 X_L \\
b_6 &= x_T + (\mathbf{t} - 1)(X_L b_3 + X_L) \\
a_5 &= -(R_L b_3 + R_L) \\
b_5 &= -b_3(x_2 + X_L) - X_L \\
a_4 &= R_L a_3 \\
b_4 &= -x_2 + x_2 a_3 + X_L a_3 \\
a_3 &= \frac{x_1 + x_{12} + x_T/\mathbf{t} + x_2}{x_2} \\
b_3 &= \frac{x_T}{x_2 \mathbf{t}} \\
a_2 &= \frac{-\left(b_1 + \frac{x_T}{\mathbf{t}}\right) \frac{a_1 x_T}{\mathbf{t}(\mathbf{t}-1)} + \frac{a_1 x_T}{\mathbf{t}(\mathbf{t}-1)} \left(b_1 + \frac{x_T}{\mathbf{t}} + \frac{x_T}{\mathbf{t}(\mathbf{t}-1)}\right)}{a_1^2 + \left(b_1 + \frac{x_T}{\mathbf{t}} + \frac{x_T}{\mathbf{t}(\mathbf{t}-1)}\right)^2} \\
b_2 &= \frac{\frac{a_1^2 x_T}{\mathbf{t}(\mathbf{t}-1)} + \frac{x_T}{\mathbf{t}(\mathbf{t}-1)} \left(b_1 + \frac{x_T}{\mathbf{t}}\right) \left(b_1 + \frac{x_T}{\mathbf{t}} + \frac{x_T}{\mathbf{t}(\mathbf{t}-1)}\right)}{a_1^2 + \left(b_1 + \frac{x_T}{\mathbf{t}} + \frac{x_T}{\mathbf{t}(\mathbf{t}-1)}\right)^2} \\
a_1 &= \frac{X_L x_2 R_L + R_L x_2 (x_2 + X_L)}{R_L^2 + (x_2 + X_L)^2} \\
b_1 &= \frac{R_L^2 x_2 + X_L x_2 (x_2 + X_L)}{R_L^2 + (x_2 + X_L)^2}
\end{aligned}$$

whereas the equivalent impedance is

$$Z_e = R_e + jX_e \quad (6.1.3)$$

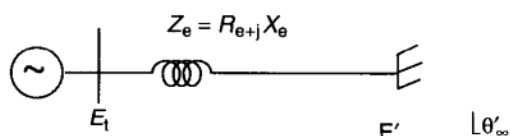


FIGURE 6.1.1 Simplified three-bus system.

with

$$R_e = \frac{-x_1 a_2 (b_2 + x_{12}) + a_2 x_1 (b_2 + x_1 + x_{12})}{a_2^2 + (b_2 + x_1 + x_{12})^2}$$

$$X_e = \frac{a_2^2 x_1 + x_1 (b_2 + x_{12})(b_2 + x_1 + x_{12})}{a_2^2 + (b_2 + x_1 + x_{12})^2}$$

APPENDIX 6.2 SINGULAR PERTURBATION METHOD FOR MODEL REDUCTION

This is a very widely used technique for model reduction when representing engineering processes that consist of subprocesses evolving at considerably different rates, that is, for a SP-based model reduction of a full-order model whose state is representable in a standard form [38]

$$\dot{y}(t) = f(y, z, \varepsilon) \quad (6.2.1)$$

$$\varepsilon \dot{z}(t) = g(y, z, \varepsilon) \quad (6.2.2)$$

given initial conditions $y(t_0) = y^0$, $z(t_0) = z^0$ and with parameter ε being a small number $\varepsilon \leq 1$.¹¹ The model in Eqs. (6.2.1) and (6.2.2) implies that the “fast” substate z evolves at a rate $1/\varepsilon$ greater than the “slow” substate y . System dynamics can be analyzed over time horizons in which changes of y are significant. Also, it is customary to develop a reduced-order model explicitly expressed in terms of the slow substate y , while taking into account the effect of changes in the fast substate.

To obtain a reduced-order model in terms of y , it is necessary to compute the following integral manifold:¹²

$$M_\varepsilon : \quad z = \phi(y, \varepsilon) \quad (6.2.3)$$

Once this relationship is obtained with certain degree of accuracy, it is used in Eq. (6.2.1) to express the reduced-order model in terms of y only. The general process for obtaining this manifold is based on defining the manifold as a Taylor-series expansion in terms of ε as follows:

$$\phi(y, \varepsilon) = \phi_0(y) + \varepsilon \phi_1(y) + \varepsilon^2 \phi_2(y) + \dots \quad (6.2.4)$$

¹¹ Obtaining a standard SP form is typically a complex process in its own right, and it is best done when combining engineering insight with mathematical procedures [38].

¹² Definition: Integral manifold for the equation $\dot{x} = X(t, x)$, where $x \in \mathbb{R}^n$, is a set $S \subset \mathbb{R} \times \mathbb{R}^n$ if for $(t_0, x_0) \in S$, the solution $(t, x(t))$, $x(t_0) = x_0$, is in S for $t \in \mathbb{R}$. If $(t, x(t)) \in S$ only at a finite interval, then we say that S is a local integral manifold [39].

Substituting Eq. (6.2.4) into (6.2.2), one arrives at the manifold condition that needs to be satisfied at all times

$$\varepsilon \frac{\partial \phi}{\partial y} \dot{y} = g(y, \phi(y, \varepsilon), \varepsilon) \quad (6.2.5)$$

Expanding Eq. (6.2.5) in ε and equating the coefficients of the powers of ε will yield the solution for $\phi_0(y)$, $\phi_1(y)$, etc.

A particular case of this general nonlinear form is the standard singularly perturbed model for linear time-invariant (LTI) models

$$\begin{aligned} \dot{y} &= A_{11}y + A_{12}z \\ \varepsilon \dot{z} &= A_{21}y + A_{22}z \end{aligned} \quad (6.2.6)$$

Condition (6.2.5) for the case of LTI systems (6.2.6) leads to

$$\begin{aligned} \varepsilon \left(\frac{\partial \phi_0}{\partial y} + \varepsilon \frac{\partial \phi_1}{\partial y} + \varepsilon^2 \phi_2(y) + \dots \right) [A_{11}y + A_{12}(\phi_0 + \varepsilon \phi_1 + \varepsilon^2 \phi_2 + \dots)] \\ = [A_{21}y + A_{22}(\phi_0 + \varepsilon \phi_1 + \varepsilon^2 \phi_2 + \dots)] \end{aligned} \quad (6.2.7)$$

Equating equal powers of ε terms leads to deriving

$$\phi_0(y) = -A_{22}^{-1}A_{21}y \quad (6.2.8)$$

$$\phi_1(y) = A_{22}^{-1}(-A_{22}^{-1}A_{21})(A_{11} - A_{12}A_{22}^{-1}A_{21})y \quad (6.2.9)$$

and higher-order terms, which are not explicitly stated here.

Based on this derivation the following results:

- *Zeroth-order approximation of system dynamics* based on approximating $z(t) \approx \phi_0(y)$ of the form

$$\dot{\bar{y}} = (A_{11} - A_{12}A_{22}^{-1}A_{21})\bar{y} \quad (6.2.10)$$

- *First-order approximation of system dynamics* based on approximating $z(t) \approx \phi_0(y) + \varepsilon \phi_1(y)$ of the form

$$\dot{\bar{y}} = (I - \varepsilon A_{22}^{-1}A_{21})(A_{11} - A_{12}A_{22}^{-1}A_{21})\bar{y} \quad (6.2.11)$$

Two block diagrams representing types of SP-based reduced-order models introduced in Ref. [38] are shown in Figures 6.2.1 and 6.2.2. The actuator form is obtained by introducing change of variables

$$\eta(t) = z(t) + L(\varepsilon)x(t) \quad (6.2.12)$$

It can be shown that two separate subsystems result when

$$A_{21} - A_{22}L + \varepsilon LA_{11} - \varepsilon LA_{12}L = 0 \quad (6.2.13)$$

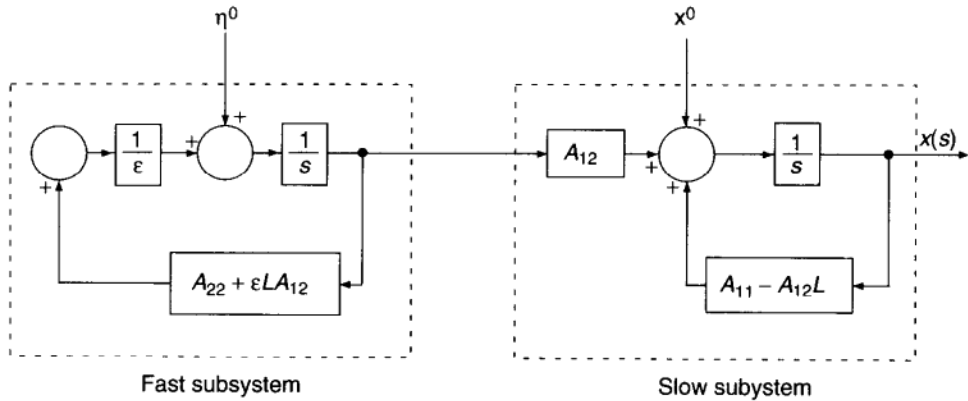


FIGURE 6.2.1 Reduced-order model in actuator form.

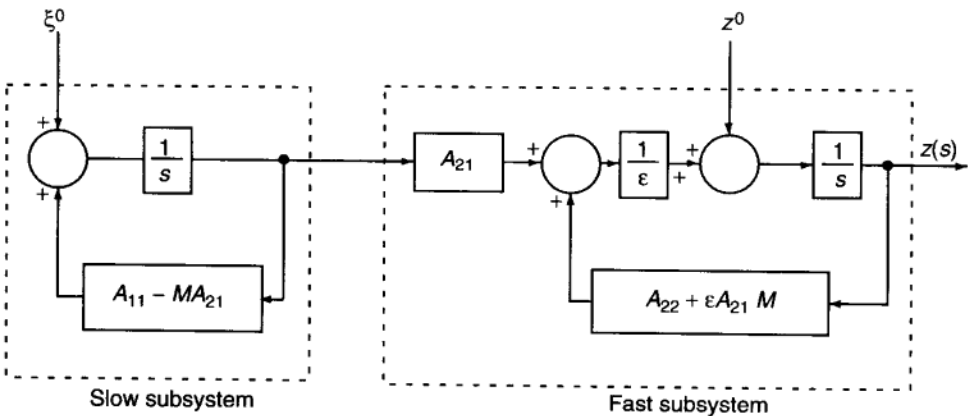


FIGURE 6.2.2 Reduced-order model in sensor form.

The fast subsystem takes on the form

$$\varepsilon \dot{\eta}(t) = (A_{22} + \varepsilon L A_{12})\eta(t) \quad (6.2.14)$$

This subsystem is often restated in scaled time $\tau = (t - t_0)/\varepsilon$ as

$$\frac{d\eta(\tau)}{d\tau} = (A_{22} + \varepsilon L A_{12})\eta(\tau) \quad (6.2.15)$$

and is known as the boundary-layer dynamics. The resulting slow subsystem takes on the form

$$\dot{x}(t) = (A_{11} - A_{12})Lx(t) + A_{12}\eta(t) \quad (6.2.16)$$

Observe that the fast subsystem in the actuator form representation is fully decoupled from the slow subsystem. Just the opposite is true in the sensor form, namely, the slow subsystem is fully decoupled from the fast dynamics. For computing methods of transformations L and M , see [33].

Generally, the reduced-order model suitable for representing the full-order dynamics becomes

$$\dot{\bar{y}} = f(\bar{y}, \phi(\bar{y}, \varepsilon)), \quad \bar{y}(0) = y_0, \quad \bar{y}(0) = \phi(\bar{y}(t_0), \varepsilon) \quad (6.2.17)$$

where \bar{y} and \bar{z} are the slow parts of y and z , respectively. The variable \bar{y} is a uniform approximation of y , that is, $y = \bar{y} + O(\varepsilon)$ for all t in $[t_0, T]$ on which $\bar{y}(t)$ exists. Observe from Eq. (6.2.17) that, by contrast with the original z , starting at the prescribed z^0 at t_0 , \bar{z} is not free to start from z^0 but instead is given by $\phi(\bar{y}(t_0), \varepsilon)$. There may be a large discrepancy between the initial value $\bar{z}(0) = \phi(\bar{y}(t_0), \varepsilon)$ and z^0 . Thus, \bar{y} cannot be a uniform approximation of z for all t in $[t_0, T]$. To remedy this situation if necessary, a boundary-layer correction is sometimes employed. The dynamics x of the boundary-layer system is given in the fast time scale $\tau = t/\varepsilon$ as [33]

$$\frac{d\hat{z}(\tau)}{d\tau} = g(\bar{y}(t), \hat{z}(\tau) + \bar{y}(t), \varepsilon) - \varepsilon\dot{\bar{y}}, \quad \hat{z}(0) = z^0 - \bar{y}(t_0) \quad (6.2.18)$$

In the case of $\varepsilon \rightarrow 0$, one obtains the limiting case

$$\frac{d\hat{z}(\tau)}{d\tau} = g(y^0, \hat{z}(\tau) + \bar{y}(t_0), 0), \quad \hat{z}(0) = z^0 - \bar{y}(t_0) \quad (6.2.19)$$

Then z can be uniformly approximated by

$$z = \bar{z}(t) + \hat{z}(\tau) + O(\varepsilon) \quad (6.2.20)$$

To justify further that for most studies it is sufficient to use the zeroth-order manifold only, the following general result [38] is important.

Theorem 6.2.1 For a system¹⁴

$$\begin{aligned} \dot{y} &= f(y, z, \varepsilon) \\ \varepsilon\dot{z} &= g(y, z, \varepsilon) \end{aligned} \quad (6.2.21)$$

the system trajectories y and z can be expressed as

$$\begin{aligned} y &= \bar{y}(t) + O(\varepsilon) \\ z &= \bar{z}(t) + \hat{z}(\tau) + O(\varepsilon) \end{aligned} \quad (6.2.22)$$

provided the following two assumptions hold.

¹⁴This theorem assumes the validity of the f and g models regardless of the velocity of movement of the y and z signals or states. One must remember, however, that modeling power-system phenomena is given in terms of quasistationary phasors. Such models lose their validity when the signal speed variation increases near or above the speed of the oscillation of the carrier. Care must be taken to ensure that the limit processes connected to $\varepsilon \rightarrow 0$ are not connected to such high-speed phenomena in the y and z signals.

Assumption 6.2.1 The equilibrium point $\hat{z}(\tau) = 0$ in the boundary-layer dynamics

$$\frac{d\hat{z}(\tau)}{d\tau} = g(y^0, \hat{z}(\tau) + \bar{z}(t_0), 0) \quad (6.2.23)$$

is asymptotically stable uniformly in y^0 and t_0 , and $\hat{z}(0) = z^0 - \bar{z}(t_0)$ belongs to its domain of attraction such that $\hat{z}(\tau)$ exists for $\tau \geq 0$.

Assumption 6.2.2 The eigenvalues of the sensitivity matrix $[\partial g / \partial z]$ evaluated for $\varepsilon = 0$ along $\bar{y}(t)$ and $\bar{z}(t)$ have real parts smaller than a fixed negative number, that is,

$$\operatorname{Re} \lambda \left\{ \frac{\partial g}{\partial z} \right\} \leq -C < 0 \quad (6.2.24)$$

A consequence of this theorem is that the existence of an asymptotically stable manifold M_0 of the system (6.2.21) implies the existence of an invariant manifold M_ε of the same system for all $\varepsilon \in [0, \varepsilon^*]$ converging to M_0 as $\varepsilon \rightarrow 0$.

The first assumption states the requirement for the fast subprocess to be asymptotically stable. This is the main condition for deriving a reduced-order model using SP-based methods. The second assumption implies exponential stability at the estimated rate.

Nonexplicit Form for Representing Subprocesses That Are Separable in Time

It is also known that a dynamic system of the form

$$\varepsilon \dot{x} = A(\varepsilon)x = [A(0) + \varepsilon A_1]x \quad (6.2.25)$$

could have substates that are separable in time. This is true only if matrix $A(0)$ is rank deficient, that is, singular. In this case the process of obtaining a standard (explicit) form for SP-based model reduction Eq. (6.2.1) and (6.2.2) requires a similarity transformation T to be applied to the original state x first.

Assume that $A(0)$ has a complete set of eigenvectors corresponding to its zero eigenvalues. Denote by $N(A_0)$ the eigenspace corresponding to zero eigenvalues, and by $R(A_0)$ the eigenspace of A_0 corresponding to the nonzero eigenvalues. It can be found in Ref. [25] that a similarity transformation defined as

$$T = [P \quad Q]^T \quad (6.2.26)$$

or

$$T^{-1} = [V \quad W]^T \quad (6.2.27)$$

where V represents bases for $N(A_0)$ and W represents bases for $R(A_0)$ applied to the old state vector as

$$[y \quad z]^T = [P \quad Q]^T x \quad (6.2.28)$$

leads through the transformation

$$T \left(\frac{A_0}{\varepsilon} + A_1 \right) T^{-1} = \begin{bmatrix} PA_1 V & PA_1 W \\ QA_1 V & \frac{QA_0 V}{\varepsilon} + QA_1 W \end{bmatrix} = \begin{bmatrix} A_s & A_{sf} \\ \varepsilon A_{fs} & A_f \end{bmatrix} \quad (6.2.29)$$

to the dynamic model in terms of transformed variables y and z , which is in the explicit SP form

$$\dot{y} = A_s y + A_{sf} z \quad (6.2.30)$$

$$\varepsilon \dot{z} = \varepsilon A_{fs} y + A_f z \quad (6.2.31)$$

Submatrices A_s , A_{sf} , A_{fs} , and A_f are submatrices as defined in Eq. (6.2.29). Matrix A_f obtained by this similarity transformation can be proven to be structurally of full rank.

Both explicit and nonexplicit singularly perturbed forms play an important role in systematic reduction of very large electric power systems. It is reviewed in what follows that the explicit form is directly used for model simplifications at each component level, as well as for model reduction of interconnected systems with different time constants governing the dynamics of individual components. In contrast, the electric connections among the components are more or less uniform. On the other hand, model reduction based on processes that are separable as a result of nonuniform electrical connections among the components require use of a nonexplicit form.

APPENDIX 6.3 EIGENMODE-BASED MODEL REDUCTION: SELECTIVE MODAL ANALYSIS

The second general approach to model reduction of very-large-scale electric power systems is based on differentiating among “relevant” and “irrelevant” modes. A designation of states and modes into these two categories depends on the specific analysis of interest. For instance, a “relevant” state may be one contributing to the unstable response in the frequency domain of interest, such as a state “participating” in interarea oscillations [25].

Techniques have been developed for model reduction that retains only a portion of the model that contributes to the relevant modes. The best-known approach of this type is the selective modal analysis (SMA), approach, which originated in Refs. [34,35,36]. The approach has since been used for analysis of very large systems, and supporting software is commercially available [36]. This section draws strongly on the work of Verghese and coworkers [34].

The SMA-based techniques are not strictly dependent on the time-scale separation among the processes and do not require restrictive assumptions on stability of irrelevant states. On the other hand, they are at present only available for LTI systems.

Suppose we write the state-space equations for the full (linearized) system as follows:

$$\begin{bmatrix} \dot{x}_r \\ \dot{x}_z \end{bmatrix} = \begin{bmatrix} A_{11} & A_{12} \\ A_{21} & A_{22} \end{bmatrix} \begin{bmatrix} \dot{x}_r \\ \dot{x}_z \end{bmatrix} + \begin{bmatrix} B_1 \\ 0 \end{bmatrix} u \quad (6.3.1)$$

$$y = [C_1 \quad 0] \begin{bmatrix} x_r \\ x_z \end{bmatrix} \quad (6.3.2)$$

The subscripts 1 and r refer to the relevant states and 2 and z to the remaining states. The general form of a reduced-order model of interest is

$$\dot{x}_r = A_r x_r + B_r u \quad (6.3.3)$$

$$y_r = C_r x_r \quad (6.3.4)$$

where $A_r = A_{11} + M$ for some M . The reduced-order model should satisfy the following two properties:

- The relevant modes of the original system (6.3.1) should be preserved in Eq. (6.3.3).
- The output y_r of the reduced system (6.3.4) should be approximately the same as the output y of the original system (6.3.2).

This model reduction process results in a reduced-order model whose block diagram is shown in Figure 6.3.1 [31].

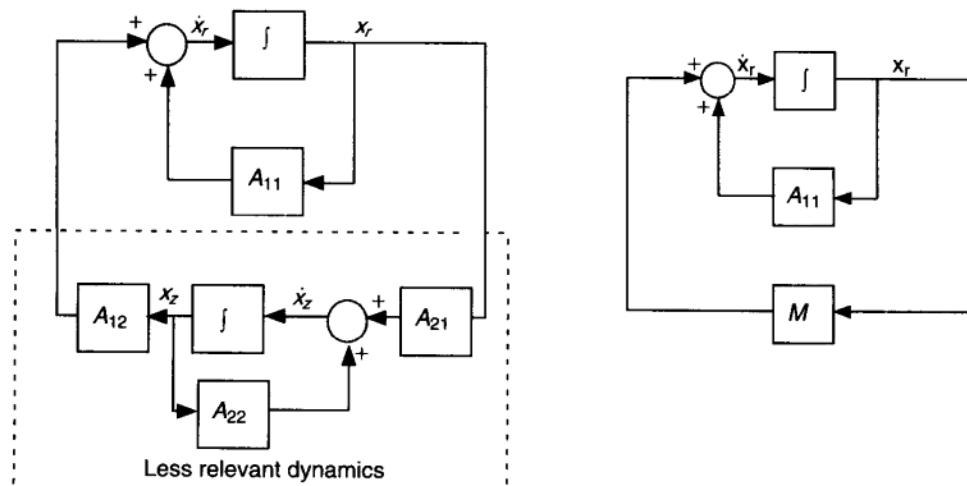


FIGURE 6.3.1 Block diagram representing SMA-based dynamics.

The SMA-based approach is to look for a relationship of the form

$$x_z = Kx_r \quad (6.3.5)$$

that holds when only the relevant modes are excited. This definition of K and the relationship between relevant and irrelevant states has been proposed very recently as a generalization of the strict coherency-based requirements that groups of states move in an identical manner in response to an arbitrary perturbation. This property is defined in Refs. [4, 26, 27] as a synchronic response and can be viewed as a generalization of a coherent response, which rarely takes place in reality. The actual derivation of matrix K is based on the selective modal analysis introduced earlier. The SMA is a comprehensive framework for accurate and efficient modeling of a reduced-order model of the form (6.3.3). These objectives are achieved by developing the following [31]:

- Sensitivity measures, which are named *participation factors* for identifying the state variables that contribute significantly to the selected modes x_r .
- Algorithms for efficient and accurate computing of a few selected modes of interest.

The fundamentals of the approach are best introduced by assuming zero input $u = 0$, which leads to the analysis of a simple LTI system:

$$\dot{x} = Ax \quad (6.3.6)$$

The eigenvalue λ_i and the right v_i and left w_i eigenvectors for the i th mode are defined by the equations

$$Av_i = v_i\lambda_i \quad (6.3.7)$$

$$w_i^T A = \lambda_i w_i^T \quad (6.3.8)$$

assuming the standard normalization

$$w_i^T v_i = 1 \quad (6.3.9)$$

Participation Factors

The time-domain response of a system (6.3.6) written in modal form is

$$x(t) = \sum_{i=1}^N \alpha_i v_i \exp(\lambda_i t) \quad (6.3.10)$$

The coefficients α_i are determined by the initial conditions x_0 . Each term in this sum represents a contribution of a specific mode λ_i to the system response, and

the entries of the right eigenvector v_i determine the level of activity of each state when only one mode is excited. The left eigenvector defines a linear combination of the original states into a single variable associated only with the i th mode.

This can be seen by considering the same system after a similarity transformation that diagonalizes the original system (6.3.6) into a model

$$\dot{\xi}_i = \lambda_i \xi_i \quad (6.3.11)$$

in which the transformed state ξ_i is associated only with one mode. To determine which state variables are significant in the i th mode, the expression of ξ_i is written in terms of all variables when only the i th mode is excited:

$$\xi_i(t) = w_i^T x(t) = \alpha_i \sum_{j=1}^N w_{ji} v_{ji} \exp(\lambda_i t) \quad (6.3.12)$$

This expression suggests the definition of the participation factors p_{ij} of the j th variable in the i th mode as

$$p_{ij} = w_{ji} v_{ji} \quad (6.3.13)$$

It is important to observe that the participation factors are dimensionless and therefore independent of a particular choice of units associated with states x .

It can be shown that a participation factor p_{ij} also measures the sensitivity of the i th mode with respect to the changes in the diagonal element in the system matrix A in Eq. (6.3.6), that is,

$$p_{ji} = \frac{\partial \lambda_i}{\partial a_{ii}} \quad (6.3.14)$$

A specific SMA algorithm can be found in Ref. [34].

APPENDIX 6.4 SOME RELATIONS BETWEEN SP- AND SMA-BASED MODEL REDUCTION TECHNIQUES

While the results of model reduction based on SP and SMA approaches often lead to similar conclusions, it is hard to compare the two approaches directly. The underlying question is concerned with the conditions for approximating the eigenvalues of a full matrix

$$A = \begin{bmatrix} A_\alpha & A_\beta \\ A_\gamma & A_\delta \end{bmatrix} \quad (6.4.1)$$

by the eigenvalues of matrices A_α and A_δ , on one hand, and with the conditions for existence of time-scale-separated processes in the dynamic system defined as

$$\dot{x} = A(\varepsilon)x \quad (6.4.2)$$

on the other hand.

Relations between these conditions were described in [40] by means of a powerful Gershgorin's theorem. To begin, it is suggested in [40] that a matrix A can be thought of as having been obtained from a matrix

$$A_{\text{decoupled}} = \begin{bmatrix} A_\alpha & 0 \\ 0 & A_\delta \end{bmatrix} \quad (6.4.3)$$

by continuously increasing the off-diagonal blocks from zero to A_β and A_γ , respectively, causing the eigenvalues to move from those of A_α and A_δ to those of A .

This suggests that if the coupling between the eigenstructures induced by presence of the off-diagonal submatrices is small relative to the separation between these eigenstructures, then the eigenstructure of A will consist of two relatively separated parts, one centered around the eigenstructure of A_α and the other around that of A_δ . Gershgorin's theorem states this fact in a precise sense and is re-stated here for its importance.

Theorem 6.7.2: Gershgorin's Theorem Let λ_0 be any eigenvalue of A , $\lambda_{\alpha i}$ any eigenvalue of A_α , and $\lambda_{\delta j}$ any eigenvalue of A_δ . Then the following holds:

$$\min_i |\lambda_0 - \lambda_{\delta i}| \leq k_\delta \|A_\gamma\| \quad (6.4.4)$$

and

$$\min_i |\lambda_0 - \lambda_{\alpha i}| \leq k_\alpha \|A_\beta\| \quad (6.4.5)$$

Coefficients k_α and k_δ are defined as

$$k_\alpha = \|V_\alpha\| V_\alpha^{-1} \| \quad (6.4.6)$$

Similarly,

$$k_\delta = \|V_\delta\| V_\delta^{-1} \| \quad (6.4.7)$$

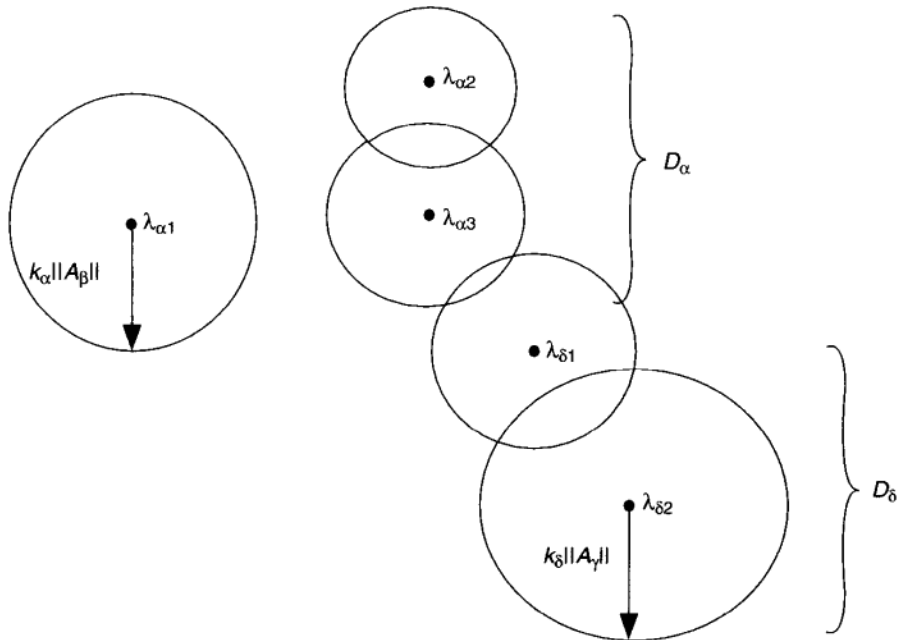
with $\|M\| = \max_{x \neq 0} \|Mx\|/\|x\|$ being the norm of matrix M . Matrices V_α and V_δ , respectively, are the similarity transformations that diagonalize matrices A_α and A_δ ,

$$A_\alpha = V_\alpha \Lambda_\alpha V_\alpha^T \quad (6.4.8)$$

and

$$A_\delta = V_\delta \Lambda_\delta V_\delta^T \quad (6.4.9)$$

Coefficients k_α and k_δ are dimensionless and are known as modal condition numbers of matrices A_α and A_δ , respectively. Gershgorin's theorem is illustrated in Figure 6.4.1. D_α and D_δ in this figure represent sets containing the actual eigenvalues of the full matrix A . One of the implications of this theorem is as follows.

**FIGURE 6.4.1** Gershgorin's theorem.

Theorem 6.7.3 Suppose

$$k_\alpha \|A_\beta\| + k_\delta \|A_\gamma\| \leq \min_{i,j} (|\lambda_{\alpha i} - \lambda_{\delta j}|) \quad (6.4.10)$$

then the sets D_α and D_δ are disjoint.

This condition is not as powerful as the one needed to answer the question concerned with conditions for eigenstructure separation in processes separable in time. This can be seen from the fact that when Eq. (6.4.10) is applied to the matrix

$$A(\varepsilon) = \begin{bmatrix} A_{11} & A_{12} \\ A_{21} & A_{22} \\ \hline \varepsilon & \varepsilon \end{bmatrix} \quad (6.4.11)$$

both sides of Eq. (6.4.11) are of order $1/\varepsilon$. Instead, the following stronger condition is suggested in Ref. [40].

Theorem 6.7.4 The modified Gershgorin theorem condition

$$\frac{k_\alpha k_\delta \|A_\beta\| \|A_\gamma\|}{(\min_{i,j} |\lambda_{\alpha i} - \lambda_{\delta j}|)^2} \leq 0.25 \quad (6.4.12)$$

allows for D_α and D_δ to be disjoint, implying that processes separable in time that meet this modified condition have simultaneously disjoint eigenstructures.

This condition was proven in Ref. [40] by recognizing that the eigenvalues of matrix A are the same as the eigenvalues of matrix

$$A_c = \begin{bmatrix} A_\alpha & cA_\beta \\ \frac{1}{c}A_\gamma & A_\delta \end{bmatrix} \quad (6.4.13)$$

For matrix A_c the sets D_α and D_δ can be defined as before, except that their radii are $|c|k_\alpha\|A_\beta\|$ and $(1/|c|)k_\delta\|A_\gamma\|$.

Now, if

$$|c|k_\alpha\|A_\beta\| + \frac{1}{|c|}k_\delta\|A_\gamma\| \leq \min_{i,j} |\lambda_{\alpha i} - \lambda_{\delta j}| \quad (6.4.14)$$

for some $|c|$, then the sets are disjoint.

This problem reduces to the question of existence of a real-valued positive $|c|$ such that this inequality holds. One could further show that for this to occur it suffices to have

$$r_1 r_2 \leq 0.25 \quad (6.4.15)$$

where

$$r_1 = \frac{k_\delta\|A_\gamma\|}{\min_{i,j} |\lambda_{\alpha i} - \lambda_{\delta j}|}, \quad r_2 = \frac{k_\alpha\|A_\beta\|}{\min_{i,j} |\lambda_{\alpha i} - \lambda_{\delta j}|}$$

This follows from the condition for solvability of quadratic equation (6.4.14) for $|c|$.

This result is very helpful for interpreting reduced-order models based on eigenvalue-based approaches in terms of time-scale separation, and vice versa.

In this chapter we have applied these general model-reduction methods for purposes of model reduction and small-signal stability analysis in power systems.

BIBLIOGRAPHY

1. Proposed Terms and Definitions for Power System Stability, Task Force Report, *IEEE Trans. Power Apparatus Syst.*, PAS-101: 1894–1898, 1982.
2. Allemong, J., A singular perturbation approach to power system dynamics, Ph.D. thesis, University of Illinois at Urbana-Champaign, 1978.
3. Mak, F. K., *Analysis and control of voltage dynamics in electric power systems*, Ph.D. thesis, University of Illinois at Urbana-Champaign, 1990.
4. Rajagopalan, C., Lesieutre, B., Sauer, P., and Pai, M. A., Dynamic aspects of voltage/power characteristics, *IEEE Trans. Power Syst.*, 7: August 1992, pp. 990–1000.
5. Mak, F. K., and Ilić, M. D., Classification of voltage problems in electric power systems, *Electrical Power Energy Syst.*, 15, pp. 377–385, 1993.
6. Vournas, C. D., Sauer, P., and Pai, M., Relationships between voltage and angle stability of power systems, *Electrical Power Energy Syst.*, 18, 493–500, 1996.

7. Van Cutsem, T., and Vournas, C., *Voltage Stability of Electric Power Systems*, Kluwer Academic Publishers, Boston, MA 1998.
8. Rees, J., *On-line identification of reduced-order subsystem models for selective modal analysis*, M. Sci. thesis, MIT, 1992.
9. Ladde, G., and Siljak, D., Multiparameter singular perturbations of linear systems with multiple time scales, *Automatica* **19**: 385–394, 1983.
10. Abed, E., Decomposition and stability of multiparameter singular perturbation problems, *IEEE Trans. Automat. Control* **AC-31**: 1986.
11. Concordia, C., Private correspondence to the PES Dynamic Performance Subcommittee Task Force on Voltage Instabilities, August 21, 1985.
12. Tavora C. J., and Smith, O. J. M., Equilibrium analysis of power systems, *IEEE Trans. Power Apparatus Syst.*, **PAS-91**: 1131–1137, 1972.
13. Barbier C., Barret, J. P., An analysis of phenomena of voltage collapse on a transmission system, *Revue General d'Electricite*, **89**: 672–80, 1980.
14. Di Caprio, U., Practical and Structural Coherency in Multimachine Power Systems, *Intl. J. Electrical Power Energy Syst.*, **7**, 147–153, 1985.
15. Sauer P., and Pai, M., Power system dynamics and stability, Course notes EE476, University of Illinois.
16. Medanić, J., Ilić M., and Christensen, J. Discrete models of slow voltage dynamics for under load tap changing transformer coordination, *IEEE Trans. Power Syst.*, **PWRS-2**, 873–82, 1987.
17. Ćalović, M. S., Modeling and analysis of under load tap changing transformers in voltage and var control applications, University of Illinois, Report No. PAP- TR-83-3, 1983.
18. Ćalović, M., *Regulation of Electric Power Systems*, Vizartis, Belgrade, Yugoslavia, 1997 (in Serbian).
19. Liu, X. S., Structural modeling and hierarchical control of large-scale electric power systems, Ph.D. thesis, MIT, 1994.
20. Ilić, M., and Liu, S. X. A simple structural approach to modeling and analysis of the inter-area dynamics of the large electric power systems: Part I—Linearized models of frequency dynamics, *Proc. 1993 North Am. Power Symp.*, Washington, DC, 1993, pp. 560–569.
21. Ilić, M., and Liu, S.X., A simple structural approach to modeling and analysis of the inter-area dynamics of the large electric power systems: Part II—Nonlinear models of frequency and voltage dynamics, *Proc. North Am. Power Symp.*, 1993, pp. 570–578.
22. Ilić, M. D., and Liu, S.X.. *Hierarchical Power Systems Control: Its Value in a Changing Electric Power Industry*, Advances in Industrial Control, London: Springer-Verlag, 1996.
23. Zaborszky, J., Rittenhouse, *Transmission Systems*, Reynolds, 1954. Available in paperback at the Rensselaer University Bookstore, Troy, NY.
24. Campbell, S. L., Differentiation of constraints in differential-algebraic equations, *J. Mech. Struct. Mach.*, **19**: 19–39, 1991.
25. Chow, J. H. (ed.), Time-Scale of Dynamic Networks with Applications to Power Systems, Lecture Notes in Control and Information Sciences, vol. 46, Springer-Verlag, NY, 1982.
26. Kundur, P., *Power System Stability and Control*, New York, Mc-Graw Hill, 1993.

27. Chapman, J. C., and Ilić, M. D., *Large-Signal Generator Control and its Impact on Improved Power Transfer Flexibility*, Final Report under the Empire State Electric Energy Research Co. (ESEERCO), Project No. EP90-45, New York, 1990.
28. Ramaswamy, G. N., Modal structures and modal reduction, with application to power system equivalencing, Ph.D. thesis, Department of Electrical Engineering and Computer Science, MIT, 1995.
29. Ramaswamy, G. N. Verghese, G. C. Rouco, L. Vialas, C., and DeMarco, C. L., Synchrony, aggregation and multi-area eigenanalysis, Paper No. 95WM192-5PWRS, IEEE PES Winter Meeting, New York, 1995.
30. Ramaswamy, G. N., Rouco, L., Fillatre, O., Verghese, G. C., Panciatici, P., Lesieutre, B. C., and Peltier, D., Synchronic modal equivalencing (SME) for structure-preserving dynamic equivalents, Paper No. 95WM113-1PWRS, IEEE PES Winter Meeting, New York, 1995.
31. Chow, J. H., Winkelman, J. R., Pai, M. A., and Sauer, P., Application of singular perturbations theory to power system modeling and stability analysis, *Proc. Am. Control Conf.*, 1985.
32. Podmore, R., Identification of coherent generators for dynamic equivalents, *IEEE Trans. Power Apparatus Syst.*, **PAS-97**: 1344–1354, 1978.
33. Othman, H., *Decoupled stability analysis of power systems with slow and fast dynamics*, Ph.D. thesis, University of Illinois at Urbana-Champaign, Urbana, IL, 1988.
34. Perez-Arriaga, I., Verghese, G. C., Pagola, L. F., Sancha, J. L., and Schweppé, F. C., Developments in selective modal analysis of small-signal stability in electric power systems, *IFAC Automatica*, **26**: 215–231, 1990.
35. Verghese, G. C., Perez-Arriaga, I. J., Schweppé, F. C., and Tsai, K.W.-K., *Selective Modal Analysis in Electric Power Systems*, EPRI EL-2830, Research Project No. 1764-8, Final Report, January 1983.
36. Eigenanalysis and Frequency Domain Methods for System Dynamic Performance, IEEE Tutorial No. 90TH0292-3-PWR, IEEE 1989.
37. DeMarco, C. L., and Wassner, J., A generalized eigenvalue perturbation approach to coherency, Technical Report No. ECE-95-5, Department of Electrical and Computer Engineering, Univ. of Wisconsin-Madison, Madison, WI, 1995.
38. Kokotović, P., Khalil, H. K., and O'Reilly J., *Singular Perturbation Methods in Control: Analysis and Design*, Orlando, FL: Academic Press, 1986.
39. Sobolev, V. A., Integral manifolds and decomposition of singularly perturbed systems, *Syst. Control Lett.*, **5**: 169–179 (1984).
40. Verghese, G. C., 6.238 Class Notes, MIT, Fall 1986.

7 Introduction to the Concepts and Structure of Comprehensive Power-System Dynamics

Power systems prior to 1950 were small interconnections of at most a couple of dozen generating stations with a few relatively weak ties to their neighbors. The technology of operation and analysis still posed difficult problems, then at the forefront of electrical engineering. Impressive solutions developed earlier in the century such as the phasor and Blondel (direct and quadrature axis) transformations provided a solid foundation.

The power industry was leading in the industrial use of analog computers called network analyzers with up to a few dozen analog generator models with variable interconnections. These were used in the pressing problems of the times: load-flow analysis for stationary purposes and as steps in numerically integrating transients of these small systems.

The appearance in the 1950s of (slow) digital computers made these computations much faster and use became more widespread. In fact, the power industry seems to have produced the first industrial use of digital computers. That in turn encouraged an increase in interconnections, loading levels, and the development of the automatic generation control (AGC), based on the use of these industrial computers. Analytic techniques for dynamic problems, however, remained confined essentially to stationary conditions and small-signal (linearized) type analysis. The only crucial full-scale large-signal nonlinear problem, that of transient stability, continued to be analyzed by numerical integration of trajectories on faster and faster digital computers.

The use of precise mathematical analysis without numerical integration of the full nonlinear large-signal problems that arise with the ever increasing interconnection and loading levels of recent decades has emerged in the late 1980s and the 1990s. This is a complex theoretical development involving relatively advanced mathematics and the evolution of new concepts. A full theory has emerged in recent years. These developments are described here in Chapters 7 to 11. They should play important roles in developing more effective technologies for the future.

Using the technique applied earlier in this text for introducing such developments the presentation is divided into two steps.

Chapter 7, which is aimed for readers who are not familiar with these developments, uses small models. A "minimum" (second degree) and a "rudimentary"

(third degree) power-system type models introduce the new concepts and their analysis in a precise but intuitively comprehensible manner. Using second and third degree examples is quite advantageous because all results on such systems can be clearly and precisely represented graphically on a sheet of paper.

After acquiring such conceptual understanding the reader can readily follow the full rigorous mathematical treatment offered in Chapter 8 for systems of any size and any smooth nonlinear dynamics. A truly large-scale illustration of practical use of the theory on a real-life event on a 7500-bus system is presented in Chapter 9. Chapter 10 extends these results to systems that contain nonsmooth elements such as hard limits or tap changers. After the full presentation of the theory in Chapter 8, and 10 the analyses on small models presented in Chapter 7 become simple illustrative examples of the theory.

The theory is very general in system size, nonlinearity type, and physical character of the system, but the voltage dynamics of the power system are specially emphasized. In this chapter, a graphically illustrated and fully intuitive introduction to the theory on the minimal and rudimentary models is given in two sections (7.1 and 7.2, respectively), which serve as stepping stones to the working-level material of Chapter 8.

Two appendices may help the reader to review the necessary background on smooth dynamics of nonconstrained differential equation systems (Appendix 7.1) and/or bifurcations (Appendix 7.2). Dynamic concepts are introduced here as general concepts but developed for specific power system models of minimal size. In Chapter 8 the model is only specified in type but not in specific detail or size, as it does not even need to be a power system.

The senior author with Gargi Huang and graduate students, particularly Baohua Zheng and Tin Chi Leung, started a comprehensive study in the 1980s of the dynamics of the power system modeled by smooth nonlinear differential equations. The results of this work are summarized in Appendix 1 of this Chapter based mostly on [6].

Then the senior author with Baohua Zheng initiated the investigation of algebraically constrained models in power systems for the “minimal” power system model summarized in Section 7.1, [6] [17].

The foundations of a comprehensive theory and precise study of the dynamics of the power system modeled by smoothly constrained nonlinear differential equations were then laid in the thesis work of V. Venkatasubramanian with H. Schättler and J. Zaborszky starting with a detailed intuitive, but also mathematically precise, study of the “rudimentary power system model” as summarized here in Section 7.2, from [1, 2, 3, 30]. The further development into a “Taxonomy Theory” of the DAE systems with or without discontinuous limits follows in Chapters 8–11 where more specific attributions are also presented.

7.1 NONLINEAR DYNAMIC ANALYSIS OF A MINIMAL POWER SYSTEM

To be described as a power system, the combination of a generator feeding a load would certainly be the minimum size arrangement (Fig. 7.1). It will be assumed that the generators' voltage dynamics are represented by a simplified one-axis model, that is, type IV, defined in Section 3.3.3.7. In addition, a fixed excitation E_{fd} and a perfect match of power generation with load are assumed. For simplicity, the load considered is a constant-power model for both active and reactive components. The load will be assumed to possess no significant inertia.

Because there is only one inertia in this system (the turbine generator rotor) the assumption that the load P is always matched by the generation produced $P_T \equiv P$, with no initial stored transient energy, implies that $\dot{\delta} = 0$ and $T = \text{const}$, as there is nothing to excite any mechanical transients in this model. Thus the voltage dynamics is isolated from the angle dynamics. A "physical" representation of this situation may consist of a generator feeding into an infinite or slack bus. Thus this assumption is a voltage-dynamics counterpart for the so-called "classical" model, which isolates the rotor-angle dynamics by assuming constant voltage behind the transient reactance (i.e., $\dot{E}' = 0$); see Table 3.3 in Section 3.3.3.7.

7.1.1 A Minimal Power System Model with (Loss-less) Generator and Matched Load

This simple example for which everything can readily be displayed and analyzed is used here to help the reader to understand a variety of concepts involved in the large-scale dynamic analysis of nonlinear systems that will be needed in Section 7.3 but is obscured there by multidimensionality. Readers who are already familiar with these concepts may scan Sections 7.1 and 7.2 and proceed to Section 7.3.

The minimal power system model as defined consists of the following:

1. Dynamic state equation for the generator (type IV model, Sec. 3.3.3.7):

$$T'_{d0}\dot{E}' = -\frac{x_d}{x'_d}E' + \frac{x_d - x'_d}{x'_d}E \cos(\delta - \delta') + E_{fd} \quad (7.1)$$

from Eqs. (3.3.77), and (3.3.78) with $ri_q = 0$.

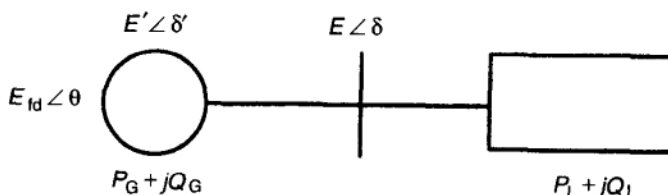


FIGURE 7.1 "Minimal" power system.

2. Algebraic constraint equations for the power transmission line (Sec 3.3.7):

$$P = -\frac{E'E}{x'_d} \sin(\delta - \delta') \quad (7.2)$$

$$Q = \frac{E'E \cos(\delta - \delta') - E^2}{x'_d} \quad (7.3)$$

P and Q are given as instantaneous inputs or operating parameters. Observe that this system has one dynamic state variable $x = E'$, two algebraic state variables $y_1 = E$ and $y_2 = \delta - \delta'$, two system parameters $p_1 = x_d$ and $p_2 = x'_d$, and three operating parameters $p_3 = P$, $p_4 = Q$, and $p_5 = E_{fd}$. So the specific form of Eqs. (7.1) and (7.2) becomes here

$$\dot{x} = f(x, y_1, y_2, p_1, p_2, p_5) \quad (7.4)$$

$$0 = g_1(x, y_1, y_2, p_2, p_3) \quad (7.5)$$

$$0 = g_2(x, y_1, y_2, p_2, p_4) \quad (7.6)$$

Because of the decoupling of mechanical dynamics through the $P_T = P$ assumption, $\delta - \delta'$ is a free instantaneous variable that can be eliminated (for $|\delta - \delta'| < \pi/2$, the practical range) using the reduced model. This leaves only one dynamic equation and algebraic equation, described as next.

3. Dynamic system equation:

$$\dot{E}' = \frac{1}{T'_{d0}} \left(-\frac{x_d}{x'_d} E' + \frac{x_d - x'_d}{x'_d} \frac{E^2 + x'_d Q}{E'} + E_{fd} \right) = f(x, y, p) \quad (7.7)$$

4. Algebraic system equation:

$$0 = E'^2 E^2 - (x'_d P)^2 - (x'_d Q + E^2)^2 = g(x, y, p) \quad (7.8)$$

So after eliminating $\delta - \delta'$ which is constant because of the assumption $P_T = P$ there remains just one dynamic state variable $x = E'$ and one algebraic state variable $y = E$. All five parameters are free to take on values within their practical ranges. Note that in this example, the algebraic equation simply describes the fact that the generator output P_T and the load input at the bus P must strictly match as assumed.

The advantage of studying this smallest possible example of a “power system” is that a major portion of the properties of dynamics can be observed and identified within this microcosmos in a most concise manner. In fact, all three aspects of voltage stability, that is,

- Parameter space
- State space
- Time histories of the various states

can be presented for this system on a single page, as is done in Figure 7.2.

Since the purpose of using the minimal system is to develop insight into the structure of the voltage dynamics problem, a descriptive study of the three aspects of voltage stability just listed and shown in Figure 7.2 will first be given. More mathematical details are then presented in Section 7.2. The text in this section is based mostly on Refs. [1, 2, 6, 14, 17].

A systematic display of all specified cores is shown in Figure 7.2. This is not just an abstract display but a tool for introducing and illustrating such

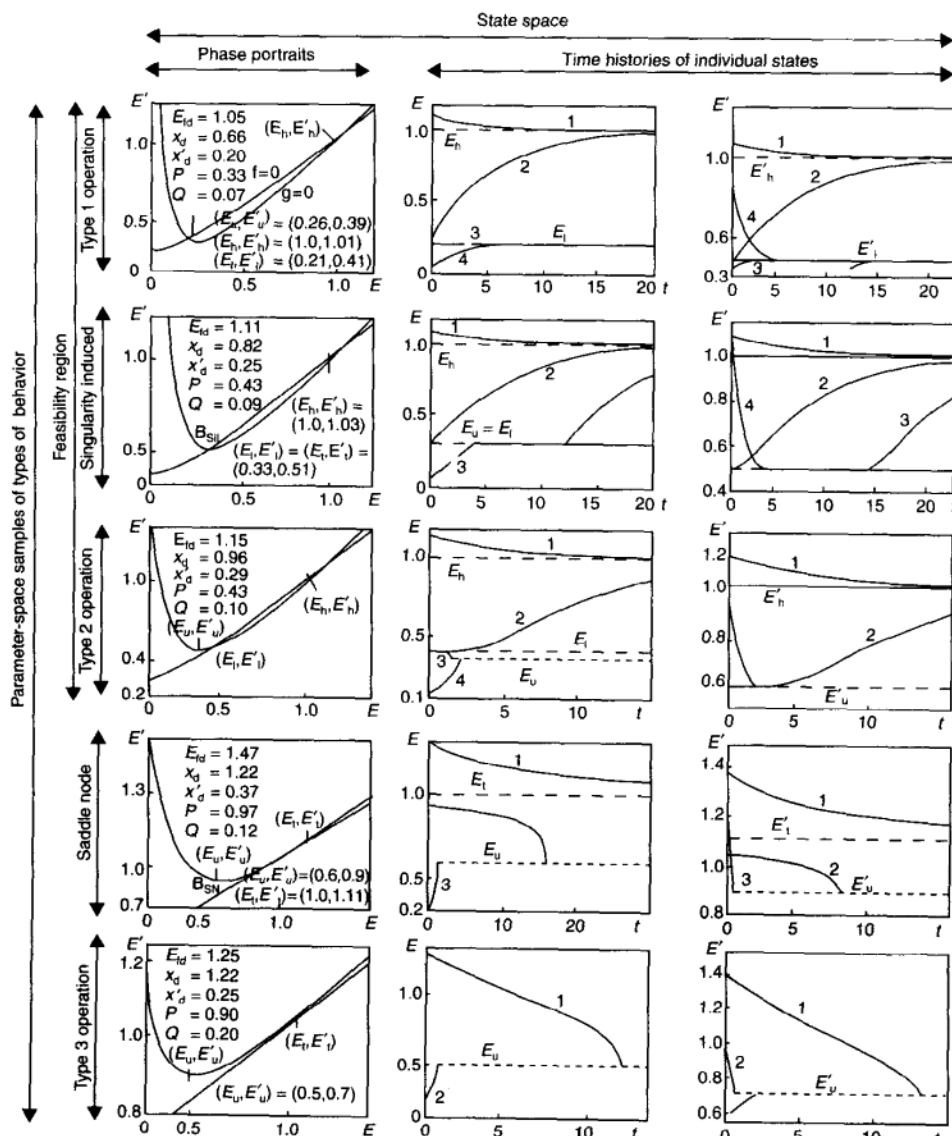


FIGURE 7.2 Three possible types of operating behavior in the three typal regions of the parameter space and at their bifurcation boundaries.

concepts as segments of the stability and feasibility boundaries. Figure 7.2 will be referred to as practical illustrations of such concepts for theoretical formulations in Section 7.3.

7.1.2 Parameter Space

The *parameter space*, which, for this small example, is still five-dimensional ($P, Q, E_{fd}; x_d, x'_d$), will be represented by the vertical axis, that is, the columns in Fig. 7.2. As will become apparent, there are only three open regions (1, 2, and 3) in this five-dimensional space in which uniform behavior occurs in the state space (meaning the same number and stability status of equilibrium points) for systems with parameter sets taken from the same region. These regions with a uniform type of state-space behavior patterns will be called *typal regions*. They are separated by two boundaries B_{S1} and B_{S2} respectively, in the parameter space, which are actually bifurcation boundaries [by definition, as they separate regions where equilibria have different stability properties (see Appendix 7.2)]. The three types and two boundaries are represented by the five rows in Figure 7.2 as marked.

Note that other than selecting a set that makes the size of the higher-voltage stable equilibrium point $E_h = 1$ p.u., in each typal region and boundary in Figure 7.2, all five parameter sets are arbitrarily picked. Hence, the five cases are chance samples from the various parameter regions and their boundaries. Since the parameter space is still five-dimensional, no attempt will be made here to display the geometry of the regions and their boundaries. Such a study for a parameter subspace will be given in Section 7.2.

7.1.3 State Space

The *state space* for this example is two-dimensional (E, E'). E is an instantaneous state variable with no dynamics to restrain it; hence its velocity \dot{E} may vary from $-\infty$ to ∞ smoothly or by jumps. E' is a dynamic state variable that changes only smoothly.

Phase portraits (for background see Appendix 7.1) in the state-space eliminate time and show the trajectories or orbits that are the loci or curves traced in the state space emanating from any initial state. Such a trace is known as a *phase portrait*, which is two-dimensional here (E and E') and hence is readily represented in the plane as is done in the five two-dimensional phase portraits, one for each typal region and each boundary in the first column of Figure 7.2. The phase-portrait approach is quite inclusive because it identifies history of the state-space sequence from any initial state but without the specific time history of each state variable.

Equilibrium points play a vital role and, of course, the stable points represent the only candidates for operating points. At equilibrium points the system is in a stationary condition; that is, all time derivatives are zero (in this case $\dot{E}' = 0$). This assumption leaves two algebraic equations (7.7) with $\dot{E}' = 0$ and (7.8), which define the equilibrium state. In this simple case, a closed-form solution

could be found when it exists for a given parameter set p . However, it will prove enlightening to study first the interplay of the two loci defined by Eq. (7.7) with $\dot{E}' = 0$ and (7.8), respectively. These loci will be called

1. The constraint or flow manifold (locus):

$$E'^2 E^2 - (x'_d P)^2 - (x'_d Q + E^2)^2 = g(x, y, p) = 0 \quad (7.9)$$

2. The stationary manifold (locus):

$$\frac{1}{T'_{d0}} \left(-\frac{x'_d}{x'_d} E' + \frac{x'_d - x'_d}{x'_d} \frac{E^2 + x'_d Q}{E'} + E_{fd} \right) = f(x, y, p) = 0 \quad (7.10)$$

A glance at Figure 7.2 reveals the dominant role of the relative topology of these two curves on the types of system behavior.

1. The designation *constraint manifold* in Figure 7.2 is automatic because this is the locus at which the constraint equations are satisfied [the pair of Eqs. (7.2) and (7.3) or Eq. (7.9)]. Physically by Eqs. (7.2) and (7.3) they represent the balance of active and reactive power at the bus. However, from another viewpoint the name *flow manifold* is also logical. This latter label refers to the flow of the vector field representing the dynamic movement of the state that is constrained to this manifold since the state is constrained to it.

In the power industry the terms *load flow* or *power flow* have a special meaning. Correspondingly the term *load-flow manifold* will designate here a special case of the flow manifold in which the bus voltages and corresponding real or reactive power are the coupling variables y . This is the conventional use of the term '*load flow*' (with *PV* or *PQ* buses). Flow manifold as used here, on the other hand, is more general. In fact, even in this simple example, the coupling variables, y , include only one bus voltage, E , the other one is an excitation, E' . In more complex systems, the latter could even be replaced by a control set point or an internal voltage such as E_{fd} .

2. The designation *stationary manifold* as used in Figure (7.2) is logical for the locus of all states where all time derivatives are zero. Mathematical definitions will be given in Section 7.2.2.

In this simple two-dimensional example, both manifolds are one-dimensional that is, lines, as is shown in the five phase portraits in the first column of Figure 7.2. By Eqs. (7.9) and (7.10), the equilibria, if any, will occur at the intersections of these two lines.

7.1.3.1 Constraint or Flow Manifold This manifold contains all states that are physically and/or mathematically permissible under the model in Eqs. (7.1) to (7.3). This automatically follows from the constraint concept. The model as

stated defines no solution that is, no state outside the constraint manifold—a line as shown in Figure 7.2.

E' is a dynamic state that can change only smoothly, whereas E is nondynamic and thus capable of instant change. Thus E would instantly jump to a point of the constraint surface along an $E' = \text{const}$ line (direction not defined). Physical systems typically possess some, usually fast, dynamics applicable to conditions outside the constraint, but these may not be easy to model. Furthermore, on the power system no quasistationary model exists for this fast dynamics range (i.e., phasor, impedance, reactive power, and all the other familiar concepts cease to exist in this range) as analyzed in detail in Chapter 8. On the other hand, most phenomena of practical interest (such as various types of stability) are quite precisely defined by the quasi stationary model as given in Eqs. (7.1) to (7.3). Thus it is reasonable to study this type of model in a strict sense as will be done in Sections 7.1 and 7.2. In parts of Chapter 8, a deeper study of events outside the regular part of the constraint surface will be included.

Given a model system consisting of algebraically constrained ordinary differential equations such as Eqs. (7.7) and (7.8) that have the general form of

$$\begin{aligned}\dot{x} &= f(x, y) \\ 0 &= g(x, y)\end{aligned}\tag{7.11}$$

where p is considered as given and omitted for notational convenience, it is tempting to try to convert it into a set of ordinary differential equations

$$\dot{x} = f(x, y)\tag{7.12}$$

$$\dot{y} = \gamma(x, y) = -\left(\frac{\partial g}{\partial y}\right)^{-1} \frac{\partial g}{\partial x} f(x, y)\tag{7.13}$$

by differentiating $g = 0$ as

$$\frac{\partial g}{\partial y} \dot{y} + \frac{\partial g}{\partial x} \dot{x} = 0\tag{7.14}$$

This indeed is possible if the Jacobian $D_y g = (\partial g / \partial y) = (\partial g / \partial E)$ is nonsingular (the determinant of $D_y g \neq 0$) and thus it is invertible (discussed later). For now, as observed from Figure 7.2, even in this simple case there is a point E_u on the $g = 0$, line, that is, the constraint manifold where $D_y g$ is singular. $D_y g = \partial g / \partial E$ in one dimension is proportional to the slope of the tangent of the line (manifold) $g = 0$, which is indeed horizontal at E_u and hence $(\partial g / \partial E)|_u = 0$. Thus point E_u is a singular point at which the behavior of the state is not defined (E cannot be solved for). Such *singular points* (*manifolds* in high dimensions) play an important role and will be discussed extensively later. Let it just be observed at this stage that the singular point E_u separates the constraint surface into two “*components*” to the left and right of E_u . All points are *regular* ($D_y g$ nonsingular) within the components, and indeed within these components the

system does behave like a smooth system of the type in Eqs. (7.12) and (7.13), but the singularity at E_u separates the components from each other (details given later). Note: Eq. (7.14) appears in the literature with both + and - signs. The sign depends on selection of the reference directions and so it is arbitrary, but it must be considered.

7.1.3.2 Stationary Manifold This manifold, expressed by Eq. (7.10), is defined by the dynamic equations when all derivatives are set to zero. States on this locus attain physical reality only at intersections with the constraint manifold because only points on the latter have such reality. Also, by definition, such points are equilibria. It follows from the shape of the two loci that there can be two, one, or no equilibria in this problem corresponding to the three typical regions 1, 2 and 3 in Figure 7.2.

7.1.3.3 Trajectories As the state is confined to the flow manifold, all trajectories are confined there. Furthermore, because the manifold is a one-dimensional line, in this case individual trajectories can differ only in their initial states in this minimal problem. Direction of the flow can be established intuitively by observing the sign of \dot{E}' and the shape of the flow manifold. First, we observe that $\dot{E}' = 0$ on the stationary manifold; Hence it would be one sign ($\dot{E}' < 0$) above this manifold and the other sign ($\dot{E}' > 0$) below.

Expressed in equations, the flow manifold can be written as

$$E' = v(E) = \frac{1}{E} \sqrt{(x'_d Q + E^2)^2 + (x'_d P)^2} \quad (7.15)$$

Therefore

$$\frac{dE'}{dE} > 0 \quad \text{if } E > E_u \quad (7.16)$$

$$\frac{dE'}{dE} < 0 \quad \text{if } E < E_u$$

Also note that

$$\frac{\partial g}{\partial E} = -\frac{\partial g}{\partial E'} \frac{dE'}{dE} = -2E'E^2 \frac{dE'}{dE} \quad (7.17)$$

$$\dot{E} = \dot{E}' \left/ \frac{dE'}{dE} \right. \quad (7.18)$$

Anywhere within the flow manifold the state is moving at a rate corresponding to the dynamic value of \dot{E}' . The direction of this motion is easily identified from Eq. (7.16), as shown in Figure 7.2.

7.1.3.4 Equilibria Equilibrium points where the state is converging from both sides are, of course, *stable*. Points where the state diverges from both sides are *unstable* (see Fig. 7.2). More precisely,

1. Equilibria where the intersection of the two manifolds is transversal [typical regions 2, points (E_l, E'_l) and (E_u, E'_u)] at a regular point are *hyperbolic* because the full system Jacobian $J = D_{x,y}(f, g)$ is nonsingular—there is no zero eigenvalue—trajectories converge or diverge from both sides.
2. Equilibria where the intersection is tangential at a regular point [boundary case B_{SN} , point (E_l, E'_l)] form a nonhyperbolic equilibrium point with a zero eigenvalue of the system Jacobian J . Here the trajectory converges from one side and diverges from the other.
3. Equilibria where a transversal intersection occurs at a singular point [boundary case B_{SiL} , point (E_u, E'_u)] result in a combination of an equilibrium with a singularity but it is neither one nor the other. These points will play an important role in the algebraically constrained system and will be discussed extensively under the name *pseudoequilibria*, denoted by Ψ .
4. Other points like a tangential intersection at a singular point will be observed on more complex cases later.

7.1.4 Time Histories of Individual State Variables

Plotting individual *state* variables as *functions of time* represents the third aspect (besides the parameter and state spaces) of global representation for voltage stability. All three aspects fit on one sheet, in Figure 7.2, for this minimal system, and the five rows represent the types associated with parameter regions and their boundaries. The first column represents the phase portrait for each type. Finally, the last two columns give example time histories for the two individual state variables E and E' . For larger systems the trajectories will be families of curves that fill a space both in the state space and in the time histories. Here, however, the dynamics are constrained on the one-dimensional flow manifold and hence individual trajectories necessarily overlap. Individual trajectories differ only in their initial state, that is, how much of the potential early history is cut off. Specifically, in Figure 7.2 moving the $t = 0$ point right or left represents individual trajectories with zero values for negative time. In the phase portrait the initial state—a point—will be moving along the flow manifold.

An important feature of the time-domain representation is that the time history for each individual state variable can be presented separately in two dimensions (the individual state and time, respectively) regardless of the dimension of the system. However, of course there is such a plot for every state variable. For larger systems this means numerous plots, which are hard to scan for visualization. However, this aspect gives the only specific display of changes in time and their rates. These are the reasons for the dominant concentration on the time aspects in the literature and in practice with the almost complete neglect of the other two. This is not really desirable because the phase-portrait and parameter-space

analyses provide a wealth of information that is nearly impossible to obtain from time histories. In this text the three will be treated in a balanced manner for clearest understanding of a very complex field.

7.1.5 A Guided Tour Through the Parameter and State Spaces and the Time Histories

Now that all the components have been identified and examined, the overall analysis of the events on the minimal system can be summarized, based on Figure 7.2. There are only three typal regions 1 to 3 in the parameter space that are distinguished by topologically different types of phase portraits. Within each region the topology (roughly the number, relative position, and character of equilibria and basic manifolds) is uniform. Two bifurcation surfaces B_{S1} and B_{S2} separate the three regions. Even in this minimal case the parameter space is still five-dimensional, so it still would be rather complicated to study the geometry of these regions and surfaces. Instead, for this study, only five parameter sets are chosen arbitrarily, one from each region and one from each boundary surface. All parameters are arbitrarily shifted from one typal region to another to emphasize the uniformity of the events within each region and boundary. One exception, the high equilibrium point (E_u, E'_u) , if any, is adjusted always to 1 p.u. so this would be a feasible operating point. The five examples in Figure 7.2 are nevertheless presented in a logical flow of progression to illustrate the gradual change of types. Mostly the examples are given in rough order of increasing power, especially reactive power. In Section 7.2, the geometry of the parameter space for a somewhat larger system will be analyzed systematically for a two-dimensional subspace of the parameter space.

The sequence here reveals the following. At low loads in typal region 1 there are two equilibrium points, both stable. Thus the system state converges to a stable equilibrium point from any arbitrary initial state that may occur say after a disturbance. The regions of attraction are the half lines on either side of (E_u, E'_u) ; hence the singularity is the stability boundary (this role of the singular surface is a special feature for this type of problem). The high equilibrium point (E_h, E'_h) at 1 p.u. is a feasible operating point. The lower equilibrium point (E_l, E'_l) , however, while stable is of low voltage and hence probably nonviable. In fact, if the system should reach the lower equilibrium after a disturbance, it will get trapped by the stability boundary and stay at this possibly much too low voltage, a type of voltage collapse requiring system breakup. Note that the singularity (E_u, E'_u) is a source of trajectories that emerge from the singularity at finite speed, that is, at a finite slope in time-domain plots on the right. So here the singularity is a source of trajectories. It is also a barrier dividing the state space into two components, on the left and right of (E_u, E'_u) . There is no predictable way to take the state from one component to the other. This latter character of the singularity persists through all five cases.

When the parameter set is approaching the boundary, the low equilibrium (E_l, E'_l) is moving close to (E_u, E'_u) and overlaps it at the singularity-induced

bifurcation B_{Sil} (to be analyzed in Section 7.2 and Appendix 7.2). The high equilibrium remains stable normally but the low equilibrium essentially ceases to exist as such and becomes a case of a *pseudoequilibrium* point ψ , where a singularity overlaps an equilibrium (Fig. 7.2).

Passing into region 2 on the other side of the singularity-induced bifurcation boundary the lower equilibrium becomes a normal unstable equilibrium (its character was changed; hence a bifurcation occurred). The singularity, now again free standing, becomes a sink of the trajectories. It still isolates the left and right components. The high equilibrium point (E_h, E'_h) remains stable but its stability boundary on the left has changed to the unstable local equilibrium, which replaces the singularity as the anchor point of the stability boundary and also the boundary itself in this one-dimensional case.

Approaching the boundary toward region 3 the two equilibria approach each other and eventually merge in nonhyperbolic equilibrium point (E_t, E'_t) and a saddle-node bifurcation. The latter term indicates a bifurcation point at which the operating equilibrium point ceases to exist (detail will be given later).

Across the border in region 3 there are no equilibria; all trajectories fall into the singularity representing the ultimate voltage collapse. Note that singularity (E_u, E'_u) still isolates the left and right components of the state space even in this extreme case.

There is one equilibrium point (E_h, E'_h) in each of the typal regions 1 and 2 in Figure 7.2 that is stable and is located at $E = 1$ p.u. bus voltage. Operation at such a point is then stable and feasible. There is no stable or unstable equilibrium point in region 3; hence operation in typal region 3 is nonfeasible. As shown in Figure 7.2 the combination of typal regions 1 and 2 is the feasibility region for operation at the high equilibrium point (E_h, E'_h) for this system. This means that the high equilibrium point (E_h, E'_h) can be moved as such from any point in this *feasibility region* to any other point of the region smoothly by normal operator action, such as load change.

In this minimal example, there are still two state variables E and E' ; hence the time-domain representation still requires two columns versus one for the phase portrait. They are essentially self-explanatory. Each illustration contains four different time response examples numbered 1, 2, 3, and 4. It is readily observed how two traces (1–2 and 3–4) from either side converge to all stable equilibria asymptotically, that is, to (E_h, E'_h) in regions 1 and 2 and into (E_l, E'_l) in region 1. Both trajectories 2 and 3 diverge from the unstable equilibrium point (E_l, E'_l) in region 2. One of these, trajectory 2, which is increasing in time, has an inflection point and then converges to the stable point (E_h, E'_h) . The other, trajectory 3 drops into the singular point (E_u, E'_u) at infinite speed in E , that is, with vertical tangent. Trajectories 2 and 3 in saddle node and 1 and 2 in region 3, also reach the singularity (E_u, E'_u) . However, trajectories reach the singularity with the finite and bounded dynamic speed \dot{E}' (less than vertical slope) in these cases. At the singularity-induced bifurcation B_{Sil} one trajectory (2) rises out of the singularity at finite speed in E and then converges to the stable equilibrium asymptotically, while the other (3) from the left converges to the singularity

asymptotically. At the saddle-node bifurcation B_{SN} there is one trajectory (1) that still approaches the stable equilibrium from above asymptotically, while the other two (2 and 3) both fall into the singularity at infinite speed in E , but at finite, high speed in E' .

7.1.6 Some Observations

The preceding analysis of the minimal system was done through descriptions to enhance the intuitive insight of the reader. Mathematical aspects, even commonly known ones, were played down. A few of these will be mentioned briefly here for maintaining the continuity of thought. Sections 7.2 and 7.2.4 and Chapter 8 are increasingly mathematical in nature. Of course, keeping of intuitive insight becomes increasingly difficult at high dimensions.

The *phase portrait* depicts the flow of the vector field representing the rate of change of the state; in other words, this means all the trajectories in the (E, E') state space. However, the trajectories must stay within the subspace defined by the flow manifold, so the actual state space consists of this manifold. Furthermore, here this manifold is one-dimensional — a line — hence all trajectories are within this line. In fact, they are identical beyond their starting points, that is, the initial state $(E, E')|_{t=0}$ on the load flow manifold. In this sense then, each point on the load-flow manifold with few exceptions is the starting point of an individual trajectory (as it should be). The exceptions are typically connected with singularities and equilibria.

7.1.6.1 Singular Points (E_u, E'_u)

The Jacobian of g is from Eq. (7.8),

$$\frac{\partial g}{\partial y} = \frac{\partial g}{\partial E} = 2E'^2E - 4(x_d'Q + E^2)E \quad (7.19)$$

At *regular points*, this Jacobian is nonsingular and so, by the implicit function theorem, a solution y (in terms of x) will exist at least locally. By substituting y in f , the problem becomes equivalent (locally) to the non-constrained differential equations (7.12), and (7.13).

At the *singular point* $E = E_u$ such that $(dE'/dE)|_{E_u} = 0$ [equivalently, $(\partial g/\partial E)|_{E_u} = 0$; see Eq. (7.17)], the state of the complete system becomes ill-defined. This can actually be seen quite directly for this minimal case. At (E_u, E'_u) , the load-flow manifold as defined by $g = 0$, Eq. (7.8) or (7.15), has a horizontal tangent $(dE'/dE)|_{E_u} = 0$, so the dynamic state E' is constrained to move horizontally, that is, $E' = \text{const}$. Yet in general $\dot{E}'|_{E_u} \neq 0$ as defined by Eq. (7.7). (The $\dot{E}' = 0$ special case will be discussed later.) Thus at this singular point there is no \dot{E}' value that would satisfy both Eqs. (7.9) and (7.10), that is, both $\dot{x} = f$ and $g = 0$.

In fact, the dynamic state E' will cause the state to leave the load-flow manifold vertically at a rate \dot{E}' . This means that the system state is undefined at the singular point. Furthermore, E would arrive at (E_u, E'_u) with infinite speed \dot{E} as is apparent

from Eq. (5.22), which reverses its sign at E_u . Infinite speed results because the slope of the flow manifold decreases to zero at E_u , thus the instantaneous E must move faster and faster along the curve to maintain a slow dynamic \dot{E}' . This foreshadows violent and unpredictable events near the singularity in the physical system, although the singularity itself is a mathematical concept rather than a physical reality. These matters will be studied further in Sections 7.2 and 7.2.4.

7.1.6.2 Equilibrium Points (E_l, E_h) Equilibrium points occur at transversal intersections at a regular point of $g = 0$ of the load-flow and stationary manifolds where $\dot{E}' = 0$, that is no dynamic event occurs. If the Jacobian J of the complete system $\dot{x} = f$, $0 = g$ defined in Eqs. (7.7), and (7.8),

$$J = \begin{pmatrix} \frac{\partial f}{\partial x} & \frac{\partial f}{\partial y} \\ \frac{\partial g}{\partial x} & \frac{\partial g}{\partial y} \end{pmatrix} \quad (7.20)$$

is nonsingular, that is, there are no zero eigenvalues, then the equilibria are *hyperbolic*. It is easy to show from Eqs. (7.7) and (7.8) that this happens when the two manifolds intersect transversally as they do in Figure 7.2 in regions 1 and 2 operations.

7.1.6.3 Intersections Two special kinds of intersections of the manifold separate the three basic regions 1, 2, 3.

Nontransversal (Tangential) Intersections If the Jacobian (7.20) is singular and it possesses one zero eigenvalue, then there is an equilibrium that is *nonhyperbolic*. As can be observed at the saddle-node bifurcation in Figure 7.2 such an equilibrium occurs at (E_l, E'_l) where the two manifolds are tangential, that is, the intersection is nontransversal. (E_l, E'_l) is not stable or unstable in the ordinary sense; the trajectory is converging to it on one side, and diverging from it on the other.

Equilibrium Overlapping Singularity (Pseudoequilibrium) When the two manifolds intersect transversally at a singular point (E_u, E'_u) (where then $f = 0$ and the Jacobian of the flow manifold, J_g , is singular) a special point arises that is called a *pseudoequilibrium point* denoted by Ψ . It plays a major role in voltage stability as will be seen in Sections 7.2 and 7.2.4. It is neither a singularity, (because $\dot{E}' = 0$ there and hence the state is not pushed off the load-flow manifold), nor is it an equilibrium (with the singular Jacobian the state y is also not properly defined). As can be observed at $\Psi = (E_u, E'_u)$ at the singularity-induced bifurcation in Figure 7.2, the trajectory again converges from one side and diverges from the other.

7.2 VOLTAGE STABILITY ANALYSIS OF THE RUDIMENTARY POWER SYSTEM

The “minimal power system”, a generator and a load, has the advantage for study purposes that a complete analysis of its global behavior could be presented on a single sheet as in Figure 7.2. This makes it possible to introduce in a concise manner the many interesting features that determine voltage stability, most of which were not noted until recently. The shortcoming of the minimal model approach is that it is not really a power system. So in preparation for the presentation of the general mathematical structure in Chapter 8 and because of the complexity and “strangeness” of the latter, another stepping stone will be studied: a system composed of generation, transmission, load, and dynamic voltage control. The latter can be either excitation control or controlled reactance [Static Var Compensator (SVC)] or automatic tap-changer control (OLTC). This system is marginally a power system (it is referred to here as a rudimentary system) because it contains all the rudiments of the general power system. It could be viewed as a simplified representation of an actual power system. The simplification comes from the smallest possible number of components simply modeled so that all pertinent features can be visualized in three dimensions.

Even the study of the minimal system in Section 7.1 gives a hint that the global dynamic behavior over the practical operating range of a power system under both normal and emergency conditions is very complex. The state space contains regions of attractions of stable equilibria and other regions in which stable operation is not possible. Typically the parameter space breaks up into several open connected regions, corresponding to particular behavior patterns of the system in the state space, separated by boundaries. The topology of the state space changes as parameters move across the boundary from one open region into another. The boundaries between the regions typically correspond to bifurcation phenomena.

Only recently has the significance of the role played by the boundaries between different regions of structurally stable behavior in the parameter space been realized (e.g., Refs. [4] to [6]). The bulk of today’s literature is still devoted to the study of the saddle-node bifurcation, which occurs at the tip of the $P-V$ curve. Not always identified as a bifurcation (for an introduction, see Appendix 7.2), this phenomenon has been studied for a long time (for example, it is described and analyzed in one of the senior author’s 46-year-old textbook [7]). A few papers dealt with the Hopf bifurcation, which is related to the creation of limit cycles in the state space ([8 to 10]). Saddle-node and Hopf bifurcations are the most commonly studied local codimension-one bifurcations in the power system literature. Because of the multitude of parameters present in the system, further bifurcation types will occur. For instance, a homoclinic orbit was observed as part of a simulation study in the aftermath of a Hopf bifurcation in Refs. 8, 11. Here this particular phenomenon will be explained as the occurrence of a saddle-connection bifurcation in the vicinity of a local codimension-two bifurcation when Hopf and saddle-node bifurcations merge. Furthermore, power-system dynamics

are typically constrained by load-flow equations, resulting in a mathematical model that is differential-algebraic. As a consequence, the dynamic system has singularities. The great importance of these singularities has been pointed out by Zaborszky in [6], by Hill, Hiskens, and Mareels (impasse surfaces) in [12], [13], and was rigorously analyzed in [2]. As will be seen later, singularities can act as stability boundaries, can be sources or sinks of trajectories, and can cause further bifurcations. The presence of some of these singularity-related bifurcations has been noted in the power-system literature Refs. [1, 4, 5, 6, 14], and a rigorous analysis of it was presented for the rudimentary system in Ref. 3. A full and general discussion of it is presented in Chapter 8.

In this section, a comprehensive study of a third-order rudimentary model for the power system will be established based on earlier work at Washington University [3, 6, 14]. While the model has to be quite simplified to be mathematically tractable, it retains the rudiments of the four principal components of the power system that affect the stability, namely, the generator, voltage control, transmission, and load. In this section a comprehensive analysis for variations of control gain and loading will be given and correlated to the dynamic behavior in the state space. Even in this low order, an amazingly rich collection of practical behavior patterns emerges. In fact, the interacting structure observed in the state space and the parameter space for this rudimentary system is largely preserved even for general differential algebraic systems, as is shown in [2, 16, 14] and in Section 7.2.4. However, the low degree of the system has the advantage that results can be readily displayed graphically, fostering both understanding and insight.

The dynamic behavior in the state space is studied here mostly through phase portraits rather than the more conventional time histories for individual states. The phase portrait is interpreted in a general and multi-dimensional sense as the flow of a vector field, that is, as the totality of all integral curves. For this rudimentary system the phase portraits are directly visualizable in a perspective projection in the plane. Hence concepts such as instability and damping of trajectories can easily be observed and the regions of attractions and the regions of voltage collapse can be identified.

This section is organized as follows: Section 7.2.1 gives a mathematical description of the model; a physical-mathematical description of the observed phenomena follows in Sections 7.2.2 and 7.2.3, whereas the mathematical foundations are developed in Section 7.2.4. The material presented in this is based mostly on Venkatasubramanian, Schättler, and Zaborszky [3, 1], and by Zaborszky and B.H. Zheng [6, 7].

7.2.1 Power-System Model with Generator, Voltage Control, Transmission and Matched Load

Voltage dynamics for the rudimentary case of a generator with load at the end of a transmission line as shown in Figure 7.3 will be considered. Three types of voltage control, (1) excitation; (2) thyristor-controlled reactance (SVC); and (3) automatic tap changers (OLTC) will be explored. Since there is only one inertia

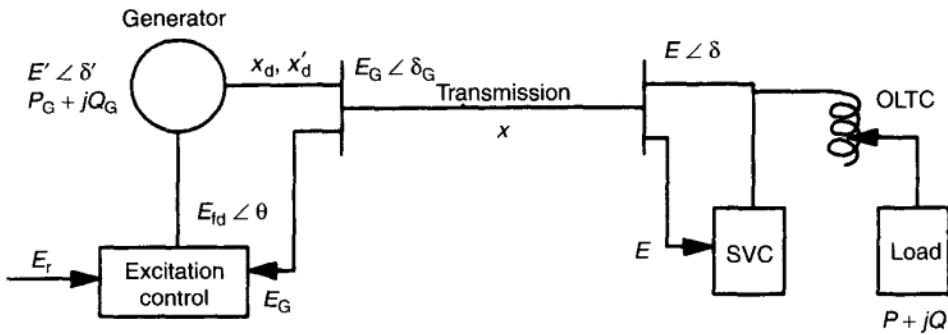


FIGURE 7.3 Rudimentary power-system model. Only one excitation control, SVC or OLTC, is used at any time.

and no losses in this system the assumption $P = P_G$ with no initial stored energy implies that $\delta = 0$ and $\delta = \text{constant}$. This decouples voltage dynamics, and this decoupled model will serve here as a demonstration case study.

Using a simplified one-axis generator model (type IV₂) from Section 3.3.3.4, Eq. (3.3.7.8b) and a first-degree control dynamics, which is a simplification of the IEEE Type 1 excitation dynamics [18], Section 3.2.4, the model for this rudimentary case can be stated as follows:

$$T'_{d0}\dot{E}' = -\frac{x_d}{x'_d}E' + \frac{x_d - x'_d}{x'_d}E_G \cos(\delta_G - \delta') + E_{fd} \quad (7.21)$$

$$T\dot{E}_{fd} = -(E_{fd} - E_{fd}^0) - K(E_G - E_r) \quad (7.22)$$

$$\begin{aligned} 0 &= \frac{E'E_G}{x'_d} \sin(\delta_G - \delta') \\ &\quad + \frac{E_G E}{x} \sin(\delta_G - \delta) \end{aligned} \quad (7.23)$$

$$\begin{aligned} 0 &= \frac{1}{x'_d}[E_G^2 - E_G E' \cos(\delta_G - \delta')] \\ &\quad + \frac{1}{x}[E_G^2 - E_G E \cos(\delta_G - \delta)] \end{aligned} \quad (7.24)$$

$$0 = \frac{EE_G}{x} \sin(\delta - \delta_G) + P \quad (7.25)$$

$$0 = \frac{1}{x}[E^2 - E_G E \cos(\delta - \delta_G)] + Q \quad (7.26)$$

$$Q = Q_0 + HE + BE^2 \quad (7.27)$$

Note that the load model includes an algebraic dependence of the reactive load on voltage in the form of Eq. (7.27) as explained in Section 3.2.3. The quantity E_r is the set-point voltage, E_{fd}^0 is the nominal field excitation, and T and K are excitation control coefficients. The other notations are conventional and are used throughout this text.

The excitation control [Eq. (7.22)] will be replaced in some instances by an equation for an SVC (a thyristor-controlled reactance) at a load of the form

$$T\dot{B}_S = -B_S + K(E - E_r) \quad (7.28)$$

and then Q can be redefined as

$$Q = Q_0 + HE + BE^2 + B_S E^2 \quad (7.29)$$

Control by an automatic tap changing (OLTC) transformer will also be studied in Chapter 10.

Note that with these three basic types of control this study covers a wide range of time scales from about 0.1 sec to several minutes, that is, from fast to midrange.

Since the angle variables always appear in the form $\delta_G - \delta$ or $\delta_G - \delta'$ in Eqs. (7.21) to (7.26), using algebraic elimination, one can obtain the following equations.

Dynamic Equations

$$\begin{aligned} \dot{E}' &= \frac{1}{T'_{d0}} \left(-\frac{x + x_d}{x'} E' + \frac{x_d - x'_d}{x'} \frac{(E^2 + x'Q)}{E'} + E_{fd} \right) \\ &= f_1(x, y, p) \end{aligned} \quad (7.30)$$

$$\begin{aligned} \dot{E}_{fd} &= \frac{1}{T} \left[-(E_{fd} - E_{fd}^0) - K \left(\frac{1}{E} \sqrt{(x'_d)^2 + (xQ + E^2)^2} - E_r \right) \right] \\ &= f_2(x, y, p) \end{aligned} \quad (7.31)$$

Constraint or Flow Equations

$$\begin{aligned} 0 &= E'^2 E^2 - (x'P)^2 - (x'Q + E^2)^2 \\ &= g(x, y, p) \end{aligned} \quad (7.32)$$

The general form of the model is therefore a system of ordinary differential equations subject to algebraic constraints:

$$\dot{x} = f(x, y, p) \quad (7.33)$$

$$0 = g(x, y, p) \quad (7.34)$$

For the power-system model, f and g are, respectively, 2 and 1-vectors of smooth, real analytic, functions; x and y are, respectively, the dynamic and instantaneous state variables that span the state space $\mathcal{X} \times \mathcal{Y}$. For the rudimentary system (Fig. 7.3) $x = \{E', E_{fd}\}$, $y = \{E\}$, p denotes parameters and (secondary) controls that jointly span the parameter space $\mathcal{P} = \mathcal{P}_S \cup \mathcal{P}_O$ where $\mathcal{P}_S = \{x_d, x'_d, x\}$, $\mathcal{P}_O = \{P, Q_0, H, B, K, T, E_r\}$ are, respectively, the system parameters and the operating parameters. E_1 is a control reference, or setpoint that is, a secondary control output.

7.2.2 Basic Features of the Structure of the State-Space—Parameter Spaces

Equation (7.32) defines the admissible points in the state-space—parameter-space for the rudimentary power system. These are located in the *algebraic constraint or flow locus* $0 = g(x, y, p)$ for given parameters p (a manifold for this simple case). The designations constraint and flow and their connection to conventional load flow were introduced and discussed in Section 7.1 and Appendix 7.1. The set of points (x, y, p) that satisfy $0 = f(x, y, p)$ is called the *stationary manifold* (or locus), indicating the absence of dynamic events. Points that lie on both the stationary manifold and on the flow manifold are the equilibrium points (see Fig. 7.4). The state space for the rudimentary system is three-dimensional with the variables E , E' , and E_{fd} . Accordingly, manifolds can be directly visualized. In Figure 7.4, this is shown for one specific set of parameters that corresponds to what will be called type 1" later. The flow manifold, which here is diffeomorphic to a plane, is a curved vertical wall in E_{fd} for this example because E_{fd} does not appear in g . Since the state is constrained within the flow manifold, all trajectories on the flow manifold can be displayed in a planar view by projecting into the (E, E_{fd}) subspace as displayed in Figures 7.5, 7.6 and 7.7.

The flow manifold is readily computed at or around regular points where the Jacobian of g with respect to E is nonsingular ($\partial g / \partial E \neq 0$) and $g = 0$ can be solved for E locally by the implicit function theorem. The remaining points are singular. (The terminology *noncausal* has also been used by other authors in this context [4, 19]). The singular points are the solutions of Eq. (7.32) and the following relation:

$$\frac{\partial g}{\partial E} = (1 + Bx')^2 E^4 + Hx'(1 + Bx')E^3 - (HQ_0E + P^2 + Q_0^2)x'^2 = 0 \quad (7.35)$$

which states that the Jacobian of the constraint equation is singular.

It is easily seen that these equations have a unique solution and hence the singularity exists, unless both P and Q_0 are zero, which would represent an unrealistic model. For the special case considered later, when $Q = Q_0$, a simple explicit solution for the singularity can be given as the positive square roots for

$$E_{\text{sing}}^2 = x' \sqrt{P^2 + Q^2}, \quad E'_{\text{sing}}^2 = 2x'(Q + \sqrt{P^2 + Q^2}) \quad (7.36)$$

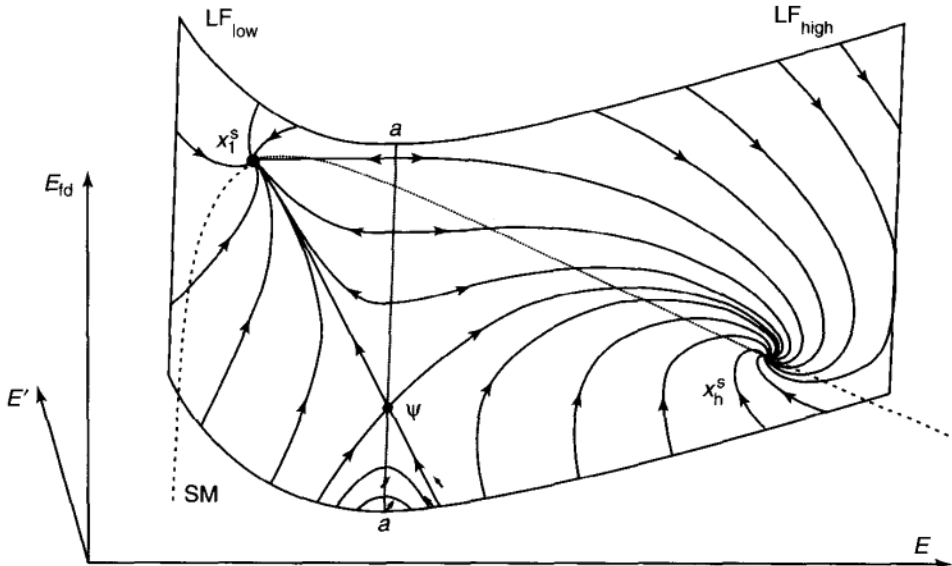


FIGURE 7.4 Dynamics on the flow manifold for parameters $T'_{d0} = 10$, $T = 1.75$, $E_{fd}^0 = 1.6$, $E_r = 1.0$, $x_d = 1.0$, $x'_d = 0.2$, $x = 0.1$, $P = 0.5$, $Q_0 = 0.2$, $H = 0.1$ and $B = 0.1$.

Hence the set of singular points is precisely the line

$$S = \{(E'_{\text{sing}}, E_{\text{fd}}, E_{\text{sing}}) : E_{\text{fd}} \in \mathbb{R}_+\} \quad (7.37)$$

denoted by $a-a$ in Figure 7.4 and in all of the Figures 7.5 to 7.7. This singular line divides the flow manifold FM into two half-spaces FM_{high} and FM_{low} (see Fig. 7.4), which have been called the *components* [2] or *causal domains* [19] of the state space. Each has its own dynamics, which is identified by substituting the solution of Eq. (7.32) within the component into Eqs. (7.30) and (7.31). As has been discussed in Section 7.1 and will be further analyzed in Section 7.2, trajectories *cannot* predictably progress across the singular line. Mathematically, the model in Eqs. (7.30) to (7.32) implies that trajectories enter into or emerge from singular points with infinite speed in the algebraic variable E . Hence in the vicinity of the singular point the analysis based on the quasistationary model in Eqs. (7.30) to (7.32) cannot proceed, and the validity of conventional AC dynamics collapses (Chapter 8). It is therefore apparent that the singular line, $a-a$, plays a fundamental role in the study of voltage dynamics. In the real system this behavior is governed by the ultrafast distributed-parameter dynamics of the transmission lines and other non-AC type fast dynamics [2]. In the enlarged dynamic space $\mathcal{X} \times \mathcal{Y}$, the flow manifold itself becomes a dynamic feature, which then raises the question of the stability of the components. This is an unsolved problem currently because of the unconventional nature (boundary-value problems with a network structure for the boundary values) of the model for the fast y dynamics. Discussion follows later in the book.

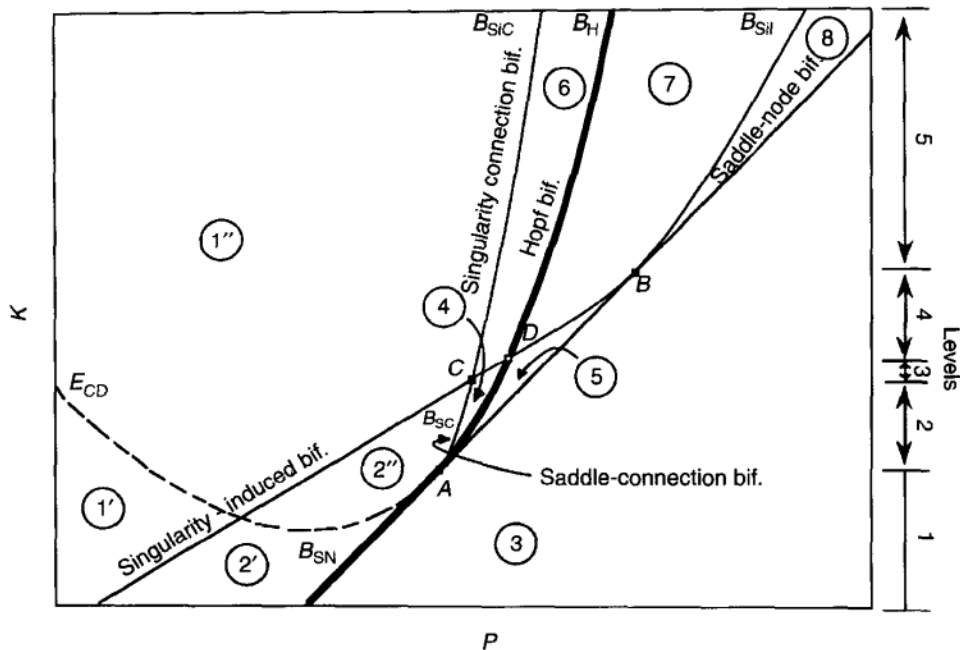


FIGURE 7.5 Qualitative representation of the bifurcation diagram (on the $K \times P$ of the projection in the parameter space).

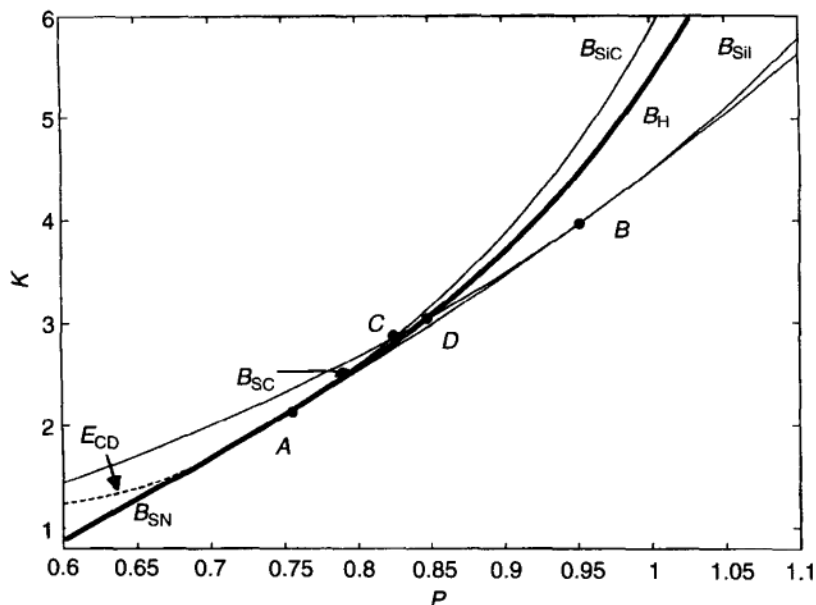


FIGURE 7.6 Bifurcation diagram for parameters $T'_d = 5$, $T = 1.5$, $E_f^0 = 1.6$, $E_r = 1.0$, $x_d = 1.2$, $x'_d = 0.2$, $x = 0.1$, $Q_0 = 0.5P$, $H = 0$ and $B = 0$.

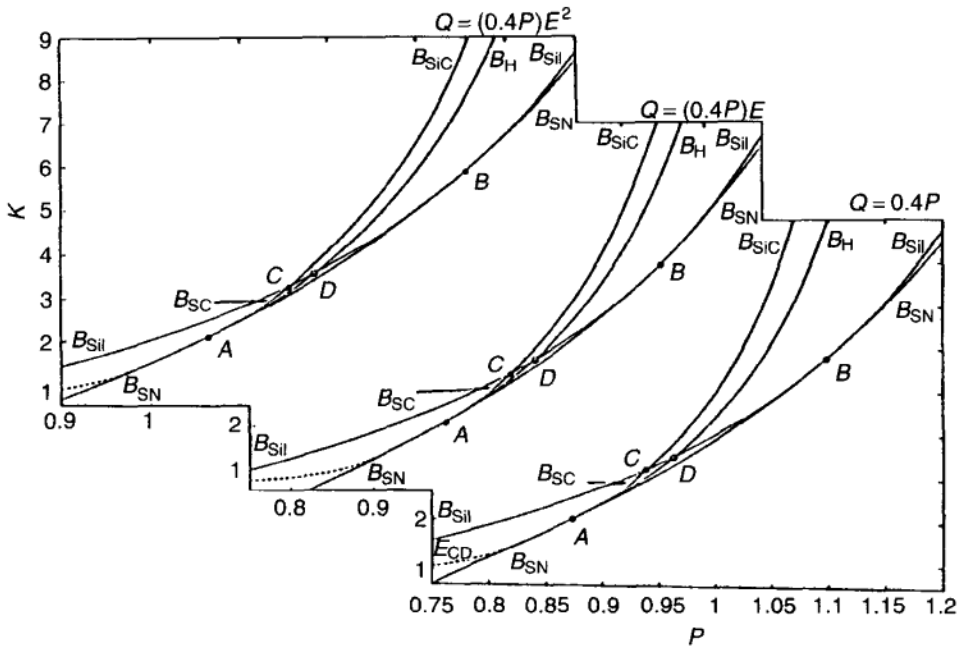


FIGURE 7.7 Comparative bifurcation diagrams for the three basic reactive-load types for parameters $T'_{d0} = 5$, $T = 1.25$, $E_{fd}^0 = 1.5$, $E_r = 1.0$, $x_d = 1.0$, $x'_d = 0.15$, $x = 0.2$ and $q = 0.4$.

Voltage dynamics (and indeed system stability) depends on properties of both the state space and the parameter space, which play equally important roles. Roughly, the position of the operating point in the parameter space determines the type and topology of state-space behavior and the position of equilibria. State-space events (Figs. 7.8 to 7.10) dictate the specific trajectories (i.e., time histories of E , E' , or E_{fd}) that come into play. Even in this simple example the operating parameter space is seven-dimensional, $\mathcal{P}_O = \{P, Q_0, H, B, K, T, E_r\}$. It is realistic to assume for study purposes that the control set point is $E_r = 1$ p.u. at the operating point and that the nominal reactive power at 1 p.u. voltage is proportional to the real power $Q/P = q = \text{const}$, which means a constant power factor. Experiments show that performance is much more sensitive to control gain K than to T . Accordingly a two-dimensional parameter subspace consisting of power P (or equivalently Q) and control gain K is selected for study. This choice represents the most active and hence most informative subset of the operating parameter space. The presentation here is not challenged by exploratory variations of other parameters such as T or the power factor, that is, q .

At this point the problem has been reduced to a dynamic state space (E , E_{fd}) and an active parameter space (P, K) [equivalently (Q, K) under the constant power factor assumption] that are both two-dimensional and can thus be presented in a plane. Note that for the state space the plane is the projection of the roll-shaped flow manifold (Fig. 7.4) onto the (E, E_{fd}) plane.

7.2.2.1 Typical Regions of the Voltage Dynamics in the Rudimentary Power System The objective in this section is to establish the system behavior across parameter space and state space. Each point in the parameter space defines a flow manifold and a corresponding phase portrait (Fig. 7.4). With increasing load, for a fixed value of the control gain, the type of operation changes as bifurcations occur. Figure 7.5 gives the qualitative structure of the bifurcation diagram for the parameters P and K . In Figures 7.6 to 7.7 an actual simulation is given for a specific set of values. P and K of course represent an (active) cross section of the seven-dimensional parameter space.

For simplifying the analysis, it will be assumed in the rest of the section as in Figures 7.5 and 7.6 that the reactive power load is represented by a constant injection, that is, $Q = Q_0$. As can be seen from, Eq. (7.35), *singular points exist as long as either P or Q_0 is nonzero*, that is, as long as a constant-power injection term is part of the load model. Furthermore, as long as $P \neq 0$, the results for the constant-reactive-load case are not challenged by simulation even for the general composite load type shown in Eq. (7.27) and even when the three terms in Eq. (7.27) are arbitrarily used separately (see load-modeling issues discussed in Chapter 3). Figure 7.7 shows the bifurcation diagrams for the three individual load types, that is, the reactive power is represented as a constant load Q_0 in Figure 7.7a, a constant-current source H in Figure 7.7(b), and as a constant impedance $1/B$ in Figure 7.7(c). In all three cases, the reactive power Q in Eq. (7.27) is varied proportionately to the real power P (constant power factor) as assumed before. These bifurcation diagrams clearly indicate that *the structure in the parameter space is the same for the three basic types*, and the various bifurcations even occur at values well approximating each other at different values. Specifically, the singularity is present for each special case, including a pure reactance for reactive load. One may conclude that the choice static load model beyond the presence of a nonservo-active or reactive-power injection component typically is not a crucial issue for the dynamics. DAE dynamics load-modeling issues are discussed in Chapter 3.

7.2.2.2 Survey of the Dynamic Behavior Across Parameter Space and State Space In this section a complete set of behavioral types are illustrated for the rudimentary system in Figures 7.5 through 7.12. This is a large number of graphs but the reader is urged to look at these as a systematically structured survey of the phenomena that are encountered on a rudimentary system designed to help the reader to develop the comprehensive feel and intuition needed to work with this kind of dynamics. It is a disservice to dismiss this material simply as a chaotic avalanche of graphs with no overall content. The following text will lead readers through the panoramic and typical pictures and help them understand the connections and interactions. In Chapter 8 the corresponding theoretical results are presented precisely and the various special cases shown here will serve as illustrative examples by reference.

The main features of the bifurcation diagram of Figures 7.5 and 7.6 are discussed here, but most proofs will be deferred until Section 7.2.4. Several

different phenomena, represented by five bifurcation loci corresponding to three local bifurcations (B_{SN} , B_H , B_{SiI}) and two global bifurcations (B_{SC} , B_{SiC}), occur even for this rudimentary model. (Some basics of bifurcations are presented in Appendix 7.2). To a large extent, special points labeled A to D in Figure 7.5 determine the sequence of structural changes. These points give rise to five different levels of control gain indicated in Figure 7.5. Among them these levels produce all possible sequences of types of operation (*typal regions* 1 to 8) depicted in circles and intervening bifurcations as also illustrated on the P - V curves of Figure 7.12, which will be discussed later. Examples of state-space behavior (phase portraits) for all eight typal regions are displayed in Figures 7.8 to 7.10. Note that there are no stable equilibria for operating parameter values in typal regions 3 and 5. Moreover, the normal operating point x_h^s is stable only in regions 1, 2, 4, and 6, where $1 = 1' \cup 1''$ and $2 = 2' \cup 2''$. The boundary E_{CD} , shown as a dashed line in Figures 7.5 and 7.6, is not a bifurcation since it only represents a change of x_h^s from a node ($1'$, $2'$) to a focus ($1''$, $2''$). Within the larger region composed of regions 1, 2, 4, and 6, the position of x_h^s can be shifted by changing operating parameters within normal operating procedures (e.g., load increases) from any point to any other point without loss of stability. This region is called the *feasibility region* of the operating point x_h^s . Feasible operation at the high equilibrium ends at the boundary denoted by a heavy line in Figure 7.5. This boundary, called the *feasibility boundary*, is composed of segments of saddle-node and Hopf bifurcation loci, joined at point A . Remember that the full boundary is defined in the combined state and parameter spaces. Here we are looking at a cross section in the $P \times K$ plane of the projection of the feasibility boundary into the parameter space. The projection into the state space will not be discussed here.

The phase portraits for all eight *typal regions*, in particular their regions of stability, are illustrated in Figures 7.8, 7.9 and 7.10 in sequences along constant values of the control gain K at three levels (1, 2, and 5). All types of operations and all transitions among the types of operations, are covered among these three regions. This then provides a complete set of illustrations. Our discussion will concentrate on the types encountered in sequence within level 2 (Fig. 7.9), because this gain level is most typical. However, we will simultaneously comment on comparable events in levels 1 and 5. For the parameter values shown in Figure 7.6, let us proceed from the left in Figure 7.5 at the gain value $K = 2.5$.

7.2.2.2.1 Type I' Behavior Examples: Figure 7.9(a) for level 2; Figure 7.10(a) for level 5 with $P = 0.7$; Figure 7.10(b) for level 5 with $P = 1.0$.

Among these three examples listed and all other examples in this section, Figure 7.9(a) is a maverick. All other examples shown in this chapter are excitation control, except Figure 7.9(a) where the system of Figure 7.3 is under SVC control. Even so it can be observed that the topology is quite similar except that the singular line $a-a$ is a curve instead of a straight line. There are two stable equilibria x_l^s and x_h^s , both nodes. There is a pseudoequilibrium x . Trajectories emerge from the singularity above Ψ and return to the stable equilibria or to the singular surface below Ψ in a fashion visible in Figure 7.10(b) [or Fig. 7.9(c)].

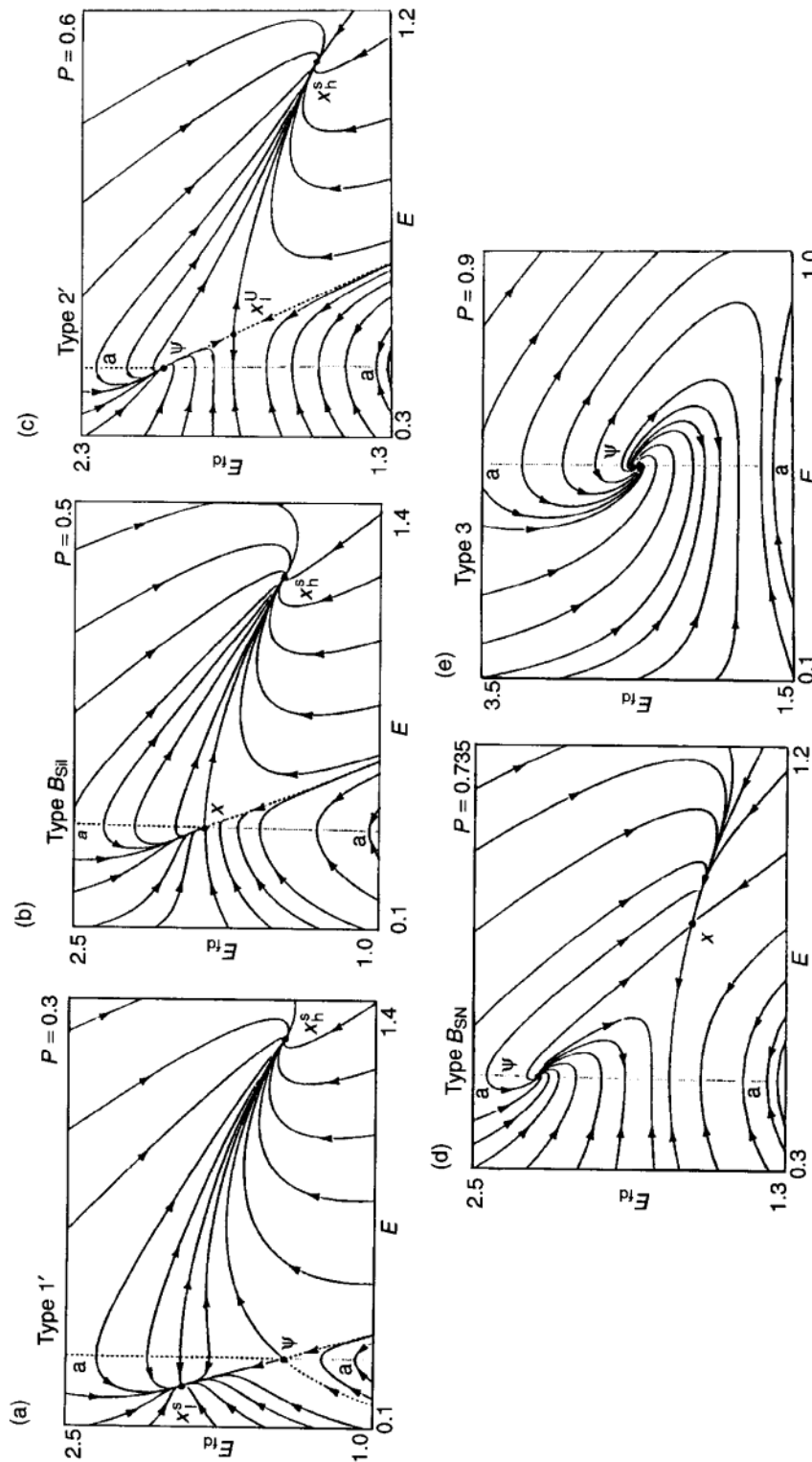


FIGURE 7.8 Phase portraits for the control gain $K = 0.5$ in level 1 with other parameters as listed in Figure 7.8.

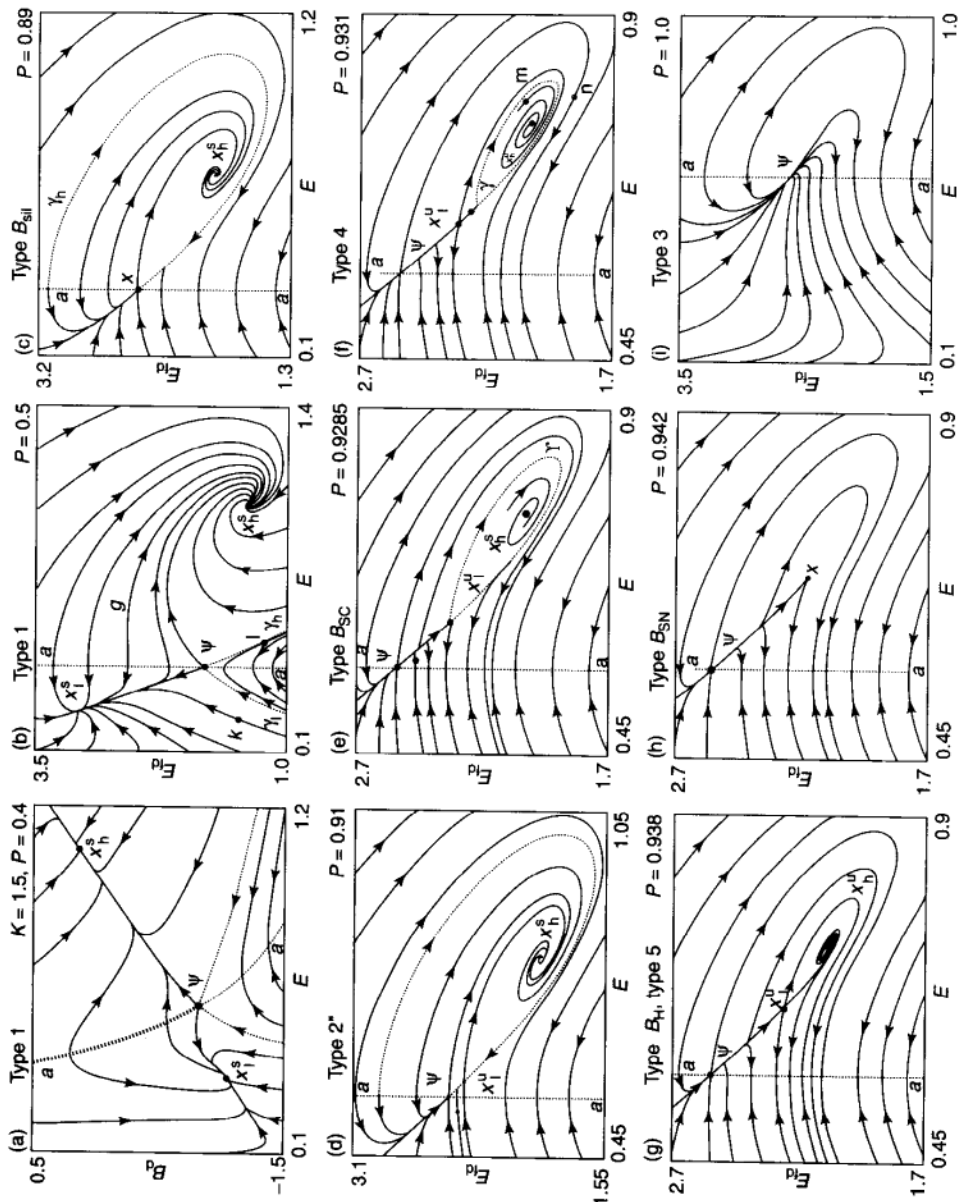


FIGURE 7.9 Phase portraits for the control gain $K = 2.5$ in level 2 with other parameters as listed in Figure 7.8.

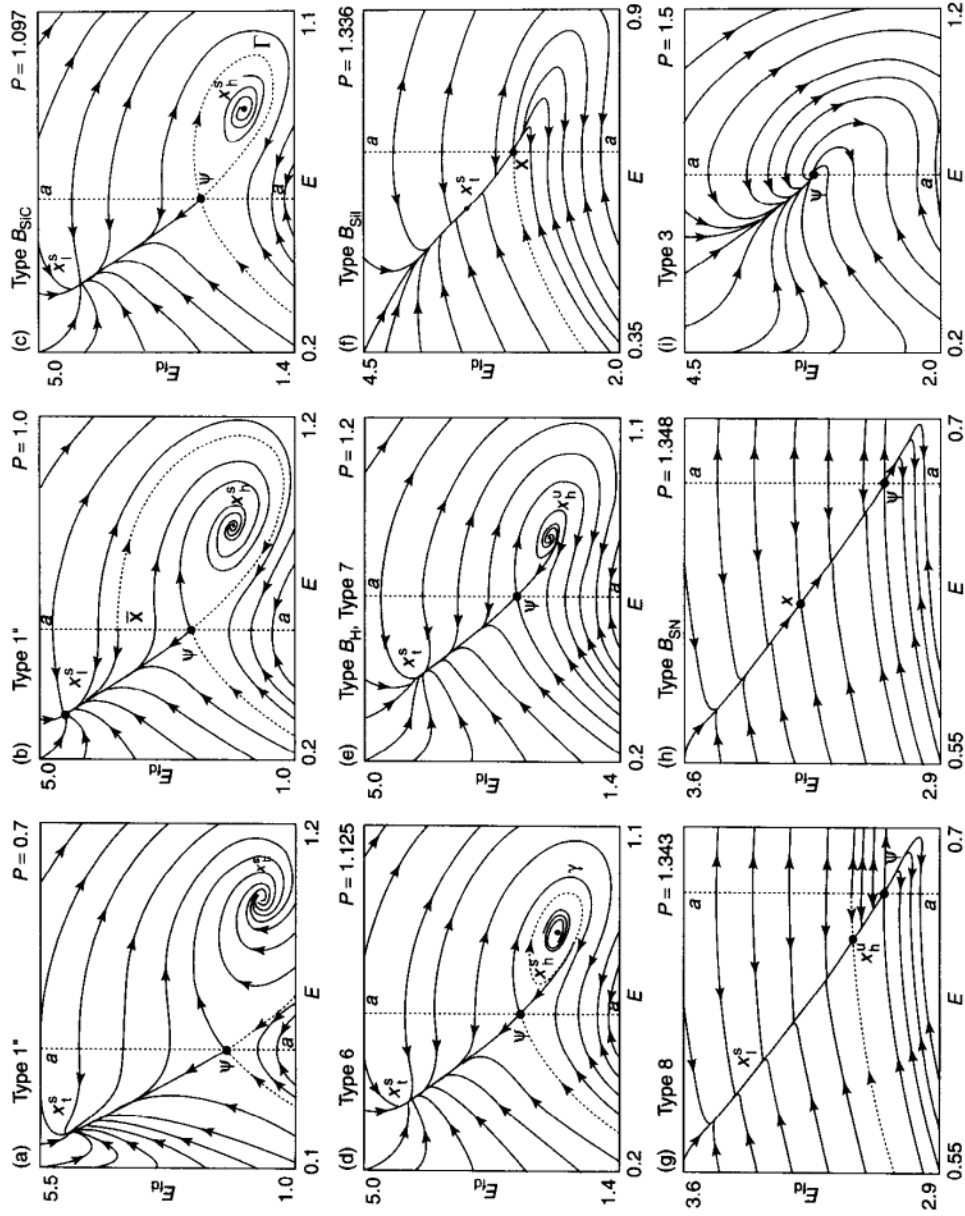


FIGURE 7.10 Phase portraits for the control gain $K = 7.0$ in level 5 with other parameters as listed in Figure 7.8.

The same pattern would be seen in the other graphs if a larger part of the plane were used.

7.2.2.2.2 Type I'' Behavior Examples: Figure 7.9(b) for level 2; Figure 7.8(a) for level 1, Figure 7.10(a) for level 5.

At these light loads there are two stable equilibria, x_h^s and x_l^s , one on each side of the singular surface ($a-a$); x_h^s is a focus for parameter values above line E_{CD} in Figure 7.5. There are three regions, two of which correspond to the regions of attractions of the stable equilibria (stability boundaries are shown by heavier dotted lines in Figs. 7.8 to 7.10). The region to the right of $a-\psi-\gamma_h$ is the region of attraction of the stable equilibrium point, x_h^s , and the region to the left of $a-\psi-\gamma_l$ is the region of attraction of the other stable equilibrium point x_l^s . The third region contains no equilibria and all trajectories sink into the singular line, resulting in voltage collapse. The pivotal role is played by the point ψ on the load-flow manifold where $\dot{E}' = 0$, but $\dot{E}_{fd} \neq 0$, which will be called *pseudoequilibrium*. As will be shown in Chapter 8, this point ψ becomes an additional equilibrium point if the time scale is singularly transformed to eliminate the singularity. This fact already explains the special role of ψ as the limit point of infinitely many trajectories or as anchor for stability boundary segments like the one under consideration at the moment. There exist unique trajectories γ_l and γ_h on the left and right components of the load-flow manifold that converge to ψ . These two trajectories, together with the singular line above ψ form the stability boundaries of the three regions.

All stability properties can be read off the phase portrait immediately. Upon clearing a disturbance, the system state may be initially anywhere in the state space. If the initial state is, for example, at point j [in Fig. 7.11(b)], then the system state will follow a trajectory with acceptable damping back to the stable equilibrium point at x_h^s , the operating point of the system, following the time history in Figure 7.11(a). Hence the system has *transient voltage stability* in the traditional sense of power engineering for the disturbance, which is cleared at the initial point from state j . If the system should be at state k in Figure 7.11(b) after

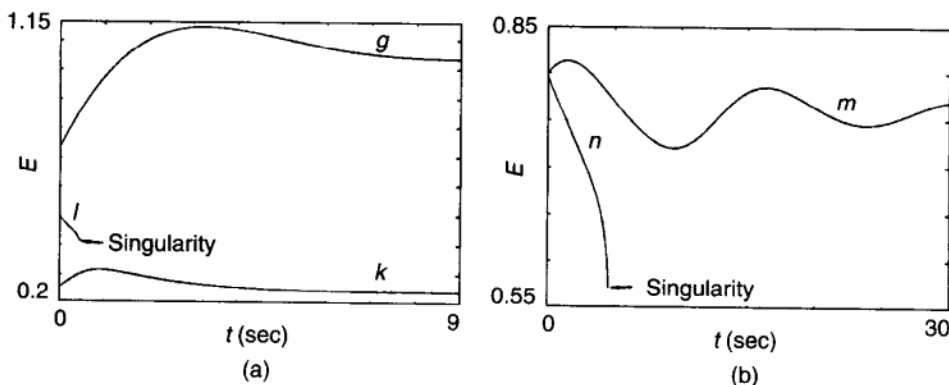


FIGURE 7.11 Time histories for the bus voltage E .

the disturbance, then it will move on a trajectory to the low stable equilibrium point x_l^s . The equilibrium x_l^s is at too low a bus voltage for operation (it is not viable); [Fig. 7.9(b)], but the system gets trapped there since x_l^s is stable. A system breakup by selective protection will follow. Industrial experiences of such entrapments have been reported [6]. However, as already mentioned, a valid proof of the stability of the components themselves in the full dynamic (x, y) space does not exist because of modeling difficulties [6].

Finally, from an initial state at l , in Figure 7.9(b) the system will move to a voltage collapse at a singular point on the line $\psi-a$ [Fig. 7.11(a)]. Note that with increasing gain K both equilibria gradually change from nodes to foci across line ECD . Also, note that in Figure 7.10(b), the stability boundary γ_h bends back to a source point \bar{x} on the singular line, restricting the stability region of x_h^s . This also portends the birth of a closed orbit in Figure 7.10(c) at a higher load P as in Figure 7.9(f), where the trajectory of point v inside the closed orbit (which bounds the stability region) and point w outside of it converges or diverges to the singularity as shown in Figure 7.11(b), Figure 7.9(c) for level 2; Figure 7.10(f) for level 5; and Figure 7.8(b) for level 1.

7.2.2.2.3 Type B_{SIL} Bifurcation Behavior Examples: Figure 7.9(c) for level 2; Figure 7.10(f) for level 5; Figure 7.8(b) for level 1. As the load increases to $(K, P) \in B_{SIL}$, the lower stable equilibrium x_l^s crosses from the left to the right half-space and changes into a saddle, that is, a *singularity-induced bifurcation* occurs. For parameter values on the bifurcation curve B_{SIL} , the equilibrium point lies on the singular line at the point ψ in the state space, which coalesces with x_l here. All the trajectories in the left component (LF_{low}) converge to the singular line. The behavior of the stable equilibrium point x_h^s on the right component (LF_{high}) is not affected by the singularity-induced bifurcation. It still is a stable focus with the region of attraction bounded by the curve $a-x-\gamma_h$, where γ_h denotes the unique trajectory on the right half-space, which converges to the point $x = \psi = x_l$. The trajectory γ_l-x_l loses its significance as stability boundary, but it still separates trajectories converging to x_l or to the singular line. The same remarks apply to Figure 7.8(b) except that for the high equilibrium there is a node. In Figure 7.10(f), the high equilibrium $x_h \in B_{SIL}$ (originally a focus) moves to the low side component LF_{low} , resulting in the presence of a stable node x_l^s and a saddle x_h^u on the low side in Figure 7.10(g) (region 8), while no equilibria exist on the high side there.

7.2.2.2.4 Type 2'' Behavior Examples: Figure 7.9(d) for level 2; Figure 7.8(c) for level 1 (type 2').

Upon increasing the load further, the lower equilibrium point x_l^s moves into the right half-space and becomes a saddle x_l^u . The high equilibrium point x_h^s is still stable. Part of the stability boundary consists of the stable manifolds of the saddle x_l^u . The point ψ itself becomes both a sink and a source for infinitely many trajectories on the left and right half-spaces. The only difference to note in Figure 7.8(c) is that x_h^s is a node.

No further changes occur in the phase portrait with increasing load in the left half-space component (right half-space in Fig. 7.10) and therefore only the right half-space (left in Fig. 7.10) is described henceforth.

7.2.2.2.5 Type B_{SC} or B_{SiC} Bifurcation Behavior Examples:

Figures 7.9(e) for level 2; Figure 7.10(c) for level 5:

As the load increases, a saddle-connection bifurcation (B_{SC}) occurs at the transition from region 2'' into region 4. For values $(K, P) \in B_{SC}$, one each of the stable and unstable manifolds of the saddle x_l^u coincide and form the *homoclinic orbit* Γ . This homoclinic orbit together with the equilibrium point x_l^u forms the stability boundary for the stable focus x_h^s . Trajectories that lie inside converge to x_h^s and the trajectories that lie outside. Those that do not lie on the stable manifolds of the saddle x_l^u converge to the singular line, that is, they experience voltage collapse. Because of the infinite "period" of the homoclinic orbit, the motion of the state is very slow near Γ . This bifurcation is not encountered in levels 1 and 5, but the behavior at the singularity-connection bifurcation $(K, P) \in B_{SiC}$ in level 5 [Fig. 7.10(c)] where the trajectory Γ of the stability boundary that closes on itself at ψ is quite similar to what happens at the homoclinic orbit. This orbit Γ in Figure 7.10(c) actually becomes a homoclinic orbit in a transformed system in which time has been rescaled.

7.2.2.2.6 Type 4 and Type 6 Behavior Examples:

Figure 7.9(f) for type 4 in level 2; Figure 7.10(d) for type 6 in level 5:

The structural changes upon moving from region 2'' to region 4 through the *saddle-connection bifurcation* (B_{SC}) in Figures 7.9(c) to 7.9(e) and from region 1'' to region 6 through the *singularity-induced bifurcation* (B_{SiC}) in Figures 7.10(b) to 7.10(d) are of a global nature. The local phase portraits near the two equilibria do not change at all.

x_l^u stays a saddle in Figure 7.9(e) and the pseudoequilibrium ψ also stays the same in Figure 7.9(d); x_h^s remains a stable focus in either case. The bifurcation occurs in the form of global rearrangements of the stable and unstable manifolds of x_l^u at B_{SC} . They approach [region 2'', Fig. 7.9(c)] and slide over each other, forming a homoclinic orbit [Fig. 7.9(d)] where they coincide. Upon continuing increase of parameters, they emerge in opposite relative position [Fig. 7.9(e)], whereas a limit cycle replaces the homoclinic orbit in region 4 in Figure 7.9(e). Similarly the closed orbit in Figure 7.10(c), where the origin and the end point of the stability boundary meet on the singularity at ψ is replaced by a limit cycle in Figure 7.9(d) upon an increase of load, whereas x_h^s and x_l^u retain their character. Global structural changes of this type are considerably harder to analyze and detect than local bifurcations, but they have been intensively studied recently in connection with chaotic behavior of dynamical systems. The presence of homoclinic orbits even in this low-order model along with the fact that the dynamics is considerably more complex near the singularity strongly indicates the possible presence of chaotic behavior for certain parameter values in the general large-power system. If so, such behavior would represent another form

of voltage collapse regardless of detail. Reported results should, however, be carefully analyzed for the physical realism of the model.

As the load increases in region 4 or in region 6, the periodic orbit and hence the stability region for the high equilibrium x_h^s shrink. Concurrently, the period of the limit cycle decreases from ∞ (for parameter values $(K, P) \in B_{SC}$ corresponding to the homoclinic orbit) to ω (for parameter values $(K, P) \in B_H$, corresponding to a Hopf bifurcation with eigenvalues $\pm i\omega$). Figure 7.11(b) shows time histories for points v and w that lie inside and outside the limit cycle shown in Figure 7.9(e). One should observe the poorly damped character of the time history of point v .

7.2.2.2.7 Type B_H Bifurcation Behavior Examples: Figure 7.9(g) for level 2 (type 5); Figure 7.10(e) for level 5 (type 7).

The phase portrait for region 5 or 7 operation given in Figure 7.9(f) or 7.10(e) and for the Hopf bifurcation is qualitatively the same. The stability behavior of the high equilibrium point x_h at the bifurcation value B_H is already that of an unstable focus. Hence, except for the points on the stable manifold for x_l^u , all trajectories converge to a point on the singular line in the high component LF_{high} , resulting in voltage collapse.

7.2.2.2.8 Type B_{SN} Bifurcation Behavior Examples: Figure 7.8(d) for level 1, Figure 7.9(h) for level 2; Figure 7.10(h) for level 5.

For $(K, P) \in B_{SN}$ the well-known saddle-node bifurcation occurs: the two equilibria merge at $x = x_h^s = x_l^u$. There are a variety of different combinations that occur at this point among the three gain levels 1, 2, and 5 studied. In level 2, which is our primary subject, the two merging equilibria are a saddle and an unstable node. The unstable focus in Figure 7.9(f) becomes an unstable node (which is not a bifurcation) before reaching the saddle in Figure 7.9(g). At the two other levels a stable node meets a saddle in the high component in case of level 1 [Fig. 7.8(d) following Fig. 7.8(c)] and in the lower half-plane in case of level 5 [Fig. 7.10(h) following 7.10(g)]. In all cases, a nonhyperbolic unstable equilibrium results at x .

7.2.2.2.9 Type 3 Behavior Examples: Figure 7.8(e) for level 1; Figure 7.9(i) for level 2; Figure 7.10(i) for level 5.

Finally, if P is increased beyond its value on B_{SN} , the equilibrium disappears and all the trajectories on both the high and low sides converge to the singular line from where they also originated. Now every trajectory results in voltage collapse. This trivial situation occurs in region 3 and exemplary phase portraits are given in Figures 7.8(e), 7.9(i) and 7.10(i).

7.2.2.3 Role of the PV or PQ Curves In the approach of this text the analysis is based on the entire state space and the entire parameter space or its more active subspace (in this chapter, three state variables and a two-dimensional parameter subspace). For a general system both of these will be very large, but between them, they give all the data needed to study the whole system and give results

that are well defined and meaningful. Traditionally it is customary to attempt to use the PV curve as the basis for analyzing even large and complex systems. The PV (or QV) curve originated in the steady-state analysis of a single transmission line, for which it is well suited. It is discussed in this role in the 1954 textbook of one of the present authors [27]. It is unsuitable for analyzing the general large dynamic system or even the rudimentary system of this example. It retains a single variable from the state space and from the parameter space—a woefully inadequate database. Researchers using this approach seem to put a major obstacle in their way even before they start.

On the other hand, the $P-V$ curve can be used for displaying the output of results in an effective way once such results are obtained by using the appropriate general analytical tools. This is illustrated in Figure 7.12 for each of the eight typical regions of the rudimentary system. For instance, the results of level 1, Figure 7.8, are illustrated on the $P-V$ curve of Figure 7.12(a). At these low gains, the upper branch is stable up to the saddle-node bifurcation at the tip. The lower branch also has a stable (but nonviable) branch at loads up to the singularity-induced bifurcation. No solution exists beyond the saddle node. As summarized in Figure 7.12(b) at level 2 stable operation ends on the upper branch at the Hopf bifurcation ahead of the saddle node. The Hopf bifurcation is preceded by a section where, though still stable, the region of attraction of x_h^s is restricted to the interior of an unstable limit cycle beyond B_{SC} (compare Fig. 7.9). On the lower branch, stability still ends at B_{SII} .

Finally Figure 7.12(e) summarizes the results at level 5 and Figure 7.10. Stability on the upper branch, that is, for the high equilibrium, ends at the Hopf bifurcation, preceded by a section of shrinking region of attraction (starting at B_{SIC} instead of B_{SC}). The lower branch or low equilibrium is stable everywhere up to the tip, B_{SN} . The singularity-induced bifurcation now occurs on the upper branch when the high equilibrium crosses the singularity into the low side. Note that the other two illustrations, Figures 7.12(c) and 7.12(d), display the sequence of events at levels 3 and 4 as also easily seen in Figure 7.5.

This shows how the PV curve, or equivalently, the QV curve, can be useful as a tool for displaying results after they are obtained by proper analytical methods. The PV curve is, however, a serious drawback when used for analysis, as is common practice.

7.2.2.4 Overview of the Two-Level Cellular Structure of the State Space and the Parameter Space as Revealed by the Rudimentary Power System. The preceding analysis reveals a two-level cellular structure in the parameter space and the state space: The two governing features of the voltage dynamics problem are (1) *the region of attraction* and its stability boundary in the state space (Table 7.1 and Fig. 7.4); (2) *the feasibility region* and its feasibility boundary in the parameter space (Table 7.2). Each stable equilibrium point has a stability region and its boundary in the state space, as shown by dashed lines in Figures 7.8 to 7.10. Each stable equilibrium has a feasibility region and its boundary in the

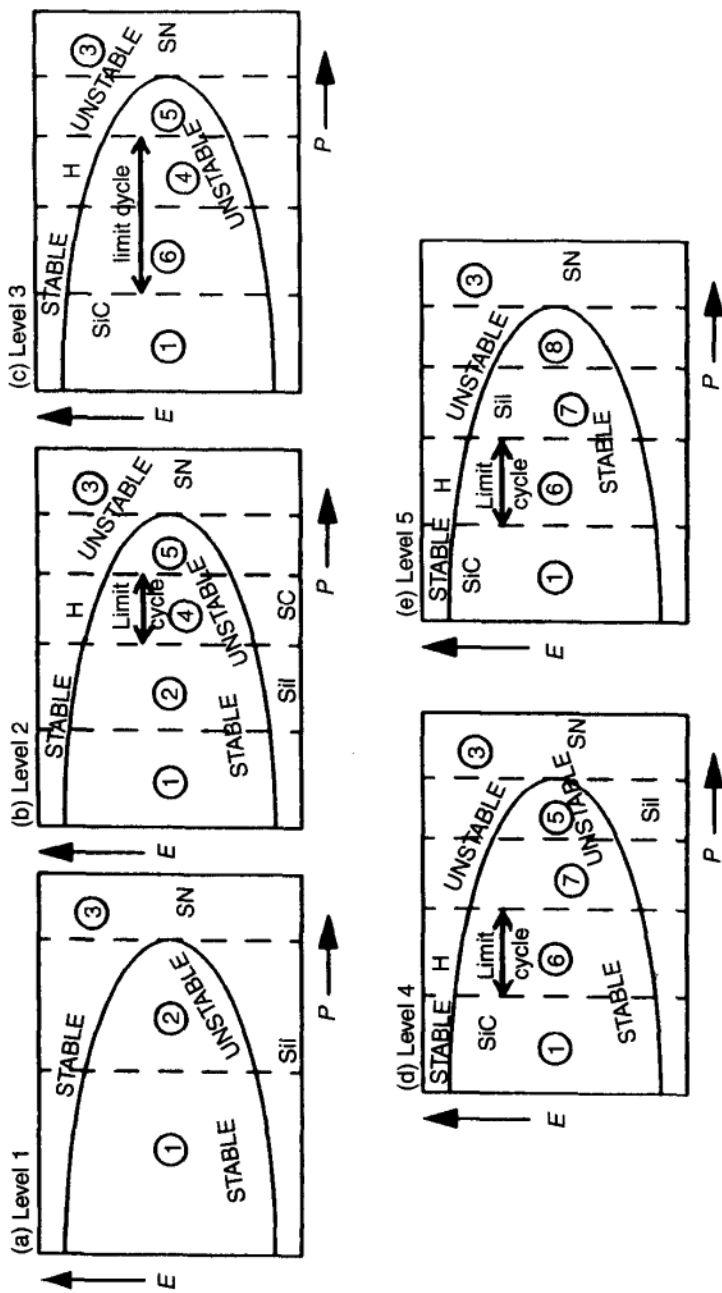


FIGURE 7.12 P - V curves in qualitative display.

TABLE 7.1 Two-Level Cellular Structure of the State Space

Region	Sections of the boundary
<i>Component</i>	<i>Singular Surface</i>
State moves on predictable trajectories over regular points	Source and termination of predictable trajectories
1. Region of attraction	<i>Quasi-stability Boundary</i>
2. Region of no convergence	1. Stable manifolds of four types of anchors
3. Region of voltage collapse near singularity	a. Unstable equilibria b. Unstable limit cycles c. Pseudoequilibrium surface d. Semisingular surface
4. Additional types	2. Singular points

TABLE 7.2 Two Level Cellular Structure of the Parameter Space

Region	Sections of the boundary
<i>Feasibility Region</i>	<i>Bifurcations</i>
Operating point movable continuously as a stable equilibrium	1. Saddle node 2. Hopf 3. Singularity induced
<i>Typical Region</i>	Various kinds of bifurcation surfaces consisting of local and global bifurcations

parameter space, as shown for the high equilibrium by a thick line in Figures 7.5 and 7.6.

A certain type of phase portrait in the state space persists for operating conditions within open regions of the parameter space, Labeled *typal regions* 1 to 8. Each typal region has a type of phase portrait with a given topology that is a transient behavior, displayed in Figures 7.5 to 7.10 for each of the eight typical regions of the parameter space of the rudimentary system used here as an example. Changes in the type of the phase portrait occur as parameters cross the bifurcation curves shown in Figure 7.5. Some of the typal regions can be grouped together into a *feasible region* where operation at a specific stable equilibrium point is feasible in the sense that the reference equilibrium can be shifted smoothly through normal operating practices from any point in the region to any other point, retaining its stable character. The boundary of the feasibility region is called *feasibility boundary*. The feasibility boundary for the high equilibrium x_h

is shown in Figures 7.5 and 7.6 as thick lines and also in Figure 7.13. It consists of a curve, $B_{SN}-A-B_H$ connecting the lower half of the saddle-node bifurcation curve B_{SN} with the Hopf bifurcation curve B_H at the codimension-two bifurcation point A . In the upper left half-plane (regions 1, 2, 4, and 6) operation is feasible at the high equilibrium point x_h , which is stable there. For the low equilibrium point x_l the feasibility boundary $B_{SIL}-B-B_{SNL}$ is actually wider at high gains than that for x_h . It consists of regions 1, 6, 7, and 8, bounded by the lower half of the singularity-induced bifurcation B_{SIL} up to a point B and beyond point B by the upper half of the saddle-node bifurcation B_{SN} as shown in Figure 7.13. The lower equilibrium is stable throughout this region but is typically not viable, mostly because of large voltage differences and heavy currents. Note that between them the stability boundaries for x_h^s and x_l^s consist of segments of saddle-node, Hopf, and singularity-induced bifurcations. It will be seen in Section 7.2.4 that these three still form the feasibility boundary for the very large system and also when different types of equipment such as automatic tap changing or saturation are involved. The latter also leads to the presence of several disjoint segments of, say, saddle-node bifurcations in the boundary, each connected to a different physical experiment such as tap changes.

Following the clearing of a fault in the state space, all initial states that lie within the region of attraction of the equilibrium that serves as the operating

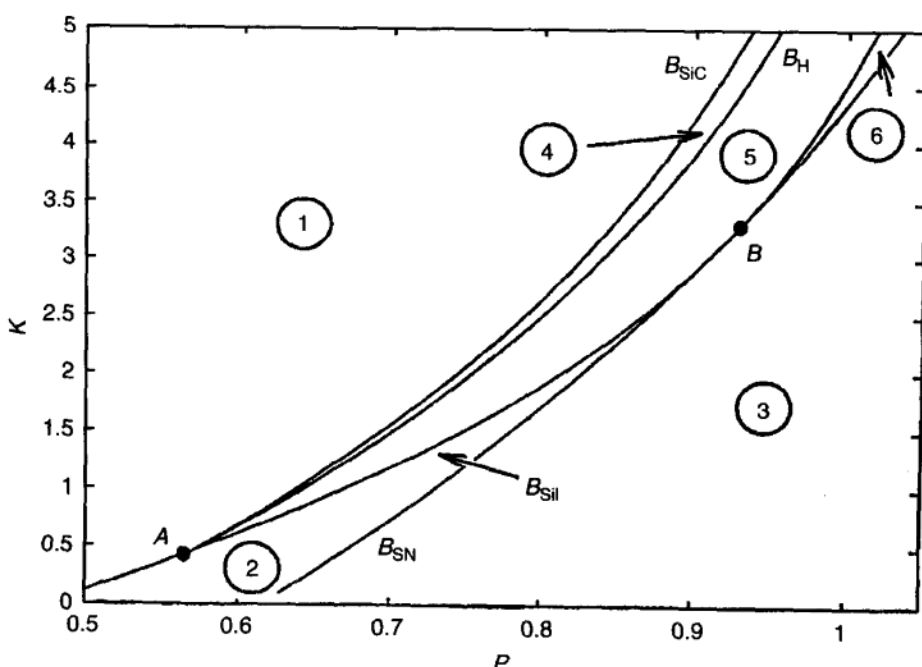


FIGURE 7.13 Bifurcation diagram for the rudimentary system with SVC control for parameters $T'_{d0} = 10$, $T = 1.75$, $E_{fd}^0 = 1.6$, $E_r = 1.0$, $x_d = 1.0$, $x'_d = 0.2$, $x = 0.1$, $Q_0 = 0.25p$, $H = 0.12p$ and $B = 0.12p$.

point converge back to the equilibrium. So the system has transient stability for such faults. Stability boundaries are designated in each of Figures 7.8 to 7.10 by dashed lines. It should be observed in Figures 7.8 to 7.10 that the region of attraction of x_h^s , the usual operating point, gradually shrinks in size with increasing load and disappears at the feasibility boundary when one of the saddle-node or Hopf bifurcations is crossed.

Equilibria are potential operating points provided they (1) are feasible, (2) have transient stability, (3) are viable (that is, their voltages and currents are within specified tolerances) (see Chapters 4, 5, and 6). These points are secure in the sense that they have feasibility, viability, and transient stability with adequate margin for any first-order contingency, that is, any one single fault that may occur on the system.

7.2.2.5 Voltage-Collapse Phenomena Voltage-collapse phenomena can be classified as dynamic (state space), parametric (parameter space), and equipment related. A detailed analysis will be presented in Section 7.2.4 for the general large system. It is quite instructive, however, to identify occurrences on the rudimentary system as observed in this section.

Dynamic voltage collapse occurs when the postfault state lies outside the postfault transient stability region and thus the high equilibrium is not regained. At least three subtypes exist: (1) The transient simply diverges out of practical range because after a saddle-node bifurcation, a descent on the center manifold, occurs (the term *voltage collapse* is applied to this case exclusively in some of the literature). (2) The transient converges at infinite speed to a singular surface where practical operation ends, as in Figures 7.11(a) and 7.11(b) for the trajectory from point l in the Figure 7.9(b) and w in Figure 7.9(f). (3) The transient to the low equilibrium, which is stable [Fig. 7.11(a) transient from point k , of Fig. 7.9(b)]. Because of its stability *the state is trapped* at this impractical operating point and the system is then broken up by selective protection.

Parametric voltage collapse occurs when the system (or its postfault composition) is located (as a result of load change or loss of transmission, generation, etc.) in a region of the parameter space from which it cannot return to a stable operating point. Two subtypes occur: (1) A stable operating point does not exist (regions 3 and 5 for this example). (2) A stable equilibrium does exist, but it is not practical for operation (such as the stable lower equilibrium in regions 7 and 8, e.g., because of low, nonviable voltage).

Equipment-related voltage collapse will be observed later in this chapter, especially those connected with tap-changer operations.

The literature sometimes associates voltage collapse exclusively with the slow descent on the center manifold following a *saddle-node* bifurcation—this is beyond the type of the mode of the P–V or Q–V curves.

7.2.3 Exploration of Changes Caused by Variations in the Load Model and the Type of Control Used

The study in Section 7.2.2 was based on a load model of one particular type and of voltage control through generator excitation. Actually the load-modeling question is rather unsettled and the control type influences the speed for time response quite decisively. All restrictions to specific modeling assumptions except nonlinear and smooth differential-algebraic equations models are eliminated in Chapter 8 for the general large system. But again the results in Chapter 8 are general in nature and hence not readily visualizable. Thus it is desirable to analyze the effects of modeling and control type in the context of the rudimentary system from which results can be directly visualized.

7.2.3.1 How the Load Model Affects the Results Modeling of composite loads is in a rather rudimentary state (as analyzed in Chapter 3). Only a few remarks pertinent to the rudimentary system examples of this section need to be emphasized here. The assumption of real load matching $P_G = P$ was used here to separate the voltage stability from the angle stability and create a clear counterpart to the “classical”, voltage behind the transient reactance ($E' = \text{const}$) model (in Chapter 3). This assumption is dropped in the general Section 7.2.4, which includes both electromagnetic (voltage) and electromechanical (angle) stability. It is desirable, however, to explore the effects of the form of the instantaneous load model, as shown in Eq. (7.27), on the results of Section 7.2.4 and particularly on the singularity. The special case of $H = B = 0$ in Eq. (7.27), that is, a constant reactive load Q_0 , is considered mostly in Section 7.2.2 along with constant power factor $Q_0 = qP$ with $q = \text{const}$. Singular boundaries were observed in that section. However, it can be seen from Eq. (7.35) that *singular points exist only as long as either P or Q_0 is nonzero*.

Furthermore, the results for the constant-reactive-load case are not challenged by simulation even for the general composite-load type. Figure 7.7 shows the bifurcation diagrams for the three special load types in Eq. (7.27), that is, the reactive power is represented as a constant reactive load in Figure 7.7(a) constant current source in Figure 7.7(b) and as a constant impedance in Figure 7.7(c). In all three cases, the total reactive power Q is varied proportionally to the real power P (constant power factor). Hence the two are equivalent. The bifurcation diagrams in Figure 7.7 clearly indicate that *the structure in the parameter space projection is the same for the three basic types of models*, although the various bifurcations occur at different parameter value sets, which, however, still remain reasonable approximations of each other. Furthermore, the singularity is present for each special case (including a pure resistance load) for reactive load as long as there is a constant component in either the active or reactive power (P_0 or Q_0). The presence of such components was conclusively shown in detailed studies on large real systems [21, 22].

7.2.3.2 How the Type of Voltage Control Used Affects the Results The sketch in Figure 7.3 shows three different types of controls, each connected with different

time scales from fast to middle range. These will now be discussed individually assuming that only one is active at a time.

Automatic Excitation Control In this case, which has been the one studied so far, the typical response time, depending on equipment, ranges from a tenth of a second to a few seconds. The model for the rudimentary system is given in Eqs. (7.21) to (7.27). Section 7.2.1 has presented a detailed analysis of events, which will be used here as the norm in describing other time scales.

Automatic Thyristor Control of Reactance (SVC) The time scale is basically instantaneous, but a linear filter of a time constant of about 0.1 sec is usually incorporated to cut down fast noise-type reactions. This is about the fastest time scale encountered in this situation. Equations (7.30) to (7.32), (7.28), and (7.29) present the rudimentary model when SVC is used.

Comparison of Figures 7.14 and 7.6 show that the general nature of the results presented in Section 7.2.2 remains the same in case of a rudimentary system regulated via automatic thyristor, that is SVC control, instead of excitation control. Equations (7.28) and (7.29) represent the model for the thyristor control. It is important to note that the structure of the parameter space and that of the state space [Fig. 7.9(a) gives an example for the SVC case] are qualitatively the same

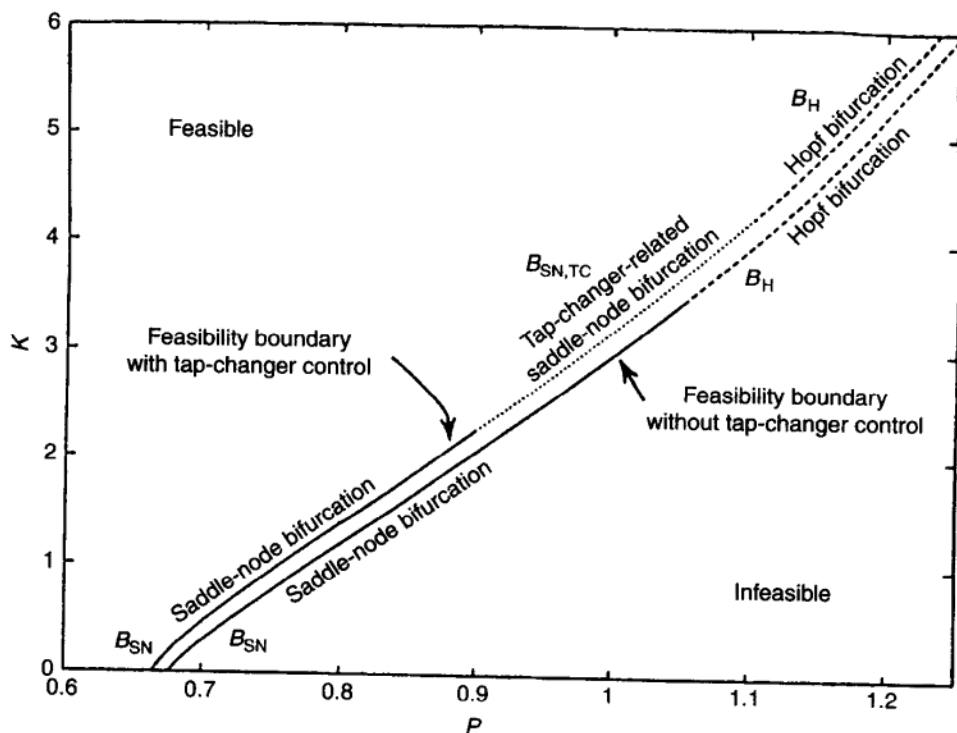


FIGURE 7.14 Composition of the feasibility boundary with or without tap changer.

with either of the controls. To facilitate comparison, coordinated labeling is used between Figures 7.6 and 7.14. Of course, there is some warping, for instance, the singular line $a-a$ is not a straight line [Fig. 7.9(a)] any more and the typical region 8 does not appear in Figure 7.13. Also, the typical regions occur in somewhat rearranged sequences. But certainly the basic features and the two local cellular structures of Tables 7.1 and 7.2 remain the same as with excitation control.

Automatic Tap-Changer-Based Control Automatic tap-changer control is a nonsmooth nonlinear control and as such it will be discussed in Chapter 10. The reader may be interested in [23] in which this material is supplemented by a section on mathematical analysis containing introduction of additional concepts on one- and two-dimensional bifurcations and global bifurcations. Figure 7.14 is included to give an overall effect of the tap changer control.

7.2.4 Bifurcation Analysis for the Rudimentary Power System

In the preceding segments of Section 7.2 a mostly qualitative or numerical discussion of the parameter- and state-space structure of the rudimentary power system was given. Utilizing the low degree of this system it was possible to represent almost everything graphically. This provides a very convenient basis for gaining insight into a very complex situation. Discussion of Figures 7.3 through 7.14 was used for this purpose. The mathematical origin of the illustrations was only briefly mentioned. Now the necessary mathematical background to understand the genesis of the various bifurcation loci in these curves and especially in Figures 7.15, and 7.16 can be provided.

7.2.4.1 Equivalent Smooth Dynamic System Model Achieved Through a Singular Transformation In all the phase portraits that occur in Figure 7.3 to 7.16 a singular surface is present. This singularity is a very physical presence in the sense that no predictable continuation of trajectories will enter its vicinity. Efforts to bridge this by singular-perturbation-type approaches are of dubious reliability, mostly because of the breakdown of quasistationarity and the randomness of the end point of the quasistationary behavior, as will be discussed later. This leaves the components of the state space such as the two half-planes, that is, two *components*, separated by singular line $a-a$ in Figures 7.8 to 7.10 without any structural connection in a physical or engineering sense. Nevertheless, looking at these pictures it appears that a certain structural connection does exist at least in a mathematical sense. This indeed turns out to be the case. Mathematically, the connection is possible by using a special nonlinear transformation, a nonlinear rescaling of time, which smooths out the singularity in a strictly mathematical sense. It should not be forgotten, however, that no physical nature is attributed to this transformation. On the other hand, the mathematical analysis of the entire system is facilitated very effectively by this process. The process itself is carried out in two steps. First, through straightforward algebraic manipulations, the pair of dynamic variables E' and

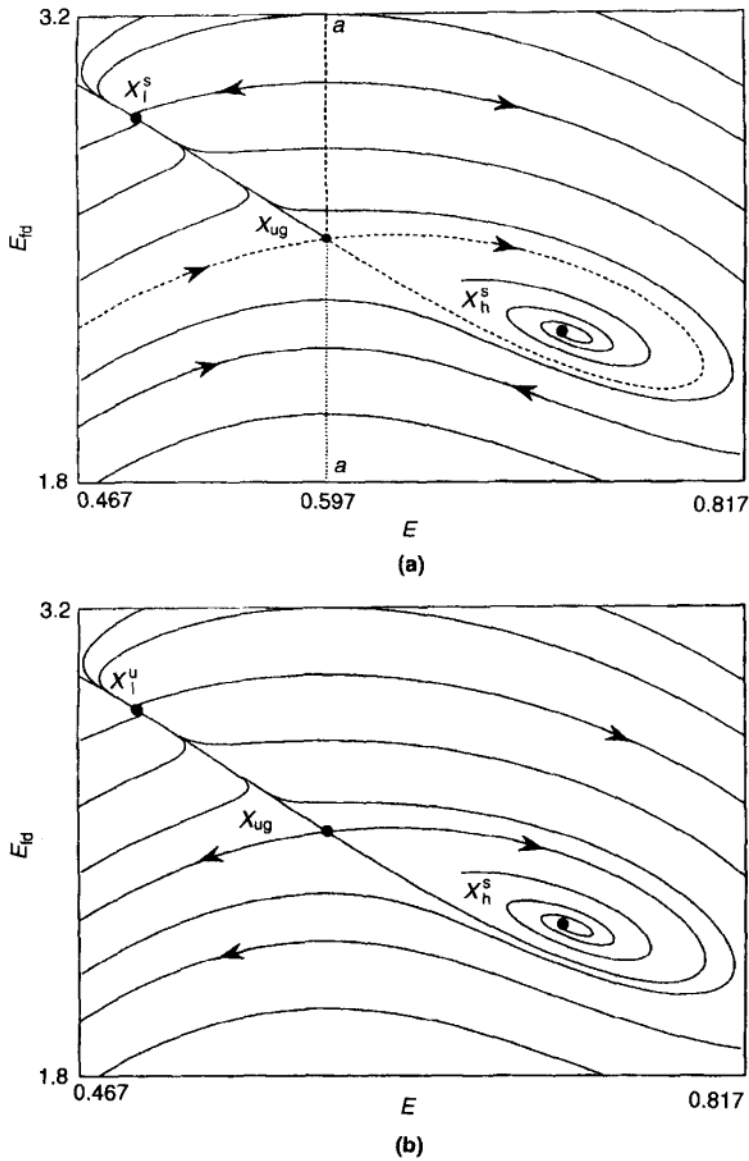


FIGURE 7.15 Phase portraits for (a) the system Z and (b) the system Z^T . The line $a-a$ represents the singularity S .

E'_{fd} as shown in Eqs. (7.30) and (7.31) are replaced by the pair E and E_{fd} , resulting in the following pair of dynamic equations, which replace Eqs. (7.30) and (7.31):

$$\dot{E} = \left(-\frac{x + x_d}{T_{d0}x'_d} v(E, P) + \frac{x - x'_d}{T'_{d0}x'_d} \frac{E^2}{v(E, P)} + \frac{x_d - x'_d}{T'_{d0}} \frac{qP}{v(E, P)} + \frac{E_{\text{fd}}}{T'_{d0}} \right) \frac{1}{v'(E, P)} \quad (7.38)$$

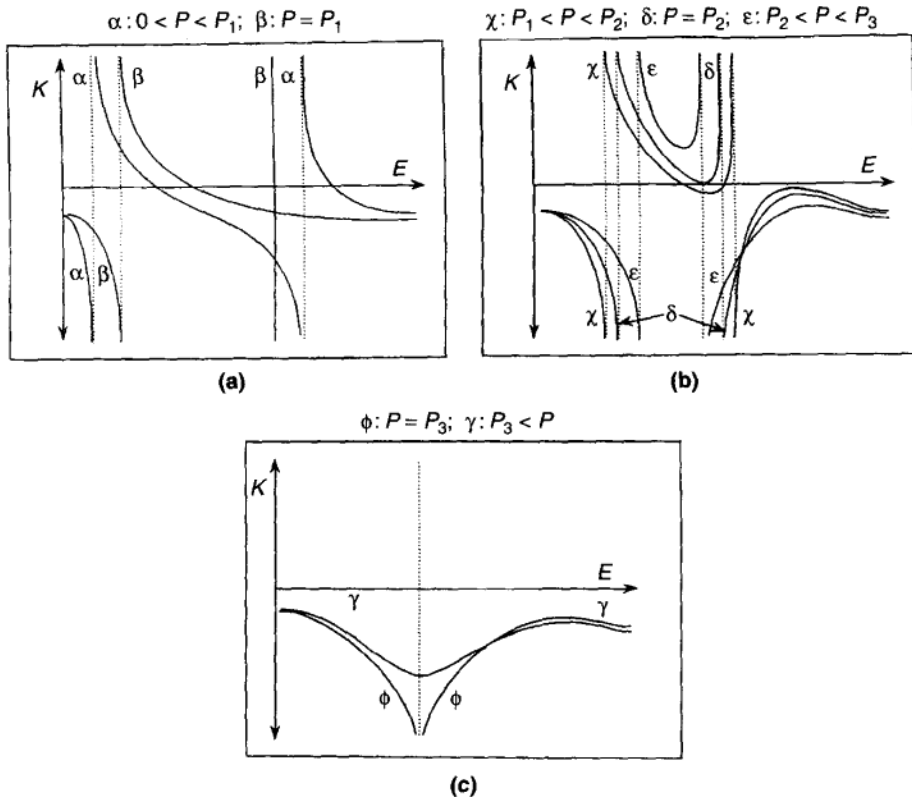


FIGURE 7.16 Cross-sections of the equilibrium manifold EQ .

$$\dot{E}_{fd} = -\frac{E_{fd}}{T} - \frac{1}{T} u(E, P) + \frac{E_{fd}^0 + E_r}{T} \quad (7.39)$$

where

$$E' = v(E, P) = \frac{1}{E} \sqrt{x'^2[P^2 + (qP)^2] + 2x'E^2(qP) + E^4} \quad (7.40)$$

$$E_G = u(E, P) = \frac{1}{E} \sqrt{x^2[P^2 + (qP)^2] + 2x'E^2(qP) + E^4} \quad (7.41)$$

Second, it can be shown that Eqs. (7.38) and (7.39) become singular along the line $v(E, P) = 0$, that is, for

$$E_{sing}^4 = x'^2[P^2 + (qP)^2] \quad (7.42)$$

The singularity can be eliminated by a nonlinear transformation—a rescaling of the time variable t into τ —as follows:

$$\frac{dt}{d\tau} = v'(E(\tau), P) \quad (7.43)$$

where the prime on v' represents partial differentiation with E (this notation will be applied throughout the rest of this subsection). The transformed dynamic equations in τ then read

$$\dot{E} = -\frac{x+x_d}{T'_{d0}x'}v(E, P) + \frac{x_d-x'_d}{T'_{d0}x'_d}\frac{E^2}{v(E, P)} + \frac{x_d-x'_d}{T'_{d0}}\frac{qP+Q_{L0}}{v(E, P)} + \frac{E_{fd}}{T'_{d0}} \quad (7.44)$$

$$\dot{E}_{fd} = \left(-\frac{E_{fd}}{T} - \frac{K}{T}u(E, P) + \frac{E_{fd}^0 + E_r K}{T} \right) v'(E, P) \quad (7.45)$$

Note that, for notational convenience, the same letters E and E_{fd} are used to denote the state variables in Eqs. (7.38), (7.39) and Eqs. (7.44), (7.45) even though the time scale has changed from t in Eqs. (7.38) and (7.39) to τ in Eqs. (7.44) and (7.45) according to the transformation (7.43). Also the dot denotes the time derivative in either t or τ . The phase portrait of the system Σ in Eqs. (7.44) and (7.45) is exactly the same as that of the system given by Eqs. (7.38) and (7.39) except for the following interpretational changes (see Fig. 7.15): (1) The singular line no longer plays a special role. Points on it are now regular points in the state space. (2) The time orientation of the trajectories is reversed to the left of the singular line. (3) The state (E, E_{fd}) moves along the same trajectories but with speeds of, respectively,

$$\frac{dE}{d\tau} = \frac{dE}{dt}v'(E(\tau), P) \quad \frac{dE_{fd}}{d\tau} = \frac{dE_{fd}}{dt}v(E(\tau), P) \quad (7.46)$$

Away from the singularity, the collection of integral curves is identical for the systems given by Eqs. (7.38) and (7.39) and for Σ . In the system given by Eqs. (7.38) and (7.39) the variable E approaches the singular line with infinite speed. For Σ this speed is finite and the speed of E_{fd} at the singular line becomes zero. Hence, at every point where $\dot{E} \neq 0$, the direction field is transversal to the singular line and there exists a unique trajectory passing through this point, connecting half-trajectories on $E < E_{sing}$ with corresponding half-trajectories on $E > E_{sing}$. Therefore, the phase portrait of Σ gives a canonical extension of the phase portrait of the system with singularity given by Equation (7.38) and (7.39) to the singular line. It follows from Eq. (7.44) that at $E = E_{sing}$ the derivative \dot{E} vanishes at a unique point ψ given by

$$E_{fd} = \frac{x+x_d}{x'}v(E_{sing}, P) - \frac{x_d x'_d}{x'}\frac{E_{sing}^2}{v(E_{sing}, P)} - \frac{(x_d - x'_d)gP}{v(E_{sing}, P)} \quad (7.47)$$

This point ψ becomes an isolated equilibrium point for the new system Σ . Observe that for the original system, \dot{E}_{fd} in Eq. (7.39) does not vanish at ψ , so that ψ is not an equilibrium of the original system. This justifies naming ψ a *pseudoequilibrium* point. More general analysis follows.

7.2.4.2 Equilibrium Manifold The static structure of equilibria away from the singular line will be analyzed next. It follows from Eq. (7.45) that when $\dot{E}_{\text{fd}} = 0$, then

$$E_{\text{fd}} = E_{\text{fd}}^0 + E_r k - u(E, P)k \quad (7.48)$$

and substituting this relation into Eq. (7.44) with $\dot{E} = 0$ gives

$$\frac{x + x_d}{x'} v(E, P) - \frac{x_d - x_d}{x'} \frac{E_{x_d}'^2(qP)}{v(E, P)} - E_{\text{fd}}^0 + K(u(E, P) - E_r) = 0 \quad (7.49)$$

Since Eq. (7.48) gives an explicit formula for E_{fd} as function of (E, K, P) , the set of equilibria can be visualized in (E, K, P) space. This set is denoted by EQ and called the *equilibrium manifold* [with the understanding that the E_{fd} component is defined by Eq. (7.48)]. Away from the set $\{(E, P) = E_r\}$, EQ is a smooth two-dimensional manifold. This can be seen by solving Eq. (7.49) for K as

$$K = \frac{1}{E_r - u(E, P)} \left(-E_{\text{fd}}^0 + \frac{x + x_d}{x'} v(E, P) - \frac{x_d - x_d}{x'} \frac{E^2 + x'(qP)}{v(E, P)} \right) \quad (7.50)$$

The geometric shape of EQ will now be summarized in the following statements. The proofs consist of straightforward and elementary, though tedious, manipulations, which will not be included here. Set

$$k_1(E, P) = \frac{1}{E_r - u(E, P)} \quad (7.51)$$

$$k_2(E, P) = \frac{x + x_d}{x_d'} v(E, P) - \frac{x - x_{dd}'}{x_d'} \frac{E^2 + x_d' qP}{v(E, P)} - E_{\text{fd}}^0 \quad (7.52)$$

1. Let P_3 be the (unique) positive root of the equation

$$E_r^4 - 4x(qP)E_r^2 - 4x^2P^2 = 0$$

For $P < P_3$ the function k_1 has two poles $E_{p,\pm}$, which are the positive roots of

$$2E_{p,\pm}^2 = E_r^2 - 2x(qP + QL_0) \pm \sqrt{E_r^4 - 4xqPE_r^2 - 4x^2P^2}$$

For $P = P_3$ a unique pole is given by

$$2E_{p_3,0}^2 = E_r^2 - 2xqP_3$$

and there are no poles for $P > P_3$. The function k_2 is strictly convex for all parameter values. There exists a unique parameter value $P_2 < P_3$ with the property that k_2 has two zeros $E_{z,\pm}$ for $P < P_2$, a double zero for $P = P_2$

and no zeros for $P > P_3$. Furthermore, there exists a unique parameter value $P_1 < P_2$ where $E_{p,+}$ and $E_{z,+}$ cancel in a pole-zero cancellation (Fig. 7.16).

2. Let $P \in (0, P_2)$. Then two load-flow solutions with positive K exist. For $P = P_1$ one of the two load-flow solutions is always given by $E_{p,+} = E_{z,+}$ independently of K . Additional load-flow solutions that represent control with positive feedback exist for negative K (as shown in Fig. 7.16). Some of these are stable, but they are associated with impractical voltage and current combinations.
3. Let $P \in (P_2, P_3)$. Then the function $K(\cdot, P)$ is positive on $(E_{p,-}, E_{p,+})$ and negative on $(0, E_{p,-})$ and $(E_{p,+}, \infty)$. For all $E \in (E_{p,-}, E_{p,+})$ we have that $(\partial K / \partial P)(E, P) > 0$.

Furthermore, K is quasiconvex in E over the interval $(E_{p,-}, E_{p,+})$. In particular, in this interval K has a unique global minimum at the stationary point where $(\partial K / \partial E)(E, P) = 0$. If $K_{\min}(P)$ denotes this minimum value, then there are two load-flow solutions for levels $K > K_{\min}(P)$, a unique one for $K = K_{\min}(P)$ and none for $K < K_{\min}(P)$. There exist no load-flow solutions with K positive for $P \geq P_3$.

Load-flow solutions corresponding to typical control gain values, K , are shown in Figure 7.16, which displays the warping of the $K(E, P)$ curve with a gradual increase of P from 0 to P_3 including the history of transitions at P_1 , P_2 , and P_3 . They imply the shape of the equilibrium manifold EQ (Fig. 7.17).

7.2.4.3 Bifurcation Loci

7.2.4.3.1 Parameter Values, $P_2 < P < P_3$ Here the structure of the equilibrium manifold will be analyzed further for parameter values P between P_2 and P_3 . Let

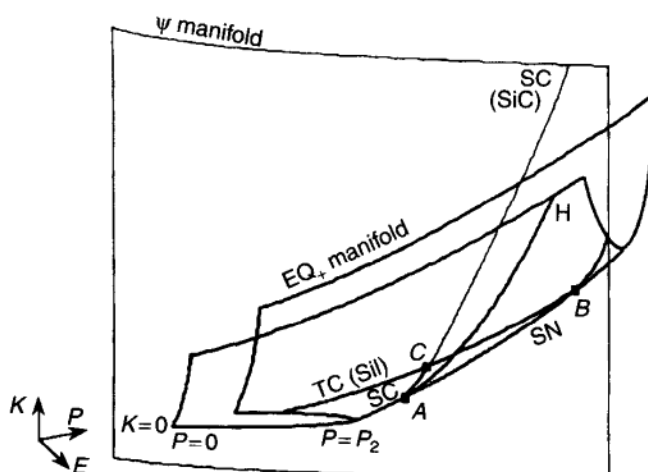


FIGURE 7.17 Bifurcation loci and the equilibrium manifolds.

$$\text{EQ}_+ = \{(E, K, P) \in \text{EQ}: K > 0, P \in (P_2, P_3)\} \quad (7.53)$$

The geometric shape of EQ_+ (Figure 7.16) follows from statements 1 to 3 above. For $P \in (P_2, P_3)$ fixed, the graph of K is strictly quasiconvex and these graphs are increasing with P for E fixed. Let

$$\text{SN} = \{(E, K, P) \in \text{EQ}_+: K'(E, P) = 0\} \quad (7.54)$$

denote the crest of the equilibrium manifold. (Here K' again denotes the partial derivative with respect to E .) Notice that SN divides EQ_+ into two halves (Fig. 7.17). According to the value of the E -coordinate, they will be called the high and low side, respectively. Furthermore, since $(\partial K / \partial P)(E, P) > 0$, the equation $K(E, P) = \text{const}$ can always be solved for P as a function of E . Since

$$\frac{dP}{dE} = -\frac{K'(E, P)}{(\partial K / \partial P)(E, P)}, \quad (7.55)$$

It also follows that this function is increasing for points (E, K, P) on the high side and decreasing for points on the low side. This establishes the structure of the popular PV curves as a slice of constant control gain K (see Fig. 7.17).

In this section, the bifurcation loci on the manifold EQ_+ will be established. The bifurcation diagram given in Figure 7.15 is simply the projection of this set into the parameter space. First the loci where the Jacobian Df of the system Σ given by Eqs. (7.44) and (7.45) has an eigenvalue 0 will be computed. A direct calculation shows that

$$\det(Df)|_{x \in \text{EQ}_+} = \frac{E_r - u(E, P)}{T T'_{d0}} K'(E, P) v'(E, P) \quad (7.56)$$

Since $E_r \neq u(E, P)$ for this parameter range, the only zeros occur for SN and for

$$\text{TC} = \{(E, K, P) \in \text{EQ}_+: v'(E, P) = 0\} \quad (7.57)$$

Each of these loci is the image under the map $K = K(E, P)$ of the graph of a smooth function $E = E(P)$ in (E, P) space. For TC an explicit expression of this function is given by Eq. (7.42), which also shows that this function is increasing in P . For SN the implicit function theorem has to be involved. Since K is strictly quasiconvex, it has a strict minimum at the stationary point. Hence $K''(E, P) > 0$ and so the equation $K'(E, P) = 0$ can be solved for E as a smooth function of P . Verifying that $(\partial K' / \partial P)(E, P)$ is positive, it follows from

$$\frac{dE}{dP} = -\frac{(\partial K' / \partial P)(E, P)}{K''(E, P)} \quad (7.58)$$

that the resulting function is decreasing in P . In particular, there exists a unique point of intersection B of the curves SN and TC .

For the two-dimensional system, the Jacobian Df has a double eigenvalue at zero or purely imaginary eigenvalues if and only if the trace of Df ,

$$\text{tr}(Df) = \frac{\partial f_1}{\partial E} + \frac{\partial f_2}{\partial E_{\text{fd}}}, \quad (7.59)$$

vanishes. The equation $\text{tr}(Df) = 0$ is equivalent to a quartic polynomial equation in E^2 of the form

$$h(E, P) = -h_4 E^8 - h_3 E^6 + h_2 E^4 + h_1 E^2 + h_0 = 0 \quad (7.60)$$

where all the coefficients h_i are positive. The h_i can easily be computed [16]. The function h is the product of $\text{tr}(Df)$ and a positive function. Since there is exactly one change of sign in these coefficients, it follows from Descartes' rule that, for any given P , these equations have a unique positive real root that is simple. Since the polynomial is quartic in E^2 , this root can in principle be calculated explicitly.

Furthermore, because the root is simple, $h'(E, P) \neq 0$ [in fact, $h'(E, P) < 0$ because the coefficient $h_4 > 0$] and so the equation $h(E, P) = 0$ can be solved for E as a smooth function $E = E(P)$. Hence

$$\tilde{H} = \{(E, K, P) \in \text{EQ}_+: h(E, P) = 0\} \quad (7.61)$$

is a smooth curve embedded in EQ_+ . It can also be verified that this function $E = E(P)$ is increasing in P over the parameter range $P_2 \leq P < P_3$ by showing that $(\partial h / \partial E)(E, P)$ is positive at $h(E, P) = 0$ [16]. As a consequence, there also exists a unique intersection of the curve \tilde{H} with SN and this point will be denoted by A . The curves \tilde{H} and TC do not intersect. This can easily be seen by substituting the relation (7.42), which defines TC (Figure 7.17) in terms of the polynomial h . The result is always positive. A sketch of these curves on the equilibrium manifold EQ_+ (together with a curve SC , which will be discussed later) is given in Figure 7.17.

Let H be the portion of \tilde{H} that lies on the high side of EQ_+ . It will now be shown that the curves shown in Figure 7.17 constitute the bifurcation set of the dynamic system Σ . The curves SN , TC , and H correspond to a saddle-node, a transcritical, and a Hopf bifurcation, respectively. In the Σ model, the transcritical bifurcation takes over the role of the singularity induced bifurcation described in Section 7.2.1. All three are local codimension-one bifurcations. The points A and B correspond to local codimension-two bifurcations, and the curve SC indicates a global saddle-connection bifurcation. The *bifurcation diagram* in Figure 7.5 is the projection of these bifurcation loci into the parameter space. In Figure 7.5 the corresponding projected curves are denoted B_{SN} , B_{Sil} (for TC) and B_H , while the labeling of the points is the same. It is an immediate consequence of the geometric shape of the equilibrium manifold that the curves B_H and B_{Sil} are tangent to B_{SN} at points A and B of intersection. Notice that Figure 7.17 gives more precise information about the bifurcation loci since it also identifies whether

the bifurcations are on the low or on the high side. For instance, the curves TC and H do not intersect on EQ_+ , but in the projection into the parameter space an intersection point that was labeled D in Figure 7.5 arises. It is clear from Figure 7.17 that D has no special significance since the corresponding equilibria lie on different sides of EQ_+ . The local codimension-1 bifurcations happen to occur simultaneously at different equilibria. This can, of course, also be seen analytically, but the geometry of the equilibrium manifold and the bifurcation curves beautifully illustrates this point. Also, the popular PV curves are obtained as slices of EQ_+ for constant K . The intersections of these PV curves with the various bifurcation curves on the surface EQ_+ identify the occurrence of the various bifurcations on the PV curve as displayed for various K values in Figure 7.12. These in turn can be connected over a sequence of PV curves at fixed gain values K to present bifurcation loci in the hybrid space composed of P and E .

7.2.4.3.1.1 SADDLE-NODE BIFURCATION The curve SN corresponds to the crest of EQ_+ , that is for P fixed the corresponding K value is the minimum of the function $K(E, P)$ on $(E_{p,-}, E_{p,+})$. It is clear from the geometric shape of the equilibrium manifold that a saddle-node bifurcation occurs along SN. Also, if the control gain K is kept constant and if P is varied as parameter, then Sotomayor's theorem (e.g., in Refs. [21, 24] or Theorem 3.4.1) applies at points $(E, P, K) \in \text{SN}$ where the Jacobian Df has 0 as simple eigenvalue and where a certain technical transversality condition is satisfied. Since the trace of Df vanishes only at A on SN , it follows that all points away from A have 0 as simple eigenvalue (whereas 0 is a double eigenvalue of Df at A). Furthermore, it can be verified that the transversality condition for the saddle-node bifurcation is only violated at the point B [16]. Hence in all points on SN except for A and B a saddle-node bifurcation occurs (see Figure 7.17).

7.2.4.3.1.2 TRANSCRITICAL BIFURCATION For fixed parameters (K, P) , the equation $v'(E, P) = 0$ also defines the singular line in the state space of the original model [see Eqs. (7.30) to (7.32)]. Hence for points in TC one of the two equilibria has merged with the pseudoequilibrium ψ . The pseudoequilibrium ψ gives rise to a second equilibrium manifold shown as Ψ in Figure 7.17. Since the location of ψ is independent of K , Ψ simply is a vertical wall over the curve $v'(E, P) = 0$ in (E, P) space. It intersects EQ_+ in TC and this curve corresponds to the singularity induced bifurcation described in Section 7.2.1. If K is kept fixed and P is varied, then it is again evident from the geometric shape of the equilibrium manifold EQ_+ that a transcritical bifurcation occurs at all points on TC except for B [the two curves of equilibria are given by $\text{EQ}_+ \cap \{K = \text{constant}\}$ and the curve $v'(E, P) = 0$ lifted in the plane corresponding to this level of K]. An analytical justification can be given by verifying the conditions of the transcritical bifurcation theorem (Section 3.4 and Ref. [21]). Like Sotomayor's theorem for a saddle-node bifurcation, this theorem requires that 0 is a simple eigenvalue of the Jacobian Df and that a certain technical transversality condition holds. Since

\tilde{H} and TC do not intersect, 0 is always a simple eigenvalue on TC and it can be verified that, like for SN, the transversality condition is only violated at the point B . Hence the local structure of the phase portraits (in state and parameter spaces) for points near TC is known.

7.2.4.3.1.3 LOCAL CODIMENSION-TWO BIFURCATION AT B — A PITCHFORK BIFURCATION For the parameter values corresponding to the point B , a nongeneric codimension-two bifurcation occurs as a result of a simultaneous occurrence of a saddle-node and a transcritical bifurcation. (Note that both of these bifurcations occur for fixed K when only the parameter P is varied. Therefore this is not a generic situation.) The two equilibria of EQ_+ merge and disappear in a standard saddle-node bifurcation. The saddle-node bifurcation just happens to occur in the same location in the state space that is taken by ψ . The result is a so-called pitchfork bifurcation [21]. The typical pitchfork diagram arises as the intersection of EQ_+ with the equilibrium manifold for ψ in the level set $K = K_B$ corresponding to the value at B .

7.2.4.3.1.4 HOPF BIFURCATION A Hopf bifurcation occurs when the Jacobian Df has a simple pair of complex eigenvalues that cross the imaginary axis (while no other eigenvalues have zero real parts). These conditions hold on H . By construction $\text{tr}(Df) = 0$ on \tilde{H} , and H is the part of \tilde{H} where $\det(Df) > 0$. Hence Df has a simple pair of imaginary eigenvalues on H . Fix K and let P be the varying parameter. Recall that near H the intersection of the cross section $\{K = \text{const}\}$ with the equilibrium manifold can then be described by a decreasing smooth function $E = \tilde{E}(P)$. Furthermore, as was explained earlier, if $(\tilde{E}(P_H), K, P_H) \in H$, then $h'(\tilde{E}, P) < 0$ and $(\partial h / \partial P)(\tilde{E}, P) > 0$ [16]. Therefore

$$\frac{d}{dP} h(\tilde{E}(P), P) = h'(\tilde{E}, P) \frac{d\tilde{E}}{dP} + \frac{\partial h}{\partial P}(\tilde{E}, P) > 0 \quad (7.62)$$

for the parameter value P_H corresponding to H . Since $h(E, P)$ is a positive multiple of $\text{tr}(Df)$, this implies that the eigenvalues of Df cross the imaginary axis from the left to the right, that is, the required transversality condition is satisfied. Hence the Hopf bifurcation theorem (e.g., Ref. [21], Theorem 3.4.2.) applies at every point on H . If a certain coefficient a does not vanish, this theorem gives the existence of a surface of periodic solutions that are stable if $a < 0$ and unstable if $a > 0$. In the appropriate coordinates (x, y) this surface of periodic solutions agrees up to second order with the paraboloid

$$P - P_H = -\frac{a}{d}(x^2 + y^2), \quad d = \frac{d}{dP} \text{Re} [\lambda(P)]|_{P=P_H} \quad (7.63)$$

Up to a positive multiple, d agrees with $(d/dP)[h(\tilde{E}(P), P)]$ and hence is positive. It is well known how to calculate a (e.g., [21, p. 152]) and it can be verified

(numerically) that $a > 0$. It follows that there exist unstable periodic orbits for $P < P_H$ and no periodic orbits for $P > P_H$ for P close to P_H (Figs. 7.9 and 7.10).

At point A in the frontier of H the two purely imaginary eigenvalues merge at zero and Df has 0 as a double eigenvalue. The interplay of the Hopf bifurcation with the saddle-node bifurcation gives rise to a local codimension-two bifurcation at A , which has global consequences. Since both parameters K and P are relevant for this behavior, this is still a generic bifurcation.

7.2.4.3.1.5 LOCAL CODIMENSION-TWO BIFURCATION AT A The curves H and SN intersect in A . The local structure of the bifurcation set and the corresponding phase portraits of the system near A are well understood under certain generic assumptions that relate to the normal form of the dynamic system near the equilibrium (E'_A, E_{fd_A}) [21, Sections 7.2 and 7.3].

If these conditions are satisfied, then periodic orbits are generated (or destroyed) in a saddle connection bifurcation that occurs along a curve SC that originates at the point A . This structure will be analyzed at least numerically, and such analysis of the example system is presented in Refs. [1] and [3] based on Section 7.3 in Ref. [21]. These results establish therefore the local structure of the bifurcation diagram in Figure 7.5 near point A . In Figure 7.17 the curve B_{SC} (near A) has been lifted to a curve SC on the low side of EQ_+ . This, of course, is arbitrary, but it seems reasonable since the homoclinic orbit is homoclinic to the low equilibrium.

7.2.4.3.1.6 GLOBAL PROPERTIES The discussion given in Section 7.2.4.3.1.4 establishes the existence of a curve SC near A with the property that for $(E, K, P) \in SC$ there exists an orbit homoclinic to x_l . This analysis is local and not valid far away from A . Numerical calculations show that the saddle-connection bifurcation persists. For a fixed value of K , unstable periodic orbits are created around the high equilibrium in the Hopf bifurcation (Fig. 7.5). For decreasing P the periods increase and become unbounded for P approaching a value P_{SC} where they change into a homoclinic orbit. For values of K in level 2 of Figure 7.5, this orbit is homoclinic to the low equilibrium (saddle connection); for values of K in higher levels it is homoclinic to the pseudoequilibrium ψ (singularity connection). The switch occurs at the point C , where the low equilibrium and the pseudoequilibrium merge.

Furthermore, for $P \in (P_{SC}, P_H)$ there exists a unique unstable limit cycle and no periodic orbits exist for $P < P_{SC}$. Hence the same behavior that holds near A is valid for all levels K . Currently these statements are only based on numerical evidence not on a mathematical analysis. Also, global aspects of the phase portrait have not been established yet. But our numerical calculations are sufficient to establish the dynamical behavior of the system Σ for the power system over the practically relevant regions of the state and parameter spaces.

7.2.4.3.2 Parameter Values $0 < P < P_2$ The equilibrium structure of the system for all power values P discussed in Section 6.4.2.3.1 is summarized

in Figure 7.17. From the geometric shape of the equilibrium surface and by Sotomayor's theorem, it can be seen that the saddle-node bifurcation occurs at the local minimum of the equilibrium surface EQ in Figure 7.17. Note that the load $P = P_2$ has been defined as the load value when this minimum occurs for $K = 0$, that is, the load that corresponds to a double zero for the EQ surface in Figure 7.17. Then the structure of the equilibrium surface directly implies that the surface EQ has no minima for positive control-gain K values (i.e., negative feedback) when $P < P_2$. Hence the saddle-node bifurcation does not occur for positive control gains for all low loads ($P < P_2$). For $P_1 < P < P_2$ the saddle node occurs at negative control-gain values, and below $P = P_1$, there is no saddle-node bifurcation (as there is no minimum for the surface EQ). So for positive control-gain values, which correspond to the practically interesting case, *the system always has two equilibria* for low loads, that is, when $0 < P < P_2$. Let us restrict the stability analysis which follows next to positive control-gain values $K > 0$.

As shown in the previous subsections, the high equilibrium point x_h is stable up to the saddle-node or Hopf bifurcations, whichever occurs first. The saddle node does not occur in this range as discussed previously. The Hopf bifurcation disappears at the codimension-two bifurcation, point A. For typical system parameter values, the load at point A, P_A , is higher than the load P_2 [16]. Hence, Hopf bifurcations do not occur at these low-load values. So *the high equilibrium point is stable for all practical control gains for low loads* ($P < P_2$).

For the low equilibrium point x_l , the feasibility boundary consists of pieces of saddle-node and singularity-induced bifurcations. Again for the equilibrium point x_l , the saddle node never occurs in this parameter range. The transcritical (or singularity-induced) bifurcation occurs under generic conditions at the points in the zero set TC defined in Eq. (7.57). Define P_{TC}^0 as the load when the transcritical bifurcation occurs at $K = 0$. Then under light-load conditions, that is, for $P < P_{TC}^0$ and $P < P_2$, *the low equilibrium is also stable for all practical control-gain values*.

APPENDIX 7.1: SOME ASPECTS OF THE PHASE PORTRAIT (THE FLOW OF THE VECTOR FIELD)

In this book, the subject is mainly the algebraically constrained system of ordinary differential equations, which is applicable to many problems of the large electric power system including voltage stability. The simpler, unconstrained, problem

$$\dot{x} = f(x, p), \quad x \in X \subset \mathbb{R}^n, \quad p \in P \subset \mathbb{R}^p \quad (7.1.1)$$

is applicable to some models for the angle-stability problem, and its analytical features are quite familiar at least for low-order systems. The summary of these simpler results should be a desirable introduction to the study that follows. The material presented here is mostly based on Ref. [25], in the items project of B.H. Zhang and T.C. Leung advised by Garg Huang and John Zaborszky.

Points where $\dot{x} = 0$, that is, points defined by $f = 0$ are *equilibrium points* (unless they are singular). No closed orbits (limit cycles) occur in the angle

stability problem with viscous damping present [25] (but they do when line resistances are present and are known as *hunting*).

At *stable* or *order-n equilibrium points* x_0^s the Jacobian $J_f = (\partial f / \partial x)$ is non-singular with eigenvalues of nonpositive real parts. J_f is nonsingular on the power system as long as the reference is fixed, for example, a slack-bus phasor voltage, or in other words, as long as any drift of the center of angle is excluded from the state space. Remember that this lowers the dimension of the state space by one or two. Equilibria so defined (nonsingular J_f) are called hyperbolic [21].

On the power system, stability is generally *global*, which means that a unique trajectory (or orbit) $x(t)$ passes through each state x within an open set A_0^s containing a stable equilibrium point x_0^s , which converges to a local neighborhood of x_0^s and hence asymptotically to x_0^s . The open set A_0^s is the *region of attraction* or *stability region* of x_0^s . A_0^s has the full rank n of the state space.

At *unstable equilibrium points* the Jacobian J_f has eigenvalues with positive real parts. If there are j such eigenvalues the unstable equilibrium is order $n - j$. For instance, an $(n - 1)$ -order unstable equilibrium x_0^{n-1} is the source of one pair of unstable trajectories that asymptotically diverge from x_0^{n-1} to either a stable equilibrium point or infinity. These form a line, or one-dimensional manifold, the *unstable manifold* of x_0^{n-1} . For an $(n - j)$ -order unstable equilibrium point, there is a j -dimensional unstable manifold composed of trajectories diverging from x_0^{n-j} . The remaining $(n - j)$ -dimensional subspace is composed of trajectories converging to x_0^{n-j} . These then form the *stable manifold* of x_0^{n-j} .

It was shown [25, 26] that the stability boundary around the open stable manifold of $(n - j)$ -order equilibria is a union of $(n - j - 1)$ -degree stable manifolds (open) of $n - j - 1$ equilibria with the boundaries of the latter being supplied in hierarchical order by the $n - j - 2, n - j - 3, \dots$ equilibria. Such a structure is known in mathematics as a stratification. The conceptual sketch of Figure 7.18 attempts to depict this situation graphically for an angle-stability problem. The stable equilibria of order- n equilibria reside uniquely within tubelike structures because the angle variable is periodic (trajectories are functions of $\delta \pm k2\pi$). Hence the region of attraction is bounded in δ between $+\pi$ and $-\pi$ but unbounded in $\dot{\delta}$. Most of the boundary is supplied by the stable manifolds of the x_0^{n-1} unstable equilibria (shown as surfaces in Fig. 7.18). The single unstable trajectories of the $n - 1$ equilibria enter the region of attraction of x_0^s and converge there along with the multitude of trajectories coming in through the pipe. The "cracks" so to speak, between the boundary components around each $n - 1$ equilibrium are filled by stable manifolds of $n - 2, n - 3, \dots$ equilibria in a hierarchy (such a structure identifies a stratification). It is hoped that Figure 7.18 will help to understand this hierarchy. However, Figure 7.18 must be interpreted very cautiously since it is an attempt to give intuitive insight into a multidimensional situation through a perspective view of three-dimensional representation.

In addition to equilibria being hyperbolic, it is assumed in the preceding, as usual, that various stable manifolds intersect transversely as sketched in Figure 7.18 (they are not tangential) and that these assumptions will apply in the following discussion unless otherwise specified. For more details, see [26].

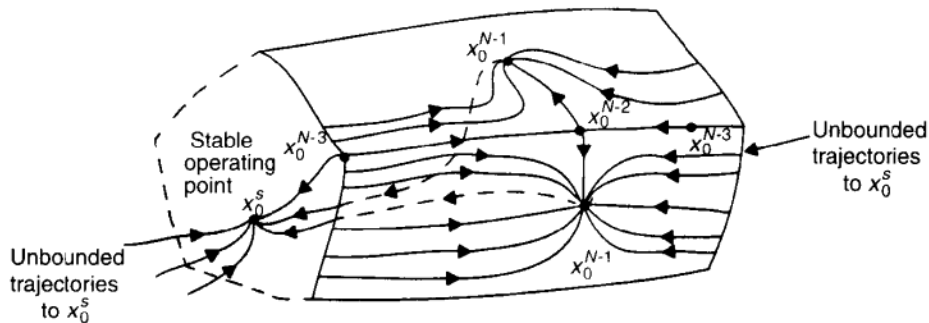


FIGURE 7.18 Qualitative sketch of the structure of the phase portrait of the power system.

Note that not every open set in the state space composed of trajectories contains an equilibrium point. In the absence of such a point trajectories in such sections do not converge (start and end at infinity).

In summary, as it may be in angle stability, the state space is divided by stability boundaries into open stability regions or regions of attraction and regions where trajectories do not converge. No equilibria reside in the latter regions. Stability boundaries are composed hierarchically from stable manifolds of unstable equilibria of descending orders. Interested readers may wish to study Ref. [25] for full detail.

This orderly structure is disturbed when the set $g = 0$ is nonempty, that is, when there are explicit algebraic constraints present. This is the case of prime interest for voltage stability, which is the subject here. The principal difference is the appearance in the state space of another element. Singular surfaces or manifolds join the stable and unstable manifolds. The latter are smooth surfaces consisting entirely of smooth trajectories. By contrast on singular surfaces that state is not defined. On the other hand, such surfaces play a variety of roles. They can be sources or sinks of trajectories; they also can form segments of stability boundaries. It is the objective of part of this chapter to unravel the structural features of the state space for this situation. While the preceding description of the structure of the region of attraction is rather complex and may appear baffling at first sight, it will be evolving in the next chapters through a series of studies designed for gradually developing insight and theoretical knowledge. Interested readers may wish to study [25].

APPENDIX 7.2: SOME ASPECTS OF BIFURCATIONS

Because of the large role played by bifurcations on the parameter space and since these concepts are relatively less current in the engineering experience, a summary sketch of types of bifurcations encountered in this chapter follows here. Readers seeking deeper background are referred to the mathematical literature, particularly [21, 27] namely, local and global.

Local Bifurcations

Local bifurcations occur when the character of an equilibrium changes within an arbitrarily small local neighborhood of a critical parameter set. Local bifurcations can be further classified depending on the specific way in which the critical parameter value is defined. Local changes of this type are often effectively studied by analyzing changes of the eigenvalues in response to parameter variations.

Studying the effects of variation of a single parameter, $\mu \in P$, on the structure of the eigenvalues is most effectively done by using a generalized form of the popular root-locus technique. In a conventional root (i.e., eigenvalue) locus the parameter is $\mu = k$, that is, the control gain. As applied here the parameter will be any single system or operating parameter of the power system but the branch of the locus connected with the bifurcation still will track the movement of one critical real eigenvalue or a pair of complex eigenvalues (Fig. 7.19). Moreover, note that since the model here is nonlinear the equilibrium point itself is changing continuously along the root locus. Movements of the other eigenvalues are not shown but in some situations it could be also advantageous to study these other root locus branches.

The various types of local bifurcation points generally will form surfaces or manifolds in the multidimensional parameter space. These surfaces serve in the parameter space as boundaries separating regions where a certain type of system operation (as characterized by equilibria and trajectories) persists. A point on such a surface can be identified by fixing one parameter or coordinate $\mu = \mu_0$ (a specific choice of many possibilities). In recognition of this fact these bifurcations are designated as *codimension one*. Important events also take place at intersections of two or more bifurcation surfaces. Two or more parameters or coordinates must be specified to designate a point on such an intersection. Hence these will be designated as *codimension-two* bifurcations.

The separation of the state space into components of regular points and singular surfaces as described previously must be considered. It does make a

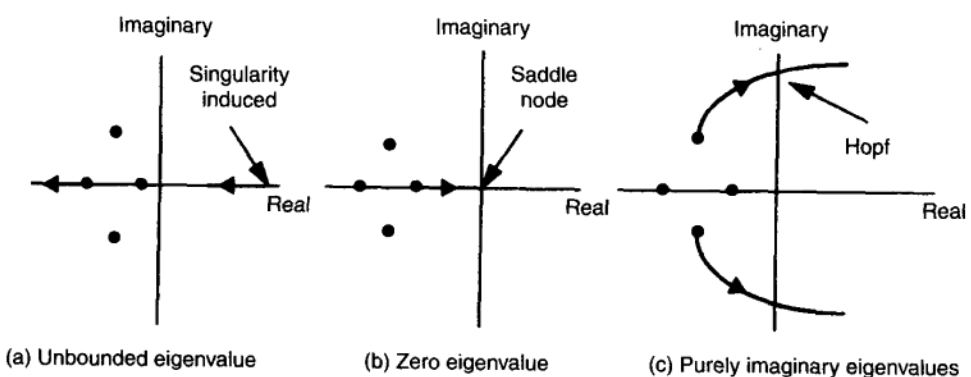


FIGURE 7.19 Locus of the eigenvalues for varying parameter near the three local bifurcations operating on the feasibility boundary.

major difference in which of these two state-space regions the bifurcation actually takes place, even though the bifurcation locus is defined in the parameter space.

1. Local codimension-one bifurcations

- A. Bifurcations at regular points (points within one component C) of the constraint surface where the Jacobian of the constraint surface $J_g = (\partial g / \partial y)$ is nonsingular.
 - i. *Saddle-node bifurcation* [Fig. 7.19(a)]; see Ref. [4]. The Jacobian of the system,

$$A = \frac{\partial f}{\partial x} - \frac{\partial f}{\partial y} \left(\frac{\partial g}{\partial y} \right)^{-1} \frac{\partial g}{\partial x}$$

has a (geometrically) simple eigenvalue with right eigenvector v and left eigenvector w , and there is no other eigenvalue in the imaginary axis. Furthermore, the following inequality conditions called the “transversality conditions” [21] are satisfied:

$$\omega^T A \neq 0 \quad (7.2.1)$$

and

$$\omega^T \frac{\partial A}{\partial x} (v, v) \neq 0 \quad (7.2.2)$$

- ii. *Hopf bifurcation* [Fig. 7.19(b)]; see Refs. [11, 28]. The Jacobian A of the system has an algebraically simple pair of purely imaginary eigenvalues and there are no other eigenvalues on the imaginary axis. As the parameter changes, certain inequality conditions need to hold that ensure that this pair of critical eigenvalues crosses the imaginary axis. They can be formulated as

$$\frac{\partial}{\partial \mu} \operatorname{Re} [\lambda(\mu)] \neq 0 \quad (7.2.3)$$

where $\operatorname{Re}(\lambda)$ denotes the real part of the eigenvalue λ , which moves across the imaginary axis, and $(\partial / \partial \mu)$ denotes the derivative with respect to the parameter μ .

- B. Bifurcations at singular points (points within the singular surface S) of the constraint surface (J_g is singular).

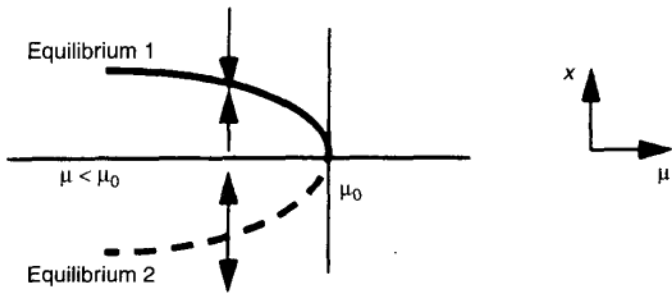
- i. *Singularity-induced bifurcation* Fig. 7.19(c), [3]. A singularity-induced bifurcation occurs when one real eigenvalue (or one pair of pure imaginary eigenvalues) of A moves from the left to right half-space or vice versa by diverging through infinity (and when certain inequality conditions are satisfied that guarantee the least degenerate behavior). The precise conditions are given in [2, 16, 29]. Figure 7.19 reveals some of the details of the movements of the critical eigenvalues over the

three special cases A i, A ii, and B i. Figure 7.20 gives a conceptual sketch of the accompanying events for the saddle-node and Hopf bifurcations. The singularity induces bifurcation—first analyzed by us—is more complex and interested readers are referred to Ref. [3]. For saddle-node and Hopf bifurcations, assume without loss of generality that the operating point under consideration is locally stable or stable against small signals that is, all eigenvalues lie in the open left-half complex plane. Then, in general, when the bifurcation occurs within a component C in the state space, the critical eigenvalues will be shifting toward the imaginary axis as μ approaches μ_0 and will reach the imaginary axis at $\mu = \mu_0$ either at the origin $\lambda = 0$ or at a pair of imaginary eigenvalues (Fig. 7.19).

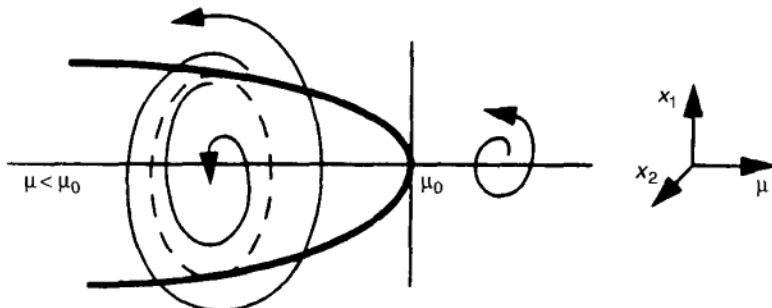
1. Saddle-node bifurcation. At a saddle-node bifurcation [Figs. 7.19(a) and 7.20(a)] by the Sotomayor theorem [21] the root locus ends at $\mu = \mu_0$ and at the origin. In other words, the equilibria connected with λ cease to exist when μ moves beyond μ_0 . Correspondingly in the state space x , two equilibria approach each other as μ approaches μ_0 ; then at μ_0 they fuse in a nonhyperbolic equilibrium (with a zero eigenvalue at $\lambda_{C_z} = 0$). The latter disappears as μ moves beyond μ_0 .

Under certain additional transversality (nondegenerate) conditions, the presence of the simple zero eigenvalue of the Jacobian essentially characterizes this bifurcation. In second-order systems, this bifurcation corresponds to the annihilation of a saddle point and a node, hence the name saddle-node bifurcation. A conceptual sketch depicts this situation in Figure 7.20(a). Note that this sketch combining a state x and a parameter μ can be seen as a generalized form of the popular $P-V$ curve. There is no equilibrium solution (for the second-order system) beyond $\mu = \mu_0$.

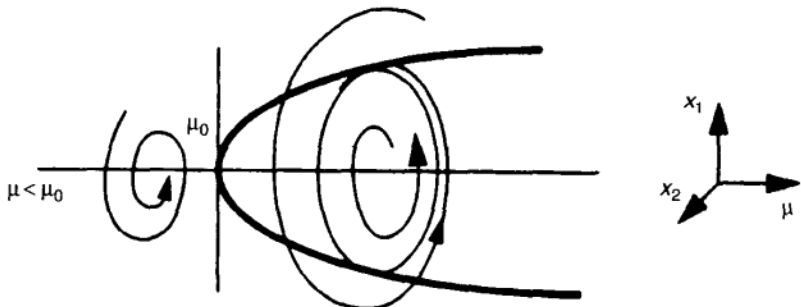
2. Hopf bifurcation. When a parameter μ reaches a *Hopf bifurcation* at $\mu = \mu_0$, the system has a Jacobian with a pair of pure imaginary eigenvalues. Typically, this means that for $\mu \neq \mu_0$ the system has an equilibrium and a closed trajectory; a limit cycle [Figs. 7.20(b) and 7.20(c)] exists near this equilibrium for one side of the parameters ($\mu > \mu_0$ or $\mu < \mu_0$). This limit cycle can be unstable (or stable), that is, trajectories diverge (converge) from (to) it from both the inside and the outside. The inside trajectories converge to (diverge from) a stable (unstable) internal equilibrium point. In Figure 7.20(b), the limit cycle is unstable and the internal equilibrium is stable. As μ approaches the critical value, μ_0 , the limit cycle shrinks into the stable equilibrium within. After passing μ_0 only the unstable region outside the limit cycle survives, now as a regular (hyperbolic) unstable equilibrium point [Fig. 7.20(b)]. Hence the local effect is that the stability of the equilibrium at the origin is destroyed at μ_0 . Conversely there may be an unstable equilibrium surrounded by a stable limit cycle in the



(a) Saddle node bifurcation



(b) Hopf bifurcation – subcritical (unstable limit cycle)



(c) Hopf bifurcation – supercritical (stable limit cycle)

FIGURE 7.20 Conceptual sketch for two of the local bifurcations occurring on the feasibility boundary.

right-half plane and a single real stable node on the left. Then this is known as a supercritical Hopf bifurcation. Therefore, the supercritical Hopf bifurcation corresponds to a transition in the system operating condition from a small-signal stable equilibrium point for $\mu < \mu_0$, and a small-signal stable limit cycle for $\mu > \mu_0$. That is, when the system undergoes a supercritical Hopf bifurcation at $\mu = \mu_0$, the system operating condition changes to sustained oscillation for $\mu > \mu_0$. This type of supercritical Hopf bifurcation appears and plays a fundamental role in

the oscillating event experienced by Union Electric in 1992. Accordingly, Hopf bifurcations are classified as subcritical and supercritical according to the dynamic behavior. At a subcritical Hopf bifurcation [Fig. 7.20(b)], an unstable periodic orbit shrinks into a stable equilibrium to disappear and only an unstable equilibrium survives. For a supercritical Hopf bifurcation [Fig. 7.20(c)], this scenario is reversed. Now a stable equilibrium becomes unstable, and a stable periodic orbit is created at the bifurcation.

3. Singularity-induced bifurcation with one real eigenvalue. When a parameter μ approaches a critical value μ_0 for a singularity-induced bifurcation, the system equilibrium x_0^s approaches a singular point (surface) in the state space. Typically, after passing the singular point, the stability order of the equilibrium changes by one. In systems up to second order this amounts to reversal of stability x_0^s to instability x_0^u , or vice versa [see Fig. 7.20(d)].

Figures 7.19(c) and 7.20(d) reveal that the system response becomes faster and faster as the value of μ is approaches μ_0 and hence the singularity S where system behavior becomes unpredictable and λ_S becomes zero. Events become more complex for systems of order higher than 2.

4. Singularity of complex eigenvalues. This case is included here for the sake of completeness, although it appears to occur only in degenerate situations. The figures reveal that the system behavior in this case is not fundamentally different from case 3 with only one critical eigenvalue. Of course, with two imaginary eigenvalues, the system responses now will be oscillatory, and the phase portraits change from nodes and saddles to foci.

The preceding gives an intuitive summary of what occurs at the various bifurcations. Mathematical details and practical conditions are given precisely in Section 8.2.

Global Bifurcations

Unlike a local bifurcation, global bifurcations are characterized by global changes in the trajectories. The local behavior of the system near the equilibria remains unchanged.

In two characteristic examples of such global bifurcations, two equilibria in a *saddle-connection bifurcation* may be involved [Figs. 7.21(a) to 7.21(c)] or one equilibrium and a singular boundary in the state space in a *singularity-connection bifurcation* [Figs. 7.21(d) to 7.21(f)]. In either case, the stable equilibrium (a focus) remains unchanged in character while parameter μ_0 passes through the bifurcation value. Also unchanged in their nature is either the unstable saddle or the singular boundary. So these cases certainly differ from the local bifurcation of Figures 7.20 and 7.22. The change here is global in the sense that it alters the overall pattern of the trajectories away from either equilibrium (or singularity).

Specifically, in the *saddle-connection bifurcation* with increasing μ , a stable trajectory from the saddle closes back on itself and returns to the saddle as an

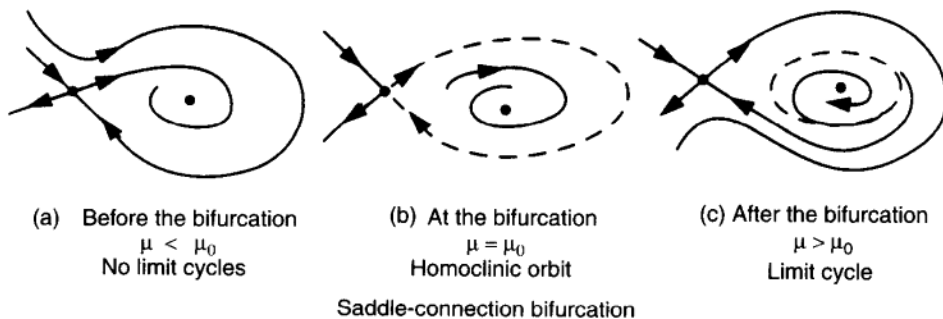


FIGURE 7.21 Two examples of global bifurcation.

unstable one. A *homoclinic orbit* results, which is closed except for the saddle point itself. It could be viewed as a limit cycle with infinite cycle time. In fact, with increasing μ , that is, after the bifurcation in Figures 7.21(a) to 7.21(c), a regular limit cycle peels off of the homoclinic orbit and is gradually shrinks with further increase of μ , usually ending in a Hopf bifurcation. Note that throughout the sequence depicted in Figures 7.21(a) to 7.21(c) there was no change in the characters of the local field near either equilibrium.

When a singular boundary is present trajectories may originate from the singular boundary and also terminate on it as shown in Figures 7.21(a) to 7.21(c) for $\mu < \mu_0$. With changing μ the starting and end points may coalesce at some $\mu = \mu_0$ value, generating an orbit rather like a homoclinic orbit. Thus a sequence such as Figure 7.21(c) results for a *singularity-connected bifurcation*. In fact, it will be seen later that the character of the two global bifurcations becomes indistinguishable when a singular transformation is applied to the system.

The various types of local bifurcation points generally will form surfaces or manifolds in the multidimensional parameter space. These surfaces serve in the parameter space as boundaries separating regions where a certain type of system operation (as characterized by equilibria) persists. A point on such a surface can be identified by fixing one parameter or coordinate $\mu = \mu_0$ (a specific choice of many possibilities). In recognition of this fact these bifurcations are designated as *codimension 1*.

Important events also take place at intersections of two or more bifurcation surfaces. Two or more parameters or coordinates must be specified to designate a point on such an intersection. Hence these will be designated as *codimension 2* bifurcations. Interested readers may like to study Refs. [21, 25]. For examples, see Refs. [1, 2, 4, 18].

BIBLIOGRAPHY

1. Venkatasubramanian, V., Schättler, H., and Zaborszky, J., Global voltage dynamics: Study of a generator with voltage control, transmission and matched MW load, Proc. 29th IEEE Conf. Decision Control, Honolulu, Hawaii, 1990, pp. 3045–3056.

2. Venkatasubramanian, V., Schättler, H., and Zaborszky, J., A taxonomy of the dynamics of the large electric power system with emphasis on its voltage stability, *Proc. NSF Intl. Workshop Bulk Power Syst. Voltage Phenom.—II*, 1991, pp. 9–52.
3. Venkatasubramanian, V., Schättler, H., and Zaborszky, J., Voltage dynamics: Study of a generator with voltage control, transmission and matched MW load, *IEEE Trans. Automatic Control*, 1717–1733, 1992.
4. Kwatny, H. G., Pasrija, A. K., and Bahar, L. Y., Static bifurcations in electric power systems: Loss of steady state stability and voltage collapse, *IEEE Trans. Circuits Syst., CAS-33*: 981–991, 1986.
5. Schlueter, R. A., Hu, I., Whang, M. W., Barry, R., Arndt, C., Ray, R., and Podwoiski, N., Reactive supply on-line security criteria, *Proc. Bulk Power Syst. Voltage Phenom.—Voltage Stability and Security*, Potosi, MO, 1988, pp. 7.1–7.39.
6. Zaborszky, J., Some basic issues in voltage stability and viability, *Proc. Bulk-Power Voltage Phenom.—Voltage Stability Security*, *Proc. NSF Intl. Workshop Bulk Power Syst. Voltage Phenom.—II*, Potosi, MO, 1988, pp. 1.17–1.60.
7. Zaborszky, J., and Rittenhouse, J. W., *Electric Power Transmission*, Reynolds 1954. Available in paperback at Rensselaer University Bookstore, Troy, NY.
8. Abed, E. H., and Varaiya, P. P., Nonlinear oscillations in power systems, *Intl. J. Electric Power Energy Syst.*, **6**: 37–43, 1984.
9. Sauer, P. W., and Pai, M. A., Power system steady state stability and load-flow Jacobian, *IEEE Trans. Power Syst.*, **PAS-5**: 1374–1383, 1990.
10. Salam, F. M. A., Marsden, J., and Varaiya, P. P., Arnold diffusion in swing equations of a power system, *IEEE Trans. Circuits Syst.*, **30**: 199–206, 1984.
11. Abed, E. H., Alexander, J. C., Wang, H., Hamdan, A. M. A., and Lee, H.-C., Dynamic bifurcations in a power system model exhibiting voltage collapse, *Proc. IEEE Intl. Symp. Circuits Syst.*, San Diego, CA, 1992, pp. 2509–2512.
12. Hill, D. J., Hiskens, I. A. and Mareels, I. M. Y., Stability theory of differential/algebraic models of power systems, Technical Report No. EE8941, University of New Castle, Australia.
13. Hiskens, I. A., and Hill, D. J., Energy function, transient stability and voltage behavior in power systems with nonlinear loads, *IEEE Trans. Power Syst.*, **4**: 1525–1533, 1989.
14. Venkatasubramanian, V., Schättler, H. and Zaborszky, J., A stability theory of large differential algebraic systems—A Taxonomy, Report No. SSM 9201, Washington University, Dept. of Systems Science and Math., St. Louis, MO.
15. Sauer, P. W., and Pai, M. A., Modeling and simulation of multimachine power dynamics, in C. T. leondes (ed.), *Advances in Control and Dynamics Systems*, New York: Academic, 1991, Vol.43.
16. Zaborszky, J., and Zheng, B., Structure features of the dynamic state space for studying voltage-reactive control, *Proc. Power Syst. Comput. Conf.*, Graz, Austria, 1990, pp. 319–326.
17. IEEE Committee Report, *Excitation system models for power system stability studies*, *IEEE Trans. Power Apparatus Syst.*, **PAS-100**: pp. 494–509, 1981.
18. Hill, D. J., and Mareels, I. M. Y., Stability theory for differential/algebraic systems with applications to power systems, *IEEE Trans. Circuits Syst.*, 1416–1423, 1990.
19. Brenan, K. E., Campbell, S. L., and Petzold, L. R., *Numerical Solution of Initial Value Problems in Differential-Algebraic Equations*, Amsterdam: North-Holland, 1989.

20. Guckenheimer, J., and Holmes, P., *Nonlinear Oscillations, Dynamical Systems and Bifurcations of Vector Fields*, New York, Springer, 1983.
21. Kalinowsky, S. A., and Forte, M. N., Steady state load-voltage characteristic field tests at area substations and fluorescent lighting component characteristics, *IEEE Trans. Power Apparatus Syst.*, **PAS-100**: 3087–3094, 1991.
22. Venkatasubramanian, V., Jiang, X., Schättler, H., and Zaborszky, J., Current status of the taxonomy theory of large power system dynamics—DAE systems with hard limits, L. H. Fink (ed.), *Proc. NSF Intl. Workshop Bulk Power Syst. Voltage Phenom. — III*, Davos, Switzerland, 1994, pp. 15–103.
23. Palis, J. Jr., and de Melo, W., *Geometric Theory of Dynamical Systems, An Introduction*, New York: Springer, 1982.
24. Zaborszky, J., Huang, G., Zheng, B. H., and Leung, T. C., On the phase portraits of a class of large nonlinear dynamic systems such as the power system, *IEEE Trans. Automatic Control*, **33**: 4–15, 1988.
25. Chiang, H.D., Hirsch, M., and Wu, F., Stability regions of nonlinear autonomous dynamical systems, *IEEE Trans. Automatic Control*, **33**: pp. 16–27, 1988.
26. Chow, S.-N., and Hale, J. K., *Methods of Bifurcation Theory*, New York: Springer, 1982.
27. Rajagopalan, C., Sauer, P. W., and Pai, M. A., An integrated approach to dynamic and static voltage stability, *Proc. Am. Control Conference*, 1989, pp. 1231–1235.
28. Venkatasubramanian, V., *A taxonomy of the dynamics of large differential-algebraic systems such as the power system*, Ph.D. thesis Washington University, St. Louis, MO, August 1992.
29. Venkatasubramanian, V. and Zaborszky, J., Dynamics of Large Constrained Nonlinear Systems—A Taxonomy theory. Invited paper in the Special Issue of the IEEE Proceedings, Vol. 83, Nov. 1995, pp. 1530–1561.

8 Smooth Nonlinear Dynamics of the Large Power System

In Chapter 7 we have analyzed in detail the dynamics, that is, the state- and parameter-space behavior of a second-degree (minimal) and a third-degree (rudimentary) power system. These simplified examples with still highly recognizable physical features were used actually to introduce the various features and concepts of the constrained general power system for examples in which everything can be tied to physical and graphical representations. Although both the minimal (Sec. 7.1) and the rudimentary (Sec. 7.2) examples are formulated as voltage dynamic problems, the reader should know that this text is not limited to voltage stability in any sense. The same arguments could have been presented for examples of angle dynamics. Chapter 8 will be presented in a general form not biased to either the angle or voltage side. In fact, the results are applicable to any constrained dynamic system with smooth differential equation models, although the motivation is clearly that of the power system. It is hoped that with the preparation of Chapter 7 (and possibly with perusal of its two Appendixes written in casual style) the reader will find the contents of Chapter 8 to be enlightening and a useful foundation for work on the dynamics of the large nonlinear system with constraints.

Two types of constraints are of major importance on the power system.

1. *Smooth “algebraic” constraints* such as those of the transmission network power-flow or load-flow equations. These will be discussed in Chapter 8.
2. *Hard limits* (or inequality constraint) such as limits on certain control outputs or maximum generator output or tap chargers. These will be discussed in Chapter 10.

Interestingly these two types of constraints, although being quite different in their overall effect, also share basic features. For instance, both produce a two-level structure both in the state and parameter spaces as we shall see. Also, both can lead to sustained oscillations, that is, limit cycles in the general dynamic analysis in Chapter 10.

No restriction is assumed for the overall system structure except the generic and commonly understood separation into a network, coupling the individual buses and the sets of equipment (generator, transformer, composite load, SVC, HVDC, FACTS, etc). These components are coupled at individual buses but disjoint from bus to bus as sketched in Figure 7.1 and described

in Figures 3.1 to 3.3. This illustration also exhibits the presence of various mathematical languages in which the system states and parameters are described in various segments of the system that is, quasistationary phasors (Chapter 2) or time-varying phasors (Chapter 11), Blondel-type direct- and quadrature-axis components (Chapter 3), or direct time-domain simulation (Chapter 2). In other words, these languages are discussed in detail in preceding chapters. Structural subdivisions such as the generating station, area, and power pool enter naturally into the formulation of the problem for the analysis by the theory presented in Chapter 8.

The inherent division into network and station equipment results in part from the structural differences [network structure $0 = g(x, y, p)$ versus buswise decoupled structure $\dot{x} = f(x, y, p)$] and in part from the fact that in many problems the network equations are effectively instantaneous (their transients in traveling waves are very fast compared to those for the station equipment). This leads to system models composed of ordinary differential equations under differential, “algebraic” equation constraints (DAEs), which are mostly studied in this chapter.

Of course, the DAE model is a very close approximation at most points of the parameter space where the state trajectories are dominated by the solutions of the DAE equations (Fig. 8.1). However, in a band around the singular points of the DAE (where its set of equations is not invertible for the network states), the solution of the DAE model loses its dominance or validity for either or both of two reasons.

1. Physically in this area, the trajectories are dominated by the very fast modes associated with capacitance and inductance and with the traveling waves for the transmission lines. If these are neglected as customary (and justified outside these regions), then the DAE solution loses physical validity in this region. The fast moving parts of the system could be included in the model symbolically but not in practical reality.
2. If the DAE model is written in quasistationary phasors (Chapters 2 and 9) as customary, then this model loses validity because the quasistationary (that is, slow) assumption is grossly violated in these regions of physically fast movements. Hence any solutions based on quasistationarity lose their validity and the entire model fails. One consequence is that the condition of the trajectories across the singular surface cannot in general be identified.

This raises important and often overlooked problems with singular perturbation, which is the alternative approximation for the DAE formulation. These will be discussed in Section 8.1.4 and elaborated later in the book.

A comprehensive theory providing solutions within the scope described can realistically deal with essentially all dynamic problems of the real-life large power system in a practical way. Such a theory of large proportions was introduced within this decade for the first time in a sizable literature under the name of taxonomy theory.

The first phase of this project, mostly in the late 1980s, produced an organized analysis of the state-space behavior of systems modeled by smooth nonlinear differential equations. Results of this phase are summarized in Appendix 7.1. Attributions are given in the Introduction of Chapter 7.

The second phase is concerned with the realistic DAE model of sets of nonlinear differential equations constrained by nonlinear “algebraic” (i.e., nondifferential) equations. Extensive progress was made in the thesis of V. Venkatasubramanian, who was advised by professors H. Schättler and John Zaborszky. V. Venkatasubramanian was the primary contributor to the mathematical theory of differential-algebraic equations and his research collaboration with Washington University continued after his graduation when he moved to Washington State University. Students Xin Jiang and Kiyong Kim later joined the project and worked under the guidance of J. Zaborszky, Heinz Schättler, and V. Venkatasubramanian whose key advising, particularly for Xin Jiang, continued after he moved to WSU.

Most of the material in this chapter comes from Refs. [1 to 5, 46 and 59]. Specific attributions will be made where appropriate for the individual sections, including other work in the literature dealing with some of the details covered by this recent theory.

Most of the material presented in this chapter is applicable to any large nonlinear DAE system, and such DAE problems will occur across all time ranges of the power system. Accordingly the presentation in Section 8.2 is in general terms, although the power-system interactions and motivations are noted throughout. Some of the general issues connected with the power system will now be pointed out.

Security of System Operation: Security Region

The power system is considered *secure* if it has regions of feasibility, viability, and transient stability of adequate shape and size such that (1) continued system operation is ensured, (2) the system is returned to the operating point, or (3) (in case of equipment loss) the shift occurs to an alternate feasible, viable, and transiently stable equilibrium point following any “first contingency” from a prespecified set of first contingencies. The following definitions hold.

1. *Viability*, that is, all voltages, currents, frequency, etc., are within the applicable tolerances. This defines an open *viability region* V in the parameter space.
2. *Feasibility*, that is, the operating point exists as a locally (in the mathematical sense) stable equilibrium that is continuously movable as such over an open *feasibility region* F in the parameter space.
3. *Transient stability*, that is, when subjected to any of a specified set of (first) contingencies, trajectories converge back to the operating point. This defines an open *transient stability region* in the parameter space.

In other words, the *region of security*, that is, the safe operating region, is defined as the intersection of the regions of viability, transient stability, and feasibility. Our attention here will be devoted primarily to feasibility and transient stability because viability has no direct dynamic features.

Note that all three of these concepts need to be defined in the cross section of the state and parameter spaces but we will often study their projections in one or the other space. Note that transient stability is a special and traditional term in the power system in that it depends on a set of specified contingencies. This term will be used in its traditional meaning within this book. Specifically an equilibrium point, say, x_s , is transient stable if the system converges back to the stable equilibrium condition after it is subjected to any one of a specified set of first contingencies. This implies that the postcontingency initial state lies within the region of attraction of a suitable stable equilibrium point for the post-contingency parameter values. This postulates a knowledge of the stability boundary of the relevant region of attraction for checking transient stability, which is a difficult problem analytically and computationally. Traditionally, transient stability is evaluated without knowing the stability boundary by numerically computing the pre- and postcontingency trajectories.

In this chapter, issues connected with system security including computation of the above boundaries with mathematical precision and practicality are studied extensively.

Direct Method

A very large effort has been in progress for decades in the literature (hundreds of papers illogically referred to as the *direct* method) to “bypass” the trajectory computation by various approximations often connected with Lyapunov theory and to estimate the minimum distance to the security margin, from the postcontingency state to the stability boundary (an often restrictive sufficient condition). This book is not directly concerned with this part of the literature. The emphasis here is on establishing the precise structure of the stability boundary. Equipped with this knowledge of boundary composition, suitable approximations of the boundary can be developed. Some developments in this direction [6] are discussed here.

Limits on the Validity of Using Singular Perturbations on Conventional Phasor Models

In Chapter 11, we observe the limitations connected with the conventional quasistationary phasor representation in lumped-parameter *RLC* models for the transmission lines and *dq*-axis models for the generator, etc. This lumped-parameter transmission-line model is indeed a good approximation in analysis assuming that (1) the dynamics is not faster than in the common transient stability variety [7], and (2) lines are not excessively long. However, many voltage-stability and emerging voltage-control events are so fast that the quasistationary assumption, which is the basis for the traditional DAE phasor model, simply

loses validity. So, for instance, the conventional phasor model cannot predict realistically the fast events in the vicinity of the singularities of the DAE model, and the trajectories lose their identity.

The conclusion is that an approximation of the dynamics by $\dot{x} = f$, $\varepsilon \dot{y} = g$, $\varepsilon \rightarrow 0$ would be valid around a point substantially far away from singular point given in the existence of a fast smooth dynamics but it would be *totally false* in conjunction with the conventional phasor $\dot{x} = f$, $0 = g$ model. Fast nonphasor models (for stray capacitances, inductors, etc) can be formulated conceptually but it is not practically possible to identify their constants or parameters. Another remedy may be built on the time varying phasor defined in Chapter 11.

Singular perturbation is a very useful tool in the analysis of power systems and other large dynamic systems. Unfortunately, power-system dynamics is mostly written in quasistationary phasors, and so it has become so much a second nature of us that most of us have forgotten that its validity as an approximation depends on the quasistationary assumption, that is, the speed of variation of the event must be slow compared to 60 Hz. Hence, as explained before, the $\dot{x} = f$, $\varepsilon \dot{y} = g$, $\varepsilon \Rightarrow 0$ approximation written with quasistationary phasors, that is, the common type of phasors, is automatically without any validity in regions of the state space around the singularity of the phasor model (Fig. 8.1). Forgetting this fact has led to erroneous publications in the literature.

The conceptual sketch in Figure 8.1 displays in two dimensions the basic behavior of the trajectories in the state space. Trajectories starting at points within the region of attraction converge to a stable equilibrium point (a potential operating point provided it is viable). Trajectories starting outside the region of attraction of a particular stable equilibrium may converge to another stable equilibrium (not shown in Fig. 8.1) or keep diverging toward infinity or being dissolved and lose identity or predictability at a singular boundary. The DAE model [$\dot{x} = f(x, y, p)$, $0 = g(x, y, p)$] predicts such singular section of the boundaries where the $f = 0$, $g = 0$ equation is not invertible for y .

Such points typically define singular boundary surfaces (curves in the conceptual sketch of Fig. 8.1). What the quasistationary model implies in this singular boundaries is an instant jump of the state from $+\infty$ to $-\infty$ or vice versa. Such an event, of course, does not physically occur but it physically implies the existence of a band of very-high-speed events in a band around the “singularity surface” in the state space (Fig. 8.1). In these bands the validity of the quasistationary assumption, the foundation of conventional phasor equations, would be grossly violated, hence the common $\dot{x} = f$, $0 = g(x)$ model totally loses its validity.

8.1 HISTORICAL SKETCH OF THE DEVELOPMENT OF ANALYTIC TOOLS FOR LARGE COMPREHENSIVE POWER-SYSTEM DYNAMICS

A brief history of recent analysis of nonlinear phenomena in power systems is presented now with special emphasis on constrained power-system models. More

extensive citations appear throughout the text on relevant subject areas. These are intended to help the reader with extended studies.

The first major step in the direction of developing a stability theory was a systematic analysis in Refs. [8 to 11] of the large nonlinear (unconstrained) smooth system in a Morse–Smale-like formulation that observed the composition of the stability boundary. As in Morse–Smale theory [12, 13] a stratification of the stability boundary as a union of the stable manifolds of unstable equilibria (in a descending order) was proved in Ref. [9] while the explicit contribution to the boundary analysis from the presence of periodic orbits was established in Ref. [10]. A novel concept of a “quasistability boundary” was introduced in Refs. [9, 11], which eliminated impractical interior segments of the boundary and by so doing importantly simplified the analysis and engineering use of the boundary. Specifically based on the concept of the quasistability boundary, it was proved in Ref. [9] that it is sufficient to consider only the order one unstable equilibrium points (the type one equilibria) for precise and practical analysis of the stability boundary.

In the parameter-space analysis, a static notion of feasible regions was proposed in Ref. [14] introducing the concept of regions as a tool in analyzing the general feasibility of load-flow solutions. The significance of nonlinear dynamic phenomena such as bifurcations in smooth unconstrained power system models was identified in Ref. [15], which studied the occurrence of Hopf bifurcations, while other early works [15, 16] analyzed global bifurcations and complex behavior in angle-stability models. On the voltage side, the relationship between the singularity of the load-flow Jacobian, proximity to multiple load-flow solutions, and voltage-instability phenomena was recognized in Ref. [18], and the precise mathematical connection between these three events was established in Ref. [19] using the Sotomayor theory of the saddle-node bifurcation [20]. Reference 19 also observed the occurrence of a special bifurcation arising in a constrained power-system model related to the noncausal nature of the algebraic constraints.

The importance of the differential-algebraic formulation in voltage-stability studies was demonstrated in Ref. [1] in which several new phenomena were introduced related to the singular points (called noncausal points in Ref. [19]). These include observations in small-scale power-system models on new contributions to the stability boundary from certain special singular points and the presence of certain bifurcations directly connected with the singularity. The interaction of the state space and the parameter space with initial beginnings of a taxonomy were presented in Ref. [21] on some minimum-size power-system models.

The constrained nature of detailed power-system models has been well known in power-system analysis. For instance, Refs. [22] and [23] (see Sec. 7.2) state the dynamic problem as a “coupled” set of differential equations, coupling via the power-flow equations and variables. Explicit models of the constrained nature were introduced in Ref. [24] for transient stability analysis of *non-constant-impedance* type load models. These non-“classical” power system models were given the

name *structure-preserving power-system models* [24, 26], which directly reflected the network structure of the power system in the form of algebraic equations within the model.

There exists a rich history of “direct” stability methods based on energy function concepts and using Lyapunov theoretic tools [26 to 28]. Development of Lyapunov theoretic techniques to constrained power-system models can be seen in Ref. [29]. An extensive Lyapunov stability theory for DAE systems has been proposed in Ref. [30] in which some effects of singular points (called impasse points in Ref. [34]) are considered. Recent work in Ref. [6] uses Lyapunov theory tools, the stability boundary characterization [1], and the static bifurcation properties of the singularity in deriving transient stability algorithms for DAE models.

The first detailed geometric analysis of a rudimentary constrained power-system model was carried out in Refs. [1, 31] in which the rich interactions of the state-space features (such as those related to the singularity) and parameter-space phenomena (including the occurrence of several local and global bifurcations) were rigorously analyzed. Moreover, it was proved that these individual details indeed fit in an organized overall structure, what was later called the taxonomy in Ref. [1]. Ref. [31] included an analysis of a special local bifurcation that arises when an equilibrium crosses the singularity called *the singularity-induced bifurcation* and a new global bifurcation called the *singularity connection bifurcation* [3] in which periodic orbits were annihilated.

The full-fledged taxonomy theory for analyzing the dynamics of large differential-algebraic nonlinear models was presented in Refs. [1, 2, 3]. A precise two-level intertwined cellular structure for the state space and the parameter space was proved there.

DAE models have also been analyzed in singular control theory with applications in robotics [32] among other areas. Differential-algebraic systems have also been studied with much interest in nonlinear network theory. Reference [33] analyzed certain jump phenomena in singularly perturbed large-scale models, whereas Ref. [34] proved that in general large DAEs, impasse points where the trajectories of differential-algebraic equations cannot be continued are generic within the set of all singular points.

In mathematical theory, Ref. [35] first posed the problem of special phenomena arising in constrained nonlinear systems. A jump phenomenon in a class of constrained gradient vector fields was analyzed in Ref. [36], which also studied the generic dynamic structure near certain singular points in two- and three-dimensional systems. Later mathematical works in this context appear to be focused on the concept of canards, which are complicated jump phenomena leading to duck cycles or canard oscillations [37]. Canards occur near certain special singular points under singular perturbations of the DAE models. (Remember that the quasistationary phasor model disappears near the singularity.) These methods are based on nonstandard mathematical analyses [38] and are restricted to two- and three-dimensional systems [25, 37].

Systematic investigation of large nonlinear systems modeled by differential equations with algebraic equality conditions (DAEs) started around 1990 [15, 21]. A team led by one of the authors has proceeded to develop a theory that was introduced in Ref. [1] under the name of *taxonomy*¹ [1, 2]. Taxonomy theory has intensively developed since that time and it currently covers both the state and parameter spaces for DAEs, and now also for large systems with many different types of system hard limits [5], that is, inequality constraints. In taxonomy theory, all major and minor analytical and structural aspects of these classes of systems are analyzed in detail by the team of [1]–[5], as described in Chapters 7–10. (See also Tables 7.1 and 7.2.)

Analysis of the state and parameter spaces for large constrained nonlinear systems in this work have revealed that both these spaces have a two-level cellular structure (in the form of regions and subregions) in a topological sense. This structure is summarized below.

Briefly the state space is divided at the upper level by the singular surface into open components so that the constrained dynamics restricted to individual components is smooth. However, the trajectories when reaching the component boundaries, namely, the singularity surface, typically undergo loss of existence or uniqueness and hence lose analytical tractability in the sense of the DAE model. The components in turn contain possibly several stability regions and other instability regions in the lower level of the state-space structure. Among these subregions of a component, the dominant and most interesting region is the region of attraction of the stable operating point. It is proved that the boundary of the region of attraction (under certain Morse–Smale-like assumptions) consists of, among other segments, some that derive from the singularity surface itself and also from stable manifolds anchored at special very-high-dimensional subsets of the singularity surface (Table 7.1).

The parameter space at the upper level is divided into feasibility regions of various operating points by the feasibility boundaries. Operating points cannot cross the feasibility boundaries without losing their local stability in a generic sense. The feasibility boundary consists of three types of principal bifurcation segments including a new bifurcation called the singularity-induced bifurcation, which was first rigorously studied in Ref. [1]. The subregions in the parameter space are called *typal regions* because the state-space topology is uniform at parameter values within these typal regions. The boundaries of the typal regions consist of local bifurcations and global bifurcations (Table 7.2).

Within the taxonomy theory of DAEs, a special role is played by the singularity both in the form of singular boundaries in the state space and in the form of bifurcations connected with the singularity in the parameter space. The complexity encountered accordingly in the study of these is a major aspect of the theory. New bifurcations both local and global are observed here and are precisely analyzed (Sec. 8.2) [1, 2, 5].

¹ The term *taxonomy* was first used in this context by Les Fink in his call for papers for Ref. [39].

8.2 DYNAMICS OF THE DAE SYSTEM*

As explained in Chapter 7, a large class of physical systems including the quasi-stationary (slow with respect to the 60-Hz carrier frequency) dynamics of the large electric power system can be modeled (as illustrated in Secs. 7.1 and 7.2) by a parameter-dependent differential-algebraic system of the form

$$\Sigma: \dot{x} = f(x, y, p), \quad f: \mathbb{R}^{n+m+p} \rightarrow \mathbb{R}^n \quad (8.1)$$

$$0 = g(x, y, p), \quad g: \mathbb{R}^{n+m+p} \rightarrow \mathbb{R}^m \quad (8.2)$$

$$x \in X \subset \mathbb{R}^n, \quad y \in Y \subset \mathbb{R}^m, \quad p \in P \subset \mathbb{R}^p$$

The formulation of the model, Eqs. (8.1) and (8.2), is as follows. In the state space $X \times Y$, dynamic state variables x and instantaneous state variables y are distinguished. While the (dynamic) x variables have their associated dynamics explicitly modeled by Eq. (8.1), the dynamics of the (instantaneous) y variables is assumed to be so fast that the constraints $g = 0$ [Eq. (8.2)] are always satisfied. Even though formally the variables y and p appear to be of similar nature in Eqs. (8.1) and (8.2), they play fundamentally different roles in the formulation of Σ . As just stated, the variables y are *state* variables that change instantaneously with variations in the x states, whereas the variables p are parameters that are assumed to have no dynamics and their values depend on outside (typically slow varying) input of operating conditions (e.g., power generation of individual units) and structural features (e.g., which units or lines are in service).

For the electric power system, typical dynamic state variables x are the time-dependent values of internal generator voltages and rotor phases, control states, and load dynamic variables. They are detailed extensively in Chapter 3. Typical instantaneous variables g are the load-flow variables (the bus voltages and angles) so that the power-balance equations or the load-flow equations, also detailed in Chapter 3, typically form the set of constraints $g = 0$. The parameter space P is composed of system parameters (the system topography, i.e., what is energized, and equipment constants, e.g., inductances) and operating parameters (such as loads, generation, and voltage set points).

For a fixed parameter p_0 , the state variables describe the time behavior of the system, the stationary solution, or the transients. The equality constraints $g = 0$ limit the state to a constraint set L ,

$$L = \{(x, y) \in X \times Y: g(x, y, p_0) = 0\} \quad (8.3)$$

at all times. Through every point $q \in L$ with the exception of points in a singular subset S ,

$$S = \{(x, y) \in L: \Delta(x, y) := \det D_y g(x, y, p_0) = 0\} \quad (8.4)$$

* Reader should remember that because of space limitation full proofs are not given for all theorems. However these are available at the end of the naming of the theorem.

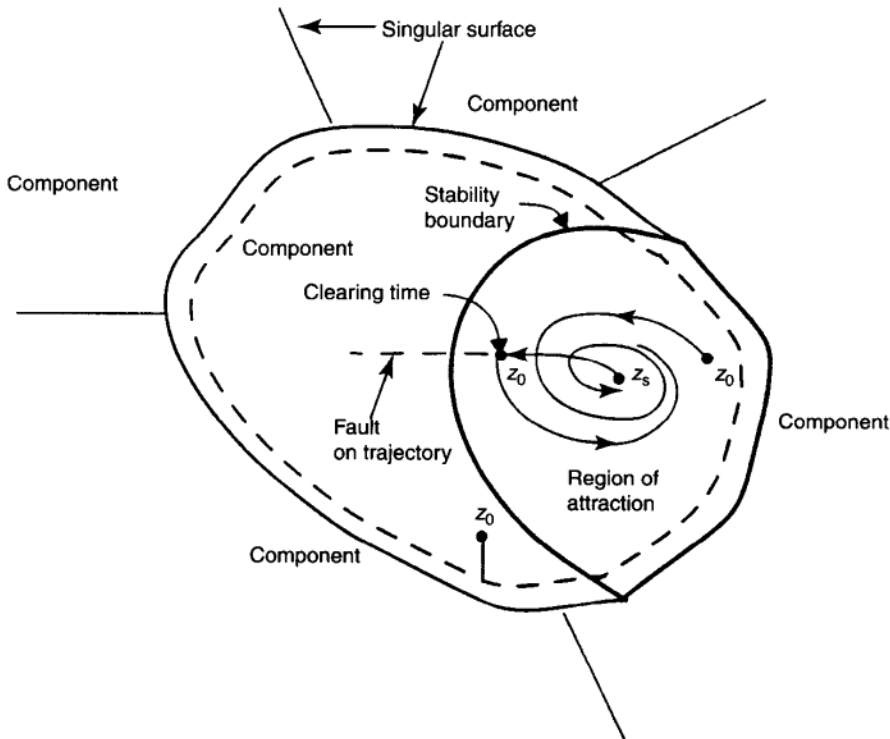


FIGURE 8.1 Simple conceptual sketch of the general state space shown in a two dimensional equivalent.

there exists a unique trajectory (i.e., transient) that passes through q and lies in L . Here $D_y g$ stands for the matrix of partial derivatives of g with respect to y , that is, $(\partial g)/(\partial y)$. The singular set S is defined as the set in which the conditions of the implicit function theorem for eliminating y from the algebraic constraint are violated. Typically S is a stratified set of maximal dimension $n - 1$ embedded in L , and L is separated by S into open regions, the components C of the state space. The state space is confined to the complement of S in L . A simple conceptual sketch is indicated in Figure 8.1.

The *state space* (see Fig. 8.1) is separated into *connected components* by singular surfaces (the first level of Table 7.1), shown in Section 7.2. Within each component, stable equilibria and other stable limit sets have their *regions of attractions* bounded by stability boundaries along with other *instability regions* (the second level of Table 7.1). The stability boundary of the region of attraction of a stable equilibrium can be characterized for the DAE system Σ as shown in Appendix 7.1. This assumes that the system admits a dissipating energy function and the ω -limit set² for any trajectory in the stability boundary consists only

² \hat{z} is defined as ω -limit points for a trajectory $z(t)$ if there exists a diverging sequence $\{t_k\}$ such that $z(t_k) \rightarrow \hat{z}$ as $t \rightarrow \infty$. The set of all ω -limit points for the trajectory $z(t)$ is defined as its ω -limit set.

of equilibrium points and periodic orbits. Under Morse–Smale-like assumptions, it can be shown that the stability boundary of the singular system Σ consists of trajectories that converge to the anchor points, along with sections of the singular surface. Unstable equilibria, unstable periodic orbits, and special subsets of the singular surface called the semisingular surface and the pseudoequilibrium surface constitute the set of anchor points. The detailed analysis of the singular dynamics Σ is summarized from Refs. [1, 2, 46 and 59] in Section 7.6.1.

The *parameter space* (Table 7.2) is composed of *typal regions* (regions of structural stability) bounded by bifurcation surfaces (first level of Table 7.2). Typal regions are grouped into *feasibility regions*. The feasibility region consists of all operating points that can be reached from the given operating point by continuous variations of parameters without loss of local stability (second level of Table 7.2). The boundary of the feasibility region is mostly composed of three types of codimension-1 [roughly $(q - 1)$ -dimensional in a q -dimensional parameter space] bifurcation surfaces, namely the well-known saddle-node and Hopf bifurcations [40], and a new bifurcation called the singularity-induced bifurcation [1, 2]. At the singularity-induced bifurcation, one eigenvalue along the equilibrium locus changes its stability status by diverging through infinity, while the other eigenvalues remain bounded. It can be shown that the feasibility boundary for Σ can be solved for as common zeros (called zero sets hereafter) of three different sets of functions. Each zero set corresponds to the closure of one of the three bifurcation surfaces mentioned earlier, that is, the saddle-node, Hopf, and the singularity-induced bifurcations. Therefore generically the loss of local stability at the operating point is completely characterized by these three local bifurcations. Moreover, it can be shown [41] that some of the interior feasibility boundary segments that correspond to the common boundary of the saddle-node- and Hopf-bifurcation segments are also interesting because global bifurcations such as the saddle connection bifurcation will also be present near these points. However, for large nonlinear systems, analysis of other global bifurcations, which may be related to complicated system behavior, appears to be a formidable task owing to analytical and numerical difficulties. Nevertheless, considerable progress along these lines has been reported recently [41].

An analysis of the main structural features of the constrained dynamics with emphasis on those aspects caused by the presence of the algebraic constraints is given in Section 8.2.1. Since the analysis of the overall structure in Section 8.2.1 is necessary for both the state-space analysis of stability regions and the parameter-space analysis of bifurcations generating typal and feasibility regions, these issues are treated here. Section 8.2.2 deals with stability regions in the state space, and the main objective is to characterize the stability boundary ∂A of the region of attraction A of a stable equilibrium point.

The structure of the parameter space is summarized in Section 8.2.3. The concept of a feasibility region is defined. The singularity-induced bifurcation, which arises when the equilibrium is at the singularity, is rigorously analyzed in Sections 8.2.3.3 and 8.2.3.4. A brief introduction to the concept of typal regions is presented in Section 8.2.3.6.

Note that the proofs for all the Lemmas and Theorems stated in this chapter were published in the form of a technical report [2] and in several other publications [1, 5, 46 and 59]. Here only the salient results are summarized.

8.2.1 State-Space Structure of the DAE Dynamics, Σ

A fixed parameter p_0 is considered in Eqs. (8.1) and (8.2) and the parameter p is not shown for notational simplicity. The equations are written in the form

$$\Sigma: \dot{x} = f(x, y), \quad f: \mathbb{R}^{n+m} \rightarrow \mathbb{R}^n \quad (8.5)$$

$$0 = g(x, y), \quad g: \mathbb{R}^{n+m} \rightarrow \mathbb{R}^m \quad (8.6)$$

8.2.1.1 Notation and the Structure of the State Space A conceptual introduction using the state-space structure of the rudimentary system is given in Sections 7.2.2 and 7.2.3 and even more extensively in Section 7.2.4. A precise mathematical analysis follows here. The following sets largely define the structure of the state space:

$$L = \{(x, y) \in \mathbb{R}^{n+m}: g(x, y) = 0\} \quad (8.7)$$

$$M = \{(x, y) \in L: \text{rank}(D_x g(x, y), D_y g(x, y)) = m\} \quad (8.8)$$

$$S = \{(x, y) \in L: \Delta(x, y) := \det D_y g(x, y) = 0\} \quad (8.9)$$

$$\Psi = \{(x, y) \in S: \kappa(x, y) := \text{adj}[D_y g(x, y)]D_x g(x, y)f(x, y) = 0\} \quad (8.10)$$

$$\Xi = \{(x, y) \in S \setminus \Psi: D_y \Delta(x, y)\kappa(x, y) = 0\} \quad (8.11)$$

$$R = S \setminus (\Psi \cup \Xi) \quad (8.12)$$

L is the constraint surface determined by the algebraic constraint. The system must stay on L and henceforth, all topological definitions are relative to L . M is a regular subset of L , which, by the implicit function theorem, is an n -dimensional manifold. S is called the singular surface or the singularity. Typically no solution exists for points in S . Ψ is called the *pseudoequilibrium surface*. This high-dimensional subset displays the behavior of an equilibrium surface for the vector field Z [Eq. (8.17)] induced by the system Σ and indeed becomes an equilibrium surface for an “equivalent” smooth dynamical system defined by a transformed vector field Z^T [Eq. (8.18)]. Z and Z^T are related by a singular transformation. The details of this transformation follow in Section 8.2.1.2. The pseudoequilibrium surface is a true equilibrium surface for the transformed vector field Z^T . It is useful to distinguish the following subsets of Ψ :

$$N_\psi = \{(x, y) \in \Psi \cap M: \text{rank}(D_y g) = m - 1 \text{ and the Jacobian of } Z^T \text{ has exactly two eigenvalues with nonzero real parts}\} \quad (8.13)$$

$$B_\psi = \Psi \setminus N_\psi \quad (8.14)$$

Typically, the Jacobian of Z^T (restricted to M) has at least $n - 2$ zero eigenvalues at a point in Ψ (see Sec. 8.2.4). Hence, N_ψ corresponds to the subset of Ψ in which the most regular type behavior takes place. It will be shown that near every point in N_ψ the integral curves of the system locally behave similar to a linear system, and the points in the set N_ψ will be called the *nice* pseudoequilibrium points. The local dynamics near the points in the set B_ψ is more complex, and we call these points the *bad* pseudoequilibrium points. Finally, Ξ corresponds to points where Z^T is tangent to the singularity (see Sec. 8.2.1.5). Henceforth points in Ξ will be called *semisingular*. Let

$$N_\xi = \left\{ (x, y) \in \Xi : \text{rank} \begin{pmatrix} D_x g & D_y g \\ D_x \Delta & D_y \Delta \end{pmatrix} = m + 1 \text{ and } D_y \{(D_y \Delta) \kappa\} \kappa \neq 0 \right\} \quad (8.15)$$

$$B_\xi = \Xi \setminus N_\xi \quad (8.16)$$

We call the points in the set N_ξ the *nice* semisingular points, and the points in the set B_ξ the *bad* semisingular points. The condition on the second derivative in the definition of N_ξ ensures that trajectories do not cross over as they touch the singularity. R is the complement of Ψ and Ξ in S and it consists of ordinary singular points named here the *transversal singular points*, that is, at each point z in R either two trajectories originate from z or converge to z at infinite speed, and the two trajectories approach z transversal to R at z . The properties of these various subdivisions of the state space are summarized in the next theorem.

Theorem 8.2.1: Singular Dynamics Hierarchy Theorem [1] If the subsets are not empty, then

1. $L \setminus S$ is an n -dimensional manifold. The solutions of the system (8.5) and (8.6) are the integral curves of the vector field Z on $L \setminus S$.
2. R is an $(n - 1)$ -dimensional manifold. At each point in R two trajectories either approach or leave the singularity transversally.
3. N_ψ is an $(n - 2)$ -dimensional manifold. Ignoring orientations, the solution curves are locally equivalent to those of a linear system near the origin.
4. N_ξ is an $(n - 2)$ -dimensional manifold. Trajectories are tangent to the singularity at N_ξ , but do not cross over.

The proof of this theorem is presented in the form of several lemmas, and these lemmas constitute precise statements of the structure of the singular dynamics. First, in Section 8.2.1.2, the singular transformation is introduced. Using the transformation, then we will analyze the constrained dynamics Σ in a hierarchical fashion by starting with the constraint surface L . At each step, we leave out a lower-dimensional subset with a more degenerate behavior, thus identifying the most regular behavior for that level in the analysis.

8.2.1.1 Codimension-0 Dynamics

Lemma 8.2.1 Restricted to $L \setminus S$, the dynamics defined by Eqs. (8.5) and (8.6) is locally induced by the vector field Z (i.e., described by a set of ordinary differential equations),

$$Z = \begin{pmatrix} f(x, y) \\ -[D_y g(x, y)]^{-1} D_x g(x, y) f(x, y) \end{pmatrix} \quad (8.17)$$

For any point in the set $L \setminus S$, the Jacobian $D_y g$ is nonsingular and hence $L \setminus S \subset M$. Therefore, the set $L \setminus S$ is an n -dimensional manifold, and the dynamics Σ restricted to this set $L \setminus S$ is smooth. For any point $z \in L \setminus S$, there exists a unique trajectory that passes through z . When $z \in L \setminus S$ is not an equilibrium point for the vector field Z , it is well known that the flow defined by Z can be nicely characterized locally near z (flow-box theorem [42]) as shown in Figure 8.2. In the illustrations, the corresponding dimension for each set is shown in square brackets. The connected components of the set $L \setminus S$ will be called in this book the *components* of the state space. See the conceptual sketch in Figure 8.1 and compare the behavior of the singularity (in $M = \sqrt{5}$) in Figures 7.6 and 7.8 to 7.10 for the rudimentary system.

8.2.1.2 Singular Transformation Note that the vector field Z is not defined at points in S since $D_y g$ is singular. For analyzing the behavior near S , define the transformed vector field Z^T to be

$$Z^T := \begin{pmatrix} f(x, y)\Delta(x, y) \\ -\text{adj}(D_y g)D_x g(x, y)f(x, y) \end{pmatrix} \quad (8.18)$$

which is a global extension [1, 2] of a singular transformation introduced in Ref. [36]. The flow of the vector field Z describes the dynamics of the system. The transformed vector field Z^T is *globally* smooth and leaves the constraint

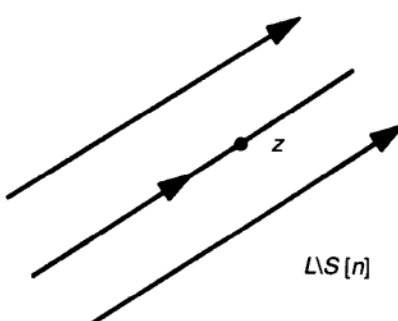


FIGURE 8.2 Dynamics near regular points in $L \setminus S$.

surface invariant. Z^T will be used in the proofs thus facilitating standard nonlinear analysis. The results for the singular systems can be readily reinterpreted for the DAE system Σ as implied by the next lemma. Therefore, this singular transformation serves as a powerful tool for analyzing the *singular* dynamics of Σ using *standard* (i.e., not nonstandard [38]) mathematical analysis. This formulation makes it possible to analyze both local and global properties of the *singular* dynamics in *large* DAEs.

The vector field Z^T is obtained when the vector field Z is pointwise scaled by the determinant $\Delta(x, y)$. Define

$$(L \setminus S)_+ = \{(x, y) \in L \setminus S : \Delta(x, y) > 0\} \quad (8.19)$$

$$(L \setminus S)_- = \{(x, y) \in L \setminus S : \Delta(x, y) < 0\} \quad (8.20)$$

Clearly, $(L \setminus S) = (L \setminus S)_+ \cup (L \setminus S)_-$ as $\Delta(x, y) \neq 0$ in $L \setminus S$. A detailed and intuitive example in Section 7.2.4 will help to develop a clear conceptual picture of the singular transformation and the behavior in the transformed vector fields.

Lemma 8.2.2 [1, 2] The vector fields Z and Z^T , restricted to $(L \setminus S)_+$, are equivalent. When restricted to $(L \setminus S)_-$, Z and $-Z^T$ are equivalent.

In particular, if (x_0, y_0) is an equilibrium point for the vector field Z , then it is also an equilibrium for the new vector field Z^T , and the eigenvalues in the transformed system are simply scaled by $\Delta(x_0, y_0)$. As curves, the trajectories of Z and Z^T are identical in $L \setminus S$. Whereas Z is not defined on S , Z^T defines a smooth vector field on all of the constraint surfaces L . The transformed vector field Z^T has an additional set of equilibrium points in the pseudoequilibrium surface Ψ (for a conceptual interpretation see Fig. 7.16 in Sec. 7.2.3.1).

The subset M of L is an n -dimensional manifold by implicit function theorem. By definition $L \setminus M \subset S$. Moreover, it is interesting that all such “nonmanifold” points on the constraint surface are pseudoequilibrium points. Again see the detailed example in Section 7.2.4.1 for insight.

Lemma 8.2.3 [1, 2] $L \setminus M \subset \Psi$.

The next lemma (8.2.4) states that the transformation Z^T provides a canonical extension of the vector field Z to the singularity. It should be noted that the orientation of the trajectories is reversed for the points in $(L \setminus S)_-$, as $\Delta(x, y) < 0$.

Lemma 8.2.4 [1, 2] Any integral curve of the vector field Z that approaches the singular surface has a unique limit on the singularity and this limit agrees with the limit of the solution curve in the transformed system.

8.2.1.3 Codimension-1 Dynamics In Section 8.2.1.1, we could easily show that the Σ dynamics is smooth when restricted to $L \setminus S$. Now let us consider the next degenerate subset $S \subset L$.

Lemma 8.2.5 [1, 2] $R = S \setminus (\Psi \cup \Xi)$ is an $(n - 1)$ -dimensional embedded submanifold of M and Z^T is transversal to R .

Since $R \cap \Psi = \emptyset$, by Lemma 8.2.3, we conclude that $R \subset M$. Thus by Lemma 8.2.5, it follows that $R \subset S$ is a codimension one submanifold of M . Let us consider any point $z \in R$. Then since $z \notin \Psi$, z is a regular point for the flow of the transformed vector field Z^T . Therefore, by the flow-box theorem [42], there exists a unique trajectory of Z^T that passes through z . Again by Lemma 8.2.5, the vector field Z^T is transversal to R at z and so, the trajectory that passes through z crosses the singular surface R transversally at z .

Next, we claim that the determinant $\Delta(x, y)$ must change sign at $z \in R$ when the trajectory crosses $z \in R$. This is because along the trajectory $(x(t), y(t))$ which passes through $z \in R$, by transversal intersection, we have that

$$\frac{d}{dt} \Delta(x(t), y(t))|_z = (D_x \Delta, D_y \Delta) Z^T|_z = -(D_y \Delta) \kappa|_z \neq 0 \quad (8.21)$$

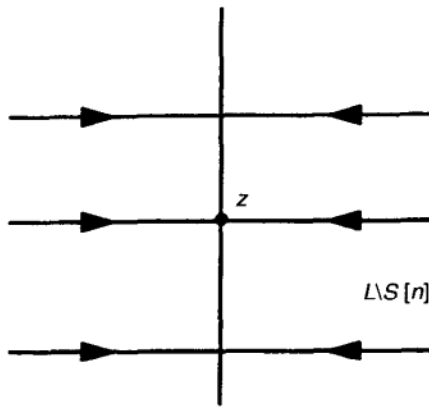
Transforming back to the original system Σ , we conclude that for each $z \in R$, two trajectories of Z either approach or leave z transversal to R . Hence, depending on the sign of the term $(D_y g)\kappa$, we define the first case as singular sinks R_{si} or singular sources R_{so} , respectively, that is,

$$R_{si} := \{(x, y) \in R : (D_y \Delta) \kappa(x, y) > 0\} \quad (8.22)$$

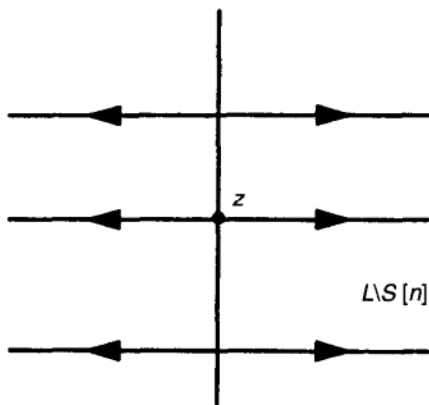
$$R_{so} := \{(x, y) \in R : (D_y \Delta) \kappa(x, y) < 0\} \quad (8.23)$$

By Eq. (8.21), we conclude that for any point $z \in R_{si}$, the determinant $\Delta(x(t), y(t))$ decreases along the transformed system trajectory $(x(t), y(t))$. Hence, for Σ , two trajectories approach $z \in R_{si}$ transversally as shown in Figure 8.3(a). Similarly we conclude that at any $z \in R_{so}$, two trajectories of Σ leave z transversally away from R as shown in Figure 8.3(b). Since the vector field Z^T is nonzero at $z \in R$ and $\Delta = 0$ at $z \in R$, it is clear that the two trajectories for the vector field Z (which is obtained by dividing Z^T by Δ) will have unbounded velocities as they approach the point $z \in R$ (see the conceptual sketch in Fig. 8.1) on or near the singular surface $(a-a)$ (see Figs. 7.4 and 10.8 to 10.10 and the accompanying text in Section 7.2).

Special singular points such as the transverse sources and transverse sinks above have been a subject of much interest in the theory of nonlinear networks. In Ref. [34], points where positive (negative) time continuation of solutions is not possible are defined as *forward (backward) impasse points*. Using Lyapunov–Schmidt reduction arguments, it is proved in Ref. [34] that impasse points (forward and backward as just defined) must be generic within the set of singular points S . The analysis in this section proves that *transverse sources are backward impasse points and transverse sinks are forward impasse points for the DAE system Σ* . In our geometric analysis of codimension-1 dynamics, the transverse sources and transverse sinks have been derived analytically with



(a) Traverse sinks



(b) Traverse sources

FIGURE 8.3 Dynamics near (a) singular sources R_{so} and (b) singular sinks R_{si} .

explicit easily verifiable algebraic formulas (by construction), and these naturally emerge as the least degenerate objects within the singularity S . In other words, transverse sources and transverse sinks tell us *how* to identify the forward impasse points and the backward impasse points of Ref. [34] for the model Σ (generically) by simple formulas.

Simple numerical examples illustrating this concept are given in Figure 7.4 and Figures 7.8 to 7.10 with $a-a$ above Ψ being backward and $a-a$ below Ψ being forward impass. The accompanying text gives a less mathematically precise intuitive explanation than is offered here. Now we, proceed with the analysis of the next level of the hierarchy, namely, with the codimension-2 dynamics.

8.2.1.4 Codimension-2 Dynamics We left out the subsets, the set of pseudoequilibria Ψ , and the set of semisingular points Ξ for establishing the principal

structure R of the singular set S . In this section, we will look at the “nice” subsets of Ψ and Ξ and show that locally near these points, the singular dynamics Σ is well understood.

8.2.1.4.1 Nice Semisingular Points

Lemma 8.2.6 [5] If nonempty, then N_ξ is an $(n - 2)$ -dimensional embedded submanifold of M . The vector field Z^T has a nonzero normal component at every point in N_ξ .

Since Z^T has a normal component for any point $\xi \in N_\xi$, the trajectories of Z^T that reach any $\xi \in N_\xi$ strictly leave the set N_ξ . Let us proceed with a detailed analysis of the local picture near these points. First, we construct a special set of chart coordinates, which reduce the dynamics of Z^T to a canonical form near the singular points.

Define the coordinates η_1 and η_2 in (x, y) coordinates as

$$\eta_1 = \Delta(x, y), \quad \eta_2 = D_y \Delta(x, y) \kappa(x, y) \quad (8.24)$$

and complete the coordinate system η_i in a suitable way. This is possible because the Jacobian, say, J_{ss} involved in the coordinate change, is of full rank [2]. In η_i coordinates, let the system be described as

$$\dot{\eta}_1 = \beta_1(\eta_1, \eta_2, \eta_r) \quad (8.25)$$

$$\dot{\eta}_2 = \beta_2(\eta_1, \eta_2, \eta_r) \quad (8.26)$$

$$\dot{\eta}_r = \beta_r(\eta_1, \eta_2, \eta_r) \quad (8.27)$$

Then, the singular surface S is locally given as $\{\eta_1 = 0\}$ and N_ξ is the coordinate plane $\{\eta_1 = 0, \eta_2 = 0\}$. Furthermore, since $(D_y \Delta) \kappa = 0$ in Ξ ,

$$\beta_1(0, 0, \eta_r) = (D_y \Delta) \kappa|_{N_\xi} = (D_{y1} \Delta_1) g_1|_{N_\xi} = 0, \quad (8.28)$$

and since $D_y \{(D_y \Delta) \kappa\} \kappa \neq 0$ in N_ξ ,

$$\beta_2(0, 0, \eta_r) = D_y \{(D_y \Delta) \kappa\} \kappa|_{N_\xi} = (D_{y1} \varphi_1) g_1|_{N_\xi} \neq 0. \quad (8.29)$$

Since $\Xi \cap \Psi = \emptyset$, there are no equilibrium points of Z near the singularity. Hence, the local picture is as shown in Figure 8.4.

As observed earlier, it is clear that the flow of Z^T is tangent to the singularity at any point $\xi \in N_\xi$. But due to our assumption on the second derivative,

$$\ddot{\eta}_1 = \frac{d}{dt} |_{(0,0,\eta_r)} \beta_1(\eta_1, \eta_2, \eta_r) = D_y \{(D_y \Delta) \kappa\} \kappa|_{N_\xi} \neq 0 \quad (8.30)$$

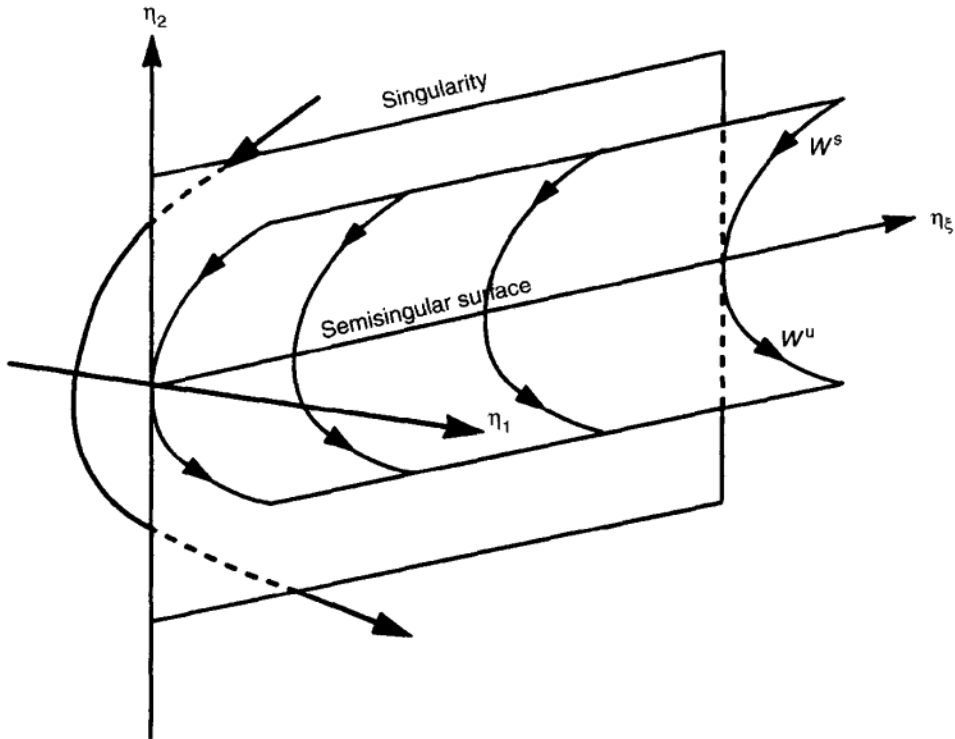


FIGURE 8.4 Dynamics near nice semisingular points N_ξ .

Suppose we look at one side of the singular surface first, say at a component C . Without loss of generality, assume that $\Delta(x, y) > 0$ in C (otherwise redefine Δ as $-\Delta$). If $D_y\{(D_y\Delta)\kappa\}\kappa > 0$ at ξ , then

$$\frac{d}{dt} \Big|_{\xi} \Delta(x, y) = 0, \quad \frac{d^2}{dt^2} \Big|_{\xi} \Delta(x, y) > 0 \quad (8.31)$$

In C there exists a unique trajectory that reaches ξ in finite time and immediately leaves the singularity again to the same side. Combining this fact with the flow-box theorem [42] for the transformed vector field Z^T at ξ , we have established that the local phase portrait near ξ is as shown in Figure 8.4.

8.2.1.4.2 Nice Pseudoequilibrium Points The pseudoequilibrium surface Ψ , which is an equilibrium surface for the transformed vector field Z^T , can be split into a nice set N_ψ and a bad set B_ψ as defined in Eqs. (8.13) and (8.14). The properties of the set N_ψ will be explored in this section.

Lemma 8.2.7 [1, 2] If nonempty, then N_ψ is an $(n - 2)$ -dimensional embedded submanifold of M .

Lemma 8.2.8 [1, 2] For every point $\psi \in N_\psi$, there exists a neighborhood U of ψ in M , and a coordinate chart (η_1, \dots, η_n) defined on U , such that

1. The chart is centered at ψ , i.e., $\eta_i(\psi) = 0$ for all i .
2. The dynamics take the form

$$\dot{\eta}_i = f_i^1 \eta_1 + f_i^2 \eta_2 \quad (8.32)$$

for some functions f_i^k : $\eta(U) \subset \mathbb{R}^n \rightarrow \mathbb{R}$, $k = 1, 2$ and $i = 1, \dots, n$.

3. $S \cap U = \{\eta_1 = 0\}$.
4. $N_\psi \cap U = \{\eta_1 = 0 \text{ and } \eta_2 = 0\}$.

In these coordinates, the origin is the pseudo equilibrium and the Jacobian of the vector field Z^T has $n - 2$ zero eigenvalues and 2 nonzero eigenvalues. Hence, the equilibrium points in the set N_ψ are nonhyperbolic. But they are special in the following sense:

Lemma 8.2.9 [1, 2] The local center manifold for any point $\psi \in N_\psi$ in the nice set is N_ψ itself.

The set N_ψ can be split into three different subsets, depending on the stability status. Define

$$N_{\text{so}} := \{\psi \in N_\psi : \text{Jacobian of } Z^T \text{ has two eigenvalues in } C^+\} \quad (8.33)$$

$$N_{\text{sa}} := \{\psi \in N_\psi : \begin{aligned} &\text{Jacobian of } Z^T \text{ has one eigenvalue in } C^- \\ &\text{and one in } C^+ \end{aligned}\} \quad (8.34)$$

$$N_{\text{si}} := \{\psi \in N_\psi : \text{Jacobian of } Z^T \text{ has two eigenvalues in } C^-\} \quad (8.35)$$

So $N_\psi = N_{\text{so}} \cup N_{\text{sa}} \cup N_{\text{si}}$. Note that any component of N_ψ entirely lies in one of the three sets. Let us call the points in N_{so} , N_{sa} , and N_{si} *pseudosources*, *pseudosaddles*, and *pseudosinks*, respectively. This definition is motivated by the next lemma, which shows that the local dynamics for Z^T near the nice pseudoequilibrium manifold N_ψ looks like the linear dynamics of a $(n - 2)$ -dimensional continuum of second-order systems.

Lemma 8.2.10 [1, 2] For $\psi \in N_\psi$, the flow of Z^T is locally *equivalent* to a linear system defined as

$$\dot{x}_u = x_u, \quad \dot{x}_s = -x_s, \quad \dot{x}_c = 0, \quad x_c \in \mathbb{R}^{n-2} \quad (8.36)$$

The dimensions of x_u and x_s depend on the particular set in N_ψ , that is,

$$\dim(x_u) = 2, \quad \dim(x_s) = 0 \quad \text{when } \psi \in N_{\text{so}}$$

$$\begin{aligned} \dim(x_u) &= 1, & \dim(x_s) &= 1 & \text{when } \psi \in N_{sa} \\ \dim(x_u) &= 0, & \dim(x_s) &= 2 & \text{when } \psi \in N_{si} \end{aligned}$$

TRANSVERSE PSEUDOSADDLES The dynamics for the transformed vector field Z^T locally is equivalent to the dynamics of the linear system (8.36) near the pseudosaddle manifold with $\dim(x_u) = \dim(x_s) = 1$ and $\dim(x_c) = n - 2$, by Lemma 8.2.10. Consider any $\psi \in N_{sa}$. Since the equivalent linear system has a one-dimensional stable and unstable manifolds, it directly follows that ξ has one-dimensional stable and unstable manifolds for Z^T . But we are interested in analyzing the dynamics of Z . Locally near ψ , the singular set is a manifold by Lemma 8.2.8, and the determinant Δ changes sign at the singular set in a local neighborhood. Therefore, the trajectories of Z^T need to be reversed on one side of the singular set for finding the integral curves of Z by Lemma 8.2.2. Hence, we need to carefully look at the relative position of the singular set, compared to the stable and unstable manifolds.

A pseudosaddle is called *transverse* if its stable and unstable manifolds are not tangent to the singularity. Define the set of transverse pseudosaddles as $N_{tr,sa}$. Let us analyze the local dynamics near pseudosaddles using the chart in Lemma 8.2.8. Locally near any pseudosaddle $\psi \in N_{sa}$, the singular surface is described by setting $\eta_1 = 0$ and the pseudoequilibria (which locally are pseudosaddles) are characterized by setting $\eta_1 = 0$ and $\eta_2 = 0$. Clearly, the Jacobian of the dynamics evaluated at ψ has $n - 2$ zero eigenvalues. Define e_k as the unit vector along the η_k axis. Then it is easy to see that $\{e_3, e_4, \dots, e_n\}$ form the set of eigenvectors for the zero eigenvalues. If the stable (unstable) manifold is tangential to the singularity at ψ , then the eigenvector for the stable (unstable) eigenvalue lies on the singular surface $\eta_1 = 0$. Hence, in particular at ψ , f_1^2 must be zero for nontransverse pseudosaddles. Hence, generically, tangentiality of the stable (unstable) manifold to the singularity occurs only at a lower-dimensional subset of N_{sa} . In other words, generically, pseudosaddles are nontransverse only at lower dimensional subsets. In the general spirit of our approach, let us first look at the transverse pseudosaddles as the most regular structure in N_{sa} .

The local dynamics for the vector field Z near transverse pseudosaddles is shown in Figure 8.5. Near any transverse pseudosaddle, as the stable and unstable manifolds are transversal to the singularity, the singularity divides a neighborhood of ψ into two parts, each containing one stable and one unstable trajectory as shown in Figure 8.5. Since the trajectories get reversed on one side of the singular set from Z^T to Z , the unstable and stable manifolds of the pseudosaddles for Z^T become continuous trajectories for Z as shown in Figure 8.5. A simpler conceptual example of Ψ as a pseudosaddle and the only component present for Ψ in the rudimentary system is again shown in Figures 7.6 and 7.8.

PSEUDOSINKS AND PSEUDOSOURCES Let us consider pseudosinks first. By definition, the Jacobian of Z^T has two stable eigenvalues at a pseudosink. By Lemma 8.2.10, it follows that the local dynamics of Z^T near a pseudosink is topologically equivalent to the dynamics of the linear system $\dot{x}_1 = -x_1$ and

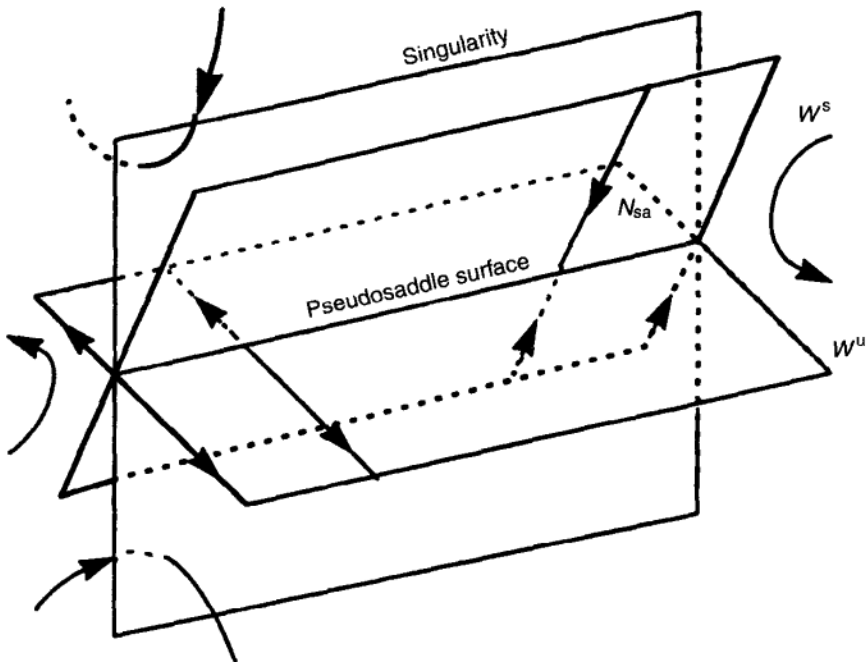


FIGURE 8.5 Dynamics near transverse pseudosaddles $N_{\text{tr},\text{sa}}$.

$\dot{x}_2 = 0$, where x_1 is two-dimensional and x_2 is $(n - 2)$ -dimensional. For the transformed system defined by Z^T , then the local picture near N_{si} will look like that of an $(n - 2)$ -dimensional continuum of stable two-dimensional nodes or two-dimensional stable foci, and this will depend on the nature of the two nonzero eigenvalues. Lemma 8.2.10 is not sufficient to distinguish between the node and focus, but using standard arguments for second-order systems such as in Ref. [43], it can be proved that locally the dynamics for these cases (for nodes and foci) are both well understood and are topologically different. This is not shown here due to space limitations. The local picture near pseudosources follows from the analysis of the pseudosinks by reversing the time scale.

8.2.1.5 Codimension-3 and Higher

8.2.1.5.1 Bad Semisingular Points When $\xi \in B_\xi$, since semisingular points can not be equilibria by their definition, there still exists a unique nontrivial trajectory for Z^T that passes through any $\xi \in \Xi$ and is tangential to the singular surface.

8.2.1.5.2 Nontransverse Pseudosaddles Consider any non-transverse pseudo saddle ψ . By the local equivalence Lemma 8.2.10, for Z^T , there exist two stable trajectories and two unstable trajectories for the nontransverse pseudosaddle ψ . The actual dynamics of Σ depends on the relative position of the singular set at ψ . When the stable manifold is tangential to the singularity different possibilities arise, depending on one, two, or three of the four stable and unstable trajectories

on one side of the singular set. Also, a stable or unstable trajectory may lie entirely in the singular set when bad semisingular points are nearby.

8.2.1.5.3 Bad Pseudoequilibrium Points Certainly the most interesting elements of the codimension-3 subsets are the bad pseudoequilibrium points. Here we have defined the nice pseudoequilibria as the set in which the Jacobian has exactly two nonzero eigenvalues [$n - 2$ are zero since generally Ψ is $(n - 2)$ -dimensional]. Generally at a bad pseudoequilibrium, one or two of the remaining two eigenvalues lie on the imaginary axis. When the Jacobian has exactly one nonzero eigenvalue and certain inequality conditions are satisfied, we define the points to be *pseudosaddle nodes*. The dynamics near these points has a rich structure, but will not be discussed here due to space limitations. The bad pseudoequilibria where the two eigenvalues are purely imaginary may also be interesting. More degenerate bad pseudoequilibria such as when all the eigenvalues are zero may be quite difficult to analyze, and it is an open question whether the dynamics near those points will have any nice structure.

8.2.2 Analysis of the Stability Regions

The objective of this section is to study the stability boundary ∂A of the region of attraction A of a stable equilibrium point. Instead of restricting the analysis to the region of attraction A defined above, it is practically more meaningful to consider the bigger region, the interior of the closure, $\text{int}(\bar{A})$. With small perturbations always present in the system, any trajectory in this region $\text{int}(\bar{A})$ will converge to the stable equilibrium point [9]. Hence, we will analyze the quasistability boundary $\partial \bar{A}$, which is the boundary of the region $\text{int}(\bar{A})$.

The tools used in the analysis are (1) standard geometric tools such as the λ lemma [13] and its extensions for pseudoequilibria and semisingular points [1, 2], (2) the invariance properties [2], and (3) a technical result called here the basic anchor theorem (see Sec. 8.2.2.1). After making some assumptions in Section 8.2.2.2, the necessary and sufficient conditions for testing the presence of anchor points on the stability boundary ∂A will be developed in Section 8.2.2.3. The characterization of the quasistability boundary $\partial \bar{A}$ follows in Section 8.2.2.4. Energy-function-based stability tests are developed in Section 8.2.2.5.

8.2.2.1 Basic Properties Equilibrium points and periodic orbits are defined as usual for the singular dynamics Σ , with the proviso that they do not intersect the singular set S . Stable equilibrium points define the system operating points for general physical systems of the form Σ such as the large power system. Given a stable equilibrium point z_s , the set of all trajectories that converge to the point z_s generally defines the region of attraction for z_s . These matters are summarized intuitively in Appendix 1 of Chapter 7 based on Ref. [9]. However, for the singular system of the form Σ , we restrict our definition of the region of attraction and other stable and unstable manifolds to the state space component C (connected component of $L \setminus S$) which contains z_s [1] (see also the related notion of *causal regions* proposed in Refs. [25, 30], where a state-space decomposition

is proposed based on the eigenproperties of the Jacobian $D_y g$). This definition is strongly motivated by the dynamics of the large power system in which the singular set signals the onset of unpredictable system behavior [1].

The *region of attraction* of a stable equilibrium z_s is defined as

$$A = \{z \in C: \Phi_t(z) \in C \quad \forall t \geq 0, \quad \Phi_t(z) \rightarrow z_s \text{ as } t \rightarrow \infty\} \quad (8.37)$$

Similarly define the stable and unstable manifolds for equilibria and periodic orbits in the usual way, but with the restriction to the component. The stable and unstable manifolds for a pseudoequilibrium Ψ and a semisingular point ξ is similar to those for the equilibrium, but the convergence may occur in finite time. More details can be found in Refs. [1, 2].

Note that ignoring the speed, the trajectories of the vector fields Z and Z^T are identical (topologically equivalent) in C by Lemma 8.2.2 (see Fig. 7.15 for a conceptual illustrative example). Since the trajectories (integral curves to be more precise) of Z coincide with the trajectories of Z^T within the component C , the stability regions defined above for the flow Φ_t of Z can be equivalently redefined in terms of the flow Φ_t^T of the transformed vector field Z^T , by restricting the trajectories of Z^T to the component C as shown for the region of attraction A :

$$A = \{z \in C: \Phi_t^T(z) \in C \quad \forall t \geq 0, \quad \Phi_t^T(z) \rightarrow z_s \text{ as } t \rightarrow \infty\} \quad (8.38)$$

Hence, the boundary of the region of attraction ∂A (with respect to L) can be analyzed equivalently using the transformed vector field. Note that the trajectories of Z^T demand a more careful analysis near the singular surface to be consistent with the DAE Σ , as explained in Section 8.2.1.

In this section, we present results on the internal structure of the stability boundaries. This analysis then paves the way for characterization of the stability boundary ∂A in the next section. The results presented in this section are extensions of the results for unconstrained systems in Refs. [7, 9, 10, 13]. The results presented here cover the boundary characterization results for smooth systems in Refs. [9] and [10] as the special case when the singular set S is empty. Although most of the results use the transformed vector field Z^T and its flow Φ_t^T , it should be emphasized that the results stated in the following are directly valid for stable manifolds and stability boundaries for the vector field Z .

For some of the results, we will assume that the intersections of stable and unstable manifolds are transversal. Let N_C denote a connected component of either N_ψ or N_ξ . Let B_C denote a connected component of the set of bad pseudoequilibria B_ψ . The assumption can be precisely stated as follows:

- (A) Restricted to \bar{A} , stable manifolds from the set $\{W^s(z_0), W^s(\gamma_0), W^s(N_C), W^s(B_C)\}$ intersect transversally with unstable manifolds from the set $\{W^u(z_0), W^u(\gamma_0), W^u(N_C), W^u(B_C)\}$.

Equilibrium points, periodic orbits, pseudoequilibria, and semisingular points in the boundary of the region of attraction will be called *anchor points*.

The objective in this section is to study the properties of the stable and unstable manifolds of anchor points, when they are present on the stability boundaries. This preliminary analysis sets up the basis for stronger conditions to be developed below. *The main results are summarized here.*

Theorem 8.2.2: Basic Anchor Theorem [2, 31] Suppose the equilibrium z and the periodic orbit γ are hyperbolic and all pseudoequilibria ψ and semi-singular points ξ lie in the nice sets in the statement below. Let η stand for any of (1) hyperbolic equilibrium, (2) a hyperbolic periodic orbit, (3) a connected component of the nice set, or (4) a connected component of the bad set. For the equivalences marked with an asterisk, also assume that assumption (A3) on the transversal intersections of stable and unstable manifolds holds. Furthermore, v is used to label pseudosaddles or semisaddles, and $v \notin \partial\eta$. Then

1. For an equilibrium point z_0

$$\begin{aligned} z \in \partial W^s(z_0) &\iff [W^u(z) \setminus \{z\}] \cap \overline{W^s(z_0)} \neq \emptyset \\ (*) \quad z \in \partial W^s(z_0) &\iff [W^s(z) \setminus \{z\}] \cap \partial W^s(z_0) \neq \emptyset \\ \gamma \in \partial W^s(z_0) &\iff [W^u(\gamma) \setminus \{\gamma\}] \cap \overline{W^s(z_0)} \neq \emptyset \\ (*) \quad \gamma \in \partial W^s(z_0) &\iff [W^s(\gamma) \setminus \{\gamma\}] \cap \partial W^s(z_0) \neq \emptyset \\ v \in \partial W^s(z_0) &\iff W^u(v) \cap \overline{W^s(z_0)} \neq \emptyset \end{aligned} \tag{8.39}$$

If z_0 is stable, no transversality assumptions are required.

2. For a periodic orbit γ_0

$$\begin{aligned} z \in \partial W^s(\gamma_0) &\iff [W^u(z) \setminus \{z\}] \cap \overline{W^s(\gamma_0)} \neq \emptyset \\ (*) \quad z \in \partial W^s(\gamma_0) &\iff [W^s(z) \setminus \{z\}] \cap \partial W^s(\gamma_0) \neq \emptyset \\ \gamma \in \partial W^s(\gamma_0) &\iff [W^u(\gamma) \setminus \{\gamma\}] \cap \overline{W^s(\gamma_0)} \neq \emptyset \\ (*) \quad \gamma \in \partial W^s(\gamma_0) &\iff [W^s(\gamma) \setminus \{\gamma\}] \cap \partial W^s(\gamma_0) \neq \emptyset \\ v \in \partial W^s(\gamma_0) &\iff W^u(v) \cap \overline{W^s(\gamma_0)} \neq \emptyset \end{aligned} \tag{8.40}$$

3. For a connected component N_C of the nice set, with $v \notin \partial N_C$,

$$\begin{aligned} z \in \partial W^s(N_C) &\iff [W^u(z) \setminus \{z\}] \cap \overline{W^s(N_C)} \neq \emptyset \\ (*) \quad z \in \partial W^s(N_C) &\iff [W^s(z) \setminus \{z\}] \cap \partial W^s(N_C) \neq \emptyset \\ \gamma \in \partial W^s(N_C) &\iff [W^u(\gamma) \setminus \{\gamma\}] \cap \overline{W^s(N_C)} \neq \emptyset \\ (*) \quad \gamma \in \partial W^s(N_C) &\iff [W^s(\gamma) \setminus \{\gamma\}] \cap \partial W^s(N_C) \neq \emptyset \\ v \in \partial W^s(N_C) &\iff W^u(v) \cap \overline{W^s(N_C)} \neq \emptyset \end{aligned} \tag{8.41}$$

4. For a connected component B_C of the bad set, with $v \notin \partial B_C$,

$$\begin{aligned} z \in \partial W^s(B_C) &\iff [W^u(z) \setminus \{z\}] \cap \overline{W^s(B_C)} \neq \emptyset \\ (*) \quad z \in \partial W^s(B_C) &\iff [W^s(z) \setminus \{z\}] \cap \partial W^s(B_C) \neq \emptyset \\ \gamma \in \partial W^s(B_C) &\iff [W^u(\gamma) \setminus \{\gamma\}] \cap \overline{W^s(B_C)} \neq \emptyset \quad (8.42) \\ (*) \quad \gamma \in \partial W^s(B_C) &\iff [W^s(\gamma) \setminus \{\gamma\}] \cap \partial W^s(B_C) \neq \emptyset \\ v \in \partial W^s(B_C) &\iff W^u(v) \cap \overline{W^s(B_C)} \neq \emptyset \end{aligned}$$

8.2.2.2 Assumptions In this section, we state certain assumptions that are extensions of the assumptions for the Morse–Smale systems of smooth dynamical systems. It will be assumed that the following assumptions are satisfied in the closure of the region of attraction \bar{A} :

(A1) The nice sets N_ψ and N_ξ are dense in Ψ and Ξ , respectively. Furthermore, at every point $\psi \in \Psi$ or $\xi \in \Xi$, the sets B_ψ and B_ξ have dimension at most $n - 3$.

(A2) (a) Equilibria z_0 and periodic orbits γ_0 in the boundary of the region of attraction, ∂A , are hyperbolic.

(b) Except for sets of dimension at most $n - 3$, all pseudosaddles in ∂A are transverse.

(A3) Stable manifolds from the set $\{W^s(z_0), W^s(\gamma_0), W^s(N_C), W^s(B_C)\}$ intersect transversally with unstable manifolds from the set $\{W^u(z_0), W^u(\gamma_0), W^u(N_C), W^u(B_C)\}$. Here N_C stands for a connected component of either N_ψ or N_ξ and B_C stands for a connected component of B_ψ or B_ξ .

(A4) All trajectories converge to an equilibrium point, a periodic orbit, a pseudoequilibrium point, or a semisingular point.

It can be shown that generally assumptions (A1) to (A3) will be satisfied for the system Σ [2, 31]. However, assumption (A4) is not generic, but will be satisfied if there exists a suitable dissipating energy function [1].

Lemma 8.2.11 If there exists a Lyapunov function $V = V(x, y)$ such that

1. $D_x V f - D_y V(D_y g)^{-1} D_x g f \leq 0$ in A
2. V is proper in the closure of A
3. The ω -limit set in \bar{A} consists only of equilibria and periodic orbits

then assumption (A4) is satisfied. All trajectories in ∂A converge to equilibria, periodic orbits, pseudoequilibria, or semisingular points.

8.2.2.3 Analysis of the Stability Boundary ∂A In the following assumptions (A1) to (A4) will be in effect in this chapter, unless stated otherwise. The composition of the stability boundary is established first.

Theorem 8.2.3 Stability Boundary Theorem [2, 31] Under assumptions (A1) to (A4) the stability boundary is composed of

1. Stable manifolds of unstable equilibria $z_0 \in \partial A$
2. Stable manifolds of unstable periodic orbits $\gamma_0 \subset \partial A$
3. Stable manifolds of transverse pseudosaddles $N_{\text{tr},\text{sa}} \cap \partial A$
4. Stable manifolds of semisaddles $N_{\text{se},\text{sa}} \cap \partial A$
5. Stable manifolds of other pseudoequilibria $(\Psi \setminus N_{\text{se},\text{sa}}) \cap \partial A$
6. Stable manifolds of other semisingular points $(\Xi \setminus N_{\text{se},\text{sa}}) \cap \partial A$
7. Singular boundary pieces $S \cap \partial \bar{A}$

In other words,

$$\begin{aligned} \partial A = & \bigcup_{z_0 \in \partial A} W^s(z_0) \bigcup_{\gamma_0 \in \partial A} W^s(\gamma_0) \cup W^s(N_{\text{tr},\text{sa}} \cap \partial A) \\ & \cup W^s(N_{\text{se},\text{sa}} \cap \partial A) \cup [W^s(\Psi \setminus N_{\text{tr},\text{sa}}) \cap \partial A] \\ & \cup [W^s(\Xi \setminus N_{\text{se},\text{sa}}) \cap \partial A] \cup (S \cap \partial \bar{A}) \end{aligned} \quad (8.43)$$

We next state a set of necessary and sufficient conditions for distinguishing the anchor points (that anchor the stable manifolds within ∂A) from among the various candidates such as unstable equilibria, unstable periodic orbits, pseudosaddles, and semisaddles. First, we consider order-1 equilibria on the stability boundary ∂A .

Lemma 8.2.12 Suppose z_0 is an order-1 equilibrium point. Then

$$z_0 \in \partial A \iff [W^u(z_0) \setminus \{z_0\}] \cap A \neq \emptyset \quad (8.44)$$

$$z_0 \in \partial A \iff W^s(z_0) \subset \partial A \quad (8.45)$$

Note that for a general unstable equilibrium, a necessary condition is already available in the basic anchor theorem; however, this is weaker than for the order-1 equilibria in Lemma 8.2.12. The sufficient condition is of the same nature in general.

Lemma 8.2.13 Suppose z_0 is a hyperbolic unstable equilibrium point. Then

$$z_0 \in \partial A \iff W^s(z_0) \subset \partial A \quad (8.46)$$

A similar result follows for unstable periodic orbits.

Lemma 8.2.14 Suppose γ_0 is a hyperbolic unstable periodic orbit. Then

$$\gamma_0 \in \partial A \iff W^s(\gamma_0) \subset \partial A \quad (8.47)$$

The conditions for pseudosaddles and semisaddles are presented for convenience as part of the quasistability boundary analysis that follows.

8.2.2.4 Analysis of the Quasistability Boundary $\partial\bar{A}$ To simplify the proofs in this section, the role of periodic orbits as anchor points on the quasistability boundary will not be investigated. We only consider the set of anchor points consisting of equilibria, pseudoequilibria, and semisingular points. The basic structure of the periodic orbits on the stability boundary ∂A has been illustrated by the stability boundary theorem (Theorem 8.2.3). The contribution of the stable manifolds of the periodic orbits to the quasistability boundary $\partial\bar{A}$ can also be established in an analogous way. Such an extension will be presented elsewhere.

More precisely, in addition to assumptions (A1) to (A4), we make the following assumption:

(A5) The ω -limit set for any trajectory in ∂A consists only of equilibrium points.

Assumptions (A4) and (A5) together imply that all the trajectories on the stability boundary converge to equilibrium points, pseudoequilibria, or semisingular points. (no periodic orbits on $\partial\bar{A}$). The energy-function lemma (Lemma 8.2.11) can be restated to guarantee both assumptions (A4) and (A5) as shown next and the proof is exactly same as for Lemma 8.2.11. Note that all the existing energy functions for constrained power system models of the form Σ do not permit the presence of periodic orbits anyway [25, 39], hence this assumption (A5) is not restrictive.

Lemma 8.2.15 If there exists a Lyapunov function $V = V(x, y)$ such that

1. $D_x V f - D_y V(D_y g)^{-1} D_x g f \leq 0$ in A
2. V is proper in the closure of A
3. The ω -limit set in \bar{A} consists only of equilibria

then assumptions (A4) and (A5) are satisfied. All trajectories in ∂A converge to equilibria, pseudoequilibria or semisingular points.

8.2.2.4.1 Anchor Characterization Theorem The basic structure of the anchors on the boundary $\partial\bar{A}$ is considered first. A set of necessary and sufficient conditions for some of the anchor points on the quasistability boundary are summarized as a Theorem below.

Theorem 8.2.4: Anchor Characterization Theorem [2, 31]

$$\begin{aligned} z_0^1 \in \partial\bar{A} &\iff W^u(z_0^1) \cap A \neq \emptyset \quad \text{and} \quad W^u(z_0^1) \cap \bar{A}^c \neq \emptyset \\ z_0^1 \in \partial\bar{A} &\iff W^s(z_0^1) \subset \partial\bar{A} \end{aligned} \quad (8.48)$$

and

$$\begin{aligned} v \in N_{n-1}^v &\iff \text{there exists a } \delta_0 > 0 \text{ such that for every } \delta < \delta_0, \\ &\quad W^u(\delta(v)) \cap A \text{ is dense in } W^u(\delta(v)), \text{ for any} \\ &\quad \delta\text{-sized neighborhood, } \delta(v), \text{ in } N_v \end{aligned} \quad (8.49)$$

$$v \in N_{n-1}^v \iff W^s(v) \subset \partial\bar{A} \quad (8.50)$$

where

$$N_{n-1}^\psi = \{\psi \in N_{\text{tr,sa}} \cap \partial\bar{A}: \text{there exists a } \delta > 0 \text{ such that the } \delta\text{-sized} \\ \text{neighborhood of } \psi \text{ in } N_\psi, \delta(\psi) \subset \partial\bar{A}\} \quad (8.51)$$

and

$$N_{n-1}^\xi = \{\xi \in N_{\text{se,sa}} \cap \partial\bar{A}: \text{there exists a } \delta > 0 \text{ such that the } \delta\text{-sized} \\ \text{neighborhood of } \xi \text{ in } N_\xi, \delta(\xi) \subset \partial\bar{A}\} \quad (8.52)$$

Here v labels either ψ or ξ .

8.2.2.4.2 Quasistability Boundary Theorem Recall that the order of an equilibrium point z_0 is the dimension of its unstable subspace and is denoted by a superscript.

Theorem 8.2.5: Quasistability Boundary Theorem [2, 31] Under assumptions (A1) to (A5), the boundary of the closure of the region of attraction $\partial\bar{A}$, the quasistability boundary, is composed of the following principal elements,

1. Stable manifolds of order 1 equilibria $z_0^1 \in \partial\bar{A}$
2. Stable manifolds of transverse pseudosaddles $N_{n-1}^\psi \cap \partial\bar{A}$
3. Stable manifolds of semisaddles $N_{n-1}^\xi \cap \partial\bar{A}$
4. Stable manifolds of bad anchors B_{n-1}
5. Singular boundary pieces $S \cap \partial\bar{A}$

More precisely

$$\partial\bar{A} = \overline{\bigcup_{z_0^1 \in \partial\bar{A}} W^s(z_0^1) \cup W^s(N_{n-1}) \cup [W^s(B_{n-1}) \cap \partial\bar{A}] \cup (S \cap \partial\bar{A})} \quad (8.53)$$

where $N_{n-1} = N_{n-1}^\psi \cup N_{n-1}^\xi$.

Note: Unstable limit cycles are not included to avoid major complications in the proof. They are, however, genuine components of the quasistability boundary [2].

By inspection of the stability boundary composition (8.43) with the quasistability boundary structure (8.53), the simplification in using the quasistability boundary is apparent. A qualitative representation of the boundary $\partial\bar{A}$ is shown in Figure 8.6 (periodic orbits are also included for conceptual clarity).

For the power-system model, only polynomials and polynomial functions of sinusoidal functions are present. If the angles are restricted to a variation of 2π , it follows from algebraic stratification theory (essentially, from the Tarski–Seidenberg theorem [44], that the numbers of equilibria and the numbers of connected components of N , B , and S are finite. Therefore suppose assumptions (A1) to (A5) hold. Then for a power-system model there are only finitely many terms in the union

$$\partial\bar{A} = \bigcup_{z_0^1 \in \partial\bar{A}} \overline{W^s(z_0^1)} \cup \overline{W^s(N_{n-1})} \cup [\overline{W^s(B_{n-1})} \cap \partial\bar{A}] \cup (S \cap \partial\bar{A})$$

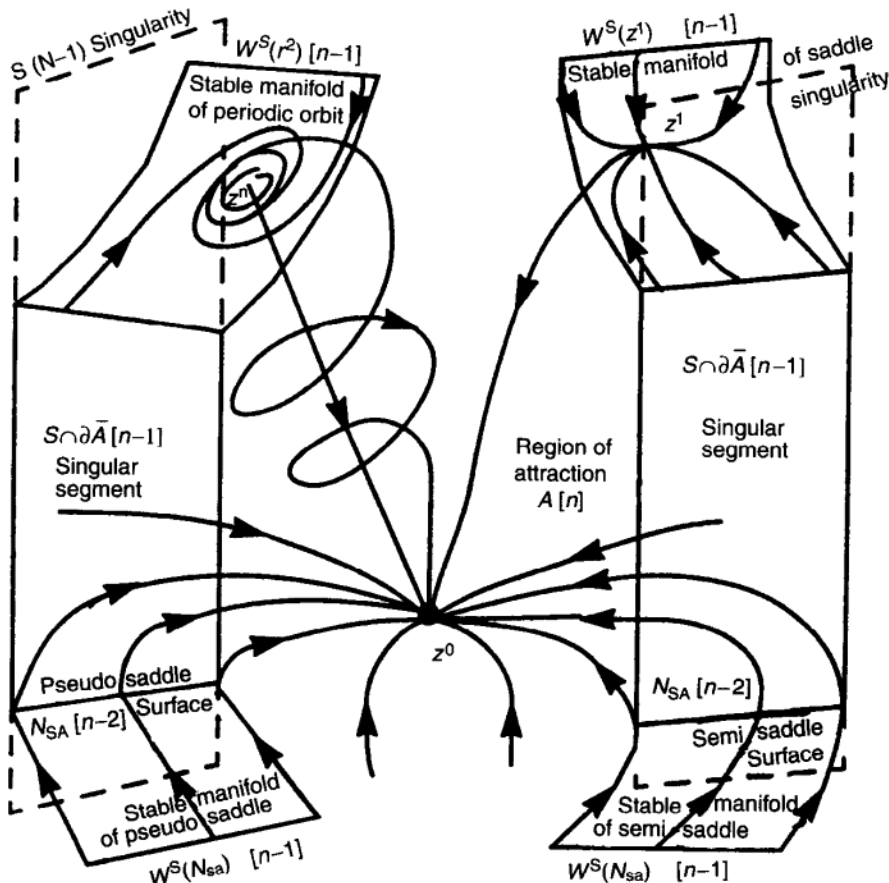


FIGURE 8.6 Qualitative representation of the boundary of the region of attraction $\partial\bar{A}$.

8.2.2.5 Energy-Function Results Suppose an energy function V with the properties as defined in Lemma 8.2.15 is available. Then, define the set $\mathcal{R}(e)$ as the connected component of the set

$$\{z \in C: V(z) < e\} \quad (8.54)$$

that contains the stable equilibrium point z_s .

Lemma 8.2.16 [2] Suppose e_{\max} is the largest number such that $\overline{\mathcal{R}(e_{\max})}$ does not intersect with the set of unstable equilibrium points, pseudoequilibrium surface, and the semisingular surface. Then

$$\mathcal{R}(e_{\max}) \subset A \quad (8.55)$$

It follows by Theorem 8.2.5 and the definition of \mathcal{P} that the quasistability boundary is composed of the closure of the stable manifolds of the principal anchors and the singular set $S \cap \partial\bar{A}$. The energy V decreases along the trajectories. Suppose α and β are anchor points. Then, by continuity, if $\alpha \in \partial W^s(\beta)$, then $V(\alpha) \geq V(\beta)$. By Theorem 8.2.5, every anchor point that is not principal belongs to the boundary of the principal anchor points or the boundary of their stable manifolds. Hence we have proved the next result:

Lemma 8.2.17 The energy function attains its lowest values at the closure of the set of principal anchor points in the quasistability boundary.

The next result provides an energy function based estimate of the stability region \bar{A} .

Lemma 8.2.18 [2] Suppose α is an anchor point. Then $\mathcal{R}(V(\alpha)) \subset \bar{A}$ if and only if α is the point in the set, $\bar{\mathcal{P}}$ with the lowest energy.

In the previous lemma, we have developed a method for computing a conservative estimate of the region $\text{int}(\bar{A})$ (which better serves as the region of attraction A due to practical considerations [9]). However, given an initial condition z_0 , for testing whether z_0 belongs to the region of attraction or more generally to $\text{int}(\bar{A})$, we need to compute the stable manifolds of the principal anchors along with the singular segment (see Theorem 8.2.5) for a rigorous stability test. To provide a practical tool for judging the stability of the given point, next an energy-function-type method is developed for finding the “critical” sections of the stability boundary (which has multitudes of sections on a large system) where the boundary may be breached. Among all the principal anchor points, we will prove that those with energy higher than the energy of the given initial state can be ignored for the stability test. The result thus considerably reduces the complexity of a rigorous stability test. This concept was originally introduced and analyzed in Ref. [9] and stability monitoring schemes based on this concept

have been developed in Ref. [45]. Here we extend those results to include new segments in the quasistability boundary for our problem, such as the singularity and the pseudosaddles.

DEFINITION 1 Given an initial condition z_0 , the critical anchor points are the principal anchor points with energy lower than $V(z_0)$.

So, \mathcal{P} can be divided into two sets \mathcal{P}_c and \mathcal{P}_{nc} defined as

$$\mathcal{P}_c(z_0) := \{\alpha \in \mathcal{P}: V(\alpha) \leq V(z_0)\} \quad (8.56)$$

$$\mathcal{P}_{nc}(z_0) := \{\alpha \in \mathcal{P}: V(\alpha) > V(z_0)\} \quad (8.57)$$

The next lemma enables us to consider only the critical anchor points \mathcal{P}_c for stability tests.

Lemma 8.2.19: Critical Anchor Lemma Suppose $z_0 \in C$ is an initial condition. Then, z_0 is inside (outside) $\bar{A} \Leftrightarrow z_0$ is inside (outside) the portion of the stability boundary defined by the closure of stable manifolds of the critical anchor points

This method is still conservative because typically the stability boundary is at a lower level than the anchor point. But it is not as conservative as the typical “direct method” techniques, since it only analyzes stability segments near the actual state Z_0 .

8.2.3 Structure of the Parameter Space

The parameter space can be broadly divided (functionally) into the set of all system parameters (that do not change during system operation) and the set of operating parameters (that can change during operation). When these parameters change, the state space (consisting of system trajectories or transients) associated with each parameter value undergoes changes; however, the structure of the state space remains topologically equivalent unless we encounter certain boundaries in the parameter space, namely, the bifurcation boundaries. In other words, the bifurcation surfaces in the parameter space divide the parameter space into open connected regions called the typal regions [1, 30] within which the structure of the state space remains identical. This includes the static properties such as the equilibrium structure, dynamic local properties such as the stability status of equilibria, and dynamic global properties such as the composition of the stability boundary. Therefore, this knowledge on the properties of typal regions would provide us with a sort of “complete” overview of the current system operation for security studies. However, unfortunately, at the present time, such an overview seems to be impossible even theoretically for large nonlinear systems. This is because the boundary of the typal regions consists of local and global bifurcations. Specifically, the global bifurcations in general can themselves be dense in open

sets of projection into the parameter space (see [28, 40], complex behavior), which then renders the problem extremely difficult to analyze the large system. Analysis of a three-dimensional system, the rudimentary system, is presented in Section 7.2 in which a detailed analysis is presented of the typical regions in Figures 7.8 and 7.10. These and the associated discussions give wide conceptual insight. The analysis in this section for the reasons described is restricted to the study of a simpler yet more practical concept in the parameter space called the notion of feasibility regions. (This concept is also introduced and demonstrated in Section 7.2 on a small system.)

The concept of feasibility regions in the solution space of nonlinear problems has existed for a long time (for instance, refer to the optimization theory). In the power-system context, Jargis and Galiana [14] introduced the notion of load-flow feasibility for quantifying the solvability of the load-flow equations in parameter space. Later work [43] extended this concept to include the effects of small-signal stability by restricting the analysis to those solutions in which the system is stable against small signals. The boundary of this region then consists of points where an operating point undergoes change in its eigenstructure, and these points therefore correspond to local bifurcations. In unconstrained system models, it is well-known that the generic local bifurcations are the saddle-node bifurcation (connected with zero eigenvalue of the system Jacobian) and the Hopf bifurcation (related to purely imaginary eigenvalues of the system Jacobian). The first case of zero eigenvalues and the saddle-node bifurcation has been studied extensively in the recent past connected with the voltage-collapse phenomena. The Hopf bifurcation can be generally associated with oscillatory phenomena [4, 46] leading to either stable oscillations (supercritical Hopf, [60]) or oscillatory divergence (subcritical Hopf [60]). Recently, occurrences of oscillatory voltage disturbances have been reported by the industry, even though this phenomenon is not wellunderstood in general. Chapter 9 will be devoted to the analysis of such a real life Hopf-related event on a very large system (7500 buses) using the theory base presented in Chapter 7 for a practical lower-scale computational study. There has been extensive research progress recently (e.g., [37, 47 to 49]) on the problem of computing the nearest saddle-node- and Hopf-bifurcation points in the parameter space.

In Refs. [1, 30], the notion of a feasibility region is proposed in the combined state and parameter spaces as the set of all operating points in the parameter space that can be reached by quasistatic parametric variations as part of the system operation. This region projected into the parameter space then naturally identifies a safe operating region in the parameter space within which the operation can be shifted around freely (by slow continuous parameter changes) without imminent danger of losing local stability. Of course, it has to be remembered that the size of the region of attraction (roughly the size of the region of transient stability) decreases to zero as one approaches the feasibility boundary (see loss of stability theorem [2] and Section 8.2.3.1); therefore, the proximity to the feasibility boundary, that is, the boundary of the feasibility region, could indicate potential emergence of transient-instability problems. So in summary, while the

system operation has to stay inside the feasibility region for sustained small-signal stability, it is also desirable to stay well inside the region and away from the boundary to lessen the danger of transient instability phenomena. All this demands a careful analysis of the feasibility boundary for gaining insight into its structure and for developing techniques to compute them.

We will show that the boundary of the feasibility region as defined here typically consists of three types of bifurcation surfaces, namely the saddle node, Hopf, and the singularity-induced bifurcations (Sec. 8.2.3.2). The saddle-node-bifurcation boundary segments can be computed by solving for a zero set of explicit functions [20, 60], which forms the basis for computational methods that exploit the rank deficiency [50] (point of collapse methods, [37]). Computational methods have been developed for computing the distance to the saddle-node- (a small sample-[19, 37, 47]) and Hopf-bifurcation boundaries [49]. Here in Section 8.2.3, it will be shown that all three bifurcation surfaces can be characterized as zero sets of explicit functions, and hence the whole feasibility boundary should be amenable to computational methods for system security of the large system (this will be demonstrated on a very large 7500-bus system in Chapter 9). Note that combined with model-reduction techniques such as dynamic clustering approaches [51] and/or participation-factor approaches [52] for developing practical computer algorithms, the efficiency of such computations could be greatly increased.

8.2.3.1 Feasibility Regions and Feasibility Boundary In Section 7.2, the concepts of the feasibility region and feasibility boundary were introduced and thoroughly analyzed for a small three-dimensional system. Such a study is useful for developing conceptual understanding, yet the power system is a very large and complex system. Hence only a comprehensive and general theory for the system without limitation of its size and the details of its modeling is really useful for the real-life power system. Such a feasibility theory will now be introduced. Let

$$\begin{aligned} \text{EQ} &= \{(x, y, p) \in X \times Y \times P: f(x, y, p) = 0, g(x, y, p) = 0\} \\ \text{OP} &= \{(x, y, p) \in \text{EQ}: D_y g \text{ is nonsingular and } J = D_x f - D_y f(D_y g)^{-1} D_x g \\ &\quad \text{has eigenvalues with negative real part}\} \end{aligned} \quad (8.58)$$

Here $D_x f$, etc., denote the matrix of partial derivatives of the components of f with respect to x . EQ is the set of equilibrium points and OP is the subset of stable equilibria. Note that the full Jacobian in x and y is nonsingular for $(x, y, p) \in \text{OP}$ and therefore, by the implicit function theorem, the equations $f(x, y, p) = 0$ and $g(x, y, p) = 0$ can theoretically be solved uniquely for x and y as functions of the parameter p . Hence OP is a p -dimensional submanifold embedded in $\text{EQ} \subset X \times Y \times P$.

DEFINITION 2 Given a stable equilibrium $z_s^0 = (x_0, y_0)$ (a load flow solution) for parameter value p_0 , the connected component F of OP that contains

(x_0, y_0, p_0) is called the feasibility region of z_s^0 . Its boundary (relative to EQ) is the feasibility boundary.

Note that the feasibility region is defined as a subset of $X \times Y \times P$, not as a subset of the parameter space. This way, *all possible stable equilibrium points that can be reached from (x_0, y_0, p_0) by continuous variations of the parameter while maintaining stability form the feasibility region*. Furthermore, the feasibility regions directly interact with the regions of viability and transient stability. The intersections of these three define the region of security as explained in Section 8.3.2.1.

Theorem 8.2.6: Feasibility Boundary Theorem [46] For a system defined in Eqs. (8.1) and (8.2), the feasibility boundary of a feasibility region F consists of three zero sets:

$$\partial F = (\partial F \cap C_S) \cup (\partial F \cap C_Z) \cup (\partial F \cap C_H) \quad (8.59)$$

where

$$C_S = \{(x, y, p) \in \text{EQ}: \det D_y g = 0\}, \quad (8.60)$$

$$C_Z = \left\{ (x, y, p) \in \text{EQ}: \det D_y g \neq 0, \det \begin{pmatrix} D_x f & D_y f \\ D_x g & D_y g \end{pmatrix} = 0 \right\} \quad (8.61)$$

and

$$C_H = \left\{ (x, y, p) \in \text{EQ}: \det D_y g \neq 0, \det \begin{pmatrix} D_x f & D_y f \\ D_x g & D_y g \end{pmatrix} \neq 0, \det [H_{n-1}(J)] = 0 \right\} \quad (8.62)$$

where

$$J = D_x f - D_y f (D_y g)^{-1} D_x g \quad (8.63)$$

and H_{n-1} is the Hurwitz matrix [52] corresponding to the coefficients of the characteristic polynomial of J .

The three zero sets, which constitute the feasibility boundary, correspond to specific conditions on the eigenvalues of the system. As a point on EQ approaches C_S some eigenvalues diverge to infinity. The equilibrium has zero eigenvalues in the set C_Z and purely imaginary eigenvalues for points in the set C_H (see Fig. 8.7). Under generic conditions local bifurcations occur at all these points, namely, a singularity-induced bifurcation in C_S , a saddle-node bifurcation in C_Z , and a Hopf bifurcation in C_H . Moreover, generically these bifurcations constitute a dense subset of the feasibility boundary for Eqs. (8.1) and (8.2). Saddle-node and Hopf bifurcations are well known in the literature, and accordingly

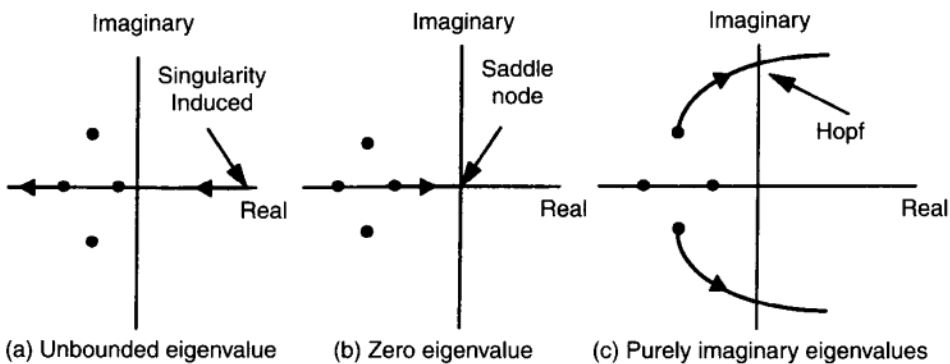


FIGURE 8.7 Locus of the eigenvalues near the three feasibility boundary segments.

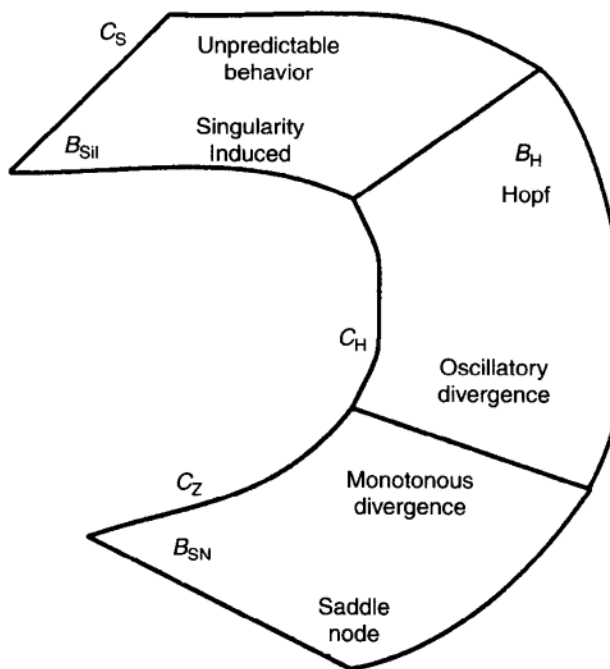


FIGURE 8.8 Qualitative representation of a segment of the feasibility boundary.

results will be simply stated for these. The singularity-induced bifurcation will be analyzed.

A qualitative representation of the feasibility boundary is shown in Figure 8.8. Specific numerical examples for a small system are presented for these results in Figure 7.14 and the accompanying text.

8.2.3.2 Principal Bifurcations on the Feasibility Boundary The feasibility boundary ∂F may contain some internal segments of the boundary, that is, in

$\text{int}(\overline{F})$ (closure is with respect to EQ, the set of all equilibrium points). Since such boundary segments $\partial F \cap \text{int}(\overline{F})$ lie in the interior, they do not correspond to loss of stability of the operating point. If $(z, p) \in \partial F \cap \text{int}(\overline{F})$, then we can find a neighborhood U of (z, p) in EQ such that most of the operating states in U are stable. Hence, with the model equations (8.1) and (8.2), the feasibility boundary segments in the interior $\partial F \cap \text{int}(\overline{F})$ do not imply loss of stable operation at the present operating equilibrium state. Next theorem states that generically there are no internal segments of the feasibility boundary, that is,

$$\partial F \cap \text{int}(\overline{F}) = \emptyset \quad (8.64)$$

In other words, generically indeed the local stability at the operating equilibrium is lost at most of the feasibility boundary points.

Theorem 8.2.7: Loss of Stability Theorem [2, 46] Suppose system (8.1), (8.2) satisfies assumptions (A2) to (A4) [1, 2]. Then the saddle-node bifurcation, the Hopf bifurcation, and the singularity-induced bifurcation occur on a dense subset of the boundary ∂F . The feasibility boundary ∂F coincides with the quasifeasibility boundary $\partial\overline{F}$, that is, the stability of the equilibrium is lost at most of the boundary points.

Moreover, for a power-system model, as observed earlier, only polynomials and polynomial functions of sinusoidal functions are present. If the angles are restricted to a variation of 2π , it follows from algebraic stratification theory (essentially, from the Tarski–Seidenberg theorem [44]) that there are *finitely* many connected components of codimension one bifurcations in the quasi feasibility boundary.

Lemma 8.2.20 [46] For the power-system model, there are finitely many connected components in the union,

$$\partial F = \partial\overline{F} = (\overline{\partial F \cap B_H}) \cup (\overline{\partial F \cap B_{SiL}}) \cup (\overline{\partial F \cap B_{SN}}) \quad (8.65)$$

In short, the feasibility boundary can be computed as zero sets. Generically, for the system (8.1) and (8.2) most of the boundary points lead to a saddle-node, Hopf, or a singularity-induced bifurcation.

8.2.3.3 Analysis of the Singularity-Induced Bifurcation When the steady-state solution or the equilibrium defined by EQ approaches the singularity S , it has been observed that some eigenvalues of the system Jacobian at the equilibrium point become unbounded [3, 12, 19, 30, 54]. In Refs. [3, 30], it was shown that this case generally is “equivalent” to a transcritical bifurcation (“exchange of stability” bifurcation [60]) for a two-dimensional system. In this section, we analyze this scenario for the general system, Eqs. (8.1) and (8.2), will be analyzed, when the equilibrium approaches the singularity. As the change in

the structure is caused by the presence of the singular surface, we call this bifurcation the *singularity-induced bifurcation*. For analyzing the bifurcation, we use the singular transformation, which was introduced in Section 8.2.1.2. By analyzing the transformed system Z^T under certain transversality conditions, the local eigenstructure of the equilibrium point is established near the bifurcation point.

Theorem 8.2.8: Singularity-Induced Bifurcation Theorem [5, 46] Consider the system Σ_s with a one-dimensional parameter (say, μ) space. Suppose the following conditions are satisfied at $(0, 0, \mu_0)$.

(SI1) $f(0, 0, \mu_0) = 0$, $g(0, 0, \mu_0) = 0$, and $D_y g$ has a simple zero eigenvalue

(SI2) $\begin{pmatrix} D_x f & D_y f \\ D_x g & D_y g \end{pmatrix}$ is nonsingular

(SI3) $\begin{pmatrix} D_x f & D_y f & D_\mu f \\ D_x g & D_y g & D_\mu g \\ D_x \Delta & D_y \Delta & D_\mu \Delta \end{pmatrix}$ is nonsingular.

Then there exists a smooth curve of equilibria, say $\text{EQ}(\mu) := (x(\mu), y(\mu), \mu)$ in \mathbb{R}^{n+m+1} that passes through $(0, 0, \mu_0)$ and is transversal to the singular surface S at $(0, 0, \mu_0)$. When μ increases through μ_0 , one eigenvalue of the system, (that is, an eigenvalue of

$$J = D_x f - D_y f (D_y g)^{-1} D_x g \quad (8.66)$$

evaluated along the equilibrium locus, moves from the open left-half complex plane C^- to the open right-half complex plane C^+ if $b/c > 0$ (respectively from C^+ to C^- if $b/c < 0$) along the real axis by diverging through ∞ . The other eigenvalues remain bounded and stay away from the origin. Here c is defined as the derivative of Δ along $\text{EQ}(\mu)$:

$$c := \frac{d}{d\mu} \Big|_{\mu=\mu_0} \Delta(x(\mu), y(\mu), \mu) \quad (8.67)$$

and b is defined as the only nonzero eigenvalue of the Jacobian $-D_y f \text{adj}(D_y g) D_x g$ at $(0, 0, \mu_0)$, where $\text{adj}(A)$ stands for the classical matrix adjoint of the matrix A .

8.2.3.4 Local Dynamics near the Three Principal Bifurcations A detailed study of the qualitative behavior of the system Σ near the three principal boundaries, namely the saddle-node, Hopf, and the singularity-induced bifurcations would provide us with insight on how the instability develops as the system operation approaches one of the feasibility boundary segments. For the saddle-node-bifurcation boundary, such an analysis was presented in Ref. [55]

using center-manifold theory for certain unconstrained power-system models. It was shown that the occurrence of the saddle-node bifurcation is related to the voltage-collapse phenomenon under some conditions. In Refs. [4, 5, 46], all the three principal local bifurcations for the large constrained system Σ were considered and established the qualitative local behavior of Σ for the three cases. These results are briefly stated below. Details can be found in Refs. [4, 5, 46].

1. The saddle-node-bifurcation segments of the feasibility boundary correspond to monotonic divergence as shown conceptually in Figure 8.9.
2. The supercritical Hopf bifurcation implies the transition from stable equilibrium to sustained oscillations. (Fig. 8.10). Near the subcritical Hopf segments, the transients will be diverging in an oscillatory fashion (see Fig. 8.11).
3. For the singularity-induced bifurcation, it can be shown that generically even when the equilibrium is at the singularity, there exists an $(n - 1)$ -dimensional invariant manifold W^{reg} that passes through the singularity such that the singular dynamics Σ restricted to the invariant manifold is smooth. (see Fig. 8.12). Moreover, this invariant manifold is locally “attracting” on one side of the singular surface and “repelling” on the other side, thereby providing a “conduit” for the trajectories from one side of the singular surface to cross over to the other side at finite speed, possibly either diverging towards a new steady-state condition or ending at the singular surface, where a different model takes over. The constrained model Σ does not provide sufficient information to distinguish between the two different types of behaviors, so the singularity-induced bifurcation denotes a true barrier to *predictable* behavior with the model Σ from a mathematical as well as an engineering viewpoint. Moreover, the loss of reliable system prediction using Σ at this bifurcation follows for any constrained model of the form Σ under certain generic transversality assumptions and is not related to the limitations of the quasistationary assumption in phasor power-system models. A detailed description of the local dynamics near the singularity-induced bifurcation can be seen in Refs. [4, 5, 46].

8.2.3.5 *Typal Regions* A feasibility region consists of possibly several open subregions, called *typal regions*, and some of the respective boundaries. Typal regions are defined by the property that the phase portraits of the system are topologically equivalent (i.e., structurally stable) within one subregion. The boundaries between these regions are determined by various local and global bifurcation surfaces. The possibility of complex behavior connected with global bifurcations has been noted in angle [16, 17] and voltage [30, 55, 56] power-system models. For a rudimentary power system model [with $n = 2$ and $m = 1$ in Eqs. (8.1) and (8.2)], a complete classification of the typal regions has been given in Refs. [3, 31] for a realistic range of two parameters (power and control). However, for a general n -dimensional system defined by Eqs. (8.1) and (8.2), for

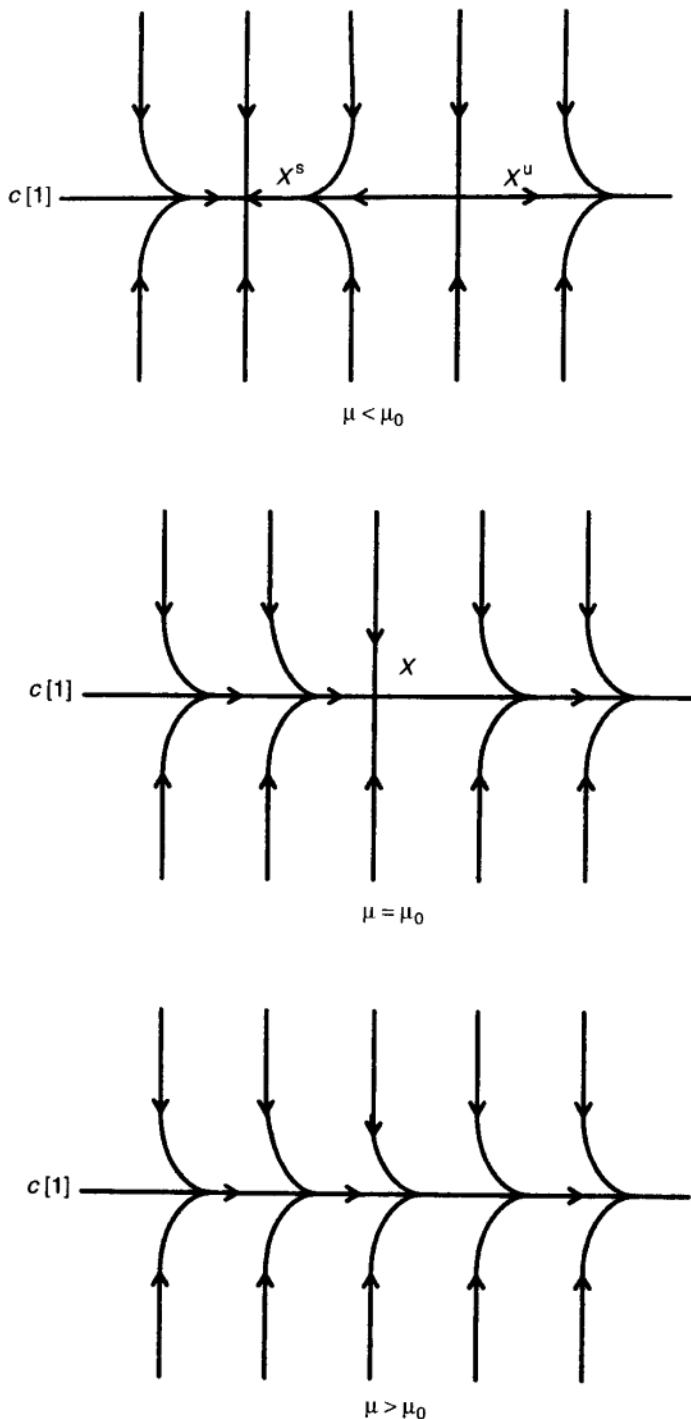


FIGURE 8.9 Instability mechanism of the saddle node bifurcation boundary: annihilation of the operating point results in monotonous divergence.

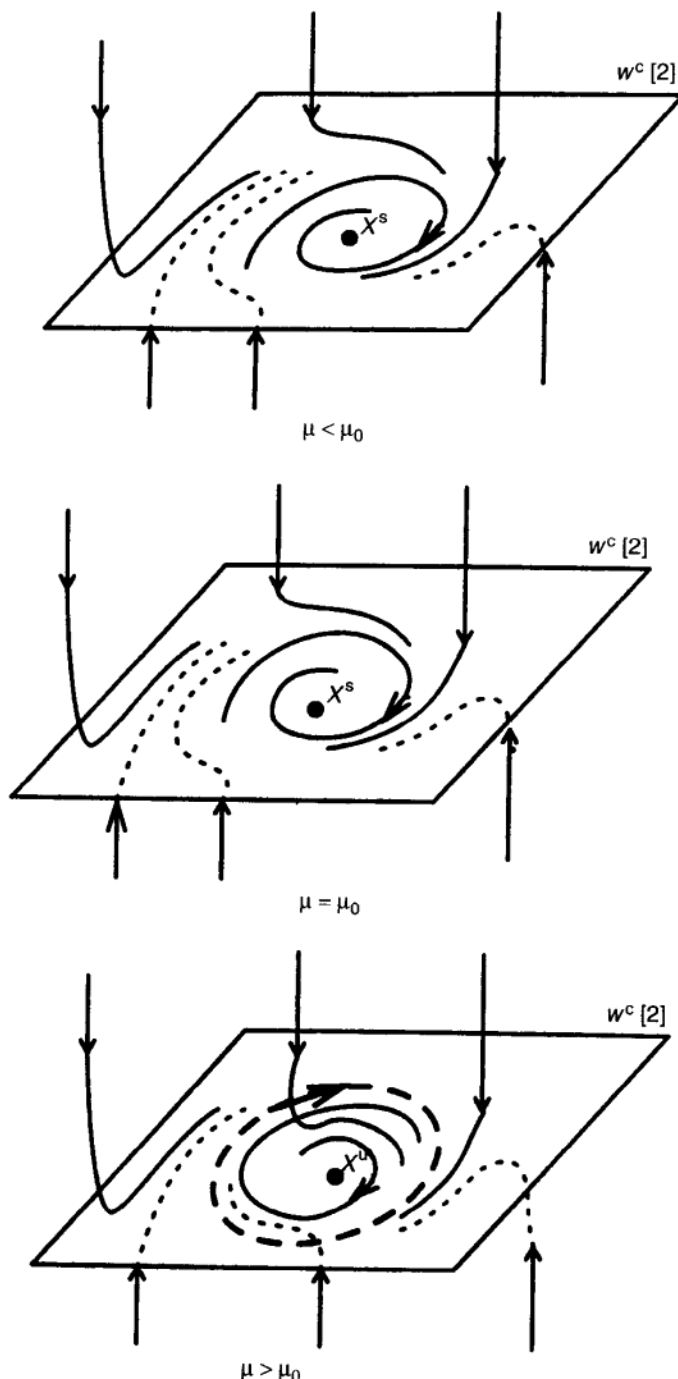


FIGURE 8.10 Instability mechanism of the supercritical Hopf-bifurcation boundary: Operation changes from an operating point to stable oscillations.

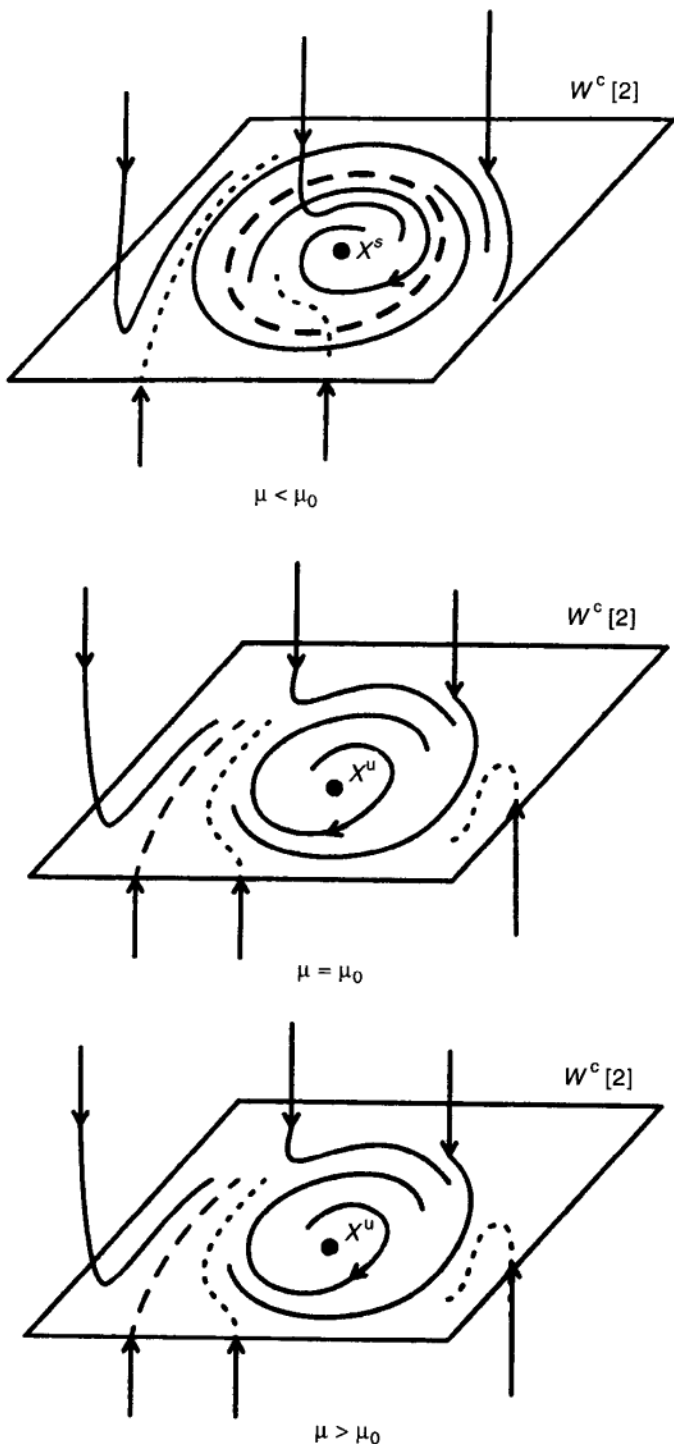


FIGURE 8.11 Instability mechanism of the subcritical Hopf-bifurcation boundary: Annihilation of the operating point leads to oscillatory diverging transient.

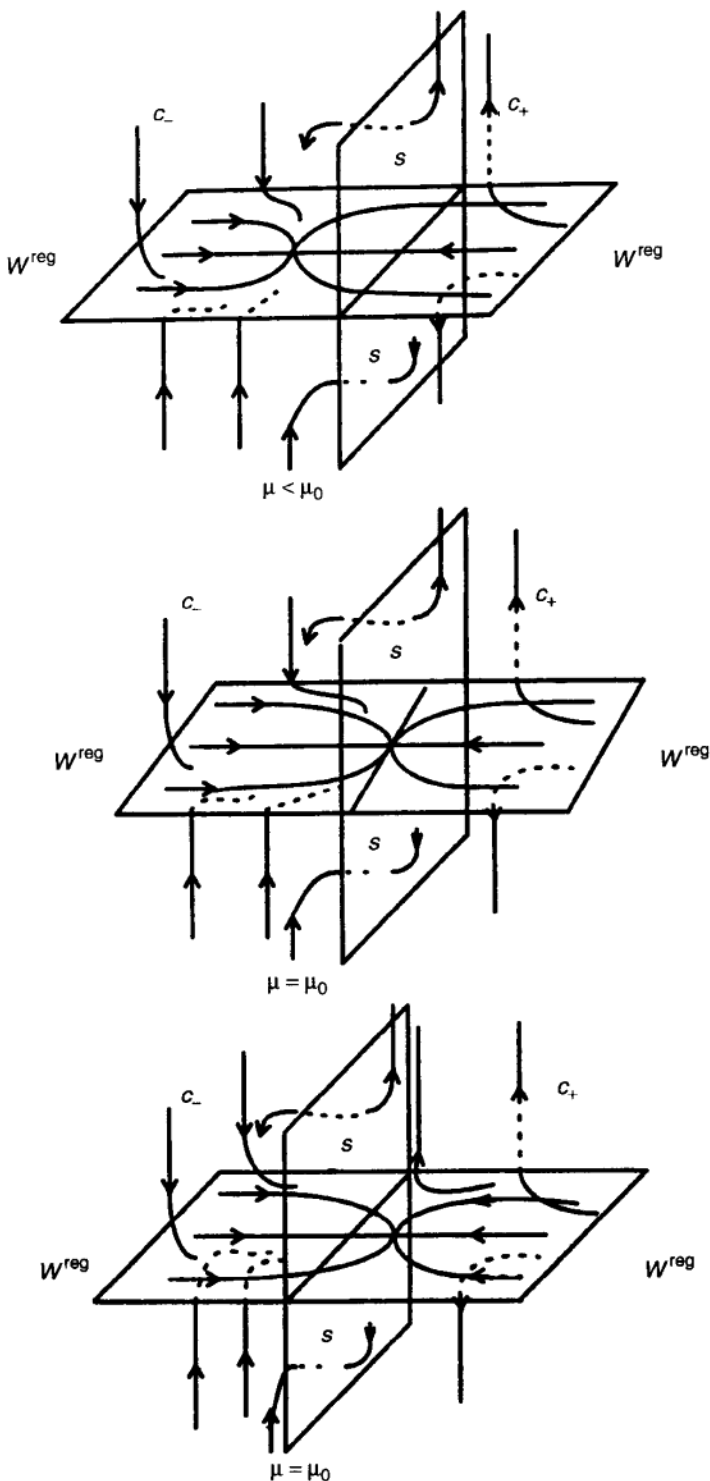


FIGURE 8.12 Instability mechanism of the singularity-induced bifurcation boundary: unpredictable system behavior.

reasons of dimensionality and because of the difficulty connected with complex system behavior, a similar complete description is unrealistic.

BIBLIOGRAPHY

1. Venkatasubramanian, V., Schättler, H., and Zaborszky, J., A taxonomy of the dynamics of the large electric power system with emphasis on its voltage stability, *Proc. NSF Intl. Workshop Bulk Power Syst. Voltage Phenom.—II*, 1991, pp. 9–52 (Editor Les Fink).
2. Venkatasubramanian, V., Schättler, H., and Zaborszky, J., A stability theory of large differential algebraic systems—a taxonomy, Report No. SSM 9201 Dept. of Systems Science and Math., Washington University, Saint Louis, MO.
3. Venkatasubramanian, V., Schättler, H., and Zaborszky, J., Voltage dynamics: Study of a generator with voltage control, transmission and matched MW load, *IEEE Trans. Automatic Control*, 1717–1733, 1992.
4. Venkatasubramanian, V., Schättler, H., and Zaborszky, J., Analysis of local bifurcation mechanisms in large differential-algebraic systems such as the power system, *Proc. IEEE Conf. Decision and Control*, 1993, pp. 3727–3733.
5. V. Venkatasubramanian, Jiang, X., Schättler, H., and Zaborszky, J., Current status of the taxonomy theory of large power system dynamics—DAE systems with hard limits, in L. H. Fink (ed.), *Proc. NSF Intl. Workshop Bulk Power Syst. Voltage Phenom.—III*, Davos, Switzerland, 1994, pp. 15–103.
6. Prapost, K. L., and Loparo, K. A., An energy function method for determining voltage collapse during a power system transient, *IEEE Trans. Circuits Syst.*
7. Zaborszky, J., Schättler, H., and Venkatasubramanian, V., Limitations of the quasi-stationary dynamics and error due to phasor computations in network equations, *Proc. Power Systems Comput. Conf.*, France, 1993, pp. 721–729.
8. Variaya, P. V., Wu, F. F., and Chen, R., Direct methods for transient stability analysis of power systems: Recent results, *Proc. IEEE*, 73: 1703–1715, 1985.
9. Zaborszky, J., Huang, G., Zheng, B., and Leung, T. C., On the phase portraits of a class of large nonlinear dynamic systems such as the power system, *IEEE Trans. Automatic Control*, 33: 4–15, 1988.
10. Chiang, H. D., Hirsch, M., and Wu, F., Stability regions of nonlinear autonomous dynamical systems, *IEEE Trans. Automatic Control*, 33: 16–27, 1988.
11. Zaborszky, J., Huang, G., and Zheng, B., A counter-example on a theorem by Tsolas et. al. and an independent result by Zaborszky et al., *IEEE Trans. Automatic Control*, 33: 316–318, 1988.
12. Smale, S., Differential dynamical systems, *Bull. Am. Math. Soc.*, 73: 747–817, 1967.
13. Palis, J., On Morse-Smale dynamical systems, *Topology*, 8: 385–405, 1969.
14. Jargis, J., and Galiana, F. D., Quantitative analysis of steady state stability in power networks, *IEEE Trans. Power Apparatus Syst.*, PAS-100: 318–326, 1981.
15. Abed, E. H., and Varaiya, P. P., Nonlinear oscillations in power systems, *International J. Electric Power Energy Syst.*, 6: 37–43, 1984.
16. Kopell, N., and Washburn, R. B., Chaotic motions in the two degree of freedom swing equations, *IEEE Trans. Circuits Syst.*, CAS 29: 738–746, 1982.

17. Salam, F. M. A., Marsden, J., and Varaiya, P. P., Arnold diffusion in swing equations of a power system, *IEEE Trans. Circuits Syst.*, **30**: 199–206, 1984.
18. Tamura, H., Mori, H., and Iwamoto, S., Relationship between voltage instability and multiple load flow solutions in electric power systems, *IEEE Trans. Power Apparatus Syst.*, **PAS-102**: 1115–1125, 1983.
19. Dobson, I., Observations on the geometry of saddle node bifurcation and voltage collapse in electric power systems, *IEEE Trans. Circuits Syst.*, **39**: 240–243, 1992.
20. Sotomayor, J., Generic bifurcations of dynamical systems, In M. M. Peixoto (ed.) *Dynamical Systems*, New York: Academic, 1973.
21. Zaborszky, J., and Zheng, B., Structure features of the dynamic state space for studying voltage-reactive control, *Proc. Power Syst. Comput. Conf.*, Graz, Austria, 1990, pp. 319–326.
22. Zaborszky, J., Subramanian, A. K., Tarn, T. J., and Lu, K. M., A new state space for emergency control in the interconnected power system, *IEEE Trans. Automatic Control*, **AC-22**: 505–517, 1977.
23. Anderson, P. M., and Fouad, A. A., *Power System Control and Stability*, Ames, IA: Iowa State Press, 1977.
24. Bergen, A. R., and Hill, D. J., A structure preserving models for power system stability analysis, *IEEE Trans. Power Apparatus Syst.*, **PAS-100**: 25–35, 1981.
25. Benoit, E., *Canards Thesis Et Enlancements*, Paris: Publications I.H.E.S., 1991.
26. Pai, M. A., *Power System Stability Analysis by Direct Method of Lyapunov*, New York: Elsevier North-Holland, 1981.
27. Ribbens-Pavella, M., and Evans, F. J., Direct methods for studying dynamics of large-scale electric power systems—A survey, *Automatica*, **21**: 1–21, 1985.
28. Anosov, D. V., and Arnold, V. I. (eds.), *Ordinary Differential Equations and Smooth Dynamical Systems*, Vol. I of Encyclopedia of Mathematics, New York: Springer, 1980.
29. Narasimhamurthi, N., and Musavi, M. R., A general energy function for transient stability analysis of power systems, *IEEE Trans. Circuits Syst.*, **CAS-31**: 637–645, 1984.
30. Hill, D. J., and Mareels, I. M. Y., Stability theory for differential/algebraic systems with applications to power systems, *IEEE Trans. Circuits Syst.*, 1416–1423, 1990.
31. Venkatasubramanian, V., A taxonomy of the dynamics of large differential-algebraic systems such as the power system, Ph.D. thesis, Washington University, Saint Louis, MO, August 1992.
32. Brenan, K. E., Campbell, S. L., and Petzold, L. R., *Numerical Solution of Initial Value Problems in Differential-Algebraic Equations*, Amsterdam: North-Holland, 1989.
33. Sastry, S., and Desoer, C., Jump behavior of circuits and systems, *IEEE Trans. Circuits Syst.*, **CAS-28**: 1109–1124, 1981.
34. Chua, L. O., and Deng, A. C., Impasse points—Part II: Analytical aspects, *Intell. J. Circuit Theory*, 1989.
35. Takens, F., Implicit differential equations: Some open problems, in *Singularités d'Applications Differentiables*, Plans-sur-Bex, 1975, Vol. 535 of *Lecture Notes in Mathematics*, Springer, 1976, pp. 237–253.

36. Takens, F., Constrained equations: a study of implicit differential equations and their discontinuous solutions, in *Structural Stability, The Theory of Catastrophes and the Application in the Sciences*, Vol. 525 of *Lecture notes in Mathematics*, Berlin: Springer, 1976, pp. 143–234.
37. Alvarado, F. L., and Jung, T. H., Direct detection of voltage collapse mechanisms, *Proc. Bulk Power Voltage Phenomena*, Potosi, MO, 1988.
38. Zvonkin, A. K., and Shubin, M. A., Non-standard analysis and singular perturbations of ordinary differential equations, *Russian Math. Surv.*, **39**(2): 69–131, 1984.
39. Hill, D. J., Hiskens, I. A., and Mareels, I. M. Y., Stability theory of differential/algebraic models of power systems, Technical Report No. EE8941, Department of Electrical Engineering and Computer Science, University of New Castle, Australia.
40. Bergen, A. R., *Power Systems Analysis*, Englewood Cliffs, NJ: Prentice-Hall, 1986.
41. Venkatasubramanian, V., Schättler, H., and Zaborszky, J., Homoclinic orbits and the persistence of the saddle connection bifurcation for the large electric power system, *Proc. Intl. Symp. Circuits Syst.*, 1993.
42. Abraham, R., Marsden, J. E., and Ratiu, T., *Manifolds, Tensor Analysis, and Applications*, 2nd ed., New York: Springer, 1983.
43. Andronov, A. A., Leontovich, E. A., Gordon, I. I., and Maeir, A. G., *Qualitative Theory of Second-Order Dynamic Systems*, New York: Wiley, 1973.
44. Jacobson, N., *Basic Algebra I*, San Francisco: Freeman, 1974.
45. Zaborszky, J., Huang, G., and Zheng, B., New results on stability monitoring on the large electric power systems, *Proc IEEE Conf. Decision Control*, Los Angeles, 1987, pp. 30–40.
46. Venkatasubramanian, V., Schättler, H., and Zaborszky, J., Local bifurcations and feasibility regions in differential-algebraic systems, *IEEE Trans. Automatic Control*, Vol. 40, 1995, pp. 1992–2013.
47. Ajjrapu, V., and Christy, C., The continuation power flow: A tool for steady state voltage stability analysis, *IEEE PICA Conf. Proc.*, 1991, pp. 304–311.
48. Dobson, I., and Lu, L., New methods for computing a closest saddle node bifurcation and worst case load power load margin for voltage collapse, *IEEE Power Eng. Soc. Summer Meet.*, Seattle, WA, 1992.
49. Dobson, I., An iterative method to compute a closest saddle node or Hopf bifurcation instability in multidimensional parameter space, *Proc. Intl. Symp. Circuits Syst.*, San Diego, 1992, pp. 2513–2516.
50. Seydel, R., *From Equilibrium to Chaos*, City: Elsevier Science, 1988.
51. Varghese, G. C., Perez-Arriaga, I. J., and Sheweppe, F. C., Selective modal analysis with applications to electric power systems, *IEEE Trans. Power Apparatus Syst.*, **PAS-101**: 3117–3134, 1982.
52. Zadeh, L. A., and Desoer, C. A., *Linear System Theory: The State Space Approach*, New York: McGraw Hill, 1963.
53. Chow, J. H., and Gebreselassie, A., Dynamic voltage stability analysis of a single machine constant power load system, *Poc. IEEE Conf. Decision Control*, 1990, pp. 3057–3062.
54. Zaborszky, J., Whang, K. W., Huang, G. M., Chiang, L. J., and Lin, S. Y., A clustered model for a class of linear autonomous systems using simple enumerative sorting, *IEEE Trans. Circuits Syst.*, **CAS 29**: 1982.

55. Chiang, H.-D., Liu, C.-W., Varaiya, P., Wu, F. F., and Lauby, M. G., Chaos in a simple power system, *IEEE/PES Winter Power Meeting, Paper No. 92 WM 151-1 PWRS*, 1992.
56. Dobson, I., and Chiang, H. D., Towards a theory of voltage collapse in power systems, *Syst. Control Lett.*, **13**: 253–262, 1989.
57. Schlueter, R. A., Hu, I.-P., and Huo, T.-Y., Dynamic/static voltage stability security criteria, *Proc. NSF Intl. Workshop Bulk Power Syst. voltage phenom.—Voltage Stability Security*, 1991, pp. 265–303.
58. Wang, H., Abed, E., and Hamdan, A. M. A., Bifurcations, chaos and crises in voltage collapse of a model power system, *IEEE Trans. Circuits Syst.*, 294–302, 1994.
59. Venkatasubramanian, V., Schättler, H., Zaborszky, J., Dynamics of Large Constrained Nonlinear Systems—A Taxonomy theory. Invited paper, Special Issue of the Proc. of IEEE, vol. 83, Nov. 1995, pp. 1530–61.
60. Guckenheimer, J., and Holmes, P., *Nonlinear Oscillations, Dynamical Systems and Bifurcations of Vector Fields*, New York, Springer Verlag, 1983.

9 Dynamic Computation Analysis on Realistic Size (Thousands of Buses) Systems with Real-Life Examples

Large-size power systems in dynamic conditions have been analyzed using computers throughout most of the century (transient stability). Such analyses were originally carried out by computing trajectories using numerical integration by special analog computers (network analyzers). During the 1960s digital computers took over, and today giant commercial programs (by EPRI and others) are available. The state-of-the-art approach though is still accomplished by numerically integrating time variations of various voltages and angles. When the number of buses rises into the thousands and the number of variables approaches a million, this approach still will tell us if the system preserves stability and gives some indication on damping. However, no deeper analysis can be performed on a large system. Furthermore, the computation time becomes very long even with the ever-improving computer technology.

Chapter 8 laid down the basis for direct analysis of systems with unlimited size, avoiding numerical integration, and minimal-size numerical examples were given in Chapter 7. The latter examples serve mostly to give a conceptual understanding to readers of a new approach, which may contain concepts that are new or unfamiliar to some readers. Little more can be learned from slightly larger but still small size (9, 39, or 118 buses) systems which the reader can easily study and demonstrate for himself or herself by following the progress of the rudimentary system in Chapter 7, so that range is skipped in this book. Instead, a realistically large example involving 7600 buses is used to analyze a real-life event that was felt throughout the midwestern United States. This example was selected because the event was analyzed by the utility with unusual thoroughness using conventional methods. This gave an opportunity to verify the results both ways. These results were published in two EPRI reports. Part 1 [1] deals directly with the computation of the feasibility boundary and analyzing with its use the event and its sensitivity of various aspects and structural changes. Part 1 is discussed in this chapter. Part 2 of the EPRI report worked out by professor V. Venkatasubramanian and his students at Washington State University [2] concentrates on computing the center manifold for large systems and using it for the analysis, for example, of the sub- and supercritical nature of a

Hopf bifurcation and other matters now in the forefront of interest, like strange attractors and chaos. A short version of Part 1 of the EPRI Report is presented in Refs. [4] and [5]. The event which was selected for study because of its practical size and instructive nature happens to involve a Hopf bifurcation. So this chapter is concerned with the Hopf segment of the feasibility boundary. The computational analysis was developed in Kiyong's Kim's PhD thesis research as an example [4] under the advisorship of V. Venkatasubramanian, H. Schäffler, and J. Zaborszky. Kirit Shah and David Takach of Union Electric also contributed substantially. Some computational aspects including the development of new algorithms for analyzing the Hopf segment will be presented first in Section 9.1 and then applied to the Rush Island example in Section 9.1.6. It will only be possible to provide a sketchy summary of this example but details are available mostly in Refs. [1, 4, 5, 16, 17].

9.1 COMPUTATIONAL ASPECTS OF THE HOPF-BIFURCATION-RELATED SEGMENT OF THE FEASIBILITY BOUNDARY

9.1.1 System Description

Several FORTRAN programs were developed, including the modified EPRI Program for Eigenvalue Analysis of Large Systems (PEALS) (in Refs. [1] and [2]). These experimental programs and commercial programs, such as PTI's Power System Simulator Load Flow (PSSLF4), are used for computing a local segment of the feasibility boundary and particularly its Hopf segment, which is pertinent to the Rush Island example given later. The computation of a Hopf bifurcation point is performed in the level of job control command (or Unix shell programming). A continuation method is then used for calculating the Hopf-bifurcation-related segment of the feasibility boundary. It effectively computes the Rush Island example on a network model as large as the 7500-bus regional system covering the entire midwestern United States. It serves as an example of using the taxonomy theory approach on a very large, real-life power-system problem. Please observe that the computation time was not an (issue in this) demonstration example. Commercial software would be developed for use in industrial practice without using existing software.

The smooth quasistationary dynamics of the large electric power system can be modeled by a parameter-dependent differential-algebraic equation (DAE) system Σ of the form as established in Chapter 8:

$$\Sigma: \begin{cases} x = f(x, y, p), & f: \mathbb{R}^{n+m+r} \rightarrow \mathbb{R}^n \\ 0 = g(x, y, p), & g: \mathbb{R}^{n+m+r} \rightarrow \mathbb{R}^m \\ x \in X \subset \mathbb{R}^n, & y \in Y \subset \mathbb{R}^m, \quad p \in P \subset \mathbb{R}^r \end{cases} \quad (9.1)$$

In the state space $X \times Y$, dynamic state variables x and instantaneous state variables y are distinguished. While the (dynamic) variables x have their associated

dynamics explicitly modeled by Eq. (9.1), the dynamics of the (instantaneous) variables y is assumed to be so fast that the constraints $g = 0$ in Eq. (9.1) are always satisfied. The parameters p define a specific system configuration and the operating condition.

For the power system, typical dynamic state variables are the time-dependent values of generator voltages, rotor angles, and control states; load dynamic variables and instantaneous variables are the transmission-line power-flow variables (the bus voltages and angles). The parameter space P is composed of system parameters (which describe the system topography, that is, which lines, buses, etc., are energized, and which include equipment constants such as inductances and transformation ratios) and operating parameters (such as loads, generation, and voltage set points). The dynamics of the generators, control devices, and the load dynamics together define the f equation. Typically the constraints $g = 0$ are defined by the power-balance equations of the transmission system presented in Chapter 3.

9.1.2 Some Aspects of the Hopf Bifurcation and Its Vicinity

A mathematical analysis of the DAE system Σ in chapter 8 shows that the operating equilibrium point remains stable, that is, valid within a feasibility region [5]. Given a stable equilibrium point (x_0, y_0) for parameter value p_0 , the *feasibility region* of (x_0, y_0, p_0) is defined as the set of all stable equilibrium points that can be reached quasistatically (or in a stationary sense) from (x_0, y_0, p_0) by continuous parameter variations without losing local stability. The boundary of the feasibility region is called the *feasibility boundary*. Note that the feasibility region is defined as a subset of $X \times Y \times P$, not a subset of the parameter space (Details in Chapters 7 and 8.).

The significance of the Hopf bifurcation in power-system models was first identified in Ref. [6]. Hopf bifurcations have been studied in many recent papers, including Refs. [3, 5, 7]. Computational methods for calculating nearest Hopf bifurcations have been studied in Ref. [3]. More general algorithms for computing critical eigenvalues of a power system model have been proposed in Refs. [8, 9, 10] for studying small-signal stability problems.

In preparation for computing the Hopf-bifurcation-related segment of the feasibility boundary, we first consider an effective method for computing the Hopf bifurcation point. We propose an indirect method similar to Hassard's method [11].

Let μ be a specific but arbitrarily selected parameter such as a generator output or a gain in the control of a generator (preferably a parameter to which the bifurcation is sensitive). Let μ^H be a value of parameter μ at which a Hopf bifurcation occurs in the system. Assume that μ is sufficiently close to the Hopf bifurcation point μ^H . The full Jacobian matrix

$$\begin{pmatrix} f_x & f_y \\ g_x & g_y \end{pmatrix}$$

of the functions f and g evaluated at $\mu = \mu^H \pm \varepsilon$ is then nonsingular for sufficiently small ε . (Here f_x , f_y , g_x , and g_y denote the matrices of partial derivatives of f and g with respect to x and y .) Thus, by the implicit function theorem, there exists a smooth curve of equilibrium points, that is, stationary solutions (x^e, y^e) of Eq. (9.1) that can be solved in terms of μ [5]. The equilibrium point (x^e, y^e) depends continuously on μ . So do the elements of the system matrix $A = f_x - f_y g_y^{-1} g_x$ evaluated at (x^e, y^e) . Hence, the eigenvalues λ of A also depend continuously on μ . Furthermore, there is a pair of purely imaginary complex eigenvalues (Hopf-bifurcation eigenvalues) for the Jacobian matrix A evaluated at μ^H . It follows that for some value $\mu = \mu^H + \varepsilon$, with sufficiently small $\varepsilon > 0$, there will be a pair of complex eigenvalues that become Hopf eigenvalues as μ approaches to μ^H . These eigenvalues will be called the critical eigenvalues. This implies that the Hopf-bifurcation point can be determined by testing the real parts of the eigenvalues λ of the system matrix A . This method requires repeated evaluation of the eigenvalues for a sequence of starting points generated by some continuation method. We shall assume that among the eigenvalues in some neighborhood of μ^H only the Hopf eigenvalues have a zero real part. Thus, the Hopf-bifurcation point can be characterized by the following set of conditions:

$$f(x, y, \mu) = 0 \quad (9.2)$$

$$g(x, y, \mu) = 0 \quad (9.3)$$

$$h(x, y, \mu) \equiv \text{Re}[\lambda(\mu)] = 0 \quad (9.4)$$

where $h(x, y, \mu) = 0$ denotes a suitably chosen equation that characterizes the purely imaginary eigenvalues of the system matrix A .

9.1.3 Critical Eigenvalue

When the system matrix A is transformed using a bilinear transformation [9, 10] to $\tilde{A} = (A + wI_n)(A - wI_n)^{-1}$, where w is a weighting factor assumed to be a real number (which determines the eigenvalue distribution in the z plane), the Hopf eigenvalues lie on the unit circle and all other eigenvalues are inside the unit circle (see Figs. 9.1 and 9.2). That is, the Hopf eigenvalues become the dominant eigenvalues (the eigenvalue with the largest magnitude), which can be easily computed using the power method. The power method (for example, in Ref. [12] is best suited for computing dominant eigenvalues of a large matrix for which nonpower methods would not be practical. Thus the bilinear transformation allows the effective use of the power method on a system that has all eigenvalues with negative real parts, except possibly one pair of unstable complex conjugate eigenvalues. It follows that for some value $\mu = \mu^H + \varepsilon$, with sufficiently small $\varepsilon > 0$, the pair of critical eigenvalues that will probably become the Hopf eigenvalue also become the dominant eigenvalues in the z plane. Then an algorithm can be designed:

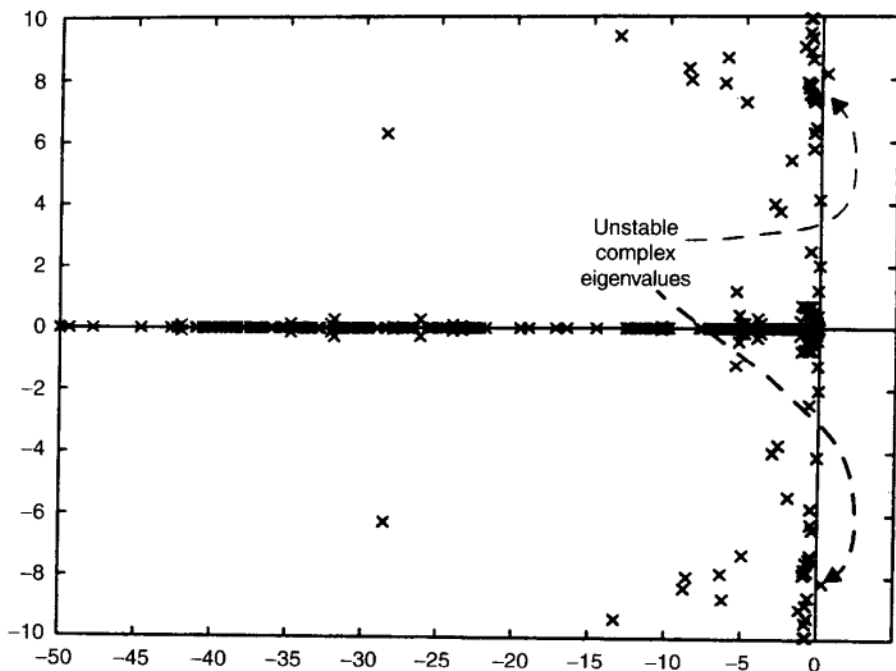


FIGURE 9.1 Eigenvalue distribution in the s domain for a 100 bus realistic approximate model.

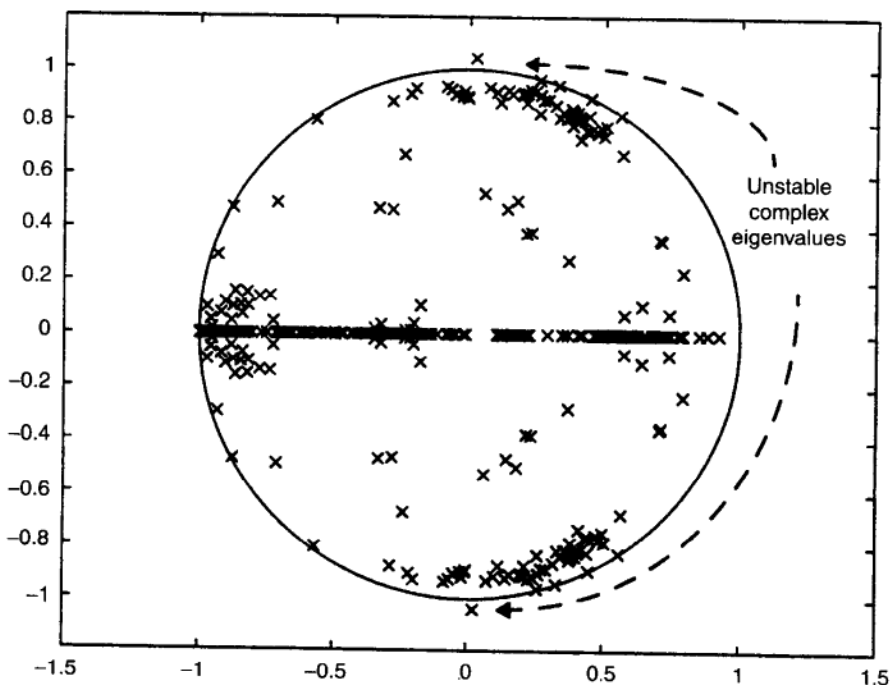


FIGURE 9.2 Eigenvalue distribution in the z domain for Figure 9.1.

1. Use the power method and find a pair of critical eigenvalues at parameter sufficiently small $\varepsilon > 0$ (after the Hopf bifurcation).
2. Use a method of successive approximations to guide μ towards μ^H and thus identify a Hopf bifurcation.

This approach greatly simplifies the computational burden for selecting the critical eigenvalues for a large power system. For comparison, in order to find the critical eigenvalue in the Hassard method [11], all the eigenvalues of the Jacobian matrix are calculated in order to select the critical eigenvalues.

More specifically, the magnitude of the Hopf eigenvalues is 1.0 in the z plane. Thus the Hopf bifurcation point can be located by solving Eqs. (9.3), (9.4) and

$$\tilde{h}(\mu) = 1 - r_\sigma(\tilde{A}) = 0 \quad (9.5)$$

where $r_\sigma(\tilde{A})$ is the spectral radius, that is, the largest absolute value of all eigenvalues of \tilde{A} . Based on the sufficient conditions (9.5) together with Eqs. (9.3) and (9.4), we describe an iterative technique for finding a Hopf bifurcation point (x^H, y^H, μ^H) on the feasibility boundary.

9.1.4 Iterative Technique for Finding a Hopf-Bifurcation Point

Let us assume that there exists only one pair of critical eigenvalues (poorly damped or unstable eigenvalues, which will probably become the Hopf eigenvalues). Then a pair of critical eigenvalues can be obtained using the power method [12] in the z plane, that is, a power iteration with bilinear transformation $\tilde{A} = (A + wI_n)(A - wI_n)^{-1}$ with weighting factor $w = 8$ (see Ref. [1] for details on the choice of w). We select the parameter most sensitive (μ) to these critical eigenvalues (see Refs. [4, 6] for a detailed method). Then a point μ^H on the feasibility boundary can be found by an iterative sequence. The detailed procedure for computing a Hopf bifurcation point is summarized from Ref. [1] as follows:

Step 1. Compute the equilibrium $(x_m^e, y_m^e) = (x^e(\mu_m), y^e(\mu_m))$ satisfying $f = 0$ and $g = 0$ for μ_m . This process requires an iterative process such as the Newton–Raphson method. To handle the large-size system as well as various types of dynamic devices, we directly use EPRI's PSAPAC programs and power-flow programs.

Step 2. Evaluate the coefficient matrices f_x , f_y , g_x , and g_y at (x_m^e, y_m^e) . For this process, we directly use EPRI's PSAPAC programs.

Step 3. If a priori information on λ_{m-1}^c is available, compute the critical eigenvalue using the inverse power iteration [12], that is, by power iteration of $(A - \lambda_{m-1}^c I_n)^{-1}$. If the critical eigenvalue is not available, do the bilinear transformation with weighting factor $w = 8$, that is, $\tilde{A} = (A + wI_n)(A - wI_n)^{-1}$,

and compute the critical eigenvalue using the power method or the modified Arnoldi method (see Ref. [1] for details). The eigenvalue obtained is tested using the convergence criterion $|\lambda_m^e - \lambda_{m-1}^e|/\lambda_{m-1}^e \leq e_\lambda$.

Step 4. Compute the participation factors p_{ic} [1] and verify whether or not it has the same state mode as in the previous iteration step. If so, go to Step 5; otherwise go to Step 6 after replacing a weighting factor κ with 0.5κ and $\tilde{h}_m = \tilde{h}(\mu_m)$ with $\tilde{h}(\mu_{m-1})$.

Step 5. Compute the quantity $\tilde{h}_m = \tilde{h}(\mu_m)$ representing the distance of this critical eigenvalue from the unit circle.

Step 6. Test the stopping condition for μ_m . If either $|\tilde{h}(\mu_m)| \leq \varepsilon_h$ or $|\mu_m - \mu_{m-1}|/|\mu_{m-1}| \leq \varepsilon_\mu$ is satisfied, the secant iteration stops. If not, go back to Step 1 after determining a parameter for the next step using $\mu_{m-1} = \mu_m - \kappa \tilde{h}_m (\mu_m - \mu_{m-1}) / (\tilde{h}_m - \tilde{h}_{m-1})$.

9.1.5 Method for Computing a Hopf-Bifurcation-Related Feasibility Boundary

In Section 9.1.4, we introduced an iterative method for finding a Hopf bifurcation point. This method is used for a one-dimensional parameter vector μ . For a two-dimensional parameter subspace, a Hopf-bifurcation-related segment is a connected curve consisting of points in the parameter subspace (μ^1, μ^2) that are solutions of

$$\tilde{h}(\mu^1, \mu^2) = 0 \quad (9.6)$$

where $\mu^1, \mu^2 \subset P \in \mathbb{R}^r$. Using the algorithm described in Section 9.1.4, one solution of Eq. (9.6) has been determined. Let us denote this first solution by $\mu_1 = (\mu^1, \mu^2)$. For further solutions, $\mu_2, \mu_3, \dots, \mu_N$, we use predictor–corrector methods (for examples, in Refs. [13, 14]). Then the Hopf-bifurcation segment can be determined by the set of these points, that is, by simply connecting these solutions.

The predictor provides an approximation of the k th solution $\tilde{\mu}_{k+1}$ of Eq. (9.6) using the solutions obtained in the previous steps (Figure 9.3). The $(k+1)$ th solution μ_{k+1} can be found by the corrector iterations with a predicted point $\tilde{\mu}_{k+1}$.

Details of the predictor–corrector method used in this section are described by the following four parts

1. Predictor. An approximate solution $\tilde{\mu}_{k+1}$ of Eq. (9.6) is obtained using the secant prediction, which can be expressed as

$$\tilde{\mu}_k^j = \mu_k^j + \beta_k \left(\mu_k^i - \mu_{k-1}^j \right) - \mu_k^i + \Delta \mu_k^i, \quad i = 1, 2 \quad (9.7)$$

where the quantity β_k is a weighting factor.

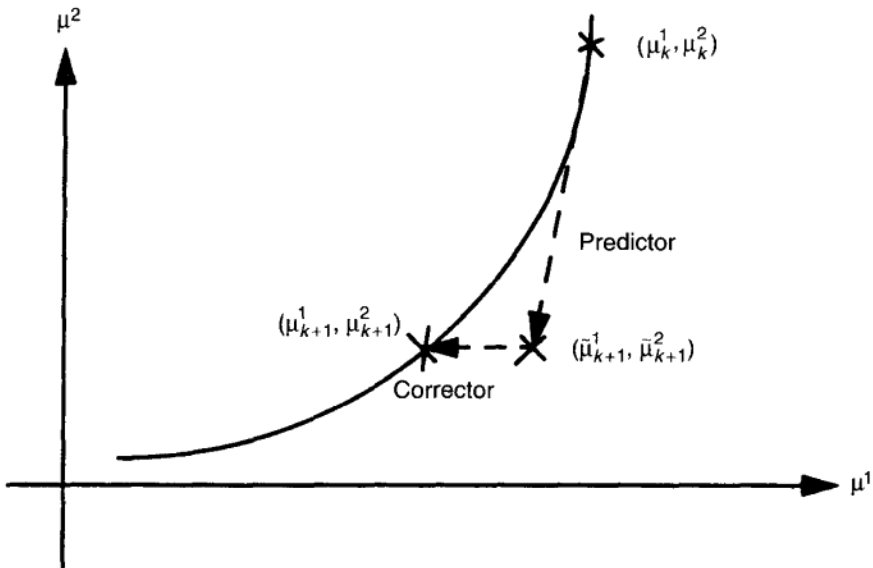


FIGURE 9.3 Basic scheme of a predictor–corrector method.

2. Parametrization. In this example, the local parametrization method is actually used. That is, one of the variables in $\mu_k = (\mu_k^i, \mu_k^j)$ is used as active parameter. This leads to the parametrizing equation

$$\mu_k^i - \eta = 0 \quad (9.8)$$

with index i and a suitable value of step length η . The index i and the step-length parameter η are locally determined at each continuation step in order to keep the continuation flexible. Hence, we have the augmented equations

$$\begin{pmatrix} \tilde{h}(\mu_k^j, \mu_k^2) \\ \mu_k^i - \eta \end{pmatrix} = 0, \quad i = 1 \text{ or } 2 \quad (9.9)$$

Based on the secant predictor (9.7), i is determined such that the relative changes $\delta\mu_k^i$ are maximal in μ_k ,

$$\Delta\mu_k^i = \max(\Delta\mu_k^1/\gamma^1, \Delta\mu_k^2/\gamma^2) \quad (9.10)$$

where γ^i is a scale factor for the normalization of the i th parameter.

3. Step length. We use an adaptive step length $\eta = \Delta\mu_{\max}^i$, where $\Delta\mu_{\max}^i$ is the maximum variation of the i th parameter. $\Delta\mu_{\max}^i$ is adjusted during the iteration. If the corrector iteration fails, the previous iteration is repeated with $\eta = 0.5\Delta\mu_{\max}^i$. Once a local parameter from use of Eq. (9.10) has been selected,

say the i th parameter, then the k th step length is determined by

$$\beta_k = \eta / \Delta\mu_k^i \quad (9.11)$$

Note that $\Delta\mu_{\max}^i$ and γ^i for $i = 1, 2$ should be specified. Basically the k th parameter is stretched to the maximum length specified and the other parameter is stretched proportionally.

4. Corrector. The k th continuation step starts from an approximation $\tilde{\mu}_{k+1}$ of a solution μ_{k+1} of Eq. (9.6). In general, the $\tilde{\mu}_{k+1}$ is not a solution of Eq. (9.6). The predictor merely provides an initial guess for corrector iterations that home in on a solution of Eq. (9.6). The augmented equation (9.9) is solved with a suitable index i and value of η by the proposed method for computing a Hopf bifurcation point described in Section 9.1.4.

9.1.6 Computational Analysis

A complete algorithmic computational process was developed and programmed by incorporating the use of large commercial programs (EPRI's PSAPAC programs and PTI's PSS/E programs). This is summarized in Section 9.1.5. Computational illustrations follow in this section.

Models of all types of equipment in the power systems, except the composite loads as seen at the transmission buses, are well understood. Very highly detailed, physically based dynamic models for equipment such as generators and transformers are presented in Chapter 3 and programmed with a somewhat different perspective in EPRI's software packages (SSSP, ETMSP, etc.). System loads are modeled by constant-impedance representation. The results do not change appreciably when different types of load models are considered as shown in Ref. [1] or chapter 3.

Computation of the Hopf segment of the feasibility boundary as projected into the parameter space (which describes the system composition) and operating conditions will be now presented in an illustrative example that analyzes a real-life event on an 7600-bus system model.

Summary of an Oscillatory Disturbance on the U.S. Interconnection on June 12, 1992 On June 12, 1992, at 12:46 pm, a standup insulator failed at Union Electric Company's Tyson 345-V substation [15]. This was followed by a sequence of relaying and switching actions that left an unusual system configuration as shown in Fig. 9.4. In this postfault condition, both Rush Island generating station units were connected to the transmission system through only one outlet circuit with two major north-south transmission ties severed. Generation at Rush Island was at about 1100 MW at the time of the fault.

After the condition shown in Fig. 9.4 set in, Union Electric and neighboring generating units experienced an oscillation in the magnitude of power output and

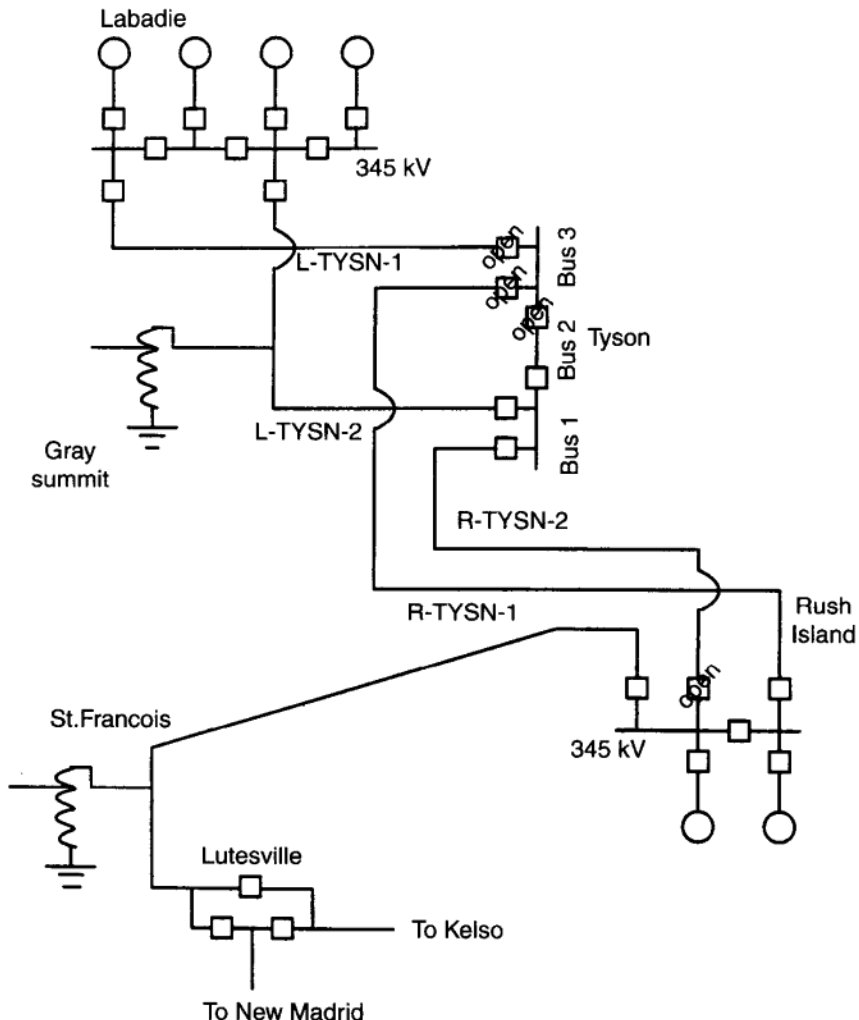


FIGURE 9.4 Postfault system configuration.

of voltage for about 38 minutes. At Rush Island, the total plant output was oscillating about 280 MW, swinging between a peak value of about 1200 MW and a minimum of about 920 MW. The frequency of the oscillation at the Rush Island plant was observed to be about 1 Hz. Other plants on the Union Electric system and surrounding systems experienced MW oscillations of a lower magnitude in the range of 25 MW to 75 MW.

The only major operating adjustment in progress at a Union Electric plant prior and during the event was the gradual lowering of the MW output level of Rush Island Unit 2 [see Fig. 9.5(b)]. This operation continued until it was sped up by the operators in the last 8 to 10 minutes. Unit 1 was carrying constant load at the beginning which was then reduced in a complex manner [Fig. 9.5(a)].

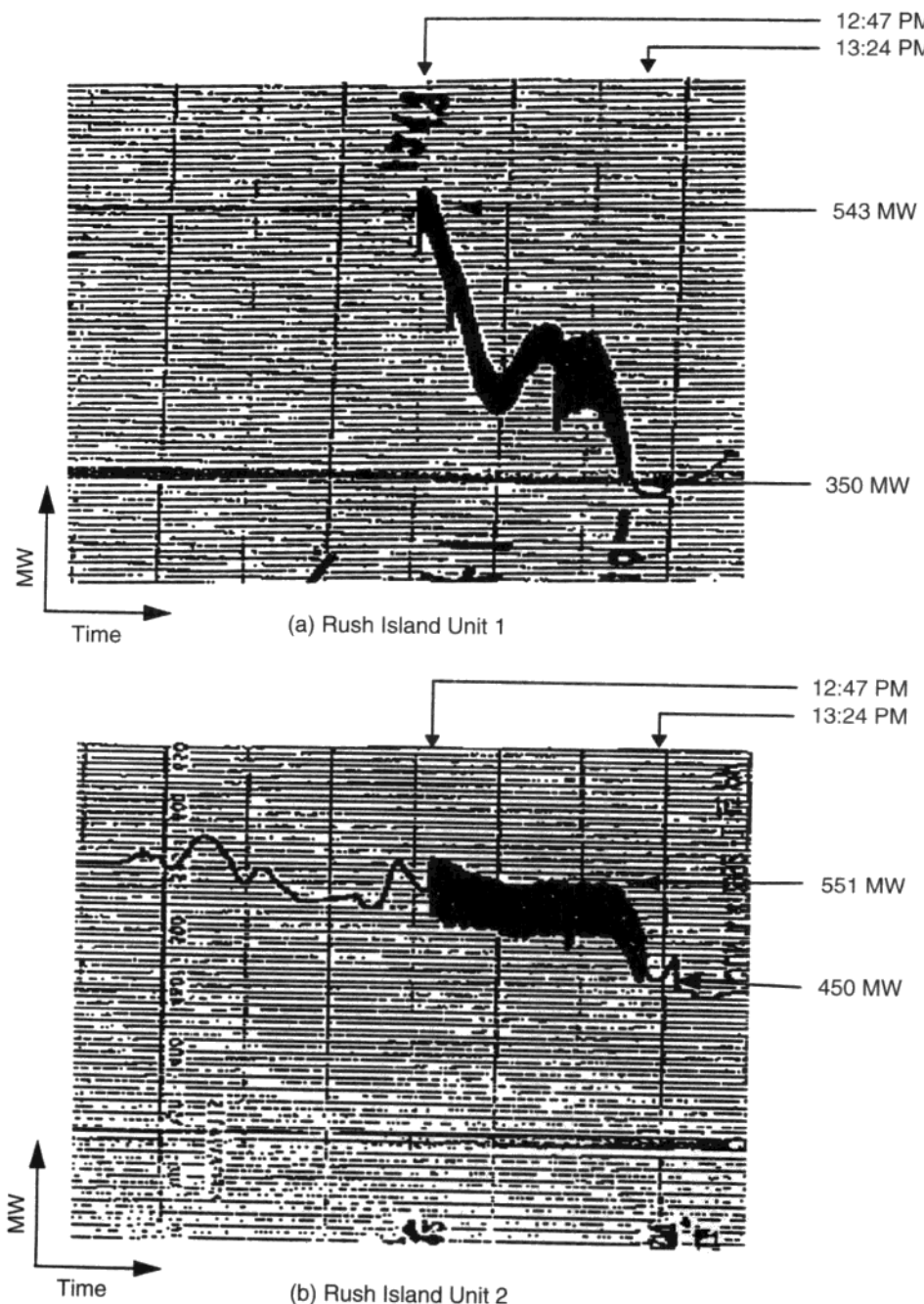


FIGURE 9.5 Chart record of the Rush Island Event on June 12, 1992.

Reduction of the Rush Island generation has been verified to be the principal cause of oscillation cessation.

This event is well documented by simulation and other studies as well as the original recordings of the event [15]. A comprehensive analysis conducted by the Union Electric engineers showed that the operating equilibrium point was unstable against small signals for the postcontingency configuration and moreover, that the time-domain simulation using the EPRI Extended Transient/Midterm Stability Package (ETMSP) program illustrated the existence of a stable limit cycle. This combination indicates the existence of a possible supercritical Hopf bifurcation. Here we analyze the event using results from Chapter 8 and Section 9.1.6, establish its characterization, and compare the conclusions with the known physical facts. The algorithms introduced will in general be useful for predicting small-signal stability and security near Hopf-bifurcation-related segments of the feasibility boundary for any general large-power-system model like the 7600-bus model used here. The computational algorithms should prove to be useful in general. Such a study could be the basis of developing commercial software in this area. Our results demonstrate the applicability of Hopf-bifurcation-related methods proposed in Refs. [1, 4, 16] on real systems of large size.

Problem Formulation for the Rush Island Event

System Modeling We consider a regional system that represents the midwestern United States power interconnected system. Rush Island is in this regional system. Thus by using the regional system model the system is modeled in its entirety. This is a large system of 7600 buses and 5700 dynamic states, and realistic system models are used. Knowledge of detailed system operating conditions in and around the Union Electric area at the fringes of the system are also assumed as in Refs. [1, 16]. This is then an illustration of the feasibility boundary theory on systems of real life size.

Selection of System Parameters for Computational Analysis While an oscillation is present on the system, the first action taken by the operator may be changing the status, controls, and/or settings of both the excitation and boiler systems in an effort to eliminate the oscillation. This is what happened at Rush Island.

Among parameters to which critical eigenvalues are most sensitive, we select three operating parameters at the Rush Island plant, real-power generation P_g , forward gain K_a , and feedback gain K_f , of the automatic voltage regulator (AVR) for the excitation system for computing the Hopf-bifurcation segments (see Refs. [1, 4] for details on the choice of these parameters). There are two generator units at Rush Island. Both units have the same governor and excitation systems. However, to make the display of results more effective, the variation of three parameters (P_g , K_a , and K_f) for only Rush Island Unit 1 (where most of the activities concentrated) will be considered as follows:

Case 1. Real-power generation (P_g) at Rush Island Unit 1 and forward gain (K_a) of the AVR of Rush Island Unit 1.

Case 2. Forward gain (K_a) and feedback gain (K_f) of the AVR of Rush Island Unit 1.

Note that Figure 9.5 shows that major activity was concentrated in Unit 1 among the two generators during the time of the actual event.

9.1.7 Computation of the Hopf-Bifurcation-Related Segment

The system operating conditions used for all computational results following are based on calculated design values and postfault operating conditions for the June 12, 1992 event. In order to get an initial Hopf point on the feasibility boundary, the method described in Section 9.1.4 is used. For computing the Hopf-bifurcation-related segment of the feasibility boundary, a continuation algorithm described in Section 12.1.5 is used.

Case 1: (P_g , K_a) Subspace The Hopf-bifurcation-related segment of the feasibility boundary is computed here in the two-dimensional parameter subspace (P_g , K_a), where P_g is real-power generation and K_a is the forward gain of the excitation system AVR for Rush Island Unit 1. Generation at Rush Island was at about 1100 MW at the time of the fault (543 MW for Unit 1 and 551 MW for Unit 2). The calculated value (design value) of the forward gain K_a of the AVR in the excitation system for Rush Island Unit 1 is 730. To get the Hopf-bifurcation-related segment, the ranges of these two parameters must be defined. For convenience, we select a practical range for each parameter as $200 \leq P_g \leq 600$ and $200 \leq K_a \leq 900$.

All other parameters for Unit 1 such as K_f and T_a are fixed with the design operating values. All parameters for Unit 2 are fixed as well. First we locate the Hopf-bifurcation point P_g^H of the given system for $K_a = 900$ fixed using the proposed method described in Section 9.1.6. This point is used as the starting point for the continuation method proposed in Section 9.1.5. Results obtained by this procedure for the regional system are illustrated in Figure 9.6. Note that, as shown in Figure 9.6, the initial operating points of both units are in the infeasible region, which signals a Hopf oscillation.

Time-domain simulations are performed at two operating points, one with a parameter inside the feasible region and the other with a parameter outside the feasible region. EPRI's ETMSP was used. Figure 9.7 shows the MW outputs of the Rush Island Unit 1 from the time-domain simulation. When the governor set point is changed from 0.8 p.u. to 0.5 p.u. at a time of 10 seconds (the parameter is outside the feasibility boundary), the time-domain simulations showed a stable limit cycle [Fig. 9.7(a)]. This limit cycle disappeared as the parameter crossed the feasibility boundary into the feasible region, that is, the governor set point is changed from 1 p.u. to 0.6 p.u. at time 10 seconds [Fig. 9.7(b)]. The corresponding phase portraits for each case are also shown in Figures 9.8(a) and 9.8(b), respectively.

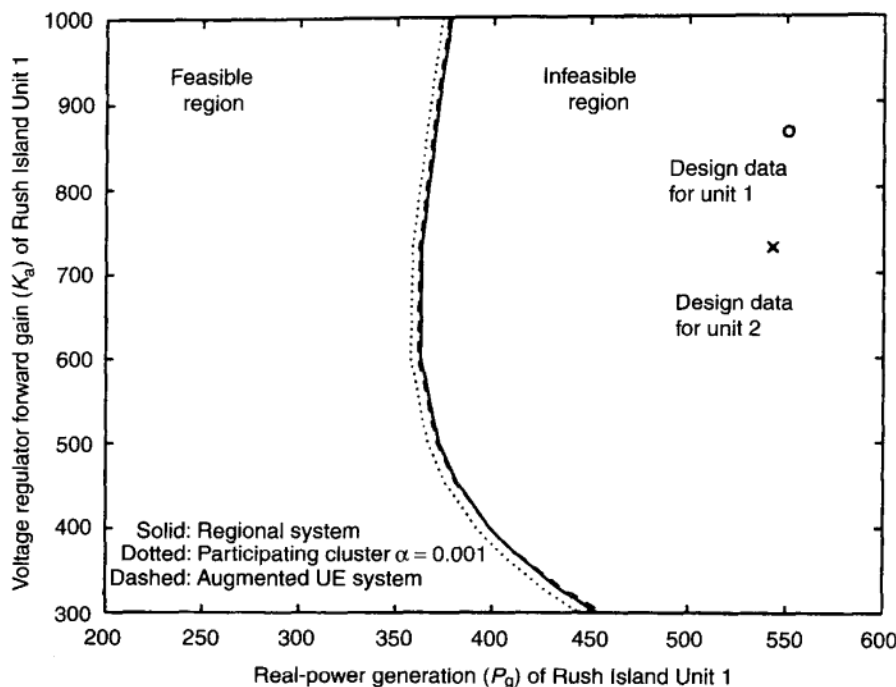


FIGURE 9.6 Hopf-bifurcation-related segment of the feasibility boundary in the parameter subspace (P_g, K_a) of the Rush Island Unit 1 for postfault parameters settings.

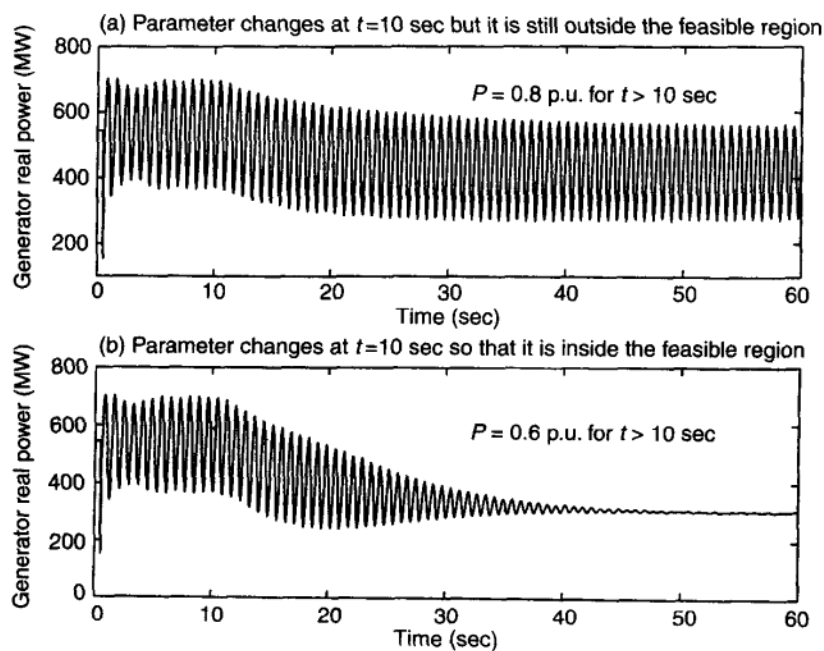


FIGURE 9.7 Time-domain simulation of the Rush Island Unit 1.

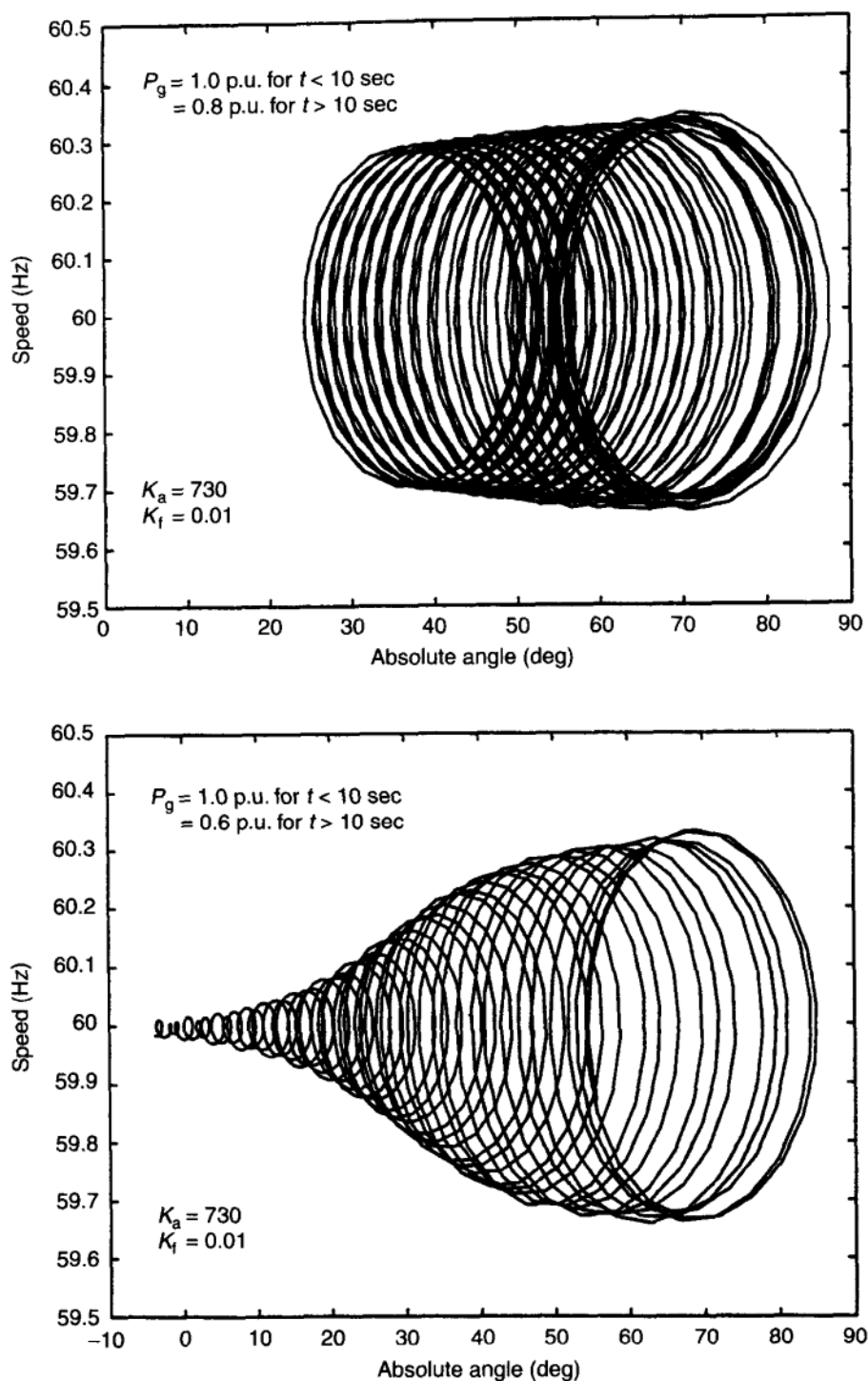


FIGURE 9.8 Phase portrait of the Rush Island Unit 1.

In the Rush Island event the real-power generation of Unit 2 was reduced slowly compared to Unit 1 apparently following a schedule, then in about the last 10 minutes it was reduced much faster. The total change during the oscillation was about 200 MW for Unit 1 and about 80 MW for Unit 2. To explore this type of event the feasibility boundary was computed with the Unit 1 output variable and the Unit 2 output fixed at either the pre- or postdisturbance value at 80 MW below the value before the disturbance. The results are shown for comparison in Figure 9.9.

The postfault system conditions and the system conditions at the termination of the system oscillation are indicated with a cross \times respectively in the right and the left sides of Figure 9.9. From Figure 9.9, the sustained oscillation of the Rush Island event following the system disturbance can be explained. The system resided in the infeasible region after fault clearance at $K_a = 730$ and $P_g = 543$ MW. The system trajectory therefore approaches a stable limit cycle present after the supercritical Hopf bifurcation. As the power generation was reduced the oscillation stopped at about $P_g = 350$ MW after the state of the systems regained the stable equilibrium point.

Case 2: The (K_f, K_a) Subspace The Hopf-bifurcation-related segment of the feasibility boundary is computed here in the two-dimensional parameter subspace (K_f, K_a) , where K_f and K_a are, respectively, the feedback gain and the forward

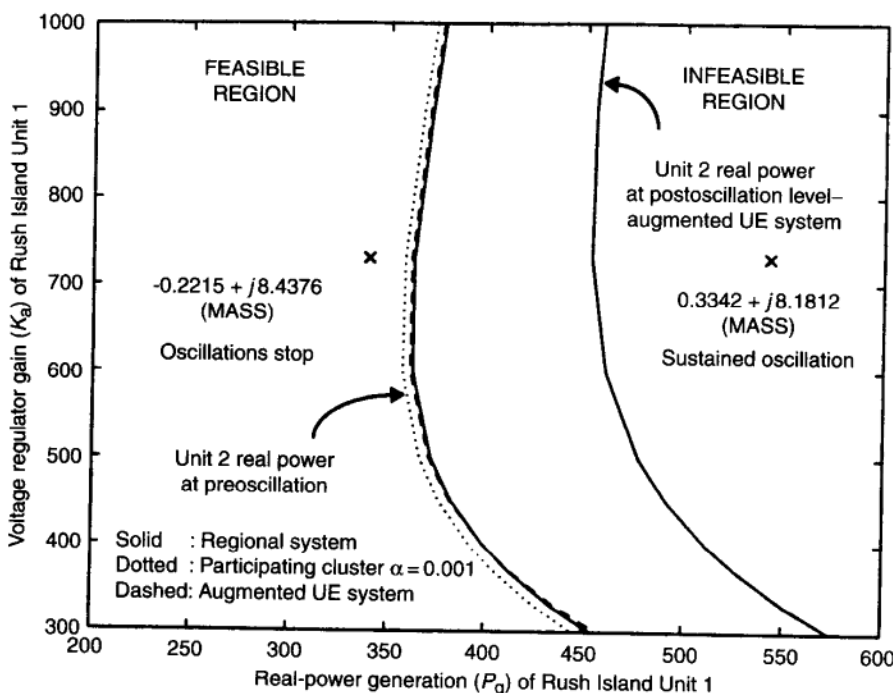


FIGURE 9.9 Interpretation of the Rush Island event based on the feasibility boundary.

gain of the excitation system AVR for Rush Island Unit 1. Based on the actual control setting data at the time of the event, excitation system model parameters were calculated by the excitation system manufacturer [15]. The calculated values (design value) of K_f and K_a were 0.01 and 730, respectively, for Unit 1.

For convenience, we select a practical range for each parameter as $0.005 \leq K_f \leq 0.05$ and $200 \leq K_a \leq 900$. All other parameters for Unit 1 such as P_g , and T_a are fixed to the values designed for operation. All parameters for Unit 2 are fixed as well. Results obtained by this procedure for the regional system are illustrated in Figure 9.10. Again, a constant-impedance load model was assumed for the results shown in Figure 9.10 (see Ref. [1] for the effect of different types of static load models). The design data for Units 1 and 2 at postfault system conditions (actual values during the event) are indicated with a cross and circle, respectively, in Figure 9.10.

Time-domain simulations at each parameter point, one in the feasible region and the other in the infeasible region, were also performed using EPRI's software ETMSP, and the results are shown in Figure 9.11. The parameter values for Unit 1 are described in each figure. The parameter values for Unit 2 are fixed at postfault conditions. The corresponding phase portraits are given in Figures 9.12(a) and 9.12(b), respectively. Here we interpret this

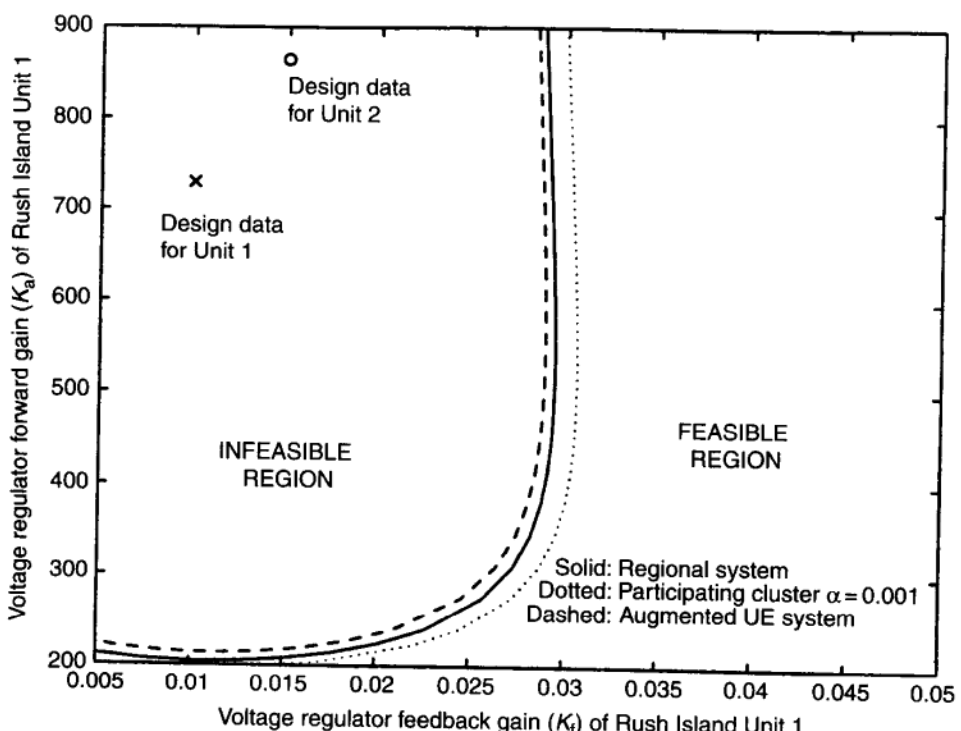


FIGURE 9.10 Hopf-bifurcation-related segment of the feasibility boundary in parameter subspace (K_f, K_a) of Rush Island Unit 1.

oscillation in two-dimensional parameter subspace (K_f , K_a). Figure 9.10 shows the Hopf segment including the design gain setting indicated with a cross. From Figure 9.10, it is clear that the AVR gains were set outside the feasible region at the time of the Rush Island event (postfault condition). Also it is clear that this oscillation could be prevented if the exciter gains were set to the values inside the feasible region in this two-dimensional parameter subspace (K_f , K_a). This fact indicates a valuable application of the feasibility region context for determining a gain setting of the exciter system. In fact, Union Electric planning engineers have successfully used the feasibility boundary computational methods described in this example together with other tools such as transient stability methods for selection and tuning of exciter control gains in the Union Electric system.

The good matching between the records of the original event of the extensive simulation studied by Union Electric and the analytically based results of this section mutually verify these data and approaches. It also demonstrates the relative efficiency of the computational techniques offered in this chapter based on the analysis of large-system dynamics presented in Chapter 8 and the Hopf analysis.

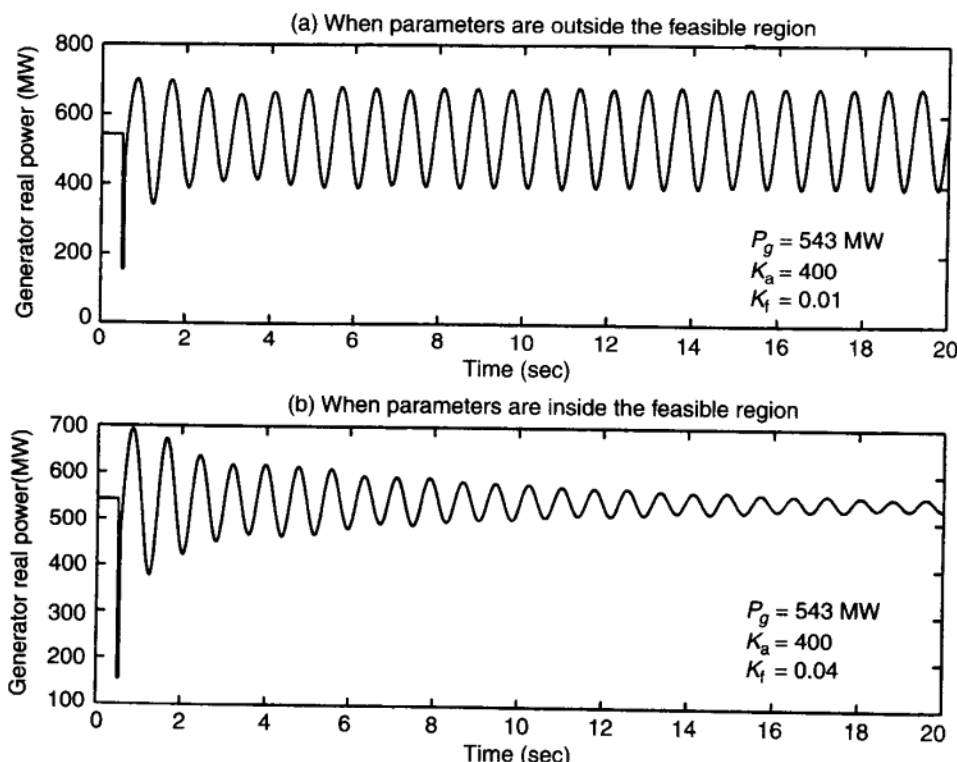


FIGURE 9.11 Time-domain simulation of the Rush Island Unit 1 for parameters K_f and K_a of Rush Island Unit 1.

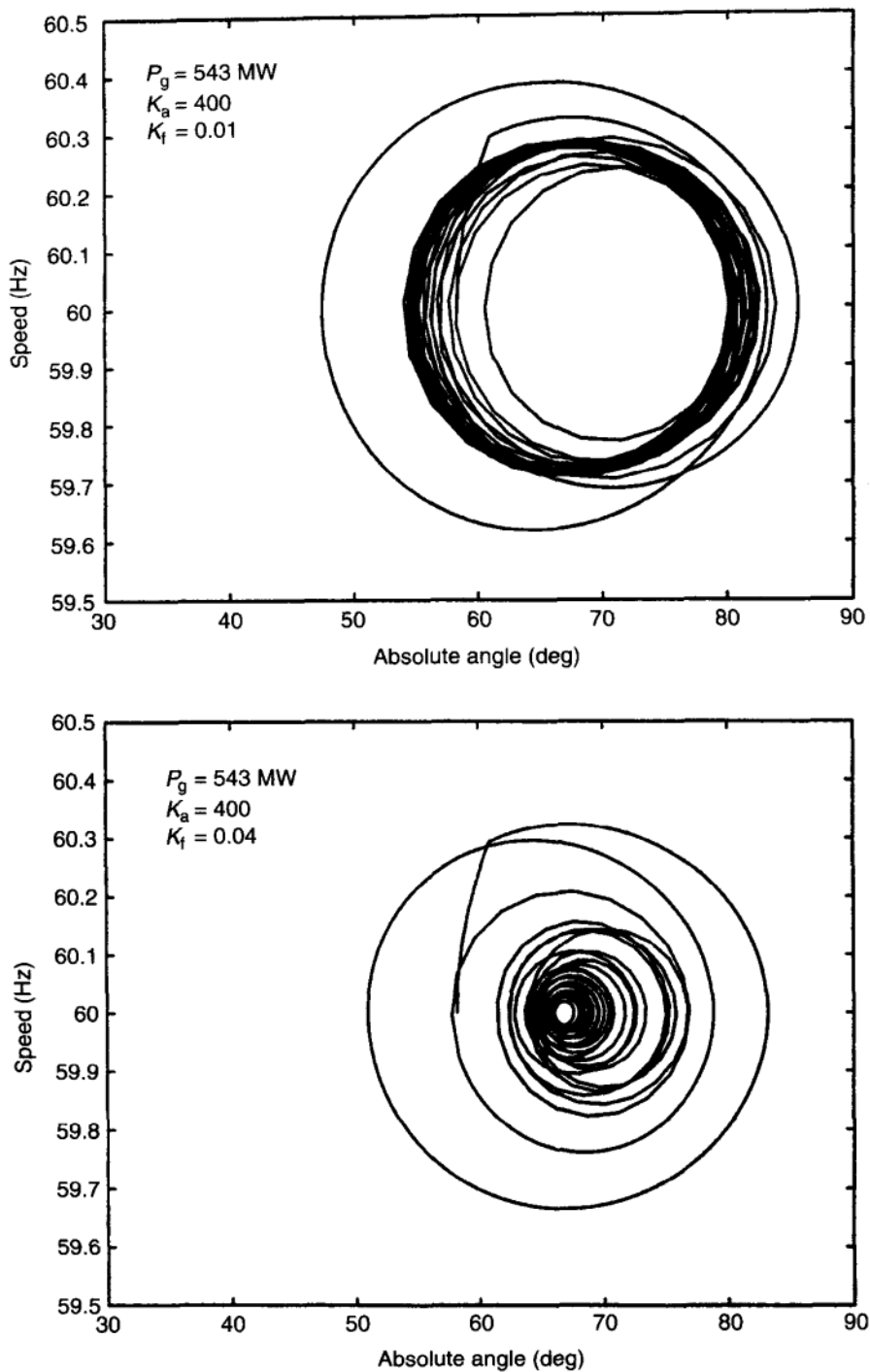


FIGURE 9.12 Phase portrait of the trajectory for the Rush Island Unit 1.

9.2 USE OF LARGE-SCALE COMPUTATION RESULTS FOR STUDYING THE NATURE AND INTERACTIONS NEAR THE FEASIBILITY BOUNDARY

Conventional methods typically utilizing time-domain simulation can give answers to the questions about verifying the presence of sustained oscillations, indicating the possible presence of Hopf bifurcations, and generally those connected with transient stability. However, these methods are highly demanding on computation time and not well suited for studying system behavior because of the need to sort through voluminous time responses and the lack of analytical guidance.

In the preceding section, the efficiency of the analytically based methods was demonstrated in obtaining answers for the conventional questions for a very-large-scale real-life occurrence. This section gives a few examples of how the analytically based computations introduced in Chapter 8 and here can be used for efficient and informative studies of phenomena in general around the feasibility or stability boundaries.

This will be accomplished by asking a series of individual questions, which are logical in a systematic study of the kind described here, showing how they can be answered and interpreting the answers. Numerous additional items and discussions can be found in Refs. [1, 4].

9.2.1 Effect of Using Lower-Degree Approximations

The computations presented in this chapter utilize the full size of the 7600-bus midwest region model. Whereas the computations proposed here are highly efficient, one would prefer to use a lower-order cluster if the approximation is sufficient. This question can really be answered only for individual problems of individual systems. Two approximate clusters were tried here:

1. The Participation-factor-based clustering approach at a sensitivity ratio of $\alpha = 0.001$
2. An augmented Union Electric system derived by engineering intuition.

Comparing the results shown in Figure 9.13 indicates that for this system and this problem, potentially acceptable approximations of the feasibility boundary can be computed by using either of the reduced-order models.

9.2.2 Substantiation of the Feasibility Boundary by the Presence of Critical Eigenvalues in Its Neighborhood

For verifying the Hopf-bifurcation segment on the feasibility boundary, the eigenvalues at some points near this segment were computed using EPRI's Program for Eigenvalue Analysis of Large Systems (PEALS). The parameter values are illustrated in Figure 9.14. Note that the stable eigenvalues are computed for the parameters in the feasible region and unstable eigenvalues for the parameters in the

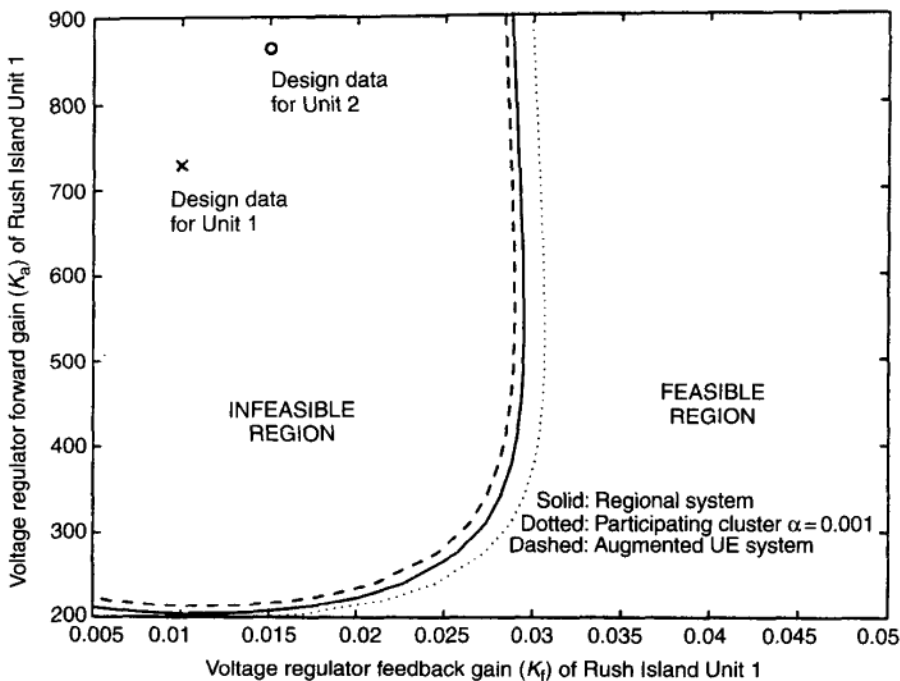


FIGURE 9.13 Hopf-bifurcation-related segments of the feasibility boundary for various system models in the two-dimensional parameter subspace (K_f, K_a) of Rush Island Unit 1.

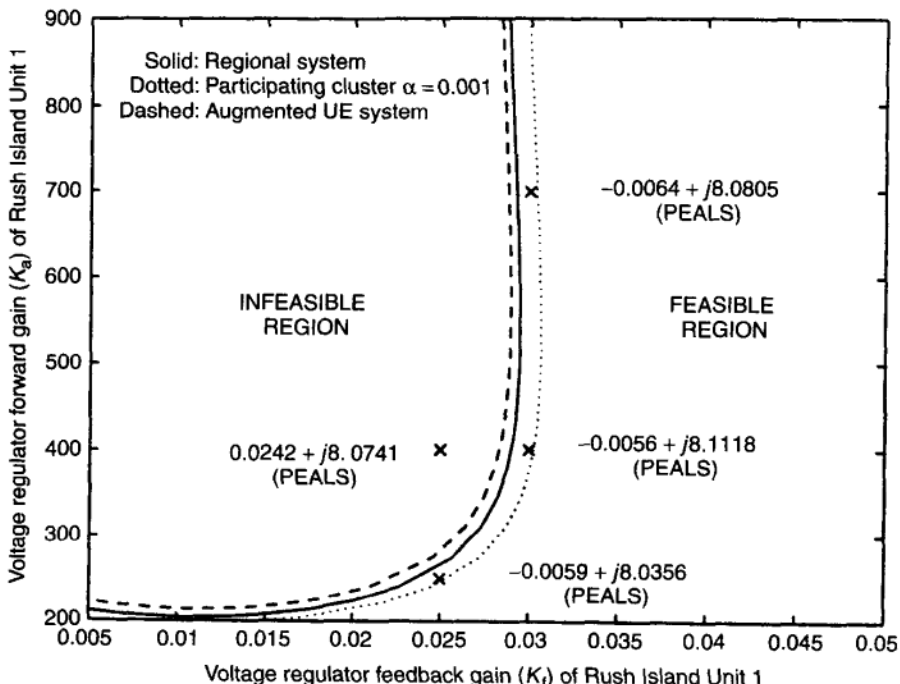


FIGURE 9.14 Eigenvalues near the Hopf-bifurcation feasibility boundary for parameters K_f and K_a of Rush Island Unit 1.

infeasible region are computed as expected. An extensive analysis of the behavior of a very large electric power system analyzed in the manner of the examples in Figures 9.13 and 9.14 is carried out and reported in [1, 2], [4, 5], [16] for readers who would be interested. These studies bring mathematical and intuitive insights into the behavior of the Hopf bifurcation in response to variations of the parametric and operating classes of the large power systems.

BIBLIOGRAPHY

1. Zaborszky, J., Schättler, H., Kim, K., Venkatasubramanian, V., Dehkordi, N., and Ji, W., *Application of Taxonomy Theory—Part 1: Computing the Hopf Bifurcation Related Segment of the Feasibility Boundary*, Part 1, EPRI Report No. RP3573-10, 1995.
2. Venkatasubramanian, V., Dehkordi, N., and Ji, W., *Application of Taxonomy Theory—Part 1: Computing the Hopf Bifurcation Related Segment of the Feasibility Boundary*, Part 2 EPRI Report No. RP3573-10, 1995.
3. Dobson, I. An iterative method to compute a closest saddle node or Hopf bifurcation instability in multidimensional parameter space, *Proc. Intl. Symp. Circuits Syst.*, San Diego, 2513–2516, 1992.
4. Kim, K., Computational methods for the Hopf bifurcation related segment of the feasibility boundary for large power systems, D.Sc. thesis, Washington University, St. Louis, 1995.
5. Venkatasubramanian, V., Schättler, H., and Zaborszky, J., A taxonomy of the dynamics of the large electric power system, in L. Fink (ed.), *NSF Proc. Intl. Symp. Bulk Power Voltage Phenomena—II*, Maryland, 1991.
6. Abed, E. H., and Varaiya, P. P., Nonlinear oscillations in power systems, *Int. J. Electric Power Energy Syst.*, **6**: 37–43, 1984.
7. Rajagopalan, C., Sauer, P. W., and Pai, M. A., An integrated approach to dynamic and static voltage stability, *Proc. Am. Control Conf.*, pp. 1231–1235, 1989.
8. Kundur, P., Rogers, G. J., Wong, D. Y., Wang, L., and Lauby, M. G., A comprehensive computer program package for small signal stability analysis of power systems, *IEEE Trans. Power Syst.*, **5**: 1076–1083, 1990.
9. Lima, L., Bezerra, L., Tomei, C., and Martins, N., New method for fast small-signal stability assessment of large-scale power systems, 1995 IEEE/PES Winter Meeting, New York, 1995, Paper 95 WM 190-9 PWRS.
10. Uchida, N. and Nagao, T., A new eigenvalue-analysis method of steady-state stability studies for large power systems: s-matrix method, *IEEE Trans. Power Syst.*, **3**: 706–714, 1987.
11. Hassard, B. D., Kazarinoff, N. D., and Wan, Y. H., *Theory and applications of the Hopf bifurcation*, Cambridge: Cambridge University Press, 1981.
12. Golub, G. H., and Van Loan, C. F., *Matrix Computations*, Baltimore: Johns Hopkins University Press, 1989.
13. Ajjarapu, V., and Christy, C., The continuation power flow: a tool for steady state voltage stability analysis, *IEEE Trans. Power Syst.*, **7**: 416–423, 1992.
14. Seydel, R., *From Equilibrium to Chaos-Practical Bifurcation and Stability Analysis*, City: Elsevier Science, North-Holland, 1988.

15. Shah, K. S., Bhrubh, G. R., and Beaulieu, R. E., Testing and modeling of the Union Electric generator excitation systems, submitted to the Missouri Valley Electrical Association Engineering Conference, Kansas City, April 1995.
16. Kim, K., Zaborszky, J., Schättler H., Venkatasubramanian, V., and Hirsch, P., Methods for calculating oscillations in large scale power systems, *IEEE Trans. Power Syst.*, **12**: 1639–1648, 1997.
17. Venkatasubramanian, V., Schättler, H., Zaborszky, J., Dynamics of Large Constrained Nonlinear Systems—A Taxonomy theory. Invited paper in Special Issue of *Proc. of IEEE*, Vol. 83, Nov. 1995, p. 1530–1561.

10 Large Smooth Systems with Embedded Discontinuous Nonlinear Constraints

Detailed and systematic theoretical analysis of smooth nonlinear systems modeled by ordinary differential equations with “algebraic” (that is, non-dynamic) smooth nonlinear constraints was presented in Chapters 7 and 8. A large-scale computational analysis along those lines was presented in Chapter 9 for a very-large-size (7600-bus) system experiencing a real-life supercritical Hopf-type bifurcation. This shows that valid practical results can be obtained even for very large systems from such smooth models. Nevertheless, it is true that the power system is full of nonsmooth elements particularly in the form of tap changers, hard limits, and relays, which can result in strongly altered behavior. This necessitates a thorough study of the behavior of the effect of such discontinuous events, which is the purpose of this chapter. Tap changers and hard limits exert different types of influences. Accordingly they will be treated in two separate subsections. Also they were developed at two different branches of the project and by somewhat different personnel.

On load tap changers (OLTC) on transformers produce small discontinuous parameter jumps at a rate determined by their construction (slow rate is the type most common in the US). This makes it possible to analyze their effect in a manner similar to Chapter 8, out modified with a sampled data like view. Such an analysis is presented in Section 10.1. In the small signal range other approaches are possible as presented in Chapter 6. This work was done in Washington University by the personnel described in Chapter 8.

The hard limit study at Washington University presented in Section 10.2 was mostly carried out in the framework of Xin Jiang’s thesis at a time when the original team has divided with V. Venkatasubramanian having moved to Washington State University where he carried out an extensive study of the hard limit problem, but still continued cooperating with the group at Washington University and played a key role in advising Xin Jiang.

10.1 AUTOMATIC-TAP-CHANGER-BASED CONTROL EMBEDDED IN DIFFERENTIAL-ALGEBRAIC EQUATION SYSTEMS

For the type of tap-changer control commonly used in the United States, the operating time is up to 40 sec to 100 sec. Faster devices around 3 sec to 10 sec are

available with resistor switching, and even faster ones with thyristor control are now installed. The range of 10 sec to 100 sec, would be commonly considered a midrange time scale, so it is desirable to extend the study of the rudimentary system to this area. The modeling here differs from the dynamic model in Eqs. (7.30) to (7.32) in more ways than that for the static var compensator (SVC) so it will need to be studied at some length. The emphasis in this section is on the way in which tap-changer control blends into the mathematically precise taxonomy of voltage dynamics established in Section 7.3.

10.1.1 Physical Features

Traditionally, to operate a tap changer under load, it will be necessary first to bridge two transformer taps through appropriate inductors or resistors with center taps and then interrupt the circulating current at the old tap, leaving a circuit through the new tap and the center tap. The latter then may be directly connected to take the bridge fully out of the main circuit. This involves considerable mechanical operation of contacts and switches and the use of small interrupters (often vacuum type). Operating these mechanisms takes a considerable and fixed amount of time that is independent of the deviation of the bus voltage from the set point.

The point is that the system experiences one (or two) fixed-magnitude step jumps of the transformation ratio per tap change (usually less than 1% total) and a minimum time interval, also of fixed magnitude of many (up to 100) seconds between consecutive changes. It is clear that the response to small-step increases, placed many seconds apart, will break down to two decoupled phenomena (the step is small and hence the behavior is linear).

- A transient response is made to the small-step jump. Normally this response is quite harmless, unless the system is operating with inadequate security and is much too close to its feasibility or stability boundary, in which case the question becomes moot. This transient decays during a small initial part of the minimum delay preceding the next tap change.
- The success of a tap change is expressed by the steady-state voltage $E_{Li}^s(i+1)$ reached after the last tap change and before the next one (Fig. 10.1). This voltage is independent of the transient, which has died out by that time. So typically only the steady-state value is significant.

The traditional tap-changer operating control is a simple device that switches one step up or down when the deviation between the steady-state load voltage E_{Li}^s and the reference setting E_{ri} reaches or exceeds the tolerance value ΔE :

$$n_{k+1} = \begin{cases} n_k + \Delta n & \text{if } E_{Li}^s - E_{ri} < -\Delta E \\ n_k & \text{if } |E_{Li}^s - E_{ri}| \leq \Delta E \\ n_k - \Delta n & \text{if } E_{Li}^s - E_{ri} > \Delta E \end{cases} \quad (10.1)$$

where Δn is the tap step size (usually equal or slightly less than ΔE) and E_{Li}^s is the steady-state voltage at the load i and as such the solution of

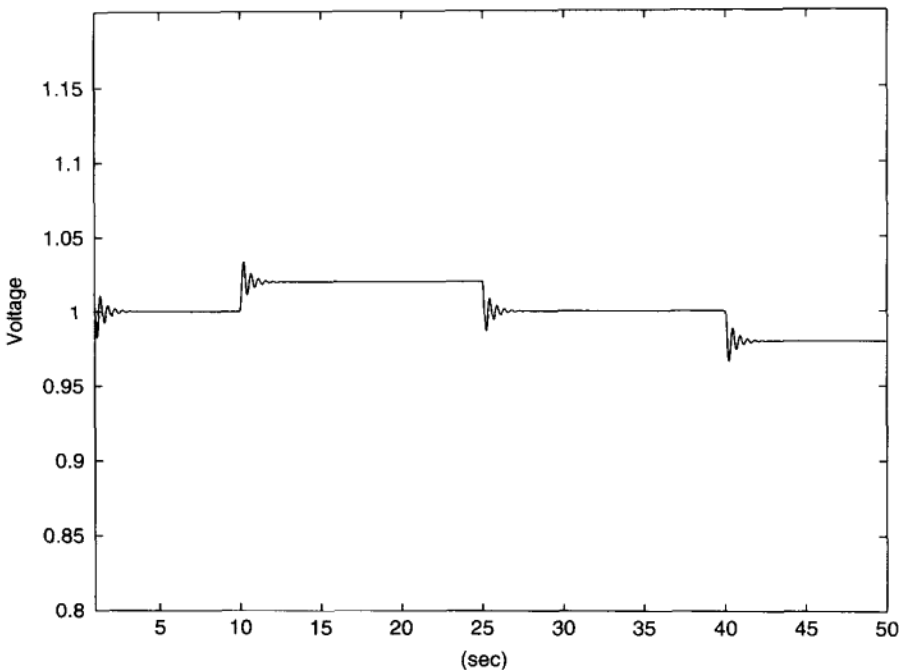


FIGURE 10.1 Voltage during a step change in a OLTC control.

$$0 = f(x, y, n, p), \quad 0 = g(x, y, n, p) \quad (10.2)$$

For convenience, the vector n of tap positions is displayed separately from states and parameters. Its nature may vary depending on the problem. If we denote the bus voltage by $x_1 = \{E_i^s\}$, the load voltages (secondary of tap changers) by $x_2 = \{E_{L_i}^s\}$, and the remaining (dynamic and instantaneous) state variables by x_3 (for brevity, the algebraic y_3 is included in x_3 since it plays no different role in this problem) and if all the parameters are grouped as p , then the system at steady state can be written comprehensively as

$$0 = h(x_1, x_2, x_3, n, p) \quad (10.3)$$

Note that this analysis applies to the traditional type of a slow tap changer. Thyristor-controlled tap changers are simply and directly part of the system dynamics covered in Section 7.2. These actually require no special solutions but will be discussed further.

10.1.2 Effect of the Automatic Tap Changer on the Feasibility Boundary in Parameter Space

Model (10.3) will now be analyzed for the restriction of the feasibility region caused by these types of tap changers. Let d denote the number of transfers with tap changers. If bus i is equipped with a tap changer, then $X_{2i}^k = x_{1i}n_i$, so that

$d = \dim(x_1) = \dim(x_2) = \dim(n)$. Substituting $x_{1i} = x_{2i}/n_i$ in Eq. (10.3) gives

$$0 = h_i(x_2, x_3, n, p) \quad (10.4)$$

Here the number of equations is equal to the sum of the dimensions of x_2 and x_3 . Suppose n and p are within the feasibility region and away from the feasibility boundary. Then (since $D_{x_2}h_i$, $D_{x_3}h_i$ is nonsingular), locally near any such point the solutions to Eq. (10.4) can be represented as

$$x_2 = x_2(n, p), \quad x_3 = x_3(n, p) \quad (10.5)$$

The tap changer continues switching until $x_{2i} = E_{ri}$ for all load buses. Hence, for the system with automatic tap changer control, the solution of Eq. (10.4) with $x_{2i} = E_{ri}$ defines the equilibrium state. The stability of the tap-changer control is determined by the Jacobian

$$J_d := -D_n x_2 = (I_d, 0)(D_{x_2}h_1, D_{x_3}h_1)^{-1} D_n h_1 \quad (10.6)$$

The equilibrium is stable if $-D_n x_2$ is stable (negative definite), and stability is lost when it has eigenvalues on the imaginary axis. This can be demonstrated by approximating the discrete dynamics of the tap changer tap size by a small step if the voltage differs from the set-point voltage by more than the allowed tolerance value. Usually, the tap-step size and the tolerance values are small, less than 1%. Hence, we can approximate the discrete model by a continuous model of the form

$$\dot{n}_i = f_i(x_{2i}) = \begin{cases} c & \text{if } x_{2i} < E_{ri} \\ -c & \text{if } x_{2i} > E_{ri} \end{cases} \quad (10.7)$$

where c is a suitable positive constant. The system described by Eq. (10.7) is not smooth at $x_{2i} = E_{ri}$, but the “slope” $D_{x_2}f_i$ can be taken to be arbitrarily large and negative. To analyze the local stability, choose a suitable smooth function \tilde{f}_i that approximates f_i to the desired accuracy and, in addition, is such that $D_{x_2}\tilde{f}_i = -kI_d$, where k is a positive constant. The Jacobian of the system $\dot{n}_i = \tilde{f}_i(x_{2i})$ is then given by kJ_d . Hence, the approximated system is stable if all the eigenvalues of J_d are in C^- , and is unstable if there exists at least one eigenvalue in C^+ . Considering the limiting case for $f_i(x_{2i})$, as the slope goes to $-\infty$, the result follows. Hence, the segment(s) of the feasibility boundary induced by the tap changer are pinpointed (at least after taking the closure, if necessary) by the parameters where the sensitivity matrix $(-J_d)$ has eigenvalues on the imaginary axis.

The new feasibility boundary is then where J_d loses stability, that is, where the eigenvalues of J_d cross the imaginary axis (as we stay away from ∂F , eigenvalues do not blow up) for either $\det(J_d) = 0$ (zero eigenvalue) or $\det[H_{n-1}(J_d)] = 0$

(purely imaginary eigenvalues) [1]. The Jacobian J_d can be simplified as

$$J_d(x_2, x_3, n, p) = J_d\left(E_{ri}, x_3, \frac{E_r}{x_1}; p\right) = \tilde{J}_d(x_1, x_3, p) \quad (10.8)$$

Essentially, the tap changer tries to track the solutions of

$$0 = h(x_1, x_2, x_3, n, p), \quad x_{2i} = E_{ri}, \quad n_i = \frac{E_{ri}}{x_{1i}} \quad (10.9)$$

Rewriting these equations, the steady-state solutions with the tap-changer control are the solutions of

$$0 = h_2(x_1, x_3, p) \quad (10.10)$$

and the new feasibility boundaries are defined by the conditions

$$0 = \det(\tilde{J}_d), \quad 0 = \det[H_{n-1}(\tilde{J}_d)] \quad (10.11)$$

Note that the first condition in Eq. (10.11) implies a saddle-node bifurcation that is separate from but identical in nature to the saddle-node bifurcation identified in Section 7.2.1 for the model applicable to excitation control or SVC control. Beyond this border the voltage will collapse by repeated step increases leading to diminishing voltage, because every upward switch actually results in the reduction of the voltage E_L . The second condition in Eq. (10.11) indicates a Hopf bifurcation, again similar to those observed in Figures 7.9 and 7.10 but involving diverging swings of the tap changer at various buses.

Figure 10.2 illustrates the existence of the two types of saddle-node bifurcations and the effect on the feasibility boundary of changing from excitation control to automatic tap-changer control on the rudimentary system.

10.1.3 Transient Phenomena Connected with the Tap Changer in the State Space

The traditional slow tap changer has no real dynamic characteristics beyond Eqs. (10.1) to (10.5); in other words, when the voltage is off the reference by the tap size, a tap change is implemented regardless of anything else. So on this type of device, there is no \dot{n} , that is no tap-rate term. In fact, the tap change is always strictly one tap at a time regardless of the size of the deviation. So this is a discrete element. For computing trajectories and analyzing stability by a discrete-continuous analysis [10,8], it is usually assumed that the tap-switching times are synchronized systemwide; however, the tap changer has the option of not switching when the voltage is within the neutral band $|E_L^s - E_r| \leq \Delta E$. This is a quite realistic approximation, but it still leaves a rather difficult hybrid analytical problem. So it is tempting to introduce a continuous approximation of the form

$$\dot{E}_L^s = \frac{1}{T}(E_L^s - E_r) \quad (10.12)$$

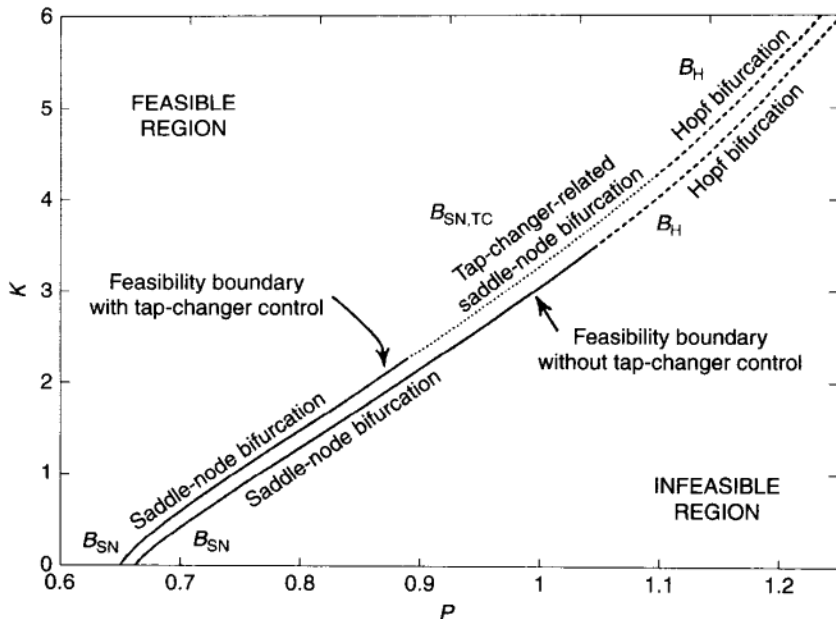


FIGURE 10.2 Comparison of feasibility boundaries with excitation and tap-changer control.

or

$$\dot{n} = \frac{1}{T}(E_L^s - E_r) \quad (10.13)$$

Justification of this latter step of approximation seems less convincing for the traditional slow tap changers. In fact, often it is simply stated as an unsupported assumption [4]. Since the normal dynamic elements (generator excitation control, load dynamic, etc.) are much too fast to couple into the tap-changing cycle the practical meaning of this assumption is dubious unless a much slower f, g system is considered, like boiler dynamics or some automatic generation control (AGC) action.

On the other hand, by using very fast thyristor-type tap changers, it would be quite easy to implement an actual controller with the control law of Eq. (10.12) or (10.13) in the usual transient stability range. In the latter case, if such a control dynamics exist, then the system itself would need to be modeled in its full dynamic form, that is, $\dot{x} = f(x, y, p)$, $0 = g(x, y, p)$, where now \dot{x} includes \dot{E}_L^s or \dot{n} and f includes Eq. (10.12) or (10.13). The results of this text are directly applicable for such studies, so nothing more needs to be said here.

10.2 DYNAMICS OF THE LARGE DAE POWER SYSTEM WITH EMBEDDED HARD LIMITS

In studying large physical systems, which is the objective of this section, we need to consider hard limits, which are always present (in very large numbers) in

a real physical system. The significance of analyzing these hard limits has been emphasized in recent IEEE Committee Reports on voltage stability.

In this section the analysis of smooth systems presented in Chapters 7 and 8 will be extended briefly to such system containing hard limits. Some of the more important publications on this area are Refs. [7–15, 25, 26, 27].

The material in Section 10.2 is based on research by the Washington University team and by V. Venkatasubramanian at Washington State University. In this study important work was developed in the thesis work of X. Jiang [16] under the advisorship of V. Venkatasubramanian, H. Schättler, and J. Zaborszky, [12]–[15], [22]–[25], and in the subsequent research work of V. Venkatasubramanian. The material presented in this section is based on mostly on Refs. [11, 12, 14].

10.2.1 Modeling the Large Power System with Hard Limits

The dynamics of the large interconnected power system can be formally represented by parameter-dependent differential-algebraic equations as shown later. These equations are also subject to various types of hard limits stated therein. The significance of the different variables, functions, and hard limits in the mathematical model will be explained following the description of the model itself.

$$\Sigma : \dot{x} = f(x, y, z, p) \quad (10.14)$$

$$0 = g(x, y, p) \quad (10.15)$$

$$x_{\ell_i} \leq x \leq x_{u_i}, \quad i = 1, \dots, n \quad (10.16)$$

$$z_i = \bar{h}_i(x, y, p) \\ := \begin{cases} z_{\ell_i} & \text{if } h_i(x, y, p) \leq z_{\ell_i} \\ h_i(x, y, p) & \text{if } z_{\ell_i} < h_i(x, y, p) < z_{u_i} \\ z_{u_i} & \text{if } h_i(x, y, p) \geq z_{u_i} \end{cases} \\ i = 1, \dots, s \quad (10.17)$$

where $x \in X \subset \mathbb{R}^n$, $y \in Y \subset \mathbb{R}^m$, $p \in P \subset \mathbb{R}^q$, $z \in \mathbb{R}^s$, and f , g , and h are analytic functions with appropriate dimensions. In the Σ model Eqs. (10.14) describe the dynamics of power-system equipment including generators, composite dynamic loads, and the control devices. The variables x in Eq. (10.14) then correspond to the dynamic state variables of the respective power-system equipment, and the examples are generator internal fluxes, rotor angles and frequencies, load dynamic states, and control state variables. The algebraic equations (10.15), on the other hand, describe the network power-flow equations or the traditional load-flow equations written in the form of the network coupling equations. The algebraic variables y are typically the power-flow variables such as bus voltages and bus angles. The parameters p can be largely divided into system parameters (which define the power-system configuration and equipment parameters) and the operating parameters such as loads and reference set points (which define a specific operating condition). Together Eqs. (10.14) and (10.15)

constitute the traditional differential-algebraic power system model (DAE model). These equations form the model analyzed in Chapters 7 and 8.

However, in the Σ model also notice the presence of two types of hard limits, namely, the actuator or *windup limits* (10.17) on the *actuation* variable z_i , which is a function of a few states and represents an internal actuation such as an internal control output z , and the *nonwindup limits* (10.16) on the dynamic state variables x . The distinction between the two types of hard limits, namely, the windup and nonwindup types, has long been recognized in power-system literature [5, 6]. In the case of the nonwindup limits (10.16), the limits, say, $x_{\ell i}$ and x_{ui} on the state variable x_i forces this state variable x_i to strictly stay within these limits with no windup involved. For instance, when x_i tries to increase past x_{ui} the nonwindup limiter would prevent such an action so that the state x_i would get stuck at x_{ui} with no windup, that is, no energy storage in this process. Therefore the nonwindup limits (10.16) constitute hard limits on the state variables x_i ; hence these are called the *state limits* in Ref. [14].

On the other hand, the mechanics of the windup limits (10.17) are very different. For instance, consider the simple case of a windup limit directly on just one state variable (this case arises frequently), say, $z_i = \bar{h}_i(x_i)$, which acts on the control, that is, actuation signal. This limits the internal states, then, when state x_i increases past the limiting value z_{ui} , the output $z_i = \bar{h}_i(x_i)$ indeed gets stuck at the limit z_{ui} . However, the input or the state variable x_i does not stop but instead moves past the limit to some potentially much higher value before it starts winding back in the course of the system dynamics. Even when the state starts to wind back, note that the output z_i would remain at z_{ui} until that time when state x_i itself has returned to where $h(x_i)$ drops below the limit z_{ui} . Therefore, the windup limit primarily acts on the output of an actuation device such as a controller. Therefore windup limits are equivalently called *actuation limits* [14].

The word *windup* tries to imply the fact that the dynamics of the complete n th-order system is progressing freely except for a temporary system modification that keeps a quantity (a function of the state) fixed until this dynamic process moves h of the limit. In nonwindup limits a state variable is directly frozen at a constant value temporarily, which means that the system order is reduced by one. However, the dynamics again proceeds on its course in the reduced-order system until this dynamic has this variable pects to the unconstrained side smoothly and reverts from a parameter to a state variable again.

A third type of hard limit that will not be discussed here in detail is represented by *switching limits*. Reaching the limits initiates preprogrammed structural action, which then in turn can change the whole system, its state, and/or the parameter space. These switching actions are initiated by relay mechanisms and protective limiters in the physical system, which monitor certain states or certain functions of several states of the system (thus relay-type limits can also be of state or actuation types). Depending on their preprogrammed logic, protective actions are taken when certain (disruptive) events are sensed. For the power system, detailed models for including the effects of relays in system dynamic studies have been

recently proposed in Refs. [5, 6]. Essentially the relay elements can be included in the analysis by modelling their internal logic mechanisms as state dynamic equations. In general, the switching-type limits can be modeled by introducing certain internal variables say, $s_i = \bar{v}_i(x, p)$ where the function $\bar{V}_i(x, p)$ takes only two values, either zero or one [14] [23, 24].

Each of these hard limits can be introduced into the DAE model resulting in an overall system representation that is a hard-limit-constrained set of differential-algebraic equations. By separately considering the three types individually, it can be shown [14] that the two-level cellular structure of the DAE dynamics introduced in earlier sections is preserved in this case, though somewhat different in details. In this chapter, we summarize some of the results from Ref. [14] for the special case of windup limits or actuation limits. The results for nonwindup limits are presented in Ref. [14]. It should be mentioned that this treatment covers events at hard limits inside individual components.

10.2.2 Conceptual Introduction on Small Systems

The plan followed in Sections 7.2 and 7.3 in describing and studying DAE dynamics was first to study a small, rudimentary system (Section 7.2). This is only a third-order system and as such lends itself to two-dimensional graphical representation. This makes it an excellent tool for explaining the rather complex geometrical and analytic features involved in this nonlinear dynamics. A conceptual understanding of the DAE problem was developed in Chapter 7. This then facilitated the precise exposition of the dynamics of the very large system modeled in refined detail in Chapter 8.

The same process will be followed here. First, in the next (section 10.2.2.1), the rudimentary system is again used for developing conceptual understanding about a small but representative example. This then will be followed in later sections by a precise study of the state space and the parameter space of the realistically very large power system, modeled in a careful and representative manner [11].

10.2.2.1 A Rudimentary Power-System Example A rudimentary power system including generation, voltage control, transmission, and matched load (see Fig. 10.3) is used in this section to illustrate various dynamical phenomena related to hard limits. The phase portraits shown in this section provide an overview of the state-space and the parameter-space phenomena for the hard-limit-constrained DAE system. In Figure 10.3(a), a one-axis generator model and a constant power load are connected by a lossless transmission line. We assume the active load is always matched by the mechanical input to the generator, thus eliminating the rotor-angle dynamics. The generator in Figure 10.3(a) has a first-degree voltage control block [see Figs. 10.3(b) and 10.3(c)], which is a simplification of the IEEE Type 1 excitation system [6].

The rudimentary power system introduced in Section 7.2 can be represented by the following differential algebraic equations.

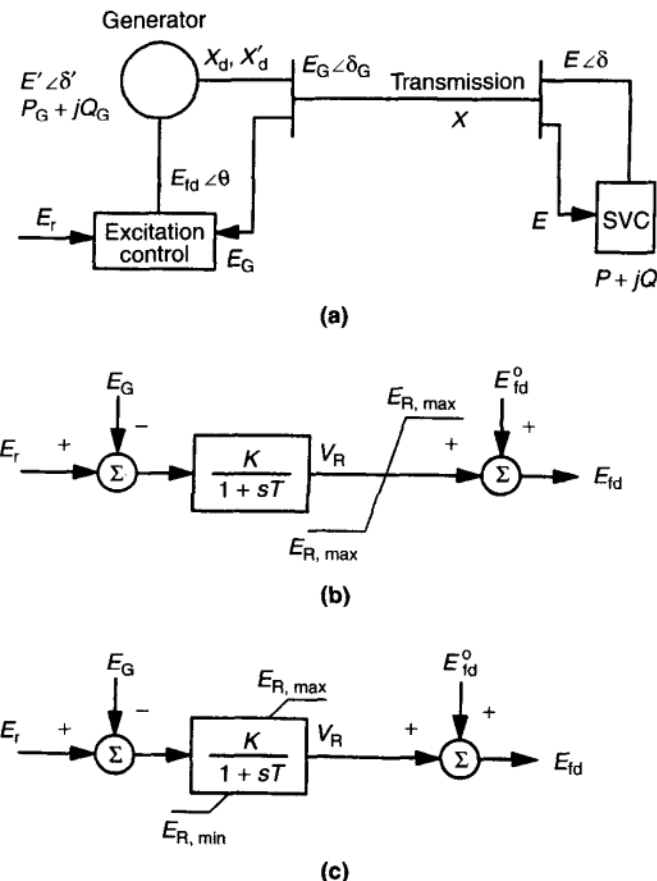


FIGURE 10.3 Rudimentary power system. (a) One-line diagram; (b) excitation system with windup limits; (c) excitation with nonwindup limits.

Dynamic equations

$$T'_{d0}\dot{E}' = -\frac{x+x_d}{x'}E' + \frac{x_d-x'_d}{x'}\frac{E^2+x'Q}{E'} + E_{fd} \quad (10.18)$$

$$T\dot{V}_R = -V_R - K \left(\frac{1}{E} \sqrt{(xP)^2 + (x'Q+E^2)^2} - E_r \right) \quad (10.19)$$

Algebraic Equation

$$0 = E'^2 - (x'P)^2 - (x'Q+E^2)^2 \quad (10.20)$$

The output V_R of the voltage control will be limited by either a windup limit [Fig. 10.3(b)] or a nonwindup limit [Fig. 10.3(c)]. E_{fd} is obtained by summing up the limited V_R and E_{fd}^0 .

The rudimentary power-system model (without hard limits) has been studied previously in Section 7.2. A comparison of the phase portraits given in this

section with the phase portraits shown for the smooth DAE model in Section 7.2 would give valuable insight on how the windup and nonwindup hard limits affect the state-space stability regions and parameter-space bifurcations.

10.2.2.2 Nonwindup-Limit Examples Figure 10.4(a) gives the phase portrait for a system with nonwindup limits, shortly before an operating point x_h^s reaches the hard limit and is annihilated in a static limit-induced bifurcation. The figure also shows the zero sets for the underlying vector field corresponding to the control and generator equation. The operating point is a stable focus, labeled x_h^s . Its stability boundary is the dashed trajectory, which is the stable manifold of the equilibrium x_l^u induced by the hard limit. All points inside the contour formed by the dashed trajectory and the hard limit form the region of attraction for x_h^s . Note that x_l^u is unstable under the dynamics induced on the hard limit, and the part of the hard limit denoted by a solid line in Figure 10.4(a) is its local unstable manifold. This part of the hard limit is called the *active limit*. It is where the trajectories coming from the interior of the constrained state space become part of the dynamics induced on the hard limits. It can be seen from Figure 10.4(a) that with active hard limits, trajectories are not uniquely backward in time. Uniqueness is only guaranteed forward in time. The other part of the hard limit is where the flow is oriented inward. This part is called the *inactive limit*. The point q of separation called the critical limit is where the flow is tangent to the hard limit (and the order of contact is indeed 2 in this example). Here the trajectory enters into the interior of the constrained state space smoothly at q . By changing the parameter, say, the real load power, the two equilibria x_l^u and x_h^s will meet precisely at a point corresponding to q and annihilate there [see Figs. 10.4(b) and 10.4(c)]. A similar scenario arises in the windup-limit case, where two equilibrium points meet and disappear. Note that in the windup-limit case trajectories are unique anywhere, but the trajectories are usually warped at hard limits [see Figs. 10.4(d) to 10.4(f)].

Comparing these figures with Figures 10.4(g) to 10.4(i), which gives the corresponding phase portraits for the DAE system without limits, highlights another aspect of the changes that hard limits can introduce into the phase portrait. It is in general not correct that the stability boundary for the system with hard limits can be obtained by simply cutting off the stability boundary for the unconstrained system at the hard limits. The reason is that the hard limits generate additional equilibria such as x_l^u in this case [see Figs. 10.4(a) and 10.4(d)], which can cause a reduction of the region of stability. For the constrained system, the stability boundary is essentially given by the dashed line, which is the stable manifold of x_l^u . For the unconstrained system, the corresponding equilibrium x_l^s lies in the low component and its stable manifold passes through ψ , which is considerably to the left. The instability of the hard-limit-induced equilibrium x_l^u in the constrained system causes a reduction in the region of attraction of the operating point. But sometimes hard limits may also in a certain sense enlarge the region of attraction corresponding to the unconstrained system, as we will see later.

Also note that the original system shows no change in structure at all for these particular parameter values: a stable focus moves across the level corresponding

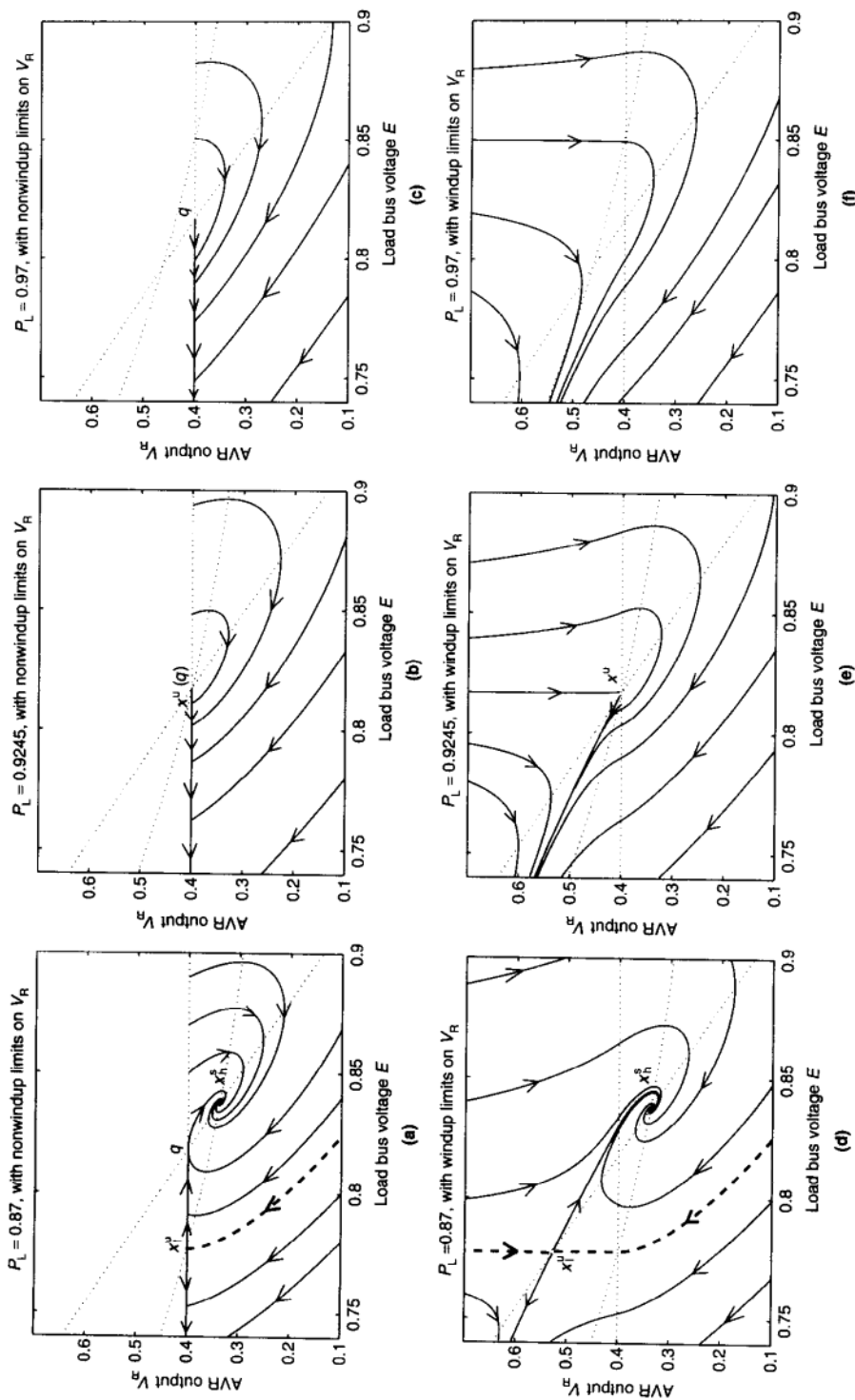


FIGURE 10.4 Phase portraits illustrating a hard-limit-induced static bifurcation: A saddle and a stable focus meet and disappear for the nonwindup limits [(a)–(c)] and windup limits [(d)–(f)]; comparative phase portraits for the unconstrained system [(g)–(i)]. Parameters: $x_d = 1, 2$, $x'_d = 0.2$, $T'_{d0} = 10$, $E_{fd}^0 = 1.6$, $K = 1.6$, $T = 3.5$, $E_r = 1.75$, $x = 0.1$, $Q = 0.5$, $V_{R,\text{MAX}} = 0.4$, $V_{R,\text{MIN}} = -0.4$.

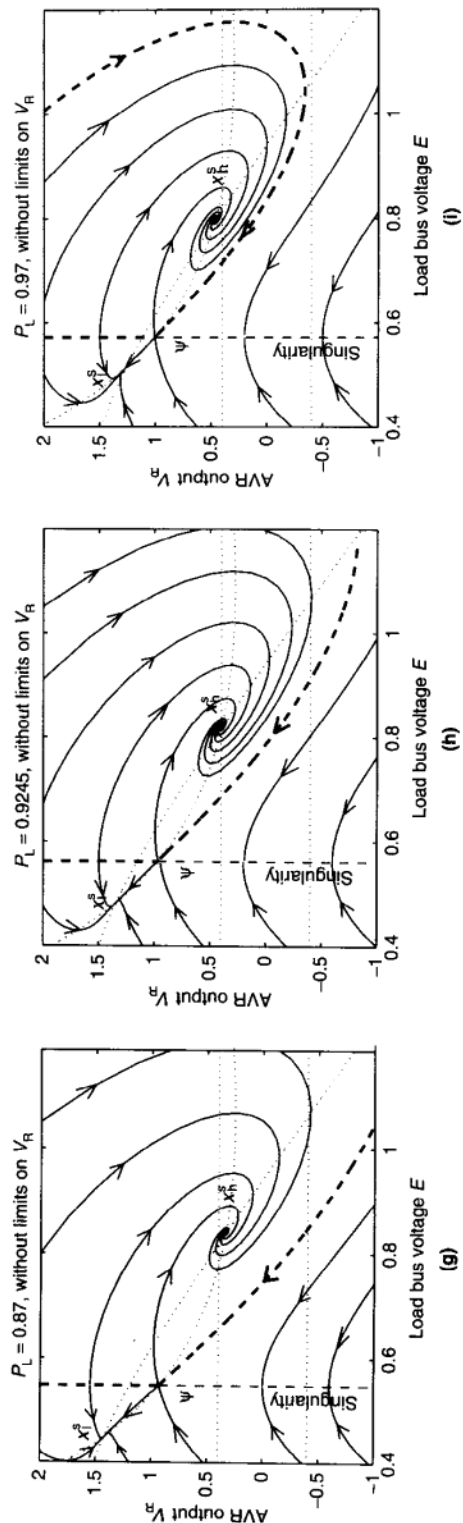


FIGURE 10.4 (Continued)

to the hard limit. In the constrained system, the equilibrium x_1^u is “brought in,” and this causes the annihilation of the two equilibria at the bifurcation. In a certain sense the hard limit generates a bifurcation that has the same effect as a saddle node of the smooth system [17], but here the stable equilibrium is in fact a focus.

Another interesting phenomenon is depicted in Figure 10.5, which shows how an operating point (here a stable node) moves onto the hard-limit surface and persists as an operating point there. In this case stability is sustained. It is also possible that the equilibrium becomes unstable as it reaches the hard limit and this therefore leads to a loss of stability.

Figure 10.6 shows the emergence and disappearance of hard-limit-induced oscillations. In Figure 10.6(a), the equilibrium point x_h^s is locally stable with the dashed line as its stability boundary, which is the stable manifold of the hard-limit-induced saddle point x_1^u . It is interesting to note that the unconstrained system has an unstable limit cycle [see Fig. 10.7(a)], but this limit cycle is cut through by the hard limit at the point s . The trajectory then follows the hard limit toward the critical limit q , where the trajectory enters the interior of the constrained state space tangentially and converges to the stable equilibrium x_h^s . It is important to note that the region of attraction of x_h^s for the system with hard limits is, in a certain sense, larger than that for the unconstrained system.

Figure 10.7 shows that the trajectory for the constrained system, starting from point A , converges with time, while the trajectory for the unconstrained system though starting from the same point diverges with time. As the parameter changes, for the system without limits, the limit cycle moves towards the hard limit from the outside. After it touches the hard limit at the critical limit q , this limit cycle also appears in the constrained system [see Fig. 10.6(b)]. The limit cycle is stable from outside and unstable from inside. If the parameter changes further, a second limit cycle, which is induced by the hard limit, emerges [see Fig. 10.6(c)]. What Figures 10.6(a) to 10.6(c) demonstrate is actually a nonsmooth version of cyclic fold bifurcation induced by hard limits. At point r , the system reaches the hard limit and follows the induced dynamics until again point q is reached, where the flows are tangential, and the trajectory enters the inside smoothly at this point q . Then the oscillatory behavior of the trajectory makes it return to the hard-limit surface at r . This nonsmooth limit cycle even persists after the smooth limit cycle disappears [see Fig. 10.6(d)]. As the parameter changes further, x_h^s undergoes a subcritical Hopf bifurcation and becomes an unstable focus afterwards (see Fig. 10.6).

In the unconstrained system the instabilities take over (the transient hits the singularity to be precise) [see Fig. 10.7(b)] and operation is not possible. But for the nonwindup-limit system, this is not the case. The stable nonsmooth limit cycle forms a “boundary” for the unstable region of x_h^u [see Fig. 10.6(d)], which absorbs the unstable transients diverging from the unstable focus x_h^u . In fact, this phenomenon appears to be quite persistent even in more detailed power-system models. However, in large systems, the interaction of more than one hard limit appears to be decisive on the transient behavior [18].

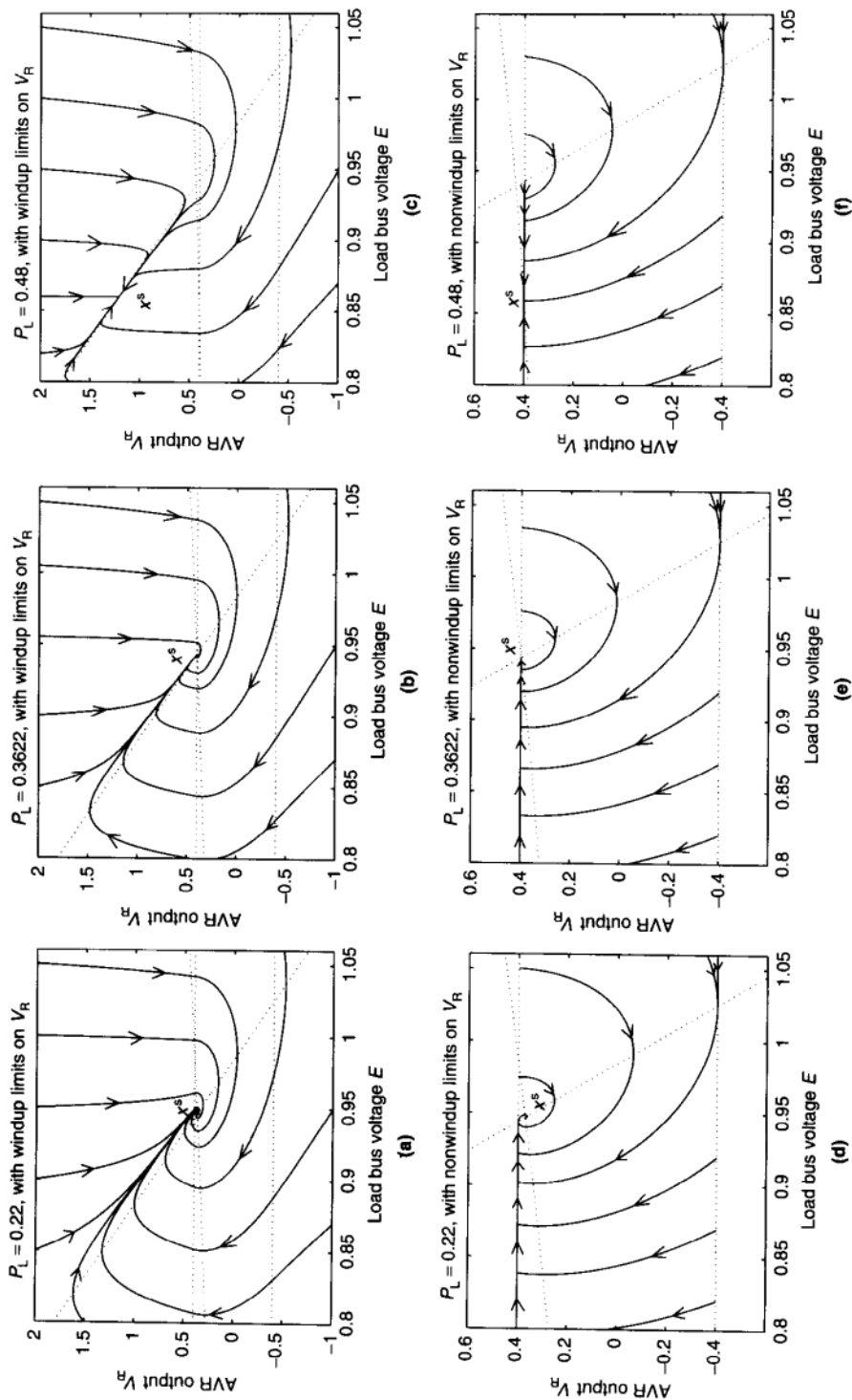


FIGURE 10.5 Phase portraits showing stable system operation continues even after the operating point reaches the windup limits [(a)–(c)] and nonwindup limits [(d)–(f)]. Parameters: $x_d = 1.2$, $x'_d = 0.2$, $T'_{d0} = 0.8$, $K = 10$, $T = 1.75$, $E_r^0 = 10$, $E_{\text{fd}} = 0.8$, $V_{R,\text{MAX}} = 0.4$, $V_{R,\text{MIN}} = -0.4$, $x = 0.1$, $Q = 0.15$.

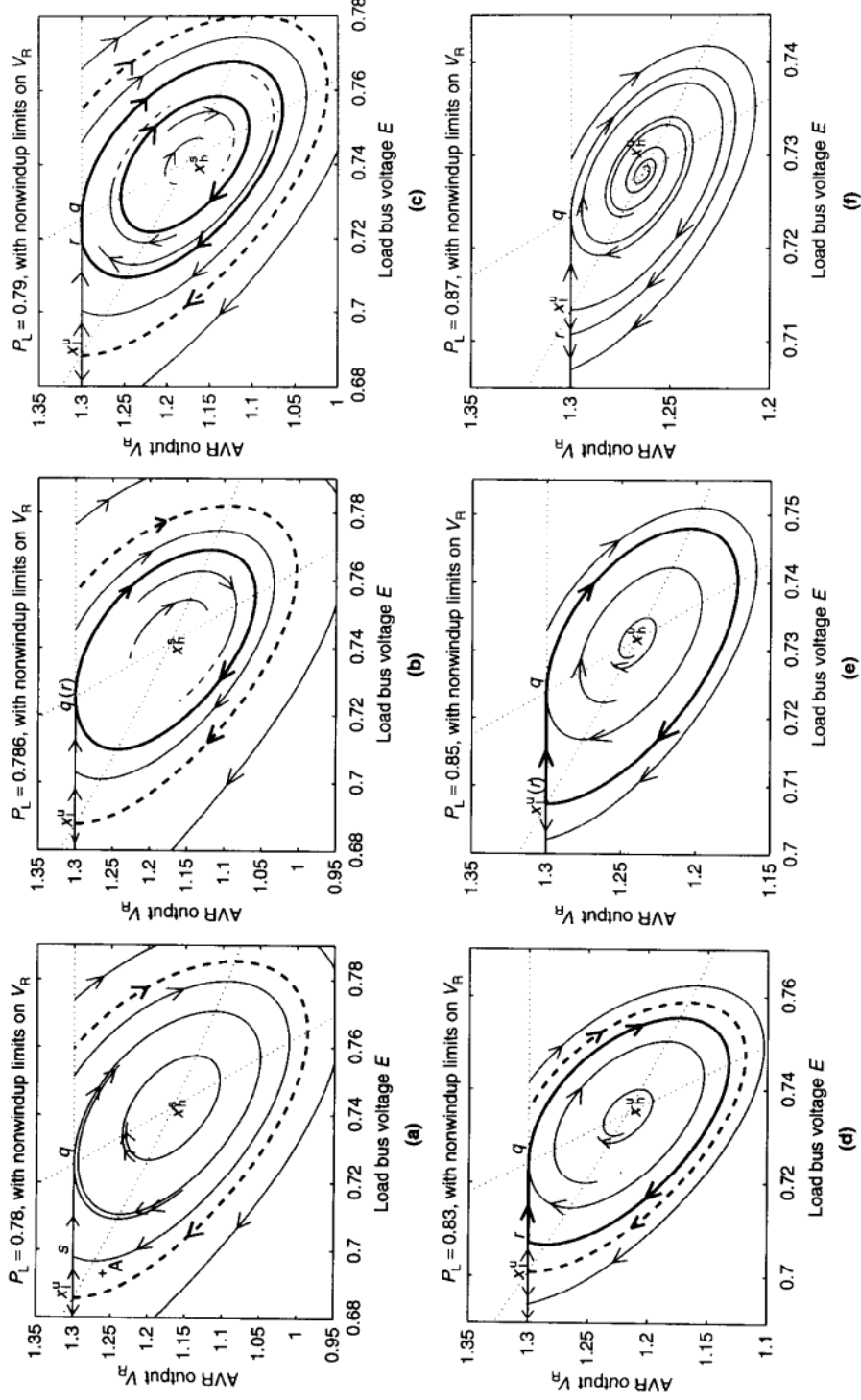


FIGURE 10.6 Phase portraits showing the emergence of a nonsmooth limit cycle [(a)–(c)] and nonsmooth homoclinic orbit [(d)–(f)] around a subcritical Hopf bifurcation. Parameters: $x_d = 1.2$, $x'_d = 0.2$, $T'_{d0} = 0.2$, $K = 10$, $E_{id}^0 = 1.6$, $E_r = 1.5$, $T = 10$, $E_t = 1.5$, $V_{R,\text{MAX}} = 1.3$, $V_{R,\text{MIN}} = -1.3$, $x = 0.1$, $Q = 1$.

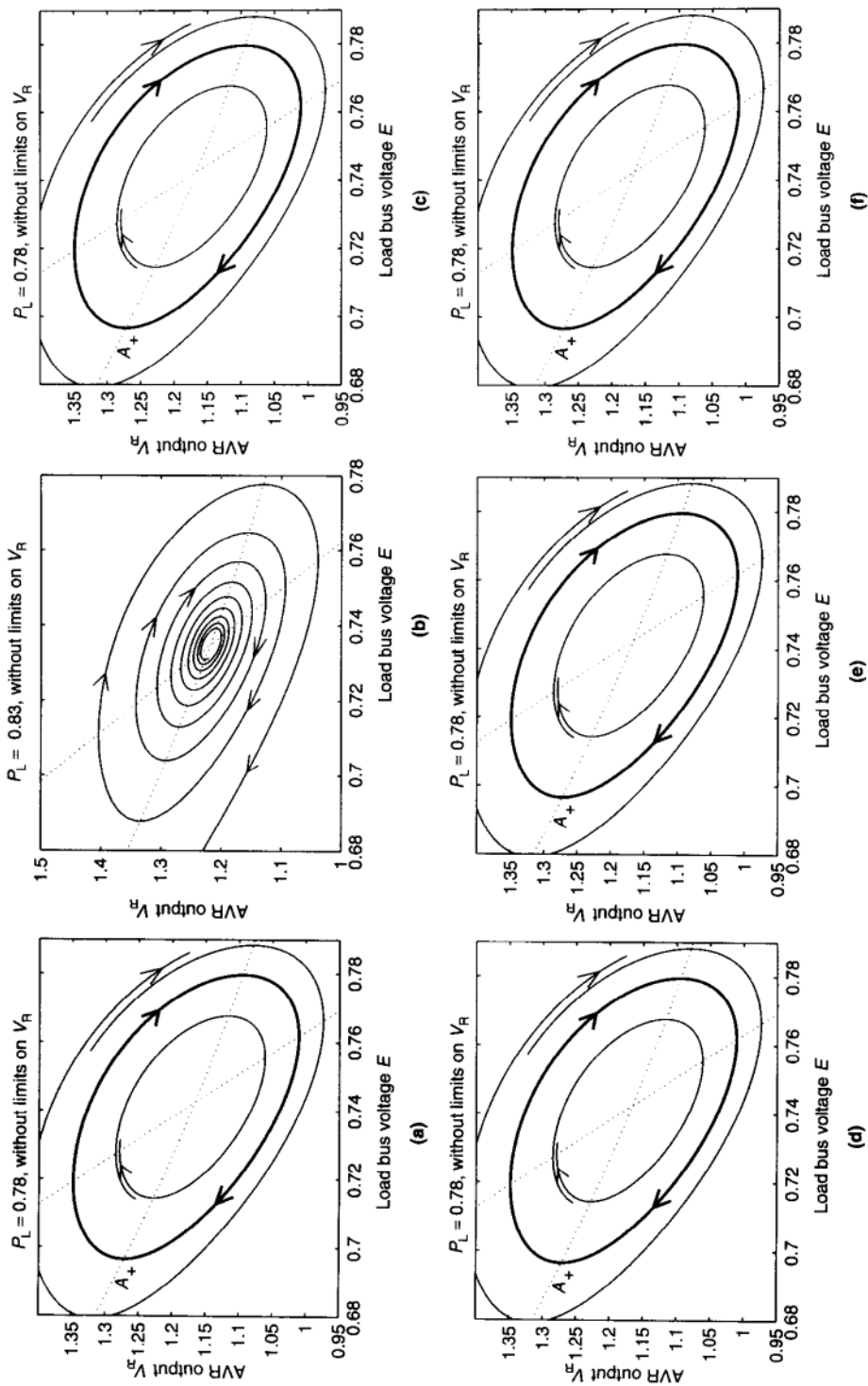


FIGURE 10.7 Comparative phase portraits showing only a subcritical Hopf bifurcation occurs if there are no limits on the automatic voltage regulator (AVR) output V_R : (a) stable operating point and unstable limit cycle; (b) unstable operating point.

Figures 10.6(e) to 10.6(f) show the disappearance of the hard-limit-induced limit cycle when it touches the unstable equilibrium point x_1^u on the hard-limit surface. This constitutes the formation of an exotic limit set, namely a hard-limit-induced (nonsmooth) homoclinic orbit at the equilibrium x_1^u , which is locally attracting from the interior. However, the mere existence of such stable homoclinic orbits in hard-limit-constrained power-system models is significant for investigating the possibility of chaotic behavior. Note that as in smooth systems, the limit cycle disappears in Figure 10.6(e) after the homoclinic bifurcation (also called the saddle connection bifurcation; see Ref. [17]) in Figure 10.6(d). A detailed analysis of this nonsmooth homoclinic orbit can be found in Ref. [13].

More generally we can show that the observed hard-limit-induced cyclic fold bifurcations observed in Figures 10.6(a) to 10.6(c) are in fact generic bifurcation phenomena in planar systems with state (nonwindup) limits. Specifically, it can be proved that when a hyperbolic unstable-limit cycle of a planar system touches a state limit under parametric variation, generically this will lead to a state-limit-induced cyclic fold bifurcation. On the other hand, when a stable hyperbolic limit cycle of a planar system approaches a state limit, the phenomenon will be quite different. In this case, it can be shown that generically a stable limit cycle exists locally around the parameter for which the limit cycle touches the state limit. However, the smoothness of the limit cycle will change at that parameter.

10.2.3 Hard Limits in the Power-System Model

The DAE system Σ_{DAE} is widely viewed as a realistic model for events in power systems [10,19] with midterm stability. As we mention in Section 10.2.1, power systems contain various types of hard limits [5,6,20]. Although hard limits have been routinely modeled in transient, midterm, and long-term stability simulation programs, they are seldom taken into account in analytical approaches or computer programs based on these approaches. Neglecting hard limits except in computer simulations is largely attributable to the difficulties in developing a mathematically rigorous theory for systems involving nonsmooth elements such as hard limits and to the fact that until recently power systems were relatively less heavily loaded and thus had less a chance of being operated at or near such hard limits. Recently, for regulatory and economical reasons, power systems are being operated at an increasingly high level of loading, or being increasingly stressed. As a result, it becomes necessary to develop a stability theory incorporating hard limits and examine the consequences of these hard limits for the system security.

After taking hard limits into consideration, the basic model of the power-system dynamics becomes

$$\Sigma_{\text{HL}} : \quad \dot{x} = f(x, y, z, p) \quad (10.21)$$

$$0 = g(x, y, z, p) \quad (10.22)$$

$$x_{l_i} \leq x_i \leq x_{u_i}, i = 1, \dots, n \quad (10.23)$$

$$z_i = \sigma_i(h_i(x, y, p)), i = 1, \dots, s \quad (10.24)$$

$$:= \begin{cases} z_{l_i} & \text{if } h_i < z_{l_i} \\ h_i & \text{if } z_{l_i} \leq h_i \leq z_{u_i} \\ z_{u_i} & \text{if } h_i > z_{u_i} \end{cases} \quad (10.25)$$

where $x \in X \subset \mathbb{R}^n$, $y \in Y \subset \mathbb{R}^m$, $z \in Z \subset \mathbb{R}^s$, $p \in P \subset \mathbb{R}^q$, and f , g , and h are smooth functions with appropriate dimensions. In Eq. (10.23) we allow $x_{l_i} = -\infty$ and $x_{u_i} = \infty$ (i.e., only some components of x may have limits).

The limits given by Eqs. (10.23) and (10.24) are called, respectively, state (nonwindup, in IEEE usage) limits and the signal (windup, in IEEE usage) [1]. In the case of nonwindup limits, a state x_i is constrained within a window ($x_{l_i} \leq x_i \leq x_{u_i}$), and the dimension of the state space is reduced when this state gets stuck at the limiting value. In the windup-limit case, a window ($z_{l_i} \leq z_i \leq z_{u_i}$) is imposed on a “dummy” state z_i for the function h_i . But the order of the system never changes. Generally, nonwindup and windup limits can be associated with integrator blocks, single-time constant blocks, and lead-lag blocks [10, pp. 358–361, and 1].

The mathematical model of DAE equations with embedded hard limits was presented in Eqs. (10.8) to (10.12) and the types of state (nonwindup) and actuation (signal, windup) limits was explained. Using these formulations the rudimentary system example of Chapter 7 was again used in Section 10.2.1 to introduce the reader to new concepts and new types of events generated by the presence of hard limits.

To simplify the analysis and to better visualize new phenomena connected with hard limits, we will assume the following assumptions.

Assumption 1 The system stays on one component and keeps a sufficient distance from the singular surfaces [therefore a DAE system essentially reduces to an ordinary differential equation (ODE) system].

We are allowed to do so because the hard limits will only affect the differential equations while the algebraic equations are valid all the time. In other words, the algebraic equations are defined on the unlimited composite space, and therefore all the concepts and results to the algebraic constraint equations are still valid as if the hard limits were not there. Specifically, the system model we will study in the following sections is

$$\Sigma_R : \quad \dot{x} = f(x, p), \quad (x, p) \in \bar{X} \times P \quad (10.26)$$

where f is called the underlying vector field and \bar{X} is the constrained state space given by

$$\bar{X} := \{x \in X : \quad x_{l_i} \leq x_i \leq x_{u_i}, i = 1, \dots, n\} \quad (10.27)$$

10.2.4 State-Space Structure: Region of Attraction and Stability Boundary

In this section, a fixed parameter p_0 is considered in the system Σ_R and is dropped for notational simplicity. We first describe the constrained dynamics induced by

nonwindup limits and then proceed to point out some of the interesting and significant changes that the nonwindup limits force on the structure of region of attraction and stability boundary. The basic premise in constructing the induced dynamics is that [6] if the underlying vector field f in Eq. (10.26) postulates a value x_i that is outside the window $x_{l_i} \leq x_i \leq x_{u_i}$, then x_i will be physically stalked at one of the limit (one would say x_i now is a parameter and the order of the vector field f is reduced by one after f_i is excluded). In this condition, the physical value of the state $x \setminus x_i$ (x excluding x_i) is determined by the truncated vector field $f \setminus f_i$ (f excluding f_i), and the state space is accordingly truncated down to the window in x_i . However, as soon as the underlying vector field f produces (mathematically) a state x_i that returns into the window, the physical x_i will follow the underlying vector field without delay, hence the name *nonwindup*. The underlying vector field f then gives the physical state x until x_i again reaches its limits. A formal definition follows.

DEFINITION 3: NONWINDUP OR STATE LIMITS Let $x_0 \in \bar{X}$. A nonwindup limit is defined as [6]

$$\dot{x}_i = \begin{cases} f_i & \text{when } \begin{cases} x_{l_i} < x_{0_i} < x_{u_i}, \\ x_{0_i} = x_{l_i} \text{ and } f_i(x_0) > 0, \text{ or} \\ x_{0_i} = x_{u_i} \text{ and } f_i(x_0) < 0 \end{cases} \\ 0 & \text{when } \begin{cases} x_{0_i} = x_{l_i} \text{ and } f_i(x_0) < 0 \text{ or} \\ x_{0_i} = x_{u_i} \text{ and } f_i(x_0) > 0 \end{cases} \end{cases} \quad (10.28)$$

Definition 3 motivates the following division of a hard-limit surface into three mutually disjoint sets based on whether or not the dynamics f_i will be annihilated for a state variable x_i .

DEFINITION 4: LIMIT SURFACE DIVISION

Hard limit surface $H_i = H_{l_i} \cup H_{u_i}$

Active Set $H_{A_i} = H_{l_i}^{(-)} \cup H_{u_i}^{(+)}$

Inactive Set $H_{I_i} = H_{l_i}^{(+)} \cup H_{u_i}^{(-)}$

Critical Set $H_{C_i} = H_{l_i}^{(0)} \cup H_{u_i}^{(0)}$

(10.29)

where

$$H_{l/u_i} = \{x \in \bar{X} : x_i = x_{l/u_i}\}$$

$$H_{l/u_i}^{(+)} = \{x \in H_{l/u_i} : f_i(x) > 0\}$$

$$H_{l/u_i}^{(-)} = \{x \in H_{l/u_i} : f_i(x) < 0\}$$

$$H_{l/u_i}^{(0)} = \{x \in H_{l/u_i} : f_i(x) = 0\}$$

It follows from Definition 4 that

$$H_i = H_{A_i} \cup H_{I_i} \cup H_{C_i} \quad (10.30)$$

Referring to Definition 3, it is apparent that an active set is where the dynamics f_i will be annihilated while an inactive set is where f_i will be kept. In fact, Definition 3 essentially introduces reduced-order flows in active sets. However, the dynamics for points in the critical set is not defined in Definition 3. We can show that generically the critical set serves as the boundary of the active set. Therefore, it is reasonable to extend the flows in active sets to critical sets so that points in the critical set become either originating or ending points for the reduced order flows. With this extension, the following result holds.

Theorem 10.2.1: Positive Semiflow Under generic assumptions ([14, Theorem 17]) there exists a unique induced vector field \bar{f} that is compatible with the hard limits. This vector field is piecewise smooth in the sense that there exists a decomposition of \bar{X} into connected embedded submanifolds with the property that the restriction of \bar{f} to these submanifolds are smooth vector fields. For every point $q \in \bar{X}$ there exists a unique solution γ_q forward in time to the ODE $\dot{x} = \bar{f}(x)$ that is defined over a maximal interval $[0, T(q))$. We say that \bar{f} generates a positive semiflow.

Theorem 10.2.1 shows that under generic assumptions (i.e., for vector fields in an open and dense set), the trajectory is indeed unique (but not smooth) in forward time; however, the uniqueness in backward time is lost. The nonsmoothness and loss of backward uniqueness are the two main difficulties in analyzing the nonwindup-limit-constrained dynamics. It can be shown [1] that with a windup limit, the trajectory uniqueness will be preserved in both forward and backward time. We will assume from here on that the generic assumptions of Theorem 10.2.1 are in effect so that \bar{f} generates a positive semiflow.

Here, we use I (I^c) to denote the indices for hard limits reached (not reached) and $|I|$ to denote the number of hard limits reached. Apparently I is a subset of $N = \{1, \dots, n\}$ and $I^c = N \setminus I$. We also define $f^I(x^I)$ as the reduced-order vector field [($n - |I|$)-dimensional] where f^I and x^I are obtained, respectively, from f and x with components from the index set I^c . The state variables x_i from I are set to either upper or lower limits in f^I depending on which hard limit is involved. J^I denotes the Jacobian matrix $\partial f^I / \partial x^I$.

We define the equilibrium points for the system Σ_R to be the equilibria for all the reduced-order flows within their defined domain.

DEFINITION 5: EQUILIBRIUM POINTS

$$\text{EQ}^I = \{x \in \bar{X} : f^I(x) = 0, \quad (10.31)$$

$$x \in \cap_{i \in I} (H_{A_i} \cup H_{C_i})\} \quad (10.32)$$

where $I \subset N = \{1, \dots, n\}$.

Note that an equilibrium point defined by Definition 5 does not require all the f_i 's from f to be zero. Indeed, some components f_i from f may not be zero as long as the corresponding x_i of the equilibrium point is at their active hard limits so that the dynamics for these x_i has been annihilated by the respective hard limits. The equilibria involving only active hard limits are called active equilibria denoted EQ_A^I . All the other equilibria that involve critical hard limits are called critical equilibria, denoted EQ_C^I . An equilibrium is called a level- k equilibrium if it lies in the intersection of k hard limits. Generically, equilibria exist only in the interior of the constrained state space \bar{X} (these are carried over from the underlying vector field) or in the active sets of hard-limit surfaces (these are induced by the hard limits). Critical equilibria will be considered only when we study bifurcations in the parameter space when changes in parameters are considered. Therefore, in this section, we assume that EQ_C^I is empty for any $I \subset N$. The following definition identifies the generic (typical, roughly speaking) equilibria for the system Σ_R .

DEFINITION 6: HYPERBOLIC EQUILIBRIA An equilibrium $x \in \text{EQ}$ is called hyperbolic if $x \in \text{EQ}_A$ and all the eigenvalues of $J^I = \partial f^I / \partial x^I$ have nonzero real parts, where I is the index set for all the (active) hard limits involved at x .

Based on the structure of the phase portrait around a generic equilibrium, basic concepts such as the stability of equilibria and local stable and unstable manifolds of equilibria can be established. These results then allow one to pursue the structure of region of attraction for stable operating points even on hard limits. Using standard definitions for local invariant manifolds, Proposition 10.2.1 shows that the local unstable manifold of a level- k equilibrium x_0 simply is the local unstable manifold of x_0 as an equilibrium of the reduced-order vector field on the intersection of the k active sets involved at x_0 . Therefore, an active level- k equilibrium point x_0 is locally stable for \bar{f} if and only if it is locally stable for f^I . Obtaining the local stable manifolds W_{loc}^s is more technical though no less direct. Now the different flows have to be pieced together and strictly speaking, W_{loc}^s is no longer a smooth manifold, but still a topological manifold with boundaries. These are precisely formulated in the following proposition.

Proposition 10.2.1: Local Invariant Manifolds For a hyperbolic equilibrium $x_0 \in \text{EQ}_A$, we have that

$$W_{\text{loc}}^u(x_0) = W_{\text{loc}}^{u,I}(x_0) \quad (10.33)$$

where $W_{\text{loc}}^{u,I}(x_0)$ is the local unstable manifold for f^I . $W_{\text{loc}}^s(x_0)$ is a piecewise smooth manifold in the sense that it can be decomposed into a locally finite family of smooth manifolds with boundaries. It has dimension $n_s = n - n_u$,

where $n_u = \dim W_{loc}^{u,I}(x_0)$. $W_{loc}^s(x_0) \cap H_{Ai}$ is an $(n_s - 1)$ -dimensional piecewise smooth manifold for all $i \in I$.

A definition of global stable and unstable “manifolds,” however, is anything but straightforward or direct. To begin with, the sets of points converging to a particular equilibrium may not be manifolds if they involve sections on the hard limits. Because of the loss of uniqueness backward in time these definitions should be tailored carefully if one wants to avoid duplications between unstable manifolds of equilibria on different hard limits or structures that contain manifolds of different dimensions. Nevertheless, a characterization of the stability boundary of a stable equilibrium can be developed under generic assumptions relating to transversal intersection properties of the appropriately defined global stable and unstable “manifolds” and other suitable extensions of assumptions in Morse–Smale theory [9]. The stability boundary now also includes stable manifolds of hard limit induced equilibria, periodic orbits and certain “source-like” segments on the inactive and critical hard limits. The statement of the theorem however is very technical and can not be included here. Its proof rests on a careful extension of the topological arguments in Ref. [9]. We give some illustrative examples in Fig. 10.9 using the rudimentary system [11,15] with nonwindup limits on the voltage control output V_R .

Figure 10.8(a) illustrates the state-space structure of the nonwindup-limit-constrained dynamics. In Figure 10.8(a) the hard-limit surface is divided into three disjoint sets. The solid line to the left of the point q is the active set. Note that there is a hard-limit-induced flow on the active set up to the point q , which is essentially the critical set. At points on the active set, trajectories are only unique in forward time. In backward time there are two trajectories, one for the underlying flow, the other for the reduced order flow on the hard limit. Compared to the phase portrait [Fig. 10.8(b)] for the system without limits on V_R , the region of attraction of the stable focus x_h^s is reduced in Figure 10.8(a). This is because the limit on V_R induces a saddle point x_l^u on the hard-limit surface, and the stable manifold of x_l^u forms the stability region for x_h^s . However, it is not always true that a neighboring hard-limit-induced equilibrium point will reduce the size of an operating point. Figures 10.8(c) to 10.8(f) shows a scenario where the hard limit is contributing positively to the system stability. Figures 10.8(c) and 10.8(d) depict a subcritical Hopf bifurcation for the unconstrained system. Note that the operating point is stable with an unstable limit cycle as its stability boundary in Figure 10.8(c), whereas in Figure 10.8(d) the operating point becomes a unstable focus. For the case with nonwindup limits on V_R , the limit cycle in Fig. 10.8(c) is broken [Fig. 10.8(e)], and the region of attraction is enlarged in some sense by the stable manifold for the hard-limit-induced equilibrium point x_l^u . [Note the same point A is outside the region of attraction in Fig. 10.8(c), whereas it is inside the region of attraction in Fig. 10.8(e)]. In Figure 10.8(f), a stable nonsmooth limit restricts the unstable region for the equilibrium point x_h^w . A more detailed demonstration of possible interactions between hard limits and Hopf bifurcations can be seen in Ref. [11].

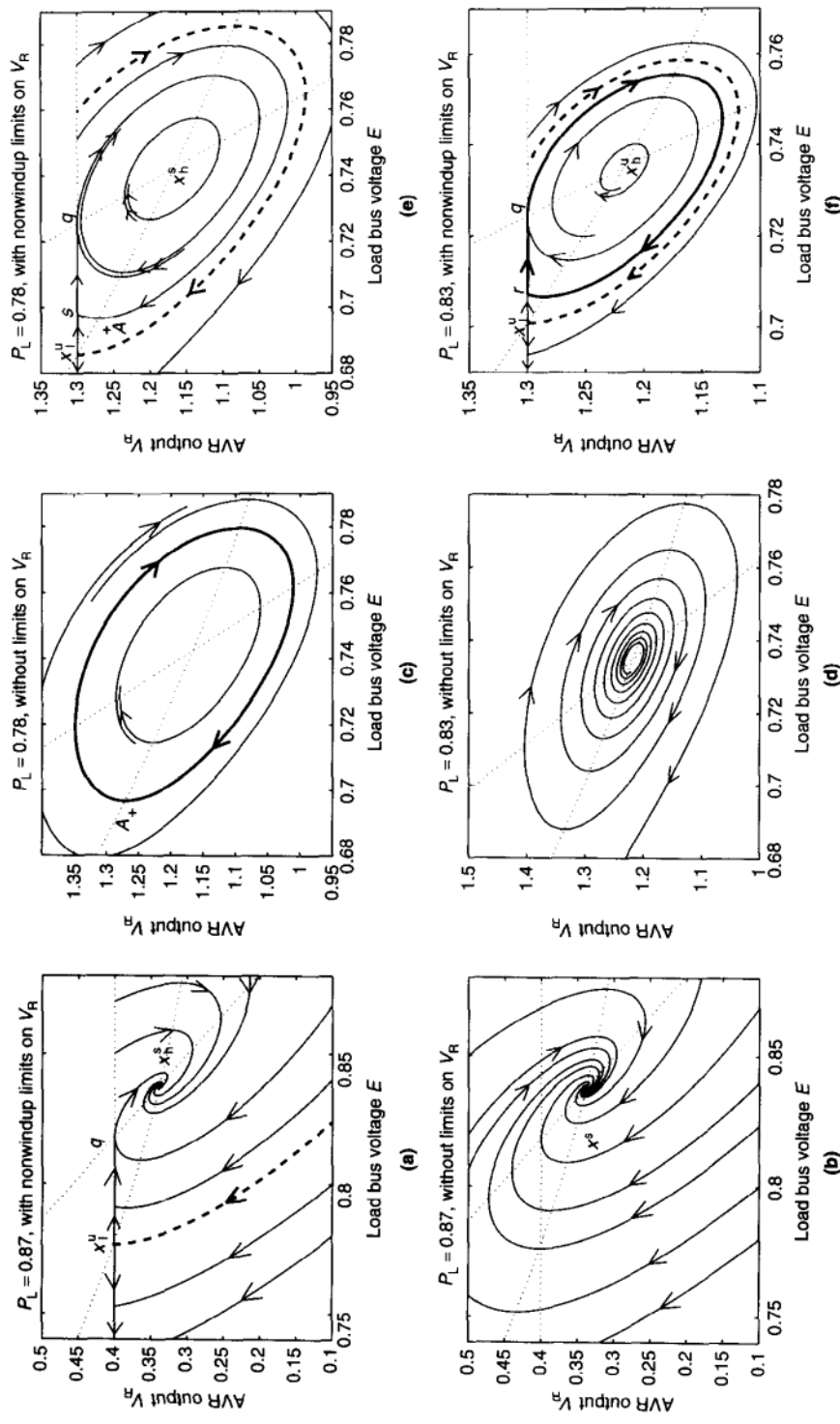


FIGURE 10.8 (a)–(b) Phase portraits showing the state-space structure of systems with nonwindup limits and the unconstrained system. Parameters: $x_d = 1.2$, $x'_d = 0.2$, $t'_{d0} = 0.2$, $E_{fd}^0 = 10$, $t'_{d0} = 10$, $K_A = 1.6$, $T_A = 3.5$, $E_r = 1.75$, $T_r = 0.4$, $x = 0.1$, $Q_L = 0.5$. (c)–(f): Interactions between Hopf bifurcations and hard limits. Parameters: $x_d = 1.2$, $x'_d = 0.2$, $T'_{d0} = 10$, $E_{fd}^0 = 1.6$, $K_A = 10$, $T_A = 1.5$, $E_r = 1$, $V_{R,\text{MAX}} = 1.3$, $V_{R,\text{MIN}} = -1.3$, $x = 0.1$, $Q_L = 1$.

10.2.5 Parameter-Space Structure: The Boundary of Small-Signal Stability

In this section, we look into the question what happens to the small-signal stability of the system when the operating point gets onto or off a hard limit. We will show that in some cases, the equilibrium becomes a hard-limit-induced bifurcation (static or dynamic) point¹ while in some other cases, stable operation will be sustained. It will be shown that a simple check involving only the Jacobians of the underlying vector field is sufficient to determine whether or not the critical equilibrium is a bifurcation point, and if it is, whether the bifurcation is static or dynamic.

We know from Section 10.2.3 that for a fixed parameter, generically equilibrium points for the system Σ_R involve only active hard limits. These equilibria are locally stable (roughly small-signal stable) if and only if they are locally stable as an equilibrium for the reduced-order system defined on the intersection of all the hard limits involved at the equilibrium. The following sets precisely identifies these stable active equilibrium points.

$$\text{OP}^I := \{(x, p) \in \text{EQ}_A : \sigma(J^I(x, p)) \subset C^-, J^I(x, p) = D_{x^I} f^I(x, p)\} \quad (10.34)$$

where $I \subset N = \{1, \dots, n\}$.

If parameters change, an equilibrium that originally lies in the interior of the constrained state space or in the intersection of active hard limits may reach the critical set of some hard-limit surface. Obviously, if a stable active equilibrium point becomes a higher-level or lower-level stable active equilibrium by passing through a critical equilibrium, from a practical point of view, it would be desirable that such a critical equilibrium point be considered as an operating point with the always present disturbances on the power system. Otherwise, the parameter region for small-signal-stable operating points will be overconservative. To include those equilibrium points with most surrounding equilibrium points stable and active in the set of operating points we use a topological operation on the set $\cup_{I \subset N} \text{OP}^I$.

DEFINITION 7: POSSIBLE OPERATING POINTS

$$\text{OP} := (\overline{\cup_{I \subset N} \text{OP}^I})^\circ \quad (10.35)$$

that is, points in the interior of the closure of the finite union are taken as operating points.

The concept of the feasibility region defined in the following then identifies the parameter region within which the operating point can move stationarily without losing small-signal stability.

¹ Roughly speaking, static bifurcation means that the system loses its equilibrium as in the case of a saddle-node bifurcation; a dynamic bifurcation means that the equilibrium still exists but becomes unstable as in the case of a Hopf bifurcation.

DEFINITION 8: FEASIBILITY REGION Given a specific operating point $(x, p) \in OP$, the feasibility region F of (x, p) is the connected component of OP that contains (x, p) . The boundary of F (relative to EQ) is the feasibility region denoted ∂F .

The next proposition shows that the feasibility boundary consists of three zero sets.

Proposition 10.2.2: Feasibility Boundary [14]

$$\partial F = (\partial F \cap EQ_C) \cup (\partial F \cap C_{SN}) \cup (\partial F \cap C_H) \quad (10.36)$$

where

$$EQ_C := \bigcup_{I \subset N} EQ_C^I \quad (10.37)$$

$$C_{SN} := \bigcup_{I \subset N} C_{SN}^I \quad (10.38)$$

$$C_H := \bigcup_{I \subset N} C_H^I \quad (10.39)$$

$f_s(x_0, y_0) = 0$ and $f_i(x_0, y_0) \neq 0$ for all $i \in I$. All eigenvalues of J^I and J^{I_s} have nonzero real parts.

$$D_p f_s - D_{x^{I_s}} f_s (D_{x^{I_s}} f^{I_s})^{-1} D_p f^{I_s} \neq 0 \quad (10.42)$$

Define α as

$$\alpha := \frac{\det(J^{I_s})}{\det(J^I)} \quad (10.43)$$

Then the equilibrium properties near (x_0, p_0) can be characterized as follows:

$\alpha > 0$: (x_0, p_0) is a static bifurcation point and $(x_0, p_0) \notin OP$.

$\alpha < 0$: If both J^I and J^{I_s} are Hurwitzian² matrices, then $(x_0, p_0) \in OP$; otherwise (x_0, p_0) is a dynamic bifurcation point and $(x_0, p_0) \notin OP$.

A detailed proof for Theorem 10.2.2 can be found in Ref. [14]. Figures 10.9(a) to 10.9(c) illustrate the cases of static bifurcation, dynamic bifurcation, and sustained stability, respectively. In Figures 10.9(a) to 10.9(c), $x^I(p)$ and $x^{I_s}(p)$ are equilibria loci for the reduced-order vector fields f^I and f^{I_s} , respectively. But x^I is an equilibrium of Σ_R if and only if x^{I_s} is within the limits on x_s ; x^{I_s} is an equilibrium of Σ_R if and only if x^{I_s} is on the active hard limits on $x_s(H_{A_s})$.

Figures 10.10(a) to 10.10(c) show a hard-limit-induced static bifurcation that occurs as a stable focus and a hard-limit-induced saddle approach each other,

² A matrix J is Hurwitzian when all eigenvalues of J have negative real parts.

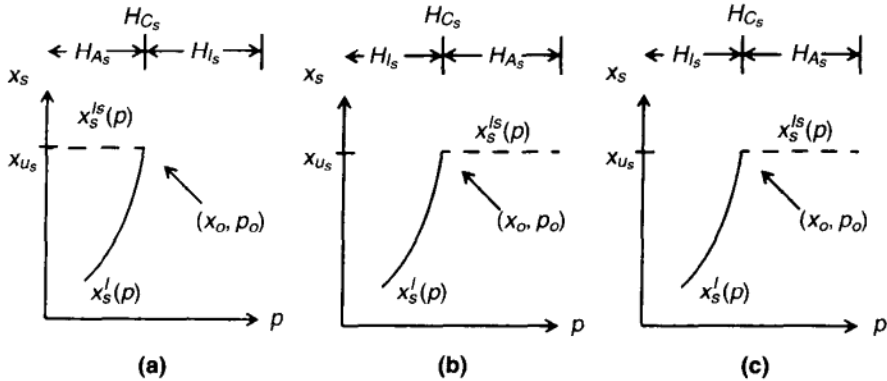


FIGURE 10.9 (a) Hard-limit-induced static bifurcation; (b) hard-limit-induced dynamic bifurcation; (c) sustained stability on hard limits.

and then both disappear after meeting. Such saddle-focus annihilations have no counterpart in the unconstrained smooth system. Figures 10.10(d) to 10.10(f) show that stable operation may be sustained as the equilibrium moves onto the hard limits.

Define

$$B_{SB} := \bigcup_{I \subset N} B_{SB}^I \quad (10.44)$$

$$B_{DB} := \bigcup_{I \subset N} B_{DB}^I \quad (10.45)$$

$$D := \bigcup_{I \subset N} D^I \quad (10.46)$$

where B_{SB}^I and B_{DB}^I are the subsets in $\overline{OP} \cap EQ_C^I$ consisting of the state-limit-induced static and dynamic bifurcation points, respectively in Theorem 10.2.2. D^I is the subset in $\overline{OP} \cup EQ_C^I$ consisting of the points in OP in Theorem 10.2.2. Similarly we define B_{SN} and B_H as the subsets in C_{SN} and C_H with appropriate transversality conditions related to saddle node and Hopf bifurcations for the reduced order system [22].

Corollary 10.2.1 (Density) Generically,

$$\partial OP \cap EQ_C = \overline{\partial OP \cap (B_{SB} \cup B_{DB})} \quad (10.47)$$

$$C_{SN} = \overline{B_{SN}} \quad (10.48)$$

$$C_H = \overline{B_H} \quad (10.49)$$

$$OP \cup_{I \in N} OP^I = OP \cap EQ_C = \overline{OP \cap D} \quad (10.50)$$

(10.50) shows that the additional equilibrium points OP besides the stable active equilibria are all connected with critical hard limits and most of them are points

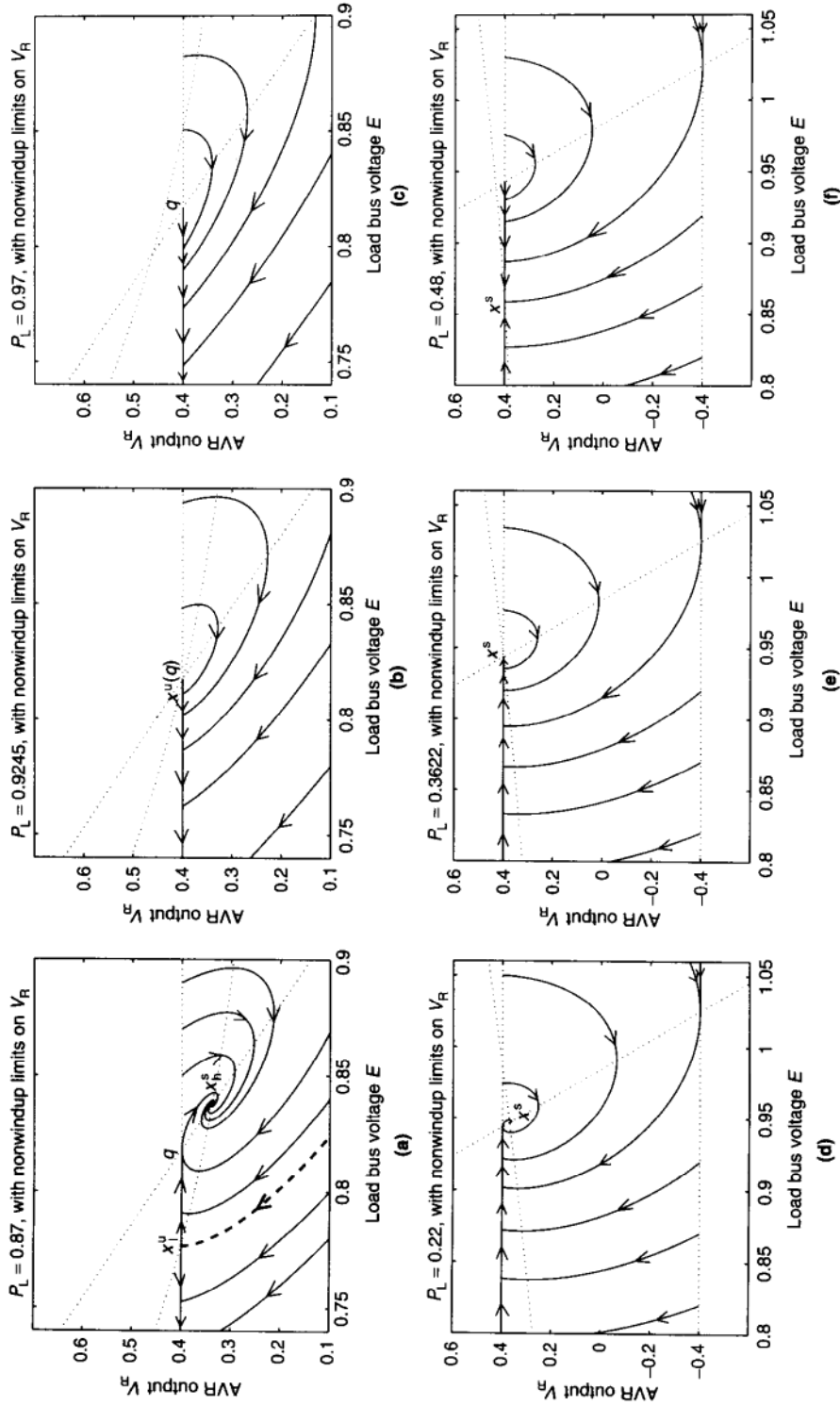


FIGURE 10.10 (a)–(c) Hard-limit-induced static bifurcation for the same parameters as in Figures 12.8(a) to 12.8(c); (d)–(f): Sustained stable operation on hard limits for the parameters $x'_d = 1.2$, $x'_d = 0.2$, $T'_{d0} = 0.2$, $E_{fd}^0 = 10$, $T_A = 10$, $K_A = 0.8$, $E_r = 1.75$, $V_{R,MAX} = 0.4$, $V_{R,MIN} = -0.4$, $x = 0.1$, $Q_L = 0.15$.

in the set D . The next theorem says that the system Σ_R loses small signal stability upon reaching the feasibility boundary mostly by undergoing four types of bifurcations, namely, hard limit induced static bifurcations, hard limit induced dynamic bifurcations, saddle node bifurcations, and Hopf bifurcations.

Theorem 10.2.3 Feasibility Boundary

$$\partial \bar{F} = \partial F \quad (10.51)$$

$$= \overline{\partial F \cap (B_{SB} \cup B_{DB})} \cup \overline{\partial F \cap (B_{SN} \cup \partial F \cap B_H)} \quad (10.52)$$

Figure 10.11 shows the parameter space structure for the system with hard limits. The feasibility boundary (solid line in Figure 10.11) consists of segments related to saddle-node (B_{SN}), Hopf (B_H), and hard limit induced (static in this case, B_{SB}) bifurcations. The dashed line in Figure 10.11 is a Hopf segment in the unconstrained smooth system which is replaced by the hard limit induced segment in the constrained system. Note that the feasibility region is reduced as a result of the hard limit induced segment.

10.3 SUMMARY

This chapter is concerned with new results for the dynamic analysis of algebraically constrained power systems which also contain nonwindup type hard limits. Such results also provide groundwork for security monitoring purposes and improving energy function methods and providing more effective stability control of large power systems.

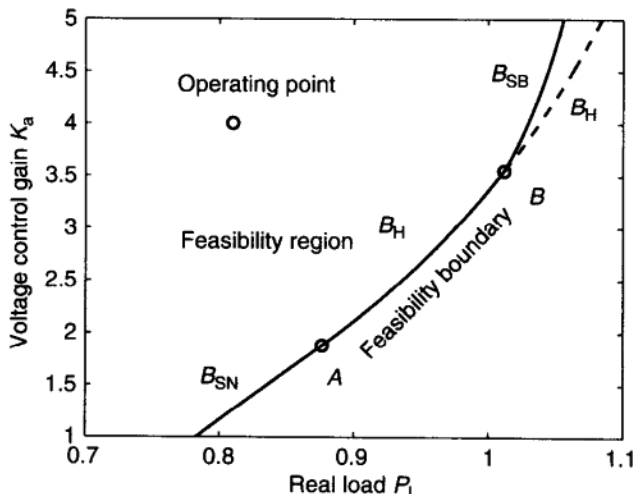


FIGURE 10.11 Feasibility boundary and the new segments related to hard limits for the parameters: $x_d = 1.2$, $x'_d = 0.2$, $T'_{q0} = 5$, $E_{fd}^0 = 1.6$, $T_A = 1.5$, $E_r = 1$, $V_{R,MAX} = 0.55$, $V_{R,MIN} = 0.55$, $x = 0.1$, $Q_L = 0.5P_L$.

In Section 10.2.4, we have seen that the hard-limit surface can be divided into three mutually disjoint sets: active, inactive, and critical sets. Active sets are where the trajectories move towards and get onto the hard-limit surfaces. Trajectories are not uniquely backward in time in this set. Inactive sets are where the trajectories originate and leave the hard-limit surfaces. Critical sets are where trajectories get onto or come off the hard-limit surfaces tangentially. Nonwindup limits will induce unconventional equilibria. These hard-limit-induced equilibria may become the anchor points in the stability boundary of the current operating point, resulting in a possible significant reduction or enlargement in the size of the stability boundary.

In Section 10.2.5, it is shown that (1) the feasibility region can incorporate hard limits, in other words, stable operation of a system can be continued on hard limits; (2) hard limits will induce additional segments in the feasibility boundary where the system will typically undergo either static or dynamic bifurcations; (3) saddle-node segments and Hopf segments are still in the feasibility boundary but they may happen on the (active) hard limits. Whether or not small-signal stability will be maintained when the operating point gets onto or off a hard limit is determined by the two Jacobians related to the underlying vector field. Note that the power system does not necessarily lose small-signal stability when the operating point reaches a hard limit. This is in contrast to the singularity-induced bifurcation for the DAE system in which the system behavior becomes unpredictable after the operating point crosses the singularity.

This chapter is relatively short on detail compared to Chapters 7 and 8 because of space limitation, but it at least introduces the conceptual aspects of the changes produced by the presence of hard limits in the DAE systems of Chapters 7 and 8. More details can be found in References [12 to 15]. Only the nonwindup type of hard limit is treated here in any detail. Details of the windup case were worked out by Venkatasubramanian in Ref. [27] and other of his recent publications on related topics.

BIBLIOGRAPHY

1. Venkatasubramanian, V., Stability boundary computations in large differential-algebraic models with hard-limits of the electric power system, in preparation.
2. Ilic-Spong, M., and Mak, F., Mid-range voltage dynamics modeling with the load controls present, *Proc. IEEE Conf. Decision Control*, 1987, pp. 45–52.
3. Medanić, J. Ilic-Spong, M., and Christensen, J., Discrete models of slow voltage dynamics under load tap-changing transformer coordination, *IEEE Trans. Power Syst.* **PWRS-2** 873–882, 1987.
4. Kwatny, H. G., Pasrija, A. K., and Bahar, L. Y., Static bifurcations in electric power systems: Loss of steady state stability and voltage collapse, *IEEE Trans. Circuits Syst., CAS-33*: 981–991, 1986.
5. IEEE Committee Report, Dynamic models for steam and hydro turbines in power systems studies, *IEEE Trans. Power Apparatus Syst.* 1904–1915, 1973.

6. IEEE Committee Report, Excitation system models for power system stability studies, *IEEE Trans. Power Apparatus Syst.* **PAS-100** 494–509, 1981.
7. Zaborszky, J., Some basic issues in voltage stability and viability, in L. H. Fink (ed.), *Proc. NSF Intl. Workshop Bulk Power Syst. Voltage Phenom.—I*, Potosi, MO 1988, pp. 1.17–1.60.
8. Zaborszky, J., and Zheng, B., Structure features of the dynamic state space for studying voltage-reactive control, *Proc. Power Syst. Comput. Conf.* Graz, Austria, 1990, pp. 319–326.
9. Venkatasubramanian, V., Schättler, H., and Zaborszky, J., A taxonomy of the dynamics of the large electric power system with emphasis on its voltage stability, in L. H. Fink (ed.), *Proc. NSF Intl. Workshop Bulk Power Syst. Voltage Phenom.—II*, Deep Creek Lake, MD, 1991, pp. 9–52.
10. Hill, D. J., Hiskens, I. A., and Mareels, I. M. Y., Stability theory of differential/algebraic models of power systems, Special Issue of *Sadhana*, M. A. Pai, (ed.), *Acad. J. Eng. Sci. India*, **18**: pt. 5, 731–748, 1993.
11. Jiang, X., Venkatasubramanian, V., Schättler, H., and Zaborszky, J., Hard limit related stability phenomena in the power system, *Proc. 1995 IEEE Conf. Control Appl.*, Albany, New York, 1995.
12. Jiang, X., Venkatasubramanian, V., Schättler, H., and Zaborszky, J., On the dynamics of the large power system with algebraic constraints and hard limits, *12th Power Syst. Comput. Conf. (PSCC)*, Dresden, Germany, 1996, pp. 440–449.
13. Jiang, X., Schättler, H., Zaborszky, J., and Venkatasubramanian, V., Hard limit induced oscillations, *Proc. 1995 IEEE Int. Sympo. Circuits Syst.*, Seattle, WA 1995, Vol. 1, pp. 146–150.
14. Venkatasubramanian, V., Jiang, X., Schättler, H., and Zaborszky, J., Current status of the taxonomy theory of large power system dynamics—DAE systems with hard limits, in L. H. Fink, (ed.), *Proc. NSF Intl. Workshop Bulk Power Syst. Voltage Phenom.—III*, Davos, Switzerland, 1994, pp. 15–103.
15. Venkatasubramanian, V., Schättler, H., and Zaborszky, J., Voltage dynamics: study of a generator with voltage control, transmission and matched MW load, *IEEE Trans. Automatic Control*, 1717–1733, 1992.
16. Jiang, X., Stability analysis of large power systems with hard limits on dynamic state, Ph.D. thesis, Washington University, Saint Louis, MO, 1996.
17. Guckenheimer, J., and Holmes, P., *Nonlinear Oscillations, Dynamical Systems and Bifurcations of Vector Fields*, New York: Springer, 1983.
18. Dehkordi, N., Analysis of Hopf bifurcation and voltage oscillations in power system models, M.Sci. thesis, Washington State University, Pullman, WA 1994.
19. Fischl, R., Decision support framework for evaluating voltage collapse criteria, Proc. Bulk Power System Voltage Phenomena—Voltage Stability and Security, Potosi, MO, 1988, pp. 7.59–7.109.
20. Kundur, P., *Power System Stability and Control*, New York: McGraw-Hill, 1994.
21. Venkatasubramanian, V., Schättler, H., and Zaborszky, J., Local bifurcations and feasibility regions in differential-algebraic systems, *IEEE Trans. Automatic Control*, **40**: 1992–2013, 1995.
22. Abed, E. H., and Varaiya, P. P., Nonlinear oscillations in power systems, *Int. J. Electric Power Energy Syst.*, **6**: 37–43, 1984.

23. Perez, L. G., Flechsig, A., Venkatasubramanian, V., Modeling the protective system for power system dynamic analysis, IEEE Winter Power Meeting, 1994.
24. Perez, L. G., Modeling and analysis of transient stability of power systems with special emphasis on the effect of protective relaying, Doctoral dissertation, School of Electrical Engineering and Computer Science, Washington State University, Pullman, WA 99164–2752, May 1994.
25. Jiang, X., Venkatasubramanian, V., Schättler, H., and Zaborszky, J., Basic structure of the dynamics with saturation limits on states, Proceedings of the 1996 IEEE Conference on Decision and Control Kobe, Japan, December 1996, Vol. 1, pp. 1103–1112.
26. Venkatasubramanian, V., Schättler, H., Zaborszky, J., Dynamics of Large Constrained Nonlinear Systems—A Taxonomy theory. Invited paper. Special Issue Proceedings of IEEE Vol. 83, 11 Nov. 1995, p. 1530–1561.

11 Beyond Quasistationarity and the Lumped-Parameter Model

During the last few decades, the nature of the power system has gradually changed by growing loads on the transmission and generation, increasing interconnections, increasing use of power electronic devices such as HV DC, Static Var Compensator (SVC), and thyristor-controlled motors. The result, among others, is an emergence of voltage stability (voltage collapse) and voltage control as critical problems connected with some much faster moving phenomena than those in the traditional rotor-angle transient stability. Some of the power electronic devices act as fast as cycle by cycle, but since this is a periodic intrusion, they will create harmonics in the steady state and can be handled by the harmonic approach which is presented in Chapter 2 and is not a concern here. Thus the theoretical and practical questions connected with the validity of phasor formulation now need to play a fundamental role in the dynamic theory of the modern AC system. Awareness of this situation has now been raised by practical occurrences and also in the literature [1,2]. A clear-cut comprehensive understanding of phasor dynamics, is offered in this chapter based on recent results in this area [1 to 9].

The senior author noted the presence in the literature of questionable results [10] arising from forgetting the limitations of the quasistationary assumption in the analysis of phenomena much faster than covered by this assumption [2,10,11] and with V. Venkatasubramanian established the need for fast time-varying phasors as reported in Refs. [6 and 1] on which the following presentation is based. V. Venkatasubramanian carried on the work after moving to Washington State University by establishing connections to similar concepts in circuit theory [8]. He also analyzed the effect of distributed parameters on long transmission lines being described by boundary-value problems and the line specific propagation time delay as an equivalent alternative to the boundary-value representation. Distributed parameters are the second major issue discussed in this chapter.

Other approaches (e.g. [4]) use physical reasoning and intuitive deduction to try to reach a general time-dependent phasor concept. Under the assumption that the system (including the transmission network and the loads) only consists of resistors and inductors, detailed power-system models purely in terms of flux linkages (without the quasistationary approximation) have been proposed for a large system in [5]. A concept of transient algebraic circuits is introduced in Ref. [5], which model the impedance variations as functions of frequency deviations, and the resulting singularly perturbed dynamics is simplified using the

integral-manifold theory. Some of the fundamental limitations connected with the general time-varying phasor concept have been recognized in Ref. [7]. Based on a filtering approach, it is shown in Ref. [7] that time-varying power-flow equations can be rewritten as autonomous differential equations in the phasor domain under certain bandwidth restrictions. An elegant method for formulating these phasor-domain equations using a notion of *phasor-domain circuits* is proposed in Ref. [7], which is related to the concept of *transient algebraic circuits* in Ref. [5] for the *RL* networks.

The main difference in the approach introduced in Refs. [1,2,6,8,9] from other work is the recognition that phasors essentially represent a mathematical transformation. This transformation can lead to tremendous simplification in analysis (for all cases: stationary; quasistationary; fast transients) provided necessary caution is exercised in establishing it rigorously. The mathematical properties of the phasor transformation have been proved recently in Refs. [6,8]. The results in Ref. [6] are based on the Blondel transformation in which the time-varying phasor transformation is established precisely for the balanced system. These results are summarized here in Section 11.3.1. In Ref. [8], the methodology of time-varying phasors is extended to the general large system (valid for both balanced and unbalanced conditions and not constrained to R-L circuits) using the long-existing notion of time-varying phasors from the communication theory under certain low-pass bandwidth assumptions.

Here we provide a structured overview (essentially a taxonomy) of the various phasor concepts and their implications for power-system dynamic analysis. Finally, in Section 11.6, these results are applied to a number of special cases and the question of approximation is expressed in a manner painting the way for moving into problems beyond quasistationarity and the lumped parameter model.

11.1 GENERALIZED TIME-VARYING PHASOR TRANSFORMATION

Current engineering practice involving modulated signals such as AC voltages and currents, $e(t)$ and $i(t)$, is largely based on transforming modulated signals into a phasor form, $\hat{E}(t)$ and $\hat{I}(t)$ through the relationship

$$\begin{aligned} e(t) &= E(t) \cos[\omega_c t + \delta(t)] \\ &= \operatorname{Re} [\hat{E}(t)e^{j\omega_c t}] = \operatorname{Re} [E(t)e^{j[\omega_c t + \delta(t)]}] \quad \forall t \in \mathbb{R} \end{aligned} \quad (11.1)$$

In this formulation, the phasor definition is tacitly conceived as a mathematical operator, say, \mathcal{P} , which maps the modulated signals to those time-varying phasor signals that satisfy the modulation equation (11.1).

Notation: Lowercase characters such as $e(\cdot)$ and $i(\cdot)$ denote modulated signals. Uppercase characters with hats such as $\hat{E}(\cdot)$ and $\hat{I}(\cdot)$ stand for the phasor signals. Capital letters such as $E(t)$ and $I(t)$ denote the magnitudes of the phasors or equivalently the amplitudes of the modulated signals. For notational convenience $E(t)$ and $I(t)$ will be interpreted as rms values [$E(t) = (1/\sqrt{2})\mathcal{E}(t)$, $I(t) = (1/\sqrt{2})\mathcal{I}(t)$], where $\mathcal{E}(t)$ and $\mathcal{I}(t)$ are the actual peak values of the modulated sinusoids for

voltage and current]. This is customary in power engineering. Lowercase Greek letters such as $\delta(t)$ and $\phi(t)$ denote the phases of the phasors.

Note that the frequency of the carrier signal ω_c is itself time varying in general. In this analysis, the reference frequency (e.g., $\omega_c = 60$ Hz) and ω_c is assumed fixed. Essentially since the actual frequency of the signal $e(t)$ [assuming that the amplitude $E(t)$ is constant] is $\omega = \omega_c + \delta$, the actual carrier frequency will be time varying even with the reference frequency ω_c defined as a constant. The concept of a *signal frequency* becomes more difficult when the amplitude is also time varying, such as in emerging voltage problems. Therefore, the notion of a time-varying phasor needs to be carefully thought out starting from the fundamentals, and this will be done in the next section. Time-varying phasors and the associated tools of manipulation such as time differentiation were casually introduced in Chapter 2. However in Chapter 2 only the stationary and quasistationary (i.e., slow) special cases were actually studied.

To develop a precise dynamic time varying phasor for the general system, the following definitions are now made.

DEFINITION 11.1: Phasor Signal; the set of all functions

$$\hat{E}(t) = E(t)e^{j\delta(t)} = E(t)\angle\delta(t) \quad (11.2)$$

which are complex-valued functions of time (i.e., $\hat{E} : \mathbb{R} \rightarrow C$ and \hat{E} is C^∞) is defined as the set P of phasors.

DEFINITION 11.2: Modulated Signal; the set of all functions

$$e(t) = E(t) \cos[\omega_c t + \delta(t)] \quad (11.3)$$

which are real-valued smooth functions of time (i.e., $e : \mathbb{R} \rightarrow \mathbb{R}$ and e is C^∞) is the set M of modulated functions.

Because power-system engineering is mostly about moving power around, the modulated and phasor form of the instantaneous power $p(t) = e(t)i(t)$ through

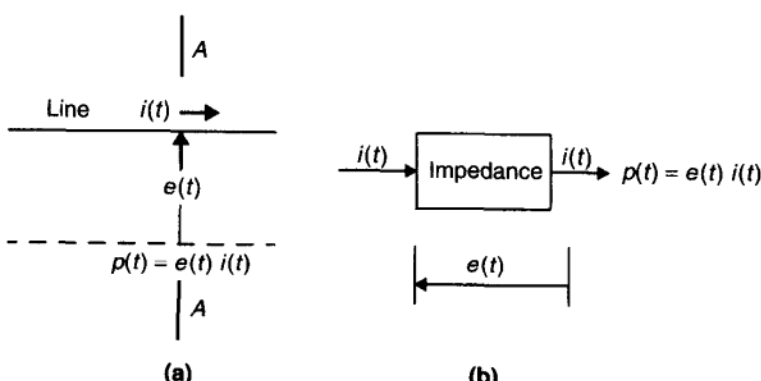


FIGURE 11.1 (a) Instantaneous power flow through the cross section A–A of a single phase (of a) line; (b) instantaneous power flow into an impedance.

a cross section or cut set or into an impedance (Fig. 11.1) is equally important to voltage and current (Definitions 11.1 and 11.2). In this respect, phasor use in power systems differs from most other applications. The following readily results by simple manipulation.

DEFINITION 11.3: Complex Power; Given a voltage signal $e(\cdot) \in \mathcal{M}$ and a current signal $i(\cdot) \in \mathcal{M}$ the phasor power operator $\hat{S}(e, i)$ is given by

$$\hat{S}(e, i) := \mathcal{P}(e)\mathcal{P}(i)^* = \hat{E}\hat{I}^* = P + jQ \quad (11.4)$$

where \hat{I} denotes the complex conjugate of \hat{I} . The real-power operator P is the real part of $\hat{S}(e, i)$:

$$P(e, i) := \operatorname{Re} [\hat{S}(e, i)] = \operatorname{Re} (\hat{E} \cdot \hat{I}^*) \quad (11.5)$$

Similarly the reactive-power operator Q is the imaginary part:

$$Q(e, i) := \operatorname{Im} [\hat{S}(e, i)] = \operatorname{Im} (\hat{E} \cdot \hat{I}^*) \quad (11.6)$$

Suppose $\hat{E}(t) = E(t)\angle\delta(t)$ and $\hat{I}(t) = I(t)\angle[\delta(t) + \varphi(t)]$. Then it is easily seen that the real power $P(e, i) = EI \cos(\varphi)$ and the reactive power $Q(e, i) = -EI \sin(\varphi)$. Definitions locally follow from Eqs. (11.1), to (11.3), which leads to the equation,

$$\begin{aligned} p(t) &= e(t)i(t) \\ &= E(t)I(t) \cos[\varphi(t)]\{1 + \cos 2[\omega_c t + \delta(t)]\} \\ &\quad - E(t)I(t) \sin[\varphi(t)]\{\sin 2[\omega_c t + \delta(t)]\} \\ &= P(e(t), i(t))\{1 + \cos 2[\omega_c t + \delta(t)]\} \\ &\quad + Q(e(t), i(t))\{\sin 2[\omega_c t + \delta(t)]\} \end{aligned} \quad (11.7)$$

which could be interpreted as a phasor relationship at double the carrier frequency ω_c .

Remarks: Note that the sign of $P(e(t), i(t))\{1 + \cos 2[\omega_c t + \delta(t)]\}$ always matches the sign of P and, in the stationary case where E, I, δ, φ , and P are all constants, P represents a net cumulative power flow, which is thus a “real” or “active” transfer of energy. On the other hand, $Q(e(t), i(t))\{\sin 2[\omega_c t + \delta(t)]\}$ does not generally match the sign of Q and in the stationary case it represent a fixed amount of energy swinging across the cross section A–A, at double frequency with no net exchange over time periods of integer number of half cycles of ω_c . This latter property is denoted by the name *reactive* (which probably derives from the word reactance or vice versa), as discussed in Chapter 2.

Definitions 11.1, 11.2, and 11.3 define the phasor form for voltage current and power in a manner applicable whether the modulating signals E and δ are time varying or constant. As originally defined only for the stationary case, where

time derivatives of E , I , δ , φ , P , and Q are identically zero, this concept is precise as commonly formulated in problem areas such as power-flow computation. In traditional engineering practice the stationary relations are also used under the name of quasistationary (or quasistatic) cases, as approximations for slowly varying E and δ , that is $\dot{E} = 3\eta_E \neq 0$ and $\dot{\delta} = 3\eta_\delta \neq 0$, where η_E and η_δ are small. The limits of the necessary slowness for a good approximation were established both by experience and simulation and recently also analytically [3,10] to cover conventional *transient stability* analysis primarily for angle (electromechanical) dynamics and marginally also for voltage (electromagnetic) dynamics. New problems resulting from new equipment and practice result in voltage dynamic conditions for which the quasistationary approximation is no longer valid [1]. Often this fact is obscured by the deeply ingrained status of phasor representation in our engineering thinking resulting in some dubious results reported in the literature.

This situation clearly calls for a precise analysis of the properties of phasors introduced through Eqs. (11.1) to (11.3) for the entire time and frequency domain. Such an analysis is presented here.

Two classes of assumptions which will assure the validity of the phasor transformation of Definition 11.3 are

1. Limiting the frequency band of the modulating signal
2. Assuming that the system is balanced three phase.

These concepts will now be defined.

11.1.1 Low-Pass Phasor Signals

The sets \mathcal{M} and \mathcal{P} are easily seen (Definitions 11.1 and 11.2) to be vector spaces. By the engineering definition of phasors, an element, say, $\hat{I}(\cdot) \in \mathcal{P}$ can be considered to be the corresponding time-varying phasor for a modulated signal $\hat{I}(\cdot)$ provided \hat{I} and i satisfy the modulation equation (11.1). Therefore in this formulation, the phasor definition becomes a mathematical operator, say, \mathcal{P} , which maps the modulated signals in the space \mathcal{M} to those time-varying phasor signals \mathcal{P} that satisfy the modulation equation (11.1). Precisely, $\hat{I} \in \mathcal{P}_i$ provided Eq. (11.1) holds. However, even a simple signal may be mapped to an infinite number of time-varying phasor signals. The phasor operator \mathcal{P} based on the modulation property (11.2) is one-to-one provided the bandwidth is smaller than the carrier frequency. But, as mentioned before, from a practical viewpoint, it is realistic to restrict the phasor analysis to those cases that satisfy the latter assumption.

DEFINITION 11.4: Low-Pass Phasor; A signal $\hat{E}(\cdot) \in \mathcal{L}$ is a low-pass phasor if its Fourier transform $\hat{E}(\omega)$ satisfies

$$\hat{E}(\omega) = \mathbf{0}, \quad \omega \geq \omega_c, \quad \omega \leq -\omega_c \quad (11.8)$$

The set of all low-pass phasors is defined as \mathcal{L} and clearly $\mathcal{L} \subset \mathcal{T}$ is a subspace. An assumption that is inherent in the definition of low-pass phasors is the existence of its Fourier transform.

Notation: The Fourier transforms of time-varying phasors are denoted by corresponding boldface capital letters such as $\hat{\mathbf{E}}$, denoting the Fourier transform of \mathbf{E} . Similarly plain bold capital letters such as \mathbf{E} denote the Fourier transform of modulated signals such as $e \in \mathcal{M}$.

The corresponding subset of \mathcal{M} which is related to \mathcal{L} through the property (11.3) can be defined as the set of band-pass signals.

DEFINITION 11.5: Band-Pass Signal; A signal $e(\cdot) \in \mathcal{M}$ is a band-pass signal if its Fourier transform $\mathbf{E}(\omega)$ satisfies

$$\mathbf{E}(\omega) = \mathbf{0}, \quad \omega \leq 0, \quad \omega \geq 2\omega_c \quad (11.9)$$

The subset of band-pass signals within the space \mathcal{M} is defined as the space of band-pass signals, denoted by \mathcal{B} . Restriction to these subspaces will establish the phasor transformation precisely as a linear operator, as presented in Section 11.2.

11.1.2 Three-Phase Balanced Phasor Signals

Consider a three-phase signal $\underline{e}(t)$ of the form

$$\underline{e}(t) = \begin{pmatrix} e_a(t) \\ e_b(t) \\ e_c(t) \end{pmatrix} = \begin{pmatrix} \sqrt{2}E_a(t) \cos[\omega_c t + \delta_a(t)] \\ \sqrt{2}E_b(t) \cos[\omega_c t + \delta_b(t)] \\ \sqrt{2}E_c(t) \cos[\omega_c t + \delta_c(t)] \end{pmatrix} \quad (11.10)$$

Clearly $\underline{e}(\cdot) \in \mathcal{M}^3 := \mathcal{M} \times \mathcal{M} \times \mathcal{M}$. Among these three phase signals, the set of all balanced three phase signals can be distinguished. Precisely we say that $\underline{e}(t) \in \mathcal{M}^3$ is balanced if there exist smooth scalar functions $E : \mathbb{R} \rightarrow \mathbb{R}$ and $\delta : \mathbb{R} \rightarrow \mathbb{R}$ such that

$$\begin{aligned} \underline{e}(t) &= \begin{pmatrix} e_a(t) \\ e_b(t) \\ e_c(t) \end{pmatrix} = \begin{pmatrix} \sqrt{2}E(t) \cos[\omega t + \delta(t)] \\ \sqrt{2}E(t) \cos[\omega t + \delta(t) - 2\pi/3] \\ \sqrt{2}E(t) \cos[\omega t + \delta(t) + 2\pi/3] \end{pmatrix} \\ &= \sqrt{3}B(t) \begin{pmatrix} E(t) \cos \delta(t) \\ E(t) \sin \delta(t) \\ 0 \end{pmatrix} \end{aligned} \quad (11.11)$$

where $B(t)$ is the orthonormal matrix,

$$B(t) := \sqrt{\frac{2}{3}} \begin{pmatrix} \cos(\omega t) & -\sin(\omega t) & \frac{1}{\sqrt{2}} \\ \cos\left(\omega t - \frac{2\pi}{3}\right) & -\sin\left(\omega t - \frac{2\pi}{3}\right) & \frac{1}{\sqrt{2}} \\ \cos\left(\omega t + \frac{2\pi}{3}\right) & -\sin\left(\omega t + \frac{2\pi}{3}\right) & \frac{1}{\sqrt{2}} \end{pmatrix} \quad (11.12)$$

The set of all three-phase balanced signals satisfying Eq. (11.11) is the set \mathcal{M}_B^3 . Since the operation (11.11) is linear, it follows that $\mathcal{M}_B^3 \subset \mathcal{M}^3$ itself is a vector space.

Now for the balanced signals $\underline{e}(\cdot) \in \mathcal{M}_B^3$, we can define the associated time-varying phasor $\hat{E}(\cdot)$ by inverting the linear transformation $B(t)$ in Eq. (11.11). To distinguish the definition for the balanced three-phase signals from the single-phase band-limited signals of the previous section, we represent the phasor operator by \mathcal{P}_B (here B stands for the balanced case).

DEFINITION 11.6: The phasor representation $\mathcal{P}_B(\underline{e}(t)) := \hat{E}(t)$ of a balanced sinusoidal three-phase signal $\underline{e}(t)$ is

$$\mathcal{P}_B(\underline{e}(t)) = (1 \quad j \quad 0) \frac{B^{-1}(t)}{\sqrt{3}} \underline{e}(t) \quad (11.13)$$

or in alternate (and conventional) notations

$$\begin{aligned} \mathcal{P}_B(\underline{e}(t)) &:= \hat{E}(t) := E_d(t) + jE_q(t) \\ &:= E(t) \cos \delta(t) + jE(t) \sin \delta(t) \end{aligned} \quad (11.14)$$

$$= E(t)e^{j\delta(t)} + E(t)\angle\delta(t) \quad (11.15)$$

Remarks

- Given a balanced three-phase signal $\underline{e}(t)$, the preceding phasor operation essentially identifies the associated phasor $\hat{E}(t)$ by exploiting the invertibility of the Blondel transformation matrix (11.11).
- The Blondel transformation described before has been routinely used in machine theory for decades for simplifying the rotating flux equations within the machine by defining a rotating reference frame B in which the entries of the matrix are usually functions of the machine angle from a synchronous reference, say, θ , electrically. Physically for multiple machines an electric angle of 2π correspond to $2\pi/N$ mechanical angles, where N is the number of pole pairs. Mainly this transformation identifies the direct-axis (the d axis for

short) and quadrature-axis (the q axis for short) components that are stationary with respect to the rotor, thus considerably simplifying the electromagnetic equations. However, when multimachine models are considered, the d and q axes of the various machines are each rotating at different reference frames resulting from different machine speeds. To unify the analysis in the computation of stator transients, under the quasistationary assumption, it is customary to transform all the different machine references to a common reference that is rotating with the 60-Hz synchronous speed of $2\pi\omega/N$, where N is the number of poles.

Recent work [4,5] extends this approach to a more general formulation by transforming the transmission network and the loads into equivalent RL networks in d and q axes in the form of flux equations. Under the assumption that the network with the loads only consist of resistors and inductors, it is shown in Ref. [5] that all the machine equations along with the network-load-flux equations can be transformed to a common $d-q$ axis reference frame in which the computations of stator transients are carried out. However, such an approach by requiring equivalent physical networks in the d and q axes becomes restrictive. Among other factors, they have been forced to exclude capacitors and general load types.

It is preferable to approach the problem of phasor analysis as one of a convenient mathematical transformation. The motivation is to facilitate the problem solution in the transformed domain. It is important to realize that the states of the transformed system need not have direct physical meaning. If properly solved mathematically, however, they will give the correct physical result after inverse transformation. Think of the Laplace transformation. The transforms do not have direct physical meaning (although after working with them for some time, one may have the feeling that they do—as it also happened in the phasor case), yet the inverse Laplace transform of the solution gives the correct physical time-domain results. Understanding this fact opens up a wide horizon as it does here, yielding a set of dynamic load-flow equations for analyzing fast transients.

These methods were developed in [3] [6] and [8] mostly by V. Venkatasubramanian using precise mathematical proofs long existing for time-varying phasor results in communication theory for the problem of the power system dynamics presented here. Only some summaries of these results will be included here.

11.2 TIME-VARYING PHASOR AND ITS PROPERTIES

It is now possible to establish that *unique* time-varying transformation exists for two classes of systems: (1) bandwidth-limited systems (where the frequency range of the modulating signal is constrained) and (2) balanced three-phase systems (where the speed of the modulation need not be constrained). This will now be sketched in three forms.

Theorem 11.2.1: Low Pass Phasor Transformation Operation Assume that Definitions 11.1 to 11.5 apply and that $e(t)$ is restricted to \mathcal{L} , that is, $e(t) \in \mathcal{B}$ [and

so also $\hat{E}(t) \in \mathcal{L}$], then the map

$$\mathcal{P} : \mathcal{B} \rightarrow \mathcal{L} \quad (11.16)$$

defined in Eq. (11.1) is a linear operator that possesses the Properties 1 to 4 stated and proved in the following.

Note: In the statement of the theorem, the symbols such as $e(t)$ and $\hat{E}(t)$ correspond to any voltage e , current i , power p , etc. Each Property to be stated will be proved individually.

Theorem 11.2.2: Balanced Three-Phase Phasor Transformation Operator The map $\mathcal{P}_B : \mathcal{M}_B^3 \rightarrow \mathcal{T}$ defined by Eq. (11.13) is a linear operator and is one-to-one. Moreover, it satisfies properties 1 to 4.

The *proof* of the theorems will be given property by property first for Theorem 11.2.1 followed by a discussion of differences in the proofs for Theorem 11.2.2. Note, however, that the same properties hold in both types of systems.

PROPERTY 1 $\mathcal{P} : \mathcal{B} \rightarrow \mathcal{L}$ is a one-to-one and onto map. Moreover $\mathcal{P} : \mathcal{B} \rightarrow \mathcal{L}$ (or simply \mathcal{P}) is linear.

Proof One-to-One Property Let $e(\cdot) \in \mathcal{B}$. First it will be proved that there exists a unique $\hat{E} \in \mathcal{L}$ that satisfies $\mathcal{P}(e) = \hat{E}$. The proof directly follows from the concept of analytic signal from communication theory and is summarized here for continuity. Let $\tilde{e}(t)$ denote the Hilbert transform of the signal $e(t)$, and define the preenvelope or the analytic signal $e_+(t)$ by $e_+(t) := e(t) + j\tilde{e}(t)$. By the assumption on the band-pass signals in \mathcal{B} , it follows that the Fourier transform of e_+t is nonzero only within the interval $0 < \omega < 2\omega_c$. Therefore the signal $e_+(t)$ can be defined as $e_+(t) = \hat{E}(t) \exp(j\omega_c t)$ for a unique function $\hat{E}(t)$ the Fourier transform of which can be seen to be

$$\hat{E}(\omega) = \begin{cases} 2\mathbf{E}(\omega + \omega_c), & -\omega_c < \omega < \omega_c \\ 0, & \text{otherwise} \end{cases} \quad (11.17)$$

Since the preenvelope $e_+(t)$ by construction satisfies $e(t) = \operatorname{Re}[e_+(t)]$, the function $\hat{E}(t)$ satisfies Eq. (11.1); hence $\hat{E} \in \mathcal{P}(e)$. From the Fourier transform property (11.1) and the band-pass property (BP), it follows that $\hat{E} \in \mathcal{L}$. The fact that \hat{E} is the only such function in \mathcal{L} with this property can be easily seen by the following equivalent construction of \hat{E} based on the classical demodulation technique (Fig. 2.35a in Refs. [7,12]): (1) The real part $e_d(t)$ of the signal $\hat{E}(t)$ denoted the *in-phase component* [12] or the direct component is recovered from $e(t)$ by passing the product $e(t) \cos \omega_c t$ through an ideal low-pass filter with cutoff frequency at $\omega = \omega_c$. (2) Similarly the imaginary part $e_q(t)$ of $\hat{E}(t)$ denoted the *quadrature component* [12] can be reconstructed by passing the product

$-e(t) \sin \omega_c t$ again through an ideal low-pass filter with the cutoff frequency at $\omega = \omega_c$. This demodulation technique is significant for real-time practical implementations because low-pass filters can be effectively emulated in real-time using standard digital signal-processing techniques. The converse that a phasor signal $\hat{E} \in \mathcal{L}$ maps into a unique e under the inverse of the phasor operator is straightforward from Eq. (11.1). It is easily seen that \mathcal{P} is also onto. Q.E.D.

Proof: Linearity The linearity follows simply by the linearity of the construction of real and imaginary parts of \hat{E} using the low-pass filter shown previously. Q.E.D.

PROPERTY 2 Assume that $e(\cdot) \in \mathcal{B}$ and $i(\cdot) \in \mathcal{B}$, then instantaneous power-balance equations can be equivalently rewritten in terms of the real-power and reactive-power balance equations.

Proof Because all the signals are in \mathcal{B} , it follows that the phasor operator \mathcal{P} is linear by Property 1 and so is the complex conjugate operator and therefore the composition $\mathcal{P}(\cdot)^*$. By the generalized form of Tellegen's theorem [13] and applying the linear operator \mathcal{P} on the voltages and the linear operator \mathcal{P}^* on the currents, it follows that

$$\begin{aligned} \sum_{k=1}^n e_k(t) i_k(t) = 0 &\Leftrightarrow \sum_{k=1}^n \hat{E}_k(t) \cdot \hat{I}_k(t) = 0 \\ \sum_{k=1}^n P(e_k(t), i_k(t)) = 0 & \\ \Leftrightarrow & \\ \sum_{k=1}^n Q(e_k(t), i_k(t)) = 0 & \text{Q.E.D.} \end{aligned} \tag{11.18}$$

Note: It will be shown in Section 11.3 that stronger results can be obtained for various specific problem areas defined by additional assumptions.

PROPERTY 3 Suppose $e(\cdot) \in \mathcal{B}$ and $(d/dt)e(\cdot) \in \mathcal{B}$. Then

$$\mathcal{P}\left(\frac{d}{dt}e(t)\right) = \frac{d}{dt}\mathcal{P}(e(t)) + j\omega_c\mathcal{P}(e(t)) \tag{11.19}$$

Proof Suppose $e(\cdot) \in \mathcal{B}$ and let $\hat{E} = \mathcal{P}(e)$. Then these two are related in a unique way by ([4], see the proof of Property 1)

$$e(t) = \operatorname{Re} [\hat{E}(t)e^{j\omega_c t}] \tag{11.20}$$

By direct differentiation, we find

$$\frac{d}{dt}e(t) = \operatorname{Re} \left(\frac{d}{dt}\hat{E}(t) + j\omega_c \hat{E}(t) \right) e^{j\omega_c t} \quad (11.21)$$

On the other hand, since the derivative $\dot{e} \in \mathcal{B}$, there exists a unique derivative in the phasor domain $\mathcal{P}(\dot{e})$ that satisfies

$$\dot{e}(t) = \operatorname{Re} [\mathcal{P}(\dot{e}(t)) e^{j\omega_c t}] \quad (11.22)$$

Since the phasor operator is one-to-one (Property 1), comparing Eqs. (11.21) and (11.22), the result follows. Q.E.D.

Remarks: (1) Note that for the conventional stationary or quasistationary phasor calculus the derivative consists of only the second term. (2) Using Property 3, the instantaneous equations for a linear capacitor C , and a linear inductor L (and a linear resistor) elements in the network are easily rewritten using the preceding derivative rule.

PROPERTY 4

1. Capacitor: The current $i_C(t)$ flowing through a capacitor C with the terminal voltage $e_C(t)$ can be represented by

$$\hat{i}_C(t) = C \frac{d}{dt} \hat{E}_C(t) + j\omega_c C \hat{E}_C(t) \quad (11.23)$$

in the phasor domain when i_C and e_C belong to \mathcal{B} .

2. Inductor: The voltage $e_L(t)$ across an inductor L when current $i_L(t)$ is flowing through can be represented by

$$\hat{E}_L(t) = L \frac{d}{dt} \hat{i}_L(t) + j\omega_c L \hat{i}_L(t) \quad (11.24)$$

in the phasor domain when i_L and e_L belong to \mathcal{B} .

3. Resistor: The voltage $e_R(t)$ across a resistor R when the current $i_R(t)$ is flowing through can be represented by

$$\hat{E}_R(t) = R \hat{i}_R(t) \quad (11.25)$$

Remark

1. These three equations (11.23) to (11.25) along with Eq. (11.18) provide the relationships needed for writing the dynamic models in the time-varying representation. These properties are summarized in the form of a table (Table 11.1) for convenience.

TABLE 11.i General Taxonomy of the Time-varying Phasor Calculus

Property	Instantaneous Signal Domain		Quasistationary Domain		Low Pass Phasor Domain		Balanced Three-Phase Domain	
	Assumptions	None	Signal bandwidth very small compared to ω_c (quasistationary assumption)	Signal bandwidth less than ω_c (assumption BP and LP)	Filter	Filter	Filter	Filter
Estimation	$e(t)$	$e(t)\cos\omega_0 t$	$e(t)\cos\omega_0 t$	$e(t)\cos\omega_0 t$	$E/\delta = e_{Rb} + e_{Im}$	$E/\delta = e_{Rb} + e_{Im}$	$E/\delta = e_{Rb} + e_{Im}$	$E/\delta = e_{Rb} + e_{Im}$
		$e(t)\sin\omega_0 t$	$e(t)\sin\omega_0 t$	$e(t)\sin\omega_0 t$	$E/\delta = e_{Rb} + e_{Im}$	$E/\delta = e_{Rb} + e_{Im}$	$E/\delta = e_{Rb} + e_{Im}$	$E/\delta = e_{Rb} + e_{Im}$
Power concept	$p(t) = e(t)i(t)$	Instantaneous power	Complex power $S = \hat{e}i^*$	Complex power $S = \hat{e}i^*$	Complex power $S = \hat{e}i^*$	Real power $P = \text{Re}(\hat{e}i^*)$	Real power $P = \text{Re}(\hat{e}i^*)$	Complex power $S = \underline{ei}^*$
			Reactive power $Q = \text{Im}(\hat{e}i^*)$	Reactive power $Q = \text{Im}(\hat{e}i^*)$	Reactive power $Q = \text{Im}(\hat{e}i^*)$	Reactive power $Q = \text{Im}(\hat{e}i^*)$	Real power $P = \text{Re}(\underline{ei}^*)$	Real power $P = \text{Re}(\underline{ei}^*)$
								Reactive power $Q = \text{Im}(\underline{ei}^*)$

Time differentiation	$\frac{d}{dt}e(t)$	$j\omega_c \hat{e}$	$\frac{d}{dt}\hat{e}(t) + j\omega_c \hat{e}(t)$	$\frac{d}{dt}\hat{e}(t) + j\omega_c \hat{e}(t)$
Capacitor equation	$i_c(t) = C \frac{d}{dt}e_c(t)$	$\hat{i}_c = j\omega_c C \hat{e}_c$	$\hat{i}_c = j\omega_c C \hat{e}_c + \frac{d}{dt}\hat{e}_c(t)$	$\hat{i}_c = j\omega_c C \hat{e}_c + \frac{d}{dt}\hat{e}_c(t)$
Inductor equation	$e(t) = L \frac{d}{dt}i_L(t)$	$\hat{e}_L = j\omega_L L \hat{i}_L$	$\hat{e}_L = j\omega_L L \hat{i}_L + \frac{d}{dt}i_L(t)$	$\hat{i}_L = j\omega_L L \hat{e}_L + \frac{d}{dt}\hat{e}_L(t)$
Resistor equation	$e(t) = R i_R(t)$	$\hat{e}(t) = R \hat{i}_R(t)$	$\hat{e}(t) = R \hat{i}_R(t)$	$\hat{e}(t) = R \hat{i}_R(t)$
Network equations	$\sum_{k=1}^n e_k(t) = 0, \quad \text{KVL}$ $\sum_{k=1}^n i_k(t) = 0, \quad \text{KCL}$	$\sum_{k=1}^n \hat{e}_k(t) = 0, \quad \text{KVL}$ $\sum_{k=1}^n \hat{i}_k(t) = 0, \quad \text{KCL}$	$\sum_{k=1}^n \hat{e}_k(t) = 0, \quad \text{KVL}$ $\sum_{k=1}^n \hat{i}_k(t) = 0, \quad \text{KCL}$	$\sum_{k=1}^n \hat{e}_k(t) = 0, \quad \text{KVL}$ $\sum_{k=1}^n \hat{i}_k(t) = 0, \quad \text{KCL}$
Power-balance equation	$\sum_{k=1}^n e_k(t)i_k(t) = 0$	$\sum_{k=1}^n \hat{e}_k \hat{i}_k = 0$	$\sum_{k=1}^n \hat{e}_k \hat{i}_k = 0$	$\sum_{k=1}^n \hat{e}_k(t) \hat{i}_k(t)^* = 0$

2. Note that the fundamental properties, Properties 1 through 4, on linearity (Property 1), on the complex power-balance equations (Property 2), on the differentiation rule (Property 3), and on the linear network equations (Property 4) are exactly the same for the two notions of time-varying phasors introduced namely for low-pass phasors \mathcal{P} and the three-phase balanced time-varying phasor. This is to be expected since when the three-phase balanced signals are also band-limited signals and the network is symmetric, the results from the two definitions must coincide so that they are consistent. The first case of low-pass phasors \mathcal{P} , which is not requiring the balanced symmetric operation, is more useful when unbalanced conditions, such as asymmetric fault conditions, are considered (see an extension of the symmetrical components method in Ref. [8]). The Blondel transformation approach \mathcal{P}_B , on the other hand, is not restricted by any bandwidth assumption and hence is suited for analyzing faster transients such as the fast electromagnetic transients arising in transmission networks. For these reasons, the first concept is denoted as *low-pass phasors* (connected with band-limited signals), and the latter one *fast balanced phasors* (connected with balanced three-phase signals). From Properties 1 to 4, both concepts are powerful ways for simplifying the analysis. Specifically the fast balanced phasors will be used in the next few sections for deriving a set of time-delay algebraic equations (11.26) and (11.27) that describe the network dynamics of the interconnected transmission system. In Table 11.1 then four ways are summarized for solving problems of four classes by good approximation in each case of network type systems such as the power system:

1. Modulated time-domain signals
2. Traditional quasistationary phasor signals
3. Time-varying low-pass phasor signals
4. Fast time-varying balanced phasor signals

Important questions arise when one looks into such details as three-phase balance or the lack of it, bandwidths of modulating signals, and the presence of distributed-parameter components in the power network. A quick look at the familiar structure of the power system in Figure 3.31 will help to identify domains of phasor calculus on this system. For details see [6,8].

11.3.1 Parts of the Power System for which Phasors Apply

The large electric power system consists of these fundamental elements:

1. *Transmission*, that is, a network of high-voltage transmission lines connecting buses (nodes), is at the core of the system (see sketch in Figure 3.31). All states or signals within are modulated AC (or appear to be such at the end points for high-voltage DC lines and SVC). It has a sparse connection matrix

(typically from 2 to 10 lines per bus) even for large systems. This part is represented by a set G of equations.

2. *Equipment* such as generators, loads, and various power electronic (thyristor, SVC, HV DC) devices are connected to individual buses. Each item has its own dynamics in various forms, usually differential equations (e.g., Park equations for the machines). None of the equipment is physically in modulated AC form, and there is no direct coupling between individual items outside their connection to the buses (Figure 3.31). Accordingly, the equipment dynamics is defined mostly by a set F (Figure 3.31) of ordinary differential equations and need not be discussed in this chapter.
3. Since the mathematical form of describing the dynamics is thus quite different for transmission and the attached equipment, conversion equations (e.g., Blondel) are typically needed for the interaction between the G and F sets (Figure 3.31).

Our interest is here directed to the dynamics of the transmission system that is, the G set for which phasor representation naturally applies. It will be proved in Sections 11.4 to 11.7 that the G set under certain assumptions can be represented by a set of differential-algebraic equations in the phasor domain. These equations have time-delayed contributions from various transmission lines.

In a stationary or steady-state condition (a normal operating condition), a large power system is defined by two sets of algebraic equations:

$$F \text{ set: } f(x, y) = 0, \quad x \in \mathbb{R}^n, \quad f : \mathbb{R}^{n+m} \rightarrow \mathbb{R}^n \quad (11.26)$$

$$G \text{ set: } g(x, y) = 0, \quad y \in \mathbb{R}^m, \quad g : \mathbb{R}^{n+m} \rightarrow \mathbb{R}^m \quad (11.27)$$

When the system enters a dynamic condition, equations of the F set naturally change into ordinary differential equations in the x states ($\dot{x} = f(x, y)$). A special feature of the power system is that interconnections of x variables for individual pieces of equipment occurs exclusively at individual buses. Bus-to-bus interconnections are by transmission lines through the y states. Each transmission line represented by a single-phase circuit for a balanced system has four terminals (three if the circuit is represented by one phase and a neutral for balanced system). The differential equations of the F set are not set with phasors, generally (e.g., the generators), because their state variables are not modulated signals (although a transformation to phasors via the Blondel transformation may be convenient, as explained previously). Phasors should be typically used in the G set, that is, the transmission network. For balanced networks, this set consists of buses interconnected dynamically by the four-terminal networks of the transmission line. Each such four-terminal network for our transmission line is a boundary-value problem. This dichotomy of representations between the F and G set calls for a (mathematical) transition layer consisting of the Blondel transformation and others. In the following, our interest is the G set and its representation.

11.3.2 Phasors in the G Set the Transmission System

The electric power transmission system is an electric network that connects the buses. A simplified approximate example of one bus i and two neighbors j and k is shown in Figure 3.31. In a general and precise sense the G set has two types of components:

1. Buses, or simply nodes, which must balance flows of all connected branches
2. Transmission lines, which are basically four-terminal networks that may involve mutual inductances and may be in distributed-parameter form, which produce time-delay effects

In linear system theory, Kirchoff's well-known laws,

1. The sum of all currents at every node is zero at every instant of time.
2. The sum of all voltages around every loop is zero at every instant of time.

are invoked to define the dynamics of such a system. However, since the power system is about moving electric power around, the power-balance equations that follow are preferable:

1. At the buses the sum of instantaneous power flowing into a bus from all connected equipment and all connected transmission lines is zero. Buses have no appreciable storage ability.
2. The difference of instantaneous power at the two ends of a line is stored in the line or dissipated as heat for loss.

These are easily shown to be equivalent or homeomorphic to the Kirchoff laws by Tellegen's theorem [14, 13] or just by direct manipulation of the equations.

There is little that can be added to the equation described in item 1. The general three-terminal definition of the line assumes balanced three-phase operation and is used here to save space and improve clarity. In phasor form, the solution of the four-terminal network reads as

$$\hat{I}_i = \hat{Y}_{ij}(\hat{E}_i, \hat{E}_j, \tau_{ij}, \dots) \quad (11.28)$$

$$\hat{I}_j = \hat{Y}_{ji}(\hat{E}_i, \hat{E}_j, \tau_{ij}, \dots) \quad (11.29)$$

where τ_{ij} are line-specific delays. This solution can be quite a bit more complex than the familiar linear admittance constant case:

$$\hat{I}_i = \hat{Y}_{ii} \times \hat{E}_i + \hat{Y}_{ij} \times \hat{E}_j \quad (11.30)$$

$$\hat{I}_j = \hat{Y}_{ji} \times \hat{E}_i + \hat{Y}_{jj} \times \hat{E}_j \quad (11.31)$$

In more complex situations, the solution of boundary-value problems may be needed to get a form like Eqs. (11.28) and (11.29) and the presence of nonlinearities may be involved. Furthermore, the power-balance form

$$\hat{S}_{ij} = \hat{E}_i \times \hat{I}_{ij}^*, \hat{S}_{ji} = \hat{E}_j \times \hat{I}_{ji}^*$$

is nonlinear even if the line as an E, I circuit is linear as it is on the power system with sufficiently short lines.

Overall then the broad general form of the equations to define the G set is in phasor form, as follows.

1. The bus i power balance in phasor form is

$$\begin{aligned} \sum_i \hat{S}_{G_i} + \sum_i \hat{S}_{\mathcal{L}_i} + \sum_i \hat{S}_{\text{SVC,HVDC}_i} + \sum_i \hat{S}_{\text{mix}_i} \\ + (j\omega C_i E_i^2 + C_i \hat{E}_i \dot{\hat{E}}_i^*) - \sum_j \hat{S}_{ij} = \hat{O} \end{aligned} \quad (11.32)$$

2. The line (ij, ji) power-balance equations if the modulation is averaged out by the balanced nature of the three-phase system or by some other means (see the complex power-balance equations, Property 2) are

$$\hat{S}_{ij} = \hat{E}_i \hat{Y}_{ij}(\hat{E}_i, \hat{E}_j \tau_{ij}, \dots) = \hat{E}_i \times \hat{I}_i^* \quad (11.33)$$

$$\hat{S}_{ji} = \hat{E}_j \hat{Y}_{ji}(\hat{E}_i, \hat{E}_j \tau_{ij}, \dots) = \hat{E}_j \times \hat{I}_j^* \quad (11.34)$$

Here subscript G refers to the generator, \mathcal{L} to the load, SVC, HV DC to thyristor controls; subscript mix means an unspecified equipment; C_i is a capacitor bank (if any) at bus i ; Y_{ij} and Y_{ji} are generally nonlinear functions of the voltages (but for G sets consisting of simple short AC transmission lines, they are closely approximated by elements of the familiar admittance matrix or Y bus matrix used in power-flow analysis) at the two line ends, time delay, and potentially other parameters.

11.4 ANALYSIS OF THE TRANSMISSION-LINE DYNAMICS INCLUDING DISTRIBUTED CONSTANTS AND LINE LOSSES

Important components of both power and communications systems are transmission lines, which are distributed-parameter systems modeled precisely by a special type of partial differential equation known as a wave equation because it defines traveling waves along the line. Typically in power-system networks, the line length is an (often small) fraction of the wavelength of the carrier on the line. In communications, however, the reverse situation prevails with thousands or millions of carrier wavelengths along the line (a wave guide). The basic

problem is the same but the situation is more complex on the power system. Wave equations and their solutions are well known in the literature, including the engineering use of phasors for the stationary system (e.g., Chapter 6 in Ref. [15] 1955 which also observes the line specific time delays). A time-delay solution of the wave equations in the instantaneous time domain was proposed in Ref. [16] under the assumption of lossless transmission lines, commonly known (in electromagnetics or transmission-line theory) under the name of *the Branin algorithm*. In fact, it appears that such time-delay solutions were known earlier in the power-system context, and Ref. [11] appears to be one of the first references. In this chapter, our aim is to derive explicit solutions for the wave equations using time-varying phasors so that we can formulate the dynamics of the distributed-parameter-type interconnected transmission network all from within the familiar phasor analytical domain.

A mathematically precise formulation of the time-varying phasors was established in Sections 11.2 and 11.3. In this section, the construction of time-delay-type exact solutions to the wave equation is briefly summarized to demonstrate our claim that the general phasor operator will apply directly to solving the partial differential equation problem as well.

Looking at a short segment $\Delta\ell$ of the transmission line ij (Fig. 11.2), it is readily approximated as an ordinary linear circuit for which relations between Δe , Δi and $\Delta\ell$, Δt are readily written. Taking limits for $\Delta\ell \rightarrow 0$, the wave Eqs. (11.35) and (11.36) are of general validity, not depending on conditions like stationarity. They also account for line losses

$$\frac{\partial e(\ell, t)}{\partial \ell} = R_{ij}i(\ell, t) + L_{ij}\frac{\partial i(\ell, t)}{\partial t} \quad (11.35)$$

$$\frac{\partial i(\ell, t)}{\partial \ell} = G_{ij}e(\ell, t) + C_{ij}\frac{\partial e(\ell, t)}{\partial t} \quad (11.36)$$

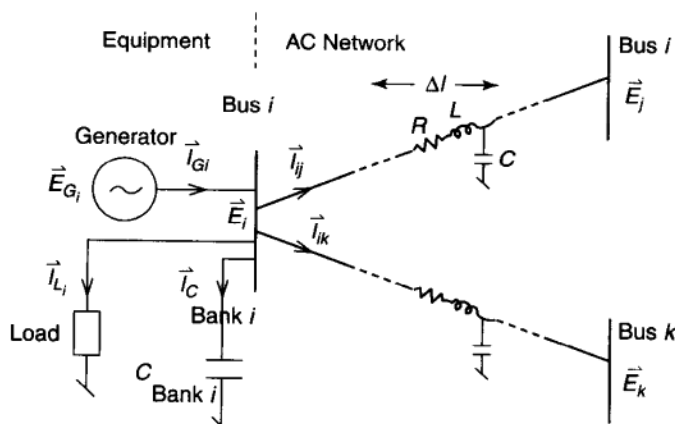


FIGURE 11.2 Sketch for the power-balance equation.

When these are combined with the conditions at the line ends i and j ,

$$e(0, t) = e_i(t), \quad e(\ell_{ij}, t) = e_j(t) \quad (11.37)$$

$$i(0, t) = i_{ji}(t), \quad i(\ell_{ij}, t) = -i_{ij}(t) \quad (11.38)$$

then the dynamics of the line is defined in terms of the boundary-value problem of Eqs. (11.35) to (11.38) and one pair of the four conditions in Eqs. (11.37) and (11.38). The other pair represents the free variables of Eqs. (11.37) and (11.38). Assuming zero initial conditions, a solution for the lossless case ($R_{ij} = G_{ij} = 0$) can be obtained in the form [11, 16]

$$e_i(t) = \tilde{R}_{ij}i_{ij}(t) + \tilde{R}_{ij}i_{ji}(t - \tau_{ij}) + e_j(t - \tau_{ij}) \quad (11.39)$$

$$e_j(t) = \tilde{R}_{ij}i_{ji}(t) + \tilde{R}_{ij}i_{ij}(t - \tau_{ij}) + e_i(t - \tau_{ij}) \quad (11.40)$$

$$\tilde{R}_{ij} = \sqrt{\frac{L_{ij}}{C_{ij}}}, \quad \tau_{ij} = \frac{\ell_{ij}}{C} \quad (11.41)$$

The actual solution also includes some terms corresponding to nonzero initial values for line voltages and currents, but these technical issues will be postponed for the moment. Note that these equations depend on the characteristic line impedance \tilde{R}_{ij} and include a time delay τ_{ij} that is line specific: it is the time the wave takes to pass through the line at the speed of light c . So when precisely calculated, each line is described by a (rather simple, in the lossless case) algebraic equation with a time delay that depends on the line length but not on any state variable. For three-phase or parallel lines, mutual impedances need to be considered, but again these can be eliminated precisely from the symmetry in balanced three-phase lines [15].

These are classical results for the time domain although the form becomes more complicated when modulation is considered.

Using fast balanced time-varying phasors as just defined, it is seen that in general the phasor transformation is interchangeable with the $\Delta\ell \rightarrow 0$ limit process. Accordingly a set of wave equations incorporated in a boundary-value problem directly corresponding to Eqs. (11.35) to (11.38) results in

$$\frac{\partial \hat{E}(\ell, t)}{\partial \ell} = R_{ij}\hat{I}(\ell, t) + L_{ij}\frac{\partial \hat{I}(\ell, t)}{\partial t} + j\omega_c L_{ij}\hat{I}(\ell, t) \quad (11.42)$$

$$\frac{\partial \hat{I}(\ell, t)}{\partial \ell} = G_{ij}\hat{E}(\ell, t) + C_{ij}\frac{\partial \hat{E}(\ell, t)}{\partial t} + J\omega_c C_{ij}\hat{E}(\ell, t) \quad (11.43)$$

$$\hat{E}(0, t) = \hat{E}_i(t), \quad \hat{E}(\ell_{ij}, t) = \hat{E}_i(t) \quad (11.44)$$

$$\hat{I}(0, t) = \hat{I}_{ij}(t), \quad \hat{I}(\ell_{ij}, t) = -\hat{I}_{ij}(t) \quad (11.45)$$

Again for the lossless case this boundary-value problem can be solved:

$$\begin{aligned}\hat{I}_{ij}(t) = & \hat{I}_{ij}(t - 2\tau_{ij})e^{-j2\tilde{\theta}_{ij}} - \tilde{G}_{ij}\tilde{E}_i(t) + 2\tilde{G}_{ij}\hat{E}_j(t - \tau_{ij})e^{-j\tilde{\theta}_{ij}} \\ & - \tilde{G}_{ij}\hat{E}_i(t - 2\tau_{ij})e^{-j2\tilde{\theta}_{ij}}\end{aligned}\quad (11.46)$$

$$\begin{aligned}\hat{I}_{ji}(t) = & \hat{I}_{ji}(t - 2\tau_{ij})e^{-j2\tilde{\theta}_{ij}} - \tilde{G}_{ij}\hat{E}_j(t) + 2\tilde{G}_{ij}\hat{E}_i(t - \tau_{ij})e^{-j\tilde{\theta}_{ij}} \\ & + \tilde{G}_{ij}\hat{E}_j(t - 2\tau_{ij})e^{-j2\tilde{\theta}_{ij}}\end{aligned}\quad (11.47)$$

where $\tilde{G}_{ij} = 1/\tilde{R}_{ij}$ is the characteristic admittance of the line ij and $\tilde{\theta}_{ij} = \omega_c\tau_{ij}$ is the phase shift introduced by the line ij . Note that Eqs. (11.46) and (11.47) are more complex than Eqs. (11.39) and (11.40). However, remember that Eqs. (11.39) and (11.40) are less specific. They are not restricted to modulated signals, whereas the phasor form in Eqs. (11.46) and (11.47) implies modulation.

When the line losses are included, then attenuation terms enter along with the time delays. Thus finding exact solutions to the phasor wave equations is much more difficult. However, quite precise solutions can be found under certain assumptions such as when the line resistance R_{ij} is much smaller than the line reactance $X_{ij} = \omega_c L_{ij}$. Actual practice typically satisfies this assumption very well. Laplace transform can then be used to find the solution.

In the Laplace domain, denoting the complex Laplace transforms of the phasors $\hat{E}(z, t)$ and $\hat{I}(z, t)$ by $\hat{\mathbf{E}}(z, s)$ and $\hat{\mathbf{I}}(z, s)$, the complex phasor wave equations (11.42) and (11.43) can be Laplace-transformed to

$$\frac{d^2\hat{\mathbf{E}}(z, s)}{dz^2} = \gamma_{ij}^2 \hat{\mathbf{E}}(z, s) \quad (11.48)$$

where

$$\gamma_{ij} = \sqrt{(R_{ij} + (s + j\omega_c)L_{ij})(s + j\omega_c)C_{ij}} \quad (11.49)$$

Also let

$$Y_{0_{ij}} = \sqrt{\frac{(s + j\omega_c)C_{ij}}{R_{ij} + (s + j\omega_c)L_{ij}}} \quad (11.50)$$

Then solutions to Eq. (11.48) can be found in the Laplace domain rather easily, but the challenge is to find valid inverse Laplace transforms for establishing the time-domain solutions. Specifically the variables γ_{ij} and $Y_{0_{ij}}$ need to be simplified. Under the assumption that $R_{ij} \ll X_{ij}$, these quantities can be approximated as

$$\gamma_{ij} \approx (s + j\omega_c)\sqrt{L_{ij}C_{ij}} + \frac{R_{ij}}{2} \sqrt{\frac{C_{ij}}{L_{ij}}} \quad (11.51)$$

$$Y_{0_{ij}} \approx \sqrt{\frac{C_{ij}}{L_{ij}}} \left(\frac{s + j\omega_c}{R_{ij}/2L_{ij} + s + j\omega_c} \right) \quad (11.52)$$

Note that when the line losses are set to zero (with $R_{ij} = 0$), the quantities $Y_{0_{ij}} = \tilde{G}_{ij}$ and $\gamma_{ij} = \sqrt{(s + j\omega_c)L_{ij}C_{ij}}$ are the lossless counterparts, hence equations (11.51) and (11.52) are indeed consistent. With these approximations, an explicit solution to the wave equations (11.25) to (11.42), which now includes transmission-line attenuation effects can be shown to be

$$\begin{aligned}\hat{I}_{ij}(t) &= \tilde{G}_{ij}\hat{\phi}_i(t) + \hat{I}_{ij}(t - 2\tau_{ij})e^{-2(\tilde{\alpha}_{ij} + j\tilde{\theta}_{ij})} \\ &\quad - 2\tilde{G}_{ij}\hat{\phi}_j(t - \tau)e^{-(\tilde{\alpha}_{ij} + j\tilde{\theta}_{ij})} + \tilde{G}_{ij}\hat{\phi}_i(t - 2\tau_{ij})e^{-2(\tilde{\alpha}_{ij} + j\tilde{\theta}_{ij})}\end{aligned}\quad (11.53)$$

$$\begin{aligned}\hat{I}_{ji}(t) &= \tilde{G}_{ij}\hat{\phi}_j(t) + \hat{I}_{ji}(t - 2\tau)e^{-2(\tilde{\alpha}_{ij} + j\tilde{\theta}_{ij})} \\ &\quad - 2\tilde{G}_{ij}\hat{\phi}_i(t - \tau_{ij})e^{-(\tilde{\alpha}_{ij} + j\tilde{\theta}_{ij})} + \tilde{G}_{ij}\hat{\phi}_j(t - 2\tau_{ij})e^{-2(\tilde{\alpha}_{ij} + j\tilde{\theta}_{ij})}\end{aligned}\quad (11.54)$$

where $\tilde{\alpha}_{ij} = (R_{ij}\ell_{ij}/2)\sqrt{C_{ij}/L_{ij}}$ is the attenuation factor of the line. The phasor functions $\hat{\phi}_i(t)$ and $\hat{\phi}_j(t)$ are given by the equations

$$\dot{\hat{\phi}}_i = -j\omega_c\hat{\phi}_i - \frac{R_{ij}}{2L_{ij}}\hat{\phi}_i + \dot{\hat{E}}_i + j\omega_c\hat{E}_i \quad (11.55)$$

$$\dot{\hat{\phi}}_j = -j\omega_c\hat{\phi}_j - \frac{R_{ij}}{2L_{ij}}\hat{\phi}_j + \dot{\hat{E}}_j + j\omega_c\hat{E}_j \quad (11.56)$$

Note that for the lossless case (by setting $R_{ij} = 0$), it is easily seen from Eqs. (11.55) and (11.56) that the phasor variables $\hat{\phi}_i$ and $\hat{\phi}_j$ coincide with the bus voltages \hat{E}_i and \hat{E}_j , respectively. Therefore when the line losses are neglected, that is, if we set $R_{ij} = 0$ (hence $\tilde{\alpha}_{ij} = 0$) in Eqs. (11.53) and (11.54), these equations reduce to the lossless counterparts (11.46) and (11.47). Also better approximations to these solutions for the lossy case can be derived by considering finite series expansions for quantities γ and Y_0 in the derivation, whereas only the first terms were used in the derivation thus far, given by the relations (11.51) and (11.52).

Equations (11.32) to (11.34) define the nature of the $g(x, y)$ equations shown in Figure 3.31. The actual form here would vary widely depending on the circumstances, ranging from the simple linear circuit relations to complex nonlinear algebraic equations with time delays. In fact, the G -set representation may have to remain a boundary-value problem if suitable analytic solutions cannot be found.

It is the objective of this chapter to develop the basic models of Eqs. (11.32) to (11.34) for the G set, thus opening the way for load-flow (power-flow) computations for lossy systems with long lines and beyond the dynamics for such systems. Such basic models will be developed in the next section for the most complete representation of the transmission line and then in consecutive sections for various simplifying approximations such as the commonly used RLC or π -circuit representation.

11.5 TRANSMISSION-SYSTEM EQUATIONS (POWER BALANCE)—MODELS FOR THE G SET USING TIME DELAYS TO REPRESENT PARTIAL DIFFERENTIAL EQUATIONS

The form (11.32) to (11.34) of the power-balance equations that constitutes the model of the G set composed of distributed-constant lines can now be given explicitly with reference to Eqs. (11.32) to (11.34).

1. Bus power-balance equation [see Eq. (11.32) for details]

$$\sum_i \hat{S}_{G_i} + \sum_i \hat{S}_{L_i} + \sum_i \hat{S}_{\text{SVC},\text{HVDC}_i} + \sum_i \hat{S}_{\text{mix}_i} + (j\omega C_i \hat{E}_i + C_i \hat{E}_i \hat{E}_i^*) - \sum_j \hat{S}_{ij} = \hat{0} \quad (11.57)$$

2. Line power-balance equation.

Let $\tilde{G}_{ij} = 1/\tilde{R}_{ij}$ represent the wave admittance of the transmission line between i and j let τ_{ij} be its time delay, and let $\tilde{\theta}_{ij}$ (\tilde{s} are dropped in the equations below for notational simplicity) be its phase shift, as defined. Then after simple algebraic manipulations, Eqs. (11.23) and (11.24) can be rewritten as

$$\begin{pmatrix} \hat{I}_{ij}(t) \\ \hat{I}_{ji}(t) \end{pmatrix} = \begin{pmatrix} \tilde{G}_{ij} \frac{\cosh \theta_{ij}}{\sinh \theta_{ij}} & -\tilde{G}_{ij} \frac{1}{\sinh \theta_{ij}} \\ -\tilde{G}_{ij} \frac{1}{\sinh \theta_{ij}} & \tilde{G}_{ij} \frac{\cosh \theta_{ij}}{\sinh \theta_{ij}} \end{pmatrix} \begin{pmatrix} \hat{E}_i(t) \\ \hat{E}_j(t) \end{pmatrix} + \begin{pmatrix} \Delta \hat{I}_{ij}(t) \\ \Delta \hat{I}_{ji}(t) \end{pmatrix} \quad (11.58)$$

where

$$\begin{pmatrix} \Delta \hat{I}_{ij}(t) \\ \Delta \hat{I}_{ji}(t) \end{pmatrix} = -\tilde{G}_{ij} \frac{\cosh \theta_{ij}}{\sinh \theta_{ij}} \begin{pmatrix} \hat{E}_i(t) - \hat{E}_i(t - 2\tau_{ij}) \\ \hat{E}_i(t) - \hat{E}_i(t - 2\tau_{ij}) \end{pmatrix} - \tilde{G}_{ij} \frac{1}{\sinh \theta_{ij}} \begin{pmatrix} \hat{E}_i(t) - \hat{E}_i(t - \tau_{ij}) \\ \hat{E}_i(t) - \hat{E}_i(t - \tau_{ij}) \end{pmatrix} - \frac{e^{-j\theta_{ij}}}{\sinh \theta_{ij}} \begin{pmatrix} \hat{I}_{ij}(t) - \hat{I}_{ij}(t - 2\tau_{ij}) \\ \hat{I}_{ji}(t) - \hat{I}_{ji}(t - 2\tau_{ij}) \end{pmatrix} \quad (11.59)$$

Together Eqs. (11.57) to (11.59) completely describe the voltage–current relationships of the transmission system, which is now the exact set of solutions for the lossless transmission system. By setting the current correction terms $\Delta \hat{I}_{ij}$ and $\Delta \hat{I}_{ji}$ terms to zero in Eq. (11.58) (which will be justified where $\tau_{ij} \rightarrow 0$, as it would on short lines) Eqs. (11.58) and (11.59) simplify to the well-known bus admittance matrix or Y matrix formulation used in software for

load-flow or power-flow computations. So Eqs. (11.57) to (11.59) present the base for load-flow software on systems with long lossy lines. Also, the correction terms drop out naturally for steady-state computations: Under steady-state conditions, the quantities $\hat{E}(t) = \hat{E}(t - \tau) = \text{const}$, so $\Delta\hat{I}_{ij}$ and $\Delta\hat{I}_{ji}$ reduce to zero. However, these terms become significant under transient conditions, depending on the line lengths, which determine the time delays τ and the speeds of the trajectories (how much they change within the τ time delay period). Note that the simplification of the equations for the lossy lines would be similar, starting from Eqs. (11.53) and (11.54).

While in this context the basic model in Eqs. (11.32), (11.58), and (11.59) takes the role as the defining equations of static events in the G set, that is, in the transmission system, these equations are also partners to the dynamic F set $\dot{x} = f(x, y, p)$ in Figure 3.31. Together they define the precise dynamic behavior of the overall interconnected power system now generalized to lossy transmission lines with long lines.

11.5.1 Transients in the G Set

By tacit assumption Eqs. (11.32), (11.58), and (11.59) of Section 11.4, the variation of the modulation signal is smooth and the system does not undergo sudden changes. As there are no transients, the trajectory is not dislocated from the current state. This type of operation is realistic most of the time on the power system. Note that the model in Eqs. (11.58) and (11.59) will automatically incorporate the dynamic contributions of the distributed-parameter line itself to the path taken by the system trajectory. However, this contribution will be minor (negligible) because of the fast internal response of the line.

When the trajectory is abruptly dislocated from the current state because of a disturbance or switching action, this information can be incorporated into the Laplace transform and can be evaluated, at least in principle. This is not included here, and because of its complexity and its small effect associated with the speed of these transients, it is conventionally neglected. This implies instant internal response within the network.

11.6 POWER-SYSTEM DYNAMIC MODELS

Two major issues arise in analyzing and establishing dynamic models for a power system and especially its transmission network, the G set:

1. What are the important details that need to be incorporated to ensure proper and precise results?
2. What, if any, limitations exist on the nature of the dynamic quantities, especially their velocities given the fact that on the transmission system all transfers of “signals” such as voltage, current, and power are via the modulated carrier?

These are discussed in the following sections.

11.6.1 Some Details and the Precision of the Model; Available Approximations

In Section 11.4, a complete and precise model of the G set, the transmission system, was established in the form of power-balance equations for the individual buses (11.32) and the individual transmission lines (11.58) and (11.59). Note here that the terms *bus* and *transmission line* should be interpreted broadly. Bus simply means a node where data are available to establish a bus power-balance-type condition. This may be the terminal of a generator or load, where such formulation is desirable. Likewise, transmission lines may incorporate transformers, tap changers, or generator internal impedance, or they may be of the HV-DC type. Furthermore, as defined earlier, this complete model for the G set accounts for the time-varying nature of the modulating signals, the presence of distributed-parameter components, transmission-line losses, and other fine points (the effect of hard limits is discussed in Chapter 10). So Eqs. (10.43), (11.58), and (11.59) present a model for transmission lines as detailed, as broad, and as precise as possible. When combined with the dynamic equations $\dot{x} = f(x, y, p)$ (F set) for the equipment (generators, loads, etc.), which are typically ordinary differential equations, the precise model of the power system is of the general type

$$\sum_{\text{TD}} : \quad \dot{x} = f(x, y, p), \quad x \in R, \quad y \in \quad (11.60)$$

$$0 = \tilde{g}(x(t), y(t), x(t - \tau), y(t - \tau), p) \quad (11.61)$$

consisting of differential equations $\dot{x} = f$ for the equipment (F set) and algebraic equations $0 = g$ for the transmission system (G set). Also incorporated are line-specific time delays in the form of time-delayed TD variables $x_i(t - \tau_j)$ and $y_i(t - \tau_k)$. The latter account for wave propagation on transmission lines.

It is interesting, and will come as a surprise to many, that *the precise model of the power system is still a DAE type, albeit with time delays* in the algebraic constraints. In fact, further studies show that singularities still occur in the constraint manifold even with the time delays (if the speed of the internal transients is considered instantaneous); however, these appear to result in jump phenomena. Parasitic effects are modeled using time-varying phasors (Tables 11.2 and 11.1). Note that time-delayed constraints are well suited for numerical integration but a difficult problem for analytic solution.

At this point, one also needs to point out certain potential problems associated with a prevalent practice in the literature of introducing *arbitrary singular perturbations* of the $\varepsilon \dot{y} = g(x, y)$ dynamics type into the DAE equations, under the justification that the singular perturbations in the form of $\varepsilon \dot{y}$ model the dynamics of the transmission network and other parasitic effects. Typically the load-flow equations in the form of $0 = g(x, y)$ are arbitrarily modified to be $\varepsilon \dot{y} = g(x, y)$ by

introducing a voltage derivative term in the reactive-power-flow equations and a phase-derivative term in the real-power equations. Such singular perturbation representations, which convert the DAE model Σ into a convenient analytical entity, are then used for continuing the trajectory near singular points S and for tracking jump phenomena outside the constraint $g = 0$. This approach is of questionable validity for a number of different reasons:

1. The constraints $0 = g(x, y)$ for the power system are typically written in quasistationary phasor form. Also, these equations will have singular points, placed on singular surfaces, where their Jacobian has a zero determinant. Mathematically at these points very fast dynamics is implied with a trajectory flipping over from $-$ to $+\infty$. Such an event of course cannot happen physically because of the presence of stray capacitances and inductances, delays over transmission lines etc, but even considering these additional features the implication mathematically of very fast transients around the singular points of $g(x, y)$ remains. No such implication exists outside the singular surface and its neighborhood, assuming that the frequencies of the trajectories stay well below 60 Hz, say about 3 Hz which is typical for transients in angle. Voltage transient frequencies are higher but still tend to be in the quasistationary range at least marginally.
2. All this means that on the singular surface of g and its neighborhood the computational quasistationary model loses validity. Hence, $\varepsilon \dot{y} = g(x, y)$ formulation becomes meaningless in that region.

11.6.2 RLC-Circuit Approximation

The difficulties of analyzing the full distributed-parameter model in either its partial differential equation (column 1 of Table 11.2) or time-delay (column 2) representations are conducive for seeking approximations. Fortunately, on the power system the typical line lengths of 100 to 200 miles produce small time delays. In other words, the difference made by considering these delays is quite small and thus may be set to zero as an approximation in the absence of much longer lines in many problems.

When the time delay associated with transmission lines is neglected, Eqs. (11.58) and (11.59) will collapse into a quite conventional *RLC*-type circuit, a three-terminal network representation (for balanced three-phase systems). Conventional practice further approximates this to a simple nominal π circuit by simply lumping total line resistances, capacitances, and inductances in the three branches of the π circuit.

This last step is questionable because it puts a lumped capacitor at all line ends at the bus, which is not there. Remember that charge and energy pass freely into a capacitor but must enter a line (like a pipe) at a fixed rate. This can cause erroneous results in certain problems, as pointed out in the previous section.

TABLE 11.2 General Taxonomy of the Time-Varying Phasor Calculus

Assump- tion on signal speed	Formulation of dynamic model	Lines are boundary-value problems on four terminal networks		Lines are approximated by lumped RLC or Y-Z matrices	
		Include PDEs	Time-delay equivalent	Nominal π or $Y - Z$ matrices	General linear network
General	$\dot{x} = f(x, y, p)$ $0 = g\left(x, y, p, \frac{dy}{dt}, \frac{dy}{dl}\right)$	$\dot{x} = f(x, y, p)$ $0 = g(x, y, p, T)$	$\dot{x} = f(x, y, p)$ $0 = g(x, y, p)$	$\dot{x} = f(x, y, p)$ $\dot{y} = A \begin{pmatrix} x \\ y \end{pmatrix}$	$\dot{x} = f(x, y, p)$ $\dot{y} = A \begin{pmatrix} x \\ y \end{pmatrix}$
Exact ①	Precise equivalent to exact ②	Constraints are algebraic equations with line-specific time delays T	Constraints are approximated by algebraic equations	Not usable directly for power systems ④ dynamics is coded for lines ③	Alternative: $\dot{x} = f(x, y, p)$ $\dot{y} = g(x, y, p)$

Steady-state special case	$0 = f\left(x, y, p, \frac{dy}{dt}\right)$	$0 = f(x, y, p)$ $0 = g(x, y, p, T)$	$0 = f(x, y, p)$ $0 = g(x, y, p)$	$0 = f(x, y, p)$ $0 = A \begin{pmatrix} x \\ y \end{pmatrix}$
$\dot{x} = 0$	Boundary-value problems in t only	Alternative: equivalent π for the lines	Nominal π or $Y - Z$ matrices	
		$\dot{x} = f(x, y, p)$ $0 = g(x, y, p)$	NA	
		Exact	Exact no time delays needed	Approximate
		$\dot{x} = f(x, y, p)$ $0 = g(x, y, p, T)$	$\dot{x} = f(x, y, p)$ $0 = g(x, y, p)$	NA
Quasistationary approximation	$\dot{x} = f(x, y, p, \frac{dy}{dt})$ $0 = g\left(x, y, p, \frac{dy}{dt}\right)$	Variation of x slow (less than 3-Hz bandwidth)	Questionable although the accuracy in time is improved over ③	Approximation in both t and l
		Frequency band of signals x less than ± 3 Hz	Questionably precise in l Approximate in t	Approximation in both t and l
Unbalanced system	Approximate	$\dot{x} = f(x, y, p)$ $0 = g\left(x, y, p, \frac{dy}{dt}, \frac{d^2y}{dt^2}\right)$	Widely used $\dot{x} = f(x, y, p)$ $\dot{y} = g(x, y, p)$	(continued)

TABLE 11.2 (Continued)

Assumption on signal speed	Formulation of dynamic model	Lines are boundary-value problems on four terminal networks	Lines are approximated by lumped RLC or Y-Z matrices
	Include PDEs	Time-delay equivalent	Nominal π or $Y - Z$ matrices
Bandwidth limitations	Time-varying phasors produce precise results if the bandwidth of signal x is ± 60 Hz	Time-varying phasors produce precise results if the bandwidth of signal x is ± 60 Hz	x, y bandwidth limited 0 to 60 Hz π or $Y - Z$ model symmetrical components apply ⑤
Balanced three-phase system	Exact	$\dot{x} = f(x, y, p)$ $0 = g(x, y, p, \frac{dy}{dt}, \frac{d^2y}{dt^2})$	$\dot{x} = f(x, y, p)$ $\dot{y} = g(x, y, p)$ NA
No limit on bandwidth of signal x	Exact	Time-varying phasors produce precise results on balanced three-phase system	Time-varying phasors produce precise results on balanced three-phase system No bandwidth limitation on x Approximation ④

Note ⑤ identifies cases discussed in text

The customary nominal π -circuit approximation can be pretty crude, even in the steady state when lines are relatively long. So when abandoning the time-delay representation, it would be desirable to retain some correction terms. This can be done in the steady state [15] when an “equivalent” π circuit is applied as follows:

$$Z_\pi = Z \left(1 + \frac{Z}{6Z'} + \frac{Z^2}{120Z'^2} + \dots \right) \quad (11.62)$$

$$Z'_\pi = 2Z' \left(1 + \frac{Z}{12Z'} + \frac{Z^2}{120Z'} + \dots \right) \quad (11.63)$$

where $Z = \omega_c L$, $Z' = 1/\omega_c C$ for the whole line, and Z'_π are the columns and Z_π is the bridge of the π circuit. The fully converged series will give the exact solution for a line of any length but unfortunately only in the steady case. The existence of such correction terms for the steady state raises some hope that an improved RLC circuit could be developed from exact forms such as Eq. (11.59). When the time delays τ_{ij} are small, the correction terms of the form $\hat{E}_i(t) \rightarrow \hat{E}_i(t - \tau_{ij})$ can be very well approximated as

$$\hat{E}_i(t) - \hat{E}_i(t - \tau_{ij}) \approx \tau_{ij} \dot{\hat{E}}_i(t)$$

under certain assumptions. In other words, it may be possible to rewrite the time-delay equations (11.46) and (11.47) [or (11.53) and (11.54)] as singularly perturbed dynamic equations with proper validity under certain assumptions. Otherwise, the conventional RLC or π -circuit approximation is well known.

Power-balance equations in the general format of Eq. (11.61) (with $\tau = 0$) for the equipment $\dot{x} = f(x, y)$ and for transmission-system π circuits to define load flow on individual lines are used in the fashion of conventional power-flow software. Such equations, although they are traditionally written for steady-state conditions, are still applicable for good approximate solutions for dynamic conditions as long as the dynamics is not faster than conventional “transient-stability” analysis of electromechanical oscillations. This range is known as the *quasistationary range*.

11.6.3 Limitations Imposed by the Time-Varying Phasors

It should be emphasized that the primary aim of this section is the study of the effect of the time-varying nature of the time-varying phasors as defined in Theorems 11.2.1 and 11.2.2. This is a very vital feature when dynamic speeds on the system exceed those of historical transient stability.

Here we should point out that the system equations, whether in distributed-constant form [Eqs. (11.32), (11.58), and (11.59)] or in an approximation, are written in time-varying phasors that were defined in Theorems 11.2.1 and 11.2.2 (Properties 1 through 4). These are limited by one of two factors: (1) the modulating signal (\hat{E} and \hat{I}) variations are contained in a frequency band of ω_c that

is slower than the carrier (the low-pass phasor), or (2) the three-phase signal is balanced and the network is symmetric (fast balanced phasors). Note that in the instantaneous-time domain, the power-balance equations of the form (11.7) are not easy to work since the carrier is still present in the terms $1 + \cos 2[\omega_c t + \delta(t)]$ and $\sin 2[\omega_c t + \delta(t)]$ in the power-flow equation. On the other hand, by the time-varying phasor properties (Property 2, to be precise), it is possible to rewrite these equations purely in the form of real power $P(t)$ and reactive power $Q(t)$. Hence the problem is analytically much simpler to handle. For instance, in Eq. (11.7), if the three-phase system is balanced, then in the three-phase power (which in per unit is the same as single phase power), the term $1 + \cos 2[\omega_c t + \delta(t)]$ becomes 1 and the term $\sin 2[\omega_c t + \delta(t)]$ becomes 0 as a result of adding three symmetrically spaced phasors. This indicates the importance of studying the power-flow equations in terms of the respective time-varying phasors. The rest of this section is devoted to studying some important special cases.

Table 11.2 is included to support the reader in developing an organized view of the various cases that occur. In this table the complete and precise model is located in the upper left corner box 1. In its general form, Eqs. (11.32), (11.58), and (11.59), this model uses boundary-value problems with partial differential equations for the lines, allows fast variation of modulating signals, considers line losses, and treats fast time-varying events along distributed constant transmission lines. Next to it on the right is located the time-delay formulation (box 2), which is equivalent to the PDE version box 1. The other columns depict various approximations and special cases that allow special solutions. In box 3 an *RLC* linear approximation of the transmission system is introduced, and this approximation, which includes the customary nominal π circuit, is used in the rest of the cases in boxes 4 to 5 for simplicity of presentation, although the results also apply to the full distributed model of Eqs. (11.32), (11.58), and (11.59).

The second row of Table 11.3 displays special features of each case for stationary conditions of the system. The third row acknowledges possible usefulness of the stationary model under a quasistationary label for relatively slow events. The last two rows provide sketches of the cases connected, respectively, with Theorems 11.2.1 and 11.2.2.

A brief set of equations modelling the dynamics of the large power system is shown in Table 11.3 in which the G set is represented by two sets of equations for easy comparison. All the equations in Table 11.3 are written under the assumption of a three-phase balanced-power system. In addition, if we impose the quasistationary phasor assumption, then using the nominal π circuit, the G set (the power-balance equations) simplifies to a simple set of algebraic equations shown on the left-hand side of Table 11.2. It is easily seen that these equations reduce to the traditional Y_{bus} formulation. On the other hand, by using the fast balanced time-varying phasors introduced previously in this chapter, the power-balance equations now possibly include derivative terms from the presence of capacitors (see the right-hand side of the G set in Table 11.3). Moreover, when the distributed nature of the lines are considered, the algebraic nominal π -circuit equation on the left side of the line ij becomes a set of time-delay equations

TABLE 11.3 Illustrative Example: A Large Balanced-Power System Model

F set: Dynamic equations nonmodulated

(highly simplified model, detailed models can be equally used)

- Generator electromagnetics simplification from Park and Concordia

$$T_{d0}\dot{E}' = -\frac{x_d}{x'_d}E' + \frac{x_d - x'_d}{x'_d}E_G \cos(\delta_G - \delta') + E_{fd}$$

- Generator excitation control simplification from IEEE Type I model

$$T\dot{E}_{fd} = -(E_{fd} - E_{fd}^0) - K(E_G - \delta') + E_r$$

- Generator electromechanics swing equation

$$J_i\ddot{\theta}_i + b_i\dot{\theta}_i = p_{Ti} - \frac{x_d}{x'_d}e_G \sin(\delta_G - \delta'_i)$$

- Load

$$P_{L_i} = P_{S_i} - P_{D_i}, \quad Q_{L_i} = Q_{S_i} - Q_{D_i}, \quad S_{L_i} = P_{L_i} - jQ_{L_i}$$

$$P_i = P_i^o + M_i(E_i) + G_i(E_i)^2, \quad Q_i = Q_i^o + H_i(E_i) + B_i(E_i)^2$$

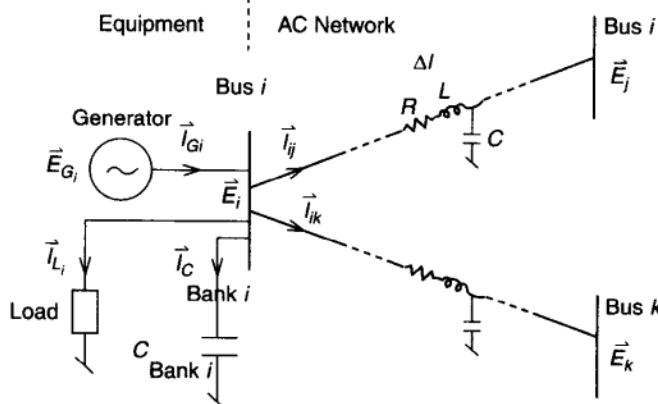
$$P_{D_i} = P_{D_i}(x_{D_i}, E_i, \delta_i), \quad Q_{D_i} = Q_{D_i}(x_{D_i}, E_i, \delta_i)$$

$$\dot{x}_{D_i} = f_{D_i}(x_{D_i}, E_i, \delta_i)$$

G set: Network equations (modulated phasor)

Power-balance equations

$$E_{G_i} = E'_i \angle \theta_i, \quad J_{G_i} = J_{G_i} \angle \theta_i, \quad E_i = E_i \angle \theta_i, \quad J_{ij} = J_{ij} \angle \theta_i$$



Quasistationary phasor equations

Bus i :

$$E_{G_i}I_{G_i} - S_L - j\omega C_i E_i^2 - \sum_{j=i}^m C_{ij}E_i I_{ij}^* = 0$$

$$E_{G_i} - E_i - i\omega L_{D_i} J_{G_i} = 0$$

Line ij :

$$E_i = E_j - (R_{ij} + j\omega L_{ij})I_{ij} = 0$$

Time-varying phasor time-delay equations

Bus i : $0 = g(x, y, x(t - \tau), y(t - \tau), p)$

$$E_{G_i}J_{G_i} - S_{L_i} - j\omega C_i E_i^2 - \sum_{j=i}^m C_{ij}E_i I_{ij}^* = C_i E_i \frac{dE_i}{dt}$$

$$E_{G_i} - E_i - i\omega L_{D_i} J_{G_i} = L_{D_i} J_{G_i} \frac{dI_{G_i}}{dt}$$

Line ij :

$$E_i - E_j - (R_{ij} + j\omega L_{ij})I_{ij} = L_{ij} I_{ij}^* \frac{dI_{G_i}}{dt}$$

shown on the right side [which also includes certain flux quantities $\hat{\phi}_i$ from modeling the line losses, see Eqs. (11.53) to (11.56)]. If we set the derivative terms to zero and the time delays to zero in the equations shown on the left side in the G set, then these equations precisely reduce to the corresponding equations for the nominal π representation after the well-known conversion, Eqs. (11.62) and (11.63), from the equivalent π to nominal π circuit.

11.7 CHAPTER SUMMARY

In the previous chapters of this book extensive and comprehensive treatment is given to the fundamental problems of the large power system: modeling of the structure and components of the system in an analytical and a computed manner; stationary operation; small-signal (linearized) environment; and full nonlinear dynamics for the DAE model incorporating hard limits and stepwise control. All are given in the language of common phasors [quasistationary and in lumped (*RLC*) approximations], which actually still covers the vast majority of practical problems. The limits of validity of this (quasistationary) approximation are carefully identified in this text.

This chapter then lays the foundation on how solutions can be found when phenomena are too fast for assuming quasistationarity and how to utilize lumped-constant approximations.

BIBLIOGRAPHY

1. Venkatasubramanian, V., Schättler, H., and Zaborszky, J., A taxonomy of the dynamics of the large electric power system with emphasis on its voltage stability, *Proc. NSF Intl. Workshop Bulk Power Syst. Voltage Phenom.—II*, 1991, pp. 9–52.
2. Zaborszky, J., Schättler, H., and Venkatasubramanian, V., Limitations of the quasi-stationary dynamics and error due to phasor computations in network equations, *Proc. Power Syst. Comput. Conf.*, Avignon France, 1993, pp. 721–729.
3. Venkatasubramanian, V., Jiang, X., Schättler, H., and Zaborszky, J., Current status of the taxonomy theory of large power system dynamics—DAE systems with hard limits, in L. H. Fink (ed.), *Proc. NSF Intl. Workshop Bulk Power Syst. Voltage Phenomena—III*, Davos, Switzerland, 1994, pp. 15–103.
4. Sauer, P. W., and Pai, M. A., Modeling and simulation of multimachine power dynamics, in C. T. Leondes ed. *Advances in Control and Dynamic Systems*, City: Academic, 1991, Vol. 43.
5. Sauer, P. W., Lesieutre, B. C., and Pai, M. A., Transient algebraic circuits for power system dynamic modeling, *Int. J. Electric Power Energy Syst.*
6. Venkatasubramanian, V., Schättler, H., and Zaborszky, J., Fast time varying phasor analysis in the balanced large electric power system, *IEEE Trans. Automatic Control*, AC-40: 1992–2013, 1995.
7. DeMarco, C. L., and Verghese, G. C. Bringing phasor dynamics into the power system load flow, *Proc. North Am. Power Symp.* 1993.

8. Venkatasubramanian, V., Tools for dynamic analysis of the general large power system using time varying phasors, *Int. J. Electric Power Energy Syst.*, 365–376, 1994.
9. Venkatasubramanian, V., Schättler, H., and Zaborszky, J., Time-delay differential-algebraic phasor formulation of the large power system dynamics, *IEEE Int'l. Symp. Circuits Syst.*, 1994.
10. Zaborszky, J., Some basic issues in voltage stability and viability, *NSF Proc. Bulk-Power Voltage Phenom.—Voltage Stability Security*, Potosi, MO, 1988, pp. 1.17–1.60. (Editor L. Fink)
11. Althammer, P., and Glavitsch, H., On the matching of Bergeron's method and the two-reaction theory to calculate transients in synchronous machines connected to transmission lines, *Proc. Power Syst. Comput. Conf.*, Stockholm, 1966.
12. Haykin, S., *Communication Systems*, 2nd ed., New York: Wiley 1983.
13. Penfield, P., Jr., Spence, R., and Duinker, S., *Tellegen's Theorem and Electrical Networks*, Research Monograph No. 58, Cambridge, MA: MIT Press, 1970.
14. Bergen, A. R., *Power Systems Analysis*, Cliffs, NJ: Prentice-Hall, 1986.
15. Zaborszky, J., and Rittenhouse, J. W., *Electric Power Transmission*, Reynolds 1954. Available in paperback at the Rensselaer University Bookstore, Troy, NY.
16. Branin, Jr., F.H., Transient analysis of lossless transmission lines, *Proc. IEEE lett.* 55: 2012–2013, 1967.

PART III

Control and Stabilization

12 Primary Control of Electric Power Systems

In this chapter, we revisit the dependence of power-system dynamics on the type of primary control used and analyze the role of primary control on an interconnected power system for achieving desired performance. While much research has been done on particular aspects of planning and operations in large electric power systems, it has remained difficult to provide a reliable, flexible methodology for automated tuning and switching of a variety of control equipment spread throughout the system. In addition to the problem of high dimensionality, the development of such general tools is particularly challenging for this class of systems because of the nonuniformity of control components, reflected in their uneven spatial distribution throughout the system as well as a large spread of response times.

In order to respond to the need for an integrated, intelligent monitoring and control methodology, one needs to take a global look at the state of the art in tuning and switching of all classes of power-system controllers currently available on the system, as well as the newly evolving classes that are considered to be potentially very powerful for improving dynamic performance of the large interconnected system.

In this chapter, we provide potentially useful classifications of the available primary controllers. First, generation-based control is described. Present state-of-the-art control designs are briefly reviewed. It is suggested that these controllers are generally effective for stabilizing system deviations in response to relatively small disturbances. Improvement in control design is needed when the system is under stress. We provide a brief literature survey of several recently proposed nonlinear controllers that are potentially useful when the system is under stress.

Next, primary control of the transmission lines and loads is briefly reviewed. Both mechanically switched reactive compensation of various types, and the power-electronic-switched technologies known as flexible AC transmission systems (FACTS) are analyzed for their impact on system performance.

The emphasis of this chapter is on an assessment of primary controllers for their impact on power-system performance. This question is viewed as a control design problem. This approach is in sharp contrast with typical studies concerned with the performance of a candidate controller for improving system performance in a particular part of the system under a critical contingency [1]. The remaining conceptual challenges in designing primary controllers so that their systemwide

effect is acceptable under both normal and emergency operating conditions are highlighted.

12.1 AVAILABLE TYPES OF PRIMARY-CONTROL DEVICES

All primary-control devices are, at least in principle, fully automated devices that respond to deviations of system conditions from scheduled events.

These deviations are caused

1. By deviations in demand under normal operating conditions
2. By unexpected equipment failures on the generation and transmission sides.

In Chapter 3 we introduced a variety of components that are used as primary control throughout the interconnected system. Among these, three qualitatively different classes of primary controllers can be found on present power systems. They are

1. Primary controllers, which form an integral part of prime power sources, such as turbine-generator sets
2. Controllers that change characteristics of a transmission network at selected locations
3. Load controllers

Most representative types of primary controllers in the first category are governors and exciters. They are installed as an integral part of each large generator-turbine unit. More recently, power-system stabilizers (PSSs) are being added to the automatic voltage regulators (AVRs) as supplementary controls. The function of exciters, governors, and power-system stabilizers is to regulate frequency and terminal voltage locally at each generator level, in response to deviations of these variables from their set values. The primary system control regulates deviations of real-and reactive-power generation sent into the system around their scheduled values. This control also responds to fast deviations in demand from the scheduled demand, so that voltage and frequency remain within the prespecified operating limits. A primary control-generator-turbine set is an active device that injects energy into the transmission network to be transferred to the demand points. The closed-loop system dynamics, as well as its stationary conditions, are significantly affected by the control of generators and turbines.

In the second and third categories of primary controllers one finds a variety of qualitatively different types of primary controllers; these are passive devices that change effective impedances at various locations within a transmission system. They do not inject real power into the grid. Most conventional primary-control devices of this type are shunt capacitor and inductor banks. The number of banks connected between the system bus and the ground varies as the operating conditions change. Some other devices of this type are phase-shifting transformers for direct regulation of power line flow and on-load tap-changing transformers

for voltage regulation. An extreme form of this type of control is line opening and closing, which some utilities use under unusual demand conditions.

12.1.1 Time-Scale-Separation-Based Classification

The design of a wide variety of currently implemented primary-control devices can be classified according to their time-scale-separation effects on closed-loop system dynamics. It is helpful to assess the role of various primary-control devices in context of the system dynamics to which they are designed to respond. This sometimes tends to be forgotten, and it leads to false expectations of primary-control performances. Some technologies are inherently slow, and moreover, they are intended to regulate the system in response to small deviations under normal operating conditions. These cannot be expected to be effective under emergency conditions when system dynamics vary quickly and the deviations from the scheduled conditions are large. In this situation, fast primary-control devices, the control logic of which is adapted to make most out of existing resources, are essential.

In the past, most of the switching has been done at a slow rate relative to the 60-cycle system dynamics. The switching has been mechanical. The main objective of mechanically switched devices, such as shunt and series capacitors and inductors as well as slowly switched phase-shifting transformers, is to regulate system voltages and flows (phase-angle differences across the transmission lines) at selected locations throughout the system within operationally acceptable limits. This is done in response to slow, unpredictable deviations from the scheduled demands. These devices are effective as long as no dynamic or transient instabilities occur as the system conditions change.

The FACTS device technologies are generally more useful for stabilizing system dynamics with truly dynamic and transient instabilities. More recently, important breakthroughs have been made in power-electronic-based fast switching technologies for changing critical transmission characteristics at the 60-cycle rate. These technologies are generally known as FACTS device technologies. Many of these have already been installed and proven to be useful. Typical devices of this sort are static Var compensators (SVC), rapidly adjustable phase shifters (RAPS), and rapidly adjustable series capacitors [2,3]. SVCs have been in use the longest and represent possibly the earliest type of FACTS device technologies currently under development [4].

Most primary-control devices are designed to regulate system voltage and frequency in response to relatively slow and small demand deviations under normal operating conditions. Effective system regulation in response to contingencies requires a systematic adjustment of a viable postfault set point. This is in addition to the need for advanced stabilizing control logic. Adjusting a post-fault set value on the control devices is challenging because under contingencies, one usually does not have much time to perform extensive systemwide computations. To deal with this basic problem, a system operator usually relies on lookup tables that are based on extensive off-line simulations for the emergency

scenario of interest. As a future alternative, one could design intelligent primary control devices that compute a postcontingency target by learning locally about the system state. The observation-decoupled state space (ODSS) [5] and more recently the work in Ref. [6,7] provide some theoretical basis for adjusting post-fault set values in real time using only local measurements.

In this chapter, the emphasis is on describing local control logic, assuming the set values are assigned. It turns out that this is a justifiable approach in normal system operation. Limits on available control are critical in this case and, although a primary-control logic may be fast and adaptive, there simply may not be enough control to regulate the system back to a precontingency situation.

12.2 GENERATION-BASED PRIMARY CONTROL UNDER NORMAL OPERATION

It is assumed here that under normal operation, system conditions deviate from scheduled mainly as a result of small unexpected changes in demand. These deviations in demand have a very fast, random fluctuation component in real power $P_{L_i}(t)$, and reactive power $Q_{L_i}(t)$ at all load buses $i \in NL$. They also have a slower, sustained component $P_{L_i}(\tau)$ and $Q_{L_i}(\tau)$, again at all load buses in the interconnected system $i \in NL$. If the amplitude of these deviations is small relative to the scheduled load, linearized system models are sufficiently accurate to represent a system response to such disturbances and also for a systematic tuning and switching of primary controllers. We review here typical primary controllers in use at present.

12.2.1 Fast Continuous Primary Controllers

Consider a simple three-bus system, consisting of one generator and two loads. The generator is equipped with a turbine–governor and exciter or automatic voltage regulator needed to regulate generator frequency ω_1 and generator terminal voltage E_{t1} in response to deviations in demand, $\underline{d}(t) = [P_L(t) \ Q_L(t)]$ and $\underline{d}(\tau) = [P_L(\tau) \ Q_L(\tau)]$. The governor is typically designed to suppress deviations in $P_L(\tau)$, and the exciter or voltage regulator responds to fast fluctuations in $\underline{d}(t)$. Deviations in $Q_L(\tau)$ are generally regulated by a mechanically switched reactive compensation at the load location or on transmission lines, as described later in this chapter.

Under a typically made assumption, that the exciter or voltage regulator would stabilize terminal voltage to its set value before the governor responds to frequency deviations (see Chapter 6), one could use two separate, lower-order models for their tuning.

12.2.1.1 Tuning an Exciter or Voltage Regulator Consider a linearized model of this system, introduced earlier in Chapter 6. The vector of relevant state variables of the generator is $\underline{x}(t) = [\delta_G \ \omega_G(t) \ e'_q]$; the mechanical power out of

the turbine is assumed to be a given parameter in the time range of interest for designing the exciter or voltage regulator.

The basic primary-control problem here is to design a feedback $u(x) = e_{fd}$ so that the terminal voltage E_{tl} is regulated quickly to its set value E^{ref} , despite disturbance in demand $d(t)$. This problem is a textbook example of a single-input-single-output control problem. A standard proportional-integral-differential (PID) controller design directly applies in this case.

Here we use the same notation as in Ref. [8], since this is a seminal paper that addressed small-signal-stability consideration when designing excitation control for voltage regulation. It turns out that the representative literature on supplementary control, such as PSS [9]–[11], uses the same notation introduced by Concordia and DeMello [8]. This was the first paper concerned with small-signal (dynamic) instabilities of a closed-loop linearized system dynamics, as affected by a controller design.

A block diagram representing linearized small perturbation relations of a single generator supplying an infinite bus through external impedance x_e is shown in Figure 12.1. The coefficients in this block diagram are defined as $K_1 = \partial T_e / \partial \delta$, $K_2 = \partial T_e / \partial e'_q$, $K_3 = x'_d + x_e / x_d + x_e$, $K_4 = (1/K_3)(\partial e'_q / \partial \delta)$, $K_5 = \partial E_t / \partial e'_q$, and $K_6 = \partial E_t / \partial \delta$. Coefficients K_1 and K_2 represent sensitivities of the electric torque with respect to rotor angle and flux linkage, respectively. K_3 is the impedance factor, under the assumption that resistive losses are neglected. K_4 represents

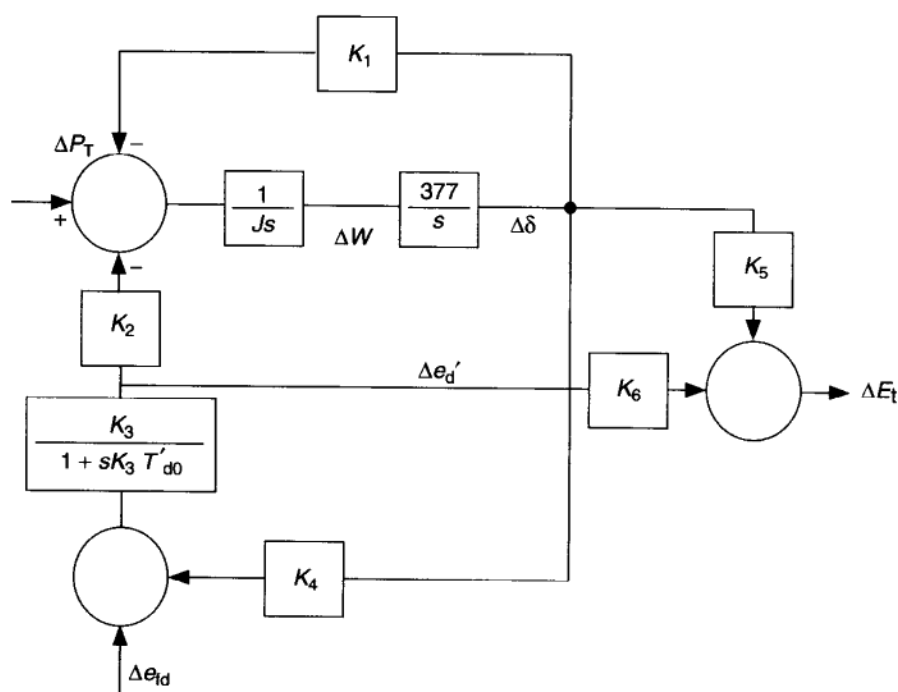


FIGURE 12.1 Block diagram corresponding to a linearized model of a generator connected to an infinite bus.

sensitivity of flux linkage with respect to rotor-angle change. Finally, K_5 and K_6 represent sensitivity of terminal voltage with respect to rotor-angle and flux linkage change, Ref. [8].

Using the block diagram in Figure 12.1, one can analyze particular various dynamic effects in the closed-loop dynamics. The simplest scenario is the dynamics of the classical model, which is obtained with K_2 to K_6 identically zero. The block diagram in this case takes on the form shown in Figure 12.2.

The system dynamics in this case is given as

$$J \frac{d^2\delta}{dt^2} + D \frac{d\delta}{dt} + K_1 \delta = 0 \quad (12.1)$$

As analyzed in Chapter 6, the eigenmodes of this dynamic system are

$$s_{1,2} = -\frac{D}{2J} \pm \sqrt{\left(\frac{D}{2J}\right)^2 - \frac{K_1}{J}}$$

Although in most cases K_1 is positive, it is possible in the case of heavy loading to have negative K_1 . The natural, undamped frequency $\omega_n = \sqrt{K_1/J}$ when $D = 0$, and for $\zeta = \frac{1}{2}D/\sqrt{JK_1}$, the damped natural frequency of this second-order system is $\omega_n \sqrt{1 - \zeta^2} = \omega_d$ [12]. The natural mode is typically smaller than 2 Hz.

The term $D\omega$ in system dynamics (12.1) is called a *damping torque*, while the term $K_1\delta$ is often called a *synchronizing torque* [8]. System oscillations caused by any particular means are often analyzed from a viewpoint of their contributions to the damping and synchronizing torque. Observe for purposes of discussion that system modes could be in the right-hand side complex plane if either $K_1 \leq 0$ or

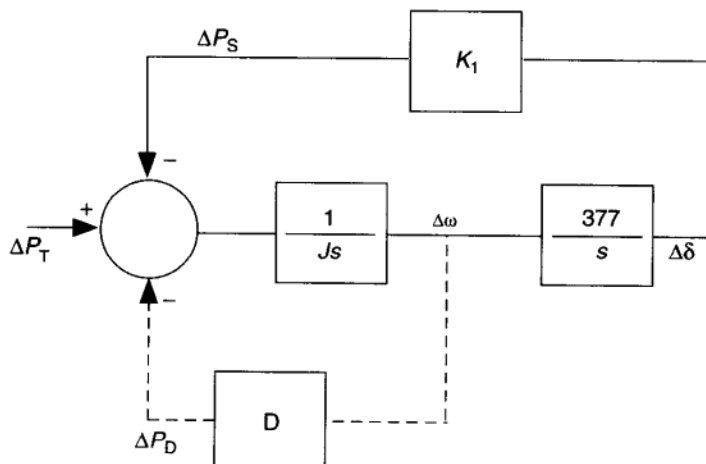


FIGURE 12.2 Block diagram representing the torque-speed loop.

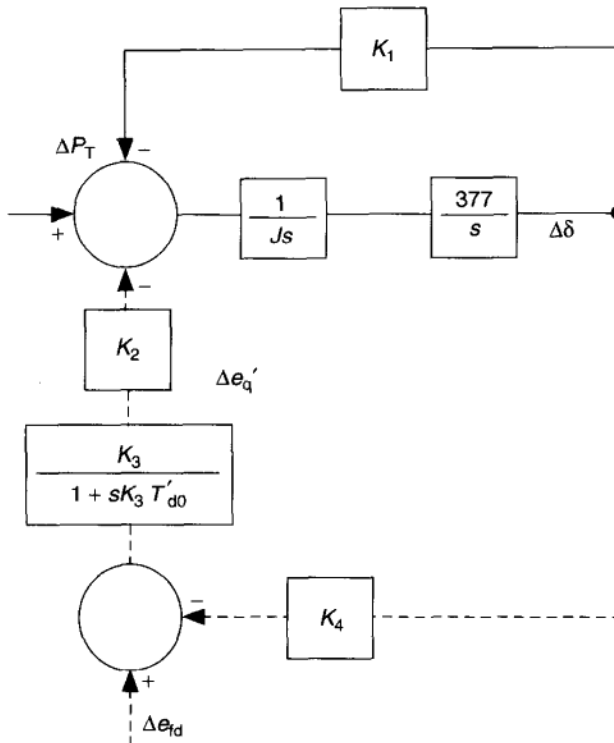


FIGURE 12.3 Block diagram without a voltage regulator.

$D \leq 0$. Typical practical design is focused on ensuring positive K_1 . The instabilities caused by $D \leq 0$ are often seen in sustained, low-frequency oscillations and are often associated with high gain of a voltage regulator [8].

To analyze the impact of changes in field voltage on the basic torque-angle transfer function, consider a block diagram given in Figure 12.1 without a voltage regulator. This block diagram is shown in Figure 12.3.

In the case of slow oscillations ($sK_3 T'_{d0} \ll 1$) and constant field voltage, the characteristic equation can be approximated by

$$Ms^2\delta + (K_1 - K_2 K_3 K_4)\delta = 0 \quad (12.2)$$

In the case when $K_1 - K_2 K_3 K_4 \leq 0$, the system response is unstable against constant field voltage, and it is necessary to have excitation control to change e_{fd} accordingly.

12.2.1.2 Effect of a Voltage Regulator Here we consider a standard IEEE Type 1 exciter or voltage regulator described in Section 3.2. An even simpler version is a very fast exciter with one time constant T_A with a transfer function

$$\frac{e_{fd}}{E_t} = -\frac{K_A}{1 + sT_A} \quad (12.3)$$

The choice of gain K_A must be made carefully in order to provide a well-damped closed-loop dynamics. It is shown in Ref. [8] that for a typical value of $T_A = 0.05$ sec and $T'_{d0} = 5$ sec, this gain should not exceed 5. This result is based on a requirement to maintain the crossover frequency of less than $1/2T_A$. It is shown in Ref. [13] that an approximate two-time constant transfer function

$$\frac{E_t}{E^{\text{ref}}} \approx \frac{1}{(1 + sT'_{d0}/K_A K_6)(1 + sT_A)} \quad (12.4)$$

To analyze the impact of a voltage regulator on system stability, one could compare the transfer function relevant for the synchronizing torque in two cases: (1) without a voltage regulator and (2) with the voltage regulator. This transfer function is approximately [13]

$$\frac{\partial T_e}{\partial \delta} \approx -\frac{K_2 K_4}{K_A K_6 (1 + sT'_{d0}/K_A K_6)} \quad (12.5)$$

One could see that the negative component in a synchronizing torque is smaller by a factor $1/K_A K_6 K_3$ with a voltage regulator present. Also, since the effective time constant has been reduced with a high regulator gain from $K_3 T'_{d0}$ to $T'_{d0}/K_A K_6$, this reduces the damping torque.

Following an analysis similar to this, one could study the impact of K_5 on synchronizing and damping torques. It is shown in Ref. [8] that a dilemma arises here, since a positive K_5 contributes to a positive synchronizing torque, which is desirable; yet at the same time, it could be detrimental to the damping torque. A block diagram with a voltage regulator is shown in Figure 12.4.

12.2.1.3 Power-System Stabilizer Since the effect of K_5 could lead to unexpected negative damping despite natural effects of damper windings, supplemental control has been introduced to deal with this problem by means of PSSs.

The basic function of a PSS is to extend the stability limits by modulating the generator excitation to provide damping for the oscillations of synchronous machine rotors relative to one another [9] to [11]. To provide damping, the power system must produce a component of electrical torque on the rotor that is in phase with speed variations.

The block diagram in Figure 12.5 illustrates, in terms of a few very basic small-signal transfer functions, the relationship between the applied torques on the turbine-generator shaft and the resulting generator rotor speed ω and rotor displacement δ . The electrical torque may be considered to have two components, (1) one produced by the power-system stabilizer solely by modulation of the generator flux and (2) one that results from all other sources, including shaft motion.

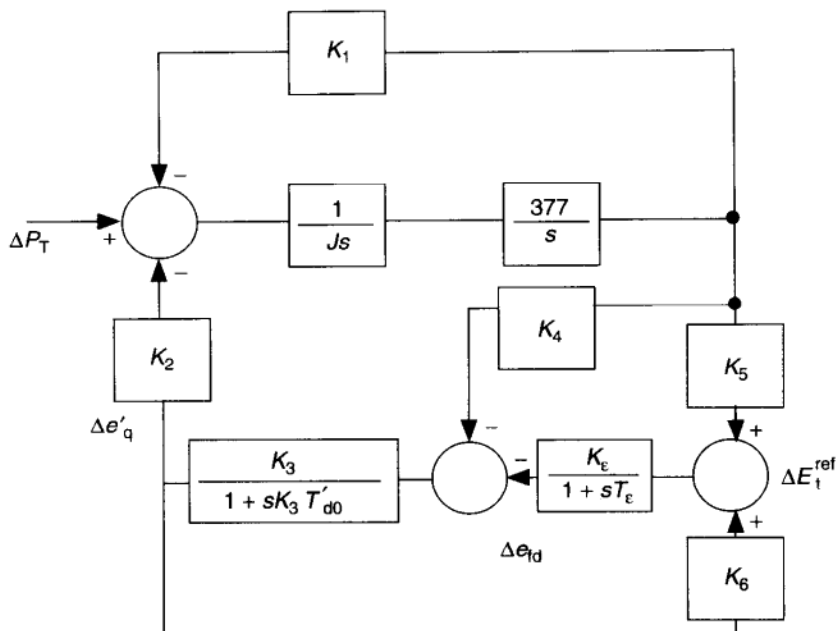


FIGURE 12.4 Block diagram with a voltage regulator.

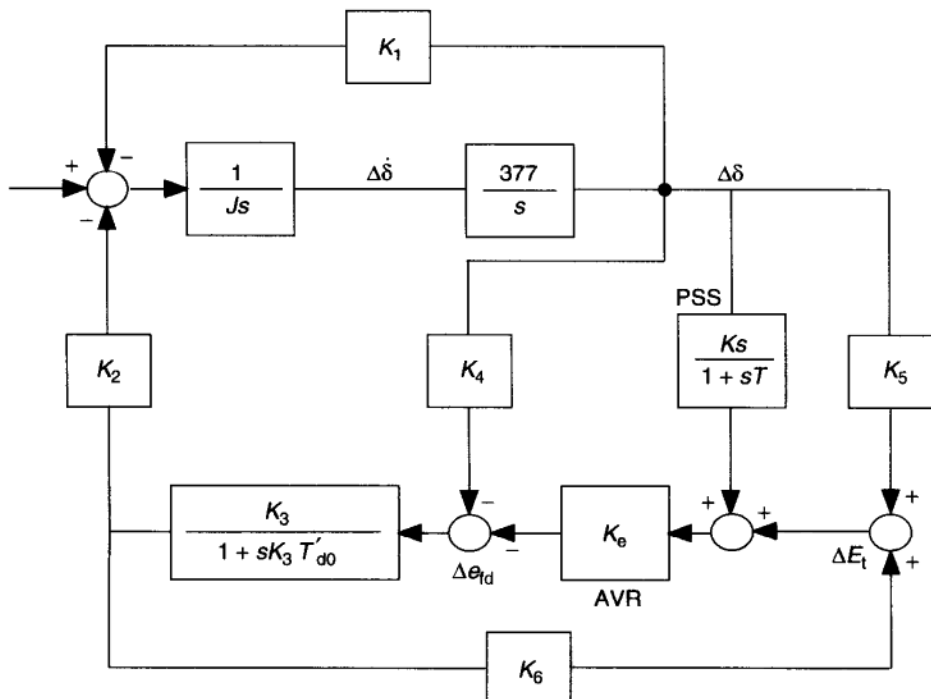


FIGURE 12.5 Simplified model of a single machine with a PSS.

The contribution of torque due to the stabilizer path is

$$\frac{\partial T_{EP}}{\partial \omega_G} = PSS_\omega(s)GEP(s) \equiv P(s) \quad (12.6)$$

The transfer function GEP(s) represents the characteristics of the generator, the excitation system, and the power system. It has been shown in Ref. [9] that

$$GEP(s) \approx \frac{K_2}{K_6} \frac{\partial E_t}{\partial E^{\text{ref}}} \quad (12.7)$$

This relation is routinely used for tuning procedures that involve measurement of the closed-loop voltage regulator characteristic to determine the phase compensation needed by the stabilizer [9,10]. The variation of GEP(s) with exciter gain K_A , generator loading, and the AC system strength plays a dominant role in power-system stabilizer tuning requirements and performance.

It is important to keep in mind that the stabilizer is intended to provide damping for small variations around a steady-state operating point and not to enhance transient stability, that is it has no ability to recover from a severe disturbance. As a matter of fact, the stabilizer design does not show good impact on transient stability [10]. Several practical considerations are also essential when tuning a PSS, the most important being a danger of torsional interaction and the filtering needed to prevent this problem. In addition, a typical PSS design is sensitive to various noise problems.

12.2.1.4 Eigenmode-Based Tuning Both the automatic voltage regulator design and a PSS design could be done without a physical interpretation of gains K_1 to K_6 and K_A in such a way that the closed-loop system matrix of the linearized dynamic model in a standard state space form has all eigenmodes in the left side of the complex plane.

It is derived in Ref. [13] that the linearized closed-loop dynamics with the IEEE Type 1 excitation control takes on the form [13].

$$\begin{bmatrix} \dot{e}'_q \\ \dot{\delta} \\ \dot{\omega} \\ \dot{e}_{fd} \end{bmatrix} = \begin{bmatrix} -\frac{1}{K_3 T'_{d0}} & \frac{K_4}{T'_{d0}} & 0 & \frac{1}{T'_{d0}} \\ 0 & 0 & 1 & 0 \\ \frac{K_2}{M} & \frac{K_1}{M} & 0 & 0 \\ \frac{K_A K_6}{T_A} & \frac{K_A K_5}{T_A} & 0 & \frac{1}{T_A} \end{bmatrix} \begin{bmatrix} e'_q \\ \delta \\ \omega \\ e_{fd} \end{bmatrix} \quad (12.8)$$

For this system to be stable, it is necessary that all eigenmodes be in the left side of the complex plane. Many systematic methods exist for such a design [14]. If

this system is unstable, one could consider a supplementary control. The supplemental control is effectively a *dynamic* feedback given by [13]

$$\frac{dx_5}{dt} = -\frac{1}{T}x_5 + \frac{d\omega}{dt}\frac{du}{dt} = -\frac{K_6 K_2 T_1}{MT_2} e'_q - \frac{K_c K_1 T_1}{MT_2} \delta + \frac{K_c}{T_2} \left(1 - \frac{T_1}{T_2} x_5 - \frac{1}{T_2} u \right) \quad (12.9)$$

Proper tuning of additional parameters K_c , T_1 , and T_2 can be carried out to ensure stability of the closed-loop dynamics with the supplemental control [15].

A qualitatively different approach to supplemental control can be found in Ref. [16]. This design is known as a four-loop control and has been successfully used in practice on the French power system.

Current practice performs PSS tuning by means of field measurements and focuses on damping only one local mode (i.e., oscillation of the plant of interest against the rest of the system) [17, p. 88]. We return to this important issue in the section concerned with primary-control problems for multibus power systems.

12.2.1.5 Tuning a Governor The problem of governor design or tuning for normal operating conditions is a fairly straightforward control problem, as well. The relevant state vector in this case is $\underline{x}(\tau) = [\omega(\tau) P_T(\tau) a(\tau)]$ where $a(\tau)$ is a turbine valve position and $P_T(\tau)$, is the mechanical power produced by the turbine for some $\tau \in [t_1, T]$ where t_1 stands for the settling time of a voltage regulator. The control problem is one of regulating $u(\tau) = a(\tau)$ so that frequency $\omega(\tau)$ follows closely the set frequency $\omega^{\text{ref}}(kT_s)$.

Present operating problems with governor control under normal operation are attributable primarily to the model and parameter uncertainties of a turbine–generator–governor unit, and also to disabling (often intentionally) the governor by setting the error band within which the governor responds to be large. Conceptually, present state-of-the-art governor control is based on a basic PID controller design.

12.2.2 Generator-Based Control as a Full-State Optimal Control-Design Problem

It can be deduced from the preceding analysis that early work on voltage regulators is heavily based on physical interpretation of the effects of feedback designed. For example, in Ref. [8] a voltage regulator is analyzed to detect when it could lead to destabilization of the torque-angle dynamics, in addition to regulating the terminal voltage. Recall from the preceding that a PSS was introduced as a “supplemental” control to mitigate this potentially detrimental effect of a voltage regulator.

It was suggested in Ref. [15] that the problem of designing a generator voltage regulator could be viewed, to start with, as the problem of optimal feedback design for linear systems [12,14]. Solutions are available for designing an optimal full-state feedback of the form

$$u = -Fx = -R^{-1}B^T Kx \quad (12.10)$$

for any linear system in its standard state-space form

$$\dot{x} = Ax + Bu \quad (12.11)$$

so that a performance index

$$J = \frac{1}{2} \int_0^{\infty} (x^T Q x + u^T R u) dt \quad (12.12)$$

is minimized. Here matrix K is simply a steady state solution to the Riccati equation

$$-KA - A^T K + KBR^{-1}B^T K = 0 \quad (12.13)$$

Theoretically, as long as system (12.11) is fully controllable, a unique solution to Eq. (12.13) exists. At present, the MATLAB package [18] could be used to obtain such a solution without having to be an expert on optimal control theory. More difficult is the appropriate choice of matrices Q and R so that the dynamic performance of the controller is acceptable (e.g., real parts of dominant eigenvalues within the desired specifications) subject to constraints on control cost.

In the context of generator control, this approach would result in designing a single controller for the entire state space (mechanical and electromagnetic), for example, $x = [\delta \omega e'_q]^T$, and matrix K would be a full (3×3) matrix. This approach basically results in a single controller instead of a voltage regulator and its supplemental PSS.

The same approach further applied to the generator–turbine state space requires a design using an even higher-order full state. It effectively needs a two-input (e_{fd} , P_T) governor, a PSS, and a voltage regulator simultaneously [19]. This, however, may be an overly complex approach if one considers that control design beyond a single input becomes more involved and, moreover, the fact that turbine dynamics is slower than generator dynamics by an order of magnitude. One may consider using lower-order models introduced in Chapter 6 for designing composite control consisting of fast e_{fd} control and slower governor control.

12.2.2.1 Optimal Output Feedback While an optimal full-state feedback approach guarantees desired performance, it is often not implementable in practice because many states are either unmeasurable or very hard to obtain with acceptable precision. In the case of a synchronous generator, measurements of flux linkages are generally most difficult; some devices for measuring the rotor angle exist; however, control designers prefer to avoid the expense of installing this measuring device whenever possible.

Consequently, most of the feedback designs for power systems are based on output feedback instead of full state. This obviously reduces the performance of the designed feedback relative to the full-state-based design. One could view, for example, present state-of-the-art voltage regulators as an output-feedback problem. It should come as no surprise that a particular, not directly regulated,

state could destabilize under an output feedback that does not respond to this state directly. (Recall that ω becomes potentially unstable when the regulator gain K_A is high.)

The formulation of the basic optimal output feedback design [15] for a dynamic system

$$\begin{aligned}\dot{x} &= Ax + Bu + Dd \\ y &= Cx \\ y_m &= C_m x\end{aligned}\tag{12.14}$$

where y_m are the output variables available for measurement and y are output variables whose performance is of interest, is based on designing a control law of the form

$$u = -F y_m\tag{12.15}$$

so that a performance index

$$J_y = \frac{1}{2} E \left(\int_0^\infty (y^T Q y + u^T R u) dt \right)\tag{12.16}$$

is minimized. E in (12.16) stands for the expected value with respect to the disturbance vector d whose effect a controller should counteract.¹

It can be shown that Eq. (12.16) amounts to

$$J_y = \text{tr} [D^T K(F) D]\tag{12.17}$$

where $K(F)$ satisfies the Lyapunov matrix equation

$$K \tilde{A} + \tilde{A}^T K = -\tilde{Q}\tag{12.18}$$

and

$$\tilde{Q} = C^T Q C + C_m F^T R F C_m\tag{12.19}$$

The problem then becomes the one of minimizing J_y by choice of feedback matrix F . In theory, if system (12.14) is fully controllable and observable, it is possible to design optimal output feedback without deteriorating the performance of the states that are not directly controlled.

An example of this approach could be found in the pioneering work by Davison for a three-machine case [19]. It is essential to recognize that a straightforward use of optimal full-state or output-feedback design for systems with more than

¹ Typically only performance in response to a zero-mean, uniformly distributed disturbance d can be guaranteed; this does not include large unexpected outages in power systems.

one machine leads to the need for on-line communications among the machines. As will be discussed later, this leads to the question of the minimal coordination necessary to stabilize power-system dynamics and, furthermore, to the question of the effectiveness of a present-day decentralized generator control relative to a fully coordinated design. Although recognized, this issue has not been actively pursued in power systems until very recently, with the new influx of reliable, inexpensive phasor-measurement ideas [20] to [22].

12.3 GENERATION CONTROL OF POWER SYSTEMS UNDER STRESS

In order to make full use of control design for regulating and stabilizing power systems under stress, several questions should be studied. For purposes of control design, a power system is considered to be under stress when the implemented control is not capable of responding adequately to variations in operating conditions.

The main objective of primary control in the power industry has historically been to respond to relatively minor disturbances in an automated fashion and to stabilize the system to a prespecified regime, defined by the set points of the primary controllers. Primary control is inadequate when changes in system conditions exceed ranges for which the control is proven to meet this task.

This occurs in two qualitatively different scenarios: (1) when unexpected equipment outages occur, and/or (2) when demand patterns deviate significantly from the anticipated, causing the “normal” operating point to move far from the conditions for which primary controllers are tuned and expected to operate. The latter is caused by either unusually high or unusually light system load.

Both scenarios create challenges to the present state-of-the-art primary controllers that are typically based on constant-gain-control design, as described previously, and that are typically tuned to respond to deviations around the normal loading.

Initially, under an assumption that an unusual situation arises as a consequence of unexpected equipment outage, one must, at least in concept, attempt to relate to the control design necessary to prevent transient instability [6]. To design the “best” excitation control, it is necessary to identify some of the mechanisms by which excitation control impacts the system energy function and its component quantities of kinetic and potential energies. Some time-scale separations have been proposed that divide the objectives of controls acting on the transient time scale into distinct components. These could be the immediate postfault period in which the primary objective is to convert kinetic energy (KE) into potential energy (PE) effectively and the period following the first swing, during which the concern is to prevent the conversion of PE to KE and restore nominal equilibrium in a secure manner. It has been only recently that an attempt was made to propose metrics to quantify security-related control performance and provide design objectives [6]. Many challenges are identified in this work: finding the

most appropriate functions for expressing the system energy, generalizing the method to include a wider range of control devices, and providing a possible framework for deriving a more meaningful optimization of control design.

The general idea of allowing a postfault equilibrium to differ from the prefault value is potentially essential when attempting to maximize the effects of available control. Recently, this idea was formalized in Ref. [23]; a similar idea can be found in the study of general variable structure control based on a free-order switching concept [24,25].

In the second scenario, when significant deviations from expected conditions occur as a result of unusual generation or demand patterns, it may be more straightforward to design nonlinear control than in the case when topological changes take place as a result of equipment outage. Several nonlinear control techniques have recently been proposed for improved generator control [26,6,27,28,29].

12.3.1 Remaining Challenges in Designing Primary Control of Generators

Most of the early work on excitation systems and governor control is presented for the simple case of a two-bus power system. It is useful to understand control principles using the simplest topology first. To understand the challenge of designing this control, one must consider a general multimachine power system. In this case at least three basic issues arise:

1. Problems related to using a linear system design for controlling nonlinear dynamics.
2. Problems caused by the lack of or accuracy of state variable measurements; consequently, instead of full-state feedback, only output feedback is implemented.
3. Problems caused by a lack of coordination of primary controllers. A pragmatic, effective approach to the fast primary control of generators has so far been decentralized control.

It is critical to assess the performance of a particular design while keeping in mind that the issues just described are qualitatively different in nature, and that potential problems should be related to the correct causes. The reasons for introducing supplemental generator control in the form of a PSS even for a simple two-bus power system can be attributed to the first two issues. The problem of coordination of any primary controller (excitation systems, PSS), on the other hand, is primarily the question of the effectiveness of solely decentralized control designs in large-scale electric power systems, that is the third issue in the preceding list.

12.3.1.1 Problems Caused by Using Linear Control Design for Nonlinear Dynamic Systems It was shown in the analysis in Ref. [8], for example that an IEEE Type 1 voltage regulator could destabilize the frequency response of the closed-loop dynamics if the regulator gain is high. The analysis shows that this

only happens, however, when the system is regulated around operating conditions for which certain critical sensitivity parameters have signs opposite from the signs expected in normal operations. In particular, when parameters K_1 and K_3 defined in Refs. [15] and [8] change from being positive to negative, frequency instability could arise, caused by the high-gain voltage regulator attempting to maintain voltage regardless of the type of operating conditions.

It is critical for users of this control technology to realize that an IEEE-type exciter cannot be expected to regulate the terminal voltage of a generator over an arbitrary range of changes in operating conditions. Its coefficients are chosen to meet a certain performance level around a prespecified operating point; the coefficients of a linearized model of the plant being controlled closely represent the behavior of the nonlinear power system dynamics only in a relatively small range around the specified operating point. In other words, the main objective of this regulator is to stabilize terminal voltage in response to small changes.

This problem is clearly identifiable with the problem of designing constant gain control assuming that a linearized model does not change significantly, an assumption that cannot be generally made for nonlinear dynamic systems. This type of problem could be dealt with in practice either (1) by understanding that a constant gain controller performs well only in response to relatively small perturbations in operating conditions away from those for which the linearized model was obtained, or (2) by designing controllers capable of responding as expected within a wider range of changes in operating conditions. Several newly proposed methods for voltage and frequency control of generators based on control design for nonlinear systems are described in Section 12.3.2, devoted to primary controls for abnormal (emergency) operating conditions. It is also possible to approach this design as a problem of simultaneous stabilization of (linear) systems with multiple operating conditions Ref. [30].

12.3.1.2 Problems Related to the Type of Measurements Available: Output versus Full-State Feedback The simplest way to consider this issue is for the case of a single-machine infinite-bus system, since the system states are identical to the states of the machine (subsystem). Therefore, no coordination questions among the machines (subsystems) arise. The main objective of the output control design is to design F in Eq. (12.15) so that no instability takes place, that is, so that a performance criterion of the form (12.12) is minimized. In Ref. [19] algorithms for determining optimal constant output-feedback gains can be found. Algorithms of this sort have not been applied directly to the generator control design yet. It is an important exercise prior to designing the controller of one's choice to check basic controllability and observability condition [31,32,33,40,41]. This is not done routinely in power systems, and it should be.

It has been shown in Ref. [34] that a PSS is a special case of an observer of the form

$$\dot{x}_s = D_2 x_s + D_1 y_m \quad (12.20)$$

which describes the behavior of a dynamic controller whose input is y_m and state is x_s . The optimal feedback controller of the form

$$u = -F_1 y_m - F_2 x_s \quad (12.21)$$

It follows then that a simultaneous PSS–voltage-regulator design is a special case of the control in Eq. (12.21), designing an observer to be used by a voltage regulator. This reference confirms that the fundamental reason for introducing a supplemental PSS is associated with the problem of insufficient observability when designing an output-feedback-based voltage regulator.

12.3.1.3 Problems Caused by Insufficient Control Coordination in Multimachine Systems It will be described in the later part of this chapter that many recently introduced techniques for nonlinear control design, notably feedback linearizing and variable structure control, are directly applicable to the full-state control design of electric power systems. Replacing the constant gain generator control design by these designs is likely to eliminate partially issues concerning the fact that a controller is required to respond in an effective way to a wide range of variations in operating conditions and that the straightforward optimal feedback for linear systems cannot respond to this request.

Generally the problem of output versus full-state feedback in the case of multiple-input–multiple-output (MIMO) systems is closely related to the third question of minimal real-time measurements for the control to perform satisfactorily. However, in large-scale dynamic systems, such as electric power systems in which individual subsystems have their own control, it makes sense to differentiate the two questions. The question of output versus full-state feedback is more applicable to the problem of single-subsystem control, whereas the question of minimal coordination concerns the amount of communication among different subsystems, often across geographical distances that are too great for the individual controllers not to misoperate when connected to the system. The latter is of direct interest here, under the assumption that all subsystems (A_i, B_i, C_i) are controllable and observable for the range of operating conditions of interest. A rather encouraging answer to this question can be found in the literature that is directly concerned with this general problem of structural controllability and observability of composite systems. With a composite system, one generally considers a system consisting of a number of subsystems interconnected in an arbitrary way. It is reported that a system (A, B, C) is structurally controllable and observable if and only if it is connectable and that a certain nonpathological rank condition holds. It would be useful to understand the implications of these theoretical results on basic controllability and observability of electric power systems. This approach is potentially simpler to use than to check basic controllability and observability conditions [12],[14] directly.² In Refs. [31,32] an illustration

² This is potentially very useful because reachability and observability of specific subsystems can be checked even for nonlinear models of electric power systems; the connectability condition is structural and is not a function of operating conditions.

of such a general approach to determining the controllability of nonlinear power systems is studied. More research is needed in this general area.

Several research efforts can be found that report on an entirely decentralized control design for multimachine power systems. Stabilization of system dynamics via such systems can only be guaranteed under certain conditions. An interesting application of the M -matrix theory used to establish stabilizability conditions for composite power systems is carried out in the literature Ref. [35]. It has been suggested here that a linearized dynamic model for the i th generator of a multimachine system introduced in Chapter 6 can be used for control design purposes as

$$\dot{x}_i(t) = A_{1i}x_i(t) + A_{2i}y_i(t) + B_iu_i(t) \quad (12.22)$$

where $y_i(t)$ is a local (to a machine i) output variable and it is generally expressed in the form³

$$y_i(t) = M_{ii}x_i(t) + \sum_{j=1, j \neq i}^n M_{ij}x_j(t) \quad (12.23)$$

where M_{ii} and M_{ij} are constant matrices. For the purposes of applying general results of this type from Ref. [35], the model in Eqs. (12.22) and (12.23) is restated as

$$\dot{x}_i(t) = A_i(t)x_i(t) + B_iu_i(t) + h_i(t) \quad (12.24)$$

with

$$h_i(t) = \sum_{j=1, j \neq i}^n A_{ij}x_j(t) \quad (12.25)$$

expressing the interaction terms that describe the effects of other machines on the i th machine, and $A_i = A_{1i} + A_{2i}M_{ii}$ and $A_{ij} = A_{2i}M_{ij}$.

The performance index for each subsystem i is

$$J_i = x_i^T(T)F_i x_i(T) + \frac{1}{2} \int_0^T [x_i(t)^T Q_i x_i(t) + u_i^T(t) R_i u_i(t)] dt \quad (12.26)$$

If P_i is the solution of the Riccati matrix equation for each machine i ,

$$A_i^T P_i + P_i A_i - P_i B_i R_i^{-1} B_i^T P_i + Q_i = 0 \quad (12.27)$$

a suboptimal control law of the form

$$u_i(t) = -R_i^{-1}B_i - A_i^T P_i x_i(t) - B_i^T (P_i B_i R_i^{-1} B_i^T - A_i^T)^{-1} P_i h_i(t) \quad (12.28)$$

³ Strictly speaking, this is only true for a model after nondynamic components, such as loads, have been suppressed.

is proven to stabilize the interconnected systems as long as

$$\max_i \lambda_M(P_i) \sum_{i=1}^n \sum_{j=1}^n \lambda_M^{1/2}(A_{ij}^T A_{ij}) \leq \frac{1}{2} \min_i \lambda_m(S_i) \quad (12.29)$$

where $S_i = P_i B_i R_i^{-1} P_i + Q_i$ and λ_M and λ_m are the maximum and minimum eigenvalues of the matrices of interest.

If machines (subsystems) are strongly coupled the term $A_{ij}^T A_{ij}$ is large enough so the condition (12.29) may not be met. In this case, the decentralized control (12.28) is not guaranteed to stabilize the interconnected system. An application of this result to a decentralized voltage-regulator design of multimachine power systems can be found in the literature. It would be interesting to test condition (12.29) for light- and heavy-load operations.

It is important to explore all possibilities for reliable decentralized control design first. The alternative is to provide real-time measurements and pursue optimal feedback design without any restrictions on coordination among the individual machines. Given the complexity of a typical power system, it is almost impossible to envision systemwide data exchange among all machines participating in control. Methods of projective controls introduced in Ref. [36] are potentially very useful for reducing the number of machines whose coordination is required.

Another interesting avenue to explore is to consider time-varying feedback laws for decentralized control when decentralized constant gain control is not effective. Much progress has recently been made in this general area of control; however, no applications to power systems have been tried out.

Finally, and potentially most interesting, is to view the question of decentralized feedback for power systems using ideas from Ref. [37]. This can be viewed as the problem of several control agents having nonidentical information on the system structure, state vectors, parameters, etc., being involved in controlling the same system. The questions of nonstandard information exchange among local controllers, such as the direct exchange of information among local agents and the implications of the pattern of information exchange on system performance, has not been studied much in the traditional hierarchical control of large-scale systems [38]. These aspects of decentralized control will have to be studied for power-system operations under competition in which the pattern of direct information exchange between only two parties is very typical.

12.3.1.3.1 Phasor Measurements as a Means of Coordination A qualitatively new approach to systemwide coordination in operating large interconnected power systems was recently introduced by assuming that fast, synchronized state measurements across such systems would be available in real time. Much progress has been made in developing these “phasor measurements” [20,21,22]. If such measurements are made readily available, the question of control coordination for stabilization and regulation becomes grossly simplified.

12.3.2 Nonlinear Control Design for Generators

To deal with the question of designing control for wide ranges of variations in operating conditions, there has been considerable exploratory work on nonlinear control design over the past several years. In this section, only two representative nonlinear control approaches are described as applied to power-system control. They are

1. Feedback linearizing control
2. Variable structure, or sliding mode, control

These are briefly described next.

12.3.2.1 Feedback Linearizing Excitation Control for Enhanced Power-System Stability The transformation used for feedback linearizing excitation control was developed in Refs. [39,40], and the details of this derivation are not repeated here. The model in the transformation is the third-order single-axis model (type II₃, Chapter 3). A new state space is then defined as

$$\underline{z} = T(\underline{x}) \quad (12.30)$$

where, for a system with N generators,

$$\underline{x} = [\delta_1 \omega_1 e'_{q1} \cdots \delta_N \omega_N e'_{qN}] \quad (12.31)$$

and

$$\underline{z} = [\delta_1 \omega_1 \dot{\omega}_1 \cdots \delta_N \omega_N \dot{\omega}_N] \quad (12.32)$$

After some algebraic manipulation, the state equations can be written in affine form

$$\begin{aligned} \dot{\delta}_i &= \omega_i \\ \dot{\omega}_i &= \alpha_i \\ \dot{\alpha}_i &= f_i(\underline{x}) + b_i(\underline{x})e_{fdi} \end{aligned} \quad (12.33)$$

where $f_i(\underline{x})$ and $b_i(\underline{x})$ are defined as

$$\begin{aligned} \underline{f}(\underline{x}) &= -\frac{\omega_0}{2H} \left([(x_q - x'_q)i_d + e'_q]\dot{i}_q + e'_d\dot{i}_d + \frac{D}{\omega_0}\dot{\omega} \right. \\ &\quad \left. - [(x_q - x'_q)i_d + e'_q]\frac{\partial i_q}{\partial e'_q}\dot{e}'_q - e'_d\frac{\partial i_d}{\partial e'_q}\dot{e}'_q \right) \\ &\quad + \frac{\omega_0}{2HT'_d} \left([x_q - x'_q)i_d + e'_q]\frac{\partial i_q}{\partial e'_q} + e'_d\frac{\partial i_d}{\partial e'_q} + i_q \right) \\ &\quad [e'_q + (x_d - x'_d)i_d] \end{aligned} \quad (12.34)$$

and

$$\underline{b}(\underline{x}) = -\frac{\omega_0}{2HT'_{d0}}[(x_q - x'_q)i_d + e'_q]\frac{\partial i_q}{\partial e'_q} + e'_d\frac{\partial i_d}{\partial e'_q + i_q}[e'_q + (x_d - x'_d)i_d] \quad (12.35)$$

We now define a *feedback linearizing control law*

$$e_{fdi} = \frac{1}{b(x)}[v(z) - f(x)] \quad (12.36)$$

and

$$v(z) = a_0(\delta - \delta_0) + a_1(\omega - \omega_0) + a_2\alpha \quad (12.37)$$

resulting in a linear closed-loop dynamic system in a block-diagonal form

$$\dot{x} = (A_1 \cdots A_N)x \quad (12.38)$$

with

$$A_i = \begin{bmatrix} 0 & 1 & 0 \\ 0 & 0 & 1 \\ a_{0i} & a_{01} & a_{02} \end{bmatrix} \quad (12.39)$$

This control effectively decouples machine dynamics from the dynamics of the system as a whole. From Eq. (12.37) it can be seen that the equilibrium point is well defined for ω and $\dot{\omega}$, but the reference angle δ_0 can be determined only by full-scale load-flow computation of the postcontingency conditions. Assuming for the moment that the proper angle reference can be found, the feedback linearizing controller (FBLC) allows for arbitrary pole placement via the choice of coefficients in Eq. (12.37), and the resulting subsystem is decoupled and not very sensitive to disturbances. It can be expected to operate predictably over a wide range of operating conditions, provided that an equilibrium exists within the operating constraints of the machine and the excitation system.

Since the feedback linearizing transformation brings the original nonlinear model into a controllable Brunovsky form, one can generally use any linear control design to chose coefficients in Eq. (12.37), that is to tune the FBLC Ref. [41,42]. A common linear quadratic Gaussian (LQG) optimal control approach is directly applicable to tuning the FBLC for a multimachine power system. Many recent references have appeared world wide on this subject, including the work in Refs. [26,27], which stressed a decentralized implementation.

12.3.2.2 Variable Structure Excitation Control for Enhanced Power-System Stability Another nonlinear control design potentially useful for enhancing power-system stability is variable structure control [42]. This is a discontinuous feedback control strategy that only depends on the sign of the sliding surface S . For a nonlinear system whose output variable is defined as $y = h(x)$, a typical

stabilization task is to maintain the output variable close to such sliding surface defined as

$$S = \{x \in \mathbb{R}^n | y = h(x) = 0\} \quad (12.40)$$

The control law is of the form

$$u = \begin{cases} 1 & \text{for } y \leq 0 \\ 0 & \text{for } y \geq 0 \end{cases}$$

A sliding regime is said to exist around a sliding surface, resulting in system stabilization, if for each operating point in the vicinity of S

$$\dot{y} = \begin{cases} \frac{\partial h}{\partial x} \dot{x} \leq 0 & \text{for } y \geq 0 \\ \frac{\partial h}{\partial x} \dot{x} \geq 0 & \text{for } y \leq 0 \end{cases} \quad (12.41)$$

Condition (12.41) is sufficient for the state to return to the sliding surface, and it simply reflects the fact that if the state is above the sliding surface, it should be driven towards it by decreasing its derivative, and vice versa.

The equivalent control $u_{eq}(x)$ Refs. [42,43,44] is defined as the continuous control once the state is on a sliding surface, that is

$$\dot{y} = \frac{\partial h}{\partial x} [f(x) + g(x)u_{eq}(x)] = 0 \quad (12.42)$$

and is

$$u_{eq}(x) = - \left(\frac{\partial h}{\partial x} g(x) \right)^{-1} \frac{\partial h}{\partial x} f(x) \quad (12.43)$$

It has been shown [43] that a sliding regime exists locally if and only if the equivalent control satisfies

$$0 \leq u_{eq}(x) \leq 1 \quad (12.44)$$

The ideal switching dynamics is

$$\dot{x} = \left[I - g(x) \left(\frac{\partial h}{\partial x} g(x) \right)^{-1} \frac{\partial h}{\partial x} \right] f(x) \quad (12.45)$$

It is also known that the sliding regimes are quite insensitive (robust) to the parametric changes provided that the following structural condition, known as matching condition, is met:

$$\gamma(x) \in \text{span } \{g(x)\} \quad (12.46)$$

where $\gamma(x)$ is the additive uncertainty in the system function $f(x)$ [43].

Recently, there have been extensive efforts to formulate variable structure control for the generation-based control designs [45,46,47].

12.3.2.3 Equivalence of Feedback Linearizing Control and Variable Structure Control: High Gain Control It has been shown in Ref. [48] that feedback linearizing control and sliding-mode control both belong to the class of so called high gain control. In particular, typical hardware implementation of FBLC uses power-electronic-based switching characteristic of sliding-mode-type control laws [47]. High gain control is generally suited to respond to large signal deviations in system dynamics. This is one possible intuitive explanation of the effectiveness of FBLC, for example, in stabilizing inter area voltage oscillations when the system is under stress [27,28]. Increased fundamental understanding of the potential role of high gain control in stabilizing power-system dynamics under stress is needed. At present, only particular designs are introduced and demonstrated to be more powerful than the standard AVR–PSS set of generators. Even carrying out this comparison can be difficult since the conclusions depend on how is an AVR–PSS set tuned. In general, establishing metrics for comparison of various control designs for generation-based control is very challenging Ref. [6]. These comparisons are usually done for particular cases of interest, and it is hard to establish conditions under which a high gain nonlinear control is more effective than the conventional PID control of an AVR–PSS set. As described before, the specific control law implemented plays only a partial role in achieving the effective control of the dynamics in an interconnected electric power system. Some other important factors are the choice of output variables controlled and the level of coordination of individual controllers.

12.3.2.4 On-line Stabilizing Control of the Large Power System Using Observation Decoupled State Space and Nonlinear Control Tools After major disturbances a large power system may be swinging system wide and so be in danger of breaking up with loss of service over wide areas. This leaves a need for means to lead a system which is swinging toward disintegration back to a normal stable and viable operating point. This need was long recognized and serious studies were conducted in the early and mid seventies to satisfy it. During that period the senior author and his colleagues proposed the concept of an observation decoupled (originally called local) state space [49] to guide the system back to security. The theory of such a transformation and its properties were developed rigorously for control of the individual machines [50,51] and coherent dynamic clusters [52,53] and a summary in matured presentation was offered in the Special Issue on FACTS of the Int. J. on Energy and Power Systems [72]. The limiting factor for its wide use at the time was the absence of flexible control tools. Flexible tools, mostly thyristor based, are currently under development by major manufacturers stimulated by the current FACTS movement in the power industry. As described above, theory of large nonlinear control system (e.g. linearization by nonlinear feedback) also made major strides.

In this new climate the observation decoupled transformation becomes a major resource of effective new solutions. Such developments are indeed progressing.

Results of a major industrial study for a 5000 bus system will be briefly discussed at the end of this summary.

Here we summarize the theoretical foundations, properties, and practical potential of the observation decoupled concept. This development introduces for large, nonlinear systems with a network structure such as the power system a specific transformation of the customary state space $Z = \{z\}$ into an *observation decoupled* state space $Z_e = \{z_e\}$. This transformation is diffeomorphic under proper and practical assumptions including that the generators are modeled by the classical model of Type IV, in Chapter 3 (as proven in Refs. [49,50]), so the two spaces are equivalent.* Individual state vector of the two are distinct everywhere except at the stable equilibria where their coordinates coincide pair by pair for each state variable. Furthermore in the customary state space states are directly associated with specific physical quantities at specific locations. Hence the observation decoupled state, z_e , of the system can be treated as a moving target (without direct physical identity) to be tracked by the physical state z . When z catches up with z_e at each of the states z_i then the system is at its stable equilibrium. No knowledge of the equilibrium state is needed during the tracking process. This is of great practical importance because the equilibrium state cannot be computed or otherwise located on the time scale where it is needed—but the tracking finds it anyway. Even better, because of the structure of the power system model, subsets z_{ei} of the target state z_{el} connected with a particular bus (node) can be computed at the local bus i using information which can be measured at this local bus itself. So z_e is decoupled as far as its observation is concerned. The tracking process itself is not so decoupled hence a fully optimal tracking control needs to be done centrally. However because of the network structure, the controls u_i within the subsets z_i associated with bus i dominate the process of tracking. Hence good suboptimal tracking control can be designed which operates entirely locally that is within subset z_i associated with bus i . This means decoupled operation and control.

12.3.2.4.1 Basic Characteristics of the Model of the Power System Recall from Chapter 4 that a general model of a large power system has a particular structure. Its dynamics was shown to be modeled by parameter dependent differential-algebraic equations of the form

$$\sum: \quad 0 = f(x, \dot{x}, y, u), \quad f: \mathbb{R}^{n+m+p} \rightarrow \mathbb{R}^n \quad (12.47)$$

$$0 = g(x, y, u), \quad g: \mathbb{R}^{n+m+p} \rightarrow \mathbb{R}^m \quad (12.48)$$

$$x \in X \subset \mathbb{R}^n, y \in Y \subset \mathbb{R}^m, u \in P \subset \mathbb{R}^p$$

where functions f and g are smooth and \dot{x} can be given explicitly in f .

* This is an approximate model so computations and conclusions based on it are not of high accuracy. High accuracy, however, is not required to actually track the system back to a stable equilibrium. As long as the moving target is in the region of attraction of a stable equilibrium, the approach is effective.

In the state space $X \times Y$ dynamic state variables x and instantaneous state variables y are distinguished, $z = \{x, y\}$ $Z = \{X, Y\}$. The dynamics of the states x is directly defined by (12.47) while the dynamics of the y variables is such that the system satisfies the constraints (12.48). The controls produce inputs u into the buses. Recall from Chapters 3, 4 and 6 that typical dynamic state variables x are the time dependent values of generator internal voltages and rotor phases, instantaneous variables y are bus voltages and other load flow variables. Typically state variables have direct physical meaning associated with a specific location on the system (e.g. bus i voltage: rms magnitude and phase angle). Furthermore, in the network structure dynamic variables x_i of equipment (such as generators) connected to a bus are not directly coupled to any equipment at other buses. Each generator bus has its own specific stabilizing control input u_i . Note that dynamics of normal state operating controls (e.g. excitation control or turbine governor) are incorporated in the f set where they have their own equations and own dynamic states x .

Exploiting this structure (12.47)–(12.48) can be equivalently restated as

$$h(x, \dot{x}, y, u) = 0 \quad \text{where} \quad (12.49)$$

$$h_i(x_i, \dot{x}_i, y_i, C_{ij}y_j, u_i) = \{f_i(x_i, \dot{x}_i, C_{ij}y_j, u_i), C_{ij}g_i(x_i, y_i, C_{ij}y_j, u_i)\} = 0 \quad (12.50)$$

where $C_{ij} = 1$ only if buses i and j are directly connected and 0 otherwise, thus $C_{ij}y_j$ are the instantaneous states of neighboring buses j connected to bus i directly.

Note that in h_i each bus i and all buses j connected to it are displayed as a separate group of equations. Note that x_i, \dot{x}_i, u_i will occur only in one set, that is in h_i . The y_i will appear in other equations h_j where $C_{ij} = 1$ so to this extent the h_i are interconnected.

But (12.49)–(12.50) is simply a rearrangement of (12.47), (12.48) and readily reduces back to it.

Physically h_i could be interpreted simply as a statement of the dynamic problem for one bus i and its associated equipment at a time given the phasor voltages at the neighboring buses and the control input u_i .

Systems Σ where such rearrangement is possible are suggested to be called *sectional*.

12.3.2.4.2 Definition of the Observation Decoupled State Space

Now make the following assumptions;

1. Each h_i will be considered separately.
2. $C_{ij}y_j$, that is the neighboring bus voltages, are known at bus i and expressed on the local phase reference of y_i
3. Assume that the neighboring bus voltages, $C_{ij}y_j$, can be determined from local measurements at bus i . This characteristic is called *observation decoupled*. It is assured in case of the power system by using local voltage and current measurements and knowledge of transmission line characteristics.

So far this is still equivalent to (12.47)–(12.48) provided all i buses are covered by $h \in \mathbb{R}^m$ and the measurements are exact.

Note however that the equilibrium state, z_0 of the system is defined by the equation

$$h(x_0, \dot{x}_0 = 0, y_0, u_0 = 0) = 0$$

Even if information on the current status and composition of the system were instantly available at the control center (which is not quite true) it would still require an enhanced load flow solution to find equilibrium z_0 . This is impractical on the time scale demanded by the stabilizing controls. This problem is often ignored in the literature, but it is verified by the statements made in a large industrial study, Refs. [7,27]. To break this impasse a transformation is introduced next which produces a transformed state z_e obtainable in local segments at each bus i (hence observation decoupled). State z_e , as will be explained, can serve as a moving target. When it is tracked (centrally or, as an approximation, locally, segment wise, at each bus i) successfully with the system state z being guided to $z = z_e$ it produces also $z = z_0$. Hence successful tracking of z_e leads the system to its stable equilibrium without knowing where it is until formed by tracking z_e . This motivates the following.

DEFINITION 12.1 *The local segment of the observation decoupled reference vector*

$$z_{ei} = \{x_{ei}, y_{ei}\}, i = 1, 2, \dots, m \quad (12.51)$$

is defined by

$$h_i(x_{ei}, \dot{x}_{ei} = 0, y_{ei}, C_{ij}y_j, u_i = 0) = 0 \quad \forall z_{ei} \in Z_C \quad (12.52)$$

where

$$Z_C = \{z_{ei} | z_{ei}^l \leq z_{ei} < z_{ei}^h\} \quad (12.53)$$

where m is typically the number of the buses (two equations in g_i at each bus i for active and reactive power balance respectively) and Z_C is a set of constraints.

Note that formally z_{ei} would be the equilibrium of x_i and y_i in the static condition $\dot{x}_i = 0$ with no on line stabilizing control $u_i = 0$. However such an interpretation has no physical meaning unless $z_{ei} = z_i$ for all i . It is meaningless to refer to z_e as stable or unstable.

Note also that in z_e in (12.51) to (12.53) x_{ei}, y_{ei} are states (same dimension as x_i, y_i). $C_{ij}y_j$ play the role of inputs into (12.51) to (12.53) in this definition.

The concept of observation decoupled reference has some properties which can make it exceptionally useful. These properties will now be stated.

PROPERTY 1. Individual segments or subspaces z_{ei} of Z_e belong to each bus i . All individual z_{eik} within the local segment z_{ei} can be computed entirely from measurements taken locally (at bus i). First $C_{ij}y_j$ are computed from measurements and line data at bus i (these are not states in z_{ei}), then x_{ei}, y_{ei} are computed from $C_{ij}y_j$ with (12.51) to (12.53). (these are the states in z_{ei}).

PROPERTY 2. The observation decoupled vector space $z_e = \{x_e, y_e\}$ exists uniquely if the constraints are properly selected (e.g. phase of y_i is less than $\frac{\pi}{2}$) and is diffeomorphic to the state vector $z = \{x, y\}$. So (12.51) to (12.53) defines a transformation

$$T_z \leftrightarrow z_e \quad (12.54)$$

and establishes z_e as a precise equivalent of the state z .

PROPERTY 3. If an equilibrium state $z_0 = \{x_0, y_0\}$ exist within the constraints set, $Z_E, \forall i$, then $z_{oi} = z_{ei}, \forall i$, and z_{ei} exists. The system is in equilibrium.

These properties were rigorously proven (for a system model using the “classical” generator dynamics and impedance loads) in a set of theorems and lemmas in Refs. [49,50]. The proof is nontrivial because (12.52) is an implicit function.

12.3.2.4.3 Stabilizing Control Based on Tracking the Observation Decoupled Reference It follows from these properties that the system state z will coincide with the observation decoupled reference z_{ei} at all i (at each bus) only when the system is at a stable and viable equilibrium z_0 (i.e. an equilibrium within the constraint set z_e) that is $z_{oi} = z_i, \forall i$, if and only if z_0 is a stable equilibrium. This establishes z_e as a *moving target vector* in the state space. If this target is being successfully tracked by the system state to coincidence by properly using the stabilizing controls u_i then the system has reached a stable and viable equilibrium *without any need to know its location* during the control process.

The later fact is very important. Other proposed approaches usually make the assumption that the stable operating equilibrium is known and the stabilizing control simply needs to guide the system to it. However this assumption in most cases will not be satisfied. The disturbance usually changes the system composition or its loading or generation so the original equilibrium would not be applicable to the post fault system. A new equilibrium target needs to be computed from the post fault system data but those would not be usually available fast and precisely enough mostly because the entire control event may last only a couple seconds so z_0 would be needed in something like 10 m seconds.

Recall from Chapter 3 that currently there is a movement for flexible equipment and non linear control theory using power electronic switching in the power industry. This opens up an entirely new environment for this approach. In fact work along these lines is progressing and it is bearing fruit as briefly summarized next.

12.3.2.4.4 An Industrial Level Large Scale Simulation Study on Stabilization with Observation Decoupled Target Tracking Using New Nonlinear Control Technology Recently [7,27] MIT and the New York Power Pool conducted an intensive simulation study on a very large (5000 bus) model of the Northeast Power Coordinating System to evaluate an on line stabilizing control technique which tracks a form of the observation decoupled moving target with a control system

using the recently developed linearization by nonlinear feedback technique with decentralized reference coordinates (DRC). The extensive tests were quite successful in proving the effectiveness of the method. It will be only possible in this summary to give two brief quotations from Ref. [7,27]. More details can be found in the full papers.

"the determination of the proper rotor reference angle would normally require the equivalent of a full-scale load-flow calculation, updated continuously. This is obviously not practical in real time. An alternative method of generating a reference angle is the decentralized reference calculation or DRC (referred to as the ODSS calculation in [7]), which provides a moving reference angle, calculated using local measurements, that converges to the desired reference as the DRC is iterated. One very important characteristic of the DRC is that it allows the measurement of voltage phasors and the rotor angle with respect to a locally-produced 60-Hz reference, so that no centralized reference signal is required for these measurements."

and from the conclusion of Ref. [27].

"the ability of the FBLC/DRC to hold the system together following an extreme multiple fault seems to be an unequivocal advantage, provided that the rise in steady-state terminal voltage that was seen is not a problem in the more moderate situations. Our experience has been that it is not, however more exhaustive testing of this phenomenon is called for."

All of which indicates that in the new environment of flexible tools and sophisticated control theory the moving target of the observation decoupled reference is emerging as a valuable foundation of system stabilization, under stress.

12.4 FACTS-BASED TRANSMISSION SYSTEM CONTROL

If one considers a typical electric power system consisting of a relatively small number of large electric machines supplying a much higher number of loads, it becomes intuitively clear that under certain operating conditions the interconnected system may experience lack of adequate control. This is particularly pronounced when major loads are electrically distant from the controlled generation. In the case of poorly damped power-system dynamics, any minor disturbance could cause the machine angles to oscillate around their steady-state value at a natural frequency of the electromechanical system.

This general concern for potential oscillations leads to system design such that for the anticipated normal operation, the system is well within its stability margins. This results in a certain underutilization of the existing transmission facilities. This general lack of adequate control is also reflected through the fact that with the conventional generation-based control technologies it is almost impossible to control the power flow fully through a specific transmission path as desired.

Electrical distances between generation and load have been typically reduced in the past by adding new transmission lines where necessary. With the impediments for building new transmission lines due to economic and environmental

constraints, this is no longer possible. It is for these reasons primarily that FACTS technologies are beginning to play a major role in enhancing system performance, and although still expensive, are often justifiable. FACTS devices described in Chapter 3 enable fast power electronic based modulation of parameters at various locations of the transmission system, including loads. Whereas conventional AC electric power systems are not easily controlled to direct the flow of power, some of the FACTS devices and HV-DC transmission are ideally suited for this purpose. FACTS technology makes the vision of a controlled power-flow mode, or the concept of an electric valve on a transmission line, a reality. FACTS includes solid-state means for phase-angle, impedance, and voltage control. The possibility of changing the transmittable power by transmission-line series compensation also implies a potential application of these devices for damping of power-system oscillations.

In this section we consider control design aspects of FACTS devices and their potential impact on the dynamic performance of the system. We first briefly analyze the impact of one of the most mature power electronic based controls, that is, a static Var compensator (SVC) on the steady-state and dynamic performance of the system.

12.4.1 Static Var Compensator as a Control Means

Recall from Chapter 3 that an SVC is a shunt thyristor controlled reactance, connected between ground and bus i with the objective of regulating its voltage magnitude. This is done, for example, by having a fixed-capacitor–thyristor-controlled reactor (FC-TCR) and varying the firing angle of the TCR in such a way that the bus voltage magnitude is regulated to within a threshold of its desired set value.

Its primary objective is to increase power transmission capability with a given transmission network from the generators to loads. An SVC does not generate or absorb reactive power; real-power transfer is affected indirectly through voltage control. The reactive-power output of an SVC is varied to control the voltage at given terminals of the transmission network so as to maintain the desired power flow under possible system disturbances and contingencies. Because of its high cost, it is expected that this device would be effective particularly when the system is subject to large disturbances, that is, for transient stabilization in addition to small-signal stabilization.

A thorough analysis showing how are these goals achieved can be found in Refs. [54,55]. As with all other controls, the analysis is typically presented only for the simplest two-bus power system. Here only a very brief summary of the principles on which two-bus system regulation rests is given first. More emphasis is set on the systems control aspects in a general power system.

12.4.1.1 Impact of an SVC on the System Stability Limit Here we briefly assess the impact of the SVC on a system's steady state, small signal, and transient stability. Consider, as in Ref. [55], an SVC located in the middle of a transmission line connecting buses 1 and 2. Recall from Section 4.2 the definition of a steady-state stability limit for a two-bus power system. The maximum power that can

be transferred from a sending bus 1 to a receiving bus 2 is

$$P_2^{\max} = \frac{E_1 E_2}{X} \quad (12.55)$$

Now, consider an SVC placed in the middle of a transmission line between buses 1 and 2, regulating voltage E_m to the fixed value. Now, the maximum real power transferable from bus 1 to bus m is

$$P_m^{\max} = \frac{E_1 E_m}{X/2} \quad (12.56)$$

and the maximum real power transferable from bus m to bus 2 is

$$P_m^{\max} = \frac{E_m E_2}{X/2} \quad (12.57)$$

It can be seen by comparing Eqs. (12.55) and (12.57) that the maximum power transferred to the receiving bus 2 has almost doubled if the voltage magnitude at bus m is regulated as being as close as possible to E_1 . The basic effect of an SVC on improving small-signal stability (damping) is more involved [55]. To see this, start with the basic equation in Table 3.3 of Chapter 3:

$$M \frac{d^2\delta}{dt^2} = P_T - P_e \quad (12.58)$$

It is assumed here that the mechanical power P_T does not change in response to a small-signal disturbance within the time interval of interest. Therefore, the dynamics of the rotor angle δ can only be influenced by changes in ΔP_e ,

$$\Delta P_e = \frac{\partial P_e}{\partial E_1} \Delta E_1 + \frac{\partial P_e}{\partial E_m} \Delta E_m + \frac{\partial P_e}{\partial \delta} \Delta \delta \quad (12.59)$$

Assuming that generator at bus 1 has a fast voltage regulator, the change in this voltage is $\Delta E_1 = 0$; similarly, if the SVC maintains voltage E_m so that $\Delta E_m = 0$, there is no effect of voltage regulation on small-signal stability. Therefore, in order to make the power oscillations damped, the midpoint voltage E_m must be varied as a function of $d\delta/dt$, that is,

$$\Delta E_m = K \frac{d\delta}{dt} \quad (12.60)$$

The swing equation (12.58) with the SVC closed-loop control (12.60) takes on the form

$$M \frac{d^2\delta}{dt^2} + \frac{\partial P_e}{\partial E_m} K \frac{d\delta}{dt} + \frac{\partial P_e}{\partial \delta} = 0 \quad (12.61)$$

whose characteristic equation is

$$S^2 + 2\zeta s + \omega_0^2 = 0 \quad (12.62)$$

and

$$\omega_0 = \sqrt{\frac{1}{M} \frac{\partial P_c}{\partial \delta}} \quad (12.63)$$

With the assumed $P_T = \text{const}$, $d\delta/dt$ can be expressed from Eq. (12.59) as a function of transmitted electric power

$$\frac{d\delta}{dt} \sim \int \Delta P_e dt \quad (12.64)$$

Finally, an SVC has a positive effect on transient stabilization, which is simply due to the increase in steady-state stability limit [55].

12.4.1.2 Thyristor-Based Control as a Variable Structure Control Problem

It is well recognized in low-power applications that the power-electronic-based switching offers an excellent means for implementing so called variable structure (or sliding-mode) control (VSC) [42]. As a matter of fact, while the theory of VSC was introduced long ago, its use has been rather limited prior to the emergence of fast switching technologies. Here we set stage a for variable structure control model of an SVC first. Recall (Chapter 3) that a FC-TCR is controlled in such a way as to make the SVC a controllable shunt reactance defined as follows:

$$X_C = -\frac{1}{u} X_{\text{SVC}} \quad (12.65)$$

where X_{SVC} is the SVC reactance rating and $u \in [u_{\min}, u_{\max}]$ is the control variable (when the inductive and capacitive SVC ratings are equal, $u_{\min} = -1$ and $u_{\max} = 1$) [56].

The problem of optimal switching of an SVC becomes the problem of optimizing the performance criterion of choice with respect to u . In Ref. [56] this is defined as the problem of designing $u \in [u_{\min}, u_{\max}]$ for a dynamic system:

$$\begin{aligned} \dot{\delta} &= \omega \\ \dot{\omega} &= \frac{1}{J} P(\delta, u) \end{aligned} \quad (12.66)$$

so that, for example the transient-stability margin defined by the area enclosed by the power-transfer characteristic above the steady-state power-transfer level given as

$$E_s = \int_{\delta_s}^{(\pi - \delta_s)} [P(\delta) - P(\delta_s)] d\delta \quad (12.67)$$

is maximized.

12.4.1.3 Effect of Capacitors, Phase Shifters, and other FACTS Connected in Series As described in Chapter 3, another possible way to modulate properties of the transmission grid is by means of electronic-power-modulated reactive devices (reactances, capacitors connected in series with the transmission lines). The most important representatives in this group are series capacitors and phase-shifting transformers. An analysis similar to the analysis of the effects of an SVC on system stability could be made to understand the effect of FACTS devices connected in series with transmission lines.

It is fairly straightforward to understand that when a series capacitor is placed in series with a primarily reactive transmission line, the effective reactance of the line is much smaller, resulting in a reduced electrical distance between the buses to which the line is connected. At first sight, this effect is similar to that seen when connecting an SVC in the middle of a transmission line. However, recall from Chapter 5 that the most effective way of changing the characteristics of a transmission line is by adding a series compensation. Consequently, this type of controlling the transfer capabilities of lines has been of great interest over some time. It has been only recently that the actual use of series compensation has increased after improvements in protection systems based on metal oxide arresters and triggered air gap Refs. [2] to [7], [56].

12.4.1.4 Average modeling of FACTS devices In this section we draw reader's attention to the recent modeling work in Refs. [57] to [59]. While power electronic based switching forms the basis of a variety of low power electronics devices, as well as, of more recently, higher power FACTS devices, their modeling and control present an interesting challenge because of the inherent discontinuous on—off thyristor control (Chapter 3).

The problem of power conversion in electrical networks has attracted attention in the systems control community for quite some time, as reportedly, notably in the early work in Ref. [60].

FACTS devices are generally intended to aim to take advantage of the rather fast (single cycle) controllability of these devices, directly contributing state dynamics to the model. In [58] the phasor dynamics approach is used to develop simple, natural and powerful models for a major FACTS component, the thyristor—controlled series capacitor (TCSC). The model leads to improvements by factors of around 30 in simulation times for transients of interest, compared with EMTP (Electromagnetic Transient Program)-style simulations, Ref. [2]. This improvement is obtained by focusing on the dynamics of the voltage and current phasors rather than dealing with instantaneous voltages and currents (the EMTP extreme) or quasi-static voltage and current phasors (treated algebraically, via impedance—domain computations).

The phasor dynamics model of the TCSC is well—structured, involving the same phasor quantities that are used to characterize other power system components, particularly generators. This model opens up several possible avenues for non-linear, large-signal control design. The work in [61] shows how phasor dynamics models can be effectively used for the analysis of subsynchronous

resonance problem and the effect of feedback linearizing control in eliminating this problem. Much more work is needed toward systematic FACTS-based control design. The modeling described here naturally lends itself to incorporating the effects of FACTS on the generator dynamics.

We provide next an example of typical modeling of the type described; this example was fully contributed by the MIT graduate student Vahe Caliskan. This example illustrates the averaged modeling of FACTS (Flexible AC Transmission Systems) devices. The concepts of generalized averaging go hand-in-hand with the time-varying phasor approaches. Here we will utilize the Fixed Capacitor Thyristor Controlled Reactor (FC-TCR) to illustrate the modeling concepts and provide some insights into the modeling and what it provides. The FC-TCR is one of many static VAr compensators that appear in either series or shunt. The ultimate goal is to be able to capture the dynamics of the model which can then be used in standard data flow simulation languages such as MATLAB, Ref. [18].

12.4.1.4.1 FC-TCR Model The circuit diagram for the Fixed Capacitor Thyristor Controlled Reactor (FC-TCR) is shown in Figure 12.6. It consists of a fixed capacitor C , inductor L and a pair of anti-parallel thyristors Q_1 and Q_2 . The thyristors are controlled by varying their firing angle α . The thyristors are usually activated by sending a short pulse of current into their gate terminals. If the anode to cathode voltage of a thyristor is positive when the gate current is applied, it will turn on. Thyristor turns off much like a diode, that is, when its anode to cathode voltage tries to reverse. As can be seen in Figure 12.6, the line voltage $v(t)$ is taken as the reference signal and the control angle α is measured with respect to the peak of this voltage. One can easily see from this diagram that α must satisfy the following inequality:

$$0 \leq \alpha \leq \pi \quad (12.68)$$

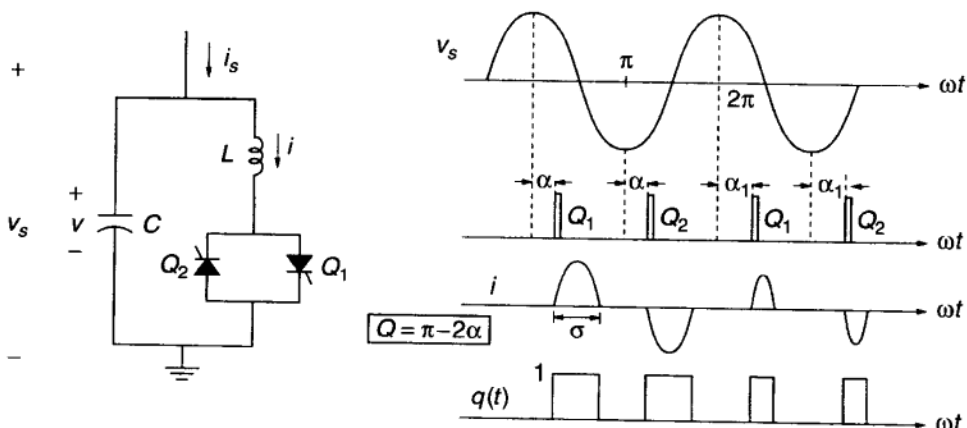


FIGURE 12.6 Modeling an FC-TCR.

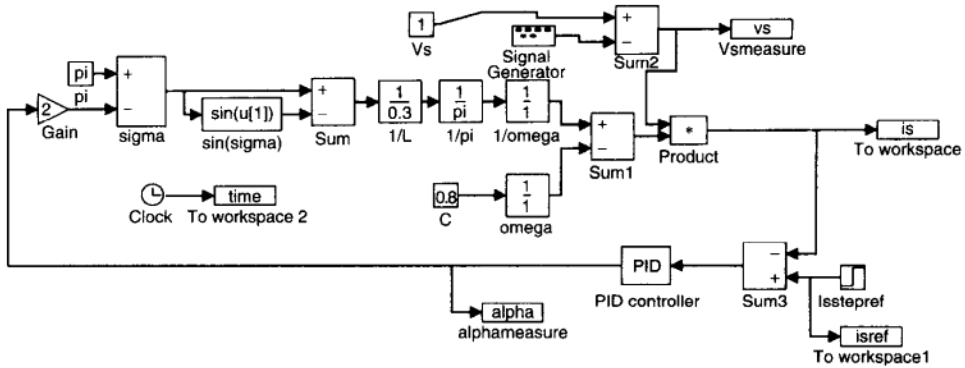


FIGURE 12.7 Simulation diagram for FC-TCR.

Based on the circuit diagram and the waveforms shown in Figure 12.6, it is quite straightforward to write down the governing differential equations for this system:

$$\frac{di(t)}{dt} = \frac{1}{L}[q(t)v(t)] \quad (12.69)$$

$$\frac{dv(t)}{dt} = \frac{1}{C}[i_s(t) - i(t)] \quad (12.70)$$

In the above description of the system, $i(t)$ is the inductor current, $v(t)$ is the capacitor voltage, $i_s(t)$ is the composite current in the FC-TCR. There also is a binary switching signal $q(t)$ which is unity when either Q_1 or Q_2 is on and is zero otherwise. The above set of equations is interesting since we have a sort of hybrid system. That is, the state variables $v(t)$ and $i(t)$ are continuous-time whereas the signal $q(t)$ (which may be considered as the control input) is a discrete-time variable.

12.4.1.4.2 Review Of Frequency-Selective Averaging In this section, we review some of the results of frequency-selective averaging and their implications [57]–[59], [62]. This averaging method is based on the representation of a signal $x(t)$ on the interval $[t - T, t]$ by the Fourier series

$$x(t - T + \tau) = \sum_{k=-\infty}^{\infty} \langle x \rangle_k(t) e^{jk\omega(t-T+\tau)} \quad (12.71)$$

where $\omega = 2\pi/T$ and the $\langle x \rangle_k(t)$ are the complex Fourier coefficients. Notice that these coefficients are functions of time and are given by

$$\langle x \rangle_k(t) = \frac{1}{T} \int_{t-T}^t x(\tau) e^{-jk\omega\tau} d\tau \quad (12.72)$$

The k th coefficient of the Fourier series is also referred to as the *index- k* average or the *k -phasor*. To reconstruct $x(t)$ from its Fourier coefficients, we can use Eqn. (12.71) with $\tau = T$, giving the following expression:

$$x(t) = \langle x \rangle_0 + 2 \sum_{k=1}^{\infty} (\Re\{\langle x \rangle_k\} \cos(k\omega_s t) - \Im\{\langle x \rangle_k\} \sin(k\omega_s t)) \quad (12.73)$$

where we have dropped the time argument from the $\langle x \rangle_k$, for notational simplicity. In (6), $\Re\{\langle x \rangle_k\}$ and $\Im\{\langle x \rangle_k\}$ refer to the real and imaginary parts of $\langle x \rangle_k$, respectively. Note that the classical state-space average can be derived [62] by considering the one-cycle averaged model of the state variable $x(t)$, given by

$$\langle x \rangle_0(t) = \frac{1}{T} \int_{t-T}^t x(\tau) d\tau \quad (12.74)$$

where T period; this average is nothing more than the DC term of the Fourier series representation.

There are two key properties that allow us to apply the procedure of frequency-selective averaging. The properties relate to: (i) differentiation of the index- k average with respect to time, and (ii) computation of the index- k average of the product of two signals. We discuss these properties in the next two subsections.

A. Differentiation with Respect to Time

The derivative with respect to time of the k th coefficient of the Fourier series can be calculated by the following formula, which is easy to verify:

$$\frac{d\langle x \rangle_k(t)}{dt} = \left\langle \frac{dx}{dt} \right\rangle_k (t) - jk\omega_s \langle x \rangle_k(t) \quad (12.75)$$

For linear circuit elements such as resistors, inductors and capacitors, the implications are very clear:

$$\langle v \rangle_k = R\langle i \rangle_k \quad (12.76)$$

$$\langle v \rangle_k = L \frac{d\langle i \rangle_k}{dt} + jk\omega_s L \langle i \rangle_k \quad (12.77)$$

$$\langle i \rangle_k = C \frac{d\langle v \rangle_k}{dt} + jk\omega_s C \langle v \rangle_k \quad (12.78)$$

B. Computation of Average of Product

The index- k average of the product of signals $x(t)$ and $q(t)$ can be computed by the following (discrete convolution) relationship:

$$\langle qx \rangle_k = \sum_{i=-\infty}^{\infty} \langle q \rangle_{k-i} \langle x \rangle_i \quad (12.79)$$

Consider the case where $q(t)$ and the variable $x(t)$ can be well approximated by the sum of their index-0 and index-1 averages (DC + fundamental), with all other index- k averages assumed negligible:

$$\begin{aligned} q(t) &\approx \langle q \rangle_0 + \langle q \rangle_{-1} e^{-jw_s t} + \langle q \rangle_1 e^{jw_s t} \\ x(t) &\approx \langle x \rangle_0 + \langle x \rangle_{-1} e^{-jw_s t} + \langle x \rangle_1 e^{jw_s t} \end{aligned} \quad (12.80)$$

Applying (12.79), we get the following expressions for various averages of the product:

$$\langle qx \rangle_0 = \langle q \rangle_0 \langle x \rangle_0 + \langle q \rangle_{-1} \langle x \rangle_1 + \langle q \rangle_1 \langle x \rangle_{-1} \quad (12.81)$$

$$\langle qx \rangle_1 = \langle q \rangle_0 \langle x \rangle_1 + \langle q \rangle_1 \langle x \rangle_0 \quad (12.82)$$

$$\langle qx \rangle_{-1} = \langle q \rangle_0 \langle x \rangle_{-1} + \langle q \rangle_{-1} \langle x \rangle_0 \quad (12.83)$$

In what follows, we shall assume that all other index- k averages of the product are negligible. Here we have to note that quantities representing the fundamental components, for example $\langle x \rangle_1$ and $\langle q \rangle_{-1}$, are in general complex quantities. Furthermore, positive and negative indices are complex conjugates of each other. Mathematically, we have

$$\langle q \rangle_1 = \langle q \rangle_1^R + j\langle q \rangle_1^I = \langle q \rangle_{-1}^* = (\langle q \rangle_{-1}^R + j\langle q \rangle_{-1}^I)^* \quad (12.84)$$

$$\langle x \rangle_1 = \langle x \rangle_1^R + j\langle x \rangle_1^I = \langle x \rangle_{-1}^* = (\langle x \rangle_{-1}^R + j\langle x \rangle_{-1}^I)^* \quad (12.85)$$

where the superscripts R and I denote the *real* and the *imaginary* parts of the defined quantities and $(*)$ denotes complex conjugation. Using these facts, it is easy to show that

$$\langle qx \rangle_0 = \langle q \rangle_0 \langle x \rangle_0 + 2(\langle q \rangle_1^R \langle x \rangle_1^R + \langle q \rangle_1^I \langle x \rangle_1^I) \quad (12.86)$$

$$\langle qx \rangle_1^R = \langle q \rangle_0 \langle x \rangle_1^R + \langle x \rangle_0 \langle q \rangle_1^R \quad (12.87)$$

$$\langle qx \rangle_1^I = \langle q \rangle_0 \langle x \rangle_1^I + \langle x \rangle_0 \langle q \rangle_1^I \quad (12.88)$$

C. Implications of Averaging

In most cases, $q(t)$ is a binary switching function and $x(t)$ is a state variable such as a capacitor voltage or an inductor current. The first of the above expressions is useful in the index-0 model, whereas the last two are necessary for constructing the index-1 model. In PWM converters, one usually is interested in the index-0 models, namely the average values of the state variable. In resonant converters and FACTS devices, however, one is usually interested in the index-1 models since these models describe the evolution of the amplitudes of the state variables. This fits in well with the concept of time-varying phasor analysis. We will now apply generalized averaging to the FC-TCR.

12.4.1.4.3 Application Of Frequency-Selective Averaging Taking the index-1 averages of our FC-TCR state equations results in the following *complex* differential equations:

$$\frac{d\langle i \rangle_1}{dt} = -j\omega\langle i \rangle_1 + \frac{1}{L}\langle qv \rangle_1 \quad (12.89)$$

$$\frac{d\langle v \rangle_1}{dt} = -j\omega\langle v \rangle_1 + \frac{1}{C}(\langle i_s \rangle_1 - \langle i \rangle_1) \quad (12.90)$$

This differential equation describes the evolution in time of the fundamental component of the *Complex Fourier Series*. We can now simplify $\langle qv \rangle_1$ by noting that

$$\langle qv \rangle_1 = \frac{1}{\pi} \int_{\alpha}^{\pi-\alpha} \langle v \rangle_1(\theta) e^{-j\theta} d\theta \quad (12.91)$$

Assuming that the *amplitude* of the phasor voltage $\langle v \rangle_1(\theta)$ does not vary much over the integration limits $\alpha \leq \theta \leq \pi - \alpha$, we can pull it out of the integral to obtain the following approximation for $\langle qv \rangle_1$:

$$\langle qv \rangle_1 \approx \langle v \rangle_1 \left(1 - 2 \left(\frac{\alpha}{\pi} \right) - \frac{1}{\pi} \sin(2\alpha) \right) = \langle v \rangle_1 \frac{\sigma - \sin(\sigma)}{\pi} \quad (12.92)$$

where we have defined $\sigma \triangleq \pi - 2\alpha$. We now define the impedance Z of the FC-TCR as follows:

$$Z = Z(\alpha) = jX \quad (12.93)$$

where we have

$$X \triangleq \frac{\omega L_{eq}}{1 - \omega^2 C L_{eq}} \quad L_{eq} \triangleq \frac{L\pi}{\sigma - \sin(\sigma)} \quad (12.94)$$

The equivalent inductance L_{eq} represents the inductive impedance that is in parallel with the fixed capacitor C . This clearly illustrates why the impedance Z is a function of the firing angle α . In effect, the FC-TCR is a controlled impedance. To illustrate this, look at the extreme value of the firing angle. If $\alpha = 0$, the thyristors are never turned on and the inductive leg of the FC-TCR is essentially an open circuit and only the capacitor is connected to the line. The capacitor then will *inject* reactive power into the line. Once we start increasing α toward its maximum value ($= \pi$), the inductor will start drawing more and more current from the line. This has the effect of reducing the reactive power that is injected into the line. When α is identically π , the anti-parallelled thyristors are essentially a short circuit. In other words, $L_{eq} = L$. If one selects the inductor and the capacitor such that the resonant frequency $\omega_0 \triangleq 1/\sqrt{LC}$ coincides with the line frequency $\omega \approx 377$ rad/s and the firing angle is π , then the FC-TCR is essentially an open circuit. Consequently, no reactive power is injected into

the line. One often uses the following conventions when describing the reactive power compensation: $\alpha = 0$ (full compensation), $\alpha = \pi$ (no compensation).

12.4.1.4.4 FC-TCR Averaged Model Separating the above differential equations of (12.89) and (12.90) into their real and imaginary parts yields a fourth-order nonlinear model:

$$\begin{aligned}\frac{d\langle i \rangle_1^R}{dt} &= \omega\langle i \rangle_1^I + \langle v \rangle_1^R \left(\frac{\sigma(\alpha) - \sin(\sigma(\alpha))}{L\pi} \right) \\ \frac{d\langle i \rangle_1^I}{dt} &= -\omega\langle i \rangle_1^R + \langle v \rangle_1^I \left(\frac{\sigma(\alpha) - \sin(\sigma(\alpha))}{L\pi} \right) \\ \frac{d\langle v \rangle_1^R}{dt} &= \omega\langle v \rangle_1^I + \frac{1}{C} (\langle i_s \rangle_1^R - \langle i \rangle_1^R) \\ \frac{d\langle v \rangle_1^I}{dt} &= -\omega\langle v \rangle_1^R + \frac{1}{C} (\langle i_s \rangle_1^I - \langle i \rangle_1^I)\end{aligned}$$

The above equations describe the $i - v(i_s - v)$ characteristics of the compensating device. Firing angle is the control variable in the above equations since σ is directly related to α .

A. Comments

The implications for modeling of FACTS devices is that one must define certain variables as ‘inputs’ and others as ‘outputs’. For example, since the line current is usually assumed to be known, we can declare it as an input to our system. On the other hand we can make the capacitor voltage (the voltage across the FC-TCR) as an output. The discrete signal $q(t)$ may be modeled as a disturbance input which controls the time interval σ .

12.4.1.4.5. Simulations To exercise the model developed, a simulation was executed. The FC-TCR parameters are $C = 0.8$ p.u. and $L = 0.3$ p.u. To check the transient dynamics of the system, it assumed that there is a change in the reactive power demand in the system. This was accomplished by having a control reference signal $I_{s,\text{ref}}$ for the compensator current i_s . In the simulation, $I_{s,\text{ref}}$ is stepped from 1 to 1.5 p.u. at $t = 10$ s. To make things a little more complicated, the line voltage is not assumed constant but has a low frequency variation in its amplitude. The amplitude of v_s varies as

$$|\langle v \rangle_1| = 1 + 0.1 \sin(0.6t) \quad (12.95)$$

The loop is closed by feeding the error in the compensator current into a PI controller with the transfer function:

$$H(s) = 5 + \frac{3}{s} \quad (12.96)$$

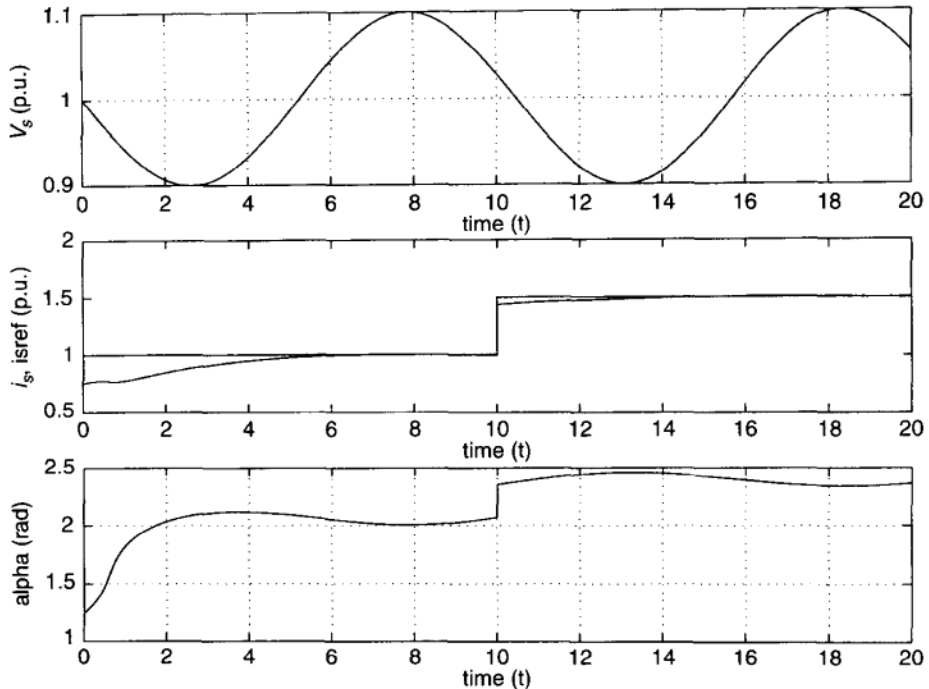


FIGURE 12.8 Simulation results for FC-TCR using a PI controller.

The results of the simulation are shown in Figure 12.8. The three plots show the variation in the line voltage amplitude $|\langle v \rangle_1| = V_s$, the reference signal for the compensator $I_{s,ref}$, the actual compensator current i_s and the firing angle α . As can be seen from the figure, the compensator current is able to follow the command signal. The performance can be optimized by changing the controller parameters or by using a different controller—such as a nonlinear controller. It should be noted that the low frequency variations in the control variable α are due to the fact that the line voltage amplitude was not assumed constant.

The noise performance of the model is shown in Figure 12.9. A high frequency noise signal of amplitude 0.01 p.u. was added to the 1 p.u. nominal amplitude of the line. As can be seen from the results, the controller still performs well although there is some more variation in the control signal α which is due to the fact that PI controller does not filter out all of the noise signal. However, the controlled signal still has good performance.

The detailed model derived here can be used to study a variety of problems: specifications of the power electronics components—for example, the VA rating of the thyristors and the control logic; closed-loop dynamics of the SVC—since the model is general and is derived independent of the controller, virtually any control scheme can be implemented and simulated; dynamic stability (using linearized model)—one can linearize the fourth order nonlinear model that we developed to study the dynamic (small signal) stability of the FC-TCR around an operating point.

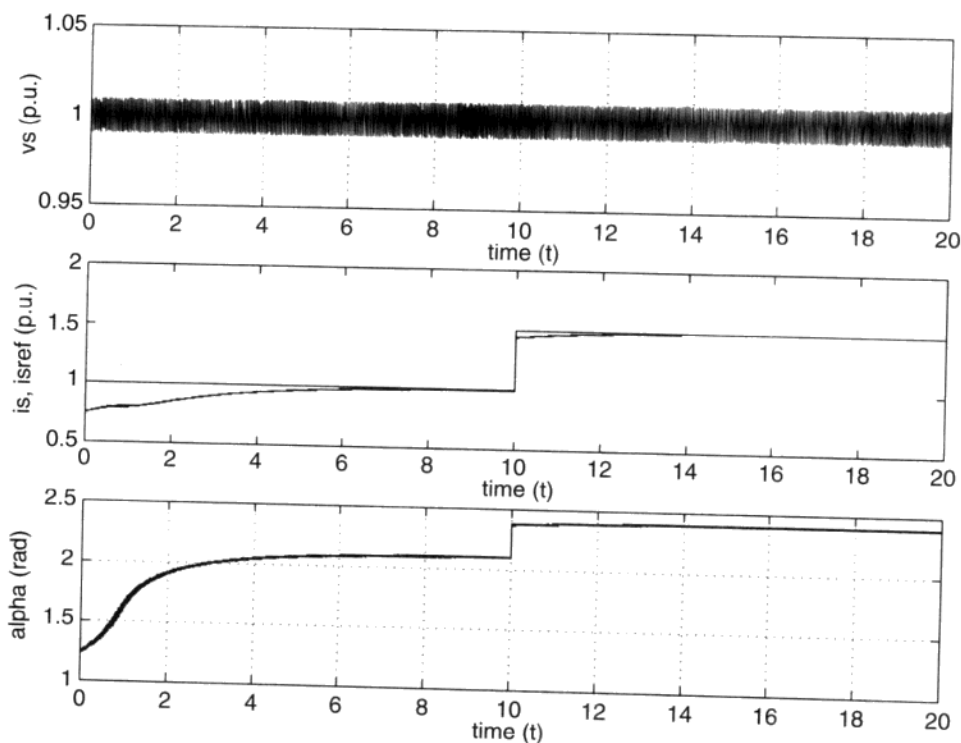


FIGURE 12.9 Noise performance of the FC-TCR model using a PI controller.

12.4.1.5 Major challenges in FACTS-based control FACTS-based control has brought new challenges to controlling large scale power systems. Some of these are: (1) the need for fundamental understanding of the impact of fast reactive power compensation on frequency stabilization, particularly under large disturbances, (2) the need for fundamental understanding of direct line power flow control in a large power system, already controlled at its inputs by generation-based primary controllers; (3) the need to coordinate network (FACTS) controllers with the port (generator) controllers. For the first time there exists technology for direct flow control on transmission lines, and this calls for major re-assessment of the control objectives. (4) Finally, nonlinear control designs are needed for these devices which do not require full state measurements. The early work in Refs. [63] to [65] holds high promise for decentralized control of FACTS devices. (5) One of the major problems in the control of the electric power systems relates to the fact that very little work has been done on systematic control design for which certain performance bounds can be stated. With the influx of a variety of fast switching-based network (including load side) controllers, it is necessary to begin re-assessing the present state-of the art in orders to avoid coordination problems among primary controllers evolving at different rates and of different type (PID designs, nonlinear continuous and nonlinear discontinuous-switching-types).

12.5 LOAD-BASED CONTROL

Finally, it is worthwhile mentioning that, in addition to generation-based and network-based control, a development of automated distributed load controllers will become necessary in the future. Some major power companies are already using load control as a means of keeping the system together under unusual stress [66]. The problem of automated under-frequency and under-voltage load shedding will take on a new importance as a result of steady tendency toward more control at a local (distribution system) rather than at a backbone (transmission) level control, as well as the result of the major breakthroughs in distributed generation, Ref. [67].

The overall area of basic objectives underlying load control of a large power system, and the tradeoffs between system control by generation-based, transmission-based or load-based control remains wide open for future investigations.

12.6 MECHANICALLY SWITCHED CONTROL

Under normal operating conditions an assumption is made that fast continuous primary controllers located on large synchronous machines provide for stable return to the steady state in response to fast disturbances $d(t)$. In addition, fast FACTS devices controlling transmission equipment is starting to be used under more stressful conditions. Moreover, the continuous governor control responds to slower unpredictable changes in real-power demand $P_L(\tau)$.

If this assumption is met, a major remaining objective of automated controls is to maintain *voltages* at various demand buses throughout a large system, as the reactive power varies around the scheduled demand. This variation is denoted as $Q_L(\tau)$, and it evolves at the rates similar to the real-power variation $P_L(\tau)$, or slower. Many mechanically switched devices, ranging from on-load tap changers, shunt inductors and capacitors, through series capacitors, have the main objective to regulate load voltages at the specified buses in response to these deviations in reactive-power demand. Since the response to the reactive-power disturbance in the steady state is fairly localized, one needs many devices of this type. The control logic on which their function is based reflects this property; they are all decentralized, in the sense that they respond to local output and regulate it by local means. Moreover, the typical control logic is common to all technologies; the effective local impedance varies as a function of voltage deviations following the simple logic of increasing or decreasing a fixed portion of impedance as the voltage leaves acceptable ranges of operation. This switching is done with a typical duty ratio of a minute or longer. The slow activity is intentional so that the mechanical switching does not damage the device and excessive switching losses are avoided. This, in turn, allows for a time-scale-based separation of effects in closed-loop dynamics caused by fast primary controllers on one hand and mechanically switched devices on the other hand.

These devices have been used successfully with very little concern for their control logic. It has been only recently, in the era of facing voltage-related

problems, that certain malfunctioning of these devices has been detected [68,69]. The observed difficulties are reflected in situations of increased shunt capacitance, not increasing load voltage, and on-load tap changers leading to severe deficiencies in reactive-power support at a system wide level. These occurrences were representative of heavy reactive-power demand conditions when the reactive-power reserves out of generators were approaching their limits.

The reported curious events of this kind have led to recent research activities whose output provides some basic insights regarding quantification of these unusual operating conditions under which the common switching logic may worsen, rather than improve voltage support on the system. Once such conditions are detected, it is necessary either to disable temporarily (lock) the automatic switching or to change the control logic. The most accepted practice is to disable the automatic functions.

The analysis here provides a brief summary of the recent research that forms a basis for quantifying steady-state (scheduled) operating conditions under which abnormal performance of mechanically switched controllers could be expected.

12.6.1 Modeling of Switched-Control-Driven Voltage Changes

It is interesting to recognize that all switched-control-driven changes in response to deviations of reactive-power demand from nominally scheduled values can be described as a control-driven process, subject to the common algebraic constraint imposed by the need to meet basic flow balance at each quasistationary step. For instance, changes associated with the capacitor bank switching are according to the automated logic

$$C_i(l+1) = C_i(l) - f_i(z_i^C(l), z_{i,\text{ref}}^C) \quad (12.97)$$

where $i = 1, 2, \dots, M^C$, and $l = 1, 2, \dots$. Vector z^C represents a subset of system outputs (voltages), locally controlled by capacitor banks, and is related to the system voltages y as

$$z^C = C^C y \quad (12.98)$$

The value of the capacitance switched between the node and the ground is $C(l)$, at discrete times l , and changes according to the relay-type logic function. Similarly, a representative type of discrete process defined by the automatic actions of on-load tap changing (OLTC) transformers connected between transmission nodes i and j , and directly controlling the nodal voltage at i , is carried out by changing their tap positions according to

$$a_{ij}(m+1) = a_{ij}(m) - f_i(z_i^T(m), z_{i,\text{ref}}^T) \quad (12.99)$$

where $i = 1, 2, \dots, M^T$ and $m = 1, 2, \dots$. Similar to the capacitor switching case,

$$z^T = C^T y \quad (12.100)$$

Note also that the relay-type function is common to all mechanically switched devices, including typical human operator decision making, since operators typically assume the qualitative network response to be such that any increase in demand or decrease in generator voltage decreases the load voltage. Note that in the case of human operator actions the discrete process is typically asynchronous.

The algebraic constraint that needs to be met at any switching instant l and/or m represents the reactive-power balance at load nodes everywhere on the system. It is of the form

$$0 = g(y, u, p) \quad (12.101)$$

In Eq. (12.101) variables y correspond to all nodal load voltages, directly controlled or not, u are system inputs representing terminal voltages at generators and reactive-power demand at the loads, and p are transmission network parameters, such as line inductances, and shunt capacitances. Parameters $C_i^c(l+1)$ and $a_{ij}(m+1)$ in Eqs. (12.97) and (12.99), respectively, are a subset of other transmission network parameters that are not directly controlled. While the reactive-power balance is studied first as the algebraic constraint on controllers that directly respond to voltage changes, a decoupling assumption could be relaxed.

The discrete processes (12.97) and (12.99) result in parametric changes of the transmission-system interconnections. Modeling and analysis of the quasistationary closed-loop processes of these types as discrete, quantized control-driven dynamic sequences was introduced to the power-system area for the first time in Refs. [70,71]. This was done in the context of OLTC analysis and is briefly summarized next. Here we suggest to generalize this approach as fundamental unifying modeling and control of all other mechanically switched processes. This could enable one to analyze and control changes over midterm horizons in much the same fashion as has been done for very-short-horizon continuous dynamics up to now. The stability properties of discrete sequences defined previously interpreted as their convergence to within the desired threshold of directly controlled variables [70,71].

A clearer understanding of the qualitative changes of the discrete processes of interest can be obtained by linearizing the algebraic constraint (12.101) at each control step. For example, a dynamic process with capacitor switching, while disabling the switching of OLTCs, the linearization of Eq. (12.101) after rearranging terms, and with the assumption that the system Jacobian

$$J = \left(\frac{\partial g}{\partial y(l)} \right)^{-1} \quad (12.102)$$

as $l = 0, 1, \dots$ remains nonsingular, yields an explicit time-varying process of the form

$$z^c(l+1) = z^c(l) - C^c \left(\frac{\partial g}{\partial y}(l) \right)^{-1} \left(\frac{\partial g}{\partial C}(l) \right) [C(l+1) - C(l)] \quad (12.103)$$

Also, the discrete process associated with automatic tap-position changing on transformers is describable as

$$z^T(m+1) = z^T(m) - C^T \left(\frac{\partial g}{\partial y}(m) \right)^{-1} \left(\frac{\partial g}{\partial a}(m) \right) [a(m+1) - a(m)] \quad (12.104)$$

It was shown in Ref. [70] that as long as the system Jacobian in Eq. (12.103) remains positive definite, the conventional switching logic of the relay type will bring the closed-loop discrete process to within the threshold of system outputs z_{thresh}^T . This condition is fundamental for the desired regulation of other discrete processes, such as shunt capacitor switching defined in Eq. (12.103).

This result suggests the need for developing pragmatic ways of obtaining information about the qualitative nature of the system Jacobian given in Eq. (12.102). We observe immediately that if this question is attempted independently from the very rich underlying structure of the load-flow equation studied in Chapter 5, this task quickly becomes hopeless for any on-line use. Therefore, we suggest to explore more than one avenue that would allow a solution of this fundamental problem by intelligent use of our knowledge of Eq. (12.102) describing transmission-system constraints on controllers.

12.8 CHAPTER SUMMARY

A basic premise here is that the power system must be recognized as a constantly evolving, time-varying process, which requires integrated coordination of all types of controllers, including the human operators and system protection, over diverse time horizons. This leads to defining classes of problematic operating conditions on present power systems, which could be improved significantly by solving the underlying control problems. They can be summarized as often evolving over longer time horizons, at different rates, and/or in response to unusually large deviations away from nominal operating conditions.

The available control actions range from tuning (of set points, gains, etc.) to switching (of on-line tap-changing transformers, capacitor banks, etc., as well as their associated logic). A key objective of intelligent control will be generation of relevant information on-line that will allow individual local controllers to operate in an effective manner. This is typically a straightforward problem when designing controllers for a given linear system that are synchronized and either discrete or continuous. The nonstandard control problems of power systems are due to a large variety of controllers, which pose serious challenges to their performance when the system operates over a wide range of changes.

Practical concerns favor schemes that use information available locally to each controller, and in which the appropriate control responses can be determined primarily at this local level. The coordination of switching and tuning controllers, operating at different locations and time scales, constitutes a key task as well.

It is suggested in this chapter that state-of-the-art control is effective for a power system operating close to its nominal conditions. Yet, many nonstandard

control problems have evolved recently on modern power transmission grids. This situation highlights the need to enhance existing control hardware and logic to enhance performance under unusual operating conditions.

Additional complexity has already been introduced by a variety of high-technology control (such as FACTS) and communications hardware, viewed as necessary for improving the performance of the system operating under stress. A major remaining challenge is to provide intelligent coordination of this hardware under a variety of operating conditions.

In particular, newly evolved voltage problems can be used to define and illustrate operating scenarios that create challenges to the controllers currently used on power systems. By making the same controllers more intelligent, it appears possible to regulate system operation in much larger regions than those used now. The benefits of doing this can be measured in terms of achieving better economic and secure system operation by smarter controls, instead of overdesigning physical transmission and generation capabilities of the system.

BIBLIOGRAPHY

1. Pasternack, B., Flexible AC transmission system: Transmission limitations — A planner's viewpoint of the needs, EPRI FACTS Workshop, 1991.
2. Flexible AC Transmission Systems (FACTS): Scoping Study, Vol. 1, Part 1: Analytical Studies, EPRI EL-6943, 1990.
3. Flexible AC Transmission Systems (FACTS): Scoping Study, Vol. 2, Part 1: Analytical Studies, EPRI EL-6943, 1991.
4. Application of Static Var Systems for System Dynamic Performance, IEEE Special Publication No. 87TH0187-5-PWR.
5. Zaborszky, Whang, K. W., Prasad, K. V., and Katz, I. N., Local feedback stabilization of large interconnected power systems in emergencies, *Automatica*, **17**: 673–686, 1981.
6. Chapman, J. W., Power system control for large-disturbance stability: Security, robustness and transient energy, Ph.D. thesis, MIT, Department of Electrical Engineering and Computer Science, 1996.
7. Chapman, J. W., Ilić, M. D., and King, C. A., Stabilizing a multimachine power system via decentralized feedback linearizing excitation control, *IEEE Trans. Power Syst.*, PWRS, August 1993, pp. 830–839.
8. DeMello, F. P., and Concordia, C., Concepts of synchronous machine stability affected by excitation control, *IEEE Trans. Power Apparatus Syst.*, **PAS-88**: 316–328, 1968.
9. Larsen, E. V., and Swann, D. A., Applying power system stabilizers. Part I: General concepts, *IEEE Trans. Power Apparatus Syst.*, **PAS-100**: 3017–3024, 1981.
10. Larsen, E. V., and Swann, D. A., Applying power system stabilizers. Part II: Performance objectives and tuning concepts, *IEEE Trans. Power Apparatus Syst.*, **PAS-100**: 3025–3034, 1981.
11. Larsen, E. V., and Swann, D. A., Applying power system stabilizers. Part III: Practical considerations, *IEEE Trans. Power Apparatus Syst.*, **PAS-100**: 3034–3046, 1981.

12. Brockett, R., *Linear Dynamic Systems*.
13. Sauer, P., and Pai, M. A., Lecture notes on power system modeling and analysis, University of Illinois, 1984.
14. Doyle, J., and Stein, G., Multivariable feedback design: Concepts for a classical/modern synthesis, *IEEE Trans. Automatic Control*, **AC-26**: 4–16, 1981.
15. Bergen, A., Analytical methods for the problem of dynamic stability, *Proc. IEEE Intl. Symp. Circuits Syst.*, pp. 864–871.
16. Hugoud, P., Benejean, R., Irving, E., Barret, J-P., Blanchet, P., Herouard, M., and Meyer, J-P., Improving system stability by field voltage control of synchronous machines, *RGE Special Issue*, July 1980, pp. 64–92.
17. Eigenanalysis and Frequency Domain Methods for System Dynamic Performance, *IEEE 90TH0292-3-PWR*.
18. MATLAB, User's Guide, The Math Works, Inc., Natick, MA.
19. Davison, E., and Rau, N. The optimal output feedback control of a synchronous machine *IEEE Trans. Power Apparatus and systems*, Vol. PAS-90, 1971, pp. 2123–2134.
20. Rovnyak, S., Kretsinger, S., Thorp, J., and Brown, D., Decision trees for real-time transient stability prediction, *IEEE Trans. Power Syst.*, **9**: 1417–1426.
21. Rovnyak, S. M., Taylor, C. W., and Thorp, J. S., Real-time transient stability prediction—Possibilities for on-line automatic database generation and classifier training, 2nd IFAC Symp. Control Power Plants Power Syst., Cancun, Mexico, 1995.
22. Rovnyak, S. M., Taylor, C. W., Mecham, J. R., and Thorp, J. S., Plans To demonstrate decision tree control using phasor measurements for Hvdc fast power changes, Fault Disturbance Analysis Precise Meas. Power Syst. Conf., Arlington, VA, 1995.
23. Chapman, J., and Ilić, M., Some robustness results for feedback linearizing control of generator excitation, *Proc. 31st IEEE Conf. Decision and Control*, Tuscon, AZ, 1992, pp. 1123–28.
24. Hung, J. Y., Gao, W., and Hung, J. G., Variable structure control: A survey, *IEEE Trans. Ind. Electron.*, **40**: 1993.
25. Gao, W., and Hung, J. C., Variable structure control of nonlinear systems: A new approach, *IEEE Trans. Ind. Electron.*, **40**: 1993.
26. Chapman, J. W., Feedback linearizing generator excitation control for enhanced power system stability, M.Sci. thesis, M.I.T., and 1992.
27. King, C. A., Chapman, J. W., Ilić, M. D., “Feedback linearizing excitation control on a full-scale power system model,” *IEEE Trans. Power Syst.*, **PWRS-9**, May 1994, pp. 1102–1109.
28. Cao, Y., Jiang, S., Chen, D., Malik, O. P., and Hope, G. S., A nonlinear variable structure stabilizer for power system stability, *IEEE Trans. Energy Conv.*, 1994, Vol. 9, No. 3,
29. Huang, T. L., Chen, S. C., and Yang, W. T., Power system output feedback stabilizer design via optimal subeigenstructure assignment, *Electric Power Systems Research*, **21**: 107–114, 1991.
30. Chow, J. “A pole—placement design approach for systems with multiple operating conditions, prod. of the IEEE conf. on Decision and control, 1988.

31. Marino, R., Feedback equivalence of nonlinear systems to applications to power system equations, D.Sc. thesis, Washington University, St. Louis, MO, 1982.
32. Marino, R., On the stabilization of power systems with a reduced number of controls, *Lecture Notes in Control and Information Sciences*, New York: Springer, 1984, Vol. 62.
33. Noroozian, M., Exploring benefits of controllable series compensators in power systems, TRITA-EES-9402, Royal Institute of Technology, Stockholm, Sweden, 1994.
34. Quintana, V. H., Zohdy, M. A. Anderson, J. H., "On the desire of output feedback excitation controllers of synchronous machines," *The IEEE Trans. Power App. Syot.*, **PAS-95**: pp. 954–961, June 1976.
35. Siljak, D., *Decentralized Control of Complex Systems*, New York: Academic, 1991.
36. Diong, B., and Medanić, J., Dynamic output feedback variable structure control for system stabilization, *Int. J. Control.*, **56**: 607–630, 1992.
37. Aoki, M., On feedback stabilizability of decentralized dynamic systems *IFAC Automatica*, Vol. 8, pp. 163–173, Pergamon Press, 1972.
38. Ilić, M., Liu, S., "*Hierarchical Power Systems Control: Its value in the Changing Industry*, Sponser Verlag Advanced Control Series, London, 1996.
39. Mak, F. K., and Ilić, M. D., Towards most effective control of reactive power reserves in electric machines, *Proc. 10th Power Syst. Comput. Confe.*, Graz, Austria., pp. 359–367, 1990.
40. Mak, F. K., Analysis and control of voltage dynamics in electric power systems, Ph.D. thesis, University of Illinois at Urbana-Champaign, 1990.
41. Su, R., "On the linear equivalents of nonlinear systems," *Systems Control Letters*, Vol. 2, no 1, July 1982.
42. Utkin, V. I., Variable structure systems with sliding mode, *IEEE Trans. Automatic Control*, **AC-22**: 212–222, 1977.
43. Drazenović, B., The invariance conditions in variable structure systems, *Automatica*, **5**: 287–295, 1969.
44. Yu, X., Sira-Ramirez, H., and Ledwich, G., Switching control strategy for the power system stabilization problem, *Int. J. Control.*, **62**: 1021–1036, 1995.
45. Cao, Y., Jiang, S., Chen, D., Malik, O. P., and Hope, G. S., A nonlinear variable structure stabilizer for power system stability, *IEEE Trans Energy Conversion*, **9**: 1994.
46. Smith, J., et al, An enhanced LQ adaptive Var unit controller for given power system damping, *IEEE Trans. Power Syst.*, **4**: 443–451, 1989.
47. Taylor, D., Ph.D. thesis, Department of Electrical Engineering, University of Illinois, 1987.
48. Marino, R., High-gain in nonlinear control systems, R-84.04, 1984, Dipartimento Di Ingegneria Elettronica, Seconda Universita di Ingegneria Elettronica, Roma, Italy.
49. Zaborszky, J., Subramanian, A. K., Tarn, T. J. and Lu, K. M. A New State Space for Energy Control in the Interconnected Power System, *IEEE Transactions on Automatic Control*, August 1977, Vol. AC-22, No. 4, pp. 505–517.
50. Zaborszky, J., Whang, K. W., Prasad, K. V., and Katz, I. N. Local Feedback Stabilization of Large Interconnected Power Systems in Emergencies, *Automatica*, September 1981, p. 673–686.

51. Zaborszky, J., Whang, K. W., and Prasad, K. V. Stabilizing control in Emergencies. Part I: Equilibrium Point and State Estimation, Part II: Control by Local Feedback, IEEE-PES Transactions on Power Apparatus and Systems 1981, Part I: pp. 2374–2380, Part II: pp. 2381–2389.
52. Zaborszky, J., Whang, K. W., Huang, G., Chiang, L. J., and Lin, S. Y. A Clustered Dynamic Model for a Class of Linear Autonomous Systems Using Simple Enumerative Sorting, Special issue of IEEE Transactions on Circuits and Systems, Vol. CAS-29, No. 11, November 1982, pp. 747–758.
53. Zaborszky, J., Huang, G. and Chiang, L. J. Stabilizing the Large Power System by Tracking the Observation Decoupled Reference Through Cluster Feedback, Proceedings of the IEEE-SCS International Symposium on Circuits and Systems, May 1983, pp. 1405–1409.
54. Miller, T., *Reactive Power Control in Electric Systems*, New York; Wiley, 1982.
55. Gyugyi, L., Reactive power generation and control by thyristor circuits, *IEEE Trans. Ind. Appl.*, **1A-15**: 521–532, 1979.
56. Gavrilović, M., *Int. J. Power and Energy Syst.*, FACTS Special Issue, Vol. 17, 1995, pp. 199–205.
57. Sanders, S. R., Noworolski, J. M., Lim, X. Z., Verghese, G. C., “Generalizcol averaging method for power conversion circuits,” *IEEE Trans. on Power Electronics*, **6**(2), pp. 251–259, April 1991.
58. Mattavelli, P., Verghese, G. C., Stanković, A. M., “Phasor dynamics of thyristor-controlled series capacitor systems,” *IEEE Trans. on Power Systems*, **12**(3), pp. 1259–1267, Aug. 97.
59. Caliskan, V. A., Verghese, G. C., Stanković, A. M., “Multi-frequency averaging DC/DC converters,” IEEE Workshop on Computers and Power Electronics, Portland, OR, August 1996.
60. Wood, J. R., “Power Conversion in Electrical Networks”, NASA CR-120830 Topical Report, Harvard University, 1972.
61. Allen, E., Chapman, J. W., Ilić, M. D., “Effects of torsionel dynamics on nonlinear generator control,” *IEEE Trans. on Control Systems Technology*, Vol. 2, pp. 125–140, March 1996.
62. Kassakian, J. G., Schlecht, M. F., Verghese, G. C., *Principles of Power Electronics*, Addison-Wesley, 1991.
63. DeCarlo, R. A., Saeks, R. *Interconnected Dynamical Systems*, Marcel Dekker, New York, 1981.
64. Mathews, G. P., DeCarlo, R. A., Hawley, P., Lefebvre, S. “Toward a feasible variable structure control design for a synchronous machine connected to infinite ions”, *IEEE Trans. on Automatic Control*, Vol. AC-31, Dec. 1986, pp. 1159–1163.
65. Lefebvre, S., Richter, S., DeCarlo, R., “The Component connection model and decentralized control: theory and application” TR-EE 82–15, June 1982, Purdue University, Lafayette, IN.
66. Trudel, S., Bernard, S., Scott, G. “Hydro–Quebec defence plan against extreme contingencies” IEEE paper no. PE-211-PWRS-0–06–1998, IEEE Under Power Meeting, NY, 1998.
67. Cardell, J., Ilić, M., “The control and operation of distributed generation in a competitive electric market,” pp. 451–516, in Ilić, M., Galiana, F., Fink, L., (eds.), *Power*

- Systems Restructuring: Engineering and Economics, Kluwer Academic Publishers, Boston, MA, 1998.
- 68. Calvaer, A., Voltage stability and collapse: A simple theory based on active and reactive currents, *Revue Generale de l'Electricite* No. **8**: 1–17, 1986.
 - 69. Donohue, T., and Rana, R., Analytical study of the loadability of AEP's Amos-Matt Funk 345-kV circuit, *Proc. Am. Power Conf.*, 1988, Vol. 50, p. 395.
 - 70. Medanić, J., Ilić, M., and Christensen, J., Discrete models of slow voltage dynamics for under load tap changing transformer coordination, *IEEE Trans. Power App. Syst.*, **PWRS-2**: 873–882, 1987.
 - 71. Ilić, M., and Medanić, J., Modeling and control of slow voltage dynamics in electric power systems, *Proc. IFAC Symp. Large-Scale Systems*, Switzerland, 1986.
 - 72 Zaborszky, J. “On the road towards FACTS”, *Int. J. Power and Energy Systems*, Special Issue on FACTS, Vol. 17, 1995, pp. 165–171.

13 Stationary Generation Control (Ignoring Congestion)

With a model of an electric power system developed in Chapters 3 and 4, we are in a position to formulate the main objectives of power-system operation and its monitoring and control. To understand the underlying basis of the computer-aided decision and control process, we first recognize that a power system is never at a true equilibrium. Instead, its state is constantly changing in response to fluctuations in load demand, and less frequently, in response to unexpected equipment failures (contingencies). The main (technical) objective of real-time power system operation is then to provide power to the varying loads, while maintaining frequency and voltages within prespecified limits.

Meeting the objective of real-time power system operation naturally requires a process guided by control and decisions based on constant monitoring of the system condition. As the power system is operated the process breaks up into two levels in a natural way. Discrete computer-type process measurements are taken and actions are commanded in a sequence of discrete time instances spaced with a fixed interval.

Level 1: Monitoring and Decision The condition of the system is continuously observed in the control centers by protective relays for faults or contingencies caused by equipment trouble and failure, by instruments on the broad security monitoring programs, etc. If any of these monitoring devices identifies a sufficiently severe problem at the sample time, then the system is in an abnormal condition. If no such abnormality is observed, then the system is in a normal condition.

Level 2: Control At each sample, then, the proper commands are generated for correcting the abnormality or protecting the system from its consequences. If no abnormality is observed, then the normal operation proceeds for the next sample interval.

These matters will be further elucidated in Section 13.1. Particular emphasis is placed on the decision phase concerning the nature of the current operating mode of a power system. A major distinction is drawn between the normal and all other operating modes. The normal operating mode generally lends itself to the well-established analytic tools for its on-line control. The analysis and control of other operating modes is much harder to automate using strictly analytic models.

Note that the data for the decision or monitoring process are automatically present in parallel time sequences, and indeed the decision on mechanisms also exists. The latter might be unified and more specifically organized with the idea of decision making. This activity, however, will not be pursued further in this book.

13.1 PRINCIPLES OF OPERATION OF THE LARGE INTERCONNECTED SYSTEM BY DECISION AND CONTROL

The U.S. structure of power-system operation was developing generally during this century without much awareness or attention to the implications of the evolution of the power-system structure. With the gradual infiltration of the computer into on-line operation in the 1950s, a surge of interconnections developed for utilizing the potential for improved efficiency and economy. As is typically the case in human activities, the development took the form of designs for individual cases of construction based only on the local situation of the case and only during normal, stationary system operation. The vital questions of the effects of the addition of new construction on the entire system and the effects of off-nominal conditions were essentially ignored. A striking example is the omission in new construction of self-starting house units and the total dependence for starting large generators and power plants (new or blacked out) on power drawn from transmission lines to neighboring stations (all of which, of course, can also be blacked out). This general attitude was the root cause of the famous "Northeast Blackout," a cascading system collapse that disabled ten states for about a week in 1964 followed by a few other large events, such as that occurring in Manhattan in 1967.

After this rude awakening, consciousness of the importance of the structure of the complete system (the interconnected U.S. electric power system) started to gradually creep into the awareness within the field. It was Dy Liacco [1], when he presented his now-famous chart in 1967, who formally introduced a view of power-system operation in terms of its principal states (operating modes), normal, alert, emergency, and restoration, and the transitions, spontaneous or forced, between these states (Fig. 13.1). The *in extremis* state or system failure was added by Fink and Carlsen [2] (Fig. 13.2).

This view thoroughly influenced the thinking of the power-system community since then. Given a large power system operating with the aid of advanced control, microwave communications, and micro-, mini-, and macroframework computer hardware, all under the authority of a control center with satellite local control centers, a *decision and control* approach emerges (Fig. 13.3) as a natural way to approach efficient system operation [3]. Computer operation inherently runs in discrete time, and so at each new sample time a decision must be made on what the system state is and what action is needed called the *decision phase*. Then the *control phase* carries out the actions that were decided on. Or more specifically, the *decision phase* consists of a continuous surveillance, monitoring, and decision on (1) the condition of the system and (2) decisions of selecting the

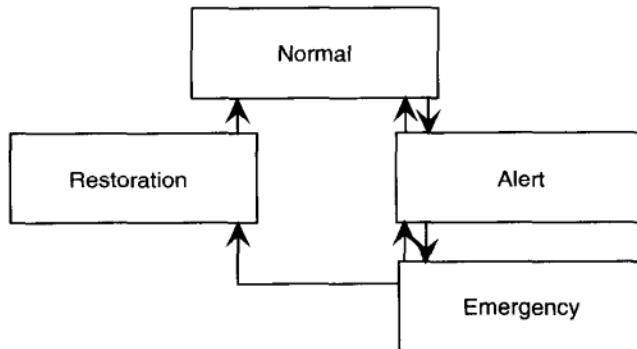


FIGURE 13.1 Dy Liacco's diagram representing the main operating modes of a power system.

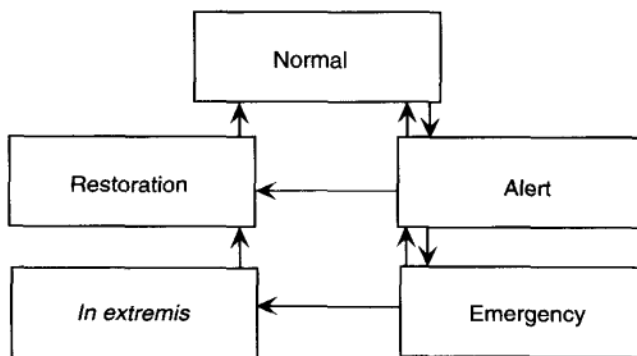


FIGURE 13.2 Fink–Carlsen diagram representing the main operating modes of a power system.

best regime of actions, specifically preventive, corrective, and/or control actions in order to move the system back towards its normal condition.

The *control phase* then proceeds with the algorithms and actions (including selective protection relaying [4,5]), comprising the control regime selected during the decision phase and carries out the control actions, which are commanded by the algorithms. Some of the actions are fully automated, and others are assisted by a human operator.

13.1.1 Some Details of the Decision and Control Phases

A decision on system conditions and applicable algorithms is made at every time step and the applicable control algorithm is carried out. The basic decision is between normal and abnormal conditions or, more precisely, on the degree and nature of abnormal operation. The applicable control algorithms are then aimed at maintaining normal operation or leading the system back to normal operation by least objectionable actions. The word *abnormal* is used to avoid semantic arguments over the meaning of *emergency*. For instance, one could argue whether

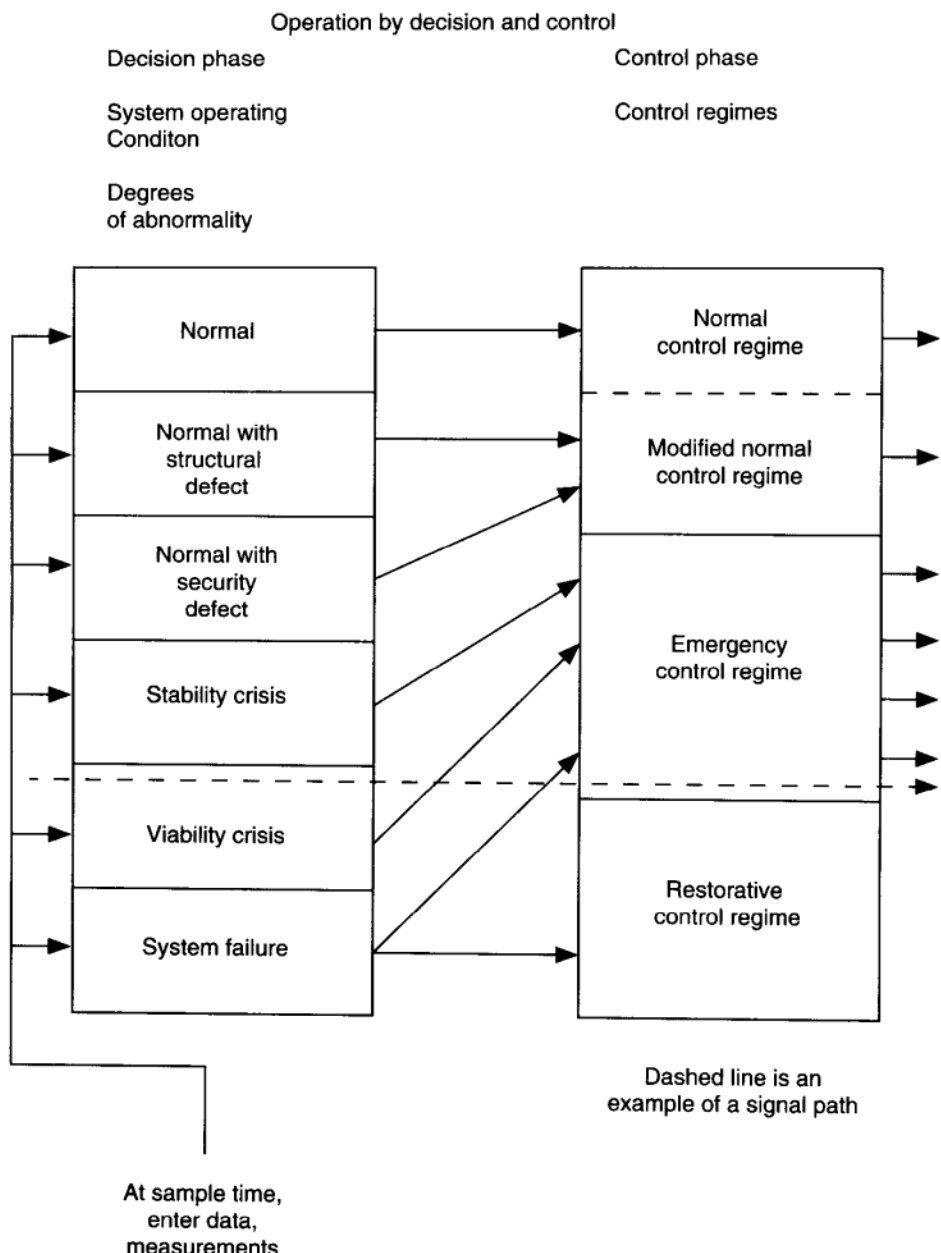


FIGURE 13.3 System operation by decision and control

loosing a line or a generator when adequate reserve is present is or is not an emergency. It clearly is an abnormal condition, however. Abnormal conditions simply mean that everything is not as expected. There are many degrees and many time scales of abnormal operation that can be roughly claimed as follows [3,6] (Fig. 13.3):

I. Normal operating conditions

- A. Decision phase: Conditions are normal when they are stationary and as expected. All equipment is working that is supposed to work; loads, fuel supplies, water and weather conditions are within the expected ranges. Principal computer-based algorithms for this phase are for
 - 1. Monitoring and estimation of load and generation
 - 2. Static state estimation
 - 3. Monitoring of the system loading conditions and security
- B. Control phase: Some principal algorithms used in normal control are
 - 1. Unit commitment (UC)
 - 2. Economic dispatch (EC) or optimal power flow (OPF)
 - 3. Automatic generation control (AGC) to match area load and system frequency [in some parts of the world, also automatic voltage control (AVC)]
 - 4. Load management

II. Alert operating conditions

- A. Decision Phase: Conditions are normal; the system is viable and within the acceptable operating constraints. However, the structure has been altered from what was expected by an earlier event—a line is missing, for example. The principal operating algorithms are as for the normal operating mode, but, in addition, future consequences of the structural change must be evaluated and, if necessary, remedied. For example, the structural change may violate security constraints during an approaching peak load. The present industry practice is preventive in this operating mode in the sense that the system is operated so that it meets normal operating constraints when any one of the most likely and most severe unexpected structural changes (contingencies) [7] takes place. This accepted preventive mode is known as the “ $(n - 1)$ ” criterion [3]. It is often cost inefficient because it does not allow for least-cost use of resources without considering future events. To get around this problem, the operating limits under structural changes are allowed to be less restrictive in the alert mode than in the normal mode. For example, typically accepted voltage variations under the normal operation are within $\pm 2\%$ or 0.002 p.u., and in the alert mode they are relaxed to $\pm 5\%$.¹ When a more severe structural change occurs, it may bring the system very close to the limits of acceptable operating constraints. For such conditions economic criteria are overruled by the security criteria. Different ancillary algorithms for readjusting network flows, bringing

¹ These are not uniformly set in all parts of the system.

on new, more expensive generation, modifying load dispatch, etc., are used to assist the operator under these conditions.

- B. Control Phase:** Since the system operation is still normal under the alert state the control tools and actions of the normal state are used. The special alert-state control actions consist primarily of equipment switching and changes in control set points and schedules to improve security.

III. Emergency or abnormal conditions

These conditions are divided into stability crisis, viability crisis, and system failure (*in extremis* [2], integrity crisis). This division, however, is not clearcut. The conditions overlap but normally one dominates. Take in sequence:

A. Stability crisis

- 1. Decision phase:** The system is in a momentary dynamic state, typically caused by a fault, which is sufficiently violent to endanger the integrity of the system.
- 2. Control phase:** Some of the principal control tools can be
 - a. Local structural control** or protective relaying to eliminate faulty components and local control actions to preserve system stability.
 - b. Stability augmentation** utilizing the FACTS technologies, breaking resistors, load skipping, etc.
 - c. Load dropping** or major structural changes to separate the system into the least objectionable manner when integrity cannot be maintained. Note that this action pushes the system into an integrity crisis mode or an *in extremis* condition.

B. Viability crisis

- 1. Decision phase:** The system in its present condition is incapable of operating within voltage, current, frequency, etc., operating constraints given the available generation and transmission capability for the existing load demand. This condition can result from a fault and is then frequently preceded by a stability crisis. Nonviable conditions can, however, come on quietly; for instance, major generation or other equipment does not become available when it is scheduled to come on line for a peak. A very interesting situation here is in the context of currently pursued competitive energy markets. Often a control center cannot schedule in a fully informed way, since some types of independent power producers are not required to coordinate their technical activities with the systemwide functions. It is easy to imagine a quietly emerging crisis of this sort [8].
- 2. Control phase:** Principal algorithms in an approximate order of undesirability include

- a. Frequency reduction of the AGC type
- b. Use of spinning reserves or cold reserves
- c. Special measures such as fast turbine run back
- d. Help from neighboring areas
- e. Exploiting time-limited overload capability of the equipment
- f. Special measures such as voltage reduction
- g. First-stage structural control such as starting a new generation, returning equipment from maintenance, or load dropping (for minutes or hours)
- h. Second-stage structural control-islanding involving separation of a power network into parts, some of which are not supplied with power.

C. Integrity crisis, system failure, or *in extremis* operating mode

1. Decision phase: The integrity of the system is violated, for instance, load was dropped or the system is islanded. Principally this is a severe and extensive accumulation of stability and viability crises or the damage left by them with islanding and blacked-out patches in the system. During the crisis phase, events are still occurring and a struggle is still going on to avoid as much disintegration as possible.
 2. Control phase: The tools are mostly the same as in the stability and viability crisis.
- D. Restoration:** This is an extensive and collective control (generally interpreted) effort to remedy the damage left by any combination of the three crisis (Fig. 13.1). The main processes taking place during restoration are
1. Reconnection of the islands
 2. Restoration of loads

This is of course an operation by itself, and it has been researched extensively in recent years [9]-[12]. The author's contribution is summarized in Refs. [13,14] but it will not be further discussed in this text.

13.2 BASIC STRUCTURE OF THE GENERATION-DISPATCH CONTROL

In this chapter we are concerned with the basic structure of controlling the dispatch of generation to cover consumer demand in a way that is the best under the objectives and policies followed by national legislative decisions. These result in operating rules that are changeable and usually have desirable and undesirable features. Their effect on the available equipment and system composition is relatively indirect but the control operation must follow and implement these changes directly and flexibly. The result is a structure (Fig. 13.4) that is reminiscent of the structure of the classical feedback-control scheme but is more complex and sophisticated in its nature. Let us make brief comments on the

various blocks including a somewhat more detailed discussion of the active dispatch segment (blocks 2, 3, and 6). Block 1 is the definition of the operating rules, principles, and objectives set politically through legislative processes of various nations. In the United States now a major change is in progress, moving from heavily government-regulated operation of an industry, the components of which are in private ownership, to a way that effectively injects a framework of commodity market-style competition usually described as *deregulated*. Note that European countries have developed their own dispatching practices with great variety from straight state ownership (England, France, and Italy) to relatively free-acting private ownership. These varied developments are quite individualistic with moderate links in their developments. Future changes will continue to occur. All these varied industry structures are reflected in varied approaches in blocks 2, 3, and 6, all of which are built on top of the fundamental system structure of the physical composition of the system and its real-time operation sketched in blocks 4 and 5. Accordingly the material described in this text indeed gives a precise and detailed foundation for studying any control activity from fast to slow and including any type of operating principles and practices as implied in Figure 13.3.

The various types of operating rules manifest themselves in the processes in boxes 1, 2, 3, and 6. These will now be briefly sketched and then illustrated by two current examples.

Operating Rules

Box 1: Political–Philosophical Background Box 1 shows that the type of dispatching is a political output of the philosophies dominating the thinking of the government at the time. In the 1950s and 1960s power companies were interconnected at increasing rates by tie lines for power exchange utilizing the development of computers. So a very large and nonlinear system arose that needed to be organized for operation. Those were still the post-Roosevelt liberal years, so the organization was based on heavy government regulation to deal with the inherently monopolistic character of selling power to multitudes of customers. Well, now we are in the years of free enterprise, a still-booming economy, and a fast rising stock exchange. So logically a new electric power industry structure is required to fit the times.

The classical generation dispatch and control practice is well established and is described in this chapter. The new deregulated structure is being gradually established but not yet fully developed theoretically or practically far enough. Only its framework will be presented and shown how it fits into the same setting of Figure 13.4.

The point of box 1 is that, regulated or deregulated, it takes government action to set the organizational framework and objectives. In any operation the same functions need to be performed to satisfy the needs of the operation as shown in Figure 13.4.

Blocks 4 and 5: Physical System Blocks 4 and 5 summarize the model, dynamics, and statics of the physical system itself. The *f* and *g* division properly

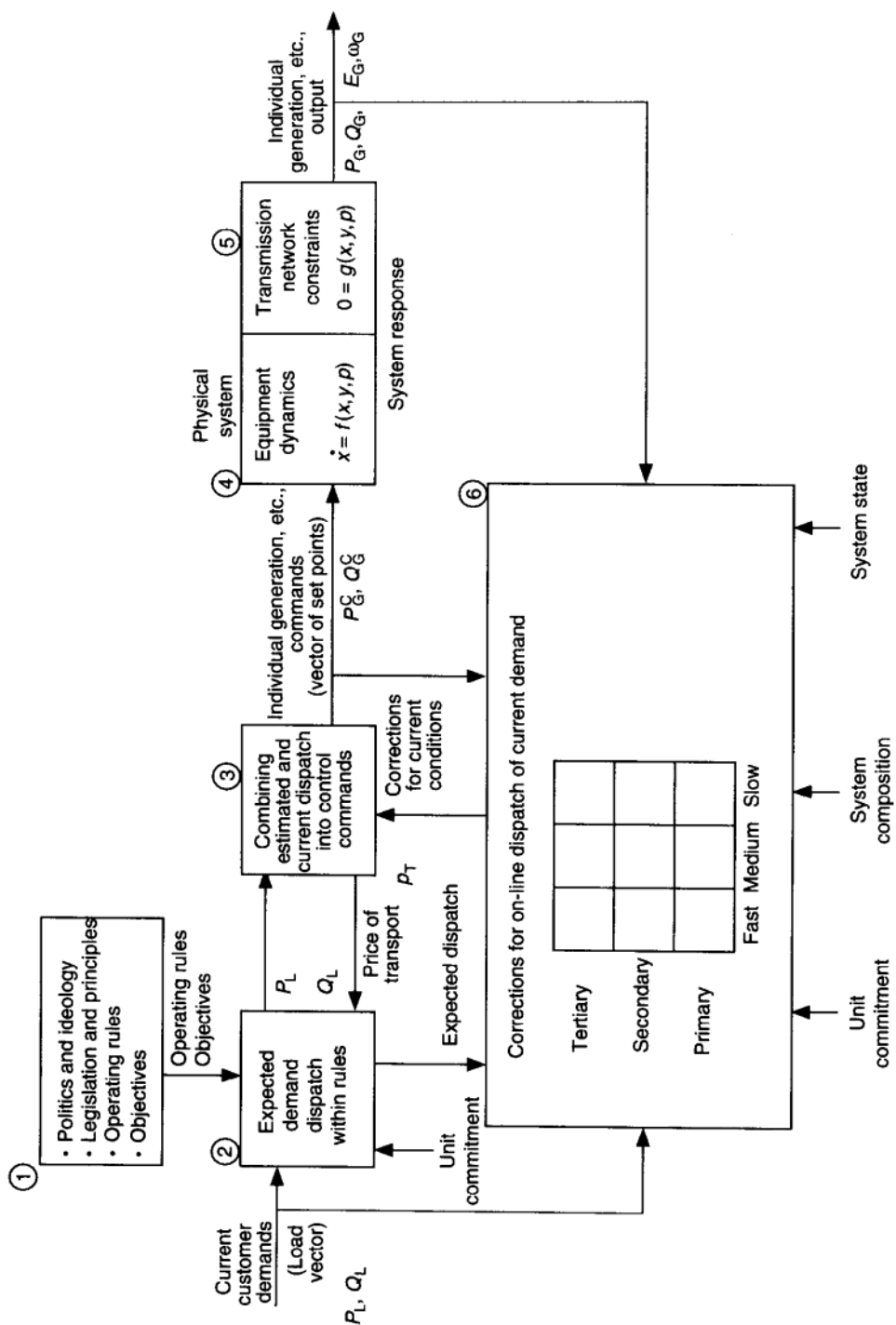


FIGURE 13.4 Structure of generation dispatch and control in normal operation.

emphasizes the inherent and rudimentary structural division of the system into a transmission network (box 5) and the equipment section (box 4). Dynamics of the transmission-line network is very fast compared to most equipment, as is implied by the $\dot{x} = f$, $0 = g$ type modeling in boxes 4 and 5 with exceptions, for example, response of boilers would be “medium fast” while most equipment would be fast. The superfast response of the transmission system is represented as static (instantaneous), but for lightning and switching transients and very long lines they must be considered.

Control devices (governors, excitors, etc.) are part of the physical system. Primary control is typically “fast,” secondary control (e.g., overall control of the areas) is medium, and tertiary control (e.g., frequency or generation control at the system interconnection level) is slow.

The physical system modeling and behavior under varying conditions is treated in Chapters 6 to 10. This material should be the foundation of any work on dispatch control under any circumstances. In Chapters 3 to 10 the models used are smooth but realistically nonlinear, of very large size (tens of thousands of buses), and based on the quasistationary phasor representations. Matters of hard limits are discussed in Chapter 10 and breakdowns of the quasistationary assumption in Chapter 11.

Blocks 2 and 3: Determination of the Systemwide Set Points These are the blocks that assure that the solutions of the problems of dispatch as solved in block 6 and implemented in blocks 4 and 5 comply with the objectives and operating rules as described in block 1. Inherently these problems involve the economic details of pricing and responsibilities for paying the bill. Also in these blocks the dispatch process follows different tracks depending on the politics, economics, and principles on which objectives and the rules are based as discussed in block 1. As mentioned, these typically differ from country to country. Currently they are subject to major change or reversal in the United States.

Only the regulated and deregulated examples will be sketchily discussed here. Considerable details of the regulated and deregulated generation dispatch are described in Section 13.3 of this chapter.

Part 1: Objectives of the Operation in Boxes 2 and 3

Regulated System For the regulated system the objective is to cover the consumer’s demand for power using available generating sources systemwide in such a way that the following is upheld.

1. The total operating cost of the full system including transmission losses is minimal.
2. The price the customers pay for power is subject to government regulation and control in such a way that the total cost of estimated power production is covered with adequate profit margin.
3. There is enough power available on the system (in running steam generators, etc.) to cover the current load estimated statistically based on the past

year's records plus adequate reserves to cover deviations of the current load from the estimated values and for emergencies of a first contingency class.

4. The power quality is adequate for consumer satisfaction, that is, voltage and frequency are kept within an adequate viability band and kept sufficiently steady. Note that synchronous time frequency is a courtesy to the customers. Much less precision would be enough for engineering purposes.
5. The system has security that minimizes outages.

Deregulated System For the deregulated system the objective is to cover consumer demand for power using available generating sources system wide in such a way that the following is upheld.

1. Suppliers of power can get the maximum price for their product competitively established in a free commodities market-type economy restricted only in the sense of the rules of the exchange.
2. Consumers of electric power can pay the lowest prices for their purchase competitively established in a free commodities market-type economy restricted only in the sense of the rules of the exchange. *Note:* This may work fine for the large consumers who can effectively trade at the commodities market to their advantage. Small customers cannot effectively do that, which raises the difficult question of how to establish the price of the power at individual homes or dwellings, with a potential outcome to retain some kind of government regulation in this area.
3. There is enough power available on the system to cover the current load of the system for emergencies of a first contingency class.
4. The power supply quality is adequate for consumer satisfaction, that is, voltage and frequency are kept within an adequate viability band and sufficiently steady (see also the Note in item 2).
5. The system has security to minimize outages (see also the Note in item 2).

Part 2: Transportation in Blocks 2 and 3 In addition to the direct economic problems of prices of the commodity of electric power, an additional problem arises connected with the cost of transporting this commodity from the seller to the buyer. This is a puzzling problem even for economists who are thinking normally of loading the truck (train, ship) at the seller and unloading it at the buyer. Electric power, however, is transported by or on the transmission network where it disperses and flows on alien territory, adding to or reducing the congestion and the losses on the lines. So what is the price of transportation (Fig. 13.4) of this? In Chapter 14 we describe possible operating and financial mechanisms for ensuring that the physical flows remain within the line constraints, that is, there is no "congestion" on the system.

Regulated System The regulated system is divided into areas that are owned by individual power companies that are responsible for providing for their customers'

needs and for the losses that develop during this operation. The losses develop on the transmission lines and depend on the flow on these lines. The latter is composed of the load that supplies the area customers' demand and the loss caused by transport of power exchange among other areas. Even if computed in detail (possible, in principle), the division is obscured by the nonlinear definition of power [15]. Because in the regulated system such exchanges are not explicitly identified, this problem cannot be properly formulated with ease, and no published solution of precision seems to exist.

Deregulated System As discussed further in the next section on block 6, it may probably be advantageous to retain the area concept in a reduced capacity for the individually owned distribution systems in a reduced role. These distribution systems may trade with the generating companies for electric power to distribute to the customers. However, some of the large customers may buy their power directly from the generators, and such companies may or may not be supplied from the area network. This would make the untangling of how much of whose power is flowing on individual transmission lines and who must pay for creating transmission constraints (congestion) and transmission losses very complex. This question is studied in detail in Chapter 14 together with several conceptual solutions under consideration.

These results are then fed into the physical system, blocks 4 and 5, to set the controls, and also fed back through block 6 along with the data on current demand and system states to be used in the dispatch process.

Alternatives of the Dispatch Process The classical AGC process is (block 6) thoroughly developed and was used exclusively in the United States until very recently. It is treated in considerable detail in Section 13.4.

Currently the major issue in electric-power-system theory and practice is a period of transition into reduced government regulation with different objectives and with many of the actual detailed activities still very much in a development stage. A sketch of the two alternatives follows.

Part 3: Determination of Set Points in Blocks 2 and 6 In order to control the system practically within the rules, a three-level process is needed. On the first level the system must be prepared by estimation based on past records of the daily variation of the load for today's date. The most economical set of generators must be committed to cover this load with an adequate margin for deviation of the current load from the estimate and for emergencies. Then the estimated load needs to be economically distributed to the committed units in a way that makes it transportable within congestion on the network. This is illustrated in block 2.

At the second level, corrective adjustments must be made (of relatively small size) to adjust the estimated dispatch to the current actual load. This level of dispatching is more demanding, sophisticated, and time critical, although the dispatching should be of relatively small amplitude. This task as presented here is assigned to block 6.

However, the two levels described could also be combined in either block 6 or block 2. On the other hand, they are quite different in character and possibly are better suited to separate but interacting organizations. Unit commitment is carried out in the regulated system for the previous day. However, with the time interval between sales time and delivery shrinking, there is bound to be a trend toward pushing unit commitment closer and closer to be on line.

The corrective dispatch for the current load will be further discussed under block 6. The estimated dispatch from block 2 is then combined in block 3 with the correction for the current load from block 6 and developed into a set of control set points for generators, network controls, etc. This vector then transmits to the physical system in blocks 4 and 5. This determination of set points collectively becomes the active physical control of the system.

The third level deals with provisions for unexpected shortages of power and faults. Dealing with shortages will require arrangements not necessary in normal state operation. These are discrete events which may occur at unpredictable times.

Regulated, AGC Power-Dispatch Control Implementation of the corrective adjustments in response to deviations of the actual load from its forecast is carried out for the three speed ranges as follows:

1. Primary control of individual machines assures that the output of the various generators, reactive power sources, HV DC lines, and other power-electronically-switched devices stabilizes the local output variables (frequency and voltage) as close to the assigned (set point) value as possible. Also, primary control smooths the fast random fluctuations of the composite load of a typical amplitude of about 1% of the total load [16].
2. The secondary control generates the assigned values of about an hourly rate, adjusting the load forecasting results and the system frequency target (to maintain synchronous time) assigned on the tertiary level. In AGC this task is fully decentralized in an ingenious manner by driving an area control error (ACE) to zero. An ACE is a linear combination of deviations of frequency and area generation from the schedules. If all areas succeed in driving their ACEs to zero then both the system frequency and the sum of their tie-line exchange powers maintains their tertiary assigned set points. No interaction between areas is required; this process is fully decentralized. Furthermore, when one of the areas does not have enough power to meet its $ACE = 0$ condition, other areas across the system will contribute. This system is fully decentralized at the expense of the deviations in the system frequency and the normal total area generation dictated by $ACE = 0$. This ingenious decentralization greatly simplifies the control of the system. It also provides an opportunity for some cheating by faking a need. The total load is determined so as to minimize generation including transmission losses. This optimizes the income of the company who owns the area.

3. The tertiary level control (NERC) in the United States covers the entire system and it also is slow in a day-to-day sense. Time error correction is done at this level to compensate for the integral of system frequency drift.

Deregulated Power-Dispatch Control The basic structure of the new operation needs to be the same in the sense that primary, secondary, and tertiary control needs to be provided through the fast, medium, and slow dynamic ranges of the system. Details, however, differ for different objectives, and numerous alternatives exist. With the new organization (see Fig. 3.1), power companies will still exist as power distribution companies with many large and small customers, so it may be desirable to still treat these as areas that will trade directly with companies owning generators for buying and transporting power over the transmission system. Since the main transmission system may be owned by a different, systemwide organization, the distributing company network would break up into segments, corresponding to what is called subtransmission networks in connection to Figure 3.1.²

This assumes that power is bought by these remaining distribution areas through one single bus, implying small areas. If, on the other hand, areas buy power over the transmission-system lines at several buses, then difficult questions arise since in this situation lines within the area are also part of the transmission system.³ Power then is sold from generation companies to these redefined areas and some very large consumers, not in any area.

A possible arrangement and the question it raises will be sketched here to parallel the descriptions in the section titled “Regulated, AGC Power-Dispatch Control” with the details in Section 13.4.2.

1. Primary dispatch control of individual machines will still remain basically as described in item 1 of the section just noted.
2. Secondary dispatch control will still have the task of distributing power inside the area and still have the objective of distributing the power bought by the distributing company over several buses on its network [17]. This would be a similar but more complex question than the secondary control described for the regulated AGC power-dispatch control, still with the aim of reducing cost of total power delivered including losses. On the other hand, secondary control would disappear or more precisely merge with tertiary control for areas buying through a single bus and for very large loads buying directly from a generating station through the transmission network.
3. Tertiary control can merge with the secondary level. It is now a “free” commodities market situation with the tandem objective for the seller to get the

² It is still unclear if these will be small individual companies or several (from the old area) in common ownership. There will still be here some fairly large consumers and multitudes of small ones (households).

³ The ownership and payment questions are still unresolved at this stage.

highest price for energy delivered, including losses, and for the buyer to pay the lowest price for the power received. By itself this should be a dynamics that is a straightforward application of commodities market economics that would have been worked out by economists. One consequence would be, however, a speedup of tertiary control. Buyers would still prepare estimates a day in advance of their needs to mirror how much to buy, but the purchases would need to be made on very short time scale (about an hour). Someone is needed to assure that enough power is available to supply the demand. This latter question may force retaining some measure of regulation.

These questions can be simply stated here but their proper solutions are complex and difficult problems. This leaves a very challenging research area without clear answers at this time, while the industry is moving ahead without a clear understanding and wide perspective. Some preliminary concepts are described in this chapter.

Another version of the general structure of generation and operation can be found in a very recent Ref. [85]. In this reference the emphasis is on differentiating market and technical processes in both operations and planning of the power systems.

13.2.1 Basis for Hierarchies in Regulated Generation Control

A power system is considered to be in normal operation when all equipment (generation and transmission) is functional as expected, and the only major changes are the result of load dynamics (blocks 2 and 6). Therefore power-systems dynamics in normal conditions are driven primarily by changes in demand. Typical demand curves are shown in Figures 13.5 to 13.7 [18].

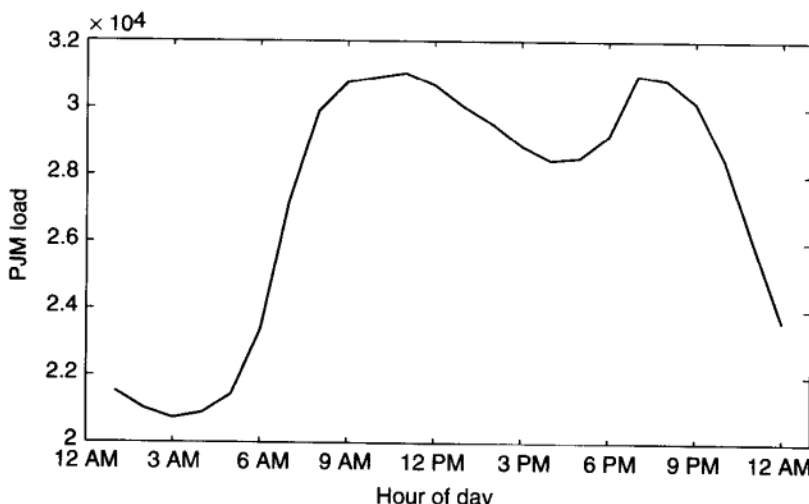


FIGURE 13.5 Typical daily load curve Pennsylvania-New Jersey-Maryland ((PJM) system).

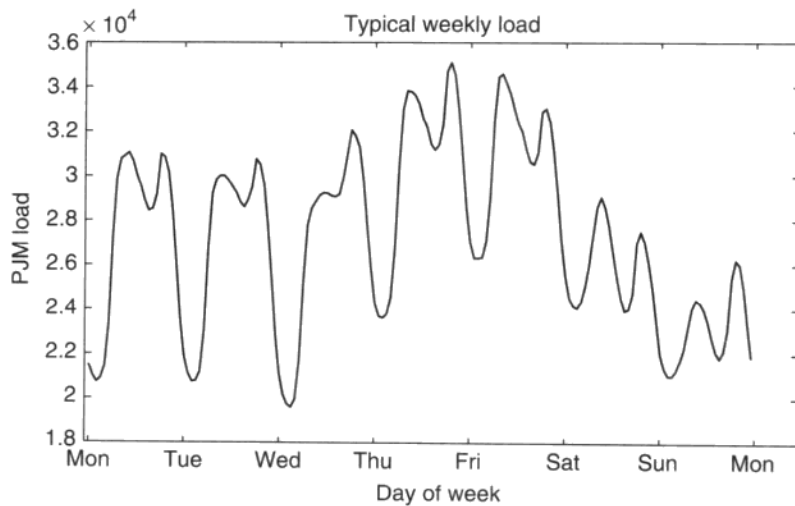


FIGURE 13.6 Typical weekly load curve (PJM system).

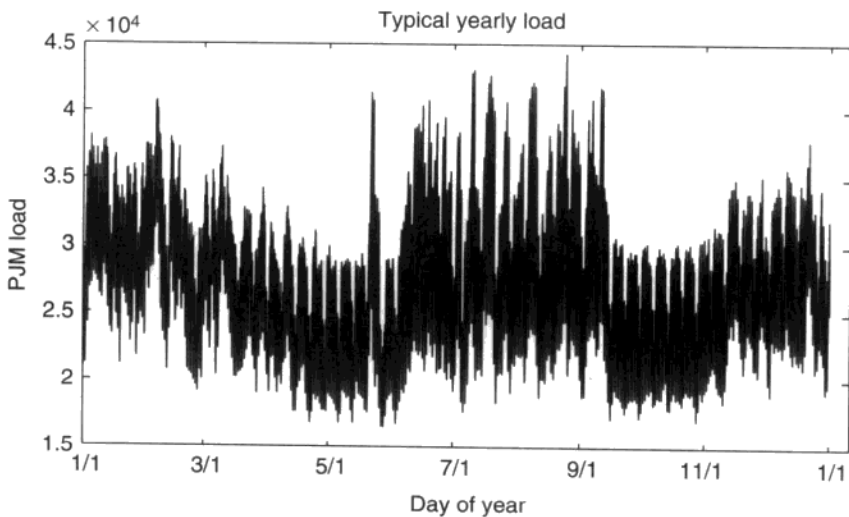


FIGURE 13.7 Typical yearly load curve (PJM) system.

It can be seen from these figures that load dynamics exhibit several rates of response, ranging from very fast random variations (order of seconds), through hourly, daily, weekly, and seasonal patterns of larger deviations. In today's hierarchical organization shown in Figure 13.8 generation-based scheduling is open loop, while the secondary level control is closed loop and automated. Variations of this can be found throughout the world; for example, the U.K. system does *not* have automatic frequency regulation, and, moreover, since the entire system is effectively a single control area, tertiary and secondary levels merge into a single level.

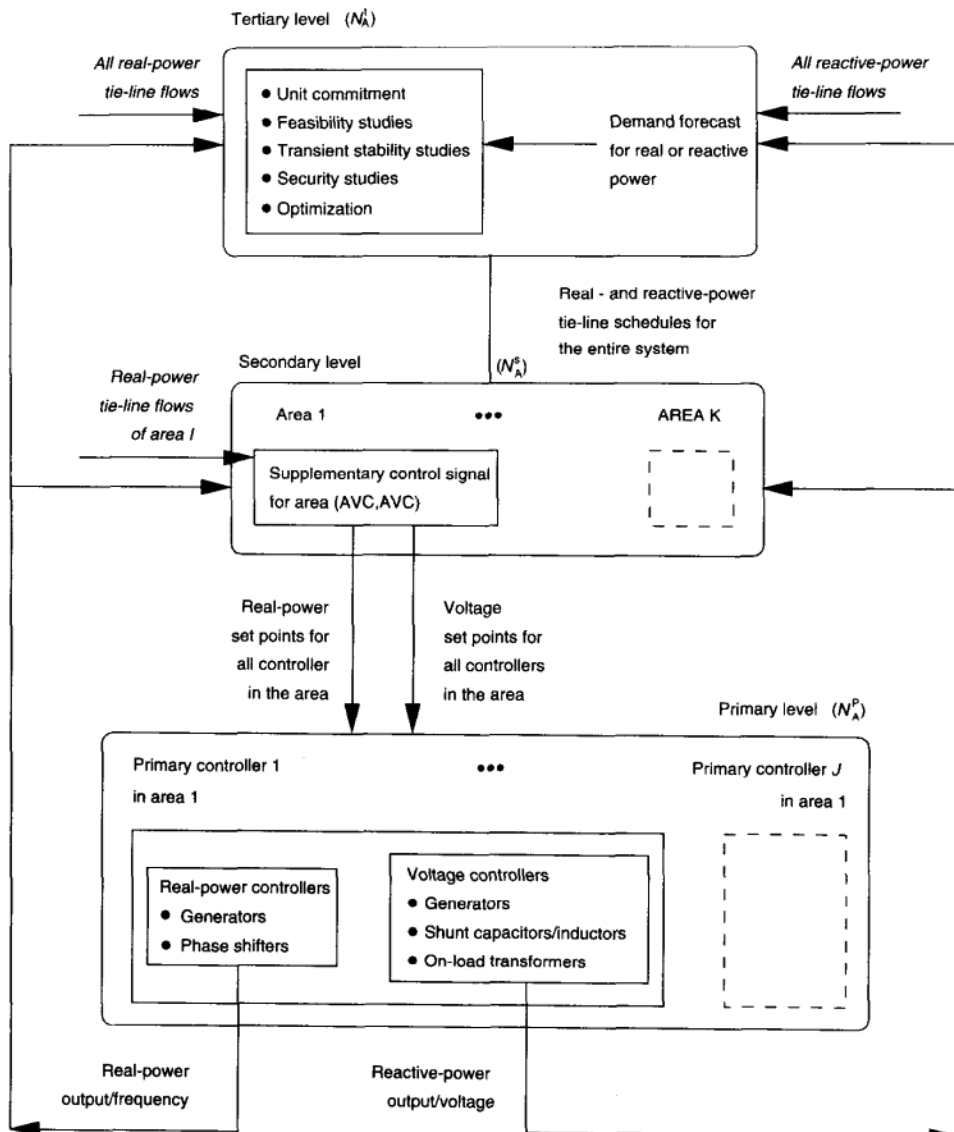


FIGURE 13.8 Hierarchical measurement and control structure in regulated industry [8].

13.2.2 Basis for Hierarchies in Deregulated Generation Control

In addition to the temporal decomposition-based hierarchies present in load dynamics, further temporal decompositions are emerging by establishing electricity markets whose on-line decision making evolves at daily, through hourly and even 5 minute rates (blocks 2 and 6). Two observations are relevant here for effective on-line use of generation in deregulated industry, as follows: (1) The distinction between predicted and real time is no longer as pronounced as when

unit commitment is done, assuming demand to be known for the next day, (2) It is therefore difficult to “unbundle” the economic generation scheduling process, assuming the predicted load from the on-line control function for responding to unexpected load fluctuations.

Furthermore, some customers are willing to accept power interruptions in exchange for a lower price of electricity, that is, generation is beginning to be provided to some customers on a nonfirm basis. This is a qualitative change from the utility’s unconditional obligation to charge its connected customer the same price for electricity. This raises a fundamental question about the inherent temporal decomposition of load dynamics.

It is possible that near-real-time electricity markets will develop (currently in the experimental phase in California) and that the temporal separation between generation scheduling for the predicted demand and generation control responding to still unexpected real-time demand fluctuations is no longer as pronounced as in deregulated industry. However, we emphasize the conceptual need for a closed-loop market for ensuring that frequency quality specifications are met. It is for this reason that in Section 13.4.2 we describe a possible framework for deregulated frequency control. The deregulated frequency control framework described is very simple to implement as long as attention is paid to the contract specifications. We propose that this market lends itself to an entirely decentralized implementation.

Moreover, the creation of effective markets for frequency control implies dynamic scheduling, that is, participation of regulating units from outside the control area. By definition, today’s horizontal structures are making room for open access areas of electricity provision. The fundamental function of the ACE signal, which has formed the basis for hierarchical control based on spatial separation into control areas, is shown to be gone. Frequency control is beginning to be redesigned in response to system frequency deviations, and not in response to individual ACEs of present control areas [19–22].

13.2.2.1 Economic versus Operating Objectives The unit commitment and economic dispatch are basic computer-aided tools for optimizing total variable operating cost in today’s industry. This is done by using the least expensive units to supply base load and more expensive units for load following and (load) frequency control. Important to recognize is the role of accurate short-term load forecasting; the more accurately and more frequently the load is projected, the more efficient use of available generation will be (more balancing of power in real time will take place in block 2 rather than in block 6).

In what follows, we describe the unit commitment (UC) and economic dispatch (ED) as the main means of generation dispatch essential for balancing supply and demand. While doing so, we emphasize that they are still an integral part of a single complex function whose economic and technical performance depend on the actual interdependencies of UC and ED, on one side, and frequency control, on the other. For example, it was recently estimated that the main inefficiency when doing UC comes from leaving unused generation on some regulating

units [20]. One could envision, with sufficient computing power, that generation control based solely on dynamic economic dispatch and stochastic unit commitment would be sufficient to balance supply and demand in real time without violating frequency quality specifications [22].

These normal-state standard systems control functions are summarized as follows:

Time Frame	Function
2 to 3 sec	Inertia, loads, excitation systems
7 to 10 sec	Governors
5 to 10 min	Automatic generation control (AGC)
5 to 30 min	Economic dispatch (ED)
1 to 10 hours	Unit commitment, restarting and shutting off units

In what follows, we provide a theoretical formulation of economic dispatch in regulated and deregulated industry first. This is followed by the section concerning generation-based frequency control that is necessary for delivering high-quality (frequency) power to the customers.

13.3 GENERATION-DISPATCH ECONOMY

In regulated industry generation follows demand in real time by scheduling the most economic generation in an open-loop manner for the forecasted demand (say, a day or an hour ahead) (block 2), as well as by the closed-loop hierarchical generation control (block 6).

At a control center level, the most cost-effective units are scheduled on and off to optimize generation use over daily or weekly time intervals in accordance with coordinated unit commitment. The function is open loop, performed only for anticipated, not actual, system conditions.

The longer-term operating efficiency is determined by how power plants are turned on and off, and cost optimization in real time is achieved by performing economic dispatch as the information about system loads becomes available through a supervisory control and data acquisition (SCADA) system.

In the traditional regulated approach, statistics derived from observations of many past years is used in the unit-commitment processor (carried out on the previous day) to assign an estimated load requirement hour by hour to day by day for each of the areas (power companies, pools etc.) and to assign the needed generation equipment to be available for supplying load unit by unit on the system. On the interconnected system this process includes an estimated net tie-line exchange for each area hour by hour during the current day. If everything is normal, if the load is exactly as estimated, and if the system frequency is at its nominal value, then each area is responsible for covering the sum of its connected load and the assigned tie-line exchange as economically as possible.

Pioneering work on the automatic generation control of the large power system during normal or stationary conditions was carried out by the Washington University team in the early 1970s and was published with the usual delay of a few years [23 to 27]. In this work the nature of the area load variation during stationary (or quasi stationary) conditions was carefully studied, and its decomposition into three components, separated by type and time scale, was established. The conventionally (at that time) considered static and separately treated control of area load and system frequency (LFC, box 6), on the one hand, and generation economic dispatch (box 2), on the other, were interwoven dynamically areawise by this work in a manner to utilize the available area generation optimally and to do so dynamically in a way moving toward AGC. The results were published in a three-part paper [25 to 27] of special character in the sense that the development of this approach was in progress while Parts I and II were written. The reader may prefer to start with Part III, which includes a well organized summary of the approach. This remains the most comprehensive treatment of stationary and, for the first time, dynamic generation control as a single problem.

At this point of the process it is possible to make sales of blocks of power between areas one day in advance under close government regulation. Such actions then are expressed in the scheduled network tie-line exchange amounts for the next day.

The competitive nature of a deregulated power industry has so far been primarily seen through creating markets to sell and purchase power, so-called electricity markets. Only residual imbalances resulting from market-based trades (block 2) must be controlled on line, typically in response to frequency deviations (block 6).

In the competitive power industry, balancing power supply and demand in real time is generally market-based. Two qualitatively different market mechanisms are of interest: (1) primary electricity market(s) for supplying anticipated demand (block 2) and (2) frequency-control market(s) for ensuring that system frequency remains within prespecified limits as demand deviates in real time from its anticipated pattern (block 6). Both types of markets are necessary for ensuring that the system frequency remains within its technically acceptable limits as power is provided competitively.

To reproduce, through an ensemble of markets, a response to changing load demands similar to that achieved under the traditional industry structure, one could specify a long-term bilateral market for the supply of base load power and a weekly (or daily) market for subsequent load power that would, according to contractual specifications, respond to frequently updated short-range forecasts of diurnal load trajectory (as used in dynamic dispatch programs). Alternatively, a more conventionally conceived mix of markets could include a long-term bilateral market for meeting base-load requirements a week or more ahead, a weekly or daily market for dispatch to follow daily load forecasts, and an hourly spot market to meet departures from the daily forecast [21].

For conceptual discussion herein, these differences are not critical. However, the overall dynamics and efficiency comparison of primary electricity markets

are largely unknown since these markets (block 2) are just evolving. It is of great importance to understand the interplay between electricity price dynamics (volatility) and the average efficiency effects. This will ultimately determine how much temporal unbundling of electricity markets is effective. This remains a challenging open question for both its modeling and data support.

13.3.1 Generation Dispatch in the Regulated Industry

Economic dispatch and unit commitment are functions that generally incorporate some measure of anticipation in change. The economic dispatch function generally evolves over a 5 min to 30 min period and is used to schedule generation outputs of the power plants in service every 5 minutes to follow the hourly system load trend.

In the present system the coordinator must project which units should be operated in subsequent periods. Unit-commitment programs are used to fulfill this function. Operating capacity additions must be planned in advance given the fact that it may take from 1 hour to 10 hours to restart all available steam plants, for example. Other conditions, such as hydro storage facilities, may require that weekly concerns be included (for example, start the week with full storage, end the week with no storage, and pump the storage full over the weekend). For purposes of analysis in this chapter, we consider a day-ahead unit-commitment decision for each day as a discrete time process taking place each hour.

At present various utility control centers respond to their anticipated demand and perform economic dispatch and unit commitment. The units under the jurisdiction of a particular control center generally schedule their own units for the *preagreed-upon* power exchange with the neighboring companies. Tie-line flow scheduling among different companies is done bilaterally without any overall systemwide coordination.

13.3.1.1 Conventional Economic Dispatch The economic dispatch program is routinely used for changing the power generated every 5 min to 15 min to fit the anticipated demand in near-real-time. Mathematically, this is the problem of minimizing the total generation cost:

$$\min_{P_g} \left(\sum_{i=1}^{nG} C_i(P_{Gi}) \right) \quad (13.1)$$

such that total generation equals total load,⁴

$$\sum_{i=1}^{nG} P_{Gi} = \sum_{i=1}^{nL} P_{Li} \quad (13.2)$$

⁴ In this formulation real-power transmission loss is neglected for simplicity. Transmission-loss-related issues are briefly addressed in Chapter 14 as the issue directly relevant for transmission flow control.

This basic version of unconstrained economic dispatch easily finds a solution to this optimization problem for a system of arbitrary size. A necessary condition for solving this basic economic dispatch problem is

$$\frac{dC_1}{dP_{G1}} = \dots = \frac{dC_{nG}}{dP_{G1nG}} = \lambda \quad (13.3)$$

This condition defines the least generation cost for meeting given demand. The term λ is known as the short-run marginal cost (SRMC) and at the optimum of Eq. (13.1) all unit marginal costs are equal to it.

Notice that conventional economic dispatch assumes demand to be a given input for which generation use is optimized under the constraint that total generation meets total demand [Eq. (13.2)]. It is straightforward to generalize this formulation to account for demand-price elasticity. This important generalization is described next.⁵

13.3.1.2 Generalized Economic Dispatch In the formulation of the economic dispatch given in Eq. (13.1) we assume that only generation is price responsive, while the demand is prespecified. It is straightforward to extend this formulation to account for demand-price elasticity. The generalized economic dispatch is then the problem of scheduling *both generation and demand* so that the total generation and demand cost is minimized as follows:

$$\min_{P_G, P_L} \left(\sum_{i=1}^{nG} C_i(P_{Gi}) + \sum_{j=1}^{nL} C_j(P_{Lj}) \right) \quad (13.4)$$

such that total generation equals total load [Eq. (13.2)]. A necessary condition for solving this basic economic dispatch problem is

$$\frac{dC_1}{dP_{G1}} = \dots = \frac{dC_{nG}}{dP_{n,Gn}} = \frac{dC_{L1}}{dP_{L1}} = \dots = \frac{dC_{nL}}{dP_{L,nL}} \quad (13.5)$$

Criterion (13.4) is used as a general measure of static efficiency in any competitive industry and is often referred to as the (negative of) the *social welfare*. Both generation and demand cost functions $C_i(P_{Gi})$ and $C_i(P_{Li})$ are analogous and can be represented as a single function as shown in Figure 13.9. In addition, since both generation and load have hard upper and lower limits, the optimum must account for such restrictions. One way of accomplishing this is by assuming that at the limits the costs are infinitely high, as depicted in Figures 13.10 and 13.11.

An important degenerate case of price-elastic cost functions is the problem of a generalized economic dispatch subject to must-run and must-serve constraints

⁵ Formulating both produced and consumed power as decision variables allows customers to play an active role in responding on line to the price of electricity in a deregulated industry.

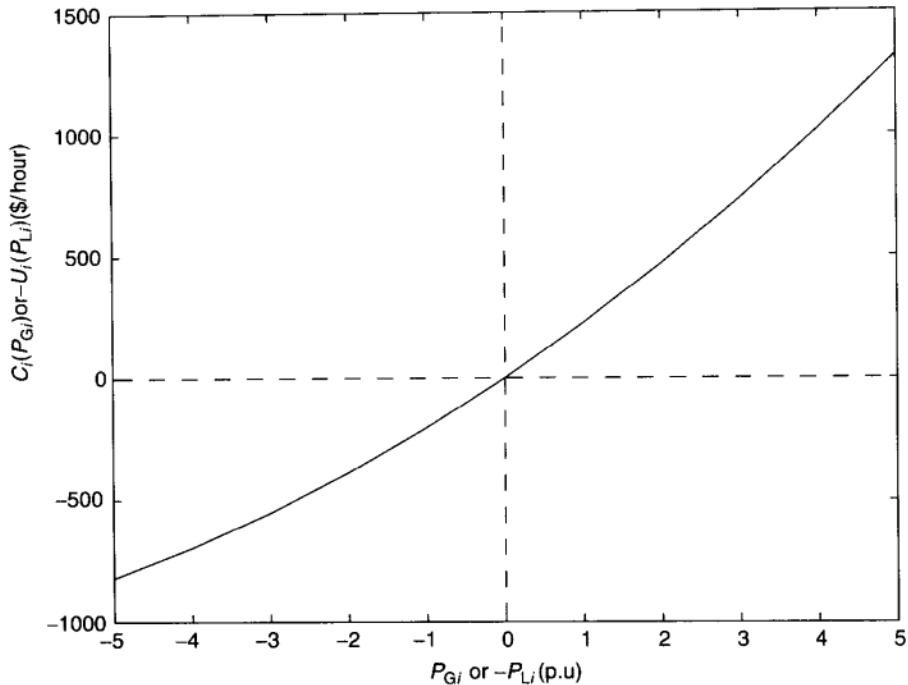


FIGURE 13.9 Simplified generation and demand cost function.

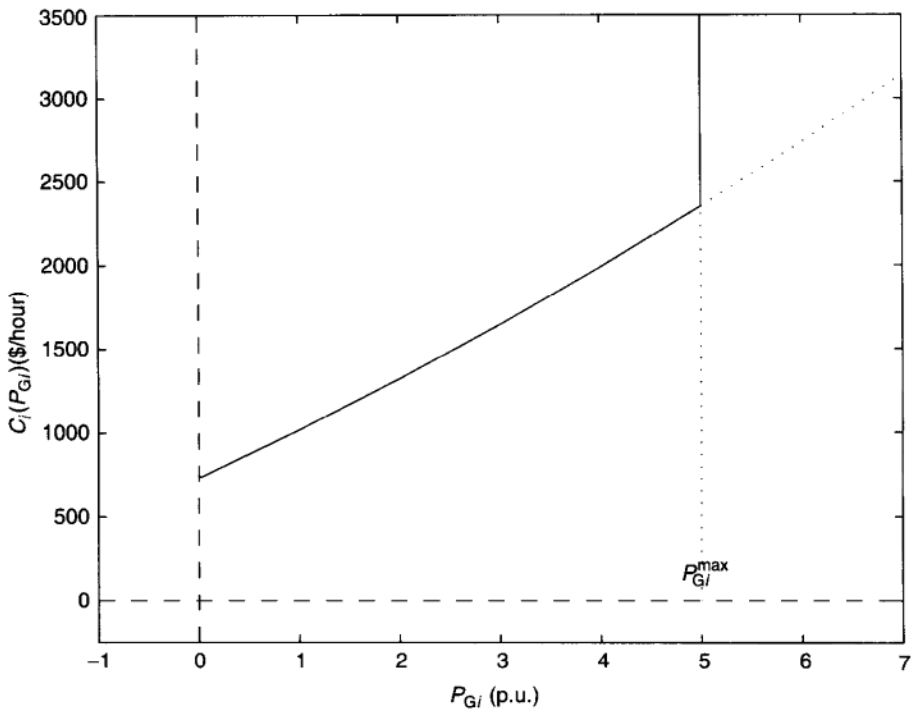


FIGURE 13.10 Generation cost function with capacity limits accounted for [40].

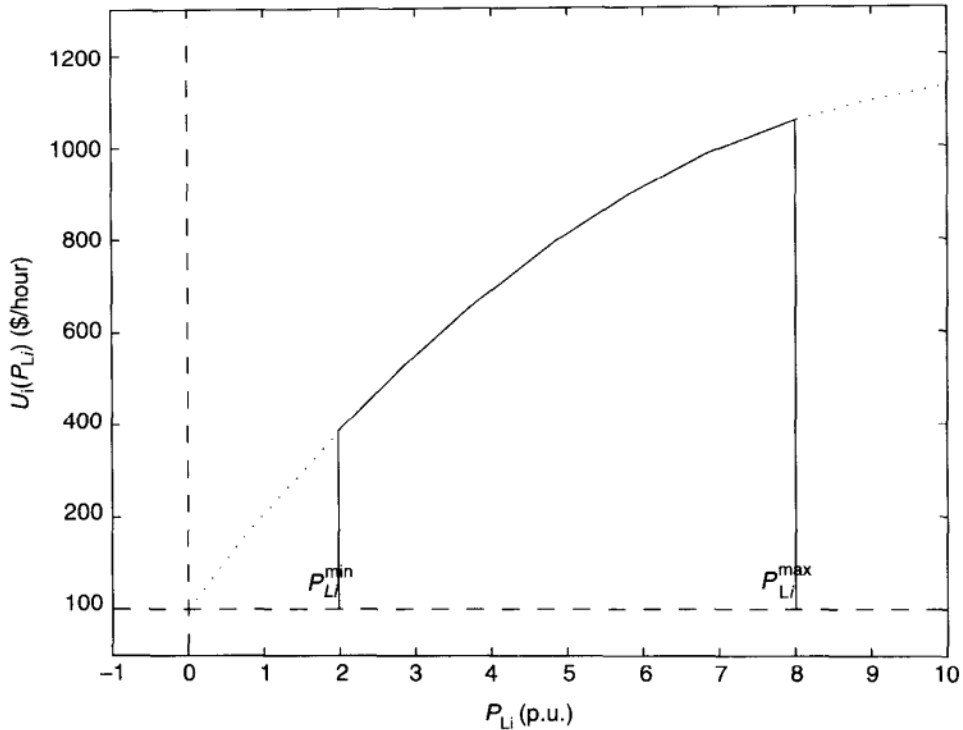


FIGURE 13.11 Demand utility function with capacity limits accounted for [40].

for some generation plants and some loads. See Refs. [28, 29] for implications of this on market outcomes.

13.3.1.3 Simplest Unit Commitment The basic unit-commitment problem (without start-up costs or minimum down-time constraints) is as follows:

$$\min_{u, P_G} \sum_{i=1}^{nG} u_i C_i(P_{Gi}) \quad (13.6)$$

subject to

$$\sum_{i=1}^{nG} P_{Gi} = P_L \quad (13.7)$$

where u_i equals 0 or 1 depending on whether the unit is off or on. Following the Lagrangian relaxation method [30, 31], one first forms the Lagrangian function,

$$L(u, P_G, \lambda) = \sum_{i=1}^{nG} u_i [C_i(P_{Gi}) - \lambda P_{Gi}] + \lambda P_L \quad (13.8)$$

By minimizing Eq. (13.8) over P_G first, one obtains the conventional economic dispatch equal-incremental condition, that is,

$$\frac{dC_i}{dP_{Gi}} = \lambda, \quad \forall i \quad (13.9)$$

which permits one to solve for P_{Gi} in terms of λ , the system incremental cost or

$$P_{Gi} = P_{Gi}(\lambda) \quad (13.10)$$

Equation (13.10) is then substituted into Eq. (13.8) so that the Lagrangian becomes

$$L(u, \lambda) = \sum_{i=1}^{nG} u_i (C_i(P_{Gi}(\lambda)) - \lambda P_{Gi}(\lambda)) + \lambda P_L \quad (13.11)$$

Finally, the Lagrangian method minimizes $L(u, \lambda)$ with respect to u giving the *switching-curve law*:

$$u_i = \begin{cases} 0 & \text{if } C_i - \lambda P_{Gi} > 0 \\ 1 & \text{if } C_i - \lambda P_{Gi} < 0 \end{cases}$$

that is, the unit is off if the average cost $C_i/P_{Gi} > \lambda$ and on otherwise. Essentially, this says that the unit should be off if the average unit cost is too high, that is, higher than the system incremental cost. This simple rule is used to decide if the unit should be turned on and off. Once on, a conventional economic dispatch is used to adjust to demand changes if these are monitored more frequently. Observe that the same λ is obtained when simply doing conventional economic dispatch, namely, that both unit commitment and economic dispatch result in the same marginal cost when the demand is assumed to be known and no intertemporal effects in starting and running power plants are accounted for.

13.3.1.4 Generalized Unit Commitment A possible generalization of the conventional-unit commitment formulation to include turning on and off price-responsive loads is straightforward, at least in principle. This problem generalization is as follows:

$$\min_{u, P_G, P_L} \left(\sum_{i=1}^{nG} u_i C_i(P_{Gi}) + \sum_{j=1}^{nL} u_j C_j(P_{Lj}) \right) \quad (13.12)$$

subject to

$$\sum_{i=1}^{nG} u_i P_{Gi} = \sum_{j=1}^{nL} u_j P_{Lj} \quad (13.13)$$

where u_j is 0 or 1 depending on whether the load is on or off. The result is a *generalized switching curve law* for both power suppliers and price-responsive

demand; the switching law is identical for power plants as in the conventional-unit commitment case, while the switching law for loads is

$$u_j = \begin{cases} 0 & \text{if } C_j - \lambda P_{Lj} > 0 \\ 1 & \text{if } C_j - \lambda P_{Lj} < 0 \end{cases}$$

that is, the load should be off if its average benefit is too low, that is, lower than the price of electricity λ . If the utility (benefit) functions of loads are made known to the operator making unit-commitment decisions, this is implementable in a very similar way as it is done for the power plants at present.

13.3.1.5 Deterministic Unit Commitment That Accounts for Various Cost Components In its very general form, the unit commitment problem may be written as follows [32]:

$$u_k^* = \arg \min_{u_k} E_{w_k} \left(\sum_{k=1}^N C_k \right) \quad (13.14)$$

that is, a unit commitment is the problem of computing decisions u_k^* that minimize the total *expected* cost over some future horizon while satisfying all constraints. Here E_{w_k} stands for the expected value with respect to the random variable w_k . For unit commitment, w_k is typically real power demand, as well as the availability of generators and transmission lines. Unit-commitment decisions are made at periodic intervals k . The time period between decisions is referred here as a *stage*. The future horizon of interest is N stages long.

Because of the enormous computational complexity of the stochastic unit commitment, many simplifications are made in practice. The possibility of generator and line failures is typically handled by providing an adequate reserve margin [30, 31, 33], so that all loads are served with very high probability.

A simplified version of the general unit-commitment problem formulation results when the optimization is performed assuming that the *demand is equal to the forecasted value* [31, 34]. In this case a random load is replaced by its predicted value. Even under this assumption, the real-life unit-commitment problem is a complicated problem with a large number of possible decisions [32]. In particular, the rate of response of units, start-up and shutdown costs, must-run times, etc., result in a complicated production cost function. The total cost incurred during stage k , denoted as C_k , is

$$\begin{aligned} C_k = \sum_{i=1}^{n_G} & \left(\int_0^{h_k} C_{Gi}(P_{Gi}(t)) dt + u_k(i) I(x_k(i) < 0) S_i \right. \\ & \left. + [1 - u_k(i)] I(x_k(i) > 0) T_i \right) \end{aligned} \quad (13.15)$$

Here I is a conditional statement and it has value of 1 if the statement is true and 0 if it is false. h_k stands for the number of hours in stage k , and S_i and

T_i are start-up and shutdown costs for generator i , respectively. x_k is the state variable (in the simplest case, the only state is the on or off status of plants as the decision is being made for the next stage).

Given a predicted system demand over the future horizon of interest T (T is a week or longer in Figs. 13.5 to 13.7), typically used unit-commitment software computes the turn-on and turn-off times for various plants taking into consideration the start-up cost, rate of response of plants, must-run time, etc.

13.3.1.6 Stochastic Unit-Commitment Problem Many unit-commitment methods in use are deterministic with respect to the load, meaning that the optimization is performed assuming that the actual demand is equal to its forecasted value [31, 34]. It can be shown that a schedule obtained by replacing a randomly varying demand by its expected value would be suboptimal when compared with the result obtained using the stochastic unit-commitment problem formulation given in Eq. (13.14). Because of this, some power companies have developed unit-commitment methods that allow for a probabilistic load distribution [33, 35].

We stress in the later part of this chapter that probabilistic (multistage) decision making is possibly the most critical part of becoming a successful market participant in the new power industry. While much of such decision making will be made by the marketers, it is important to understand the necessary decision-making process of this type by the system operators themselves. An effective day ahead, or week ahead, coordinated forward spot market is in many ways equivalent to using a stochastic unit commitment in today's industry [32]. The seemingly unnecessary distinctions in formulating the unit-commitment problem must be understood to appreciate issues such as causes of real-time electricity price volatility and inefficiency in the new industry.⁶

The stochastic unit-commitment problem is the problem of finding a sequence of optimal unit-commitment decisions (for example, for the next 24 hours) $u[1], u[2], \dots, u[24]$ where $u[k] = [u_1[k] \ u_2[k] \ \dots \ u_{nG}[k]]^T$ is a decision vector for all generating units at stage $[k]$ so that

$$\min_{u[1], u[2], \dots, u[24]} E_{P_L[1] \dots P_L[24]} \sum_{k=1}^{24} \sum_{i=1}^{nG} C_i[k] \quad (13.16)$$

Mathematically, the stochastic unit-commitment problem can be expressed as a dynamic programming problem including control inputs, system states, and uncertain random variables [31, 32, 36]. Time is broken down into a series of stages, and a control decision is made at the beginning of each stage. The system

⁶The same issues exist in today's industry, except that these are masked from the power consumers since only average charge is stated.

can be described by the following equations:

$$x_{k+1} = f_k(x_k, u_k, w_k) \quad (13.17)$$

where $k = 0, 1, \dots, x_k$ is the state vector at time k , u_k is the control input at time k , and w_k is a random disturbance. The state transition equation (13.17) defines how the state changes from one stage to the next [31]. At each stage, there is a cost to be paid. The problem is to determine a control policy u_k that minimizes the cost (or maximizes the reward).

In the case of finite number of stages N , at each stage k there is cost $g_k(x_k, u_k, w_k)$ incurred. Additionally, there is a terminal cost $g_N(x_N)$ that depends on the final value of the state vector. The objective of the problem is to find the control policy that minimizes the total expected cost over N stages, known as the *optimal policy*. Dynamic programming is a method for finding such policy, and it is expressed mathematically as [36]

$$\begin{aligned} J_N(x_N) &= g_N(x_N) \\ J_k(x_k) &= \min_{u_k \in U_k(x_k)} E_{w_k}[g_k(x_k, u_k, w_k) + J_{k+1}(f_k(x_k, u_k, w_k))] \end{aligned} \quad (13.18)$$

where $J_k(x_k)$ denotes the optimal expected cost when beginning at stage k . An optimal policy u_k^* is obtained so that it attains the minimization in Eq. (13.18) for each x_k and k .⁷

While this formulation is complex and generally not solvable exactly in real time for large electric power systems, potential benefits from such *multistage decision making* must be kept in mind. This fact was recognized some time ago in Ref. [22] and recommendations were made to perform so-called dynamic dispatch that incorporates active load prediction.

The most critical distinction between the simplified unit-commitment methods in today's industry and the solution obtained using a dynamic programming approach comes from the assumption that the events at various stages are not correlated [21]. This assumption cannot be made with any significant uncertainties present (demand forecast, generation and transmission lines availability, etc.)

13.3.2 Generation Dispatch in the Deregulated Industry

It is helpful to view the primary electricity markets as replacements for co-ordinated generation dispatch for the expected load at a control center level in today's industry. Functions such as unit commitment and economic dispatch may be accomplished through various forms of primary electricity markets, ranging from the long-term bilateral through spot markets, and possible others.

The electricity markets often take the form of an auction whereby many sellers and buyers submit bids to supply or receive power. An auctioneer then selects a

⁷ Note that an optimal policy need not be unique.

subset of the bids according to a set of rules. If the auctioneer is buying power from the generators on behalf of the pool, as in the United Kingdom, then the auctioneer's job is to minimize the pool purchase cost. If the auctioneer, as in the Alberta pool, receives both selling and buying bids, then the auctioneer's function is to match the aggregate generation-price curve to the aggregate load-price curve as closely as possible. If the structure is one of private bilateral contracts, then the two partners (or brokers on their behalf) carry out the role of the auctioneer by matching individual buyers and sellers.

The (independent) system operator and the electricity market could be separate bodies, as is the case in California [37]. The system operator is concerned with maintaining system security without knowledge of contract prices, while the main job of the electricity market is to match supply and demand most economically. In some instances, however, the two functions are carried by the same body, for example, in the United Kingdom, or are proposed to be done this way, such as in New York and New England. Concerning Figure 13.4, the system operator approves technically feasible transactions (block 3) requested at the electricity market level (block 2).

13.3.2.1 Electricity Markets There exist a number of approved and proposed competitive structures for the trading of electricity [38].

1. Wholesale competitive generators bid to supply power to a single pool. Load-serving companies buy wholesale power from the pool at a regulated price and resell it to the retail loads.
2. Wholesale competitive generators bid to supply power to a single pool, while load-serving companies then compete to buy wholesale power from the pool and resell it to the retail loads.
3. Combinations of structures 1 and 2 with bilateral wholesale contracts between generators and load-serving entities.
4. Combinations of all previous structures plus contracts between all entities and retail loads.

13.3.2.2 Trading Entities It is useful to define a number of commercial entities in a competitive power system structure. These are as follows.

1. Generator-serving entities (GSEs). The goal of these is to trade on behalf of one or a group of generators.
2. Load-serving entities (LSEs). Their goal is to trade on behalf of the loads.
3. Pure trading entities or marketers. The basic function of the evolving power exchanges and marketers is to facilitate certain level of aggregation for trading power on a complex system consisting of thousands of physical loads and hundreds of suppliers. The role of these is to trade on behalf of any generator, load, or other trading entity. One can think of a pool as one type of trading entity.

Under competition, generation, loads, and flows are not the only system decision variables. To these, one must add the contracts among trading entities. Such contracts are defined by the market conditions, and, together with the bus loads, they can be considered as the system inputs driving the power system. The transaction network introduced in Refs [39, 40] is a useful general tool for representing the information flow among trading entities as well as the contracts among them under any competitive structure. Figure 13.12 shows a general form of a transaction network where the arrows represent matrices of transactions among the various types of trading entities. We note that marketers, generators, and load-serving entities can also trade with each other as shown by the arrows starting and ending in the same circle. In this section we provide only the basic mathematical formulation of decentralized economic dispatch and unit commitment for the restructured industry.

13.3.2.3 Economic Dispatch and Unit Commitment in Deregulated Industry

When competitive bilateral transactions take place, the main objective of each party is to maximize its profit,

$$\max_{P_i} \pi_i(P_i) \quad (13.19)$$

where P_i represents net (generation and demand) power traded, $\pi_i = pP_i - C_i(P_i)$ stands for the profit made by the market participant i through some sort of trading process, given a (known) price of electricity p . If the market participant is a generator, then

$$\pi_i(P_{Gi}) = pP_{Gi} - C_i(P_{Gi}) \quad (13.20)$$

while if it is a load,

$$\pi_i(P_{Li}) = -[pP_{Li} - C_i(P_{Li})] \quad (13.21)$$

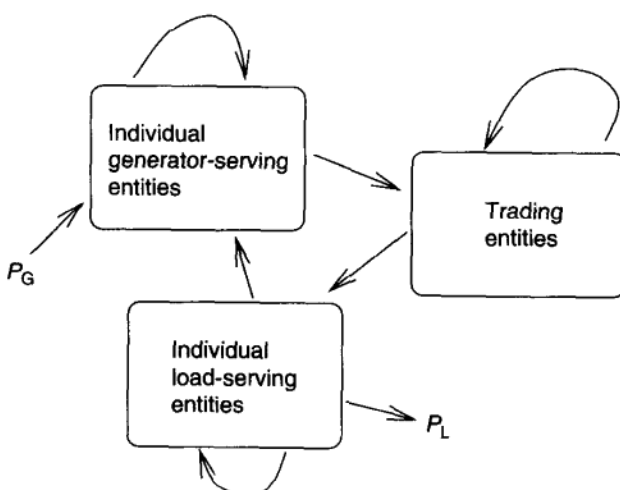


FIGURE 13.12 General transaction network, Ref. [40].

In these equations, p is the price paid and C_i is the cost function. Thus, under perfect conditions, when the market converges to a single electricity price for both sellers and buyers, p , one can maximize π_i to yield

$$\frac{dC_{G1}}{dP_{G1}} = \dots = \frac{dC_{nG}}{dP_{nG}} = \frac{dC_{L1}}{dP_{L1}} = \dots = \frac{dC_{nL}}{dP_{nL}} = p \quad (13.22)$$

This is simply obtained by each market participant optimizing its own profit and/or benefit for the assumed (exogenous) market price p . The process of bilateral decisions will stabilize at the systemwide economic equilibrium under a perfect information exchange among all decision makers.

Thus, because the necessary conditions (13.3) and (13.22) are identical under perfect market conditions,⁸ both the currently used unconstrained economic dispatch and a competitive market process should lead to the same power quantities traded and to the same total social welfare optimum. Most importantly, in this case the optimal electricity price is reached under the same conditions for which the social welfare is maximized. The performance objectives of the individual market participants (price) and the total operating cost are consistent.

13.3.2.4 Decentralized Unit Commitment Consider first a simplified situation with a single generator owner that sells electricity into a day-ahead spot market. This problem is much simpler than the stochastic unit-commitment problem in today's industry, as there is only one generator to consider, and all of the random disturbances are presumed to be reflected by the price at which power is sold.⁹ The generator owner is assumed to be a price-taker in a competitive market place.

The generation owner must make unit-commitment decisions typically by a certain time one day ahead, *before* actually knowing the spot price of the next hour. After the spot price is known, the generator decides how much power to sell (dispatch) in order to maximize profit. The only control for the problem is $u_k(1)$, whether to turn on or off at stage k . The generation level \hat{P}_{Gi} may be regarded as a function of the control $u_k(1)$ and the expected price \hat{p}_k . If $u_k(1) = 0$, then $\hat{P}_{Gi} = 0$. If $u_k(1) = 1$, then \hat{P}_{Gi} at stage k is set to maximize the *expected* profit,

$$\hat{\pi}_k = \hat{p}_k \hat{P}_{Gi} - C_i(\hat{P}_{Gi}) \quad (13.23)$$

For a quadratic cost function $C_i(P_{Gi}) = a_i P_{Gi}^2 + b_i P_{Gi} + c_i$ and not taking into consideration the generation limits the power quantity that maximizes profit at stage k is easily found to be $\hat{P}_{Gi} = (\hat{p}_k - b_i)/2a_i$.

Notice that here an assumption is made that \hat{p}_k is an *exogenous* input to the decision-making process, namely, that the market prices are uncorrelated at

⁸ Technical definition of a perfect market implies symmetric information and no gaming.

⁹ For this formulation, we assume that the generator is capable of selling as much power as desired at the market equilibrium price p_k . For analyzing the impact of generation constraints on decision making and a numerical example illustrating inter temporal effects, see Refs. [18, 32].

different decision-making stages. The same process gets computationally more involved when the price is modeled as a state variable. The result, that is, the overall profit, should be higher with this additional variable. The problem, of course gets computationally more involved. For examples of this, see Ref. [41].

13.3.2.5 Theoretical Equivalence of a Coordinated and Decentralized Economic Dispatch Here we state a fairly straightforward way of confirming the conclusions drawn before that optimizing the total cost by the integrated utility is theoretically equivalent to the decentralized profit maximization by the power suppliers. This can be done by posing a dual problem of the primary optimization problem and showing the claim by simply exchanging the order of two suboptimization problems. This proof is contributed by Jean-Pierre Leotard, MIT.

The real-power generation-dispatch problem in the regulated industry

$$\min_{P_i} \left(\sum_i C_i(P_i) \right) \quad (13.24)$$

subject to the equality constraints

$$\sum_i P_i = 0 \quad (13.25)$$

and the inequality constraints

$$P_i \leq P_i^{\max} \quad (13.26)$$

can be restated as a the following minimum–maximum (min-max) problem:

$$\max_{\lambda, \sigma_i} \min_{P_i} \sum_i C_i(P_i) - \lambda \sum_i P_i - \sum_i \sigma_i (P_i^{\max} - P_i) \quad (13.27)$$

Now, the proof for the theoretical equivalence between the real-power economic dispatch in the regulated and deregulated industries is based on the simple mathematical fact that

$$\max_{x_1, x_2, \dots, x_n} \sum_i f_i(x_i) = \sum_i \max_{x_i} f_i(x_i) \quad (13.28)$$

A simpler problem is when the inequality constraint is inactive (no capacity constraints). In this case, the min-max problem can be rewritten as

$$\max_{\lambda} \min_{P_i} \sum_i [C_i(P_i) - \lambda P_i] \quad (13.29)$$

or, by applying Eq. (13.28),

$$\max_{\lambda} \sum_i \min_{P_i} [C_i(P_i) - \lambda P_i] \quad (13.30)$$

Thus, given the price of electricity (λ), individual power producers could choose their output by minimizing $C_i(P_i) - \lambda P_i$, which is equivalent to the decentralized profit maximization.

The same reasoning applies to the economic dispatch subject to the generation capacity constraints; in this case the min-max problem is formulated as

$$\max_{\lambda} \max_{\sigma_i} \min_{P_i} \sum_i [C_i(P_i) - \lambda P_i - \sigma_i(P_i^{\max} - P_i)] \quad (13.31)$$

After applying the property (13.28) twice, one obtains

$$\max_{\lambda} \sum_i \left(\max_{\sigma_i} \min_{P_i} [C_i(P_i) - \lambda P_i - \sigma_i(P_i^{\max} - P_i)] \right) \quad (13.32)$$

The optimization problem (13.32) consists of n decentralized optimization problems, each of which is interpretable as a single constrained profit maximization problem. Thus, given price λ , power producers can choose their outputs the same way as one would obtain these by solving a generation-capacity-constrained economic dispatch in a coordinated way.

13.3.2.6 Theoretical Equivalence of a Coordinated and Decentralized Unit Commitment As the coordinated-unit commitment of today's industry is being partially replaced by the decentralized scheduling in a bilateral way, an important question arises concerning similarities and differences of the two solutions. In the simplest case of assuming deterministic (known) price, and ignoring start-up costs, must-run time constraints, etc., it can be shown that an individual decision-maker would arrive at the *same average cost versus market price decision rule as the rule often used by a system operator scheduling plants in a coordinated way*, reviewed in the preceding section.¹⁰ The proof for this is as follows. This proof provided by Eric Allen, M I T.

Given a generator i with cost curve $C_i(P_{Gi}) = a_i P_{Gi}^2 + b_i P_{Gi} + c_i$ and fixed cost C_{Fi} , its profit while on is

$$\hat{\pi}_{on} = \hat{p}\hat{P}_{Gi} - C_i(\hat{P}_{Gi}) - C_{Fi} \quad (13.33)$$

The profit while off is

$$\hat{\pi}_{off} = -C_{Fi} \quad (13.34)$$

After determining the value of P_{Gi} that maximizes the "on" profit, the decision to turn on or off is made. The generator will turn on only if $\hat{\pi}_{on} > \hat{\pi}_{off}$, or

¹⁰ An important assumption here is that cost curves are smooth convex functions; when this is not true, this proposition fails.

$\hat{p}\hat{P}_{Gi} - C_i(\hat{P}_{Gi}) > 0$, which is equivalent to

$$\hat{p} > \frac{C_i(\hat{P}_{Gi})}{\hat{P}_{Gi}} \quad (13.35)$$

which is the average cost rule used for coordinated unit commitment. Notice that generation limits do not affect this result. A generation limit may preclude a more profitable choice of \hat{P}_{Gi} , but as long as the average cost rule is satisfied, the generator will turn on.

One can conclude based on this derivation that under perfect market assumptions and when neglecting minimum run times, startup costs, etc., a system operator would schedule the *same units* to what would be decided in a decentralized way by the individual power producers.

13.3.2.7 Generation Dispatch at a Spot-Market Level A bilateral trading process can be interpreted as a *decentralized* unit commitment that at least partially provides generation to supply system demand. However, this process does not guarantee that the generation sold will meet the predicted system demand, and an additional unit commitment must be done in near-real-time (on a day-ahead spot market) to supply the remaining generation.

This day-ahead unit commitment at a spot-market level is generally done in a coordinated way, except that it relies on price bids resembling supply functions that are not necessarily the same as cost functions. In that sense, the only difference with the unit commitment decision-making is that this process is based on price instead of cost. For example, such a combined unit-commitment–economic-dispatch feature in the U.K. pool company is presently done according to the average cost rule [42]; the only difference is that in a competitive pool company the decision is based on the relative comparison of the average unit cost and the system price p instead of cost λ .

The demand at a spot market is generally estimated by a power-exchange (PX) coordinator (or, alternatively, a system operator) who attempts to purchase just enough power from the GSEs to meet the load required by the LSEs. However, some GSEs and LSEs (for example, scheduling coordinators in the California market) may also sell or buy power from the spot market if they cannot cover their long-term contracts with their native generation, or if they wish to respond to real-time price changes on the spot market while still meeting their long-term power contracts. Once spot-market demand has been determined, the generator bids are stacked, starting with the lowest price. The point at which the stack of bids intersects the cumulative load specifies the clearing price, defined as the price demanded by the most expensive bid accepted. This price will be awarded to all accepted bids as shown in Figure 13.13.

13.3.2.8 Hourly Spot Submarket In the case in which a sufficient information structure is in place for accurate demand estimates on an hourly basis or shorter, one could consider having yet another spot market that operates 1 to

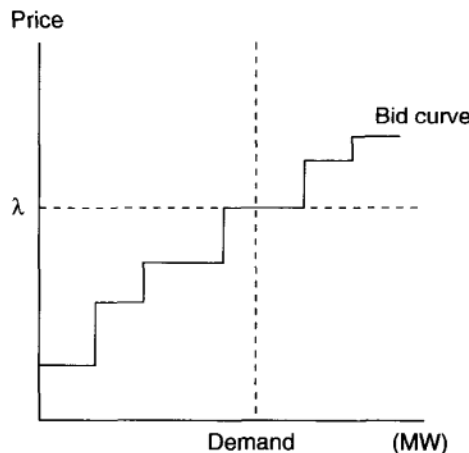


FIGURE 13.13 Spot-market price determination.

2 hours ahead.¹¹ In principle, the existence of such a market could contribute to an improved short-term price efficiency when compared with the efficiency of the combination of a day-ahead market and the on-line frequency-control market.

At present, the system has no accurate load estimators at the substation level. This level is being replaced by the LSEs, and it would be highly desirable to provide short-term (1- or 2-hour horizon) forecasts of load trajectories, updated at 5-min intervals. Requiring the frequency-control market instead to follow differences between actual load and daily forecasts would put a burden on that market that would cause very inefficient use of regulating energy.

13.3.2.9 Market Power-Related Questions One of the basic problems with forming electricity markets is the presence of market power [43, 44]. The large utilities, owners of generation, become large participants in bid-based generation dispatch. The derivations mentioned earlier assumed that all market participants (sellers and buyers) are price “takers,” in other words, their actions are not significant enough to influence the market price of electricity. Consequently, they will not be in a position to sustain bids that are higher than their operating cost, and the price of electricity, as derived earlier, would be determined by the price of the highest bid used. If this is not the case, some market participants may be very large (as a result of either small total power needed, or because of their relative capacity, or because the number of market participants is small) and therefore in a position to influence the price of electricity through their bids.

¹¹ Equivalent to the U.S. Federal Energy Regulatory Commission's (FERC's) load-following function.

These issues are essential when comparing the performance of the regulated generation dispatch to the deregulated dispatch and may be significant enough to offset potential benefits of competition. They are not covered in this book, but the reader must be aware of this very real problem.

13.4 GENERATION-BASED FREQUENCY CONTROL

Of course the actual current load will virtually never match its statistically estimated value for which generation dispatch is done and the system frequency is also subject to small fluctuations. Consequently some form of on-line control will be needed to keep the system frequency close to nominal. The specific control design block 6 in Fig. 13.4 generally depends on the horizontal structure of the given electric power system, and it could range from a manual frequency control of an isolated system as in the United Kingdom through a hierarchical generation control in a multicontrol area setup as in the United States.¹²

An important observation concerning frequency control is that even the most advanced hierarchical frequency control is strikingly simple with respect to its on-line information and coordination requirements. Most of the early engineering literature on this topic provides an explanation for this simplicity using static power or frequency thinking valid only at a system equilibrium. An important exception to this is the early work by Concordia and Kirchmayer [45, 46]. In the later work by Elgerd and others this issue is recognized and the problem is formulated using a detailed model of governor–turbine–generator dynamics and viewing the control design as a single (PI) proportional integral optimal controller design problem [40, 47–49].

However, these formulations do not lend themselves to a direct separation of subcontrol tasks ingrained in the hierarchical generation-based control design shown in block 6. Here primary controllers only stabilize the local generator frequency to its set-point value, defined at the slower rate at each control area (secondary) level, with very little, even slower, adjustment of these set points in response to a coordinating signal given from the interconnection (tertiary) level. Only recently was such a formulation developed in Refs. [8, 50–53].

Here we pose a hierarchical frequency-control design problem based on this latest work. The emphasis is on developing models directly relevant for each specific level of hierarchy (primary, secondary, and tertiary) and on using these models for systematic frequency-control design. This general structure-based hierarchical modeling and control design approach is reviewed in Appendices 13.1 and 13.2. It is summarized there how, given an arbitrary horizontal structure of a large dynamical system, models relevant for the higher-level (secondary and tertiary) control could be introduced first. The secondary and tertiary control design levels are then defined using these higher-level models.

¹² The U.S. implementation is often referred to as the automatic generation control (AGC).

13.4.1 Frequency Control in the Regulated Industry

In this section we introduce a hierarchical design for frequency control based on the linearized decoupled real-power–frequency dynamic model in Chapter 6, Eq. (6.93). Here we take an approach that provides a sufficiently general model for capturing changes in system state variables caused by the slow and small demand fluctuations. We show how this method could be used for hierarchical real-power–frequency control design. Then we reinterpret the rationale for the currently used ACE signal in the U.S. AGC scheme by analyzing the relations defining equilibrium of the general model.

The emphasis is on understanding the fundamental need for minimal systemwide coordination necessary to maintain (load) frequency quality. To introduce these fundamentals, models directly relevant for processes evolving over the midterm and long-term time horizons are derived.¹³

13.4.1.1 Basic Hierarchies Monitoring and control of large-scale power systems currently have three distinct levels (block 6):

- **Primary control:** This level is most often entirely localized in the sense that controllers respond to the local output variable changes only. The main function of primary control is to correct for small, fast output deviations caused by fast load disturbances. Excitation and governor systems of generating plants are the main primary controllers responsible for voltage and frequency stabilization, respectively.
- **Secondary control:** This level is concerned with controlling deviations from schedules at each area level. Its main function is to eliminate frequency and voltage deviations at certain critical locations over the midterm time horizon. These deviations are caused by slow load deviations and the deviations in net generation exchange with the neighboring areas. Adjusting speed-changers of the governors and terminal voltages of the generators are the main automatic generation control means at this level of hierarchy.
- **Tertiary control:** This level is concerned with the coordination of secondary controllers by incorporating effects of interactions on the quasistatic changes of the interconnected system over the long-term time horizon. The ultimate goal of this coordination is to achieve a desired long-term systemwide performance.

The present design is hierarchical in its basic nature. Fast primary controllers are local, intended to respond to random fast load fluctuations $P_L(t) = d(t)$. The area level is intended to reset the set points of the primary controllers at a significantly slower rate than the rate at which primary control acts. Its main

¹³ This approach to power-system modeling is particularly relevant for operating power systems under competition, in which the slow interplay between system changes and economic signals has to be evaluated in a meaningful way for pricing purposes.

purpose is to regulate area performance in response to slow disturbance component $d[kT_s] = P_L[(k+1)T_s] - P_L[kT_s]$.

13.4.1.2 Basis for Temporal and Spatial Hierarchies of Generation Control

One approach to introducing temporal separation to modeling and control of very large power systems is to view loads as the main drive of open loop system dynamics. As described earlier in Chapter 3 and illustrated in Figures 13.4 to 13.6, a small component (about 2%) of the loads exhibit very fast, random fluctuations continuously, or at the very fast rate $1/T_p$. Here T_p represents the relevant sampling time for both measuring and control (stabilization) of this load component. The bulk of the load varies in a quasistationary manner at the rate $1/T_s$, where T_s is of the order of minutes. Most significant changes are the slowest rate $1/T_t$.

One possible representation of the real- and reactive-power load deviations of any load, is of the form

$$P_L = P_L(t) + P_L[k] + P_L[K] \quad (13.36)$$

$$Q_L = Q_L(t) + Q_L[k] + Q_L[K] \quad (13.37)$$

Note that this model is effectively a constant-power model described in Chapter 3. As such, it just represents time variations in power, and it does not show explicit dependence of P and Q on variations in voltage and frequency.

More complex models could be used to reflect the self-stabilizing effect of load demand, such as the frequency-dependent real-power load model in Eq. (3.250) and the voltage-dependent reactive-power model in Eq. (3.251) introduced in Chapter 3. The model in Eq. (13.36) could be rewritten for purposes of more rigorous frequency-control design, which accounts for the self-stabilizing load effect, as [27]

$$P_L = -\beta_L \omega + P_L(t) + P_L[k] + P_L[K] \quad (13.38)$$

In normal operation the transmission system responds instantaneously to these deviations in demand. The generation-based control design is done in a multi-level setting to regulate different components of frequency and voltage deviations caused by these load fluctuations. The fast, random, component of load deviations $P_L(t)$ is compensated by the control equipment distributed throughout the system, which is highly decentralized in the sense that the control $v(t)$ responds strictly to the deviations of the local output variable from the set point of the controller $v[kT]$. The set points of the controllers are adjusted at the areawide level to compensate for area load deviations $P_L[kT_s]$ and $P_L[KT_t]$. Two different subprocesses for adjusting these set points are also found in a multiutility environment in which individual utilities regulate their power and voltage at the rate $1/T_s$ while maintaining power flows with the neighboring utilities unchanged. At the slowest rate $[KT_t]$ the set points of controllers are adjusted to correct for imperfect decentralized areawide frequency control; this is done in response

to the integral of frequency deviations (time error) and it is not automated at present.

This general multilevel control approach to regulating frequency and voltage in large-scale power systems results in closed-loop dynamics that can be separated under certain conditions into very fast, primary processes evolving at the rate $1/T_p$, quasistationary, midrange processes with typical rate $1/T_s$, and the slowest quasistationary, long-term process (tertiary) evolving at the typical rate $1/T_t$. The primary process corresponds to the fast, continuous closed-loop dynamics of units, the secondary process is associated with the adjustments of set values for regional controllers over midterm horizons, and the tertiary process is associated with the slowest adjustments of the systemwide setting of controllers relevant for the entire interconnected system.

Since the secondary and tertiary processes are activated only at discrete times, a generation-based control vector can be thought of as a composite control [54] of the form

$$v = v(t) + v[k] + v[K] \quad (13.39)$$

Any process of interest is represented in terms of general multitime scale subprocesses as shown in Figure 13.14. Note that in a regulated (horizontally structured) electric power system the temporal separation typically maps into spatial separation; the fastest and medium fast generation control are designed around the objective that the generation in each area meets its connected load.

13.4.1.3 Basic Hierarchical Model Development In what follows next, we use Eq. (6.93) as the starting model for posing the problem of hierarchical generation-based frequency control at secondary and tertiary system levels. We use the general thinking reviewed in the Appendices 13.1 and 13.2 to introduce effective models for hierarchical generation-based frequency control design for normal operation of the horizontally structured electric power systems. The decoupled linearized real-power–frequency model of the large interconnected system Eq. (6.93) developed in Chapter 6 is used as the starting model. A (quasistationary) secondary-level model is derived by starting from this model and making the assumption on temporal separation among the subprocesses at the primary, secondary, and tertiary levels induced by the basic character of load-demand fluctuations. The basic idea followed in today's hierarchical frequency-control design is that primary controllers (governors) stabilize generator frequency locally to the set-point value of the governor's speed-changer; this

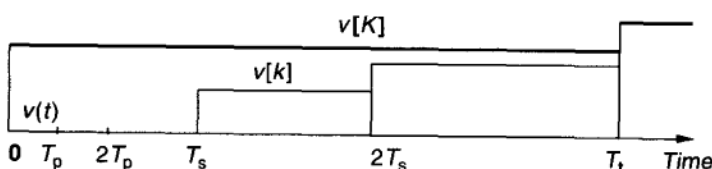


FIGURE 13.14 Multiple time scales.

is done to cancel the fastest random deviations in load. Obviously, the frequency-control design at this level requires the entire model in Eq. (6.93). The treatment of this primary control is provided in Chapter 12. Here a strong assumption is made that the primary control stabilizes these deviations. Only the secondary - or tertiary-level frequency-control design problems concerned with the systematic adjustments (regulation) of the speed-changer settings $\omega_G^{\text{ref}}[kT_s]$ at a slower rate to balance supply and demand at each control area (secondary) level in response to the slower (and presumably still small) deviations in load demand are treated. The main subprocess of interest concerns changes in generation power outputs of the area I units participating in the secondary control $P_{Gj}^I[kT_s]$. These changes are driven by the closed-loop control of the set points of the speed-changers $\omega_G^{I,\text{ref}}[kT_s]$ in response to the area frequency deviations at this rate created by the load-demand changes $P_{Lj}^I[kT_s]$ and the deviations in the net tie-line flows of power into the area $F^I[kT_s]$ from the scheduled values at the level of block 2 in Fig. 13.4. The model capturing this subprocess at the rate of interest $[kT_s]$ turns out to be very effective and simple.

The problem of tertiary-level frequency control is viewed as the question of minimal coordination of the entire interconnected system to correct for fully decentralized secondary-level controllers at the rate $[KT_1]$ and eliminate possible drift of system frequency resulting from the very slow deviations in demand $P_L[KT_1]$ and the resulting cumulative frequency deviations. Using the structure-based modeling approach, one could develop a low-order model for automating the tertiary level of control as well [52,53]. However, this has not been automated in practice today; this is partly a consequence of the fact that if the secondary-level control were to operate perfectly (that is, keep the system always at its equilibrium), one could show that there would be no need for tertiary level control at all. This is only possible because frequency at an equilibrium is the same at each point in the system (not necessarily nominal), and as such it is observable and controllable from each level of the hierarchy interchangeably.

13.4.1.4 Quasistatic Model for Secondary-Level Frequency Control The purpose of the areawise secondary control is to update the frequency set-point values (ω_G^{ref} of governors, in particular) for each participating generator–turbine–generator (G-T-G) unit at discrete times $[kT_s]$ so that frequency deviations are eliminated in agreement with the engineering standards. The model derivation here is an example of the conceptual hierarchical modeling summarized in Appendix 13.1.

Let us start with the closed-loop primary dynamical model in Eq. (6.93) described in Chapter 6,

$$\begin{bmatrix} \dot{x}_G \\ \dot{P}_G \end{bmatrix} = \begin{bmatrix} A_G & -c \\ K_P E & 0 \end{bmatrix} \begin{bmatrix} x_G \\ P_G \end{bmatrix} + \begin{bmatrix} b \\ 0 \end{bmatrix} \omega_G^{\text{ref}} - \begin{bmatrix} 0 \\ F_e \end{bmatrix} + \begin{bmatrix} 0 \\ D_P \dot{P}_L \end{bmatrix} \quad (13.40)$$

Assume that the governors are designed so that the closed-loop dynamics are fast relative to the rate of updating their set-point values. Under this assumption one

can write $\dot{x}_G = 0$, at kT_s , $k = 0, 1, \dots$, that is, the system settles to steady state at these discrete time instances kT_s [54]. Let us first consider the local dynamics of each G-T-G unit,

$$\dot{x}_G = A_G x_G + b\omega_G^{\text{ref}} - cP_G \quad (13.41)$$

The assumption of fast dynamics¹⁴ yields at kT_s

$$A_G x_G[k] = -b\omega_G^{\text{ref}}[k] + cP_G[k] \quad (13.42)$$

or

$$x_G[k] = -A_G^{-1}b\omega_G^{\text{ref}}[k] + A^{-1}cP_G[k] \quad (13.43)$$

since A is invertible. One can further calculate

$$A_G^{-1} = \frac{1}{\Delta} \begin{bmatrix} -rM & -rT_u & -(e_T + K_t)T_G \\ K_t M & -(rD + e_T)T_u & -DK_t T_G \\ M & T_u & -DT_G \end{bmatrix} \quad (13.44)$$

with $\eta = \gamma D + e_T + K_t$. Substituting this back into Eq. (13.43) simply gives

$$\begin{bmatrix} \omega_G[k] \\ P_T[k] \\ a[k] \end{bmatrix} = \frac{1}{\eta} \times \begin{bmatrix} e_T + K_t \\ DK_t \\ D \end{bmatrix} \times \omega_G^{\text{ref}}[k] + \frac{1}{\eta} \times \begin{bmatrix} -\gamma \\ K_t \\ 1 \end{bmatrix} \times P_G[k] \quad (13.45)$$

Because we are interested in the frequency variations, let us consider only the first row of this relation,

$$\omega_G[k] = \frac{e_T + K_t}{\eta} \omega_G^{\text{ref}}[k] - \frac{\gamma}{\eta} P_G[k] \quad (13.46)$$

or

$$\omega_G[k] = \left(1 - \frac{\gamma}{\eta} D\right) \omega_G^{\text{ref}}[k] - \frac{\gamma}{\eta} P_G[k] \quad (13.47)$$

Define the *droop constant* of a G-T-G unit as

$$\Sigma \triangleq - \left. \frac{\partial \omega_G[k]}{\partial P_G[k]} \right|_{\omega_G^{\text{ref}}[k]=0} \quad (13.48)$$

A droop constant represents the sensitivity of the steady-state frequency to the real-power output of a G-T-G unit when the frequency setting is kept constant (deviation $\omega_G^{\text{ref}}[k] = 0$), or the secondary-level control is inactive. A small droop constant indicates that real-power output variations have a small effect on the

¹⁴ For simplicity, kT_s is replaced by k throughout this text; similarly, KT_t is replaced by K .

steady state frequency variations. A flat droop characteristic, i.e., $\Sigma = 0$, implies that the steady-state frequency always reaches the set-point value, no matter how the real-power output varies. Clearly, an integral control must be involved in the primary controller in this case, so that the steady-state error of the primary local control vanishes.

With this general definition, one simply obtains the droop constant for the G-T-G unit discussed here as

$$\Sigma = \frac{r}{\eta} = \frac{r}{rD + e_T + K_t} \quad (13.49)$$

It then follows from Eq.(6.73) that the steady-state transfer function of the G-T-G unit for specified $P_G[k]$ is

$$\omega_G[k] = (1 - \Sigma D) \omega_G^{ref}[k] - \Sigma P_G[k] \quad (13.50)$$

where D is the generator damping constant. This is a quasistatic relation between the frequency deviation ω_G , set-point value ω_G^{ref} , and real-power output variation P_G of each G-T-G set. This relation gives the basic insight for the decentralization in the sense that no coupling among different G-T-G units occurs except through the local output variables P_G . This complete decentralization (decoupling) is transparent only if the real power output of each G-T-G unit is chosen as a state variable [50]. Real-power output variations of all G-T-G units in the network are coupled through the network constraints formulated in Chapters 3 and 4 earlier.

Let us derive the secondary level relation for an area consisting of m such G-T-G units. Since Eq. (13.50) is completely decentralized and true for each G-T-G unit, the secondary-level relation for all units in the area is simply obtained by combining Eq. (13.50) for each G-T-G unit. To do this, we define the generator frequency vector and power output vectors as

$$\omega_G \triangleq \begin{bmatrix} \omega_G^1 \\ \vdots \\ \omega_G^m \end{bmatrix} \quad (13.51)$$

$$P_G = \begin{bmatrix} P_G^1 \\ \vdots \\ P_G^m \end{bmatrix} \quad (13.52)$$

and the diagonal droop matrix and damping matrix as

$$\Sigma \triangleq \begin{bmatrix} \Sigma_1 & & \\ & \ddots & \\ & & \Sigma_m \end{bmatrix}, \quad D = \begin{bmatrix} D_1 & & \\ & \ddots & \\ & & D_m \end{bmatrix} \quad (13.53)$$

Then a decentralized quasistatic model for all m G-T-G units can be obtained as

$$\omega_G[k] = (I - \Sigma D) \omega_G^{\text{ref}}[k] - \Sigma P_G[k] \quad (13.54)$$

where I is an $(m \times m)$ identity matrix.

Recall from Chapter 6 the linearized network constraint, Eq. (6.85),

$$P_G[k] = K_P \delta_G[k] - F_e[k] + D_P P_L[k] \quad (13.55)$$

Equation (13.54) is combined with Eq. (13.55) to yield

$$\omega_G[k] = (I - \Sigma D) \omega_G^{\text{ref}}[k] - \Sigma(K_P \delta_G[k] - F_e[k] + D_P P_L[k]) \quad (13.56)$$

Writing Eq. (13.56) at two successive sampling instances kT_s and $(k+1)T_s$, one obtains

$$\begin{aligned} \omega_G[k+1] - \omega_G[k] &= (I - \Sigma D)(\omega_G^{\text{ref}}[k+1] - \omega_G^{\text{ref}}[k]) \\ &\quad - \Sigma K_P(\delta_G[k+1] - \delta_G[k]) + \Sigma(F_e[k+1] - F_e[k]) \\ &\quad - \Sigma D_P(P_L[k+1] - P_L[k]) \end{aligned} \quad (13.57)$$

Since

$$\delta_G[k+1] - \delta_G[k] \approx T_s \omega_G[k] \quad (13.58)$$

the model in Eq. (13.57) expressed in terms of $\omega_G[k]$ only takes the form

$$\begin{aligned} \omega_G[k+1] &= (I - \Sigma K_P T_s) \omega_G[k] + (I - \Sigma D)(\omega_G^{\text{ref}}[k+1] - \omega_G^{\text{ref}}[k]) \\ &\quad + \Sigma(F_e[k+1] - F_e[k]) - \Sigma D_P(P_L[k+1] - P_L[k]) \end{aligned} \quad (13.59)$$

The model in Eq. (13.59) is defined in terms of system variables at discrete times kT_s , $k = 0, 1, \dots$ only.

An alternative model for load following at a secondary level can be derived in terms of P_G as state variables. This model takes on the form [8].

$$\begin{aligned} P_G[k+1] &= (I - K_P \Sigma T_s) P_G[k] + K_P(I - \Sigma D) T_s \omega_G^{\text{ref}}[k] \\ &\quad - \Sigma(F_e[k+1] - F_e[k] - D_P(P_L[k+1] - P_L[k])) \end{aligned} \quad (13.60)$$

As pointed out in Ref. [8], there exists an important qualitative difference between the model in terms of frequencies $\omega_G[k]$ as state variables (13.59) and the model in Eq. (13.60) in which $P_G[k]$ are state variables. The model in Eq. (13.59) is solely control-driven, since when there are no disturbances in load and tie-line flows the secondary control is zero. The secondary level dynamics model in Eq. (13.60), however, is not a control-driven model because of the droop characteristics of the generator primary control. An in-depth analysis shows that

this lack of full controllability in the P_G state space is a direct consequence of the modeling singularity of the real-power–frequency model discussed earlier (Chapters 3 and 4). The system is autonomous, and power can still change with time even when the system is not subject to tie-line and load disturbances and $u_s[k] = 0$, as a consequence of generator dynamics [55]. The discrete-time corrective signal ($\omega_G^{\text{ref}}[k+1] - \omega_G^{\text{ref}}[k]$) is the control action for the secondary level.

To allow for generating units not participating in the secondary level control, partition ω_G as

$$\omega_G = \begin{bmatrix} \omega_s \\ \omega_n \end{bmatrix} \quad (13.61)$$

where ω_s and ω_n represent the participating and nonparticipating, generators, respectively. The term $\omega_G^{\text{ref}}[k+1] - \omega_G^{\text{ref}}[k]$ can now be written as

$$\omega_G^{\text{ref}}[k+1] - \omega_G^{\text{ref}}[k] = \begin{bmatrix} \omega_s^{\text{ref}}[k+1] - \omega_s^{\text{ref}}[k] \\ \omega_n^{\text{ref}}[k+1] - \omega_n^{\text{ref}}[k] \end{bmatrix} \quad (13.62)$$

By definition, for the nonparticipating generators

$$\omega_n^{\text{ref}}[k+1] - \omega_n^{\text{ref}}[k] \equiv 0 \quad \forall k \quad (13.63)$$

Let us define the actual secondary frequency-control signal as

$$u_s[k] \triangleq \omega_s^{\text{ref}}[k+1] - \omega_s^{\text{ref}}[k] \quad (13.64)$$

From these definitions, we can rewrite the control term as

$$\omega_G^{\text{ref}}[k+1] - \omega_G^{\text{ref}}[k] = \begin{bmatrix} u_s[k] \\ 0 \end{bmatrix} = \begin{bmatrix} I \\ 0 \end{bmatrix} u_s[k] \triangleq B_s u_s[k] \quad (13.65)$$

where I is an $(p \times p)$ identity matrix with p being the number of participating generators.

Let us further define the net tie-line flow effect as

$$F_s[k] = F_e[k+1] - F_e[k] \quad (13.66)$$

and also define the disturbance at the secondary level as

$$d_s[k] = P_L[k+1] - P_L[k] \quad (13.67)$$

With these definitions, we derive the discrete-time dynamics of the generator frequencies at the secondary level as

$$\begin{aligned} \omega_G[k+1] &= (I - \Sigma K_P T_s) \omega_G[k] + (I - \Sigma D) B_s u_s[k] + \Sigma F_s[k] \\ &\quad - \Sigma D_P d_s[k] \end{aligned} \quad (13.68)$$

This is the secondary-level dynamical model for all generator frequencies in terms of the frequency set-point changes and tie-line flow changes.

Load frequencies ω_L are expressed in terms of the generator frequencies ω_G by Eq. (6.82):

$$\omega_L = C_\omega \omega_G + J_{LL}^{-1}(\dot{F}_L - \dot{P}_L) \quad (13.69)$$

which leads to, with all time derivatives vanishing at discrete times kT_s ,

$$\omega_L[k] = C_\omega \omega_G[k] \quad (13.70)$$

This relation defines changes in load frequencies in terms of changes in generator frequencies.

The output variables for the secondary control include part or all of the generators and possibly some loads. Inclusion of load frequencies allows for demand-side control for the secondary level frequency regulation. Let us define the output variables as

$$\omega_o[k] = C_1 \omega_G[k] + C_2 \omega_L[k] \quad (13.71)$$

where C_1 and C_2 are matrices with 0's and 1's to pick up the desired output variables. Using Eq. (13.70) to express $\omega_L[k]$ in terms of the state variables $\omega_G[k]$, we obtain the output equation of the secondary-level frequency control as

$$\omega_o[k] = C_s \omega_G[k] \quad (13.72)$$

where the output matrix is simply $C_s = C_1 + C_2 C_\omega$.

Equations (13.68) and (13.72) constitute a simple discrete-time dynamical model for variables of interest at the secondary level. This simple model forms a basis for the secondary-level frequency control.

13.4.1.5 Conventional Frequency-Control Design The quasistatic dynamic model of frequency changes caused by deviations from scheduled area demand, Eq. (13.68), could be used for designing decentralized secondary-level controllers. As explained in the Appendix 13.2, a linear quadratic performance criterion for the area can be chosen as

$$J_s = \sum_{k=0}^{\infty} (\omega_o^T[k] Q \omega_o[k] + u_s^T[k] R u_s[k]) \quad (13.73)$$

for $Q = Q^T \geq 0$ and $R = R^T > 0$. Depending on the relative importance of the quality of frequency control and the fuel cost associated with specific G-T-G sets, the weighting matrices Q and R in the performance criterion will vary.

The secondary-level control signal $u_s[k]$ is used to cancel the effect of the load and tie-line flow variations to eliminate steady-state frequency deviations

$$u_s[k] = G_s(\omega_o[k] - \omega_o[K]) \quad (13.74)$$

The optimization with respect to the secondary control $u_s[k]$ determines the optimal gain G_s . The performance criterion reflects specifications of the output variables at the area level. It is sufficiently general to allow for specifying different frequency quality requirements at different individual generators or loads throughout the area, if so chosen.

Of course, frequencies in the area are very close numerically at different locations in the area. Because of this, a potentially more useful model for regulating power imbalances at each area level by updating the set values of governor speed-changers $\omega_G^{\text{ref}}[k]$ would be the secondary-level model in Eq. (13.68) expressed in terms of $P_{Gi}[k]$ as the state variables of interest. The locational differences among P_{Gi} and P_{Li} within the area are generally much more observable than the differences among ω_{Gi} 's in the area. A control law $u_s[k]$ similar to the control law (13.74) could be designed for optimizing a performance criterion expressed in terms of deviations in real-power variables. Designing a control law of this type may lend itself to a better understanding of cause and effect in power imbalances within each area.

13.4.1.6 Improved Frequency-Control Design The conventional control design described above does not fully guarantee the specified area performance independently of the fluctuations in the tie-line flows into the area $F_s[k]$. To get around this problem, one could design an improved control scheme for each area, as explained in Appendix 13.2. Since the number of tie lines is small, and tie-line flows are monitored in practice, an improved control law at the secondary level of the form

$$u_s[k] = G_s(\omega_o[k] - \omega_o[K]) + H_s F_s[k] \quad (13.75)$$

could be used. The gain matrices G_s and H_s are to be determined.

Under this control law, the closed-loop dynamics at the secondary level become

$$\begin{aligned} \omega_G[k+1] &= (I - \Sigma K_P T_s) \omega_G[k] + (I - \Sigma D) B_s G_s (\omega_o[k] - \omega_o[K]) \\ &\quad + (I - \Sigma D) B_s H_s + \Sigma F_s[k] - \Sigma D_p d_s[k] \end{aligned} \quad (13.76)$$

Using the output equation $\omega_o[k] = C_s \omega_G[k]$, one obtains

$$\begin{aligned} \omega_G[k+1] &= A_s \omega_G[k] - (I - \Sigma D) B_s G_s \omega_o[K] \\ &\quad + [(I - \Sigma D) B_s H_s + \Sigma] F_s[k] - \Sigma D_p d_s[k] \end{aligned} \quad (13.77)$$

where

$$A_s \triangleq (I - \Sigma K_p T_s) + (I - \Sigma D) B_s G_s C_s \quad (13.78)$$

is the closed-loop system matrix of secondary-level dynamics.

The purpose of the additional term $H_s F_s[k]$ in the control law is to cancel the effect of tie-line flows from the neighboring areas, so that each area has effectively decoupled dynamics. Full decoupling can be achieved if

$$(I - \Sigma D) B_s H_s + \Sigma = 0 \quad (13.79)$$

In general, both generator damping and the droop constants are very small, so that matrix $I - \Sigma D$ is invertible. In this case, to derive a unique solution for H_s from Eq. (13.79), one must require that B_s be nonsingular. From the structure of B_s defined in Eq. (13.65), it is clear that the nonsingularity of B_s is equivalent to all generators participating in secondary-level frequency control. In this case, $B_s = I$, and we can simply choose

$$H_s = - (I - \Sigma D)^{-1} \Sigma \quad (13.80)$$

to cancel the effect of neighboring areas. With this choice of H_s , the area under study looks as if it were disconnected from the rest of the system. The closed-loop dynamics of the area take on the form

$$\omega_G[k+1] = A_s \omega_G[k] - (I - \Sigma D) B_s G_s \omega_0^{\text{ref}}[k] - \Sigma D p d_s[k] \quad (13.81)$$

with no coupling among different areas. Unless all generators participate in the secondary control, complete cancellation of tie-line flows is not possible. In this case, only partial cancellation for some state variables can be achieved.

The gain matrix G_s can be determined by specifying the desired closed-loop dynamics or by formulating an optimal control problem.

Note that the conventional and improved control designs described here clearly separate the governor controllers at the primary level and at the secondary level, while the earlier formulations [47,48] combine the two levels into one single PI controller design; the proportional part comes from the primary level, and the integral part from the secondary. Physically these are two different control loops, and the formulation here for the first time provides two separate mathematical models for them, Eq. (6.93) and Eqs. (13.68) to (13.72).

A further comparison of the proposed formulation for secondary-level frequency control with ACE-based AGC implementation shows that the two formulations are actually consistent in terms of the measurement structure employed at the area level. Note, however, that the need for defining the frequency bias for the ACE signal is entirely eliminated with the control scheme proposed here. The gain G_s is designed according to the desired frequency quality at different locations in the area ω_0 . The gain H_s is a function of the transmission network parameters and is computed according to Eq. (13.80).

The same five-bus example illustrated in Figure 13.23 is used here to illustrate the proposed control scheme. To simplify the computation, we choose all three generators to participate in secondary-level frequency control. In this case, $B_s = I$. The output variables are simply the three generator frequencies, so that $C_s = I$. The gain H_s is chosen according to Eq. (13.80). In this case, Eq. (13.81) is simplified to

$$\omega_G[k+1] = A_s \omega_G[k] - (I - \Sigma D) G_s \omega_o^{\text{ref}}[K] - \Sigma D p d_s[k] \quad (13.82)$$

with $A_s = (I - \Sigma K_p T_s) + (I - \Sigma D) G_s$. To simplify calculations further, the gain G_s is chosen such that the three generator frequencies have decoupled identical dynamics, that is, $A_s = \lambda I$ for some scalar constant λ . With this choice of A_s , one simply obtains

$$G_s = (I - \Sigma D)^{-1} [(\lambda - 1)I + \Sigma K_p T_s] \quad (13.83)$$

Figure 13.15 shows the same linearly varying load at bus 4 as in Figure 13.16 and the generator frequency responses to this load change with and without secondary-level frequency control. The scalar constant λ is chosen to be $\lambda = -1$. Figure 13.16 clearly indicates that the proposed secondary-level control scheme eliminates the of frequencies inversely following load variations, as depicted in Figure 13.16. The control scheme also significantly reduces the steady-state frequency errors.

13.4.1.7 Tertiary-Level Frequency Control A decentralized secondary-level control design of one or the other type [Eqs. (13.74) and (13.75)] still leaves us with the question concerning necessary coordination at the interconnected (tertiary) system level. An important objective of tertiary-level control is to coordinate the area secondary-level controllers in such a way that the interconnected system operates as specified. To be more specific, the objective is to adjust tie-line flows in response to the load variations $P_L[K]$ while maintaining the system frequency. This could be done using units dedicated to this level of frequency control and adjusting their governor speed-changers systematically.¹⁵ Such tertiary-level control is envisaged as particularly effective when the load-generation mismatch in a specific control area exceeds the capacity of secondary-level controls. When certain control or output limits are reached in the stressed area, the scheduled exchange should be adjusted to facilitate help from the neighboring areas. At present, this is done in an asynchronous, ad hoc manner. If this process were to become automated, it could be implemented in much the same way as the areawise frequency control, only at a much slower sampling rate T_t . We observe that the presence of slow deviations in the average

¹⁵ At present, this task is carried out by agreement among several areas when needed. The concept is referred to in Ref. [57] for example, as “central AGC.”

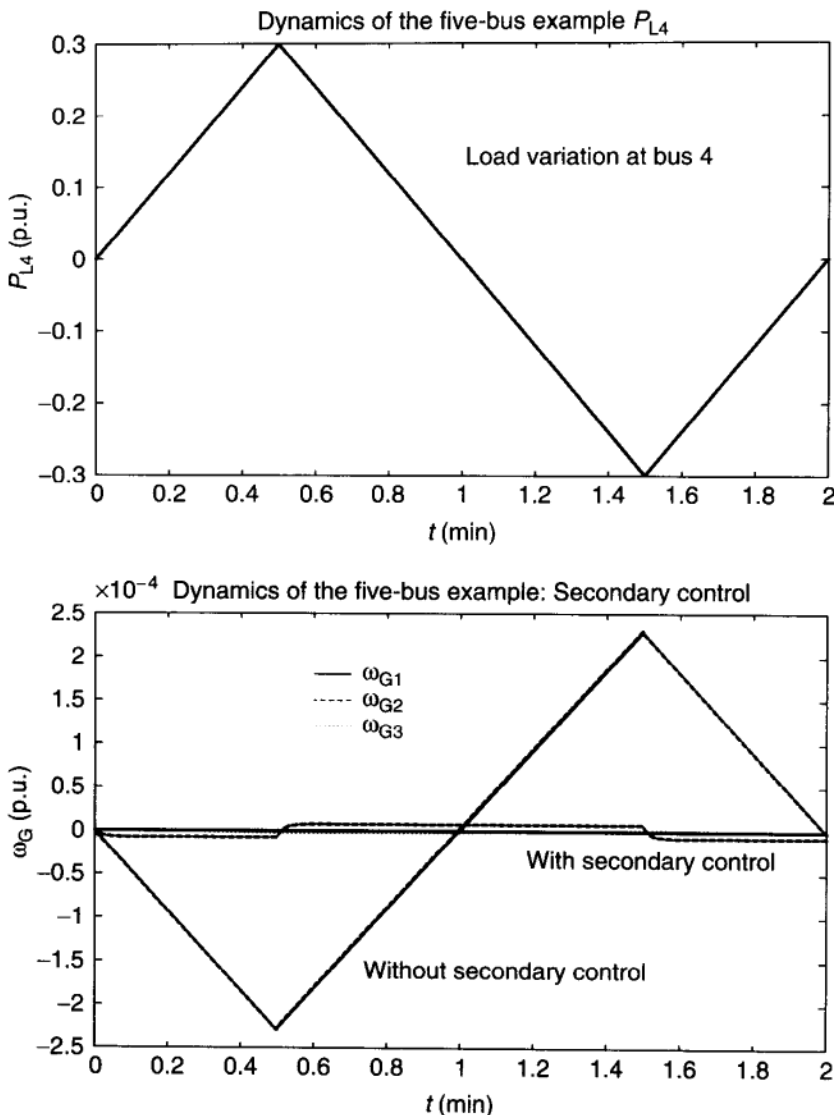


FIGURE 13.15 Load variation and frequency response with secondary control.

frequency documented in Ref. [57] can be explained by inadequate tie-line flow schedules.

The relevant output variables at the tertiary level are the power outputs from the units participating in tertiary-level system frequency control and the tie-line flows. The tertiary-level model could be used to regulate tie-line flow exchanges, including inadvertent energy exchange, according to given prespecifications among the very large interconnected systems, such as large portions of the United States, while requiring certain fringe control at each control area level [56]. The coordination at the interconnected system level by means of tertiary level

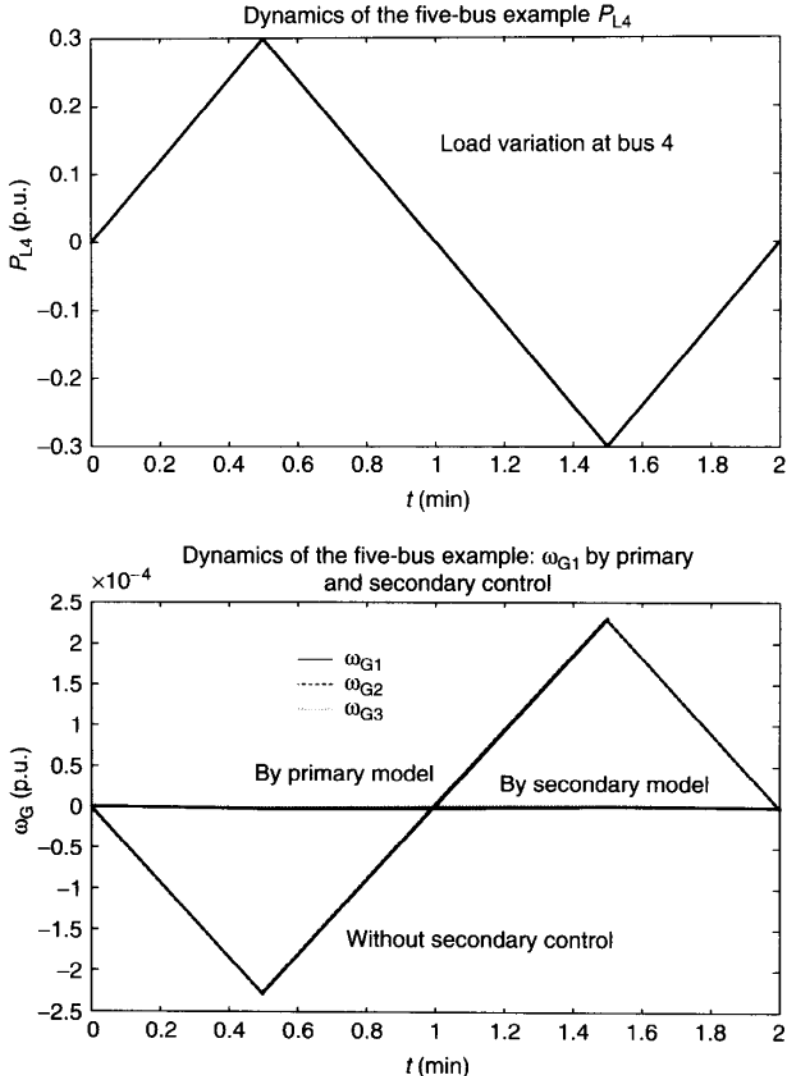


FIGURE 13.16 Load variation and frequency response without secondary control.

is minimal [56]. For the-tertiary level model and control design, see Refs. [51 to 53].

13.4.1.8 Static AGC: Particular Case of Structure-Based Frequency-Control Design Here we use the modeling developed before to state conditions explicitly under which the ingenious ACE-based AGC of today works and show how it directly follows as a particular case of the hierarchical frequency-control design presented. Consider first a single (isolated) control area I . It follows from the basic electromechanical generator model in Eq. (3.202) that at an equilibrium its frequency is determined by the mismatch between the mechanical power P_{Tj}^I

produced and the electrical power P_{Gj}^I sent to the area, that is, the frequency deviation from nominal ω_{Gj}^I is determined as (P_{Tj}^I unadjusted for the moment)

$$\omega_{Gj}^I = -\frac{1}{D_j^I} P_{Gj}^I \quad (13.84)$$

This is true for all generators j in the area I . Assuming that the system is at an equilibrium, the frequency is the same everywhere,¹⁶ and the simple summation of characteristics in Eq. (13.84) over all $j \in I$ leads to the basic power or frequency static characteristic of the area I

$$\omega^I = -\frac{1}{\beta^I} P_G^I \quad (13.85)$$

Coefficient β^I is known as the natural response of the area I . Consider next two control areas, I and K interconnected by a tieline. The power or frequency response in these areas is, respectively,

$$\omega^I = -\frac{1}{\beta^I} (P_G^I - F) \quad (13.86)$$

$$\omega^K = -\frac{1}{\beta^K} (P_G^K + F) \quad (13.87)$$

At the system (interconnection) equilibrium $\omega^I = \omega^K$ and

$$T = -\frac{\beta^I P_G^K + \beta^K P_G^I}{\beta^I + \beta^K} \quad (13.88)$$

The main objective of the present ACE-based AGC is to adjust (regulate) the set-point values of the AGC units and, consequently, change their mechanical power outputs P_{Tj}^I to maintain frequency close to its nominal value. As described earlier, this is currently done in a decentralized way at each area level; control areas I and K respond to their own error signals ACE^I and ACE^K , respectively,

$$ACE^I = F^I - \frac{10B^I}{2\pi} \omega^I \quad (13.89)$$

$$ACE^K = F^K - \frac{10B^K}{2\pi} \omega^K \quad (13.90)$$

It is the responsibility of the controlling units to regulate the ACE according to the prespecified control performance criteria. Currently in the United States the recommended control criterion is the so-called criterion A_1 , which states that

¹⁶The proof for this directly follows from the rank 1 deficiency of system matrix K_p in Eq. (6.125).

under normal operating conditions the ACE of each control area (CA) crosses zero every 10 min [58]. The parameters B^I and B^K (frequency biases) are weighting coefficients of area frequency and the tie-line flow deviations from their specified values. The area frequency bias determines a trade-off between quality of frequency regulation in the area and the tie-line flow deviations. It is straightforward to see from Eqs. (13.86) and (13.87) that if a frequency bias B^I of each area is chosen to correspond to its natural response coefficient β^I of the same area, the ACE^I provides a measure of the *local* power imbalance in a specific control area. Consequently, if ACE^I of the area is zero, the area I generation and demand are identical. The frequency, however, may still deviate from its nominal value, but such deviations are entirely due to tie-line flow deviations and as such, are the result of power imbalances in other control areas. Therefore, ACE^I is a measure of the local (areawise) imbalance between power produced P_T^I and power consumed by the system P_G^I .

13.4.1.9 Decentralized Control in Response to ACE^I When viewing a single control area, the ACE^I seems like an unsuitable output variable to regulate frequency, since it does not guarantee that frequency returns exactly to its nominal value. However, viewed from the entire interconnected system level, the ACE^I allows for a rather elegant decentralized control scheme. This design is based on the idea of assigning a group of generators in each control area to the task of regulating the ACE^I in this control area. The trade-off parameter in the formula for the ACE^I of each control area is chosen as $B^I = \beta^I$. When the parameters are chosen in this way, forcing the ACE^I to zero corresponds to balancing power exactly at each control area level. If the regulating units succeed in driving the ACE to zero, there will be no power imbalance in the interconnected system and therefore no tie-line flow and frequency deviations from nominal. For a two-area system

$$\text{ACE}^I = F - \frac{10\beta^I}{2\pi}\omega^I = 0 \quad (13.91)$$

and

$$\text{ACE}^K = -F - \frac{10\beta^K}{2\pi}\omega^K = 0 \quad (13.92)$$

Consequently,

$$\text{ACE}^I + \text{ACE}^K = -\frac{10(\beta^I + \beta^K)}{2\pi}\omega = 0 \quad (13.93)$$

Based on this, there are two reasons for using a decentralized control scheme based on the ACE output variable:

1. *Simplicity.* Under ordinary operating conditions there is no need for system operators in different areas to communicate data for on-line frequency control. Each regulating unit has a simple criterion for the performance of its own control area based on the data that can be gathered in that control area.

2. *Accounting.* The beauty of an ACE-based controller is that when one sets the trade-off parameter (bias, B) properly, the control units will compensate only for the mismatch of load and generation in their own control areas. Thus, there is no need to redistribute control cost charges between the subsystems. Each area ideally takes care of its own problems.

There are also some disadvantages of using this scheme, such as:

1. The decentralized control scheme works well as long as *each* control area is able to maintain its ACE near zero. However, if one control area fails to meet this ACE-based criterion, the net disturbance will propagate throughout the entire system. Furthermore, the regulating units in the neighboring control areas are tuned so as *not* to respond to disturbances that originate elsewhere on the system. Thus the disturbance will not be canceled by any area, which in turn may lead to long-term frequency deviations. To resolve this problem, the so-called time-error correction is practiced at present so that the inadvertent disturbance is compensated over a long period of time while being consistent with the prevalent time error.
2. Although it was shown above that in a steady state, with each control area meeting its ACE, system frequency will be nominal. This provides no insight into the dynamic interactions of the independent regulating units. For questions of robustness of this design see Ref. [59].
3. While each system operator has the freedom to assign control responsibilities within the control area to minimize regulation costs, this does not necessarily lead to a systemwide minimal frequency regulation cost. It may be possible for a subsystem to reduce its cost by delegating its control responsibility to generators *outside the control area*. The effect of this process on system performance is discussed next.

13.4.1.10 Flat Frequency Control Observe that if each control area uses its own generation to drive its ACE to zero, then this is sufficient to ensure that system frequency stays at its nominal value. However, if the ACE is not properly regulated in one area, this leads to a systemwide frequency deviation. Now, we derive a condition for how to reset the frequency bias coefficients in area I without any control in area K and still maintain stable frequency.

Start again with the nominal conditions. Introduce a disturbance in area K , $P_G^K = P^d$. Since there are no regulating units in area K , the generation in this area remains at $P_G^K = P^d$. The regulating units in area I , however, will respond to the disturbance $P_G^I = P^c$. The regulating generator will set its output level to drive the ACE in its region to zero. Thus, in a steady state we have a constraint

$$\text{ACE}^I = F - \frac{10B^I}{2\pi}\omega = 0 \quad (13.94)$$

We combine this constraint with the general expressions for natural frequency responses in each area and enforce the constraint of uniform frequency in the

steady state. This allows us to specify the level of regulation as a function of the disturbance and the frequency bias as follows:

$$P^c = \frac{\beta^I - B^I}{\beta^K + B^I} P^d \quad (13.95)$$

Choose $B^I = \beta^I$, which was proven earlier to be optimal in a decentralized control case. With this value, $P^c = 0$, which should not come as a surprise. We have argued that a controller is tuned in a decentralized scheme to respond only to a disturbance in its own area.

The real question here is how to tune the regulating units in area I if we want them to compensate for the disturbances on the entire system. In this case, we require that $P^c = -P^d$. Incorporating this condition into the above constraint gives us the following relation:

$$\frac{\beta^I - B^I}{\beta^K + B^I} = -1 \quad (13.96)$$

Since both β^I and β^K are positive, the only way of satisfying this constraint is to let B^I go to infinity. This result also should not be surprising. Letting B^I go to infinity corresponds to ignoring the tie-line flows and focusing on regulating the systemwide frequency only. In the case when one must control the entire system with one regulating unit, the ACE signal is no longer applicable, and one must respond directly to frequency.

Note: These derivations are essential for mathematical explanation of the qualitative difference between the newly proposed criterion CPS_1 and A_1 [58]. The point is proven here that it is actually impossible to fully “trade” frequency-regulation responsibilities if regulating units respond to the ACE; instead, a control performance criterion such as the CPS_1 criterion is needed to make such a process technically feasible [60].

13.4.1.11 Partial Dynamic Scheduling We have examined the situation in which one control area takes over the regulating responsibilities of the entire system. We now examine the case in which the control areas redistribute partial responsibility for the frequency regulation. This is done by altering (“trading,” selling and/or buying) frequency biases between the areas. In order to quantify how one should change frequency bias, one should look beyond the static model. Driving the ACE to zero in both control areas will always imply zero tie-line flow (deviations) in the steady state, regardless of how one sets the frequency biases for individual control areas. Zero tie-line flow deviations imply that each control area takes care of its own imbalance, and thus there is no way of redistributing regulating responsibilities in the steady state by altering the ACE parameters. In order to appreciate the effect of such changes, one has to examine dynamic

interactions of the two regulators. For this, consider the following model:

$$\omega^I[k] = -\frac{1}{10\beta^I}(P_G^I[k] - F[k]) \quad (13.97)$$

$$\omega^K[k] = -\frac{1}{10\beta^K}(P_G^K[k] + F[k]) \quad (13.98)$$

and impose the constraint (now, an assumption since the system is away from the equilibrium)

$$\omega^I[k] = \omega^K[k] = \omega[k] \quad (13.99)$$

This leads to the following frequency and tie-line flow dependence:

$$\begin{aligned} \omega[k] &= -\frac{1}{10(\beta^I + \beta^K)}(P_G^I[k] + P_G^K[k]) \\ &= -\frac{1}{10\beta}(P_G^I[k] + P_G^K[k]) \end{aligned} \quad (13.100)$$

$$F[k] = \frac{\beta^K}{\beta^I + \beta^K}P_G^I[k] - \frac{\beta^I}{\beta^I + \beta^K}P_G^K[k] \quad (13.101)$$

Recall the definition of the ACE at each step [k]:

$$\text{ACE}^I[k] = F[k] - \frac{10B^I}{2\pi}\omega[k] \quad (13.102)$$

$$\text{ACE}^K[k] = -F[k] - \frac{10B^K}{2\pi}\omega[k] \quad (13.103)$$

We now tune our regulating units in each control area to compensate for their respective ACE signals as

$$P_T^I[k] = -\text{ACE}^I[k] \quad (13.104)$$

$$P_T^K[k] = -\text{ACE}^K[k] \quad (13.105)$$

Assume the disturbance on the system originates in area K ; the total generation in each area then becomes

$$P_G^I[k+1] = P_T^I[k] \quad (13.106)$$

and

$$P_G^K[k+1] = P_T^K[k] + P^d[k] \quad (13.107)$$

This leads to a discrete time (quasistationary) model that defines system frequency changes:

$$\omega[k+1] = -\frac{1}{\beta}(B^I + B^K)\omega[k] - \frac{1}{10\beta}P^d[k] \quad (13.108)$$

Although very simple in structure, this model is the *key* to understanding the trade-off involved in altering the parameters in ACEs. The main observation is that the dynamic behavior of the frequency depends only on the *sum* of individual frequency biases. This leads to an easy way of measuring the necessary trade-offs between B^I and B^K . One area simply takes over part of the frequency bias from the other control area. Since they both react to the *same* frequency, the increase in the frequency bias for the system is exactly equal to the decrease in the frequency bias of the other area. This can be rewritten as

$$\text{ACE}^I[k] = F[k] - \frac{10(B^I + b)}{2\pi}\omega[k] \quad (13.109)$$

$$\text{ACE}^K[k] = -F[k] - \frac{10(B^K - b)}{2\pi}\omega[k] \quad (13.110)$$

The other significant factor to consider when trading frequency biases is the robustness of system response. This condition depends on the properties of the constant $(B^I + B^K)/(\beta)$, as determined from the dynamic model given in Eq. (13.108). As long as

$$\left| \frac{B^I + B^K}{\beta} \right| > 1 \quad (13.111)$$

(the strict inequality) is met, it follows from this above model that the system will be robust with respect to the choice of frequency bias. Otherwise, it could be marginally stable ($= 1$), or unstable when ≥ 1 . An interesting observation is that when frequency bias is chosen to correspond to the natural response of each area, the system is only marginally stable. Higher gains would lead to oscillations among the control areas, and reducing the gain would provide for a robustly stable response but a somewhat slower regulation of frequency. In addition to being marginally stable, the ACE-based regulation exhibits some other fundamental problems when one attempts to use it in a competitive industry [59].

13.4.1.12 Ingenious AGC: Summary Thinking in terms of hierarchies, a very ingenious formulation in the original load frequency control, devised for stationary conditions without dynamic effects, grossly simplified the problem of balancing generation and demand in real time. By defining the ACE concept as the sum of

1. The weighted difference between the actual present system frequency and the system frequency scheduled for the present time and

2. The difference between the actual and scheduled net tie line exchange for the present time for each of the areas.

when this linear sum, the ACE, is zero for each area, then the system is running exactly on schedule. If each area independently controls its generation economically to drive its own ACE to zero, then:

1. The actual load for the system is covered.
2. The system frequency is as scheduled.
3. All net tie-line exchanges are at their scheduled values area by area, thus satisfying the trades struck yesterday among areas under government regulation.
4. If an area is unable to supply its scheduled net tie-line exchange and drive its own ACE to zero, then system frequency will drop and net tie-line exchanges at other areas will rise to cover the deficiency in the load at the deficient area.

This amounts to a hierarchical system which is very easy to operate:

1. The top level (NERC, in the United States) can simply adjust the set-point frequency to drive the actual system frequency and synchronous time (as a courtesy toward the customers, the system itself is quite tolerant in this sense) back to normal. This one piece of information needs to be communicated to the areas. This minimal central action will rearrange the area net tie-line exchanges to cover the actual system load.
2. Each area individually acts on the change of frequency set point by keeping its ACE to zero. No communication is needed between areas.
3. The system is *fully decoupled*; the areas do not need to communicate with each other or the center. The center only needs to watch the synchronous time to generate its single control command.

This combination of the original load-frequency control and economic dispatch came into use around 1960 when the computers were in their initial phase, just fast enough to handle the areawise economic dispatch computations. Yet this development was the basis for the fact that on-line computer control in industrial systems was pioneered by the power industry.

13.4.2 Frequency Control in the Deregulated Industry

It is straightforward to conclude from the secondary-level frequency model in Eq. (13.68) that it is not possible to meet frequency specifications exactly through an open-loop generation dispatch, regulated or deregulated. It follows from this model that as long as the load disturbance $P_L[kT_s]$ is nonzero, the frequency is generally away from its nominal value. Since each load-serving entity is likely to

create such a load disturbance, purchase of frequency regulation should be made mandatory.

Moreover, in a competitive electric power industry one could easily envision frequency control as being provided on a market basis. Today one such successfully working example of a market-based frequency control can be found in Northern Europe [60]; there are also several such experiments in the United States in progress [16]. Very recently the U.S. Federal Energy Regulatory Commission (FERC) has issued an order allowing all power plants the right to sell frequency control competitively.

As mentioned earlier, the rationale for unbundling generation-based activities into the generation-dispatch level (block 2) from the frequency-control level (block 6) is no longer as straightforward as it has been in the regulated industry. [In particular, the unbundling of block 2 into several submarkets (daily, hourly, and even 5 minutes) is likely to impose an unnecessary burden created by the huge number of transactions attempting to be processed in real time. It is important to observe that in the regulated industry the economic dispatch is computed at the rate of 5 min to 30 min and the results are implemented on line. All other load fluctuations are balanced in a closed-loop manner by the secondary-level frequency control units. As the industry deregulation takes its course, one must assess trade-off between excessive labor and technologies needed to automate the fast evolving markets (hourly and shorter) versus possible inefficiencies created if these are not in place, and the fast real-power balancing is done indirectly by controlling frequency.]

However, by default, this unbundling has taken its course; all real-time supply–demand mismatches created through the primary electricity market activities and through the unintended small deviations in demand are compensated separately [61]. Without making any judgments if this is the right course, we address the main conceptual question whether the market could ensure the desired control of system frequency by auctioning out a set of contracts that require generators to respond to frequency deviations in a decentralized fashion. The answer to this question is affirmative, and we describe next a theoretical basis for one such possible design. The results presented here are a direct summary of our recent research [19, 21].

13.4.2.1 Physical Delivery of the Scheduled Power The economic dispatch is done under the assumption that system frequency is tightly controlled and that the electric power output from a generator is a fully controllable quantity by each power plant. Recall that this power output is actually determined by a three-way relation [droop characteristic, Eq. (13.50) [8,55]] between the power generated $P_{Gi}[kT_s]$, secondary control $\omega_{Gi}^{ef}[kT_s]$, and the frequency $\omega_{Gi}[kT_s]$. In the regulated industry it is not essential to *unbundle* actual power output into (1) the component caused by the frequency changes resulting from systemwide power imbalances and (2) the component directly controllable by each G-T-G unit.

In the competitive environment, however, it is important to relate cause and effect, and it is potentially useful to rewrite Eq. (13.50) as [22]

$$P_{Gi}(\omega)[kT_s] = P_{Gi}^c[kT_s] - \frac{1}{\sigma_{Gi}}\omega[kT_s] = P_{Gi}^c[kT_s] - \beta_{Gi}\omega[kT_s] \quad (13.112)$$

where

$$P_{Gi}^c = \frac{(1 - \sigma_{Gi}d_{Gi})\omega_{Gi}^{\text{ref}}}{\sigma_{Gi}} \quad (13.113)$$

and

$$\beta_{Gi} = \frac{1}{\sigma_{Gi}} \quad (13.114)$$

P_{Gi}^c is the component of power generated under the direct control of each power plant. The remaining component $\beta_{Gi}\omega$ depends on everyone else's activities and it reflects how a governor changes P_{Gi} to control system frequency ω to its set-point value ω_{Gi}^{ref} ¹⁷.

Observe that the component P_{Gi}^c is directly controllable by each G-T-G unit through adjusting the set-point value ω_{Gi}^{ref} ; in today's industry only AGC units adjust this value. We show next why is the distinction between P_{Gi} and P_{Gi}^c critical under the market-based provision of power.

13.4.2.2 Ensuring that the Power Contracts are Physically Deliverable The droop characteristic of a power plant defined in Eq. (13.50) above is a strong complicating factor when power provision and frequency control are attempted through market means. Since the power produced by any given plant can be decomposed into the part fully controllable by the producer P_{Gi}^c and the component that varies with the system conditions $\beta_{Gi}\omega$ according to Eq. (13.112). Each power supplier should be responsible for specifying $P_{Gi}^c(t)$ only and not the actual $P_{Gi}(t)$.

Recall also from Chapter 3 [Eq. (3.251), section on load modeling] that each load is characterizable similarly as

$$P_{Lj}(\omega) = P_{Lj}^c + \beta_{Lj}\omega \quad (13.115)$$

where P_{Lj}^c is the load component independent of system frequency (that is, other system users' activities), and the remaining component changes as a function of system frequency. This formula represents the well-known self-stabilization of loads in today's industry; since they are not elastic with respect to price, the

¹⁷ In this section an approximation is made for simplicity that the frequency is the same at each location, even when slightly away from an equilibrium. It is possible, however, to use a more detailed model in Eq. (13.68). This may be particularly relevant to do when designing markets for load-following in a deregulated industry [51].

demand naturally decreases as the system frequency decreases, leading to smaller demand shortage, and therefore they contribute to the system frequency increase [24, 55]. Each power consumer (could be aggregated at a LSE level) requests a delivery of $P_{Lj}^c(t)$ from the primary electricity market. Since the load inherently deviates from its intended use, the band of expected deviations, $\Delta P_{Lj}(t)$, also must be part of the contract, and each LSE must purchase frequency-control service to compensate for its likely deviations.

Specifying power contracts in terms of P_{Gi}^c and P_{Lj}^c ensures that all that can be controlled by the system users themselves is specified. This, in turn, ensures that the power contracts specified in the primary markets can be physically delivered independent from the activities of the others. This contract specification is *the key* to designing separate submarkets for balancing power and ensuring frequency control and must be done at the level of block 6 when a transaction is allowed for physical implementation.

13.4.2.3 Possible Market for Frequency Control Depending on the specific user's characteristics, one would need to purchase more frequency control than the other user. For example, it is well known that an arc furnace creates more unexpected power imbalances than residential equipment, and thus the arc furnace owner should therefore pay more for the system frequency-control service.

A meaningful frequency-control market should capture these distinctions among system users and the tariffs for system control should further reflect these differences. Possibly the simplest way to achieve this is by establishing a mandatory contract format, which in a transparent way provides the information to the market coordinator about each system user's need for system frequency control. One such possible format is described next and is based on Ref. [21].

In order to develop a meaningful market for frequency control and charge accordingly for this service, we suggest that, at least, each contract on the electricity market should specify an anticipated load-power requirement as a function of time¹⁸ and an estimate of the expected band of super-imposed load fluctuations. We demonstrate here that this is sufficient for developing a well-defined frequency control market. A representative contract curve suggested is shown in Figure 13.17. If no restrictions are placed on the source of frequency control, market coordination will be required, and all system users, GSEs, and LSEs, who do not choose to self-provide their control, will be required to provide information to the frequency-control market as a prerequisite to connecting to the system. The general information would be in the form shown in Figure 13.17. All LSEs would be expected to specify a nonzero band $\pm \Delta P_{Lj}(t)$; generators not participating in the frequency-control market would be required to provide information about their power $P_{Gi}^c(t)$ to be sold into the primary electricity markets.

¹⁸ Using currently established utility language, this means that the load profile needs to be specified.

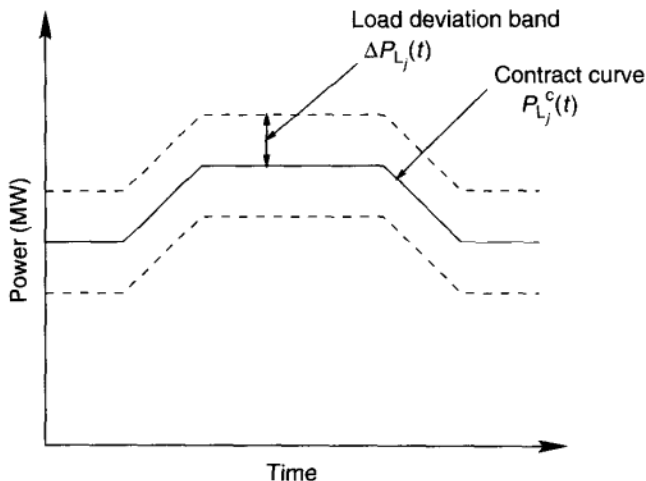


FIGURE 13.17 Recommended structure for contracts.

This information can, in turn, be used by the system (or frequency-control market) operator to estimate the maximum cumulative power mismatch that must be compensated through purchasing control on this market. Using this estimate, a coordinator of the frequency-control market can decide how much power to purchase for control. We describe next how this could be done.

13.4.2.4 Service Providers in the Frequency-Control Market Power producers selling their services to the frequency-control market are required to provide different type of contractual specification. A system user participating in the frequency-control market sells an obligation to adjust its directly controllable power P_{Gm}^c in response to frequency deviations, within a preset band of power, according to

$$P_{Gm}^{control}[kT_s] = P_{Gm}^c[(k+1)T_s] - P_{Gm}^c[kT_s] = G_{Gm}\omega[kT_s] \quad (13.116)$$

for some

$$P_{Gm}^{c,min} < P_{Gm}^c < P_{Gm}^{c,max} \quad (13.117)$$

A sample of such contract specification is sketched in Figure 13.18.

13.4.2.5 Meeting the Frequency-Control Objective The function of the market for frequency control is to guarantee that frequency remains close to 60 Hz at all times. We write this systemwide control objective as

$$\omega^{\min} < \omega < \omega^{\max} \quad (13.118)$$

How, then, can the purchase of control contracts on the market, as just defined, guarantee that this objective is met? To answer this question we first rederive the

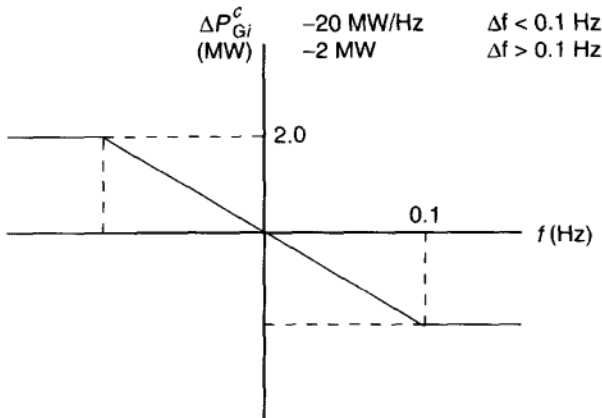


FIGURE 13.18 Structure of contracts traded on the control market.

control objective in terms of the load–generator power imbalance. Because of the droop characteristic, the net real power injected at the generators will always match the net power extracted at the loads:

$$\sum_m P_{Gm}(\omega) - \sum_i P_{Li}(\omega) = 0 \quad (13.119)$$

Therefore the popular notion that system frequency deviates because of a mismatch in power between load and generation is not quite accurate. In order to observe this imbalance we have to disregard the droop characteristic and consider only the controllable part of the power output (P_{Gi}^c and P_{Li}^c). This gives us a linear relationship between the cumulative mismatch in load and generation and the deviation in system frequency from 60 Hz:

$$\omega = [1/(\beta_G + \beta_L)] \left(\sum_m P_{Gm}^c - \sum_i P_{Li}^c \right) \quad (13.120)$$

where $\beta_G = \sum_m \beta_{Gm}$ and $\beta_L = \sum_i \beta_{Li}$. We also define P_{imb} such that

$$\omega = [1/(\beta_G + \beta_L)]P_{imb} \quad (13.121)$$

Having derived the relationship between power imbalance and frequency deviation we can now rewrite the control objective (13.118) in terms of power imbalance:

$$P_{imb}^{\min} < P_{imb} < P_{imb}^{\max} \quad (13.122)$$

where $P_{imb}^{\min} = (\beta_G + \beta_L)\omega^{\min}$ and $P_{imb}^{\max} = (\beta_G + \beta_L)\omega^{\max}$. On the actual system the generators are required to have the controllable portion of their power output track a contract curve, while the load is allowed to deviate within specified

margins (see contract structure, Fig. 13.17). The power imbalance on the system will therefore be due to unpredicted deviations of the loads (and imperfect generator controls). Since only generators participating in the frequency-control market will respond to this imbalance we assume that P_{Gm}^c is as specified by the contract curve for all nonparticipating generators.¹⁹ Participating generators will respond according to the control law specified in the previous section, Eq. (13.116). Furthermore, we introduce the notation P_{Li}^{dev} to denote the deviation of the i the load from the contract curve. Under these assumptions, the power imbalance of the closed-loop system will be given by

$$P_{imb}[k] = \sum_m P_{Gm}^c[k] - \sum_i P_{Li}^{dev}[k] \quad (13.123)$$

Then the system imbalance after additional generation provided by the frequency control market is

$$P_{imb}[k+1] = \sum_m P_{Gm}^{control}[k] + \sum_m P_{Gm}^c - \sum_i P_{Li}^{dev}[k] \quad (13.124)$$

Using the control law defined in Eq. (13.116) this expression becomes

$$P_{imb}[k+1] = \sum_m G_{Gm}\omega[k] + P_{imb}[k] \quad (13.125)$$

We now substitute Eq. (13.121) for ω ,

$$P_{imb}[k+1] = \left(\sum_m G_{Gm} \right) [1/(\beta_G + \beta_L)] P_{imb}[k] + P_{imb}[k] \quad (13.126)$$

This relation clearly spells out how control gains must be set in order to balance the overall system. By selecting gains such that

$$\sum_m G_{Gm} = -(\beta_G + \beta_L) \quad (13.127)$$

the net imbalance will be zero and system frequency is expected back to nominal. This simple constraint on the sum of the control gains therefore spells out the steady-state requirement for balancing frequency on the system. When auctioning control contracts, the frequency-control market will need to match the sum of droop constants for all loads and generators in its area.

¹⁹ Otherwise, high penalties for not meeting contractual obligations should be in effect.

13.4.2.6 Estimation of Frequency-Control Capacity Needs So far we have shown how to specify the gain on the control contracts traded on the frequency-control market. We still have to determine how to set $P_{Gm}^{c,\min}$ and $P_{Gm}^{c,\max}$ for each contract. To do this the power-exchange operator uses the information provided in the bands around the contract curves in the primary electricity market. As described earlier, each contract specifies a maximum deviation (ΔP_{Li}) from the contract. This provides the system operator with an upper bound on the maximum cumulative imbalance on the system:

$$P_{\text{imb}} < \sum_i \Delta P_{Li} \quad (13.128)$$

A simple and safe strategy would be for the system operator to purchase sufficient control capacity to cover this worst-case scenario. This strategy could be expressed as

$$\sum_m (P_{Gi}^{c,\max} - P_{Gi}^{c,\min}) = 2 \sum_i \Delta P_{Li} \quad (13.129)$$

In reality, however, this would be an overly conservative and thus economically inefficient approach. The deviations of the individual loads will tend to cancel each other to some extent. In the regulated environment, the utilities took advantage of this effect by forecasting the load in a control area as a single unit. Because the same supplier (the utility) covered all loads in the area, it was not necessary to distinguish among the deviations of individual consumers. In the deregulated industry, however, the stochastic behavior of each load-serving entity must be extracted. This is critical so that loads will be charged in proportion to the disturbance they induce on the system. The function of the frequency-control market is to relay the cost of purchasing control contracts to the loads that make up the demand (or need) for frequency control. The demand for control is represented by the width of the band around the bilateral contract, and the charge for the frequency-control service is set in proportion to this width. Specifically, if the unit clearing price for a control contract is given by P_{FC} and m contracts are purchased, the mandatory frequency-control charge (MFCC) to each LSE i for frequency control will be given by

$$\text{MFCC}_i = m P_{\text{FC}} \left[\Delta P_{Li} / \left(\sum_j \Delta P_{Lj} \right) \right] \quad (13.130)$$

If this charge is passed on to all LSEs, the total amount of money paid to the frequency control market coordinator is:

$$\sum_i \text{MFCC}_i = m P_{\text{FC}} \quad (13.131)$$

This is exactly equal to the amount paid by the market coordinator to the generators participating in frequency control, so the market manages to recover its cost fully while providing individualized economic feedback to the load-serving entities.

We still have not answered how the market determines how many frequency contracts to purchase. Clearly, purchasing control capacity equal to the sum of the contract bounds [see Eq. (13.129)] is overly conservative. In order to improve on this strategy the market needs some measure of the degree to which the deviations of the loads will cancel each other out. Such a measure is given by the correlation between the stochastic behavior of the LSEs. The closer the loads are to being fully uncorrelated, the less control capacity needs to be purchased through the market. Consider the case in which we have n bilateral contracts, each with an identical deviation band of ΔP_L around the contract curve. In the worst-case scenario, if the deviations of the loads were fully correlated, then we have to purchase the full amount of control capacity given in Eq. (13.129). The other limiting case is given when the load fluctuations can be modeled as independent identically distributed (IID) processes. Under this assumption the necessary control capacity, based on the standard deviation of the cumulative disturbance, is given by:

$$\sum_m (P_{Gm}^{c,\max} - P_{Gm}^{c,\min}) = (2/\sqrt{n}) \sum_i \Delta P_{Li} \quad (13.132)$$

This clearly is a significant improvement in the economic efficiency of the controls market. In a market with hundreds of LSEs, the necessary capacity may be reduced by a factor approaching 10. According to the pricing scheme provided in Eq. (13.131) this saving will be directly passed on to the loads.

13.4.2.7 Introducing the Λ Function The stochastic analysis sets bounds on the effect of the correlation between individual load fluctuations on the overall (system) load volatility. In order to achieve full efficiency, however, it will be necessary to define this impact over the full range of load correlations. To measure this effect, we introduce the Λ function. $\Lambda(\text{cov}(P_{L1}^c, \dots, P_{Ln}^c))$ determines the proportional relation between the sum of the deviation bands and the required amount of control capacity:

$$\sum_m (P_{Gi}^{c,\max} - P_{Gi}^{c,\min}) = 2\Lambda \sum_i \Delta P_{Li} \quad (13.133)$$

Λ is a monotonically increasing function of load correlation, starting at $\Lambda = 1/\sqrt{n}$ for IID loads, and bounded by $\Lambda = 1$ for fully correlated loads. The introduction of this function illustrates the necessity for market participants to provide more information, to the extent possible, to market facilitators in order to ensure efficient operation.

Example 13.4.1 Here a simple four-bus system, [21] shown in Figure 13.19, is used to illustrate theoretical ideas for creating market-based frequency control. The system consists of two generators and two loads. For simplicity, the two loads, L_3 and L_4 , are assumed not to vary with frequency and also to be statistically uncorrelated. Two loads are characterized by different deviation bands around their contract curves: L_3 has a ± 0.5 p.u. deviation band; L_4 has a relatively larger, ± 2 p.u., deviation band as shown in Figure 13.20. The set points of generator governors are changed every 30 sec., corresponding to the P_{Gm}^c needed to fulfill the control contracts. Since the droop characteristics, \sum_{Gm} , of both G_1 and G_2 are 5% (rad/sec)/p.u. based on Eq. (13.127), the total control gains needed for frequency regulation should be

$$\sum_{m=1}^2 G_{Gm} = \beta_1 + \beta_2 = 2\pi \times 40 \text{ p.u./Hz} \quad (13.134)$$

In this simulation, we choose $G_{G1} = (2\pi/3) \times 40$ and $G_{G2} = (4\pi/3) \times 40$ so that the control gain of G_2 is twice as large as that of G_1 . This way G_2 obtains twice as many control contract units as G_1 does. Figure 13.21 shows the real-power response of G_1 and G_2 participating in the frequency control market. It shows that G_2 increases (or decreases) twice as much its real power compared with G_1 when balancing the system. Generator G_2 must have a fast enough ramping rate in order to qualify to bid for more control contracts, and also it needs to reserve more of its real-power capability for frequency control. Furthermore, since L_4 deviates more from its contract curve, it should take more responsibility than L_3 for the system-frequency deviation. These verify the charge and payment mechanism described in Section 13.4.2.6.

Figure 13.22 shows system-frequency response to the system disturbances. It can be seen that without any coordination the average frequency deviates in an uncontrolled way. In contrast, with a well-defined frequency-control market and regulating power provided by G_1 and G_2 , the system frequency deviation is reduced to less than ± 2 mHz.

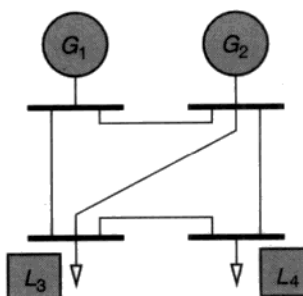


FIGURE 13.19 Simple four-bus system.

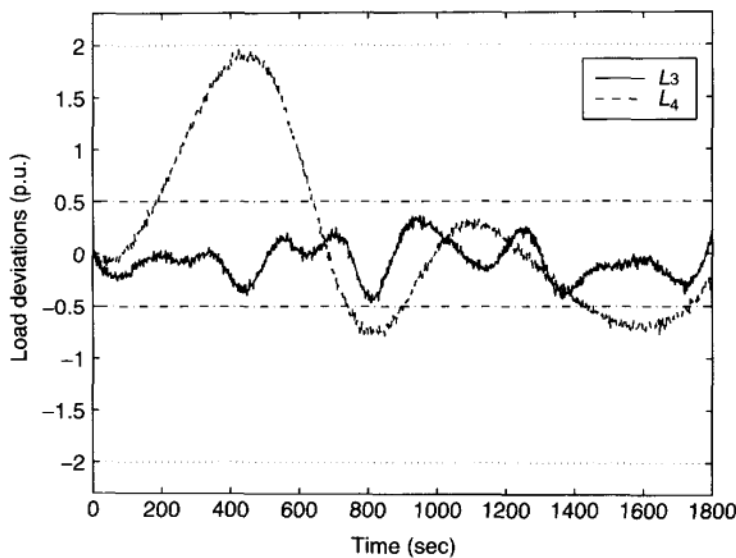


FIGURE 13.20 Deviations from contract curves at L_3 and L_4 .

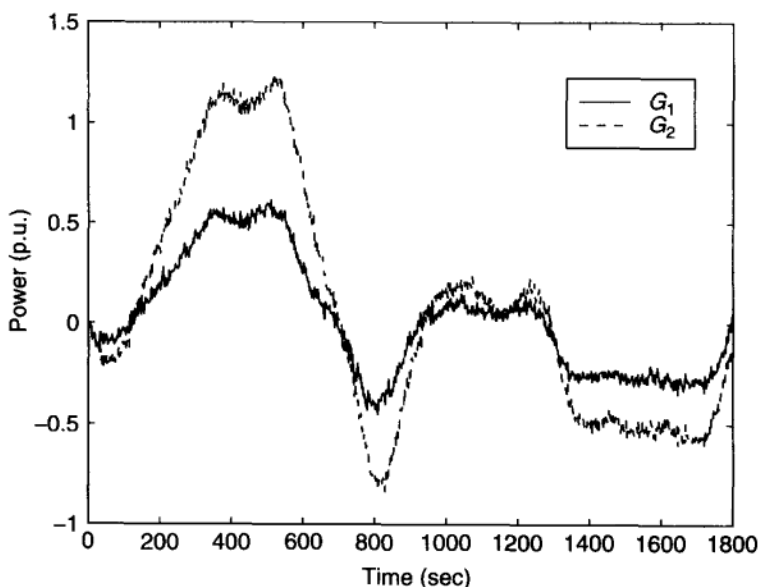


FIGURE 13.21 Real-power outputs of G_1 and G_2 .

13.4.2.8 Frequency Control in a Multicontrol Area Creating markets for frequency control in an interconnection comprised of several control areas appears at first sight to be much more complex than creating a frequency-control market for an isolated, single control area system described previously. Depending on a specific historic horizontal structure of an electric interconnection as well as on

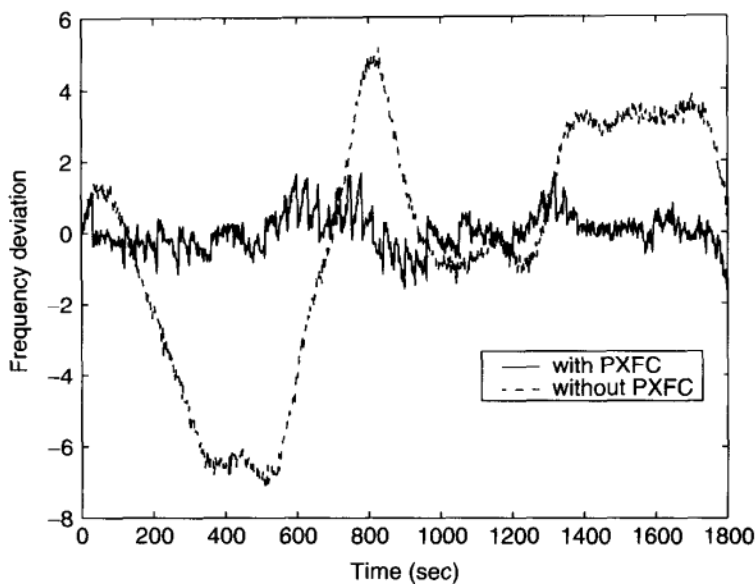


FIGURE 13.22 System-frequency response with power exchange for frequency (PXFC).

the type of newly formed primary electricity markets in the same interconnection, many architectures are possible. These range from operating the interconnection as a single control area, whose boundaries are identical with the boundaries of a frequency-control market, through having a frequency-control market in charge of several control areas, or even having a situation in which a frequency-control market is in charge of a portion of a control area only.

To deal with this variety of architectures without creating excessive complexity, it is important to recognize two major facts:

1. The boundaries of a control area are not essential for balancing power in real time, nor for regulating frequency of the entire interconnection.
2. It is essential, however, to develop a frequency-control market in which control criterion is measured in terms of system-frequency deviations and *not* in terms of the traditional ACE.

As explained earlier, the ACE has been used historically as a means of allocating responsibilities for balancing supply and demand at each control area level. In a competitive industry this is no longer a requirement; instead, active contracts for selling power from outside of a control area to the load directly connected to the grid in this area are routinely attempted under competition. Therefore, there is no functional role left for a control area concerning unexpected balances created by both system users and the users from the outside of the area.

In what follows we describe several conceptual difficulties with using ACE for system-frequency control under open access first. Next, we suggest that NERC

has already moved into the direction of changing the frequency-control criterion from ACE-based to CPS1-based [20]; the CPS1 criterion recently recommended by NERC was designed with a different motivation in mind; however, it directly lends itself to being useful for systematic design of a frequency control market which is not restricted to a single control area.²⁰ Once the case is made for creation of a frequency-control market beyond a single control area, we describe how this could be implemented. The concepts are identical to the concepts described previously for a single control area.

In the proposed market for frequency control, we have, in addition to moving from a centrally dispatched system to a competitive market, also shifted the technical criteria of the control algorithm from the area control error to an algorithm based only on the system frequency. This shift makes the control system more robust to inaccurate tie-line flow schedules. In fact, we will show that the performance of the frequency-based controller is independent of the scheduled flow of base load power. This, in turn, will allow more flexibility in the spot-market trade, without having to coordinate last-minute changes with the generators participating in frequency control.

13.4.2.9 Potential Problems with Using ACE to Regulate System Frequency

The deregulation of the electric utility industry provides a drastic change in the conditions under which a frequency-control system must operate. With the introduction of independent power producers (IPPs), and a number of aggregators both on the load and generation side, the number of active participants in the market has increased significantly. In addition, the complexity of the market structure is growing. Generators are demanding the right to enter into bilateral contracts with loads in different control areas. Power brokers are looking to take advantage of differences in spot-market prices by moving large quantities of power on short notice. Each of these transactions could potentially produce a real power imbalance on the system. The question is who is responsible for this mismatch, physically as well as financially, and how the costs of balancing the system should be recovered. If we apply ACE to the deregulated market, we quickly run into a coordination problem.

Each time a trade is completed involving a generator and load in different control areas, the scheduled values of the tie-line flow will change. If trades on the spot market are conducted at an hourly rate, the system operator will be forced to recompute the tie-line schedule, update the operating point for the ACE measurement and redispatch this information to generators participating in frequency control each hour. If an update in the schedule is delayed or inaccurate, the controller will be functioning with the wrong operating point, potentially causing it to add a further disturbance rather than balancing the system. We will show the effects of inaccurate scheduling through the following example.

²⁰ It is our understanding that most of the control areas experimenting with CPS1 use this measure as an accounting mechanism and not as a tool for real-time frequency control.

Example 13.4.2 To illustrate the differences between a control algorithm based on the area control error and that based on flat frequency control, we consider a simple five-bus system with three generators and two loads, separated into two control areas (see Fig. 13.23) [21]. Note that the two tie lines, G_2-G_3 and L_4-L_5 , have the same impedance and inductance as the intra-area lines. These two areas simulated are strongly connected. Assume a single bilateral contract between generator G_2 and load L_5 . The structure of the contract is the same as described earlier: a nominal contract curve bounded by upper and lower limits on load deviations. The actual load is set to deviate from the contract curve sinusoidally, but it remains within the contractual bounds. The complete contractual setup of the contract and the actual load is shown in Figure 13.24. In order to have a point of comparison for the performance of the control system, we begin by simulating the system in the absence of any AGC. In this case the system frequency will deviate freely in proportion to the net real-power imbalance. The

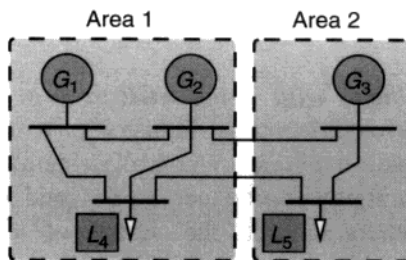


FIGURE 13.23 Five-bus system for multicontrol area simulations.

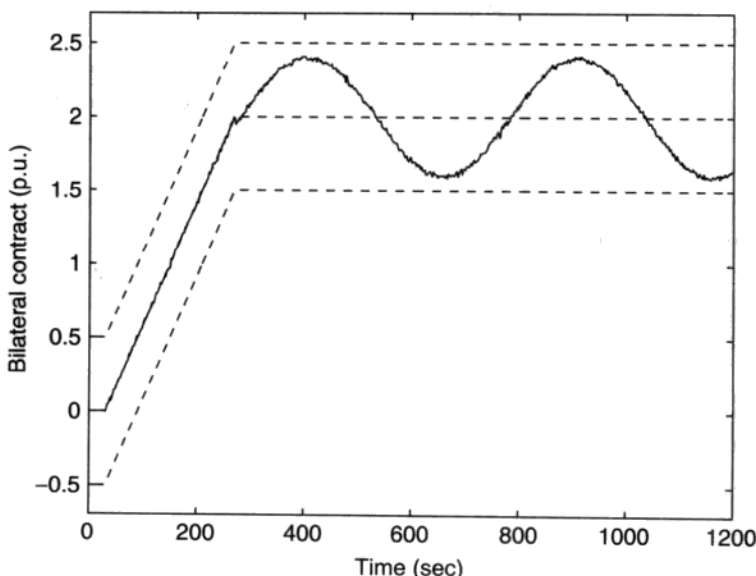


FIGURE 13.24 Bilateral contract between G_2 and L_5 .

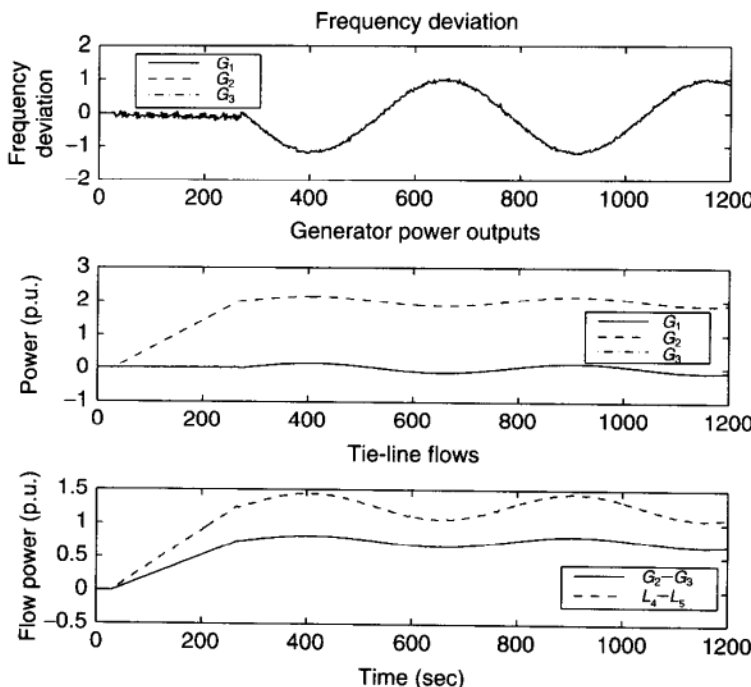


FIGURE 13.25 Uncontrolled frequency response.

magnitude of the deviation will depend on the natural response of the system as described earlier. We can also see how the output of the generators varies slightly in inverse proportion to frequency. This is due to the droop characteristic of the generators. An increase in system frequency will cause a decrease in net power output, and vice versa. The uncontrolled system response is shown in Figure 13.25.

We now consider the response of the system with a controller based on the area control error. In order to illustrate the effects of an error in tie-line scheduling on system performance, we will consider two cases. The first will assume a perfect schedule for the tie line, while the second assumes an approximate schedule. The difference in the two schedules is shown in Figure 13.26.

We now simulate the closed-loop response of the system controlled by the area control error using first the exact and then the approximate tie-line schedule. As can be seen by comparing Figures 13.27 and 13.28 the impact of the scheduling error is quite significant. The maximum frequency deviation increases from less than 1 mHz for the perfect schedule to almost 4 mHz for the approximate schedule. It is interesting to note that such a significant deterioration in performance occurred strictly due to an approximation error. If, instead, there had been a failure to add or remove several transactions from the schedule, the impact would have been disastrous.

We now simulate the system driven by the same disturbance but with our proposed frequency-based controller. From the perspective of the controls market

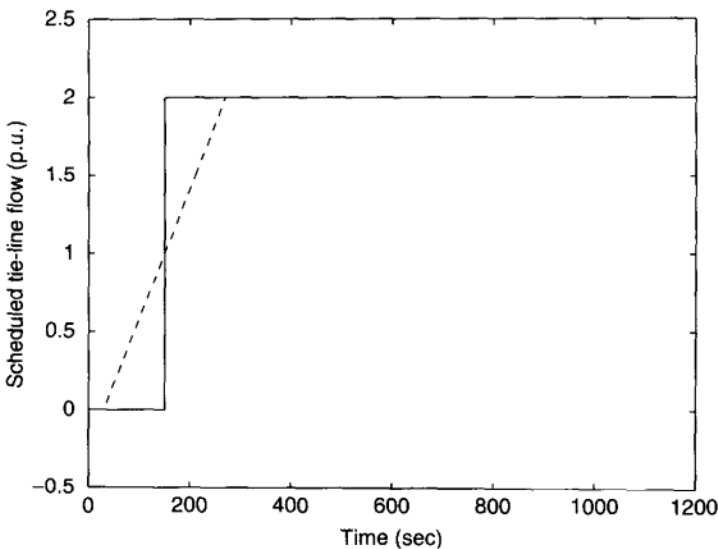


FIGURE 13.26 Exact and approximate tie-line flow schedules for ACE-based control.

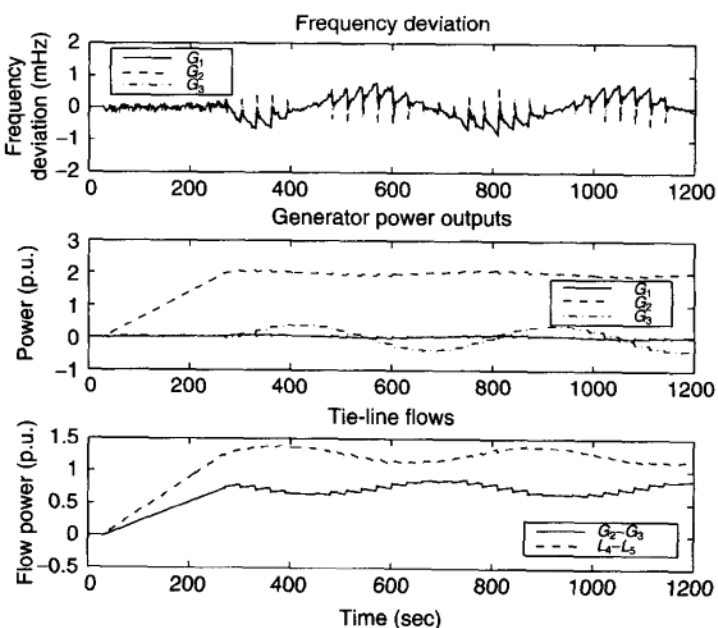


FIGURE 13.27 Exact tie-line flow schedules for ACE-based control.

there is a single control contract offered by generator number 3. The system response illustrated in Figure 13.29 shows that the deviations in frequency are the same as in the case of the ACE-based controller with perfect scheduling. This illustrates how a shift from ACE- to frequency-based control provides for increased robustness without any deterioration in performance. An additional

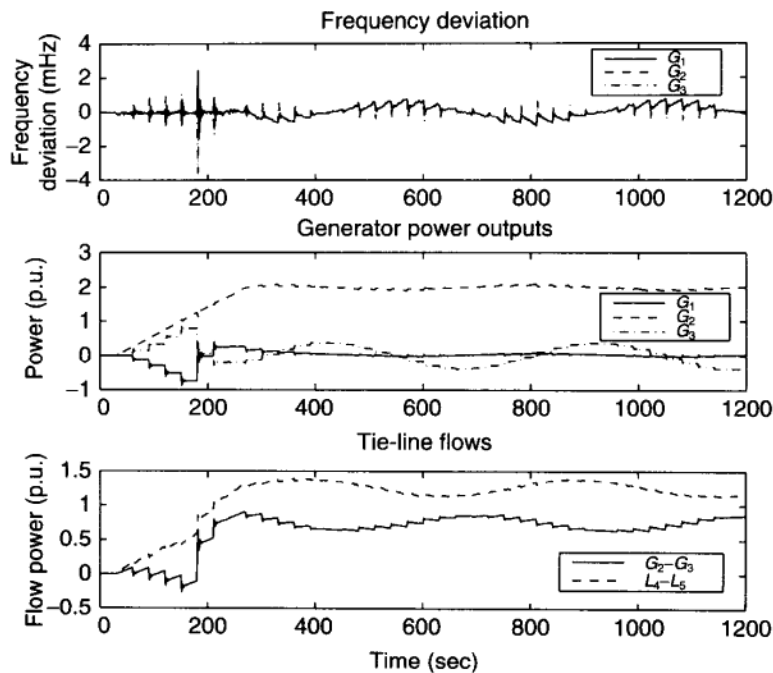


FIGURE 13.28 Approximate tie-line flow schedules for ACE-based control.

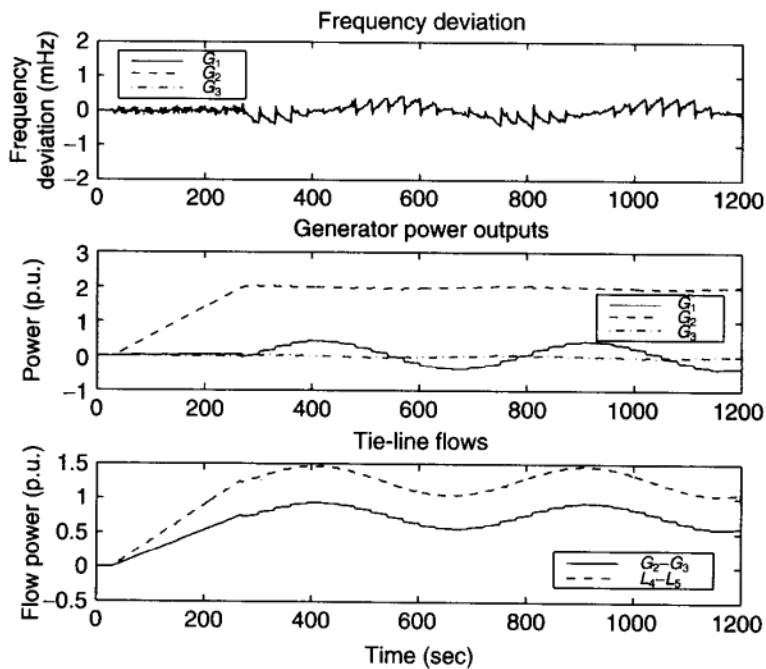


FIGURE 13.29 System response for frequency-based control.

advantage of the new control law is that it lends itself easily to the interarea trade of control generation. Suppose that generator G_1 is able to offer the same control contract as G_3 at a lower bidding price. Figure 13.30 shows the system response after the control contract has been shifted from generator G_3 to generator G_1 . As we can see, there is no noticeable deterioration in the performance of the control system.

13.4.2.10 Market-Based Flat Frequency Control: Summary In closing, here we propose a possible market structure for frequency control necessary to balance power imbalances created through the electricity market activities. It is shown that it is theoretically possible to balance power and guarantee frequency quality through a very simple market structure. If the rules, rights, and regulations for primary markets are well structured, it is possible to establish a market-based provision of frequency regulation in which the role of a system operator would be mainly supervisory.

This proposed scheme allows different loads, with different characteristics and variabilities, to be charged differently — according to their actual impact on the system. This property is very appealing as a way to promote economic efficiency.

This scheme, of course, will not work perfectly. For implementation, and moving it toward real policy, there would need to be some enforcement or monitoring (quality control) to make sure people do not misrepresent their load-generator characteristics and thus avoid actually paying for their true impact.

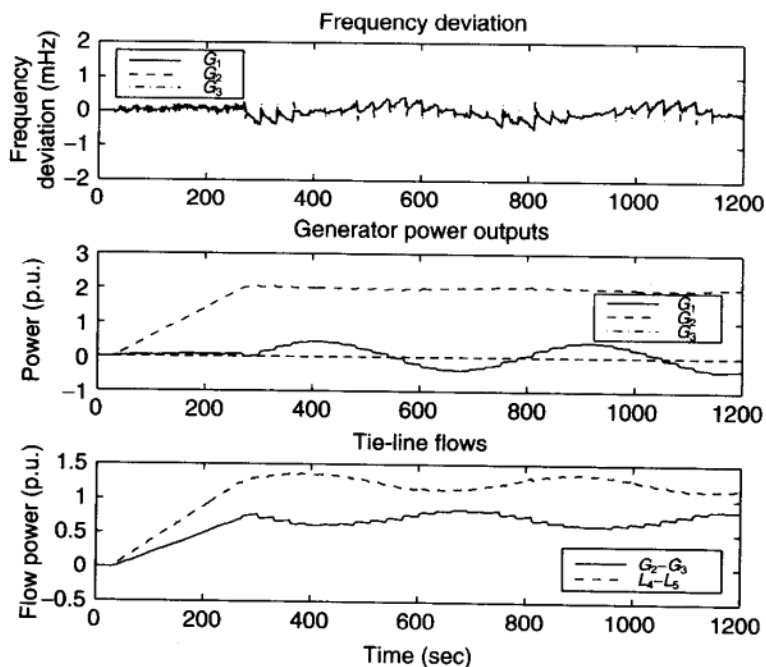


FIGURE 13.30 System response after the control contract of G_3 is shifted to G_1 .

on the system. There will probably need to be some form of sanction or penalty for users who significantly and/or repeatedly make contracts, for example, with a deviation band that is more narrow than their true deviation. Also, the robustness of the proposed market to the accuracy at which generator and load droop characteristics are known will have to be studied further to gain confidence in the proposed concept.

Nevertheless, it is somewhat exciting to have reached the point that indicates that market forces could balance power in real time with minimal coordination. This is conceptually possible because system frequency is more or less the same everywhere, and therefore the actual location of power imbalance becomes secondary.

In the context of an open access comprised of several control areas, the conclusion is that when the ACE is replaced by the frequency criterion, the fundamental role of control area is also lost. In an open-access market, boundaries between control areas are no longer relevant (nor legal) as power is traded within the interconnection. The proposed frequency-control market described in detail for a single control area can be directly generalized to the multicontrol area open systems.

13.4.2.11 Time-Error Correction in the Deregulated Industry It is worthwhile to observe that, similar to the regulated industry, the system-frequency deviations will accumulate over time no matter how small. Viewed mathematically, this inability to control the total supply–demand imbalance of an isolated system by entirely decentralized controllers directly follows from the singularity of the K_P matrix of the interconnected system as described earlier. Consequently, as shown earlier in this chapter, there exists an interarea variable that is not controllable. Viewed physically, the entire interconnection is still a floating system with the cumulative errors in frequency reflecting the fact that no firm physical reference bus exists.

This situation will further result in the deviation of synchronous time or so-called time error [62]. This problem does not go away with the implementation of the market-based flat frequency control described earlier. Because of this, some form of tertiary–(interconnection) level correction will be required to correct for this cumulative frequency error, if maintaining synchronous time is to remain part of the power-system operation. Of course, the rate at which system synchronous time will deviate in a deregulated industry may be considerably different than that in the regulated industry. One could envision that the time error correction may be managed in response to the difference between the wholesale-level electricity price and the price which small users are willing to pay.

13.5 REACTIVE-POWER DISPATCH ECONOMY

The real-power economic dispatch, regulated or deregulated (block 2 in Fig. 13.4), is a fairly straightforward optimization process. It should be clear

from Section 13.3 that the economic dispatch is in many ways analogous to the process of balancing supply and demand in any other industry.

The balancing of reactive power on an interconnected power system, on the other hand, is unique to the electric power industry. Recall from Chapter 2 that any real-power production, transport, and/or consumption is at the same time accompanied by the production, transport loss, and/or consumption of reactive power. In particular, each load consumes certain reactive power Q_L as it consumes real power P_L . Because of this, it is necessary to balance reactive power.

Conceptually, the reactive-power balancing is carried out in a way analogous to the process of real-power dispatch and frequency control. Similar to real power, the stationary reactive-power consumption exhibits deviations from the expected reactive-power consumption at various rates. The same temporal separation of real-power demand described earlier is applicable to the reactive-power fluctuations according to formula (13.37). Based on this temporal separation, the reactive power out of power plants is scheduled at the level of block 2 for anticipated customer needs. Since reactive power consumed is not identical to its expected value, closed-loop voltage control takes place at various rates, as indicated in block 6.

The reactive-power compensation for the power consumed by loads and reactive power lost in transport could be provided by the loads themselves, by the reactive-power-compensating devices on the transmission system (such as shunt and series capacitor banks), and/or by the power plants. In the regulated industry these methods are used without explicitly separating shares of power plants, generators, and customers' responsibilities for providing reactive-power support. In the deregulated industry the rules for reactive-power provision are likely to become more explicitly defined.

In what follows we formulate the reactive-power dispatch for the anticipated reactive-power demand for the regulated and competitive industry, respectively. This is followed by the description of hierarchical (load) voltage control in Section 13.6.

13.5.1 Reactive-power Dispatch in Regulated Industry

As explained in Chapter 5, for an interconnected power system to remain viable, the reactive power must balance at each bus (recall the load-flow equations). In this chapter only the generation-based reactive-power dispatch is of direct interest. The schedules are implemented by changing the set-point values E_{Gi}^{ref} of power plants, similar to the way the real power P_{Gi} is indirectly set by changing the setting of the governor speed-changer ω_{Gi}^{ref} .

The problem of reactive-power dispatch in the regulated industry is generally bundled with the problem of maintaining (load) voltages within the prespecified limits. The (generator) voltage set-point values E_{Gi}^{ref} are optimized with respect to certain performance criteria subject to the reactive-power-balance constraints, the load-voltage acceptable limits, and the availability limits on the reactive power generated and the limits on generator voltages. The generation-based reactive-power dispatch falls under the category of the optimal power flow

(OPF) [63]. Depending on the actual choice of the optimization criterion, two formulations are of interest:

1. The cost function is the total fuel cost required to supply a given demand.
2. The cost function is total transmission loss that occurs as power is delivered from the power plants to the customers.

The conventional OPF formulation is reviewed briefly next for completeness.

Consider an electric power system whose total number of generator buses is $N = k + 1$ and number of loads is n , with bus number 0 being system slack bus. In the general (coupled real-power reactive-power) case, the *control variables* u are

1. Real power:

$$P = [P_0 \quad P_{n+1} \quad P_{n+2} \quad \dots \quad P_{n+k}] \quad (13.135)$$

generated by the power plants.

2. Generator voltages

$$[E_0 \quad E_{n+1} \quad E_{n+2} \quad \dots \quad E_{n+k}] \quad (13.136)$$

The optimization problem of interest is the problem of minimizing a cost function J [eq. (13.1)]

$$J = F(u) = F(P_0, P_{n+1}, \dots, P_{n+k}) \quad (13.137)$$

subject to upper (max) and lower (min) constraints

$$\begin{aligned} P_i^2 + Q_i^2 &\leq S_i^2, \quad i = 0, n+1, \dots, n+k \\ P_i^{\min} &\leq P_i \leq P_i^{\max}, \quad i = 0, n+1, \dots, n+k \\ Q_i^{\min} &\leq Q_i \leq Q_i^{\max}, \quad i = 0, n+1, \dots, n+k \\ E_i^{\min} &\leq E_i \leq E_i^{\max}, \quad i = 0, 1, 2, \dots, n+k \\ B_{ij}|\delta_i - \delta_j| &\leq P_{ij}^{\max}, \quad i, j \in 0, 1, 2, \dots, n+k \end{aligned} \quad (13.138)$$

so that the load flow equations (5.10) to (5.12) on the entire system are satisfied. This optimization is done with respect to either real-power generation and/or settings of voltages at buses the voltage magnitude of which is directly controllable.

This problem falls under the category of basic static optimization problems subject to equality and inequality constraints. The necessary optimality conditions provided by the theorem of Kuhn and Tucker are stated as follows.

Theorem 13.5.1 Given

1. Cost $F(u)$ of the control variable u
2. Inequality constraints of the form

$$G(x, u) \leq 0 \quad (13.139)$$

3. Equality constraints of the form

$$H(x, u) = 0 \quad (13.140)$$

and assuming convexity for F , G , and H , the necessary conditions under which $F(u)$ reaches minimum are given by the condition

$$dL = 0 \quad (13.141)$$

where the Lagrangian is defined as

$$L(x, u) = F(u) + \alpha^T G(x, u) + \beta^T H(x, u) \quad (13.142)$$

Typically when the cost function represents the cost of real-power generation, the control variables with respect to cost minimization are the real power P in Eq. (13.135). Kuhn and Tucker conditions applied to this problem then result in Lagrangian of the form

$$\begin{aligned} L(x, u) = & F(P_0, P_{n+1}, \dots, P_{n+k}) + \sum_i \alpha_i^P (I_i - P_i + P_{Di}) \\ & + \sum_i \alpha_i^Q (K_i - Q_i + Q_{Di}) \\ & + \sum_i M_i (P_i^2 + Q_i^2 - S_i^{2,M}) + \sum_i m_i (P_i^{\min} - P_i) + \sum_i M_i (P_i - P_i^{\max}) \\ & + \sum_i e_i^{\max} (Q_i - Q_i^{\max}) + \sum_i e_i^{\min} (Q_i^{\min} - Q_i) \\ & + \sum_i \mu_i^{\max} (E_i - E_i^{\max}) + \sum_i^{\min} \mu_i^{\min} (E_i^{\min} - E_i) \\ & + \sum_{i,j} \mu_{ij} (P_{ij} - P_{ij}^{\max}) \end{aligned} \quad (13.143)$$

Here I_i and K_i stand for the real- and reactive-power injections into bus i from the transmission grid.

It has been shown by Carpentier [64] that at the optimum the dual variables α_i^P and α_i^Q measure the marginal or incremental cost of active and reactive consumption at node i , that is,

$$\alpha_i^P = \frac{\partial F}{\partial P_i} \approx \frac{\Delta F}{\Delta P_i} \quad (13.144)$$

and

$$\alpha_i^Q = \frac{\partial F}{\partial Q_i} \approx \frac{\Delta F}{\Delta Q_i} \quad (13.145)$$

Similarly, the other dual variables M_i , m_i , e_i^{\min} , e_i^{\max} , μ_i^{\max} , μ_i^{\max} , and μ_{ij} in the Lagrangian (13.143) measure the marginal cost associated with the inequality constraints (13.139). For example, the dual variable

$$\mu_i^{\max} = \frac{\partial F}{\partial E_i^{\max}} \approx \frac{\Delta F}{\Delta E_i^{\max}} \quad (13.146)$$

relates the saving ΔF due to relaxation in ΔE_i^{\max} in the upper voltage bound E_i^{\max} at bus i . This formulation is useful for real-power rescheduling to minimize cost of real-power generation, while meeting operating constraints. In this sense it can be interpreted also as a security-constrained economic dispatch problem [1].

When the cost function represents total transmission losses,

$$J = P_{\text{loss}} = F(\underline{E}, \delta) \quad (13.147)$$

optimization is typically done with respect to directly controlled (generation) voltages, Eq. (13.136). In this case control variables u are voltages at directly controlled buses. The solution to this problem obtains optimum changes in E_i at generators, within the constraints, such that transmission losses are minimized for given load. The optimization of the performance criterion J_{loss} with respect to voltage magnitudes complements a constrained economic-dispatch-type optimization of real power $u = [P_0 \ P_{n+1} \ P_{n+2} \ \dots \ P_{n+k}]$ that explicitly minimizes the fuel-cost-related performance criterion in Eq. (13.137). The choice of the “right” performance criterion is a complex, system-dependent problem [65 to 67].

13.5.1.1 OPF-Based Approaches to Voltage and Var Problems An increased severity of voltage-related operating problems has resulted in an effort to make OPF-based formulations more directly related to these problems than the general OPF methods. Among many developments, three are worthy describing in detail:

1. An improved formulation by Carpentier [64] of the decoupled OPF.
2. OPF-based optimization of reactive power margins by Van Cutsem and Vournas [68].

3. An OPF targeted on improving the energy transfer over far electrical distances.

A transformation introduced in Ref. [64] forms a basis for a more accurate OPF solution of reactive-power controls under the decoupling assumption than the one commonly practiced. This transformation is based on eliminating from the load-flow equations the individual branch phase-angle differences. To do this, each real-power line-flow relation is considered as a function of E_i , E_j , and $\delta_{ij} = \delta_i - \delta_j$,

$$P_{ij} = f_P(E_i, E_j, \delta_{ij}) \quad (13.148)$$

and is used to express

$$\delta_{ij} = f_P^{-1}(E_i, E_j, P_{ij}) \quad (13.149)$$

which is substituted into the corresponding reactive-power line-flow equation, resulting in

$$Q_{ij} = f_Q(E_i, E_j, \delta_{ij}) = f_Q(E_i, E_j, f_P^{-1}(E_i, E_j, P_{ij})) \quad (13.150)$$

to yield

$$Q_{ij} = \tilde{f}_Q(E_i, E_j, P_{ij}) \quad (13.151)$$

Details of these relations can be found in Ref. [64], in which it is shown that fixing individual active power flows P_{ij} is an approximation in the sense that when voltages change, the real-power flows are also somewhat redistributed; the real-power losses also change. However, this is a more adequate approximation than the conventional real reactive-power decoupling approximation defined in Chapter 5. The OPF-based reactive-power optimization that uses this transformation, Eqs. (13.148) to (13.151), to reduce the complexity of the problem can be found in Ref. [64]. This formulation provides for an interesting separation between the optimization of real-power resources, on one hand, and the reactive-power resources, on the other, without sacrificing accuracy in a significant manner. An important extension of the optimization of reactive power resources by Van Cutsem and Vournas based on this formulation can be found in Ref. [68].

13.5.2 Reactive-Power Dispatch in the Deregulated Industry

Opinions about reactive-power management and its value in the restructuring of industry range from emphasizing the variable cost of generators associated with system voltage and reactive-power constraints based on OPF computations [64], through claims that implementing capacitors to support voltage may be sufficient and inexpensive [69]. Only recently was it recognized that voltage-support-related questions are potentially more complex than envisioned in the early documents and that they may have significant impact on the success of competitive power provision. Technically, when voltage support is not provided,

this creates a major obstacle to the implementation of the energy transactions; this, in turn, has an impact on market efficiency [70].

Moreover, there exists a significant difference between the cost of the reactive-power-voltage provision and its value to the market. This raises a question concerning possible markets for reactive-power compensation and voltage control.

To establish a systematic framework for voltage-support and reactive-power compensation under open access, one must address the same two questions as in the regulated industry [71]. Namely, as the reactive-power dispatch and voltage scheduling are attempted in the restructuring of industry, one must keep in mind the distinction between security-related rules and standards and the impact of voltage support on market efficiency (optimal voltage profile question). The two are briefly described next.

13.5.2.1 Reactive-Power Scheduling for Reliability: Technical Standards

There are two conceptually different starting approaches one could consider for reliable voltage-support and reactive-power compensation:

1. Each subsystem is characterized by the nominal patterns of generation and demand, including prespecification of power-exchange levels among the subsystems. The voltage-support and reactive-power compensation is designed for these patterns. As the generation patterns change (or even demand, in the case of price-responsive users), the relative impact of the deviations from the nominal conditions for which the subsystems were originally designed must be determined for further enhancements of an open-access system with the objective of maintaining the same level of technical reliability.

A transmission provider is responsible for either procuring reactive-power support from generators and/or building reactive network compensation to maintain voltages close to their nominal values. Loads pay for this provision.

This approach critically depends on clear quantification of nominal (optimal) voltage schedules. (This notion is difficult because there are many different subobjectives [67].)

2. A transmission provider could define a new simple technical objective for all to ensure reliable voltage support in a rather noncontroversial way. The concept rests on the following *uniform* requirement (standard) for all users, generators, and loads equally: Either the net reactive-power consumption at each bus i should be zero, or the bus is equipped with some form of direct voltage control to maintain voltage at 1 p.u.²¹ Any transmission system whose bus characterization is like this will always have assurance that it is reliable with respect to voltage support [71].

²¹ Possibly a more relaxed requirement could be imposed allowing for a very small deviation around unity power factor and 1 p.u. voltage specifications.

Short of this, serious technical problems arise with respect to the fundamental solution existence to the problem. In particular, recall from Chapter 5 that methods for quantifying bounds on maximum power Q_{Li}^{\max} for which reactive-power steady-state stability limits are exceeded are basically nonexistent beyond a simple two-bus system. On the other hand, bounds are known on the maximum capacitor limits C_i^{\max} which could be installed at bus i to avoid (statically) unstable voltage solutions [72].

These two technical facts point into the direction that it would be very safe, from a reliability point of view, to require loads to have effective zero reactive-power impact on the system and therefore not expect any reactive-power compensation from a system provider. In addition, a good technical standard would be for *all* users with direct voltage control capabilities (generators, in particular) to maintain their voltages to the same voltage level, say 1 p.u. The zero impact of loads on the interconnected system could be achieved in two different ways:

- By installing local capacitive support to compensate for its own reactive-power use (within well-defined limits on capacitive compensation C_i^{\max} determined by a system provider) or
- By purchasing from a generator reactive power Q_{Gj} to compensate for the power consumed Q_{Li} and for the *estimated reactive-power (transmission) loss* created by injecting this power at bus i . Generator j would have to produce $Q_{Li} + Q_{Gj}^{\text{loss}}$ (Q_{Gj}^{loss} is the reactive-power transmission loss induced on the grid by G_j while selling a Q_{Li} amount); the load would use $Q_{Gj} - Q_{Li}^{\text{loss}}$.

The latter approach critically depends on the reactive-power consumers and sellers estimating the transmission loss they would induce while doing this. Recent results in Refs. [73 to 75] provide algorithms for doing this effectively. The only information needed is the injection at the location for which the loss estimate is computed, the entire transmission network topology, its parameters, and a nominal voltage profile of the system to which user is connected. While not all of this information is made available on-line at present, this is the basic information that should be provided in the future for various purposes. We illustrate in Appendix 7.3 the basis for this result.

13.5.2.1.1 Likely Reliable System Architecture of the Future This system would have many loads compensating their own reactive-power consumption by either their own (shunt) capacitive support or by many distributed network controls for maintaining load voltage at 1 p.u. at relatively low voltage levels (a load whose voltage is directly controlled does not have to compensate for reactive power). A very interesting concept of HV-DC light recently launched by ABB, Inc. has exactly such a purpose of equipping low-voltage level transmission and distribution systems with reactive-power-compensating devices located on the grid to control load voltage directly [76]. Many FACTS-like devices at lower voltage levels would provide the system with firm 1-p.u. voltage support. In

addition, as small distributed generation gets implemented at low voltage levels, it could also be used to support voltage where implemented.

Note: A more advanced and effective approach to defining technically acceptable voltage profile would be based on a bottom-up approach. For instance, as the LSEs specify their real power needs, they could specify voltage deviations around 1 p.u. at their own locations acceptable by their customers. This would set a basis for customer-based power quality, in this case voltage specifications. The providers of the voltage quality needed could be market-based, as outlined here, and it could be provided by the LSE itself, by the wire company and by a generator. The power quality specifications provided by the LSEs under open access are essential for meaningful linking with the wholesale electricity markets.

13.5.2.2 Possible Markets for Voltage support and Reactive-Power compensation A starting premise here is that it is conceptually impossible for a system provider to define “optimal” standards for voltage support in restructuring the industry. This claim should be clear based on the preceding section concerning fundamental issues with optimal voltage scheduling in the regulated industry. It is fairly obvious that the systemwide criterion in the new industry will be attempted by optimizing generation-dependent, load-dependent, and network-dependent criteria. Moreover, it is difficult to coordinate the trade-offs between these subcriteria in a nondiscriminatory way.

We propose here that a sufficient basis exists to create a market for reactive-power provision. This assumes a clear specification of the responsibilities of different parties with respect to system reliability. Keeping in mind the two distinct approaches to reliable voltage support under competition proposed here, one could envision two different setups for market-based reactive-power and voltage control:

- A spot market for voltage or reactive power in which a transmission provider charges users for deviating from their nominal voltage schedules and collects these charges to enhance the system and/or purchase reactive power from generators beyond their nominal reactive-power outputs. The performance measure of a good transmission provider is how well it maintains voltages close to those determined by present practices.
- A more interesting approach would be to have system users connected at each bus meet the standard reliability requirement of either keeping the bus voltage at 1 p.u. or compensating for reactive power absorbed at the bus while mutually competing for reactive-power resources.

Reactive-power sellers would make value-based bids to sell reactive power as shown in Figure 13.31. The maximum amount of real power that a generator can produce depends on how much reactive power Q_G it generates, that is,

$$P_G^{\max} = P_G^{\max}(Q_G) \quad (13.152)$$

where P_G^{\max} is the maximum power output by a generator as this generator produces reactive power Q_G . Based on historic data, a generator should be able to

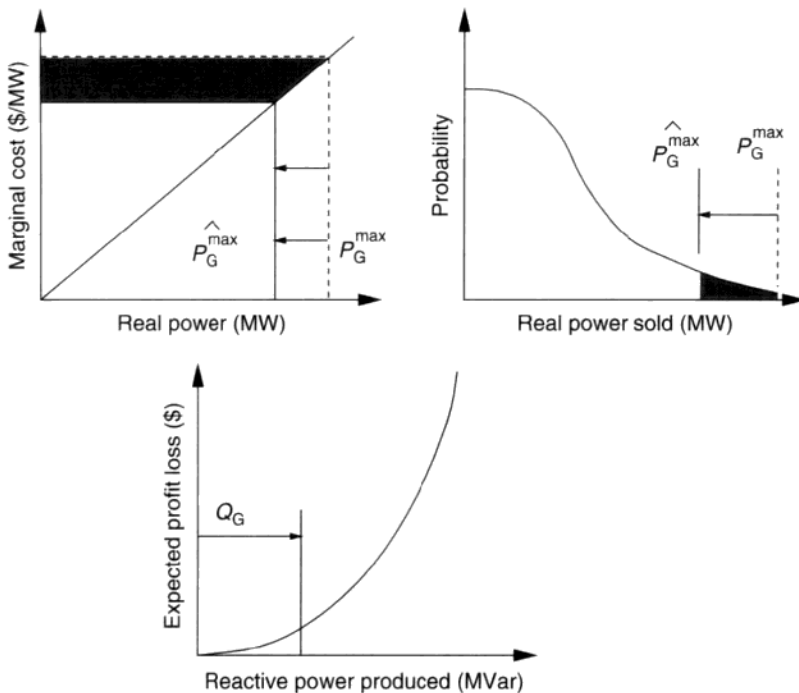


FIGURE 13.31 Expected profit loss of a generator due to reactive-power production.

build a function describing the probability $S(P_G)$ of how much real power it will sell.²² Then a generator would bid in the reactive-power-compensation market based on $P_G^{\max}(Q_G)$, $S(P_G)$, and its marginal cost curve $MC(P_G)$, according to

$$L(Q_G) = \int_0^{Q_G} MC(P_G^{\max}(Q_G))S(P_G^{\max}(Q_G))dQ_G \quad (13.153)$$

where $L(Q_G)$ reflects the lost opportunity to sell more real power because of reactive power produced.

The transmission provider could sell voltage control to the system users who need to meet the standard of maintaining voltage at 1 p.u.* This could be done by means of many new devices for network-controlled reactive-power provision; it is straightforward to see that the lower the cost is, the more distributed, and the smaller these devices are (therefore on lower voltage levels of the grid, including subtransmission), the more competitive will be the price of reactive power sold by generators.

Loads themselves could also provide their own reactive-power compensation. The need to purchase more compensation because of the reactive-power

²² This estimation process could be updated frequently by updating market data.

* The entire market setup could be generalized if a bottom-up specification of a desired voltage quality is in place.

loss created when compensation is provided by other parties would therefore be avoided. However, in some cases if reactive power from generators is inexpensive, it pays off to purchase compensation for losses as well. As long as the market takes the covering of transport loss, the compensation is not too far beyond consideration. This is how one gets around the problem of localized response. The reactive-power support is “optimal” to the buyer as long as it is cheaper to purchase from a generator than to build its own capacitive support or to purchase voltage control from a transmission provider.

One could now view this market as the process of buying and selling reactive-power compensation and/or voltage support with clearly defined capacity limits of the products purchased. For example, the limit on maximum capacitor size at bus i for given transmission topology and parameters [72] is observed by all to avoid reliability problems. These limits are a function of transmission-line parameters; as these limits change over time because of the network control devices are added, the limits change. However, this could be made public information, since it is strictly a technical feature and trades must observe it.

Assuming progress is made toward systematic technical designs, the truly novel questions concern pros and cons of developing a market for reactive power and voltage support. Viewed from a consumer's point (who ultimately pays all charges), it is essential to understand reasons for the amount of reactive power or voltage for which each user is responsible. Depending on the transmission structure of the future, a consumer may have more or less flexibility in controlling the charge for this support. We suggest that there are many choices for each customer to make provision of reactive-power or voltage control based on value. This, in turn, will have considerable impact on the transmission business of the future (particularly at the lower voltage levels [76]) as well.

A proposed market structure achieves three objectives:

- The structure manages to avoid the issue of optimal voltage “standards” on an interconnected system, which is for all practical purposes an unsolvable problem.
- The structure lets all potential providers of reactive power and voltage support compete for service, similar to the way competitive electricity markets work.
- By clearly defining each user's (equal) responsibility for reliability reasons only, the structure lets market work for meeting these in a competitive way. (This could be modified to accommodate power quality requirements, as suggested above.)

Once the market is in place, this will lead to significant improvements in the flexibility of the transmission grid because incentives will be in place to enforce it wherever it is beneficial to the market.

An important starting point in developing markets for voltage support is the fact that most of the *low-voltage* support equipment does not have significant fixed cost. Namely, cost of the equipment changes as a function of capacity, or, in other words, the economies of scale are not pronounced.

This sets the basis for usage-based pricing capable of recovering investment costs [77]. (This situation is in sharp contrast with the investment for large transmission lines for which the economies of scale are very pronounced and points in the direction of HV-DC-like transmission technologies of the future for low voltage levels.)

13.5.2.3 Voltage-Related Market Power Issues Voltage problems, as any other technical obstacle to implementing the requested market transactions, are often viewed by regulators as an exercise in a system provider's barrier to entry. To deal with this regulatory issue, it is critical to develop ways of demonstrating the technical option selection process.

A possible approach for reactive-power market design suggested here establishes means that differentiate technical necessity (reliability, and, possibly, power quality) from the market-related actions. In the case of reactive power it is effectively impossible to have a single optimal performance criterion (optimal standard). Instead, market users decide themselves what is best.

Here we omit a formal proof that the proposed market would converge to the minimal systemwide charges for meeting the preset minimal reliability standard of either compensating fully for the reactive-power impact on the system or maintaining bus voltage at 1 p.u. The proof simply reflects the basic law of (reactive power or voltage) supply and demand.

One of the main claims we make is that different options exist for achieving the same technical goal. For example, as demonstrated in our study of the New England voltage problems, there is a choice of supporting voltage by a power plant or by enforcing the grid [78]. These two are economic substitutes, and, as long as there are well-developed rules, regulations, and responsibilities for selling and buying reactive power and voltage support, they could be provided on a competitive basis. Moreover, must-run units under the minimal technical standard recommended are no longer a necessary concept.

The choice in the envisioned reactive-power market will be much larger at low(er) voltage levels. The real competition for voltage support in the future will take place between distributed generators willing to sell reactive power and DC light-like transmission technologies as recently introduced in Ref. [76].

13.5.2.4 Two Different Subproblems As the industry restructuring evolves, it may be helpful to separate two qualitatively different types of systems for which voltage support is needed:

1. A transmission system that still remains a link between its connected load and generation within a well-defined entity (state or utility), similar to the way before restructuring started. Such systems are typical in parts of the U.S. system where competition is still slow to evolve, or in subareas whose interface with the neighboring systems is already fully utilized.
2. A large open-access transmission system comprising several control areas characterized by active energy trades between distant users and producers.

Such systems are typical of areas where restructuring has advanced and where transmission access is given to all.

In the first type of system the line-flow patterns are very similar to the patterns for which the system was designed. Reactive-power and voltage-support problems are primarily technical; methods for preventing voltage collapse and design of on-line voltage control to ensure prespecified technical performance remain active challenges.

The second type of system is subject to many new industry restructuring-related open issues. Here, technical, economic and regulatory aspects are closely interwoven.

Systems in which restructuring is very active must resolve several fundamental questions triggered by this process, particularly:

1. Separation of responsibilities for reactive power and voltage support among functionally separate transmission, distribution (load), and generation entities (questions regarding "standards" [79]).
2. Defining minimal technical criteria that each user must meet.
3. Coordination of performance criteria for voltage scheduling among the neighboring areas within an open-access transmission territory to avoid inadvertent flows.
4. Development of charging mechanisms to encourage solutions most useful to the system users.

Here only one possible approach to solving these challenges has been described. Much future development is expected on this topic.

13.6 GENERATION-BASED VOLTAGE CONTROL

Compared with the generation-based frequency control, the generation-based reactive-power or voltage control is less standardized and less automated (block 6). Only a handful of countries in the world have semiautomated voltage control of generators.

A close look into this problem would indicate, however, that the objectives of a hierarchical voltage-control scheme are analogous to the objectives of frequency control; the main objective at the secondary- (area) level voltage control is, for example, to update set points of generator exciters to maintain voltages at critical ("pilot" points [80]) within the prespecified deviations as the reactive-power demand and generation deviate from their scheduled (anticipated) values. In this section we provide a treatment of hierarchical reactive-power or voltage control for the regulated industry based on the systematic implementations in several European countries; this scheme is sometimes referred to as automatic voltage control (AVC) [8,80].

13.6.1 Voltage Control in the Regulated Industry

While the voltage control of an interconnected large-scale power system is widely recognized as a very important problem, its basic formulation and solutions are often utility-specific. In the United States voltage control at the secondary and tertiary levels is viewed as an entirely static problem, the solution of which is identical to centralized open-loop optimization-based reactive-power–voltage dispatch. The most common tool for solving this optimization problem is an algorithm based on optimal power flow (OPF), as described earlier in Section 13.5.1.

A qualitatively different approach to the voltage-control design is hierarchical and it is based on temporal separation of reactive-power fluctuations and corresponding control levels as defined in Eqs. (13.37) and (13.39), respectively. Similar to the hierarchical real-power–frequency-control scheme described in Section 13.4.1, the approach is based on the decomposition of a large system into control areas equipped with decentralized closed-loop secondary-level voltage controllers.

Here we introduce this hierarchical approach to the generation-based voltage control. As in the case of hierarchical frequency-control design, we introduce the models directly relevant for voltage control over the mid- and long-term horizons first. These models are load variation- and control-driven models, in the sense that any variations in voltages with time are caused by the control signal or the disturbances only. The conventional and improved secondary-level voltage controls are described next using these models.

13.6.1.1. Quasistatic Model for Secondary-Level Voltage Control The objective of the secondary-level reactive-power or voltage control is to regulate load voltages by controlling settings of terminal voltages on generators $E_G^{\text{ref}}[k]$. To derive the relation between load voltages and generator terminal voltages, let us consider an administrative area within an interconnected system. From the network relation (6.114) one can obtain the following quasistatic discrete-time model, by integrating Eq. (6.114) from the secondary time instant kT_s to the next instant $(k+1)T_s$,

$$\begin{aligned} E_L[k+1] - E_L[k] &= C_V(E_G[k+1] - E_G[k]) + J_{LL}^{-1}[(F_L[k+1] - F_L[k]) \\ &\quad - (Q_L[k+1] - Q_L[k])] \end{aligned} \quad (13.154)$$

As in the frequency-control case, we define the secondary corrective control signal as

$$u_s[k] \triangleq E_G[k+1] - E_G[k] \quad (13.155)$$

the tie-line flow changes as

$$F_s[k] \triangleq F_L[k+1] - F_L[k] \quad (13.156)$$

and the secondary-level load disturbances as

$$d_s[k] \triangleq Q_L[k+1] - Q_L[k] \quad (13.157)$$

Eq. (13.154) then becomes

$$E_L[k+1] - E_L[k] = C_V u_s[k] + D_s(F_s[k] - d_s[k]) \quad (13.158)$$

with $D_s \triangleq J_{LL}^{-1}$. This is the desired secondary-level discrete-time dynamic model for a region within an interconnected system.

To write this using standard state-space model formulation [81], let us define the secondary-level states as

$$x_s[k] \triangleq E_L[k] \quad (13.159)$$

Then Eq. (13.158) is rewritten as

$$x_s[k+1] - x_s[k] = C_V u_s[k] + D_s(F_s[k] - d_s[k]) \quad (13.160)$$

where $F_s[k]$ and $d_s[k]$ act as the disturbances to the system with control $u_s[k]$. The difference between $F_s[k]$ and $d_s[k]$ is that the flow can be measured, while the loading variations are rarely measured in practice. They are either estimated or simply treated as a real disturbance.

It is emphasized that the discrete-time dynamic model in Eq. (13.160) is a control- or disturbance-driven model in the sense that if no disturbances (including tie-line flows) are present and the corrective control is inactive, then $x_s[k] = \text{const } \forall k$. Clearly, control actions are needed to bring the system (13.160) back to the nominal operation if the system is perturbed away from the nominal operation by disturbances.

13.6.1.2 Quasistatic Interaction Variables Observe next that the dimension of the sensitivity matrix C_V in the secondary-level voltage model in Eq. (13.158) is $n \times m$, where n is the number of load buses and m is the number of generator buses that participate in the secondary-level regulation. In general, it is true that $n > m$, that is, the number of load buses is larger than the number of generator buses participating in secondary-level control.

Under the condition of $n > m$, one can verify that the closed-loop system using any feedback control is singular, because matrix C_V has a maximum rank of m . This structural singularity is due to the relative numbers of controls and states. This is a general property for any control-driven system. Based on this inherent rank deficiency in the quasistatic voltage dynamics, we introduce the following definition first.

Definition 13.6.1: Quasistatic Interaction Variables Any linear combination of the states, $z[k] = T x_s[k]$, $T \neq 0$, that satisfies

$$z[k+1] - z[k] \equiv 0 \quad \forall k \quad (13.161)$$

for any secondary control actions, and in the absence of interactions among regions and disturbances, that is $F_s = 0$ and $d_s = 0$, is defined as the quasistatic interaction variable of the administrative area under study.

The same notation as the continuous interaction variables in Chapter 4 is used here to indicate the similar characteristics of the two. The meaning is clear from the context under study. As with the continuous interaction variables, the quasistatic interaction variables do not vary with time when interconnections are removed and load disturbances are not present. For the interconnected system, therefore, any variations of the interaction variables with time are entirely due to the interactions among regions or load disturbances. Note from the definition that the interaction variables are not unique. In fact, any combinations of the interaction variables are still interaction variables.

Let us derive the condition for the transformation matrix T . Combining Eq. (13.161)

$$z[k+1] - z[k] = T(E_L[k+1] - E_L[k]) = TC_V u_s[k] + TD_s(F_s[k] - d_s[k]) \quad (13.162)$$

Under the conditions in the definition, $F_s[k] \equiv 0$ and $d_s[k] \equiv 0$, we arrive at

$$z[k+1] - z[k] = TC_V u_s[k] \quad (13.163)$$

In order to have $z[k+1] - z[k] \equiv 0$ for any control $u_s[k]$, matrix T must satisfy

$$TC_V = 0 \quad (13.164)$$

This is the equation for calculating T . Note that matrix C_V has maximum rank $m < n$, and therefore Eq. (13.164) has nonzero solutions for T . We can solve T from Eq. (13.164) because it is a simple algebraic equation that can be solved with a Gaussian elimination method. The need for eigenstructure analysis is completely avoided.

Note that the definition for interaction variables holds independent of the specific secondary control. Equivalently, the secondary control cannot affect the interaction variables. Any variations of the interaction variables are due to the interactions with other areas or are result of the load fluctuations in the area for which control is designed. The matrix T , as a result, will not be dependent on the specific form of the secondary control.

An interesting difference between the continuous and quasistatic interaction variables can be noted. For any single area, the dimension of the continuous interaction variables in the reactive-power–voltage model is generally 0, because the system normally has a full rank. For the quasistatic interaction variables, as shown previously, the dimension is the difference between the number of states and the number of controls. This difference between the interaction variables indicates the fundamentally different causes for the existence of two types of interaction variables.

Once the interaction variables are determined from Eq. (13.164), one can further derive the dynamic model for these interaction variables.

Equations (13.162) and (13.164) lead to

$$z[k+1] - z[k] = TD_s(F_s[k] - d_s[k]) \quad (13.165)$$

This simple model relates the interaction variables to the tie-line flows and load variations. This model is basic to effective secondary-level voltage control and tertiary-level coordination.

Notice that the definition for the quasistatic interaction variables does not assume numerically weak interconnections. Rather, it reflects a structural property of the system—different numbers of states and controls. It is interesting to relate the interaction variables defined previously to the slow variables in singular perturbation analysis, which assumes weak interconnections. It can be seen from the interaction dynamic model in Eq. (13.165) that, in the weak-interconnection case, the interaction variables do vary more slowly than the rest of the states. One can rigorously prove that, in the weak-interconnection case, the interaction dynamics derived here will be the slow subsystem in the singular perturbation analysis. (The only assumption made here is that the voltage regulators/excitation system stabilize E_G to E_G^{ref} .)

Let us now demonstrate the interaction variables and their properties on a small nine-bus example network, given in Figure 13.32 [8]. Region I consists of buses 1 and 7; the rest is area II. The pilot points are buses 1, 2, and 3. The feedback gain G_s is designed such that the pilot voltages settle exponentially in 3 min. The load is assumed to have a step increase at bus 5 at $t = 0$; thus the effect of $d_s(k)$ is seen in changes of the initial conditions for all load voltages. The numerical data used in the simulations for the nine-bus system are given in Table 13.1. The sensitivity matrix for area I, which has only one generator bus and one load bus, is simply

$$C_V^I = 1 \quad (13.166)$$

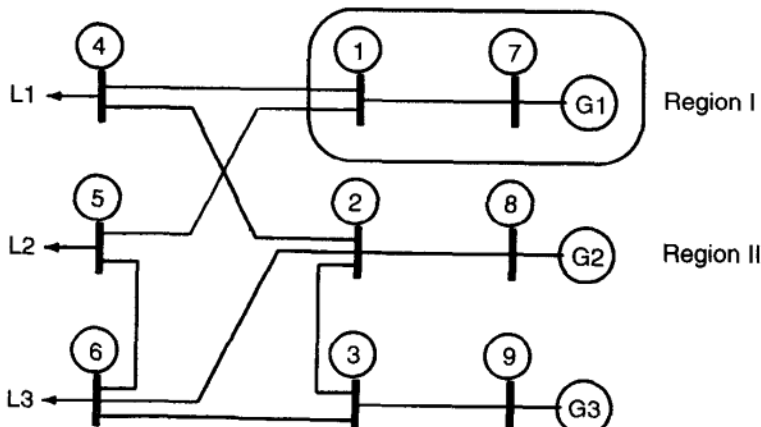


FIGURE 13.32 Nine-bus example.

TABLE 13.1 Per-Unit Data of the Nine-Bus Example

Line Parameters										
	1-4	1-5	1-7	2-3	2-4	2-6	2-8	3-6	3-9	5-6
B_{ij}	5	7	7.69	15.67	21.55	13.19	8.33	12.49	10	9.8
G_{ij}	0	0.15	0	0	1.02	0.34	0	0.31	0	0
Nominal Operating Point										
	1	2	3	4	5	6	7	8	9	
E	1	1	1	1	1	1	1	1	1	
δ	0	0	0	0	0	0	0	0	0	

The sensitivity matrix for area II, which has two generator buses and five load buses, is calculated as

$$C_V^{II} = \begin{bmatrix} 0.55 & 0.45 \\ 0.37 & 0.63 \\ 0.55 & 0.45 \\ 0.44 & 0.56 \\ 0.44 & 0.56 \end{bmatrix} \quad (13.167)$$

Let us use condition (13.164) to calculate the matrix T . For region I, condition $T^I C_V^I = 0$ simply gives $T^I = 0$. This means that region I does not have any interaction variables. For area II, condition $T^{II} C_V^{II} = 0$ leads to one independent solution

$$T^{II} = \begin{bmatrix} 21.55 & 0 & -21.55 & 0 & 0 \\ 0 & 0 & 0 & 9.8 & -9.8 \\ 13.19 & 12.49 & 0 & 9.8 & -29.48 \end{bmatrix} \quad (13.168)$$

There are three independent interaction variables given by

$$z^{II} = \begin{bmatrix} 21.55(x_2 - x_4) \\ 9.8(x_5 - x_6) \\ 13.19x_2 + 12.49x_3 + 9.8x_5 - 29.48x_6 \end{bmatrix} \quad (13.169)$$

To see the physical meaning of these interaction variables, let us rewrite the preceding equation as

$$z^{II} = \begin{bmatrix} 21.55(x_2 - x_4) \\ 9.8(x_5 - x_6) \\ 13.19(x_2 - x_6) + 12.49(x_3 - x_6) + 9.8(x_5 - x_6) \end{bmatrix} \quad (13.170)$$

Note that the interaction variables are given in terms of differences of bus voltages, with the coefficients being exactly the line inductances. Therefore, these interaction variables represent the power flows on the lines, because the power flow on each line is exactly the voltage difference across the line multiplied by the line inductance for the nominal operating conditions given in Table 13.1. Preservation of the physical meaning of the interaction variables is important for both regional control and tertiary coordination.

13.6.1.3 Secondary-Level Voltage Control The simple control-driven model (13.160) is basic to developing decentralized secondary-level voltage controllers. This control level is referred to in France and Italy as the automatic voltage control (AVC) [80]. Its main function is to respond to reactive power load disturbances $d_s[k] = Q_L[k+1] - Q_L[k]$. AVC is implemented on generator units whose voltage set points $E_G^{\text{ref}}[k]$ are automatically changed to respond to deviations in load voltages $E_L[k]$ at the chosen subset of loads, the critical pilot point loads, $E_c[k] = C_s E_L[k]$. Because the maximum number of states that can be fully controlled is equal to the number of active controls (the number of participating generators), the number of pilot point loads is always less or equal to the number of participating generators.

As with AGC, AVC at the secondary level should be designed to keep operation of subsystems as autonomous as possible, given control constraints. Its main objectives are to

- Reschedule $E_G^{\text{ref}}[k]$ at each subsystem level to balance reactive-power load deviations $Q_L[k]$, $k = 0, 1, \dots$
- Control critical load voltages $E_c[k]$ to $E_c[K]$
- Maintain $F_S[K] \approx 0$ as long as reserves within each area are available (area control principle)
- Optimize area performance (total reactive reserve or total transmission losses)

Consider, within an interconnected system, an area with n load buses and m generators participating in secondary-level control. In the secondary-level model in Eq. (13.158) assume $n > m$. Under this condition, one can prove the following:

Proposition 13.1: Controllability The dynamic system given in Eq. (13.158) is not fully controllable.

Proof Let us write the controllability matrix for the model given in Eqn. (13.158) as

$$Q_c = [B \quad AB \quad \cdots \quad A^{n-1}B] = [C_V \quad 0 \quad \cdots \quad 0] \quad (13.171)$$

since $A = 0$ for the control-driven system. Because the sensitivity matrix C_V has maximum rank m , the system is not fully controllable.

As a result, not all load voltages can be fully controlled. Only the same number of loads as the number of generators can be fully controlled. This leads to the idea of pilot load voltages, the number of which does not exceed the number of generators participating in the secondary-level voltage control.

Because of this controllability issue, the maximum number of loads that can be controlled is equal to the number of active controls. Let us choose m output variables, or pilot loads, as

$$E_c[k] = C_s E_L[k] \quad (13.172)$$

The control-driven dynamic model for these pilot loads can be obtained as

$$E_c[k+1] - E_c[k] = C_c u_s[k] + D_c(F_s[k] - d_s[k]) \quad (13.173)$$

where $C_c = C_s C_V$ is the sensitivity matrix of the critical pilot voltages relative to the control and $D_c = C_s D_s$. This is the basic model for secondary-level control design. Note that C_c is now a square matrix.

13.6.1.4 Conventional Secondary-Level Control The automated secondary-level voltage control is based only on areawide measurements, that is, area pilot-point load voltages (in France and Italy). The effect of interconnecting flow changes due to changes in the neighboring areas is not considered directly. One consequence of this is that under certain conditions a secondary-level controller may cause a significant overshoot or not reach the set value within the prespecified time intervals. The goal of secondary-level control is to maintain the pilot load voltages (output variables) at their prespecified set values when the system is under disturbances. A simple proportional feedback law takes on the form

$$u_s[k] = G_s(E_c[k] - E_c[K]) \quad (13.174)$$

where $E_c[K] \equiv E_c(KT_t)$ is the value for the pilot load voltages assigned at the tertiary level. This value is adjusted by the tertiary-level control on an even longer time scale T_t and is a constant for the secondary-level control process.

Under this control law, the secondary-level closed-loop model becomes

$$E_L[k+1] - E_L[k] = C_V G_s(C_s E_L[k] - E_c[K]) + D_s(F_s[k] - d_s[k]) \quad (13.175)$$

and the pilot-point voltage dynamics are

$$E_c[k+1] - E_c[k] = C_c G_s(E_c[k] - E_c[K]) + D_c(F_s[k] - d_s[k]) \quad (13.176)$$

Let $A_s = C_c G_s$. We then rewrite Eq. (13.175) as

$$E_c[k+1] - E_c[k] = A_s(E_c[k] - E_c[K]) + D_c(F_s[k] - d_s[k]) \quad (13.177)$$

One requirement for the choice of pilot load voltages E_c is that the resulting matrix C_c must be nonsingular. If matrix C_c is singular, then A_s will be singular for any gain matrix G_s . The discrete-time closed-loop system matrix $(I + A_s)$ will always have an eigenvalue of 1. The consequence of this is that the system will have a linear combination of the pilot voltages that cannot be moved by any control actions, that is, not all pilot voltages can be fully controlled. In other words, steady-state errors are inevitable for the chosen pilot voltages. To control the pilot voltages fully, it is required that the pilot points are selected such that C_c is of full rank.

The secondary-level control design is to choose the appropriate gain G_s . The conventional control design neglects the effect of neighboring areas, that is, it assumes $F_s[k] = 0$. Under this simplification, the model for pilot-load-voltage dynamics becomes

$$E_c[k+1] - E_c[k] = A_s(E_c[k] - E_c[K]) - D_c d_s[k] \quad (13.178)$$

where $d_s[k]$ is treated as disturbances to the system. The problem of determining the feedback matrix G_s can be formulated as an optimal control problem with given performance criterion. An alternative way is to specify the desired closed-loop dynamics for the pilot voltages. The choice commonly used is to specify the closed-loop dynamics so that all pilot load voltages are fully decoupled from each other and exponentially reaching their set values within a specified time constant. This can be easily done by choosing the closed-loop system matrix $(I + A_s)$ to be a fully decoupled diagonal matrix with desired time constant. An example for the choice of time constant typically used in France is 3 min. Equivalently, this is achieved by choosing

$$A_s = \lambda I \quad (13.179)$$

where λ is a scalar such that the pilot voltages settle to their steady state within the given time. For the specified decoupled dynamics, the time-domain response of all pilot voltages will be purely exponential and no overshoot or undershoot will occur. Using the given A_s , one can solve for the gain matrix as

$$G_s = C_c^{-1} \lambda \quad (13.180)$$

under the assumption that pilot voltages are well chosen such that matrix C_c is nonsingular.

Under conventional control, the actual dynamics of the pilot voltages become

$$E_c[k+1] - E_c[k] = \lambda(E_c[k] - E_c[K]) + D_c(F_s[k] - d_s[k]) \quad (13.181)$$

The flow $F_s[k]$ is a function of the state variables. Therefore the effective dynamics of the pilot load voltages are not purely exponential. In fact, overshoot or undershoot have been observed in some cases.

13.6.1.5 Improved Secondary-Level Voltage Control We propose in this section possible ways to improve secondary-level voltage control by taking into consideration the effect of interconnections while preserving its decentralized nature. The proposed control laws will be such that they cancel out the effect of interactions based on additional feedback signals that use the reactive power flow measurements.

In Eq. (13.175) or (13.177) the tie-line flows are viewed as an independent external input to the area voltage dynamics. The conventional design of secondary control, that is, the design of G_s , is typically done by neglecting the interconnections with neighboring areas because of the large scale of the system and the desire to maintain the decentralized nature of secondary-level control. The “optimal” control designed this way will in general not be optimal when implemented on an actual system where interconnections are indeed present. To compensate for the effect of interconnections fully, we propose a new control feedback law in the form

$$u_s[k] = G_s(E_c[k] - E_c[K]) + HF_s[k] \quad (13.182)$$

where the first term is the same as for conventional secondary-level control. The additional term $HF_s[k]$ cancels the tie-line flows on the dynamics of the pilot voltages. It will be shown that complete cancellation of the tie-line flows for the dynamics of the pilot load voltages is possible with an appropriate choice of the matrix H . Substituting this improved control law into Eq. (13.173) leads to

$$E_c[k+1] - E_c[k] = A_s(E_c[k] - E_c[K]) + (C_c H + D_c)F_s[k] - D_c d_s[k] \quad (13.183)$$

It is clear that when C_c is invertible, the tie-line flows can be fully eliminated in the pilot-load-voltage dynamics by choosing

$$H = -C_c^{-1}D_c \quad (13.184)$$

With this choice of H , Eq. (13.183) reads

$$E_c[k+1] - E_c[k] = A_s(E_c[k] - E_c[K]) - D_c d_s[k] \quad (13.185)$$

with no flows entering the equation. In other words, the area under study looks as if it were completely isolated from the rest of the system, as far as pilot-load-voltage dynamics are concerned.

It is noted that because of the controllability issue of Proposition 13.1, tie-line flows can be fully canceled only for as many as m (the number of active controls) load voltages. Since we choose m pilot points, flows can be canceled for all pilot load voltages.

Note that the control scheme presented here is fully decentralized, assuming the tie-line flows are locally measurable at each area level. No detailed information about neighboring areas is needed; only tie-line flows, which

aggregate the net effect of detailed dynamics of the neighboring areas, are required.

13.6.1.5.1 Nine-Bus Example Let us now illustrate the results on a small nine-bus example network given in Figure 13.32. Figure 13.33(a) shows the pilot-load-voltage responses using the conventional feedback law given in Eq. (13.174). It is seen that because of tie-line interactions, overshoot occurs, and the settling time is longer than supposed. Figure 13.33(b) shows the pilot-load-voltage responses with the improved feedback control given in Eq. (13.182).

It is clear that the additional term $HF_s(k)$ improves the responses, both eliminating the overshoot and ensuring the prompt settling. This improvement is expected to be significant when tie lines are strong and meshed.

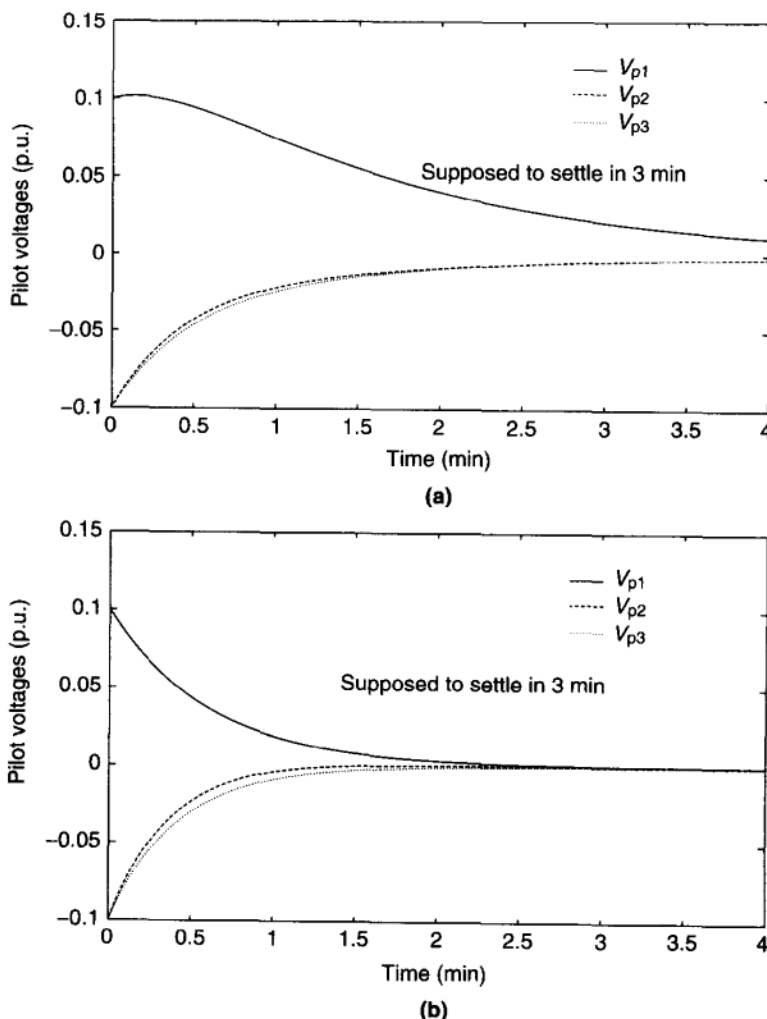


FIGURE 13.33 Pilot load voltages: (a) conventional and (b) improved.

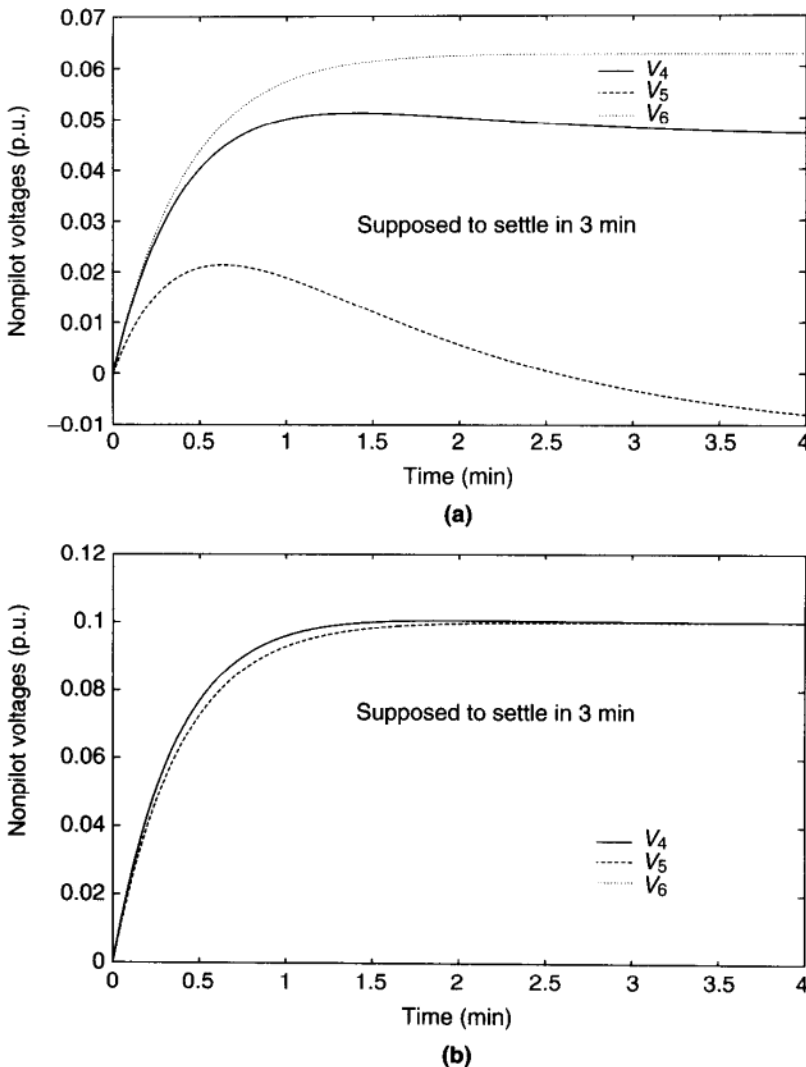


FIGURE 13.34 Nonpilot load voltages: (a) conventional and (b) improved.

Figure 13.34 shows the comparison between the non-pilot-load-voltage responses using the conventional and improved feedback controls. Again improvement is appreciable. These figures also show that no oscillatory modes exist in the time-domain responses of the load voltages, for either conventional secondary control or improved secondary control.

13.6.1.6 Tertiary-Level Voltage Coordination With an increased tendency toward large energy transfers over far distances, the problem of maintaining voltages within acceptable operating specifications has emerged in operating and planning power systems throughout the world. The main purpose of tertiary-level

voltage control is to optimize systemwide performance in response to the slow load deviations $Q_L[K]$, $K = 0, 1, \dots$. This could be done on an hourly basis or more often. The idea behind the coordination of areawide controllers is to establish feasible schemes for maintaining voltages throughout the interconnected system within the prespecified limits, subject to available reactive power resources.²³

The determination of the optimal set values for the pilot load voltages is formulated as an optimization problem. However, the notion of *optimal* voltage profiles remains an open research question, even for the simplest possible network with one generator supplying power to a single load [66]. This is because the optimal operation of the transmission network with respect to voltage cannot be uniquely defined. The main performance candidates are concerned with

- System reactive reserves
- Transmission losses
- Voltage proximity to the prespecified limits
- Flow scheduling

We recognize that some performance criteria may be more relevant for normal operating conditions and others for emergency conditions. Therefore, coordination strategies may depend on the type of system operating mode described in Section 13.1. In this sense, there should be a certain degree of adaptation to the operating mode. Conventional thinking is that under normal operation one wishes to minimize transmission loss, assuming that the system is well within the reactive reserve and voltage limits.

13.6.1.7 Question of Tertiary-Level Voltage Performance Criteria Assuming that secondary-level control is carried out properly, the objective of the tertiary-level control is to determine the values for the pilot load voltages, or equivalently the set values for the generator voltages, at the slowest rate KT_t , so that the system as a whole operates optimally according to a certain performance criterion. In this section, we discuss some general aspects of the performance criteria that have been used for this optimization process.

Since the system is composed of three major components—the generators, the transmission network, and the loads—the overall performance criterion can be written as

$$J = J_{\text{gen}} + J_{\text{net}} + J_{\text{load}} \quad (13.186)$$

²³ Although in this chapter only reactive-power reserves of generators are of direct interest, the coordination is directly applicable to all other sources of reactive energy that have primary controls responding to local voltages, such as static Var compensators and on load tap-changing transformers. This is described in Chapter 14 which is directly concerned with the transmission flow control.

where J_{gen} , J_{net} , and J_{load} are the performance criteria corresponding to each of the three major components of the power system. Specifically, using the above performance criterion, we can achieve the following:

- *Generation alignment* in an attempt to equalize the ratios of actual generation to the maximum capacity of all or part of the generators (reactive-power reserve)
- *Flow scheduling* to adjust the tie-line flows among the interconnected areas so that the system operates in a coordinated fashion
- *Security enhancement* to ensure that the generators stay within their limits as much as possible
- *Loss minimization* to reduce the losses on the transmission network

13.6.1.7.1 Generation-Dependent Criteria For the generators, we need to deal with both the reactive-power generation and the terminal voltages. Therefore, the choice for the generator performance criterion can be further decomposed as

$$J_{\text{gen}} = J_Q + J_V \quad (13.187)$$

with J_Q pertaining to reactive-power generation and J_V to the voltage limit problem. The term J_Q is introduced to ensure that the reactive-power generation remains within physically permissible limits. One simple quadratic form, for example, can be

$$J_Q = (Q_G[K] - Q_G^{\text{nom}})^T W_Q (Q_G[K] - Q_G^{\text{nom}}) \quad (13.188)$$

where Q_G^{nom} is the desired nominal point inside the limit band of the reactive-power generation, and the weighting matrix $W_Q = W_Q^T \geq 0$. The term J_V is primarily used to ensure that the generator terminal voltages stay within the allowable bounds. The simple quadratic form for J_V is expressed as

$$J_V = (E_G[K] - E_G^{\text{nom}})^T W_V (E_G[K] - E_G^{\text{nom}}) \quad (13.189)$$

where E_G^{nom} is the desired nominal point inside the limit band of the generator terminal voltages, and the weighting matrix $W_V = W_V^T \geq 0$. This kind of performance criterion tends to keep the generation outputs and terminal voltages close to their desired nominal values, if heavy weights are assigned to these terms. The justification for this type of performance criterion is that it can eliminate the situation of some generators hitting their physical operating limits under heavy loading conditions.

13.6.1.7.2 Transmission-Network-Dependent Criteria Similarly, for the transmission network, we can decompose the performance criterion into a term involving the total losses on the transmission network and a term involving rescheduling the tie-line flows.

13.6.1.7.3 Load-Dependent Criteria For the loads, the primary concern is also for the critical pilot node load voltages to remain within acceptable bounds. An expression similar to Eq. (13.189) can be written for the load voltages:

$$J_{\text{load}} = (E_c[K] - E_c^{\text{nom}})^T W_c (E_c[K] - E_c^{\text{nom}}) \quad (13.190)$$

where E_c^{nom} is the desired point inside the limit band of the load voltages, and the weighting matrix $W_c = W_c^T > 0$. This performance criterion tends to keep load voltages close to the desired point E_c^{nom} .

13.6.1.8 Reactive-Power Tie-Line Flows and the Interaction Variables In the process of solving the optimal control problem given in Eq. (13.186), network constraints defining relations between the tie-line flows, unit generation outputs, losses, and the set values for the pilot load voltages are needed. These constraints for the time K involve the values of these quantities at the previous time ($K - 1$). As a consequence, the optimal solution for the time K involves quantities at the previous time $K - 1$. Therefore, the pilot-load-voltage settings as a result of the optimal control problem form another discrete-time sequence on the very slow time scale T_t . The basic requirement for the optimization process is that it must guarantee the stability of this discrete event process.

It is emphasized that this process of tertiary-level control involves only information about the generators participating in secondary-level control and about the pilot point loads, plus the tie-line flows if they are to be rescheduled. The amount of data and computation involved is much less than that needed for full-scale optimal power-flow calculation, where information about all loads is necessary. As an example, two regions of the French network have 259 buses, while the number of pilot points for the two regions is only 9. Because of this reduced information needed, it is possible that this tertiary-level control scheme can be implemented on line as closed-loop control. For a detailed description of the tertiary-level voltage models and tertiary-level voltage coordination, see Refs. [8,53].

A particularly interesting technical result concerns the relation between reactive-power tie-line flows and the quasistationary interaction variables $z[K]$ defined in Eq. (13.161). This result is repeated here because of its unique importance.

The model in Eq. (13.165) used to define interactions between the areas at the slow rate KT_t as a function of tie-line flows $F_s(KT_t)$ is restated here as follows:

$$z[K + 1] - z[K] = S(F_s[K + 1] - F_s[k]) - S(d[K + 1] - d[K]) \quad (13.191)$$

where

$$S \triangleq TD_s \quad (13.192)$$

Define $d_t[K] \triangleq d[K + 1] - d[K]$ as the tertiary-level disturbance. Equation (13.191) becomes

$$z[K + 1] - z[K] = S(F_s[K + 1] - F_s[K]) - Sd_t[K] \quad (13.193)$$

Matrix S as defined in Eq. (13.192) has a special structure and can be constructed by inspection. Recall the definition of $C_V = -J_{LL}^{-1}J_{LG} = -D_s J_{LG}$ and the condition $TC_V = 0$ in Eq. (13.164). One simply has

$$SJ_{LG} = TD_s J_{LG} = -TC_V \quad (13.194)$$

Therefore we derive the important relation for the S matrix as

$$SJ_{LG} = 0 \quad (13.195)$$

This gives a simple method to construct the S matrix. Suppose that there are n load buses and m generator buses in the area under consideration, and assume that $n > m$. Then there are $n - m$ independent solutions for S , or S has $n - m$ independent rows. If load bus i is not connected to a generator bus, then the corresponding i th row of J_{LG} is all zero because J_{LG} is the connection matrix between the load buses and the generator buses. In this case, vector

$$v = [0 \quad \cdots \quad 0 \quad 1 \quad 0 \quad \cdots \quad 0] \quad (13.196)$$

$\uparrow \text{ } i^{\text{th}} \text{ element}$

will satisfy $vJ_{LG} = 0$ because the i th row of J_{LG} is all zero. In other words, matrix S will have v as one of its rows. Therefore, for all load buses not connected to generator buses, we construct S by selecting 1 at the corresponding locations and 0 elsewhere. If the number of load buses not connected to generator buses is equal to $n - m$, then we have found all $n - m$ independent solutions for S . If this number is less than $n - m$, then there are more independent solutions to be determined. In this case, one needs to solve Eq. (13.195) to get all the independent solutions.

Because of the special structure of the S matrix, we see from Eq. (13.193) that the interaction variables are just the tie-line flows into all load buses that are not connected to generator buses. Understanding this relation is essential for effective tertiary-level voltage control coordination.

13.6.2 $P-\delta$ and $Q-V$ control: Similarities and Differences

In the case of real-power or frequency regulation, as the actual real-power flow into loads and out of generators deviate slowly from the anticipated, the objective of real-power or frequency regulation is to maintain system output variables of direct interest within their specifications. Most of the interconnected power systems in the world are equipped with this function, referred to as load frequency control regulation (LFC) or automatic generation control [82]. Present state-of-the-art frequency control design responds to an aggregate output variable at each subsystem (control area) level, known as the area control error (ACE), which leads to fully decentralized control of each area.

It is fairly straightforward to show that because of singular K_P in the system matrix A [Eq. (6.93)] at the steady-state system frequencies at all buses are

the same. This frequency, however, is not necessarily equal to the nominal 60 cycles. The system frequency is determined by the total generation–demand mismatch, and when this is nonzero, the steady-state frequency deviation from 60 cycles is nonzero. This, again, is a direct consequence of properties of the K_P matrix. By definition, the interarea variable $z(t)$, which is in the case of lossless transmission system identical to the generation–demand mismatch [Eq. 6.133], is not controllable by decentralized primary G-T-G controllers, such as governors without readjusting their set points in a coordinated way at each area level.

These observations, straightforward to see when taking a closer look at the properties of the linearized real-power–frequency dynamic model in Eq. (6.93), create a natural lead into the frequency regulation by each area in response to their own interarea variables with the neighboring areas.

The reactive-power–voltage regulation, on the other hand, is less standardized and less automated. Only a handful of countries in the world have semiautomated voltage regulation of generators. The objective of this automated voltage control (AVC) is to update set points of generator exciters to maintain voltages at critical (“pilot” points) within the prespecified deviations as the reactive-power demand and generation deviate from their scheduled (anticipated) values. In this sense, there exists a definite analogy between angle and voltage control with the common feature that it is for the deviations of power-flow specifications from their anticipated and/or planned values that one needs real-time slow closed-loop system control.

However, there exists a fundamental difference between the $P-\delta$ and $Q-V$ models, respectively. While K_p is always rank-deficient (resulting in single system frequency at an equilibrium), matrix K_Q generally has full rank. Consequently, at an equilibrium bus voltage magnitudes differ from bus to bus. This is a mathematical explanation of the physical characteristics such as localized response to the reactive-power disturbance, the reactive power not traveling far or not having inter-area oscillations in voltages. Therefore, only as many load voltages are controllable as there are directly controlled voltage buses on the system.

Altogether conceptually different operating and control paradigms in the restructured industry may emerge as described in this chapter. It is interesting to recognize that the minimal technical requirement for voltage or reactive-power support in the new industry proposed earlier rests on the well defined nominal voltages everywhere on the system. This would bring the $Q-V$ control closer to today’s $P-\delta$ control concepts.

13.7 CHAPTER SUMMARY

The major portion of this chapter concerns the normal operating mode only. We start by describing in Section 13.2 the basic structure of the generation dispatch control in context of operating rules and objectives dictated by the specific government policies. The main means of implementing control decisions in real-time operation is generation-based. The objectives of this control are twofold, that is, (1) to ensure that supply meets anticipated customer demand,

and (2) to maintain high-quality frequency and voltage at the customer side as the demand fluctuates. Real-power generation dispatch to meet the anticipated load is generally viewed as an economic function, as it is done with the objective of minimizing the total cost. We describe the principles of real-power generation dispatch for regulated and competitive power industry cases (Sec. 13.3). This is followed by Section 13.4, which introduces hierarchical frequency control for normal operation of the regulated electric power systems first. It is shown that this control scheme is a particular example of a more general structure-based hierarchical control design reviewed in Appendices 13.1 and 13.2. The principles of the ingenious ACE-based frequency control are explained by analyzing the equilibrium conditions of the hierarchical real-power–frequency model used. The function of LFC evolved as primarily an operating function for which units most suited technically were used. The two functions [economic dispatch (ED) and the LFC] are an integral part of one single objective of balancing generation and demand in real time (also known as the AGC). If this is done properly the system frequency naturally settles at its nominal value. In Section 13.4.2 we describe a possible approach to market-based provision of frequency control in a deregulated industry.

We next introduce principles of generation-based reactive power dispatch in Section 13.5 and (load) voltage control in Section 13.6. Although the main objective of supply meeting demand is characterized in terms of real-power dispatch (Sec. 13.3), this process is unavoidably accompanied by the presence of reactive-power generation, consumption, and (reactive-power) transmission loss. Similarly as in the case of real-power balancing, reactive-power dispatch for the anticipated reactive-power consumption does not compensate for random reactive-power demand fluctuations; (load) voltage control is needed for this purpose. Both reactive-power dispatch and voltage control functions are generally less standardized and automated than is the case with the real-power dispatch and frequency control, respectively. One technically systematic approach to hierarchical voltage control has been implemented in several European countries; here we refer to this approach as the automatic voltage control (AVC) function. We use this implementation to formalize a structure-based approach to the hierarchical voltage control for regulated industry in Section 13.6.1; the basis for this approach is the same general structure-based approach whose summary is provided in Appendices 13.1 and 13.2. Moreover, the economic implications of specific technical solutions to voltage-control problem have not been studied much in the regulated industry. While this is likely to change under competition, no conceptually new approaches are known at present.

In Section 13.6.2 we point out qualitative differences between the minimal information structure needed for generation-based frequency and voltage-control schemes described in Sections 13.4 and 13.6, respectively. Controllability and observability properties of the structure-based relevant models are used to explain these fundamental differences.

BIBLIOGRAPHY

1. Dy Liacco, T. E., The adaptive reliability control system, *IEEE Trans. Power Apparatus Syst.*, **PAS-86**: 517–531, 1967.
2. Fink, L. H., and Carlsen, K., Operating under stress and strain, *IEEE Spectrum*, March: 48–53, 1978.
3. Zaborszky, J., Prasad, K., and Whang, K. W., Operation of the large interconnected system by decision and control, *IEEE Trans. Power Apparatus Syst.* **PAS-99**: 37–45, 1980.
4. Phadke, A. G., and Thorp, J. S., *Computer Relaying for Power Systems*, New York: Wiley, 1988.
5. Zaborszky, J., Ilić, M., Huang, G., and Dobraca, F., Computer control of the large power system during faults for inherently adaptive selective protection, *IEEE Trans. Power Apparatus Syst.*, **PWRS-2**: 494–504, 1987.
6. Zaborszky, J., A large system approach toward operating the electric power system by decision and control, Proc. Am. Control Conf., 1984, pp. 1143–1155.
7. Brown, H. E., *Solution of Large Networks by Matrix Methods*, New York: Wiley, 1985.
8. Ilić, M. D., and Liu, S. X., *Hierarchical Power Systems Control: Its Value in a Changing Industry*, City: London Springer Verlag, 1996.
9. M. M. Adibi and L. H. Fink: Power system restoration planning, *IEEE Trans. Power Syst.*, **PS-1**: 22–28, 1994.
10. Fink, L. H. Liou, K. L. and Liu, C. C. From generic generation actions to specific restoration strategies, *IEEE Trans. Power Syst.*, **PS-10**: 745–52, 1995.
11. Morin, G. Service restoration following a major failure on the hydro-Quebec power system, *IEEE Trans.*, v.PD-2/2, pp. 454–463, 1987.
12. Kearsley, R. Restoration in sweden and experience gained from the blackout, *IEEE Trans. Power Syst.*, **PS-2**: 422–28, 1987.
13. Zaborszky, J., Huang, G., Lin, S. Y., and Liu, B. J., Restoration of the large power system using a computer generated sequence of target systems, Proc. IFAC Symp. Power Syst. Power Plant Control, Beijing, China, 1986.
14. Zaborszky, J., Huang, G., Clelland, P., and Fagnan, D., Optimal partnership of operator and computer for power system restoration, Proc. IFAC, Tallin, Estonia, 1990.
15. Zobian, A., and Ilić, M., Unbundling of transmission and ancillary services. Parts I and II, *IEEE Trans. Power Syst.* **PWRS-12**: 539–558, 1997.
16. Singh, H., and Papalexopoulos, A., Auctions for ancillary services, Proc. Conf. Syst. Sci., Hawaii, 1998.
17. Cardell, J., and Ilić, M., Modeling and stability analysis for distributed generation systems, Proc. North Am. Power Sympo. MIT, Cambridge, MA, 1996, pp. 239–347.
18. Allen, E. H., and Ilić, M., *Price-Based Commitment Decisions in the Electricity Market*, Advances in Industrial Control, London: Springer Verlag, 1998.
19. Skantze, P., *Closed-loop market dynamics for a deregulated electric power industry*, Ms. Eng. thesis, MIT, 1998.

20. Hoffman, S., and Illian, H., Control performance criteria, Proc. Am. Power Conf., Chicago, IL, 1996.
21. Ilić, M., Skantze, P., Yu, C-N, Fink, L., and Cardell, J., Power exchange for frequency control (PXFC), Proc. Bulk Power Syst. Dynamics Control—IV: Restructuring, Santorini, Greece, 1998.
22. Fink, L. H., and Erkman, I., Economic dispatch to match actual data to the actual problem, Proc. EPRI 1987 Power Plant Performance Monitoring Syst. Dispatch Conf., EPRI CS/EL-5251-SR, pp. 4/23–43.
23. Chiang, T. Y., and Subramanian, A. K., Modeling and estimation of the load demand of an area, IEEE Power Engineering Soc. Summer Meeting, Mexico City, 1997, Paper No. A 77 580-4.
24. Chiang, T. Y., and Subramanian, A. K., Economic Areawise Generation Control, IEEE Power Eng. Soc. Summer Meeting, Mexico City, 1977, Paper No. A 77 581-2.
25. Zaborszky, J., and Singh, J., A reevaluation of the normal operating state of the power system using computer control and system theory. Part I: Estimation, Proc. Power Industry Computer Appl. Conf. (PICA), Cleveland, OH, 1978.
26. Zaborszky, J., Mukai, H., Singh, J., and Spare, J. H., A reevaluation of the normal operating state of the power system using computer control and system theory. Part II: Dispatch Targeting, IEEE PES Trans., pp. 309–317, 1980.
27. Zaborszky, J., Mukai, H., Kambale, P., and Spare, J. H., A reevaluation of the normal operation state control (AGC) of the power system using computer control and system theory. Part III: Tracking the dispatch targets with unit control, *IEEE PES Trans.*, pp. 1903–1912, 1983.
28. Smith, V. L., Regulatory reform in the electric power industry, *Regulation*, **1**: 33–46, 1996.
29. Backerman, S. R., Rassenti, S. J., and Smith, V. L., Efficiency and income shares in high demand energy networks: Who receives the congestion rents when a line is constrained?, Univ. Ariz. Working Paper, 1997.
30. Bertsekas, D., Lauer, G., Sandell, N., and Posbergh, T., Optimal short-term scheduling of large-scale power systems, *IEEE Trans. Automatic Control*, **AC-28**: 1–11, 1983.
31. Shaw, J., A direct method for security-constrained unit commitment, *IEEE Trans. Power Syst.* **10**: 1329–1342, 1995.
32. Allen, E., and Ilić, M., Stochastic unit commitment in a deregulated utility industry, Proc. North Am. Power Symp. Univ. Wyoming, 1997.
33. Takriti, S., Birge, J., and Long, E., A stochastic model for the unit commitment problem, *IEEE Trans. Power Syst.*, **11**: 1497–1506, 1996.
34. Erwin, S., et al, Using an optimization software to lower overall electric production costs for Southern Company, *Interfaces*, **21**: 27–41, 1991.
35. Hara, K., Kimura, M., and Honda, N., A method for planning unit commitment and maintenance of thermal power systems, *IEEE Trans. Power Apparatus Syst.* **PAS-85**: 427–436, 1966.
36. Bertsekas, D., *Dynamic Programming and Optimal Control*, Belmont, MA: Athena Scientific, 1995, Vol. I.

37. Gaebe, G. P., California's electric industry restructuring, Proc. EPRI Workshop Future Power Delivery 21st Century, La Jolla, CA, 1997.
38. Hunt, S., and Shuttleworth, G., Unlocking the grid, *IEEE Spectrum*, July, 20–25, 1996.
39. Galiana, F. D., and Ilić, M. D., A mathematical framework for the analysis and management of power transactions under open access, *IEEE Trans. Power Syst. PWRS-13*: 681–687, 1998.
40. Ilić, M., Galiana, F. D., and Fink, L. (eds.) *Electric Power Systems Restructuring: Engineering and Economics*, City: Kluwer Academic, 1998.
41. Allen, E. H., Stochastic unit commitment in a restructured electric power industry, Ph.D. thesis, MIT, 1998.
42. Gross, G., and Finlay, D. J., Optimal bidding strategy in competitive electricity market, Proc. Power Syst. Comput. Conf. Dresden, Germany, 1996, pp. 815–823.
43. Gibbons, R., *Game Theory for Applied Economists*, Princeton University Press: Princeton, NJ, 1992.
44. Joskow, P., and Schmalensee, R., *Markets of Power: An Analysis of Electric Utility Deregulation*, Cambridge, MA: MIT Press, 1983.
45. Concordia, C., and Kirchmayer, L. K., Tie-line power and frequency control of electric power system, *AIEE Trans. Part III, Power Apparatus Syst.*, **72**: 562–572, 1953.
46. Concordia, C., and Kirchmayer, L. K., Tie-line power and frequency control of electric power system—Part II, *AIEE Trans. Part III, Power Apparatus Syst.*, **73**: 133–141, 1954.
47. Elgerd, O. I., and Fosha, C. E., Optimum megawatt-frequency control of multiarea electric energy systems, *IEEE Trans. Power Apparatus Syst.*, **PAS-89**: 556–571, 1970.
48. Davison, E. J., and Tripathi, N. K., The optimal decentralized control of a large power system: Load and frequency control, *IEEE Trans. Automatic Control*, **AC-23**: 312–325, 1978.
49. Ćalović, M.S., Automatic generation control: Decentralized areawise optimal solution, *Electric Power Syst. Res.* **7**: 115–139, 1984.
50. Liu, X., Structural modeling and hierarchical control of large-scale electric power systems, Ph.D. thesis, MIT, 1994.
51. Eidson, B., and Ilić, M., Advanced generation control: Technical enhancements, costs, and responses to market-driven demand, Proc. Am. Power Conf., Chicago, IL, 1995.
52. Eidson, B., State estimation and control of electric power systems, Ph.D. thesis, MIT, 1995.
53. Ilić, M. D., Eidson, B., Liu, X., Vialas, C., and Athans, M., A structure-based modeling and control of electric power systems, *IFAC Automatica*, **33**: 515–531, 1997.
54. Kokotović, P., and Khalil, H., (eds.), *Singular Perturbations in Systems and Control*, City: IEEE Press, 1986.
55. Zaborszky, J., and Rittenhouse, J., *Electric Power Transmission*, Reynolds 1954. Available in paperback at Rensselaer University Bookstore, Troy, NY.
56. Ilić, M. D., and Yu, C-N., Minimal system regulation and its value in a changing industry, Proc. IEEE Intl. Conf. Control Appl., Dearborn, MI, 1996.

57. Ewart, D., Performance under normal conditions, Proc. Syst. Eng. Power: Status and Prospects, Henniker, NH, 1975.
58. Interconnected Operations Services, NERC WG Report, 1996.
59. Ilić, M. D., Skantze, P. L., and Yu, C-N., Market-based frequency regulation: Can it be done, why and how?, Proc. Am. Power Conf., Chicago, IL, 1997.
60. Bakken, B. H., and Grande, O. S., Automatic generation control in a deregulated power industry, IEEE PES Summer Power Meeting, San Diego, CA, 1998, Paper No. PE-183-PWRS-0-11-1997.
61. U.S. Federal Energy Regulatory Commission's (FERC) Rule 888, 1996.
62. Van Slyck, L. S., Jaleeli, N., and Kelley, W. R., A comprehensive shakedown of an automatic generation control process, *IEEE Trans. Power Syst.* **4**: 771–781, 1989.
63. Talukdar, S., and Wu, F. F., Computer-aided dispatch for electric power systems, Proc. *IEEE*, **69**: 1981.
64. Carpentier, J., Multi method optimal power flow at EDF, IFAC Intl. Symp. Power Syst. Plants, Seoul, Korea, 1989.
65. Carpasso, A., Mariani, E., and Sabelli, C., On the objective functions for reactive power optimization, IEEE Winter Power Meeting Paper No. A 80WM 090-1, 1980.
66. Ilić, M., Liu, X., and Vialas, Ch., Some optimality notions of voltage profile for the steady-state operation of electric power systems, Proc. Symp. Bulk Power Syst. Voltage Phenomena III: Voltage Stability and Security, Davos, Switzerland, 1994.
67. Fink, L. H., Concerning power systems control structures *ISA Adv. Instrum.* **26**, Part 1: 1/1–11, 1971.
68. Van Cutsem, T., and Vournas, C., *Voltage Stability of Electric Power Systems*, Boston Kluwer Academic Publishers, 1998.
69. Kahn, E., and Baldick, R., Reactive power is a cheap constraint, *Energy J.* **15**: 191–201, 1994.
70. Banales, S., Ilić, M., On the role and value of voltage support in a deregulated power industry, Proc. North Am. Power Symp., Laramie, WY, 1997, pp. 471–478.
71. Ilić, M., and Yu, C-N., A possible framework for market-based voltage/reactive power control, Proc. IEEE Winter Power Meeting, New York, NY, 1999.
72. Ilić-Spong, M., Thorp, J., and Spong, M., Localized response performance of the decoupled Q - V , network, *IEEE Trans. Circuits Syst.*, **CAS-33**: 316–322, 1986.
73. Wu, F. F., and Varaiya, P., Coordinated multilateral trades for electric power networks—theory and implementation, Univ. Calif. Berkeley, CA, Report No. PWR-031, 1995.
74. Cordero, R., Estimation of transmission losses in a changing electric power industry, EECS thesis, MIT, 1996.
75. Ilić, M., and Cordero, R., On providing interconnected operations services by the end user: Case of transmission losses, Proc. NSF Conf. Unbundled Power Quality Services Power Ind. Key West, FL, 1996, pp. 28–38.
76. Asplund, G., Eriksson, K., and Svensson, K., HV-DC light—DC transmission based voltage sourced converter, *ABB Rev.*, **1998**: 4–7.
77. Ilić, M., Leotard, J-P., Rochlin, C., and Stoft, S., On the objectives of transmission pricing, Proc. Intl. Symp. Bulk Power Syst. Dynamics Control—IV: Restructuring, Santorini, Greece, 1998.

78. Yu, C-N., Yoon, Y. T., Ilić, M., and Catelli, A., On-line voltage regulation: The case of New England, *IEEE Trans. Power Apparatus Syst.* (to be published) (also paper number PE-082-PWRS-0-02-9-1999).
79. Report on Interconnected Operation Services (IOS), North American Electric Reliability Council (NERC), 1997.
80. Paul, J. P., Leost, J. Y., and Tesseron, J. M., Survey of the secondary voltage control in France, *IEEE Trans. Power Syst.*, **PWRS-2**: xx–xx 1987.
81. Athans, M., and Falb, P., *Optimal Control*, New York: McGraw-Hill, 1966.
82. Cohn, N., Research opportunities in the control of bulk power and energy transfers on interconnected systems, Special Report on Power System Planning and Operations: Future Problems and Research Needs, EPRI EL-377-SR, 1977.
83. Siljak, D., *Large-Scale Dynamic Systems*, New York: Elsevier North-Holland, 1978.
84. MATLAB Manual.
85. Zaborszky, J., and Ilić, M., General structure of the regulated, deregulated and other generation dispatch, *IEEE Power Tech '99 Conference*, Hungary, 1999, paper # BPT-440-21.

APPENDIX 13.1: STRUCTURE-BASED MODELING FOR HIERARCHICAL CONTROL DESIGN

Posing the system regulation problem as a multilevel (hierarchical) problem directly lends itself to the modeling framework of Chapter 4 and the resulting structure introduced there. This approach is also useful for providing algorithmic tools to the operator over a variety of time horizons, because it allows for direct specifications in terms of power inputs to the system, both at the supply and demand side.²⁴

Because the updating of set-point values of output variables is done typically more slowly than the rate at which closed-loop primary dynamics evolve, different time scales exist in the system dynamics over the long-time horizon. Time-scale separation techniques can be used to simplify higher-level control designs.

In the linearized dynamical model for an administrative area given in Eqs. (4.81) and (4.82), vector F represents the tie-line flows into this area from its neighboring regions. The set point output value y^{ref} is updated at discrete instances to regulate the profiles of output variables of direct interest so that a predefined performance is met. Due to physical limitations and practical considerations, the updating is typically done more slowly than the rate of the closed-loop primary dynamics. This process of updating the set-point values of individual controllers is often called the *secondary control* [80].

Let us denote the sampling time interval of the secondary control as T_s , denoting that a set-point value is updated at instances kT_s , $k = 0, 1, \dots$. Thus the set point value y^{ref} is constant in the interval $kT_s < t < (k + 1)T_s$. Let us

²⁴ This designation of equipment in terms of power provides also a direct link between the technical processes and cost, at least for real-power dynamics [51].

further denote $y^{\text{ref}}[k] = y^{\text{ref}}[kT_s]$ as a discrete time sequence of the reference value. With this notation, Eqs. (4.81) and (4.82) can now be linearized around an operating point and written as²⁵

$$\dot{x} = Ax + By^{\text{ref}}[k] + UF + V\dot{F} \quad (13.1.1)$$

The main objective of secondary control is to provide an appropriate discrete time sequence $y^{\text{ref}}[k]$ to meet some prespecified performance criterion, as will be further discussed. Because the discrete sequence $y^{\text{ref}}[k]$ varies more slowly than the closed-loop primary dynamics, relatively low-order models can be derived to assist the secondary-control design.

The secondary-level control $y^{\text{ref}}[k]$ is designed to eliminate the slow drifting of some critical variables of the area such as frequency of an area or critical load voltages inside an area. Let us express these critical variables for the secondary level as

$$x_s = Dx \quad (13.1.2)$$

The dimension of x_s is in general much lower than the dimension of x . The set-point value $y^{\text{ref}}[k]$ is updated each T_s time units so that the slower steady-state offset in x_s on the time scale T_s is eliminated. To derive the relation between $x_s[k]$ and $y^{\text{ref}}[k]$, we distinguish two important cases, a singular model and nonsingular model. As shown in Chapter 6 a structurally singular model of Eq. (6.93) corresponds to the real-power–frequency dynamics, and a (structurally) nonsingular model Eq. (6.114) corresponds to the reactive-power–voltage dynamics.

For a *singular* model, that is, where matrix A in Eq. (13.40) is structurally singular, the relation between $x_s[k]$ and $y^{\text{ref}}[k]$ is quite complicated. As described in Chapter 6 (section 6.6.2) and in Chapter 3, Section 3.2.1.1., several fairly straightforward methods are generally used to eliminate this modeling singularity. This matter is explained and illustrated on the basic transmission network with its singular \hat{Y}_{bus} matrix in Chapter 3, Sections 3.2 and 3.2.1. In the case of a *nonsingular* system, with either the voltage dynamics or the frequency dynamics with some means of maintaining system reference angle, a desired relation between $x_s[k]$ and $y^{\text{ref}}[k]$ can be easily determined from Eq. (13.1.1) as

$$x[k] = -A^{-1}By^{\text{ref}}[k] - A^{-1}UF_s[k] \quad (13.1.3)$$

and therefore

$$x_s[k] = B_s y^{\text{ref}}[k] + M_s F_s[k] \quad (13.1.4)$$

with $B_s = -DA^{-1}B$ and $M_s = -DA^{-1}U$.

²⁵This model should be interpreted as a dynamical model whose state vector representing closed-loop primary dynamics is x , $y^{\text{ref}}[k]$ is some general secondary-level control acting each kT_s time interval in response to the disturbance $d(t) = UF + V\dot{F}$. Furthermore, if deviations in area load are modeled, $d(t) = UF + V\dot{F} + W\dot{P}_L$. Specific examples of these models are introduced in Chapter 6 for controlling real-power–frequency and reactive-power–voltage dynamics.

Model derivation (assuming nonsingularity) for secondary-level control uses the fact that the time constant of the closed-loop primary dynamics is much shorter than the secondary-control time interval T_s . Because of this, one can assume that the fast transients settle within each kT_s time interval, that is $\dot{x} \approx 0$ at kT_s . Equation (13.1.1) then reduces to

$$Ax + By^{\text{ref}}[k] + UF = 0, \quad t = kT_s \quad (13.1.5)$$

or

$$Ax[k] + By^{\text{ref}}[k] + UF_s[k] = 0 \quad (13.1.6)$$

Equation (13.1.6) determines a static relation between the steady-state equilibria of the system and the set-point values to be adjusted by the secondary control, that is, between $x_s[k]$ and $y^{\text{ref}}[k]$. This quasistatic relation is best utilized for the secondary-control design when formulated as a discrete-time model. This model is generally obtained by subtracting Eq. (13.1.4) at two consecutive time instances kT_s and $(k+1)T_s$:

$$x_s[k+1] - x_s[k] = B_s(y^{\text{ref}}[k+1] - y^{\text{ref}}[k]) + M_s(F[k+1] - F_s[k]) \quad (13.1.7)$$

and further defining the update of the set-point value, or the corrective control for the secondary level as

$$u_s[k] = y^{\text{ref}}[k+1] - y^{\text{ref}}[k] \quad (13.1.8)$$

and the change of tie-line flows as

$$F_s[k] = F[k+1] - F_s[k] \quad (13.1.9)$$

This results in a discrete-time model of the form

$$x_s[k+1] - x_s[k] = B_s u_s[k] + M_s F_s[k] \quad (13.1.10)$$

The model in Eq. (13.1.10) is introduced as the simplest model for designing output feedback-based secondary-level controllers at a regional level. This model can also be interpreted as representing a discrete event process of a moving equilibrium $x_s[k]$ driven by the discrete control actions $u_s[k]$ and the tie-line flow increments $F_s[k]$ [83]. Variables $x_s[k]$ will be referred to as *secondary-level states*.

It should be pointed out that the corrective control signal $u_s[k]$ defined in Eq. (13.1.8) represents an implicit integral control, because, from Eq. (13.1.8),

$$y^{\text{ref}}[l] = \sum_{k=0}^{l-1} u_s[k] + y^{\text{ref}}[0] \quad (13.1.11)$$

for any integer l . It is this implicit integral control that rejects the steady-state error in the output variables at the secondary level.

APPENDIX 13.2: STRUCTURE-BASED HIERARCHICAL CONTROL DESIGN

In this section we present a hierarchical control design using the low-order model of each area [Eq. (13.1.10)].

13.2.1 Controllability

Let us first establish the controllability of the model in Eq. (13.1.10) is determined, which is an entirely secondary-control-driven model (no system matrix). In this case the controllability is simply determined by the relative dimensions of the states and control. Assume that the dimension of the secondary-level states $x_s[k]$ is n , and the dimension of the secondary-level controls $u_s[k]$ is m . Observe that the controllability matrix of Eq. (13.1.10), with $F_s[k]$ treated as an external input (disturbance) is of the form

$$[B_s \quad 0 \quad \cdots \quad 0] \quad (13.2.1)$$

This matrix has maximum rows of m and therefore a maximum rank of m . If the number of controls m is less than the number of states n , as is typically the case, this controllability matrix is always singular, and the system is not fully controllable. This property is structural since it is independent of the numerical values of the system.

As a result of this structural nature of controllability, only at most m states can be controlled independently. Let us choose m critical states as the output variables to be regulated by the secondary control, expressed as

$$y_s[k] = C_s x_s[k] \quad (13.2.2)$$

with matrix C_s having dimension $m \times n$. Variations in the output variables $y_s[k]$ can be easily obtained from Eq. (13.1.10) as

$$y_s[k+1] - y_s[k] = C_s B_s u_s[k] + C_s M_s F_s[k] \quad (13.2.3)$$

Define the $m \times m$ square matrix $U_s = C_s B_s$. Then the preceding can be written as

$$y_s[k+1] - y_s[k] = U_s u_s[k] + C_s M_s F_s[k] \quad (13.2.4)$$

13.2.2 Conventional Secondary Control

The goal of the secondary-level control is to regulate the output variables $y_s[k]$ over the secondary time horizon to an optimal value determined by the tertiary

control in an optimal sense. The conventional secondary control for normal operation takes on a simple proportional form

$$u_s[k] = G(y_s[k] - y_s[K]) \quad (13.2.5)$$

where $y_s[K] = y_s(KT_t)$ is the value for the output variables set over the slowest time scale T_t . This value is calculated by the tertiary control, and is quasi-constant for secondary processes.

Under this conventional feedback control, secondary-level closed-loop dynamical model for output variables is obtained as

$$y_s[k+1] - y_s[k] = U_s G(y_s[k] - y_s[K]) + C_s M_s F_s[k] \quad (13.2.6)$$

The gain matrix G can be chosen to optimize a performance index at the area level as

$$J_s = \sum_{k=0}^{\infty} (y_s^T[k] Q y_s[k] + u_s^T[k] R u_s[k]) \quad (13.2.7)$$

for some matrices $Q = Q^T \geq 0$ and $R = R^T > 0$ specified by each area. The optimization is with respect to $u_s[k]$, and the result is the optimal gain matrix G . In this process, tie-line flows with neighboring areas are viewed as independent disturbances by this decentralized control. The gain G is computed in a straightforward way using general linear quadratic regulator theory [81]. To obtain G one needs to specify system matrices and the matrices defining quality of response desired Q and its cost R , respectively. MATLAB [84] has a readily usable subroutine that solves Riccati equation in order to compute G [81].

Notice that other performance objectives could also be attempted, such as the worst-case deviation of the output variable of interest and a given range of disturbances.

13.2.0.2 Improved Secondary Level Control

It is clear from Eq. (13.2.6) that tie-line flows viewed as an independent external input to the area affect the dynamics of its output variables. The conventional “optimal” control designed with interconnections neglected will no longer be optimal when implemented to the actual system in which interconnections are indeed present. To compensate the effect of interconnections fully, a modified feedback control law of the form

$$u_s[k] = G(y_s[k] - y_s[K]) + H F_s[k] \quad (13.2.8)$$

has been proposed [8,50], where the term $H F_s[k]$ is introduced to cancel out the effects of $F_s[k]$ on output variables. Substituting Eq. (13.2.8) into (13.2.6) yields

$$y_s[k+1] - y_s[k] = U_s G(y_s[k] - y_s[K]) + (U_s H + C_s M_s) F_s[k] \quad (13.2.9)$$

It is clear that if U_s is invertible, then the effects of the tie-line flows can be fully eliminated by simply choosing

$$H = -U_s^{-1}C_sM_s \quad (13.2.10)$$

With this choice of H , Eq. (13.2.9) reads

$$y_s[k+1] - y_s[k] = U_sK_s(y_s[k] - y_s[K]) \quad (13.2.11)$$

with no flows entering into the model. In other words, the area could meet its own objective by cancelling out the effects of the other areas. (This control, of course, would be more expensive relative to the conventional secondary control.) The area under study looks as if it were fully isolated from the rest of the system, as far as the output variables are concerned.

Notice that the condition that U_s is invertible should not be viewed as restrictive; instead, it ought to be taken as one of the requirements for the choice of output variables. This is due to the fact that the matrix $(I + U_sK_s)$ is the system matrix for the output variables $y_s[k]$ seen from Eq. (13.2.6) or (13.2.11); therefore, if the matrix U_s were singular, the closed-loop system matrix $(I + U_sK_s)$ would always have an eigenvalue of 1. The consequence of this is that steady-state errors are inevitable for the chosen output variables. To fully control all output variables, it is required that they are selected such that U_s is of full rank.

Notice also that the control scheme presented here is totally decentralized at each area level, assuming that tie-line flows are locally measured at each area level. No detailed information about the areas is needed; only tie-line flows are required, since they aggregate the net effect of detailed dynamics in the neighboring regions. It is not an unrealistic assumption that tie-line flows are locally measurable.

13.7.0.3 Tertiary-Level Control Design

As mentioned earlier, the tertiary-level control is mainly concerned with regional coordination over the long time scale T_t . The ultimate goal of this level is to ensure that the interconnected system as a whole operates in an acceptable fashion. It could be implemented by adjusting the values y_s of the secondary output variables over the time horizon T_t . Since inter-regional effects take place through the tie-line flows, regulating these flows is of direct concern for the tertiary control. In fact, the goal of tertiary-level design, as proposed here, is to regulate the tie-line flows according to a systemwide performance criterion.

There exists a trade-off between the settings of flows and the secondary-level output variables. An ideal optimal operation at the tertiary level may require unrealistic setting at the secondary level, due to physical limitations and constraints. Thus, a typical performance criterion at the tertiary level should take into consideration the trade-off between the regulated flow and the optimal settings for the secondary-level outputs. To solve this problem, one should know

TABLE 13.2 Reactive-Power Loss Changes due to Changes in Injection at Node 2

Tier	From–To	$\Delta Q_{\text{loss}}(\text{estimated})$	$\Delta Q_{\text{loss}}(LF)$
I	1–2	0.0280	0.0316
II	2–3	−0.0055	−0.0060
	2–4	−0.0046	−0.0048
	3–4	−0.0021	−0.0024
III	3–5	0.0043	0.0053
	3–6	−0.0025	−0.0028
IV	6–7	0.0004	0.0005
	5–8	−0.0007	−0.0006
	5–9	0.0014	0.0016
V	7–10	0.0002	0.0002
	7–11	−0.0001	−0.0001
	8–12	0.0001	0.0001
	8–13	0.0020	0.0027
	8–14	0.0002	0.0003
	11–12	0.0002	0.0002
VI	10–15	0.0001	0.0001
	10–16	−0.0001	−0.0002
	10–17	0.0010	0.0013
	10–18	−0.0004	−0.0003
	12–19	−0.0006	−0.0007
	14–20	0.0002	0.0003
VII	15–21	−0.0001	−0.0001
	16–22	0.0003	0.0004
	21–22	0.0000	0.0000
	17–23	−0.0007	0.0009
	17–24	0.0000	0.0000
	18–25	0.0001	0.0001
	19–26	0.0002	0.0002
	20–27	0.0002	0.0003
	19–25	−0.0001	−0.0002
	21–28	0.0005	0.0006
VIII	22–29	0.0009	0.0012
	24–30	0.0003	0.0004
	25–31	0.0001	0.0001
	26–32	−0.0001	−0.0001s
	26–33	0.0000	0.0000
	27–32	0.0003	0.0003
	31–34	0.0001	0.0001
IX	31–35	0.0000	0.0000
	34–35	0.0000	0.0000
	32–36	0.0000	0.0000
	33–37	0.0000	0.0000
	33–36	−0.0001	−0.0001
	33–38	0.0009	0.0014

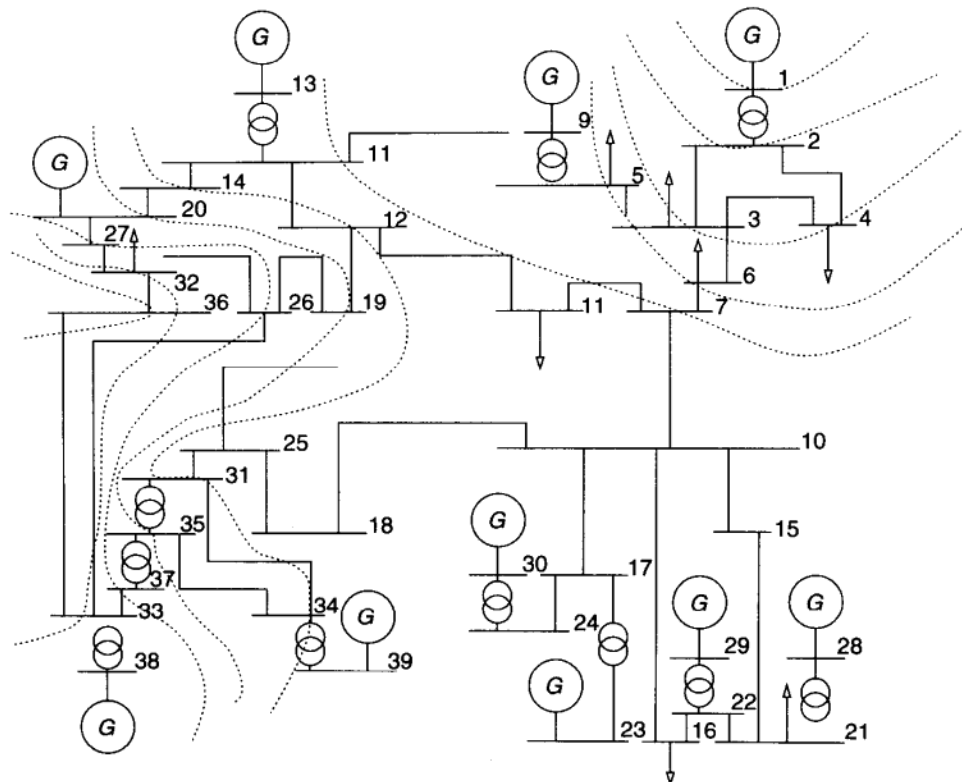


FIGURE 13.35 IEEE 39-bus system.

a relation between the setting $y_s^{\text{set}}[K]$ and the tie-line flows. This relation, which reveals the effect of tie-line flows on the output variables of each region, is the aggregate model on the tertiary level [51, 56].

APPENDIX 13.3: LOCAL ESTIMATION OF REACTIVE-POWER LOSSES

A numerical simulation on the standard IEEE 39-bus system, Figure 13.35, is provided to demonstrate local losses estimation algorithm developed in Ref. [74]. Detailed system data and the nominal load-flow solution are documented in Ref. [74]. In this simulation, we introduce 50% reactive-power change ($\Delta Q_2 = 0.6345$ p.u.) at bus 2. Due to the injection change, the reactive-power loss in each transmission line is different from its nominal value. The estimated reactive-power losses change and the exact load-flow solution are listed in Table 13.2. These results indicate that the method developed in Ref. [74] could estimate the reactive-power losses locally with high accuracy.

14 Stationary Generation Control (with Congestion)

As the electric power industry begins to restructure, it is becoming increasingly clear that the most attractive electricity market transactions (block 2 in Fig. 13.4) may not be implementable because of the various system constraints. The transmission-system-related constraints are often referred to in the current restructuring debate as the transmission *congestion*.

Methods for modifying generation or demand patterns computed in block 2 online to avoid system constraints are the subject of this chapter. Depending on the particular industry structure in place (regulated or deregulated) and on the specific electricity market design (coordinated or bilateral), constrained generation control for anticipated demand is either computed in block 2, or the process consists of two steps, with the first step being an unconstrained generation optimization for the anticipated demand (subject of the Chapter 13, block 2) and the second step a separate task of modifying the result of step one to adjust to the physical constraints (block 3).

The methods described in this chapter are applicable to the stationary operation only. It is assumed that the system is in normal (stable) operation. As the system inputs (generation and demand) vary slowly, steady-state operating limits for bus voltages and line currents may be exceeded. The issue of stationary generation control with congestion becomes a problem of slow adjustments of system inputs (generation, primarily) to prevent the line currents and bus voltages from exceeding the prespecified limits.

Most of these constraints (thermal and steady-state voltage) are not hard constraints in the sense that their violation will not lead to immediate emergency conditions. Therefore, the methods described here play a significant role in system economics. As such, the methods for stationary generation control with congestion usually have the objective of optimizing a prespecified performance criterion subject to system constraints.

The efficiency of such algorithms is measured in two ways.

- The first measure is concerned with the computational efficiency.
- The second measure is concerned with the minimum number of least disruptive modifications of the system inputs determined at the level of block 2.

Both measures are essential for technical implementation of these methods in near-real-time.

Many algorithms of this type are routinely used in present control centers, such as a constrained economic dispatch. Their prime use has been for scheduling of real power, while assuming insignificant voltage changes. Recently, more emphasis has been given to scheduling for voltage support in addition to real-power scheduling. This has required use of algorithms similar to the constrained economic dispatch-type algorithms, which include scheduling of voltage resources.

The first part of this chapter concerns basic problem formulation for managing thermal constraints, Section 14.1. Methods for regulated industry are introduced in Section 14.1.1. This is followed by a summary of emerging methods for so-called transmission congestion management in the deregulated industry in Section 14.1.2. We demonstrate using simple examples a new concept that it is possible to manage thermal constraints by providing a meaningful on-line price for using the system.

The second part of this chapter concerns computer methods for efficient management of system congestion (thermal and/or voltage) for very large power systems. Two qualitatively different approaches are possible when attempting efficient computations:

1. Develop tests for checking if conditions under which the network response to demand and/or control changes is limited to the nearby buses. If the conditions are met, proceed with simplified methods based on this property.
2. Assume that any change always affects everything else on the system and develop methods for parallel computing.

Methods described in this chapter could be classified according to this distinction. In Section 14.3.1 several methods are summarized for testing conditions under which reactive-power or voltage changes are localized. This is followed by Section 14.3.1.3, devoted to a specific method for identifying portions of a large system most affected by a change in reactive-power injection of interest (load increase, generator loss) and for computing least disruptive corrective actions for bringing voltages close to their values before the change occurred. This method is described in some detail to illustrate typical steps necessary to manage voltage congestion. A computationally effective clustering method is introduced next. This method is illustrated in the context of reactive-power or voltage congestion management. A potential use of a similar clustering approach for thermal congestion management in the deregulated industry is described thereafter.

In Section 14.4 a novel computationally efficient method for systemwide congestion management is described. This method is known as the textured model or algorithm and is applicable to parallel computing in other classes of large systems in addition to the power networks. The conclusion of this chapter is that sufficiently effective computing methods have been introduced for congestion management in large power systems. The main challenge is the development of high-quality software for enabling use of these techniques.

14.1 METHODS FOR TRANSMISSION CONGESTION FLOW CONTROL

In the past the problem of line flow control within transmission line limits has been an integral part of the stationary generation-control process subject to various equality and inequality system constraints. As the economic dispatch of generators is solved to meet the estimated demand, only technically viable solutions are implemented. This generally results in a suboptimal use of power because some out-of-merit units must be used to avoid system constraints. This is known as a constrained economic dispatch (CED) [1]. With regard to Figure 13.4, a CED is computed in block 2 for the anticipated demand.

A more common approach still practiced in today's industry is to first compute an unconstrained economic dispatch (with transmission loss estimate minimized, at best) in block 2 and then in block 3 redispatch certain units to ensure that thermal limits on transmission lines are observed.

Depending on the software tools available in a specific control center, the algorithms for ensuring that thermal limits are met range from the most complex (based on optimal power flow), by using sensitivity factors to estimate the effect of various units on the line constraints, all the way to the methods based on nonanalytic rules unique to each specific system.

There are many obstacles to implementing optimal-power-flow-based solutions. However, the major problem is related to the computational complexity of a very large number of equality and inequality constraints in real-life power systems. The challenge is then to develop computationally efficient methods that obviate this problem.

In this section we first state the problem of thermal congestion control mathematically for both regulated and deregulated industries. This is followed by describing computationally efficient methods to do this for large power systems.

Depending on the type of the method used to manage line flow limits, the relevant information consists of one or more of the following:

- Sensitivities of flows in congested lines P_l with respect to critical injections P_i
- Sensitivities of the total optimal cost of meeting demand with respect to the capacity of the congested line P_l^{\max}

These sensitivities can be used to screen for most critical contingencies as system injections determined in block 2 vary and also to adjust these in block 3 so that the limits are not violated. Generally the adjustments determined using strictly technical criterion based on sensitivities do not result in the most efficient use of power, as measured in terms of total generation cost.

To optimize cost under line flow constraints, it is necessary to solve an optimal power flow. It is shown in what follows how sensitivities of both types could be used for reaching optimum cost under constraints. Depending on how the optimum (unconstrained) dispatch is implemented, the sensitivities of flows in

congested lines with respect to system inputs and/or cost sensitivities with respect to line capacities could be used as essential information for optimizing system performance under constraints. The latter type of sensitivity could be used to provide the on-line price for using the transmission system to the decision makers in the (primary) electricity market (block 2). These coordinating signals could serve as incentives for the decision makers to adjust their requirements for transmission use at time of scarcity (likely congestion) and indirectly to prevent the occurrence of technical congestion. This is an important new concept evolving in the deregulated industry. By providing a meaningful on-line price signal for using transmission (p_T , block 3 in Fig. 13.4), an optimal load-flow solution is solved by the system users themselves. These ideas are described next for the two cases of regulated and deregulated power industries.

14.1.1 Transmission Line Flow (Congestion) Control in Regulated Industry

Congestion control practices in today's industry for computing real power and voltage support for anticipated demand are such that if *any single contingency* occurs, the system still remains within the normal operating inequality constraints. This operating philosophy is known as meeting the $n - 1$ security criterion and has been fully adopted by the industry.

In order to apply the scheduling techniques described in this chapter and meet this operating practice, a system operator usually needs to follow several steps:

- Simulate one contingency at a time.
- Apply a scheduling technique of interest for given demand and under the simulated contingency.
- Repeat the process for *all* contingencies from a predefined list.
- Suggest scheduling that satisfies operating constraints for the most critical conditions.

These steps require computer-aided methods to carry out when managing a constrained transmission system, such as:

- Determining on-line the most critical changes in system topology and system injections for which line flow limits of some lines may be violated, and also determining lines most likely to become congested.
- Determining on-line the most effective remedial actions to avoid likely congestion.
- Determining on-line system input changes that are economically the most effective when attempting to avoid congestion.

These steps are briefly described next.

14.1.1.1 Critical Contingencies Creating Congestion All system operators have acquired over the years contingencies specific to their own systems that

are most likely to create congestion in certain parts of the systems. Most of today's transmission systems are designed in a sufficiently robust way, meaning that under normal conditions (all major equipment status as planned) there is no congestion. (This situation may change as smaller, new power plants replace large, older power plants in the deregulated industry, unless the existing grid is enhanced.)

The important step carried out in most control centers today is so-called contingency screening. Out of a huge number of likely contingencies only very few may cause congestion. There are many well-established computer algorithms available at present for determining possible critical contingencies. The basis for these methods are the so-called distribution factors described in Chapter 5. These are simply linearized sensitivities of line flows P_l with respect to changes in generation inputs P_i and are easily computed in the on-line operating environment.

An important missing step is typically the reinterpretation of the huge distribution factor matrix for purposes of effective congestion management. Only recently was an organized method proposed for deriving so-called congestion clusters for grouping sets of buses. The distribution factors of these sets that reflect sensitivity of a particular transmission line flow of interest with respect to changes in their inputs are similar. The conceptual aspects of such clustering are identical to the clustering technique proposed some time ago by the senior author in Ref. [2]; this method is described in detail in this chapter under the methods for managing voltage constraints.

An additional complication when computing sensitivities of line flows with respect to changes in the real-power injections comes from the presence of a slack bus; this was recognized some time ago by the senior author of this book in Ref. [2]. As a possible remedy, a transformation of system inputs was proposed, resulting in distribution factors the magnitudes of which decay with the electrical distance between the line flow and the injections causing it. A similar transformation was recently reported in Ref. [3] and its use illustrated on a New England 2000-bus power system.

14.1.1.2 Technically Most Effective Congestion Control Once the distribution-factor matrix is defined, and groups of buses are organized (clustered) according to their relative impact on the line flow of interest, one can compute controls (injections) at the set of buses with strongest effect on the line flow of interest. This conceptual procedure is again illustrated with methods for efficient management of constraints later in this chapter.

14.1.1.3 Economically Most Effective Congestion Control (Spot Pricing) The basic formulation of real-power generation control with line flow limits (congestion) included is the problem of maximizing social welfare with respect to net injections P_i at all system nodes i ,

$$\max_{P_i} \sum_i [-c_i(P_i)] \quad (14.1)$$

subject to

$$\sum_i P_i = 0 \quad (14.2)$$

and

$$-P_l^{\max} \leq P_l \leq P_l^{\max} \quad (14.3)$$

The Lagrangian for this optimization problem is

$$\begin{aligned} \mathcal{L}(P, \mu, \nu) = & \sum_i [-c_i(P_i)] + \lambda \sum_i P_i + \sum_l \mu_l \left(P_l^{\max} + \sum_i D_{li} P_i \right) \\ & + \sum_l \nu_l \left(P_l^{\max} - \sum_i D_{li} P_i \right) \end{aligned} \quad (14.4)$$

The optimal solution satisfies

$$\sum_i P_i = 0 \quad (14.5)$$

$$\nu_l \left(P_l^{\max} - \sum_i D_{li} P_i \right) = 0 \quad (14.6)$$

$$\mu_l \left(P_l^{\max} + \sum_i D_{li} P_i \right) = 0 \quad (14.7)$$

and

$$\lambda = \rho_i + \sum_i D_{li} (\nu_l - \mu_l) \quad (14.8)$$

The D_{li} terms represent distribution factors defined in Chapter 5, Eq. (5.105). Transmission capacity has a paramount influence on the overall efficiency in power systems. A congestion caused by the line-flow constraint generally leads to inefficiencies. As an illustration, consider a simple three-bus system with the cost functions $c_1(P_{G1}) = P_{G1}^2 - P_{G1} + 0.5$, $c_2(P_{G2}) = P_{G2}^2 + P_{G2} + 1$, and the load benefit function $U_{L1}(P_{L1}) = 214.66P_{L1} + 10P_{L1}^2$. The optimal dispatch without line-capacity constraints results in the cost function (Eq. (14.1)) of 1065. If the line between buses 1 and 2 has a thermal limit 3, then the optimum would be 968, that is, this line constraint is a cause of 10% decrease in efficiency.

The dual approach to the problem in Eqs. (14.1) to (14.3) is

$$\begin{aligned} \min_{P_i} & \sum_i [-c_i(P_i)] + \sum_l \mu_l \left(P_l^{\max} + \sum_i D_{li} P_i \right) + \sum_l \nu_l \left(P_l^{\max} - \sum_i D_{li} P_i \right) \\ & - \lambda \sum_i P_i - \sum_i P_i \left(\frac{\partial c_i}{\partial P_i} + \sum_l \nu_l D_{li} - \sum_l \mu_l D_{li} - \lambda \right) \end{aligned} \quad (14.9)$$

subject to

$$\lambda + \sum_l D_{li}(\nu_l - \mu_l) = \frac{\partial c_i}{\partial P_i} = \rho_i \quad (14.10)$$

and $\nu_l \geq 0$, $\mu_l \geq 0$. The cost function (14.9) after simplifications becomes

$$\min \sum_l (\mu_l + \nu_l) P_l^{\max} + \sum_i \left(P_i \frac{\partial c_i}{\partial P_i} - c_i(P_i) \right) \quad (14.11)$$

It follows from Eq. (14.10) that at the optimum a marginal cost at bus i equals the marginal cost of electricity λ obtained when ignoring transmission constraints modified by the term reflecting the impact of the active constraint. The simplest interpretation of this formula is when there is only one nonzero μ_l , indicating that line l is overloaded. This line overload has impact on the marginal cost at each bus i as given in this formula.

The nodal prices $\rho_i = \partial c_i / \partial P_i$ are the marginal costs of production at each node at the optimum. Equivalently, the difference of nodal prices between two nodes represents the shadow price of the line-capacity constraint for the total cost function.

We note that at the optimum the objective functions of the primal and the dual problems are equal; thus

$$\sum_i [-c_i(P_i)] = \sum_l (\mu_l + \nu_l) P_l^{\max} + \sum_i \left(P_i^* \frac{\partial c_i}{\partial P_i} - c_i(P_i^*) \right) \quad (14.12)$$

which is equivalent to

$$\sum_l (\mu_l + \nu_l) P_l^{\max} = - \sum_i P_i \frac{\partial c_i}{\partial P_i} \quad (14.13)$$

The net revenue from injecting power P_i at price $\partial c_i / \partial P_i$ is the term on the right-hand side (RHS) of this equality. This formula provides a basic relation between the net revenue (merchandise surplus) and the possible “rent” for using the system on the LHS. Furthermore, taking partial derivatives of both sides of Eq. (14.12) with respect to the line capacity P_l^{\max} , one obtains the following relation at the optimum

$$\frac{\partial c^*}{\partial P_l^{\max}} = -\frac{\partial \text{rent}^*}{\partial P_l^{\max}} + \sum_i \frac{\partial}{\partial P_l^{\max}} \left(c_i(P_i^*) - P_i^* \frac{\partial c_i(P_i)}{\partial P_i} \right) \quad (14.14)$$

In the case of linear $c_i(P_i) = a_i P_i$ it follows from Eq. (14.14) that

$$\mu_l = \frac{\partial c^*}{\partial P_l^{\max}} \quad (14.15)$$

This gives a direct interpretation of the Lagrangian coefficients μ_l and ν_l associated with the thermal limits of a power network; in the case of linear $c_i(P_i)$ these coefficients are sensitivities of optimal cost with respect to the line-capacity limits [4].

We observe here that because of the electricity pricing based on average costs the economic signals such as μ_l and ν_l have not been explicitly used in the regulated industry for enhancing short-term efficient use of the available transmission capacity. This is in sharp contrast with the strong emphasis on the role of transmission pricing in the deregulated industry. Various proposals for transmission pricing in the deregulated industry based on these basic formulas are described next.

14.1.2 Transmission Line Flow (Congestion) Management in Deregulated Industry

It is well known that an unconstrained primary-market solution may not be implementable because it may lead to violations of line-flow constraints or bus voltage limits (generally referred to as the security constraints). This will have impacts on the profits or benefits of market participants.

Given that generation and transmission are qualitatively different, separate, businesses in the deregulated industry, the objectives of a transaction management system are often viewed differently by a system provider (block 3) than by a system user (block 2).

14.1.2.1 Objectives of a System Provider A system provider (block 3) in charge of maintaining system integrity as market-driven bus power injections vary is primarily concerned with maintaining secure system conditions in its area. The provider is also interested in coordination of its real-time operation with the neighboring systems so that the operation of a large interconnection comprising several electricity markets also remains secure. When some of the economic transactions are not implementable in real time, a system provider will need standby tools for systematic adjustment of proposed transactions to ensure that security constraints are met.

The role of a system operator in facilitating primary-market efficiency is less clearly defined. To a large extent, it depends on the primary-market structure in place and on the explicit incentives given to a system operator to develop computer software for assessing and posting the most likely and most critical system limitations.

14.1.2.2 Objectives of a System User In contrast to the system providers, a system user (or a group of system users requesting simultaneous access, block 2), sees the system security requirement as yet another uncertainty in its basic decision-making concerning supply and demand trades in the primary electricity market. Depending on how the transactions are managed, some market participants either may not be given permission to use the system at certain times or may be charged for effecting security margins.

The main concerns of system users are (1) to make sure that they are served equitably and (2) to minimize uncertainties imposed by system constraints. These uncertainties can be reduced either by a system provider actively posting most likely technical constraints (including the probability of their occurrence) [5] and/or by system users purchasing financial insurance for transmission [6].

14.1.2.3 Congestion Control Based on Technical Signals The basic approach to congestion control under deregulation is identical to the control techniques in the regulated industry. As requests for implementing specific market transactions are given, the operator (block 3) attempts to implement as many requests as it possibly can without endangering system security. The only active control action a system provider can take is to reject certain requests. This can be done using the same methods based on strictly technical signals described for the regulated industry.

14.1.2.4 Congestion Control Based on Economic (Price) Signals A qualitatively different approach in the deregulated industry is the use of on-line price feedback p_T sent from a system provider (block 3) to the market participants (block 2). Several ideas for on-line transmission service pricing as a means of managing thermal congestion are briefly summarized next.

This is a more difficult scenario than just providing for reliability; a system provider (block 3) is expected to facilitate market efficiency (block 2) in addition to making sure that the system remains intact. A system provider could do this in several ways, the most obvious being public posting of system conditions and the projected critical constraints. However, since a system provider is not necessarily in charge of generation scheduling and therefore is not likely to have full access to economic data, the operator must develop tools for "learning" the market trends based on the past and the ongoing real-time market activities.

Methods for projecting system bottlenecks based on market activities are potentially useful for all types of primary-market structures. In a pool-company type primary-market structure in which economic dispatch and system operator are the same entity (blocks 2 and 3 become one), market inefficiencies created by transmission-system constraints are reflected in the nonuniform locational nodal prices ρ_i [Eq. (14.8)]. As a consequence of these unequal nodal prices, a so-called merchandise surplus is created, which is the difference between what consumers pay and what the suppliers are paid. This raises the issue of congestion pricing. Opinions concerning merchandise surplus allocation are diverse, such as having (1) proposals to use these funds as insurance against system uncertainties for those system users who hold unconditional transmission rights to either use the system or be compensated for not using it [7] or (2) proposals to use this money toward enhancing the system in the future to eliminate the most likely major obstacles to facilitating unconstrained market transactions [8].

The three methods described in the following illustrate some possible variations for managing transactions to ensure secure operation; method (1) is applicable for transmission pricing in a mandatory pool company [7], method (2)

requires adjustments of power quantities facilitated by the system, without any charges related to system constraints [9], and method (3) introduces a real-time transmission-price feedback to the system users that helps the users adjust their requests as the security margins vary [10 to 12]. These techniques enable system users to value the transmission system and adjust their requests for service accordingly. The earliest ideas suggesting methods of this type can be found in Refs. [9,10,13].

A conceptual scheme for the setup in which decisions for transmission service and its use are decoupled from the electricity market could be illustrated using Figure 13.4 with block 2 representing the electricity market and block 3 representing a system provider as separate entities. Methods (2) and (3) are of this type.

These methods are in sharp contrast with the bundled, nodal pricing-based approach to congestion management [method (1)] in which the financial impact of transmission constraints is generally bundled together with the value of the energy market bids as illustrated in Figure 13.4 by having blocks 2 and 3 merge into one entity. This approach to transmission-congestion management has been advocated in Refs. [7,14]. A system provider performs a bundled management of energy bids subject to transmission constraints and evolves with a bundled price indicator. In this approach energy-market decisions and transmission-market decisions are not separable, and, moreover, no iterations are allowed in which system users would respond to the transmission charge. Once the bids are made, it is the system provider who determines which bids are used and the price.

14.1.2.4.1 Pool-Company (Poolco)-Based Congestion Pricing [Method (1)]

The so-called nodal pricing approach is based on the theory of spot pricing [15]. In the case of line-flow-constraint-related security charges, the transmission flow constraints (14.3) in particular are considered when performing generalized economic dispatch. As described in Section 14.1.1, because of line-flow limits P_l^{\max} , the solution to this problem leads to different nodal prices ρ_i at each bus; these are also known as spot prices, originally introduced in Ref. [15]. The basic proposal is then to charge each market participant i price ρ_i , hence according to their location in the network. As a result, loads located in remote areas where the transfer capability is limited will pay comparatively higher rates.

As an example, consider a simple three-bus network shown in Figure 4.4. Assume that, based on the bids, a system operator is given the following cost–benefit functions: $C_1(P_{G1}) = P_{G1}^2 + P_{G1} + 0.5$, $C_2(P_{G2}) = 2P_{G2}^2 + 0.5P_{G2} + 1$, and $U_1(P_{L1}) = 214.167P_{L1} - 10P_{L1}^2$. Without any transmission-line-flow constraints, the generalized economic dispatch (Chapter 13) results in the optimal power produced $P_{G1} = 6.58$ p.u., $P_{G2} = 3.42$ p.u. and power consumed $P_{L1} = -10$ p.u.

Next, consider the same supply functions subject to the flow limit $P_{G1-L1}^{\max} = 5$ p.u. A simple load-flow calculation shows that the real-power line flow would be $P_{G1-L1} = 5.5$ p.u. for the bus injections just mentioned. The system λ defined in Eq. (13.22) is in this case $\lambda = 14.17$. However, since this solution violates

the line-flow constraint, a system operator would perform a price-bid-based constrained economic dispatch and calculate the nodal prices. The result of a transmission-constrained economic dispatch just described is $P_{G1} = 5.41$ p.u., $P_{G2} = 4.16$ p.u., and $P_{L1} = -9.583$ p.u. The corresponding nodal prices are $\rho_{G1} = 11.84$, $\rho_{G2} = 17.16$, and $\rho_{L1} = 22.49$. The nodal price differences reflect the impact of the active transmission-line constraint relative to the unconstrained market price $\lambda = 14.17$. The proposal in Ref. [7] is to use this approach for ex post transmission use charges, computed at the end of each day, for example.

14.1.2.4.2 Multilateral Markets [Method (2)] A qualitatively different approach to managing system constraints is to *unbundle* primary electricity market activities (block 2) from the system constraint-imposed adjustments (block 3). This was proposed by Wu and Varaiya as a way of creating coordinated multilateral markets [9]. The basic idea is for a system operator to adjust transactions initially so that the line flow is at its limit and to provide market participants with a set of equations that will have to be observed as further trading evolves. The coordination is achieved by the participants observing the technical constraints defined by the system provider. Market participants are left alone to decide on their transactions without having to reveal any economic data to the system provider (block 2). The technical constraints use the distribution-factor-based line-flow allocation formulas that define how much each bus injection contributes to a line flow. For every line whose limit is reached, one such constraint is provided. This approach is qualitatively different from the nodal-pricing-based transaction management since there is *no monetary charge* related to system constraints (block 3).

To illustrate this method, consider the same three-bus system as before. Since the line flow T_{G1-L1} exceeds the operating limit P_{G1-L1}^{\max} , a system operator first adjusts the transactions requested by the market to ensure that $P_{G1-L1} = P_{G1-L1}^{\max}$ and imposes the following equality constraint:

$$P_{G1-L1} \approx \frac{2}{3}P_{G1} + \frac{1}{3}P_{G2} \quad (14.16)$$

This is *strictly technical information* that generators G1 and G2 must observe as they pursue further trades. In this case, if P_{G2} is increased at twice the rate of decrease in P_{G1} , then the flow in the previously congested line is unchanged. Therefore, generator G1 can sell additional power to the load if generator G1 *simultaneously buys* twice as much power from generator G2. The initial adjustment is arbitrary. To show sensitivity of profits or benefits of the individual market participants to the initial adjustment, consider two different initial adjustments: (1) reduce both P_{G1} and P_{G2} by the amount of the excess line flow (0.53 p.u.). (2) curtail only P_{G2} because this unit has a higher marginal cost; for the line flow to remain at its limit, $P'_{G2} = 1.83$ p.u., while $P'_{G1} = P_{G1} = 6.58$ p.u. Consequently, $P_{L1} = 8.42$ p.u.

Of course, there exist many other combinations of bilateral trades that are completely equivalent and satisfy the line-flow limit. For example, generator G2

can increase its sales to the load if generator G1 sells half of that amount to generator G2. Alternatively, generator G1 can increase these sales to the load if generator G2 decreases its sales to the load by twice as much.

This trilateral (generally multilateral [9]) trade can be viewed as three coordinated bilateral markets: one, for exchanges between generator G1 and load L1, another between generators G1 and G2, and a third between generator G2 and load L3 [16]. The submarkets are coordinated because the price in one market affects the demand or supply in the other.

Generator G2 and load L1 make their decision to trade in the same way as before the congestion is reached, that is they follow the rule of their own profit or benefit maximization as given by Eq. (13.9). Generator G2 continues to sell power to generator G1 as long as the price is greater than its marginal cost. The load's demand for power in the G1–L1 (sub)market is determined by the same strategy: Continue to buy power until the price is equal to his marginal benefit.

The strategy for generator G1 is a bit more complicated, however. The profit for generator G1 in the trilateral market is a function of the prices p_{G1-L1} and p_{G1-G2} in the two postcongested markets, and the quantity that is sold after congestion is affected by this fact [16].

At the new equilibrium generator G1 sells 5.42 and generator G2 will produce 4.17 units of power. The load purchases 9.58 units of power. The bilateral prices are $p_{G1-L1} = 22.5$ and $p_{G1-G2} = 17.17$. It can be shown that this equilibrium is reached *independently* of the initial adjustment.

However, total profits or benefits of generators G1 and G2 and load L1 are generally affected by the initial adjustment since the actual amounts sold at pre- and postcongested price are different. Because the individual profits are affected by the initial adjustment rule used by a system operator, this seemingly free-market approach is prone to the so-called *quantity control* (this could be contrasted to the nodal-pricing-based approach that is sometimes qualified as a *price-control-based method* because the system users are required to provide their economic information.)

Notice, however, that if the primary-market accounting is done only at the end (and not at both precongested and congested prices), there is no difference between individual profits when applying method (1) [7] and method (2) [9]. Technical feedback that reflects system constraints [method (2)] and price feedback [method (1)] result in identical quantities and prices [17].

However, in an industry structure in which bilateral transactions take place inside the secure operating regions without any charges for reducing security margins, trading will be done in two stages for quantities traded prior to congestion and at the end when an equilibrium is reached subject to an active line constraint. In this case, as long as a system operator has direct control over how much can be sold, the profits are affected by the initial adjustments.

In contrast with methods (1) and (2), which are inactive before the security limit is reached, method (3) [10] provides transmission-price feedback that reflects the relative contribution of individual market participants to the reduced

system security as the system constraints are being approached. This should give sufficient warning to system users to adjust their transactions. Consequently, the probability of violating security limits is reduced considerably. This method is briefly described next.

14.1.2.4.3 Soft-Constraint-Based Congestion Pricing [Method (3)] One of the basic questions in the new industry is whether price feedback can be used to induce system security sufficiently fast in real-time operation. Generally the *rate* at which the price feedback is used will determine how fast the self-adjusting process will evolve.

A version of a possible congestion market that leaves enough room for system users to value transmission is based on the concept of a transmission provider signaling to all users a short-term (hourly) congestion price based on their current relative impact. The price is proportional to the square of the deviation in flows from nominal¹ caused by their relative contribution to the total flow in a line approaching congestion. The premise here is that the system users will adjust iteratively (hour by hour) in response to these signals, and this will prevent congestion from occurring. The error signals are based on soft, rather than hard, transmission constraints [18,19].

A real-time (hourly) transmission-price feedback is based on using the error vector $\{E(t)\}$, the elements of which reflect the amount of the individual line flows beyond their nominal values,

$$E_l(t) = \begin{cases} P_l - P_l^{\text{nom}} & \text{if } P_l > P_l^{\text{nom}} \\ 0 & \text{otherwise} \end{cases}$$

for all lines l , where P_l^{nom} is a value smaller than the thermal limit P_l^{max} by certain safety margin. Next one can compute the vector of transmission-congestion charges according to

$$\{CC(t)\} = \{E(t)\}^T [\text{diag}(\{R\})] \{E(t)\} \quad (14.17)$$

where $[\text{diag}(\{R\})]$ is a diagonal matrix with coefficients that reflect the relative importance of maintaining flow in various transmission lines within their nominal values. The total charge for congestion is the sum over all lines

$$TC = \{1\}^T \{CC(t)\} \quad (14.18)$$

The usage-based charge allocation method is then applied for this charge allocation to individual users.

¹ The definition of a nominal flow in a multi-control area under open access remains an open problem [20].

This price-feedback design is based on usage in the sense that the transmission-congestion charge to a market participant at bus i is proportional to the relative contribution of its injection to the line flow. The larger the rate, the faster will system users respond to the security conditions. However, if the price feedback is too large, oscillations may occur. The conceptual use of real-time price feedback to regulate technical processes is known to have a potentially destabilizing effect. To avoid these problems, one has to engage in systematic feedback design for regulating system conditions in response to the expected ranges of system disturbances.

Rather than informing the user that he or she has to be suddenly disconnected from the system, the user is given, in real-time operation, a price feedback for effecting security margins. This price, of course, unavoidably depends on all other system users, and all users are expected to adjust to the system conditions over time by either paying for effecting system security and/or by adjusting power quantities traded to avoid this charge.²

Example 14.1.1[19] We illustrate next on a five-bus example shown in Figure 14.1 the feasibility of this approach. Simulations of this scenario were done by Chien-Ning Yu, MIT [19]. Soft-constraint-based price feedback is used to avoid transmission constraints in real time. Assume that there are only two bilateral contracts present on the system: $T_{1,5}$, between G_1 and L_5 , and $T_{2,4}$, between G_2 and L_4 . The scheduled (nominal) values for $T_{1,5}$ and $T_{2,4}$ are 8 p.u. and 10 p.u., respectively. Over time, at the end of the first hour, at $t = 1$ h, $T_{2,4}$ starts to deviate from its scheduled value in anticipation of an improved profit by generator G_2 and benefit at load L_4 . The quantity requested for approval by $T_{2,4}$ adjusts every 15 min, and the maximum change is $\pm 20\%$ of its nominal value. Around $t = 2.25$ h, $T_{2,4}$ settles to its optimal value $T_{2,4} = 15$ p.u. At $t = 3$ h,

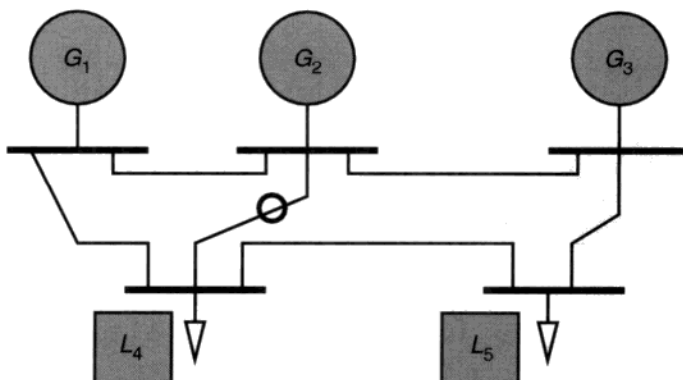


FIGURE 14.1 Five-bus system.

² The transmission charges collected here are probably best used for future system enhancements to maintain P_l close to P_l^{nom} .

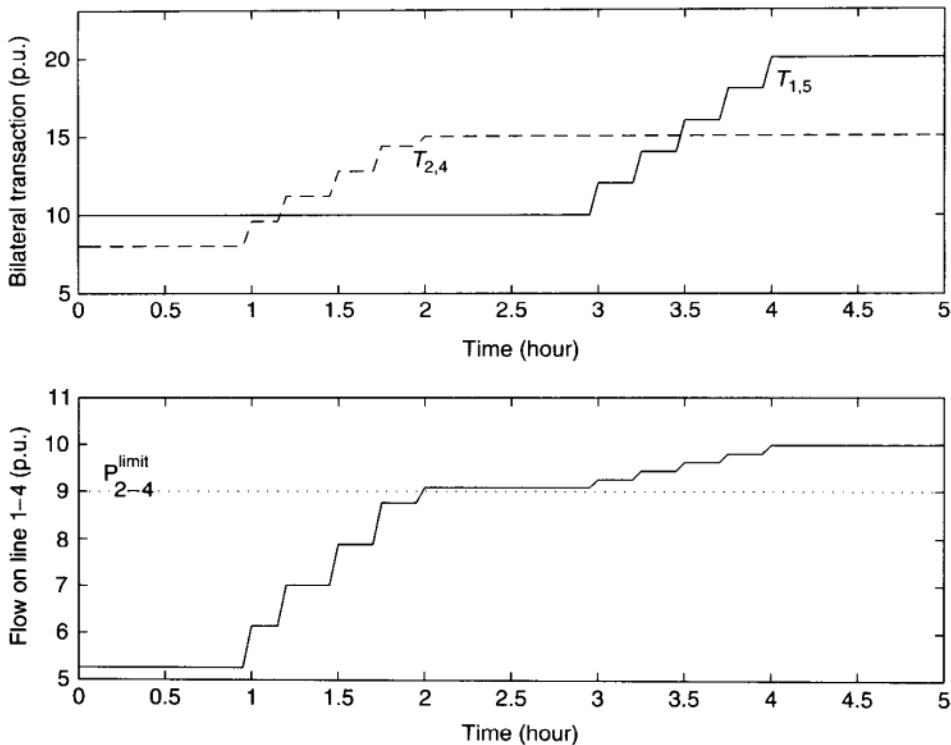


FIGURE 14.2 Transactions without charge for constraint.

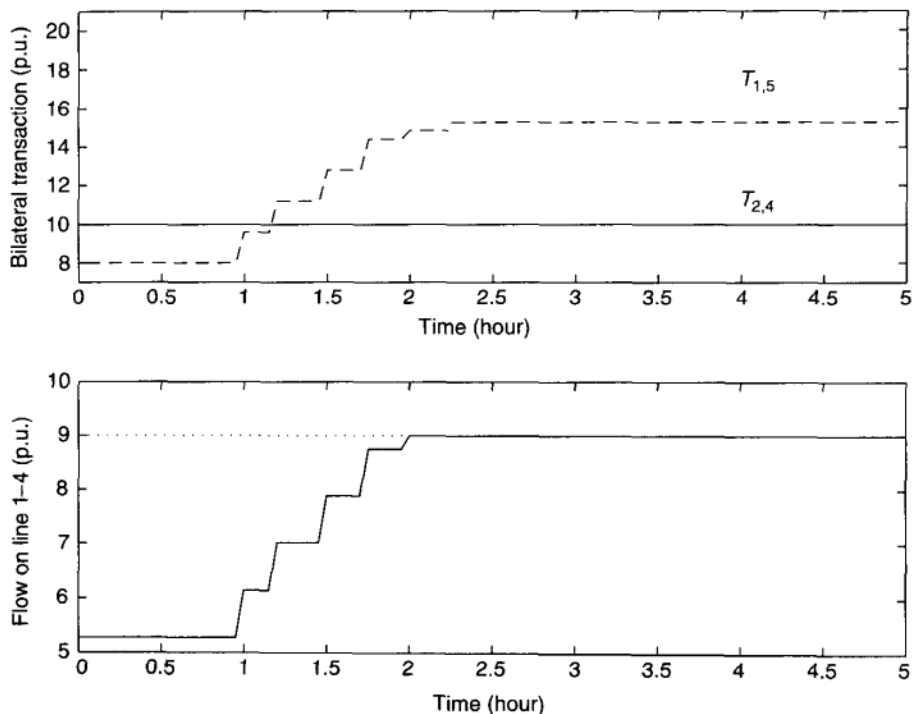
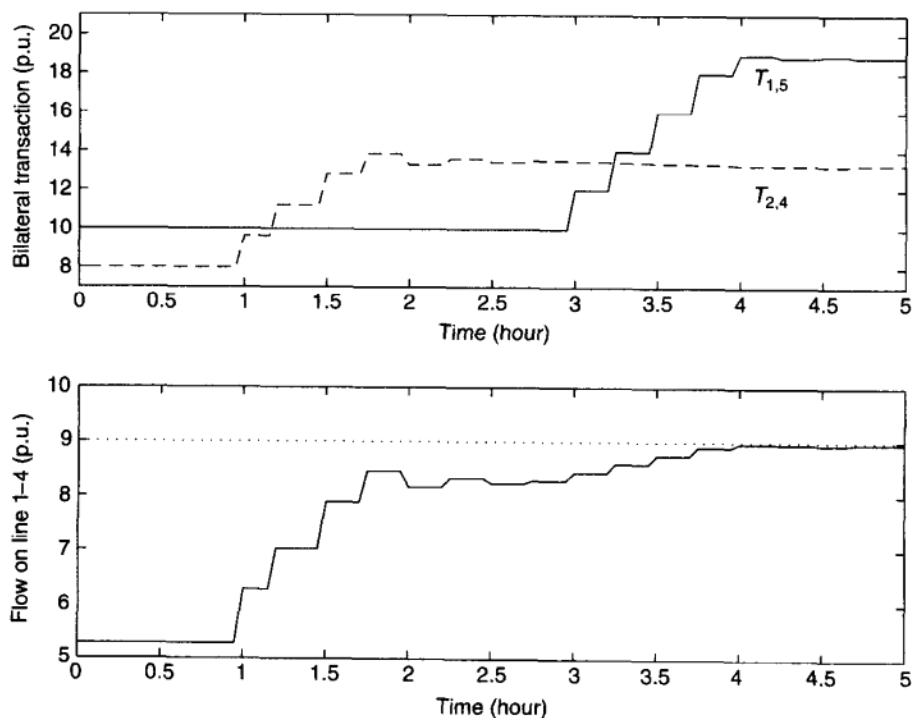
$T_{1,5}$ starts changing the quantity traded and it finally settles to its optimal value $T_{1,5} = 20$ p.u. (Fig. 14.2).

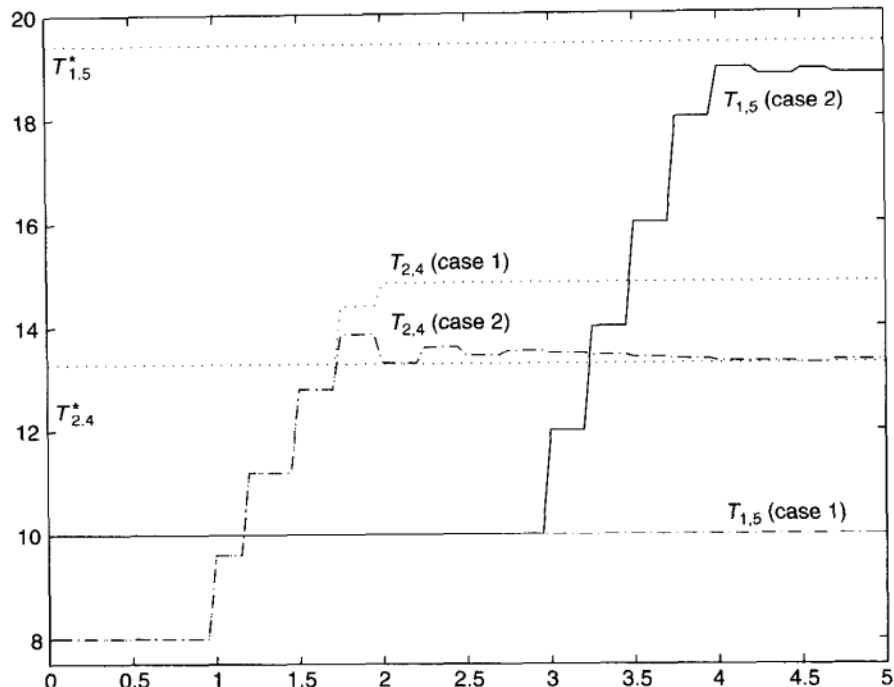
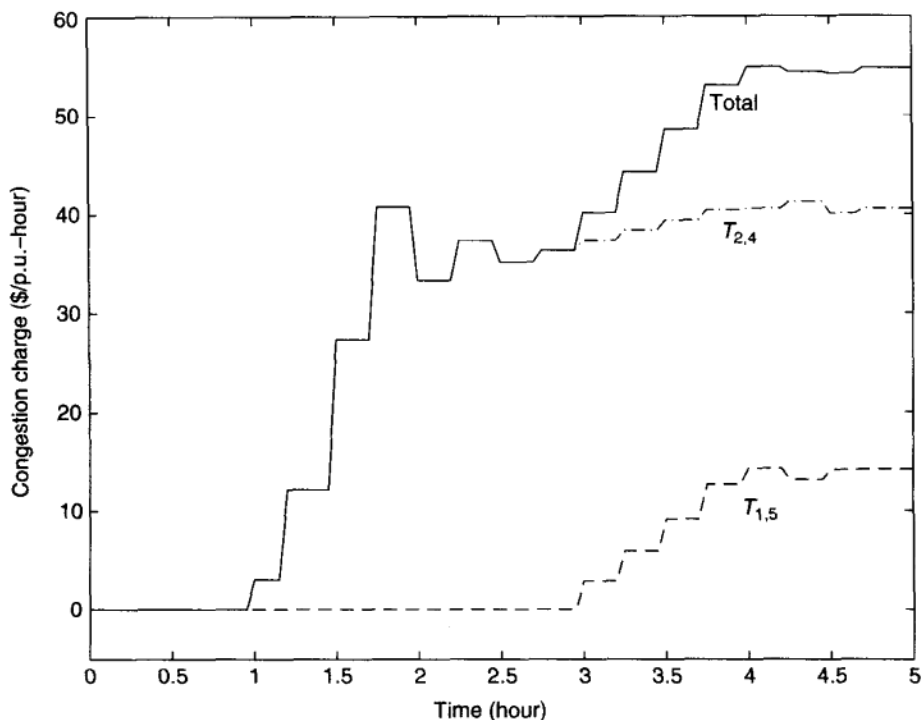
Now, assuming that the thermal limit of line 2–4 is 9 p.u., the line constraint will be obviously violated in the absence of any price feedback p_T between blocks 2 and 3, reflecting the proximity of the line flow to its limit. Shown in Figure 14.3 is the result of an obvious physical adjustment; transaction $T_{2,4}$ is curtailed to the value 9 p.u. (case 1).

Shown in Figure 14.4 is an application of the soft-constraint-based price feedback described here. Each transaction is given a price signal based on its relative contribution to the line constraint. It can be seen that since the proximity to a line-flow constraint depends on both transactions, $T_{2,4}$ will *self-adjust* as $T_{1,5}$ changes, so they collectively result in an acceptable line flow.

In Figure 14.5 a comparison of cases 1 and 2 is summarized. This figure shows the result of case 2 actually approaching the optimal value $T_{1,5}^* = 19.43$ p.u. and $T_{2,4}^* = 3.28$ p.u. when both transactions are scheduled simultaneously to minimize the total cost subject to a given line constraint. This figure is an illustration of a *self-adjusting* process by primary-market participants in response to the system-constraint-based price feedback.

The transmission charges for $T_{1,5}$ and $T_{2,4}$ are shown in Figure 14.6.

**FIGURE 14.3** Case 1: Obvious physical adjustment.**FIGURE 14.4** Case 2: Applying soft constraints.

**FIGURE 14.5** A comparison of cases 1 and 2.**FIGURE 14.6** Congestion charge.

For the five-bus example, the transmission service charge TS reflecting the proximity of the line flow P_{2-4} to its limit is computed as⁴

$$TS = \begin{cases} \alpha(P_{2-4} - P_{2-4}^{\text{nom}})^2 & \text{if } P_{2-4} > P_{2-4}^{\text{nom}} \\ 0 & \text{otherwise} \end{cases} \quad (14.19)$$

$$(14.20)$$

and it is further distributed to transactions currently using the system according to the relative contributions of transactions $T_{1,5}$ and $T_{2,4}$ to this line flow (using distribution factors $\partial P_{2-4} / \partial T_{1,5}$ and $\partial P_{2-4} / \partial T_{2,4}$),

$$\Delta P_{2-4} = \frac{\partial P_{2-4}}{\partial T_{1,5}} \Delta T_{1,5} + \frac{\partial P_{2-4}}{\partial T_{2,4}} \Delta T_{2,4} \quad (14.21)$$

$$= 0.0912 \Delta T_{1,5} + 0.4360 \Delta T_{2,4} \quad (14.22)$$

$$= \Delta P_{2-4}^{T_{1,5}} + \Delta P_{2-4}^{T_{2,4}} \quad (14.23)$$

Corresponding transmission charges for $T_{1,5}$ and $T_{2,4}$ are

$$TS^{T_{1,5}} = \frac{\Delta P_{2-4}^{T_{1,5}}}{\Delta P_{2-4}} TS \quad (14.24)$$

$$TS^{T_{2,4}} = \frac{\Delta P_{2-4}^{T_{2,4}}}{\Delta P_{2-4}} TS \quad (14.25)$$

Each system user applies a very straightforward formula when deciding how to adjust its transaction request in response to changing system security constraints. The decision-making formula is effectively identical to the formula (13.19) used in decentralized economic dispatch or unit commitment, *except* for the additional term reflecting its relative transmission service charge [Eq. (14.25)], that is, in case of a power producer i , for example,

$$\max_{P_{Gi}} \left(pP_{Gi} - C_i(P_{Gi}) - \sum_k \sum_n TS^{kn} P_{Gi} \right) \quad (14.26)$$

where TS^{kn} is the charge to P_{Gi} for effecting a security margin in a transmission line kn . This adjusting process is applied in the five-bus example for the utility functions at the five buses as follows,

$$C_1(P_{G_1}) = P_{G_1}^2 + P_{G_1} + 0.5 \quad (14.27)$$

$$C_2(P_{G_2}) = 2P_{G_2}^2 + 0.5P_{G_2} + 1 \quad (14.28)$$

⁴ In this case, we choose $\alpha = 4 / p.u.^3\text{-hour}$. The choice of nominal line flows, in this case P_{2-4}^{nom} , is critical in this method; an “anchor” nominal point for which the open access is designed must be defined, and all inefficiencies and transmission charges for new system enhancements should be measured relative to the nominal system design.

for generators 1 and 2, and for loads

$$U_4(P_{L_4}) = 360.5P_{L_4} - 10P_{L_4}^2 \quad (14.29)$$

$$U_5(P_{L_5}) = 241P_{L_5} - 5P_{L_5}^2 \quad (14.30)$$

Since $P_{G_1} = P_{L_5} = T_{1,5}$ and $P_{G_2} = P_{L_4} = T_{2,4}$, the cost or utility functions can be rewritten in terms of $T_{1,5}$ and $T_{2,4}$.

$$C_1(T_{1,5}) = T_{1,5}^2 + T_{1,5} + 0.5 \quad (14.31)$$

$$C_2(T_{2,4}) = 2T_{2,4}^2 + 0.5T_{2,4} + 1 \quad (14.32)$$

$$U_4(T_{2,4}) = 360.5T_{2,4} - 10T_{2,4}^2 \quad (14.33)$$

$$U_5(T_{1,5}) = 241T_{1,5} - 5T_{1,5}^2 \quad (14.34)$$

These simulations indicate the basic preaching of competitive economics: Given the right price feedback p_T for creating congestion (in this case $TS^{T_{1,5}}$ and $TS^{T_{2,4}}$), the primary market (process in block 2) will adjust in a decentralized way to the near theoretically optimal conditions *without* requiring a coordinated primary market. System users are likely to learn the value of their transaction being implemented and compare this value with the charge being assessed. If the difference between the two is big, this gives an incentive to the system user to adjust to the situation by seeking longer-term solutions (trade different power quantities, invest in system enhancements, or purchase some sort of insurance against system uncertainties). *In theory*, assuming perfect market conditions, one will have exactly the same situation as when comparing performance of real-time spot markets and their competitive market equivalents, that is, there will not be much difference between the two. Recall that the long-term market adjustments are in response to the observation of the real-time electricity prices. Following identical thinking, one can argue that if an adequate real-time signal about system security status is given to the market participants, they will respond to it and converge to the market conditions in which constraints are directly coordinated with the primary-market processes.

In summary, it is possible to manage transactions within system security constraints in more than one way. If market-information delays and intertemporal effects are neglected, all three methods lead to an identical market outcome. Further studies are needed to investigate market performance away from perfect market conditions. Both theoretical and experimental studies are needed on this subject.

14.1.2.5 Dealing with System-Constraint Related Market Uncertainties

System constraints are basically external to the primary electricity markets. Their effect could be reduced considerably by system providers posting projected system constraints and/or by developing financial instruments for hedging against

these uncertainties. Very little has been done so far in developing software tools by system providers to inform market participants about probabilities of technical limitations. If these were made known, system users could account for the risks related to system provision when making market decisions. An initial effort in this direction was reported in Ref. [5]; however, rather than assuming that all market transactions are equally probable, as assumed in this work, it is necessary to develop *conditional probabilities* about the system constraints in terms of most likely market events.

Since probabilistic information about system security status is not made readily available, market participants are considering a possible means of hedging against system related uncertainties. One possible approach proposed by the Federal Energy Regulatory Commission (FERC) in Ref. [21] suggests creation of primary and secondary markets for purchasing *transmission rights*. Taking this path brings up many unresolved technical questions; see Ref. [22,23]. More work is needed to come to some resolution concerning the feasibility of this idea.

The second idea is to establish transmission-congestion contracts between a market participant and a transmission system provider [7]. This idea was originally conceived as part of the nodal pricing for transmission congestion, in particular the controversy surrounding the question of who should be paid the merchandise surplus resulting from unequal nodal prices [4,24]. This surplus is often significant as constraints are violated.

This issue has been discussed quite actively. One possible solution would be to collect this surplus for future system enhancements to avoid congestion. A peak-load pricing for transmission was recently proposed in Refs.[8,25] as one possible method for implementing this idea. The second approach to using merchandise surplus is by introducing financial instruments for hedging against system-constraint induced market uncertainties. This is briefly described next.

14.1.2.5.1 Transmission-Congestion Contracts One possible approach to distributing the merchandising surplus suggested is to use it to compensate market participants who own *transmission congestion contracts* (TCCs) [7] to inject into the system a prespecified amount of power in a point-to-point fashion. If TCCs are not feasible in a real-time operation, the owners of these transmission rights would be compensated *ex post* for not being able to exercise their transaction in such a way that they are indifferent to the fact if they have produced power themselves or have been compensated for not selling it. The TCCs should be viewed strictly as a financial instrument for dealing with transfer-capability-related uncertainties, much in the same way as the contracts for differences are used to deal with the primary-market uncertainties. They are effectively the same mechanism between the system provider and the system user who owns these contracts.

As an illustration of a TCC, consider the same three-bus example and an existing TCC to transfer 7.5 p.u. from bus 1 to bus 3. This could represent a financial right of generator G1 to sell 7.5 p.u. to load L1. Consider then the following actual dispatch of $P_{G1} = P_{L1} = 7.5$ p.u. and $P_{G2} = 0$ p.u., which results in line flows $P_{1,3} = 5$ p.u. = $P_{1,3}^{\max}$, and $P_{2,3} = 2.5$ p.u. The corresponding

nodal prices are $p_1 = \$16$, $p_2 = \$0$ and $p_3 = \$64$. Since the congestion is not binding yet, the capacity right of 7.5 p.u. is implementable at the production cost of $7.5 \times \$16$, equaling \$120. Transmission cost is \$0; congestion rent is \$0. Now, after solving the optimization problem for this case, we obtain quantities and nodal prices $P_{G1} = 5.76$ p.u., $P_{G2} = 3.74$ p.u. $P_{L1} = -9.5$ p.u., $p_1 = \$12.52$, $p_2 = \$15.44$ and $p_3 = \$24.17$. To derive the effect of the transmission constraint, take the difference between unconstrained and constrained prices $t_1 = \$13.5 - \$12.53 = \$0.97$ and $t_3 = \$24.17 - \$24.17 = \$0$. The congestion payment to bus 1 is $(\$0.97 - 0)5.76 = \5.59 , the congestion rent is $(\$0.97 - 0)(7.5 - 5.76) = -\1.736 , production cost equals $12.53 \times 5.76 = \$72.23$, and the purchase at bus 3 costs $\$24.17 \times (7.5 - 5.7645) = \41.94). The algebraic sum of the congestion payment, rent, production cost, and the payment by the load amounts to \$118.02, which is approximately \$120.00 (within the numerical error).

The initialization of transmission-congestion rights in electricity markets that are far from being liquid and the impact of this on the overall market inefficiency are open questions.

14.1.2.5.2 Priority-Based Insurance for Transmission Services Depending on the specific objectives of various market participants, their needs for transmission vary considerably. To some system users it is critical to have insurance for near-unconditional use of the system, independent from what other users are requesting. Other users are willing to take the risk of not being served and therefore are paying less for transmission service [26].

Moreover, a transmission provider typically does not have access to the economic data associated with energy market decisions. This makes it quite difficult to estimate the demand function for transmission by a system provider.

It has been suggested in the literature that one way of circumventing this conceptual issue would be to let system users make decisions themselves about the amount and type of insurance for transmission service they would need and the value they would associate with it. The system provider would then develop mechanisms for facilitating the needs of the system users, without interfering with their financial decisions once the two sides have agreed on the price for transmission service requested. The actual implementation of such concepts could vary, again: (1) A transmission provider would sell firm transmission rights on a seasonal basis and have a secondary transmission market develop for trading these rights by the system users themselves. 2) A transmission provider would sell priority-based transmission service instead of firm transmission rights, again with an active secondary market for transmission playing a decisive role in efficient real-time use of these rights [6,27]. (3) Transmission rights would not be sold by a transmission provider; instead, the transmission provider would play a major role in auctioning the use of transmission as the requests evolve. Here, both transmission provider and system users actively estimate the value of transmission for the contract duration and iterate to a compromise [28].

14.2 RE-EXAMINATION OF VOLTAGE CONTROL

As described before, in the area of system congestion and its control a major attention has been given only to the problem of managing thermal line flow limits in the deregulated industry. The problem of generation-based control for maintaining voltages within their prespecified limits (to prevent voltage-related system congestion) is not the focus of interest at present. As explained in Chapter 13, Section 13.5, the problem of power dispatch for balancing reactive power is typically done by taking voltage constraints into consideration. In other words, no equivalent step to the unconstrained economic dispatch (block 2) is carried out for reactive-power management. As explained in the same section, (Sec. 13.5.2) this situation is likely to change in the deregulated industry as technical standards for system users with respect to reactive-power–voltage-support requirements are adopted.

In the remainder of this chapter the formulation of the constrained reactive-power dispatch introduced in Chapter 13, Section 13.5.1, is used as a starting point for purposes of introducing efficient computer methods. Furthermore, at present both the regulated industry and the industry undergoing restructuring base their voltage control primarily on technical signals and not on economic signals. Nevertheless, much in the same way as μ_l in Eq. (14.5) reflects the sensitivity of optimal cost with respect to the thermal capacity of a congested transmission line, the OPF-like formulation that takes into consideration voltage limits provides Lagrangian coefficients in Eq. (13.143) that could be used as economic signals for voltage control [29].

14.3 METHODS FOR EFFICIENT CONGESTION CONTROL IN VERY LARGE POWER SYSTEMS

It can be seen from the preceding discussion that the basic formulations of congestion (thermal and/or voltage) problems are straightforward. They can be identified as particular examples of nonlinear programming problems [30] that have been studied in considerable depth over many years. Optimality conditions and assumptions under which the existence and uniqueness of a solution can be guaranteed are also known from the general theory of nonlinear programming.

The real obstacle to efficient transmission-congestion management in large electric power systems is related to the amount of data that must be processed in near-real-time.* The remainder of this chapter is written with this issue in mind. An integral part of the methods described is data compression for creating useful information.

Unique characteristics of the propagation of a disturbance in response to changes in real- and reactive-power injections were described in Chapter 5 as localized response properties. They are used in today's industry to simplify an

* This problem is in addition to the problem of defining meaningful technical standards with respect to reactive-power-voltage-support requirements (Section 13.6).

operator's decision-making in real time either implicitly by the operator or as part of computer algorithms implemented in modern control centers.

An early idea of clustering was introduced by the senior author of this book for efficient real- and reactive-power management in regulated power systems [2,31]. This method is essential for displaying critical information to the market participants in the deregulated industry regarding the proximity of the system to the thermal line limits as well. Basically the same approach was recently used in Ref. [3] to propose on-line information that is essential for effective management of thermal constraints in the new industry. It has been suggested in this work that the same information is important when the price for using the system is determined by a transmission provider as well as when strictly technical information is used for intelligent adjustment of market participants to the system conditions.

It appears that the simplifications of this type may become essential in the deregulated industry characterized by a large number of price-driven changes in system inputs [32]. It is then the operator's basic responsibility to respond in a flexible and somewhat transparent way to the electricity market needs (block 2) as he or she attempts to manage system congestion (block 3).

It is important that new operating and control paradigms be created using the tremendous flexibility and simplicity offered by implementing methods described in this chapter. This will avoid unnecessarily rigid approaches of grouping system users into "zones" that do not vary with system conditions [32].

Changes of operating conditions and equipment status either could create a somewhat localized effect on the rest of the system or, less frequently, could affect the entire system significantly. It is quite effective to have decision-making tools to assist the operator in recognizing the extent to which the system is affected by the changes. In the remainder of this chapter, we first describe several such decision-making tools for the voltage-reactive-power congestion control. This is followed by a section describing methods for finding the most effective control actions when the effects are localized. The flexible clustering approach introduced in Refs. [2,31] is described as an essential method for congestion management.

Next, an analogous method for managing thermal congestion on the system is illustrated for the deregulated industry, in which requests for system service are balanced. Here again we recognize an interesting relation with the earlier work of the senior author concerning asymmetries created by having a slack bus; in Ref. [2] a transformation was introduced to circumvent this problem. We illustrate how a similar transformation was applied in Ref. [3] for defining clusters of buses with similar effects on a particular line of interest.

14.3.1 Monitoring Tests for Determining the Localized Nature of Voltage Problems

In reactive-power studies, sensitivity to changes of reactive-power injection at a given bus does not necessarily drop tierwise, but on viable systems it will

generally drop sharply beyond a closed cut set across those *PV* buses* that are nearest to that bus. In other words, one should not count on monotonic tier-by-tier dropoff of sensitivities, but local sensitive regions roughly defined by the nearest *PV* buses around the disturbance that would be present. In this sense then, with a typical scattering of directly controlled buses throughout the system, every location of a disturbance or a control action will generally be surrounded by a region of affected locations that are sensitive above some preset threshold. This property underlies the clusterwise voltage-control techniques, referred to as *viabilization techniques* [2,31].

In this section three monitoring tests are described as a means for detecting the extent of reactive-power disturbance propagation. They are based on the echelon concept, and the bus reactive-load excess and the deviation vector \underline{D} notions. Using these notions corrective strategies for eliminating local problems are described.

The analysis results from Chapter 5 suggest that determining the basic nature of bus-voltage and phase-angle changes in response to any given event could be based on the following measures:

1. The echelon structure is an effective way for bounding changes on network parameters and system inputs under which the response remains localized.
2. The components of vector \underline{D} (Chapter 5, Eq. (5.247)) represent normalized reactive-power imbalance at each load bus. This is also an indicator of possible localized differences of the reactive-power sources and demand.
3. The bus reactive-load excess (BRE) measure proposed in Ref. [33] is effectively a heuristic measure of the worst-case reactive-power bus imbalance. It is computed as a hypothetical imbalance obtained when the actual net injection is replaced by the maximum possible imbalance when voltages are at their limits.

14.3.1.1 Conditions for Reactive-Power Imbalance over Local Segments Using the Echelon Concept Given the components of the imaginary part of the bus reactance matrix $X = B^{-1}$ with all shunt admittances set to zero, then if the shunt capacitors satisfy the inequality introduced in Chapter 5 [34]

$$C_{ii} \leq \frac{1}{X_{ii} + X_{ij} \frac{X_{mi} - X_{ji}}{X_{jj} - X_{mj}}} \quad (14.35)$$

it follows that any change at bus j will not cause a change ΔE_j that is larger than ΔE_m . Proof for the inequality (14.35) was given in Chapter 5. This means that as long as the size of shunt capacitors at each bus i is constrained by the (transmission-network-dependent) bound in Eq. (14.35), change in injections

* Recall from Chapter 5 that *PV* buses are generators whose voltage E_G^{ref} is directly controlled. Any other type of bus equipment with direct voltage control (SVCs, for example) plays the same role in supporting system voltage.

may cause a change in voltage that decreases with distance away from the injection change. However, under excessive capacitive support quantified by violating relationship (14.35), it is possible to have voltage disturbance propagation larger somewhere else on the system than at the location where a disturbance took place. Using inequality (14.35) straightforward conditions could be employed for the computer-aided monitoring of a large power system. They fall under the category of knowledge-based rules, which have evolved as a result of a detailed mathematical analysis of the reactive-power disturbance propagation in Chapter 5. With the basic definition of echelons being that all directly controlled voltage buses on the system form echelon 1, buses directly connected to buses in echelon 1 form echelon 2, etc, one could establish the following rules:

- *Rule 1* The choice of capacitive support should be such that the imaginary part of the admittance matrix of the entire interconnected system does not have any negative row sum, a condition equivalent to Eq. (14.35). If this is not the case, even on the systems that have a good echelon structure, that is, large numbers of buses subject to uniformly distributed direct voltage control, a nonlocalized voltage response may occur.
- *Rule 2* Systems with many echelons are proven to have a potentially nonlocalized propagation of voltage deviations. A good system design with respect to its voltage support is characterized by having as many buses with direct voltage control as possible if the economic constraints allow for it.

Using these rules, a system operator could monitor whether the voltage problem is local. If so, control actions are needed that are simpler than those used when the entire system is affected. Such an echelon-based algorithm for finding the extent of disturbance spreading was first suggested in Ref. [35,p.91]. The flowchart for a possible computer-aided algorithm of this type is given in Figure 14.7. It should be understood that any bus that is directly voltage controlled (even using on-load tap-changing transformers, static Var capacitors, etc.) is classified as belonging to the first echelon. It can be seen that the only on-line data needed to be sent to the system operator are the following:

- Signals that capacitors have changed their values at some bus i by value ΔC_i in the system comprising n buses
- Disturbance (fault) location at bus i , or line outages between buses i and k (DL)
- Signals that a voltage controller has reached its operating limit (EL)

The flowchart in Figure 14.7 is relatively simple; it illustrates very little effort needed for computing a new row sum (RS) corresponding to the bus at which capacitors are switched or line outages occurred.

14.3.1.2 Conditions for Reactive Power Imbalance over Local Segments Using the BRE Measure

A heuristic indicator of possible localized deficiencies of

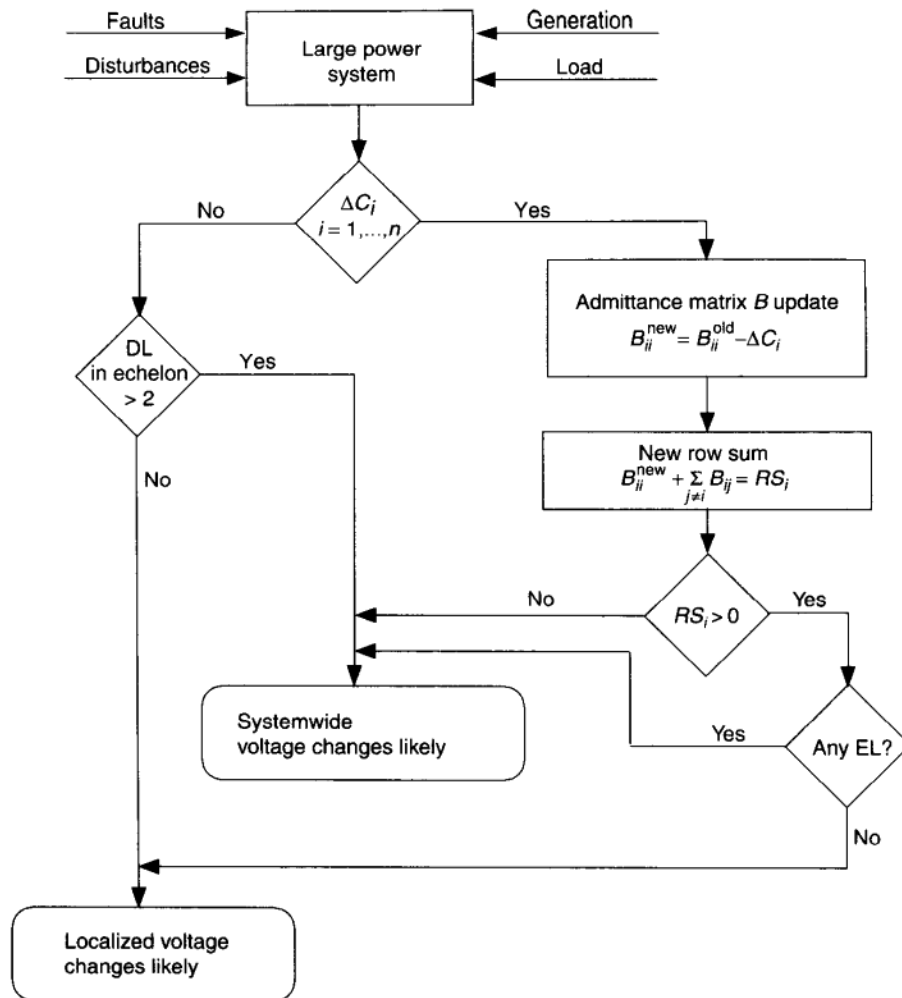


FIGURE 14.7 Echelon-based algorithm for determining localized voltage response.

the reactive-power sources, the bus reactive power excess (BRE) was proposed in Ref. [33]. In the absence of actual voltage violations, imbalance does not necessarily indicate an actual problem, although it would pinpoint a deviation from most technically desired system operation. The BRE at bus i is defined by

$$\begin{aligned}\Delta Q_i = \text{BRE}_i &= Q_{\text{Di}} - Q_i + \sum_{j=1}^N C_{ij} \frac{E_i}{Z'_i} \sin \zeta'_{ij} \\ &\quad - \frac{E_i E_j \sin(\delta_{ij} + \zeta_{ij})}{Z_{ij}} + \frac{E_i^2}{Z_{ij}} \sin \zeta'_i\end{aligned}\quad (14.36)$$

where E_i and E_j are the bus voltage set points at buses the voltage of which is directly controlled or the minimum permissible voltages (except the maximum

at i) at PQ buses. Q_i is the available reactive-power generation of bus i (including synchronous and static condensers or reactors, static Var control, etc.); Q_{Di} is the actual reactive power demand at bus i , C_{ij} is 1 and 0, respectively, when buses i and j are connected and not connected by a transmission line. Quantities E_i , E_j and Q_i are subject to inequality constraints of the form

$$\begin{aligned} E_i^{\min} \leq E_i &\leq E_i^{\max} \\ Q_i^{\min} \leq Q_i &\leq Q_i^{\max} \end{aligned} \quad (14.37)$$

As is well known, voltage problems could result from violations of either the upper or the lower limits. High voltages tend to occur at light loads with an excess of capacitive (negative) demand. The low voltage occurs during heavy inductive (positive) load periods. Only the latter case is explicitly treated in Ref. [33]. Much notational complexity can be avoided by this restriction, whereas equations for the high-voltage case are still easily obtained by changing a few signs and reversing a few inequalities. Note that if the load-flow values are substituted in Eq. (14.37) for E_i , E_j , Q_i , Q_{Di} , and the angles $\delta \Delta Q_i = 0$. This, of course, is not what is meant here. As defined, BRE _{i} compares the actual available reactive injection ($Q_i - Q_{Di}$) with the maximum demand that can be impressed on bus i through the network, assuming that the voltages and reactive-power injections are at their set points or within their tolerance bands [Eq. (14.37)]. This then represents the worst-case imbalance. If the BRE is monitored for all buses i and found to be nonpositive, then it is clear that no viability problem exists. Any value of BRE exceeding a preassigned threshold would indicate a potential reactive-power shortage at bus i . If it is coupled with a violation of permissible voltage limits, it would constitute a local reactive-power imbalance.

If BRE is monitored for all buses i and is found to be small, then it is clear that no significant reactive-power imbalance exists. Any large value of BRE would indicate a potential reactive-power shortage at bus i even if it is not currently coupled with a violation of permissible voltage limits.

Of course, reactive-power flow can be rearranged over a local area. Consequently, more information is needed to judge local reactive-power balance than BRE at a particular bus. One process for such judgment proposed in Ref. [33] is based on BRE and its first- and second-tier [36] sums

$$\begin{aligned} \Delta Q_i^I &= \Delta Q_i + \sum_j C_{ij} \Delta Q_j \\ \Delta Q_i^{II} &= \Delta Q_i^I + \sum_k C_{ik} \Delta Q_k \end{aligned} \quad (14.38)$$

where the tier I around bus i is defined as all buses j , connected directly to bus i , and tier II is defined as all buses k , connected directly to buses j of the first tier, except, of course, bus i , etc. If it is found that ΔQ_i , ΔQ_i^I , and ΔQ_i^{II} are large for some i , this is an indication of local weak-reactive-power support that

pinpoints i as a potential site for the static voltage problem and the potential initiating voltage collapse. This would indicate the need for checking security and, if actual violations exist, emergency viabilization [37]. Intermediate cases in which some ΔQ_i , ΔQ_i^I and ΔQ_i^{II} are non-negative are less directly clear but it would seem that at least marginal reactive balance and an even texture exists if one of the three is negative. The approach to reactive power balance on the local level proposed here is quite arbitrary, that is, no rigorous theoretical basis for the conclusions, is offered in Ref. [31]. Nevertheless, it should be quite useful as a practical index of the uniformity of the reactive texture, or conversely, any weak spots in this texture.

14.3.1.3 Conditions for Reactive-Power Imbalance Using \underline{D} Vector This method is based on the use of sufficient conditions for the existence of the unique solution to the nonlinear reactive-power–voltage problem described in Chapter 5. The deviation vector \underline{D} , is used to show where reactive-power shortages occur after a reactive-power input change. Recall the formulation of the \underline{D} vector given in Chapter 5, Eq. (5.247)

$$\underline{D} = (H - \hat{\lambda} I)\underline{E}^{\min} - \underline{c} + \underline{g}(\underline{e}) \quad (14.39)$$

where

$$H_{i,i} = B_{i,i} - b_i \quad (14.40)$$

$$H_{ij} = -B_{ij} \cos \delta_{ij} - G_{ij} \sin \delta_{ij} \quad \text{for } i \neq j \quad (14.41)$$

$$\lambda_i = \frac{|Q_i|}{(E_i^{\min})^2}, \quad \hat{\lambda} = \max_i \lambda_i \quad (14.42)$$

$$\hat{\lambda}_i = \hat{\lambda} - \lambda_i \quad (14.43)$$

The deviation vector \underline{D} can be used to identify locations of most severe reactive power shortages⁵ following major changes in system inputs or system topology. The formulation of the \underline{D} vector is such that the effects of raising voltages for the reactive-power imbalance are quickly and clearly identifiable. Hence, the algorithm is able to use knowledge of the available shunts and the reactive-power limits of generators to suggest control actions that will restore the reactive-power balance and thereby recover voltages at or above prefault levels. Such an algorithm is described next.

14.3.2 \underline{D} Vector-Based Algorithm

Initially, the low bound for the target voltage E_{lb}^t is set equal to load voltages from the most recent load flow, \underline{E}_t . Hence, all of the \underline{D} -vector elements start

⁵ On the other hand, reactive-power excess is associated with high-voltage problems. A generalization of the results to the high-voltage problems is straightforward and is omitted here.

out at zero, indicating perfect reactive-power balance. After a fault, the resulting shortage of reactive power is recognized through the \underline{D} vector. The algorithm then uses the numerical system data to determine whether the load voltages that existed before can be recovered through available control actions. If the prefault voltages cannot be recovered, the algorithm then suggests that some load voltages be reduced by a small amount. The possible control actions that the computer algorithm is able to suggest are the following:

- Switching in capacitive shunt at nodes where it is available
- Raising generator voltages
- Lowering the voltage at those load buses in which the desired voltage cannot be maintained (this is referred to as browning the voltage)

It should be noted at the outset that the order in which events occur internally to the algorithm is in no way meant to reflect the chronological occurrence of the physical events being simulated. The description of the algorithm's internal flow is for the edification of the reader only. Usage of the algorithm entails entering a scenario and receiving a list of suggested control actions.

14.3.2.1 Localized Response Immediately after a fault, only the nodes that are directly connected to the fault are flagged by the \underline{D} vector as having a reactive-power shortage. That is, in the case of a line outage, there is a reactive-power shortage at most at both ends of the line. In the case of a generator outage, only those nodes that are directly connected to the generator are seen as having a reactive-power shortage. Clearly, if these directly affected nodes have reactive-power shortages, some nodes that are directly connected to them will also experience a shortage of reactive power. However, the algorithm always begins with controls that are nearest to the fault. So, the algorithm first attempts to restore reactive-power balance to those nodes directly affected by the fault.

14.3.2.2 Urgency Determined by \underline{D} Magnitude From the formulation of the \underline{D} vector it can be seen that a shortage of reactive power is indicated by a positive \underline{D} -vector element. The magnitude of the \underline{D} element is within 10% of the magnitude of the reactive-power shortage at that node. Assuming a serious fault or set of faults, the algorithm determines the node that is in most urgent need of restored reactive power support by selecting the node whose corresponding \underline{D} element is most highly positive. The algorithm will continue to try to restore reactive-power balance to this node until it is no longer the node whose \underline{D} element is largest. Then the most urgent reactive-power mismatch is somewhere else, so the algorithm suspends consideration of the starting node and moves on to the new center of urgency. It should be stressed that until all elements of the \underline{D} vector are once again at or below zero, the E'_{lb} voltages are not an accurate representation of the current system load voltages. One large \underline{D} element might correspond to a whole region of low voltages. The algorithm suggests actions that it automatically takes internally. Only when these actions drive all of the \underline{D} elements back down to zero can the E'_{lb} voltages be taken as an accurate prediction.

14.3.2.3 Controls Are Located Using Tiers Once the algorithm has decided on which node to work on first, it next finds the closest controls. Any system can be redrawn with a designated node, say node i , as its “center” point. The nodes that are directly connected to i are said to be on the first “tier” away from i . All of the nodes that are directly connected to the nodes on the first tier, excluding other nodes on the first tier and i , are on the second tier, and so forth. When the system has been represented in this way, the tiers can be used to approximate which of the controls are closest. Clearly, a node that is on the third tier away from i could be closer in electrical distance to i than a node that is on the second tier. However, a node that is on the fifth tier away from i is not likely to be closer to i in electrical distance than a node that is on the first or the second tier. Once a list of the closest controls has been found using the tiers, some smart routine can be used to determine which of the closest 10 generators, for example, is electrically closest to i . Finally, it should be remembered that the electrical distance is not the only measure of a control’s effectiveness; the amount of reactive-power support available at the node must also be considered.

The algorithm does not try to determine which of the controls are closest across different tiers. The potentially inaccurate assumption is made that the controls that are on tiers closest to i should be applied first. Additionally, no attempt has been made to determine which of several controls on the same tier should be applied first. Neither of these issues is thought to be of critical importance. However, new versions of efficient searches based on different concepts of electrical distance [38] could be developed.

14.3.2.4 Browning Voltages and Partial Voltage-Based Load Shedding If the reactive power cannot be restored by raising the nearest generator voltages and by switching in the nearest shunts, then it is claimed that the voltage at i is not maintainable at the level indicated by E'_{lb} . When this has been determined, E'_{lb} , is lowered (or “browned”) by the amount necessary to drive \underline{D} at i to zero. An absolute lower bound on all load voltages E'^{abs}_{lb} is assumed to exist. If all control actions near i have been exhausted and browning E'_{lb} does not restore \underline{D} at i to zero without violating the bound E'^{abs}_{lb} , then the algorithm instructs the user so that E'_{lb} cannot be maintained without shedding load.

The importance of recognizing when load shedding has to be done is far reaching, since there are no other algorithms with this option. If for no other reason, this is an extremely important decision for political reasons. The algorithm can be used to provide the necessary technical evidence to justify unpopular actions, such as load shedding.

14.3.2.5 Flow of the Algorithm After the system numerical data has been read in and E'_{lb} has been set equal to E_i , the algorithm is ready for a fault simulation. When a fault has been selected, the algorithm begins to find control actions for recovering load voltages. Once the matrices H and $H - \hat{\lambda}I$ and the vectors $\hat{\lambda}$, c , and $g(1)$ defined in Section 14.3.1.3 have been built, $\hat{\lambda}$ can be determined and the \underline{D} vector can be calculated. The \underline{D} vector is then recorded so that D_1 is the

largest of the D elements, D_2 is next largest, etc. A second vector keeps track of the nodes to which each D element corresponds.

Let D_1 be located at bus i . The algorithm proceeds by representing the portion of the system directly surrounding i as a set of tiers. Because control actions taken at a great distance from i are unlikely to restore reactive-power balance at i , it is only necessary to represent the system around i to a depth of several tiers. At this point, the nearby shunts and generators can be found, as described earlier, and the control actions can be tried.

The algorithm proceeds by selecting one by one the nearest locations at which there are shunt capacitances available. At each capacitor bank, shunt is added incrementally until the location of D_1 changes. After all of the shunt at a particular bank has been used up, if neither the location of D_1 has changed nor the magnitude of D_1 has been reduced by at least some specified percentage, then that capacitor bank is marked as being relatively useless at restoring reactive power to i . To conserve reserve reactive power, the shunts at that node are switched back out and the next shunt location is considered. Once all nearby shunts have been either switched in or marked as useless, the algorithm proceeds on to raising generator voltages.

As with the shunts, the generators nearest to i are found and one by one each generator's voltage is raised until either the location of D_1 changes or the generator reaches its reactive power limit. Because raising a generator voltage is not inherently an incremental procedure, the process of raising voltages exactly the right amount is more involved. Initially, the algorithm raises the voltage by a very small increment. If that voltage increase is not sufficient to decrease D_1 at all, the generator voltage is further raised until there is some change in D_1 . Given the amount by which the generator voltage increase has decreased D_1 , it is possible to estimate the voltage increase required to drive D_1 to zero. As a rough approximation, this desired voltage increase $\Delta E_{\text{gen}}^{\text{new}}$ is

$$\Delta E_{\text{gen}}^{\text{new}} = \Delta E_{\text{gen}}^{\text{old}} \frac{D_1^{\text{new}} - D_1^{\text{old}}}{D_1^{\text{new}}} \quad (14.44)$$

As might be expected, the voltage change calculated in this way tends to be more than enough to drive D_1 to zero. It is preferable not to attempt a larger generator voltage increase than is necessary, thereby driving D_1 below zero, because of the reactive-power limits of the generator. Hence the generator voltage is increased by a fraction of the calculated amount and the procedure is repeated until either the generator hits its reactive-power limit or the location of D_1 changes. Once again, when the generator's reactive-power limit is reached, if the location of D_1 has not changed and D_1 has not been reduced by at least some specified percentage, then that generator is marked as useless at restoring reactive power. In this case, the generator voltage is returned to its previous level.

14.3.2.6 Spread of Reactive Support It remains to describe the means by which the reactive-power support spreads out from the control location to i , the location of the greatest reactive-power imbalance. Recall that a positive D

at i indicates a shortage of reactive power at i , meaning that there is currently insufficient reactive power support to recover. Similarly, a negative \underline{D} at j , where j is any load node, indicates an excess of reactive power at j , meaning that there is more than enough reactive-power support to recover $E_{lb,j}^t$. This excess reactive support will drive up the voltage at j . Let $E_{lb,j}^{t,new}$ be the new voltage at which \underline{D} at j is zero. To calculate $E_{lb,j}^{t,new}$, Eq. (14.39) is rewritten as

$$D_j = (H - \hat{\lambda}I)E_{lb,j}^t + \sum_{i=1, i \neq j} (H - \hat{\lambda}I)_{i,j}E_{lb,i}^t \quad (14.45)$$

(Note that when the \underline{D} elements are calculated, the j th element corresponds to bus j , because the \underline{D} elements have not yet been put into descending order.) If only $E_{lb,j}^t$ is adjusted, Eq. (14.45) becomes

$$\Delta D_j = (H - \hat{\lambda})_{i,j} \Delta E_{lb,j}^t \quad (14.46)$$

Because the term $(H - \hat{\lambda}I)_{i,j}$ is positive, a positive Δ_j implies a positive adjustment $\Delta E_{lb,j}^t$. Also, in this case, desired $\Delta_j = 0.0 - D_j = -D_j$. Thus

$$E_{lb,j}^{t,new} = E_{lb,j}^{t,old} - \frac{D_j^{old}}{(H - \hat{\lambda}I)_{i,j}} \quad (14.47)$$

where D_j^{old} is negative.

Upward adjustment of voltages at nodes with \underline{D} elements that are negative is made in order to drive the corresponding \underline{D} elements to zero. This adjustment will also supply further reactive-power support for the nodes that are directly connected to these nodes. Suppose the algorithm encounters a shortage of reactive power at i (\underline{D} at i is positive). Further suppose that there are no shunts available and the closest generator is in the third tier away from i . As the voltage at this generator is slowly raised, the \underline{D} elements corresponding to load buses directly connected to the generator become negative. The voltages at these buses, the j buses, are adjusted upward to drive their \underline{D} elements back to zero using Eq. (14.47). If the load buses that are directly connected to the load buses where the adjustment was made now have negative \underline{D} elements, the voltage at these load buses are also adjusted upward. This process is repeated until the adjustment made to surrounding load voltages is negligible. At this point, the evaluation is made as to whether D_1 has changed location. If it has not, the generator voltage is raised again. The whole process is repeated until the reactive-power limit of the generator is reached or the D_1 changes location.

It should be noted from the theoretical statements in Section 14.3.1.3 that the method is effective only if certain conditions on the minimum eigenvalue of the system matrix H are satisfied. This eigenvalue condition is one of the ways of expressing that common-sense remedial actions are effective, namely, that an increase in reactive-power demand always causes a decrease in voltage and vice versa. The eigenvalue condition for a small one-machine-one-load system

means that the method is fully reliable only if a postfault operating point is on the upper part of the PV curve [35,39]. The software for checking this condition is available [40]. The experience with the method reported in Refs. [41,42] suggests it be used under the assumption that the eigenvalue condition is met. For any case, a parallel execution of the eigenvalue test can be made, which is considerably slower. Test results show that the eigenvalue condition is consistently met even in the most severe cases studied.

14.3.2.7 Comparison of the D -Vector-Based Voltage Control with Other Methods It is generally hard to relate the actual value of the minimum eigenvalue of matrix H to the severity of the voltage problem. When the system has extremely low voltages, the eigenvalue often still remains positive, but quite smaller than one. If the system is operating in a robust manner with respect to voltage changes, typical order of magnitude of the λ_{\min} is 10. The fact that λ_{\min} remains positive while small, even under severe voltage reduction, indicates that methods based entirely on monitoring the character of the Jacobian are unlikely to detect the low-voltage problem. This is not the case with either the BRE method or the deviation vector D -based methods that do incorporate values of the minimum voltages suggested and monitor conditions under which voltages remain above these limits. These two methods are the only two known to the authors that allow for predicting if the voltages are below the acceptable limits, without computing the load flow.

Finally, as for the comparison between the BRE- and the D -based methods, one should recognize that the BRE method may lead to erroneous monitoring conclusions and corrective actions when the $\lambda_{\min} > 0$ condition (Theorem 5.4.3 in Chapter 5) is not met. This important detail is possible to appreciate through the fact that the BRE measure was proposed based on strong engineering insights about the power-system operation while not using theoretical developments. Scenarios in which an increase of generation, for example, does not necessarily lead to low-load-voltage corrections cannot be fully monitored and controlled by only monitoring the value of the BRE vector. This difficulty is recognized and it is suggested that the BRE be monitored at each bus and also its first and second tier sums ΔQ_i^I and ΔQ_i^{II} .

A simple analysis based on relations employed in proving conditions under which the localized response property of the QV propagation holds (section 14.3.1.1) can be used to show that scenarios in which

$$|\Delta Q_i^{II}| \leq |\Delta Q_i^I| \leq |\Delta Q_i| \quad (14.48)$$

for all $i = 1, \dots, n$ are identical to the scenarios in which the λ_{\min} remains positive. This is formally stated next as part of the convergence proof for the D -vector-based control algorithm.

Consider $k = 0$ as the starting step of the sequential (iterative) procedure described before to eliminate low-voltage problems. Then $k = 1, 2, \dots$ correspond to each set of corrective actions computed.

Claim Assuming system $\lambda_{\min} < 0$, then

$$|D_i|_{k+1}^{\max} \leq |D_j|_k^{\max} \quad (14.49)$$

for any $i, j \in 1, 2, \dots, n$. The method is completed when $|D_i|_{k+1}^{\max} \leq \varepsilon$.

The basis for Eq. (14.49) lies in the fact that as long as the minimum eigenvalue condition is met, any increase in voltage ΔE_i implies a decrease in the component of deviation vector D_i at the same bus, that is, $\Delta D_i \leq 0$. Similarly, any addition of a capacitor at i will decrease the component D_i at the same bus. The proof is outlined for corrective actions via changing terminal voltages at generators following formula (14.44) for spreading reactive deficiency. Start with $D_i \approx 0$, all $j = 1, \dots, n$ prior to load increase at bus i , for example. The load increase causes $\Delta D_i \geq 0$, and also $|\Delta D_i| = \max_{j=1, \dots, n} |\Delta D_j|$. Taking corrective actions according to formula (14.44) on the first tier results in several $\Delta E_i \geq 0$ needed to eliminate $\Delta D_i^I \geq 0$, $i \in n+1, \dots, n+k \cap I$. Each of these $|\Delta D_i^I| \leq |\Delta D_i|$ because of the way corrective actions are computed, taking into consideration that $\Delta E_i \geq 0$ always implies $\Delta D_i \leq 0$. If corrective actions are not sufficient on tier I, the same process takes place resulting in $|\Delta D_i|^{\text{II}} \leq |\Delta D_i^I|$, for $i \in n+1, \dots, n+k \cap I$, etc. If either the limit $|\Delta D_i|^{\max} \rightarrow 0$ or after all effective corrective actions are taken, load shedding occurs at buses for which $|\Delta D_i|^{\max} \geq \varepsilon$, $i \in 1, \dots, n$, this results in $|\Delta D_i|^{\max} \leq \varepsilon$ after load shedding.

Note that a rigorous proof could be provided to guarantee that the method will always converge, provided the load shedding is allowed, even in rare scenarios in which portions of the system have low-voltage problems while other portions have high-voltage problems. One such possible scenario could occur due to an outage of a very strong transmission line connecting buses i and j , shown in Figure 14.8. Assuming all elements of the \underline{D} vector are close to zero prior to the outage, with the line flow from bus i to bus j being Q_{ij} , the fault of this line results in $\Delta D_i \leq 0$ and $\Delta D_j \geq 0$.

In this scenario the method for eliminating high-voltage problems is initiated at bus i and, in parallel, the method for low voltages is started at bus j . It is most likely that the electrical distance between buses i and j after removing line ij is sufficiently high so that both methods actually converge before changes due to corrective actions for eliminating $\Delta D_i \leq 0$ actually are sensed at bus j , and

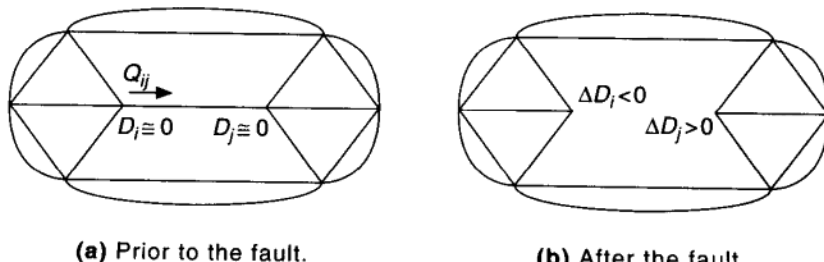


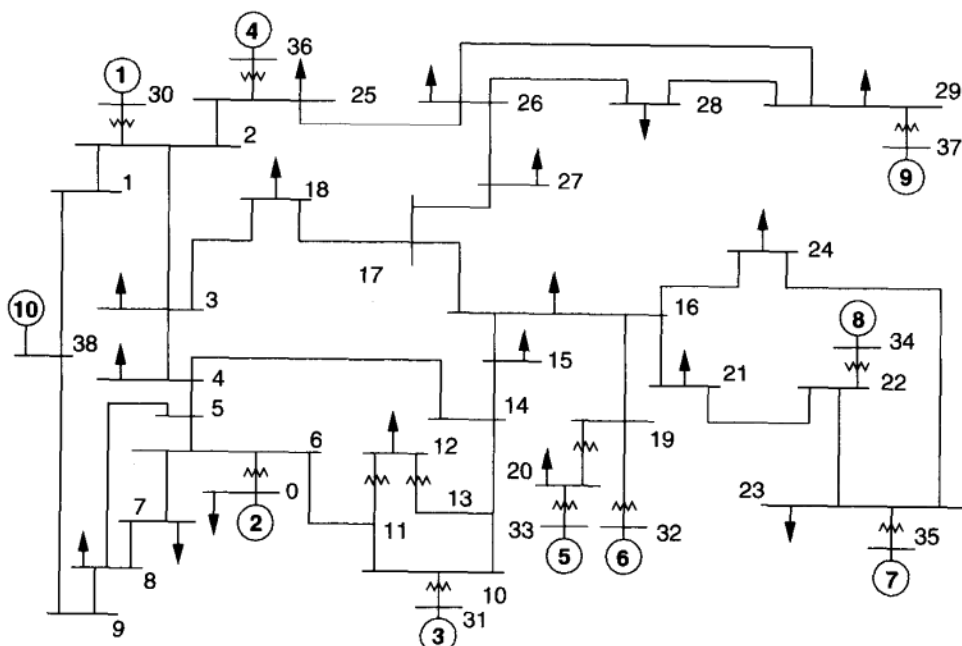
FIGURE 14.8 Line-outage scenario.

vice versa. If this electrical distance is not significant, a portion of the network in which the effects of changes from both sides are noticeable will be subject to corrective actions. This leads to some positive and some negative changes of deviations at the same buses, resulting in either high- or low-voltage problem, less severe than at the beginning.

It could be also argued that voltage problems in electrically coupled areas have to be either primarily high- or primarily low-voltage problems but not both. These are voltage problems in the sense that the deviation vector associated with either high voltages or with low voltages (but not both!) will have unacceptable components. This remains to be proven.

14.3.2.8 Test System for Illustrating the Deviation Vector D-Based Method [41] The test system used in this study has 29 load buses, 10 generators, 12 off-nominal transformers, and 46 branches. Figure 14.9 shows the one-line representation of this test system. The per-unit quantities are calculated with a 345-kV, 100-MV·A base. For the test runs described in this section, shunt capacitors were available only at buses 17 and 24. At bus 17, there is 180 MVar of shunt in 60-MVar increments and at bus 24, there is 150 MVars of shunt in 50-MVar increments.

Types of Scenarios Considered Two scenarios have been considered to demonstrate the function of the algorithm. One way to simulate a sudden shortage of reactive power is to increase the reactive power load at a bus. This action creates



a positive \underline{D} at that node. Hence, the first scenario is an increase of reactive load. The second scenario is a generator outage. The first scenario will be discussed in detail so that the reader can better understand the internal workings of the algorithm. Discussion of the second scenario will be limited primarily to its results.

FIRST SCENARIO For the first scenario, the reactive power load at bus 16 has been increased by 2 p.u. This creates a \underline{D} at 16 equal to 1.93. All other elements of \underline{D} remain at zero. In order to get rid of this reactive-power mismatch at bus 16, the system was internally “redrawn” with bus 16 at the “center.” Figure 14.10 shows how this representation of the system appears. The relatively large \underline{D} value at 16 indicates that the E'_{lb} elements corresponding to node 16 and surrounding nodes no longer accurately represent system voltages. Rather than adjusting them at this point, all efforts will first be made to drive \underline{D} at 16 to zero, thus “restoring” the voltage at 16 to its prefault value, although $E'_{lb,16}$ was never adjusted.

Control actions were investigated beginning with the shunt capacitors. From Figure 14.10, it can be seen that both bus 17 and bus 24, the locations of available

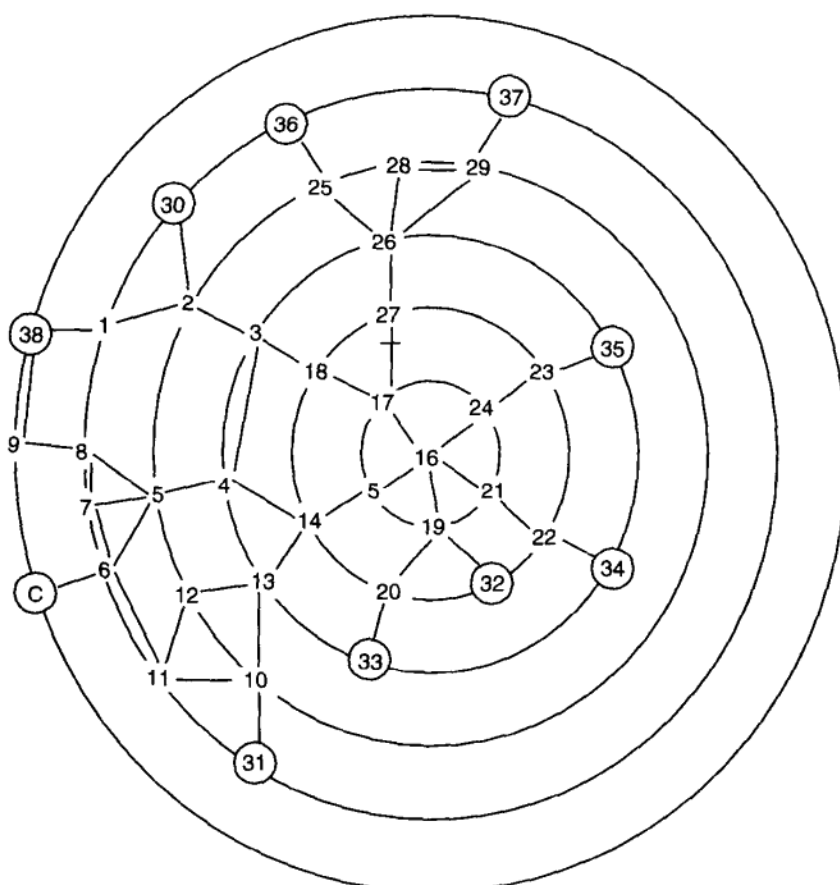


FIGURE 14.10 Alternative representation of the system showing tiers around bus 39.

shunts, are directly connected to 16. Beginning with bus 17, shunt is added in increments of 60 MVar until either all of the shunts has been used up to or \underline{D} at 16 shrinks below some other \underline{D} element. During the addition of shunt capacitance, no other positive \underline{D} elements are created, so node 16 will remain the focus of attention.

As each increment of shunt is added, \underline{D} at 17 becomes negative. This implies that $E'_{lb,17}$ is too low and it is adjusted upward until \underline{D} at 17 returns to zero. Using Eq. (14.47) and noting that for \underline{D} to return to zero after the addition of shunt, the product $(H - \hat{\lambda}I)_{17,17}E'_{lb,17}$ must remain constant, $E'^{t,new}_{lb,17}$ is found from:

$$E'^{t,new}_{lb,17} = \frac{(H - \hat{\lambda}I)_{17,17}^{old}}{(H - \hat{\lambda}I)_{17,17}^{new}} E'^{t,old}_{lb,17} \quad (14.50)$$

The new higher $E'_{lb,17}$ pulls up the voltages of buses 18 and 27 and provides more reactive-power support to bus 16. The need to adjust $E'_{lb,18}$ and $E'_{lb,27}$ upward is indicated by the negative values of \underline{D} at 18 and \underline{D} at 27. No other \underline{D} elements are negative at this point in the algorithm's flow. Because only voltages with negative \underline{D} elements are adjusted, $E'_{lb,16}$ is not adjusted unless the last control action was enough to drive the \underline{D} at 16 below zero.

To calculate the necessary adjustments to be made to a E'_{lb} element, Eq. (14.44) is used. Setting D'^{new}_{18} equal to zero,

$$E'^{t,new}_{lb,18} = E'^{t,old}_{lb,18} - \frac{D'^{old}_{18}}{(H - \hat{\lambda}I)_{18,18}} \quad (14.51)$$

Note that c_{18} and $g_{18}(1)$ have not changed. Once again, as elements of \underline{D} are being calculated, D_{18} corresponds to \underline{D} at 18. In this case,

$$D'^{old}_{18} = (H - \hat{\lambda}I)_{18,17}\Delta E'_{lb,17} \quad (14.52)$$

but in general it is possible for the negative \underline{D} to be the result of several voltage changes. Because the \underline{D} vector is used as a stepping stone in arriving at the adjusted voltages, it is not necessary to note which voltage changes are causing the negative \underline{D} elements.

Once $E'_{lb,18}$ has been adjusted, $E'_{lb,27}$ is adjusted in a similar way. Nodes 18 and 27 will then supply additional reactive-power support for nodes 3, 17, and 26. The \underline{D} elements corresponding to these nodes will be negative and the E'_{lb} elements at nodes 3, 17, and 26 need to be adjusted upward. After these adjustments have been made, the E'_{lb} elements at nodes 2, 4, 18, 25, 28, 29, and 27 will need to be adjusted. The process continues until either the negative \underline{D} elements shrink below a certain bound or the voltage adjustments become negligible.

At this point, assuming \underline{D} at 16 is still positive, the whole process is repeated. Another increment of shunt is added at 17 and all of the E'_{lb} elements corresponding to nodes with negative \underline{D} are adjusted. As has been said, this process continues until all of the shunt at 17 has been used up. Then the shunt at 16 is incrementally switched in. If all of this shunt is not enough to drive \underline{D} at 16

below zero, the algorithm begins to raise voltages. Voltage changes are dealt with in much the same way, except that the limitation on the generator voltage is the reactive-power limit of the generator. Each voltage is raised incrementally in the way described earlier. In this way the algorithm investigates the results of each control action. When all of the reactive power from a control source has been used up, if the D_1 has not been reduced by at least 10%, this control source is marked as useless in reducing D_1 . If a control source has been deemed useless, E'_{lb} and \underline{D} are reset to their values before that control source was considered, the control action is undone, and the next control source is considered.

When the algorithm has eliminated all positive \underline{D} elements, the user is supplied with a list of control actions. For the scenario described previously, the control action recommended by the computer were

- Switch in 180 MVar of shunt at node 17.
- Switch in 100 MVar of shunt at node 24.

Three voltage vectors are introduced here for the purposes of discussion. E_i is the vector of prefault voltages, $E^{lf,nc}$ is the vector of load-flow voltages that result when no corrective actions are taken, E'_{lb} is the algorithm's final estimate of the voltages that result when the suggested corrections are taken and $E^{lf,c}$ is the actual load-flow solution when the suggested corrective actions are taken. Figures 14.11, 14.12, and 14.13 show the changes in the load voltages, $E^{lf,nc} - E$, $E'_{lb} - E$, and $E^{lf,c} - E$, respectively.

Therefore, the claim of the algorithm is that the voltage levels described by Figure 14.12 are a lower bound on the actual voltage levels described by Figure 14.13. Furthermore, Figure 14.11 shows the state of the system if no actions were taken. A close comparison of Figures 14.12 and 14.13 reveals that the algorithm is performing well in estimating the voltage levels that arise after the actions are taken.

SECOND SCENARIO For the second scenario, generator 34 was switched off. Because generator 34 was only connected to bus 22, only bus 22 initially has a positive \underline{D} element. The algorithm suggests the following corrective actions:

- Switch in 150 MVar of shunt at bus 24.
- Switch in 180 MVar of shunt at bus 17.
- Raise the voltage at bus 35 by 0.008 to 1.071.

Figures 14.14, 14.15, and 14.16 show $E^{lf,new} - E$, $E'_{lb} - E$ and $E^{lf,c} - E$, respectively.

Clearly the voltages at both buses 17 and 24 rise when the shunts are added at those nodes. These voltage changes cause other nearby voltages to rise, especially at nodes 18, 27, 16, 15, and 23. E'_{lb} is again a close lower bound on $E^{lf,c}$. From Figure 14.15, it can be seen that the prefault voltage at bus 22 was exactly recovered.

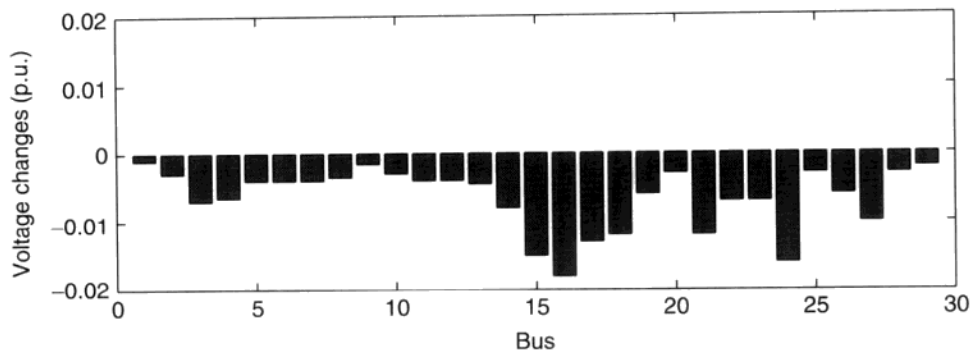


FIGURE 14.11 Scenario 1, reactive load at 16 raised by 2 p.u.; load-flow solution *without* corrective actions.

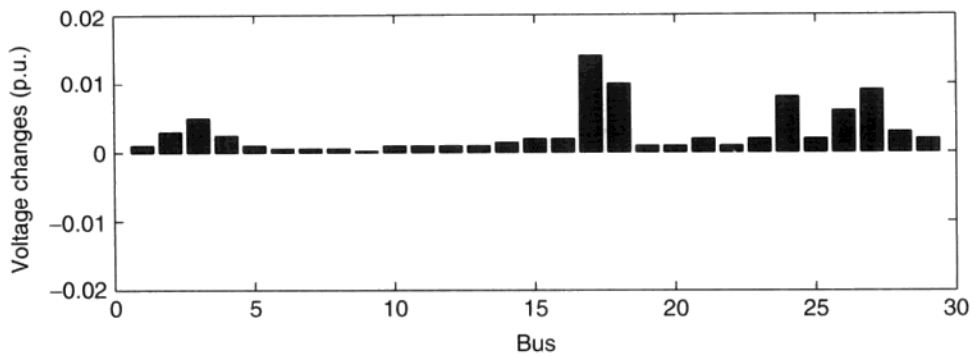


FIGURE 14.12 Scenario 1, reactive load at 16 raised by 2 p.u.; algorithm prediction with corrective actions.

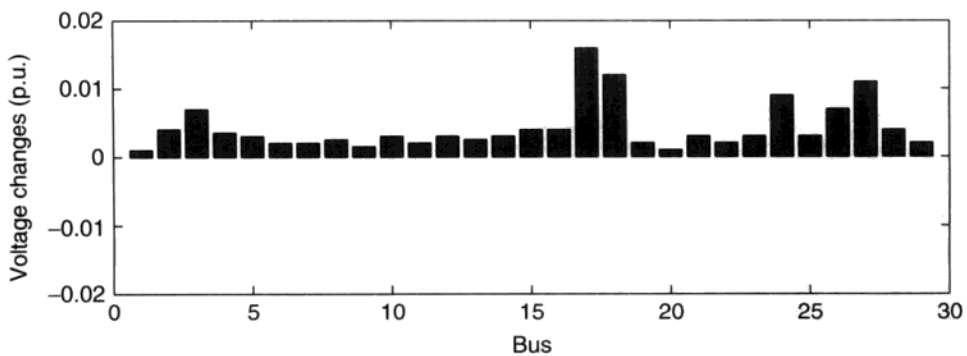


FIGURE 14.13 Scenario 1, reactive load at 16 raised by 2 p.u.; load-flow solution with corrective actions.

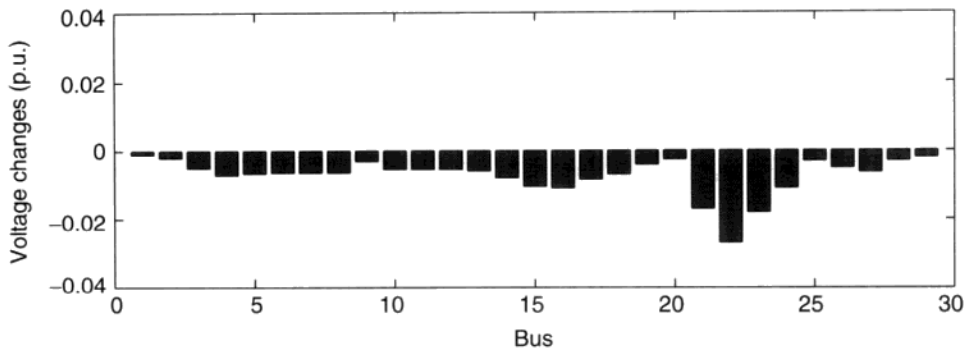


FIGURE 14.14 Scenario 2, generator 34 outage; load flow solution *without* corrective actions.

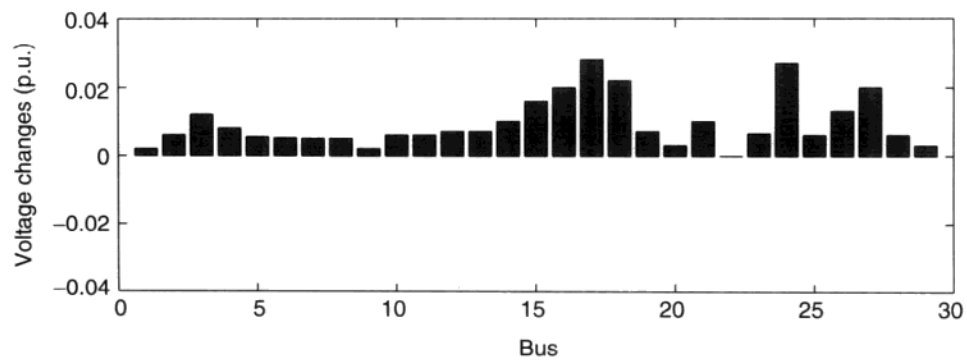


FIGURE 14.15 Scenario 2, generator 34 outage; algorithm prediction with corrective actions.

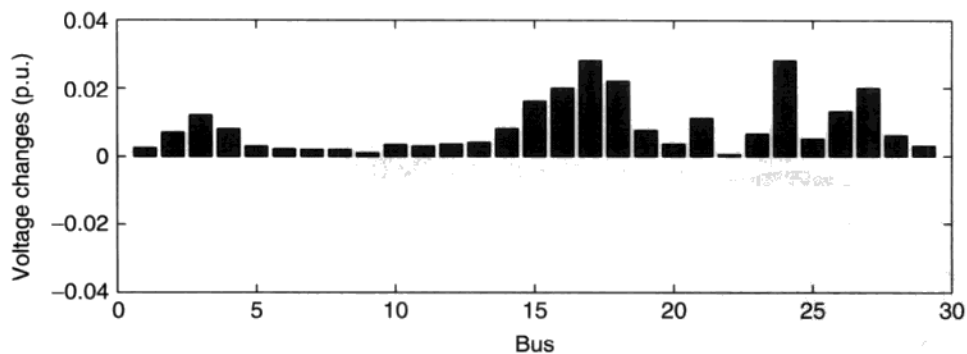


FIGURE 14.16 Scenario 2, generator 34 outage; load-flow solution with corrective actions.

Decisions about Capacitive Shunt Locations The algorithms can be used to compare the resultant voltage profiles obtainable when shunts are available at different nodes in different increments. For instance, by running the algorithm with shunts available at different locations and in different incremental amounts, decisions can be made at the planning stage about how best to distribute the capacitive shunt in terms of both absolute and incremental sizes at various locations around the network. This approach differs from just running a series of load flows in that as the algorithm runs it evaluates the best (defined loosely) set of shunts to switch in.

In conclusion, an algorithm has been presented for very effective monitoring and control of systemwide voltages. Three striking characteristics are the following:

- It is applicable for large outages.
- The computational effort for its implementation does not depend much on the power system size.
- It has the nature of rule-based (or artificial intelligence) algorithms, in the sense that it reflects inherent properties of voltage-change propagation through the system, such as localized response.

The method originally introduced in Ref. [41] has been tested for specific voltage problem scenarios on the New England Power Pool System that can be found in Ref. [42].

14.3.3 Clusterwide Approach with Full Information and Flexible Clustering

This method introduces an efficient way of controlling or “managing” the active and reactive resources of the system on line in such a way as to maintain viable voltage and current *profiles*, that is, to keep all voltages within normal limits and all currents within their thermal limits. The disruption to system operation is minimized by using tools of control in priority order. The computational burden is minimized by restricting the computations to moderate size clusters within the large system. The clusters consist of sets of violations and control tools that are effective on these violations along with such nonviolated elements that are responsive to the controls within the cluster. A novel, simple, and effective method for finding the clusters is introduced in Ref. [2,31]. Because of the limited size of the clusters the computation of the controls is inherently fast, but in addition a fast and efficient algorithm is introduced. This overall approach can be operated as an “emergency control” or an ongoing dispatch. In the latter case it will routinely handle any emergencies of the type consisting of more or less widespread voltage and current problems within segments of the system. On the other end of the spectrum, these techniques can be used effectively in establishing a restoration sequence or plan for a failed system (with or without blackout).

First, a general algorithm for real- and reactive-power corrective actions based on this clusterwide approach is introduced. A by-product of this method is yet

another method that assumes effects of real-power changes on voltage to be insignificant and was originally reported in Ref. [43]. This method forms a basis for the work reported later in Ref. [44].

The proposed approach can be summarized (Figure 14.17) as follows.

1. Monitoring bus voltages E and line currents I that violate the respective ranges of permissible values (block 1, Fig. 14.17).
2. Establishing clusters of lines and buses that contain a group of specific violations and of all associated controls (of any priority) that are effective on this group of violations and on nonviolated lines and buses within the cluster but that have negligible effect outside the cluster (block 2, Fig. 14.17).

There is an inherent tendency of such clusters to exist because of the diagonal dominant tendency of the sensitivity matrix and because specific violations themselves tend to be clustered since they are associated with some more or less localized events. Even in the case of major and widespread storm damage involving lightning and tornadoes, a clustering of violations usually occurs naturally. Often it is possible to subdivide too large clusters by omitting some controls that couple the subdivisions [45]. Of course in some cases the entire area will be found to be one cluster, which may or may not be subdivided. Notice that this also is a way of identifying a systemwide problem.

3. Establishing for each cluster a group of high-priority controls (above priority cutoff p) that can approximately cover the total control requirements on the cluster to remedy its violations. Then p can be the starting point of the algorithm. Since load dropping is the ultimate recourse as the lowest priority control, there will always exist a p (block 3, Fig. 14.17).
4. Carrying out an algorithm to find a solution for eliminating violations within the cluster using the group of controls of higher priority than p . If no solution is found the algorithm is repeated using $p + 1$ priority controls within the cluster. If a solution is found at p and if time is available, another solution may be tried to find out of a less-disruptive solution is possible (block 4, Fig. 14.17).
5. Implement solution. If the solution does not involve disruptive control (no load dropped, no reduced voltage), normal operation is reestablished forthwith. If the solution involves disruptive measures, then the restoration control regime is initiated to clear up the disruptions. The latter is outside the scope of this text (block 5, Fig. 14.17).

If operated continuously (every 5 min to 10 min) on line, this process will take care of mild violations of operating limits as well as severe emergencies, that is, both dispatch and emergency-control type situations. In fact, along with proper unit commitment it could alleviate much of the heavy computational burden of security monitoring. The same process can be quite useful in choosing or planning the restoration sequence for a failed system. The proposed methods would provide major savings in computation time since all computations are

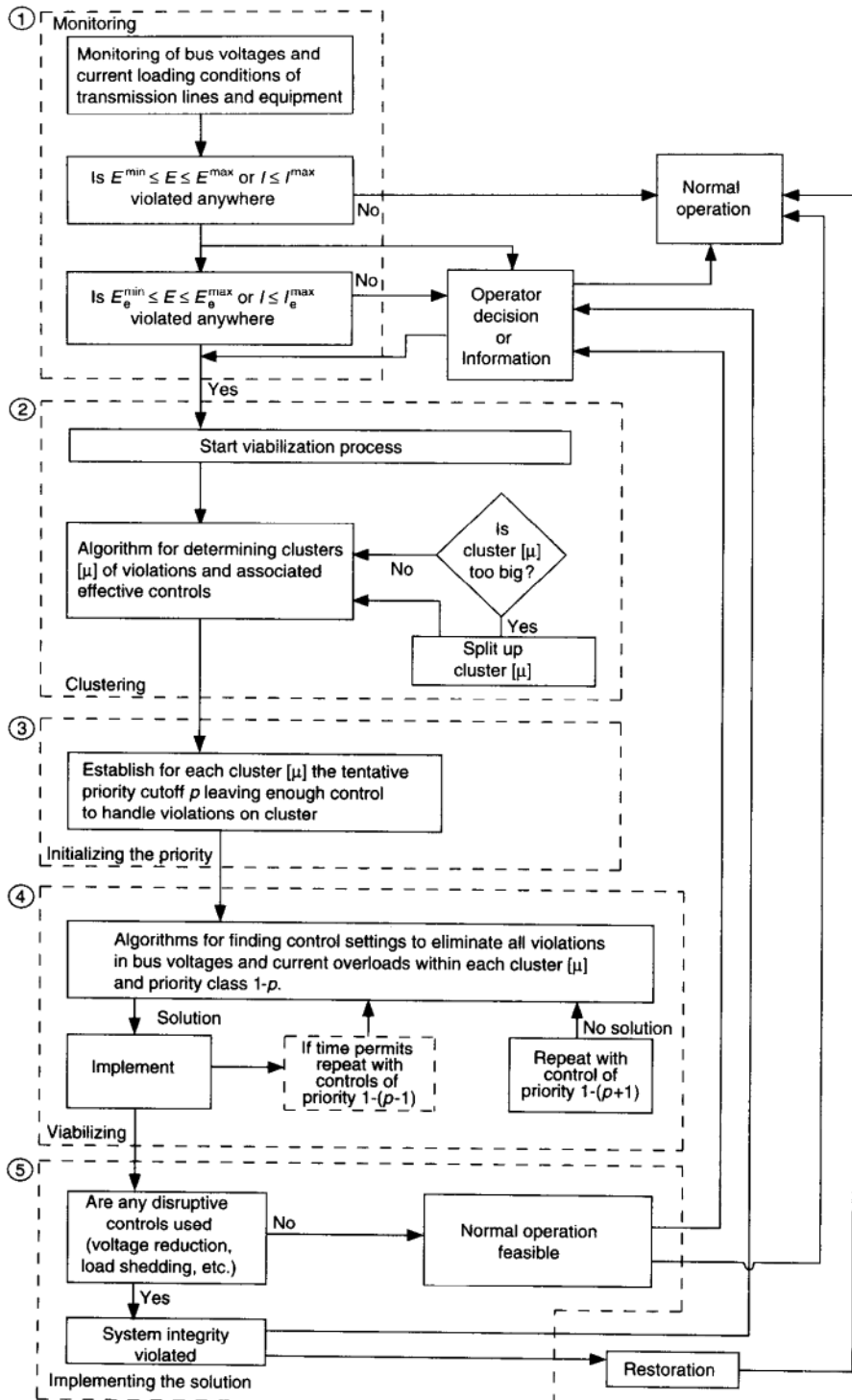


FIGURE 14.17 Block diagram for real- and reactive-power management by cluster viabilization.

carried out on moderate size clusters, even on very large systems. In fact the cluster size is largely independent of the system size.

Note: In the competitive electric power industry it would be highly desirable to post the structure of these clusters, as they modify in response to various market activities. This knowledge would create a transparent information to the system users so that they adjust over time and actively participate in maintaining acceptable system operation [3].

14.3.3.1 Least Disruptive Solution; Priorities of Controls For the purposes of the problems treated here the least disruptive solution is defined as the set of controls selected in such a manner that each priority class of controls is exhausted before the next lower one is used (other definitions are possible [2]).* This implies the existence of an interleaved priority list, incorporating both active- and reactive-power controls. Such a list of decreasing priorities may be organized as follows:

1. Reactive-power sources such as static Var compensation or capacitors
2. Active power from spinning reserves
3. Use of on-load tap changers
4. Voltage rescheduling at primary buses to normal limits E^{\min} or E^{\max}
5. Voltage rescheduling at secondary buses to normal limits E^{\min} and to emergency limits E_e^{\min} at primary buses
6. Utilizing temporary overload of lines within emergency current range I_e^{\max}
7. Reactive power from adjusted generator excitation
8. Interruptible loads
9. Voltage reduction to emergency limits at primary and secondary buses
10. Power from cold start of generators
11. Load shedding in two or more subpriority classes.

This list is, of course, purely illustrative and incomplete. Each utility would establish their own complete listing of their priorities. The tolerance ranges of bus voltage and line currents usually are defined in two steps such as

- Normal voltage range $E^{\min} \leq E \leq E^{\max}$
- Normal current range $0 \leq I \leq I^{\max}$
- Emergency voltage range $E_e^{\min} \leq E \leq E_e^{\max}$
- Emergency current range $I^{\min} \leq I \leq I^{\max}$ for T_e^{\max} minutes.

There may be more than one step of emergency line current ratings; if so, then each has its own time limit.

* In a competitive electric power industry priority class of controls is likely to be influenced by the economic decisions of the system users themselves, in addition to the system operator's decisions.

14.3.3.2 Off-Line Database Computed Once for the System In this section certain preliminary computations for the establishment of a database are discussed. These involve the computation of a sensitivity matrix. This is done off-line for some typical load conditions and stored. When network connections change, simple and fast updating procedures based on the matrix inversion lemma are available. These computations need to be done only once for the system.

14.3.3.3 Sensitivity Matrix and Its Role in Specific Viabilization The system is described by the usual load-flow equations. To monitor thermal overloads the magnitude of the line currents (which are not state variables) will need to be computed from the bus voltages and their phases as follows:

$$I_{jk} = C_{jk} \left(\frac{E_j^2 + E_k^2 - 2E_j E_k \cos(\delta_j - \delta_k)}{Z_{jk}^2} + \frac{E_j^2}{Z'_{ij}^2} \right. \\ \left. + \frac{2E_j E_k \sin(\delta_j - \delta_k + \zeta_{jk}) - 2E_j^2 \sin \zeta_{jk}}{Z_{jk} Z'_{jk}} \right)^{1/2} \quad (14.53)$$

Note that real power flow of the line instead of current can be readily substituted. Summarizing the load-flow constraints and Eq. (14.53) in general vector form

$$\begin{aligned} f(x, u) &= [f_1(x, u) & f_2(x, u) & \dots & f_n(x, u)] = 0 \\ I &= h(x) \end{aligned} \quad (14.54)$$

Equation (14.54) implicitly determines the relation

$$y = [E \quad I] = g(x, u), \quad u = [E' \quad P' \quad Q'] \quad (14.55)$$

between controls targets or outputs y , state x , and control u . y here consists of all line currents and noncontrolled bus voltages E_i . State $x = [E_i \quad Q_i \quad \delta_i]$ consists of voltage phase δ_i , noncontrolled bus voltages E_i , and noncontrolled reactive injection Q_i . The controls are (equivalent for voltage reduction, etc.) controlled real P'_i and reactive Q'_i injections and controlled bus voltage set points E'_i (either the voltage E or reactive power Q can be a control at any particular bus). Since all the relations, f , h , and g are analytic, it is feasible to write

$$\Delta y = y - g(x_0, u_0) = \frac{\partial g}{\partial u} \Big|_{x_0, u_0} \Delta u + o(\Delta u^2) = A \Delta u + O(\Delta u^2) \quad (14.56)$$

provided $u = u_0 + \Delta u$ and x_0 is the state corresponding to the initial setting u_0 of the controls. A is the sensitivity matrix. Coefficients of A can be explicitly computed, and formulas are available in [45]. In sectional viabilization large adjustments of controls are not unusual so a linearized solution is not really satisfactory. On the other hand, such crises usually affect only a limited segment

of the system so that a systemwide full nonlinear programming solution is also not justified. Hence a two-level approach is introduced here:

1. The system is divided into essentially decoupled clusters of violations and associated controls. Since the selection of controls to be used on groups of violations is a somewhat discretionary matter rather than a precise, mathematically defined problem such selection may well be based on approximate methods. The sensitivity matrix has a major role in the clustering process.
2. Computing the control amounts for eliminating violations within each cluster. Precise results are needed here, consequently full nonlinear computation is used. The computation of control amounts is not based on the sensitivity matrix unless the changes are small.

Note that the sensitivity matrix needs to be computed only once for a few typical load conditions. It can be carried as a database in the computer memory that can be updated when network connections change by updating only four elements [46]. Only those elements of the matrix that are larger than a threshold need be stored.

14.3.3.4 Control Pairs and, Special Format for Active Power Control Tools: Dealing with the Slack Bus-Induced Asymmetry When a reactive-power injection is changed for control purposes it will be effective over a limited area, that is, only nearby buses or lines will show significant sensitivity to such control. This is because reactive-power losses are large and because numerous voltage-controlled buses will absorb the excess injection. When an active-power injection is changed, however, an almost equal compensating change will occur at the slack bus. This is because active-power incremental losses are small so that the bulk of changes are taken up by the slack bus. Consequently, large sensitivity values will appear around the slack bus, which are spurious, because the slack bus is but a computational artifice, not a physical component of the system. To get around this problem, a transformation is introduced in Ref. [2] to replace individual active-power controls by self-balancing pairs that produce no activity around the slack bus. More precisely, only an activity corresponding to the small incremental loss will appear, which is then neglected. Accordingly this transformation will be based on a lossless network. This transformation can be found in Ref. [2].

14.3.3.5 On-Line Control of Real and Reactive Power for Viability in Voltage and Thermal Load After the preceding preliminaries a few details of the viabilizing process as sketched in Figure 14.17 can be discussed. In this discussion the main divisions distinguished in Figure 14.17, that is, monitoring, clustering, initializing, viabilizing, and implementing the solution will be described in sequence as subsections. The basic aim of the five operations is outlined in conjunction with Figure 14.17.

14.3.3.6 Monitoring Computer surveillance is used to note the appearance of violations of bus voltage limits or thermal overload limits (block 1, Fig. 14.17). If no abnormality is present, normal operation continues.

If one or more violations occur outside the normal voltage or current limits but within the emergency limits, the operator is notified (preferably by an easy-to-read display). The operator can then opt for continuing normal operations without taking emergency steps or for putting the viabilizing process in operation.

When violations that exceed the emergency ratings are observed by the computer program, the viabilizing process is started automatically. Of course, the operator is still notified and informed of the situation and has the ultimate option of implementing the controls.

14.3.3.7 Clustering Algorithm The sensitivity matrix, of course, will not be sparse, but most of its entries represent effects from distant control tools and thus they are very small. Such small effects have no practical significance, so it is logical to replace by zero all matrix entries that are smaller in absolute values than a threshold θ . The result is a sparse rectangular matrix, the reduced A matrix A^r , a small-scale example of which is shown in the upper left corner of Figure 14.18.

Here the rows of the reduced matrix A^r are labeled with the control target points $y_i = E_i$ or $y_i = I_{ij}$ and the columns with the independent controls u_j including reactive-power injections and active-power injection pairs. Note that there could be more independent controls than states since each bus may contain several controls of various types and priorities. The A^r matrix is always sparse if θ is selected high enough but it also is usually convertible to a block-diagonal form of decoupled clusters. An efficient algorithm to accomplish such decoupling, illustrated in Figure 14.18, is the following:

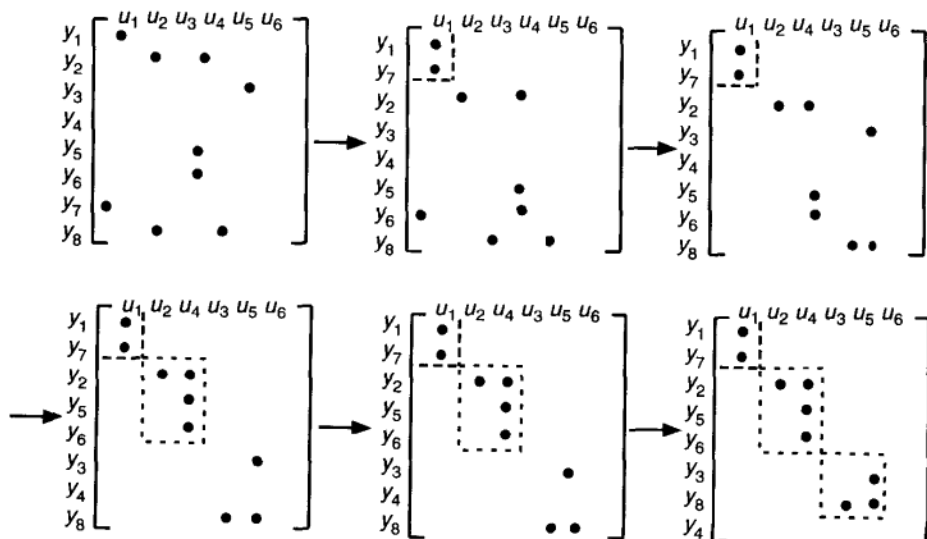


FIGURE 14.18 Illustration of the clustering algorithm.

Step 1. Termination of grouping the cluster denoted $\mu - 1$ and beginning the grouping of the cluster μ .

Step 2. Scan the first row of A^r not yet covered and collect the column indices of all nonzero elements (if none, go to the next noncovered row) into the initial column index set S_c^μ .

Step 3. Scan all columns listed in S_c^μ and collect the row indices of all nonzero elements into the initial row index S_r^μ .

Step 4. Repeat Step 1 for all rows identified in S_r^μ and produce the second (nonredundant) column S_c^μ .

Step 5. Repeat Step 2 and continue.

Termination Step. When two consecutive steps give the same S_c^μ or S_r^μ , these identify the components of cluster μ . The process is then reset to Step 0 to find cluster $\mu + 1$.

Example Apply the algorithm to the matrix A^r as listed in the top left of Figure 14.18.

Step 1. $\mu = 1$

Step 2. $S_r^1 = 1, S_c^1 = 1,$

Step 3. $S_r^1 = 1, S_c^1 = 1,$

Step 4. $S_r^1 = 1, S_c^1 = 1,$

Hence y_1, u_1 and y_7, u_1 form cluster $\mu = 1$.

Step 1. $\mu = \mu + 1 = 2$

Step 2. $S_r^2 = 2, S_c^2 = 2, 4$

Step 3. $S_r^2 = 2, 5, 6, S_c^2 = 2, 4$

Step 4. $S_r^2 = 2, 5, 6, S_c^2 = 2, 4$

Hence $y_2, u_2, y_5, u_4, y_6, u_4$ form cluster $\mu = 2$.

The final form of clustering becomes:

Step 1. $\mu = \mu_1 = 3$

Step 2. $S_r^3 = 3, S_c^3 = 5$

Step 3 and Step 4. $S_r^3 = 3, 8, S_c^3 = 3, 5$

Step 5. $S_r^3 = 3, 8, S_c^3 = 3, 5$

Hence $y_3, u_5, y_8, u_3, y_8, u_5$ form cluster $\mu = 3$.

In Figure 14.18 the process is illustrated by actually shuffling rows and columns. This of course does not imply changing storage locations in a computer implementation. Note that in this example control u_6 is not sufficiently effective on any bus y , while no control is effective enough on bus y_4 . Such occurrences may require system modification. The clustering algorithm just described makes it possible to

divide the system into clusters of violations and associated control tools that will be effective on violations within the cluster and not otherwise. Actually, since there is a possibility that the use of the controls may cause new violations, it will be necessary to include in each cluster such nonviolated buses and transmission lines which are sensitive to the controls in the cluster. This can be accomplished in the following sequence of operations.

- Stage 1 Retain all columns, that is, all controls in the reduced sensitivity matrix A^r , but only those rows that represent violated voltage and thermal overload sites. Perform the clustering algorithm.
- Stage 2 Retain all rows in A^r whether they are violated or not but only those controls (columns) that were selected for clusters in Stage 1. Perform the clustering algorithm. The results are the clusters to be used in viabilization.

The two-stage approach is necessary because using only Stage 2 the clusters would be coupled by controls that are not effective on the violations. As a result, few clusters would be identified and so the viabilizing process would require more computation than really necessary. After successful clustering the viabilization can be performed separately for the individual clusters without concern for the rest of the system. Also the clusters contain only such controls that are known to be effective on the violations. This further reduces computational demands. If the clusters turn out to be too large, and if there is enough control on the system, it is possible to split up clusters by omitting some of the controls that cause coupling [45].

14.3.3.8 Initialization Since the actual computation of viabilizing controls is to be done on a fully nonlinear model it will be desirable to search for a suitable starting point of the algorithm for the priority range that will provide approximately enough control for viabilization. Such an approximate search may logically be based on the linearized form of the problem shown in terms of the sensitivity matrix A . In fact the linearized form of the viabilizing problem for each cluster $[\mu]$ is readily written as

$$A_{[\mu]}^r \Delta u_{[\mu]} \leq \Delta y_{[\mu]} \quad (14.57)$$

Here $A_{[\mu]}^r$ is the sub-block of the reduced sensitivity matrix belonging to cluster $[\mu]$ (see Fig. 14.18). Also,

1. For violated buses and/or lines, $\Delta y_{[\mu]}$ is the difference between the nearest limit and the present, violated, value.
2. For nonviolated buses and/or lines $\Delta y_{[\mu]}$ is the difference between the present, nonviolated value and the nearest limit. Finally, $\Delta u_{[\mu]}$ is the vector of approximate control adjustments within the cluster $[\mu]$ required to put all bus voltages and line currents in the cluster $[\mu]$ back within limits.

The idea then is to find a priority level p for which enough control is available to have a feasible solution of Eq. (14.57) such that no feasible solution is found on the $p - 1$ priority level. This implies a search over various priority levels for solutions of Eq. (14.57) within each cluster $[\mu]$.

It is still not a trivial matter in general to find a solution for the problem stated in Eq. (14.57). Fortunately there was a method introduced recently for this purpose [47] that is fast enough to allow considerable searching. A search for the highest priority group $(1 - p)$ of controls to ensure a solution can then be undertaken using Eq. (14.57) without undue computational or time demand. Of course this is an approximate result for the priority class p , but it also contains an approximate solution for the control settings $\Delta u_{[\mu]}$.

14.3.3.9 Viabilizing Algorithm The viabilizing algorithm (block 4, Fig. 14.17) has the task of eliminating voltage and current violations within the cluster while preventing the creation of new violations within the cluster. Elements outside the cluster have by definition and construction only marginal sensitivity to the controls in the cluster; thus the outside system can be neglected and the boundary (the neighboring buses connected to the buses of the cluster, buses proper) bus voltages can be considered fixed (computationally a set of slack buses with fixed angle and magnitude).

The division of roles within each cluster is sketched in Figure 14.19. In each cluster there is a set of lines or line currents and a set of buses or bus voltages. Each line and/or bus is identified with a condition equation for flow balance. Each bus voltage and/or line current is subject to a set of inequality constraints. Some $[V_\mu]$ are currently violated, and others are within the constraints $[N_\mu]$, that is, nonviolated bus voltages and line currents are sensitive to the controls. Currents respond strongly to both active and reactive power and voltages mostly to reactive power—in some cases active power influence on voltage can be neglected (as indicated by dotted line in Fig. 14.19; the decoupled load flow). All controls $[C_\mu]$ are located as buses or pairs of buses that may be violated or nonviolated. A bus may contain several independent active and reactive controls of different priority rating. Either the reactive power Q^{ref} or the voltage E^{ref} (at PV buses) but not both can serve as control variables. All control power sources (active or reactive) are subject to inequality constraints. In mathematical terms the following then applies.

14.3.3.10 Problem Statement for Viabilizing

- Find E_i and controls ΔQ_i and ΔP_i such that

$$\begin{aligned} -\Delta P_i + f'_i(x, u) &= -P_i - P_{Di} - \sum C_{ij} \left(\frac{E_i^2}{Z_{ij}} \cos \zeta_{ij} - \right. \\ &\quad \left. \frac{E_i E_j}{Z_{ij}} \cos(\delta_i - \delta_j + \zeta_{ij}) \right) = 0 \end{aligned}$$

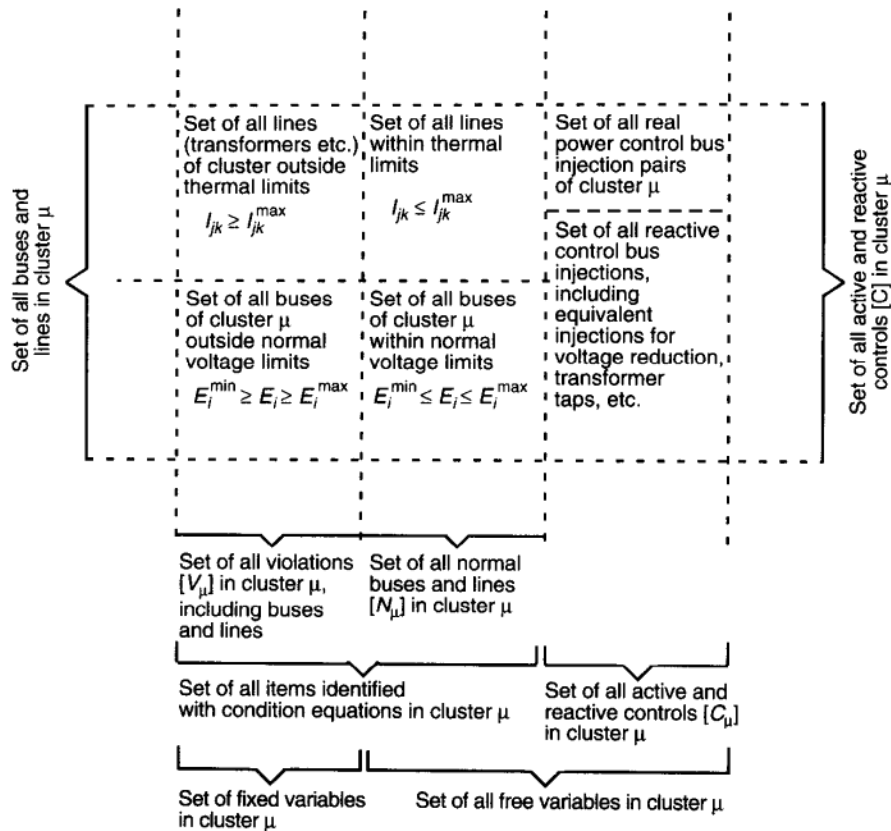


FIGURE 14.19 Division of roles within the cluster μ .

$$\begin{aligned}
 -\Delta Q_i + f''_i(x, u) &= Q_i + Q_{Di} - \sum C_{ij} \left(\frac{E_i^2}{Z_{ij}} \sin \zeta_{ij} - \right. \\
 &\quad \left. \frac{E_i E_j}{Z_{ij}} \sin(\delta_i - \delta_j + \zeta_{ij}) \right) \\
 &\quad + \frac{E_i^2}{Z_{ij}} \sin \zeta_{ij} + \frac{E_i^2}{Z_i} \sin \zeta_i = 0 \\
 I_{ij} &= \left(\frac{E_i^2 + E_j^2 - 2E_i E_j \cos(\delta_i - \delta_j + \zeta_{ij})}{Z_{ij}^2} + \frac{E_i^2}{Z'_{ij}} \right. \\
 &\quad \left. + \frac{2E_i E_j \sin(\delta_i - \delta_j + \zeta_{ij}) - 2E_i^2 \sin \zeta_{ij}}{Z_{ij} Z'_{ij}} \right)^{1/2} \quad (14.58)
 \end{aligned}$$

where P_i , Q_i , P_{Di} , and Q_{Di} are, respectively, active and reactive generation load injections at bus i and are satisfied for all buses i, j on the cluster under the following set of constraints:

Constraint set 1 For all $h, l \in [N_{[\mu]}]$, that is, for all normal buses or lines, the normal voltage range is $E_h^m \leq E_h \leq E_h^M$, the normal current range is $0 \leq I_{hl} \leq I_{hl}^M$, or optionally, the emergency voltage range is $E_e h^m \leq E_h \leq E_e h^M$, and the emergency current range is $0 \leq I_{hl} \leq I_{ehl}^M$ for T_e^M minutes.

Constraint set 2 For all $k, m \in [V_{[\mu]}]$, that is, for all violated buses or lines:

$$\begin{aligned} E_k &= E_k^M && \text{if } E_k^* - E_k^m \leq E_k^* - E_k^M \\ E_k &= E_k^m && \text{if } E_k^* - E_k^M \leq E_k^* - E_k^m \\ T_{km} &= I_{km}^M && \text{if } I_{km}^* - I_{km}^M \geq 0 \text{ and } k, m \in [V_{[\mu]}] \end{aligned} \quad (14.59)$$

where the asterisk denotes the original violated value (or the value obtained in the previous step of the algorithm). Note that these constraints set all violated values back to the nearest limit.

Constraint 3 For all $r, s \in [C_{\mu}]$, that is, all reactive-power controls and real-power control pairs at or between buses r and s

$$\begin{aligned} Q^{ref,m} \leq Q_r^* &\leq Q^{ref,M} \\ -\Delta P_{rs}^m &\leq \Delta P_{rs} \leq \Delta P_s \leq \Delta P_{rs} \end{aligned} \quad (14.60)$$

where the asterisk denotes the original value at (or the value obtained in the previous step of the algorithm).

2. Each cluster is viabilized separately. The phase and magnitude of voltages on buses connected to the boundary buses of the cluster that falls into the priority class $1 - p$ is used.
3. A subset of the controls on the cluster that falls into the priority class $1 - p$ is used. Note that this problem statement sets all violated voltages and currents back to the nearest limits (14.59) and leaves normal and control bus voltages and all normal currents to float between the chosen limits. This, of course, is not a unique way for viabilizing the system, although it is certainly a reasonable one. In fact there is no unique solution if the only aim is to maintain a voltage and current profile within set limits. Yet in most situations of system operation this is all that is required, especially in dealing with emergencies.

If desired, however, the problem statement can be easily modified to define a unique solution by requiring the minimization of some quantity such as line losses or fuel cost. Then there results an alternative problem statement.

14.3.3.11 Alternative Problem Statement for Viabilizing Omit conditions (14.59) and extend normal limits to all buses and lines within the cluster. In other words, violations are not moved back to the limits, but all buses and lines are required to stay within limits. Add the cost function

$$C = \sum C(u) \quad (14.61)$$

where u is the set of all active controls and C is the “cost,” such as the line losses or fuel cost. It is also easy to substitute line power limits for limits or line currents if desired or to add power limits.

Solving the Problem In order to deal with the somewhat unconventional features of the problem formulated in Eqs. (14.58) to (14.61), a modification of the Newton–Raphson method is introduced as follows with the aim to obtain a feasible solution with limited computational load:

1. In the initial step all violated quantities $[V_\mu]$ are set to the nearest limit and all nonviolated quantities $[N_\mu]$ are set at their predisturbance values available from state estimation.
2. The set of nonlinear equations in the problem statement, Eqs. (14.58) to (14.61) are then solved by linearization as in one step of the unconstrained Newton–Raphson method but using the pseudoinverse method when the number of controls, $[C_\mu]$, and the number of violated values, $[V_\mu]$ (or the number of condition equations, $[V_\mu] + [N_\mu]$, and the number of free variables, $[N_\mu] + [C_\mu]$) do not match. This means that each step is solved to the best mean-square approximation.
3. If any operating limits are breached after this one step at a nonviolated bus with or without controls, this bus is transferred into the violated category $[V_\mu]$. Controls that exhaust their supply of control power are removed from the control set $[C_\mu]$.
4. The changes of membership of $[V_\mu]$, $[N_\mu]$, and $[C_\mu]$ are simply tracked from one step to the next and the appropriate dimensions are used in the current step.

Note: Whereas such an approach makes good intuitive sense and works very well in experiments, it requires a different mathematical proof to establish its convergence. A sufficient condition was proven and is presented in Ref. [45]. It is straightforward to list the algorithmic steps for such a modified Newton–Raphson computation, so they will not be included here but are available in Ref. [45].

14.3.3.12 Control Variables Available in a Few Discrete Steps Only There are some controls (for instance, capacitor banks, reactors, load shedding, and tap changers) that are discrete or lumped. Their amount can only be adjusted in some fixed size steps. When such controls are present, a different computation of the amount of control is needed for viabilization.

In the beginning of each iteration of the viabilizing algorithm, such a bus i with discrete control is treated like a bus with continuous control, $[C_\mu]$. Then the control-step setting is selected to approximate the continuous result ΔQ_i as closely as possible. Clearly, the error in the control will not exceed $\frac{1}{2}$ of the control-step size, but all existing violations may not be completely eliminated in the current step.

14.3.3.13 Termination of the Viabilizing Algorithm The computation just described is carried out at the priority level $1 - p$. If a solution is not obtained,

then a new attempt is made using the next lower priority level group $1 - (p + 1)$ of control tools. If a solution is obtained at $1 - p$ and if time is available, a solution can be attempted at priority level $1 - (p - 1)$. When the final solution is available, this is fed out for implementation.

14.3.3.14 Implementing the Solution When the result of the viabilization algorithm is implemented (block 5, Fig. 14.17) the violations of voltage and current will disappear, so the remaining part of the system can operate normally. However, depending on the severity of the situation the tools used in viabilization may be more or less disruptive. They may include load shedding or voltage reduction in severe cases. If so, then the viabilization must be followed by restoration to put all loads back on line. The operator should play a role in how to proceed at this stage. For instance, he or she may conclude to forego restoration if the load is already receding in a post-peak period.

14.3.3.15 Other Uses of the Clustered Model and Relation to the Other Work The clustered model separates the system into clusters that are mostly isolated from the rest of the system in the sense that any control activity within the cluster affects the rest of the system only at a level below an arbitrarily selected threshold. So by selecting the threshold the degree of separation can be controlled in tradeoff with accuracy. Accordingly many computations essential to power-system operation can be done on a small scale within the clusters to an arbitrary approximation. Since the computation times for most numerical algorithms such as nonlinear programming, optimal control, and dynamic programming are increasing with dimension at a rate very much higher than linear, major computational savings are implied. Some areas in which such savings are possible would involve security monitoring, loss optimization, and optimal load flow.

Since cluster selection only selects the control sources to be used for a particular problem but not the control values, no on-line computation of the sensitivities is required. Prestored sensitivity values for typical load conditions will suffice. So in the proposed approach the following apply. (1) On-line computation is needed only for a handful of sensitivity values within the cluster. (2) On the other hand, the solution algorithm proposed solves the control problem within the cluster nonlinearly. Thus it can handle large deviations as would be expected in emergencies. Should the violation be small the solution algorithm will converge in one step; thus a linearized solution is obtained. In the emergency examples studied by the authors using large-scale simulation, typically 3 to 4 iterations were needed, implying significant nonlinearity.

Previously proposed linearized approaches apply systemwide linear programming solutions [48 to 51]:

1. Obtain systemwide sensitivity values on line
2. Settle for a linearized but systemwide solution even when deviations are large

Both of these requirements would limit the value of these earlier solutions in emergency conditions.

14.4 EFFICIENT METHODS FOR CONTROLLING SYSTEMWIDE CONGESTION

Any large electric power system is truly a coupled system, that is, changes in generation, load, or the transmission system are felt throughout the entire system, although the effect of a change tends to fade with distance. Computations involving the entire system are very time consuming. Thus in the past the problem of not being able to perform an efficient analysis of the whole system has led to a variety of approaches that chose to concentrate on the area of immediate interest. Also, it was assumed that the neighboring system areas were not affected much and that their effect could be approximated by small "equivalent" systems. This has also led to a rather intensive research in the area of static and dynamic system equivalents [52].

With changes in computer technology (in particular architecture and parallel-processing innovation) it has become possible to design efficient numerical algorithms for very large systems. The idea of parallel processing of weakly connected power subsystems was initiated through the work on network diakoptics [53, 54], the decomposition and coordination approach [55 to 57], and many others.

Solving algorithms such as linear or nonlinear programming or even matrix inversion for very large systems is extremely time consuming, mostly because the computation time of most such algorithms increases with system size in a fast nonlinear manner. With the possibility of parallel processing the idea readily emerges of subdividing the system into small pieces and solving individually, then piecing the solutions together. In fact this was proposed in diakoptics long before the parallel-processing age or even the computer age. The downfall is that the piecing-together part turns out to be so time consuming that it eliminates the advantages of the small-scale fast computations for the pieces.

14.4.1 Textured-Model Algorithm

The textured-model algorithm approach described here overcomes this problem through the novel idea of eliminating altogether the piecing effort and all serial time by iteratively blending the results of multiple "leaves," each containing a different set of subdivisions (i.e., groups) of the system. It works on any system that has a textured property such as a power transmission network. It works on any algorithm that retains the physical identity of the computed or optimized quantities such as most iterative mathematical programming techniques like steepest descent. The basic scheme of the textured-model algorithm is given in Figure 14.20.

In Figure 14.20, each leaf has a full rendering of buses (solid blocks for actively controlling buses, open for passive ones) and their interconnections, but only buses are shown. Buses (numbered 1 to 24) are arbitrarily assigned to overlapping groups (γ^a, γ') indicated by solid boundary lines, sized for smallest computation time for the intended algorithm (e.g., steepest descent). The effect of a controlled bus on any bus outside the group is lower than a preset threshold. Each bus belongs to at least one group. A bus is counted active on at most one leaf. Each group must

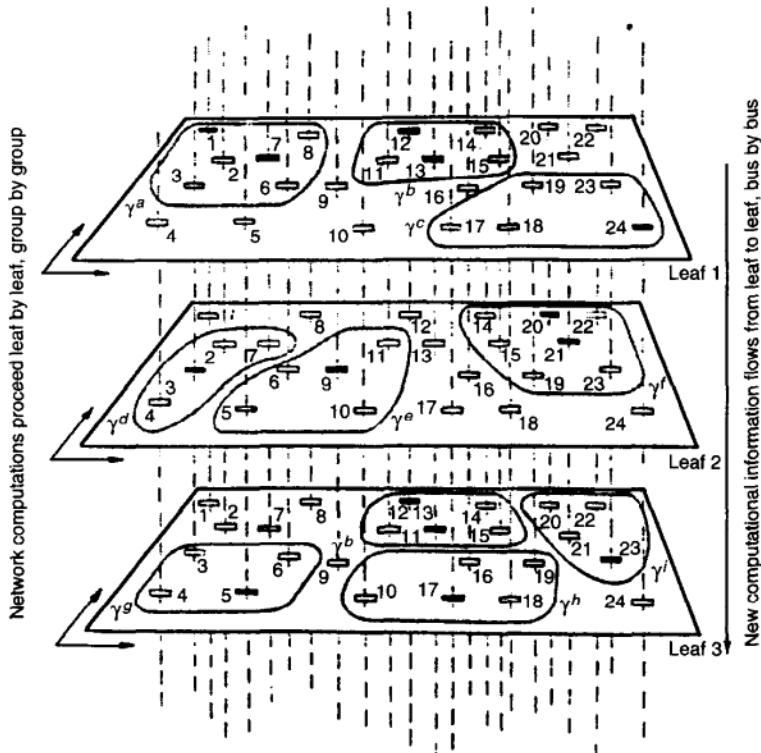


FIGURE 14.20 Conceptual sketch of the textured model and its uses.

overlap partially with at least one other group. Groups on the same leaf do not overlap. Each leaf contains approximately the same number of groups.

The algorithm is computed on parallel processors group by group on one leaf. Interactions are frozen at the group boundary at previously computed value. Results for states of buses within the group are directly passed to the same bus on the next leaf (along dashed line), and there is no intervening sequential processing. Leaves are computed in cyclic sequence. There is no waiting time if all groups are the same size and all leaves contain the same number of groups and all groups the same number of buses. While individual computation steps neglect inefficient paths, the algorithm will only stop when the exact solution is close to being reached systemwide so that corrections in the algorithm steps vanish.

A step by step explanation follows.

14.4.1.1 *Organization of the Textured-Model Algorithm*

1. Identify active elements in the system such as a place for a potential disturbance or a control located at a bus.
2. Divide the textured system arbitrarily into groups such that
 - The groups are roughly equal size.
 - Each group intersects at least one other group.

- Each element (bus) is contained in at least one group.
- Each group has at least one designated active element.
- No element is active in more than one group.
- The sensitivity of any element outside the group to any active element in the group is lower than a threshold θ .
- 3. Sort the groups into sets (leaves) of a size preferably equal to the number of parallel processors such that
 - No groups on the same leaf intersect.
 - Intersections between groups on consecutive leaves are as uniform as possible and as even between leaves as possible.

There are several matters that need coordination, to be discussed later.

14.4.1.2 Execution of the Textured-Model Algorithm

1. Take one of the leaves such as the top leaf, No. 1, of Figure 14.20. This leaf covers the entire system and contains three disjoint groups γ^a , γ^b , and γ^c . All the active, control elements on this leaf are inside the group. A number of passive elements are outside the groups but by the previous assumptions these will react weakly to active events within the groups.
It is now proposed to complete the algorithm in question (e.g., steepest descent) separately and independently over each of the three groups on leaf 1. In doing so, values at group boundary buses or line cut sets are frozen at the values currently in the memory. Initial values (representing the previous step of descent) within the group again are taken at what is currently in the memory, that is, the initialization values or the values obtained in solving the preceding leaf.
2. The results (e.g., bus voltages) of these independent groupwise computations for each group directly replace the corresponding values (e.g., bus voltages) previously recorded in the memory. No serial processing is involved.
3. Values on passive elements that are outside the groups on leaf 2 remain unchanged after the computation on leaf 2 is finished.
4. Now take the next leaf, leaf 2 in this case, and repeat the process.

Note that at the completion of computing on leaf 1 the results were put into the memory to replace previous entries; hence many values within the groups on leaf 2 have changed at the end of the computation on leaf 1. At the beginning of the computation on leaf 2, the starting values in each group (γ^d , γ^e , γ^f) of leaf 2 will be the newly computed values from the computation on leaves at such buses where the groups on the two leaves overlap. Furthermore, groups on leaf 2 such as γ^e overlap with more than one group on each leaf (γ^a and γ^b in this case). By this mechanism computational information is propagated to the next leaf and simultaneously spread over the new set of groups on the next leaf. The

greater the size of the overlap and the more different groups overlap, the more effectively and the faster the new information is spread.

Note also that the algorithm (e.g., steepest descent) is computed only over small groups within each leaf. This section takes place horizontally and in parallel in Figure 14.20 over each leaf. The new computational information, on the other hand, travels vertically down from leaf to leaf (and cyclically back to the top) as needed. This latter propagation is very direct. Memory storage is simply changed to the newest result. Serial processing is obviated by the mixing resulting from using different sets of groups from leaf to leaf and the variation of intersection between groups on different leaf.

The preceding description and Figure 14.20 provide a conceptual scheme proposed under the name of the *textured-model algorithm*. This conceptual picture implies many major advantages: parallel computation with an essentially constant number of processors, each dealing with a small part of the system and hence each taking only a short time; absence of serial processing — new computation results simply replace prior memory entries. Fitting the small network pieces together is accomplished simply by passing leaf to leaf and mixing of new information so there is no need for fitting operations or any other serial program components. Of course, beyond this conceptual picture, there are numerous hard mathematical questions of coordination, choice of parameters, and convergence. Rigorous mathematical treatment using mostly graph theory is available in Ref. [59]. A somewhat simplified summary will be presented in the following, including numerical illustration.

14.4.1.3 Off-Line Preparatory Operation Ideally a new model might be set up for each computation, that is, for each system state. However, the use of one model for a wide operating range (such as typical heavy-load conditions) seems to produce only minor deterioration, while on the other hand it eliminates all need for serial processing. With reference to the conceptual sketch of Figure 14.20, two stages are included in setting up a textured model.

Stage 1. Grouping Stage: Identifying the groups of buses.

Stage 2. Stratification Stage: Arranging the groups on leaves or levels.

A rigorous mathematical development of these processes is included in Refs. [58, 59]. A brief narrative discussion follows here.

14.4.1.4 Identifying the Groups of Buses: The Grouping Stage Again with reference to the conceptual summary of Figure 14.20 the buses are to be grouped such that

1. Interaction between active buses and any buses outside the group is below a certain preselected sensitivity threshold θ .
2. The computational time for the intended algorithm(s) is less for the group than the sum of computation times for any breakup into subgroups.

Because parallel processing is the natural way to use the proposed model, a certain uniformity of the size of the groups and the amounts of overlap between them is also important for efficient computation. Consequently a readjustment of the groups, combining some small ones and subdividing some others, should follow the basic establishment of the groups. The best way for this may be first to find the average group size and average coupling amount from the raw results. Then by adding appropriate margins of variation, upper and lower limits can be established for the sizes and intersections of groups as follows:

1. In the inequalities

$$G^m \leq G^{kk} \leq G^M, \quad G_c^m \leq G^{kj} \leq G_c^M \quad (14.62)$$

G^{kk} is the number of buses in group γ^k and G^{kj} is the number of shared buses between λ^k and λ^j .

The following two obvious requirements must also be met (see the conceptual summary in Figure 14.20).

- 2. Each bus must be a member of at least one group.**
- 3. Every group intersects at least one other group.**

First the intersection graph is obtained as follows: each group is represented by a vertex, and two vertices are connected by an edge if and only if the corresponding graphs intersect. Then, the consolidation of two groups γ^k and γ^m is called an elementary consolidation because it corresponds to the elementary contraction of the intersection graph of groups. That is, two vertices γ^k and γ^m are replaced by a vertex that connects to those vertices of groups intersecting γ^k and γ^m . Furthermore, the consolidation of more than two groups can be viewed as the result of a sequence of elementary consolidations.

In particular, the consolidation of groups preserves their incompatibilities with other groups, while the number as well as the size of the maximal incompatible set decreases.

The total computation time of a maximal incompatible set σ^i is

$$\tau(\sigma^i) = \sum_{\gamma^k \in \sigma^i} T(\gamma^k) \quad (14.63)$$

The longest total computation time of maximal incompatible sets σ^i , $i = 1, 2, \dots, N^\sigma$, is called the time span τ_S of the groups $(\gamma^k, k = 1, 2, \dots, N^\gamma)$. That is,

$$\tau_S = \max_i \tau(\sigma^i) \quad (14.64)$$

14.4.1.5 Problem Statement for the Grouping Stage Given a collection of initial groups and the computation time of the intended algorithm, the grouping stage of establishing the textured model is formulated to find a sequence of

elementary consolidations that results in groups of feasible size throughout with minimum time span. That is,

$$\begin{aligned} \min \quad & \max_i \sum_{\gamma^k \in \sigma^i} T(\gamma^k) \\ \text{subject to} \quad & G^m \leq |\lambda^k| \leq G^M, \quad k = 1, 2, \dots, N^Y \end{aligned} \quad (14.65)$$

Roughly speaking, the optimum solution would result from a sequence of elementary consolidations that contains as many computation-time-reducing consolidations as possible.

14.4.1.6 Arranging the Groups on Leaves: The Stratification State Once a collection of uniformly sized groups with the smallest time span is obtained, the establishment of the textured model can advance to the stratification stage. The objective of the stratification process is to arrange groups γ^k , $k = 1, 2, \dots, N^Y$, into leaves λ^l , $l = 1, 2, \dots, L$ in such a way that

1. The groups in each leaf should be mutually compatible and the number of groups per leaf should equal the number of available processors.
2. The number of leaves is minimized for the available amount of parallel processing.
3. The rate of computational renewal in each cycle (after which the sequence of leaves is repeated) is maximized for the intended algorithm in order to aid convergence.

The dependence of the minimum number of leaves on the amount of available processors and a measure of the computation renewal will now be discussed. The approach is based on the coloring problem in graph theory.

14.4.1.7 Minimum Number of Leaves Let P denote the number of available parallel processors. The leaf λ^l can be computed in parallel on P processors if

$$|\lambda^l| \leq P \quad (14.66)$$

Given a collection of N^Y groups and an array of processors, the *ideal number of leaves* that utilizes the maximum amount of parallel processing is

$$L^P = \min_{\gamma} \left(L \left| \frac{N^Y}{L} \leq P, \quad L \text{ is a positive integer} \right. \right) \quad (14.67)$$

Lemma 14.4.1 Given a collection of groups $(\gamma^k, k = 1, 2, \dots, N^\gamma)$ and an array of P processors, let L^* be the smallest number of leaves such that every leaf can be computed on P processors. Then

$$L^* = \max(\chi, L^P) \quad (14.68)$$

here χ is the *chromatic number* of graphs associated with $\gamma^k, k = 1, 2, \dots, N^\gamma$ as just defined. The chromatic number here is the smallest possible number of leaves on which only compatible groups will be arranged on the same leaf, and each group will be able to be assigned exactly one leaf. The concept of chromatic number originates from coloring problem in graph theory.

Proof Let $(\lambda^l, l = 1, 2, \dots, L)$ be a family of leaves for $(\gamma^k, k = 1, 2, \dots, N^\gamma)$ and every leaf be computable in parallel. Suppose $L \leq L^* = \max(\chi, L^P)$. If $L^P \geq \chi$, then $L \leq L^* = L^P$, which contradicts the definition of L^P . If $\chi \geq L^P$, then $L \leq L^* = \chi$, which contradicts the definition of L^* .

14.4.1.8 Rate of Computation Renewal For a family of leaves $\lambda^l, l = 1, 2, \dots, L$ the computation of an intended algorithm can proceed leaf by leaf on an array of P parallel processors. The computational information flows from leaf to leaf through each bus. After one computational cycle the sequence of leaves is repeated.

The *rate of computation renewal* of group γ^k on leaf λ^l is

$$R^l = G^{kk} G_l^k \quad (14.69)$$

where

$$G^{lk} = \sum_{l=1}^L G^{km}, \quad \gamma^k \in \lambda^l, \quad k \neq m \quad (14.70)$$

and $\gamma^m \in \lambda^{(l-1)}$. Note that any two adjacent leaves should contain distinct groups, otherwise the computation repeats the preceding one. In particular, no group should be allowed to repeat in any three-leaf textured model.

For a family of leaves $(\lambda^l, l = 1, 2, \dots, L)$ the cumulative computation renewal per cycle is

$$R = \sum_{l=1}^L \sum_{\gamma^k \in \lambda^l} R_l^k \quad (14.71)$$

For easier analysis of rate of computation renewal, the segments are formed by joining the maximal incompatible sets with nontrivial intersection together. Thus each segment contains one or more maximal incompatible sets. Some properties follow.

Lemma 14.4.2 For a family of segments $(\xi^n, n = 1, 2, \dots, N^\xi)$, let

$$R^n = \sum_{l=1}^L \sum_{\gamma^k \in \xi^n \in \lambda^l} G^{kk} \sum_{\lambda^m \in \xi^n \cap \lambda^{l-1}} G^{km} \quad (14.72)$$

for $n = 1, 2, \dots, N^\xi$, then

$$R = \sum_{n=1}^{N^\xi} R^n \quad (14.73)$$

Proof From Lemma 14.4.1 and the preceding definition

$$R = \sum_{l=1}^L \sum_{\lambda^k \in \lambda^l} G^{kk} \sum_{\gamma^m \in \lambda^{l-1}} G^{km} \quad (14.74)$$

Since segments associate with a partition of edges in the intersection graph of groups,

$$\begin{aligned} R &= \sum_l \sum_{\gamma^k \in \lambda^l} G^{kk} \sum_{\gamma^m \in \lambda^{l-1}} G^{km} \\ &= \sum_{l=1}^L \sum_{n=1}^{N^\xi} \sum_{\gamma^k \in \xi^n \cap \lambda^l} G^{kk} \sum_{\gamma^m \in \xi^n \cap \lambda^{l-1}} G^{km} \\ &= \sum_{n=1}^{N^\xi} \sum_{l=1}^L \sum_{\gamma^k \in \xi^n \cap \lambda^l} G^{kk} \sum_{\lambda^m \in \xi^n \cap \lambda^{l-1}} G^{km} \\ &= \sum_{n=1}^{N^\xi} R^n \end{aligned} \quad (14.75)$$

14.4.1.9 Statement of the Stratification Problem Given a collection of groups obtained from the grouping algorithm, the stratification stage of establishing the textured model is formulated to find the specific membership of groups on each leaf within one computation cycle (after which the sequence of leaves is repeated) such that the cumulative computation renewal per cycle is maximized while utilizing maximum amount of parallel processing, that is, in the standard form of mathematical programming. Maximize

$$R = \sum_{l=1}^L \sum_{\lambda^k \in \lambda^l} G^{kk} \sum_{\gamma^m \in \lambda^{l-1}} G^{km} \quad (14.76)$$

subject to

$$|\lambda^l| \leq P, \quad l = 1, 2, \dots, L \quad (14.77)$$

Although Lemma 14.4.2 implies that the objective function is separable for segments of groups, the optimal solutions for individual segments may result in an overall solution that violates the constraints. Some more details are given in Refs. [58, 59].

14.4.1.10 General Flow Chart of the Textured-Model-Based Algorithm With reference to Figure 14.20 the computation process can be described as follows:

1. On leaf 1 transmission-line flows crossed by the boundaries of the individual groups in Figure 14.20 are frozen at some initial value or at the value obtained in the previous interaction cycle.
2. Whatever the computation or optimization process, the subject of the use of the textured-model algorithm is now carried out independently and (preferably) in parallel processing for every group on leaf 1.
3. On leaf 2 transmission-line flows crossed by the boundaries of the individual groups on Figure 14.20 are frozen at the values obtained in item 2.
4. The computation or optimization process in question is now carried out independently and (preferably) in parallel processing for every group on leaf 2.
5. The computation results are used directly to update prior memory entries for bus voltages, etc.
6. Continue cyclically.

A sufficient condition for the convergence of this process was established previously [58]. An illustrative example of using this algorithm on a 118-bus IEEE test system can be found in the original reference [59].

14.5 CHAPTER SUMMARY

This chapter concerns the problem of generation-based stationary control so that the systemwide limits (such as line flows and voltages) remain within the prespecified operating limits. This problem has recently gained new importance in light of the fact that in the deregulated industry, electricity market solutions must be modified to observe system constraints. The basic problem formulation in the regulated industry falls under the category of nonlinear programming problems, for the solutions of which many general algorithms are available. The problem becomes more intriguing in the deregulated industry in which objectives of generation and transmission are separate. In this chapter we describe three possible ways of ensuring that transmission constraints are not violated in the deregulated industry; they range from simple denial of transactions leading to the violation of system constraints, through using the real-time congestion

pricing (economic feedback) to ensure system performance within the prespecified limits. The basic relation between the Lagrangian coefficients resulting from computing a constrained economic dispatch and the congestion price signals is described.

The main feature of techniques reviewed in this section is based on the fact that localized system violations are rather common. In fact these violations may be mild enough not to have an impact implied by the word *emergency* or *crisis*, although they will need correction, which may be more in the nature of dispatch or management than in the nature of emergency control. They can affect one quite limited segment of an otherwise healthy large system. It would not seem reasonable, then, to invoke a systemwide large-scale computation to find the remedies, especially because most corrective actions have a limited range as well. Controls should be found that are effective and nearby and that disrupt the system performance and service to the smallest possible degree.

In this chapter an overview of basic computer algorithms for control centers is described. The Supervisory Control and Data Aquisition (SCADA) systems together with a static state estimator are used to monitor system status (including bad data) and to estimate system voltages [57]. Basic computer algorithms have been developed for scheduling generated real-power and adjusting generator set points so that the anticipated (or estimated demand) is met in a cost-effective way. OPF-based techniques for this purpose are briefly reviewed for completeness.

Next, several methods for determining the extent of effects of system changes on system conditions are described. In particular, complexity of the scheduling methods strongly depends on how localized the effect of change is to which corrective actions need to respond. In particular, the complexity of the methods needed for scheduling real-power and voltage or reactive-power support strongly depends on whether a system input (or network topology) change for which corrective actions are needed causes localized effects or its effect is systemwide. Three simple techniques (echelon concept, BRE, and \underline{D} vector) are described for possible on-line decision-making if the effect to a known disturbance is of one or the other type.

Two algorithms, based on clustering and the \underline{D} vector, are described next for computing the most effective corrective actions to eliminate localized changes and to take the system back as closely as possible to the normal condition.

When a system is subject to a systemwide imbalance of reactive loads and sources, efficient tools are needed for taking corrective actions on the entire system. This requires use of a mathematical programming approach to select the set of controls spread over the entire system that are capable of eliminating systemwide violations. To overcome the computational burden in this situation, the textured-model algorithm is described as a potentially quite promising approach for on-line corrective actions in severe conditions when systemwide effects take place.

BIBLIOGRAPHY

1. Lugtu, R., Security constrained dispatch, *IEEE Trans. on Power Apparatus*, **PAS-98**: 270–274, 1979.
2. Zaborszky, J., et al., Reactive and real power control for computationally effective voltage and thermal management, *IEEE Trans. Power Apparatus Syst.*, 1728–1737, 1985.
3. Yu, C-N., and Ilić, M., Congestion clusters-based markets for transmission management, Proc. IEEE PES Winter Power Meet. New York, NY, 1999.
4. Wu, F. F., Varaiya, P., Spiller, P., and Oren, S., Folk theorems and transmission open access: Proofs and counterexamples, Power Report PWR-23, U. Calif. Energy Inst., 1994.
5. Cheng, J., Galiana, F. D., and McGillis, D., Studies of bilateral contracts with respect to steady state security in a deregulated environment, Proc. 20th Intl. Conf. Power Industry Computer Appl. Columbus, OH, 1998, pp. 31–36.
6. Oren, S., Economic inefficiency of passive transmission rights in congested electricity systems with competitive generation, *Energy J.*, 18: 1997.
7. Hogan, W., Contract networks for electric power transmission, *J. Regulatory Econ.*, 4: 1992.
8. Lecinq, B. S., Peak-load Pricing for Transmission in a Deregulated Electric Utility Industry, M. Sci. and Technology Policy thesis, MIT, 1996.
9. Wu, F. F., and Varaiya, P., Coordinated multilateral trades for electric power networks: theory and implementation, Power Report No. PWR-031, 1995.
10. Ilić, M. D., Hyman, L., Allen, E., Cordero, R., and Yu, C-N., Interconnected system operations and expansion in a changing industry: Coordination vs. competition, in Shimon Awerbuch and Alistair Preston (eds.), *The Virtual Utility: Accounting, Technology and Competitive Aspects of the Emerging Industry*, Series on Topics in Regulatory Economics and Policy Series, City: Kluwer Academy, 1992, pp. 307–XXX.
11. Hyman, L. S., and Ilić, M., Scarce resource, real business or threat to profitability?, *Public Utilities Fortnightly*, October 1, 1997.
12. Ilić, M., and Hyman, L. S., Transmission scarcity: Who pays?, *Electricity J.*, July: 38–49, 1997.
13. Chao, H-P., and Peck, S., A market mechanism for electric power transmission, *J. Regulatory Econ.*, **10** (1): 25–59, 1996.
14. Hogan, W., To pool or not to pool: A distracting debate, *Public Utilities Fortnightly*, January 1, 1995.
15. Scheppele, F. C., Caramanis, M. C., Tabors, R. D., and Bohn, R. E., *Spot Pricing of Electricity*, City: Kluwer Academic, 1988.
16. Ilić, M., Allen, E., and Younes, Z., Providing for transmission in times of scarcity: An ISO cannot do it all, MIT LEES WP Report No. 97–003, 1997.
17. Ilić, M., Leotard, J-P., Rochlin, C., and Stoft, S., On the objectives of transmission pricing under open access, Proc. Bulk Power Syst. Dynamics Control IV — Restructuring, Santorini, Greece, 1998.
18. Ilić, M. and Graves, F., Optimal use of ancillary generation under open access and its possible implementation, MIT Laboratory for Electromagnetic and Electronic Systems Report No. TR 95–006, 1995.

19. Ilić, M., Galiana, F., and Fink, L. (eds.), *Power Systems Restructuring: Engineering and Economics*, City: Kluwer Academic, 1998.
20. Ilić, M., and Hyman, L., Getting it right the first time: Value of transmission and high technologies, *Electricity J.*, March: 8–17, 1996.
21. Federal Energy Regulatory Commission: Capacity reservation open access transmission tariffs; notice of proposed rulemaking, Docket No. RM96-11-000, April 24, 1996.
22. Fink, L. H., Ilić, M. D., and Galiana, F. D., Transmission access rights and tariffs, *Electric Power Syst. Res.* **43**: 197–206, 1997.
23. Younes, Z., and Ilić, M., Physical and financial rights for imperfect electric power markets, MIT LEES Report No. WP 97–005, 1997.
24. Oren, S., Spiller, P., Varaiya, P., and Wu, F. F., Nodal prices and transmission rights: A crititcal appraisal, *Electricity J.*, 8 (April) 14–23, 1995.
25. Lecinq, B. S., Ilić, M., Peak-load pricing for electric power transmission, Proc. 30th Hawaii Intl. Conf. Systems Sci., 1997, pp. 624–632.
26. *The US Power Market: Restructuring and Risk Management*, London: Risk, 1997.
27. Wilson, R., Implementation of priority insurance in power exchange markets, *Energy J.*, 18: 1997.
28. Leotard, J-P., and Ilić, M., On the objectives of transmission pricing under open access, Proc. IEEE PES Winter Power Meet., New York, NY, 1999.
29. Baughman, M. L., Siddiqi, N. S., and Zarnikau, J. W., Integrating transmission into IRP, IEEE Paper No. 95 WM 200-6-PWRS.
30. Bertsekas, D., *Nonlinear Programming*, Belmont, MA: Athena Scientific, 1995.
31. Lin, S. Y., et al, Reducing cluster size for computing remedial adjustments for voltage and loading violations on the power system, Proce. 23rd IEEE Conf. Decision Control, Las Vegas, 1984.
32. Walton, S., and Tabors, R., Zonal transmission pricing: methodology and preliminary results from the WSCC, *Electricity J.*, November: 34–41, 1996.
33. Zaborszky, J., et al., Control of reactive power and voltage in emergencies, *Automatica*, VOL. **21** (3): 237–246, 1985.
34. Thorp, J. S., et al., Conditions for solution existence and localized response in the reactive power network, *Intl. J. Electrical Power Energy Syst.*, **8**: 66–74, 1986.
35. Sheble, G. (ed.), *Reactive Power: Basics, Problems, and Solutions*, IEEE Tutorial Course, 87EH0262-6-PWR.
36. Zaborszky, J., Whang, K. W., and Prasad, K. V., Fast contingency evaluation using concentric relaxation, *IEEE Trans. Power Apparatus Syst.*, **PAS-99**: 28–36, 1980.
37. Zaborsky, J., et al., Future role of the control center in the emergency state control of the power system, Proc. 8th World Congress IFAC, Kyoto, 1981, pp. 41–48.
38. Lagonotte, P., Sabonnadiere, J. C., Leost, J. Y., and Paul, J. P., Structural analysis of the electrical system: Application to the secondary voltage control in france, *IEEE Trans. Power Syst.*, **4**: 479–486, 1989.

39. Mansour, Y. (ed), *Voltage Stability of Power Systems: Concepts, Analytical Tools, and Industry Experience*, IEEE Tutorial Course, 90TH0358-2-PWR.
40. IBM package for computing eigenvalues of sparse, very large matrices.
41. Ilić, M., and Stobart, W. Development of a smart algorithm for voltage monitoring and control, *IEEE Trans. Power Syst.* **PWRS-5**: 1183–1193, 1990.
42. Zobian, A., and Ilić, M. D. A steady-state voltage monitoring and control algorithm using localized least squares minimization of load voltage deviation, *IEEE Trans. Power Syst.*, **11**: 929–938, 1996.
43. Zaborszky, J., et al., A clustered dynamic model for a class of linear autonomous systems using simple enumerative sorting, *IEEE Trans. Circuits Syst.*, **CAS-29**: 1982.
44. Schlueter, R. A., et al., Voltage stability and security assessment, EPRI Final Report, EL on Project RP 1999-8, 1988.
45. Zaborszky, J., et al., Emergency control to remedy voltage and thermal violations in a segment of the large power system by active and reactive means, SSM Report No. 8304, Washington Univ., 1983.
46. Zaborszky, J., et al., Operations of large interconnected power by decision and control, *IEEE Trans. Power Apparatus Syst.*, **PAS-99**: 37–35, 1980.
47. Hiebert, K. L., Solving systems of linear equations and inequalities, *SIAM J. Num. Anal.*, **17**: 447–464, 1980.
48. Stott, B., and Hobson, E., Power system security control calculations using linear programming, Part I, *IEEE Trans. Power Apparatus Syst.*, **PAS-097**: and 1713–1720, 1978. Part II, 1721–1731.
49. Stott, B., and Marinho, J. L., Linear programming for power-system network security applications, *IEEE Trans. Power Apparatus Syst.*, **PAS-98**: 837–848, 1979.
50. Chan, S. M., and Yip, E., A solution of the transmission limited—dispatch problem by sparse linear programming, *IEEE Trans. Power Apparatus Syst.*, **PAS-99**: 1980.
51. Hobson, E., Network constrained reactive power control using linear programming, *IEEE Trans. Power Apparatus Syst.*, **PAS-99**: 868–877, 1980.
52. Undrill, J. W., et al., “Construction of power systems electromechanical equivalents by modal analysis, *IEEE Trans. Power Apparatus Syst.*, **PAS-90**: 2049–2059, 1971.
53. Kron, G., *Diakoptics: The Precise Solution of Large Scale Systems*, London: Mac-Donald, 1963.
54. Happ, H., *Diakoptics and Networks*, New York: Academic, 1971.
55. Mansour, M. O., et al., Nonlinear Var optimization using decomposition and coordination, *IEEE Trans. Power Apparatus Syst.*, **PAS-103**: 246–255, 1984.
56. Sasson, A. M., Decomposition technique applied to the nonlinear programming load flow method, *IEEE Trans. Power Apparatus Syst.*, **PAS-89**: 78–82, 1970.
57. Schweppes, S. C., and Handschin, E. J., Static state estimation in electric power systems, *Proc. IEEE*, 972–982, 1974.
58. Lin, S. Y., A textured model, Ph.D. thesis, Washington Univ., St. Louis, MO, 1984.
59. Zaborszky, J., et al., A textured model for computationally efficient reactive power control and management, IEEE Meeting paper, No. 84SM 617–7.

GUIDE TO USING THIS BOOK

As we close, we provide the following brief indication of possible uses of this large book.

Guide to Using the Book as a Graduate Level Text

The backbone material of this book, both general and sufficiently narrow, is intended to be used as a textbook material for advanced graduate courses in the area of power systems analysis, and control. Significant portions of Chapters 2 to 6 and Chapters 12 to 14 have evolved as part of teaching Advanced Power System Analysis and Control courses at MIT and at Washington University over the past two decades. Here we provide a possible guide for using the same material in other classrooms.

Teaching dynamics and control of large electric power systems presents a unique challenge both to prospective students and teachers. The main problems are associated with the level of required background in this area.

Possibly the most successful use of this book and its unique contents would be in the scenario that the students have had senior-level courses in fundamentals of electric machines, power-system analysis, electric circuits and introductory system analysis, and control. Students with a background of this type are likely to take full advantage of the comprehensive material in the book. However, in our experience, this text has been very useful to either students with the basic training in classical power engineering or students not familiar with power engineering but with a solid background in general fields such as electric circuits, dynamic systems, and control theory. In short, this is because this book teaches the following:

- With classical power engineering as a background, learn how to pose the open engineering problems in the language of system and circuit analysis.
- With solid knowledge in general areas of circuits, systems, and control, learn how to apply these tools to many challenging power engineering problems.

The book opens wide avenues for further studies using advanced system theory beyond the tools used here, once the concepts described in this text are understood.

Some students with strong backgrounds in power engineering are likely to have seen some of the material in Chapters 2 and 3, and portions of Chapters 5, 6, 13 and 14 already. In this case they could master the rest of the book during the course of two semesters. Students at MIT and Washington University have been known to achieve this goal.

On the other hand, students without a background in power engineering are likely to go slower over the material in Chapters 2, 3, 5, 6, 13 and 14 to the extent of having to do some supplementary reading in the area of electrical

machines. Excellent supplementary texts on this subject can be found. Once the students without a power background have learned this material, they are very likely to move through Chapters 4, 7 to 10, and 12 at a faster pace than the first group of students. Chapters 5, 8, 10 and 11 are aimed at the most advanced in mathematical techniques and the most research oriented.

Both authors have taken great joy in watching students go through the process of mastering the complex field of power-system engineering in various forms during their teaching experience in the advanced power systems whose sum totals over 80 years!

It is important to recognize that the book is organized in such a way as to introduce students to the topic even without assuming a complete background at the start in power engineering and systems. The net result is that such students are likely to master only Chapters 2 through 6. In this situation there is simply not enough time in a two-semester course to master the entire material in this text. The book is organized in such a way that the nonlinear and advanced control concepts come at the later stages in Chapters 6 to 12, and can be left out. The course that covers the material, with the exception of these last chapters, still provides strong fundamentals for in-depth work in the area of large power systems. The rest of the book then becomes a reference for self-study or work beyond the basic level when challenged by problems in practice or desire for self growth. Moreover, it appears that one could also consider Chapters 7 to 12 as a text for a specialized advanced topics one-semester course on nonlinear dynamics and control in power systems as a follow-up to the first two semesters.

Last, but not least, as the industry undergoes restructuring, our future leaders in power engineering should prepare themselves for relating technical aspects of power industry to the economics and policies. Chapters 13 and 14 are a good start for understanding the foundations of these relations. Understanding this material empowers one with a perspective of general structure of power-system operations and control and helps one view regulated and competitive power industries as particular cases.

Guide to Using the Book as a Reference

The specialized material, beyond the level considered as required for introducing graduate students to the world of modern power systems, can be used for self-studies into deeper knowledge of the area. In this context, it is considered essential in preparing graduate students for doctoral research in the area of modern power systems.

The same material could be used in attempting to conduct a systematic technology transfer of academic research into new software and hardware developments. As such, it can serve as a basis for systematic recognition of specific operating problems on a given system, as well as for designing adequate software and hardware for their remedies. It can be used as an essential advanced reference by both utility- and manufacturer-type engineers as well as by many important players in the power industry under restructuring, such as the regulators,

independent system operators, transmission providers, power marketers, and load-serving entities.

It is hoped that the readers will keep the book at hand as a source once exposed to, as they have used as less advanced book written by one author 40 years ago which is still available and selling in paperback.

INDEX

- Abnormal condition, 644
AC lines, 68
Actions, control, 643
Actions, corrective, 643
Actions, preventive, 643, 645
Active power, 22, 24, 30, 53
Active power controllers, 136
Aggregate models, 371
Airgap, 83
Air-gap flux, 84
Anchored system, 71
Ancillary algorithms, 645
Angle dynamics, fast, 340, 347
Apparent power, 23
Area control error (ACE), 653, 709
Area load deviation, 678
Armature, 82
Armature current, 85
Armature leakage flux, 84, 88
Auctioneer, 668
Auctions, 668
Automatic generation control (AGC), 5, 67, 391, 645, 647, 653, 660, 690, 696
Automatic voltage control (AVC), 67, 645, 727
Automatic voltage regulator (AVR), 592, 606
Automatic voltage regulator, effect of, 597
Automatic voltage regulator, high gain, 597–598, 606
Automatic voltage regulator, tuning, 594
Available transfer capability (ATC), 245, 249
Averaging, frequency-selective, 624, 627
Averaging, generalized, 626
Axis, direct, 106
Axis, quadrature, 106

Base values, 81
Basic anchor theorem, 475
Benefit, 671, 762

Bifurcation, 290, 442
Bifurcation, Hopf, 405, 461
Bifurcation, saddle node, 402, 405, 420, 461
Bifurcation, singularity-induced, 402, 404, 420
Bilateral transmission capability, 248
Blackouts, 3, 642
Blondel matrix, 83
Boundary layer model, fast 340
Boundary value problems, 555
Breaking resistors, 646
Bus admittance matrix, 183, 219, 224, 782
Bus-connected equipment, 78
Bus, HV-AC, 62
Bus, HV-DC, 62
Bus reactive-load excess, 780
Bus, terminal, 84
Bus transmission capability (BTC), 247
Buses, 61, 67
Buyers, 668

Capacitance, stray, 455
Capacitor, 12, 14, 285, 622
Capacitor banks, 150, 632
Capacitor, energy contents of, 14
Capacitor, instantaneous power flow into, 12
Capacitor size, maximum, 725
Capacitor switching, 633, 634
Capacitor, thyristor-switched, 5, 157
Capacitor, voltage-controlled, 150
Causal domains, 410
Center manifold, 499
Center-of angle, 69
Closed-loop primary dynamical model, 680
Closed-loop system dynamics, 336, 595, 611
Clustering algorithm, 803

- Clustering, distribution factors based, 241, 762
 Clusters, 6, 241, 758
 Clusters, dynamic, 613
 Coils, rotor, 106
 Coils, stator, 106
 Complex power, 22, 59
 Components, established, 69
 Composite system, 607
 Composite system, stabilization of, 608
 Computer-aided control, 641
 Computer-aided decision, 641
 Conductance matrix, 264
 Conductance matrix, positive definiteness property, 264
 Congestion, 5
 Congestion clusters, definition, 241, 761
 Congestion distribution factors (CDFs), 244, 257
 Congestion management, 242, 249
 Congestion management in large systems, 811
 Constant flux linkage principle, 86
 Constrained economic dispatch, 759
 Constraint manifold, 397
 Consumers, 651
 Contingency, 591
 Contingency, critical, 591, 760
 Continuation methods, 291
 Contract for power, 251
 Control, 4
 Control agents, 609
 Control area, 708
 Control classification, 591
 Control, closed-loop, 680
 Control, composite, 602, 679
 Control cost, 602, 717
 Control, decentralized, 605
 Control design for nonlinear systems, 606
 Control design, large signal, 622
 Control design, systematic, 630
 Control-driven process, 632
 Control equipment, switching, 591
 Control equipment, tuning, 591
 Control gain, 405, 598, 605, 686
 Control gain, constant, 604, 606, 609
 Control, high gain, 613
 Control input, 171
 Control limits, 594
 Control, local, 190, 609
 Control, objectives, 604
 Control, on-line, 641
 Control performance, security-related, 604
 Control phase, 642, 646
 Control policy, 668
 Control policy, optimal, 668
 Control, primary, 5, 653
 Control, relay-type function, 150
 Control set point, 171, 592, 595, 650
 Control set point, postfault, 594
 Control, single input-single output problem, 595
 Control, stabilizing, 593, 616–617
 Control, supplemental, 598, 601
 Control target, postcontingency, 594, 611
 Control, thyristor, 534, 621
 Controllability, 603, 606, 684, 733
 Control law, 612
 Controlled impedance, 627
 Controller coordination, 604–605, 609, 630, 709
 Controller coordination, full, 604
 Controller coordination, minimal, 604, 607
 Controller design, 595, 605
 Controller design, optimal, 601, 608
 Controller, dynamic performance of, 602–603
 Controller,
 proportional — integral — differential (PID), 595, 601, 628, 630
 Controller, proportional integral (PI), optimal, 676
 Controller tuning, eigenmode-based, 600
 Controllers, continuous, 172
 Controllers, local, 171–172, 594
 Controllers, switching type, 172, 630
 Converters, PWM, 626
 Converters, resonant, 626
 Convex function, 674
 Coupled real power-voltage dynamic model, 192, 315
 Coupling variables, local, 171
 Criteria, scalar type, 274
 Criteria, vector type, 274
 Critical eigenvalue, 500
 Cross product, 40
 Customers, 651

- DAE dynamics, 459
 Damping, 418
 Damping, negative, 598
 DC lines, 68
 DC link, 158
 DC link, hierarchical control of, 161
 DC load flow, 223–224
 Decentralized control design, 605, 608–609
 Decentralized reference coordinates (DCR), 618
 Decision making, multi-stage, 667–668
 Decision phase, 641–642, 645–646
 Decoupled reactive power-voltage load flow, 258, 313
 Decoupled real power-angle load flow, 222–223, 227, 311
 Decoupling conditions, real and reactive power, 219, 221
 Decoupling error, 222
 Descriptor model, 187
 Diagonal dominance conditions, 265
 Differential algebraic equation (DAE), 4, 186, 392, 452, 457, 523, 614
 Discontinuous nonlinear constraints, 523
 Distribution companies, 61, 651–652, 654
 Distribution factors, 232, 239, 254, 258, 761
 Distribution factors matrix, 235
 Disturbance, large, 619, 630
 Disturbance, reactive power, 631
 Disturbance vector, 246, 418, 595, 682
 Droop constant, 681
 D vector, 272, 784
 D vector-based algorithm damper winding, 86, 97–98, 106
 Dynamic model, analytical, 61
 Dynamic programming, 668
 Dynamic scheduling, partial, 694
 Dynamics, local, 171
 Dynamic stability, 200, 629
 Dynamics, torque-angle, 601
 Echelon-based enumeration, 782
 Economic dispatch, 645, 658
 Economic dispatch, conventional, 661
 Economic dispatch, decentralized, 670
 Economic dispatch, deregulated industry, 670
 Economic dispatch, generalized, 662
 Economic dispatch, unconstrained, 662
 Economic objectives, 658
 Economy, 642
 Efficiency, 642, 721
 Eigenvalue, maximum, 609
 Eigenvalue, minimal, 609
 Electrical distance, 277, 618, 622
 Electricity market, perfect conditions, 671
 Electricity market power, 675
 Electricity market price, 671
 Electricity market, spot, 667, 723
 Electricity market, spot pricing, 761
 Electricity markets, 245, 658, 668
 Electricity markets, bilateral, 660
 Electricity price dynamics, 661
 Electricity price takers, 675
 Electricity price, volatility, 667
 Electricity pricing, 650, 670
 Electromagnetic dynamics, model, 104, 111
 Electromechanical dynamics, synchronous machine of, 79, 112
 Energy, 12, 14
 Energy, electromagnetic, 14
 Energy function, 604
 Energy, kinetic, 604
 Energy markets, 646
 Energy, mechanical, 1
 Energy, potential, 604
 Energy, stored, 14
 Energy storing components, 66
 Equilibrium point, feasible, 453
 Equilibrium point, high, 402
 Equilibrium point, hyperbolic, 404
 Equilibrium point, low, 402
 Equilibrium point, nonhyperbolic, 402
 Equilibrium point, transiently stable, 453
 Equilibrium point, viable, 453
 Equilibrium points, 396, 404, 611
 Equilibrium, postfault, 604
 Equilibrium, prefault, 604
 Equilibrium, stable, 246, 401, 405, 614
 Equipment failures, unexpected, 592, 641
 Equipment, individual types, 135
 Equipment, single-port, 170, 650
 Equipment, single-port, constituent relations of, 171
 Equipment switching, 646

- Equipment, two-port, 170
 Equipment, uniform type, 78
 Equivalent control, 612
 Estimation, 645
 Excitation control systems, 147, 359, 592, 594–595, 604
 Excitation current, 103
 Excitation systems, AC Type
 Excitation systems, brushless, 149
 Excitation systems, DC Type, 142
 Excitation voltage, 111
 Exciter dynamics, 142
 Expected load demand, 5
- Facts, decentralized control of, 630, 646
 Facts (Flexible AC Transmission Systems), 2, 5, 10, 62, 66, 138, 157, 591, 593, 619, 622
 Fast valving, 137
 Faults, 246
 Faults, multiple, 618
 FC-TCR model, 628
 Feasibility boundary, 4, 458, 484, 499, 500, 523
 Feasibility boundary, large scale computations near the, 518
 Feasibility boundary theorem, 485
 Feasibility region, 219, 402, 456, 458, 484, 500
 Federal Energy Regulatory Commission (FERC), 675, 698
 Feedback, 595, 647
 Feedback design, optimal, 601–602, 609
 Feedback, full state, 601, 605, 607
 Feedback linearizing control, 607, 610–611, 623
 Feedback matrix, 603
 Feedback, output, 605
 Feedback, time-varying, 609
 Field leakage flux, 85
 Field, rotating, 83
 Financial entities, 250
 Fink-Carlsen diagram, 643
 Firing angle, 619, 623, 627
 Firing angle, control variable as, 628
 First swing, 604
 Fixed-capacitor-thyristor controlled reactor (FC-TCR), 619, 623, 629
 Flexible parallel computing, 6
- Flux linkage, 106
 Flux linkage, measurement of, 602
 Flux, rotating, 82
 Fourier series, 624
 Frequency, 65
 Frequency control capacity needs, 704
 Frequency control charge, mandatory, 704
 Frequency control, deregulated industry, 697
 Frequency control, flat, 693
 Frequency control, flat, market-based, 714
 Frequency control market, 701
 Frequency control, market based, 698, 700
 Frequency control objective, 701
 Frequency control, primary, 353, 592
 Frequency, damped natural, 596
 Frequency dynamics, slow, 352, 358
 Frequency instability, 606
 Frequency quality, 686
 Frequency regulation, 5
 Frequency regulation, improved, 686
 Frequency regulation, market-based, 5
 Frequency regulation, performance criterion, 685
 Frequency, system, 697
 Frequency, undamped natural, 596
 Functional divisions, 66
- Gaming, 671
 Generation-based control, 591, 601
 Generation-based frequency control, 676
 Generation-based voltage control, 727
 Generation-based voltage control, regulated industry, 728
 Generation companies, 61, 652
 Generation control, regulated, 655, 677
 Generation cost, 662
 Generation cost, aggregate, 669
 Generation cost, short-run marginal (SRMC), 662
 Generation cost, shutdown, 666
 Generation cost, start-up, 666
 Generation dispatch, deregulated, 650, 657, 668
 Generation dispatch, open loop, 697
 Generation dispatch, regulated, 661
 Generation, distributed, 631
 Generation limits, 216
 Generation, must-run, 662

- Generator, 61, 66, 68
 Generator control, decentralized, 604
 Generator control, improved, 605
 Generator control, local, 336, 631
 Generator control, stationary, 235
 control, 647, 649
 Generator dropping, 137, 152
 Generator exciters, 5, 66
 Generator governors, 5
 Generator, must-run time, 666
 Generator, rate of response, 666
 Generator-serving entities (GSEs), 250,
 669
 Generator-turbine-governor unit, 336, 594,
 676
 Generator turn-off time, 667
 Generator turn-on time, 667
 Gershgorin's circle theorem, 222, 385
 Governor control, 592, 601
 Governor dynamics, 138, 336, 352
 Governor speed changer, 139
- Harmonics, 10, 30
 Hierarchical control, 5, 655
 Hierarchical control, deregulated
 industries, for, 5
 Hierarchical control, frequency, 676
 Hierarchical control, regulated industries,
 for, 5
 High voltage problems, 278
 Homotopy methods, 297
 Homotopy methods, forced, 303
 Homotopy methods, free running, 303
 Hopf-bifurcation, 4
 Hopf-bifurcation, computational aspects
 of, 500, 511
 Hopf-bifurcation, subcritical, 499
 Hopf-bifurcation, supercritical, 499
 Human operator, 643
 Hybrid systems, 624
 Hydro storage, 661
 Hydro-turbines, 139
- Implicit function theorem, 460
 Inadvertent energy exchange, 689
 Incidence matrix, 180
 Incidence matrix, reduced, 180
 Induction, combination of first and second
 kind, 109
 Induction, first kind, 107
 Induction, second kind, 108
 Inductor, 13–14, 593
 Inductor, energy contents of, 14
 Inductor, instantaneous power flow, into,
 13
 Industry structure, deregulated, 5, 652
 Industry structure, regulated, 5
 In extremis operating mode, 642,
 646–647
 Infinite bus, 69
 Information, symmetric, 671
 Instability, dynamics, 593
 Instability, long range, 208
 Instability, long range, in active power,
 208
 Instability, long range in reactive power,
 209
 Instability, medium range, 208
 Instability, transient, 593
 Instantaneous power flow, 12
 Instantaneous power flow control, 618
 Integral manifold, 343
 Integrity crisis, 647
 Interaction variables, 729
 Interaction variables, continuous, 730
 Interaction variables, quasistatic, 729
 Interarea dynamics, 334
 Interarea dynamics model, 367
 Interarea variable, computation of, 366
 Interarea variable, definition of, 364
 Interconnected system, large, 642
 Interconnected system, state-space model,
 358
 Interconnection, 391, 730
 Intra area dynamics, 334, 340, 363
 Intra area variable, 334
 Islanding, 647
 Isolated system, 71
 Isolated system, full state space, 71
- Jacobian, 403, 463, 633–634
 Jacobian, positive definite, 634
 Jacobian, singular, 321, 684
 Jump phenomenon, 457
- Kirchhoff's flow equations, 224
 Kirchhoff's laws, 179
 Kirchhoff's voltage equations, 224

- Lagrangian relaxation method, 664
 Large-scale faults, 3
 Large-scale power systems, 605
 Large-scale power systems, horizontal structure, 676
 Limiter, exciter, 148
 Limit, hard, 148, 392, 451, 523, 540
 Limit, non-wind-up, 530
 Limits, 148
 Limits, discontinuous, 392
 Limit, wind-up, 148, 530
 Line compensation, 283
 Line dropping, 137, 152, 646
 Load, 61, 68
 Load, commercial, 132
 Load compensation, 278
 Load, composite, 66, 128
 Load, constituent relations of, 176
 Load control, 592, 631, 685
 Load demand cost, aggregate, 669
 Load demand, decrease, 235
 Load demand following, 675
 Load demand, forecasted, 659
 Load demand, must-serve, 662
 Load demand price elasticity, 662
 Load demand, price-responsive, 666
 Load dropping, 137, 152, 647
 Load dynamics, 127, 655
 Load flow problem, DC, 223
 Load flow problem, deregulated industry, 245
 Load flow problem, 215–216
 Load, heavy, 596, 609
 Load, industrial, 132
 Load management, 645
 Load models, 127, 259, 427
 Load models, constant power type, 132, 261
 Load models, dynamic, 134
 Load models, impedance type, 131, 259
 Load models, parameters, 133
 Load models, static, 129
 Load, primary control of, 591
 Load, residential, 132
 Load-serving entities (LSEs), 250, 669, 700, 705, 723
 Load shedding, 152
 Load shedding, decentralized, 210
 Load shedding, under-frequency, 631
 Load shedding, under-voltage, 631
 Load voltages, 272
 Localized response, phase angle, 235
 Localized response, phase angle difference, 238, 240
 Localized response, reactive power-voltage, 631, 780
 Long-term dynamics, 337
 Losses, resistive, 224
 Loss of generators, 3
 Low-pass phasor signals, 559
 Low voltage problems, 274, 401
 Lyapunov matrix equation, 603
 Lyapunov stability theory, 457
 Marketer, 249, 667, 669
 Mathematical model, 65
 Maximum, local, 283
 Maximum power transfer, theorem, 26, 275, 277, 620
 Measurements, local, 594
 Mechanical dynamics, 67
 Mechanically switched compensation, 591, 594
 Mechanical switching, 149, 593, 631
 Merchandise surplus, 763
 Midterm dynamics, 337
 Model reduction, coherency-based, 373
 Model-reduction techniques, 334
 Modulated sinusoidal signals, 11
 Multiport power system, 278
 Multicontrol area, 707
 Multi-input-multi-output (MIMO) dynamic systems, 607
 Multiparameter singular perturbation model, 337
 Multiphase circuits with harmonics, 58
 Network analyzers, 391
 Nodal prices, 763, 765
 Nonlinear controller, 591, 605, 610, 630
 Nonlinear controllers, discontinuous, 630
 Nonlinear dynamic systems, 605
 Nonlinear network with independent sources, 261
 Normalization, p.u. 221
 Normalization, standard, 383
 Numerical instabilities, 290
 Numerical integration, 391, 499

- Observability, 603, 606
 Observation decoupled state space (ODSS), 594, 613–615
 Observer, 606–607
 ODSS reference vector, 616
 OLTC malfunctioning, 277, 632
 OLTC, mechanically switched, 150
 OLTC model, 151, 632–633
 On-load tap-changing (OLTC) transformers, 4, 136–137, 405, 523, 592, 631
 Operating objectives, 648, 650, 658
 Operating principles, 648
 Operating rules, 648
 Operation, commodity-type, 61
 Operation, deregulated, 648, 650
 Operation, government regulated, 648, 650
 Operation, hierarchical, 190
 Operation, on-line, 642
 Operation under competition, 609, 698
 Optimal power-flow, 6, 719
 Optimal switching, 621
 Outage, equipment, 604
 Outage, generator, 235
 Outage, transmission line, 235
 Output control design, 606
 Output variables, 603, 611, 678
 Output variables, measurement of, 603
 Overload capability, 647
 Overvoltages, 285
 Parameter space, 394, 396, 401, 409, 454, 460, 525
 Partial differential equations, 576
 Participation factors, 383
 Performance index, 602, 608
 Periodic current, 28
 Periodic orbit, 421, 456
 Periodic power, 28
 Periodic signals, 28, 35
 Periodic voltage, 28
 Per unit system (p.u.), 81
 Phase compensation, 600
 Phase portraits, 396, 403, 440
 Phase-shifters, rapidly adjustable (RAPS), 593
 Phase-shifting transformers, 137, 151, 592, 622
 Phase-shifting transformer, thyristor controlled, 158
 Phase voltages, 82
 Phasor calculus, quasistationary, 2–3
 Phasor calculus, stationary, 23
 Phasor, definition, 19
 Phasor dynamic model, 622
 Phasor measurements, 604, 609
 Phasors, 9
 Phasors, generalized, 33
 Phasors, time-varying, 555, 626
 Pilot point-based control, 67, 731, 734
 Pilot point loads, 274
 Power, 20
 Power, active, 16
 Power, average, 16
 Power balance equation, incremental, 256
 Power, complex valued, 558
 Power demand, deviations in, 592
 Power-electronic switched compensation, 591
 Power-electronic switched devices, 66, 69, 594, 622
 Power exchange (PX), 652, 674
 Power factor, 16
 Power factor control, 287
 Power factor, load, 283
 Power flow balance equations, 69, 218, 633
 Power-flow, basic, 17
 Power flow equations, homotopy methods for solving, 307
 Power flow equations, Jacobian of, 222, 256, 289, 302
 Power flow equations, linearized, 221, 253
 Power flow equations, numerical methods for solving, 290
 Power flow limits, 217
 Power flow problem, coupled, 285
 Power-flow, single-phase transmission lines, 13
 Power-flow, three-phase transmission lines, 17
 Power, frequency-domain, 20
 Power, imaginary, 16
 Power, imaginary total, 197
 Power industry, deregulated, 245
 Power industry, regulated, 245
 Power industry restructuring, 245
 Power, instantaneous, 557
 Power, instantaneous three-phase, 18

- Power load flow problem, 215
 Power, natural, 284
 Power network, nonlinear monotonic, 232
 Power network, nonlinear nonmonotonic, 233
 Power network response, localized, 235
 Power, phasor interpretation, 40
 Power pools, 61
 Power, Q, 16
 Power, reactive, 16
 Power, real, 16, 66
 Power, real total, 197
 Power signals, 10
 Power signals, periodic, 10
 Power system collapse, cascading, 642
 Power system compensation, 278
 Power system component, classification, 170
 Power system control objectives, 641
 Power system, deregulated, 2
 Power system, engineering, 6
 Power system equilibrium, 213
 Power system equilibrium, operationally acceptable, 214, 224
 Power system equilibrium, unconstrained, 214
 Power system equivalencing, 371
 Power system inputs, 245
 Power system input variables, 172
 Power system, minimal, 392–393
 Power system model, 65
 Power system model, analytic, 169
 Power system model, computer-aided, 169
 Power system model, lower-order, 602
 Power system model, nonlinear, 191
 Power system model, nonlinear in ODE form, 196
 Power system model, structure-preserving, 457
 Power system monitoring objectives, 641, 645
 Power system, multimachine, 607–608
 Power system, operation, 3
 Power system, operation, control-assisted, 5
 Power system operation in alert mode, 642, 645
 Power system operation, in emergency mode, 592, 604, 606, 642, 646
 Power system operation, in normal mode, 592, 594, 642, 645
 Power system operation in restoration mode, 642, 647
 Power system operation objectives, 641
 Power system operation, static, 200
 Power system operation, stationary, 200, 214
 Power system oscillations, 619
 Power system output variables, 172
 Power system performance, 591
 Power system, regulated, 2
 Power system, rudimentary, 392, 405
 Power system sensitivity matrix, input-output, 235, 733
 Power system stability problems, 198, 610
 Power system stabilizers (PSSs), 5, 592, 598–600, 607
 Power system state variables, 172, 626
 Power system tier, 235
 Power system under stress, 591, 613
 Power system viability, 247, 646
 Power-transfer capability, 3, 619, 766
 Power-transfer, existence of solutions, 3
 PQ curve, 421
 Primary controllers, 66, 135, 336, 591, 604, 606, 630
 Primary controllers, decentralized, 5
 Primary controllers, fast continuous, 594
 Primary controllers, local measurements, 5
 Primary control models, 67
 Probabilistic load distribution, 667
 Profit, 670–671, 724
 Protection devices, 161, 285, 622, 643
 Pseudoequilibrium, 402, 462
 PV curve, 421
 Quadrature-axis flux, 88
 Quasistationary assumption, 9
 Quasistationary assumption, beyond, 555
 Radial circuit, 276
 Reactance, inductive, 21
 Reactance, main field, 110
 Reactance, mutual coupling leakage, 110
 Reactance, self-leakage, 110
 Reactive power, 25, 30, 54, 627

- Reactive power compensation, 628
 Reactive power compensation, fast, 630
 Reactive power, conservation, 43
 Reactive power definitions, 55
 Reactive power demand, 628, 631–632, 716
 Reactive power dispatch, 715
 Reactive power dispatch, deregulated industry, 720
 Reactive power dispatch, economy, 715
 Reactive power dispatch, market for, 723
 Reactive power dispatch, regulated industry, 716
 Reactive power load flow problem, solution existence, 269
 Reactive power management, 6
 Reactive power management, regulated industry, in the, 6
 Reactive power matrix, 41, 43
 Reactive power transport, loss, 716, 722
 Reactive power voltage dynamics, decoupled and linearized, 359
 Reactive power voltage problem, steady state, 258, 262, 722
 Reactor, thyristor-switched, 157
 Real power transfer, 277, 283
 Real power transfer, heavy, 274
 Real-time measurements, 607
 Reference angle, 69, 611
 Reference angle, decentralized, 618
 Reference angle, moving, 618
 Reference direction, stationary, 81
 Reference signal, centralized, 618
 Region of attraction, 322, 401, 405, 454, 460, 474
 Region, quasistationary, 24, 25
 Regular points, 398, 403
 Relaxation numerical methods, 325
 Relays, 161
 Relevant modes, 382
 Reserve, cold, 647
 Reserve, spinning, 647
 Resistive network, 223
 Resistive network interpretation, reactive power load flow problem of, 266
 Resistive network interpretation, real power load flow problem of, 223, 225
 Resistive network, linear, 266
 Riccati equation, 602, 608
 Rotating vectors, 81
 Rotor-angle transient stability, 555
 Secondary control, conventional, 734
 Secondary control, 650, 653–654, 686
 Secondary control, improved, 736
 Secondary control, output variables, 685
 Secondary control, voltage, 728, 731, 733
 Secondary level model, 679, 683, 728
 Security boundary, 247
 Security constraints, 249, 613
 Security regions, 245, 454
 Selective modal analysis (SMA) method, 334, 381
 Sellers, 668
 Sensitivity, line flow wrt power input, 759
 Sensitivity, steady state frequency wrt real power, 681
 Sensitivity, terminal voltage wrt flux linkage, 596
 Sensitivity, terminal voltage wrt rotor angle, 596
 Sensitivity, torque wrt rotor angle, 595
 Sensitivity, torque wrt to flux linkage, 595
 Series capacitor compensation, 62, 137, 285, 619
 Series capacitors, controllable, 138, 156–157, 593, 613
 Series capacitors, rapidly adjustable (RASC), 593
 Set point, 652, 680
 Set point, postfault, 593, 646
 Shaft power balance, 79
 Short circuit, balanced, 86
 Short circuit current, DC component, 103
 Short circuit currents, 94, 274
 Short circuit, general load, 90
 Short circuit, inductive load, 90
 Short circuit, no load, 89
 Shunt capacitance, 264, 285, 593
 Simulations, on-line, 594
 Singular dynamics hierarchy theorem, 463
 Singular perturbation method, 109, 334, 337, 376
 Singular perturbation method, limits of validity, 454
 Singular points, 398, 403, 406
 Slack bus, 69, 224, 235
 Sliding regime, 612

- Sliding surface, 611–612
 Small signal dynamics, 333
 Small signal dynamics, closed-loop, 601, 629
 Small signal stability, 334, 595
 Small signal stabilization, 619
 Smooth constraints, 451
 Smooth nonlinear dynamics, 392, 451
 Social welfare, 662, 671
 Speed-governing systems, 139–141
 Stability, 104
 Stability boundary, 401, 456
 Stability boundary theorem, 477
 Stability, dynamic, 333
 Stability limit, steady-state, 222, 231–232, 619
 Stability margin, 219
 Stability region, 473
 Stability, small signal, 204
 Stability, transient, 205, 600, 621
 Stability, transient in active power, 205
 Stability, transient in reactive power, 206
 Stabilization, 4, 612, 618
 Stabilization, transient, 619
 Standards, technical, 721
 State space, 394, 396, 409, 454, 460
 State-space averaged model, 157, 623
 State space form, standard, 602
 State variable, local, 171
 State variable measurements, 605
 Static models, 66
 Static stability, 201
 Static stability limit, 203
 Static stability, reactive power, 201
 Static stability, real power, 201
 Static Var compensators (SVCs), 62, 68, 138, 405, 593, 619, 629
 Stationary analysis, 213
 Stationary analysis, deregulated industry in, 249
 Stationary conditions, 3
 Stationary generation control, 5, 641
 Stationary generation control, congestion included, 757
 Stationary manifold, 397
 Stationary processes, analysis of, 2
 Stator dynamics, 109
 Steady state error, primary control, 682
 Steady state stability, 285
 Steady state transfer limit, 286
 Steam turbines, 139, 661
 Storage devices, 61
 Structural changes, 499
 Structural control, 149, 607, 646
 Structure, 61, 65, 336, 609, 647
 Structure-based hierarchical control, 676, 752
 Structure-based hierarchical modeling, 676, 749
 Structure, deregulated, 648
 Structure, hierarchical measurement and control, 657
 Subsynchronous resonance, 335, 622
 Subsystem, 190, 607, 611
 Subsystems, weakly connected, 334
 Subtransient dynamics, suppressing 117
 Subtransient reactance, 97–98, 101
 Subtransient short-circuit current, 101
 Switching, duty ratio, 631
 Switching function, 172
 Switching losses, 631
 Switching signal, binary, 624, 626
 Synchronous condensers, 149
 Synchronous machine, classical model (Type IV1), 117, 122, 596
 Synchronous machine, complete (Type I) model of, 111
 Synchronous machine, constituent relations of, 173
 Synchronous machine, controllers, 137
 Synchronous machine, exciter control, 137
 Synchronous machine, governor control, 137
 Synchronous machine model, decoupled voltage model (Type IV2), 122
 Synchronous machine model, derivation, 162
 Synchronous machines, 78, 104
 Synchronous machine, secondary constants, 113
 Synchronous machine, simplified models, 114
 Synchronous machine, single axis model (Type III), 121
 Synchronous machines, state variables of, 111
 Synchronous machine, time constants, 113

- Synchronous machine, two-axis flux decay model, 121, 341
- Synchronous reactance, 90, 104
- Synchronous speed, 82
- Synchronous time, 697
- System, national, 61
- System, physical, 648, 650
- System transmission capability (STC), 247
- Target tracking, ODSS-based, 617
- Taxonomy theory, 452
- Technologies, HV-DC, 136
- Tertiary control, 650, 654, 680, 688, 690, 715, 731, 738
- Tertiary control, performance criteria, 740
- Textured model, 6, 811
- Thyristor, 62, 154
- Thyristor-controller reactor, model of, 155, 622
- Thyristor, gate-turn-off (GTO), 157
- Thyristor switching function, 155
- Tie-line currents, 191
- Tie-line power flow, 191, 659
- Tie-line power flow, net, 680, 697
- Tie-line power flow scheduling, 661
- Time constant, transient, 87
- Time-domain, current, 10
- Time-domain, energy, 10
- Time-domain, power, 10
- Time-domain, voltage, 10
- Time error, 679, 715
- Time histories, state 394, 400
- Time period, 65
- Time-scale separation, 372, 593, 679
- Time-scale separation, classification of primary controllers, 593, 654
- Time-varying phasors, limitations to, 584
- Time-varying phasor transformation, generalized, 556, 562, 623
- Time-varying process, 633
- Torque, damping, 596, 698
- Torque, synchronizing, 596
- Trading entities, 250, 669
- Transaction, 24
- Transaction, bilateral, 241, 249, 257, 669
- Transactions, analysis, 250
- Transactions matrix, 251, 253–254
- Transactions, multilateral, 258
- Transactions network, 249, 670
- Transfer function, torque-angle, 597
- Transformers, 68
- Transient impedance, 95
- Transient reactance, 90, 95, 104
- Transient time constant, 87
- Transmission company, 61
- Transmission-congestion, 6, 652, 757
- Transmission congestion control, 765, 778
- Transmission congestion control, soft-constraints based, 769
- Transmission-congestion, deregulated industry, in the, 6
- Transmission-congestion, pricing, 6, 760
- Transmission, HV-DC, 619
- Transmission line, carrying capability, 284
- Transmission line, characteristic impedance, 283
- Transmission line control, 592, 630
- Transmission line, dynamic model, 178
- Transmission line flow control, 661, 759
- Transmission line, lumped parameter model, 73, 454
- Transmission line, model, 72
- Transmission line, primary control of, 591
- Transmission lines, AC, 72
- Transmission lines, constituent relations of, 176, 225
- Transmission line, static model, 177
- Transmission loss, minimization, 26, 650
- Transmission network constraints, 5, 650
- Transmission network control, 631
- Transmission price feedback, 766, 768
- Transmission rights, 765
- Transmission system capacity, 245, 762
- Transmission system control, FACTS-based, 618
- Transmission system provider, 245, 724
- Transmission system usage, 249
- Traveling waves, 452
- Turbine dynamics, 138
- Turbine system model, general, 143
- Typal region, 402, 461, 489
- Uniform bus transmission capability (UBTC), 248
- Unit commitment, 5, 645, 658, 661
- Unit commitment, coordinated, 659
- Unit commitment, decentralized, 671
- Unit commitment, deregulated industry, 670

- Unit commitment, generalized, 665
Unit commitment, optimal decisions, 667
Unit commitment, simplest, 664
Unit commitment, stochastic, 667
Unit commitment, switching curve law, 665
Unit commitment, switching curve law, generalized, 665
- Variable structure control, 605, 607, 611, 621
Vector phasors, 28, 35
Voltage behind subtransient reactance, 101, 111
Voltage behind transient reactance, 111
Voltage collapse, 3, 277, 419
Voltage collapse, dynamic, 426
Voltage collapse, equipment-related, 426
Voltage collapse, parametric, 426
Voltage control, direct, 287
Voltage controllers, 136, 555, 592, 619
Voltage, critical, 274, 276
- Voltage dynamics, 392
Voltage dynamics, midrange, 340, 348, 359
Voltage dynamics, slow, 349, 351
Voltage dynamics, typal regions, 414
Voltage, field, 597
Voltage limits, 216
Voltage oscillations, 613
Voltage quality, 724
Voltage-reactive power compensation, 278, 716
Voltage regulation, 5, 593, 595
Voltage regulation, market-based, 5
Voltage-related market power, 726
Voltage-related problems, 632
Voltage schedule, optimal, 721
Voltage stability, 9, 337, 400, 555
Voltage stability, transient, 418
- Wave equation, time-delay solution, 572
Winding, armature coil, 106
Winding, field excitation, 106
Winding, rotor damper, 106